14th International Conference on Sustainable Energy Technologies

25th to 27th August 2015, Nottingham, UK

SUSTAINABLE ENERGY FOR A RESILIENT FUTURE

Conference Proceedings
Volume II

The University of Nottingham

UNITED KINGDOM · CHINA · MALAYSIA

Proceedings of the
14th International Conference on
Sustainable Energy Technologies – SET 2015
25th to 27th August 2015, Nottingham UK

Sustainable Energy for a Resilient Future

Volume II

Edited by

Lucelia Rodrigues

SET 2015 Co-Chair and Chair of the Scientific Committee
Architecture, Energy & Environment Research Group
Department of Architecture and Built Environment
Faculty of Engineering, University of Nottingham

Supported by the Conference Organising Committee:

Chair: Professor Saffa Riffat
Co-chair: Professor Mark Gillott
Event Manager: Zeny Amante-Roberts
Administrative Manager: Claire Hardwidge
Proceedings Support: Phil Roberts
Marketing: Guillermo Guzman
Webmaster: Johnny Mistry

Reference to a conference paper:

To cite a paper published in these conference proceedings, please substitute the highlighted sections of the reference below with the details of the article you are referring to:

Author(s) Surname, Author(s) Initial(s), 2015. 'Title of paper'. *In*: Rodrigues, L. ed., *Sustainable Energy for a Resilient Future: Proceedings of the 14th International Conference on Sustainable Energy Technologies,* 25-27 August 2015, Nottingham, UK. University of Nottingham: Architecture, Energy & Environment Research Group. Volume X, pp XX-XX. Available from: eprints.nottingham.ac.uk [Last access date].

ISBN Volume II: 9780853583141

Version: 07.07.2016

FOREWORD

Dear Reader,

I am delighted to present you with volume II of the 14th International Conference on Sustainable Energy Technologies with a theme focus on 'energy storage & conversion' and 'policies & management'. For me, volume II is the meat in the sandwich between volumes I and III. For without energy storage technologies and sound robust policies we could be hampered in our goal of achieving a sustainable world for current and future generations. Energy storage and energy conversion technologies are essential for overcoming the intermittency of the majority of renewable energy technologies and are therefore an essential part of their wide scale adoption and use.

At SET 2015 we had an excellent key note presentation from Professor Tianshou Zhao on 'Innovating Energy Storage Technologies for a Sustainable Future'. Prof Zhao highlighted how important storage technologies are in our pursuit of a low carbon world and highlighted the many advancements made by the international scientific community in innovating energy storage technologies. Many of these innovations were presented by delegates at the conference.

Chris Twinn introduced the Policies and Management section of the conference with his thought provoking excellent keynote presentation entitled 'The goal posts are changing - are we ready for the new direction?'. As scientists and engineers undertaking research in sustainable energy technologies we need sound, robust and long term policies that help support, deliver and implement their eventual use in real world applications. Science and engineering also has a role to play in informing policy in the short, medium and long term with innovations and robust scientific data. These issues were discussed and debated at length in our sessions on 'Environmental Issues and the Public', 'Energy and Environment Security' and 'Energy and Environment Policies'.

Whilst you have only reached the mid-point volume in our conference proceedings I trust you find the content both stimulating and informative. On a personal note, it was an absolute pleasure to host the 2015 conference in Nottingham and receive so many delegates from the global SET family. I hope you all enjoyed elements of what Nottingham had to offer from Robin Hood to Samba! I would like to thank all of you for your contributions and look forward to meeting up again at future SET conferences.

Professor Mark Gillott
Chair in Sustainable Building Design
SET 2015 Co-Chair

CONFERENCE PROCEEDINGS STRUCTURE

Volume I

Energy Technologies & Renewables

Volume II

Energy Storage & Conversion

Keynote Speaker Professor Tianshou Zhao: “Innovating Energy Storage Technologies for a Sustainable Energy Future”
Session 2: Heating and Cooling Systems
Session 6: Heating and Cooling Systems
Session 10: Ventilation and Air Conditioning
Session 14: Smart and Responsive Buildings
Session 18: Phase Change Materials
Session 23: Smart and Responsive Buildings
Session 30: Heating and Cooling System
Session 34: Carbon Sequestration
Poster Session A
Poster Session C
Poster Session D

Policies & Management

Keynote Speaker Chris Twinn: “The goalposts are changing – are we ready for the new direction?”
Session 4: Environmental Issues and the Public
Session 8: Energy and Environment Security
Session 12: Energy and Environment Policies
Poster Session A
Poster Session D

Volume III

Sustainable Cities & Environment

Keynote Speaker Professor Matheos Santamouris: “Urban Warming: Evidence, Impacts and Mitigation “
Keynote Speaker Professor Edward NG: “Sustainable Living in Compact Urban and Built Environment in the Tropics”
Session 3: Sustainable and Resilient Cities
Session 7: Energy Demand and Use Optimization
Session 11: Energy Efficiency in Buildings
Session 15: Green and Sustainable Buildings
Session 19: Green Buildings and Materials
Session 24: Energy Efficiency in Buildings
Session 27: Energy Efficiency in Buildings
Session 28: Energy Efficiency in Buildings
Session 31: Energy Efficiency in Buildings
Session 35: Energy Efficiency in Buildings
Poster Session A
Poster Session D
Poster Session E

CONTENTS

ENERGY STORAGE & CONVERSION

Keynote Speaker Professor Tianshou Zhao: “Innovating Energy Storage Technologies for a Sustainable Energy Future”

T S Zhao is Chair Professor of Mechanical & Aerospace Engineering at HKUST, the Director of the HKUST Energy Institute, and a Senior Fellow of the HKUST Institute for Advanced Study.

Prof Zhao combines his expertise in research and technological innovation with a commitment to creating clean energy production and storage devices for a sustainable future. He has made seminal contributions in the areas of fuel cells, flow batteries, multi-scale multiphase heat and mass transport with electrochemical reactions, and computational modeling. In addition to four edited books, 10 book chapters and over 50 keynote lectures at international conferences, he has published more than 210 papers in various prestigious journals. These papers have collectively received more than 7,300 citations and earned Prof Zhao an h-index of 50 (Web of Science). In recognition of his research achievements, Prof Zhao has in recent years received many awards, including the 2013 State Natural Science Awards, the Overseas Distinguished Young Scholars Award (NSFC), the Croucher Senior Research Fellowship Award, and the HKSUT Engineering Distinguished Research Excellence Award, among others. He is elected ASME Fellow and the Royal Society of Chemistry’s Fellow. He was named a Highly Cited Researcher in Engineering by Thomson Reuters in 2014.

In the international community, Prof Zhao serves as Editor-in-Chief of Advances in Fuel Cells, Editor-in-Chief of Aplied Thermal Engineering and Editor of the Royal Society of Chemistry (RSC)’s Energy & Environmental Science. He has served as an editorial board member for more than 10 prestigious international journals.

SESSION 2: HEATING AND COOLING SYSTEMS

51: Identification of chiller maintenance factors using Bayesian Markov Chain Monte Carlo method

PEI HUANG[1], GONGSHENG HUANG[2]

[1] City University of Hong Kong, Tat Chee Avenue, Kowloon, Hong Kong, Email: peihuang2-c@my.cityu.edu.hk
[2] City University of Hong Kong, Tat Chee Avenue, Kowloon, Hong Kong, Email: gongsheng.huang@cityu.edu.hk

HVAC systems are used in modern buildings to provide indoor thermal comfort and acceptable indoor air quality. Aging and degradation are prevalent among HVAC systems. They inevitably lead to the decrease in the efficiency and maximum cooling capacity of HVAC systems. As a result, the annual energy use will increase and the risk that the HVAC system cannot provide enough capacity will be high. Hence aging and degradation always represent a crucial consideration for designers.

In the life cycle analysis or the performance prediction of HVAC systems, the level of aging and degradation of a HVAC system or component are quantified using maintenance factor (MF). In general, good maintenance will delay the aging and degradation effects, and will therefore have a small maintenance factor. Poor maintenance accelerates the aging and degradation and will have a large maintenance factor. A conventional analysis recommends that the maintenance factor should be 0.01 for systems or components that undergo annual professional maintenance, and 0.02 for those that are seldom or never maintained. It is known that those recommendations are mainly based on a rule of thumb, and may not be accurate enough to describe the degree of aging for a given HVAC plant.

This research therefore proposes a framework of identifying the chiller maintenance factor using available in-situ cooling capacity data. The proposed method firstly employs the Bayesian inference to produce the posterior distribution of the maintenance factor, and then the Markov chain Monte Carlo method to generate samples from the posterior distribution. Using these samples, the mean, the standard deviation and some other statistical characteristics of the maintenance factor can all be obtained. The calibrated maintenance can then be used to predict the chiller plant maximum capacity, which can be used in decision making on the maintenance scheme. Details of the identification process will be provided by applying the proposed method to a real chiller plant, and results will be compared with that of a conventional analysis.

Keywords: Degradation, HVAC, maintenance factors, Bayesian Inference, Markov chain Monte Carlo

1. INTRODUCTION

Energy audit indicates that buildings consume over 40% of end-use energy worldwide, and this percentage even increases to over 90% in Hong Kong (LAM, LI, and CHEUNG 2003: page 498). In a large commercial building, its heating, ventilation and air-conditioning (HVAC) system always represents the largest primary energy end-use. One way to improve the building energy efficiency is to design HVAC appropriately. However, this is not easy since uncertainties exist inevitably in the HVAC design process (DE WIT 2003: page 35). Uncertainties easily lead to improper decision making on the sizing of HVAC components, which may result in additional energy usage/cost (if oversized) or capacity deficiency (if undersized) (HUANG, HUANG, and WANG 2015: page 33). Many studies have investigated the uncertainties in the prediction of the building peak load (DE WIT 2003: page 29; HOPFE 2009: page 27; EISENHOWER et al. 2012: page 7; HUANG, HUANG, and WANG 2015: page 28), which is one of the most important parameters to size HVAC components. However, a proper sizing is not only affected by the uncertainties associated with the building peak load but also the uncertainties associated with the effective cooling capacity provided by the HVAC system. This is because capacity loss occurs during the transmission and capacity degradation in HVAC components over the service life cannot be avoided.

In the life-cycle analysis of the maximum capacity provided by a HVAC system, aging always represents a crucial consideration for designers. The aging effect is prevalent and will inevitably lead to degradation in HVAC system performance and potential sacrifices of thermal comfort (HUNTER 1941: page 15; SMITH 1983: page 5; HU 2009: page 106; ASHRAE 2012: chapter 17.5; DONG et al. 2014: page 316). For example, material degradation may result in decreased filtration efficiency, defective seal, and system component damage (ASHRAE 2012: chapter 17.5); aged ferrous pipe has a capacity loss of 40 to 80%; and aged copper pipe has a capacity loss of 25 to 65% (HUNTER 1941: page 15). As a result, the annual energy use and the risk that the HVAC system cannot provide adequate capacity for thermal comfort may increase. Previous studies by DONG et al. (2014: page 316) indicate that HVAC systems will consume electrical energy 20% more than that in the design intent due to the equipment aging and degradation (e.g., filter or heat exchanger fouling). Therefore, how to deal with the aging and degradation effect becomes an urgent issue.

The aging effect can be quantified using different models for different components or processes (ARI 1989: page 45; MATSON et al. 2002: page 53; HENDRON 2006: page 7; ASHRAE 2012: chapter 17.5; LEE et al. 2014: page 541; TREMBLAY and ZMEUREANU 2014: page 198). For instance, the aging of photovoltaic (PV) panels can be described using a degradation range coefficient and a scale model was suggested to estimate the yearly generated power (ASHRAE 2012: chapter 17.5; LEE et al. 2014: page 541). TREMBLAY and ZMEUREANU (2014: page 198) quantified the degradation in heat exchanger effectiveness as a decaying constant and suggested a linear model to estimate the hourly heat exchanger effectiveness. The degradation in chiller plants' coefficient of performance (COP) can be modelled with a degradation coefficient and again a linear model was suggested to estimate the degraded COP (ARI 1989: page 45). Remarkably, MATSON et al. (2002: page 53) linked the aging effect in HVAC components with their maintenance and used a maintenance factor to quantify the yearly efficiency. The components' degraded capacity can then be described using an exponential model. MATSON et al.'s (2012: page 53) model has been proved to be effective, and a conventional analysis recommends that if the system or component undergoes annual professional maintenance, the maintenance factor should be considered as 0.01; otherwise, it should be 0.02 (HENDRON 2006: page 7). Unfortunately, this recommendation is mainly based on a rule of thumb, and may not be accurate enough to describe the degree of aging for a given chiller plant since the maintenance factor will be affected by many factors, such as maintenance scheme, maintenance personnel, operating condition and even the environment. Those factors are difficult to quantify and inevitably lead to an improper estimation of the maintenance factor. Therefore in this article, the author defines a parameter of degradation remaining percentage R according to the maintenance factor, and proposes a method to identify the chiller aging effect using available in-situ data in a stochastics framework.

Bayesian inference is a powerful tool for adjusting and calibrating simulation models using in-situ data. Literature review reveals that the Bayesian inference has been widely used in building simulation (HEO, CHOUDHARY, and AUGENBROE 2012: page 553; BOOTH, CHOUDHARY, and SPIEGELHALTER 2013: page 296; NOH and RAJAGOPAL 2013: volume 8692; HEO et al. 2015: page 136; KIM, AHN, and PARK 2014: page 113). For example, BOOTH, CHOUDHARY, and SPIEGELHALTER (2013: page 296) used a Bayesian method to calibrate the micro-level models with the macro-level data to improve the model accuracy. NOH and RAJAGOPAL (2013: page 5) used a Bayesian method to predict the

building next-day energy consumption. Notably, HEO, CHOUDHARY, and AUGENBROE (2012: page 553) adopted a Bayesian Markov Chain Monte Carlo (MCMC) method to calibrate uncertain input parameters for evaluating the peak thermal load, including the infiltration rate, the discharge coefficient and the indoor temperature set-point. KIM, AHN, and PARK (2014: page 113) applied the Bayesian MCMC method to balancing the construction cost of a building and its total energy consumption. Due to its wide application, the Bayesian MCMC method will be adopted in this study.

In this article, the authors propose to use the Bayesian MCMC method to identify the chiller plant aging effect using available in-situ cooling capacity data. The proposed method firstly employs the Bayesian inference to produce the posterior distribution of the degradation remaining percentage *R* (defined by Equation 3), and then uses the MCMC method to generate samples from the calibrated *R* posterior distribution. The calibrated *R* will then be used to predict the chiller plant maximum cooling capacity in the future years. The objective of this study is to assist HVAC designers to quantify the aging effect accurately and evaluate the life-cycle performance of their HVAC components. Based on the observation that (i) many HVAC researchers and engineers might not be familiar with the Bayesian MCMC method; and (ii) current relevant studies, which are found in HVAC engineering such as the references (HEO, CHOUDHARY, and AUGENBROE 2012: page 553; KIM, AHN, and PARK 2014: page 113), give a very sketchy introduction to the Bayesian MCMC method, therefore the implementation process of the Bayesian MCMC method will be introduced in detail in this paper.

2. METHODOLOGY

Capacity degradation model

From MATSON et al.'s (2002: page 53) study, the performance degradation rate of the efficiency of a cooling system is determined using Equation 1.

Equation 1: Efficiency degradation with time

$$EER = (Base\ EER) \cdot (1 - MF)^a$$

Where:

EER = energy efficiency ratio after use
$Base\ EER$ = typical energy efficiency ratio when new
MF = maintenance factor for the system
a = time in years of operation

In general, good maintenance can delay the aging effect and hence leads to a small *MF*; while poor maintenance accelerates the degradation and hence leads to a large *MF*. For a chiller plant, the degradation of its maximum cooling capacity resembles the degrading characteristics of the energy efficiency ratio: the decreasing rate is high at the beginning but becomes low after a long-term use (ASHRAE 2012: chapter 38). Therefore the yearly maximum cooling capacity supplied by the chiller plant is assumed to be described by Equation 2.

Equation 2: Capacity degradation with time

$$Q = Q_0 \cdot (1 - MF)^a$$

Where:

Q = yearly maximum cooling capacity supplied by the chiller plant (kW)
Q_0= chiller plant maximum cooling capacity when it is newly installed (kW)

In Equation 2, the term *(1-MF)* is defined as degradation remaining percentage *R*, as shown in Equation 3.

Equation 3: Degradation remaining percentage

$$R = 1 - MF$$

Where:

R = degradation remaining percentage

In general, *MF* can be quantified to follow Weibull distribution, normal distribution, log-normal distribution, or even exponential distribution (BEN-DAYA et al. 2009: page 49). To simplify the development of the likelihood function for *MF*, *R* is quantified to follow a log-normal distribution, as illustrated in Equation 4.

Equation 4: Distribution of degradation remaining percentage

$$lnR \sim N(\mu, \sigma^2)$$

Where:

lnR = natural logarithm of the degradation remaining percentage
μ = mean of natural logarithm of the degradation remaining percentage
σ =standard deviation of natural logarithm of the degradation remaining percentage

It should be noted that if available in-situ data are abundant, the prior distribution becomes less important as shown in the reference (WANG and CAO 2013: page 114).

Bayesian Markov Chain Monte Carlo

The Bayesian MCMC method is employed to calibrate *R* using the in-situ data, which has two stages: Bayesian inference and MCMC sampling. The Bayesian inference is used to generate posterior distributions for the calibrated *lnR* using the prior knowledge and available in-situ data; while the MCMC sampling is used to generate equivalent samples from the generated posterior distributions. The equivalent samples represent the statistical characteristics of the posterior distributions, and thus they will be used to evaluate the mean and deviation of *lnR* (WANG and CAO 2013: page 111; AU and WANG 2014: page 152; CAO and WANG 2014: page 5). Figure 1 illustrates the process of using the Bayesian MCMC to calibrate *lnR* in detail.

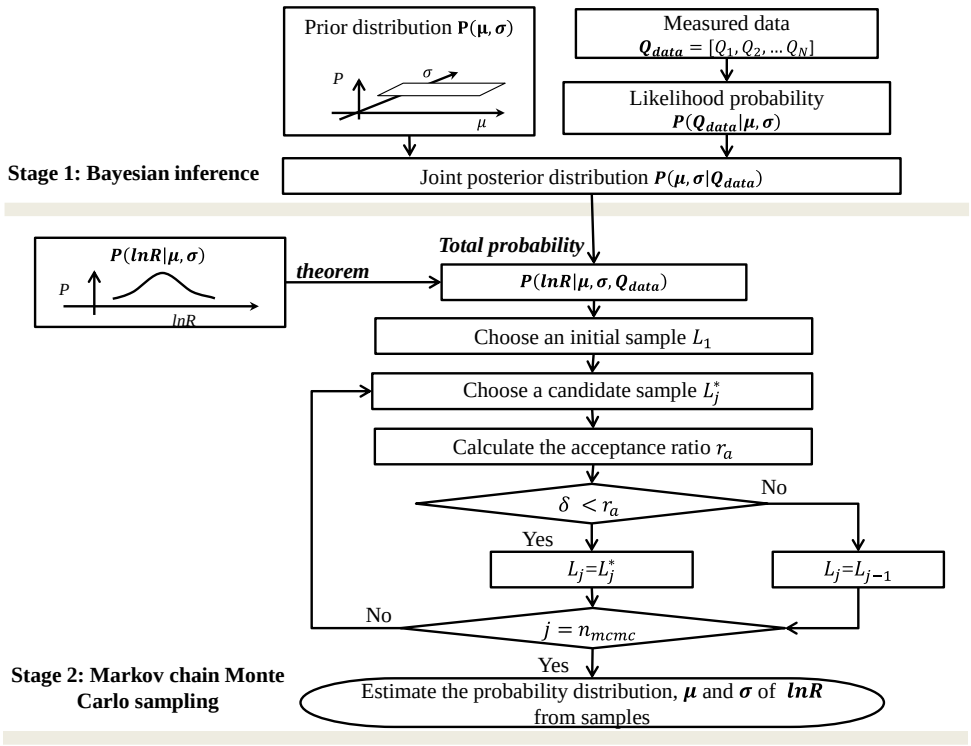

Figure 1: Flowchart of the Bayesian Markov Chain Monte Carlo method

Bayesian inference

Given a model $y=f(\theta)$ and the measured data of y_{data}, the Bayesian inference deduces the posterior probability $P(\theta | y_{data})$ by Equation 5 (BOX and TIAO 2011: page 10).

Equation 5: Bayesian inference

$$P(\theta|y_{data}) = P(y_{data}|\theta) \cdot P(\theta)/P(y_{data}) = \kappa P(y_{data}|\theta) \cdot P(\theta)$$

Where:

θ= uncertain inputs which needs to be calibrated
y_{data} = measured data
$P(y_{data}|\theta)$= likelihood probability showing the possibility of y_{data} occurring given the input θ
$P(\theta)$= prior probability representing the possibility of θ occurring
$P(y_{data})$ = probability representing the possibility of y_{data} occurring (constant)
$\kappa = 1/P(y_{data})$ = normalization constant
$P(\theta|y_{data})$ = posterior probability representing the calibrated possibility of θ occurring given y_{data}

In this study, the maximum cooling capacity Q is the output y, and the mean μ and the standard deviation σ of lnR are the inputs θ as discussed below. A non-informative joint uniform distribution of μ and σ is assumed to be the prior distribution. The joint uniform distribution is expressed as Equation 6 (WANG and CAO 2013: page 108; CAO and WANG 2014: page 3).

Equation 6: Joint prior distribution

$$P(\mu,\sigma) = \begin{cases} \frac{1}{\mu_{max}-\mu_{min}} \times \frac{1}{\sigma_{max}-\sigma_{min}} & for\ \mu \in [\mu_{min},\mu_{max}]\ and\ \sigma \in [\sigma_{min},\sigma_{max}] \\ 0 & others \end{cases}$$

Where:

μ = mean of *lnR*
σ = standard deviation of *lnR*
μ_{min}, μ_{max} = minimum and maximum values of the mean of *lnR*
$\sigma_{min}, \sigma_{max}$ = minimum and maximum values of the standard deviation of *lnR*

Based on Equations 2, 3 and 4 the likelihood probability $P(Q_{data}|\mu,\sigma)$ for available in-situ maximum cooling capacity data $Q_{data} = [Q_1, Q_2, \ldots Q_N]$ is derived as Equation 7.

Equation 7: Likelihood function

$$P(Q_{data}|\mu,\sigma) = \prod_{i=1}^{N} \frac{1}{\sqrt{2\pi}(a\sigma)Q_i} \cdot exp\left(-\frac{(lnQ_i-(lnQ_0+a\mu))^2}{2(a\sigma)^2}\right)$$

Where:

Q_i = measured maximum cooling capacity *(kW)*, which is determined by Equation 8 (ASHRAE 2012: chapter 38.2)

Equation 8: Measured maximum cooling capacity

$$Q_i = c_p \dot{m}_w \cdot (T_{return} - T_{supply}) \quad when \quad (T_{supply} > T_{rated})$$

Where:

c_p = specific heat capacity of the chilled water (kJ/(kg·℃))
$\dot{m}_w$= mass flow rate of the chilled water (kg/s)
T_{supply} = chilled water supply temperature (℃)
T_{return} = chiller water return temperature (℃)
T_{rated}= rated chilled water supply temperature (℃)

Only if the chilled water supply temperature is higher than the rated one, the supplied capacity is considered as the maximum capacity. Combing the joint prior probability (Equation 6) and the likelihood probability (Equation 7) for available in-situ data, the joint posterior distribution of μ and σ is determined as Equation 9.

Equation 9: Posterior distribution

$$P(\mu,\sigma|Q_{data}) = \frac{\kappa'}{(\mu_{max}-\mu_{min})\cdot(\sigma_{max}-\sigma_{min})} \cdot \prod_{i=1}^{N} \frac{1}{\sqrt{2\pi}(a\sigma)Q_i} \cdot exp(-\frac{(lnQ_i-(lnQ_0+a\mu))^2}{2(a\sigma)^2})$$

Where:

κ' = normalization constant

Markov Chain Monte Carlo sampling

From the joint posterior distribution of μ and σ, the probability density function of *lnR* is determined by the total probability theorem as shown in Equation 10 (WANG and CAO 2013: page 108; CAO and WANG 2014: page 4).

Equation10: Total probability theorem

$$P(lnR|\mu,\sigma,Q_{data}) = \int_{\mu,\sigma} P(lnR|\mu,\sigma)\cdot P(\mu,\sigma|Q_{data})\, d\mu d\sigma$$

Where:

$P(\ln R|\mu,\sigma)$ = possibility that *lnR* occurs given μ and σ (Equation 11)

Equation11: Probability of lnR

$$P(lnR|\mu,\sigma) = \frac{1}{\sqrt{2\pi}\cdot\sigma}\cdot\ exp\left(-\frac{(lnR-\mu)^2}{2\sigma^2}\right)$$

In general, the implementation of the MCMC sampling method involves 5 steps (WANG and CAO 2013: page 110). The details for generating the samples of *lnR* at each step are summarized as follows, where the sample generated for *lnR* is represented by *L*.

Step 1: Choose an initial sample L_1 for the Markov Chain. The initial sample can be the mean μ of its prior distribution (see Equation 4).

Step 2: Choose a candidate sample by Equation 12. There are several approaches to generate the candidate sample. For instance, the Metropolis-Hastings algorithm selects the candidate sample from a proposal distribution (METROPOLIS et al. 1953: page 1088; HASTINGS 1970: page 100; COSMA and EVERS 2010: page 53; WANG, and CAO 2013: page 109; AU and WANG 2014: page 4). In this article, the candidate sample is selected through adding a random number within a predefined range to the last selected sample (COSMA and EVERS 2010: page 56), i.e.

Equation 12: Generation of candidate sample

$$L_j^* = L_{j-1} + \varepsilon\ , \quad \varepsilon\ \in [-g, g]$$

Where:

L_j^* = candidate sample generated at the j^{th} run
L_{j-1} = sample generated at the $(j\text{-}1)^{th}$ run
ε = random variance term
g = predefined positive number

Step 3: Calculate the acceptance ratio by Equation 13. The acceptance ratio is defined as the ratio between the possibility that the candidate sample L_j* occurs with the possibility that the last sample L_{j-1} occurs.

Equation 13: Acceptance ratio

$$r_a\left(L_j^*|L_{j-1}\right) = min\left\{1\ , \frac{f(L_j^*)}{f(L_{j-1})}\right\}$$

Where:

$f(L_j^*)$= possibility that L_j* occurs given μ, σ and Q_{data} *(Equation 10)*
$f(L_{j-1})$= possibility that L_{j-1} occurs given μ, σ and Q_{data} *(Equation 10)*

Step 4: Determine a new sample according to the acceptance ratio by Euqation 14. A random number δ is selected at each run and is compared with the acceptance ratio. If r_a is greater than δ, the sample L_j generated at the j^{th} run is set to be L_j*. Otherwise it is equal to L_{j-1}.

Equation 14: Determination of new sample

$$L_j = \begin{cases} L_j^*, & r_a \geq \delta \\ L_{j-1}, & r_a < \delta \end{cases}$$

Where:

L_j = new sample generated at the j^{th} run
δ = random number within the range [0,1]

Then the number of run is compared with the number of required samples n_{mcmc} to decide whether to continue sampling or stop.

Step 5: Estimate the full distribution, including the mean μ and the standard deviation σ of *lnR* using the equivalent samples. Then, the mean *m* and the standard deviation *n* of *R* can be calculated by Equation 15 (AU and WANG. 2014:72).

Equation 15: Estimation of R

$$m = e^{\mu+\sigma^2/2}, \quad n = \sqrt{\left(e^{\sigma^2}-1\right)\cdot e^{2\mu+\sigma^2}}$$

Where:

m = mean of *R*
n = standard deviation of *R*

According to *m* and *n*, the statistical characteristics of *R* will then be determined, and the samples for *R* can be generated. These samples will be used as inputs for Monte Carlo simulation to predict the chiller plant next-year maximum cooling capacity.

Prediction of next-year maximum cooling capacity

Assume that the current year is the a^{th} year of the chiller plant putting into operation and the actual maximum cooling capacity Q_{data} in the a^{th} year is measured and stored in a building information management (BIM) database. Simultaneously, the predicted maximum capacity $Q_{a,p}$ can be calculated from the capacity degradation model (Equation 2) using a prior *lnR*. If the predicted maximum capacity $Q_{a,p}$ has close mean value and shows same trend with in-situ data Q_{data}, there is no need to calibrate the *lnR*. Otherwise, the *lnR* will be calibrated with the Bayesian MCMC method as introduced in Section 2.2.

The calibrated *lnR* (or *R*), denoted as *lnR'* (or *R'*), with its stochastic distribution is used to predict the maximum cooling capacity in the next year ($(a+1)^{th}$) using Equation 2. Using the predicted next-year maximum cooling capacity $Q_{a+1,p}$, designers and customers can evaluate the reliability of the chiller plant, i.e. to assess whether it can provide enough capacity for the load demand, and thus make a decision on the maintenance scheme for the chiller plant.

3. CASE STUDIES

In the case studies, the aging effect of a real chiller plant was analyzed. This chiller plant was equipped to provide cooling for the Green zone of the academic building 1 in City University of Hong Kong. The configuration of the chiller plant is listed in Table 1.

Table 1 Configuration of the chiller plant

Rated cooling capacity	375 TR (1318.9 kW)
Maximum cooling capacity (newly built)	426.5 TR (1500 kW)
Supply chilled water temperature	Summer: 5 ℃ Winter: 9 ℃
Maintenance	Change compressor oil per year (poor maintenance)

Operation setting	Summer: 00:00-12:00 operation; other time stop; Winter: 8:15-22:45 operation; other time stop;
Start year of operation	2007

Calibration of *lnR* in 2012

Since the chiller plant undergoes poor maintenance, *R* was set as 0.98 in the conventional analysis. In the proposed method, a non-informative prior distribution was used to describe the mean and the standard deviation of *lnR*. The minimum/maximum value μ_{min}/μ_{max} for the mean were set as -0.01 and -0.0005 respectively. The minimum/maximum value $\sigma_{min}/\sigma_{max}$ for the standard deviation were set as 0.005 and 0.1245 respectively (KIM and GODFRIED 2013: page 35).

The aging effect was not obvious in the first few years, and hence the calibration of *lnR* was conducted using the maximum cooling capacity data in 2012, when the chiller plant had been running for 5 years. In the framework of the Bayesian inference, the distribution was obtained for *lnR* using Equation 10. The MCMC method was used to generate samples from the posterior distribution. 100,000 samples were generated for *lnR*, and then these samples were put into a histogram, as shown in Figure 2. Using these samples, μ was -0.0099 and σ was 0.0062, and *lnR* was found to follow a normal distribution, i.e. $N(-0.0099, 0.0062^2)$.

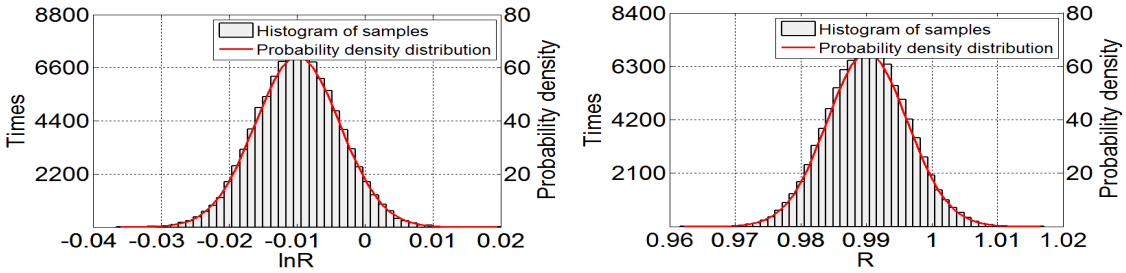

Figure 2: Posterior distribution and histogram of the samples for lnR and R

The distribution of *R* was also estimated from *μ* and *σ* of *lnR*. Figure 2 also shows the probability density distribution of *R* and the histogram of 100,000 samples generated for *R*. To simplify the analysis, *R* greater than 1 was not truncated. After calibration, *R* approximately follows a log-normal distribution instead of a deterministic constant value. The mean *m* and the standard deviation *n* of *R* were calculated using Equation 15, which gave *m*=0.9899 and *n*=0.006. This statistical distribution of *R* provided more comprehensive information than the conventional analysis (*R*=0.98).

The accuracy of the calibrated *R* was assessed by comparing the predicted maximum cooling capacity (which was calculated using *R'*, the calibrated *R*) with the measured maximum cooling capacity. The result was shown in Figure 3. The comparison indicated that the predicted maximum capacity matched the measured data very well. The measured data not only lie within the range of the predicted maximum cooling capacity but also show a similar trend. The mean of the predicted maximum cooling capacity was 1427.9kW; while the mean of the measured maximum cooling capacity was 1398.2kW. The relative error was 2.13%. The calibration using the Bayesian MCMC is effective. Besides, the calibration quantified the uncertainties associated with *R* as well.

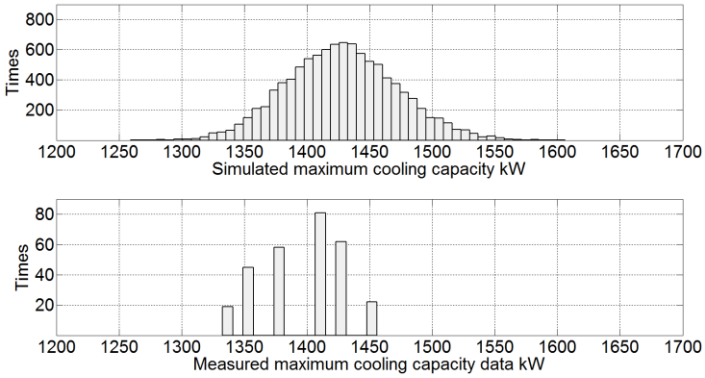

Figure 3: Comparison of the predicted maximum cooling capacity with the measured one

Prediction of the maximum capacity

Since the maintenance scheme was kept the same from 2012 to 2014, the calibrated *R* (using the data in 2012) was then used to predict the maximum cooling capacity for the years of both 2013 and 2014. Figure 4 shows the comparison of the predicted maximum cooling capacity with the measured one in 2013 and 2014. Results show that the measured data lie inside the range of the predicted maximum cooling capacity in both two cases. Moreover, the mean of the predicted maximum cooling capacity was close to the mean of the measured one. Table 2 lists the comparison of the mean, the minimum, the maximum of the measured maximum cooling capacity, as well as those of the predicted using *R*=0.98 without any calibration.

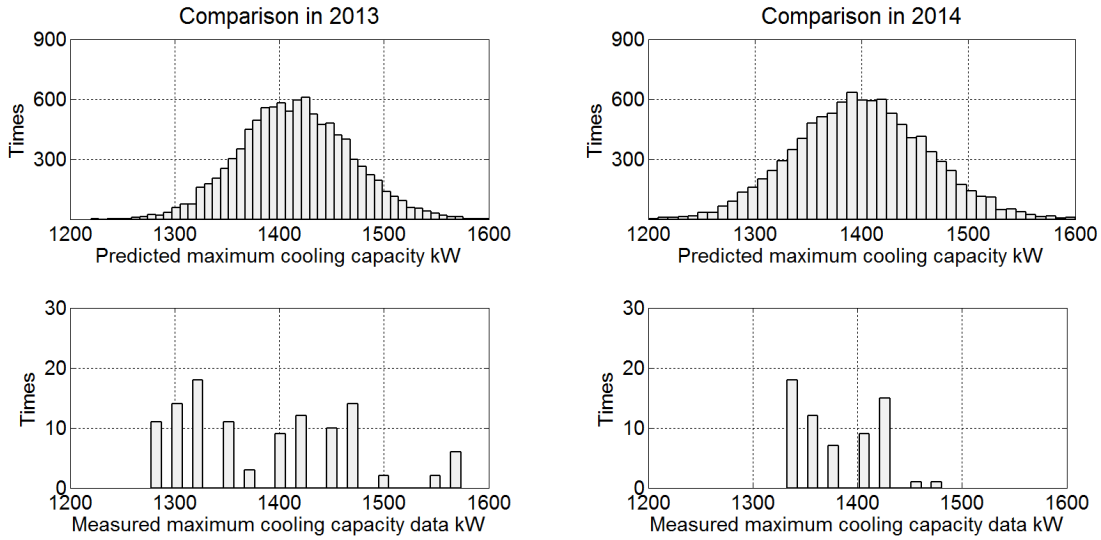

Figure 4 Comparison of the predicted maximum cooling capacity (based on the calibrated R) with the measured one in 2013 and in 2014

Table 2 Comparison between the predicted and the measured maximum cooling capacity

Year		2012	2013	2014
Measured maximum cooling capacity	Mean (kW)	1398.2	1389.2	1381.2
	Min (kW)	1332.7	1283.2	1329.6
	Max (kW)	1456.1	1573.8	1480.7
Evaluation using calibrated *R* (Confidence level 95%)	Mean (kW)	1427.9	1415.3	1402.1
	Relative error	2.13%	1.8%	1.51%
	Min (kW)	1282.5	1227.6	1190.6
	Max (kW)	1599.3	1612.4	1632
Evaluation without calibration (*R*=0.98)	(kW)	1355.9	1328.8	1302.2
	Relative error	3.03%	4.35%	5.72%

It can be seen that by applying the Bayesian MCMC method to calibrate *R*, the relative error of the evaluated maximum cooling capacity decreased from 4.35% to 1.8% in 2013, and from 5.72% to 1.15% in 2014. Therefore the calibration improved the accuracy of the prediction remarkably.

4. CONCLUSION

This study has developed a method of calibrating the chiller aging effect using the Bayesian Markov Chain Monte Carlo (MCMC) method, which consists of the main steps of generating posterior distributions and generating equivalent samples. The calibrated degradation remaining percentage (*lnR*) has been defined to predict the next-year maximum cooling capacity. Compared with the conventional analysis that uses a deterministic value of the maintenance factor to evaluate the aging effect, the proposed method can provide a much more accurate maintenance factor as well as its stochastic distribution, which will provide more information to assess the operation of the chiller plant and to select a proper maintenance scheme. Future work will focus on analyzing the life-cycle maximum capacity of

a whole HVAC system (not only the chiller plant) by taking account of various uncertainties associated with the system, such as the capacity loss during the capacity transportation, and integrate those uncertainties into the design of HVAC system.

5. REFERENCES

ARI 1989. Unitary air-conditioning and air-source heat pump equipment, Air Conditioning & Refrigeration Institute.

ASHRAE, 2012. HVAC Systems and Equipment, American Society of Heating. Refrigeration and Air-conditioning Engineers, Atlanta, GA.

AU, S., Wang, Y., 2014. Engineering risk assessment with subset simulation, John Wiley & Sons.

BEN-DAYA, M., Duffuaa, S., Raouf, A., Knezevic, J., Ait-Kadi, D., 2009. Handbook of maintenance management and engineering, Springer.

BOOTH, A., Choudhary, R., Spiegelhalter, D., 2013. A hierarchical Bayesian framework for calibrating micro-level models with macro-level data. Journal of Building Performance Simulation, 6, 293-318.

BOX, G., Tiao, G., 2011. Bayesian inference in statistical analysis, John Wiley & Sons.

CAO, Z., Wang, Y., 2014. Bayesian Model Comparison and Characterization of Undrained Shear Strength. Journal of Geotechnical and Geoenvironmental Engineering, 140.

COSMA, I., Evers, L., 2010. Markov chains and Monte Carlo methods, African Institute for Mathematical Sciences.

DE wit, S., 2003. Uncertainty in building simulation. Advanced building simulation, 25-59.

DONG, B., O'neill, Z., Luo, D., Bailey, T., 2014. Development and calibration of an online energy model for campus buildings. Energy and Buildings, 76, 316-327.

EISENHOWER, B., O'neill, Z., Fonoberov, V., Mezic, I., 2012. Uncertainty and sensitivity decomposition of building energy models. Journal of Building Performance Simulation, 5, 171-184.

HASTINGS, W., 1970. Monte-Carlo Sampling Methods Using Markov Chains and Their Applications. Biometrika, 57, 97-&.

HENDRON, R., 2006. Building America Performance Analysis Procedures for Existing Homes, National Renewable Energy Laboratory.

HEO, Y., Choudhary, R., Augenbroe, G., 2012. Calibration of building energy models for retrofit analysis under uncertainty. Energy and Buildings, 47, 550-560.

HEO, Y., Graziano, D., Guzowski, L., Muehleisen, R., 2015. Evaluation of calibration efficacy under different levels of uncertainty. Journal of Building Performance Simulation, 8, 135-144.

HOPFE, C., 2009. Uncertainty and sensitivity analysis in building performance simulation for decision support and design optimization. PhD diss., Eindhoven University.

HU, H. 2009. Risk-conscious design of off-grid solar energy houses. PhD diss., Georgia Institute of Technology.

HUANG, P., Huang, G., Wang, Y., 2015. HVAC system design under peak load prediction uncertainty using multiple-criterion decision making technique. Energy and Buildings, 91, 26-36.

HUNTER, R., 1941. Water-distributing Systems for Buildings, US Department of Commerce, National Bureau of Standards.

KIM, S., Augenbroe, G., 2013. Uncertainty in developing supervisory demand-side controls in buildings: A framework and guidance. Automation in Construction, 35, 28-43.

KIM, Y., Ahn, K., Park, C., 2014. Decision making of HVAC system using Bayesian Markov chain Monte Carlo method. Energy and Buildings, 72, 112-121.

LAM, J., Li, D., Cheung, S., 2003. An analysis of electricity end-use in air-conditioned office buildings in Hong Kong. Building and Environment, 38, 493-498.

LEE, B., Byun, J., Choi, M., Kang, B., Park, S., 2014. Degradation Diagnosis System of Photovoltaic Panels with Mobile Application. Ieee Transactions on Consumer Electronics, 60, 338-346.

MATSON, N., Wray, C., Walker, I., Sherman, M., 2002. Potential Benefits of Commissioning California Homes. Lawrence Berkeley National Laboratory.

METROPOLIS, N., Rosenbluth, A., Rosenbluth, M., Teller, A., Teller, E., 1953. Equation of state calculations by fast computing machines. The journal of chemical physics, 21, 1087-1092.

NOH, H., Rajagopal, R., Data-driven forecasting algorithms for building energy consumption. SPIE Smart Structures and Materials+ Nondestructive Evaluation and Health Monitoring, 2013. International Society for Optics and Photonics, 86920T-86920T-8.

SMITH, T., 1983. Reducing corrosion in heating plant with special reference to design considerations. Anti-Corrosion Methods and Materials, 30, 4-5.

TREMBLAY, V., Zmeureanu, R., 2014. Benchmarking models for the ongoing commissioning of heat recovery process in a central heating and cooling plant. Energy, 70, 194-203.

WANG, Y., Cao, Z., 2013. Probabilistic characterization of Young's modulus of soil using equivalent samples. Engineering Geology, 159, 106-118.

209: Experimental optimization of ci engine operated micro-trigeneration system for power, heating and space cooling

Rahul GOYAL*[1], Dilip SHARMA[2], S.L.SONI[2], Pradeep Kumar GUPTA[2], Dheeraj JOHAR[2]

[1] Mechanical Engineering Department, VGU, Jaipur, Rajasthan (India)
[2]Mechanical Engineering Department, MNIT Jaipur, Rajasthan (India)
*Corresponding author. Tel.: +91-9460763566. E-mail: rahulgg2702166@yahoo.com

Trigeneration systems use waste heat from prime movers to generate heating and cooling along with power. They are more efficient, less polluting & more economical than conventional systems. In this paper, in addition to the electricity generated from the engine genset waste heat from engine exhaust was used for heating and space cooling purpose. In this work, for space cooling, four units of Electrolux vapor absorption system, each with a capacity of 51 liters and heat input of 95 Watts, were used. Exhaust gas from the engine was the source of thermal energy to provide heat to the four generators of the VA system. A cabin (3'X5'X6') made of ply wood was fabricated as a space for cooling. The test results show that a temperature drop of 6.50C was obtained in cabin at full engine load about 6 hours after system start up. In this trigeneration or combined cooling heating and power (CCHP) mode, cooling water after extracting heat from engine block was designed to pass through the heat exchanger, where the other fluid was exhaust gas coming out from VA system generators. For the optimization of trigeneration system in CCHP mode, different VA units were operated one by one to obtain the best energy output in terms of space cooling and water heating. The test results show that in this size of set-up, using 3 units of VA system (i.e. approx. 150litres) generates an optimized trigeneration system. However, if more cooling effect is desired, then all four units of VA system should be put into operation, though sacrificing some output in terms of water heating.

Keywords: trigeneration, micro trigeneration, waste heat, vapor absorption system, space cooling.

1. INTRODUCTION

Cogeneration and trigeneration have emerged as fast growing techniques to solve energy related problems, such as increasing energy demand, increasing energy cost, energy supply security and environmental concerns. Cogeneration and trigeneration respectively mean the production of two and three useful forms of energy from the same energy source [Ryan, 2005]. Low grade waste heat available at the end of power generation process is utilized in heating and cooling / refrigeration. Cogeneration defines the simultaneous production of cooling / heating and power, while the trigeneration system defines the simultaneous production of cooling, heating and power from single energy source (i.e., the fuel only). A typical trigeneration system consists of a prime mover or the driving unit, electricity generator, thermally activated equipment and heat recovery system. There are various options for prime mover, such as, internal combustion engine, gas turbine, steam turbine, Stirling engine, fuel cells, etc. Prime mover drives a generator which provides electric power [Wu & Wang, 2006, page 459-495]. Waste heat (as a by-product) from the prime mover is recovered and used to (a) drive thermally activated components such as vapour absorption system or adsorption chiller or desiccant dehumidifier [Deng et al., 2011, page 172-203] and (b) produce hot water, steam, warm air or other heated fluid with the use of a heat exchanger. Depending upon the size, the cogeneration and trigeneration systems are classified as large, medium, small or micro cogeneration / trigeneration systems. Both cogeneration and trigeneration have application in commercial sector (office buildings, etc.) as well as in industrial sector [Ziher & Poredos, 2006, page 680-687]. A number of studies have been conducted to investigate the performance of a large scale cogeneration / trigeneration system [Kong et al., 2005, page 977-987]. However, very little work has been done in real life cases at small residential or commercial level especially for space cooling. Applying cogeneration / trigeneration technology to small scale residential use is an attractive option because of the large potential market. Khatri et al. 2010, page1505-1509 and lin Lin et al., 2007, page 576-585 designed and analysed micro trigeneration systems based on small diesel engines. The experimental results show that the idea of actualizing a household size trigeneration system is feasible and the design of such trigeneration system is successful. G. Angrisani et al., 2014, page 188-201 carried out an experimental study to investigate the performance of both micro cogeneration system and micro trigeneration system. The experimental data were analysed from energy, economy and environmental point of view and the performance of the proposed system was compared with the conventional system. Aleixo et al. 2010, page 1141-1148 investigated an experimental study of an ammonia water absorption refrigeration system using the exhaust of an internal combustion engine as energy source and result show that the cooling capacity can be improved & carbon monoxide emissions were reduced. Tiwari et al., 2012, page 337-342 have described the experimental investigation of an adsorption refrigeration system for cabin cooling of trucks using exhaust heat. J. Godefroy et al. 2007, page 68-77 have described the design, testing and mathematical modelling of a small trigeneration system based on a gas engine with 5.5 kW electricity output and an ejector cooling cycle, analysis of which shows that an overall efficiency of around 50% could be achieved. Y.Huangfu et al. 2007, page 1703- 1709 had discussed the economic and exergetic analysis of novel micro scale combined cooling, heating and power system using small scale internal combustion engine with rated electricity power 12 kW and an adsorption chiller with refrigerating capacity of 9 kW. Deepesh et al. 2013, page 1-7 presented a brief review on micro trigeneration systems and concluded that micro-trigeneration systems can be projected as strategic means to achieve energy security and efficiency, with positive impact on economy, simultaneously reducing environmental threats, leading to sustainable development. Abusoglu et. al, 2008, page 2026-2031, described the thermodynamic analysis of the diesel engine operated cogeneration system and found the thermal efficiency of the overall plant was 44.2% and exergetic efficiency was 40.7%.

The objective of the current study was to experimental optimization of CI engine operated micro-trigeneration system for power, heating and space cooling. For space cooling, four units of Electrolux vapor absorption systems, each with a capacity of 51 liters and heat input of 95 Watts, were used. Exhaust gas from the engine was the source of thermal energy for this VA system. Whereas, for production of hot water, compact type heat exchanger was used to raise the temperature of cooling water coming out of engine block with the help of exhaust gas coming from the engine/ VA system.

2. EXPERIMENTAL SET-UP

Fig. 1 (a) and (b) show the schematic layout of the experimental setup and photograph of trigeneration test rig in the laboratory respectively. The experimental setup for the study consisted of single cylinder four stroke water cooled constant speed, Kirloskar make 5 HP (3.7 kW Model AV1) diesel engine coupled with electric generator and Electrolux vapor absorption system (four units) for space cooling.

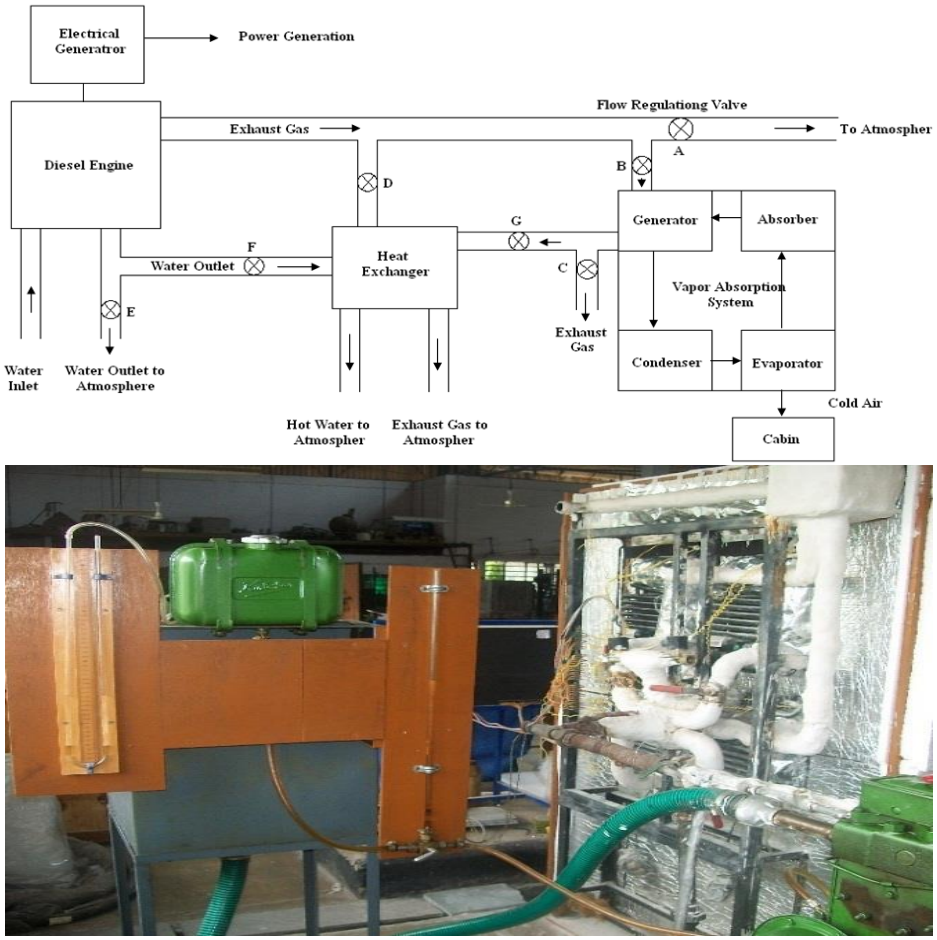

Fig. 1 (a) Schematic layout of experimental setup for trigeneration system, (b) Photograph of the trigeneration test rig in the laboratory

Four identical VA units were arranged in rectangular pattern with two rows and two columns consisting of two VA units each. Henceforth, the four VA units will be addressed as top left, top right, bottom left and bottom right VA units according to their position in the VA system while looking from the front of the VA system. Air flow rate in the engine was determined using air box method by measuring the pressure drop across a sharp edge orifice of air surge chamber with the help of a manometer. Burette method was used to measure the volumetric flow rate of diesel. Governor was used to keep engine rpm constant while varying the load on engine for creation of various test results. The load was varied by switching on the desired numbers of electric bulbs.

Digital tachometer was used to confirm that the engine speed remains constant under varying load conditions. AVL make DITEST (AVL DiGas 4000 light) 5 gas analyzer was used to analyze the exhaust emission from the engine. The exhaust emission included NOx, CO, HC, CO2 and O2, out of which, CO, HC and CO2 were measured by an NDIR technique and NOx and O2 were measured by electrochemical sensors. They give HC and NOx emissions in PPM and that of other gases in percentage. Smoke in exhaust was measured with the help of AVL smoke meter. The drop in intensity of light (lux level) between a source of light and a receiver was measured to calculate the opacity of exhaust gas. This calculation is based on Beer – Lambert Law.

Combination of four units of Electrolux vapor absorption system, each with a capacity of 51 liters and heat input of 95W, was used for space cooling. This type of cooling system is also called three fluids absorption system. The three fluids used in the system were ammonia, hydrogen and water. Ammonia was used as refrigerant because it possesses most of the desirable properties for refrigerant. Hydrogen being the lightest gas was used to increase the rate of absorption of liquid ammonia passing through the absorber. Water was used as a solvent because it has the ability to absorb ammonia readily.

Four flow regulating valves were provided for regulating the flow of exhaust coming out from the engine to the generators of each unit. Heat was to be provided to generators of the four vapor absorption units

for each unit to provide cooling effect. The exhaust flow was directed towards the four VA units one by one by opening and closing the valves (as required) of the individual VA units.

A wooden cabin of 3 feet width, 5 feet length and 6 feet height was fabricated for test of space cooling. For proper insulation of cabin, so as to minimize the loss of cooling effect, nitrile rubber was used on the rear wall of cabin, over which glass wool layer was used and further on the top of glass wool, aluminum foil was pasted, hence, giving the cabin rear a three layer firm insulation cover. The side wall of the cabin which was adjacent to the engine was provided with thermal insulation by 3 layers of 1 inch thick thermocoal sheets making it a 3 inch insulating layer of thermocoal. The cabin roof was provided with one layer of 1 inch thermocoal sheet above the ply wood ceiling. The other two walls did not need insulation as those were away from the engine. Two fans were used to reduce the excessive heat from top left and top right condensers. Also, two fans were used between VA system and cabin to suck the cold air from evaporator coil and deliver it into the cabin. The power required to run the fans (i.e. 100 Watt for four fans) was supplied by the engine genset. Exhaust gas coming out from VA system was used to further heat the cooling water coming out from the engine block. For this a compact type heat exchanger was used. The heat exchanger used was 340 mm high, 300 mm wide and 50 mm thick cross flow, multi-flattened tube and finned, made of brass tubes and copper fins.

2.1. Thermodynamic Energy Analysis

The energy analysis of the diesel engine operated single generation system, cogeneration system and trigeneration system is explained in this section. The principles of mass or energy conservation and the Second Law of Thermodynamics were applied. The following performance parameters were calculated for the system developed under single generation, cogeneration and trigeneration modes based on the energy principle:

Equation 1: Thermal energy carried by the exhaust gas:

$$E_{ex} = \dot{m}_{ex} C_{p_{ex}} \{T_{eng.ex.gas} - T_{ambient}\} \; kW$$

Where:

E_{ex} = Energy carried by the exhaust gases in kW

$\dot{m}_{ex}$ = mass flow rate of exhaust gases in kg/s

C_{pex} = Specific heat of exhaust gases at constant pressure in kJ/kg-K

$T_{eng.ex.gas}$ = Temperature of gases at engine outlet in Kelvin

$T_{ambient}$ = Atmospheric temperature in kelvin

Equation 2: Thermal energy recovered by engine cooling and exhaust gases: Total thermal energy recovered from engine cooling and engine exhaust system is the sum of the heat recovered from the run through cooling water system in engine block and extracted heat from the engine exhaust gases through the heat exchanger $E_{cw} = \dot{m}_w C_{p_w} \{T_{eng.ex.water} - T_{eng.inwater}\} + \dot{m}_w C_{p_w} \{T_{H.E.ex.water} - T_{H.E.inwater}\} kW$

Where:

E_{cw} = *Thermal energy recovered by engine cooling and exhaust gases in kW*

$\dot{m}_w$ = mass flow rate of cooling water in kg/s

C_{pw} = specific heat of water at constant pressure in kJ/kg.K

$T_{eng.ex.water}$ = Temperature of water at engine outlet in Kelvin

$T_{eng.in.water}$ = Temperature of water at engine inlet in Kelvin

$T_{H.E.ex.water}$ = Temperature of water at outlet of heat exchanger in Kelvin

$T_{H.E.in.water}$ = Temperature of water at inlet of heat exchanger in Kelvin

Equation 3: Thermal Energy recovered by VA system: It is also known as refrigeration effect produced by VA system.

$$E_{ref} = UA\{T_{ambient} - T_{cab}\}kW$$

Where:

Eref = Thermal Energy recovered by VA system in kW

U = Overall heat transfer coefficient in kW/m2k

Tambient = Atmospheric temperature in Kelvin

Tcab = Cabin temperature in Kelvin

Equation 4:Total useful energy for combined cooling, heating & power: Total useful energy output of CCHP system is calculated as the summation of electrical output, heat recovered from engine cooling and engine exhaust gases and heat recovered (or refrigeration effect)by VA system.

$$E_{tCCHP} = Electricoutput + E_{cw} + E_{ref}kW$$

2.2. Experimental optimization of the trigeneration system

Exhaust gas from engine was passed through the VA system for space cooling. In the trigeneration or CCHP mode, cooling water after extracting heat from engine block was designed to pass through the heat exchanger, where the other fluid was exhaust gas coming out from VA system generators. For the optimization of trigeneration system in CCHP mode, different VA units were operated one by one to obtain the best energy output in terms of space cooling and water heating.

It was observed that initially when only one VA unit was in operation, temperature of gases coming out from VA system generator and passing through the heat exchanger was 1250C at 1000 W and 2300C at full engine load i.e.3700 W. Similarly, the temperature of gases coming out from VA system generators and entering the heat exchanger was found to be 950C at 1000 W and 210 0C at full engine load, when the two VA units were in operation. It was also observed that if one or two VA units were in operation, then no space cooling effect was produced. Though the evaporator temperature of both the VA units (when only two VA units were in operation) reached 20C at full engine load, but it was still not sufficient to produce a cooling effect in the cabin. The total amount of heat recovered from engine exhaust and engine cooling system was 1.828 kW at 1000 W load and 4.510 kW at 3700 W engine load when only one unit of VA system was in operation and total amount of heat recovered from engine exhaust and engine cooling system was 1.70 kW at 1000 W load and 4.389 kW at 3700 W engine load when two VA units were operated. Fig. 2 shows the variation of heat from engine coolant and engine exhaust with engine load in CCHP mode when one and two VA units were in operation.

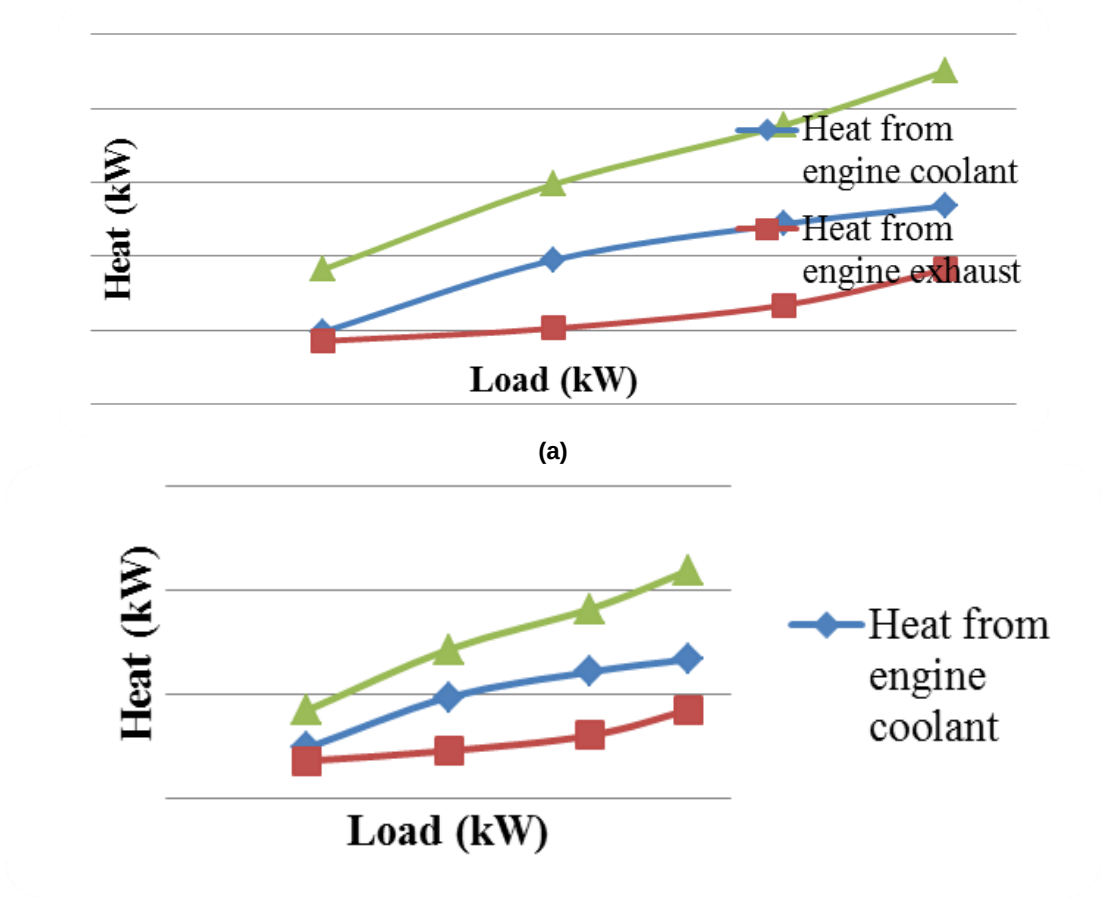

Fig.2 Variation of heat from engine coolant and engine exhaust with engine load in CCHP mode when (a) One VA unit and (b) Two VA units were in operation

When three units of VA system were in operation, then the temperature of gases coming out from VA system generators and entering the heat exchanger varied from 810C to 2000C with the variation of engine load from 1000 W to 3700 W. In that situation space cooling effect was observed only at full engine load. In the beginning, only the top left generator was operated, keeping rest of the generator valves closed. When the temperature of top left generator reached about 1000C, then the valve of top right generator of VA system was opened. In that condition, both, top left and top right units were in operation. Similarly, different permutations and combinations were applied for valves to be operated depending on the temperature condition of each VA unit's generator. There were total 7 combinations for operation of VA units when three VA units were in operation. If G1, G2, G3 and G4 are considered as the top left, top right, bottom left and bottom right generators respectively and similarly E1, E2, E3 and E4 are considered as the top left, top right, bottom left and bottom right evaporators respectively, then the observed sequence of operation of VA units, when 3 VA units are in operation, is given in table 1. At full engine load, when the three VA units were in operation, temperature difference of 4.50C was obtained between cabin and ambient. In that condition, cooling effect produced by VA system was 166 W at full engine load. The total amount of heat recovered from engine exhaust and engine cooling system varied from 1.58 kW at 1000 W to 4.26 kW at 3700 W. Fig. 3 shows the variation of heat from engine coolant and engine exhaust with engine load in CCHP mode when three VA units were in operation.

Table 1 Sequences of operation of VA units when three VA units were in operation

S. No.	1	2	3	4	5	6	7
Sequences of operation	G_1	G_1, G_2	G_2	G_2, G_3	G_3	G_1, G_3	G_1, G_2 and G_3

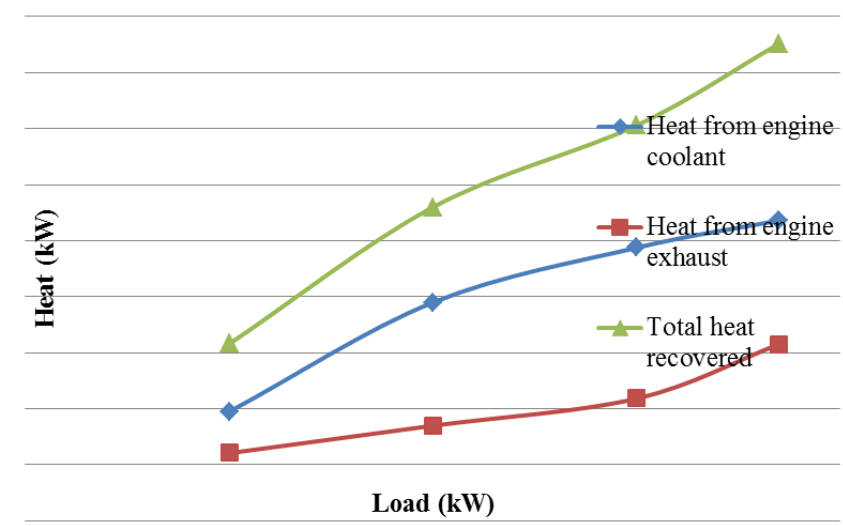

Fig.3 Variation of heat from engine coolant and engine exhaust with engine load when three VA units were in operation

When all the four units of VA system were in operation, then temperature of gases coming out from VA system generators varied from 700C to 1850C with the variation of engine load from 1000 W to 3700 W. There were total 15 combinations for operation of VA units when all the four VA units were in operation. The observed sequence of operation of VA units, when 3 VA units were in operation, is given in table 2.

Table.2 Sequence of operation of VA units with all 4 units to reach steady state condition

S. No.	1	2	3	4	5	6	7	8	9	10	11	12	13	14	15
Sequence of operation	G1	G1, G2	G2	G2, G3	G3	G3, G4	G4	G1, G3	G2, G4	G1, G4	G1, G2, G3	G2, G3, G4	G1, G3, G4	G1, G2, G4	G1, G2, G3, G4

At full engine load, when all four units of VA system were in operation, remarkable temperature difference between cabin and ambient was obtained i.e. 6.50C. In that situation, cooling effect produced inside the cabin by VA system was 240 W at full engine load. The total amount of heat recovered from engine exhaust and engine cooling system varied from 1.46 kW at 1000 W to 4.19 kW at 3700 W. Fig. 4 shows the variation of heat from engine coolant and engine exhaust with engine load in CCHP mode when all the four VA units were in operation.

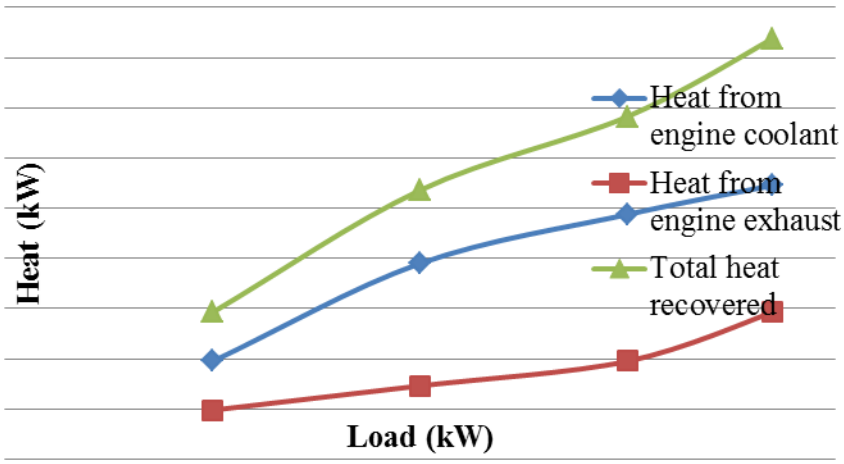

Fig.4 Variation of heat from engine coolant and engine exhaust with engine load in CCHP mode when all four VA units were in operation

Hence, with only one or two units of VA system in operation, only power and heating effect were obtained and no cooling effect was produced. Whereas, when either three or four units of VA system were in operation, it produced combined cooling, heating and power effect. Thus, trigeneration requirement was fulfilled when three or four units of VA system were in operation. Fig.5 shows the variation of total useful output with the number of VA units in operation at full load. From the figure, it was observed that total useful power output was 8.26 kW at full engine load when only one unit of VA system was in operation. Similarly, total useful power output was 8.13 kW at full engine load when two units of VA system were in operation. In both the situations, only power and heating effects were produced. Total useful output was 8.176 kW and 8.13 kW when three units and four units of VA system were in operation respectively. The cooling effect was more when all the four units of VA system were in operation. Thus, although total useful output was more when 3 units of VA system were in operation compared to that when all 4 units of VA system were in operation, however, cooling effect was substantially higher with 4 units compared to that with 3 units of VA system.

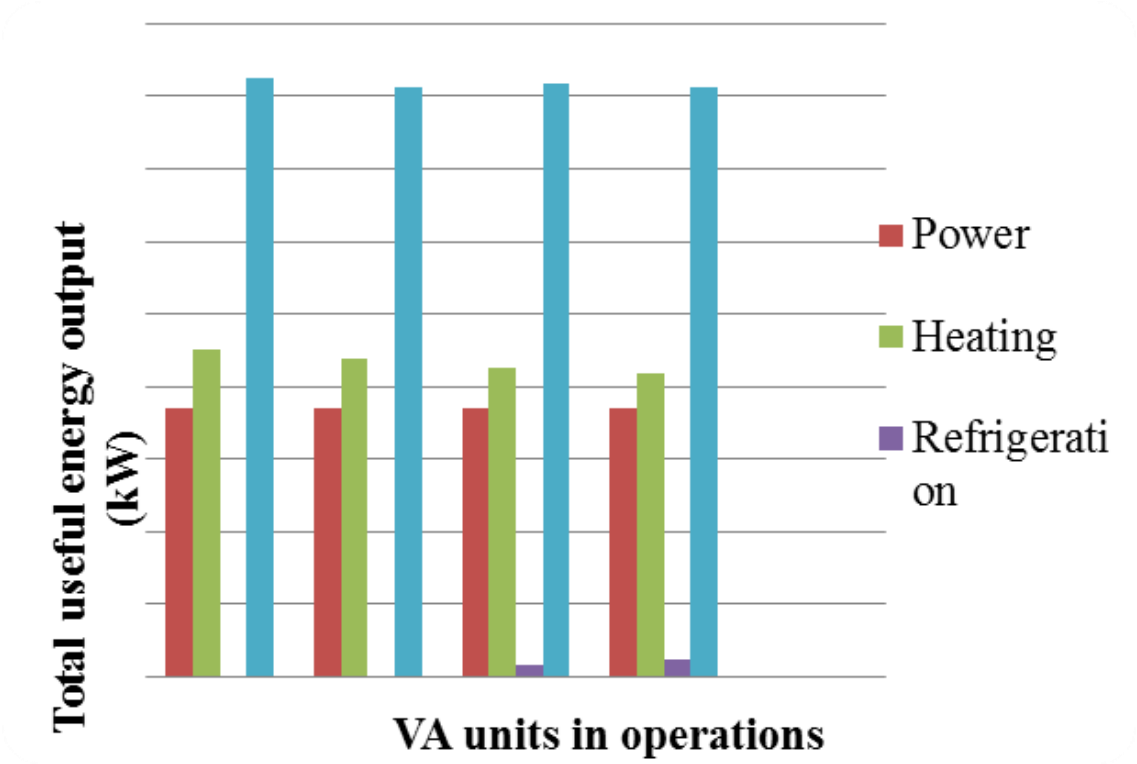

Fig.5 Variation of total useful energy output for different no. of VA units in operation

3. CONCLUSIONS

It can be safely concluded that in this size of set-up, using 3 units of VA system (i.e. approx. 150 litres) generates an optimized trigeneration system. However, if more cooling effect is desired, then all four units of VA system should be put into operation, though sacrificing some output in terms of water heating. It is important to mention that the optimum results were obtained using the suggested sequence of operation of various units of the VA system.

4. REFERENCES

RYAN Oliver Jason, “A micro cooling, heating, and power (m- CHP) instructional module”, A thesis submitted to the faculty of Mississippi State University in partial fulfilment of the requirements for the degree of master of Science in Mechanical Engineering in the Department of Mechanical Engineering Mississippi State, Mississippi December 2005.

WU D. W., Wang R. Z., “Combined cooling, heating and power: A review”, Progress in Energy and Combustion Science 32 (2006) 459-495.

DENG J.,. Wang R. Z, G. Y. Han, “A Review of thermally activated cooling technologies for combined cooling, heating and power systems”, Progress in Energy and combustion Science 37 (2011) 172-203.

ZIHER D., Poredos A., “Economics of a trigeneration system in a hospital”, Applied Thermal Engineering 26 (2006) 680-687.

KONG X. Q., Wang R.Z., Wu J., Wang X.H., Hunangfu Y., Wu D.W., Xu Y. X., “Experimental investigation of a micro combined cooling, heating, and power system driven by a gas engine”, International Journal of Refrigeration 28 (2005) 977-987.

KHATRI Kamal Kishore, Sharma Dilip, Soni S. L., Tanwar Deepak, “Experimental investigation of CI engine operated Micro Trigeneration system”, Applied Thermal Engineering 30 (2010) 1505-1509.

LIN Lin, Wang Yadong, Shemmeri Tarik Al, Ruxton Tom, Turner Stuart, Zeng Shengchuo, Huang Jincheng, He Yunxin, Huang Xiaodong, “An experimental investigation of a household size trigeneration”, Applied Thermal Engineering 27 (2007) 576-585.

ANGRISANI Giovanni, Carlo Roselli, Maurizio Sasso, Francesco Tariello, “Dynamic performance assessment of a micro-trigeneration system with a desiccant-based air handling unit in Southern Italy climatic conditions”, Energy Conservation and Management 80 (2014) 188-201.

ANDRE Alexio, Sergio Morais, Luben Cabezas Gomez, Jose Ricardo Sodre, “Using engine exhaust gas as energy source for an absorption refrigeration system”, Applied Energy 87 (2010) 1141-1148.

TIWARI Harish, Parishwad G. V., “Adsorption refrigeration system for cabin cooling of trucks”, International Journal of Emerging Technology and Advanced Engineering 2 (2012) 337-342.

GODEFROY J., Boukhanouf R., Riffat S., “Design, testing and mathematical modelling of a small-scale CHP and cooling system (small CHP-ejector trigeneration)”, Applied Thermal Engineering 27 (2007) 68-77.

HUANGFU Y., Wu J.Y., Wang R.Z., Kong X.Q., Wei B.H., “Evaluation and analysis of novel micro scale combined cooling, heating and power (MCCHP) system”, Energy Conversion and Management 48 (2007) 1703-1709.

SONAR Deepesh, Soni S.L., Sharma Dilip, “Micro-trigeneration for energy sustainability: Technologies, tools and trends”, Applied Thermal Engineering xxx (2013) 1-7.

AYSEGUL Abusoglu, Mehmet Kanoglu, “First and Second law analysis of diesel engine powered cogeneration systems”, Energy Conversion and Management 49 (2008) 2026-2031.

303: Performance assessment of residential scale solar driven adsorption cooling system in hot arid areas and gained operational experiences

AHMED HAMZA H. ALI

Mechanical Engineering Department, Faculty of Engineering, Assiut University, Assiut 71516, Egypt, ah-hamza@aun.edu.eg

This study present performance assessment of residential scales solar thermal driven adsorption cooling system as well as the gained operational experiences installed at Assiut, Egypt (hot arid and dusty climate) and in operation since summer 2012. The system consists of the following main components: evacuated tube solar collector field with apparent area of 36 m^2 modified with back high reflective parabolic surface under the vacuum tubes, adsorption chiller of 8 kW nominal cooling capacity (silica gel-water), hot water storage buffer of 1.8 m^3 effective volume and cold water storage tank of and 1.2 m^3 effective volume, 34 kW or 50 kW capacity wet cooling tower, two 4.5 kW capacity fan-coils, energy saving pumps, expansion tanks, backup gas water heater, controllers, measuring sensors and data acquisition system with impeded controller. The results show that: The daily solar collector efficiency during the reported period of system operation ranged from about 50 % to 78 %. The chiller average COP was ranged from 0.4 to 0.64 with average chilling power ranged from 3. 6 to 6.42 kW, the average cooling water temperature outlet from the cooling tower ranged from 31.4 ˚C to 23.4 ˚C and the average chilled outlet water temperature from the chiller ranged from 19 ˚C to 12.12 ˚C. For the cooling session of 2012 cooling water outlet temperature from the cooling tower of 31 ^oC, which is higher, the city water at temperature of 27.5 ˚C was used to cool the chiller directly and this experiment leads to enhancement the chiller COP by 40 % and the chilling capacity of the chiller by 17 %. In the cooling session of 2014 a 50 kW cooling capacity wet cooling tower is integrated in the system and the measurements show that the outlet cooling tower water temperature is about 23.4 ^oC at ambient air dry bulb of 35.7 ^oC and Wet Bulb temperature of about of 19 ^oC. Consequently, the chiller cooling capacity reach around 6.42 kW and COP was about 0.64 and chilled water temperature was 15 ^oC. As the heat rejection from the system has a major impact on the system performance in hot arid area, therefore, the re-cooling system should be based on alternative heat sink recourses techniques.

Keywords: Solar cooling system; Small scale adsorption chillers; Operational experiences

1. INTRODUCTION

Energy demand in Egypt is higher than production and represents one of the barriers for further development. This shortage is larger during summer time due to extra energy demand required to drive vapour compression air conditioners to cover the buildings cooling load demand. Enteria and Mizutani (2011) reported that conventional air conditioning systems(A/C) has a large contribution to the buildings energy consumption and represent more than 70 % of building energy consumption in the Middle East. In addition, the role of those A/C system refrigerants in the harmful emissions leads to the greenhouse gases effect, while, few of those systems refrigerants contribute in depletion of the ozone layer. Nowadays there are many green technologies have been used in air conditioning systems that utilize the renewable energy resources as an alternative drive solution for reducing conventional energy consumption and the harmful gasses emissions. Solar cooling systems are one of these technologies, which gain its importance from being a significant application for solar energy. This is due to fact of coincidence of cooling load time distribution with the incident solar radiation profile. Egypt is located mostly in Sun Belt and classified geographically as hot arid area with one of the world highest solar radiation intensity in Upper Egypt, therefore, the buildings need higher cooling. Therefore, solar driven cooling system can be an alternative technologies to utilize the available solar energy resource to drive a cooling machines required to cover a building cooling load demand. Solar driven or assisted cooling systems can be classified into two main categories: electrically driven and/or thermally driven systems. Solar electrically driven systems use the Photovoltaic (PV) technologies to convert portion of solar radiation spectrum into electrical power, which is mostly used to drive the compressor of vapour compression refrigeration machine. While, solar thermal driven cooling system are using the thermal energy collected by solar collectors field to the cooling machine such as sorption chillers or ejector systems. Solar thermal driven cooling sorption systems are classified into three main categories: absorption, adsorption, and desiccant cooling systems. Henning (2007) cited that the absorption cooling systems are the most widely used in case of solar thermal driven technology represent 59 % of the solar thermal driven cooling systems installed in Europe while the adsorption solar driven cooling systems represent 11 % and desiccant solar driven cooling systems represent 23 %. The absorption cooling systems have a higher specific cooling power and Coefficient of Performance COP than adsorption cooling systems. However, adsorption-cooling systems can run at low temperature level heat source started from 55 ^{o}C. Despite this fact the adsorption cooling systems advantages over the absorption cooling systems which are it doesn't need a liquid pump, has no crystallization problem at the beginning of the cooling session, noiseless and most of the commercial systems has environmental friendly refrigerants, that can the designer recommend solar driven adsorption cooling system for use in domestic buildings sector. Balaras et al., (2007) and Wang and Oliveira (2006) reported that for small cooling capacity adsorption chillers, solar cooling systems are thought to be more promising in mini-type building air conditioning systems. There are many operating parameters affecting on the performance of the solar driven adsorption cooling system. It may be seriously affected by the temperature variations of the driving heat source due to changes in the solar radiation intensity throughout the day. Wang et al. (2008) experimentally investigated the influences in variation of drive heat source temperature on the performance of the adsorption chiller. They reported that the rapid changing rate in the hot water temperature lead to large drop in the system cooling capacity and coefficient of performance. Luo et al. (2010) experimentally investigated the effects of the operating parameters on the performance of a solar driven silica gel-water adsorption. They reported that the COP and the cooling power of the solar driven adsorption system could be improved greatly by optimizing the key operation parameters such as driving temperature, heating/cooling time and chilled water outlet temperature. Zhai et al. (2010) reported that the solar adsorption cooling system with heat storage operated stably because of the regulating effect of the heat stored in the hot water tank. Higher initial capital cost is one of the hindrance for widespread of solar driven cooling technologies in residential buildings sector. In order to be competitive for integration in residential buildings Clausse et al. (2008) cited that, solar driven sorption systems has to be as simple as possible to lower their installation cost which is one of their main drawbacks for market penetration.

Throughout the literature, there are numerous pilot and demonstration solar thermal driven and/or assisted cooling systems constructed and in operation worldwide. Recently, several cold production technologies based on solar energy resources are used and developed. Therefore, for further development and implementation of solar thermal driven cooling systems into the residential sector market in hot arid areas, it is important to evaluate, report, and interpret the factors influence on performance parameters of the system as well as the gained operational experiences form a system in operation under similar operating conditions. In addition, there are remain further research and development necessity to be based on assessment of the performance parameters and reported

operational troubles of those solar driven cooling systems operated in hot arid areas. Therefore, this study aim to report performance assessment as well as gained operational experiences of residential scale solar thermal driven adsorption cooling system in operation at Assiut, Egypt (hot arid and dusty climate) since summer 2012.

2. SOLAR DRIVEN COOLING SYSTEM, MEASUREMENTS AND CONTROL, DATA REDUCTION AND EXPERMENTAL ERROR ANALYSIS

2.1 Solar Cooling System

A hybrid schematic and photos diagram of solar thermal driven adsorption cooling system supplies the cooling demand for the renewable energy lab of 80 m^2 floor area at the faculty of engineering, Assiut, Egypt (27.18^{o}N latitude and 31.19^{o}E longitude) is shown in figure (1). The system consists of the following main components: (1) evacuated tube solar collector field with apparent area of 36 m^2 modified with back high reflective parabolic surface under the vacuum tubes, (2) water hot storage (buffer) tank of 1.8 m^3 with effective volume, (3) adsorption chiller of 8 kW nominal cooling capacity (tow beds silica gel-water), (4) cold water storage tank of 1.2 m^3 effective volume, (5) 34 kW or 50 kW capacity wet cooling tower for the chiller cooling process, (6) six-energy saving pumps, (7) cooling load with two 4.5 kW capacity fan-coils, (8) intermediate heat exchanger in chiller cooling subsystem , expansion tanks, backup gas water heater, controllers, measuring sensors and data acquisition system with impeded controller.

The solar driven cooling system consists of six circuits as shown in figure (1). In this system, the water is the heat transfer carrier in the system circuits. Each circuit has variable speed pump, water flow meter and thermal expansion tank(s). The circuits are as follows: solar subsystem circuit that consists of the collectors' field and hot water storage tank, the chiller hot water driving energy circuit, which consisted of the chiller, backup hot water gas heater and the hot water storage tank. The chiller closed loop cooling water circuit that consists of the adsorption chiller condenser and adsorber and intermediate plate and frame heat exchanger, he open loop cooling water circuit that consists of the cooling tower and the intermediate plate and frame heat exchanger. The chiller chilled water circuit that consists of the adsorption chiller evaporator and the cold water storage tank, the cooling load water circuit that consists of the cold water storage tank and the fan-coils

The collectors' field that shown in figure (1) is mounted on the roof of the heat laboratory at Assiut University, Egypt consists of 36 m^2 apparent area of evacuated tube solar collectors modified with back high reflective parabolic surface under the vacuum tubes. The collators" field is facing south direction and tilted by 22-degree angle with the horizontal. The field is arranged in two sub-fields each consists of three parallel arrays and each array consists of set of three collectors connected in series to provide the required driving heat at specific water temperature.

The adsorption chiller that shown in figure (1) has two-beds of silica-gel with rated cooling capacity of 8 KW at a driving hot water temperature of 85 ^{o}C and cooling water temperature of 30 ^{o}C as reported by the manufacture. This chiller can operate with hot water supply temperature ranges from 60^{o}C to 95^{o}C, and cooling water ranges from 27 ^{o}C to 32^{o}C.

The cooling tower shown in figure (1) is installed on of the rooftop of the heat laboratory, and is selected based on the recommendation of chiller maker when using wet cooling tower with capacity of 34 KW. This cooling tower as reported by manufacture operates at 24^{o}C air Wet Bulb (WB) temperature and 5 ^{o}C range. Water outlet from the cooling tower is used to extract the heat rejected from the chiller through the intermediate plate and frame heat exchanger connected within the chiller cooling circuit. In summer 2014 higher capacity cooling tower with capacity of 50 KW replaced 34 Kw tower in the system. The new cooling tower is designed to operate at a condition of 22^{o}C air Wet Bulb (WB) temperature and 5 ^{o}C temperature range based on the weather data in system site.

Two water thermal storage tanks as can be seen from figure (1) are designed and constructed. The hot water storage tank works as a thermal buffer to avoid temperature fluctuation inlet to the chiller and store the excess hot thermal energy outlet from the collectors' field. It has effective volume of 1.8 m^3 with gross internal dimensions of 1 m inner diameter and 2.75 m height. The cold-water storage tank has effective volume of 1.2 m^3 with gross internal dimensions of 0.75 m inner diameter and 2.4 m height.

It is the system cold thermal energy storage and buffer to avoid temperature fluctuation inlet to the load (fan-coils) as well as to store the excess cold energy outlet from the chiller.

Two fan-coils each of 4.8 KW cooling capacity that shown in figure (1) are used to extract the Laboratory cooling load and they are connected to the cold tank. The covered cooling load is for the renewable energy Laboratory that has a floor area of 80 m^2 and height of 3.55 m.

Six variable speed centrifugal pumps were used in the system six circuits as shown in figure (1). The solar pump in solar collectors' field subsystem circuit used to flow the water through the solar collectors' field and hot water storage tank. It is controlled through the control system embedded in the data logger with a pulse width modulation to change its speed correspondence to the water flow rate with outlet temperature from the collectors' field with reference to the set point value. One pump for: the chiller driving hot water circuit, cooling water circuit, open loop cooling tower water circuit, chiller chilled water circuit, and those pumps were controlled by the chiller (ON/OFF) control. The chiller and load circuit pumps were controlled by the controller embedded in the logger.

2.2 Measurements and Control

The solar driven cooling system was fully automated in operation by the embedded controller in the data logger through computer interface. In addition, the data logger with computer interface was used for system monitoring and data measurements recording. System operation is done through the following steps: solar collectors' field

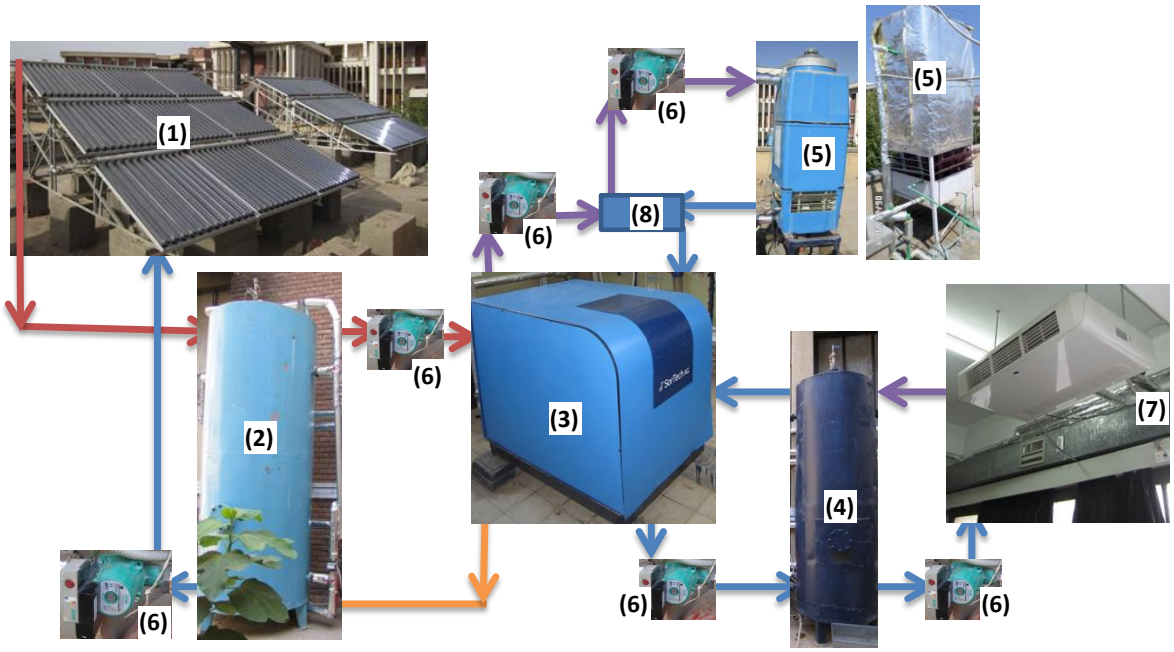

Figure 1: Hybrid schematic and photographs diagram of the main components of the solar cooling system: (1) collectors' field (2) hot water storage tank (3) adsorption chiller (4) cold water storage tank (5) cooling tower(s (6) six-variable speed pumps(7) cooling load- fan coils and (8) intermediate heat exchanger.

heats up the water in closed loop with hot storage tank until the top layers in the storage tank temperature reach to 65 ^oC. At this time the control system, send operation signal to start up the chiller and the rest of the pumps in the system except the cooling load pump. The controller send a signal to stop the solar pump when the top water layer temperature inside the hot storage tank reaches 95 ^oC also in case of the outlet water temperature from the collectors' field reach 45 ^oC the solar collectors' field pump stopped. While the chiller can continue to operate in the system using the hot thermal energy stored in the hot water storage tank until the inlet temperature to chiller reach 65 ^oC or less. The pumps in all other circuits of the system run in similar control strategies. In the system, all temperatures were measured at specific location for monitoring, control and performance analysis. Temperatures were measured by temperature sensors type PT1000. The solar radiation flux measured at the collectors plan with same tilting angle by Pyranometer with accuracy of ±0.5% in the measuring range from 0 to

2800 W/m^2, and, 1 % from normalization from 0 to 70 degree zenith angle. Ambient air relative humidity (RH) was measured by a humidity sensor with standard signal of 0-10 V correspondence to measuring range from 0 to 100% with accuracy of ± 2 % for the measured values between 30 and 90%. Water flow rate was measured by pulse meters, where six flow meters were used in the system having measuring range as follows: from 0 to 6 m^3/h for the chiller cooling water and cooling tower circuits While flow meters with range from 0 to 2.5 m^3/h are used in the solar collectors field circuit, the chiller driving hot water circuit, chiller chilled water circuit and cooling load fan coils circuit. For system control purpose, the gauge pressure at several points in the system circuits was measured by pressure transducers having measuring range from 0 to 6 bars.

2.3 Data Reduction

Assessment of solar driven cooling system performance in operation under hot arid climate requires determination of the chiller driving thermal power, the chiller chilling capacity, and collectors' filed useful gained thermal power. The quantities of those parameters are determined as follows:

$$Q = \dot{m} \times Cp \times \Delta T \quad (1)$$

Where:

- Q= heat rate (kW)
- $\dot{m}$= water mass flow rate (kg/s)
- C_p= water specific heat (kJ/kg.^{o}C)
- ΔT= temperature difference (^{o}C)

The chiller coefficient of performance is determined by $COP = \frac{Q_{chw}}{Q_{hw}}$ (2)

Where:

- COP= chiller coefficient of performance
- Q_{chw}= chiller chilling capacity (kW)
- Q_{hw}= chiller driving thermal power (kW)

The collectors' field overall efficiency is determined by $\eta = \frac{Q_{cll}}{G_T \times A_{cf}}$ (3)

Where:

- η= collector field overall efficiency
- Q_{cll}= collectors' filed output thermal power (kW)
- G_T= total measured incident solar radiation flux on the collectors field surface (kW/m^2)
- A_{cf}= apparent total area of the solar collectors' field (m^2)

2.4 Experimental Error Analysis

In this study, the uncertainty in the determined quantities based on the measured values and the instrumentation accuracy were calculated using the formulas of Coleman and Steele (1999). The uncertainty reported by the manufacturers' sheets of the instrumentation used to measure temperature, solar radiation, water mass flow rates were used in experimental error analysis. Throughout all experiments, it is found that the average uncertainties are as follows: in the temperature was 0.29%, heat transfer rates was 4.2%, COP was 4.8% and collectors' efficiency was 2.6%.

3. RESULTS AND DISCUSSION

3.1 System Performance

The solar driven adsorption cooling system is in operation since summer 2012 until now, therefore, large amount of data and results were obtained. However only sample of performance assessment results for few days during those years presented and discussed. This has done by selecting performance results of operation days in the cooling sessions of 2102, 2014 and 2014, respectively. The performance of the system is expressed in terms of the solar collector field efficiency, cooling tower outlet temperature, chiller chilling capacity, temperature of chilled water outlet the chiller and the chiller coefficient of performance (COP). The main weather data affect the system performance from the measurements at the system site is shown in figure (2). The figure shows the variations of incident solar radiation flux, ambient air-dry bulb temperature and ambient air relative humidity during selected test days. As can be seen from figure (2) the measured solar radiation flux around noon at the collectors' field surface for the presented days is ranged between 900 to 1000 W/m^2, ambient air-dry bulb temperature varied between 25 to 50 ^{o}C, and the ambient air relative humidity varied between 5 to 73%. The presented measured weather data clearly indicate that the system site has a combination of weather resources apparently is ideal for the system to operate efficiently. The measurements also show that for summer 2013 the daily insolation during the experiments was ranged from 21 MJ/m^2 to 27 MJ/m^2 while the maximum ambient air temperature was ranged from 33.6 to 43.7 ˚C. Figure (3-a) shows the instantaneous solar collector efficiency as a function of the mean average temperature of the water inside the collectors the collectors' filed (Tm), the ambient air dry bulb temperature, and the incident solar radiation on the collector plane according to ASHARE 93-77 Duffie and Beckman (2006). The presented data are corresponding to the measured values obtained for 2 hours before and after the noon. Clearly form figure (3-a) the collector efficiency ranged from 46.7 % to 66.4 % as the inlet water temperature ranged between 56.7 ˚C and 73 ˚C, and the outlet water temperature ranged from 67.7 ˚C to 83.5 ˚C, ambient air temperature ranged from 30 ˚C to 36 ˚C, the solar radiation flux was between 795 and 991 W/m^2. The figure clearly shows that the collectors' field efficiency was almost constant during the day. This is expected for vacuum tube collectors with a parabolic high reflective surface under the evacuated tubes in collectors. The daily solar collector efficiency during the reported period of system operation ranged from about 50 % to 78 %. Assessment of the sub-system components performance is carried out for a moderate weather day of September 3, 2103 and is presented in figure (3). The figure shows the operational characteristics of the adsorption chiller that obtained as screen shot from the data logger software. Figure (3-b) shows screen shot for the driving hot water temperature inlet and outlet from the chiller (HT), chiller cooling water temperature inlet and outlet from the chiller (MT) and cold-water temperature outlet and inlet to the chiller.

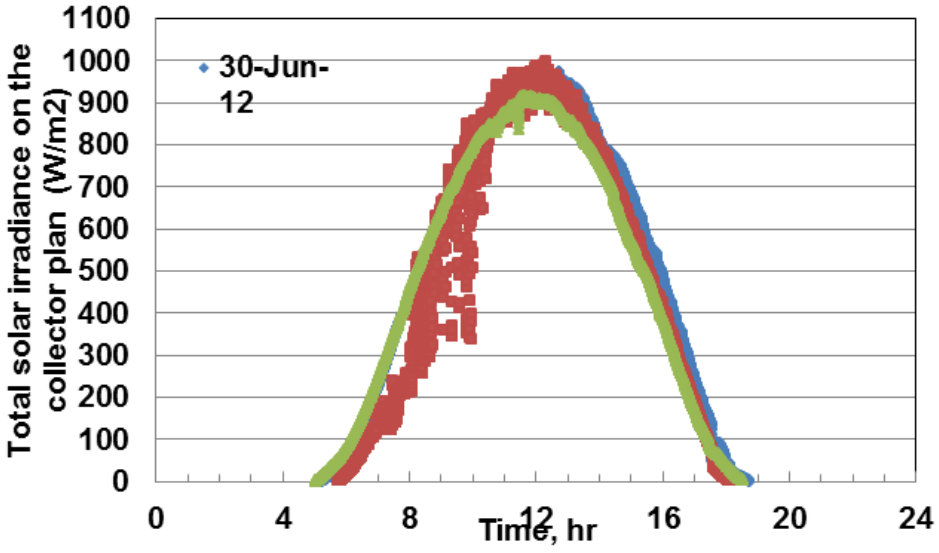

(a)

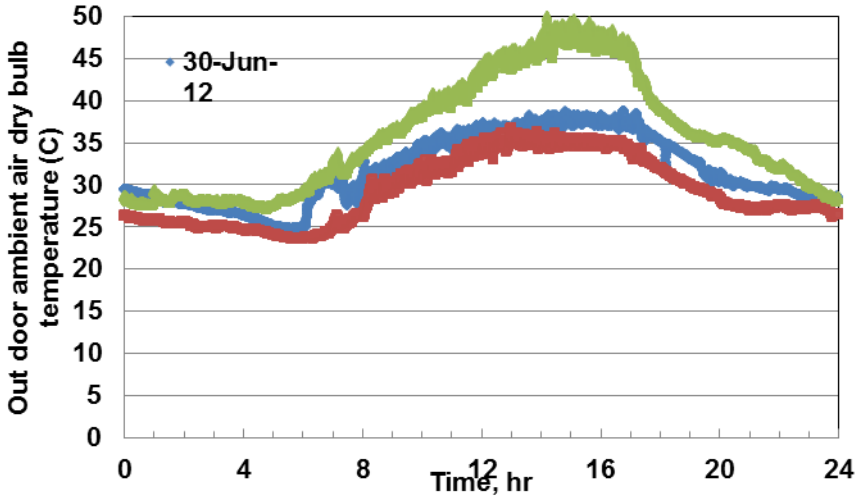

(b)

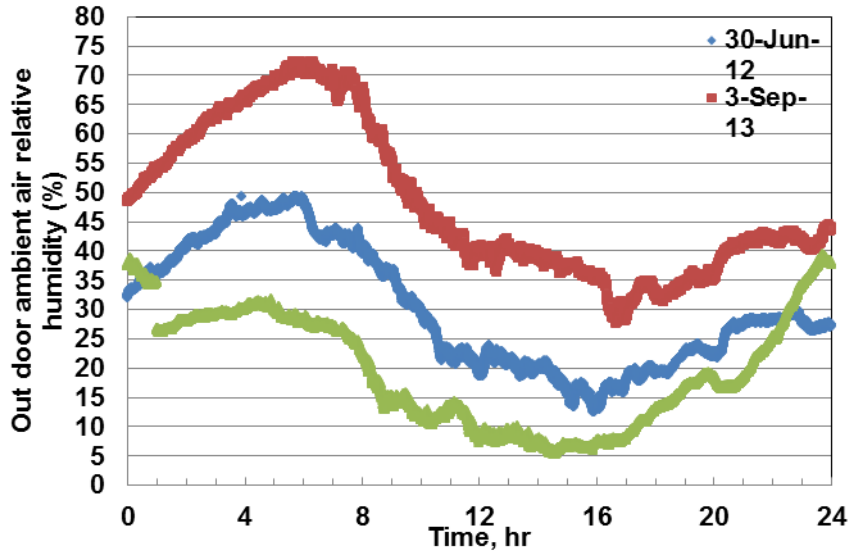

(c)

Figure 2: Main Weather data affects on the system performance measured in summer days of 2012, 2013 and 2014 (a) incident solar insolation, (b) ambient air-dry bulb temperature and (c) ambient air relative humidity.

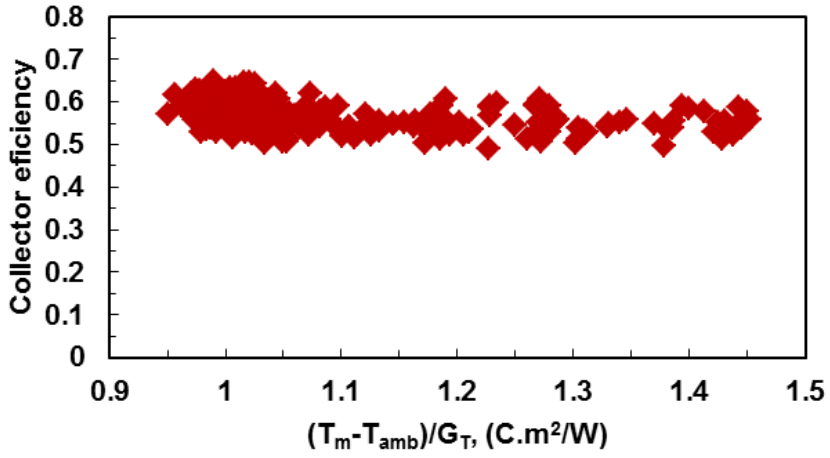

(a)

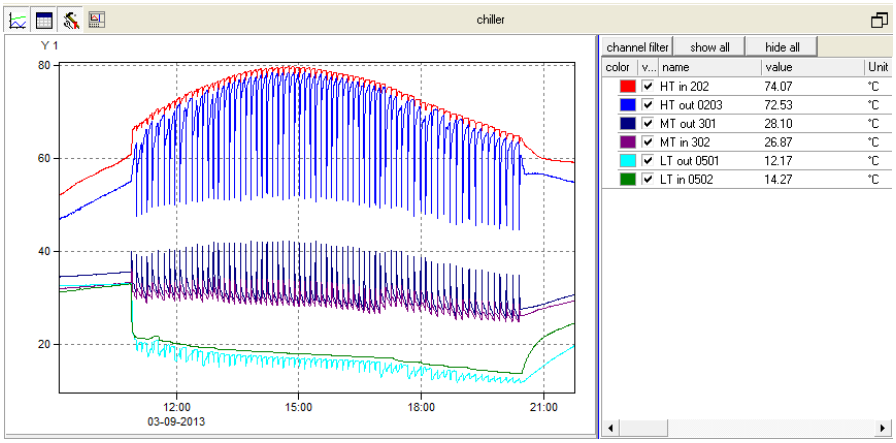

(b)

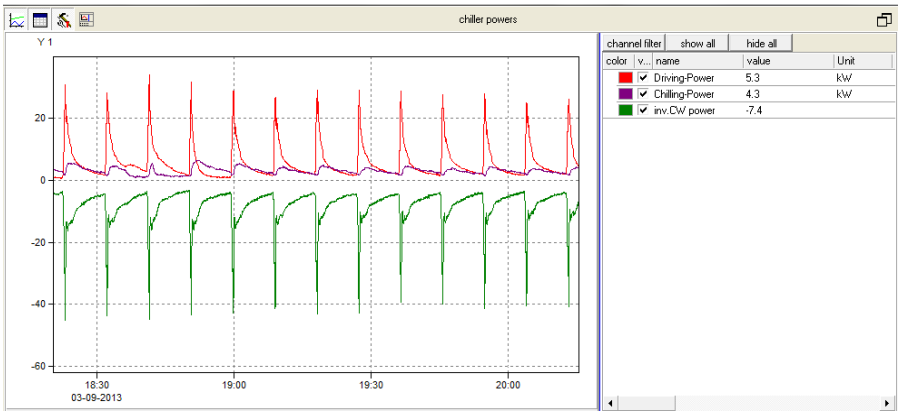

(c)

Figure 3: Sub-system components performance is for September 3, 2103 (a) solar collectors' field efficiency, (b) screen shot from the data logger for driving hot water temperature inlet and outlet from the chiller (HT), chiller cooling water temperature inlet and outlet from the chiller (MT) and chilled water temperature outlet and inlet to the chiller and (c) screen shot from the data logger for the chiller driving thermal power, chilling power and heat rejected power (CW power)

While, figure (3-c) shows screen shot for the chiller driving thermal power, chilling power and heat rejected power (CW power). Clearly, the results shown in figure (3-b and c) and figure (4) show that the chilled water outlet temperature from the chiller began from 20.6 ˚C decreases with time until 12.17 ˚C, while the chiller cooling water temperature changed from 31.4 ˚C at the beginning to became 26.87 ˚C at the end of this day experiment. The chiller driving hot water temperature was 65 ˚C at the beginning of the experiment and reaches to 80.4 ˚C around noon, and, then decreased again. For that day, the total driving heat energy supplied to the chiller was about 310

MJ, the solar energy obtained from the collectors' field was about 439.5 MJ. In that day the collector field average efficiency was 0.5 and the chiller produced about 136.1 MJ cold energy with chiller daily COP of 0.44. For the chiller working hours, the average chilling power was about 3.6 kW, which presents about 45 % of the rated chiller nominal capacity. These results mainly attributed to the higher inlet cooling water temperature to the chiller to cool both the adsorber and condenser. The overall results of cooling session for summer of 2012 were as follows: The chiller average daily COP was 0.41 with average chilling power of 4.4 kW at the cooling water outlet from the cooling tower of 31 ˚C and the outlet chilled water temperature was about 19 ˚C, correspondence to average outdoor ambient Dry Bulb temperature of about 40 ˚C and Wet Bulb temperature of about of 21 ºC. Therefore, based on cooling tower outlet water temperature of 31 ºC the city water at temperature of 27.5 ˚C was used as the chiller-cooling medium instead of the water outlet from the cooling tower, and, this process leads to enhancement the chiller COP by 40 % and the chilling capacity of the chiller by 17 %. In the results of the cooling session of 2013 presented in figure (4), clearly, it found that dust deposition on the collectors' tubes and its back reflectors should be cleaned daily, and, the cooling tower could not provide outlet cooling water less than 32 ºC with minimum chilled water outlet from the chiller of 15 ºC only at late afternoon. Therefore, this results lead to the following action. In the cooling session of 2014 a 50 kW

cooling capacity wet cooling tower is integrated in the system and the measurements show that the average of the outlet water temperature from the cooling tower is about 23.4 ^{o}C at ambient air dry bulb of 37 ^{o}C and Wet Bulb temperature of about of 19 ^{o}C. Consequently, the chiller cooling capacity reach around 6.42 kW and COP was about 0.64 and chilled water temperature was 15 ^{o}C.

3.2 Gained Operation Experiences and Recommendations

For further development of solar driven cooling systems to overcome the barriers to enter the market, it is important to report the gained operational experiences form a system working under real conditions of hot arid climate. Throughout the four cooling sessions of the recent cooling system operation including 2015 (performance result is not presented in this paper) the following can be reported:

1. Based on the results of the effect of the cooling tower capacity on the obtained results shown in figure (4), clearly, the heat rejection from the system has the higher impact the performance parameters of the chiller in hot arid area need further alternative. However, as the water normally is rare in hot arid areas therefore, the re-cooling system should be based on other heat sink recourses techniques.
2. The presented results show that the collector field has instantaneous mean efficiency value ranged from 0.50 to 0.78. These values are less than would be expected from system operating in hot arid climate condition compared with other vacuum tube collectors' performance reported in the literature. This slight degradation on the vacuum tube collectors performance can be explained based on the visual inspection of the collectors' glass tubes and back reflectors surfaces the clearly show the dust is deposited and accumulated over the surfaces as can be seen in figure (5-a). This continues dust deposition and accumulation needs a mechanism for periodical cleaning for collectors field effective surfaces as the rains on hot arid areas is rare.
3. Outside the cooling demand sessions, the collectors' field is covered from the sun. However, in some day wind removes the cover far from the field this followed by the water temperature inside the collectors' vacuum tube reach to boiling state and leads to increase the pressure inside the collectors. In this case, the steam at high-pressure leaks from the piping junctions as can be seen from figure (5-b) instead of the steam release valve. As the local market not having the accessories of the domestic heating systems, those junctions are the available on the local market and are based on gasket for sealing. Therefore, before introducing solar thermal driven cooling technologies to countries in hot arid area there is a need for establishing infrastructure of supported industries and skilled staff for such system installation and maintenance.
4. The major challenge facing solar thermal driven cooling systems are higher initial capital cost compared with conventional cooling system. One-way of cutting costs lay in the solar collection and thermal energy storage system, which are still expensive and burdensome for public use. Therefore, solar cooling driven system can be a part of solar water based heating system installed for other main use and a chiller can be integrated within this system for use excess thermal energy in the system during summer time.

4. CONCLUSION

This study present the performance assessment as well as gained operational experiences of residential scales solar thermal driven adsorption cooling system in operation at Assiut, Egypt (hot arid and dusty climate) since summer 2012. The system consists of the following main components: evacuated tube solar collector field with apparent area of 36 m^2 modified with back high reflective parabolic surface under the vacuum tubes, adsorption chiller of 8 kW nominal cooling capacity (silica gel-water), hot water storage buffer of 1.8 m^3 effective volume and cold water storage tank of and 1.2 m^3 effective volume, 34 kW or 50 kW capacity wet cooling tower for the chiller cooling process, intermediate heat exchanger in chiller cooling subsystem , two 4.5 kW capacity fan-coils, energy-saving pumps, expansion tanks, backup gas water heater, controllers, measuring sensors and data acquisition system with impeded controller. The results show that:

- The daily solar collector efficiency during the reported period of system operation ranged from 50 % to 78 %.
- The chiller average COP was ranged from 0.4 to 0.64 with average chilling power ranged from 3.6 to 6.42 kW, the average cooling water temperature outlet from the cooling tower ranged from 31.4 ˚C to 23.4 ˚C and the average chilled outlet water temperature from the chiller ranged from 19 ˚C to 12.12 ˚C, respectively.

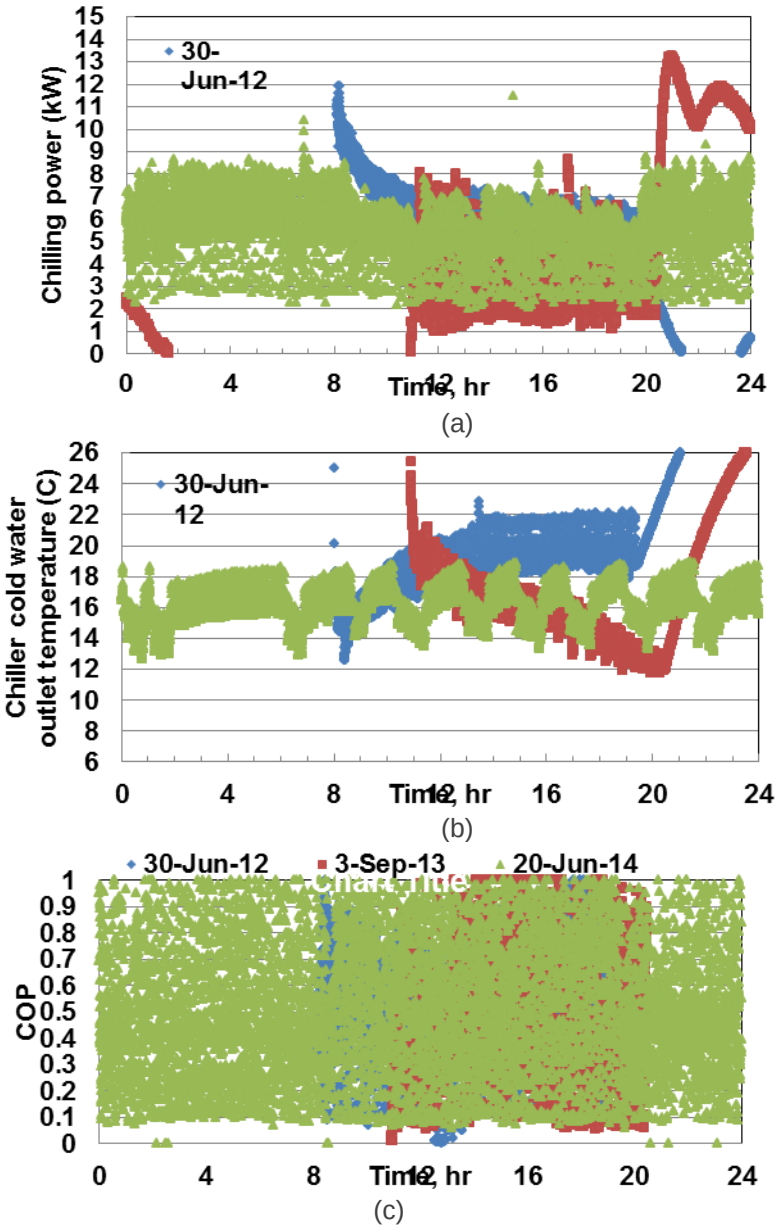

Figure 4: Operational characteristics of the adsorption chiller for some days in cooling sessions of 2012, 2013 and 2014 (a) chilling power produced by the chiller, (b) chilled water temperature outlet from the chiller and (c) chiller coefficient of performance.

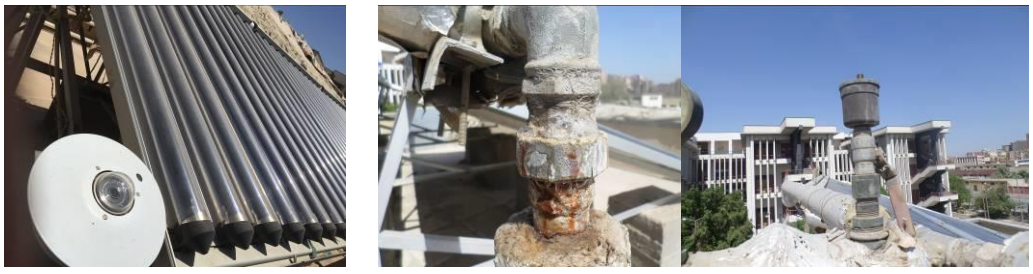

(a) (b) (c)

Figure 5: Photographs of (a) dust accumulation on the collector filed effective surfaces and (b), (c) steam leaks from the piping junction

– For the cooling session of 2012 cooling water outlet temperature from the cooling tower of 31 ºC, which is higher, the city water at temperature of 27.5 ˚C was used to cool the chiller directly and

this experiment leads to enhancement the chiller COP by 40 % and the chilling capacity of the chiller by 17 %.

- In the cooling session of 2013, clearly, it found that dust deposition on the collectors' tubes and its back reflectors should be cleaned daily, and, the cooling tower could not provide outlet cooling water less than 32 ^{o}C with instantaneous minimum chilled water outlet from the chiller of 15 ^{o}C only at late afternoon.
- In the cooling session of 2014 a 50 kW cooling capacity wet cooling tower is integrated in the system and the measurements show that the outlet cooling tower water temperature is about 23.4 ^{o}C at ambient air dry bulb of 35.7 ^{o}C and Wet Bulb temperature of about of 19 ^{o}C. Consequently, the chiller cooling capacity reach around 6.42 kW and COP was about 0.64 and chilled water temperature was 15 ^{o}C.
- The heat rejection from the system has the higher impact the performance parameters of the chiller in hot arid area, therefore, the re-cooling system should be based on other alternative heat sink recourses techniques
- Before introducing solar thermal driven cooling technologies to countries in hot arid area there is a need for establishing infrastructure of supported industries and skilled staff for such system installation and maintenance.
- Due to higher initial capital cost of solar driven cooling systems compared with conventional one for use in residential building sector. Therefore, solar cooling driven system can be a part of solar water based heating system installed for other main use and a chiller can be integrated within this system for use excess thermal energy in the system during summer time.

5. ACKNOWLEDGMENTS

The author gratefully acknowledge Science and Technology Development Fund (STDF), Egypt and the International Bureau of the German Federal Ministry of Education and Research for funding the project "Solar-Driven Adsorption Cooling for Residential Air-Conditioning - System Evaluation and Comparison to Conventional Chiller" GERF 621- IB 08/012 within 2008 Program for Bilateral Cooperation in Education and Research between Germany and Egypt through Assiut University, Egypt and Fraunhofer Institute for Environmental, Safety and Energy, Technology (UMSICHT), Germany.

6. REFERENCES

BALARAS, C.A., Grossman, G., Henning, H.M., Infante Ferreira, C. A., Podesser, E., Wang, L., Wiemken, E., (2007). Solar air conditioning in Europe-an overview. Renewable and Sustaining Energy Reviews. Vol. 11, pp. 299-314.

CLAUSSE, M., Alam, K.C.A., Meunier, F., (2008). Residential air conditioning and heating by means of enhanced solar collectors coupled to an adsorption system. Solar Energy. Vol. 82, pp. 885-892.

COLEMAN, H.W., and Steele, W.G. (1999). Experimentation and Uncertainty Analysis for Engineers, 2nd Ed., John Wiley & Sons, New York, 275 pp.

DUFFIE, J.A. and Beckman, W.A., (2006). Solar Engineering of Thermal Processes. Third ed., John Wiley & Sons, New York.

ENTERIA, N., Mizutani, K., (2011). The role of thermally activated desiccant cooling technologies in the issue of energy and environment. Renewable and Sustainable Energy Reviews. Vol. 15, pp. 2095-2122.

HENNING, H.M., (2007). Solar assisted air conditioning of buildings-an overview. Applied Thermal Engineering. Vol. 27, pp. 1734-1749.

LUO, H., Wang, R., Dai, Y., (2010). The effects of operation parameter on the performance of a solar powered adsorption chiller. Applied Energy. Vol. 87, pp. 3018-3022.

WANG, D.C., Wang, Y.J., Zhang, J.P., Tian, X.L., Wu, J.Y., (2008). Experimental study of adsorption chiller driven by variable heat source. Energy Conversion and Management. Vol. 49, pp. 1063-1073.

WANG, R.Z., Oliveira, R.G., (2006). Adsorption refrigeration-An efficient way to make good use of waste heat and solar energy. Progress in Energy and Combustion Science. Vol. 32, pp. 424-458.

ZHAI, X.Q., Wang, R.Z., (2010). Experimental investigation and performance analysis on a solar adsorption cooling system with/without heat storage. Applied Energy. Vol. 87, pp. 824-835.

SESSION 6: HEATING AND COOLING SYSTEMS

359: New composite materials based on anodic alumina for adsorption heat transformers

ALEXANDRA GREKOVA[1,2], ILYA GIRNIK[1,2], VASILY NIKULIN [1,2], MICHAIL TOKAREV [1], LARISA GORDEEVA [1,2], YURI ARISTOV [1,2]

[1] Boreskov Institute of Catalysis, Ac. Lavrentieva av. 5, Novosibirsk 630090, Russia, grekova@catalysis.ru
[2] Novosibirsk State University, Pirogova str. 2, Novosibirsk 630090, Russia

At present, due to high energy saving potential adsorption heat transformers (AHTs) – chillers and heat pumps - are considered as promising alternative to compression systems. Development of new efficient adsorbents of water and methanol specialised for AHT can essentially advance this emerging low-carbon technology. This work addresses the synthesis and study of novel composite sorbents based on inorganic salts inside pores of an anodic aluminium oxide (AAO) consolidated with aluminium support. The AAO texture is modified by varying the electrolyte nature (H2SO4, H3PO4, H2C2O4) and the current-voltage characteristics during the synthesis, and its duration. The AAO layer thickness reaches 350 □m that is superior to appropriate data presented in the literature. The AAO pore diameter can be intently varied from 30 to 70 nm, and the pore volume - between 50 and 170 cm3/m2 of the Al plate. CaCl2 and LiCl are confined into the AAO pores to increase the sorption capacity that rises up to 23 and 84 g/m2 of the plate for water and methanol, respectively. The amount of sorbates exchanged under the working conditions of a typical air conditioning cycle reaches 13 and 30 g/m2. The composites cooling capacity is estimated as 27-30 kJ/m2. Dynamics of water sorption was investigated by Large Temperature Jump method, imitating conditions of the isobaric stages of real AHT cycle. The desorption runs are found to be extremely fast and ensure the maximal power of 17 kW/m2. The results obtained have clearly demonstrated that a) these new materials can be interesting for making compact AHT units with short working cycles, and b) more R&D effort are necessary for further progress towards practical implementation.

Keywords: anodic aluminium oxide, adsorption heat transformation, energy efficiency

1. INTRODUCTION

Due to high energy saving potential and usage of environmentally benign working fluids adsorption heat transformers (AHTs) driven by low temperature heat are considered promising for cooling/heating. (MEUNIER, 2013: page 830). For successful implementation of AHTs, further improvement of transformation efficiency (Coefficient Of Performance, COP) and, especially, its Specific Cooling Power (SCP) is necessary. The SCP is essentially determined by a coupled heat and mass transfer in the "adsorbent – heat exchanger" unit (ARISTOV, 2009: page 675). An anodic aluminium oxide (AAO), produced by direct electrochemical oxidation of the surface of aluminium heat exchanger, is one of the possible solutions to enhance the SCP. Indeed, almost straight cylindrical pores of AAO are expected to promote mass transfer in the AAO layer, whereas a tight contact of the layer with the Al support can facilitate heat transfer. Filling of the pore space with an inorganic salt forming complexes with sorptive was suggested to increase the sorption ability of common adsorbents. Such Composites "Salt in Porous Matrix (CSPMs) are surveyed in (GORDEEVA, 2012: page 288). Thus, it was expected that the combination of two main AHT components, namely, the heat exchanger and adsorbent bed into a single physical and chemical structure can increase the AHT power. The synthesis of composite sorbents of water based on calcium chloride inside the AAO pores was first reported in (KUMITA, 2013: page 1564, SUWA, 2014: page 602). The AAO layers synthesized in aqueous solutions of sulphuric and oxalic acids as electrolytes exhibit the thickness $\leq$ 100 μm and the pore diameter d = 5 - 40 nm.

The aims of this work were (a) further elaboration of the AAO synthesis procedure to optimize AAO texture parameters important for AHT applications (layer thickness, pore size and volume); (b) preparation of composite sorbents based on $CaCl_2$ and LiCl inserted inside pores of the synthesized AAO layers; (c) studying equilibrium and dynamics of water and methanol sorption on the new AAO materials, and (d) evaluation of their feasibility for adsorptive air conditioning.

2. EXPERIMENTAL

The AAO layers were synthesized by electrochemical oxidation of a flat aluminium plate (thickness 0.5 mm, surface area 5-16 cm^2, purity 99.999 % Aldrich). The main components of an electrochemical rig (Figure 1) were: a power supply source able to maintain a constant current of 1 A or constant voltage up to 300 V, digital voltmeter (±0.1V), digital ammeter (±0.1 mA), carbon cathode, and aluminium anode (the Al plate to be oxidized).

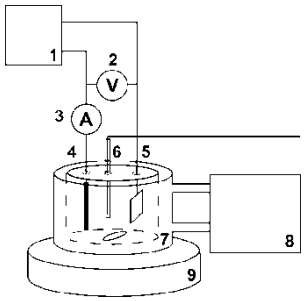

Figure 5: The scheme of the experimental setup for anodic alumina synthesis: 1 - power supply, 2 - digital voltmeter, 3 - digital ammeter, 4 – carbon cathode, 5 - aluminium anode, 6 - J-type thermocouple (±0.5℃), 7 - temperature-controlled electrochemical cell , 8 - liquid thermostat, 9 - magnetic stirrer.

In addition to sulphuric and oxalic acids used in the papers mentioned above, several preparation runs were performed in aqueous solution of phosphoric acid H3PO4. The electrolyte solution placed into temperature-controlled electrochemical cell (volume 170 or 500 cm3) was intensively stirred by a magnetic stirrer. During the Al oxidation, the main process characteristics (voltage, current, and temperature) were recorded by a data acquisition system. One side of the aluminium plate was protected from the oxidation. The AAO plates prepared were washed out with distilled water and dried at 160°C. To intently change the AAO textural characteristics, voltage, current density, synthesis temperature and time were varied in a wide range. Optimal values of the first three parameters were preliminary determined and then maintained constant (Table 1), whereas the synthesis time ts was varied.

Table 3: Experimental conditions of AAO synthesis.

Electrolyte	Voltage, V	Current density, mA/cm^2	Temperature, °C
H_2SO_4 (wt. 20%)	30	20, 26	11
$H_2C_2O_4$ (wt. 4%)	40	8	11
H_3PO_4 (wt. 3%)	185	8	25

Texture characteristics of the synthesized AAO were studied by low temperature nitrogen adsorption using a surface area analyzer NOVA 1200e. The scanning electron images were obtained with a scanning electron microscope JEOL JSM-6460. The composition of the samples was monitored using energy-dispersive X-ray spectroscopy (EDX). Since the porous AAO layer was inseparably consolidated with the aluminium plate, all AAO characteristics were related to a unit area of the plate (e.g. pore volume in [cm^3/m^2], etc). The salt ($CaCl_2$ or LiCl) was introduced into the pores by wet impregnation of the dry AAO with an aqueous solution of appropriate salt under vacuum. After the impregnation, the plate was rinsed out with distilled water in order to remove the excess of the solution from external surface of the AAO and then dried at T=160°C for 12 hrs. The salt content of the composites was calculated from the increase in the plate weight after the layer impregnation and drying. The composition of selected samples described in this communication is presented in Table 2.

Table 2: The composition of the synthesized composites.

Sample	AAO(S)/$CaCl_2$	AAO(Ox)/$CaCl_2$	AAO(Ox)/LiCl	AAO(Ph)/LiCl
Electrolyte	H_2SO_4	$H_2C_2O_4$	$H_2C_2O_4$	H_3PO_4
Salt	$CaCl_2$	$CaCl_2$	LiCl	LiCl
Mass of salt, g/m^2	21	40	40	60
Porosity	0.3	0.5	0.5	0.7

Sorption equilibrium of the new composites with water and methanol vapours was studied by thermogravimetric method using a Rubotherm thermal balance (accuracy ±0.00002g). Sorption isobars were measured in the temperature range T=28-150°C at the vapour pressure P(H_2O) = 12.3 mbar, or P(CH_3OH) = 72.8, 127.5, and 214.6 mbar. Sorption dynamics was studied by a Large Temperature Jump method (LTJ) (ARISTOV, 2008: page 4966, GLAZNEV, 2009: page 1774) which closely imitates the isobaric stages of AHT cycle. To initiate the vapour adsorption, the Al plate was subjected to a fast temperature drop from 66°C down to 30°C at P(H_2O)=12.3 mbar that is a saturated pressure of water vapour at 10°C. For desorption runs, a fast T-jump from 46°C to 90°C at P(H_2O)= 42.4 mbar (T_{con}=30°C) was realized. These boundary temperatures correspond to a typical cycle of adsorptive air conditioning (GLAZNEV, 2009: page 1774). The adsorption dynamics was characterized by the dimensionless conversion $\chi=\Delta w/\Delta w_{t\to\infty}$.

3. RESULTS AND DISCUSSION

The sorption properties of CSPMs were shown to be affected strongly by porous structure of the host matrix (GORDEEVA,2012: page 288). For this reason, the detailed study of AAO texture (layer thickness, pore size and volume) as function of the synthesis conditions was carried out. Then, selected AAO layers with the best texture characteristics were impregnated with the salts. Equilibrium and dynamics of water and methanol sorption were studied under the temperatures and pressures typical of adsorptive air conditioning cycle. On the base of the data obtained, the specific cooling capacity and power reached by using the new composite layers were evaluated and comparison with common adsorbents was made.

3.1 Texture Properties of the AAO Layers

The data on composition of the AAO layers prepared with different electrolytes (Table 3) show that besides aluminium and oxygen all the samples contain 1-3 wt.% of S and P, that could come to the layer from the appropriate electrolyte. Quite large amount of carbon (12-22 wt.%) in all the AAOs is likely to originate from the carbon cathode.

Table 3: The composition of AAO obtained in different electrolytes.

Atomic percent			
Electrolyte H_2SO_4 (wt. 20%)			
C	O	Al	S
12	62	23	3
Electrolyte H_3PO_4 (wt. 3%)			
C	O	Al	P
19	56	24	1
Electrolyte $H_2C_2O_4$ (wt. 4%)			
C	O	Al	-
22	57	21	-

A practically interesting sorption capacity of CSPMs can be obtained if the volume of the matrix's pores is large enough to accommodate inside an ample quantity of the active salt (GORDEEVA,2012: page 288). Therefore, maximizing the AAO pore volume is an important target of the synthesis procedure that can be done by increasing the AAO layer thickness L and the diameter d of its pores. Both these parameters depend on the electrolyte nature and electrolysis duration ts. At ts < 80 h the layer thickness and the pore volume growth at the increase in the oxidation duration. The further prolongation of the oxidation (ts > 85 h) does not affect the AAO layer thickness (Figure 2). The observed quasi steady-state process is likely to set in when the growth of AAO layer from the aluminium side is compensated by its partial dissolution in the acid electrolyte from the oxide side. The maximum (or steady-state) AAO thickness (150, 180, and 350 μm) is achieved at ts = 6, 70, and 86 h for sulphuric, phosphoric and oxalic acids, respectively.

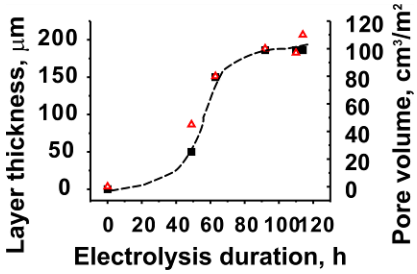

Figure 2: Dependence of AAO layer thickness (■) and pore volume (△) on the electrolysis duration in oxalic acid.

The pore size of the AAO layers depends on the electrolysis duration as well. When the electrolysis duration in oxalic acid is less than 50 h, the uniform pores of 70 nm diameter form throughout the whole layer (Figure 3 a, b). Further increase in the electrolysis duration causes the formation of larger pores of several micron size in the vicinity of the AAO external surface (Figure 4 a, b) that can be a result of the layer partial dissolution in the electrolyte.

Figure 3: SEM images of the cross-cut section of the AAO layers prepared in oxalic acid: a) magnitude 100, b) magnitude 30000.

Figure 4: SEM images of the external surface of the AAO layers prepared in oxalic acid. The electrolysis time 50 h (a) and 70 h (b).

In sulphuric acid, at t_s < 4 h the uniform pores of 40 nm diameter are observed (Figure 5 a), while the electrolysis prolongation up to 6 h leads to the formation of micron sized pores at the external surface of the AAO layer (Figure 5 b).

Figure 5: SEM images of the external surface of the sample obtained in sulphuric acid, the electrolysis time 4 h (a) and 6 h (b).

Figure 6: SEM images of the cross-cut section of the layers prepared in phosphoric acid, a) the cross-cut end, b) the external surface.

In the phosphoric acid, AAO layers with larger pores of 300-400 nm size are observed (Figure 6) that agrees with the data of (MARTíN, 2012. page 311).

The thickest AAO layer with the largest pore volume (170 cm^3/m^2) was prepared in phosphoric acid (Table 4). The usage of $H_2C_2O_4$ leads to the formation of AAO with somewhat lower thickness and pore volume, while in sulphuric acid the layer with the lowest porosity was obtained (Table 4). The maximum pore volume for layers synthesized in oxalic and sulphuric acids is 100 and 50 cm^3/m^2. Both thickness and pore volume of the new AAO layers exceed appropriate values estimated for the AAO layers obtained in (KUMITA, 2013: page 1564, SUWA, 2014: page 602**).**

Table 4:Textural characteristics of the synthesised AAO layers and the layers described in the literature

	Layer thickness, μm	Pore volume (V_{pore}), cm^3/m^2
AAO (H_2SO_4 (wt. 20%))	150	50
AAO ($H_2C_2O_4$ (wt. 4%))	180	100
AAO (H_3PO_4 (wt. 3%))	≈ 180-400	(100-170)
(H_2SO_4) (KUMITA, 2013: page 1564)	100	38
($H_2C_2O_4$) (SUWA, 2014: page 602)	100	30

3.2 Adsorption Properties of the Composites "salt/AAO"

As mentioned above, larger pore volume of the new AAO layers allows preparation of composites with larger salt content inside the pores that promotes their higher sorption ability. For this reason, the AAO layers with the largest porosity prepared in phosphoric acid, are expected to be the most advantageous for the composite synthesis. However, the sorption ability of the composites based on these AAO layers is negligible. The probable reason is an interaction of the salt with the P-containing AAO surface groups that results in the salt deactivation. Therefore, the AAO layers synthesised in sulphuric and oxalic acids were used for the composites preparation. The SEM images of the layers (Figures 7 a and b) demonstrate that the salt is spread as a thin even layer on the internal surface of the AAO indicating the strong adhesion between the salt and the AAO surface. No bulky salt particle is observed on the external AAO surface. The maximum specific salt content (40 g/m2) is found for the layer synthesized in oxalic acid (Table 1). This correlates well with the largest specific pore volume of this layer.

Figure 7: The sample prepared in $H_2C_2O_4$, a) AAO(Ox), b) AAO(Ox)/LiCl.

Water sorption isobars of AAO(Ox)/CaCl2 and AAO(S)/CaCl2 are smooth curves with the uptake gradually rising at low temperature (Figure 8 a). For both composites, no sharp steps corresponding to mono-variant formation of various CaCl2·nH2O crystalline hydrates (n = 0.33, 1, 2, and 4) are observed as reported in the literature for many CSPMs (GORDEEVA, 2012: page 288). This probably indicates a strong interaction between the salt and AAO surface (GORDEEDA, 2006: page 685) that agree with the SEM data. The water sorption capacity of AAO(Ox)/ CaCl2 reaches 23 g/m2 that is somewhat higher than the capacity of the composite AAO(S)/CaCl2 (16 g/m2). It is probably due to the fact that the calcium chloride content in AAO(Ox)/CaCl2 is larger than in AAO(S)/CaCl2 (Table 2). These capacities correspond to 4.7 mol/mol for AAO(S)/CaCl2 and 3.1 mol/mol for AAO(Ox)/CaCl2. The former value is close to the equilibrium sorption of a bulk CaCl2 under similar conditions (5.0 mol/mol), whereas the latter is significantly lower. It may indicate that some part of the salt inside the AAO(Ox) pores is deactivated or blocked, so that it can not sorbs water vapour. Probably, calcium cations react with the acidic surface centres during the Al oxidation that results in the formation of the CaC2O4 and CaSO4, which are not (or less) hydroscopic than a neat CaCl2.

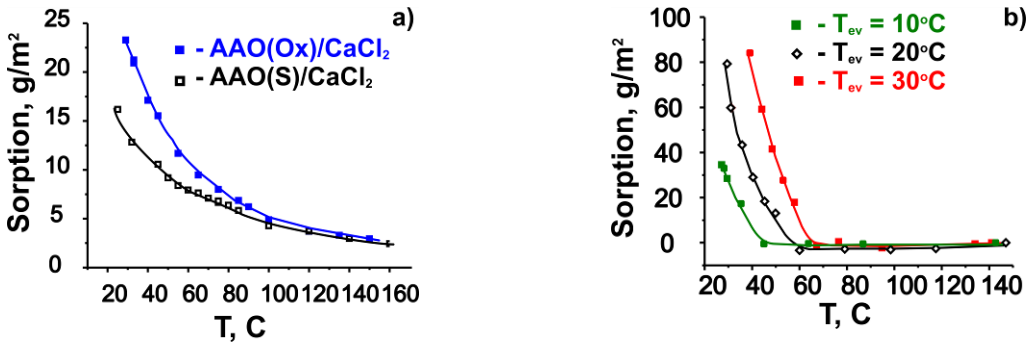

Figure 8: a) Water sorption on AAO(Ox)/$CaCl_2$ and AAO(S)/$CaCl_2$, P(H_2O)=12.3 mbar, b) Methanol sorption on AAO(Ox)/LiCl.

Isobars of methanol sorption on the composite AAO(Ox)/LiCl are very sharp at lower temperature (Figure 8b). This can be related to the formation salt-methanol complex according to the reaction LiCl + $3CH_3OH$ = $LiCl_3$•$3CH_3OH$ known from the literature (GORDEEVA,, 2008. Page 254). Indeed, the methanol sorption capacity of AAO(Ox)/LiCl reaches 84 g/m^2 that corresponds to 3.3 (mol CH_3OH)/(mol LiCl).

3.3 Evaluation of the Cooling Capacity of the Composite Sorbents

Isobars of the methanol sorption on AAO(Ox)/LiCl measured at various temperatures coincide in the coordinates "sorption capacity - free sorption energy ΔF" (Figure 9a). Hence, the sorption is a unique function of just one parameter (ΔF) instead of the common two (T and P), that is in complete accordance with the Polanyi principle of temperature invariance (POLANYI, 1932: page 316). Hence, a model adsorptive air conditioning cycle can be plotted by means of an express method suggested in (GORDEEVA, 2010: page 2703)

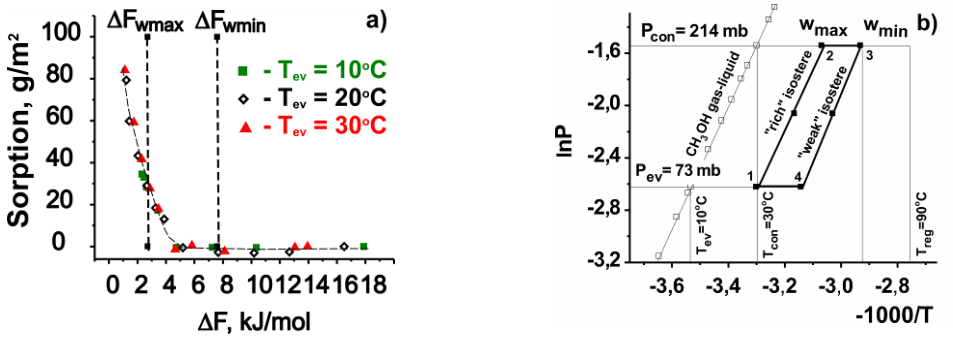

Figure 9: a) Methanol sorption on AAO(Ox)/LiC as function of the free energy ΔF, b) the AHT cycle (T_{ev} = 10°C T_{ev} = 30°C T_{ev} = 90°C) plotted for the working pair "methanol- AAO(Ox)/LiCl".

This cycle (Figure 9b) is typical for adsorptive air conditioning driven by low temperature heat (the evaporator, condenser and desorption temperatures are T_{ev} = 10°C, T_{con}= 30°C, T_{reg} = 90°C). The rich and weak isosters (lines 1-2 and 3-4 on Figure 9b) correspond to the free sorption energy 2.7 and 7.6 kJ/mol, respectively. The amount of cold that can be produced (the Cooling Capacity, CC) is estimated according as (Equation 1):

Equation 1: Specific cooling power.

$$CC = (w_{max} - w_{min}) \cdot \Delta H$$

Where:

- ΔH = the heat of sorbate evaporation
- w_{max}, w_{min} = uptake for reach and weak isosters respectively [g/m^2]

For AAO(Ox)/LiCl, the amount of methanol exchanged along the considered cycle equals 30 g/m^2 and appropriate CC = 30 kJ/m^2. For water as a sorptive, the free sorption energy corresponding to the rich and weak isosters is 3.2 and 8.6 kJ/mol, respectively, and along the cooling cycle the AAO(Ox)/$CaCl_2$ composite exchanges 13 g H_2O/ m^2 that corresponds to a CC-value of 27 kJ/m^2.

3.4 Dynamics of Water Sorption

Kinetic experiments were carried out by the LTJ method simulating the adsorbent dynamic behaviour under boundary conditions of the AHT cycles described above. The desorption run is found to be extremely fast (Figure 10). E.g., the time $\tau_{0.8}$ corresponding to a dimensionless conversion of 0.8 is short (c.a. 20 s), therefore the initial power consumed for desorption is very high (W_{max} = 17 kW/m^2) that clearly demonstrates a very fast heat transfer in the sandwich structure “Al plate – AAO”. This is probably due to the fact that the oxide layer is tightly attached to the metal plate so that the contact heat resistance between them is low. Namely the contact resistance is commonly responsible for low heat transfer rate between a granulated adsorbent bed and heat exchanger walls. The overall heat transfer coefficient α can be estimated from the initial power W_{max} as suggested in (GLAZNEV, 2010: page 1893), α = 380 W/(m^{2}K) that is larger than those reported in the literature. Thus, a fast heat transfer to the layer of porous aluminium oxide is an important advantage of the new composites.

The adsorption run is much longer, the time $\tau_{0.8}$ equals 210 s. Longer adsorption runs were observed for water and methanol adsorption on different adsorbents (silica gel Fuji RD, FAMZ01, activated carbon ACM-35, as well as composite sorbents “salt in porous matrix”(GLAZNEV, 2010: page 1893, GORDEEVA, 2011: page 1273, ARISTOV, 2013: page 841, GORDEEVA, 2014: page 127). However, the ratio of typical ad/desorption times was not more than 3-4. A strong deceleration of adsorption observed for the new material can be caused by a slow mass transport inside the long straight pores of the AAO. The adsorption is started from the pore space nearby the external surface of the AAO layer

resulting in the formation inside the pores of hydrated salt, that is either a solid salt hydrate or an aqueous salt solution. Since the volume of the hydrated salt is larger than that of the anhydrous salt, this can lead to blocking the pore entrance and strong deceleration of the adsorption. A similar phenomenon was observed for methanol adsorption on LiCl/silica gel composite studied in (GORDEEVA, 2011: page 1273). Thus, further optimization of the adsorption dynamics is certainly required.

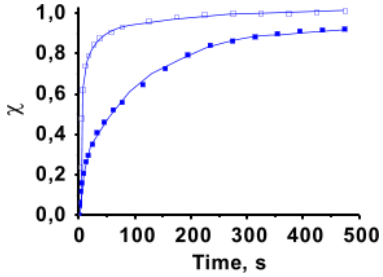

Figure 10: Dimensionless water sorption curves for AAO (Ox)/$CaCl_2$. Solid symbols – adsorption, open symbols – desorption.

The cycle specific cooling power SCP = $W_{0.8}$ realised within the AHT cycle with 80% of the final conversion is a relevant parameter for estimating the cycle dynamic efficiency (Equation 2)

Equation 2: Specific cooling power.

$$SCP = W_{0.8} = \frac{0.8 \cdot \Delta H \cdot \Delta w}{\tau_{0.8}}$$

Where:

- ΔH = the heat of water evaporation at 10°C (2477 J/g water)
- Δw = specific uptake change [g/m^2]
- $\tau_{0.8}$ = the total cycle time that corresponds to 80% of the final conversion

For AAO(Ox)/CaCl2, the cycle power is equal to 260 W/m2. This value is much larger that the specific power of a modern finned flat-tube aluminium heat exchanger studied in (FRENI, 2015: page 1). The authors reported the volumetric specific cycle power to be 93 W/(dm3 of the heat exchanger). Since the HEx volume and surface were 1 dm3 and 0.94 m2, the cycle power related to 1 m2 of fins can be evaluated as 99 W/m2. The results obtained have shown a promising potential for using AAO materials in adsorption heat transformers, however, further optimization of the process dynamics at isobaric adsorption stage, is certainly required.

4. CONCLUSIONS

The paper addresses the synthesis and study of novel composite sorbents based on inorganic salts (CaCl2 and LiCl) located inside the pores of an anodic aluminium oxide (AAO) consolidated with bulk aluminium support. These materials are intently designed to improve parameters of adsorptive heat transformations (AHTs). Variation of the electrolyte nature (H2SO4, H3PO4, H2C2O4), the current-voltage characteristics of the electrolysis and its duration, allows a target-oriented synthesis of AAO layers with improved texture characteristics (layer thickness, pore size and volume). E.g., the layer thickness and pore volume reach 350 μm and 170 cm3/m2 of the Al plate that are superior to appropriate layers presented in the literature. CaCl2 and LiCl confined into the AAO pores significantly increase the layer sorption capacity with respect to water and methanol (up to 23 and 84 g/m2). These parameters are interesting for AHT and can be further improved making the confined salt more active or available for vapours.

Very fast water desorption process was revealed for the synthesized AAO layers that is probably due to the fact that the oxide layer is tightly attached to the metal plate so that the contact heat resistance between them is low. The maximal specific power consumed for desorption reaches 17 kW/m2. The cycle averaged cooling power is much lower (230 W/m2), being, nevertheless, interesting for practical applications. The lower rate of the isobaric adsorption can be caused by inhibition of the vapour transfer inside the straight AAO pores due to the pore blockage by the hydrated salt.

The results obtained have shown an exciting potential of the new AAO layers for adsorptive heat transformation. Despite the first challenging results, more R&D efforts are still necessary for further progress towards practical implementation of consolidated salt-AAO-metal units.

5. ACKNOWLEDGEMENTS

The study was partially supported by RFBR (project number 14-08-31710 mol_a).

6. REFERENCES

ARISTOV, Yuri, 2008. A new methodology of studying the dynamics of water sorption/desorption under real operating conditions of adsorption heat pumps: Experiment. *International Journal of Heat and Mass Transfer*, 51, 4966-4972

ARISTOV, Yuri, 2009. Optimal adsorbent for adsorptive heat transformers: Dynamic considerations, *International Journal of Refrigeration*, 32, 675-686.

ARISTOV, Yuri, 2013. Experimental and numerical study of adsorptive chiller dynamics: a loose grains configuration *Applied Thermal Engineering*, 61, 841–847

FRENI, Angelo, 2015. SAPO-34 coated adsorbent heat exchanger for adsorption chillers, *Applied Thermal Engineering*, 82, 1-7.

GLAZNEV, Ivan, 2009. Kinetics of water adsorption/desorption under isobaric stages of adsorption heat transformers: the effect of isobar shape, *International Journal of Heat&Mass Transfer*, 52, 1774-1777.

GLAZNEV, Ivan, 2010. The effect of cycle boundary conditions and adsorbent grain size on the water sorption dynamics in adsorption chillers, *International Journal of Heat and Mass Transfer*, 53, 1893–1898

GORDEEVA, Larisa, 2012. Composites “salt inside porous matrix” for adsorption heat transformation: a current state of the art and new trends. *International Journal of Low Carbon Technology*, 7, 288-302.

GORDEEVA,, Larisa, 2008. Composites “lithium halides in silica gel pores”: Methanol sorption equilibrium, *Microporous and Mesoporous Materials*, 112, 254-261

GORDEEVA Larisa, 2006. Impact of phase composition on water adsorption on inorganic hybrids salt/silica”, *Journal of Colloid and Interface Science*, 301, 685–691

GORDEEVA,, Larisa, 2010. Novel sorbents of ethanol “salt confined to porous matrix” for adsorptive cooling, *Energy*, 35, 2703–2708

GORDEEVA,, Larisa, 2011. Novel adsorbent of methanol “LiCl inside silica pores” for adsorption cooling: dynamic optimization, Energy, 36, 1273-1279

GORDEEVA Larisa, 2014. Dynamic study of methanol adsorption on activated carbon ACM-35.4 for enhancing the specific cooling power of adsorptive chillers, .*Applied Energy*,17, 127–133

KUMITA, Mikio, 2013. Preparation of calcium chloride-anodized aluminium composite for water vapour sorption, *Applied Thermal Engineering*, 50. 1564-1569.

MARTíN, Jaime, 2012. In-depth study of self-ordered porous alumina in the 140-400 nm pore diameter range, *Microporous and Mesoporous Materials,* 151, 311-316.

MEUNIER, Francis, 2013. Adsorption heat powered heat pumps, *Applied Thermal Engineering*, 61, 830-836.

POLANYI Michael, 1932. Section III. Theories of the adsorption of gases. A general survey and some additional remarks, *Transactions of the Faraday Society*, 28, 316–333.

SUWA, Yuji, 2014. Impregnation of Calcium Chloride into Alumina Thin Film Prepared by Oxalic Acid Anodizing, *Journal of chemical engineering of Japan*, 47, 602-607.

362: Cooling applications with renewable energy powered resorption systems

BILSAY PASTAKKAYA[1], ERDEM CÜCE[2], PINAR MERT CÜCE[3]

[1] Uludag University Orhangazi Vocational College Machinery Program, 16800 Bursa Orhangazi Turkiye, bilsay@uludag.edu.tr
[2] University of Nottingham Institute of Sustainable Energy Technologies, Department of Architecture and Built Environment, Faculty of Engineering, NG7 2RD Nottingham, UK, Erdem.Cuce@nottingham.ac.uk
3 University of Nottingham Institute of Sustainable Energy Technologies, Department of Architecture and Built Environment, Faculty of Engineering, NG7 2RD Nottingham, UK

The use of renewable energy in cooling applications plays a key role in solving the problems related to the energy. Among the thermal energy powered sorption cooling systems, thanks to its operational features, resorption cooling systems with ammonia-water solution has more technical and economic advantages than its alternatives. It will significantly enhance the benefits of the use of the resorption cooling system if the required thermal energy for the system is obtained from the renewable energy sources or the waste heat. Moreover, reduced maximum temperature of required heat, lower pressures adjustable by ammonia concentration and supply of cooling energy below 0 °C provide considerable advantages in residential and industrial cooling applications. Also, the cooling energy can be stored by the use of ice storage tanks and can be used for cooling when the renewable energy sources are insufficient to drive the resorption system.

In this study, technical features of the resorption cooling systems were introduced and the system was compared with the other sorption cooling systems. The cooling applications and the results of the resorption cooling system were presented and the benefits of the renewable energy and waste heat powered systems were defined. The results showed that resorption cooling systems have similar COP values with the conventional absorption systems. Thus, they will have wide spread use in the future because of their advantages among its alternatives.

Keywords: Resorption, Cooling, Renewable Energy

1. INTRODUCTION

Obviously the most important problems that mankind have to challenge are related to the energy. Since these problems are increasing day by day, using clean and renewable energy sources is becoming more important. Energy requirements for industrial and residential cooling applications account for a large share of energy consumption, thus using the clean and renewable energy powered cooling system offers new alternative solutions. Energy consumption and carbon emissions during the summer season rise due to the cooling demand, and this causes many technical and environmental problems. Thus, solar cooling applications have become more attractive (Pastakkaya et al., 2012). There are many solar powered technologies used in cooling applications. Thermally driven sorption cooling systems use renewable energy such as solar, geothermal and waste heat as well. The operation costs of these systems are low, compared to the traditional air conditioning systems. Among the thermal energy powered sorption cooling systems, thanks to its operational features, resorption cooling systems with ammonia-water solution have more technical and economic advantages than its alternatives. It will significantly enhance the benefits of the use of the resorption cooling system if the required thermal energy for the system is obtained from the renewable energy sources or the waste heat. Moreover, reduced maximum temperature of required heat, lower pressures adjustable by ammonia concentration and supply of cooling energy below 0 °C, provide considerable advantages in residential and industrial cooling applications. Also, the cooling energy can be stored by the use of ice storage tanks and can be used for cooling when the renewable energy sources are insufficient to drive the resorption system.

The International Energy Agency Task 25 “Solar Assisted Air Conditioning of Buildings” (IAE, 1999), and Task 38, “Solar Air Conditioning and Refrigeration” (IAE, 2006), published several reports regarding solar assisted cooling and heating applications. Ree and Oostendorp (1980) investigated absorption and resorption heat pumps using the binary mixture ammonia-water (NH_3-H_2O) and they reported that the real advantage of the resorption heat pump in comparison with the absorption heat pump is the fact that, with in certain limits, the pressure can be freely chosen, however, in the case of NH_3-H_2O the heat ratio decreases with the pressure. Weimar (2014) presented a thermally driven resorption chiller with NH_3-H_2O solution. He reported that resorption technology has many advantages compared to conventional absorption plants with water as refrigerant and resorption chilling is more reasonable when process or waste heat is available and at the same time cold is needed. Pastakkaya (2014) demonstrated a trigeneration application with resorption cooling technology in food industry. He indicated that using resorption chiller with combined heat power systems (CHP) provides significant benefits in pasteurization and cold storage of food products besides supplies low-priced electricity for the processes. Costiuc L. and Costiuc I. (2010) investigated the relative performance of a thermally activated, environmentally friendly NH3-H_2O resorption cooling system. They reported that the system can be driving at relatively low heat source temperatures such as those achieved by solar collectors and they also presented the exergetic efficiency and the coefficient of performance (COP) of the system as a function of the degassing zone and the boiling temperature. Pastakkaya et al. (2013) represented a resorption cooling system in agricultural cold storage applications. They reported that using resorption plant as an auxiliary cooling system in cold storage for agricultural applications reduces the energy costs thus the agricultural production efficiency can be enhanced and energy independence can be improved by using renewable energy sources.

In this study, technical features of the resorption cooling systems were introduced and the system was compared with the other sorption cooling systems. The cooling applications and the results of the resorption cooling system were presented and the benefits of the renewable energy and waste heat powered systems were defined.

2. METHODS

Resorption cooling cycle is different from conventional absorption cooling cycle in some aspects. Figure 1 illustrates the resorption cooling system with NH_3-H_2O solution where the ammonia is the refrigerant and the water is the absorbent. There is a second solvent circuit in the resorption cycle where the condenser and the evaporator in the conventional absorption cycle are replaced by high pressure absorber and cold desorber, respectively. Gaseous ammonia is transferred between two ammonia-water solutions cycles of different concentrations at high and low pressure levels. The ammonia-water solvent in hot desorber is vaporized by the thermal energy from a heat source such as solar energy or waste heat. The high pressure absorber in the cold cycle absorbs the solvent vapor evaporated in the hot desorber. The heat of absorption in the absorbers is rejected by the heat rejection system such as cooling tower. The solution from high pressure absorber enters cold desorber in low pressure and

evaporates. Thus, the cooling energy is provided and can be distributed for cooling applications using a cold distribution system. The refrigerant vapour at low pressure in the cold desorber is absorbed in the low pressure absorber and the solution at low pressure in the cold desorber is pumped to high pressure absorber. There is a mix flow between the cold and hot cycles for an equalization of the concentrations to avoid an enrichment of the refrigerant in the cold cycle. Compared with conventional absorption cycles, the pressure levels are lower in the resorption cycle and can be adjusted by the alteration of the ammonia-water concentrations in both cycles. Therefore the temperature of heat source in the hot desorber can be reduce to a range of 70 – 90 °C.

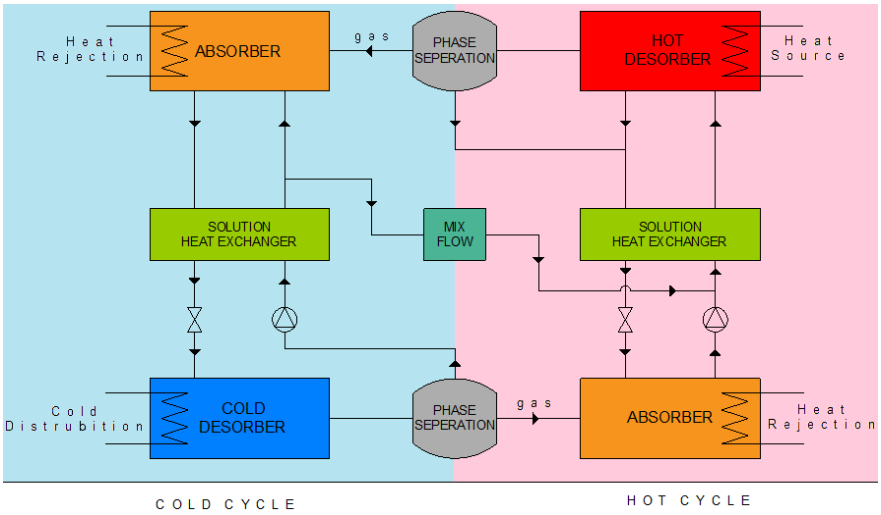

Figure 6: Resorption cooling cycle

Helle (2014) presented technical features of a resorption plant. She reported that the pressure range in the cycles varies in the range of 1,3-1,2 bar for the high pressure and 0,5-0,6 bar for the low pressure while the temperatures in the hot desorber, cold desorber and the absorbers are 70 °C, 5 °C, 20 °C, respectively. The ammonia concentrations in the low pressure absorber and hot desorber vary in the range of %35 – 30, in the high pressure absorber and cold desorber varies in the range of % 24 – 15. Figure 2 presents the maximum cooling capacity and the COP value variation with the maximum external cooling temperature of the resorption plant while the temperature for heat rejection is 20 °C.

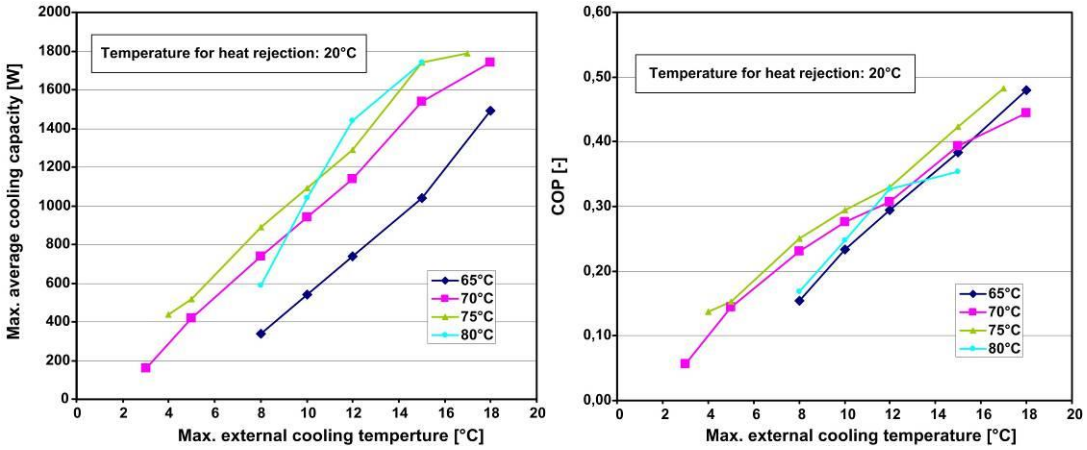

Figure 2: Maximum cooling capacity and COP value variation of resorption plant (Helle, 2014)

Weimar (2014) demonstrated resorption systems for industrial cooling applications in different cooling temperatures. He claimed that many industrial applications produce heat that is a perfect source for resorption cooling such as combined heat and power systems beyond the heating season and biogas production. He presented a diagram for resorption cooling systems for different cooling temperature ranges to show the variation of the COP of the system between cooling water temperature and the hot water temperature, illustrated in Figure 3. COP of the resorption system decreases with the increase in cooling water temperature. It is essential to use effective components in heat rejection system to maximize the COP of the cooling plant.

The COP of the system increases with the increase in cold distribution temperature. Resorption cooling system can be used in different cooling temperatures in the range of - 5 °C / 12 °C. Higher COP values can be achieved by higher cold distribution temperatures. If the thermal energy for driving the resorption plant is derived from the waste heat produced by industrial processes it is possible to set up cost effective cooling systems for industrial cooling applications. So, even if the COP of the resorption system is lower than the conventional cooling systems in low temperature cooling applications, resorption cooling systems provide more benefits than its alternatives because, they used the waste energy for the cooling.

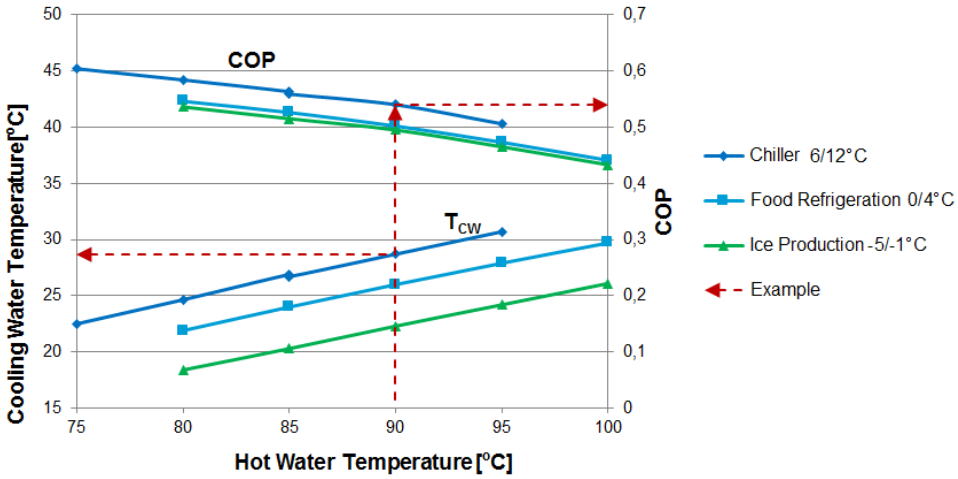

Figure 3: Variation of the COP of the resorption system (Weimar, 2014)

Since the temperature range of heat source for driving the resorption systems is lower than the conventional absorption systems, using renewable energy sources or the waste heat is more advantageous in resorption cooling in terms of technical and economic aspects. Therefore it is possible to realize more feasible projects for renewable cooling applications. Pastakkaya et al. (2013) presented Solar Resorption Cooling – SOLARES project illustrated in Figure 4. SOLARES project aims to satisfy the cooling load in agricultural cold storage application by using a solar powered resorption cooling plant with a cooling power peak of 5 kW. Five flat plate solar collectors connected in series used as heat source for hot desorber and an electric heater with 10 kW was used as the auxiliary heater. A cold storage room with 5 kW cooling load was set up to store agricultural products. There is also a vapor compression refrigerator in the plant as an auxiliary chiller. A fan coil in the cold storage room was used as cold distribution system and a wet cooling tower as heat rejection system.

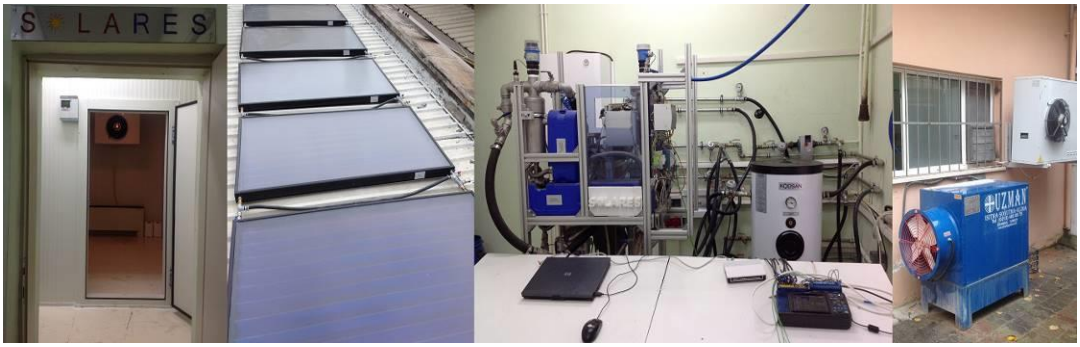

Figure 4: SOLARES project resorption plant components

Figure 5 shows the SOLARES resorption unit control system. The resorption cycle is controlled via computer program and it is possible to examine all temperature and pressure values on the interface. The resorption unit can be driven manually or automatically. Thus, the system can be operated in industrial applications effortlessly but in order to start up and stabilize the system, specialization is required. External lines, heating, cold distribution and heat rejection, temperatures affect the resorption cooling performance directly. If the heat source temperature driving the hot absorber, is below 70 °C,

vaporizing of the ammonia-water solution decreases and the system stops cooling. Likewise, if the temperature of the high and low pressure absorbers increase, the heat of absorption process cannot be discharged and COP of the system decreases. It is essential to design an effective heat rejection system for an efficient cooling application and better COP values.

Since the cooling demand increases in daytime, the solar energy is an appropriate energy source for cooling applications. However, solar energy is affected by weather conditions, and seasonal changes and can be harnessed only during clear sky hours (Pastakkaya et. al. 2012). So, if the solar energy is used as a heat source for the resorption cooling unit, an auxiliary heating system is required when the solar energy is insufficient for driving the hot desorber. It is also essential to use hot water tank as an energy storage system in solar resorption cooling applications. Geothermal energy at appropriate temperature range is a more reliable energy source for resorption cooling, since it is not affected by the meteorological conditions or seasonal changes. But still, the investment costs and availability of the geothermal sources are the main problems of the geothermal cooling systems.

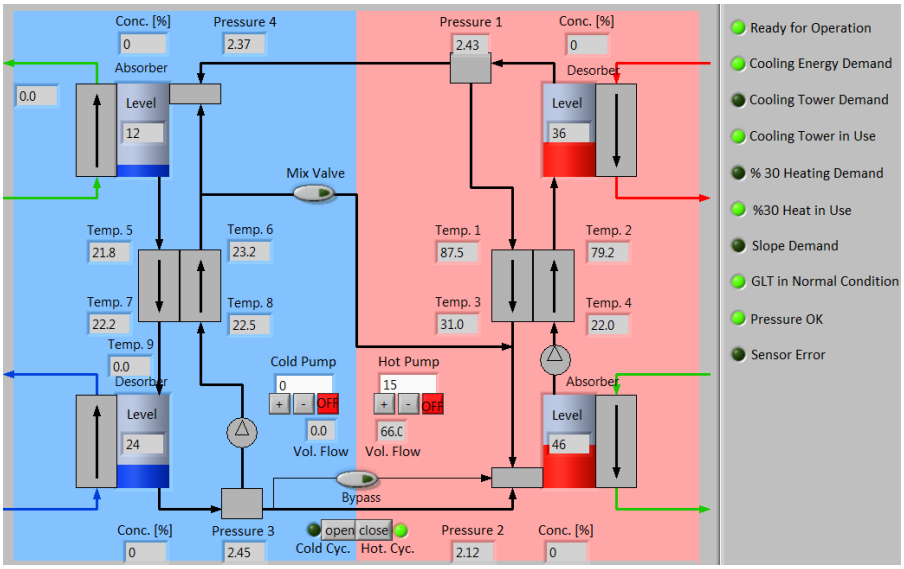

Figure 5: Resorption unit control system

Energy storage with chilled water and ice storage are other options to store energy in renewable cooling application. While the hot water storage tank experiences considerable heat loss, the chilled water storage tank has a lower rate of heat gain because of the small temperature difference between the chilled water tank and its surroundings (Li and Sumathy, 2000). The latent heat of water can be used for the system if the cooling energy stored in ice. Since the resorption cooling unit uses ammonia as refrigerant, it is possible to realize cooling applications below 0 °C and ice storage can be used as an energy storage unit. Thus, energy can be stored in ice form during the off peak periods and using ice storage units in the cooling plant allows to reduce resorption chiller capacity up to %50.

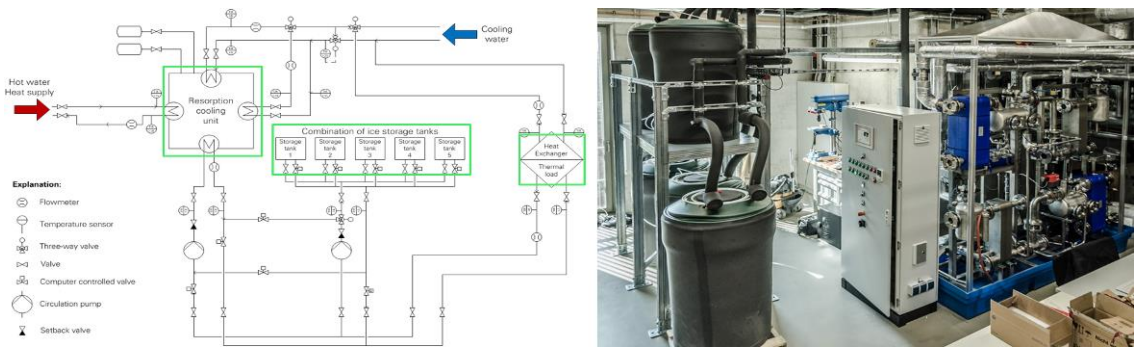

Figure 6: Resofreeze project scheme and ice storage units (Jaehner and Grund, 2014)

Jaehner and Grund (2014) presented Resofreeze, a resorption cooling project with ice storage tanks. Figure 6 illustrates the Resofreeze project scheme and ice storage units in the plant. Energy storage system consists of five ice storage tanks with total storage capacity 140 kWh. The cooling energy performance of the units is 17,5 kW lasting for 8 hours and the cooling capacity of the resorption chiller is 25 kW. It is possible to supply cooling energy in the range of -6 to +6 °C in the plant and the efficiency of the trigeneration system can be increased by using the waste heat in the CHP unit, to drive the hot desorber of the resorption chiller.

Simulation of cooling performance for Resofreeze project was also demonstrated by Jaehner and Grund (2014). Figure 7 shows the variation of COP of the resorption chiller regarding cooling water temperature, heating temperature and flow rate of the cold and hot pump. It was concluded that desired COP values can only be reached by appropriate cooling water temperature in the heat rejection system; therefore, the operation of a resorption cooling unit in the night time is very efficient. Using resorption cooling during night time also allows storing energy efficiently in the ice storage tanks and stored energy can be used as an auxiliary cooling in daytime to satisfy peak cooling demands.

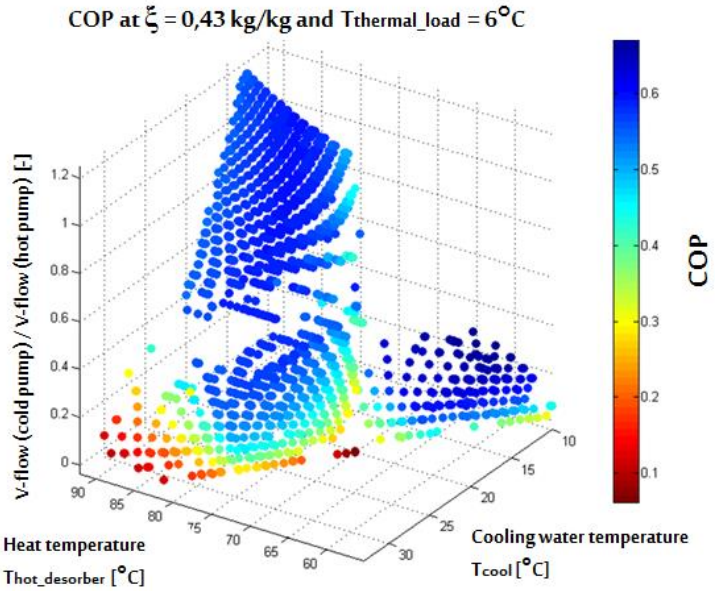

Figure 7: Simulation results for COP of the resorption chiller (Jaehner and Grund, 2014)

3. RESULTS AND DISCUSSION

Resorption cooling systems with ammonia-water solution have more technical and economic advantages than its alternatives thanks to its operational features. The temperature range of heat source is lower than the conventional sorption cooling systems; thus, using solar or geothermal energy at appropriate temperature range is more advantageous in resorption cooling in terms of technical and economic aspects. Therefore initial investment and operational costs of the resorption cooling plant are lower than its alternatives.

Since the operational pressures are significantly lower than the conventional ammonia based absorption chillers, resorption cooling is safer to use and the risk of the ammonia leakage in the system is reduced. Wall thickness of the stainless steel pipes and equipment used in the unit are lower as well, due to the lower operational pressure in the system. Therefore, it is possible to design more compact and cost effective cooling systems. It also allows realizing more feasible renewable energy powered cooling projects and decrease the payback time of the system.

The features of the external lines, heating, cold distribution and heat rejection, affect the cooling performance of the resorption unit, directly. COP of the chiller decreases with the increase in heat rejection temperature and decrease in the heating and cold distribution temperatures. It is essential to design an effective external lines for the resorption system to achieve better cooling efficiencies and better COP values. It will be beneficial to use simulation programs for determining the system features and optimal design.

Determining the control strategy of the resorption system is another important design parameter to achieve better cooling performance and reduce risks of using ammonia. Control system of the resorption unit enables to examine all temperature and pressure values. It is possible to drive the system manually and automatically, therefore the system can be operated in industrial applications effortlessly and efficiently.

Since the resorption cooling unit uses ammonia as refrigerant, it is possible to use ice storage units with resorption chillers to store energy. Thus, efficient cooling projects with the resorption systems can be realized with ice storage during the of peak periods. Stored cooling energy can be used as auxiliary to satisfy peak cooling demands and using ice storage units in the cooling plant allows reducing resorption chiller capacity.

Renewable energy powered resorption cooling systems enables to design more feasible and cost effective cooling systems by using clean and renewable energy sources. It provides new solutions for the technical and environmental problems related to the energy consumption. Using waste heat at appropriate temperature range as a heat source for the resorption system enables to realize clean and cost effective cooling applications in industry.

4. CONCLUSION

Renewable energy powered resorption cooling systems has many technical and economic advantages than its alternatives thanks to its operational features. Using ammonia as refrigerant enables to store cooling energy by the use of ice storage tanks and can be used for cooling applications, during the cooling periods that renewable energy sources are insufficient to drive the resorption system. Since the operational pressures are significantly lower than the conventional ammonia based sorption cycles, it is possible to realize safer and cost effective projects with the resorption chillers. Consequently, it is concluded that renewable energy powered resorption systems will have wide spread use in industrial and residential applications because of their advantages among its alternatives.

5. ACKNOWLEDGEMENTS

This work was partially funded by the Uludag University Scientific Research Project Association research grant, Project 2013/42 – Reducing Operational Cost of Agricultural Cooling Applications Using Resorption System in Orhangazi Region – SOLARES.

6. REFERENCES

COSTIUC L., Costiuc I., 2010. Solar Powered Resorption Cooling System, Bulletin of the Transilvania University of Brasov, Series I: Engineering Sciences Vol. 3 (52).

IEA International Energy Agency, 1999. Task 25 Solar Assisted Air Conditioning of Buildings. Website, Available online: http://www.iea-shc.org/task25/index.html, Accessed 16 April, 2011.

IEA International Energy Agency, 2006. Task 38 Solar air-conditioning and Refrigeration. Website, Available online: http://www.iea-shc.org/task38/index.html, Accessed 16 April, 2011.

HELLE K., 2014. Experimental Experiences with a Resorption Lab Plant at IUTA, Renewable & Clean Energy Workshop - U.Ü. TTO Tübitak P.No:6130034, Bursa, Turkiye.

JAEHNER T., Grund M., 2014. ResoFreeze, Renewable & Clean Energy Workshop - U.Ü. TTO Tübitak P.No:6130034, Bursa, Turkiye.

LI, Z.F., and Sumathy, K., 2000. Technology development in the solar absorption air-conditioning systems. Renewable and Sustainable Energy Reviews; 4: 267–293.

PASTAKKAYA B., Yamankaradeniz N., Kaynaklı Ö., Coşkun S., Yamankaradeniz R., 2012. Experimental analysis of a solar absorption system with interior energy storage, Journal of Energy in Southern Africa, Vol 23-2, 39-49.

PASTAKKAYA B., 2014. Renewable Energy Powered Thermal Applications in Food Industry, Uludag University IV. R&D Days, Bursa, Turkiye.

PASTAKKAYA B., Gürbüz O., Yaslıoğlu E., Gürbüz B., Ünlü K., Kılıç I., Yamankaradeniz R., 2013. Reducing Operational Cost of Agricultural Cooling Applications Using Resorption System in Orhangazi Region, Uludag University III. R&D Days, Bursa, Turkiye.

REE H., Oostendorp P.A., 1980. Resorption Heat Pumps, International Advanced Course on Heat Pump Fundamentals NATO Advanced Study Institues Programme, Espinho, Portugal.

WEIMAR T., 2014. Resorption as New Alternative for Cooling at Low temperatures, Renewable & Clean Energy Workshop - U.Ü. TTO Tübitak P.No:6130034, Bursa, Turkiye.

449: A comparative analysis of the maisotsenko cycle based air-conditioning systems: ejector cooling vs. desiccant

OLEXIY BUYADGIE[1,2], DMYTRO BUYADGIE[2], OLEKSII DRAKHNIA[2], VALERIY MAISOTSENKO[3], TAKAHIKO MIYAZAKI[4], ANDREI CHAMCHINE[5]

1V.S. Martynovsky Institute of Refrigeration, Cryogenic Technologies and Eco Energetics. 1/3, Dvoryanskaya Street, 65023 Odessa, Ukraine,
2 Wilson (Ejector Laboratory), 15/13, Mikhailiv'ska Street, 65005, Odessa, Ukraine, buyadgie@wilson-ukraine.com
3Coolerado Corp. and Idalex Inc. 4430 Glencoe Street, Denver, CO 80216, USA vm@coolerado.com
4Thermal Energy Conversion System Laboratory (TECSL), Faculty of Engineering Sciences, Kyushu University, 6-1 Kasuga koen, Kasuga-shi, Fukuoka 816-8580, Japan tmiyazak@kyudai.jp
5 University of Central Lancashire, Preston PR1 2HE, UK achamchine@uclan.ac.uk

The numerous researches of the Maisotsenko cycle (M-cycle) application for air-conditioning purposes prove 3 to 10 times (depending on air humidity) energy saving compared to the conventional vapour-compression systems. Another important value of air-conditioning through the M-cycle is the air displacement process that serves to supply fresh air into the conditioned premises continuously at the fixed energy input. Being considered as a pure heat recuperative process, the M-cycle cooling requires water makeup that is obviously high in the dry climate zones. Conversely, in the humid zones, where absolute humidity exceeds 11g/kg of the dry air, the M-cycle based air-conditioners are unable to meet the air dehumidification challenge and require the conventional or state-of-the art technologies to remove the excess moisture from the processed air before its substantial cooling to the set temperatures. In order to validate the performance of the M-cycle based air-conditioners in the humid zones and minimize the overall energy input for cooling and dehumidification processes, a comparative analysis of the latest desiccant dehumidifiers and ejector cooling systems was performed. The study is devoted to disclose the pros and cons of the existed schemes of the M-cycle based cooling systems for the habitant and technological conditions. Alternatively, it was proposed the hybrid M-cycle/desiccant/ejector air-conditioner that may serve to be one of the most energy efficient cooling system for the humid climate conditions, where 85% of the world's air-cooling demand is located.

Keywords: M-Cycle, ejector, refrigeration, humid, desiccant

1. INTRODUCTION

Reducing energy consumption for air-conditioning is a key task, because artificial cold consumes up to 20% of all generated electricity. This number tends to increase for two main reasons: global warming is most pronounced in countries where the climate was the hottest, increasing and accelerating the levelling of living standards around the world, and the new technologies development requiring climate control. M-Cycle and based on it systems development and producing various modifications conditioners contributes to solve given problem in many ways, but it cannot be recommended in pure form for all consumers. Therefore, it is necessary to decide on most cost effective options that allow to breakthrough in the field of air-conditioning.

The attention of researchers and engineers focused today on two main area: conventional vapour-compression refrigeration units, solid and liquid desiccant dehumidifiers [Buker and Riffat, 2015]. Both options require additional electricity expenditures as well as heat for recovery absorption capacity of desiccant in second case [Wani et.al., 2012, Gao et. al., 2014, Buker and Riffat, 2015, Bassuoni, 2011, Finocchiaro, 2010]. There is provided to consider sorption and jet chillers as an alternative. They consume significantly less energy and produce cold at the expense of low-grade heat. The source of this heat can be waste and solar heat.

2. FUNCTIONAL SCHEMES, THERMAL AND HUMIDITY AIR HANDLING.

The first hybrid solution for application range expanding of a new generation M-Cycle air conditioners was adding vapour compression refrigeration system (VCRC) [Buyadgie et.al, 2011, Gillan, 2008]. That increased power and material consumption (Figure 1, 2). Vapor compression chiller cold production equals 10-60% in intermediate moisture zone, where humidity lower than 50-60% and air temperature 30-35°C. However, that value rise up to 80-95% in tropical climate and it is unacceptable.

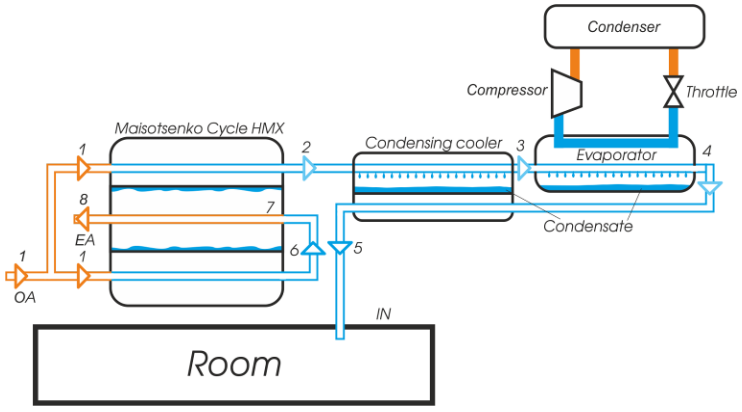

Figure 1. Hybrid M-Cycle/VCRC. 1-2 air-cooling in HMX, 1-6 working air preparing in HMX, 6-7-8 saturating working air with water and heat abstraction, 2-3 recuperative cooling by heating air before it enters the room 4-5, 3-4 air-cooling in the evaporator of vapour compression system.

An alternative method is to combine the M-Cycle with liquid and solid desiccants. Desiccants actively absorb moisture from the air when a large difference between the partial pressures, but requires recovery initial concentration of the solution or the specific moisture content in the sorbent [Gao, 2014, Buker and Riffat, 2015, Bassuoni, 2011].

In this case, the air cooling in HMX proceeds efficiently, but power consumption for circulating pumps and rotor, as well as heat for desiccant recovery quite significant (Figure 3).

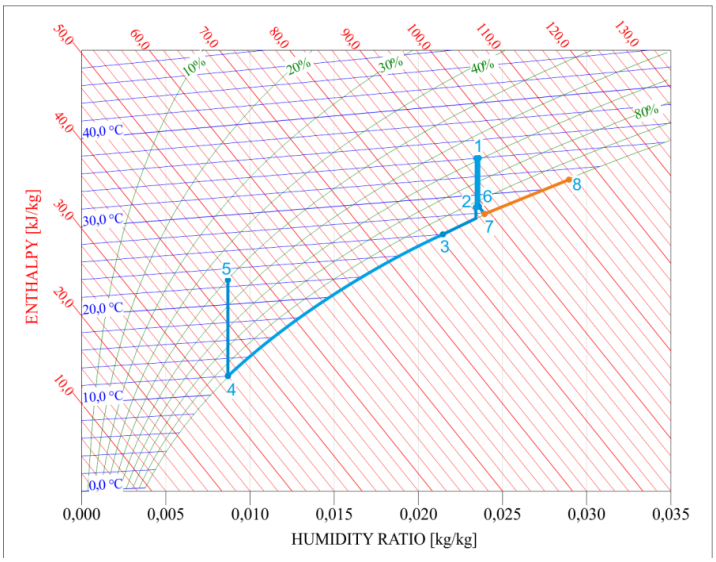

Figure 2. Process chart in M-Cycle/ VCRC.. 1-2 air-cooling in HMX, 1-6 working air preparing in HMX, 6-7-8 saturating working air with water and heat abstraction, 2-3 recuperative cooling by heating air before it enters the room 4-5, 3-4 air-cooling in the evaporator of vapour compression system.

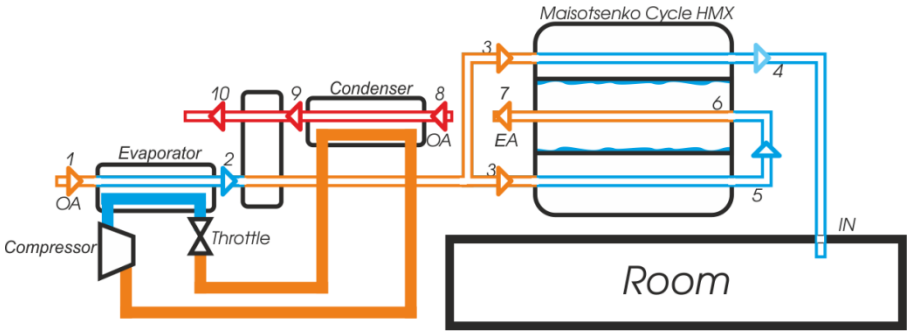

Figure 3. Combined Solid desiccant (Rotor)/M-Cycle air conditioning system. 1-2 air cooling in heat pump evaporator before rotor, 2-3 air dehumidification process, 3-4 air cooling in HMX, 3-5 working air preparing in HMX, 5-6-7 working air saturation with water and heat abstraction, 8-9 heating air in heat pump condenser for desiccant recovery, 9-10 desiccant recovery in rotor.

In addition, the evaporator load also includes cooling the heated part of rotor and desiccant through which blows coldest air in cycle. It involves additional cold losses. This results harmful air heating, which also degrades performance of air-conditioner [Buker and Riffat, 2015, Finocchiaro, 2010] (Figure 4).

Similar losses are typical for liquid desiccant [Buker and Riffat, 2015, Bassuoni, 2011]. In all last schemas with desiccant coolers use heat pump. On the one hand, it cools air before dehumidifying on the other heats air for desiccant recovery. In this case, additional heat consumption excluded [Finocchiaro, 2010].

Outside air is cooling in heat pump evaporator, and then it flows to camera where it gives excess moisture to desiccant. The dehumidified and cooled air is divided into two streams and sent to the HMX. Working air saturates by moisture and cools product air to desired temperature, after that in flows into a room. Outside air heats up in heat pump condenser and regenerates solid desiccant. In case with liquid desiccant, heated air evaporates moisture from dissipates desiccant (Figure 3, 4).

Absorption or Ejector coolers can be used for cold production and reduce power consumption. As a result, system use electricity for fan and automatics, and feed pump in absorption system. One of the advantages in ERS is thermopump. It consumes working vapour. In addition, it is possible to use water vapour-air ejector fan and vacuum pumps. System becomes completely independent of electricity. Figures 5 and 6 show two modifications of combined M-Cycle/ERS air-conditioning system. In first schema, water condensed from air during cooling evaporates in two recuperative heat exchangers. Water is spaying and evaporating in vacuum. All cold spend for water condensing returning to cycle for air-cooling. It allows to minimize required ERS cooling capacity (Figure 7).

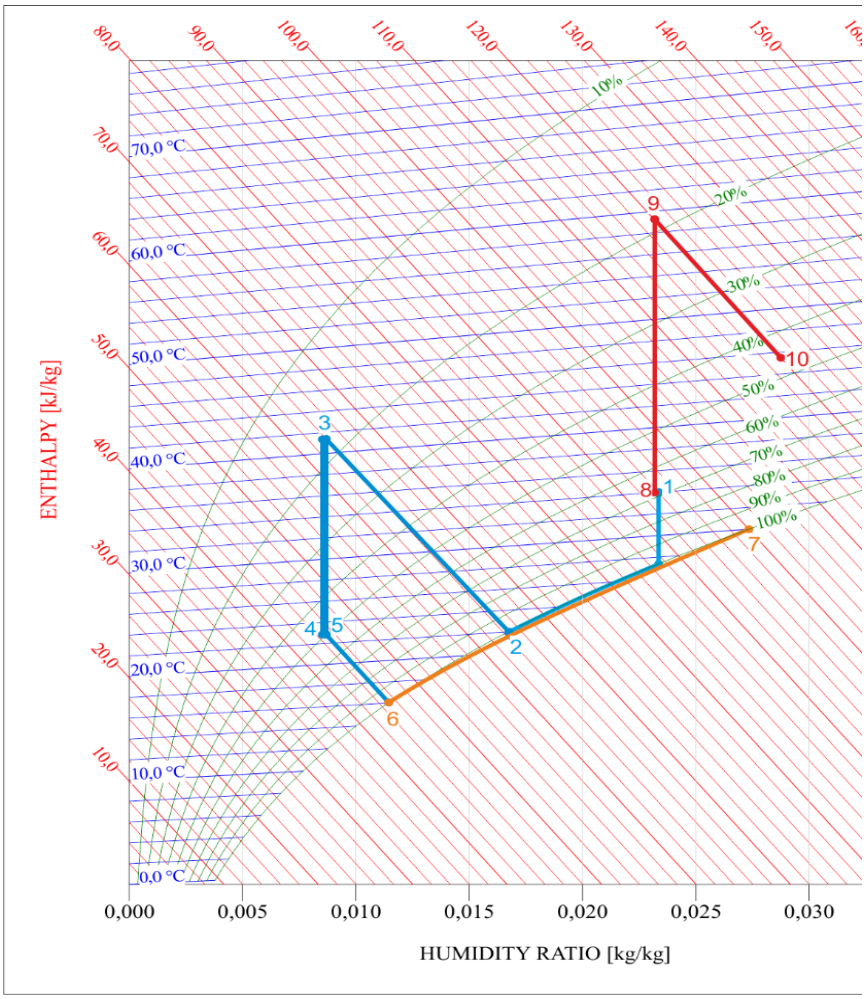

Figure 4. Process chart in Solid desiccant (Rotor)/M-Cycle system.1-2 air cooling in heat pump evaporator before rotor, 2-3 air dehumidification process, 3-4 air cooling in HMX, 3-5 working air preparing in HMX, 5-6-7 working air saturation with water and heat abstraction, 8-9 heating air in heat pump condenser for desiccant recovery, 9-10 desiccant recovery in rotor.

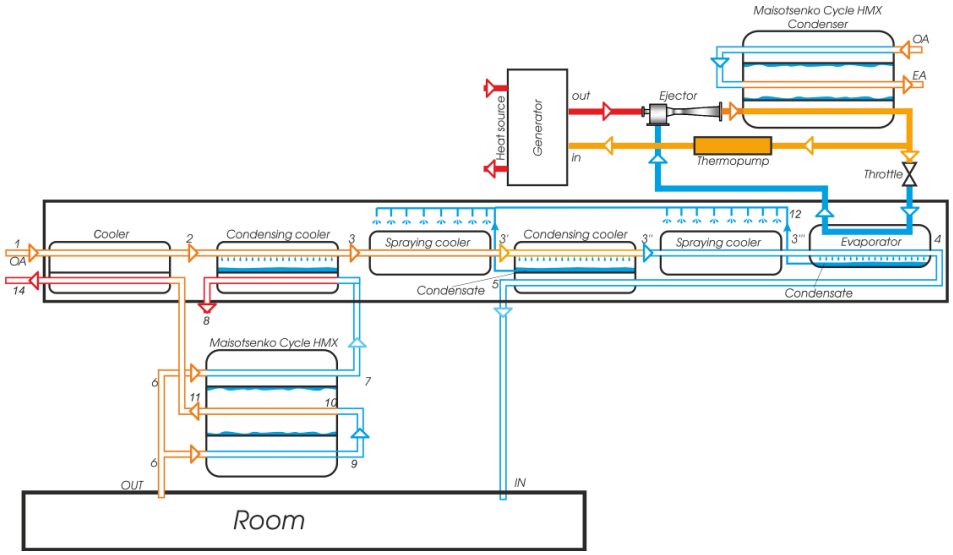

Figure 5. Combined M-Cycle/ERS air-conditioning system with full recuperation. 1-2 fresh air precooling by heating exhaust working air from HMX 11-14; 2-3 fresh air cooling by heating product air from HMX 7-8; 3-3' and 3''-3''' air cooling by precipitated moisture in process 2-4; 3'-3'' air cooling by preheating air before room air supply 4-5; 3'''-4 air cooling in ERS evaporator; 6-9 working air preparing in HMX; HMX; 6-7 HMX air cooling; 9-10-11 working air saturation with water and heat abstraction; in, out – ERS vapour generator refrigerant inlet and outlet.

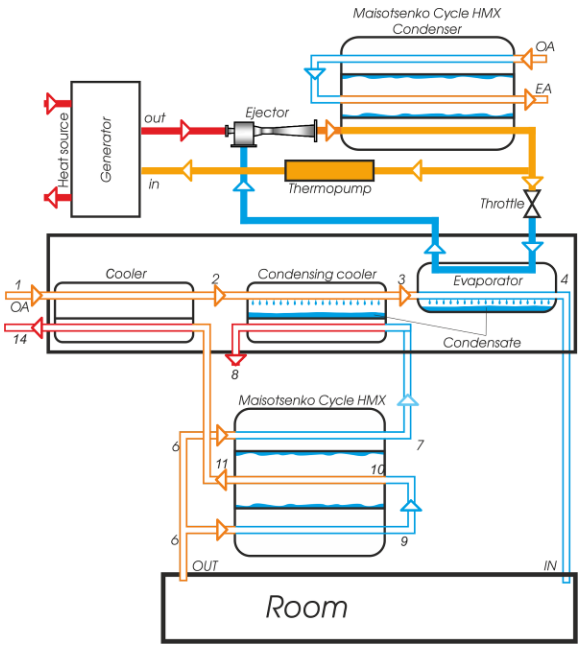

Figure 6. Combined M-Cycle/ERS air-conditioning system with partial recuperation. 1-2 fresh air precooling by heating exhaust working air from HMX 11-14; 2-3 fresh air cooling by heating product air from HMX 7-8; 3-4 air cooling in ERS evaporator, 6-9 working air preparing in HMX; HMX; 6-7 HMX air cooling; 9-10-11 working air saturation with water and heat abstraction.

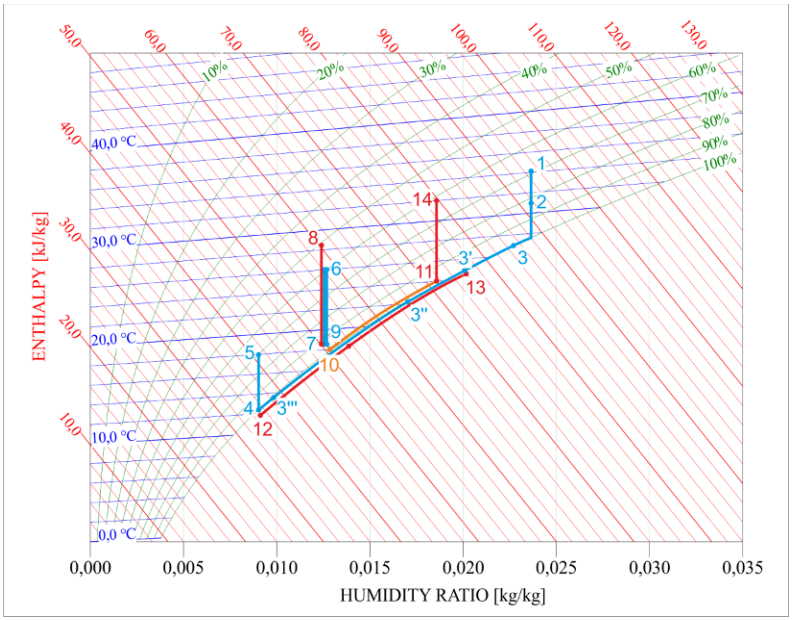

Figure 7. Process chart in combined M-Cycle / ERS system with full recuperation. 1-2 fresh air precooling by heating exhaust working air from HMX 11-14; 2-3 fresh air cooling by heating product air from HMX 7-8; 3-3' and 3''-3''' air cooling by precipitated moisture in process 2-4; 3'-3'' air cooling by preheating air before room air supply 4-5; 3'''-4 air cooling in ERS evaporator; 6-9 working air preparing in HMX; HMX; 6-7 HMX air cooling; 9-10-11 working air saturation with water and heat abstraction; in, out – ERS vapour generator refrigerant inlet and outlet.

Water vapour-air ejector provide vacuum in spraying coolers, similar ejector provide air circulation in air conditioner channels. It allows to exclude from use electric fans (not shown in schemas).

Air from cooling space direct into HMX 6, where it splits in two flows. Working flow is precooling 6-9, saturates by water 9-10-11 and heating 10-11, at the same time it cools flows 6-9 and 6-7. Fresh ambient air flows to heat exchanger where cooled 1-2 by heating HMX exhaust air 11-14. Next heat exchanger cools air 2-3 by heating HMX product air 7-8. Exhaust air 8 and 14 removes from system and can flow through ERS condenser. Cooling process 3-3' and 3''-3''' is performed by moisture evaporating in

vacuum. This moisture drops during cooling 1-4. Process 3'-3'' achieving by heating room air supply 4-5.

Table 1 shows process air parameters in combined M-Cycle/ERS system. It show that ERS and recuperation allow to reduce absolute humidity from 23.41 g/kg to 8.8 g/kg. At the same time requires ERS cooling capacity decrease from (Equation 1) to (Equation 2).

Equation 1: Specific cooling capacity $$q_{eva} = i_3 - i_4$$

Equation 2: Specific cooling capacity $$q_{eva} = i_{3''} - i_4$$

Where:

- q_{eva}= specific cooling capacity (kJ/kg)
- i_3= enthalpy at point 3 (kJ/kg)
- $i_{3'''}$= enthalpy at point 3''' (kJ/kg)
- i_4= enthalpy at point 4 (kJ/kg)

Air from point 14 can be saturated by moisture to cool to a 27°C, but usefulness of this process requires additional economic analysis.

Table 1. Process air parameters in combined M-Cycle/ERS system.

Parameters	1	2	3	3'	3''	3'''	4	5	6	7	8	9	10	11	14
Temperature, °C	34	31,1	27,1	25	22,2	13,6	12	23	26	18,5	29,1	18,5	17,9	24	32
Relative humidity, %	69	81,2	100	100	100	100	100	50	60	94,7	56,6	94,7	100	100	62,7
Enthalpy, kJ/kg	94,2	91,2	85,6	76,3	65,1	38,1	34,2	45,4	58,39	50,66	59,4	50,7	50,7	72,2	80,55
Absolute humidity, g/kg	23,4	23,4	22,8	20,1	16,8	9,8	8,8	8,8	12,6	12,6	12,6	12,6	12,9	18,9	18,9

3. CYCLE CALCULATED PARAMETERS FOR SYSTEMS WITH DESICCANTS AND ERS.

Combined system with desiccants or ERS COP is determined from following Equation 3:

Equation 3: Systems COP $$COP = \frac{Q_{eva}}{\eta_{Carnot}\sum Q_{heat} + \sum L}$$

Equation 4: Total consumed heat $$\sum Q_{heat} = Q_{gen} + Q_{desorp}$$

Equation 5: Total consumed work $$\sum L = L_{fan} + L_{pump} + L_{rotor} + L_{comp}$$

Equation 6:Cooling capacity $$Q_{eva} = G_{air,prod}\left(i_x - i_4\right)$$

Equation 7:Heat consumed for vapour generation in generator ERS $$Q_{gen} = G_{ref,gen}\left(i_{out} - i_{in}\right)$$

Equation 8: Heat consumed for desiccant restore $$Q_{desorp} = G_{air,work}\left(i_9 - i_{10}\right)$$

Equation 9: Work consumed by fans $$L_{fan} = \sum G_{air} \cdot l_{fan}$$

Equation 10: Work consumed by desiccant recirculation pump $$L_{pump} = G_{desic} l_{pump}$$

Equation 11: Specific work consumed by desiccant recirculation pump $$l_{pump} = \frac{v_{desic}\Delta p}{\eta_{pump}}$$

Equation 12: Work consumed by compressor heat pump $$L_{comp} = G_{ref} l_{comp}$$

Equation 13: Specific work consumed by compressor heat pump $$l_{comp} = \frac{i_{comp,out} - i_{comp,in}}{\sum \eta_{actual}}$$

Equation 14: Carnot cycle COP $$\eta_{Carnot} = 1 - \frac{T_{gen}}{T_{cond}}$$

Where:

- Q_{eva}= cooling capacity (kW)
- T_{gen}= generation temperature (K)
- T_{cond}= condensation temperature (K)
- $G_{ref,gen}$= refrigerant mass flow rate in ERS generator (kg/s)
- G_{ref}= refrigerant mass flow rate in compressor (kg/s)
- $G_{air,work}$= working air mass flow rate in Maisotsenko HMX (kg/s)
- $G_{air,prod}$= product air mass flow rate in Maisotsenko HMX(kg/s)
- G_{air}= total air mass flow rate in system (kg/s)
- l_{fan}= specific work consumed by fans (kJ/kg)
- G_{desic}= liquid desiccant mass flow rate (kg/s)

Heat pump working parameters: evaporation temperature teva=18°C, condensation temperature tcond=69°C. Coefficient of heat pump performance φ= 2,7. ERS working parameters: generation temperature t_{gen}=85°C, condensation temperature tcond=35°C, evaporation temperature teva=7°C. COP of ERS equals ζ =0,288 (R-142b), ζ =0,38 (R-123/Isobutane). In each system, we exclude from the expressions the quantities that not presented in it.

The results of process modeling of combined system with desiccants in Figure 8 and system with ERS shown in Figure 9.

4. COMPARATIVE ENERGY INDICATORS OF COMBINED M-CYCLE/ERS AND DESICCANT/M-CYCLE SYSTEM.

Hybrid system with compression refrigeration system is out of scope in this comparison, because with temperature and humidity raise all load lies on the compressor and M-Cycle is no longer involved in cold production.

The calculations performed for systems with solid and liquid desiccants and ERS with full heat and cold recuperation.

In schemas with solid desiccant, power consumption slightly less than in system with liquid desiccant. Rotor make 1-2 rotations in 1 hour, so operating time is small. At the same time, circulating pump works permanently. Power consumption for fans and compressor is negligibly differs. Compressor heat pump excludes additional heat consumption.

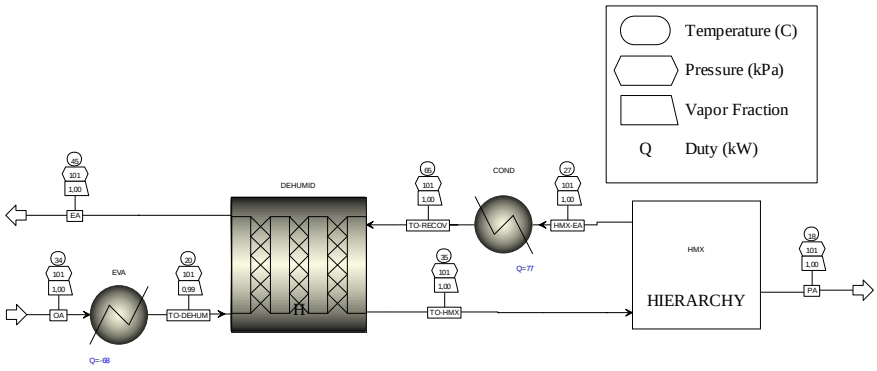

Figure 8. Process engineering of the combined Solid desiccant/M-Cycle system.

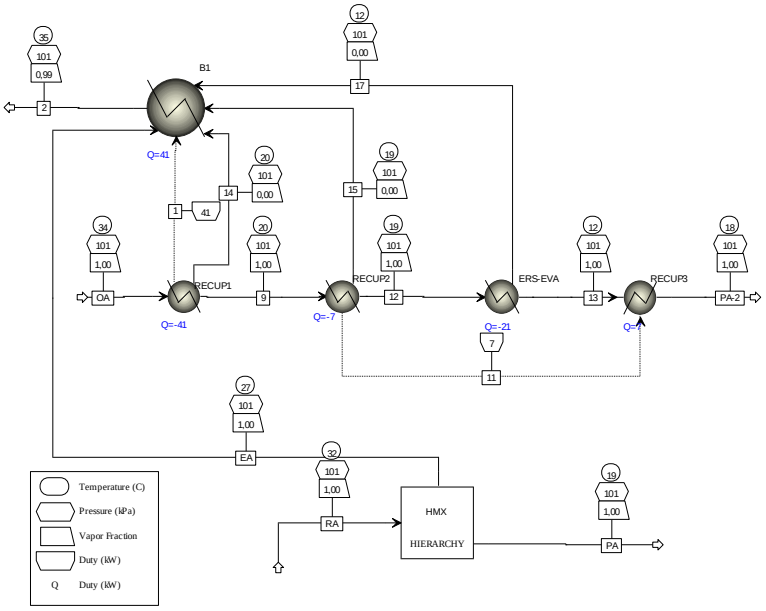

Figure 9. Process engineering of the combined M-Cycle/ERS system.

M-Cycle/ERS system consumes additional heat and electricity is only needed to drive fans. First instance is calculated at 100% fresh airflow into the room at flow rate 2700m3/h (Table 2). Air from a room flow to Maysotsenko HMX where it splits, cooled and flow to heat exchanger and precool the fresh air. M-Cycle/ERS system consumes 3.1-3.7 times less energy than Desiccant/M-Cycle system, if consumed heat recalculate to its exergy. Second instance for technical objects, system supply 60% or recirculating air, 40% fresh air at flow rate 12000 m3/h (Table 3). Cooled air from Maysotsenko HMX mixing with cooled fresh air. Exergy COP ratio of industrial air conditioners Desiccant/M-Cycle and M-Cycle/ERS equals 3.65-4.1. Vapour compression heat pump can be replaced by ejector heat pump (Figure 10). That pump utilizes heat and takes place between M-Cycle/ERS and Desiccant/M-Cycle system by energy consumption (Table 2).

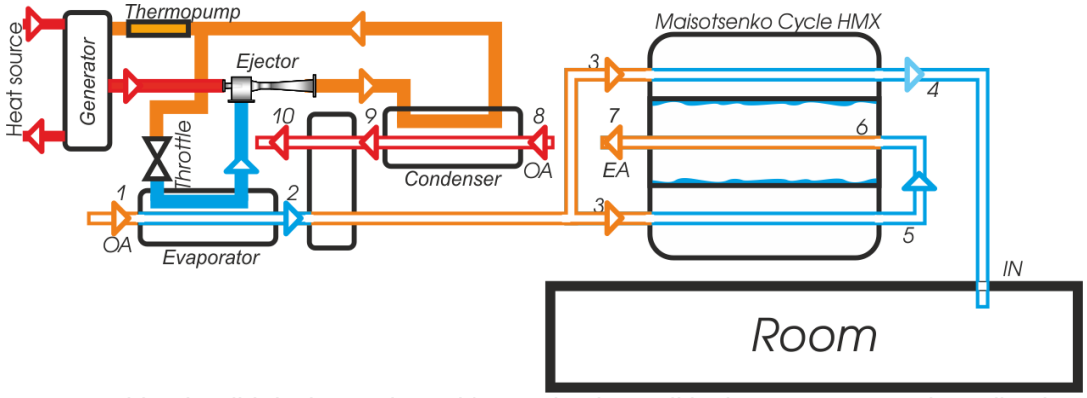

Figure 10. Combined Solid desiccant (Rotor)/M-Cycle air conditioning system. 1-2 air cooling in ejector heat pump evaporator before rotor, 2-3 air dehumidification process, 3-4 air cooling in HMX, 3-5 working air preparing in HMX, 5-6-7 working air saturation with water and heat abstraction, 8-9 heating air in heat pump condenser for desiccant recovery, 9-10 desiccant recovery in rotor.

Reduced work consumption lower by 2 times then in Desiccant/M-Cycle with vapour compression heat pump. This may be due to ERS thermal coefficient at high condensation temperatures is low and equals 0.28-0.3.

Table 2. Expenses for domestic air-conditioner operation. (2700m³/h cooled airflow, 100% fresh air).

System	Parameters						General input		
	Q_{eva}, kW	Q_{gen} / L_{comp}, kW	L_{fan}, kW	Q_{HMX}, kW	Q_{desorp}, kW	L_{pump}/L_{rotor}, kW	**Q, kW**	**L, kW**	**$L_{reduced}$, kW**
M-Cycle/ERS	5.17	19.92	3	6.47	-	-	19,92	3	5.78
Solid Desiccant/M-Cycle	40.2	14.6	3	17.26	26.25	0.4	-	18	18
Liquid Desiccant/M-Cycle	40.2	14.6	3	17.26	26.25	3,6	-	21,2	21.2
Solid Desiccant/EHP /M-Cycle	17	20	3	17.26	26.25		20	3	8.77

Table 3. Expenses for industrial air-conditioner operation. (12000m³/h cooled airflow, 60% recirculation air)

System	Parameters						General input		
	Q_{eva}, kW	Q_{gen} / L_{comp}, kW	L_{fan}, kW	Q_{HMX}, kW	Q_{desorp}, kW	L_{pump}/L_{rotor}, kW	**Q, kW**	**L, kW**	**$L_{reduced}$, kW**
M-Cycle/ERS	14,6	50,7	5,25	30,86	-	-	38	5,25	10.55
Solid Desiccant/VC HP/M-Cycle	70,4	26,08	12	45,5	78,68	0.63	-	38.7	38.7
Liquid Desiccant/VC HP/M-Cycle	70,4	26,08	12	45,5	78,68	5,47	-	43,5	43.5
Solid Desiccant/EHP /M-Cycle	30.7	35	12	45.5	65.7	0.63	35	12.63	22.73

5. M-CYCLE AIR-CONDITIONERS APPLICATION AREA.

Pure M-Cycle effective in continental climate zones with high and moderate temperature: midcontinent areas of Eurasia, Arabian Peninsula, desert zones and savannah of Africa, South and North America, inner zones of Australia. Those regions has low population. It is about 500 millions, 7-10% of total population (Figure 11).

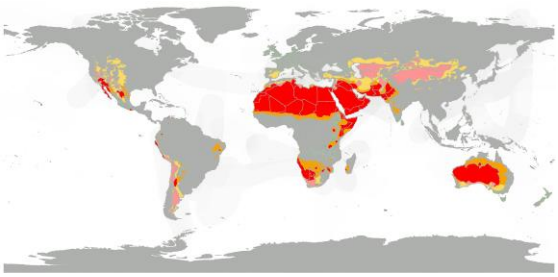

Figure 11. M-Cycle air-conditioners application area.

Application area reaches 30% of population if added zones with seasonally low humidity and where M-Cycle work is satisfying (Figure 12).

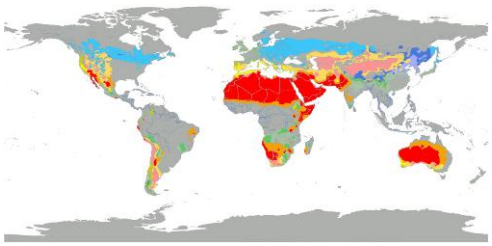

Figure 12. Zones of seasonal use of M-Cycle based air-conditioners.

Combined M-Cycle with desiccants or ERS air-conditioners can service all the regions, where air-conditioning is required. It is about 90% of population (Figure 13).

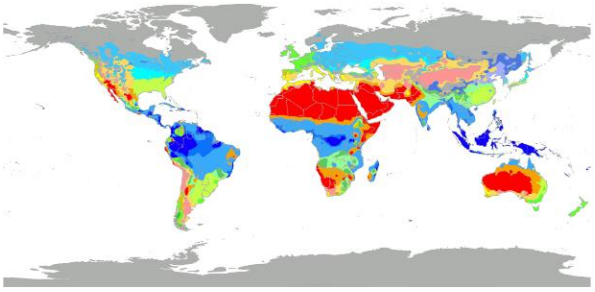

Figure 13. Application area of combined Desiccant/M-Cycle or M-Cycle/ERS air-conditioners.

New generation of air-conditioners based on M-Cycle can create comfortable conditions everywhere. It makes sense to adjust their production as an alternative to reduce electricity consumption.

6. CONCLUSION

1. Combined M-Cycle air-conditioner with ERS or desiccants can be used anywhere where air-conditioning is required.
2. Energy efficiency of M-Cycle/ERS system higher than Desiccant-M-Cycle system in 3-4 times.
3. Cold recuperation improves cycle efficiency in 1.5 times.
4. Low-grade heat source for ERS can be any waste heat, secondary heat sources and solar heat.
5. Combined M-Cycle with ERS and desiccants allow to reduce reduced work consumption in 2 times.
6. Maisotsenko HMX can effectively be used as condenser for ERS. That increase ERS efficiency by 20-35% and reduce mass-dimensional characteristics of condenser in 1.5 times due to high heat transfer coefficient.

7. REFERENCES

BASSUONI, M.M., 2011. An experimental study of structured packing dehumidifier/regenerator operating with liquid desiccant. *Energy*, 36, pp. 2628-2638.

BUKER, Mahmut Sami, RIFFAT, Saffa B., 2015. Recent developments in solar assisted liquid desiccant evaporative cooling technology—A review. *Energy and Buildings*, 96, pp. 95-108.

BUYADGIE, D., BUYADGIE, O., DRAKHNIA, O., SLADKOVSKYI, Y., ARTEMENKO, S., CHAMCHINE, A., 2011. Theoretical study of the combined M-Cycle/Ejector air-conditioning system. *International Journal of Energy for a Clean Environment*, 12(2-4), pp. 309-318.

CHANDRAKANT Wani, Satyashree Ghodke, Chaitanya Shrivastava, 2012. A Review on Potential of Maisotsenko Cycle in Energy Saving Applications Using Evaporative Cooling. *International Journal of Advance Research in Science, Engineering and Technology*, 01 (01), pp.15-20.

GAO, W.Z., CHENG, Y.P., JIANG, A.G., LIU, T., ANDERSON, K., 2014. Experimental investigation on integrated liquid desiccant - Indirect evaporative air cooling system utilizing the Maisotsenko – Cycle. *Applied Thermal Engineering*, 09, pp. 1-9.

GILLAN, L., 2008. Maisotsenko cycle for cooling processes. *Clean Air*, 9, pp. 1–18.

FINOCCHIARO, Pietro, 2010. Solar Air-Conditioning and Refrigeration Task 38, IEA-Workshop/ Solid desiccant Open Cycles and Machines. Aarhus.

280: A carbon neutral small scale district heating

MICHELE TUNZI, EDWARD COOPER, BOUKHANOUF RABAH

Department of Architecture and Built Environmen+t, University of Nottingham, University Park, Nottingham NG7 2RD, United Kingdom, ezxmt@nottingham.ac.uk.

The energy requirement of an existing small scale district heating (DH) network, connected to seven properties of mixed use (office and living spaces), located in Nottinghamshire and fuelled by a 300 kW biomass boiler, was studied in view of upgrading it. This paper presents results of heat energy simulation, monitoring and an energy audit of the existing heat network. The individual properties' heat load profiles were modelled in order to get an aggregated site profile network. In addition, on selected points of the network, the operating conditions of the network were monitored and collected: supply/return temperatures and mass flow rate are presented. The paper also summarises a recommendation for an upgraded heat network, focusing on improving the DH and to propose this as a solid technology for the future challenges of the heat energy market.

Keywords: community energy scheme, district heating, heat load profile, thermal simulation

1. INTRODUCTION

The challenging objectives of decarbonising the EU economy and achieving the long term goal of an energy system completely based on renewable sources will require massive effort in research and industrial developments of more sustainable energy processes and practices. In this direction, the EU Commission is working towards the definition of a complex strategy for achieving a sustainable society. The targets which have been set include a strategy for facing the challenging objectives over the next three decades. In the short term vision, the EU commission agreed on the "20-20-20" package solutions, in order to cut by 20% the GHG emissions from 1990 levels, increase by 20% the energy efficiency and produce 20% of energy consumed by renewable energy sources (EU, 2010). Further agreements have been achieved in the long term scenario by the definition of "the Roadmap for moving to a low-carbon economy in 2050", where a "commitment to deliver the long term low carbon society" has been defined; the core of this approach will be to cut the emissions by 85-90% compared to the 1990 levels (EU, 2011).

In this direction, considering the primary energy market, the majority of energy consumption is linked to heating requirements for space heating and domestic hot water, for a portion between 40%-50% (depending on the country considered) of the total energy generated (Olsen et al., 2008). Therefore, heating demand will have a decisive role in research and technical improvements, if the final scope is to decarbonise our economy and move towards a more sustainable society. To this extent, the promotion of future smart cities may require a more integrated approach in the provision of heating and cooling in buildings. District heating (DH) which is a widely used concept in some EU countries is a high efficiency heating process; different from the individual heat solutions, DH systems allow distribution of energy on a community basis, which includes neighbourhoods, small villages or large cities. It represents a solid technology, well developed and tested over decades in particular for northern European countries as Finland, Sweden and Denmark, where DH covers almost 60% of the heating energy demand for domestic households (Ecoheat4eu, 2011b). One of the most important characteristic is the high flexibility associated to this complex system, for both energy generation and distribution. In fact, centralising the energy generation, in one or multiple points, allows to integrate traditional fossil fuel technologies, renewable sources, as well as to recover heat from CHP plants (e.g. waste incineration) or intense industrial process which otherwise would be wasted.

In line with other European country trends, heat demand for space heating (SH) and domestic hot water (DHW) in UK covers 49% of the total energy demand, being responsible for 47% of the total carbon emissions (Ecoheat4eu, 2011c). The presence of DH technology for delivering SH and DHW in UK is in place since 1950s, with examples of large DH scheme in city like Sheffield, Nottingham, Southampton, as well as in some areas of London. The Nottingham DH for instance, fuelled by a waste CHP plant, represents a very interesting example in terms of reliability and effectiveness of the technology for the UK market. Working since 1960s, it is composed of a 14.5 MW condensing turbine and 68 km of pipelines, supplying 5000 homes and 100 businesses across several areas of the city (EnviroEnergy, 2015).

Despite the positive examples, the effective penetration in the UK compared to others EU countries is accountable for only less than 1-2% of the entire heating demand as clearly depicted in the table 1.

Table 4: EU DH development status (Ecoheat4eu, 2011a)

Status of the DH market	Market Share [%]	Examples
Consolidation	50-60	Denmark, Finland, Sweden
Refurbishment	10-50	Croatia, Czech Republic, Lithuania
Expansion	3-15	France, Germany, Italy
New development	<1	Ireland, Spain, UK

Nevertheless, an important study conducted by Euroheat & Power and BRE specifically for the UK highlights how considering a possible future scenario for the heating system between 2007 and 2030, the penetration of DH could lead to (Ecoheat4eu, 2011c):

- Reduction of annual primary energy supply: 167 PJ
- Reduction of annual national energy import: 369 PJ
- Reduction of annual carbon dioxide emissions: 34 million tonnes
- Renewable energy share: 36%

Another study conducted by Poyry Energy Consulting for UK shows how the DH market share, at the actual state of art, by simply reducing the discount rate from 10% to 3.5% and including the shadow price of carbon for the combustion of fossil fuels, could easily reach a portion between 6-14% of the total heat demand (Pöyry, 2009). However, more recently, the national authorities, differently from the past, where the decarbonisation of the UK economy was mainly focused on the electricity market, are reconsidering the strategic importance of the heat sector. As a result, the first scheme worldwide to incentivise renewable heat technologies (RHI, renewable heat incentives) was designed, from 2012 for businesses and from 2014 for domestic applications. Due to the new input given by the UK policymakers, DH technology can have a crucial role towards the challenging objectives of decarbonising the UK energy market.

From this perspective, the entire investigation is based on a detailed analysis of an existing small scale DH located in the countryside of Nottingham. The main goal of the project is on one hand, to evaluate the performances of the actual network, categorised as a medium temperature district heating (MTDH, 3rd generation) due to the supply/return temperatures of 80/50°C (Harvey, 2006); on the other hand, to assess the performances of the system in prevision of expanding the network by connecting new customers and upgrading it to the new DH concept (4th generation DH), operating at very low temperatures, supply/return 55/25°C (LTDH) (Svend Svendsen, 2014). The research part proposed in this article is focused on the energy analysis of the buildings served by the DH and the energy audit of the site, with particular emphasis on the actual operating conditions of the heating network.

2. METHODOLOGY

The research project reported in this paper was based on a case study located 30 km north of Nottingham. The system, as highlighted in figures 1 and 2, was represented by a small scale DH network fuelled by a 300 kW biomass boiler. The biomass, in form of willow and woodchip is grown and coppiced on site. The heat network delivers heat in the form of hot water to meet the space heating (SH) demand (distributed by underfloor heating), using a double pipe system (for supply and return line), while the domestic hot water preparation is provided by electric heaters. The network serves eight buildings, each of them characterised by different occupancy patterns and activity.

Figure 7: Estate Google Earth image

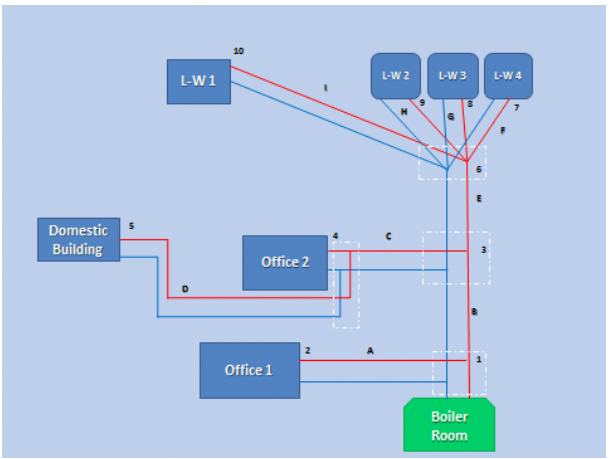

Figure 8: District heating schematic view

The strategy presented in this paper was focused on assessing and mapping the energy demand of the estate, seeking a specific methodology which can be summarised as follows:

- Building energy simulation
- Energy audit

Building energy simulation

The site is composed of eight different types of buildings, as a combination of offices, domestic properties and live/work spaces, which represented an ideal case study to perform coherent analyses on DH for UK (Table 2).

Table 5: Site Definition

Properties	Number of Occupants per Working Space	Number of occupants per Living Space	Area per Building (m^2)
Live-Work 1	4	2	256
Live-Work 2	1	3	535
Live-Work 3	5	0	535
Live-Work 4	5	1	535
Domestic Build	0	2	209
Office 1	33	0	760
Office 2	56	0	546

All the building plans, materials, HVAC and dimensions were collected and by reference to the 2006 UK Building Regulation Part L (the Estate was completely renovated during 2006), it was possible to model and simulate the energy performances of each building. The weather data from CIBSE database, for the location of Nottingham, were used as boundary condition for the simulation, as well as the definition of an occupancy plan for each building according to the specific activity.

Energy audit

In order to correctly assess the performance of the DH, on selected points of the network some loggers were installed to monitor and collect the data for temperature and mass flow rate. The flow and return temperature were collected at the boiler room and at the Live-Work 2 (see figures 1 and 2, point one and nine in the network layout) by installing two data loggers and using four RTD temperature sensors. The data collected covered the heating season 2013/14, using 15 minutes as the referenced interval. Similarly, at the boiler room (point one of the network), by using an ultrasonic sensor, it was possible to detect the total mass flow rate pumped within the DH using the standard 15 minutes interval.

3. RESULTS

The monitoring procedures produced a robust set of data for the heating season of 2013/2014; this was extremely important to define the operating conditions of the entire network and to validate the reliability of the future findings of the research project. Before using the data, those were controlled, in order to remove, if available, typical errors occurring during recording process as accidental interruptions, power cuts etc. The following figures show results for both the boiler room (point one in Figure 2) and Live-Work 2 (point nine in Figure 2) for supply and return temperatures.

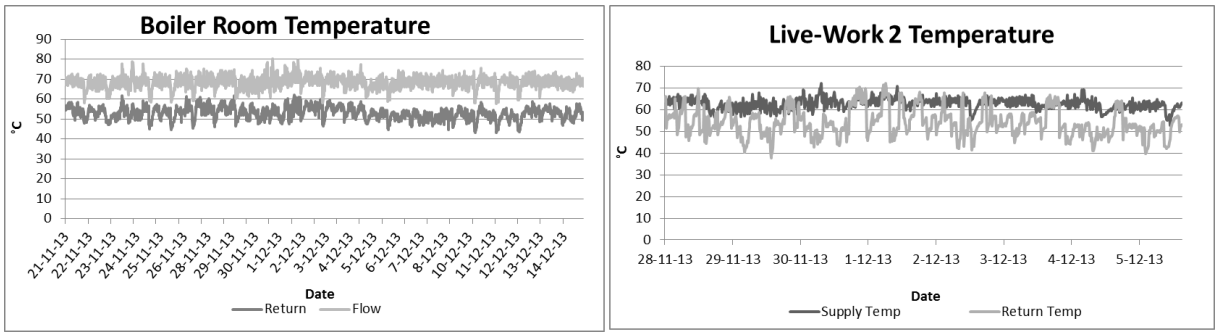

Figure 9: Recorded temperatures node one (boiler room) and node nine (Live-Work 2)

Figure 6 presents an overview of the data collected for mass flow rate. The selected point in the DH network was node 1 on the return line, in order to monitor the total flow circulating in the system.

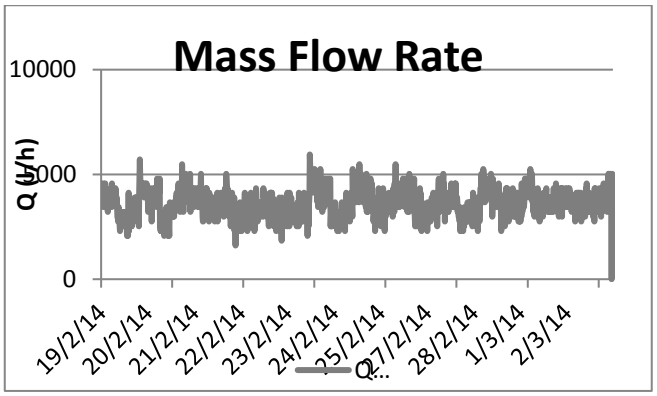

Figure 10: Recorded mass flow rate, node one (boiler room)

At the same time it was possible to collect the total energy consumption for the entire estate for the years 2007-2012 inclusive, as described in Table 3:

Table 6: Summary of Annual Energy Consumption

Ref. Year	MWh
2007/08	361.85
2008/09	349.87
2009/10	339.92
2010/11	359.04
2011/12	312.42
Average 2007-12	**344.62**

Using as a reference case the heating season of 2007/08 and considering the buildings' energy consumption individually, the simulated energy predictions were compared with the real ones. The models developed were very accurate for assessing the energy performances of the buildings, as highlighted in Table 4.

Table 7: Energy Demand Comparison

Annual Heat Consumption (MWh)		
Building	**DB**	**Recorded Data**
Office 1	114.24	121.88
Office 2	68.79	70.26
Live-Work 1	36.47	38.53
Live-Work 2	45.22	42.87
Domestic Building	21.54	26.58

Another crucial aspect of the energy analysis performed was the possibility to define the heat load profiles for each building on an hourly basis, as shown in figure 5 for the Live-work 2 and the domestic Building and figure 6 for all the buildings in a typical winter day. These results reflect on one hand, the building response to the variation of weather conditions; on the other hand, given the assumptions for the activity and occupancy in the buildings, the effect of human behaviour. These findings formed the starting point for further investigations related to this DH network.

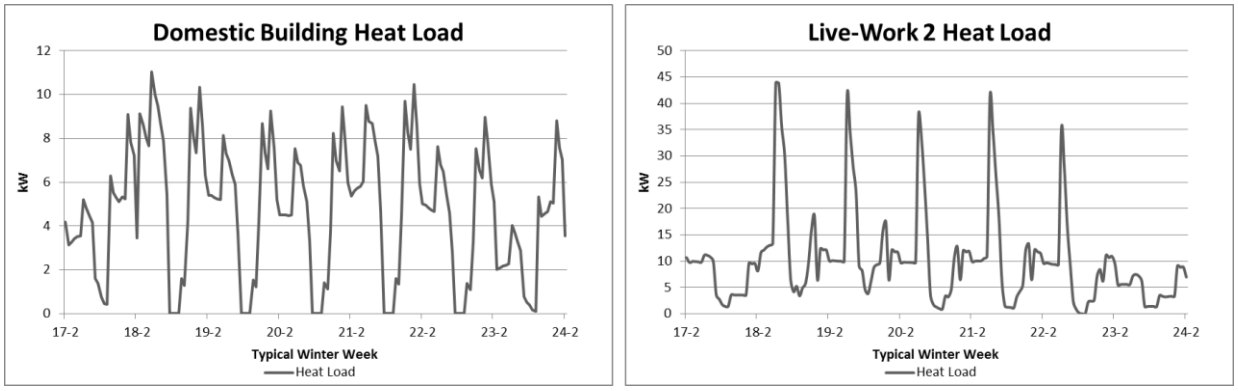

Figure 11: Simulated hourly heat load profile typical winter week (Live-Work 2 and Domestic Building)

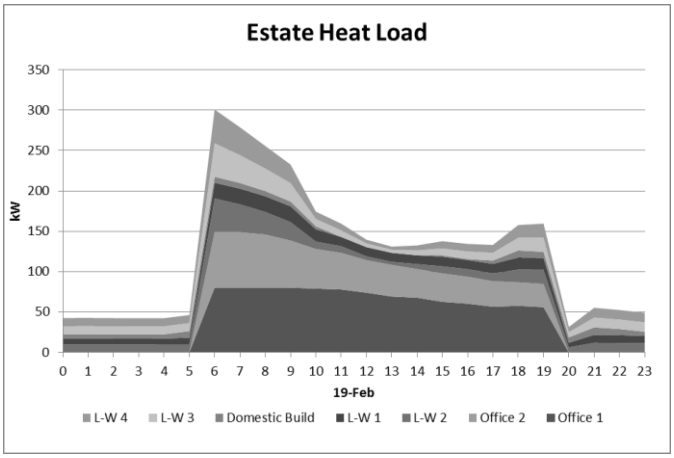

Figure 12: Simulated hourly heat load profile for the entire estate, typical winter day

4. CONCLUSION AND FURTHER WORK

The results of the investigation based on an existing DH network case study have been presented in this report. The objective was to coherently monitor the network as well as to assess the heat energy profile of the connected buildings. The analyses provided a robust set of data, which were used to generate a clear picture of the operating conditions of the DH, based on temperature and mass flow

rate. Also, the simulation outputs were used to evaluate the heat energy profile for each of the seven buildings served by the DH network, taking into account thermal envelopes, as well as occupancy and weather data. The comparison between the recorded data and simulations showed good agreement between the model results and measured operating conditions experienced in the estate during the heating season monitored.

The research will be used to highlight some crucial features for the expansion of DH technology and to address its role within the future UK heat market. To this extent, due to the characteristics of the estate, recently refurbished (following the UK Building Regulation 2006 Part L) and where space heating is provided by underfloor heating, without any major intervention it represents an ideal case study to investigate the application of the 4th generation DH in the UK context. In this direction, this most likely will represent a typical example of how future cities will challenge the heat energy market: on one hand, the improved buildings' energy performances will drastically reduce the heat demand; on the other hand, it will be decisive to define how the energy sector will efficiently adapt to this main change. To this extent, a low temperature DH network, due to the sensible reduction in the losses, improvement in the efficiency and integration with renewables, could be a viable solution for the future UK heat energy market to deliver heat to low energy buildings. Finally, the investigation will address the possibility of the network expansion, by adding new customers to the system, as well as to deliver domestic hot water by using DH instead of the actual electric heaters, making the case for a carbon neutral district heating.

5. ACKNOWLEDGEMENTS

The authors wish to thank SASIE LTD and its director Mo Kelly to provide all the support to complete this research project and Tony and Helen Strawson to allow us using the estate as case study.

6. REFERENCES

ECOHEAT4EU 2011a. Executive Summary Report. EU Commission

ECOHEAT4EU 2011b. Overview of the national DHC market.

ECOHEAT4EU 2011c. Recommendation report for the UNITED KINGDOM.

ENVIROENERGY. 2015. Available: www.enviroenergy.co.uk.

EU 2010. Analysis of options to move beyond 20% greenhouse gas emission reductions and assessing the risk of carbon leakage.

EU 2011. A Roadmap for moving to a competitive low carbon economy in 2050.

HARVEY, L. D. D. 2006. a handbook on LOW ENERGY BUILDINGS and DISTRICT-ENERGY SYSTEMS Fundamentals, Techniques and Example, London, EARTHSCAN.

OLSEN, P. K., Lambertsen, H., Hummelshoj, R., Bohm, B., Christiansen, C. H., Svendsen, S., Larsen, C. T. & WORM, J. 2008. A new Low-Temperature District Heating System for Low Energy Buildings. The 11th International Symposium on District Heating and Cooling. Reykjavik.

PÖYRY 2009. The potential and cost of district heating networks. Department of Energy and Climate Change.

SVEND SVENDSEN, J.-E. T., Morten Hofmeister, Christian Holm Christiansen, Peter Kaarup Olsen 2014. Guidelines for Low-Temperature District Heating.

SESSION 10: VENTILATION AND AIR CONDITIONING

93: Experimental study and modelling of air distribution systems and temperature control for chilled food factories in a scaled test facility

DEMETRIS PARPAS[1], CARLOS AMARIS[2], SAVVAS TASSOU[3]

1 RCUK National Centre for Sustainable Energy Use in Food Chains (CSEF), Institute of Energy Futures, Brunel University London, Uxbridge, Middlesex, UB8 3PH, UK, Demetris.parpas@brunel.ac.uk
2 RCUK National Centre for Sustainable Energy Use in Food Chains (CSEF), Institute of Energy Futures, Brunel University London, Uxbridge, Middlesex, UB8 3PH, UK, Carlos.amaris@brunel.ac.uk
3 RCUK National Centre for Sustainable Energy Use in Food Chains (CSEF), Institute of Energy Futures, Brunel University London, Uxbridge, Middlesex, UB8 3PH, UK, Savvas.Tassou@brunel.ac.uk

In this paper, an investigation on different air distribution systems at the required conditions of an actual chilled food processing factory is presented. A scaled test facility has been set-up for the analysis of air distribution systems and their energy consumption at different conditions. A three-dimensional CFD model of the scaled test room was also developed, validated and used to investigate the most appropriate air distribution approaches to create temperature stratification in the space.

Initial experiments focused on the study of an air distribution via fabric duct which is the current configuration used in an actual chilled food processing facility. Measured temperatures were found to vary between 6.7 ºC and 11.3 ºC. CFD Modelling of the air distribution system employing the SST-k-ω turbulence equation was also conducted. Results showed that the predicted temperatures and velocities were in good agreement with respect to the data measured from the scaled experimental test facility. The CFD model was then used to evaluate the performance of (a) air distribution via displacement ventilation with one horizontal diffuser, (b) air distribution with displacement ventilation system with two 1-way supply diffusers, (c) air distribution system with a half fabric duct at a medium level, and (d) air distribution system via slot diffusers at medium level.

Results from the different approaches investigated showed that the half fabric duct located at medium level provided a wider temperature gradient (from 7 ºC to 14 ºC). The most significant stratification was observed between head level and the ceiling level. It was also identified that the air distribution system via half fabric duct at a medium level provided a more homogeneous air flow over the entire production zone. The level of temperature stratification provided, air flow homogeneity and ease of implementation in a real factory situation provides a good solution for achieving thermal stratification and energy savings in a chilled food factory without compromising the thermal environment.

Keywords: Air distribution systems, Chilled food factory, Refrigeration, Efficient energy use, Computational Fluid Dynamics

1. INTRODUCTION

Chilled food industry has shown a massive growth over the last decades. Based on the Chilled Food Association (CFA) chilled food industry in UK growth from £550m in 1989 to £9,755 m in 2012. Latterly, UK overall growth of chilled food industries has been found to be at 10 % annually (CFA, 2012). Refrigeration systems in the cold food chain are estimated to be responsible for 16,100 GWh energy use and 13.7 $MtCO_2e$ Greenhouse Gas Emissions in UK. These account for approximately 28 % of final energy use and 7 % of GHG emissions of the whole food-chain (Defra, 2012). This represents a high concern taking into account that 60 % of the energy consumption in chilled food factories relies heavily on refrigeration and the maintenance of low temperatures during processing of chilled food products.

Chilled food products have short shelf lives and need to be processed in facilities at temperatures in the range between +4 to +12 ºC depending on the type of product, processing time and the desired minimum shelf time. Current chilled food processing takes place in large spaces with high ceilings. In these spaces cooling is normally provided by ceiling mounted fan coil units, air fabric ducts or diffusers. In the majority of these spaces, air temperature control is provided by convection heat transfer systems. Therefore, air distribution is an essential factor that needs to be carefully considered in order to create an environment capable of maintaining food quality without excessive worker discomfort. The air distribution system should create a temperature and humidity homogeneity around the food product in order to maintain its quality. Mixing ventilation is the most commonly used air distribution method in chilled food processing environments. In a mixing ventilation system, air is mixed through the entire room volume which results in fairly uniform environment in terms of temperature and contaminant concentration. In a chilled food facility with high ceiling height, the room volume that is needed to be conditioned is at the occupied space and where production takes place. However, these large spaces include an unoccupied volume mainly at the high levels which is also maintained at a low temperature leading to energy wastage. For the above-mentioned reason, improvement of the air-temperature distribution system is required. An efficient air-temperature distribution system would imply significant energy savings and concomitant reduction in CO_2 emissions.

The air distribution patterns in large spaces can be obtained from experimental tests including flow visualisation studies and from modelling approaches. Recent experimental investigations on air distribution systems with different approaches can be found in the open literature. Rees and Haves et al. (2013) experimentally studied the air flow mixing and overall temperature gradient in a room with displacement ventilation and chilled ceiling for office environments. Cheng et al. (2013) analysed the effect of separate location of the return and exhaust grilles on thermal comfort and energy saving. In this study, authors showed that the satisfied thermal comfort and important energy savings can be obtained when the air temperature is stratified. Meanwhile, Lin and Tsai (2014) studied the effect of the supply diffuser position and supply air flow rate on thermal environment of an indoor space. Authors reported that the temperature gradient in an indoor space becomes gentler and the indoor air stratification reduces when the supply air flow rate is increased for a given diffuser. Jurelionis et al. (2015) investigated the impact of the air supply method on the ventilation efficiency in a test chamber. In this investigation, the aerosol particle dispersion with different air distribution methods was analysed. Results showed that the one-way mixing ventilation ceiling diffuser with low flow rate was more efficient in terms of ventilation in comparison with the four-way mixing and high air exchange rates. It was also concluded that the displacement air distribution method was less efficient than the mixing ventilation in terms of air removal. Recently, Rhee et al. (2015) evaluated the performance of an active chilled beam system in terms of uniformity for an indoor thermal environment in a full-scale test bed. The authors reported acceptable thermal uniformity with the active chilled beam system even at low air flow rates.

Regarding modelling approaches, airflow modelling techniques have been developed over the last 30 years to provide a better understanding of air flow patterns and temperature distribution in large spaces including cold rooms. The most powerful of these is Computational Fluids Dynamics (CFD). Experimental results can be initially used for the CFD model validation. Once the CFD model is validated, it can be used to investigate different air distribution systems under different cooling conditions. This can lead to a better understanding of the air distribution in a space and optimum designs that minimise energy consumption and improve product quality. For example, Chourasia and Goswami (2007a,b,c) developed a three-dimensional (3-D) model to predict the airflow, temperature distribution and moisture loss in a potato loaded cold room. The authors applied the RNG k-ε turbulence model with the finite volume solution technique. The potato bulk was considered as a porous medium. The model predictions were compared with experimental data. Average overall errors of 19.5 %, 0.5 ºC and 0.61 % were found for air velocity, product temperature and moisture loss from the potatoes respectively. Smale

et al. (2006) reviewed CFD modelling applications for the prediction of airflow in refrigerated food storage applications. It was reported that the k-ε turbulence model was not accurate enough to be used in many refrigerated food storage applications. The k- ε model could not predict well the Coanda effect over the wall jets and under adverse pressure gradients. Also, none from the k -ε , LRN k-ε, two layer k-ε, two scale k-ε and RNG k-ε models could predict the presence of secondary recirculation flow. In contrast the RSM (Reynolds Stress Model) was found to be able to predict the separation between the wall jets and the airflow patterns related to primary and secondary recirculations. The authors also concluded that the Lattice Boltzmann method is a good alternative numerical method instead of CFD.

Delele et al. (2009) applied multi-scale CFD to predict air velocity, temperature and humidity distribution in a loaded cold room. The authors tested 4 different two-equation eddy-viscosity turbulence models and compared the results against experimental measurements. The 4 different models with their individual prediction accuracy regarding the air velocity are Standard k-ε model with 24.3 % accuracy, Realizable k-ε model with 23.5 % accuracy, RNG k-ε model with 22.4 % accuracy and Standard k- ω /SST k-ω models with 18.2 % accuracy. Chanteloup and Mirade (2009) developed a model to predict the local mean age of the air in a ventilated food storage space using CFD. The authors implemented 3 different modelling methods, two transient and one steady state. All predictions were compared with experimental data and the errors did not exceed 20 %. The optimum method in terms of prediction accuracy and computational time was found to be the steady-state. This method was then used to identify the ventilation efficiency of the space. The Navier-Stoke equations with the k-ε turbulence model and first-order upwind differencing discretization scheme were employed to predict the air temperature and relative humidity distribution patterns (Chanteloup and Mirade, 2009).

Delele et al. (2013) developed a 3-D model in CFD in order to predict air flow and heat transfer characteristics of a horticultural produce packaging system. In this study the authors took into account the detailed geometry and properties of the packaging material. The air flow in the space was solved using the Reynolds averaged Navier Stroke equations (RANS). A tetra-hedral hybrid mesh was applied for the discretization of the computational domain and enhanced wall functions were considered for the model. The standard k-ε, RNG k-ε and standard k-ω two equation turbulence models were considered and the SST k-ω was found to produce the most accurate predictions. Predicted cooling air pressure drop and produce temperature were compared with experimental data showing good agreement with an average relative error of 13.80 % and 16.27 %, respectively. Ho et al. (2010) studied air velocity and temperature distribution for a refrigerated space with steady state airflow and heat transfer using a 3-D and a 2-D model for comparison purposes. They used the finite element method for the CFD modelling approach in order to predict the flow and heat transfer processes. The authors considered the air inside the cold room as an incompressible fluid with constant properties. Furthermore, it was assumed that the fluid density variation affected only the temperature. From the comparison between the 3-D and 2-D model results, the authors concluded that the two models were in good agreement. As a result it was concluded that 2-D modelling can be employed with good accuracy.

Ambaw et al. (2013) reviewed the application of CFD for the modelling of post-harvest refrigeration processes. They identified the most common solution method to be the finite volume method with the upwind differencing scheme. In addition, it was reported that the Reynolds Stress Model (RSM) provides more accurate predictions compared to the conventional k-ε model but the k-ε model is more commonly used due to its lower computational requirements. For air velocity prediction, the SST k-ω model produced the smallest error compared to the RSM and k-ε models. Laguerre et al. (2014), in order to avoid the computational time of a CFD model, created a simplified model using the knowledge obtained from experimental measurements. The model was separated into zones and heat balance equations for each zone were developed. The simplified model was found to predict the product cooling rate and the final product temperature at different positions in the cold room quite well (Laguerre et al., 2014, Duret et al., 2014). Fathollahzadeh et al. (2015) studied the effect of using two types of inlet diffusers (direct and swirl) with combined and separate return and exhaust air vents on the thermal comfort, indoor air quality and energy consumption in an indoor environment. For this study, the SIMPLE algorithm was used to solve the pressure and velocity coupling. Main results showed that the energy consumption of the system decreased by reducing the height of return air vent from ceiling to floor height.

Previously, Parpas et al. (2015) investigated the air flow and temperature distribution in two actual chilled food manufacturing factories. The authors developed two 3-D CFD models to simulate the air flow and the thermal environment in the two facilities applying different turbulence equations. Results from the CFD models were compared with experimental data collected in the two factories. The predicted

temperatures from the CFD models using the SST k-ω turbulence equation showed a good agreement with the measured data.

In the present study, an experimental and modelling study on air distribution systems and temperature control in a scaled test set-up for chilled food manufacturing facilities is presented. A scaled test facility has been layout and set-up for the analysis of air distribution systems at different conditions. A 3-D CFD model of the scaled test room was also developed, validated and used to investigate the most appropriate air distribution approaches to create temperature stratification in the space.

2 PROCEDURE

The scope of this research aims to improve the efficiency of the cold air-temperature distribution in chilled food processing areas. Improved air-temperature distribution should lead to the reduction of the overall energy consumption of the refrigeration plant. Preliminary work focused on understanding, modelling and replicating the air flow and the temperature variation in existing chilled food facilities (Parpas et al., 2015). Current phase of the research deals with the development of a 3-D CFD scaled model representing a section of an actual chilled food processing room. In order to provide data for its validation, an experimental set up was build up in the laboratory. Once the CFD model was validated, different air distribution systems were investigated and modelled to identify the most appropriate air distribution approaches to create temperature stratification in the space. In future works, the most promising configuration will be build-up and installed at the laboratory to be tested.

2.1 Experimental Test Facility

In order to investigate the effect of different air distribution systems on the thermal environment of a chilled food factory and its refrigeration system energy consumption, a scaled experimental test rig representing a section of a chilled food processing room has been built up in an environmental chamber. The chamber volume, which is completely isolated, measures 2.9 m (H) x 6.6 m (L) x 3.5 m (W). The chamber was equipped with an R404a refrigeration system which consists mainly of an evaporator (Kobol CR39), and a packaged condenser unit (Silensys, with a reciprocating type compressor TAG4546Z) located outside the test rig.

Figure 1 shows an outline of the test rig. The air distribution method is via fabric duct located at ceiling level as shown in Figure 2. The fabric duct measures 50 cm in diameter and 500 cm in length. This configuration corresponds to the system currently installed in an actual chilled food factory and it is the reference case. The chamber, which was the volume under study, was divided into 4 sections as shown in Figure 1. Each section was divided into 4 sub-sections (Right-wall, Right-center, Left-center and Left-wall) where temperature sensors (T) were located at knee level, head level and ceiling level. Temperature sensors used were thermocouples with TC adapter type K with measurement uncertainty of ± 0.5 ºC. In order to simulate the thermal load released by the occupants (OC), 4 rectangular boxes with surface area of 1.6 m2 wrapped with thermal resistances were used.

Air velocity measurements were also taken close to the position of each temperature sensor using an air flow meter TSI TA465-P including a thermoanemometer articulated probe 966 with a measurement accuracy of ± 3 % from 0 to 50 m.s-1. Datascan modules 7020 were used for the data logging with logging interval of the data set to 10 second. The time for each test was 20 hrs in steady state. The air temperature in the test chamber was controlled using a temperature controller EKC 102A with the thermostat located at the back of the evaporator (suction side) and set to 9.7 ºC.

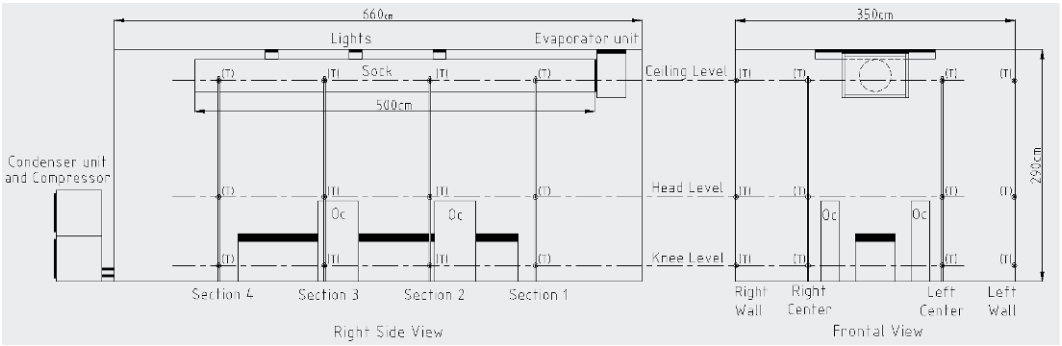

Figure 1: Outline of the experimental test facility with air distribution via fabric duct at ceiling level, reference case.

Figure 2: Experimental test facility with air distribution via fabric duct.

2.2 CFD Model Details

The dimensions of the 3-D scaled model volume are those of the experimental test room. The HVAC system consists of 1 evaporator coil initially distributing the air via fabric duct. The evaporator is operated with 100 % recirculated air and controlled by a thermostat with 9.7 ^{o}C air-of set point temperature. The steady state 3-D CFD model was solved using the commercial ANSYS FLUENT® package.

The air flow supply and return from the evaporator were set at 2825 m^3hr^{-1}. The air supply from the air fabric duct and return air at the coil boundary conditions were defined as mass flow inlets and outlets, respectively. The air supply temperature was set at 7 ºC and the occupancy density of the investigated processing area was set to be at 4 occupants taking into account the scaled model area. Each occupant was defined as a rectangular box with 1.57 m^2 surface area with 150 W sensible thermal load (Cook et al., 2011). The lighting heat load was set at 30 Wm^{-2} floor area. Other heat sources into the processing area were neglected for this phase of the research. The thermal boundary conditions of the surrounding walls were calculated taking into account the heat flow, temperature profile and thermal resistances (Rsi, Rw, Rse) over the interior and exterior of the wall. The wall boundary condition was estimated to be at 13 ºC.

The model was solved with the pressure based solution algorithm, second order upwind energy and momentum discretisation, 'Body-Force' weighted pressure discretisation, and SIMPLE pressure-velocity coupling. The air inside the food processing area was considered to be compressible and the density was allowed to vary according to the ideal gas law to account for buoyancy effects. Other thermal properties were maintained constant. The SST-k-ω turbulence model was used since it was previously found to predict actual measured data with a better accuracy in comparison to predictions with the other models (Parpas et al., 2015). The computational domain was discretized with an automatic mesh method, with mainly tetrahedral cells (with hexahedral cells in the boundary layer). The mesh density was gradually refined near the building wall, occupant surface and the air fabric duct. The final mesh size consists of 9.6 million elements, with element dimensions between 0.02-0.06 m. The finer mesh sizes were located near the wall surfaces, where a further 4 inflation layers were also employed to capture the effects of the boundary layer. The final model mesh shown in figure 3 was generated following a mesh independency study, and the simulation time for each steady-state case was 48 hours, with an average of 1900 iterations, on a 2.6GHz, 32GB RAM, Intel Xeon Processor with 12 parallel threads.

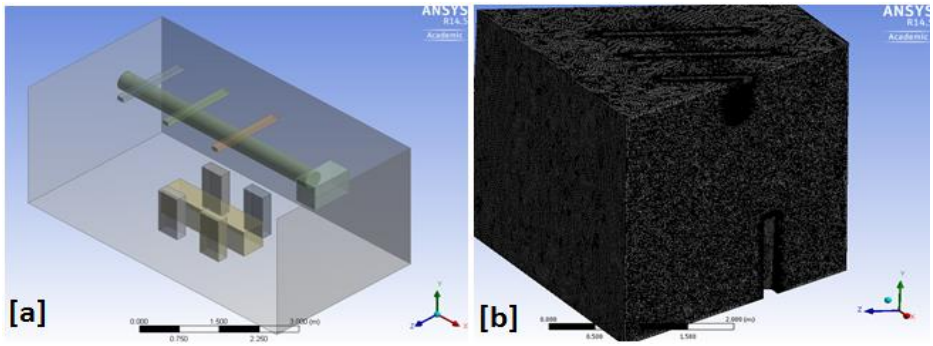

Figure 3: [a] 3-D model and [b] Model mesh cross section.

3 RESULTS AND DISCUSSION

3.1 Air Distribution via Fabric Duct, Experimental

Figure 4 shows the temperature profiles measured into the chamber from testing the air distribution system via fabric duct at ceiling level which is the reference case. The evaporator fan velocity was set at 100 % which corresponds to a measured suction air velocity of 1.52 $m.s^{-1}$.

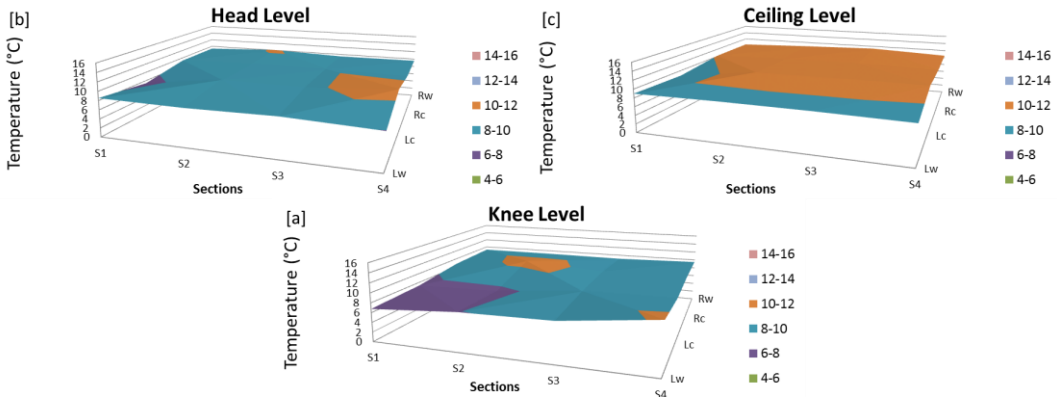

Figure 4: Temperature profiles at different heights, [a] Knee Level, [b] Head Level and [c] Ceiling Level.

Temperatures values shown in Figure 4 correspond to the average values measured in each position during a day test. According to the results, temperatures varied from 6.7 ºC and 11.3 ºC while the average temperature values measured at knee, head and ceiling level are 8.8 ºC, 9.2 ºC and 10.2 ºC, respectively. It can be observed that the lowest temperatures were measured at knee level and highest at ceiling level. Regarding the air velocities, they were very low and varied between 0.02 and 0.25 $m.s^{-1}$ with the highest values observed at knee level, Figure 5. The maximum value measured close to the fabric duct was up to 0.17 $m.s^{-1}$.

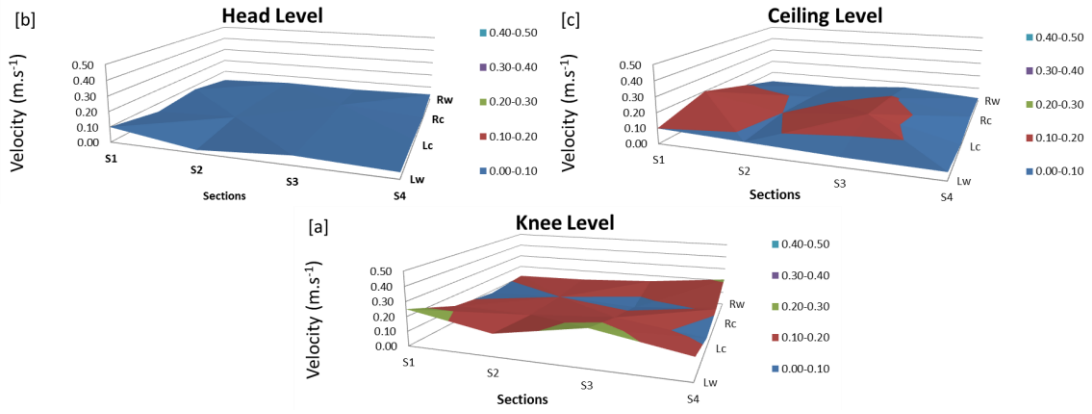

Figure 5: Velocity profiles at different heights, [a] Knee Level, [b] Head Level and [c] Ceiling Level.

3.2 Air Distribution via Fabric Duct, CFD Modelling

Figure 6 shows the velocity distribution at 4 cross sections along the space from modeling the air distribution system via fabric duct at ceiling level. Air velocities were very low and varied between 0.01 and 0.3 $m.s^{-1}$. It is also observed that the highest air flows were found directly under the fabric duct and above the occupants and production line due to the buoyancy effects. Figure 7 shows the air temperature distribution with a supply temperature from the air fabric duct at 7 ºC. The temperature in the bulk of the space varied between of 8.0 ºC and 12.0 ºC which means temperature stratification was obtained, with lowest temperatures measured at knee level and highest at ceiling level.

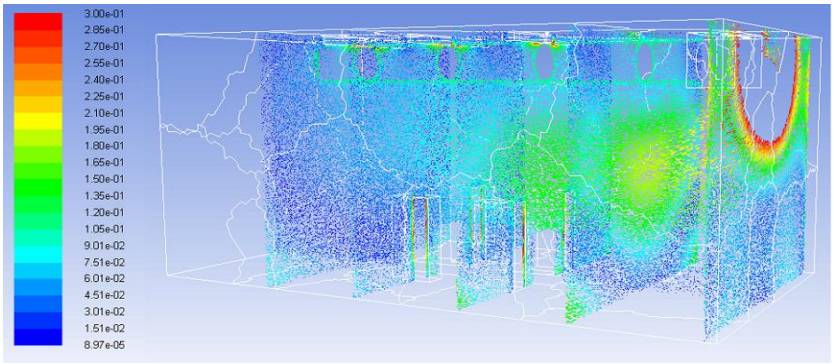

Figure 6: CFD Simulation results of air velocity in the space ($m.s^{-1}$).

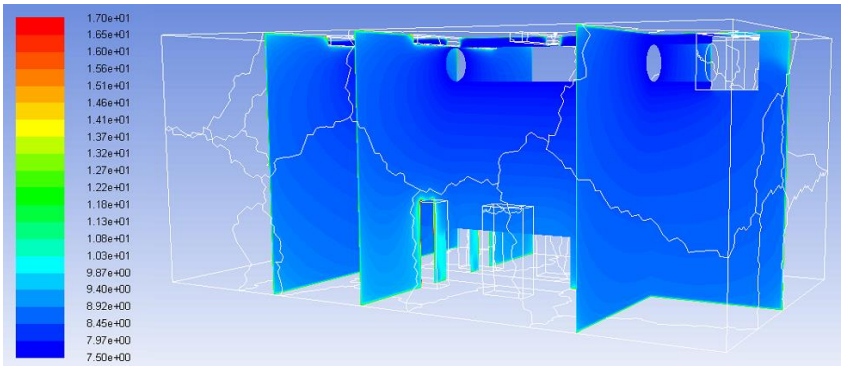

Figure 7: CFD Simulation of air temperature in the space (ºC).

To determine the validity of the model, the temperature predictions from the model were compared against temperature measurements obtained from the experimental facility. The results of this comparison are shown in Figure 8. The middle line in the graph indicates the position of 0 ºC error and the other two lines shows the maximum errors of +1.5 and -1.5 ºC respectively. From all results, 90.0 % of the points showed an absolute error lower than 1.5 ºC. The average error across all test points in the space was found to be -0.02 ºC. Considering the uncertainty of the air temperature measured shown in Figure 9 (Temperature sensor accuracy is ± 0.5 °C), the averaged absolute error is acceptable.

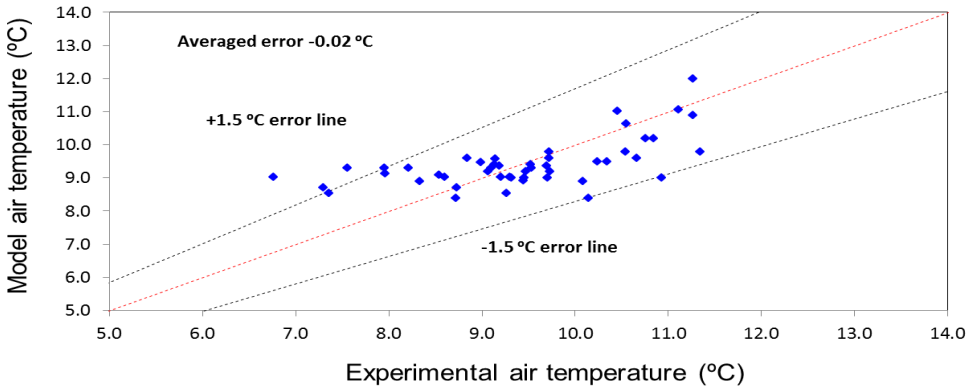

Figure 8: CFD modelling air temperature valuation.

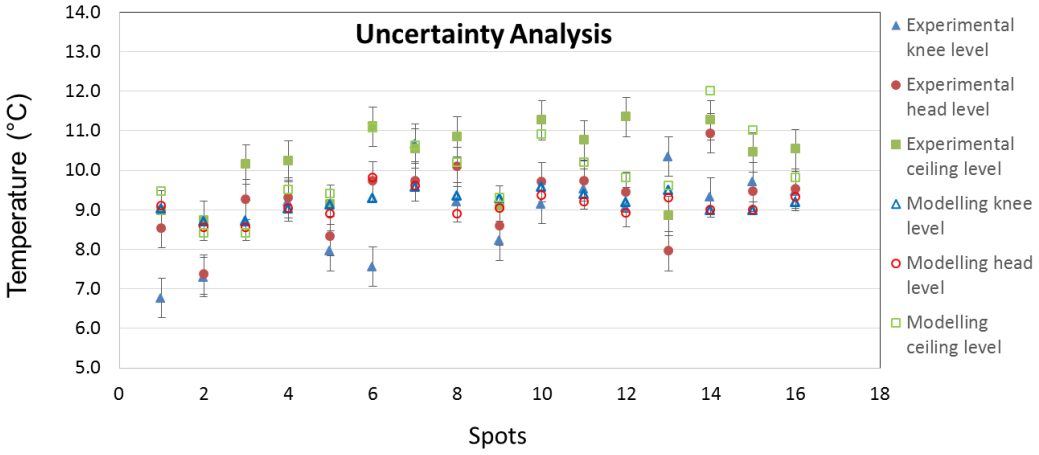

Figure 9: CFD modelling air temperature valuation uncertainty analysis.

3.3 Modelling of Different Air Distribution Systems

Once the CFD model was validated, it was then used to approach the air flow and temperature distribution from different air distribution systems. Figure 10a shows an air distribution system via displacement ventilation with one supply diffuser. In this case, the air flow rate was reduced to 300 $m^3.hr^{-1}$ to keep the supplied air under 0.2 $m.s^{-1}$. Figure 10b presents a 3-D model that uses a displacement ventilation system with two 1-way supply diffusers. Each diffuser recirculated 260 m^3hr^{-1} of conditioned air at 7.0 ºC into the space. Figure 10c corresponds to an air distribution system with a half fabric duct located at a medium level, and Figure 10d depicts an air distribution system via slot diffusers at a medium level.

Figure 11a shows the air temperature distribution at 4 cross sections along the space with air distribution system via displacement ventilation with one diffuser. With a supply temperature at 7 ºC, the temperature in the bulk of the space varied between of 7 ºC and 13.0 ºC. It was observed that temperature stratification occurs, with lowest temperatures measured at knee level and highest at ceiling level. However, it can be observed that this system does not provide homogeneous temperature gradients along the space in horizontal direction. Figure 12a shows the velocity distribution along the space. Air velocities were very low and varied between 0.01 and 0.25 $m.s^{-1}$. It was observed that the temperature stratification is driven mainly from buoyancy forces caused by the internal heat gains. Fig. 8b shows the air temperature distribution using the two 1-way supply diffusers. With a supply temperature at 7 ºC, the temperature in the bulk of the space varied between of 7 ºC and 13.0 ºC. It was observed that temperature distribution follows more homogeneous patterns at the different heights if compared with those of the preview model. Fig. 9b presents the velocity distribution in which case it was kept under 0.25 $m.s^{-1}$.

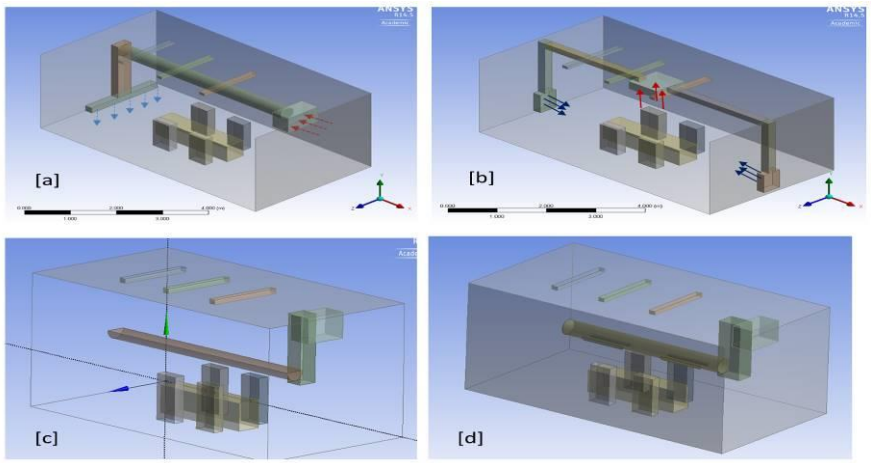

Figure 10: 3-D models [a] air distribution via displacement ventilation with one diffuser, [b] air distribution using displacement ventilation system with two 1-way supply diffusers, [c] air distribution system with a half fabric duct at a medium level, and [d] air distribution system via slot diffusers.

Meanwhile, Figure 11c shows that when the half fabric duct at a medium level was used with a supply temperature at 7 ºC, the temperature in the bulk of the space varied between of 7 ºC and 14.0 ºC. It was observed that distribution system provides a homogeneous flow pattern along the space with increased temperature stratification and a maximum air velocity of 0.3 $m.s^{-1}$ at knee level. It can also be noted that the temperature gradients were more pronounced between the head level and the ceiling level.

Otherwise, the use of the slot diffusers resulted in temperature variation between of 7 ºC and 12.0 ºC and as in the previous models (Figure 11d); the lowest temperatures were obtained at knee and head level and the highest at ceiling level. However, in Figure 12d can be noted that the use this configuration resulted in higher velocities caused by the bottom diffusers which could have an important impact on work environment.

Results from the different approaches investigated showed that the half fabric duct located at medium level is the most promising configuration. The level of temperature stratification provided, air flow homogeneity over the production zone and easy implementation in a real factory situation meet the requirements for food safety and quality and in addition, it does not compromise the work environment.

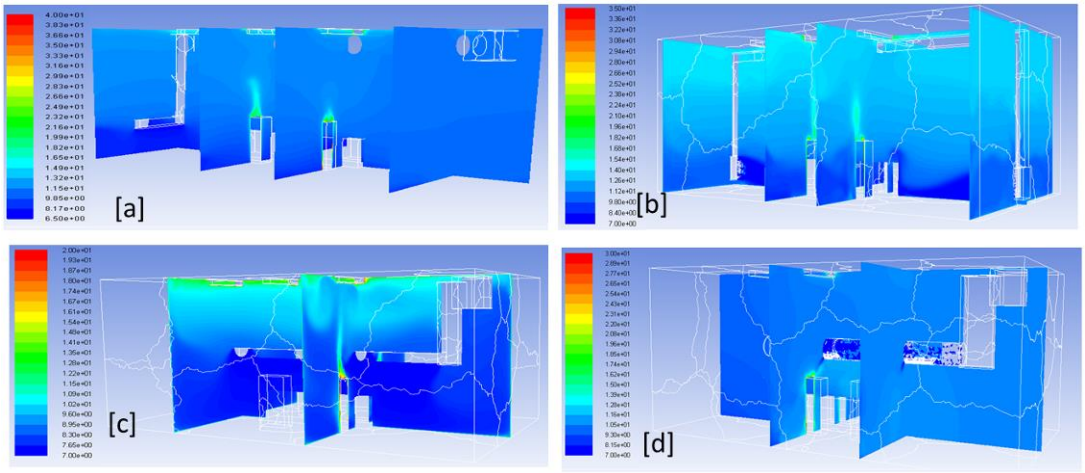

Figure 11: Air temperature distribution for [a] air distribution system via displacement ventilation with one diffuser, [b] air distribution using displacement ventilation system with two 1-way supply diffusers, [c] air distribution system with a half fabric duct at a medium level, and [d] air distribution system via slot diffusers.

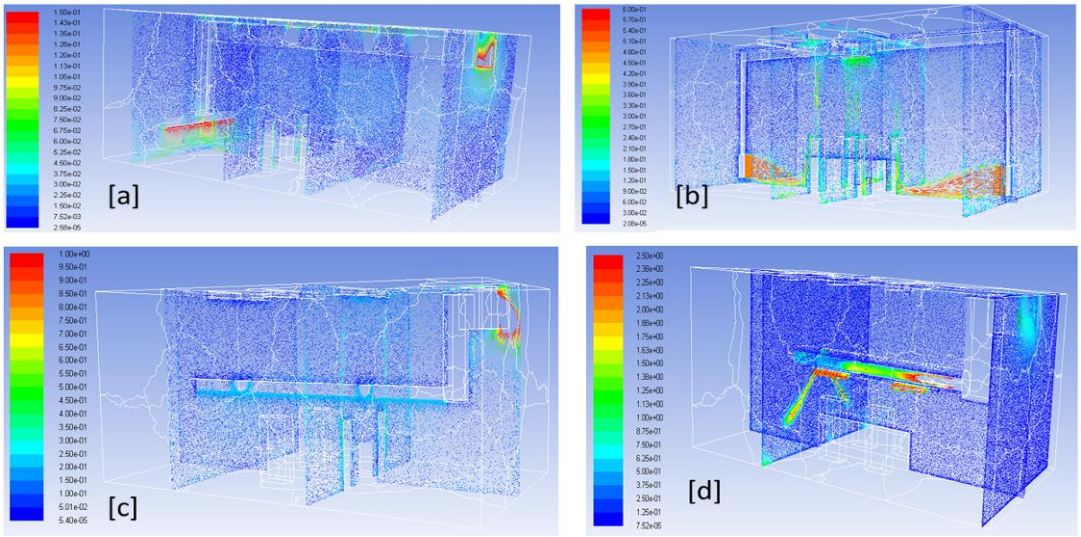

Figure 12: Air velocity profiles from [a] air distribution system via displacement ventilation with one diffuser, [b] air distribution using displacement ventilation system with two 1-way supply diffusers, [c] air distribution system with a half fabric duct at a medium level, and [d] air distribution system via slot diffusers.

4 CONCLUSIONS

In this paper, an investigation that aims to improve the efficiency of air distribution and temperature control systems in chilled food manufacturing facilities was presented. A scaled test facility was established for the investigation of air distribution systems at different conditions in the laboratory. A 3-D CFD model of the scaled test room was also developed, validated and used to investigate the most appropriate air distribution approaches to create temperature stratification in the space. Initially, the study was focused on an air distribution via fabric duct which is the current configuration used in an actual chilled food facility. Measured temperatures were found to vary between 6.7 ºC and 11.3 ºC. The 3-D CFD model was developed using a steady state solution and employing the SST k-ω turbulence model. The CFD modelling results showed a good agreement with the data measured in the scaled test facility. The CFD model was then used to evaluate four different air distribution systems: (a) air distribution via displacement ventilation with one horizontal diffuser, (b) air distribution with displacement ventilation system with two 1-way supply diffusers, (c) air distribution system with a half fabric duct at a medium level, and (d) air distribution system via slot diffusers at medium level.

Results from the different approaches investigated showed that the half fabric duct located at medium level provided a wider temperature gradient (from 7 and 14 ºC) and a more homogeneous air flow over the production zone, proving to be the most promising configuration from the ones investigated. The achievement of air stratification in a factory space operating at lower temperatures than air conditioned spaces in buildings provides opportunities for significant energy savings as only a portion of the air in the space needs to be conditioned.

Further studies will involve assessment of the performance of the half fabric duct in the manufacturing facility.

5 ACKNOWLEDGMENT

This project was co-funded by Innovate UK. The authors acknowledge the support of Innovate UK, the RCUK energy programme and the industrial collaborators Bakkavor and Waterloo Air Products PLC.

6 REFERENCES

AMBAW, A., Delele, M.A., Defraeye, T., HO, Q.T., Opara, L.U., Nicolaï, B.M., Verboven, P., 2013. The use of CFD to characterize and design post-harvest storage facilities: Past, present and future. Computers and Electronics in Agriculture, 93, 184-194.

CFA, Climate Change Agreement - Chilled Food Sector Progress and Barriers, 2012. http://www.chilledfood.org/MEDIA/campaigns (Accessed: 25/03/2015).

CHANTELOUP, V., Mirade, P., 2009. Computational fluid dynamics modelling of local mean age of air distribution in forced-ventilation food plants. Journal of Food Engineering, 90 (1), 90-103.

CHENG, Y., Niu, J., Liu, X., Gao, N., 2013. Experimental and numerical investigations on stratified air distribution systems with special configuration: Thermal comfort and energy saving. Energy and Buildings, 64, 154–161.

CHOURASIA, M.K., Goswami, T.K., 2007b. Steady state CFD modeling of airflow, heat transfer and moisture loss in a commercial potato cold store. International Journal of Refrigeration, 30 (4), 672-689.

CHOURASIA, M.K., Goswami, T.K., 2007a. Simulation of Effect of Stack Dimensions and Stacking Arrangement on Cool-down Characteristics of Potato in a Cold Store by Computational Fluid Dynamics. Biosystems Engineering, 96 (4), 503-515.

CHOURASIA, M.K., Goswami, T.K., 2007c. Three dimensional modeling on airflow, heat and mass transfer in partially impermeable enclosure containing agricultural produce during natural convective cooling. Energy Conversion and Management, 48 (7), 2136-2149.

COOK, M., Yang, T., Cropper, P., 2011. Thermal Comfort in Naturally Ventilated Classrooms: Application of Coupled Simulation Models. 12th Conference of International Building Performance Simulation Association, Sydney, Australia, 14-16 November, 2257-2262.

DEFRA, Department of Environment, Food and Rural Affairs, 2012. Food Statistics Pocketbook, 86.

DELELE, M.A., Ngcobo, M.E.K., Getahun, S.T., Chen, L., Opara, U.L., 2013. Studying airflow and heat transfer characteristics of a horticultural produce packaging system using a 3-D CFD model. Part I: Model development & validation. Postharvest Biology and Technology, 86, 536-545.

DELELE, M.A., Schenk, A., Tijskens, E. Ramon, H., Nicolaï, B.M., Verboven, P., 2009. Optimization of the humidification of cold stores by pressurized water atomizers based on a multiscale CFD model, J. of Food Engineering, 91 (2), 228-239.

DURET, S., Hoang, H.-M., Flick, D., Laguerre, O., 2014. Experimental characterization of airflow, heat and mass transfer in a cold room filled with food products. International Journal of Refrigeration, 46,17-25.

FATHOLLAHZADEH, M. H., Heidarinejad, G., Pasdarshahri, H., 2015. Prediction of thermal comfort, IAQ, and Energy consumption in a dense occupancy environment with the under floor air distribution system. Building and Environment, 90, 96–104.

HO, S.H., Rosario, L., Rahman, M.M., 2010. Numerical simulation of temperature and velocity in a refrigerated warehouse, International Journal of Refrigeration, 33 (5), 1015-1025.

JURELIONIS, A., Gagyte, L. Prasauskas, T., Ciuzas, D., Krugly, E., Seduikyte, L., Martuzevicius D., 2015. The impact of the air distribution method in ventilated rooms on the aerosol particle dispersion and removal: The experimental approach. Energy and Buildings, 86, 305–313.

LAGUERRE O., Duret, S., Hoang, H.-M., Guillier, L., Flick, D., 2014. Simplified heat transfer modeling in a cold room filled with food products. Journal of Food Engineering, 149, 78-86.

LIN, Y.J.P., Tsai, T.Y., 2014. An experimental study on a full-scale indoor thermal environment using an Under-Floor Air Distribution system. Energy and Buildings, 80, 321–330.

PARPAS, D.A., Amaris, C., Tassou, S.A., Gowreesunker, B.L., Terkuile, W., 2015. Investigation into air distribution systems and temperature control in chilled food manufacturing facilities. 3rd Sustainable Thermal Energy Management International Conference, Newcastle upon Tyne, UK, 7-8 July, 110-119.

REES, S. J., Haves P., 2013. An experimental study of air flow and temperature distribution in a room with displacement ventilation and a chilled ceiling. Building and Environment, 59, 358-368.

RHEE, K-N., Shin, M-S., Choi, S-H., 2015. Thermal uniformity in an open plan room with an active chilled beam system and conventional air distribution systems. Energy and Buildings, 93, 236–248.

SMALE, N.J., Moureh, J., Cortella, G., 2006. A review of numerical models of airflow in refrigerated fapplications. International Journal of Refrigeration, 29 (6), 911-930.

137: Numerical study of novel corrugated heat and moisture exchanging sheets applied to counter-flow dew point air cooler

PENG XU[1,2], XIAOLI MA[1],XIONG YAXUAN[2],DEYING LI[2],
YONGZHENG SHI[2],
XUDONG ZHAO[1*]

1 School of Engineering, University of Hull, UK, HU6 7RX
p.xu@hull.ac.uk; x.ma@hull.ac.uk; x.zhao@hull.ac.uk

2 Beijing Key Lab of Heating, Gas Supply, Ventilating and Air Conditioning Engineering · Beijing University of Civil Engineering and Architecture, Beijing University of Civil Engineering and Architecture, Beijing, China, 100044
xupeng@bucea.edu.cn; lideying@bucea.edu.cn; shiyongzheng@bucea.edu.cn

The authors present a numerical investigation on the performance of corrugated-sheets-stacked heat and moisture exchanger (HMX) applied to counter-flow dew point air cooler. The computational simulation software for this investigation was developed under Engineering Equation Solver (EES) environment. The results showed that the HMX could run with stably high effectiveness (generally, wet bulb effectiveness over 130% and dew point effectiveness over 85%) and supply product air at stably low temperature, as well as improve automatically the total cooling capacity with the temperature rise of the ambient air. The HMX also presented high adaptability to the various climate conditions in Southern Europe, Northern Europe and the UK. The renovation in heat exchanger configuration could lead to significant increase in the cooling capacity and COP for dew point coolers, and decrease in size and cost of the coolers at the same cooling output.

The major factor affecting the cooling performance was the relative humidity of inlet air, therefore the HMX was particularly suitable for heat-intensive places in winter, i.e. computer data centres. The optimized air-channel's geometric sizes of height and length were 0.005m and 1.0m respectively. The ideal range of operational conditions of working air ratio should be between 0.3 and 0.5 and the reasonable velocity of inlet air around 1m/s, while the inlet water temperature had little effect on the performance.

Keywords: Dew point cooling; Corrugated sheet; Heat and moisture exchanger; Counter-flow; Simulation

Nomenclature

a	side length of computational cell, m	u	air velocity, m/s
c_p	specific heat capacity, J/kg·°C	W	electric power, kW
De	equivalent diameter	***Subscripts***	
en_{steam}	latent heat, kJ/kg	dp	dew point
h	heat transfer coefficient, W/(m²·°C)	dry	dry channel
h_m	mass transfer coefficient, m/s	f	airflow
hum	moisture content, kg/kg	fan	fan
i	enthalpy, kJ/kg	$pump$	pump
l	length, m	w	wall
l_0	thermal entry length, m	wb	wet-bulb
Le	Lewis number	wet	wet channel
n	number		
$Q_{cooling}$	cooling capacity, kW	***Greek***	
Qm	volume rate, kg/s	σ	surface wettability factor
Pr	Prandtl number	Δ	difference between two states
Re	Reynolds number	μ	dynamic viscosity, kg/(m·s)
T	temperature, °C	ρ	density, kg/m³
Tf	air temperature, °C	φ	working air fraction over inlet air
Tw	channel wall temperature, °C	ε	Effectiveness

1. INTRODUCTION

Owing to the rapid growth of world energy consumption in buildings, especially in heating ventilation and air-conditioning (HVAC) systems, it is vital and urgent to develop energy-efficient and sustainable cooling systems to gradually substitute the conventional energy-intensive and CFC-refrigerant-used vapour compression refrigeration systems which domains the current corresponding cooling markets. Indirect evaporative cooling (IEC) systems, utilizing the latent heat of water evaporation without adding moisture to the product air, is desirable for the comfortable air conditioning in buildings.

With the continuous progress in technology innovation, e.g. the M-cycle (Maisotsenko and Reyzin, 2005), the IEC systems have obtained significantly enhanced cooling performance in recent decade years. The structures of the IEC heat and mass exchanger (HMX) vary from flat-plate-stack, tube and heat pipe (Duan, 2011). The heat transfer process between the air in dry and wet channels under cross-flow and counter-flow has been widely studied. Feasibility for use of IEC in various climate regions was also investigated. Meanwhile, the application and commercial markets of IEC flourish around the world, especially in the USA, Australia, west Asia and China (Duan et al., 2012).

Although great progress has been made both in IEC technology and related commercial application over the past decade years, there is still potential for further technical progress, especially in HMX structure and the airflow organization. The structures of the existing exchangers are mainly based on the flat-plate stacked form, considering their merits of easy making and cost effective. However, the flat-plate stacked structure is not the most favourite form as the heat and mass transfer space is not used effectively and the temperature of secondary air of the exchanger is not low enough to remove more heat from the primary air (Zhan et al, 2011). Contrast with the generally accepted simple structure of plane transfer surface, corrugated or irregular shape would greatly improve the heat transfer efficiency, if reasonable structure design would be developed and the fabricating cost could be controlled.

Most of the existing dew point products adopt the airflow arrangement of cross-flow, which is not the best flow pattern in terms of heat exchange. Counter-flow arrangement would obviously be more preferable as it can create a higher temperature difference (logarithmic average) between the two adjacent airstreams and a higher efficiency. A comparative study of cross-flow and counter-flow HMXs based on M-cycle for dew point cooling was conducted. Both configurations of HMXs were theoretically and experimentally investigated to indicate the counter-flow exchanger offered greater (around 20%

higher) cooling capacity, as well as greater (15-23% higher) dew point and wet-bulb effectiveness, but less energy efficient (10%) due to the increase of flow resistance, with equal physical size and under the same operational conditions (Zhan et al, 2011).

2. PHYSICAL AND NUMERICAL MODELS

The corrugated sheets could be stacked together seamlessly and supported one another. The intake air enters the dry channels from the lower part of the stack, then flows through the dry channels and is divided into two parts through the perforated top end, presenting as Fig. 1. One part keeps moving along the channels to be the final product air, while the other diverts into the adjacent channels with wet inner walls through apertures near to the end of the dry channels. The air in the wet channels flows in a reverse direction as working air and is finally discharged to atmosphere from the bottom of the HMX. Water is distributed at the top of wet channels and flows downward along the wet channel inner walls to form water film. Latent heat for water evaporation comes from the air in dry channels through the channel walls, thus the air in dry channels is cooled by the water evaporation occurring on the surface of wet channels. The vapour with the latent heat comes into the working air to be taken away.

The dry channels contain both product and working air, and the wet channel airflow just a division of the inlet air. The product air temperature of closing-to dew point of entering air can be realized by the high efficiency total heat transfer (i.e. sensible and latent heat) to the working air through water evaporation and the heat conduction of wall.

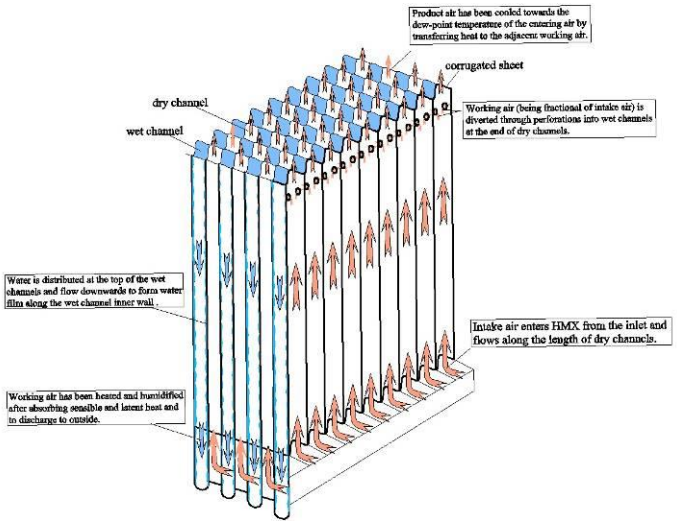

Fig. 1 working principle of counter-flow heat and mass exchanger

Corrugated surface offers more effective area for heat and mass transfer than flat surface, meanwhile it alters the state of airflow which affects the transfer rate of heat and mass. To optimize the structure of the HMX and disclose the relation among the various parameters, modelling and computational simulation of the transfer process has been carried out based on the properly simplified structure shown in Fig. 2.

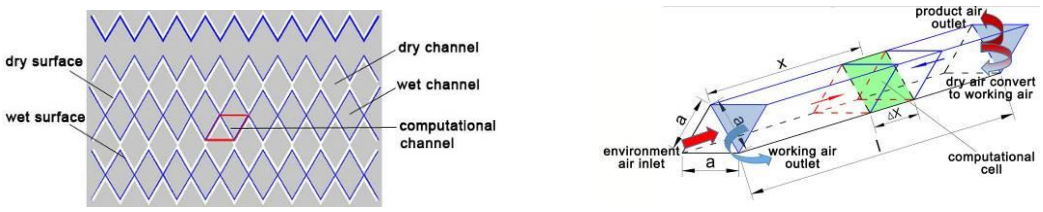

(a) Top view of the stacked corrugated sheets *(b) Computational cell in the adjacent dry and wet channels*

Fig.2 Physical model of the corrugated HMX for computation

Considering the geometric symmetry and the same boundary conditions, a computational cell, which covers the dry channel region and its adjacent wet channel counterpart (refer to Fig. 2), is taken as the basic but complete unit of heat and mass transfer to be investigated. To simplify the modelling process

and mathematical analysis, some basic assumptions are made as below. 1) Define the HMX enclosure as the system boundary. The process of heat and mass transfer was adiabatic, thus no heat transferred across the envelope between the system and the surroundings. 2) Consider the process of heat and mass transfer at steady state. 3) Heat transfer through the channel walls only occurs in the vertical direction, namely no heat and mass transfer in the airflow direction. The convective heat transfer is considered the dominant mechanism for heat transfer between the airflow and water film/channel walls. The channel walls are impervious to mass transfer. 4) The inner surfaces of wet channel are thoroughly treated with hydrophilic material for desirable water diffusivity. The temperature of the treated surface equals to the local wall temperature. 5) The thermal resistance of the wall separating the adjacent dry and wet channels is assumed to be negligible, namely ignore the temperature difference between the dry and wet sides of the wall (Zhao et al., 2008). 6) Air is treated as incompressible gas. Air velocity is considered to be uniform within a single computational cell.

Along its length, the channels are divided into numerous computational cells including the contiguous dry and wet channels. Random one of those, with a distance of x from the inlet of air inlet, is selected to be studied of the heat and mass transfer process inner and interaction with the surroundings through the corresponding interface.

Mathematical model of heat and mass transfer in the exchanging channels

The basic equilibrium equations involved are the conservation of energy and mass, which are listed below.

Equation 2: conservation of water mass volume between cell inlet and outlet

$$dQm_{water} = 2h_m \cdot \rho_{air,wet} \cdot (hum_{wall} - hum_{wet}) \cdot a \cdot \sigma \cdot dx$$

Where:

- hum_{wall} = the moisture content of the working air at wall temperature in wet channel;
- hum_{wet} = the moisture content of the working air in wet channel.

The difference between hum_{wall} and hum_{wet} is the inherent impetus for the water evaporation occurring on the wet channel surface.

Equation 2: energy balance in the dry channel cell

$$dQ_{dry} = c_p \cdot Qm_{dry} \cdot \Delta Tf_{dry} = 2h_{dry} \cdot (Tf_{dry} - Tw) \cdot a \cdot dx$$

Equation 3: mass balance in wet channel cell.

$$dhum_{wet} = 2h_m \cdot \rho_{airwet} \cdot (hum_{wall} - hum_{wet}) \cdot a \cdot \sigma \cdot dx$$

Equation 4: energy balance of airflow in the wet channel cell

$$di_{wet} = c_p \cdot Qm_{wet} \cdot \varphi \cdot \Delta Tf_{wet} = dQ_{wet} + di_{steam}$$

Where:

- $dQ_{wet} = 2h_{wet} \cdot (Tw - Tf_{wet}) \cdot \mathrm{a} \cdot dx$
- $di_{steam} = 2h_m \cdot \rho_{air,wet} \cdot (hum_{wall} - hum_{wet}) \cdot c_p^{steam} \cdot Tf_{wet,out} \cdot a \cdot \sigma \cdot dx$

Equation 5: energy balance in dry/wet cell related to water contents

$$di_{water} = dQ_{dry} - dQ_{wet} - dQ_{vap}$$

Where:

- $di_{water} = (Qm_{water,out} \cdot Tw_{out} - Qm_{water,\text{in}} \cdot Tw_{in}) \cdot c_p^{\ water}$
- $dQ_{vap} = 2h_m \cdot \rho_{air,wet} \cdot (hum_{wall} - hum_{wet}) \cdot en_{steam} \cdot a \cdot \sigma \cdot dx$
- $en_{steam} = 2446 + 1.86T_{water}$

The equations 1 to 5, through proper substitution, rearrangement and simplification, could form a differential equations set with five correlated equations and five independent parameters of Tf_{dry}, Tf_{wet}, Tw, hum_{wet} and Qm_{water}, which should be solved under certain boundary and initial conditions, thus the parameters changing along the channel length could be described.

Dedicated computational routines are developed to solve the simultaneous equations with finite difference and Newton iteration method and perform the simulation under the environment of EES (Engineering Equation Solver).

Along the length (l=1.0m), the channels, which include one dry channel and one of its adjacent wet channel, are divided into 500 computational cells. The maximum residual of iterative solutions and maximum variable change in each computational cell is less than 2.5×10^{-14} at various simulation conditions, therefore the computation is considered converged and reliable (Klein and Nellis, 2014).

3. PERFORMANCE EVALUATION STANDARDS AND CONDITIONS

The following parameters, i.e. wet-bulb effectiveness, dew-point effectiveness, cooling capacity, energy efficiency (COP), are generally applied to evaluate the performance of IEC system.

Equation 9: wet-bulb/dew-point effectiveness (Jradi and Riffat, 2014)

$$\varepsilon_{wb} = \frac{Tf_{dryin} - Tf_{dryout}}{Tf_{dryin} - Tf_{dryin\_wb}}$$

Equation 10: dew-point effectiveness (Jradi and Riffat, 2014)

$$e_{dp} = \frac{Tf_{dryin} - Tf_{dryout}}{Tf_{dryin} - Tf_{dryin\_dp}}$$

Equation 11: cooling capacity (ASHRAE, 2000)

$$Q_{cooling} = c_p \cdot (Tf_{dryin} - Tf_{dryout}) \cdot (1 - \varphi) \cdot Qm_{dryin}$$

Equation 12: Coefficient of Performance (COP) (ASHRAE, 2009)

$$COP = \frac{Q_{cooling}}{W_{fan} + W_{pump}}$$

To compare with the published results, the similar boundary and initial conditions (see table 1) are adopt to perform the simulation. The temperature of environment is taken from the typical design temperature of the UK, namely dry bulb temperature of 28℃, wet bulb temperature of 20℃ and dew point temperature of 16℃.

Table 1 Pre-set operational conditions for simulation

channel length (m)	side length of the cross-sectional channel (m)	channel number	cell number per channel	working air ratio	water temperature (℃)
1.0	0.01	2500	500	0.5	20

dry bulb temperature of inlet air (℃)	wet bulb temperature of inlet air (℃)	velocity of inlet air (m/s)	surface wettability factor	fan efficiency	pump efficiency
28	20	1.0	1.0	75%	75%

4. RESULTS AND DISCUSSION

The characteristic of inlet air is definitely the key factor affecting the performance potential of evaporative cooling, meanwhile the reasonable geometric structure of the HMX helps to acquire desirable performance. The various parameters of inlet air, i.e. temperature, moisture content, relative humidity, velocity, and the structural parameters as the channel length and height, along with the operational parameters of working air ratio have been investigated respectively below.

4.1 Inlet air temperature effect

The various parameters of air, such as relative humidity, moisture content, dry bulb temperature, wet bulb, dew point temperature, etc., are correlated and coupled with one another. In one day period, the moisture containing in the atmospheric air is considered to be constant at certain location. Thus, keeping the moisture content constant, which is 0.0015kg/kg at UK typical design weather condition, the performance of the HMX was investigated with the temperature change in one day, from 24℃ to 40℃.

It can be found in Fig.3 (b) that the HMX runs during the whole daytime with a steady performance, wet bulb effectiveness at around 120%, dew point effectiveness at about 80% and product air temperature at 19℃. However, the cooling capacity and COP both increase linearly with the outdoor temperature, Fig.3 (a). The cooling capacity at 40℃ is 3 times high as that at 24℃. Therefore, the HMX can supply product air at steady temperature with steady effectiveness during one day period, while the cooling capacity can fit for the increased cooling requirement due to the increase of outdoor temperature. In other words, the HMX presents a desirable capability that it offers stable product air of temperature and volume, despite of the change of outdoor temperature. The reason is that with the outdoor temperature increase, the relative humidity decreases, under the condition of unchanged moisture content during one day period, which leads to a faster evaporation and higher cooling rate.

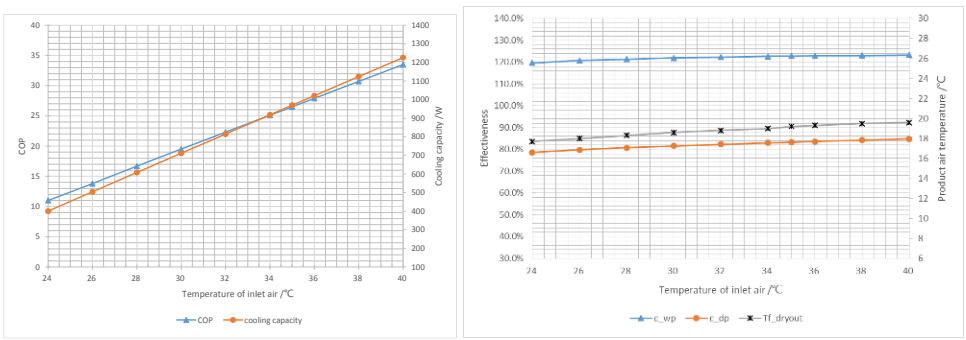

(a) Cooling capacity and COP *(b) Effectiveness and product air temperature*

Fig.3 Performance with the temperature of inlet air (moisture content constant)

4.2 Inlet air moisture effect

The moisture content of atmospheric air changes with the seasons rather than days, i.e., moisture content during one day period can be assumed to be constant. However, the season's influence on moisture content is significant. To investigate the effect of the air moisture content on the HXM performance, it was simulated by assuming the air temperature to be constant at the UK's design temperature of 28℃.

It can be seen from the Fig. 4 (a) that the cooling capacity and COP sharply fall with the increase of moisture content in atmospheric air. It implies that the air condition in cold season is more desirable for the application of IEC due to the low moisture content in the ambient air. Fig. 4 (b) shows that a low moisture content of 0.005 kg/kg could realize a cooling effect of 16℃ temperature drop, while a higher moisture content of 0.02 kg/kg could only contribute to a temperature drop of 3℃. On the other hand, the wet bulb and dew point effectiveness both present the uptrend with the increase of moisture content.

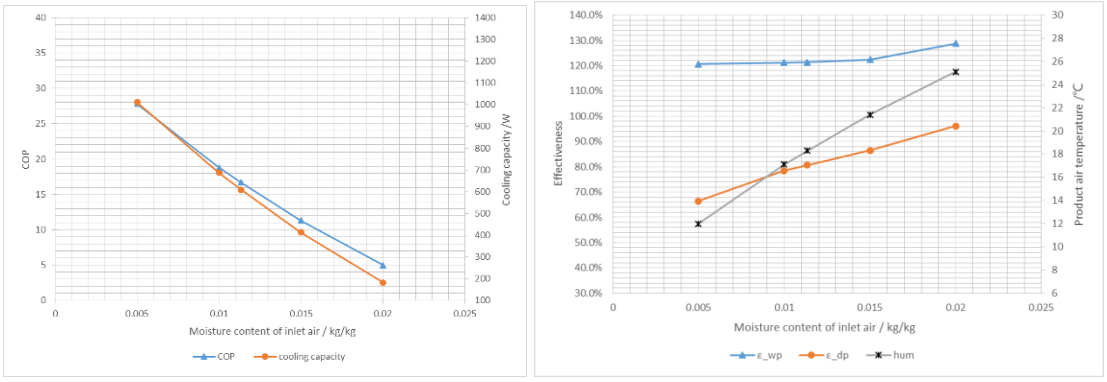

(a) Cooling capacity and COP *(b) Effectiveness and product air temperature*

Fig.4 Performance with the moisture content of inlet air

4.3 Inlet air relative humidity effect

Keeping the air temperature constant and observing the trend of cooling performance with the change of relative humidity helps to compare the performance in different geographic region with various humid air. Fig. 5 (a) presents that the dry air of 5% relative humidity could output around as 8 times high cooling capacity as the humid air of 85% relative humidity could. Fig. 5 (b) also shows the great cooling potential which could produce a temperature difference of 20℃ between the inlet and outlet air at 5% relative humidity. The wet bulb effectiveness stays stably above 120%, meanwhile the dew point effectiveness increases with relative humidity and reaches a high level of 98% at 85% relative humidity.

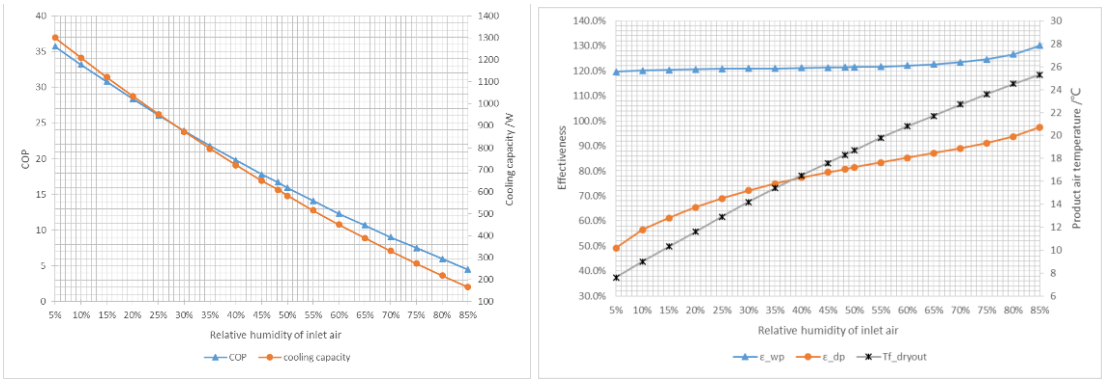

(a) Cooling capacity and COP *(b) Effectiveness and product air temperature*

Fig.5 Performance with the relative humidity of inlet air

4.4 Inlet air velocity effect

For a fixed geometric structure, the velocity of inlet air affects both the air flow rate and the flow state in the HMX channels, of which the former leads to the change of cooling capacity and the latter results in different heat and mass transfer rates and therefore the different cooling capacity.

It can be seen in Fig. 6 (a) that the cooling capacity rises with the rise of velocity from 0.3m/s to 3m/s, while COP reaches a highest point of 17.6 at the air velocity of 1.5m/s and then shows downward tendency. A non-ignorable fact is that there is just very little change during the velocity increasing from 1.0m/s to 1.5m/s. Contrast to Fig. 6 (b), the wet bulb and dew point effectiveness both decline with the increase of air velocity. When velocity below 0.5m/s, the wet bulb and dew point effectiveness could reach the levels of 140% and 93% respectively. The increase of velocity from 0.3m/s to 3.0m/s, without other air parameters change, could only contribute to a further temperature drop of 5℃. Lower velocity could bring about higher effectiveness, however the corresponding lower cooling capacity would result in worse cost effectively. Compromisingly, the velocity of around 1m/s seems to be a reasonable choice.

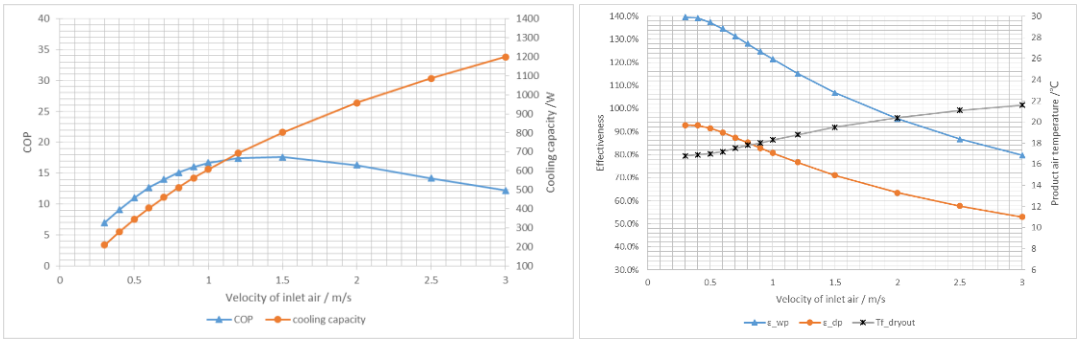

(a) Cooling capacity and COP *(b) Effectiveness and product air temperature*

Fig.6 Performance with the velocity of inlet air

4.5 Channel side length effect

The size of single channel affects the flow state and then affects the heat and mass transfer and the cooling capacity of the HMX unit. The calculation presented in Fig. 7 (a) is based on the same amount of single-channels. Comparing the simulation results for the fixed HMX unit width and thickness, the cooling capacity results show in Fig. 7 (c). It presents a perfect point at side length of 0.006m, where the web effectiveness and dew point effectiveness both reach the highest level meanwhile the product air temperature arrives at the lowest point of 16.8℃. Fig. 7(c) also shows that the cooling capacity reaches the highest point of 700W at the channel side length of 0.006m, which further confirms that the optimal size of channel side length is 0.006m.

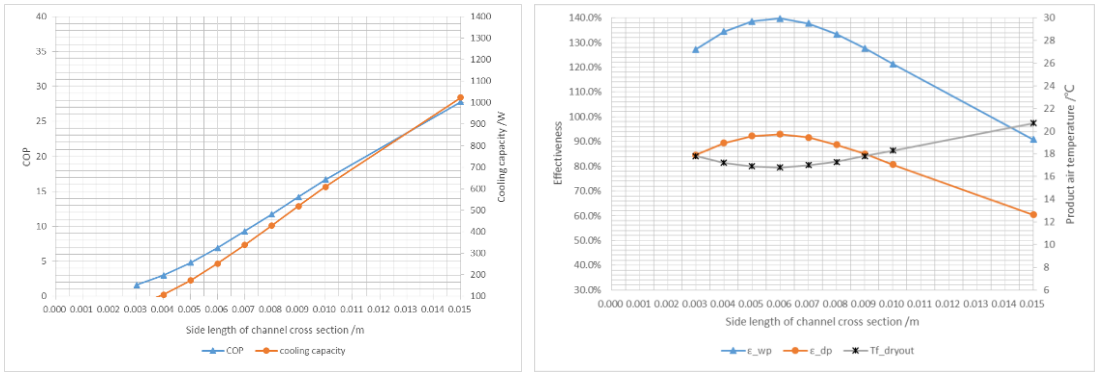

(a) Cooling capacity and COP *(b) Effectiveness and product air temperature*

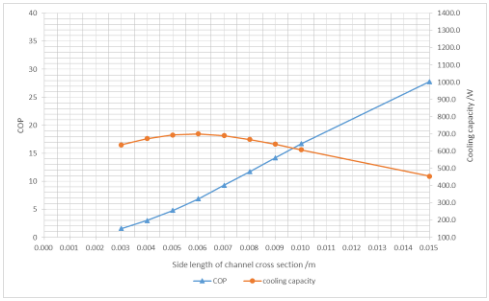

(c) Cooling capacity and COP (amended HMX volume)

Fig.7 Performance with the side length of channel cross section

4.6 Channel length effect

Longer channel length brings about more efficient heat and mass transfer inside; nevertheless it will consume more power of fan to against the flow resistance. In Fig. 8 (a), cooling capacity ascends rapidly while COP descends sharply when the length less than 2.0m. It can also be seen in Fig. 8 (b) that effectiveness ascends rapidly while COP descends sharply before the point. Overall consideration of the performance shown in the two figures, to extend the channel length to 2.0m will be worth it, while too small length, below 1.0m, will lead to undesirable results. Nevertheless, the increase of channel length results directly in the expansion of the HMX material cost proportionally. The cooling capacity would get a promotion of 15% with double cost by the channel length from 1m to 2m. Therefore, until the benefit from the HMX cost is economically more than the profit from the 15% augment of cooling capacity in practice, the channel length of 1.0m is a preferably practical option.

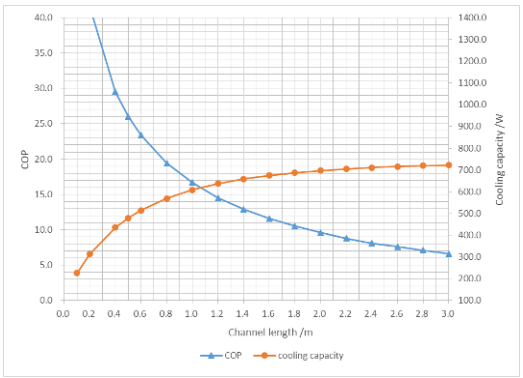

(a) Cooling capacity and COP

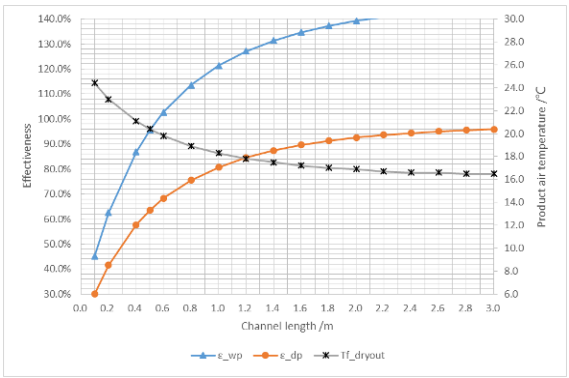

(b) Effectiveness and product air temperature

Fig. 8 Performance with the channel length

4.7 Working air ratio effect

Higher working air ratio, which is the faction of working air flow in wet channels over the total inlet air, contributes to the improvement of water evaporation rate in wet channels, while the reduced flow rate of product air decreases the total cooling capacity. Fig. 9 (a) presents an optimal point of 0.3, at which the cooling capacity and COP both reach the best levels. Contrast to Fig. 9 (b), the effectiveness and product air temperature both change rapidly before the ratio of 0.7. Considering both figures, the ideal range of working air ratio should be between 0.3 and 0.5.

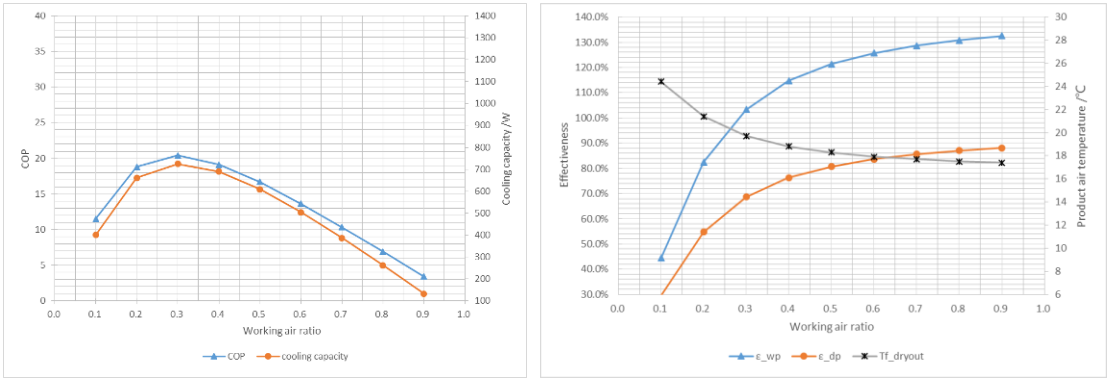

(a) Cooling capacity and COP *(b) Effectiveness and product air temperature*

Fig. 9 Performance with working air ratio

4.8 Climate adaptation

The computational simulation was conducted dedicatedly under the meteorological conditions of different European countries (see table 2) and the fixed conditions, i.e. u=1m/s; Φ=0.3; σ=1.0; Twater=16℃; a=0.006m; l=1m; HMX width=0.6m; HMX thickness=0.26m; (channels_layer=100; layers=50); n=500.

Table 2 Performance contrast among different geometric region

No.	Country	City	Dry bulb temperature (℃)	Wet bulb temperature (℃)	Dew point temperature (℃)	Relative humidity
1	UK	London	28	20	16.0	48.2%
2	Spain	San Pablo	39.9	25.1	19.2	30.3%
3	Portugal	Lisbon	32.1	19.7	12.9	31.0%
4	Italy	Catania	34.1	21.6	15.5	32.9%
5	Greece	Athens	33.8	20.8	14.1	30.5%
6	Turkey	Izmir	35.5	20.4	12.1	24.4%
7	Demark	Copenhagen	24	17.3	13.4	51.5%
8	Finland	Helsinki	26.7	19.1	15.1	48.9%

No.	Product air temperature (℃)	Wet bulb effectiveness	Dew point effectiveness	Cooling capacity (W)	Cooling capacity per unit HMX volume (kW/m^3)	COP
1	17.5	130.80%	87.00%	660.8	4.2	15.9
2	20.1	134.10%	95.80%	1201	7.7	28.8
3	16.0	129.60%	83.50%	1005	6.4	24.2
4	17.6	132.20%	88.90%	1023	6.6	29.4
5	16.8	131.10%	86.40%	1059	6.8	25.5
6	15.8	130.60%	84.20%	1220	7.8	29.4
7	15.7	123.90%	78.20%	532.9	3.4	12.9
8	16.9	128.80%	84.20%	621.9	4.0	15

The HMX shows great performance with generally the wet bulb effectiveness above 130%, dew point effectiveness above 85%, cooling capacity per unit HMX volume above 6.5 kW/m^3 and COP more than 25, in Southern Europe, i.e. Spain, Portugal, Italy, Greece and Turkey, where the relative humidity of ambient air is around 30%. Under the climate condition of Spain and Turkey, the most desirable results were gained. Under Spanish outdoor air condition, the temperature difference between inlet and outlet air was 19.8℃, the wet bulb effectiveness 134.1%, dew point effectiveness 95.8%, cooling capacity per unit HMX volume above 7.7 kW/m^3 and COP 28.8, while in Turkey the temperature difference between inlet and outlet air was 19.7℃, the wet bulb effectiveness 130.6%, dew point effectiveness 84.2%, cooling capacity per unit HMX volume 7.8 kW/m^3 and COP 29.4.

What is noteworthy is that the Northern European climates also show good adoptability. The performance under Finish outdoor air condition is very close to the one in UK. The temperature difference between inlet and outlet air is 10.5℃ and 9.8℃, the wet bulb effectiveness 130.8% and 128.8%, dew point effectiveness 87% and 84.2%, cooling capacity per unit HMX volume above 4.2 and 4.0 kW/m^3 and COP 15.9 and 15 in UK and Finland respectively.

5. CONCLUSIONS

The relative humidity of inlet air is a major fact that affects the cooling performance of the corrugated HMX. The ambient air at a lower moisture content can achieve higher cooling performance. The HMX can provide stable operation in terms of effectiveness and product air outlet temperature and its cooling capacity can increase with the rise of the ambient air during one day time. The corrugated HMX presents high adaptability to various climate conditions in Southern Europe, Northern Europe and the UK and shows great performance.

The optimum air/dimension/operation parameters of the corrugated HMX are as follow: 1) optimum dimension of the corrugated HMX's channel is 0.005m(height)×0.006m(side length)×1m(channel length); 2) optimum working air ratio range is 0.3 and 0.5; 3) optimum inlet air flow rate is around 1m/s.

6. ACKNOWLEDGEMENT

The authors would acknowledge our sincere appreciation to the financial supports from the University of Hull, Engineering and Physical Sciences Research Council (EPSRC), Innovate UK and Ministry of Science and Technology of China (EP/M507830/1) and Beijing Key Lab of Heating, Gas Supply, Ventilating and Air Conditioning Engineering.

7. REFERENCES

ASHRAE, ANSI/ASHRAE Standard 143-2000, Method of test for rating indirect evaporative coolers, American Society of Heating, Refrigerating and Air-Conditioning Engineers, Inc. GA 30329. (2000)

ASHRAE, ASHRAE handbook Fundamentals Volume: SI edition, American Society of Heating, Refrigerating and Air-Conditioning Engineers. (2009)

INCROPERA, F P., DeWitt, D P., et al., Fundamentals of heat and mass transfer, 6th edition, New York: John Wiley & Sons. (2007)

MAISOTSENKO, V. and I. Reyzin, The Maisotsenko cycle for electronics cooling, Proceedings of the ASME/Pacific Rim Technical Conference and Exhibition on Integration and Packaging of MEMS, NEMS, and Electronic Systems: Advances in Electronic Packaging, San Francisco, CA, U.S. (2005), pp. 415-424.

JRADI, M., Riffat, S, Experimental and numerical investigation of a dew-point cooling system for thermal comfort in buildings, Applied Energy 132 (2014) 524-535.

KLEIN S, Nellis G, Mastering EES, F-Chart Software, October 2014

DUAN, Z, et al, Indirect evaporative cooling: Past, present and future potentials, Renewable and Sustainable Energy Reviews 16 (2012) 6823-6850.

DUAN, Z., Investigation of a Novel Dew Point Indirect Evaporative Air Conditioning System for Buildings, PhD thesis, University of Nottingham, September 2011

ZHAN C, et al. Comparative study of the performance of the M-cycle counter-flow and cross flow heat exchangers for indirect evaporative cooling-paving the path toward sustainable cooling of buildings. Energy, 2011; 36(12):6790-805.

ZHAO X, Liu S, Riffat SB. Comparative study of heat and mass exchanging materials for indirect evaporative cooling systems. Building and Environment, 2008; 43:1902-10

262: Operation performance of separated heat pipe in data centre: testing and analysis

TAO DING, ZHI GUANG HE, ZHEN LI, ZHEN YING WANG

Department of Engineering Mechanics, Tsinghua University, Meng Min Wei Technology building, Tsinghua University, Beijing 100084 China, dingtaohang01@163.com

Data centre grows rapidly all over the world, at the same time energy consumption is also increasing. According to research, nearly 45% of the total energy in data centre is used for IT equipment while about 45% for computer room air conditioning (CRAC) system. Apparently, cooling system consumes too much energy. Badly air organization and compressor of air conditioning working all year round are the mainly two shortcomings for CRAC system. In order to save energy, a new kind of cooling system called separated heat pipe cooling system is used in data centre. This system has better airflow organization and it can use free cold ambient air as heat sink in winter. In this paper, working condition of separated heat pipe system is tested. For example, temperature at some typical points will be measured, like chilled water's inlet/outlet temperature; IT equipment's working temperature and room temperature. On dealing with temperature distribution, T-Q diagrams of CRAC and separated heat pipe system showing the temperature distribution are drawn. In T-Q diagram, temperature difference of heat transfer in every process can be easily calculated, which can be used to direct heat transfer enhancement. As for an evaluation index of data centre energy efficiency, PUE (power usage efficiency) will also be measured. In theory, the system's PUE will get the minimum value in winter, while get the maximum value in summer. Briefly, using free ambient cold air and installing evaporator inside the rack are the mainly two advantages of separated heat pipe system, which will lead to better working environment for IT equipment and more energy saving compared with traditional CRAC system.

Keywords: Separated heat pipe, CRAC, free ambient cooling, data center cooling

1. INTRODUCTION

The scale of data center develops fast all over the world, at the same time, running cost and energy consumption are also growing rapidly. Traditional data center uses CRAC (Computer room air conditioning) system for heat dissipation. Cooling system and IT equipment make up the mainly two parts of energy consumption. As is shown in figure 1[1], IT equipment consumes about 45% of the total energy while cooling system also contribute about 45% of the energy use. Apparently, it's unreasonable that cooling system consumes so much energy. In order to save energy in data center, cooling system needs to be modified.

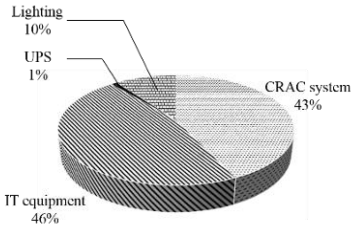

Figure 1 Energy consumption in data center

The structure of CRAC system is shown in figure 2. The racks are installed face to face to crate cold air aisle and back to back to crate hot air aisle, the floor is raised above the ground where the cold air produced by air conditioning system is sent. Cold air flows through racks and cools the IT equipment, finally, hot air flows back to air conditioning where it is cold. Although CRAC system is used widely, there are mainly two shortcomings for such system.

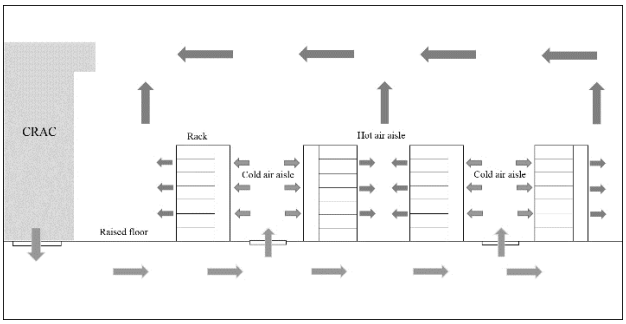

Figure 2 The scheme of CRAC system for data center

Firstly, the airstream organization is unreasonable. For example, hot air and cold air may mix at the entrance of the racks (cold and hot air mixing problem can't be solved thoroughly even the cold passage is separated from hot air passage), air mixing is harmful for heat transfer process, for it causes irreversible loss of heat transfer ability, beside, there may be some points whose temperature are extremely high in the racks, which are called local hot spots. In order to avoid air mixing and hot spots, inlet temperature of chilled water needs to be very low in order to decrease the supply air temperature. However, the lower the inlet water temperature, the higher energy consumption for chiller's compressor. In other word, in order to avoid the influence of cold and hot air mixing and local hot spots, a lot of energy is wasted by CRAC system.

Secondly, chiller needs to operate all year round even in cold winter when outside cold air temperature is far less than room temperature. These two shortcomings increase energy consumption of chiller.

In order to save energy, a new kind of system called separated heat pipe system is used in data center cooling [2,3] based on the principle of heat pipe system developed since 1960s [4]. Different from traditional heat pipe system, the evaporator and condenser are separated from each other and are connected by liquid and gas pipe. Compared with the traditional cooling system, this system can transfer heat for long distance [5], besides it can use free ambient cold air in winter or transition season.

Different from traditional CRAC system, the evaporator is installed inside the rack, once heat is generated by IT equipment, it is soon absorbed by the evaporator inside the rack, thus there is nearly

no local hot spots and the system's airstream organization condition is also improved compared with CRAC system.

2. THE SCHEME OF SEPARATED HEAT PIPE SYSTEM

Figure 3 is the scheme of the separated heat pipe system. Separated heat pipe system has mainly 4 parts. They are evaporator, condenser, gas pipe and liquid pipe. Chilled water is used as heat sink of the system. Evaporator is installed inside the rack, where Freon absorbs heat from IT equipment and changes its phase from liquid to gas, considering the low density of gas, Freon gas flows into condenser through gas pipe. In condenser, it is cooled by chilled water and changes its phase from gas to liquid. The position of evaporator is lower than condenser, by the force of gravity, liquid Freon flows back to evaporator through liquid pipe. At the same time, heat is transferred from IT equipment to chilled water. According to supply air flow direction, there are mainly two kinds of racks in the data centre. The second kind of rack is shown in figure 3(b). Evaporators are in the left and right side of the rack, air in room temperature flows into the left side of the first rack, where it is cooled by Freon coolant. Then cold air flows across IT equipment and absorb heat from them, finally, hot air flows through the evaporator in the right side where it is cooled and its temperature is equal to room temperature. There are four racks in a row, the outlet air of the first rack is the inlet air of the next rack. Different from the second kind of rack, the evaporator in the first kind of rack is installed inside the front and back plate (shown in figure 3(a)). Each rack is separated, air from room is absorbed into the rack from the front plate and flows out from the back plate.

Both kinds of racks use chilled water as heat sink. Heat generated from IT equipment is finally transferred to chilled water. In winter, as the outside air temperature is cold enough, there is a water and air heat exchanger outside, free cold ambient air is used to produce chilled water, while in summer, considering the outside air temperature is usually above 30°C, chiller is open to get chilled water. In transition season like spring, air temperature at night is cold while at noon and in the afternoon, air temperature is higher, so we can use free cooling at night and open chiller to produce chilled water when temperature is higher. According to the meteorological data (by DEST software designed by Tsinghua University) in figure 4, there are four months in a year whose average temperature is lower than 5°C in Beijing. As a result, nearly 33% of all the year free cooling can only be used.

Besides, evaporator of heat pipe is installed inside the rack. Heat generated by IT equipment is soon absorbed by evaporators in rack, thus, problems of hot spots and air mixing can be solved. A data center using separated heat pipe system as cooling method has already been built in Tsinghua University, Beijing, China. This paper will make a test about the whole system, including operating condition of the two kinds of racks, PUE at summer and winter. Besides, T-Q diagrams are used to illustrate the temperature difference of every heat transfer process for CRAC and separated heat pipe system.

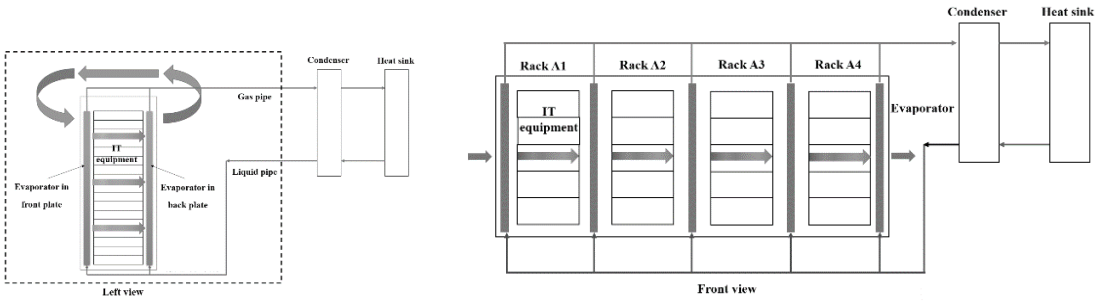

(a) The first kind of rack: Air flows from the front plate to the back plate (b) The second kind of rack: Air flows from the left plate to the right plate

Figure 3 The scheme of the separated heat pipe system

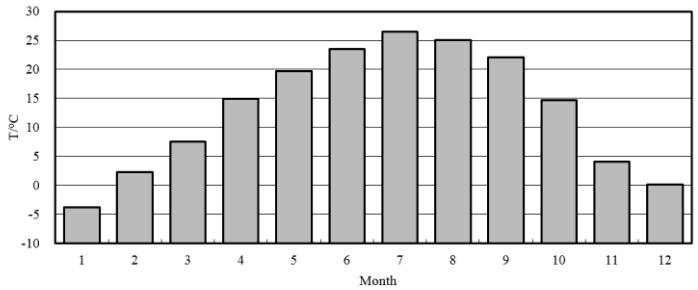

Figure 4 The meteorological data in Beijing of average temperature distribution from January to December

3. THE OPERATION CONDITION OF THE TWO KINDS OF SYSTEM IN WINTER AND SUMMER

3.1 Experiment method and testing accuracy

In the experiment, the operation condition is tested including the total heat generation of IT equipment, temperature distribution of standard points. The inlet and outlet air temperature is measured by thermal couple whose accuracy is 0.1°C after adjustment. The IT equipment's heat generation is measured by electricity meter whose accuracy is 0.1 KWh. Temperature is collected by PAC system and NI USB-9162. The temperature sample interval is one second.

3.2 Results in winter

In winter (test is carried out on March 3th to 12th, 2014), cold air is used to produce chilled water, the outdoor air temperature is stable, thus the inlet chilled water temperature is also stable. Chilled water's inlet and outlet temperature is about 12.7°C/ 14.3°C. Heat generation power of IT equipment is 20kW. In order to know the operating condition of IT equipment, one rack of the first kind of racks (B2 rack, air stream pass through front and back plate of the rack) is tested. There are 3 layers in each rack, which means one rack is separated into three parts, considering IT equipment in each layer has different heat generation rate, thus thermal couples have been laid in all the layers. In each layer, thermal couples are laid at the entrance of the front plate (also the room temperature), entrance of the IT equipment (also the outlet of front plate), outlet of IT equipment (also the entrance of back plate), outlet of back plate. The position of thermal couples and test results are shown in figure 5. The test continues 30 minutes. The results are the average temperature of 30 minutes. Heat generation of the rack is 3.8kW.

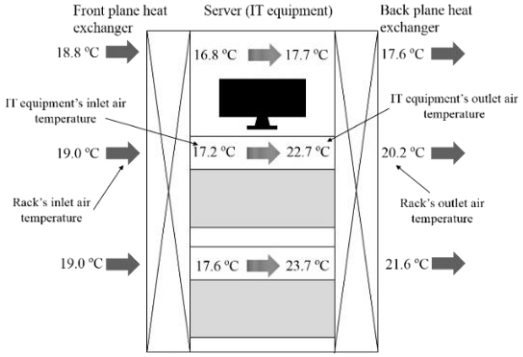

Figure 5 Temperature distribution of B2 rack in winter (left view)

The room temperature is about 19°C. After cooled by the evaporator in the front plate, air temperature decrease to 17.2°C (average temperature of three layers), because different layer has different heat generation power, the temperature difference between air's inlet and outlet are also different. At the top layer, there is a display which nearly has no heat generation, so the increase of temperature is 0.9°C. There are IT equipment in the middle and bottom layer, so the temperature difference is 5.5°C and 6.1°C. After flows through IT equipment, hot air comes into back plate of rack where it is cooled by evaporator of separated heat pipe. The outlet temperature is different at each layer, their average temperature is about 1°C higher than the inlet air temperature. IT equipment's operating temperature range is from 16.8°C to 23.7°C.

Figure 6 shows the time-average temperature distribution of 30 minutes at some typical points. Two conclusions can be obtained from the figure. 1. IT equipment's outlet average temperature is 21.4°C, and the chilled water's inlet temperature is 12.7°C, the temperature difference is just 8.7°C, that means if the IT equipment's outlet average temperature increase to 28°C, chilled water's inlet temperature just needs to be about 19°C, as a result, the time of using free cold air can be much longer. 2. Free cold ambient air is the nature heat sink, thus chiller (especially compressor) doesn't need to be open. Only water pump and fans consume electric, so the PUE can be much lower than CRAC system, according to the test, the PUE of this system is 1.20 (2014/3) and 1.25 (2015/2/28-29).

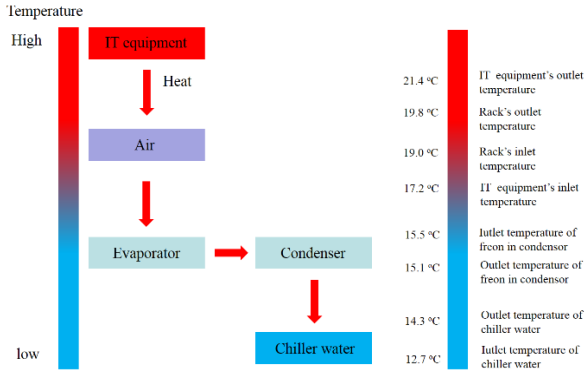

Figure 6 Time-average temperature distribution at some typical points in winter (March, The temperature of air belongs to Rack B2)

3.3 Results in summer

In summer (test is carried out from 2014/6/6-6/13 and 2015/5/16-28), as the outside air temperature is higher than data centre room temperature, chiller is open to produce chilled water. The total heat generation power of all the IT equipment is 30.5kW. Meanwhile, the nom. cooling capacity of chiller is 159.4KW, which is much higher than heat generation rate. However, the compressor's frequency is fixed, so the chiller opens and stops intermittently with the change of the inlet temperature of chilled water. Chiller opened when chilled water's inlet temperature is 18.5°C, and it closed when the temperature comes down to 12.5°C, a cycle continues about 8-10 minutes (results in 2014).

Figure 7 is the temperature distribution in two kinds of rack. Both of the results are tested at the same chilled water inlet temperature. Heat generation of B3, A1, A3, A4 racks are 3.9kW, 1.8kW, 4.5kW and 0.7kW. As can be seen from Figure 7 (a), Rack's inlet/outlet average air temperature is about 23.8°C /24.4°C, which is approach with each other. IT equipment's operating temperature is from 22.0°C to 28.0°C. Considering that there are all IT equipment in each layer of the rack, so the heat generation power are just same with each other. Uniform temperature distribution leads to less hot and cold air mix compared with figure 5.

Figure 7 (b) is the temperature distribution of the second kind of rack (air flows in from the left plate and flows out from the right). The results of (a) are tested in 2014, while (b) are tested in 2015, although heat sink temperature (chilled water inlet temperature) is just the same with each other, room temperature is not the same. As a result, rack's inlet temperature is not the same with each other in these two kinds of racks. The results show that the first kind of rack's operating condition is better than the second kind. For there exists local hot spot in A3 rack, one point of the outlet air temperature is as high as 33.7°C. The temperature distribution is not uniform. In fact, the IT equipment's placement direction and the airstream flow direction are vertical in the second kind of rack. There are fans on the front and back of IT equipment, so the air stream flow direction in IT equipment and rack are just vertical. As a result, air stream in these two direction may disturb each other, air mixing is stronger, the condition of airstream organization is bad than the first kind of rack. That's the reason why there exists local hot spots and temperature distribution is not uniform.

However, there are still one advantage for the second kind of rack. As the evaporator is installed in the left and right side of the rack, the front and back door is made of glass, they can be open easily and people can observe the IT equipment from outside through glass without open the door. Besides, when

people operate the IT equipment, cold air can still be supplied. However, considering the first kind of rack, when people want to operate IT equipment, front or back door need to be opened, thus, the rack can't produce cold air.

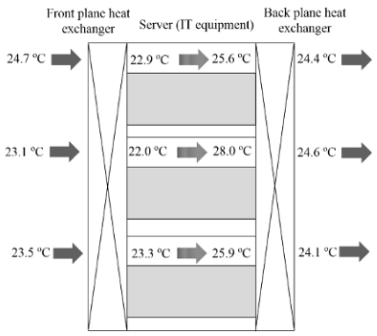

(a) Temperature distribution of B3 rack (The first kind of rack)

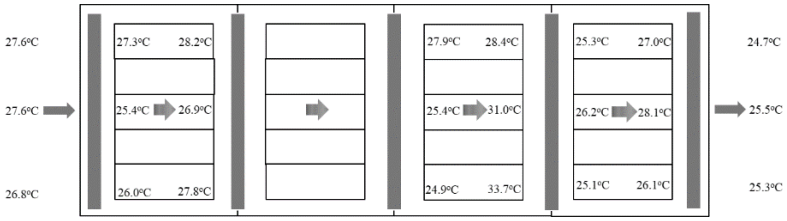

(b) Temperature distribution of the second kind of rack (front view)

Figure 7 Temperature distribution of different kinds of racks in summer

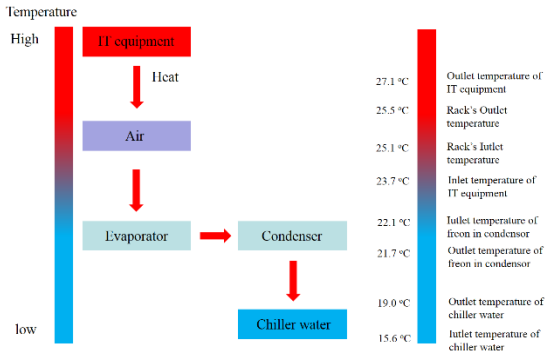

Figure 8 Time-average temperature distribution of data center room at some typical points in summer (The temperature of air belongs to Rack B2)

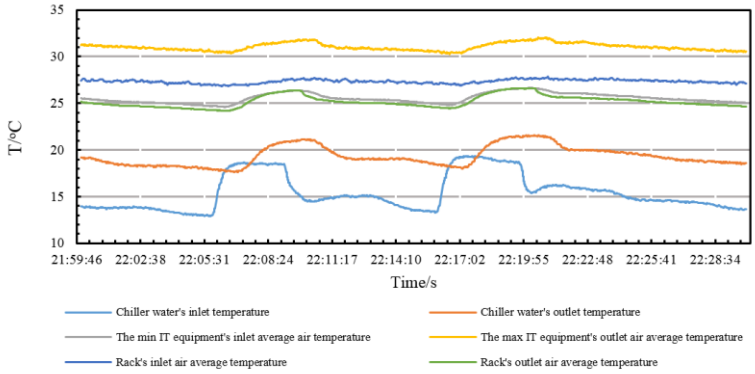

Figure 9 Temperature distribution variation at some typical points (the second kind of racks)

Figure 8 is the time-average temperature distribution at different points in summer, and figure is the variation trends for 30 minutes. In figure 9, average means the average of three temperature at different layers, temperature of air is gathered by NI and water's temperature is by PAC system. There is time difference for two gather systems. So the variation trends has the time error of few seconds after adjustment. However, this little error doesn't influence the variation trends. As can be seen from figure 9, temperature changes periodically over time. A cycle continues about 15 minutes. Although the chilled

water' amplitude of temperature variation is vary lager, the variation trends of air in racks is much gentle than chilled water temperature. As a result, the operating condition of IT equipment in summer can still be regarded as stable. The PUE in summer (June) is 1.49 and in July, PUE is 1.58.

4. COMPARISON: TRADITIONAL CRAC SYSTEM AND SEPARATED HEAT PIPE SYSTEM

In essence, the heat dissipation in data centre is a heat transfer process driven by the temperature difference of T_{chip}-T_o. T_{chip} is the air temperature around the chip when it is on operation condition, which is usually about 40ºC for CRAC system and T_o means the temperature of heat sink, in both of the computer room cooling system, chilled water is used as heat sink. As is mentioned above, compressor operating all year round and badly air flow organization are the two shortcomings of CRAC system. Cold and hot air mixing leads to irreversible loss in heat transfer, the more the mixing air, the colder the chilled water's inlet temperature. For air-conditioning, decreasing the inlet chilled water temperature means increasing the energy consumption of compressor.

Figure 10 is the T-Q diagram [6] for these two system which show the temperature distribution of some standard points. In T-Q diagram, X-axis means the total heat in the heat transfer process, Y-axis means temperature. The region bounded by the closed curves means the entransy dissipation of the heat transfer process. Entransy dissipation is a physical property used to describe the irreversible loss in heat transfer process [7]. The more the entransy dissipation, the more lost in heat transfer ability.

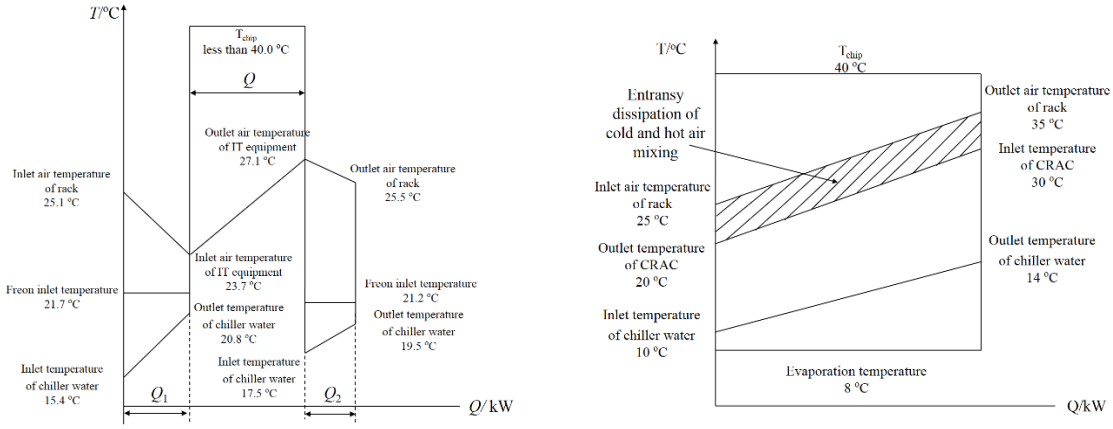

(a) T-Q diagram for separated heat pipe system *(b) T-Q diagram for traditional CRAC system*

Figure 10 T-Q diagram of heat transfer process

The T-Q diagram of separated heat pipe system is showed in figure 10 (a). The author takes the first kind of rake for example, the evaporator of the heat pipe is installed in the front and back plate of the rack. The two evaporators use different heat sink, so the inlet temperature of chilled water is different. In figure 10 (a), Q1 means the heat absorbed by evaporator inside the front plate and Q2 means the heat absorbed by evaporator inside the back plate. Q equals to Q1+Q2, which means the total heat generation of IT equipment in one rack. The lowest chilled water inlet temperature is 15.4ºC. Considering that the Rack's outlet temperature is only 0.4ºC higher than Rack's inlet temperature, there is nearly no entransy dissipation for hot and cold air mixing. Figure 10 (b) is the T-Q diagram of traditional CRAC system, temperature distribution reference from [1]. For different data center, the heat generation power is different, but the power of the distribution system (like water pump, fans) is also different. So although the heat generation is different, temperature distribution can be similar to each other for different data center. As can be seen, chilled water's inlet temperature is 10ºC which is 5.4ºC lower than 15.4ºC. As for CRAC system, the shadow zone in figure 10 (b) is the entransy dissipation of cold and hot air mixing, which consumes 15.6% of the total entransy dissipation of the whole system. For separated heat pipe system, considering that the evaporator is inside the rack, heat generated by IT equipment can be absorbed nearby. The rack's inlet and outlet air temperature are just the same with each other, so the cold and hot air mixing problem can be solved to some extent.

Besides, compare (a) and (b), the operating temperature of IT equipment for separated heat pipe system is 23.7ºC -27.1ºC, and for CRAC system is 25ºC -35ºC, which means T_{chip} for separated heat pipe system is even colder than 40ºC.

In theory, separated heat pipe system is more energy saving compared with traditional CRAC system. As it can use free cold ambient air in winter and its heat sink's temperature is also higher than CRAC system. The test result shows that the average PUE of the whole year is 1.36 (2014/06/12-2015/05/30).

5. THE TIME OF USING FREE AMBIENT COOLING IN DIFFERENT CITIES

According to the temperature distribution in figure 8, a given chilled water inlet temperature (heat sink temperature) lead to an IT equipment inlet temperature. For different data centre, the heat generation power is different, but the power of the distribution system (like water pump, fans) is also different. So although the heat generation is different, temperature distribution can be similar to each other for different data centre. In fact, if the IT equipment inlet temperature is less than 27°C, than the working condition for IT equipment is safe and reliable. In this paper, an experiment is carried out to find the relationship between the IT equipment inlet temperature and chilled water inlet temperature.

We can control the chilled water inlet temperature by setting the chiller's open temperature. The experiment is taken by the chilled water temperature range from 11°C to 20°C in B2 rack. In summer, as the chiller working in an intermittent start-stop condition, we can take time-average temperature as the chilled water temperature. The results are shown in figure 11. As can be seen there is a linear relationship between the chilled water inlet temperature and IT equipment inlet temperature. The expression is also shown in figure 11. According to the results, we can calculated that when the chilled water inlet temperature is 12.7°C, the IT equipment inlet temperature is 21.7°C. However, according to figure 6, in winter, chilled water at 12.7°C leads to the 17.2°C of IT equipment inlet temperature. The results between summer and winter are different. Because in winter, as the outside temperature is usually 15-25°C lower than room temperature, there is some part of heat transferred by building envelop. On the contrary, in summer as the outside air temperature is usually 10°C higher than room temperature, there is some part of heat transferred from outside. So the room temperature in summer is higher than the room temperature in winter although the chilled water inlet temperature is just the same. Higher room temperature leads to higher IT equipment inlet temperature.

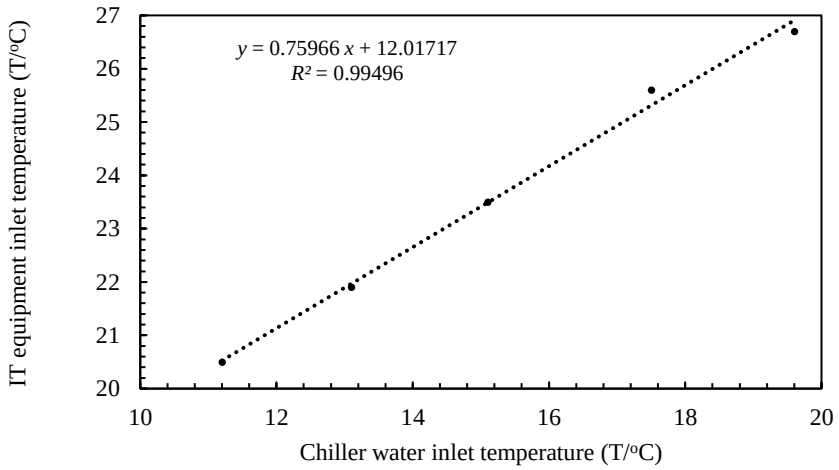

Figure 11 The relation between chilled water inlet temperature and IT equipment inlet temperature

According to figure 11, when IT equipment inlet temperature is 27°C, the chilled water needs to be 19.7°C. If the system uses cold ambient air, considering the temperature difference of cold air and chilled water heat exchanger is 5°C, then when the outside air temperature is less than 14.7°C, free cold ambient air can be used. Meteorological parameters in different cities are given by DEST software designed by Tsinghua University. The results are shown in table 1.

Table 8: Condition of using free ambient cooling in China of different cities

City	Latitude	Days number (T<14.7°C)	Percentage of all the year cold ambient air can be used
Beijing	39.9°N	180	49.3%
Guangzhou	23.2°N	58	15.9%
Harbin	45.8°N	244	66.8%
Urumchi	43.8°N	217	59.5%
Hohhot	40.8°N	229	62.7%
Shanghai	31.3°N	146	40.0%
Kunming	25.0°N	135	37.0%

As can be seen in table 1, most of the cities in north China, separated heat pipe system can use free ambient cold air to produce chilled water for half of the year. In city of middle China like Shanghai and Kunming, there are 40% of the year cold ambient air can be used. Even in south China like Guangzhou, whose climate region is near the tropical climate, there is still 15.9% of the year, when cold ambient air can be used to produce chilled water. By using cold ambient air to produce chilled water, only fans and water pump need to operate. However, when chiller is opened, compressor is also opened, which will consumes a lot of energy. Thus, the more time using free cold ambient air, the less average PUE of the whole year.

6. CONCLUSION

A separated heat pipe system for data centre cooling in Tsinghua University is tested. Different from CRAC system, evaporator of separated heat pipe system is installed inside the rack, once heat is generated by IT equipment, it is soon dissipated, which will lead to better air flow organization, and will decrease the cold and hot air mixing. Besides, the problem of local hot spots can also be solved. Separated heat pipe system can use free cold ambient air as heat sink in winter or transition season, in winter, cold ambient air is used to produce chilled water, the room temperature is about 19°C, thus chiller doesn't need to operate. As for summer, chiller is used to produce chilled water, room temperature is about 24°C. The working condition of IT equipment is safe and reliable.

T-Q diagram is drawn in this paper in order to make a compare between CRAC and separated heat pipe system, T-Q diagrams show that for CRAC system, there are 15.6% of the total entransy dissipation is for cold and hot air mixing process. However, there is nearly no air mixing for separated heat pipe system. Because of better air flow organization, the chilled water inlet temperature can be raised from 10°C (CRAC system) to 15.4°C (separated heat pipe system). Raising heat sink's temperature means less irreversible heat transfer loss and more energy saving. Because of better air stream organization and free cold ambient air using in winter, separated heat pipe system is more energy saving compared with traditional CRAC system. The average PUE of the whole year is 1.36. Such PUE is much lower than CRAC system.

Considering the IT equipment inlet temperature is 27°C, the chilled water inlet temperature needs to be less than 19.7°C. As a result, in Beijing, 49.3% of all the year, free cold ambient air can be used to produce chilled water, in middle China like Shanghai, 40% of the year free cold ambient air can be used. There are still even 15.9% of the year in Guangzhou the separated system can use cold air.

7. ACKNOWLEDGMENTS

The author gratefully acknowledges the financial support by the National Key Technology R&D Program (2012BAA13B03).

8. REFERENCES

[1] TIAN, H., 2012. Research on cooling technology for high heat density data center, doctoral dissertation, Tsinghua University.

[2] ZHOU F, Tian X, Ma G Y. 2011, Investigation into the energy consumption of a data center with a thermosyphon heat exchanger. Chinese Science Bulletin, Vol. 56. Pp. 2185-2190.

[3] ZHENG Y, Li Z, Liu X, et al, 2014. Retrofit of Air-Conditioning System in Data Center Using Separate Heat Pipe System. Proceedings of the 8th International Symposium on Heating, Ventilation and Air Conditioning. Xi'an, China, Springer. Pp. 685-694.

[4] GROVER, G. M., T. P. Cotter, and G. F. Erickson, 1964. Structures of very high thermal conductance. Journal of Applied Physics. Vol.35. Pp. 1990-1991.

[5] QIAN X, Li Z, Tian H. 2014, Application of Heat Pipe System in Data Center Cooling, the first edition, Progress in Sustainable Energy Technologies, Vol II, Springer International Publishing. Pp. 609-620.

[6] CHEN Q, Xu Y C, Guo Z Y, 2012. The property diagram in heat transfer and its applications. Chinese Science Bulletin, Vol.57: 4646-4652.

[7] GUO Z Y, Zhu H Y, Liang X G, 2007. Entransy—a physical quantity describing heat transfer ability. International Journal of Heat and Mass Transfer, Vol.50: 2545-2556.

431: A study on performance improvement of enthalpy exchanger with modified functional layers

C.Y.ZHANG[1], J.C.XU[2], T.S.GE[3], Y.J.DAI[4], R.Z.WANG[5]

1 Institute of Refrigeration and Cryogenics, Shanghai Jiao Tong University, Shanghai 200240 PR China, ZCY.123@sjtu.edu.cn
2 Institute of Refrigeration and Cryogenics, Shanghai Jiao Tong University, Shanghai 200240 PR China, xujingcui@sjtu.edu.cn
3 Research Centre of Solar Power and Refrigeration, Shanghai Jiao Tong University, Shanghai 200240 PR China, baby_wo@sjtu.edu.cn
4 Research Centre of Solar Power and Refrigeration, Shanghai Jiao Tong University, Shanghai 200240 PR China, yjdai@sjtu.edu.cn
7 Research Centre of Solar Power and Refrigeration, Shanghai Jiao Tong University, Shanghai 200240 PR China, rzwang@sjtu.edu.cn

More and more attention has been paid to the enthalpy exchanger (or total heat exchanger). The function layers, which exchange the heat and water between fresh air and exhausted air, play a demanding role in improving efficiency of the exchanger. Paper with low cost and high mechanical property is widely used as the function materials in the current enthalpy exchangers. In this study different materials have been prepared by spraying the thin paper layer with the calcium chloride solution and drying in the oven to improve the hygroscopicity of the material. The solution concentrations are 5%, 10%, 20%, 30% and 40%. The exchangers made by the modified function layers and normal structural layers are applied for test on the base of the GB standard test condition. In the case of the 0.3m/s (corresponding to 50CMH), the biggest absolute enhance of temperature efficiency, latent efficiency, enthalpy efficiency are 15%, 26%, 24% in heat condition and 23.6%, 21.8%, 22.1% in cooling condition. On the other hand, the pressure drop of the air through the exchanger increases 5 Pa in heat condition and 8 Pa in cooling condition, and it is not difficult for total heat exchanger to overcome the problems caused by increase of pressure drop

Keywords: enthalpy exchanger, function layer, enthalpy efficiency, pressure drop

1. INTRODUCTION

More and more attention has been paid to the energy conservation and environmental protection equipments. In room air control area, Zhang proposed the energy recovery ventilator (ERV)[1], which is also called the enthalpy exchanger or total heat exchanger. It has become an important energy saving device at the fresh air supplying part of the HVAC system. The core inside the enthalpy exchanger is the most important functional area, where the heat and water complete exchanging process between the fresh air into the house and exhausted air from the house, so the air from the outside can be processed in temperature and moisture in avoid of treating fresh air, such as hot and humid air in summer, by conditioner directly.

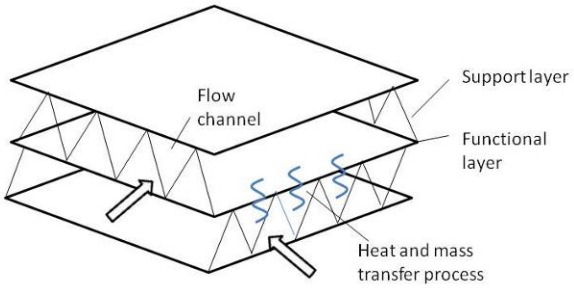

Figure 1: Schematic diagram of Enthalpy Exchanger

The exchanger core is piled up by numbers of units which consist of a functional layer and a supported layer at every unit layer as Figure 1 shows. The arrangement of neighbouring unit layers are crisscross, so it is only half surface area at one side of the exchanger core for air to enter in. Then air flows into the channel with surrounding supported layers and transfers the heat and moisture with the other side through the functional layer on the bottom. It is clear that the heat and moisture transfer processes happen on the material, namely functional layer between neighbouring flow channels, at the same time. And it is not difficult to understand that the thin functional layers have the main influence on the efficiency of the exchanger.

In general, the heat exchanging process of the exchanger always performs very well because of the compact structure and air-cross channels and it is easier for the heat to transfer through the thin layer. But the mass transfer process between the different sources of air is still difficult comparing with heat transfer. The research about enthalpy exchanger has mainly focused on the moisture transfer, which is expected to increase the latent efficiency of the exchanger. The complexity of the functional layer is that the heat and mass transfer through it simultaneously and that the layer material should meet the requirement of the both physical processes. But compared to that of the heat transfer, the low efficiency of the mass transfer has been a obvious limit of improving enthalpy of the device in the future. This study is mainly about to modify the functional layers to enhance the performance of moisture transfer process.

Many studies have been performed on the mechanism and quality of the functional layer. Zhang[1] applied the membrane used in the separation area to the total heat exchangers and built the mathematical model of the heat and moisture transferring process between the surfaces of the membrane. J.L.Niu [2] proposed dimensionless factor CMDR to determine the moisture resistance of the functional layer and provided some criterion to evaluate the materials. Yang-Ching Lee [3] discussed the operation of the total heat exchangers based on the thin functional fibrous paper and examined the great energy-saving potential of the device and the leakage effect on the efficiency. Kyungmin,Kwak [4] has studied the influence of three different types of flow passages structures on the efficiencies and pressure drop of the exchangers. The material wildly applied as the functional layer in the total heat exchanger is the thin fibrous paper (TFP). The TFP has the low cost, high mechanical proprieties, more stable quality for a long time and easily manufacturing process in the factories. These advantages make the TFP as the main material wildly used in the commerce market and HVAC systems in the buildings. But the limitation of the TFP on moisture transferring process through the membrane is also obvious compared with the composited and liquid membrane used in the gas separation. So it leads to the low latent efficiency and enthalpy efficiency during the operation.

In the case of the rotary desiccant wheel, which has similar structure and functions with enthalpy exchanger, as calcium chloride or lithium chloride have a higher hygroscopic capacity, it is always to

composite silica gel with inorganic salt as the desiccant materials to improve absorption of water[5]. So in this paper, the enhancement will be applied to enthalpy exchangers by treating the functional layers with different concentrations of calcium chloride solutions to improve the hydrophilcity of functional layers. The performance of modified exchanger cores are tested and studied in this paper.

2. TEST APPARATUS

The test was conducted in the standard psychometric rooms, in which temperature, moisture and enthalpy of air can be controlled on the certain stable values. The psychometric rooms contain two rooms, one is regarded as the indoor room and another is the outdoor room. So the two rooms can simulate the environment of indoor and outdoor air at different conditions to satisfy test requirements. The test conditions are according to the Chinese Standard 21087-2007(GB/T 21087-2007)[6]. As the Figure 2,3,4 shows, the test device is set near the separating wall in the indoor room. The test device consists of four air ducts and four flow pipes. The four air ducts made by thermal-insulated board have rectangle cross section and enclose a cubic area to set into the exchanger core. Two air pipes cross the separating wall into the outdoor room, one is to send the fresh air into the indoor room and another one is to expel the exhausted air from the indoor room. Fresh air at outdoor conditions is sent by one air blower in the outdoor room into the exchanger core at centre of device, then expelled into the indoor room, at the same time, the indoor exhausted air is provided by another air blower into the exchanger core, then expelled into the outdoor room through the air pipe. The fresh air and exhausted air exchange heat and moisture through the exchanger core set at the centre. The TMCU1 and TMCU2 areas are the function units to control the temperature and moisture in each room. The rooms have such huge volume that the enthalpy variations caused by the air flowing into rooms can be ignored. So it is assumed that the temperature and moisture keep constant while air exchanging in the core. The fences are set at to make the air flow uniformly entering ducts from round-to-square connect sections. The A, B, C, D points are the probe setting site to measure the temperature, moisture and speed of air entering and flowing out of the exchanging core. At one test condition, the average values of many points got at each tunnel cross section at each probe setting site will be regarded as the property of air into or out of the core. It always takes two hours to adjust the TMCUs to satisfy the outdoor and indoor conditions at point A and D. Besides the air blowers can provide infinitely different air speed and air pressure for the device and it is facilitate to test performances at different flow rates of entering air. All of ducts, pipes and devices are covered by the isothermal cotton materials to reduce the thermal dissipation.

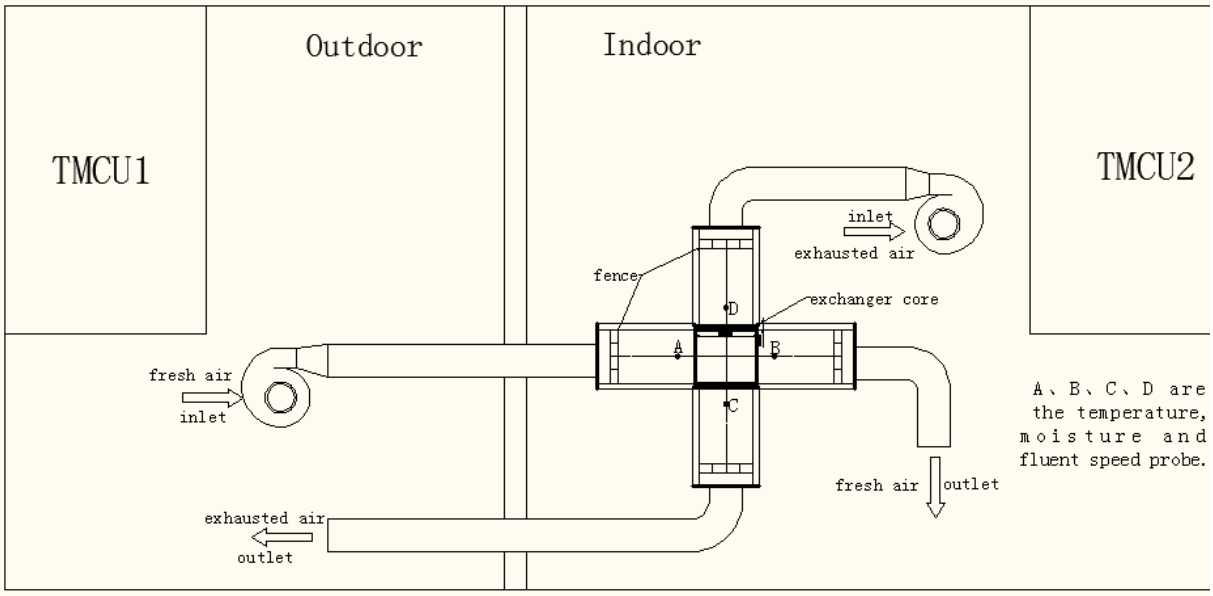

Figure 2: Schematic view of the Test Apparatus

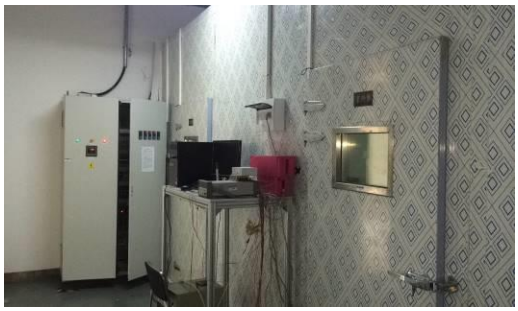

Figure 3: Psychometric rooms

Figure 4: Flow ducts in the indoor room

3. THE MODIFICATION PROCESS AND TEST CONDITONS

3.1 Modification Process

This study is to test the performances of modified exchangers treated by different concentrations of calcium chloride solutions. The treatment is to spray solutions on the materials and to dry the layers in oven for several times. As the heat and moisture transferring process only happen on the functional layers, the treatment is conducted to functional layers. The paper comes from the Tianjing Paper Inc. The calcium chloride anhydrous comes from Guoyao Chemical Reagent Company. The following is the main treatment process:

- 1. Prepare for different concentration of solution.
- 2. Spray solution on the functional layers.
- 3. Dry the layers in the oven at 80℃ for 30 minutes.
- 4. Repeat 1 and 2 for two times again.
- 5. The modified layers are spliced with gel and compressed to the exchanger core by machine.
- 6. The exchanger core is dried in the oven at 80℃ for 2 hours.

3.2 Test conditions

The size of the exchanger core is 185(mm)×185(mm)×250(mm), and the typical flow rate into the core is 0.3m/s(corresponding to 50CMH, Reynolds number 100). The flow passage of the support layer is corrugated structure, the highest and lowest points sticking with the functional layer. The height of each structure layer is 2mm and the pitch of adjacent passage is 2mm. Each side number of plates is 50.

The test standard conditions to evaluate the performance of the exchangers comes from Chinese Standard 21087-2007(GB/T 21087-2007)[6]. In the cooling condition, the bulb temperature and wet bulb temperature are 35℃ and 28℃ (corresponding air humidity is 20.91g/kg in shanghai) for fresh outdoor air, 27℃ and 19.5℃(corresponding humidity is 10.94g/kg in shanghai) for excelled indoor air, respectively. In the warming condition, the bulb temperature and wet bulb temperature are 5℃and 2℃ (corresponding air humidity is 3.08g/kg in shanghai)for fresh outdoor air, 21℃and 13℃(corresponding air humidity is 5.89g/kg in shanghai) for excelled indoor air respectively. The test flow rate into the core is from 0.1m/s to 0.5m/s.

4. DATA REDUCTION

4.1 Efficiency measurement of performance

The performance of total heat exchanger is evaluated by the efficiency of heat, moisture and enthalpy, or efficiency of sensible heat, latent heat and total heat. As we know it is difficult to remove water from air without cooling and it's hard for water to transfer through the material. So comparing with the sensible heat efficiency, the latent heat or moisture efficiency enhancement has a greater affect on the performance of total heat exchanger, especially in the cooling conditions[4].

Equation1: the definition of the efficiency.

$$e = \frac{x_{fi} - x_{fo}}{x_{fi} - x_{ei}}$$

Where:

- e indicates the efficiency of heat, moisture and enthalpy,
- x indicates the temperature, humidity and enthalpy of air measured in the test,
- subscripts fi , fo are the inlet and outlet of fresh air, subscripts
- ei is the inlet of excelled air.

4.2 Pressure drop

The pressure drop is the main index to evaluate the total heat exchanger. When the pressure drop increases, more power is needed to make sure enough ventilation volume into the room and the energy-saving effect of the exchanger decreases.

Equation2: the expression of dynamic pressure with the flow rate;

$$P_{\mathrm{d}} = \frac{1}{2}\rho v^2$$

Equation3: the expression of pressure drop of fresh and excelled air channel.

$$\Delta \mathrm{p}_f = p_{fo} - p_{fi}$$

$$\Delta \mathrm{p}_e = p_{eo} - p_{ei}$$

Where:

- ρ is density of the air, v is the flow rate of the air,
- $\Delta \mathrm{p}_f$, $\Delta \mathrm{p}_e$ are the fresh air and excelled air pressure drop,
- p_{fo} , p_{fi} , p_{eo} , p_{ei} are the dynamic pressure at outlet and inlet.

5. DISCUSSION

The functional layers are treated by the calcium chloride solutions with concentrations of 5%, 10%, 20%, 30%, 40% and compacted to be the exchanger cores by machine. Under the standard conditions, the temperature efficiency, humility efficiency and enthalpy efficiency of different cores are obtained in the test apparatus. The variations of these efficiencies with the air flow rate from 0.1 m/s to 0.5 m/s(corresponding to 18-90CMH based on the flow rate) are also tested and discussed. The results are showed in the followings.

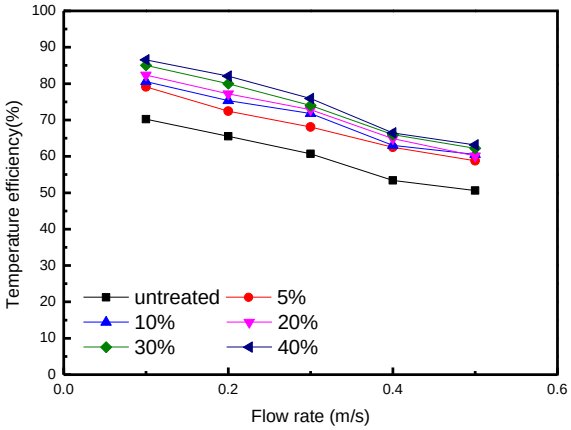

Figure.5:.The temperature efficiency for the modified exchanger cores and untreated core with air flow rate in heat condition.
Percents represents the concentrations of $CaCl_2$ solutions, the same below.

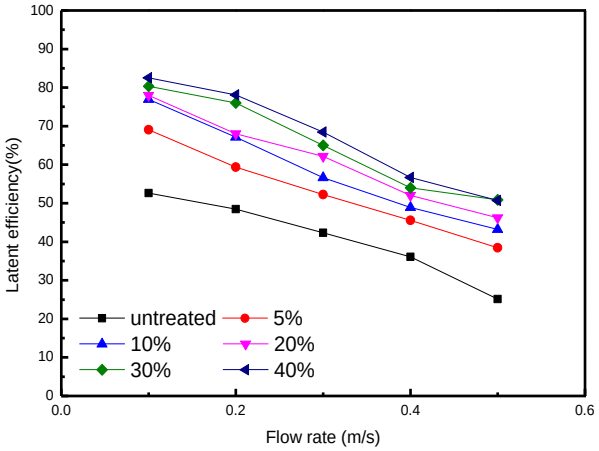

Figure.6: The latent efficiency for the modified exchanger cores and untreated core with air flow rate in heat condition

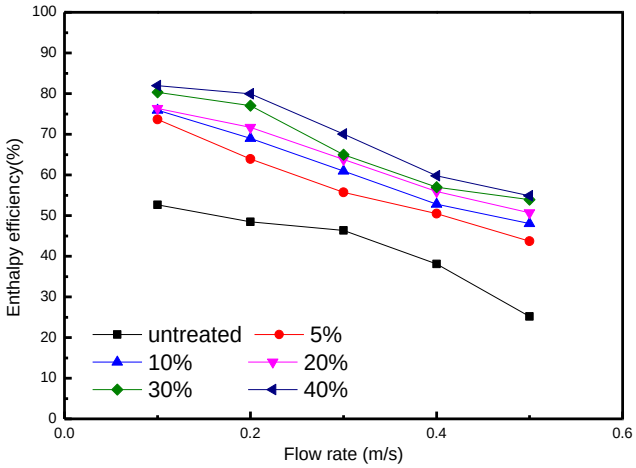

Figure.7: The enthalpy efficiency for the modified exchanger core and untreated core with air flow rate in heat condition

Figure 5 shows that the treated cores by the solutions have higher temperature efficiencies than the untreated one. At the standard flow rate 0.3m/s, the absolute enhance on temperature efficiency between the core treated by 5% solution and untreated one is 9%, the absolute enhance between the

core treated by 40% solution and untreated core is 15%. The enhance attributes to the moisture transfer process reinforced by treatment with solutions, showed in the Figure.3. At low flow rate, the difference among the different concentrations is obvious. But the at high flow rate, the efficiencies to the same area in the figure, which means the flow rate has become the limited factor for the temperature efficiencies. Figure 6 shows the latent efficiencies of modified exchanger cores and untreated one vary with the air flow rate. The efficiency decreases with increasing air flow rate. At 0.3m/s (corresponding to 50CMH, standard conditions), the absolute enhance between the core treated by 5% solutions and untreated core is 12%, the absolute enhance between the core treated by 40% and untreated core is 26%. The figure shows that the CaCl2 added into the material has obvious influence on the latent efficiency, for the water in the high humility more easily gathers in the functional layer and is taken away by the air in other channel. For the test results, it is shown that latent efficiency is always low comparing with temperature efficiency, especially at high flow rate and the air flowing speed has more effect on efficiency decreasing of humidity than that of temperature.

Figure 7 shows the enthalpy efficiencies decreases with the increasing flow rates in heat condition. At 0.3m/s, the absolute enhances between the exchanger core treated by 5%, 40% solutions and untreated core are 10%, 24%. The differences among the enthalpy efficiencies under different conditions are also very obvious. As it is known, at certain temperature, the enthalpy is mainly influenced by the humidity of air. Thus the latent efficiency is a main factor limiting the enthalpy efficiency for total heat exchangers, and enhance of latent efficiency by treating with the CaCl2 solutions will obviously improve the enthalpy efficiency.

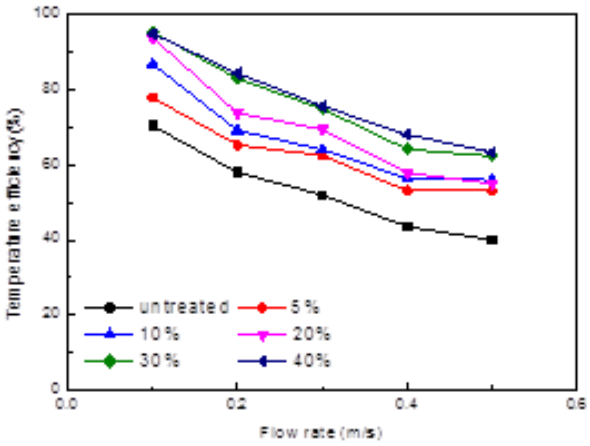

Figure.8:The temperature efficiency for the modified exchanger cores and untreated core with air flow rate in cooling condition

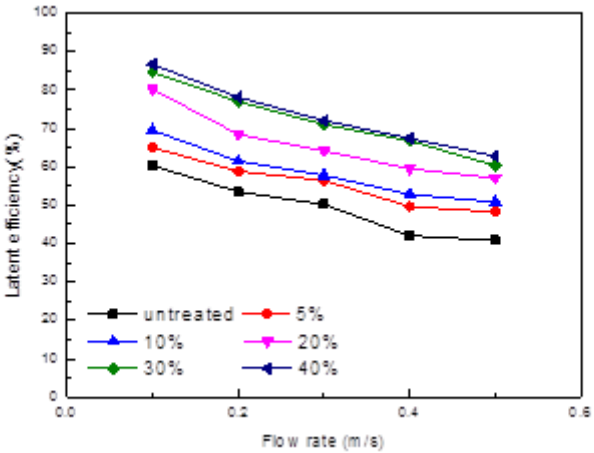

Figure.9:The latent efficiency for the modified exchanger cores and untreated core with air flow rate in cooling condition

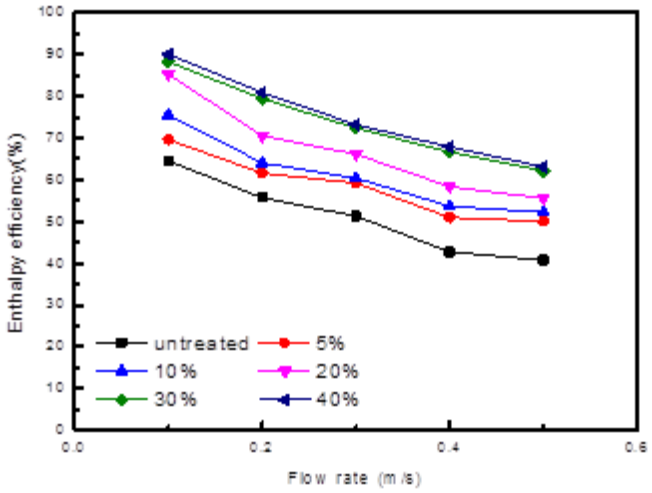

Figure.10: The enthalpy efficiency for the modified exchanger cores and untreated core with air flow rate in cooling condition

Figure 8, Figure 9, Figure 10 shows the temperature, latent and enthalpy efficiencies for the treated cores and untreated core in cooling condition. At the flow rate 0.3m/s, the absolute enhance of temperature, latent, enthalpy efficiencies between the core treated by 5% solution and untreated core are 10.5%, 6.2%, 8.0%, and that between the core treated by 40% solution and untreated core are 23.6%, 21.8%, 22.1%. Compared with that in the heat condition, the latent efficiencies for different cores in the cooling condition are higher and the differences on latent efficiencies between the treated cores and untreated core are smaller. This may account for more moisture content in summer conditions at equal relative humidity than that in winter conditions. And the function of addition of CaCl2 is more obvious in the low moisture content conditions.

Figure.11 shows the pressure drop for different cores in the heat condition. The pressure drop is defined as the dynamic pressure differences between the inlet and outlet of the channel. As Eq. (2) shown, the dynamic pressure of the air at the inlet and outlet are obtained through measuring air speed by Anemometer. The treatment with solutions does not change the flow structure inside the flow channel, so the differences of different cores are less 5 Pa, which can be ignored in heat condition. At the same time, the flow rate of air plays a dominant role on the pressure drop, which increases dramatically with the increasing flow rate. In cooling condition, as shown in Figure.12, the differences of different cores are relatively obvious for more moisture is absorbed on the material to increase the resistance of flowing over the surface. At the 0.3m/s (corresponding to 50CMH), most different values between the treated and untreated core is just 8 Pa. And it is not a big problem for total heat exchanger to overcome such increases of pressure drop.

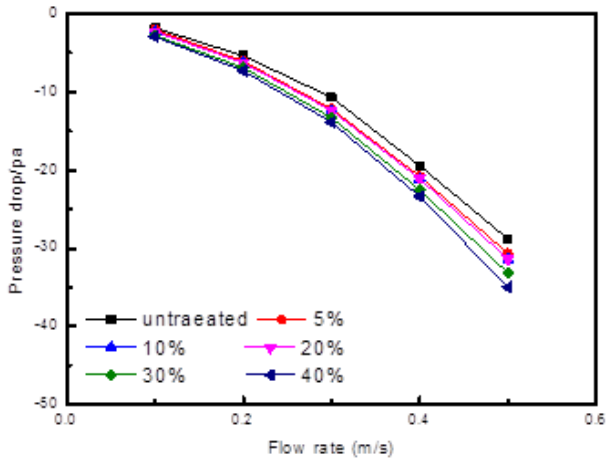

Figure.11: Pressure drop for modified cores and untreated core at different flow rates in heat condition.

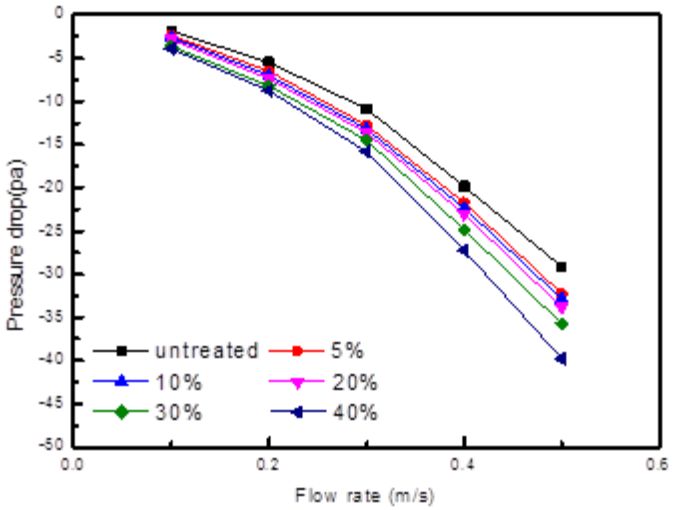

Figure.12: Pressure drop for modified cores and untreated core at different flow rates in heat condition.

6. CONCLUSION

A study has been performed to improve the efficiencies, especially latent and enthalpy efficiency of the enthalpy exchanger by modifying the functional layers with the CaCl2 solution. And the test apparatus has been built in the enthalpy difference rooms to measure the performance of different exchanger cores among the flow rate 0.1~0.5m/s. The test results and study conclusions can be summarized as followings:

- The modified exchanger cores with treated functional layers by CaCl2 solution have the higher efficiencies, especially latent and enthalpy efficiency than the untreated exchanger core. At 0.3m/s flow rate (corresponding to 50CMH, standard performance condition), the maximum absolute enhance of temperature, latent, enthalpy efficiency are 15%, 26%, 24% in the heat condition and 23.6%, 21.8%, 22.1% in the cooling condition.
- The air flow rate through the exchanger core has a remarkable influence on the efficiency of different exchangers. The efficiency would obviously decrease when the flow rate increases.
- The pressure drop increases of modified exchanger cores can be neglected in the heat condition. And compared with untreated core, the modified cores have a small improvement on pressure drop in the cooling condition.

7. REFERENCES

1. ZHANG, L.Z. and Y. Jiang, *Heat and mass transfer in a membrane-based energy recovery ventilator.* Journal of Membrane Science, 1999. **163**(1): p. 29-38.

2. NIU, J.L. and L.Z. Zhang, *Membrane-based enthalpy exchanger: material considerations and clarification of moisture resistance.* Journal of Membrane Science, 2001. **189**(2): p. 179-191.

3. LEE, Y.-C., et al., *Analysis of Cross-Flow Type of Air-to-Air Total Heat Exchangers Made of Functional Paper.* HVAC&R Research, 2005. **11**(3): p. 395-410.

4. KWAK, K. and C. Bai, A study on performance improvement of corrugated type total heat exchanger considering the structure of flow passage on surface. Journal of Mechanical Science and Technology, 2009. 23(6): p. 1528-1535.

5. LA, D., et al., Technical development of rotary desiccant dehumidification and air conditioning: A review. Renewable and Sustainable Energy Reviews, 2010. 14(1): p. 130-147.

6. 21087-2007, G.T., *Air to air enery recovery device.* 2007.

SESSION 14: SMART AND RESPONSIVE BUILDINGS

170: Numerical analysis of the humidity buffering potential of various hygrothermal coatings under extreme moisture overloading scenarios

Sean P CASEY[1]

[1] 1Division of Infrastructure, Geomatics and Architecture, Faculty of Engineering, University of Nottingham, University Park, Nottingham, NG7 2RD, UK, sean.casey@nottingham.ac.uk

Within a closed environment, (e.g. building, car, aircraft) that is hygrically isolated from the exterior climate, one approach that can help reduce the energy required for indoor climate control whilst increasing comfort levels for occupants is to use hygrothermal coatings on top of existing materials. These coatings can re-introduce hygric buffering within the isolated envelope that was lost due to application of retrofitted internal finishes (i.e. – insulation, vapour barriers, paint etc.).

The aim of this paper was to perform a parametric analysis using hygrothermal numerical software (WUFI Plus v2.1.1.73) of the humidity buffering potential of various hygrothermal coatings applied to a nominal enclosed indoor environment under extreme moisture loading scenarios and air exchange rates. Three coatings were compared: gypsum plaster, spruce timber and a 'super absorbent' desiccant under four building envelope scenarios. The location was chosen as Nottingham, UK and an external climate file was generated to sinusoidally fluctuate exterior relative humidity (RHext) about a median (50%) at constant temperature (T = 23 ºC) for a single peak to peak cycle period of t = 24h. Two sets of increased moisture profiles were applied to the model in order to represent 16 'Active Adults' present in either the morning or evening for a period of t = 4 h.

The analysis showed that there was minimal reduction of minimum indoor (RHint) levels when using traditional building materials as interior finishes (i.e. spruce and gypsum), indicating the greater influence of the external environment, RHext on the interior environment as the air exchange rate increased. In contrast, when utilising the super-adsorbent materials, RHint levels remained within the ASHRAE limits (i.e. 40% ≤ RHint ≤ 70% and T = 23 ºC) under both morning and evening overloading schedules and across the full range of air exchange rates.

Keywords: Humidity Buffering, Comfort, WUFI, Super-adsorbent

1. INTRODUCTION

Within a closed environment, (e.g. building, car, aircraft) that is hygrically isolated from the exterior climate, one approach that can help reduce the energy required for indoor climate control whilst increasing comfort levels and Indoor Air Quality (IAQ) for occupants, is to use hygrothermal coatings on top of existing materials. These coatings can re-introduce a level hygric buffering within the isolated envelope that was lost due to application of retrofitted internal finishes (i.e. – insulation, vapour barriers, paint etc.). Hygrothermal coatings can vary from clays (Liuzzi et al., 2013), timbers (Hameury, 2005), zeolites (Feng and Peng, 2005) or super-adsorbents (SA)(Sarce Thomann et al., 2015, Casey et al., 2012).

Poor occupant health can manifest as "sick building syndrome" caused by reduced levels of *RH,* whilst elevated *RH* levels can lead to irritation of the upper respiratory tract. Energy penalties can also be incurred due to the additional interior climate control required from mechanical systems such as Heating Ventilation and Air Conditioning (HVAC) (Kalamees et al., 2009, Liddament and Orme, 1998, Orme, 2001). Occupant comfort is a person's perceived comfort level in relation to their environment. According to the standard BS EN ISO 7730:2005 (BSi, 2005) comfort can be defined as the condition of mind which expresses satisfaction with the thermal environment. In the context of this research the environment is a closed space. Comfort is not determined from temperature only (Parsons, 2003), but from the interaction of other parameters including:

1. air temperature
2. mean radiant temperature
3. relative humidity
4. air velocity
5. metabolic heat generation
6. clothing

The human body is constantly subjected to the influences of the environmental factors (1, 2, 3 and 4) with utilisation of the personal factors (5 and 6) to achieve comfort. In an attempt to regulate itself at a constant temperature, the body uses biological thermoregulation processes to act against these influences; evaporation of sweat, respiratory evaporation, conduction, convection via the blood, radiation and metabolic storage. An over-occupied closed environment can result in increased fluctuations of *T* and *RH*. Combining these can lead to moisture accumulation within the indoor space due to decreased air exchange with the exterior environment, reducing IAQ. The relative impact of various pollutants, their associated biological problems and sources across the *RH* range can be seen in Figure 1.

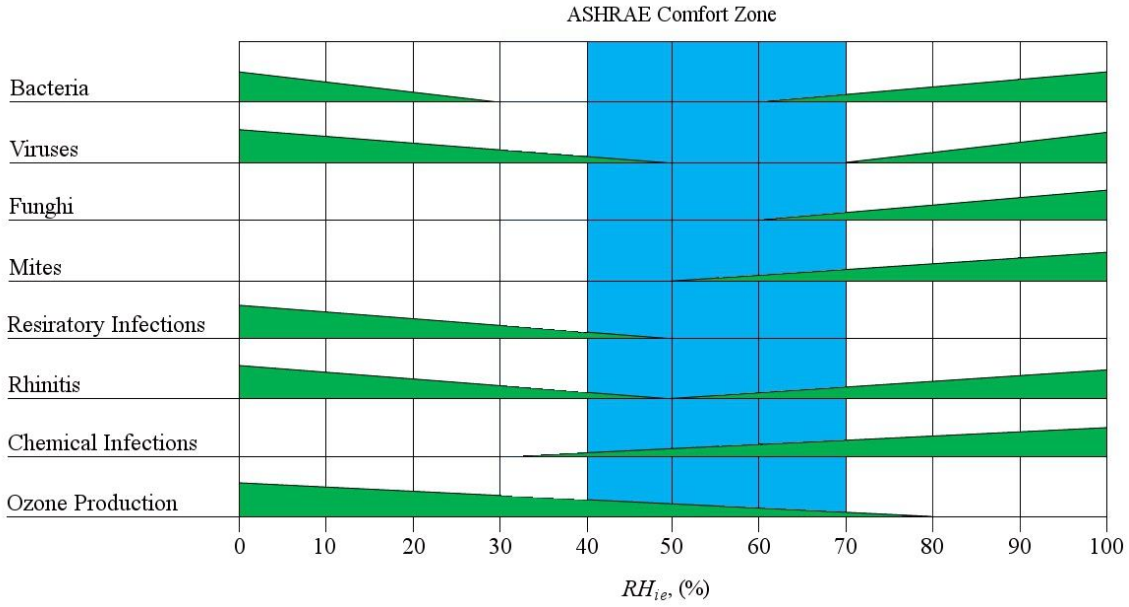

Figure 1 - Factors influencing health and hygiene showing comfort range. Adapted from: (Simonson et al., 2001).

The aim of this research was to perform a parametric analysis using hygrothermal numerical software (WUFI Plus v2.1.1.73) of the humidity buffering potential of various hygrothermal coatings applied to a nominal enclosed indoor environment under extreme moisture loading scenarios and air exchange rates.

2. METHODOLOGY

To analyse the resultant psychrometric conditions in a nominal enclosed indoor environment under extreme moisture loading scenarios and air exchange rates, the hygrothermal numerical software WUFI Plus v2.1.1.73 was used. WUFI Plus combines the analysis of all walls, floors, ceilings and other envelope components to perform 3D whole building analysis, using differential equations for transient heat and moisture (HAM) transport and storage. WUFI Plus also provides data on occupant comfort, operational energy in addition to predictive data on the hygrothermal performance of each envelope assembly.

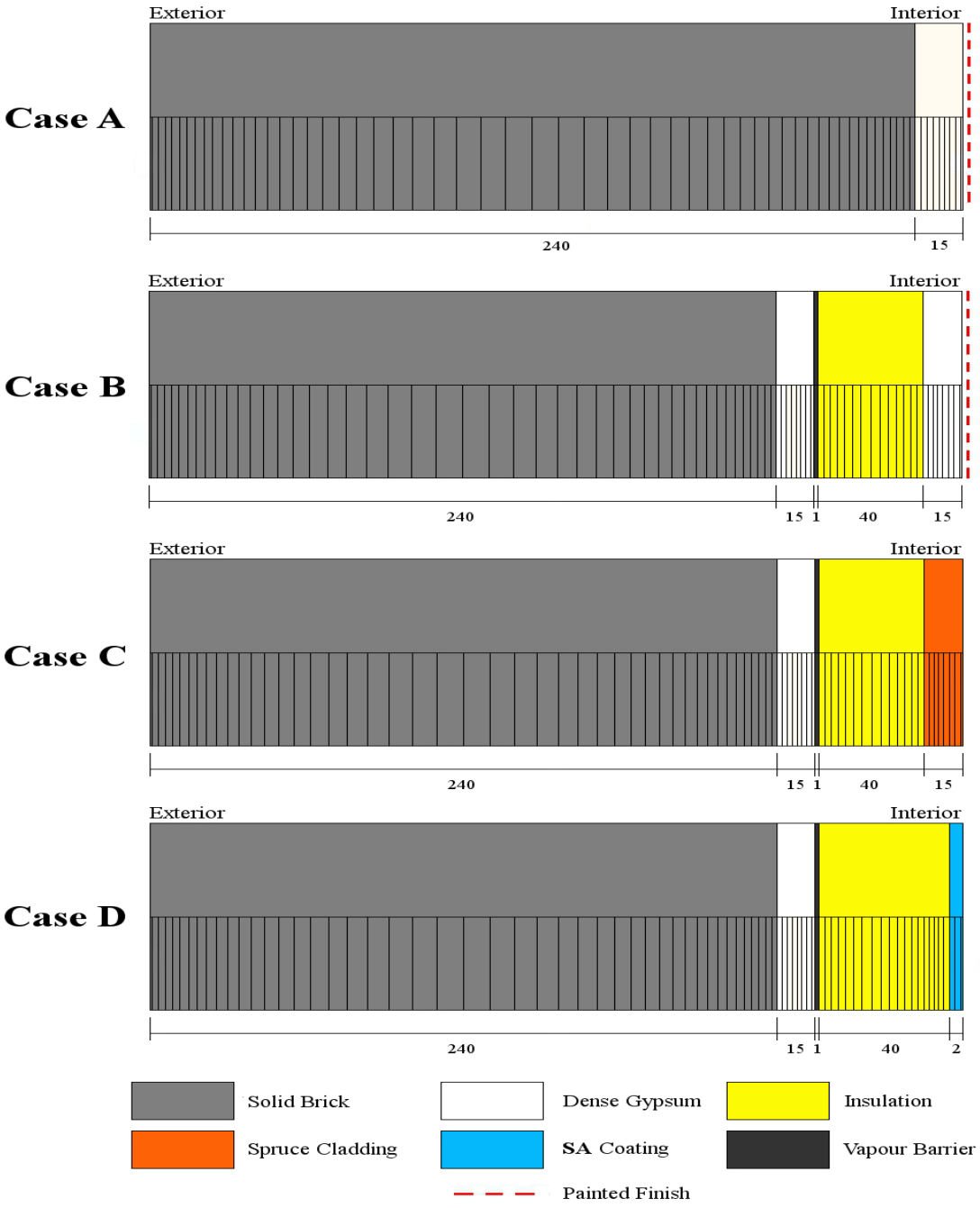

Figure 2 – Assemblies used for the numerical building retrofit model showing grid spacing.

As the main focus of interest in this research was the performance of the hygrothermal materials and to simplify the modelling and speed up convergence, it was decided to use a 1m^3 simple 'box' model rather than a complex realistic simulated building. A total of four building scenarios were simulated to represent the retrofitting of a typical building with identical material properties, parameters and dimensions (see: Figure 2). The envelope assemblies used for all walls, floors and ceilings (for each case) remained the same. The four cases were:

Case 1. Old wall - A solid brick wall with 15mm dense gypsum plaster having a painted interior surface finish.
Case 2. Retrofitted gypsum wall - A solid brick wall with dense gypsum plaster. Retrofitted internally with a vapour barrier, vacuum insulation panel and dense gypsum plaster panelling with painted surface finish.
Case 3. Retrofitted timber wall - A solid brick wall with dense gypsum plaster. Retrofitted internally with a vapour barrier, vacuum insulation panel and unfinished spruce cladding.
Case 4. Retrofitted SA wall - A solid brick wall with dense gypsum plaster. Retrofitted internally with a vapour barrier, vacuum insulation panel and a thin super-adsorbent (SA) material coating.

In the numerical model a minimum internal volume of 1m^3 is permissible due to software limits. As published occupant generation rates (heat and moisture are applicable to a standard room volume (*i.e.* 38.4 m3), it was necessary to scale the standardised moisture generation rates, to the corresponding volume of the numerical model. The volume adjusted occupant generation rates (assuming linearity) are shown in Table 1.

Standard room, V_{sr} 4m x 4m x 2.4m = 38.4m^3

Numerical model, V_{nm} 1m x 1m x 1m = 1m^3

Scaling Factor, S_f V_{sr} / V_{ib} = 38.4

Table 1 - Volume adjusted occupant loads for the 1m^3 numerical model calculated from: (BSi, 2011)

	Moisture Load (g/h)	Thermal Conductive (W)	Thermal Radiant (W)	CO2 Load (g/h)
Toddler (3 – 6 years)	2.34	0.52	0.31	0.83
Teenager (14 – 16 Years)	1.30	1.56	0.78	0.88
Adult - Sedentary	1.12	1.69	0.93	0.79
Adult – Desk Work	1.53	2.08	1.06	0.94
Adult - Active	3.20	4.11	1.22	1.57
Cooking (Gas)	3.25	---	---	---
Showering	62.5	---	---	---

The increased moisture load model was designed to assess the effects of the hygrothermal materials on the indoor conditions under a moisture 'over-loading' scenario. An example of this would be a large gathering of people in a house or use of excessive moisture generating equipment (*i.e.* steam cleaner, cooking, showering). The external climate file was generated to sinusoidally fluctuate RH_{ext} about a median (RH_{ext} = 50%) at constant temperature (T = 23 °C) for a single peak to peak cycle period t = 24h:

RH_{ext} 15% → 85% → 15% giving a ΔRH_{ext} = 70%

Two sets of increased moisture profiles were applied to the interior climate of the model in order to represent 16 'active adults' present in either the morning or evening for a period of t = 4 h. Table 2 contains the profiles of times and moisture loads, g_g. with a visual representation of the interaction of RH_{ext} and g_g shown in Figure 3. The simulation was also further expanded by running the same set of moisture load simulations under four different air exchange rates to assess the impact of air infiltration on ΔRH_{ext} sensitivity.

Table 2 - Morning and evening moisture profiles for the increased occupancy numerical model.

Morning Occupancy		Evening Occupancy	
Time (h)	g_g (g/h)	Time (h)	g_g (g/h)
0 to 8	0	0 to 18	0
8 to 12	51.25	18 to 22	51.25
12 to 24	0	22 to 24	0

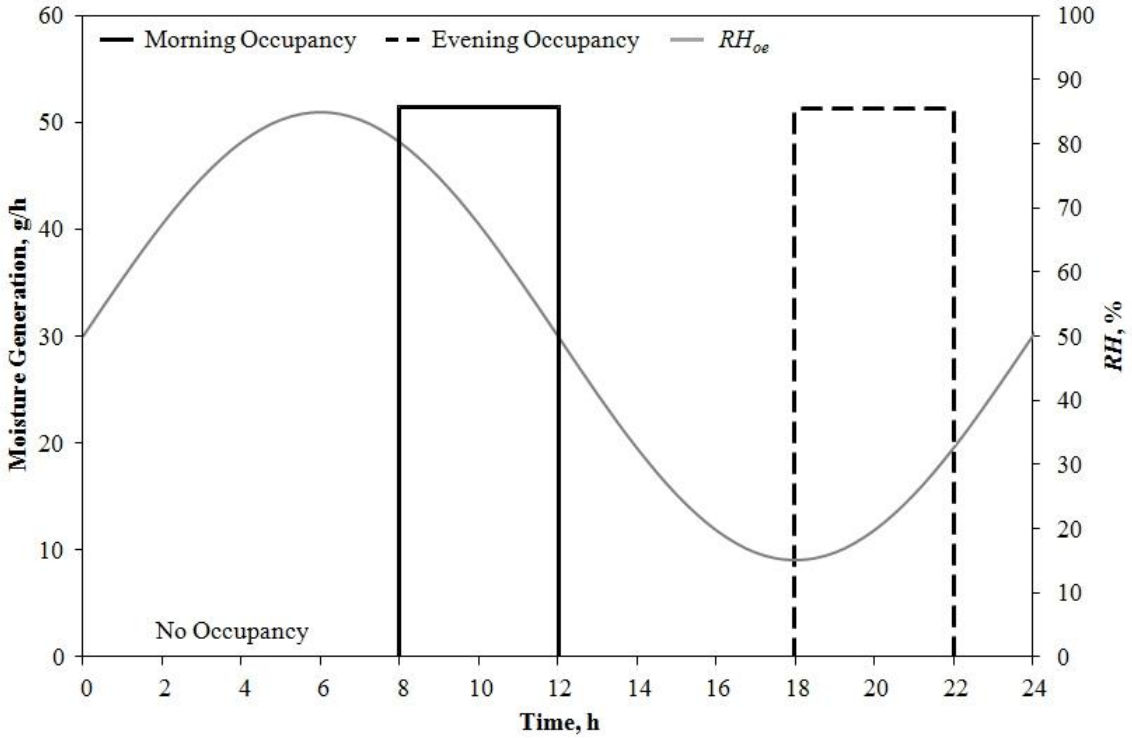

Figure 3 - Graph showing 'over-loading' occupancy schedules and sinusoidal variation of RHext for the increased moisture load model.

3. RESULTS & DISCUSSION

A series of increased moisture load simulations, designed to assess ΔRH_{ie} levels under a moisture 'over-loading' scenario were simulated using WUFI Plus as described in the previous section. The range and scale of RH_{ie} for both morning and evening schedules were plotted for an airtight scenario and across a series of different air exchange rates (AER)(see: Figure 3). Figure 4 shows an example of the full data set where the ACH was set at 1 h^{-1}.

Figure 4 shows that there is a sinusoidal nature for Case 1 (Old Wall) and Case 2 (Retrofitted Wall) with the plot of RH_{ie} tracking the exterior *RH* due to the high AER, although with a reduction in the sinusoidal peak at RH_{ie} = 67% (compared to RH_{ext} = 85%). As expected, when the moisture overload is introduced into the interior, there is a surge in RH_{ie} at t = 08:00h each day. As there is a two-way exchange between moisture in the interior and exterior environments due to the high ARE, RH_{ie} eventually resumes the sinusoidal shape again tracking RH_{ext}. For Case 3 (Spruce Timber), there is a much reduced level of fluctuation in RH_{ie} levels due to its hygric buffering potential with a maximum indoor humidity level of RH_{ie} = 87% on day seven. There is no evidence of 'tracking' as in the previous two cases, however there is some hysteresis evident (*i.e.* gradual increase in mean moisture level over the seven days) which is attributable to the greater levels of adsorption in the timber and can occur due to adsorption of the moisture vapour on the pore walls having a high enthalpy of vaporisation, requiring greater energy to desorb from the pore volume when the relative vapour pressure is negative (i.e. lower RH_{ie}). In Case 4 (Super-Adsorbent), it is clear that, even with high levels of air exchange between the interior and exterior environments, there is little variation of RH_{ie} levels over the seven days. As in Case 3, there is no evidence of 'tracking' of RH_{ext}, however there is hysteresis evident. In reality, moisture overloading scenarios would not be expected to occur every day and the interior coating would be expected to receive a 'break' allowing its moisture levels to return to their original state.

As there were a total of forty simulations run for the four interior coating cases across morning, evening overloading and five AER levels, the remaining results have been summarised into four graphs. The graphs each show one case with morning and evening moisture schedules across the five AER levels. Individual traces of RH_{ie} have been removed and are replaced with maximum and minimum levels observed over the seven cycles.

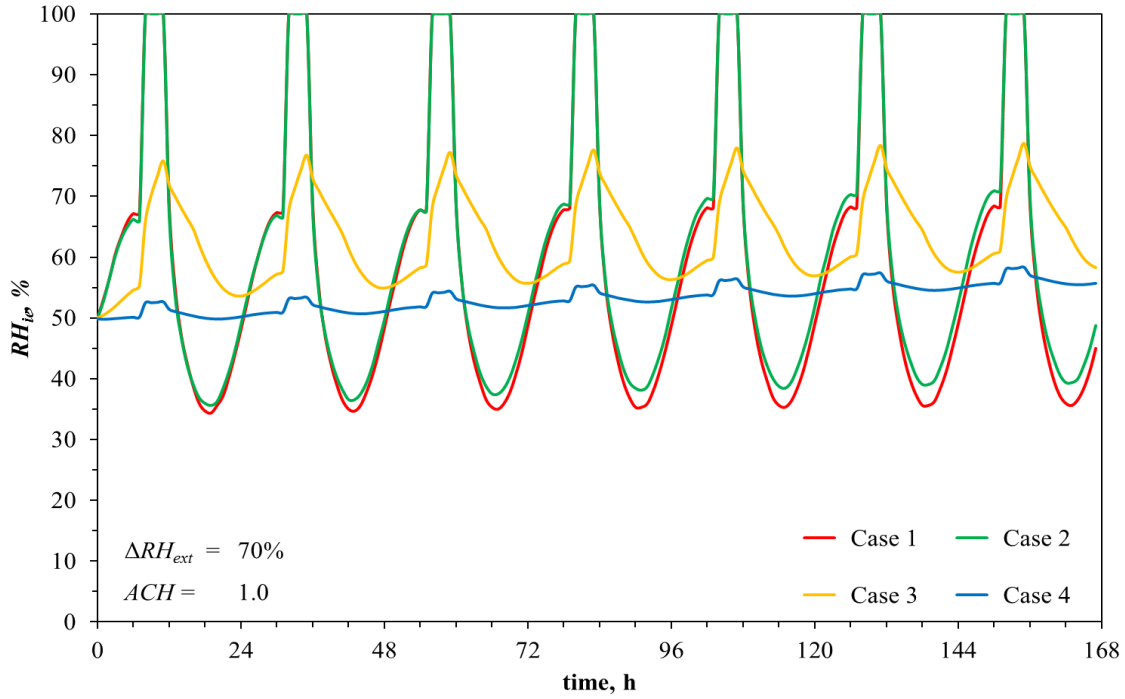

Figure 4 - Graph showing the full data set of RH_{ie} variation for four cases under increased morning moisture loads.

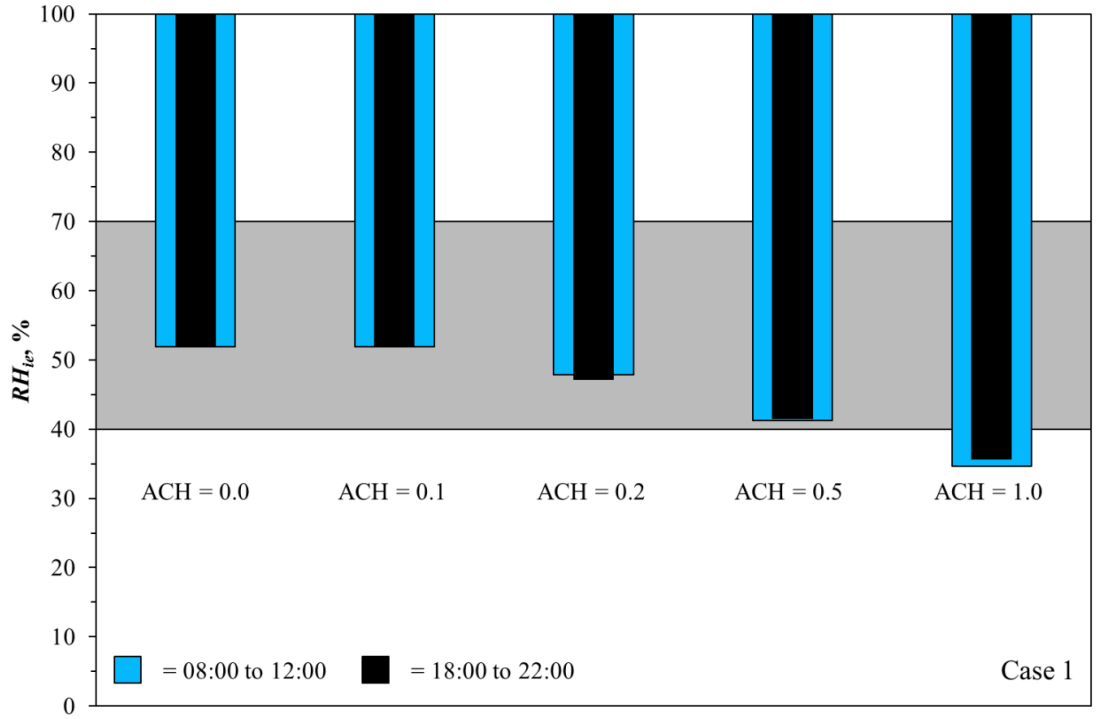

Figure 5 - Graph showing maximum and minimum RHie levels for increased moisture loads under five air exchange rates for Case 1 (Old Wall)

The results showed a general reduction of minimum RH_{ie} levels for the three non super-adsorbent (SA) cases (gypsum & timber) as the AER increased, indicating the increasing influence of the exterior

relative humidity, RH_{ext} as air exchange rate increases (see: Figure 5). Both the old and retrofitted walls displayed predicted maximum ΔRH_{ie} fluctuations of up to 67% (AER = 1.0 h^{-1}) with mean RH_{ie} values exceeding the upper ASHRAE limit (>70%) across all AER levels. In addition, upper RH_{ie} levels for both gypsum cases reached 100% for both schedules across all air exchange rates. There were minimal differences observed between Case 1 and Case 2 as both cases have the same interior coating (painted gypsum) and thus Case 2 is not shown as a figure. With RH_{ie} levels regularly reaching 100% for sustained periods of time and, in some cases, never dropping below 50%, the indoor environment would not only be uncomfortable for occupants, but also very dangerous. As mentioned in Section 1, elevated *RH* levels can have health issues for occupants including irritation of the upper respiratory system including nasal congestion, sneezing, runny or itchy nose and throat irritation, as well as coughing, wheezing and asthma. Interaction of the high vapour content of the air with the building envelope structure can also negatively affect building performance in terms of resilience. This environment can encourage mould (fungi) to form on or within the envelope, especially in Case 1 where there is no thermal isolation and also allow bacteria and viruses to thrive.

The spruce cladding (see: Figure 6) performed better with a maximum ΔRH_{ie} of 22% fluctuating about a mean RH_{ie} of 63% (AER = 1.0 h^{-1}) but with upper RH_{ie} levels outside the 40-70% ASHRAE comfort limits across all AER levels. Whilst not at the dangerous levels observed in Cases 1 & 2, this wold still prove uncomfortable for occupants, especially in the lower AER environments where peak RH_{ie} reached levels of 85% during evening overloading.

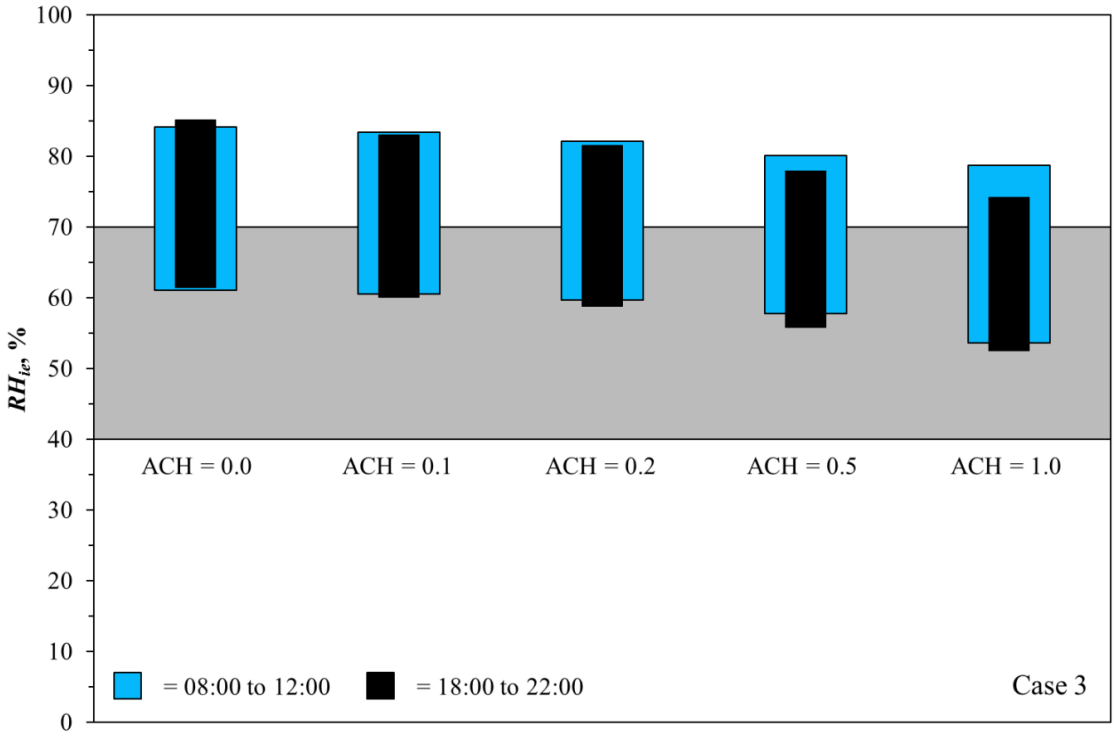

Figure 6 - Graph showing maximum and minimum RHie levels for increased moisture loads under five air exchange rates for Case 3 (Spruce Timber)

In contrast, in the super-adsorbent material (Case 4), RH_{ie} levels remained within the ASHRAE limits under both morning and evening overloading schedules and across the full range of air exchange. The SA material used in this research was composed of mesoporous silica (MS). These MS materials are highly porous silica solids with tightly controlled pore size distributions in the mesopore range (2nm ≤ $Ø_{pore}$ ≤ 50nm). Ordered MS materials were first developed during the 1990s with well researched variants MCM-41 (Beck et al., 1992) and SBA-15 (Zhao et al., 1998) developed as larger pore size variants of molecular sieves. MS materials typically display very high porosity (>90%) and specific surface area (typically 750–1500 m^2/g) and have the significant advantage of being synthesized with a controllable pore geometry (shape, diameter) (Jana et al., 2004). As a result, MS materials exhibit high moisture vapour storage levels within the hygroscopic regions of their adsorption isotherms, but with some hysteresis on desorption in subsequent cycles. This can be indicative of a slight decrease of pore size due to chemisorption of the water molecules over the initial sorption cycles. MS materials also show

very rapid sorption response times to amplitude variations of *RH*, making them inherently suitable to humidity buffering applications.

From Figure 7 we can see that the SA performed better than all the other coatings with a maximum relative humidity variation of ΔRH_{ie} = 7.5% fluctuating about a mean RH_{ie} of 53% (ACH = 1.0). These simulations demonstrate the ability of the MS materials to continually buffer RH_{ie} fluctuations even when subjected to repeated moisture overloading scenarios over a seven day period. In terms of occupant comfort, the SA material provided exceptional buffering performance which should provide a comfortable environment (within ASHRAE comfort limits) in enclosed, retrofitted spaces. The use of SA materials also suggests that a reduction in energy use (when compared to use of HVAC control) is possible due to a reduction in dehumidification energy.

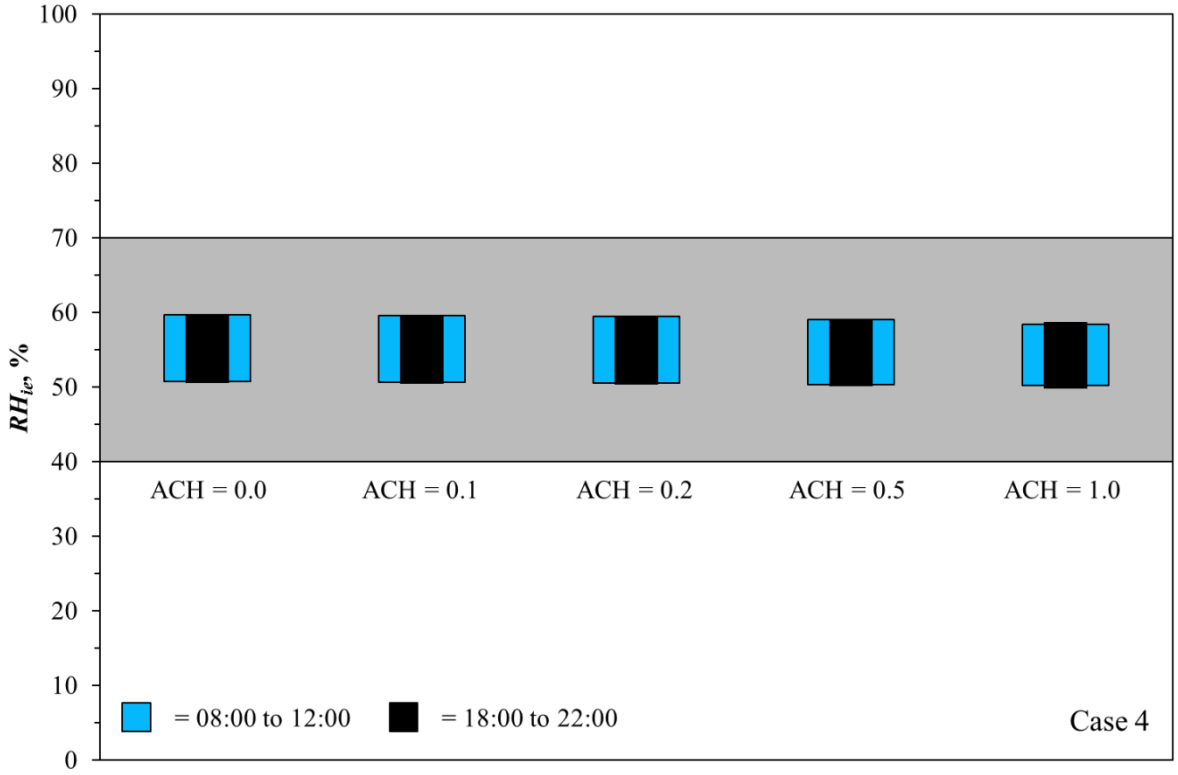

Figure 7 - Graph showing maximum and minimum RH_{ie} levels for increased moisture loads under five air exchange rates for Case 4 (Super-Adsorbent)

4. CONCLUSION

The aim of this research was to perform a parametric analysis using the hygrothermal numerical software WUFI Plus of the humidity buffering potential of various hygrothermal coatings applied to a nominal enclosed indoor environment under extreme moisture loading scenarios and air exchange rates. The main findings were:

1. In both the 'Old Wall' and 'Retrofitted' cases, with RH_{ie} levels regularly reaching 100% for sustained periods of time, the indoor environment would not only be uncomfortable for occupants, but also potentially dangerous.
2. The spruce cladding performed better than the gypsum cases with a maximum relative humidity variation of ΔRH_{ie} = 22% but with upper levels outside the ASHRAE comfort limits.
3. The Super-Adsorbent performed better than all the other coatings with a maximum of ΔRH_{ie} = 7.5% This demonstrates the ability of the SA materials to continually buffer *humidity* even when subjected to repeated moisture overloading scenarios.
4. Whilst there are documented energy savings achievable by applying retrofitting strategies to older buildings, there are clearly concerns regarding indoor environmental conditions that must be addressed in tandem with any works in order to maintain occupant comfort, indoor air quality and prevent building fabric degradation.

5. REFERENCES

BSI 2005. BS EN ISO 7730:2005: Ergonomics of the thermal environment. Analytical determination and interpretation of thermal comfort using calculation of the PMV and PPD indices and local thermal comfort criteria. London: BSI Group.

BSI 2011. BS 5250:2011: Code of practice for control of condensation in buildings. London: BSi Group.

CASEY, S. P., HALL, M. R., TSANG, S. C. E. & KHAN, M. A. 2012. Nanocomposite materials for rapid-response interior air humidity buffering in closed environments. Journal of Building Performance Simulation, 1-13.

FENG, N.-Q. & PENG, G.-F. 2005. Applications of natural zeolite to construction and building materials in China. Construction and Building Materials, 19, 579-584.

HAMEURY, S. 2005. Moisture buffering capacity of heavy timber structures directly exposed to an indoor climate: a numerical study. Building and Environment, 40, 1400-1412.

KALAMEES, T., KORPI, M., VINHA, J. & KURNITSKI, J. 2009. The effects of ventilation systems and building fabric on the stability of indoor temperature and humidity in Finnish detached houses. Building and Environment, 44, 1643-1650.

LIDDAMENT, M. W. & ORME, M. 1998. Energy and ventilation. Applied Thermal Engineering, 18, 1101-1109.

LIUZZI, S., HALL, M. R., STEFANIZZI, P. & CASEY, S. P. 2013. Hygrothermal behaviour and relative humidity buffering of unfired and hydrated lime-stabilised clay composites in a Mediterranean climate. Building and Environment, 61, 82-92.

ORME, M. 2001. Estimates of the energy impact of ventilation and associated financial expenditures. Energy and Buildings, 33, 199-205.

PARSONS, K. C. 2003. Human thermal environments: the effects of hot, moderate, and cold environments on human health, comfort, and performance, , London, Taylor & Francis.

SARCE THOMANN, F., HALL, M. R., SANGCHOOM, W. & MOKAYA, R. 2015. A hygrothermal modelling approach to water vapour sorption isotherm design for mesoporous humidity buffers. Microporous and Mesoporous Materials, 211, 113-123.

SIMONSON, C. J., OJANEN, T. & SALONVAARA, M. 2001. Improving indoor climate and comfort with wooden structures. Technical Research Centre of Finland.

148: Fabrication and commercial demands of self-cleaning hydrophobic surface for buildings

HONGXIA CHEN [1], YUYING YAN[2], YANGLI MAO [3]

1 Energy Sustainability Research Division, Faculty of Engineering, University of Nottingham, UK, NG9 2RD,
Energy Power and Mechanical Engineering, North China Electronic Power University, China, Beijing 102206, hongxia.chen@nottingham.ac.uk
2 Energy Sustainability Research Division, Faculty of Engineering, University of Nottingham, UK, NG9 2RD, yuying.yan@nottingham..ac.uk
3 Energy Sustainability Research Division, Faculty of Engineering, University of Nottingham, UK, NG9 2RD, yangli.mao@nottingham.ac.uk

The super-hydrophobic surface has been a subject of intense interest over the past several years. A considerable amount of work has been carried out to study the involved mechanisms and principles, preparation methods. With the development of economic the number of skyscraper and high-rise building is continues increasing around the world during past several years. Higher the building the cleaning working is more danger and more expensive, so many skyscrapers produce enormous demands of self-cleaning coating. While, Self-cleaning coatings play their role with two mechanisms: super-hydrophilic and super-hydrophobic. Super-hydrophobic surfaces with a contact angle bigger than 150°and a low contact angle hysteresis (less than 10°) show real self-cleaning mechanical with forming a lay of air to keep the droplet stay at the top of hierarchical structures which is different from that of hydrophilic self-cleaning surface. But in the market the super-hydrophobic self-cleaning coating has not been popular until now for multifunctional demands and technological difficulties. In this paper, advanced technologies of fabrication and the commercial demands were jointed together. With the data of the distribution of skyscrapers a huge market for self-cleaning coating is shown all over the world especially in Asia. Current advanced studies on self-cleaning super-hydrophobic coatings are summarizes especially involved in the building application for its visible rapid-increased commercial demand. According to the analysis on potential market, Super-hydrophobic self-cleaning surfaces show a numerous application potential for smart building with lowest cleaning cost. In addition, more performances such as solar control, energy conservation and thermal insulation are urgent requirements of widening commercial market; prolonged lifetime, high adhesion, transparency, wear resistance and regeneration should be got more concern to cooperate with self-cleaning character in the further research work on the super-hydrophobic coating. In the nearly future, based on the mature technology and the advanced studies, surface functional materials must be serve import role in the passive building without anything consumption.

Keywords: super-hydrophobic surface; self-cleaning; smart building; low cost; commercial demand

1. INTRODUCTION

The super-hydrophobic (hydrophobic) surface has been a subject of intense interest over the past several years. It original from the natural surfaces displayed such unconventional wettabilities against water. A considerable amount of work has been carried out to study the involved mechanisms and principles (Extrand, 2002:7991-7999,Wong et al., 2009:6500-6603), preparation methods such as plasma treatment (Fernandez-Blazquez et al., 2011:234-238), lithography(Zhang et al., 2009:7375-7382), templating (Yao and He, 2014:94-143), sol-gel process (Manca et al., 2009:6357-6362), chemical vapour deposition (Zhang et al., 2009:7375-7382), electrospinning (Tang et al., 2009:14220-14224) etc. With the gradually ripeness of the research and the fabrication technology, the applications of the super-hydrophobic (hydrophobic) surface are very wide, ranging from prevent wetting (Park and Choi, 2014:1-9) (especially in electronic device and clothing), anti-corrosion on the metal surface (Yuan et al., 2011:2738-2747), to heat transfer enhancement (Park and Choi, 2014:1-9), reduce drag (Bhushan, 2011:66-84), collect water (Park et al.,2013:13269-13277), self-cleaning (Midtdal and Jelle, 2013:126-141) et al.. Recently, some reviews reported multifunctional composite materials (Ragesh et al.,2014:14773-14797) and cleaning glazing products of today industry, while (Midtdal and Jelle, 2013:126-141), building self-cleaning industry with huge commercial potential is the important motivation of self-cleaning coating researches.

Collaboration of industries and academics has brought out the safe glass technology widely used in windshield, display counter and building windows in 1960s, which demonstrate that the cooperation model is not only a support and guide to further research but also a promotion to industry development. In the meantime, self-cleaning super-hydrophobic surfaces with dirt-removing power and friendly environment material (low VOC included in normal detergents) have an enormous commercial demand and potential because of a large cleaning saves in buildings. Therefore, there's an urgent need of an application status review on building self-cleaning surfaces from commercial perspective to inspire more brilliant researches for a broad performance and development of self-cleaning industry. The objective of this study is to attain an overview of self-cleaning research, commercial potential and analysis in order to attain an overview and perspective on self-cleaning super-hydrophobic surface to inspire more brilliant researches for a broad performance and development of self-cleaning industry.

2. SELF-CLEANING PERFORMANCES IN NATURE

The conception of self-cleaning surface comes from nature such as the lotus leaf, taro leaf, bird feather, India canna, rice leaves and other living things with hierarchical structures, these hierarchical surfaces always have high contact angle and low contact angle hysteresis. As shown in Figure , air can be trapped in the grooves by roughness and form a gas layer. When the water droplet contacts the surface, this behaviour of droplet is dependent upon the balance of water's inherent attraction to itself and its attraction to air and solid surfaces. While, Contaminants are usually larger than structure of leaves and rest on the top of the structure. These dirt particles can be adsorbed to the rolling water droplet and rushed away from the surface. The distribution pattern and direction of microstructures are also very important to the gliding of droplet. As show in As well known, Gecko can catch the wall easily and rapidly remove, all due to the attractive forces of millions of hierarchical setaes on their toes known as "frictional adhesive". The petal surface with separated islands and multi-scale structure shows hydrophobic not self-cleaning character for its called "Cassie impregnating wetting state" (Bhushan and Nosonovsky, 2010:4713-4728).this cassie impregnating wetting state endow the petal strong adhesion. That is why many crystal dews always exist on rose surface not slide away.

, butterfly edges are regularly arranged and overlapped like roof tile, the incline scutums decrease the contact chance of droplet and subtract; meanwhile, upper wings have stronger hydrophobic performance (Byun et al., 2009:63-70) with micro-and nano-scaled guiding grooves. The guiding structures give the motive force and prompt the droplet glide downward. But not all surfaces with these micro and nano-structure will have the self-cleaning performance.

As well known, Gecko can catch the wall easily and rapidly remove, all due to the attractive forces of millions of hierarchical setaes on their toes known as "frictional adhesive". The petal surface with separated islands and multi-scale structure shows hydrophobic not self-cleaning character for its called "Cassie impregnating wetting state" (Bhushan and Nosonovsky, 2010:4713-4728).this cassie impregnating wetting state endow the petal strong adhesion. That is why many crystal dews always exist on rose surface not slide away.

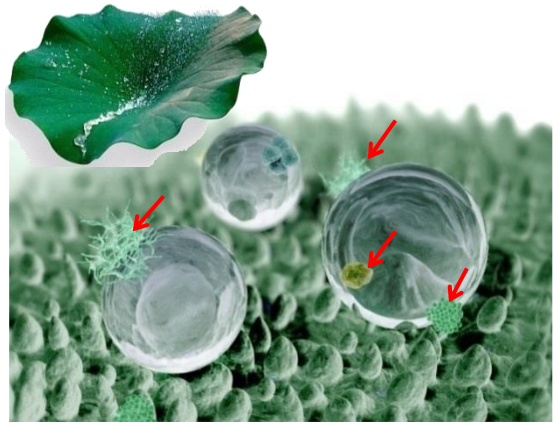

Figure 1: Lotus effect: microscopic bumps across the leaf and self-cleaning effect (Ebert and Bhushan, 2012:584-591)

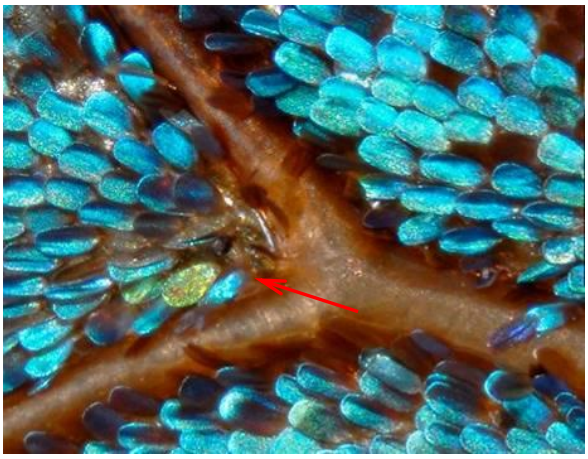

Figure 2: Butterfly wing's directional scutus (Fang et al., 2008:127-133)

3. FUNDAMENTAL THEORIES FOR SELF-CLEANING SURFACE

Wenzel equation and Cassie-Baxter equation are used to describe the relationship between roughness and contact angle. In Wenzel equation, it assumes the liquid penetrate into the roughness grooves based on hydrophilic hierarchical structures. While the Cassie-Baxter (CB) equation (Equation 1) is belonging to the other one- heterogeneous wetting regime which liquid only contact with solid surface at the top of 'sawtooth'. In CB equation, the apparent contact angle θ_w^* is a function of contact angle θ and ϕ_s. ϕ_s is a ratio of contact area at top of the sawtooth and the sum area of solid/liquid and liquid/air interfaces.

Equation 3: Cassie-Baxter (CB) equation describes the relationship between roughness and contact angel.

$$cos\theta_w^* = -1 + \phi_s(cos\theta + 1)$$

Where:

- θ_w^* = apparent contact angle (°)
- θ = contact angle (°)
- ϕ_s = a ration of contact area and the sum area

As known, the larger the contact angle, the stronger the hydrophobic. Usually, the surface with $\theta > 150^\circ$ named the super hydrophobic material. There are numbers of studies work on high contact angles of liquid droplets on artificial super hydrophobic surfaces(Gao and McCarthy, 2007:9125-9127, Yan et al., 2011:80-105).Only the maximum contact angle is not enough to define a stable super hydrophobic state, the contact angle hysteresis must be taken into account especially the destination is self-cleaning effect. The definition of hysteresis (*H*) is the difference between the advancing angel and the receding angle: $H = \theta_A - \theta_R$. A hierarchical structural surface which is close to natural super hydrophobic surface has present barriers to the motion of the liquid when it spreads and as well as when it drying. Therefore, it can cause increase in advancing angle and decrease at receding angle, then CAH (contact angel hysteresis) will increase. The really self cleaning super-hydrophobic surface needs a larger contact angle (>150°) and a low contact angle hysteresis (<10°).

4. DEMAND OF THE BOOMING CONSTRUCTION

Past several years, more and more modern high-rise building was growing over the global, increase the building height, the cleaning cost will increase. Meanwhile, since high-rise building cleaning need more professional technologies and workers, the cost is much higher than normal commercial building cleaning. For example, the tallest man-made structure on Earth, Burj Khalifa in Dubai costs £1.5 billion on construction and is covered by 120,000 m^2 glass panels, which enough to cover 17 soccer fields (National Geographic). It cost £5million of high-tech equipment, 36workers three to four months to ensure it`s shining (Marika, 2010). It is not only a dangerous work (two window cleaners died during working in 2012 (Kannan, 2012)) but always also a circle work, the moment they finish they have to start again. Abu Dhabi National Exhibition Centre will cost anything between $8,167 and $16,334 per cleaning, which means clean the building will cost at least $98,000 per year (Barnard, 2012). Another example Beijing National Stadium which is called Bird's Nest need to be cleaned twice a year and each clean takes three to four months.

The number of skyscraper and high-rise building is continues increasing around the world, as shown the total roof height of high building every year in Figure b (the point of 2015 means total height of buildings which would be completed in the year of 2015). The kingdom tower with height 1007 metres began building at April 27 2014(News, 2014). While, China developers are currently building 452 new buildings, all over 152 meters tall, and there's another 357 in the planning stages. The number of skyscrapers on the china mainland will reach 1307 in 10 years (Skyscraper Database, 2014). Higher the building the cleaning working is more danger and more expensive, more skyscrapers produce larger demands of self-cleaning coating.

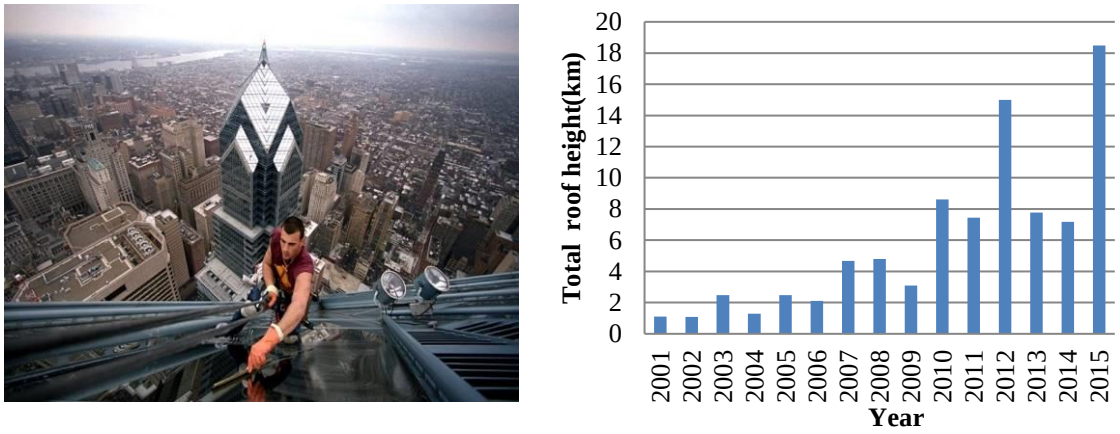

Figure 3: (a) Dangerous cleaning work out of skyscrapers, (b)Total height of new skyscrapers every year in world

List the top 100 cities with number of skyscrapers and high-rise buildings and summarize the distribution in Table 1. Asia takes account more than half of the cities, followed by North America. The total skyscrapers and high-rise building number 90428 will increase since there are still unbuilt, under construction and planned construction. Within these cities, not only large numbers of cities are located in Asia, but also these cities have high rank No. in height. All these show a huge market for self-cleaning coating especially in Asia. If the high performance self-cleaning could be applied in building widely, it would be a big conservation for energy.

Table 1: Distribution of skyscraper and high rise building in world[1]

Area	Number of city	Number of skyscrapers[2]	Number of high-rise building
Asia	54	6,929	36711
N-America	28	3105	15836
Others	10	1003	15906
Europe	8	537	10401
Total	100	11574	78854

Notes: 1: Reference from EMPORIS. 2: Definition of skyscraper in Emporis is multi-story building whose architectural height is at least 100 meters; high-rise is between 35m and 100m.

5. FABRICATION OF SELF-CLEANING COATING

In the field of surface modify technologies, several fabrication methods have shown their superiority in mimicking bio-texture of nature to achieve hydrophobic surface, such as Lithographic method, template-based technique, plasma treatment, and chemical deposition. Table 2 summarizes some of current studies on self-cleaning coatings.

Table 2: Current studies on self-cleaning coating

Method	Method/Assistance	Authors	Substrate/Film	CA/CAH
Lithography	Photolithography /UV-assisted	Jeong (Jeong et al., 2008:1913-1918, 2009:202-207)	Si/Si	CA=159~163° CAH=3~5°
	Soft lithography /chemical deposition	Kim et al. (Kim et al.,2009:095002-095009)	Si/ZnO	CA=167° CAH=4°
	Nanoimprint /sol-gel	Niedermeier et al (Niedermeier et al., 2013:7870-7873)	Si/TiO2	CA=171°
	Laser interference lithography	Li et al. (Li et al., 2014:0341091-0341096)	Si	CA=153.2°
	Anodic aluminum oxide templating/ imprinting	Huang et al (Huang et al.,2014:419-426)	Polyethylene nanofibers	CA=120~150°
Templating	Bio-skeleton templating/deposition	Wang et al. (Wang et al., 2014a:65-69)	C/ZnO	CA=164°
	Precision machining mold/ anodized alumina oxide	Ho, et al. (Ho et al., 2014:603-609)	Si/Al2O3	CA=160° CAH<10°
	Chemical skeleton templating/deposition	Wang et al. (Wang et al., 2014b:4803-4809)	Glass, paper, concernt, wood/ SiO2	CA=157~174° CAH=6°
	Plasma/chemical deposition	Vasiljevic et al (Vasiljevic et al., 2013:277-289)	Cotton Fiber/C-O-F-Si	CA=154° SA=7°
Plasma	Plasma/ self-assembly	Ellinas et al (Ellinas et al., 2014:6510-6524)	PMMA, PEEK, PDMS/SAMs	CA>153° CAH<10°
	Ar-plasma/deposition	Kylian et al. (Kylian et al., 2014:57-60)	Any/organic nano-particas	CA~180°
	Chemical vapor deposition	Rezaei et al. (Rezaei et al., 2014:11-16)	Glass, silicon, Al/organic silicon	CA>160° CAH<5°
Chemical deposition	Chemical deposition	Wu et al (Wu et al., 2014:8405-8407)	Cu/Cu-Ag	CA>165° CAH<5°
	Sol-gel	Latthe et al. (Latthe et al., 2010:115-121)	Glass/ organic silicon	CA=160° CAH=3°
	Chemical reduction of copper acetate	Sasmal et al (Sasmal et al., 2014:22034-22043)	Glass, cotton wool, Si/ Cu	CA=164°

All these fabrication methods have their advantages and disadvantages. Lithography is a relative mature technique, which copies information from a master and then copies it at second time into a replica in an opposite way. To fabricate dual-roughness structures it must copy twice with two different roughness masters, the advantage is can locate pillars precisely with designed masters (Jeong et al., 2009:202-207), but it is difficult to prepare irregular patterns or further tinier pillars. Therefore, traditional lithography always companies with chemical deposition (Kim et al., 2009:095002-095009), sol-gel (Niedermeier et al., 2013:7870-7873) methods to get the smaller roughness. While, with laser industrial development more and more elaborate processing works introduce laser technology. The beam laser interference lithography (Li et al., 2014:0341091-0341096) is a developing high efficiency and low cost technology to fabricate highly ordered super-hydrophobic structures. Template-based method is an imprint-related way which includes preparing template master, mould the replica and copying the templates. Many nature materials can be a template like natural lotus leaves, insect wings, reptile skins and rice leaf and so on. Anodic aluminium oxide (AAO) template is widely used to create Nano-line structures for well controllability. The plasma treatment can be considered as an easy and low-cost method. While, the other factors such as substrate roughness, target materials and sputtering density all affect the coating wettability. Sol-gel method is a relatively cheap wet-chemical technique used for the fabrication of both glassy and ceramic hydrophobic materials. It is facile, environment and economical for his needless of master for replication. Electrospinning, an electrostatic fiber fabrication technique has evinced more interest and attention in recent years due to its versatility and potential for applications in diverse fields. The nanoscale fibers are generated by the application of strong electric field on polymer solution or melt. Various surface patterns can be achieved by electro-spinning method

through adjusting electro-spinning time and aging time, or using hydrothermal treatment (Bhardwaj and Kundu, 2010:325-347, Tang et al., 2009:14220-14224). How to merge these fabrication methods, make use of their advantages and transform them into industrial technologies to satisfy the booming demand is the confronting problem.

6. COMMERCIAL TECHONOLOGY AND MARKET OF SELF-CLEANING COATING

6.1 Current commercial technology and market

Nowadays, commercial products of self-cleaning coating in building are mainly divided into two kinds: one is the factory-finished product (glass) which coating was added into the surface of glass during the product process (Midtdal and Jelle, 2013:126-141). The other is a user-finished product which generally is a kind of solution needed user do-it-yourself. As shown inTable , some products and corporation was summarized.

Table 3 Summary of commercial self-cleaning products and corporations

Corporation	Self-cleaning products		Other Products		Remarks
	Name	Extend functions	Name	Application property	
Pilkington Group Ltd. (UK)	Pilkington Activ™ glass	Solar control R=15% T=84%	Pilington SuncoolTM/ K Glass TM / PlanarTM/ yrodur® /OptiphonTM	Thermal insulation Noise control	Acquired by NSG (Japan) in 2006, hydrophilic
Saint Gobain Glass (UK)	SGG Bioclean® glass/Bioclean® Aqua	Thermal insulation Pro/Solar R=87%	Bioclean®/Solara/ Azura/ Natura CoolLite®/SKN/ST/ XTREME Lite Floor®/Point®/ Decorglass® Diamant®	Solar control Thermal insulation Durability Anti-reflective	Photocatalytic hydrophilic mineral layer
Fuyao Glass Industry Group Co Ltd. (China)	Self-cleaning glass	Low reflectance Low haze	Sun control coated / offline reflective /tempered glass/ curved /bended/ laminated /SGP glass	Solar control, decorative effect, energy conservation mechanical property	CVD/ magnetic sputtering /online pyrolysis spray /hydrophilic
Cardinal Glass industries (USA)	NeatTM	R=8% T=90%	LOE3 366/340, LOE3 270/272, LOE 180, LOE–i89	Selective light, saving energy	Hydrophilic/ Silicon dioxide /light selectivity
PPG industries (USA)	Sun clean®	R=19% T=79%	OEM coatng, automotive refinish, flat glass,	Antomotive refinish	Photocatalysis hydrophilic TiO2 coating
Olympic Glass Limited (UK)	Self-cleaning glass	Design, other function can be added	Insulated Glass, Solar Control Glass, Safety Glass, Acoustic Glass, Devorative Glass	Solar control, Acoustic control, decorative effect, energy conservation mechanical property	Design, manufacture supply hydophilics
Pressglass SA (Poland)	Ease of cleaning glass	Design, other function can be added	Evergy saving and solar control, Safety and security, Protection against noise, Protection against noise, against fire, façade glazing, aesthetic	Solar control Acoustic control, decorative effect, energy conservation safe function	TiO2 coating Photocalysis hydrophilic
Viridian New World Glass (Australia)	Viridian Renew™	Design, other function can be added	ComfortHushTM ComforPlusTM EnergyTechTM EnviroshieldTM, OptiviewTM, StormguardTM ThermotechTM VlamTM	Solar control, Decorative effect Energy conservation Satety guard	Hydrophilic
Balcony Systems solution Ltd. (UK)	Balco-NanoTM solution	no	Heavy duty cleaner	Clean the dirty	(DIY) super hydrophobic
RainRacer Development (UK)	Rain racer TM solution	no	House glass, bathroom, cars boats	Clean function for glass, metal, ceramic substrate	(DIY) Super hydrophobic
Sto Ltd. (German)	StoLotusan solution	no	StoTherm/StoVentec/ /StoRend /StoLit/ StoSilco/StoSilent /StoAcoustic/StoDecor	Energy conservation Acoustic control, decorative effect, finish	(DIY) Super hydrophobic

Notes: R: exterior visible reflectance; T: visible transmittance. Generally, Lower R means high saving energy, high R means solar protection which is important in desert. Higher T means lighter indoor.

The Self-cleaning character is coming into a fundamentally performance of these glasses. With demands of skyscrapers over the world more performances such as solar control, energy conservation and thermal insulation were added the self-cleaning coating. The self-cleaning character of glass almost is activated by exposure to sunlight. Photocatalysis enables the coating to gradually decompose organic material as it is exposed to sunlight, following hydrophilicity causes water drops to flatten and spread out producing a thin sheet of running water that rinses away loosened organic material and enables the glass to dry quickly. In addition to being photocatalytic and hydrophilic, the TiO_2 coating on glasses is extremely durable because the coating bonds to glass formed in the molten process. This photocatalysis and hydrophilic glass need a cleaning period generally 3~7days to catalysis and decomposition. While these products easily are combine with other functions such solar control for similar light performance.

The liquid products are silica based and create a nano-scale film that covers the microscopic valleys and peaks on the surface of glass, ceramic, concrete and so on. This type of self-clean coating prevents the contamination with the hydrophobic performance with advantages of working on organic and inorganic dirt alike and without a long reaction period. Sto-Lotusan is a typical liquid hydrophobic product of Sto Company. Its microstructure has been moulded on the lotus plant to minimize the contact area for water and dirt. Water and dirt cannot grip the surface of the wall with lotusan coating. Practical tests conducted by respected building institutes have shown that Sto-Lotusan Color can provide a reduction in soiling of up to 80%. It is reported that the maintenance cycles of Sto-Lotusan are up to 3 times longer than typical façade paint (regular maintenance cycle is 5 years). Reduced maintenance means reduced refurbishment costs for re-paints although it has higher price.

6.2 Commercial market potential

The global paints and coating market is looking forward to a bright future. In recent years, the global demand grew steadily with an average rise of 5.4% annually. Sales amount get to 41.75 million tones and sales value $127.3 billion till 2013 (WPCIA, 2014), the building coating accounts for about 40% sales volume in 2013 as listed in Table (IRFAD, 2010).Within the booming development of construction all over the world, architectural coating must be into a new leapfrog development stage. Keller expected that the global market will doubled in size by 2030.

Table 4 Paints classification yield in 2013 (Source: WPCIA)

Classification / Yield	Building	Industry	Transportation	Package	Other	Total
Sales volume (tones)	16.7	8.35	5.4275	5.01	6.2626	41.75 million
Proportion %	40%	20%	13%	12%	15%	

Advanced surface with self-cleaning property was seeded by glass companies, paints and coating companies, cleaning services companies, car industries or construction for several years. Actually, Companies must to understand the latent customer needs and own advanced techniques to meet them, so that have a shorter expected life cycle and keep their competitive advantage. As show in Table , the combination of super-hydrophobic and other solar and acoustic control et al. will be a vast investment opportunity.

7. OUTLOOK OF SELF-CLEANING TECHNOLOGY

7.1 Promising research direction

The self-cleaning mechanisms of super-hydrophobic and super-hydrophilic surface are different. Nowadays, the hydrophilic self-cleaning products were designed to satisfy the multifunction needs which generally are TiO_2 substrates easily to combine solar control performance and etc. researches on the hydrophilic self-cleaning coating companied with UV modification also brought a spotlight as show in Table . But the self-clean process carries on with spreading a layer of liquid and the catalysis of organics, decomposed organics will be cleaning away with the flowing downstream when more liquid is added

into the liquid layer. This process could not avoid reserving liquid in the hierarchical structure and a longer catalysis process.

Super-hydrophobic self-cleaning surfaces have hierarchical structures contained a lay of air to decrease the contact area between water droplets and the substrate. It is real repellency to surface attachments. As mentioned above in previous chapter, Lithographic method, template-based technique, plasma treatment all can fabricate precise multi-scale structure without the problem of transparent, In order to satisfy the day-to-day use, there are many additional requirements, improving the mechanical stability and preventing oil fouling of super-hydrophobic. Cholewinski et al. (Cholewinski et al., 2014:230-237) increased the proportion of epoxy resin to curing agent in order to prevent the added particles from fully sinking into the epoxy coating layer. The adding of particles not only can improve the roughness but also the attachment of layer between substrate. While, most glass applications must have the transparency or low scatter standards. This requires the surface corrugations with minimum roughness can allow the interested light waves passing through them (Blossey, 2003:301-306). Zhu and his partners (Zhu et al., 2012:182-186) fabricated a kind of super-hydrophobic CNTs-PTEF bulk material which remains super-hydrophobic property (contact angel is 159°) and good mechanical strength even after 20 abrasion cycles. It can regenerate the super-hydrophobicity by burning process when the material is oil fouled. But this material is not transparency for the addition of CNTs. The Self-cleaning character is coming into a fundamentally performance of these glasses. With demands of skyscrapers over the world more performances such as solar control, energy conservation and thermal insulation were added the self-cleaning coating. Meantime, such as Lithographic method, template-based technique, plasma et al. prior to manufacture a product finished in the factory stage, the chemical deposition can provide more changes to users with more flexibilities which can decrease the cost of production.

7.2 Industry-Academia collaboration model

Global cleaning services market is growing but under significant pressure to low costs and provide greater value for money. The growing market is an opportunity; in the inquired cities however, cleaning price competition will also put pressure on self-cleaning products. So, with strong support and security system research must keep up with the demand of market with novel fabrication method or material to decrease the cost. The Industry-academia collaboration is complementary. Academia like universities carries out basic research that will contribute to solutions of technical issues that occurs industry. Later, the problems found in practical experience by industry will return to academic sectors to discover a better solution. Such as Pilkington, which was a thin glass supplier of triplex at first, formed a joint company with triplex and obtained support from triplex. Sooner became a global-level safety glass company and enable to globally purchase numbers of glass companies because of its innovative cheap fabrication method. In 2006, the Pilkington with the float process technology joined into the NGS (Japan) group as one of the biggest self-cleaning glass productor. The research joins into market, technology joins into financial group is the best style for technology and social development.

8. CONCLUSION

With the development of global building industry and economy, super-hydrophobic self-cleaning surface with its special performance has a numerous application potential for smart building with lowest cleaning cost. In order to lengthen lifetime, high adhesion, transparency, wear resistance and regeneration should be got more concern to cooperate with self-cleaning character, meanwhile, more performances such as solar control, energy conservation and thermal insulation should be added in the future research work to widen commercial market. Base on the mature technology and the current studies, surface functional materials will serve import role in the passive building without anything consumption.

9. ACKNOWLEDGEMENTS

This work was supported by research grants from The Nottingham University and the Fundamental Research Funds for the Central Universities (2014MS14), the natural science foundation of china (51106050).

10. REFERENCES

BARNARD, Lucy, 2012. Window cleaning reaches for new heights in the UAE. Online/Available: http://www.thenational.ae/business/industry-insights/property/window-cleaning-reaches-for-new-heights-in-the-uae [Accessed Semptember 24 2012].

BHARDWAJ, Nandana, Kundu, Subhas C., 2010. Electrospinning: A fascinating fiber fabrication technique. Biotechnology Advances, 28, 325-347.

BHUSHAN, Bharat, 2011. Biomimetics inspired surfaces for drag reduction and oleophobicity/philicity. Beilstein Journal of Nanotechnology, 2, 66-84.

BHUSHAN, Bharat, Nosonovsky, Michael, 2010. The rose petal effect and the modes of superhydrophobicity. Philosophical Transactions of the Royal Society a-Mathematical Physical and Engineering Sciences, 368, 4713-4728.

BLOSSEY, Ralf, 2003. Self-cleaning surfaces - virtual realities. Nature Materials, 2, 301-306.

BYUN, Doyoung, Hong, Jongin, Saputra, Ko Jin Hwan, Lee, Young Jong, Park, Hoon Cheol, Byun, Bong Kyu, Lukes, Jennifer R, 2009. Wetting characteristics of insect wing surfaces. Journal of Bionic Engineering, 6, 63-70.

CHOLEWINSKI, Aleksander, Trinidad, Josh, Mcdonald, Brendan, Zhao, Boxin, 2014. Bio-inspired polydimethylsiloxane-functionalized silica particles - epoxy bilayer as a robust superhydrophobic surface coating. Surface & Coatings Technology, 254, 230-237.

EBERT, Daniel, Bhushan, Bharat, 2012. Durable Lotus-effect surfaces with hierarchical structure using micro- and nanosized hydrophobic silica particles. Journal of Colloid and Interface Science, 368, 584-591.

ELLINAS, Kosmas, Pujari, Sidharam, Dragatogiannis, Dimitrios A., Charitidis, C. A., Tserepi, A., Zuilhof, Han, Gogolides, Evangelos, 2014. Plasma micro-nanotextured, scratch, water and hexadecane resistant, superhydrophobic, and superamphiphobic polymeric surfaces with perfluorinated monolayers. ACS Applied Materials & Interfaces, 6, 6510-6524.

EXTRAND, Chuck W. 2002. Model for contact angles and hysteresis on rough and ultraphobic surfaces. Langmuir, 18, 7991-7999.

FANG, Yan, Sun, Gang, Cong, Qian, Chen, Guanghua, Ren, Luquan, 2008. Effects of methanol on wettability of the non-smooth surface on butterfly wing. Journal of Bionic Engineering, 5, 127-133.

FERNANDEZ-BLAZQUEZ, Juan P., Fell, Daniela, Bonaccurso, Elmar, Del Campo, Aranzazu, 2011. Superhydrophilic and superhydrophobic nanostructured surfaces via plasma treatment. Journal of Colloid and Interface Science, 357, 234-238.

GAO, Lichao, Mccarthy, Thomas J., 2007. A commercially available perfectly hydrophobic material (theta(A)/theta(R)=180 degrees/180 degrees). Langmuir, 23, 9125-9127.

HO, Audrey Yoke Yee, Van, Emma Luong, Lim, Chee Tiong, Natarajan, Sriram, Elmouelhi, Noha, Low, Hong Yee, Vyakarnam, Murty, Cooper, Kevin, Rodriguez, Isabel, 2014. Lotus bioinspired superhydrophobic, self-cleaning surfaces from hierarchically assembled templates. Jouranl of Polymer Science, Part B: Polymer Hypsics 52, 603-609.

HUANG, Chiung Fang, Lin, Yi, Shen, Yung Kang, Fan, YM., 2014. Optimal processing for hydrophobic nanopillar polymer surfaces using nanoporous alumina template. Applied Surface Science, 305, 419-426.

IRFAB. 2010. Specialist and Functional Architectural Coatings Market 2008 – 2018 for Europe and the Middle East, scope and samples [Online]. Available: http://www.pra-world.com /Irfab/sfacm [Accessed].

JEONG, Hoon Eui, Kwak, Moon Kyu, Park, Chan Ick, Suh, Kahp Yang, 2009. Wettability of nanoengineered dual-roughness surfaces fabricated by UV-assisted capillary force lithography. Journal of Colloid and Interface Science, 339, 202-207.

JEONG, Hoon, Eui, Kwak, Rhokyun, Kim, Jae Kwan, Suh, Kahp Yang, 2008. Generation and self-replication of monolithic, dual-scale polymer structures by two-step capillary-force lithography. Small, 4, 1913-1918.

KANNAN, Preeti, 2012. Relative of Abu Dhabi cleaner Lashes at employer for 15 storey fall. Online/Available:http://www.thenational .ae/news/uae-news/relative-of-abu-dhabi-cleaner-lashes-at-employer-for-15-storey-fall [Accessed October 19 2012].

KIM, Hyungmo, Kim, Moo Hwan, Kim, Joonwon, 2009. Wettability of dual-scaled surfaces fabricated by the combination of a conventional silicon wet-etching and a ZnO solution method. Journal of Micromechanics and Microengineering, 19.095002-095009.

KYLIAN, Ondrj, Petre, Martin, Serov, Anton, Solar, Pavel, Polonskyi, Oleksandr, Hanus, Jan, Choukourov, Andrei, Biederman, Hynek, 2014. Hydrophobic and super hydrophobic coatings based on nanoparticles overcoated by fluorocarbon plasma polymer. Vacuum, 100, 57-60.

LATTHE, Sanjay S., Imai, Hiroaki, Ganesan, V., RAO, A. Venkateswara, 2010. Porous superhydrophobic silica films by sol-gel process. Microporous and Mesoporous Materials, 130, 115-121.

LI, Wen Jun, Wang, Zuo Bin, Wang, Da Peng, Zhang, Ziang, Zhao, Le, Li, Da You, Qiu, Ren Xi, Maple, Carsten, 2014. Superhydrophobic dual micro- and nanostructures fabricated by direct laser interference lithography. Optical Engineering, 53, 0341091-1341096.

MANCA, Michele, Cannavale, Alessandro, De Marco, Luisa, Arico, Antonino S., Cingolani, Roberto, GIGLI, Giuseppe, 2009. Durable Superhydrophobic and Antireflective Surfaces by Trimethylsilanized Silica Nanoparticles-Based Sol-Gel Processing. Langmuir, 25, 6357-6362.

MARIKA, Dobbin, 2010. So you think your windows are hard to keep clean? Melbourne, Australia: The Age.

MIDTDAL, Krister, Jelle, Bjorn Petter, 2013. Self-cleaning glazing products: A state-of-the-art review and future research pathways. Solar Energy Materials and Solar Cells, 109, 126-141.

NATIONAL GEOGRAPHIC, 2014. Building the Burj Dubai: big, bigger, biggest. Online/Available: http://en.wikipedia.org/wiki/Burj_Khalifa#cite_note-cleaning-65.

NEWS. 2014. Building of Kingdom Tower to start on April 27th. Kingdom Tower Official Site. [Accessed March 27,2014].

NIEDERMEIER, Martin A., Tainter, Gregory, Weiler, Benedikt, Lugli, Paolo, Buschbaum, Peter Muller, 2013. Fabrication of hierarchically structured titania thin films via combining nano-imprint lithography with block copolymer assisted sol–gel templating. Jouranl of maerials chemistry A, 1, 7870-7873.

PARK, Kyoo-Chul, Chhatre, Shreerang S., Srinivasan, Siddarth, Cohen, Robert E., Mckinley, Gareth H., 2013. Optimal Design of Permeable Fiber Network Structures for Fog Harvesting. Langmuir, 29, 13269-13277.

PARK, Kyoo Chul, Choi, Abhijeet Wonjae, 2014. Energy efficient application using surfaces with special wettabilities. Journal of Nanotechnology and Smart Materials, 1, 1-9.

RAGESH, Prathapan, Anand Ganesh, V., Nair, Shantikumar V., Nair, ASreekumaran, 2014. A review on 'self-cleaning and multifunctional materials'. Journal of Materials Chemistry A, 2, 14773-14797.

REZAEI, Sasan, Manoucheri, Iraj, Moradian, Rostam, Pourabbas, Behzad, 2014. One-step chemical vapor deposition and modification of silica nanoparticles at the lowest possible temperature and superhydrophobic surface fabrication. Chemical Engineering Journal, 252, 11-16.

SASMAL, Anup Kumar, Mondal, Chanchal, Kumar, Arun, Gauri, Samiran S., Pal, Jaya, Aditya, Teresa, Ganguly, Mainak, Dey, Satyahari, Pal, Tarasankar, 2014. fabrication of superhydrophobic copper surface on various substrates for roll off self cleaning and water oil separation. Applied Materials &Interfaces. 6:22034-22043.

SKY SCRAPER DATABASE, 2014. http://skyscraperpage.com/diagrams/?memberID=undefined.

TANG, Hong Zhe, WANG, Hang, HE, Jun Hui, 2009. Superhydrophobic titania membranes of different adhesive forces fabricated by electrospinning. Journal of Physical Chemistry C, 113, 14220-14224.

VASILJEVIC, Jelena, Gorjanc, Marija, Tomsic, Brigita, Orel, Boris, Jerman, Ivan, Mozetic, Miran, Vesel, Alenka, Simoncic, Barbara, 2013. The surface modification of cellulose fibres to create super-hydrophobic, oleophobic and self-cleaning properties. Cellulose, 20, 277-289.

WANG, Tian Chi, Chang, Li Jing, Zhuang, Li Min, Yang, Sen, Jia, Yang, Wong, Ching Ping, 2014a. A hierarchical and superhydrophobic ZnO/C surface derived from a rice-leaf template. Monatshefte Fur Chemie, 145, 65-69.

WANG, Ya Qun, Shi, Ye, Pan, L. J., Yang, Meng, Peng, Le Le, Zong, Shi, Shi, Yi, Yu, Gui Hua, 2014b. Multifunctional superhydrophobic surfaces templated from innately microstructured hydrogel matrix. Nano Letters, 14, 4803-4809.

WONG, Tak Sing, Huang, Adam Po-Hao, Ho, Chih Ming, 2009. Wetting Behaviors of Individual Nanostructures. Langmuir, 25, 6599-6603.

WPCIA 2014. World's Top ten Paints Companies 2013 Annual Report. Washington. available: http://www.wpcia.org/news/World's%20Top%20ten%20Paints%20Companies%202013%20Annual%20Reprt.html

WU, Yun Wen, Hang, Tao, Yu, Zhe Yin, Xu, Lan, Li, Ming, 2014. Lotus leaf-like dual-scale silver film applied as a superhydrophobic and self-cleaning substrate. Chemical Communications, 50, 8405-8407.

YAN, Yu Ying, Gao, Nan, Barthlott, Wilhelm, 2011. Mimicking natural superhydrophobic surfaces and grasping the wetting process: A review on recent progress in preparing superhydrophobic surfaces. Advances in Colloid and Interface Science, 169, 80-105.

YAO, Lin, He, Junhui, 2014. Recent progress in antireflection and self-cleaning technology - From surface engineering to functional surfaces. Progress in Materials Science, 61, 94-143.

YUAN, Saojun, Pehkonen, S.O., Liang, Bin, Ting, Y. P., Neoh, K. G., Kang, E. T., 2011. Superhydrophobic fluoropolymer-modified copper surface via surface graft polymerisation for corrosion protection. Corrosion Science, 53, 2738-2747.

ZHANG, Xue Min, Zhang, Jun Hu, Ren, Zhi Yu, Li, Xiao, Zhang, Xun, Zhu, Di Fu, Wang, Tie Qiang, Tian, Tian, Yang, Bai, 2009. Morphology and Wettability Control of Silicon Cone Arrays Using Colloidal Lithography. Langmuir, 25, 7375-7382.

ZHU, Xiao Tao, Zhang, Zhao Zhu, Yang, Jin, Xu, Xiang Hui, Men, Xue Hu, Zhou, Xiao Yan, 2012. Facile fabrication of a superhydrophobic fabric with mechanical stability and easy-repairability. Journal of Colloid and Interface Science, 380, 182-186.

204: Simulated building energy savings with ventilated PCM ceiling tiles

THOMAS WHIFFEN

University of Nottingham, Dept. of Architecture and Built Environment, University Park, Nottingham, NG7 2RD, thomas.whiffen@nottingham.ac.uk

The reduction of building energy consumption is a direct target for the many governments worldwide. To date active thermal energy storage (TES) technologies have demonstrated the capability of reducing 30-40% of end-use energy demand. However traditional active TES solutions are integral to the building fabric, making retrofit due to building demand changes difficult to incorporate. Phase change material (PCM) has demonstrated comparable TES ability with five to fifty times less mass, depending on material properties and conditions. PCM solutions therefore offer lightweight TES solutions suitable for retrofit in the built environment. Traditionally PCM solutions have been fitted passively in construction layers, such as ceiling tiles or wall sections. These have suffered from poor heat transfer, leading to poor thermal cycling and performance. Novel Active-PCM solutions have been developed for AC systems saving 34%.

Through building simulation this paper investigates a novel method for improving PCM integrated ceiling tile performance. The method proposes using ventilation strategies to improve heat transfer and optimise the benefits of PCM ceiling tile retrofit. The modelled building was constructed and simulated in Design Builder using NCM templates. Ventilation strategies employed were zero ventilation, day ventilation, evening ventilation, night ventilation and twenty-four hour ventilation. The annual energy consumption for heating and cooling was analysed, as well as the total building energy savings. The results demonstrate that coupled night ventilation provided the greatest energy savings in low air-leakage buildings. Further investigation was given to enhancing heating energy savings for mechanically ventilated buildings. Simulation of combined heat recovery and PCM ceiling tile retrofit offered a 72% reduction in annual heating and cooling energy consumption in the reference building.

Keywords: Active thermal mass, thermal energy storage, sustainable built environment, phase change materials, building retrofit technology

1. INTRODUCTION

In 2011, thirty exa-joules of energy were consumed within service sector buildings, 26% of the total global built environment consumption (International Energy Agency (IEA), 2014). Assessing the end-use energy demand in such buildings, 33% of end-use energy was consumed through space heating and cooling (Figure 13). The demand for energy supply continues to rise, putting extra stress on energy markets and the environment, yet the energy intensity (energy consumption divided by contribution to GDP) has not improved since the late 1980s, suggesting a lack of improvement in energy-efficiency (Wade, 2003). To meet the UK government climate change targets (80% reduction of carbon emissions by 2050), energy-saving measures, throughout the service sector built environment are essential (Davey, 2012).

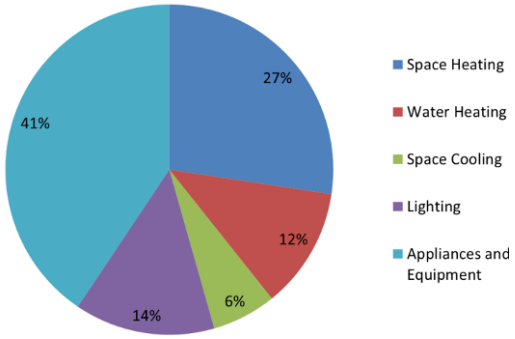

Figure 13 - Service-sector Built Environment End-use Energy Breakdown for 2011 [1]

Within the service section 74% of businesses have commissioned some level of energy-efficiency initiative. Amongst large corporations nine out of ten have commissioned work; whilst only six out of ten SMEs have commissioned projects (Jeffries, 2013). Energy efficient initiatives range from building energy management systems to behaviour change programmes.

Work done by Houssin (Houssin, 2013) suggested the two leading technologies for the reduction of building energy demand, within the EU, are advanced building envelopes (for cold regions) and heat pumps. The work also suggested the leading political measures to be enacted were; a deep renovation of existing buildings and zero-energy new buildings as standard. The work encouraged further research into the development of heat pump and thermal storage technology, as well as integration of buildings using smart grid technology. To date advanced building envelopes featuring thermal energy storage technologies have included sensible and latent thermal energy storage (TES) solutions.

1.1 Thermal Energy Storage

TES technologies utilise the residual thermal mass of the building envelope to slow the internal temperature rise, maintaining comfort within the maximum allowable room air temperature increase (ΔT_{max}), according to ISO 7730 (European Committee for Standardization, 2005). This effect works passively in buildings with thermal mass. To improve control, increase capacity and reduce energy usage, night ventilation air or chilled water is passed through the thermal mass (Littlewood, 2011, Meierhans, 1993, Winwood and Edwards, 1997, Feng, 2014).

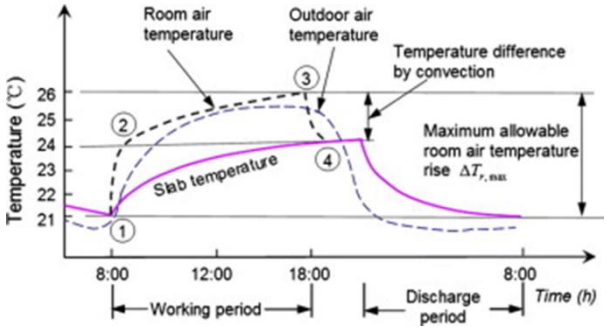

Figure 14 – Temperature variation during twenty-four hours of TES operation (Xu et al., 2014)

Airtight lightweight buildings lack residual thermal mass, thus without adequate HVAC control are subject to overheating. Latent TES materials, known as Phase Change Material (PCM), offer lightweight TES. Traditionally PCM solutions have been passive additions either as construction layers (Bio-PCM (Phase Change Energy Solutions, 2010) and Energain® (Dupont™, 2007)), impregnated in building materials (Kendrick and Walliman, 2007) or as ceiling tiles (Armstrong (Armstrong, 2012) and Datum Phase Change(Datum Phase Change, 2012b)).

PCM, incorporated as ceiling tiles, as a concept has existed within the UK for over twenty years (Feldman et al., 1989). The earliest market product dates back to 2012 (Datum Phase Change, 2012b). The RACUS, now 'ThermaCool®', product incorporated 50-70wt% BASF Micronial® 23 PCM within the tile and offers six times the energy storage density of concrete over a 20°C window (Datum Phase Change, 2014, BASF, 2011). The manufacturers quote a latent heat storage capacity of 100-140Wh/m^2.

From modelling conducted at De Montfort University, under zero-ventilation conditions a 7°C peak temperature reduction was reported, offering an average saving of 55% over traditional HVAC systems (Datum Phase Change, 2012a). The saving percentage was calculated from the difference between a room modelled with conventional HVAC system, requiring 1588.5 kWh per year for room conditioning, and a RACUS fitted room, requiring 720.5 kWh per year. This saving was multiplied across the entire floor space of Whitehall and equated to an estimated total carbon saving of 256 tonnes of carbon per year (BASF, 2011).

Further active PCM systems include; Cool-Phase™, which can reduce 90% of HVAC energy, replacing traditional air conditioning systems (Monodraught Ltd, 2014), PCM 'sails' (Susman et al., 2011) and a PCM HVAC diffuser (Gowreesunker et al., 2013). Using a limited control 22% energy savings were simulated by the diffuser. The greatest energy savings were with no night ventilation (34%) and full ventilation resulted in a 20% increase due to overcooling the space. Active cooled-ceiling solutions, using PCM, have been researched in literature (Koschenz and Lehmann, 2004, Yahay and Ahmad, 2011, Osterman et al., 2012).

1.2 Background and Hypothesis

In 2013 the author conducted a simulation based optimisation of PCM ceiling tiles. The results simulated 26% HVAC fuel energy savings were possible with a fan-coil system, although greater savings were possible at the expense of comfort, depending on the building HVAC configuration. Most noticeably the work revealed that, under UK climate conditions the PCM ceiling tile addition reduced heating fuel demand more than cooling. Following previous work, and recognising night ventilation use in sensible TES systems; the author set out to determine whether additional energy savings were achieved when PCM ceiling tiles were ventilated. Using the same PCM as in the previous work (A22H (Environmental Process Systems Ltd, 2004)) a reference model was specified.

2. METHOD

2.1 Model

Annual building energy simulation was conducted to generate annual HVAC fuel demand and total building energy usage. A fan-coil system was used throughout the simulations to ensure year round comfort temperatures were maintained. Ventilation profiles were reviewed, adjusted and simulations re-run. A reference building was specified to test the fuel energy savings. To test the hypothesis Design Builder was selected as the software tool to conduct the modelling. The software enables accurate energy and HVAC modelling through the established in-built EnergyPlus engine (Fumo et al., 2010, Boyano et al., 2013). The software also contains building templates in concordance with the National Calculation Method (NCM) in the UK. This enables accurate simulation of notional and reference building types within a trusted interface. Finally, the software also features PCM construction layers, enabling the definition and simulation of PCM integrated constructions.

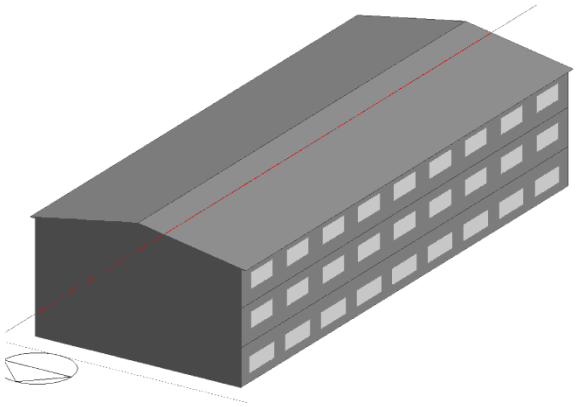

Figure 15 - Reference building model used throughout the simulations

Situated in Nottingham, UK, the 2,794m^2, three-storey building was specified as shown in Figure 15. 30% glazing was attributed to the western and eastern façades. The floor plans remained open plan generic office environments. The IWEC GBR Finningley weather file was used throughout the simulations. NCM reference templates were used where possible throughout the building simulation with the only variation being to exchange ceiling tiles for a PCM layer. Building and construction specifications were captured in Table 9 and Table 10.

Table 9 - Building Specifications

Specified Templates		Building Specifications	Activity Specifications	Environmental Control Spec.
Activity Template	Generic Office Area	3 storey 20 by 50m footprint	0.111 people/m^2 (9m^2/person)	Fan-coil System
Construction Template	NCM 2010 Reference Building	2,794m^2 internal area	NCM Open Office Occupancy Schedule	Heating COP (gas): 0.83
Glazing Template	Part L 2013 Reference Building	Pitched roof, 0.5m over hang, 10° roof slope	Metabolic Parameters: Light office work/standing/walking 123W/person, Factor 0.9, Winter 1clo, Summer 0.5clo	Cooling COP (elec.): 1.67
Lighting Template	Part L2 2010 Notional	Short side orientated to the north	Office Equipment: 11.77W/m^2	Natural ventilation: schedule varied
		No south or north glazing, 30% glazing on east and west façade		Mechanical Ventilation: Open Office Occupancy schedule
		Open floor generic offices on each level		Wide band heating and cooling set points: Heating 18°C, Cooling 28°C
		infiltration rate of 0.5 ac/h		Min Fresh Air: 10l/s per person

Table 10 - NCM 2010 Reference Building Constructions

Component	NCM 2010 Reference Building Construction Template (Part L)	U-Value (W/m^{2}K)
Walls	Brick, Insulation, Concrete, Air Gap, Plasterboard	0.306
Roof	Tiles, Air, Insulation, Plasterboard	0.236
Internal Walls	Plasterboard, Insulation, Plasterboard	0.649
Internal Floor/Ceiling	Flooring Screed, Concrete, Air Void, Ceiling Tiles	1.251
Ground Floor	Clay, Brick, Concrete, Insulation, Flooring Screed	0.345
Windows	Glazing 1 – Part L 2013 Reference Building	2.200

To simulate the PCM ceiling tile a 30.5mm layer of A22H PCM replaced the Ceiling Tiles construction layer in the *Internal Floor/Ceiling* construction component. The *PCM Internal Floor/Ceiling* component had a U-value of 1.236W/m^{2}K. The high performance A22H PCM was selected in accordance with previous background work conducted by the author (Whiffen et al. 2013). Table 11 displays the physical properties of this PCM. High-performance industry-leading PCM ceiling tiles have a mass of 25kg/m^2, therefore a 30.5mm layer of A22H PCM covered the occupied ceiling area, representing a 25kg/m^2 PCM ceiling tile retrofit.

Table 11 - A22H PCM Physical Properties

Physical Property	Value	Units
Thermal Conductivity	0.18	W/m^2K
Specific Heat Capacity	2860	J/kgK
Density	820	kg/m^3
Latent Heat	216	kJ/kg
Melt Temperature	22	°C
Melt Width	2	K

PCM performance in Design Builder was specified via a cumulative Enthalpy Curve (J/kg). Coupled Enthalpy and Temperature data points generated a hidden enthalpy profile (Figure 16) across the operating temperature, starting from a -20°C reference (Design Builder, 2013). This method leaves no room for accounting of sub-cooling, common, to differing degrees, in all PCMs (Whiffen and Riffat, 2012). To model alternative PCM within Design Builder cumulative enthalpy-temperature data points were calculated using the PCM physical properties taken from the manufacturer data sheets and the Gaussian effective heat capacity function (Darkwa and O'Callaghan, 2006). From the generated Gaussian effective heat capacity curves (J/kgK) the variable enthalpies per unit mass (J/kg) were calculated at half kelvin increments. Subsequently the cumulative enthalpy curve (Figure 16) was generated through addition of the variable enthalpies over the desired range for the PCM A22H, and specified in the construction layer properties.

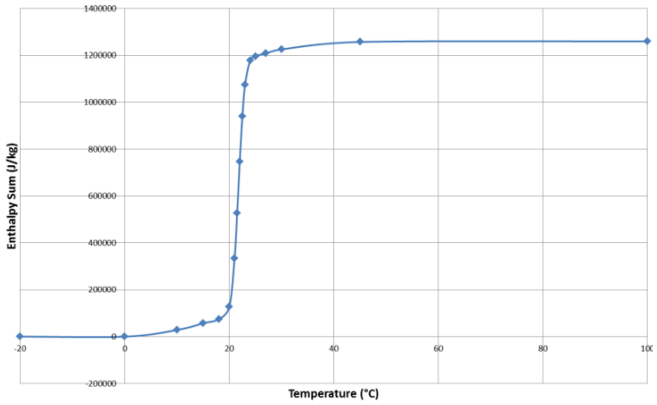

Figure 16 - A22H Theoretical Cumulative Enthalpy Curve

2.2 Simulation scenarios

Using the specified reference building model, to test the hypothesis, four time-limited natural ventilation strategies will be trialled, as well as PCM and non-PCM benchmark scenarios. Heating and cooling energy, as well as overall building fuel breakdowns were used to review energy savings. The four natural ventilation time-limited strategies were; Day Vent (9am to 5pm, 3ac/h), Evening Vent (5pm to 9pm, 3ac/h), Night Vent (7pm to 7am, 3ac/h) and 24hr Vent (9am to 9am, 3ac/h)

The ventilation profiles were displayed graphically in Figure 18. Secondly, using the same time-limited ventilation strategies, temperature limitation was added. For natural ventilation to occur the ambient temperature must fall between 12°C and 18°C, during the active ventilation times for each strategy. The temperature and time-limited ventilation profiles for a summer design week were displayed in Figure 19. Finally, maintaining the time and temperature limitations, minimum mechanical ventilation rates were investigated to determine energy saving benefits whilst occupied ventilation rates were met. The occupied mechanical ventilation lifted the basic ventilation rate to 2ac/h during occupied hours. The ventilation profiles were displayed in Figure 21.

3. RESULTS AND DISCUSSION

3.1 PCM Ceiling Tile Enhancement

As outlined, background work previously conducted simulated potential 26% heating and cooling energy saving benefit in a UK office, when PCM ceiling tiles were retrofit. Building upon the prior findings this

work initially set out the building energy profile and PCM ceiling tile enhancement energy savings, without additional ventilation. In the benchmark building, without PCM or ventilation, 13% of the building's energy usage was due to heating and cooling (Figure 17(a)).

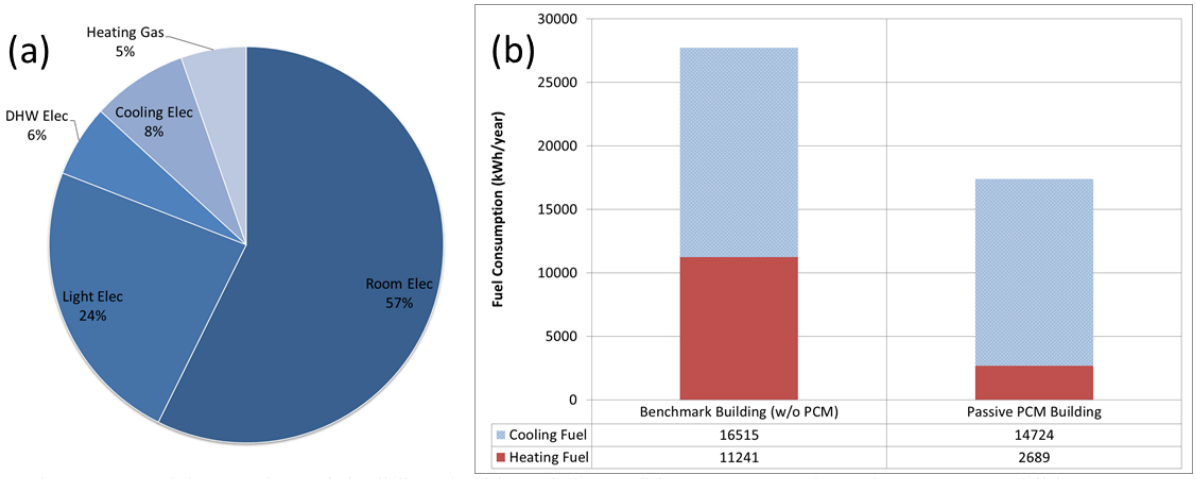

Figure 17 – (a) Benchmark building fuel breakdown (b) Energy Savings from PCM addition to an unventilated building

Figure 17(b) displays the simulated annual heating and cooling energy savings from PCM ceiling tile addition. A 37% heating and cooling fuel saving was demonstrated in the reference building, without ventilation. These cases set the benchmark for the remainder of the investigation. Since the passive PCM addition reduced the heating bill more than the cooling bill; and night ventilation has long been a well-documented technique for reducing cooling bills (Shaviv et al., 2001, Kolokotroni and Aronis, 1999, Geros et al., 2005), especially when coupled with thermal mass, the first hypothesis to investigate was thus: '*Ventilated PCM will reduce heating and cooling fuel consumption further*'.

3.2 Ventilated PCM

To test this theory, four different ventilation strategies were trialled. Each strategy was solely time dependent, operating for four to twenty-four hours per day, with no accounting for time of year or ambient temperatures. A base ventilation rate due to infiltration was set to 0.5ac/h. In addition each natural ventilation strategy added a further 3ac/h during ventilation hours (Figure 18(a)). Figure 18(b) documents the energy consumption when the ventilation profiles were simulated year round.

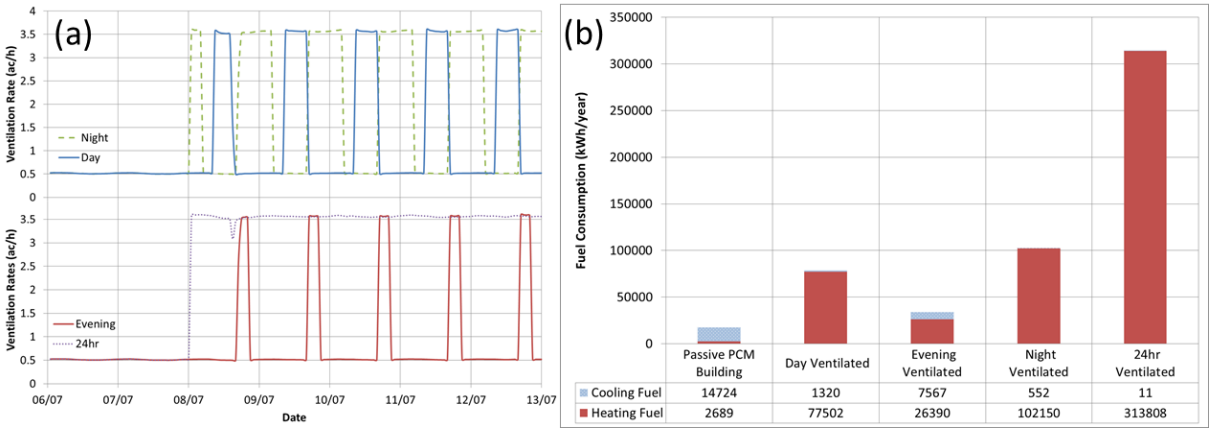

Figure 18 – (a) Time-limited ventilation profiles (b) Ventilated PCM building annual energy consumption results

The evidence from Figure 18(b) holds that ventilating thermal mass reduces cooling fuel demand. However, in each case tested, the introduction of time-limited ventilation strategies increased the heating fuel demand approximately ten to one hundred fold. Evidently, whilst the desired outcome of reduced cooling demand was achieved, an excessive increase in overall fuel consumption more than offsets any potential benefit.

Considering sensible thermal mass ventilation strategies the author decided to follow their example, introducing temperature limitations as to when additional space ventilation was conducted. Thus the hypothesis was modified: '*Temperature and time-limited ventilated PCM will reduce HVAC fuel consumption further than passive PCM addition alone*'.

3.3 Temperature Limited Ventilated PCM

The same four time-limited ventilation strategies were investigated with the addition of minimum and maximum temperature bounds. Since the cooling benefits of natural ventilation were under investigation temperature bounds, in-line with known sensible thermal mass ventilation strategies, were employed. The minimum air intake temperature was 12°C, whilst the maximum was set to 18°C. Annual heating and cooling energy consumption was again simulated.

Figure 19(a) displays an ambient temperature profile during a summer design week, coupled with the minimum and maximum temperature thresholds. When the ambient temperature was between these thresholds, during the additional ventilation time-periods (displayed in Figure 18(a)), additional ventilation up to 3ac/h was supplied. During summer design week the twenty-four hour and night ventilation strategies still provided natural ventilation and kept down cooling demand; however due to the summer temperatures evening and day strategies provided little additional ventilation.

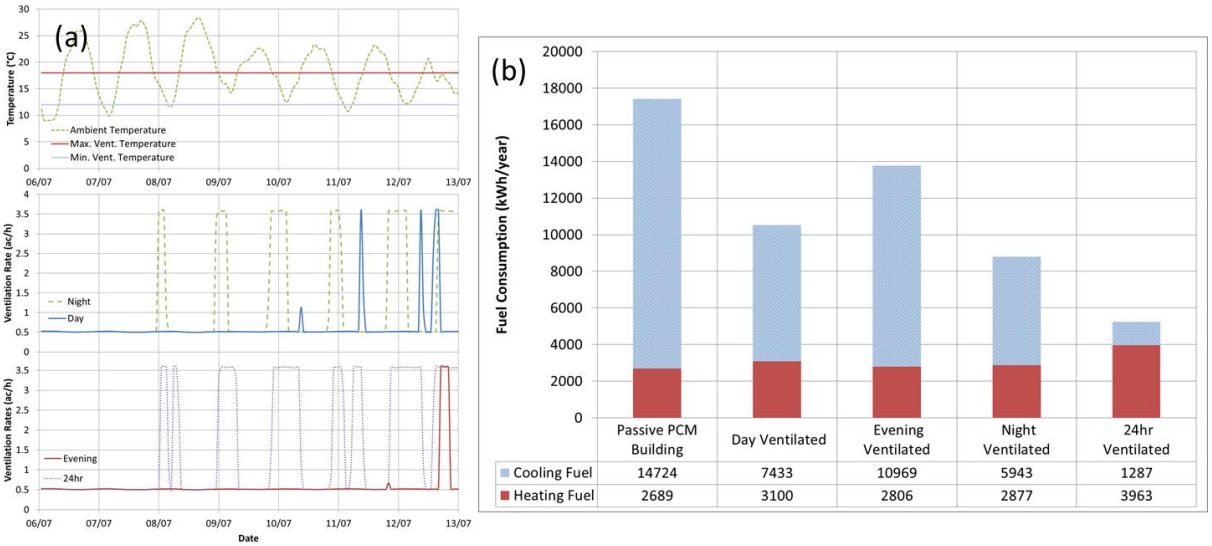

Figure 19 – (a) Temperature and time-limited ventilation profiles during a summer design week (b) Simulated annual fuel consumption under temperature and time limited ventilation strategies

By limiting the ventilation air temperature significant cooling fuel energy savings were simulated (Figure 19(b)), whilst avoiding excessive increase to the heating demand. At best the combined HVAC fuel consumption was reduced to 5,250kWh/year, from 17,413kWh/year for the PCM retrofit alone. The combined savings of PCM ceiling tiles and 24 hour, temperature-limited natural ventilation resulted in an estimated saving of 8 kWh/year/m^2, based on the 2,794m^2 simulated building. That translated to a saving of 81% in fuel demand.

3.4 Energy Saving Components

Since the temperature-limited ventilation strategies improved the energy savings, investigation sought to determine what proportion of the energy saving benefit could be attributed to the PCM retrofit and what was on account of the ventilation. Four scenarios were compared to determine the component energy saving benefits. The original benchmark, without any retrofit, was contrasted against the passive PCM building, a temperature-limited twenty-four hour naturally ventilated building without PCM, and finally the combined PCM and ventilated building as reported above.

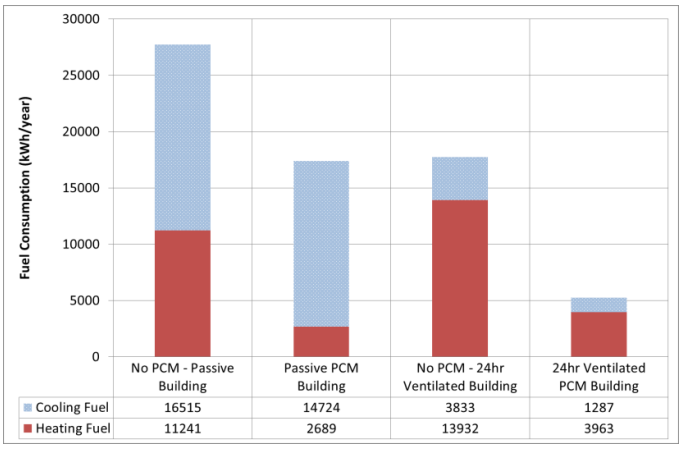

Figure 20 - Annual HVAC energy savings contrasting the component savings of retrofit strategies

As displayed in Figure 20, the PCM and ventilation strategies alone generated estimated savings of 10,343kWh/year and 9,991kWh/year. In line with previous work, the passive PCM retrofit greatly reduces heating fuel demand, with little effect on cooling fuel demand. The contrast is evident in the ventilation solution, where cooling fuel demand is significantly reduced, whilst the heating demand is increased.

The combined benefit of the solutions offered savings of more than double, reducing HVAC fuel demand by 22,506kWh/year. From these four simulations it is clear that the combined benefit of the ventilation and PCM addition works in tandem to greatly reduce fuel demand.

The evidence from these simulations strongly suggested a large fuel saving possible through retrofit and appropriate control of natural ventilation. Interrogation of the ventilation profiles however revealed that the minimum ventilation requirements of 10l/s per person, as set out by CIBSE (Butcher) (equivalent to 2ac/h in the reference building) were not always met during occupied periods. Therefore, minimum mechanical ventilation was added during occupied periods to meet the regulations.

3.5 Performance under min-ventilation requirements

The four time and temperature-limited ventilation strategies were investigated again, as well as the PCM and non-PCM benchmarks, with minimum mechanical ventilation during occupied periods. Annual heating and cooling fuel demand was observed. Figure 21(a) displays the ventilation profiles for a summer design week.

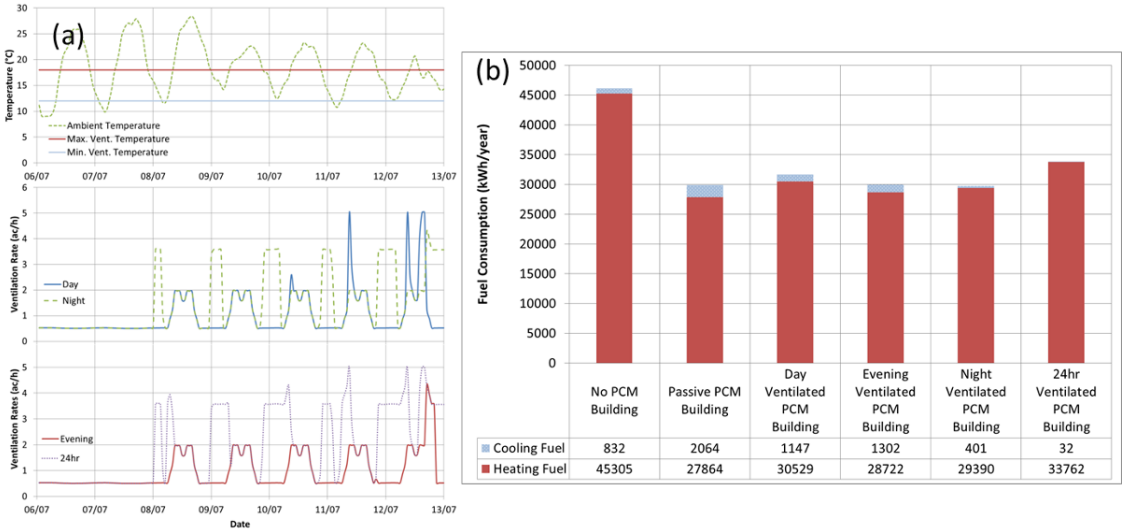

Figure 21 – (a) Ventilation profiles for a summer design week with minimum ventilation rates during occupied periods (b) Annual fuel consumption with minimum mechanical ventilation during occupied periods

The minimum occupied ventilation requirements understandably had an adverse effect on the heating fuel demand of the building (Figure 21(b)). Under these conditions only night ventilation marginally reduces the energy consumption per year compared to the PCM addition alone. Little to no benefit was observed with additional ventilation rates. PCM addition alone generated a 35% heating and cooling energy saving. Night ventilation demonstrated an additional 0.3% energy saving, with minimum ventilation guidelines.

3.6 Fraction of overall building energy usage

Further, despite the best case heating and cooling energy reduction of 81% (Figure 20), in the context of the building energy consumption, further attention now needs to be turned to reducing other building energy loads. Equipment consumption in the room and lighting energy represent the two greatest loads to address in the generic office environment.

Under the minimum occupied ventilation scenarios the ventilated PCM reduces the heating energy consumption from 20% to 13% (Figure 22 (a) and (c)), as a fraction of overall energy usage. PCM addition alone offers a similar benefit, reducing combined heating and cooling energy usage to 14% (Figure 22 (b)). PCM and temperature limited ventilation strategies alone reduce energy consumption by 6-7% of overall building energy usage. Since heating demand dominates cooling demand implementation of heat recovery technology may provide further savings.

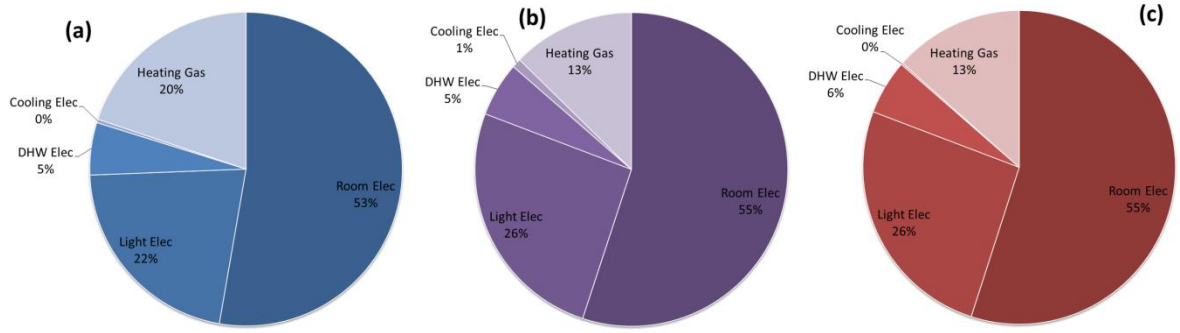

Figure 22 - Fuel breakdown under minimum mechanical ventilation during occupied periods in the (a) benchmark building, (b) PCM retrofit building and (c) night ventilated PCM building

3.7 Energy saving with heat recovery

Three scenarios were simulated with heat recovery included. They featured the minimum occupied mechanical ventilation profile. Figure 23 displays the comparative heating and cooling demand from the annual simulations. The benchmark building (No PCM) with heat recovery (+HR) reduces energy demand by 49%. PCM ceiling tile addition increases the savings to 72%, with subsequent ventilation totalling 73% heating and cooling annual energy savings.

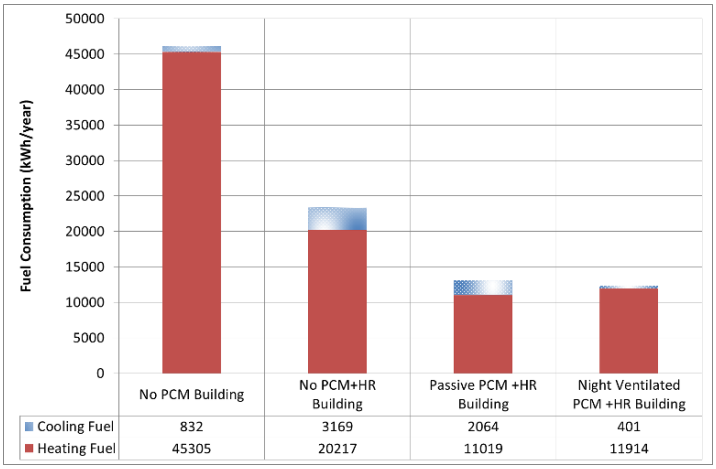

Figure 23 - Annual fuel consumption with heat recovery

4. CONCLUSIONS

In the UK climate, night ventilation can reduce the cooling load of a PCM ceiling tile building by 81%. However, with heating demand dominating buildings with adequate ventilation, the cooling demand is minimal in the scope of the whole building energy demand. Therefore, energy saving targeting heating demand reduction offered a more beneficial avenue. PCM ceiling tile retrofit reduced heating and cooling energy consumption by 35%, whilst heat recovery incorporation alone was estimated to save 49% of annual heating and cooling energy. Combined a 72% saving was estimated.

Ventilation doubled the energy savings possible when no mechanical ventilation was delivered to the building, however, when minimum ventilation requirements were considered only night ventilation offered marginal improvement on the PCM addition alone. Further, since room electricity and lighting accounts for over 80% of the building usage, even after ventilated PCM retrofit, developing energy saving solutions that focus on reducing lighting and room energy demand present the opportunity for more substantial returns.

From the evidence presented, the author suggests that in modern air-tight buildings, where overheating is a problematic occurrence, ventilated PCM ceiling tile retrofit provides a sustainable solution for minimising annual heating and cooling. However, where building ventilation rates meet CIBSE guidelines; the additional ventilation of PCM ceiling tiles offers minimal additional energy savings.

5. REFERENCES

ARMSTRONG 2012. CoolZone Technical Data Sheet.

BASF 2011. Reducing CO2 in Buildings, Energy Efficient Whitehall.

BOYANO, A., Hernandez, P. & Wolf, O. 2013. Energy demands and potential savings in European office buildings: Case studies based on EnergyPlus simulations. Energy and Buildings, 65, 19-28.

BUTCHER, K. J. CIBSE Guide A - Environmental Design (7th Edition). CIBSE.

DARKWA, K. & O'callaghan, P. W. 2006. Simulation of phase change drywalls in a passive solar building. Applied Thermal Engineering, 26, 853-858.

DATUM PHASE CHANGE. 2012a. Case Study, Department for Energy and Climate Change (DECC), London [Online]. Available: http://datumphasechange.com/index.php?department-for-energy-climate-change-decc-london [Accessed 23/04/2014.

DATUM PHASE CHANGE 2012b. RACUS Ceiling Brochure.

DATUM PHASE CHANGE. 2014. Thermal Mass: Comparison of ThermaCool(r) Ceiling TIle Performance to Standard Density Concrete [Online]. Available: http://www.datumphasechange.com/index.php?thermal-mass-8.

DAVEY, E. 2012. The Energy Efficiency Strategy: The Energy Effciency Opportunity in the UK. In: CHANGE, D. O. E. A. C. (ed.).

DESIGN BUILDER 2013. Design Builder Design Guide.

DUPONTTM 2007. Data Sheet - Measured Properties. In: DUPONT_ENERGAIN_DATASHEET.PDF (ed.).

ENVIRONMENTAL PROCESS SYSTEMS LTD 2004. Product Summary. In: LTD, E. P. S. (ed.).

EUROPEAN COMMITTEE FOR STANDARDIZATION 2005. Ergonomics of the Thermal Environment. Analytical determination and interpretation of thermal comfort using calculation of the PMV and PPD indicies and local thermal comfort criteria.

FELDMAN, D., Khan, M. A. & Banu, D. 1989. Energy storage composite with an organic PCM. Solar Energy Materials, 18, 333-341.

FENG, J. D. 2014. Design and Control of Hydronic Radiant Cooling Systems.

FUMO, N., Mago, P. & Luck, R. 2010. Methodology to estimate building energy consumption using EnergyPlus Benchmark Models. Energy and Buildings, 42, 2331-2337.

GEROS, V., Santamouris, M., Karatasou, S., Tsangrassoulis, A. & Papanikolaou, N. 2005. On the cooling potential of night ventilation techniques in the urban environment. Energy and Buildings, 37, 243-257.

GOWREESUNKER, B., Tassou, S. & Kolokotroni, M. 2013. Coupled TRNSYS-CFD simulations evaluating the performance of PCM plate heat exchangers in an airport terminal building displacement conditioning system. Building and Environment, 65, 132-145.

HOUSSIN, D. International Energy Agency Webinar. 2013.

INTERNATIONAL ENERGY AGENCY (IEA) 2014. Energy Technology Perspectives.

JEFFRIES, I., Rowlands-Rees, T., 2013. Energy Efficiency Trends Annual Report 2012/13. EEVS and Bloomberg New Energy Finance.

KENDRICK, C. & Walliman, N. 2007. Removing unwanted heat in lightweight buildings using phase change materials in building components: Simulation modelling for PCM plasterboard. Architectural Science Review, 50, 265-273.

KOLOKOTRONI, M. & Aronis, A. 1999. Cooling-energy reduction in air-conditioned offices by using night ventilation. Applied energy, 63, 241-253.

KOSCHENZ, M. & Lehmann, B. 2004. Development of a thermally activated ceiling panel with PCM for application in lightweight and retrofitted buildings. Energy and Buildings, 36, 567-578.

LITTLEWOOD, J. 2011. Recommended Specification for Non-Domestic Buildings

MEIERHANS, R. A. Slab cooling and earth coupling. ASHRAE Transactions, 1993. 511-518.

MONODRAUGHT LTD 2014. Cool-Phase(r) Natural Cooling and Low Energy Ventilation System.

OSTERMAN, E., Tyagi, V., Butala, V., Rahim, N. & Stritih, U. 2012. Review of PCM based cooling technologies for buildings. Energy and Buildings, 49, 37-49.

PHASE CHANGE ENERGY SOLUTIONS 2010. Beyond InsulationTM Bio PCM. Asheboro, NC: Phase Change Energy Solutions.

SHAVIV, E., Yezioro, A. & Capeluto, I. G. 2001. Thermal mass and night ventilation as passive cooling design strategy. Renewable energy, 24, 445-452.

SUSMAN, G., Dehouche, Z., Cheechern, T. & Craig, S. 2011. Tests of prototype PCM 'sails' for office cooling. Applied Thermal Engineering, 31, 717-726.

WADE, J., Pett, J., Ramsay, L., 2003. Energy efficiency in offices: Assessing the situation. The Association for the Conservation of Energy.

WHIFFEN, T. R. & Riffat, S. B. 2012. A review of PCM technology for thermal energy storage in the built environment: Part II. International Journal of Low-Carbon Technologies.

WINWOOD, R. B., R. & Edwards, R. 1997. Advanced fabric energy storage I: Review. BUILDING SERVICES ENGINEERING RESEARCH TECHNOLOGY, 18, 1-6.

XU, X., YU, J., Wang, S. & Wang, J. 2014. Research and application of active hollow core slabs in building systems for utilizing low energy sources. Applied Energy, 116, 424-435.

YAHAY, N. & Ahmad, H. 2011. Numerical investigation of indoor air temperature with the application of PCM gypsum board as ceiling panels in buildings. Procedia Engineering, 20, 238-248.

SESSION 18: PHASE CHANGE MATERIALS

316: Experimental study of heat transfer during mPCM slurry flow in microchannels

RABIA SHAUKAT[1,2], MUHAMMAD SAJID KAMRAN[2], SAQIB RAZA JAVANI[1], LEI CHAI[1], JIE SUN[3], TONG YANG[4], HUA SHENG WANG[1],*

[1]School of Engineering and Materials Sciences, Queen Mary University of London, E1 4NS, r.shaukat@qmul.ac.uk [2]Department of Mechanical Engineering University of Engineering and Technology, Lahore, Pakistan.
[3]Institute of Engineering Thermophysics, Chinese Academy of Sciences, Beijing 100190, China.
[4]Centre For Sustainable Energy Technologies, Faculty of Science and Engineering, The Nottingham University Ningbo, Ningbo, China

Microencapsulated phase change materials (mPCM) slurries have been used as the working fluids to enhance heat transfer compared with pure water due to their high latent heat and almost constant temperature during the phase change. A test rig has been built to measure heat transfer and pressure drop during the mPCM slurry flow in microchannels. Local surface temperature and heat flux along the channels are determined from temperatures measured at 98 precisely-known locations in the aluminum test block by inverse solution of the conduction equation (Yu et al. (2014)). The mass concentration of the mPCM slurry varies from 0 to 5%. The mass flow rate varies from 3.3 to 6.6 g/s. The results of the mPCM slurry are also compared with those of pure water. The results showed that 5% mass concentration of mPCM slurry showed local wall temperature reduction and increase in local heat flux as compared to pure water. This enhancement in heat transfer performance of mPCM slurry depends on the mass flow rate of mPCM slurry flow inside the microchannels.

Keywords: Heat transfer, microencapsulated phase change material, microchannel, inverse conduction

1. INTRODUCTION

Microchannel heat exchangers are compact in size and efficient in heat transfer due to their high ratio of heat transfer area to volume. The application of slurry of phase change materials (PCM) with high latent heats as coolant in microchannel heat exchangers has attracted much attention. The potential benefits of the PCM slurry include high heat absorption during phase change and increase of effective thermal conductivity resulting from more particle-particle and particle to fluid interactions. Since the effective heat capacity of the phase change materials is large, the temperature of the fluid remains constant during the melting or solidification of PCM particles, resulting in the constant wall temperature of electronic devices and bulk fluid temperature.

During the past decade, a lot of research has been carried out to analyse the improvement in heat transfer performance of mPCM slurry compared to pure water in macrochannels of hydraulic diameter > 4 mm (Chen et al. (2008), Yamagishi et al. (1999), Zeng et al. (2009), Wang et al. (2008)). Recently, interest has been advanced to examine the heat transfer performance of mPCM slurry for applications in microchannel heat exchangers and for cooling of electronic devices. A few experimental and numerical studies have been available for microencapsulated phase change materials (mPCM) slurry flow in microchannels. Kondle et al. (2013) numerically studied the heat transfer chracteristics of mPCM slurry in rectangular microchannels with aspect ratios ranging from 1 to 8. They observed enhanced heat transfer and constant bulk fluid temperature during the phase change process in all cases. Effects of Stefan number and melting range of mPCM slurry was numerically investigated by Ravi (2008) in smooth and internally finned circular microchannel. The results showed that decrease in Stefan number and melting range increased heat transfer. He also examined the effect of fin heights under boundary condition of constant heat flux and constant temperature. The enhanced heat transfer performance in finned tubes was observed due to increased surface area. Sabbah et al. (2008) numerically investigated the three dimensional conjugated heat transfer in microchannel heat sink with 100 μm width and 500 μm height of microchannels. The results showed that enhancement factor increased from 30-50% for 25% volume concentration of mPCM slurry. In another study, Sabbah et al. (2011) investigated the effect of mPCM particles on the development of thermal boundary layer. They found that the presence of mPCM particles delayed the development of thermal boundary layer, which has also been observed by Seyf et al. (2013).

In numerical studies, it is very easy to obtain the local temperatures and heat fluxes. But as far as experimental studies on microchannels are concerned, it is very difficult to obtain the local wall temperature and heat flux due to very small size of microchannels. Researchers used different methods to obtain the wall temperature of microchannels. Rao et al. (2007) experimentally investigated convective heat transfer performance of mPCM slurry flow in rectangular minichannels (4.2 mm height, 2 mm width and 150 mm length) under boundary condition of constant heat flux and found that mPCM slurry with 5% mass concentration showed higher Nusselt number and heat transfer coefficient with respect to water within the considered mass flow rates ranging from 0.05 to 0.35 kg/min. Six thermocouples have been placed along the flow direction inside the copper block at certain distance beneath the microchannel bottom wall. Wall temperature of microchannel was calculated by assuming one dimensional heat conduction in the copper block beneath the minichannels. Later, Dammel and Stephan (2012) modified length of test section of Rao et al. (2007) to increase residence time of mPCM slurry in microchannel. They examined that in order to take the maximum advantage of latent heat of mPCM slurry, optimum inlet temperature and the mass flow rate should be considered. Wu et al. (2013) experimentally analysed the heat transfer performance of bare and silica nanoencapsulated PCM dispersed with PAO (poly alpha olefin) in microchannel heat exchanger. Their results showed that at same velocity nanoencapsulated mPCM slurry showed 2 times better heat transfer as compared to pure PAO. Ho et al. (2013) carried out experimental study to examine the convective heat transfer characteristics of mPCM slurry in minichannels of 1.5 mm height and 1 mm width. They found about 52% enhancement in heat transfer effectiveness at $Re = 133$. Wall temperature of microchannel was calculated by the same method as Rao et al. (2006). In another study, Ho et al. (2014) developed correlation for mPCM slurry flow in microchannels. Wang and Lin (2012) did experimental study on convective heat transfer characteristics of mPCM slurry flow in rectangular channel of 0.14 aspect ratio. Wall temperature was measured by welding eight thermocouples to the shorter side of rectangular tube along the flow direction of rectangular tube. They observed about 16% dimensionless wall temperature reduction for 20% mass concentration of mPCM slurry as compared to water.

So far in the experimental studies average heat transfer was measured in microchannels. The present work is to find the local wall temperature and heat flux at inaccessible channel liquid interface by

measuring the temperature at ninety eight precisely known accessible locations inside the test block. The local wall temperature and heat flux are determined by inverse solution of conduction equation by Yu et al. (2014). An experimental test rig has been built to analyse the heat transfer characteristics of mPCM slurry flow in microchannels. Experiments have been conducted for pure water and mPCM slurry with 5% mass concentration for mass flow rates ranging from 3.3 – 6.6 g/s. The comparison of local wall temperature and heat flux along the flow direction of microchannel for mPCM slurry and pure water has been made.

2. THERMOPHYSICAL PROPERTIES OF mPCM SLURRY

The mPCM slurry Micronal DS 5037X was provided by BASF. The solid content of mPCM slurry was 43% which was diluted with distilled water to make the required concentration. The melting point of the mPCM particles was 26 °C. The scanning electron image of mPCM particles is shown in Figure 24. The nominal diameter of the particles were found from 5 to 11 µm. The phase transition and latent heat capacity of mPCM particles were measured by differential scanning calorimeter (Mettler Toledo).

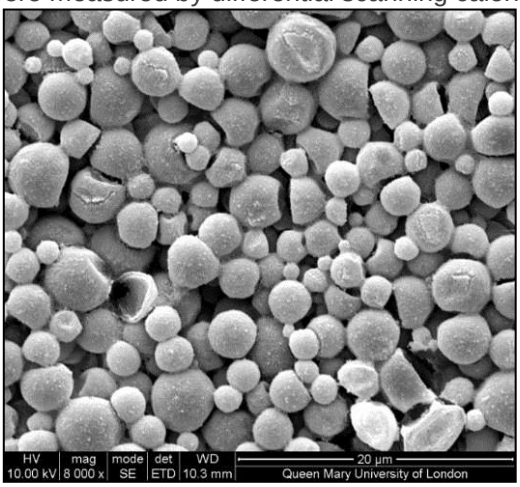

Figure 24: Microencapsulated PCM particles before thermal cycling

The phase transition and latent heat capacity of mPCM particles were measured by differential scanning calorimeter (Mettler Toledo) as shown in Figure 25 and Figure 26. Figure 25 shows that the mPCM particles started melting at 23.32 °C and completely melts at 27.65 °C. The latent heat of mPCM particles was found to be 80.36 kJ/kg.

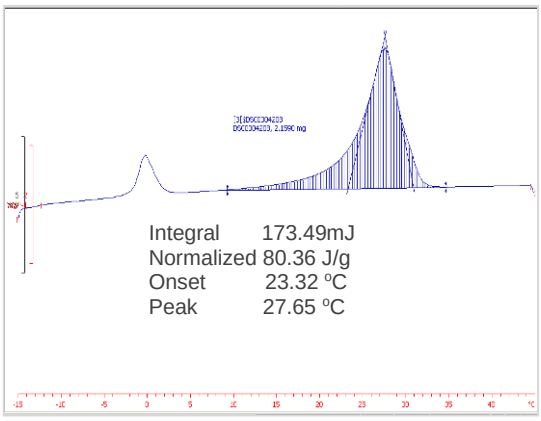

Figure 25: DSC curve of mPCM particles during heating cycle

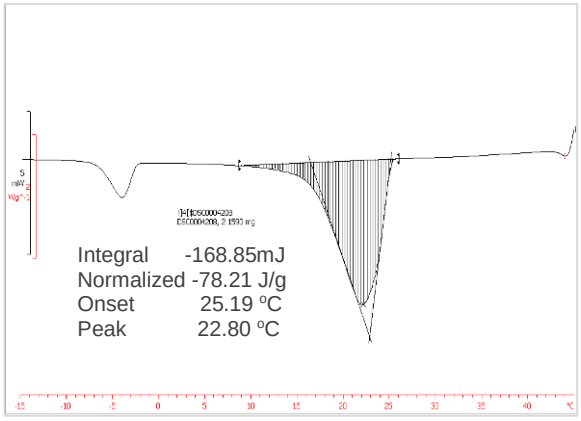

Figure 26: DSC curve of mPCM particles during cooling cycle

The thermophysical properties of mPCM slurry are given in Table 12. The density, ρ_b, thermal conductivity, k_b, dynamic viscosity, μ_b, latent heat capacity, h_{fg}, and specific heat capacity, C_b, were evaluated by the Equations 1-5.

$$\rho_b = \frac{1}{c/\rho_p + (1-c)/\rho_w} \quad (1)$$

where ρ_b is the density of bulk mPCM slurry, ρ_p is the density of solid PCM, ρ_w is the density of water, and c is the mass concentration of mPCM slurry.

$$k_b = k_w \cdot \frac{k_w + k_p + 2\emptyset(k_p - k_w)}{k_w + k_p - \emptyset(k_p - k_w)} \quad (2)$$

where k_b is the thermal conductivity of bulk mPCM slurry, k_p is the thermal conductivity of solid PCM, k_w is the thermal conductivity of water, and $\emptyset$ is the volume concentration of mPCM slurry

$$\mu_b = \mu_w(1 - \emptyset - 1.16\emptyset^2)^{-2.5} \quad (3)$$

where μ_b is dynamic viscosity of bulk mPCM slurry, μ_w is the dynamic viscosity of water.

$$h_{fg} = ch_{fgp} \quad (4)$$

where h_{fg} is the latent heat of bulk mPCM slurry and h_{fgp} is the latent heat of mPCM particles

$$C_b = cC_p + (1-c)C_w \quad (5)$$

where C_b is the specific heat capacity of bulk mPCM slurry, C_p is the specific heat capacity of solid mPCM, and C_w is the specific heat capacity of water.

Table 12:Thermophysical properties of working fluid

Fluid	c %	ρ kg/m^3	k W/mK	C_p J/kgK	μ kg/ms
Pure water	0	998	0.6	4180	1.010x10^{-3}
mPCM slurry	5	989.6	0.571	4065	1.147x10^{-3}

3. EXPERIMENTAL SETUP

3.1. Test system

Figure 27 shows the schematic of apparatus. The experimental setup consisted of two loops, one is mPCM slurry flow and the other is heating water loop represented by red and blue colour respectively. The working fluid was pumped into test section through mixing chamber. After passing through the mixing chamber working fluid was distributed into six microchannels (1.5 mm height x 1.0 mm width) which were machined on the lower block of aluminium test section. Temperatures were measured at the inlet and outlet of mixing chamber. A slot of length 16 mm, width 6 mm and height 4 mm has machined inside the aluminium block for temperature and pressure measurements at the inlet and outlet of microchannel. The test section was heated from above and below by passing pure water through jacket in counterflow direction as shown in Figure 28. Four water mixers originally designed by Krishnaswamy et al. (2006) were installed to ensure more accurate bulk fluid temperature measurement at inlet and outlet of heating water jacket. The inlet temperature of both the loops were maintained constant by heating thermostats (Lauda Ecogold 10 with accuracy ±0.01K). The flow rates for the upper and lower heating water loop were controlled by FR-4000 acrylic flow meters with accuracy of ±2%. Cooling water was circulated inside the mPCM slurry thermostat for solidifying PCM particles. Temperature of mPCM slurry thermostat was maintained at 22 ^{o}C to ensure that all PCM particles solidify before entering into the microchannel.

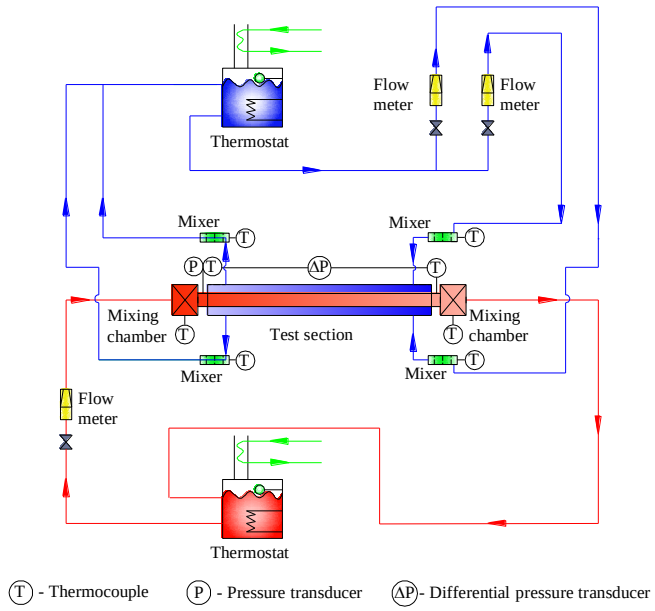

Figure 27: Schematic of apparatus

3.2. Test section

The test section consisted of two aluminium blocks (500 mm length x 40 mm width x 15 mm height). Six microchannels (1.5 mm height x 1.0 mm width x 500 mm length) were machined on the lower block of test section. Fourteen thermocouple holes, with diameter 0.6 mm, were drilled vertically in aluminium block at a depth of 20 mm. Total 98 thermocouple holes of diameter 0.3 mm were drilled at seven known locations along the length of test block. The physical model, with coordinates and boundary conditions of the test section are represented in Figure 29. *H, W* and *L* are the height, width and length of test block. *Lu* and *Ld* are the adiabatic sides of the test block. Local surface temperature and heat flux along the length of microchannel was determined by solution of inverse conduction (see Yu et al. (2014)).

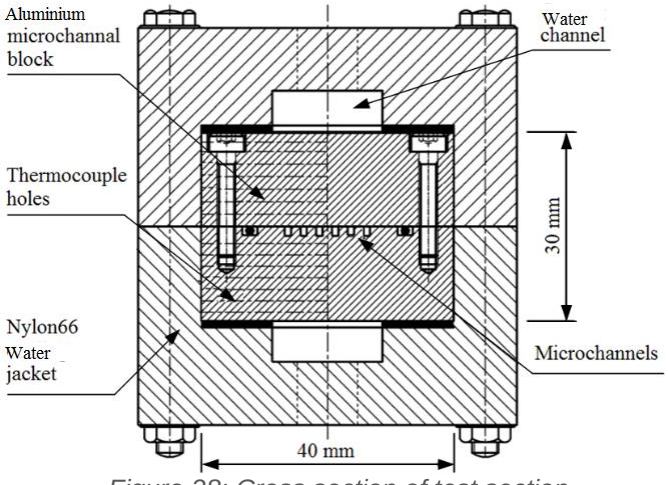

Figure 28: Cross section of test section

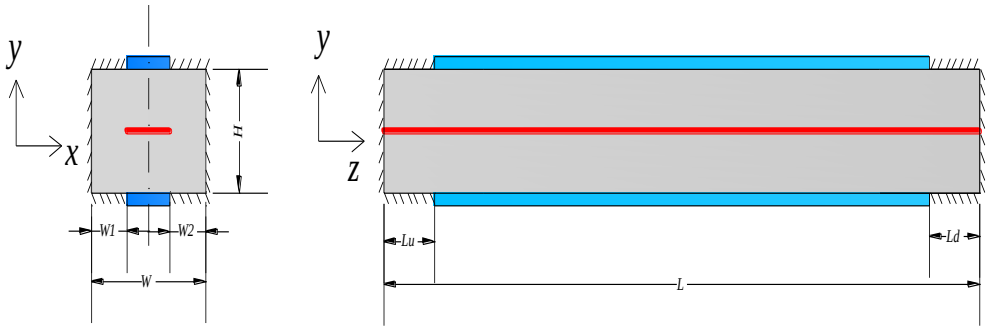

Figure 29: Physical model and coordinates

All the thermocouples were calibrated against the platinum resistance thermometer in a high accuracy constant temperature water bath. All measurements were recorded after the temperature and pressure measurements reached to steady state. An Agilent data acquisition system model 34580A with two 70 channel data cards 34980A were used for recording data.

4. EXPERIMENTAL RESULTS AND DISCUSSIONS

Heat transfer experiments were conducted with pure water and 5% mass concentration mPCM slurry. Mass flow rate of working fluid was varied from 3.3 g/s to 6.6 g/s. The inlet temperature of the working fluid was maintained at 23 ^{o}C which was close to the onset of phase change. Hot water at 60 ^{o}C were circulated inside the top and bottom jackets at mass flow rate of 29 g/s.

4.1. Temperature distribution

Temperature was measured at the 98 precisely known locations inside the test block. Figure 30 and Figure 31 show the measured temperature distribution inside the test blocks at seven locations along the flow direction of microchannel. In Figure 31 at z = 85 mm, the temperature of first point near to channel in upper block for 5% mass concentration mPCM slurry is 1.12 ^{o}C lower as compared to pure water. However, the temperature drop is only 0.37 ^{o}C at z = 415.

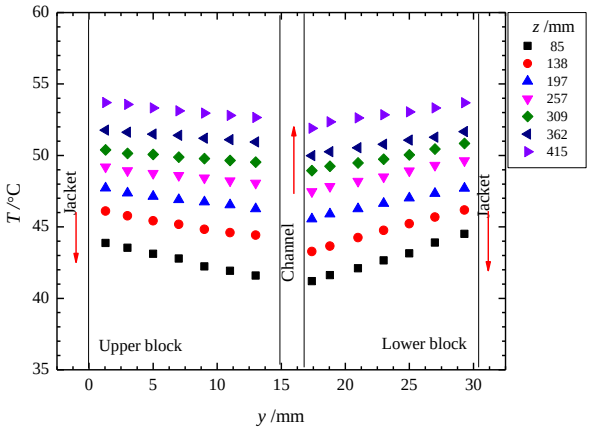

Figure 30: Temperature distributions inside the block(c = 0 %, $T_{ch} = 23\ ^{o}C, m_{ch} = 3.3g/s$, $T_{jac} = 60\ ^{o}C$, $m_{jac} = 29g/s$)

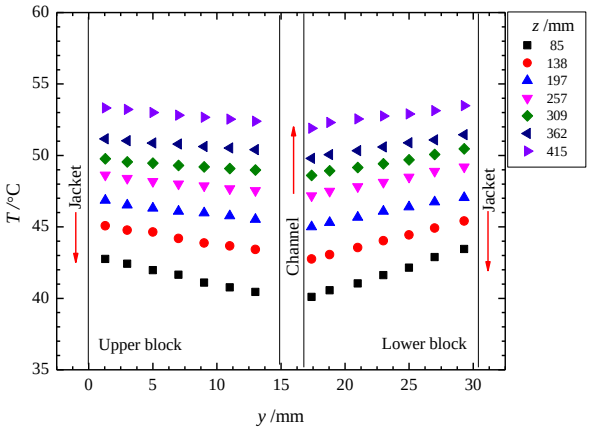

Figure 31: Temperature distributions inside the block (c = 5 %, $T_{ch} = 23\ ^{o}C, m_{ch} = 3.3g/s$, $T_{jac} = 60\ ^{o}C, m_{jac} = 29g/s$)

4.2. Local wall temperature and heat flux

The local wall temperature and heat flux were obtained by the inverse solution of conduction equation (see Yu et al. (2014)). Figure 32 and Figure 33 show the local wall temperature and heat flux at channel liquid interface along the flow direction of microchannel. It can be seen from Figure 32 that the wall temperature for 5% mass concentration mPCM slurry is 1.37 ^{o}C lower than pure water at z = 0 m. The wall temperature

difference between water and mPCM slurry is prominent till *z* = 0.4 m due to phase change of mPCM slurry. After *z* =0.4 m the wall temperature for both the water and mPCM slurry remains same.

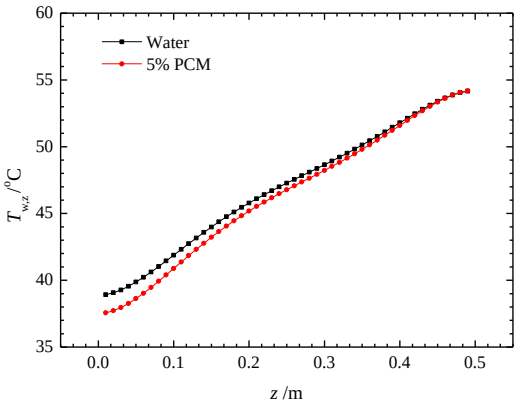

Figure 32: Temperature variation along the length of channel (T_{jac}= 60 °C, m_{jac} = 29 g/s, $T_{ch,in}$ = 23 °C, m_{ch} = 3.3 g/s)

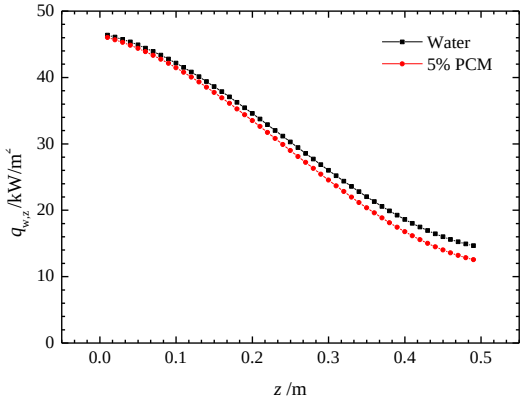

Figure 33: Heat flux variation along the length of channel (T_{jac}= 60 °C, m_{jac} = 29 g/s, $T_{ch,in}$ = 23 °C, m_{ch} = 3.3 g/s)

Figure 33 shows that the heat flux variation along the flow direction of microchannel. The heat flux for mPCM slurry is lower compared to the pure water throughout the whole length of channel. It seems after *z* = 0.2 m, the heat flux for 5% mass concentration mPCM slurry drops more as compared to pure water. This may be due to the complete melting of mPCM slurry till *z* = 0.2 m. After the complete melting of mPCM particles, heat transfer performance of mPCM slurry is poor due to lower specific heat capacity of mPCM slurry as compared to pure water.

Local wall temperature and heat flux at channel liquid interface for the case of mass flow rate of 4.9 g/s are represented by Figure 34 and Figure 35 respectively. Figure 34 shows that the wall temperature for mPCM slurry is 5.8% and 2% lower at the inlet and outlet of microchannel respectively compared to pure water. The wall temperature drops due to the increase heat absorption of mPCM slurry during phase change process. Moreover, Figure 35 depicts that the heat flux for mPCM slurry is higher as compared to pure water throughout the whole length of channel. This suggests that mPCM particles started melting near the inlet of channel and remains partially melted near the outlet of microchannel. Hence, 5% mass concentration mPCM slurry showed better performance at mass flow rate of 4.9 g/s as compared to 3.3 g/s.

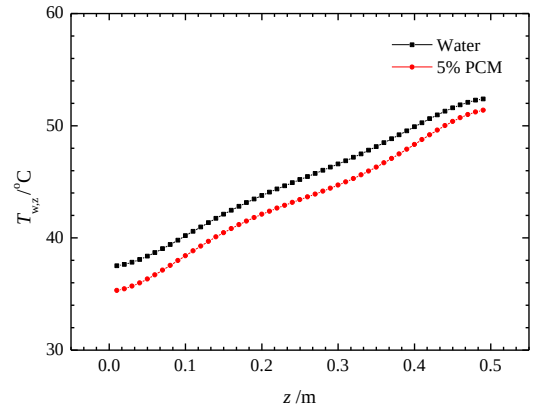

Figure 34: Temperature variation along the length of channel (T_{jac}= 60 °C, m_{jac} = 29 g/s, $T_{ch,in}$ = 23 °C, m_{ch} = 4.9 g/s)

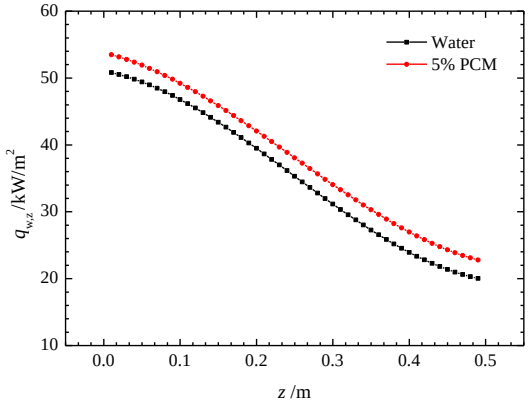

Figure 35: Heat flux variation along the length of channel (T_{jac}= 60 °C, m_{jac} = 29 g/s, $T_{ch,in}$ = 23 °C, m_{ch} = 4.9 g/s)

For the case of mass flow rate of 6.6 g/s local wall temperature and heat flux along the flow direction of microchannel are shown in Figure 36 and Figure 37 respectively. Figure 36 depicts that the wall temperature for 5% mass concentration mPCM slurry is 0.9 °C and 2 °C lower than water at inlet and outlet

of microchannel respectively. This is due to high latent heat of mPCM slurry as compared to water. However, Figure 37 shows that at the very start of microchannel the heat flux for mPCM slurry is slightly lower as compared to the water. This may be due to the mPCM slurry is still in solid phase near the inlet of microchannel. At solid phase, the specific heat capacity of mPCM slurry is less than pure water. Then, after z =0.1 m the heat flux for mPCM slurry starts increasing due to the onset of phase change. At the outlet of microchannel, the heat flux for mPCM slurry is 6% higher as compared to water. It seems that the mPCM slurry is still melting at the outlet of channel. Therefore, optimum length of the microchannel should be considered for complete melting of mPCM slurry. Three mass flow rates of working fluid ranging from 3.3 to 6.6 g/s were compared and it has been observed that the 5% mass concentration mPCM slurry shows better performance with respect to pure water at mass flow rate of 4.9 g/s

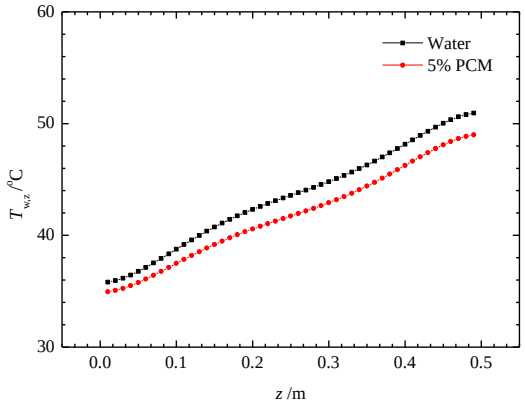

Figure 36: Temperature variation along the length of channel (T_{jac}= 60 °C, m_{jac} = 29 g/s, $T_{ch,in}$ = 23 °C, m_{ch} = 6.6 g/s)

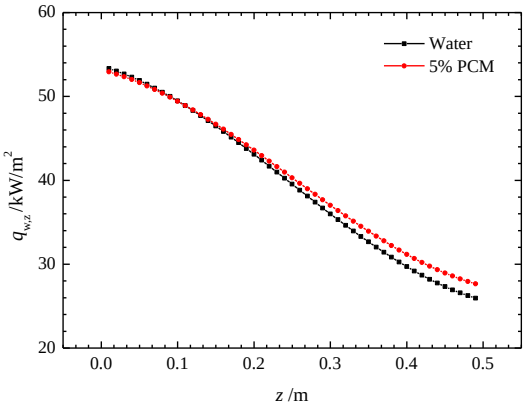

Figure 37: Heat flux variation along the length of channel (T_{jac}= 60 °C, m_{jac} = 29 g/s, $T_{ch,in}$ = 23 °C, m_{ch} = 6.6 g/s)

5. CONCLUSIONS

Heat transfer experiments were conducted for pure water and 5% mass concentration mPCM slurry at different mass flow rates ranging from 3.3 g/s to 6.6 g/s. The heat transfer performance of mPCM slurry was compared with pure water. It has been observed that heat transfer performance of mPCM slurry was strongly dependent on mass flow rate of mPCM slurry in microchannels. It was found that for low mass flow rate of 3.3 g/s the residence time of mPCM particles inside the microchannel was large enough and all PCM particles melted which results in lower heat flux because liquid PCM has lower specific heat capacity as compared to water. The mPCM slurry showed worst heat transfer performance at 3.3 g/s. For the mass flow rate of 4.9 g/s, mPCM slurry showed 5.8% local wall temperature reduction and 6% high heat flux as compared to pure water. For the mass flow rate of 6.6 g/s, mPCM particles seemed partially melted inside the microchannel. Overall, the heat transfer performance of mPCM slurry at 4.9 g/s was found superior to the other mass flow rates. Therefore, mass flow rate should be optimized for the given length of microchannel to fully utilize the latent heat capacity of mPCM particles.

6. ACKNOWLEDGEMENTS

A PhD studentship by the University of Engineering and Technology Lahore, Pakistan, EU research grant FP7-2010-IRSES-269205 and EPSRC research grant EP/L001233/1 are gratefully acknowledged.

7. REFERENCES

CHEN, B., Wang, X., Zeng, R., Zhang, Y., Wang, X., Niu, J., Li, Y. & Di, H. 2008. An experimental study of convective heat transfer with microencapsulated phase change material suspension: Laminar flow in a circular tube under constant heat flux. *Experimental Thermal and Fluid Science,* 32**,** 1638-1646.

DAMMEL, F. & Stephan, P. 2012. Heat Transfer to Suspensions of Microencapsulated Phase Change Material Flowing Through Minichannels. *Journal of Heat Transfer.*

HO, C.-J., Chen, W.-C. & Yan, W.-M. 2013. Experimental study on cooling performance of minichannel heat sink using water-based MEPCM particles. *International Communications in Heat and Mass Transfer,* 48**,** 67-72.

HO, C. J., Chen, W.-C. & Yan, W.-M. 2014. Correlations of heat transfer effectiveness in a minichannel heat sink with water-based suspensions of Al2O3 nanoparticles and/or MEPCM particles. *International Journal of Heat and Mass Transfer,* 69**,** 293-299.

KRISHNASWAMY, S., Wang, H. S. & Rose, J. W. 2006. Condensation from gas–vapour mixtures in small non-circular tubes. *International Journal of Heat and Mass Transfer,* 49**,** 1731-1737.

RAO, Y., Dammel, F., Stephan, P. & Lin, G. 2006. Flow frictional characteristics of microencapsulated phase change material suspensions flowing through rectangular minichannels. *Science in China Series E: Technological Sciences,* 49**,** 445-456.

RAO, Y., Dammel, F., Stephan, P. & Lin, G. 2007. Convective heat transfer characteristics of microencapsulated phase change material suspensions in minichannels. *Heat and Mass Transfer,* 44**,** 175-186.

RAVI, G. 2008. Study of laminar flow forced convection heat transfer behavior of a phase change material fluid. Anna University.

SABBAH, R., Farid, M. M. & Al-Hallaj, S. 2008. Micro-channel heat sink with slurry of water with micro-encapsulated phase change material: 3D-numerical study. *Applied Thermal Engineering,* 29**,** 445-454.

SABBAH, R., Seyed-Yagoobi, J. & Al-Hallaj, S. 2011. Heat Transfer Characteristics of Liquid Flow With Micro-Encapsulated Phase Change Material: Numerical Study. *Journal of Heat Transfer,* 133**,** 121702-10.

SEYF, H. R., Zhou, Z., Ma, H. B. & Zhang, Y. 2013. Three dimensional numerical study of heat-transfer enhancement by nano-encapsulated phase change material slurry in microtube heat sinks with tangential impingement. *International Journal of Heat and Mass Transfer,* 56**,** 561-573.

WANG, L. & Lin, G. 2012. Experimental study on the convective heat transfer behavior of microencapsulated phase change material suspensions in rectangular tube of small aspect ratio. *Heat and Mass Transfer,* 48**,** 83-91.

WANG, X., Niu, J., Li, Y., Zhang, Y., Wang, X., Chen, B., Zeng, R. & Song, Q. 2008. Heat transfer of microencapsulated PCM slurry flow in a circular tube. *AIChE Journal,* 54**,** 1110-1120.

WU, W., Bostanci, H., Chow, L. C., Hong, Y., Wang, C. M., Su, M. & Kizito, J. P. 2013. Heat transfer enhancement of PAO in microchannel heat exchanger using nano-encapsulated phase change indium particles. *International Journal of Heat and Mass Transfer,* 58**,** 348-355.

YAMAGISHI, Y., Takeuchi, H., Pyatenko, A. T. & Kayukawa, N. 1999. Characteristics of microencapsulated PCM slurry as a heat-transfer fluid. *AIChE Journal,* 45**,** 696-707.

YU, G. X., Sun, J., Wang, H. S., Wen, P. H. & Rose, J. W. 2014. Meshless inverse method to determine temperature and heat flux at boundaries for 2D steady-state heat conduction problems. *Experimental Thermal and Fluid Science,* 52**,** 156-163.

ZENG, R., Wang, X., Chen, B., Zhang, Y., Niu, J., Wang, X. & Di, H. 2009. Heat transfer characteristics of microencapsulated phase change material slurry in laminar flow under constant heat flux. *Applied Energy,* 86**,** 2661-2670.

441: Shape-stabilized phase change materials (SSPCM) with balanced thermal property, strength, thermal conductivity and durability

RUI YANG[1*], YI WANG[2], JIANPING WANG[3], WEIXIA WANG[4]

1 Department of Chemical Engineering, Tsinghua University, Beijing 100084, China, yangr@mail.tsinghua.edu.cn
2 Department of Chemical Engineering, Tsinghua University, Beijing 100084, China,skyret@126.com
3 Department of Chemical Engineering, Tsinghua University, Beijing 100084, China,swordabcd@163.com
4 Department of Chemical Engineering, Tsinghua University, Beijing 100084, China, sj15210957403@163.com

Energy-saving buildings appeal for the application of thermal storage materials with phase change temperature of 20-30 ℃, and paraffin is a good candidate. For the convenience of practical applications, paraffin should be encapsulated in order to prevent from leakage. Therefore, shape-stabilized phase change materials (SSPCM) were prepared by blending paraffin with high-density polyethylene (HDPE) and elastomers (e.g., ethylene-propylene-diene copolymer (EPDM) and styrene-butadiene-styrene block copolymer (SBS)). With 60 wt% paraffin, the SSPCMs exhibited good strength even when paraffin was melted. Proper crosslinking helped to increase the strength further. Due to the strong absorption ability of the elastomers, the SSPCMs showed much better durability during harsh freezing-thawing cycles. SSPCMs exhibit poor thermal conduction property and thus cannot respond to temperature changes in time. Expanded graphite (EG) and carbon nanotube (CNT) were introduced to improve the thermal conductivity of SSPCMs. Shear and/or ultrasonic treatment of EG and CNT were carried out to realize even dispersion of these fillers in SSPCMs. However, two treatment methods led to different effects on EG and CNT filled SSPCMs. Finally, thermal conductivity of SSPCMs was increased up to 1 W/m•K. Furthermore, the synergistic effect of EG and CNT was also investigated. Therefore, such SSPCMs are very promising for applications in energy-saving buildings.

Keywords: Shape-stabilized phase change material, thermal storage, strength, thermal conductivity, durability

1. INTRODUCTION

In China, energy consumption of buildings comprises about 30% of total energy consumption, and may increase further in the future, so energy-saving techniques are greatly demanded. Developing new building envelopes that can take advantage of clean, sustainable solar energy to achieve comfort is a promising way. Phase change materials are good candidates. By proper encapsulation with polymer matrix, shape-stabilized phase change materials (SSPCMs) were prepared to prevent leakage and maintain the shape before and after phase change.

For SSPCMs in energy-saving buildings, firstly we hope them to have phase change temperature of 20-30 ºC and as-high-as-possible phase change heat. Then they must be strong enough to maintain the shape. They also need to be stable after long-term phase change procedure, i.e., no chemical change and no deterioration of phase change heat. In addition, they are supposed to have proper thermal conduction so as to respond to temperature changes in time.

In SSPCMs, paraffin is the most widely used working media, and various polymers were applied as the matrices, e.g., high-density polyethylene (HDPE) [(Inaba H, 1997)], low-density polyethylene (LDPE) [(Krupa I, 2007)], polypropylene (PP) [(Krupa I, Polypropylene as a potential matrix for the reation of shape stabilized phase change materials, 2007)], styrene-butadiene-styrene block copolymer (SBS) [(Xiao M, 2001)], ethylene-propylene-diene copolymer (EPDM) [(Song G, 2010)] and ethylene-vinyl acetate copolymer (EVA) [(Cai Y, 2006)]. In most cases, paraffin with the melting point of 40-60 ºC were studied, but the phase change temperature is too high for buildings. The chemical stability of paraffin itself was proved to be perfect [(Alkan C, 2009; Sun Z, 2013)], but the durability after freezing-thawing cycles was not satisfied. For HDPE/paraffin, the weight loss after 10 cycles exceeded 3 wt%[(Luo C.Y., 2010)]. In order to improve the thermal conduction of paraffin, various metals [(Hong S., 2007)] or inorganic fillers (mainly carbon fillers [(Mills A, 2006; Kim S, 2009) (Elgafy A, 2005)], e.g., expanded graphite (EG) and carbon nanotube (CNT)) were used, but report on thermal conduction enhancement of SSPCM was still rare [(Xiao M, Thermal performance of a high conductive shape-stabilized thermal storage material, 2001) (Zhang Y, 2006) (Cheng W.L., 2010)].

Therefore, in this paper, paraffin based SSPCMs were prepared; the thermal property, mechanical property, cyclic durability and the thermal conductivity were investigated.

2. EXPERIMENTAL

2.1 Preparation of SSPCMs

Paraffin was mixed with elastomer (EPDM or SBS) and HDPE first (paraffin:elastomer:HDPE=60:30:10), and then melt-blended at 140 ºC for 6 min in a torque rheometer (Haake, Polylab QC) to prepare SSPCMs. In order to improve the mechanical property, small amount of DCP (0-4 phr) was added during the melt-blending. In order to enhance the thermal transfer, 0-7 phr EG and/or 0-2 phr MWCNT were added. Shearing or ultrasonic treatment of EG and MWCNT were carried out in paraffin first and then melt-blended with the HDPE/elastomer alloy. The SSPCMs were hot-pressed to plates or bars for further characterization.

2.2 Characterization

Phase change temperature and enthalpy were determined in N_2 by using a differential scanning calorimetry (DSC) (Q-100, TA Instruments, USA). About 5 mg samples were cooled from to -40 ºC and then heated to 60 ºC at a rate of 10 ºC/min. Cyclic durability was determined by heating samples at 60 ºC for an hour and then cooling at 0 ºC for an hour as a freezing/thawing cycle. The original weight and the weight after every five cycles were determined after the paraffin at surface was wiped by a filter paper. Tensile strength of samples were tested by a universal testing machine (GoTech, Taiwan). At least three samples were tested to obtain the average value. Thermal diffusivity α and heat capacity C_p of samples were measured by a laser flash diffusivity system (Netzsch LAF477, German), and the thermal conductivity was calculated by multiplying α, C_p and the density ρ. Microstructure of samples were observed by a scanning electron microscopy (JSM-7401, JEOL, Japan) and a transmission electron microscopy (JEM-2100, JEOL, Japan).

3. RESULTS AND DISCUSSIONS

3.1 Preparation, thermal property, mechanical property and cyclic stability

In our previous work [(Yi Wang, 2014)], four elastomers (EPDM, #1 SBS, #2 SBS and #3 SBS) were used to absorb and encapsulate paraffin. And HDPE/elastomer alloy was used as the matrix to keep paraffin inside and maintain the shape well even when paraffin melted. DSC measurements in Figure 1 proved that these SSPCMs had the same melting/freezing points (291K) with paraffin, with latent heats of 80-100 J/g.

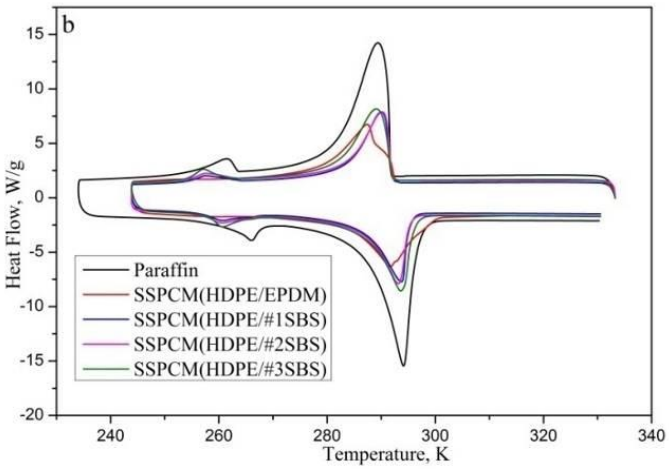

Figure 1: DSC curves of paraffin and SSPCMs with various elastomers [(Yi Wang, 2014)].

High concentration paraffin ensured enough thermal storage ability of SSPCMs. But the strength of SSPCMs with large amount of paraffin is rather weak. The tensile strength of SSPCMs was only 0.3-0.6 MPa, much lower than that of the matrix. Figure 2 showed the effect of crosslinking on the tensile strength. With DCP as the crosslinking agent, the tensile strength of EPDM/HDPE/paraffin was increased gradually to 1MPa; the tensile strength of #3SBS/HDPE/paraffin was increased up to 2MPa.

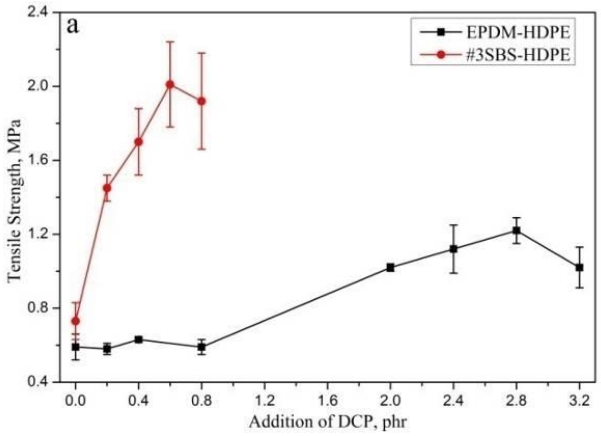

Figure 2: Effect of DCP on the tensile strength of SSPCMs with EPDM/HDPE and #SBS/HDPE as matrices [(Yi Wang, 2014)].

SSPCMs must undergo continuous phase change when they are used in buildings, so cyclic stability is quite important and required for long-term service. The melting and freezing cycle tests were carried out and the mass losses were plotted in Figure 3. All the SSPCMs showed similar mass loss behaviour, and the mass losses (due to the evaporation of paraffin) after 100 cycles were about 8-10%. In contrast, the mass loss of HDPE/paraffin, the most reported SSPCM in literatures, reached about 14% after only 40 cycles. The results demonstrated that HDPE/elastomer alloy was a good matrix to achieve long service time in buildings.

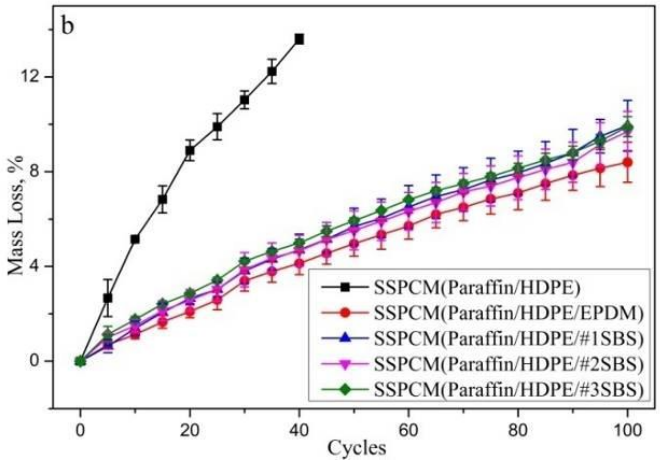

Figure 3: Mass loss ratios of SSPCMs during freezing/thawing cycles [(Yi Wang, 2014)]. (Data of paraffin/HDPE were plotted for comparison)

3.2 Thermal conductivity

SSPCMs have poor thermal conduction property, the thermal conductivity is only about 0.2 W/mK. According to the simulation result by Xu [(Xu X, 2005)], for SSPCMs in passive solar buildings, improving the thermal conductivity helped to increase the solar energy absorbing speed. Two carbon fillers with great thermal conductivity - expanded graphite (EG) and multi-wall carbon nanotube (MWCNT), were used to improve the thermal conductivity of SSPCMs. Figure 4 shows the microscopic morphologies of EG and MWCNT.

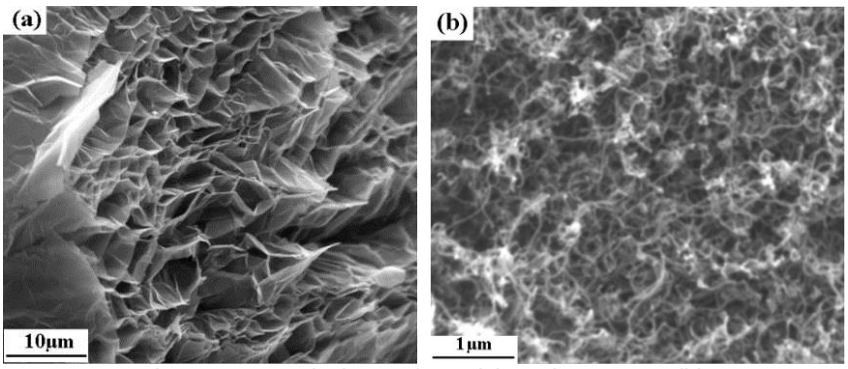

Figure 4: Morphology of EG (a) and MWCNT (b).

EG is worm-like, with nanoplatelets stacked together to form porous structure. MWCNT is thread-like, with aspect ratio of more than 1000. They are quite easy to aggregate in SSPCMs, so two pre-treatment ways to disperse them in SSPCMs were carried out, and the effects on the thermal conductivity were shown in Figure 5 and Figure 6. The ultrasonic treatment and shearing had different effects on the dispersion of EG and MWCNT. The ultrasonic treatment was effective to achieve a good dispersion of EG, so the thermal conductivity increased with the EG concentration. With 7% EG, the thermal conductivity reached 1 W/mK. But shearing after ultrasonic treatment might break the porous structure of EG, and there was nearly no improvement when 0.5-2% EG was added. In contrast, ultrasonic treatment had little effect on the dispersion of MWCNT, and there was no obvious increase of thermal conductivity when 0.2-1.2% MWCNT was added. When shearing of MWCNT after ultrasonic treatment was carried out, the dispersion of MWCNT was improved slightly. Consequently, the thermal conductivity increased in a slow speed. With 2% MWCNT, the thermal conductivity reached about 0.5 W/mK.

There was a synergistic effect between two-dimensional structure of EG and one-dimensional structure of MWCNT. They formed a more effective nanoparticle network with significantly reduced thermal contact resistance. Here MWCNT was pre-treated by shearing and sonication and EG was pre-treated by sonication before melt-blending with SSPCMs. The thermal conductivities of SSPCMs with hybrid filler (2% EG + 0-1% MWCNT) are shown in Figure 7, compared with the calculated data by the addition law. The measured thermal conductivity is higher than the calculated data. EG nanoplatelets dispersed relatively well in SSPCMs, and MWCNT served as bridges between them (Figure 8(a)). MWCNT connected EG

nanoplatelets and provided extra channels for heat flow. However, only part of EG nanoplatelets and MWCNTs formed such a connection, there were still large amount of MWCNTs aggregated, as shown in Figure 8(b). This implied a not satisfied dispersion. If all the EG nanoplatelets and MWCNTs dispersed well and connected each other, much higher thermal conductivity could be expected.

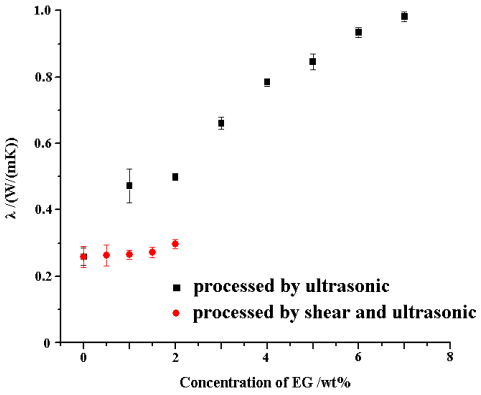

Figure 5: Thermal conductivity of SSPCM with EG as the filler.

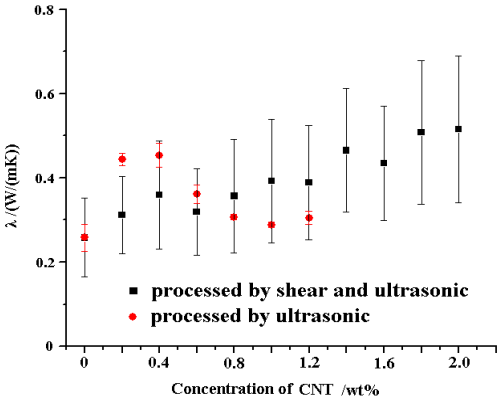

Figure 6: Thermal conductivity of SSPCM with MWCNT as the filler.

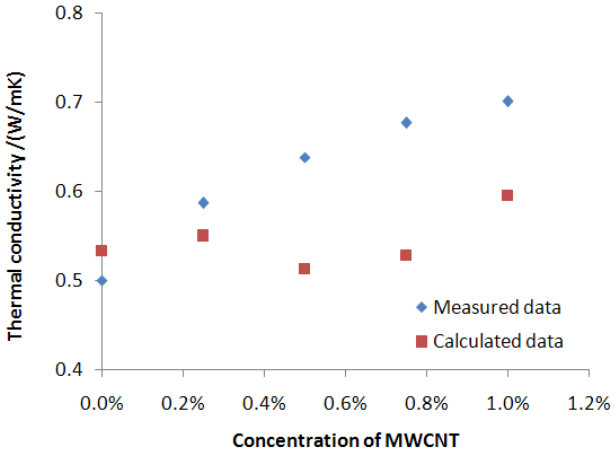

Figure 7 : Thermal conductivity of SSPCM with hybrid $EG_{2\%}MWCNT_X$ filler as a function of MWCNT concentration (X); X varies from 0 to 1%.

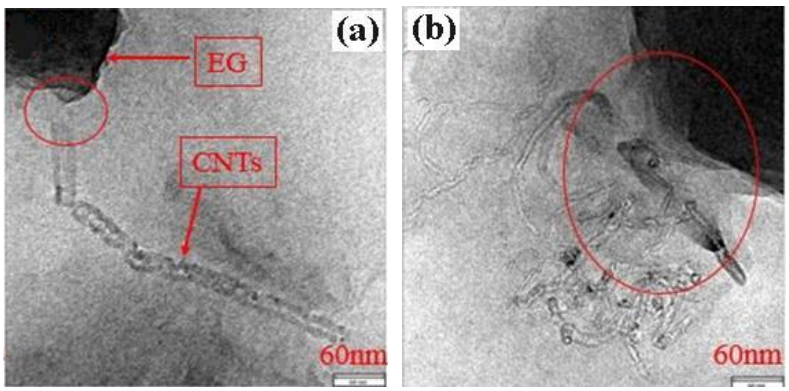

Figure 8: Microscopic morphology of SSPCMs with hybrid $EG_{2\%}MWCNT_X$ filler. (a) bridge connection between EG nanoplatelets and MWCNTs; (b) aggregation of MWCNTs

4. CONCLUSION

In this paper, SSPCMs with good processability and encapsulation ability to paraffin was prepared. They showed balanced thermal property, mechanical property, cyclic stability and thermal conductivity. SSPCMs

have poor thermal conductivity. By introducing EG and MWCNT into SSPCMs and dispersing the fillers by ultrasonic treatment and/or shearing, the thermal conductivity was increased to various extents. Furthermore, there was a synergistic effect between EG and MWCNT through the bridge connection structure. The prepared SSPCMs are promising solar energy absorbing material in energy-saving buildings. In addition, the thermal conductivity can be further increased by lessening the aggregation of MWCNT fillers.

5. ACKNOWLEDGEMENT

The authors greatly appreciate the National Science and Technology Ministry of China (Project 2013BAJ03B04) for the financial support to the work in this paper.

6. REFERENCES

ALKAN C, Kaya K, Sarı A. 2009. Preparation, thermal properties and thermal reliability of form-stable paraffin/polypropylene composite for thermal energy storage. *Polymer and Environment*, 17, 254-258

CAI Y, Hu Y, Song L, et al. 2006. Preparation and characterizations of HDPE-EVA alloy/OMT nanocomposites/paraffin compounds as a shape stabilized phase change thermal energy storage material. *Thermochim Acta*, 451, 44-51

CHENG W.L., Zhang R.M., Xie K. et al. 2010. Heat conduction enhanced shape-stabilized paraffin/HDPE composite PCMs by graphite addition: Preparation and thermal properties. *Solar Energy Materials and Solar Cells*, 94, 1636-1642

ELGAFY A, Lafdi K. 2005. Effect of carbon nanofiber additives on thermal behavior of phase change materials. *Carbon*, 43, 3067-3074

HONG S., Herling D R. 2007. Effects of Surface Area Densityof Aluminum Foamson Thermal Conductivity of Aluminum Foam-Phase Change Material Composites. *Advanced Engineering Materials*, 7,554-557

INABA H, Tu P. 1997. Evaluation of thermo physical characteristics on shape stabilized paraffin as a solid - liquid phase change material. *Heat and Mass Transfer*, 34, 307-312

KRUPA I, Mikova G, Luyt A S. 2007. Phase change materials based on low-density polyethylene/paraffin wax blends. *European Polymer*, 43, 4695-4705

KRUPA I, Mikova G, Luyt A S. 2007. Polypropylene as a potential matrix for the reation of shape stabilized phase change materials. *European Polymer*, 43, 895-907

KIM S, Drzal L T. 2009. High latent heat storage and high thermal conductive phase change materials using exfoliated graphite nanoplatelets. *Solar Energy Materials and Solar Cells*, 93, 136-142

LUO C.Y., Lin X.C., Xiao W.D., et al. 2010. Research on different polyolefin encapsulating paraffin as form-stable phase change materials. *New Chemical Materials*, 38, 100-104

MILLS A, Farid M, Selman J R, et al. 2006. Thermal conductivity enhancement of phase change materials using a graphite matrix. *Applied Thermal Engineering*, 26, 1652-1661

SONG G, Ma S, Tang G, et al. 2010. Preparation and characterization of flame retardant form-stable phase change materials composed by EPDM, paraffin and nano magnesium hydroxide. *Energy*, 35, 2179-2183

SUN Z, Kong W, Zheng S, et al. 2013. Study on preparation and thermal energy storage properties of binary paraffin blends/opal shape-stabilized phase change materials. *Solar Energy Materials and Solar Cells*, 117, 400-407

XIAO M, Feng B, Gong K. 2001. Thermal performance of a high conductive shape-stabilized thermal storage material. *Solar Energy Materials and Solar Cells*, 69, 293-296

XU X, Zhang Y P, Lin K P, et al.2005. Modeling and simulation on the thermal performance of shape-stabilized phase change material floor used in passive solar buildings. *Energy and Buildings*, 37 (10): 1084-1091

WANG Y, Wang S Y, Wang J P, Yang R. 2014. Preparation, stability and mechanical property of shape-stabilized phase change materials. *Energy and Buildings*, 77(1), 11-16

ZHANG Y P, Ding J H, Wang X, Yang R, Lin K P. 2006. Influence of additives on thermal conductivity of shape-stabilized phase change material. *Solar Energy Materials and Solar Cells*, 90 (11), 1692-1702

467: A novel building façade integrated with TIM and PCM

Numerical Study for Summer

XIN WANG[1, 2*], SAFFA RIFFAT[1], SUN XIAOYU[2], CHEN HONGXIA[1, 3]

1 Department of Architecture and Built Environment, University of Nottingham, Nottingham NG7 2RD, UK
2 Department of Building Science, Tsinghua University, Beijing 100084 China
3 Energy Power and Mechanical Engineering, North China Electric Power University, Beijing 102206 China
** Corresponding author: wangxinlj@tsinghua.edu.cn*

Transparent insulation material (TIM) not only is of similar function of opaque insulation but also can allow solar transmittance. Phase change material (PCM) can charge and discharge much heat during the phase change temperature range due to the high latent heat. A novel building façade is proposed by the combination of TIM and PCM and there are no moving parts or only a small fan in the structure. It could be used for residential and commercial buildings, providing heating and cooling for the living space as a sustainable low-carbon building. Fluent is adopted and a simple numerical model is set up to study the thermal performance of the novel structure. The fitted formula of overall transmission with solar incident angle is arrived. The numerical results for summer show that: (1) The average heat transfer rate of the exterior surface of the room wall increases with the increasing inlet velocity for the novel structure while decreases for the reference structure. (2) The ventilation heat transfer rate changes little with the increasing inlet velocity for the novel structure while increases for the reference structure. (3) When the inlet velocity is higher, the difference between the novel and reference structures is smaller. (4) The effect of Tm on the ventilation heat transfer rate is higher than that on the average heat transfer rate of the exterior surface of the room wall. (5) The suitable phase change temperature is 308-310K when the inlet velocity is 0.5 m/s and the corresponding total heat transfer rate can be decreased by 33.8% compared with that when Tm is 303-305K.

Keywords: TIM (transparent insulation material), PCM (phase change material), ventilation, building envelope, building energy

1. INTRODUCTION

Buildings represent about 40% of the EU-27 final energy consumption, and 36% of the total CO_2 emissions. A major part of this is due to heating and cooling to maintain comfortable indoor conditions. The EU has committed to meet 20% of all energy demand through the use of renewable energy sources by 2020, and a further target of 100% by 2050 is already underway (EREC, 2010). In the building sector, a recast of the European Performance of Buildings Directive is planned to enter into force by 2018, forcing all new buildings to become nearly net zero energy buildings.

Transparent insulation materials (TIMs) are small-celled honeycomb structures, made of highly transparent films, such as, polypropylene, polycarbonate, poly methyl meth acrylate (PMMA), translucent foam, and aerogels. Depending on the geometrical layout of the materials, TIMS can be classified into four generic types, which are absorber-parallel, absorber-perpendicular, cavity and quasi-homogeneous structures. Many studies have shown that heat transfer, in this kind of materials, is due to heat conduction but also to the propagation of thermal radiation while the convective heat transfer is generally negligible (Kaushika, 2003:317-351).

Transparent covers and Tromb walls have been integrated in façades (including the ventilated façades), which are one way of reducing building energy consumption in the heating season, and have been widely used in recent years. For more than 20 years, TIMs have been used extensively for a range of building applications in mostly cold climatic regions to reduce building heating and lighting loads. Transparent insulation systems when used to replace standard opaque insulation materials, not only perform similar functions to opaque insulation, reducing heat losses and making indoor temperatures easier to control, but can allow solar transmittance of more than 50% (Wong, 2007:1058-1071). A transparently insulated wall overcomes transmission losses with solar gains while at the same time passively providing low temperature wall heating (Voss, 2000:291-302).When used to south-facing external walls, transparent insulation materials with an air gap behind can be used to capture solar energy. This energy can be used either by venting the warm air inside, or by allowing the heat to conduct passively through the wall.

Wong et.al (Wong, 2015:418-425) presented a method for calculating the solar transmittance, absorptance and reflectance of a transparent insulation system. Optical interactions at each layer in the transparent insulation (TI) system were numerically modelled for five incidence angles. A direct to diffuse transmittance was calculated for solar radiation passing through the PMMA capillary cells with an incidence angle. In reference (Rockendorf, 1996:33-38), the authors presented an effective way to avoid overheating and simultaneously increase hot-water production and space heating by pumping water through a system of pipes attached to the outer wall surface, which is called transparently insulated hybrid wall. The experimental results showed that more than 75% of the absorbed heat could be removed by the fluid and the surface temperature at the inner wall remains moderate even after a long period of high irradiance. In reference (Athienitis, 1999:101-109), an explicit finite difference simulation model is developed to study the thermal performance of an outdoor test-room with one transparently insulated (TI) wall. During the summer season, shading is important to prevent overheating. Blind control is based on several criteria, including outside temperature, room-facing surface temperature of TI wall and room air temperature not to exceed a certain maximum. However, solar shading makes up about 20–30% of the glazed facade costs and proves to be necessary in all cases to guarantee summer comfort (Voss, 2000:291-302), which is costly. In the other hand, the overheating problems can be reduced to an acceptable level if it is possible to achieve good ventilation on hot days (Lien, 1997:27-35).

Due to high latent heat within a narrow temperature range, phase change materials (PCMs) can charge and discharge much heat while the temperature changes little. PCMs have been used as a means of heat or cold storage, especially in solar heating and cooling systems, in order to compensate solar radiation fluctuations as well as energy demand variations. Phase change material has more suitable features in peak shaving, tariff reduction, energy saving, equipment capacity reduction and increase thermal comfort (Cabeza, 2011:1675-1695).

Thus, the integration of TIM and PCM was presented. Based on the assumption of sinusoidal outdoor variation, the integration of transparent insulation material (TIM) with an amount of phase change material (PCM) can get high solar energy utilization and escape overheating problems, especially for south-facing surfaces in winter. The thermal lag effect in a building with a TIM wall was more pronounced than in an ordinary building (Athienitis, 1999:101-109).

In reference (Kara, 2012:243-246), the solar transmittance of the triple glazing unit (TGU) ranged from 0.45 to 0.55 during the winter and from 0.2 to 0.25 during the summer. The solar transmittance of the TGU

decreased 100% during summer compared to winter. As a result, no overheating problems for the PCM wall were observed in the summer.

However, there are still some important problems in the research. For example, most of existed research focused on the TIM effect and is lack of the relation between TIM and PCM including suitable ventilation. The indoor thermal comfort and the energy saving are not enough, which are potentially caused by the thermal mass with constant thermal properties and non-linear solar radiation and outdoor air temperature variation in the surroundings.

In this paper, a novel building facade integrated with TIM and PCM is proposed and researched by CFD (Fluent). It is necessary to determine the thermal performance of a building wall with TIM and PCM as a system. The function of solar transmittance of solar incidence is presented and the suitable thermal properties of PCM are presented. Although modelling is needed in order to reduce the cost for the measurements by reducing the necessary number of measurements, experiments are needed for validation. In this paper, it is only the numerical part for summer and the experiments will be done later.

2. STRUCTURE

The structure of the proposed novel building façade is schematically shown in Figure 1, which is composed of a south-facing TIM cover (A), solar absorption plate (B), air layer 1 (C), outer wall (D), PCM plate(E), air layer 2 (F), and an internal wall (G) from the left to the right. The thicknesses of the air layer 1, outer wall, PCM wall and air layer 2 are 0.1m, 0.24m, 0.02m, and 0.2m, respectively. The size of inlet and outlet are both 0.1m and the height of the TIM is 3m and the distance between the upper boundary and the upper outer wall is 0.2m.

The basic components are a south-facing TIM cover, which transmits solar energy dependent on the solar incident angle, and the PCM plates can charge/discharge the heat. The inlet is connected with outdoor and the temperature of inlet air is the same as the temperature of outdoor air.

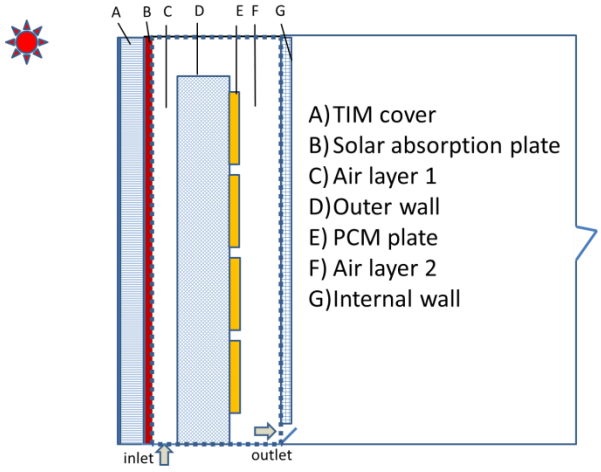

Figure 1: Schematic structure of the novel building façade

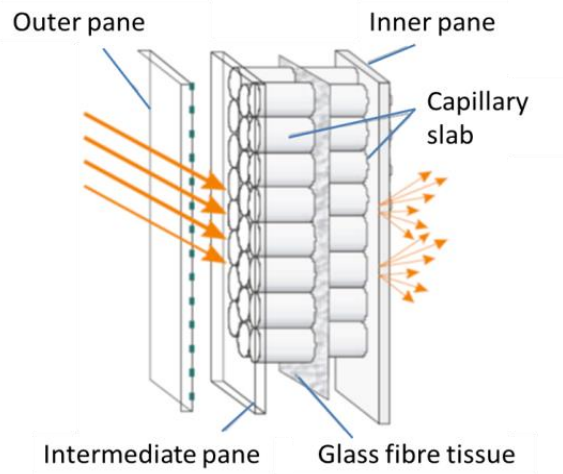

Figure 2: Schematic structure of TIM cover (http://www.skylux.ro/wp-ontent/files/i_okalux_evo_e.pdf)

The TIM cover is an important component in the novel façade. Figure 2 shows the schematic structure of one kind of TIM, which is OKALUX EVO light diffusing insulating glass made by Germany (http://www.skylux.ro/wp-content/files/i_okalux_evo_e.pdf). With the use of a translucent light diffusing capillary slab with additional glass fiber tissues in between, OKALUX EVO can achieves light transmission and total solar energy transmittance as required with very good heat insulation. The thermal transmittance U_g value for the various versions is dependent on the thickness of the capillary slab, the functional coating on outer pane, and the filling gas in the cavity between panes (air/argon/krypton). In reference (Wong, 2015:418-425), the TI cover modelled consisted of a 6mm outer glass pane, a 22mm wide PMMA capillary cell section and an 8mm inner glass pane. When solar beam radiation passed through the TI-cover, the

solar transmittance, absorptance and reflectance that occurred in the cover were calculated, which were consistent with that found in previous research.

3. MODEL

A numerical 2_D model is considered and the frame can be seen in Figure 1 (dotted line). The left boundary of the model is the interior surface of the absorption plate, the upper and lower boundaries are the surfaces of the upper and lower walls and the right boundary is the exterior surface of the internal wall. In order to emphasize the effects of the combination of TIM and PCM and simplify the numerical simulation, the following assumptions are made:

1. The thermal mass of the TIM and the absorption plate is ignored compared with the thermal mass of the wall and the PCM.
2. The absorbed solar heat and infrared radiation in TIM are ignored.
3. TIM is considered by the overall transmission and thermal resistance. The overall transmission is a function of solar incident angle and the thermal resistance is constant.
4. The thermal resistance of absorption plate is ignored due to high thermal conductivity and small thickness.

The inlet boundary is set as velocity-inlet type and the outlet boundary is set as pressure-outlet type. The SIMPLE algorithm is used to solve the pressure-velocity coupling. The spatial discretization consisted of a second-order upwind scheme for the nonlinear terms and the second-order for the viscous terms. The time integration was performed by a second-order implicit scheme. The radiation model is DO model and the realizable k- ε model is adopted for the viscous model.

3.1. Heat Transfer on TIM Cover

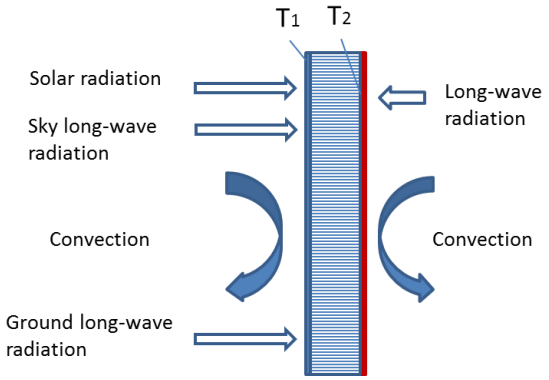

Figure 3: Scheme of heat transfer on the surfaces of TIM cover

Figure 3 shows the scheme of heat transfer on the surfaces of the TIM cover. Considering the solar radiation, long-wave radiation (sky and ground) and the convective heat transfer, the heat transfer on the exterior surface of the TIM cover q_1 is as follows:

Equation 4: Heat transfer rate q_1

$$q_1 = q_{\mathrm{r,out}} + h_{\mathrm{c,out}}(T_\infty - T_1)$$

Equation 2: Radiation heat transfer rate of $q_{\mathrm{r,out}}$

$$q_{\mathrm{r,out}} = \mathrm{q_{s1}} + q_{lw,sky} + q_{lw,groud}$$

Where:

- $\mathrm{h_{c,out}}$ = convective heat transfer coefficient of exterior surface of TIM cover (W/m^2·K)

- T_∞ =outdoor air temperature (K)
- T_1= the temperature of the exterior surface of TIM cover (K)
- $q_{s1}, q_{lw,sky}, q_{lw,groud}$= the absorbed solar radiation, sky long-wave radiation and ground long-wave radiation on the exterior surface of TIM cover, respectively (W/m^2)

For the sky and ground long-wave radiation:

Equation 3: Sky long-wave radiation

$$q_{r,sky} = \sigma\varepsilon_{0,s}\varphi_{0,s}\left(T_1^{\,4} - T_{sky}^{\,4}\right)$$

Equation 4: Ground long-wave radiation

$$q_{r,ground} = \sigma\varepsilon_{0,g}\varphi_{0,g}\left(T_1^{\,4} - T_{ground}^{\,4}\right)$$

Where:

- σ = blackbody radiation constant (5.67×10^{-8} W/(m^2·K^4))
- $\varepsilon_{o,s}$ = system emissivity between the exterior surface of TIM cover and the sky
- $\varepsilon_{o,g}$ = system emissivity between the exterior surface of TIM cover and the ground
- $\varphi_{0,s}$, $\varphi_{0,g}$ = radiation angle factors

Because the area of the sky is much more than the exterior surface of TIM components, $\varepsilon_{o,s} = \varepsilon_1$ where ε_1 is the thermal emissivity of the exterior surface of TIM components. For the vertical surface, $\varphi_{0,s} = 0.5$.

The sky background temperature can be estimated as follows (Henriques, 2002:1515-1521):

Equation 5: Sky background temperature

$$T_{sky} = \left(0.741 + 0.0062t_{dp}\right)^{0.25} T_\infty$$

Where, t_{dp} is the outdoor air dew-point temperature (℃).

For the ground long-wave radiation, the ground temperature is approximately taken as the outdoor air temperature and for the vertical surface, $\varphi_{0,g} = 0.5$.

Thus, the long-wave radiation on the surface of exterior surface of TIM cover q_r is as follows:

Equation 6: Long-wave radiation

$$q_r = q_{r,sky} + q_{r,ground} = 2\sigma\varepsilon_1\varphi_{0,s}(T_1^{\,4} - T_r^{\,4})$$

Equation 7: Equivalent long-wave radiation temperature

$$T_r = \left[0.5\left(T_{sky}^4 + T_{ground}^4\right)\right]^{1/4}$$

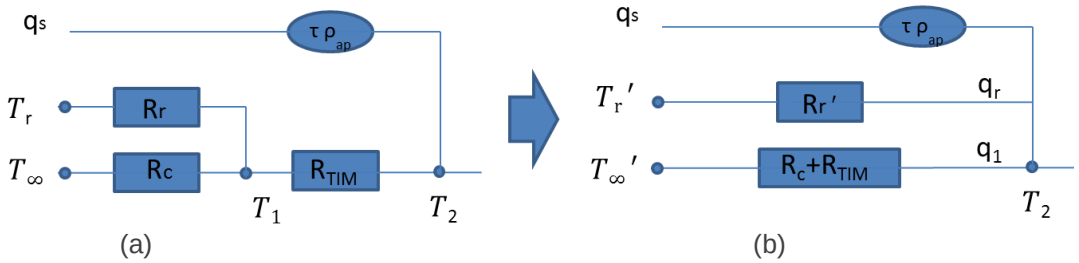

Figure 4: Schemes of thermal resistance (a) and equivalent thermal resistance (b) of TIM cover

Figure 4 shows the schemes of the thermal resistance and equivalent thermal resistance of TIM cover. In Figure 4 (a), q_s is the solar radiation on the vertical surface, τ is the overall transmission of TIM cover and ρ_{ap} is the absorptance of the solar absorption plate; T_r is the equivalent long-wave radiant temperature; R_r is the equivalent long-wave radiation thermal resistance; T_∞ is the outdoor air temperature; R_c is the convective heat transfer resistance on the TIM exterior surface; T_1 and T_2 are the temperatures of the exterior and interior surfaces of TIM, respectively; R_{TIM} is the thermal resistance of TIM cover.

For the long-wave radiation heat transfer rate q_r, it is:

Equation 8: Long-wave radiation heat transfer rate

$$q_r = \sigma\varepsilon_{0,s}\varphi_{0,s}\left(T_1^4 - T_r^4\right) = \sigma\varepsilon_{0,s}{}'\varphi_{0,s}\left(T_2^4 - T_r{}'^4\right)$$

Equation 9: Equivalent emissivity

$$\varepsilon_{0,s}{}' = \varepsilon_{0,s}c^4$$

Equation10: Equivalent temperature

$$T_r{}' = \frac{T_r}{c}$$

Where, $c = a + b\frac{T_\infty}{T_2}$, $a = \frac{R_{TIM}}{R_c + R_{TIM}}$, $b = \frac{R_c}{R_c + R_{TIM}}$.

In order to consider the most unfavourable condition, the sky long-wave radiation in summer can be ignored. For the solar radiation on the vertical wall, it is:

Equation 11: Solar radiation

$$q_s = I_{DV} + I_{dV} = \frac{I_{DH}}{\sinh}\cdot\cosh\cdot\cos\theta + \frac{1}{2}\rho_0 I_{SH}$$

Where, I_{DV} is solar directive radiation on the vertical surface (W/m^2); I_{dV} , solar diffusion radiation on the vertical surface (W/m^2); I_{DH} , solar directive radiation on the horizontal surface (W/m^2); I_{SH} , solar total radiation on the horizontal surface (W/m^2); h, solar zenith angle; θ , the azimuth angle between the sun and the wall; ρ_0 average ground reflectivity.

The solar zenith angle h is:

Equation 12: Solar zenith angle

$$\sinh = \sin\delta \cdot \sin\phi + \cos\delta \cdot \cos\phi \cdot \cos\omega$$

The solar azimuth angle θ is:

Equation 13: Solar azimuth angle

$$\cos\theta = \frac{\sinh \cdot \sin\phi - \sin\delta}{\cosh \cdot \cos\phi}$$

Where, δ is the solar declination angle, ϕ is local latitude, ω is the solar hour angle.
For the south-facing façade, the angle of solar incidence i is:

Equation 14: Solar incident angle

$$\cos i = \cosh \cdot \cos\theta$$

3.2. Thermal properties of TIM cover

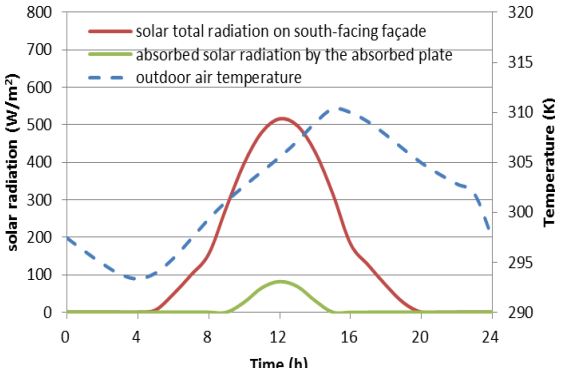

Figure: 5 Meteorological parameters of Beijing (21st June)

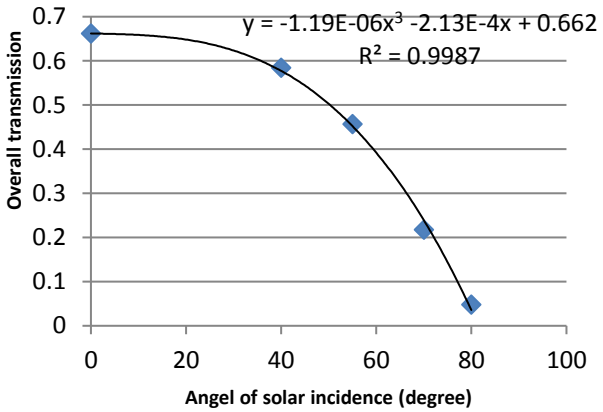

Figure: 6 Overall transmission with solar incident angle

From the DeST software, the solar radiation on the horizontal surface is available and thus the solar radiation on the vertical wall can be calculated. Figure 5 shows the outdoor air temperature, solar total radiation on the south-facing façade from DeST software and absorbed solar radiation by the absorbed plate in 21st June in Beijing. It can be seen that the solar total radiation is reduced greatly by the TIM cover, which is useful to reduce the cooling load in summer. Figure 6 shows the overall transmission of the TIM cover with the solar incident angle according to the data in reference (Wong, 2015:418-425).

Table 1 Thermal properties of TIM (Wong, 2012:253-276)

Components (outside to inside)	Thermal Resistance (m^2·K/W)	Density (kg/m^3)	Specific heat (J/kg·K)	Thermal conductivity (W/m·K)
6 mm clear float pane	0.01	2710	837	1.05
22 mm PMMA slab	0.55	30	1400	0.04
8 mm clear float pane	0.01	2710	837	1.05
20mm air gap	0.17	1.2	1.012	0.025

The fitted formula can be obtained as follows:

Equation 15 : Overall transmission with solar incident angle

$$\tau = -1.19\times10^{-6} \cdot i^3 - 2.13\times10^{-4} \cdot i + 0.662$$

where, τ is the overall transmission of TIM cover and i is the solar incident angel (degree). The mean square error R^2 is 0.9987.

Table 1 lists the thermal properties of TIM (Wong, 2012:253-276).

3.3. PCM Plate

For PCM plates, the equivalent specific heat distribution is adopted and considered as a piecewise function (Figure 7). The range of phase change temperature range is from T_1 (lower limit) to T_2 (upper limit). Table 2 lists the thermal properties of PCM (Zhou, 2007:1351-1360).

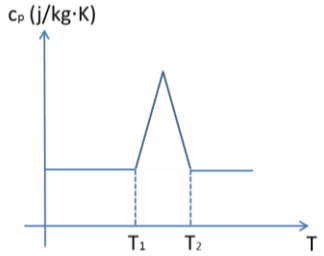

Figure:7 The equivalent specific heat distribution with temperature

Table 2 The thermal properties of PCM (paraffin)

Thermal properties	Value
Density (kg/m^3)	800
Specific heat (kJ/kg·K)	2.0
Phase change temperature (K)	303-305
Latent heat (kJ/kg)	202
Thermal conductivity (W/m·K)	0.20 (liquid) 0.15 (solid)

3.4. Other parameters

The thermal properties of other components in numerical calculation are listed in Table 3. The absorption plate is made of aluminium painted with black paint (Metacrylic) and the absorption factor for solar radiation is 0.88 (Ubertini, 2003:623-645). The outer wall is one kind of light wall and the internal wall is made of gypsum board.

Table 3 Thermal properties of other components

Components	Density (kg/m^3)	Specific heat (kJ/kg.K)	Thermal conductivity (W/m.K)	emissivity
Solar absorption plate	2719	0.871	202	0.66
Outer wall	840	1.05	0.814	0.9
Internal wall	2320	1.138	0.5	0.9

The upper and lower boundary conditions are assumed as thermal insulation and the heat transfer is very small compared to other boundaries and thus considered the heat flux is zero. The heat transfer rate on the exterior surface of the outer wall is 18.6 W/m^2·K. The thermal resistance of the internal wall is 0.53 m^2·K/W and the heat transfer rate on the interior surface of the outer wall is 5.7 W/m^2·K. The temperature of indoor air is 20℃.

4. RESULTS AND DISCUSSION

Figure 8 shows the temperatures distribution of the novel structure with time for the different surfaces, including the temperatures at the interior surface of the absorber, the exterior surface of the outer wall, the exterior surface of the PCM plates, the exterior surface of the room wall when the inlet velocity is 0.5 m/s and the phase change temperature Tm is 303-305K. From Figure 8, it can be seen that due to the latent heat, the PCM plate temperature is of relative smooth decline. However, the thermal mass is not enough because of the small quantity of the PCM used.

In order to compare the thermal performance of the novel structure, a reference structure is assumed. The ordinary glazing cover is used and the corresponding parameters are the same with the TIM cover except for the solar transmission. For the reference structure, the solar transmission of the ordinary glazing cover is 0.77 and does not change with the solar incident angle. The other components and thermal parameters are same with the novel structure.

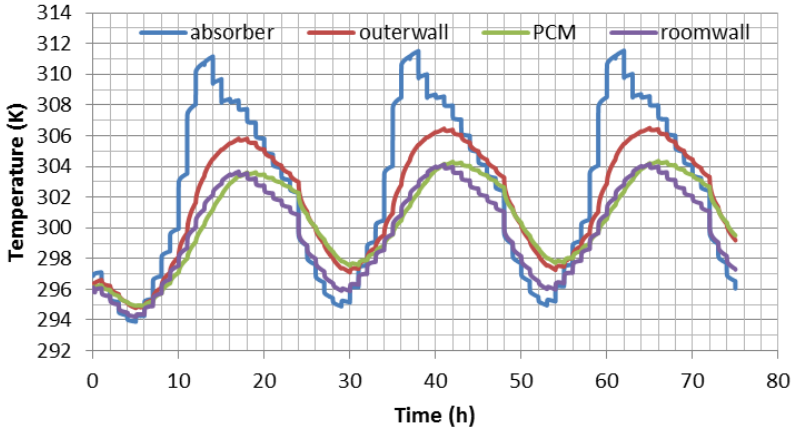

Figure: 8 Temperatures of different surfaces in the novel structure (V_{inlet}=0.5m/s ,Tm=303-305K)

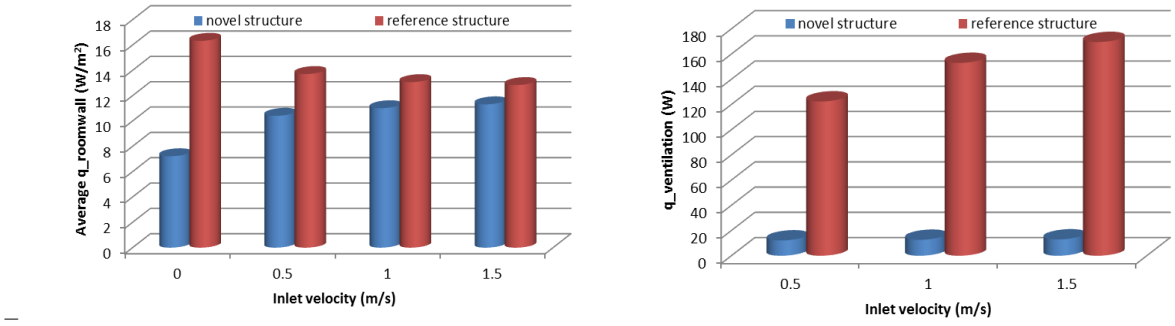

(a) (b)

Figure:9 Average heat transfer rates of the exterior surface of the room wall (a) and the ventilation heat transfer rates (b) in the novel and reference structures

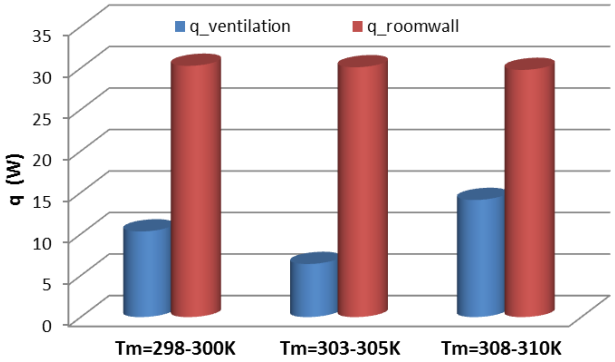

Figure: 10 Ventilation heat transfer rates and average heat transfer rates of the exterior surface of the room wall with different Tm (V_{inlet}=0.5m/s)

Figure 9 shows the average heat transfer rates of the exterior surface of the room wall and the ventilation heat transfer rates in the novel and reference structures. From Figure 9(a), it can be seen that for the novel structure, the average heat transfer rate of the exterior surface of the room wall increases with the increasing inlet velocity. When the inlet velocity increases from 0 m/s to 1.5 m/s, the average $q_{\_roomwall}$ increases from 7.22 W/m^2 to 11.32 W/m^2, which is increased by 56.8%. However, for the reference structure, the average $q_{\_roomwall}$ decreases from 16.33 W/m^2 to 12.84 W/m^2, which is decreased by 21.4% correspondingly. When the inlet velocity is higher, the difference between the novel and reference structures is smaller. For example, when the inlet velocity increases from 0 m/s to 1.5 m/s, the difference of average $q_{\_roomwall}$ of the exterior room wall surface reduces from 9.11 W/m^2 to 1.52 W/m^2 greatly. From Figure 9(b), it can be seen that the ventilation heat transfer rate changes little when the inlet velocity increases for the novel

structure. However, for the reference structure, when the inlet velocity increases from 0 m/s to 1.5 m/s, the ventilation heat transfer rate increases from 122.42 W to 169.57 W., which is increased by 38.5%.

In order to show the effect of PCM, the material of the outer wall is considered as PCM besides the PCM plates for the novel structure, which can increase the thermal mass of the structure. Figure 10 shows the ventilation heat transfer rates and average heat transfer rates of the exterior room wall surfaces with different Tm when the inlet velocity is 0.5m/s. From Figure.10, it can be seen that the effect of Tm on the ventilation heat transfer rate is higher than that on the average heat transfer rate of the exterior surface of the room wall. When Tm is 303-305K, the ventilation heat transfer rate is smallest (6.4W) and when Tm is 308-310K, it is highest (14.11W). However, the average heat transfer rates of the exterior room wall surfaces change little with different Tm. When the Tm is 303-305K, the total heat transfer rate including the ventilation heat transfer rate and the average heat transfer rate of the exterior surface of the room wall is smallest (36.5W). Because the average ventilation heat transfer rate is considered as the reduced ventilation load, it is better with higher ventilation heat transfer rate. And it is better with lower average heat transfer rates of the exterior room wall surfaces. When the Tm is 308-310K, the equivalent heat transfer rate is smallest (15.7W). Thus, the suitable phase change temperature is 308-310K and the corresponding total heat transfer rate can be decreased by 33.8% compared with that when Tm is 303-305K.

5. CONCLUSIONS

A novel building façade is proposed and there are no moving parts or only a small fan in the structure. It could be used for residential and commercial buildings, providing heating and cooling for the living space as a sustainable low-carbon building. Fluent is adopted and a simple numerical model is set up to study the thermal performance of the novel structure. The fitted formula of overall transmission with solar incident angle is arrived.

The numerical results show that:

(1) The average heat transfer rate of the exterior surface of the room wall increases with the increasing inlet velocity for the novel structure while decreases for the reference structure.
(2) The ventilation heat transfer rate changes little with the increasing inlet velocity for the novel structure while increases for the reference structure.
(3) When the inlet velocity is higher, the difference between the novel and reference structures is smaller.
(4) The effect of Tm on the ventilation heat transfer rate is higher than that on the average heat transfer rate of the exterior surface of the room wall.
(5) The suitable phase change temperature is 308-310K when the inlet velocity is 0.5 m/s and the corresponding total heat transfer rate can be decreased by 33.8% compared with that when Tm is 303-305K.

6. ACKNOWLEGEMENT

This research is financed by the Seventh Framework Program-Marie Curie Actions (PIIF-GA-2013-622117) and the 12th Five-year Plan Project of China (2013BAJ03B04).

7. REFERENCES

A.K. ATHIENITIS, H. Ramadan, 1999. Numerical model of a building with transparent insulation, Solar Energy, 67(1-3): 101–109.

L.F. CABEZA, A. Castell, C. Barreneche, A. de Gracia, A.I. Fernández, 2011. Materials used as PCM in thermal energy storage in buildings: A review, Renewable and Sustainable Energy Reviews, 15: 1675–1695.

EREC, 2010. RE-thinking 2050--A 100% Renewable Energy Vision for the European Union, European Renewable Energy Council.

FMA HENRIQUES, 2002. The effects of differential thermal insulation of walls, 30th IAHS World Congress on Housing, Housing Construction: An Interdisciplinary Task, 1-3: 1515-1521.

Y.A. KARA, A. Kurnuç, 2012. Performance of coupled novel triple glass unit and PCM wall, Applied Thermal Engineering, 35: 243-246.

N. D. KAUSHIKA, K.Sumathy, 2003. Solar transparent insulation materials: a review, Renewable and Sustainable Energy Reviews, 7: 317–351.

A. G. LIEN, A. G. Hestnes and Ø. Aschehoug, 1997. The use of transparent insulation in low energy dwellings in cold climates, Solar Energy, 59(1-3): 27-35.

G. ROCKENDORF, S. Janssen and H. Felten, 1996. Transparently insulated hybrid wall, Solar Energy, 58(1-3): 33-38.

S.UBERTINI, U. Desideri. Renewable Energy 28 (2003), 623-645.

K. VOSS, 2000. Solar energy in building renovation - results and experience of international demonstration buildings, Energy and Buildings, 32: 291–302.

I.L.WONG, P.C.Eames, R.S Perera, 2007. A review of transparent insulation systems and the evaluation of payback period for building applications, Solar Energy, 81: 1058-1071.

I.L.WONG, P.C.Eames, 2015. A method for calculating the solar transmittance, absorptance and reflectance of a transparent insulation system, Solar Energy, 111: 418–425.

I.L.WONG, P.C.Eames, R.S.Perera, 2012. Energy simulations of a transparent insulated office façade retrofit in London, UK, Smart and sustainable built environment, 1(3): 253-276.

GB ZHOU, YP Zhang, X Wang, KP Lin, W Xiao, 2007. An assessment of mixed type PCM-gypsum and shape-stabilized PCM plates in a building for passive solar heating, Solar Energy, 84(10):1351-1360.

SESSION 23: SMART AND RESPONSIBLE BUILDINGS

263: Intelligent building management system for energy demand and supply optimisation

UFUK GÖKÇE[1*], K. UMUT GÖKÇE[2]

1 R&D Director, EOS Sustainable Energy Solutions GmbH, Vahrenwalder Str. 7, 30165, Hannover, Germany. Tel: +49 511 260 304 93, Fax: +49 511 260 304 94, e-mail: ufuk.gokce@eos-ses.de
2 Managing Director, EOS Sustainable Energy Solutions GmbH, Vahrenwalder Str. 7, 30165, Hannover, Germany. Tel: +49 511 260 304 93, Fax: +49 511 260 304 94, e-mail: umut.gokce@eos-ses.de

The quality of life in Europe's cities states that although quality of life has improved in many areas, in other areas such as environmental issues and energy efficiency have deteriorated. Energy consumption for building-related services accounts for approximately 40% of European Union's total energy consumption. Total carbon emissions generated by the buildings account for 35%. In such places, people, companies and public authorities experience specific needs and demands regarding domains such as energy efficiency, environment and transportation services. These domains are increasingly enabled and facilitated by web-based applications, service oriented architectures, ubiquitous sensing infrastructure, advanced information management applications such as data warehousing and data mining technologies which generate actionable information for intelligent and predictive control for further optimised smart buildings and cities.

The research presented in this paper focuses on an innovative model-driven development approach that integrates systems in building supply-side and building demand-side to balance efficient energy production from off-the-grid systems and optimized consumption.

The research findings will be demonstrated in a residential building in Hannover, Germany integrating different energy efficient production/consumption systems addressing the renewable energy technologies coupled with energy storage systems and building energy management systems comprising scalable and robust sensing network platforms, energy performance monitoring and data warehouse technologies. The research will be carried out within the scope of State of Lower Saxony Innovation Support Program (Niedersächsischen Innovationsförderprogramms) which is funded by Ministry for Economic Affairs, Labour and Transport of State of Lower Saxony-Germany (Niedersächsisches Ministerium für Wirtschaft, Arbeit und Verkehr), Ministry for Environment, Energy and Climate Protection of State of Lower Saxony-Germany (Niedersächsisches Ministerium für Umwelt, Energie und Klimaschutz), Investment and Support Bank of State of Lower Saxony Nbank (Investitions- und Förderbank Niedersachsen – NBank) and the European Union.

Keywords: Building management system, renewable energy, holistic monitoring and analysis methodologies, scenario based control strategies, data warehouse technologies.

1. INTRODUCTION

Cities all over the world exhibit complex dynamics. As cities grow, planners devise “complex systems to deal with food supplies on an international scale, water supplies over long distances and local waste disposal, urban traffic management systems. The quality of all such urban inputs defines the quality of life of urban dwellers” (The Science Museum 2009). Notwithstanding the enormous formidable challenges and disadvantages associated with urban agglomerations, the world population has been steadily concentrating in cities. In addition, there is a substantial increase in the average size of urban areas. This has been made possible by a simultaneous upward shift in the urban technological frontier, so that a city could accommodate more inhabitants. Problems associated with urban agglomerations have usually been solved by means of creativity, human capital, cooperation among relevant stakeholders, and bright scientific ideas: in a nutshell, ‘smart’ solutions. The label ‘smart city’ should therefore point to clever solutions allowing modern cities to thrive, through quantitative and qualitative improvement in productivity and efficiency.

The concept of smart cities has different meanings. A useful definition is to call a city “smart” when “investments in human and social capital and traditional (transportation) and modern (ICT-based) infrastructure fuel sustainable economic growth and a high quality of life, with a wise management of natural resources, through participatory government” (Caragliu 2009). Other definitions identify significant characteristics such as energy efficiency, environmental issues, productive economy, and define rankings based on measurable underlying indicators. Smart cities can be also understood as places generating a particular form of spatial intelligence and innovation, based on sensors, embedded devices, large data sets, and real-time information processing and response.

The Centre of Regional Science at the Vienna University of Technology identifies six main ‘axes’ (dimensions) along which a ranking of 70 European middle size cities can be made (Komninos 2011). These axes are: a smart economy; smart mobility; a smart environment; smart people; smart living; and, finally, smart governance. These six axes connect with traditional regional and neoclassical theories of urban growth and development. In particular, the axes are based – respectively – on theories of regional competitiveness, transport and ICT economics, natural resources, human and social capital, quality of life, and participation of societies in cities.
A report of the European Environmental Agency (EEA 2009) concerning quality of life in Europe’s cities states that although quality of life has improved in many areas, in other areas such as health, environmental issues and energy efficiency have deteriorated. In such places, people, companies and public authorities experience specific needs and demands regarding domains such as healthcare, energy efficiency and the environment, as well as safety and public services. These domains are increasingly enabled and facilitated by web-based applications, service oriented architectures, ubiquitous sensing infrastructure, advanced information management applications such as data warehousing and data mining technologies which generate actionable information for intelligent and predictive control for further optimised smart cities.

On the basis of on-going research in the area of energy efficiency and legislative drivers launched by the national and international organizations, the role of integration concepts, performance monitoring and analysis methodologies and sophisticated control strategies through the seamless integration of people, ICT devices and computational resources gain significant importance for reducing the energy consumption and the operational costs for buildings as well as cities. According to European standard “EN 15232 Energy Performance of Buildings-Impact of Building Automation” building operation systems can, depending on building type and equipment standard, produce the following potential savings of energy: restaurants 31%, hotels 25%, offices 39%, shopping centres 49%, hospitals 18%, schools/universities 34% and residential 27% (DIN 2007) (VDMA 2008). This is a major contribution to the “Kyoto-Protocol-Process” in which the EU outlined the objective to reduce energy consumption by 20% by 2020. Also, it is often faster and less costly to integrate building energy systems than it is to insulate building shells. At the moment sophisticated building energy management systems are available for facilities management. Most of the larger non-residential buildings younger than 30 years are already equipped with wired building automation systems in Europe. However, their focus on energy performance rating of buildings is at best sporadic often consisting of an ad-hoc combination of off-the-shelf building management systems (BMS). This ad-hoc combination presents many difficulties for building owners in relation to the management and upgrade of these systems, as the BMS can consist of a number of components utilizing various information exchange protocols that have to be integrated within the monitoring and targeting (M&T) software packages. The optimization of these systems for energy management adds another layer of complexity to the design and management procedures (Nikolaus 2008). It requires analysing the system, developing new interfaces, replacing devices, and optimizing parameters. Furthermore the engineering and deployment of efficient energy production systems for buildings addressing the renewable energy technologies, phase change

materials, energy harvesting facades and integration of these systems with the ICT-based sub-systems becomes a necessity. Integrated IT tool support for these activities does not exist; available tools are stand-alone products, often tied to specific standards, and focus on development from scratch. There is not a procedure defined which describe information exchange between different domains for different energy generation and management systems. This lack of appropriate descriptions and tools currently outweighs the benefit of software interoperability. As this technology gap spans for all application domains, it will likely hamper further adoption of IT solutions. In this regard, the prospective consequence of the building behaviour and the needs of the building occupant/operator which would manage energy production/consumption efficiently would not be predictable with a single combined information, communication, hardware and tool platform. A promising approach, to overcome these shortcomings, is the implementation of a holistic, modular infrastructure for building energy supply and demand sides.

2. APPROACH

The agenda in this research is built on the need of integration structures, holistic monitoring and analysis methodologies, life-cycle oriented management and decision support of intelligent agents with considering two key research areas; (1) Building energy supply-side (micro grid) management which addresses the energy management systems capable of optimal integration and control of energy production addressing renewable energy technologies such as photovoltaic/hot water solar panels, geothermal heat pumps, small scale wind turbines, hydrogen fuel cells and the communication and intelligence required to work cooperatively with local authorities/grid operators and (2) Building energy demand-side management which comprises a scalable, robust wireless sensing/actuation network platform that computation and actuation to collect build-use data through advance data monitoring and data mining technologies which lead to develop optimal control algorithms that adjust Lighting, Heating, Ventilation, Cooling set points to adapt to occupancy, weather loads and their predictions, minimizing total energy consumption and balancing peak demand while maintaining the indoor environment within user preferred comfort parameters.

The proposed concept depicted in Figure 1 below consists of three parts: (1) Building Energy Supply (BES) side. This consists of conventional energy supply from the grid and Off-the-Grid energy generation systems such as photovoltaic/hot water solar panels, geothermal heat pumps, small scale wind turbines, fuel cell systems and storage technologies, (2) Building Energy Demand (BED) side which consists of HVAC systems, lighting systems and appliances, (3) Multi-Dimensional Energy Monitoring, Analysis and Optimisation System consisting of wireless sensors/meters/actuators, information management platform, intelligent control module and monitoring tools.

3. CONCEPT

Off the grid energy generation technologies are usually provided by the companies which solely focus on specific areas such as wind, solar, geothermal, fuel cell and storage as there is a very limited number of companies that provide a “total service concept”. Therefore, holistic design between various energy generation systems hasn’t been provided in an expected granularity due to the lack of integration concepts (Gökçe 2014).

Moreover, the control of energy performance of buildings is often provided by an ad-hoc combination of off-the-shelf building management components, distributed data metering equipment, glued together by M&T software tools. The absence of building management systems standardization coupled with competition for market share results in independent and non-compatible system development. In this regard BACnet™ was developed to provide an open, non-proprietary protocol specification that allows building automation controllers of different manufacturers to communicate with each other (ASHRAE 2008). However Building Management Systems / Energy Management Systems still operate on non-standardized proprietary interfaces. Consequently they are becoming more complex over time and are difficult for the average operator to understand given the educational and experience (Lowry 2002). Additional training overhead is required for each new system or system updates. Moreover Hatley et. al. (Hatley 2009) states that in the absence of compatible hardware and communication protocols maintenance can become extremely problematic as seamlessly integrating these systems is an inefficient overhead.

However, in conjunction with traditional procurement policy it is conceivable that numerous systems which would provide an integrated system chain enabling the efficient use of renewable energy resources and energy management systems in a holistic building-supply and building-demand side energy management concept complementing with a modular approach should appear, as can be seen in this research.

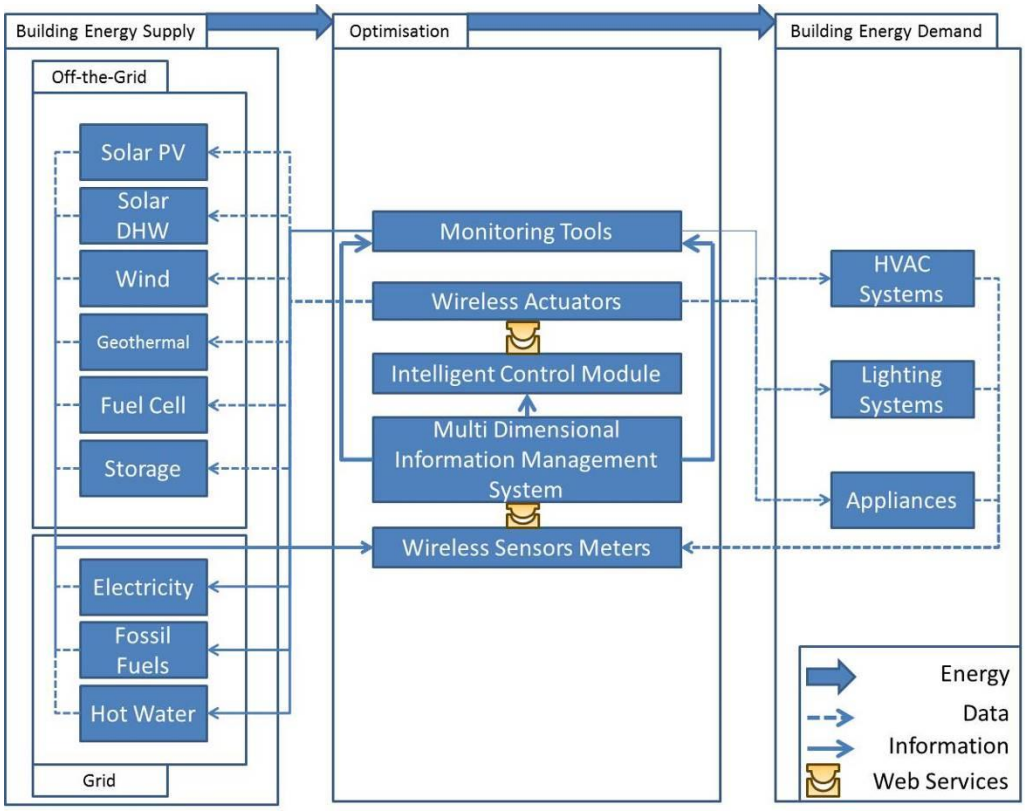

Figure 1: Hybrid Building Concept Integrated with Off-the-Grid Energy Generation Systems and Smart City Grids.

In this regard two research concepts are provided by defining: (1) Integration and optimisation of off-the-grid energy generation systems. (2) Multi-Dimensional Energy Monitoring, Analysis and Optimisation System (Gökçe 2013a).

3.1 Integration and Optimisation of Off-the-Grid Energy Generation Systems

Integration and optimisation of off-the-grid energy generation systems involves two complementing phases (1) the design of small scale house type renewable energy technologies e.g. wind, solar, geothermal, hydrogen fuel cells and storage systems for off-the-grid energy generation and storage in buildings through an integrated structure based on the requirements analysis including energy demand and grid supply patterns and (2) the development of an optimisation middleware for energy-supply, in order to control the various systems in an integrated and optimized way.

Off-the-Grid Energy Generation and Storage Systems

Off-the-grid renewable energy technologies for energy generation for buildings usually addresses individual systems integration, e.g. a wind turbine is combined with adequate storage devices or energy harvesting facades are combined with actuators or blind control systems. Several tools supporting the integration of these components exist with manufacturers having usually their own preferences.

Therefore the definition of optimal processes and interfaces allowing the integration of different systems e.g. integration of small scale battery charging wind turbines and photo-voltaic solar cells which feed a common storage system (battery bank) and control of energy production on the basis of environmental conditions e.g. wind speed, day light period, etc. can be accepted as one of the prerequisites of a holistic, modular approach.

In this research, in order to integrate different type of systems in an optimized way, the requirement and the state-of-the art analysis which would allow optimized integrations have been obtained with researching

the systems given below. This preliminary state-of-the art analysis will be used to develop the middleware for building energy supply.

i. Small Scale Battery Charging Wind Turbines

After examining, different type of home use small scale wind turbines in the market, 600W 24VDC battery charging wind turbine with 6 Blade type has been chosen to optimise small scale renewable energy output which is compatible with our application scenarios. Its cut-in speed is low in order to facilitate continuous generation and auxiliary energy source. The wind speeds in excess of 150km/h has been approved. This type of home use wind turbines generally comprises of a single axial flux permanent magnet brushless alternator. The six blade design supports a self-regulating aerodynamic rotor that achieves speed control through blade turbulence, which controls the speed of the rotor with no moving parts and no obtrusive noise. The diameter is 1.5m.

ii. Solar Panels Made of Photo-Voltaic Solar Cells

In this research, four major types of Solar Technology Panels have been examined (1) polycrystalline cells which are the most common and cheapest panels with conversion efficiency 13% to 15% (sunlight to electricity), however, under elevated temperatures of 50 degrees Celsius panel temperature, the efficiency drops by around 20%, (2) panels made from monocrystalline cells which are used in high reliability applications such as telecommunications and remote power with conversion efficiency is typically 14-17.5% (higher than the polycrystalline cells), however, at elevated temperatures, the efficiency only drops by 10-15% so they are more consistent in output (3) Panels made from amorphous cells which have been used in portable items for many years with conversion efficiency of sunlight to electricity is 5-7%, about half that of the other panels but unlike the other types, their output does not decrease in elevated temperatures. Panels made of thin film cell CIGS technology (Copper, Indium, Gallium, diSelenide) are flexible, durable, and provide slightly higher efficiency than other flexible solar cells, typical sizes less than 60W and can be mounted to curved surfaces. The critical item that delivers the current to charge the batteries is the solar controller. There are 3 major types of controller: (1) Standard single phase controller, (2) Multistage controller, and (3) Maximum Power Point Tracking Controller (MPPT). The first 2 controllers provide roughly 70% of the panels' power to the batteries as they reduce the voltage of the solar panels but do not increase the current. MPPT Controllers are true "State of the Art" technology with 96%+ output. The final critical factor is the location of the controller, the mounting the controller at the battery end of the solar panel cable allows batteries fully charged. In summary, the way to compare the relative output capacity of panels is by the current output charging batteries at around 13.5V.

In our case with considering the current systems, the high quality polycrystalline solar panels for home solar power systems and MPPT controllers are used in this research.

iii. Solar Vacuum-Tube Collectors for Hot Water

In order to heat water using solar energy, a collector, often fastened to a roof or a wall facing the sun, heats working fluid that is either pumped (active system) or driven by natural convection (passive system) through it. Residential solar thermal installations fall into two groups: passive and active systems. Both typically include an auxiliary energy source (electric heating element or connection to a gas or fuel oil central heating system) that is activated when the water in the tank falls below a minimum temperature setting such as 55 °C. Hence, hot water is always available. The combination of solar water heating and using the back-up heat from a wood stove chimney to heat water can enable a hot water system to work all year round in cooler climates, without the supplemental heat requirement of a solar water heating system being met with fossil fuels or electricity. For this research Viessmann Vitosol 300 T type SP 3A Vacuum-tube solar collectors with dry connection heat tubes have been chosen. The system has gross area of 2.88 m2 and the absorber area of 2.00 m^2.

iv. Geothermal Heat Pumps

A geothermal heat pump, ground source heat pump (GSHP), or ground heat pump is a central heating and/or cooling system that pumps heat to or from the ground. It uses the earth as a heat source (in the winter) or a heat sink (in the summer). In a fridge, heat is transferred from the inside to the outside. With a heat pump, this happens exactly the other way round. Heat from the air or the ground is transferred into

the living space via the heating system. Vapour from a refrigerant is compressed to increase the temperature, to make it high enough for central heating and DHW (Domestic Hot Water) heating. For this research, the selected Viessmann Vitocal 350-G reaches up to 72 °C. These heat pumps can therefore also be used for modernisation as they can provide a sufficiently high flow temperature for central heating with radiators. The compression process is vital for the efficiency of a heat pump. To generate heat, for example, heat is extracted from the ambient air and used to evaporate a refrigerant that boils at low temperature. Getting hotter towards the centre – from an initial temperature of between 5 and 18 °C, a flow temperature of up to 72 °C is achieved. The gas created is compressed by the scroll compressor, which causes it to heat up. The gas heated in this way transfers its heat via the condenser to the heating water or DHW heating system, and thereby condenses again. Finally, the refrigerant, which is still under pressure, is expanded in an expansion valve, and the circuit begins again. A heat pump can make use of the following energy sources: (a) Air – practically unlimited availability; lowest investment costs (b) Ground – via geothermal collector or geothermal probe. (c) Water – efficiency depends on the water temperature. (d) Waste heat – subject to availability, volume and temperature level of the waste heat. In this regard, the best heat source for each individual case depends on local conditions and the actual heat demand.

v. Fuel Cell System

A fuel cell is an electrochemical energy conversion device. A fuel cell converts the chemicals hydrogen and oxygen into water, and in the process it produces electricity. Fuel cells generate electrical power quietly and efficiently, without pollution. Unlike power sources that use fossil fuels, the by-products from an operating fuel cell are heat and water. A fuel cell provides a DC (direct current) voltage that can be used to power motors, lights or any number of electrical appliances.

In this research, polymer electrolyte membrane fuel cells (PEMFC) are used. The PEMFC has a high power density and a relatively low operating temperature (ranging from 60 to 80 degrees Celsius, or 140 to 176 degrees Fahrenheit). The low operating temperature means that it doesn't take very long for the fuel cell to warm up and begin generating electricity.

The specific system solution is Serenergy H3 5000 Methanol Power System (Serenergy 2015). The system is Methanol fuelled – integrated reformer system Liquid cooled High Temperature PEM stack with 5 kW electrical power output. The H3 5000 Methanol Power system can be used to supply an onsite, external battery pack existing on site or installed with the system. The methanol fuel cell system is ideal for combining with renewable energy sources such as wind and solar or multiple applications, both off- and on-grid, including application in critical backup power, temporary power or premium power generation. The specifications of the fuel cell are given in Table 1 below.

Table 1: Fuel Cell System Specifications.

Fuel Cell System Specifications	
Fuel Type (Mixture)	60 % Methanol, 40 % Deionized Water
Fuel Consumption (L/kWh)	0,8-0,9
Ambient Temperature (Celsius)	(-20) - (+50)
Number of Cells	120
Power Output (W)	5000
Voltage Output (VDC)	LV:48 or HV: 350-400
Turn-Down Ratio	0-100
Weight (kg)	75
Volume (l)	81

vi. Energy Storage Systems

For energy storage systems two types of batteries have been examined, (1) Lead Acid Deep Cycle Batteries which are designed to have stored current discharged between charging sessions, with very heavy non-porous battery plates to withstand repeated major discharging and charging cycles (deep cycles) and (2) Nickel Alloy Batteries Nickel Cadmium (NiCad) and Nickel Iron batteries, rather than consisting of lead plates submerged in a sulphuric acid solution, feature nickel alloy plates in an alkaline solution.

In this research, we have chosen nickel alloy battery types for our experiments with considering the facts such as they are well suited for home power use, although much less common and much more expensive than lead acid types. The nickel alloy battery can have up to 50 years of useful life, compared to 20 years with a well-maintained lead acid battery. They can also sit for extended periods of time partially or fully discharged without suffering damage, unlike lead acid types and they need lower maintenance. On the other hand a lead acid battery should never be completely discharged, meaning they need to be more closely monitored. Nickel alloy batteries operate better at lower temperatures, and can discharge more of their total amp-hour capacity as useful current.

A battery bank is the main part of the energy storage systems and enables a constant level of power to the house. Without the battery bank, the entire electrical system of a house would be limited by the immediate output of renewable energy resources. A wind turbine would be subject to constant power fluctuations as the wind speed increased, dropped or disappeared entirely. At night, a solar-run house would have no electrical power available. Therefore in order to provide a constant level of power without causing problems for households, a grid connection to the battery banks would be necessary during non-peak hours, thereby the house-use power can be available regardless of weather conditions with convenient electricity prices.

In our case, we designed our system based on three separate battery sections composed of nickel alloy batteries. The first section is connected with the small scale battery charging wind turbine, the second section is connected with the high quality polycrystalline solar panel while the third section connected to the central electricity grid. Therefore the wind generator and solar panel can deliver power to the battery bank regardless of current power usage, so excess power can be stored during low use times (generally the middle of the day and middle of the night) and be available during high use times (usually morning and evening). In our case an inverter DC-AC which is used to convert the DC power from the battery bank to AC power for the house power systems, a rectifier AC-DC which converts AC grid power to DC power for the use of battery charging, a control relay which provides a direct connection between the house and the grid in the event that all stored energy is depleted or a problem occurs in the battery bank.

vii. Optimisation Middleware for Building Energy Supply Systems

This is considered for the integration of off-the-grid power generation systems and central electricity/gas/water grid and optimal control of these systems on the basis of occupant needs and environmental factors. In order to provide this, a novel model-based system development approach is investigated that automates code development. In the model-based system development approach, we propose to adopt the software product line paradigm. It starts with requirement engineering for the envisaged systems specifying the functionality to be implemented. From these requirements the source codes are individually generated from software modules to fulfil the requirements and optimally use the system resources. Information about the implemented functions, requirements, and software function blocks are stored in the form of Electronic System Descriptions. This repository contains descriptions of individual systems for integration purposes. Consequently on the basis of specified descriptions which allow controlling of optimal management of wind turbines, solar panels, fuel cells etc. The middleware is designed with considering the functionalities given below.

The middleware is in control of charging the batteries when out of power from either the grid or renewable energy systems occurred. It will supply the hot water by taking into consideration of the occupant requirements and environmental factors. The middleware also be in control of providing stored power to the house whenever possible. It is designed for running the system in the most cost effective manner by considering carbon emissions. It would decide when to charge the batteries and from which source. The middleware is designed to provide stored power to the house whenever present and only switch to grid power if all stored power is depleted. Moreover it provides charging the batteries from the grid power during non-peak hours and only if the systems could not provide enough power for the house use.

3.2 Multi-Dimensional Energy Monitoring, Analysis and Optimisation System

Multi-Dimensional Energy Monitoring, Analysis and Optimisation System is implemented on the basis of four complementing components as (1) Building Information Model, (2) wireless sensor/meter/actuator network platform, (3) multi-dimensional information management platform, (4) Intelligent Control Module and (5) Monitoring tools.

i. Building Information Model (BIM)

In order to simplify the requirement engineering, information about the building (location, building systems, etc.) can be imported from the systems which support architectural and building systems design. Architectural designs are typically developed with the Computer Aided Design (CAD) tools such as Autodesk Revit, Microstation, ArchiCAD and DDS-CAD. They support standardised, extensible Building Information Models (BIM) based on product modelling standards such as IFC (Industrial Foundation Classes).

The concept of a BIM describes an integrated data model that stores all information relevant to a building throughout the building life cycle. In our case, it is envisioned to extend the BIM with the system design, e.g. the number and kind of wireless sensors and communication devices in order represent deployment in different rooms and their interaction within each other and with the building itself.

In order to predict and model building energy performance, energy simulation models should be considered. These models enable the building operator to perform comparisons between design intent and actual energy performance data. For example, in order to perform an energy simulation on the Revit MEP model, the IES plug-in is used in our simulations to complete BIM Model comprising energy performance aspect.

ii. Wireless Sensor/Meter/Actuator Network Platform

Wireless Sensor Network (WSN) is a wireless network consisting of spatially distributed autonomous devices using sensors that allow the physical environment to be monitored at high resolution. These sensors also called motes are installed in particular locations or can be deployed in a particular zone to gather information such as temperature, humidity, CO_2, lux level, etc. The real functionality of sensors comes with wireless sensor networks when these sensors start communicating with each other through wireless protocols. WSN can shuffle the information collected through the sensors and transfer it to the public internet and or a local area network. Finally, the information is collected in the data warehouse where it is analysed.

In this project the wireless sensor network architecture is implemented based on the recently released IETF 6LoWPAN (RFC 4944) open standard for IP communication over low-power radio links – IEEE 802.15.4 represents one such link. WSN LoWPAN networks are connected to other IP networks through one or more border routers forwarding packets between different media including Ethernet, Wi-Fi or GPRS. The IP architecture offers widespread commercial adoption and broad interoperability due to its attributes such as openness, flexibility, scalability and manageability. Many industrial standards, including BACNet, LonTalk, CIP and SCADA, introduced an IP using either TCP/IP or UDP/IP over Ethernet.

In this research the wireless sensors have been chosen to detect and measure various parameters such as temperature, humidity and water/gas/electricity meter readings. In our case the motes, mainly consists of 3 components; the sensor interface which actually measures the physical attributes like humidity level, the radio interface which communicates with other motes and the CPU which performs computations and transfers information between the two components. The used board is equipped with an Atmega1281 MCU and EM2420 radio chip. The platform includes sensors for monitoring air-temperature, air-humidity and light. Moreover incorporates electricity meters as well as the interface for controlling (on/off) an AC load are utilised. The platform runs the recently released b6LoWPAN stack. Soekris embedded PC boards (Soekris 2012) with Atheros CM9 Wi-Fi cards and a single IEEE802.15.4 node form a backbone network will be used in all the rooms of the sample building**.**

iii. Multi-Dimensional Information Management System

The objective of the data warehouse development is to provide a multi-dimensional information management platform to store integrate and analyse complex data sets from multiple information sources such as model editors, energy simulation tools and performance framework specification tools as well as data streams collected from wired and wireless sensors and meters in order to analyse building performance data and to support decision making process of the stakeholders. The data extracted from the Building Information Model and from the wireless sensor/meter/actuator network platform is aggregated in the data warehouse core in order to provide actionable information to the intelligent control module. Simultaneously aggregated data is presented through specific Graphical User Interfaces (GUIs) concerning different stakeholder requirements. The developed system is explained in detail by (Gökçe 2010).

iv. Intelligent Control Module

The actionable information generated by the Multi-Dimensional Information Management System is processed within the intelligent control module for low energy building operation in order to control and optimise both building energy supply side and building energy demand side in run time.

The intelligent control module contains algorithms for the defined building operation scenarios (e.g. heating, cooling, and lighting) and interacts with the data warehouse core to compute control parameters, which are then passed to the wireless network for actuation. The detailed description of the intelligent control module has been provided by (Gökçe 2011, 2013b).

v. Monitoring Tools

The common goal of the graphical user interfaces is to represent the building performance information to the end users at the Building Energy Demand (BED) side and to the grid operators (stakeholders) at the Building Energy Supply (BES) side concerning their roles and functions. The aim of the proposed system's monitoring tools is designing and implementing user friendly, customized and context sensitive Graphical User Interfaces (GUIs) for defined end users and stakeholders. In order to achieve this, Java and Service Oriented Architecture (SOA) based interfaces are developed which enables end users automated querying without dealing with complex SQL statements (Gökçe 2013).

4. CONCLUSIONS

In this paper an intelligent hybrid building energy management system composed of (1) Building energy supply-side and (2) Building energy demand-side management is described. The proposed concept integrates energy production systems from renewable energy sources, building energy diagnostics and predictive control, ubiquitous wireless sensing technologies, and micro grid power electronics and power control. The research focuses on an innovative model-driven development approach that integrates systems in building energy supply-side and building energy demand-side to provide optimized energy production/consumption. The research findings will be demonstrated in an appropriately selected building in Hannover, Germany with EOS Sustainable Energy Solutions GmbH (EOS 2015) integrating different energy efficient production/consumption systems addressing the renewable energy technologies, energy storage systems and building energy management systems comprising scalable and robust sensing network platforms, energy performance monitoring and data mining technologies. The initial research findings will be used to extend this research to the smart cities level.

5. REFERENCES

ASHRAE (2003). HVAC Systems and Equipment. ASHRAE Publications, ASHRAE, USA.

CARAGLIU A., Del Bo C., Nijkamp P. (2009). Smart Cities in Europe. Series Research Memoranda 0048. Free University Amsterdam, Faculty of Economics, Business Administration and Econometrics. Nederland.

DIN (Deutsches Institut für Normung e.V.) (Herausgeber) (2007). DIN EN 15232: Energieeffizienz von Gebäuden Einfluss von Gebäudeautomation und Gebäudemanagement, Deutsche Fassung EN 15232:2007. Berlin, Germany.

EEA (European Environmental Agency) (2009). Ensuring quality of life in Europe's cities and towns. EEA Report 5/2009.

EOS Sustainable Energy Solutions GmbH (2015) http://www.eos-ses.de Accessed on May 2015.

GÖKÇE H. U. (2010) Multi-Dimensional Analysis of Building Performance Data for Energy Efficient Building Operation. PhD Thesis, National University of Ireland, Cork, Ireland.

GÖKÇE K. U., Gökçe H. U. (2014). "Chapter 22: Virtual Energy Platform for Low Energy Building Operations", Book: Progress in Sustainable Energy Technologies Vol II". Springer International Publishing Switzerland. ISBN: 978-3-319-07895-3.

GÖKÇE, H. U., Gökçe K. U. (2011) Multi Dimensional Information Management Platform for Wireless Embedded Monitoring of Building Performance Data. Proc., 11th International Conference on Construction Applications of Virtual Reality, Weimar, Germany. ISBN: 978-3-86068-458-0.

GÖKÇE, H. U., Gökçe, K. U. (2013a). "Multi Dimensional Energy Monitoring, Analysis and Optimization System for Energy Efficient Building Operations" Journal of Sustainable Cities and Society, 10 (2014) 161–73. Elsevier Press.

GÖKÇE, H.U. and Gökçe, K. U. (2013b). "Integrated System Platform for Energy Efficient Building Operations." Journal of Computing in Civil Engineering, 10.1061/ (ASCE) CP.1943-5487.0000288 (Jan. 5, 2013). SCI A.

HATLEY D, Meador R, Katipamula S, Brambley M, and Lt.Cokl, C.W. (2005). Energy Management and Control System: Desired capabilities and Functionality prepared for HQ Air Mobility Command (AMC/CEO) PNNL-15074, Richland, Washington 99352.

KOMNINOS N, Schaffers H, Pallot M. (2011). Developing a policy roadmap for Smart Cities and the Future Internet. In: Proceedings of the eChallenges 2011 Conference, 24–26 October 2011, Florence. Italy.

LOWRY G. (2002) Modelling user acceptance of building management systems, Automation and Construction, 11 (6), 695-705.

NIKOLAUS K. (2008). Pictures of the Future Spring, http://w1.siemens.com/innovation/en/publikationen/publications_pdf/ Last download 2008.

Serenergy (2015) http://serenergy.com/ Accessed on May 2015.

Soekris Board (2012) http://www.soekris.com/ Accessed on June 2012.

The Science Museum. Urban Development (2013). http://www.makingthemodernworld.org.uk/learning_modules /geography/04.TU.01/?section=2. Last Accessed on 3 April 2009.

VDMA (German Engineering Federation) (2008). Energy-efficiency of Buildings. Germany. Beuth Verlag GmbH 2008, pp. 79. Berlin, Germany.

16: Applied thermal comfort control

PETER SIMMONDS

FASHRAE, Building and Systems Analytics LLC, Marina Del Rey California and Andre Jonker, WSP Group, London

A large banking facility has three trading floors, each floor has 600 occupants. Since the commissioning of the building and its systems in 2003 there have been numerous complaints from the occupants regarding conditions on each floor. The complaints had escalated so far that senior management requested the comfort conditions relative to occupants be improved. But what were the conditions which were deemed to be "uncomfortable" and what conditions needed to be created to alleviate and further complaints?

There were on-going complaints received from occupants pertaining to environmental conditions on all three of the trader floors. The complaints varied from thermal issues: Too hot, Too cold, Draft.

Detailed surveys were conducted to ascertain actual small power loads of equipment installed on a zone by zone basis. The results from these surveys in conjunction with the existing occupancy densities, lighting loads and the building façade fabric performance were recorded.

This paper will first describe the previous operating conditions and then will describe the analysis and proposed system modifications to remedy the situation. The revised HVAC system and controls would be capable of monitoring and operating zone conditions to PPD and PMV requirements.

1. INTRODUCTION

Against a background of an increasingly competitive and technologically advancing building industry serving even more demanding clients, the design function is becoming more complex. Building environmental performance is now critically assessed and the capital and running costs of the services necessary to provide the required environmental conditions come under careful scrutiny (Simmonds 1994, 1999, 2006, 2009). The purpose of most of today's calculations is to determine the correct heating and cooling capacities for a space so that the required room condition can be achieved at a given outdoor condition (Simmonds 1991). Two factors play a role:

- The first factor are the increased requirements for energy performance compliance. This increases the need for accuracy in the calculation method (ASHRAE standard 90.1-2013)
- The second factor is the increase in the requirements for Thermal Comfort compliance (ASHRAE Standard 55-2013)

The building serves as the global headquarters of the banking institution and was built in 1997 and completed in 2002 and comprises of 45 floors. The trader floors are located at Level 2, 3 and 4 of the building and the trader floor areas is 3200m².

Current occupancy levels on the 3 No floors are based on desk layouts and are approximately as follow:

- 2nd Floor – 609 persons
- 3rd Floor – 597 persons
- 4th Floor – 625 persons

Small power loads are non-standard and vary from medium to high density. This is dictated primarily by number of work stations, type of workstations, quantity of screens and type of telephone used, standard type or trader phones. There are a number of printers, 42 inch TV screens and digital display boards located on the floors.

Figure 38 shows a quadrant of one of the trading floors

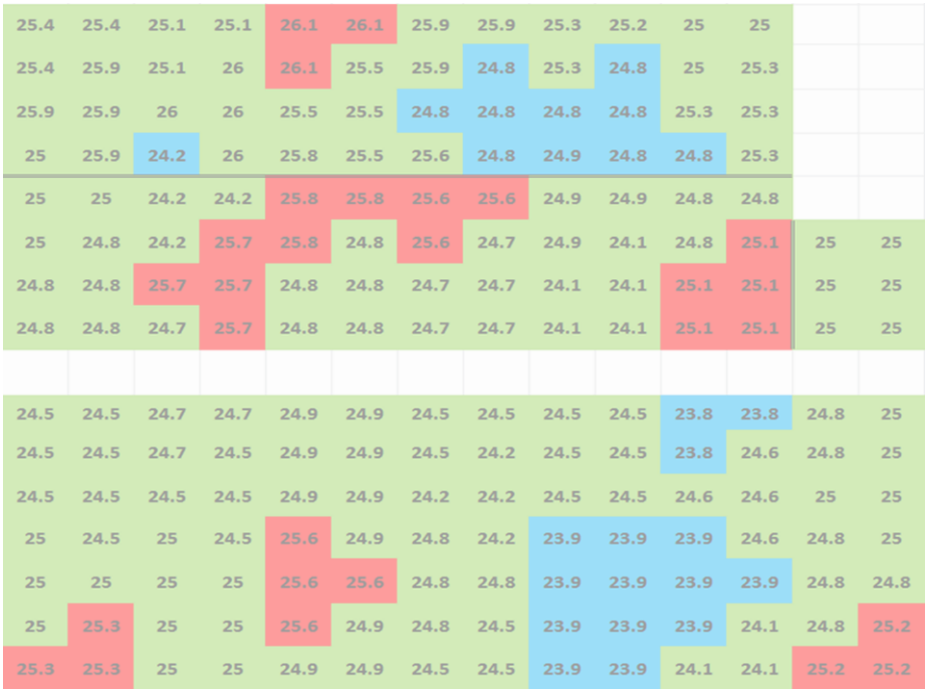

Figure 39 shows a sample of dry bulb temperatures measured on one of the floors.

2. DESCRIPTION OF HVAC SYSTEMS

2.1 Primary FA and Extract Systems

Fresh air is currently provided to the floors areas via central Air Handling Units (AHU). AHUs can supply off coil temperatures of 11°C during summer and 18°C during winter.

Fan Assisted Terminals (FAT) have been installed to provide conditioned air onto the floors. The following quantities of VAV terminals have been installed:

- 114 (Level 2),
- 121 (Level 3)
- 100 (Level 100).

The Fan Assisted Terminal (FAT) Boxes take primary and induction air from the ceiling plenum and, mix the two thoroughly and provide a constant air supply to the occupied zone of the building. Total flow from the diffuser is kept substantially constant thus giving very good air distribution even with high turn down of the primary air volume.

Design of the FAT ensures that at 100% primary air, sufficient induced air is mixed with the primary air so that the air discharged has a conventional cooling differential which will not cause draught problems in the space being conditioned.

The FAT units are self-contained and complete with flow measuring grid, motorized flow-control damper, fan, and integral controls.

Conditioned air is provided at 11°C (variable set point controlled from on floor AHU) from the main supply ductwork onto the FAT terminals and pending on the heating or cooling requirement will control the % recirculation pending the dictates of either heating or cooling by the space.

2.2 Air Terminals

Conditioned air is provided into the space via high induction swirl type diffusers. Air is returned via 4 Core type return air grilles from the space.

The critical criteria for the correct operation of the ceiling mounted swirl diffuser is the velocity Vh1. Each selection should show the velocity in the occupied zone to be lower than 0.25 m/s. if velocities are higher than 0.25m/s then occupants can possibly feel a draft sensation.

- In cooling mode the supply air temperature to the space is 12C, the space condition is 22C. From the selection the velocity is 0.13 m/s and the temperature of the air in the occupied zone is 21C. Occupants should not feel any draft or temperature sensations under these conditions.
- In heating mode the supply air temperature to the space is 26C, the space condition is 22C. From the selection the velocity is 0.13 m/s and the temperature of the air in the occupied zone is 22.4C. Occupants should not feel any draft or temperature sensations under these conditions.

2.3 Dynamic Comfort Control

In order to provide a higher degree of controllability and further information for HSBC a Dynamic Comfort Control has been integrated into the BMS.

Thermal comfort is that condition of mind that expresses satisfaction with the thermal environment. Because there are large variations, both physiologically and psychologically, from person to person, it is difficult to satisfy everyone in a space. The environmental conditions required for comfort are not the same for everyone. However, extensive laboratory and field data have been collected that provide the necessary statistical data to define conditions that a specified percentage of occupants will find thermally comfortable.

- Predicted Mean Vote (PMV).... an index that predicts the mean value of the votes of a large group of persons on the 7-point thermal sensation scale.
- Predicted Percentage of Dissatisfied (PPD).... an index that establishes a quantitative prediction of the percentage of thermally dissatisfied people determined from PMV.

Such analysis of the thermal environment requires a complete solution to the equations representing air movement and the thermal response of the building fabric under dynamic conditions. Fanger deduced a “Thermal Index” that could express a subject’s thermal sensation in a climate deviating from the optimum. Fanger assumed that thermal sensation is a function of the thermal load of the body. The Predictive Mean Vote (PMV) index can be determined when the activity (metabolic rate) and clothing (thermal resistance) are estimated and the following environmental parameters are measured:

- Air temperature (to be monitored at 72 zones on each floor)
- Mean Radiant Temperature (MRT)
- Relative air velocity
- Humidity

The PMV index is based on a thermal load and is defined as the difference between internal heat production and heat loss to the actual environment for a person with (theoretical) mean skin temperature and seat secretion at an actual activity level.

Fanger quantified the relationship from the results of experiments in which people were asked to cast a “thermal sensation” vote. The PMV scale is perhaps a little difficult to interpret. People are not identical, so in reality a group of people would report a varying range of thermal sensations. The PMV indicates the most probable sensation from the thermal load conditions. Thus the PMV gives a general indication of the level of comfort (i.e. thermal sensation) but contains no indication of the range of comfort actually experienced.

The Predicted Percentage of Dissatisfied (PPD) index establishes a quantitive prediction of the number of thermally dissatisfied persons who have voted on a seven point comfort sensation scale i.e. hot(+3), warm (+2), cool(-2) or cold (-3).

The PPD scale provides an indication of the range of comfort experienced in reality due to individual differences. The relationship between PPD and PMV was deduced by Fanger. The PPD indicates the percentage of people who when asked the question “how comfortable are you?” would say “I feel too warm” or I feel too cold”. It is impossible to satisfy all persons in a large group in the same climate. Even with a perfect environmental system, a PPD of less than 5% is rarely attainable (a point often overlooked in

practice, where any complaints however few are taken as an indication that the system is defective or badly operated).

3. FUNCTIONAL SYSTEM DESCRIPTION

The present AHU/VAV Fat Boxes control as per original design, with the exemption of the following:

- The on floor AHU set point is now fixed at 11'C instead of floating set point between 11'C - 22'C as dictated by box primary damper positions.
- There are 9 supervisory zones associated with 72 temperature zones.
- 72 New Zone Return Air Sensors have been replaced.
- 9 New Infrared Radiant Sensors have been fitted to Ceiling. (1-9 area zones)

Calculation of PPD and PMV values are achieved using the computer program shown in appendix A of the contract documents which has been integrated within the BMS.

Calculations are carried out for each zones on the second, third and fourth floors.

4. CALCULATION INPUTS

To carry out the PPD / PMV calculations the BMS uses the following six inputs

a. Metabolic Rate
b. Clothing Insulation
c. Air Temperature
d. Radiant Temperature
e. Air Speed
f. Humidity
g. Metabolic Rate

This is user selectable from the BMS. It has initially been set to a value of 1.0

Clothing Insulation

The BMS uses three values of clothing insulation (Clo) for calculation. These are 0.7, 0.85 and 1.0

For each floor and within each zone the PPD / PMV calculations are carried out at two minute intervals for the three values of Clo whilst the respective VAV box return air temperature is being sampled.

Air Temperature

For each floor and within each zone a respective VAV box return temperature sensor is sampled for six minutes to carry out the PPD / PMV calculation.

Radiant Temperature

For each floor and within each zone a respective radiant temperature sensor is monitored by the BMS

Air Speed

This is user selectable from the BMS. It has initially been set to a value of 0.13 m/s

Humidity

For each floor and within each zone a respective wall mounted humidity sensor is monitored by the

BMS

BMS Calculation of PPD / PMV Values

Each zone on each floor references a number of VAV box return air temperature sensors to carry out the PPD / PMV calculation. To carry out the calculations each VAV box return air temperature sensor is sampled consecutively and continuously for six minutes. Within this six minute period and at two minute intervals, the three different values of Clo set point are changed so that PPD / PMV calculations are carried out for three separate values of Clo.

- Once the required graphic slides have been printed the Clo set point value requires setting back to auto. The previously manually set cascade select point also requires setting back to auto.
- The calculations for PPD / PMV values will now revert back to normal auto control

Figure 40 shows a comparison of comfort conditions using the CBE [1]Thermal Comfort Tool

Data Logging

All data will be logged and recorded at 1 hour intervals for each of the 72 temperature sensors and the 9 supervisory sensors on each floor. Comfort calculations expressed as PPD/PMV for each of the 72 zones will be recorded for all three of the clothing levels listed above

5. TEST PROCEDURE

Day 1

Each zone temperature was programmed to be controlled at 22C (adj) by the BMS. The system started operation at 7 am (adj). The zone temperatures were maintained at 22C (adj) until 11am. There were 34 complaints registered during this period. At 11am a group signal was sent from the BMS to re-set each zone operating temperature to 25C (adj). All zone temperatures are to be logged at 5 minute (adj) intervals. No complaints were received during this period.

At 1:00pm a group signal will be sent from the BMS to re-set each zone operating temperature to 22C (adj). All zone temperatures are to be logged at 5 minute (adj) intervals. The conditioning system will be switched off at 10 pm (adj)

Day 2

Each zone temperature was programmed to be controlled at 24C (adj) by the BMS. The system started operation at 7am (adj).There was only one complaint during this period.

6. TEST RESULTS

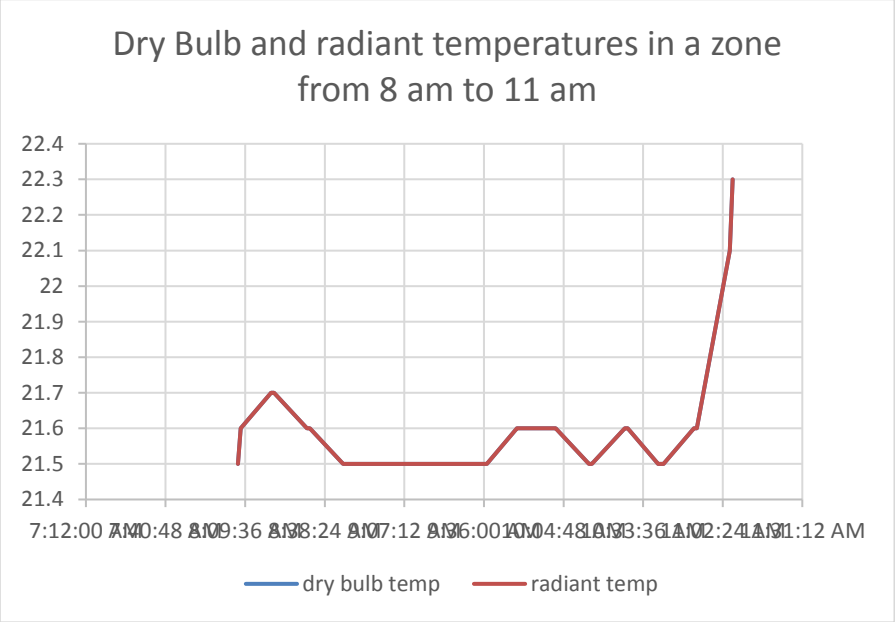

Figure 41 shows the Dry Bulb and Radiant temperatures in one of the zones from 8 am until 11am on Monday May 12, 2014

Each zone temperature was programmed to be controlled at 22C by the BMS. The system started operation at 7 am. The zone temperatures were maintained at 22C until 11am. There were 34 complaints registered during this period.

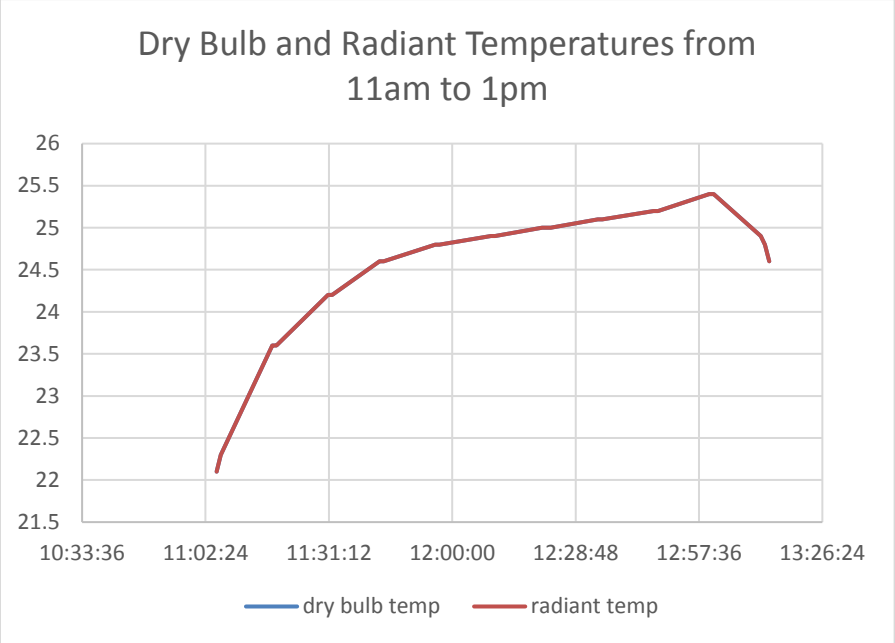

Figure 42 shows the Dry Bulb and Radiant temperatures in one of the zones from 11 am until 1:30 pm on Monday May 12th, 2014.

At 11am a group signal was sent from the BMS to re-set each zone operating temperature to 25C. All zone temperatures were logged at 5 minute intervals. Figure 3 shows how the Dry Bulb and Radiant temperatures. The temperatures rose quite rapidly, but did not increase above 25.5 C.

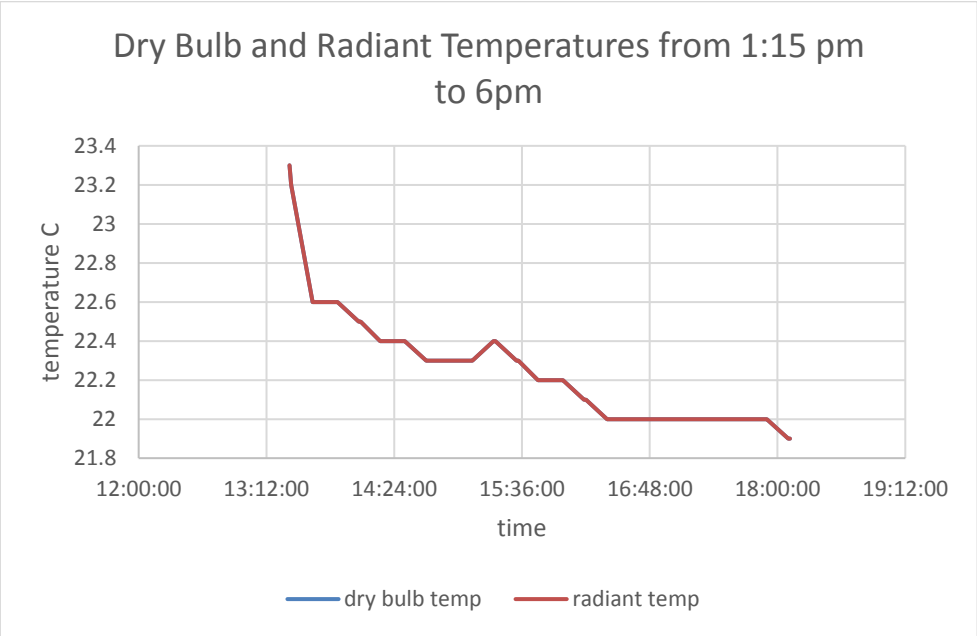

Figure 43 shows the zone Dry Bulb and Radiant temperatures from 1pm until 6 pm

At 1:00pm a group signal was sent from the BMS to re-set each zone operating temperature to 22C. All zone temperatures were logged at 5 minute intervals. Figure 4 shows the space Dry Bulb temperatures were reduced from 25C to 22C in about 15 minutes. This showed the system has sufficient capacity and also shows the controllability of the system.

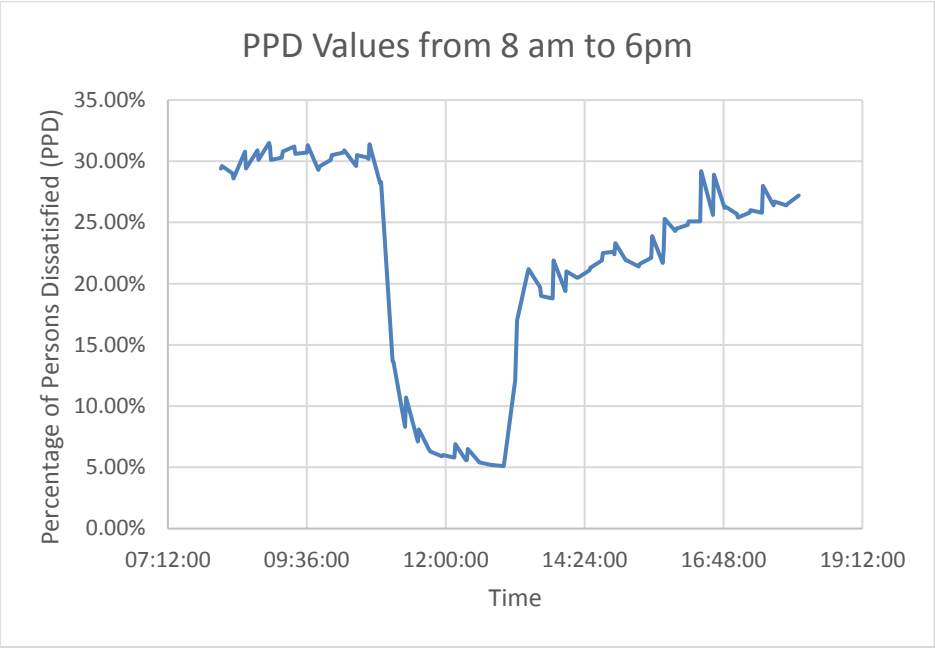

Figure 44 shows the PPD values from 8 am to 6pm.

When the space Dry Bulb temperature is controlled to 22 C (the HSBC recommended space temperature) space occupant comfort conditions are about 30% PPD. When the space Dry Bulb temperature is increased to 25-26C the comfort conditions increase to below 10% PPD. As the zone Dry Bulb temperature if reduced to the required operating Dry Bulb temperature of 22C, occupant comfort conditions are reduced down to 25%.

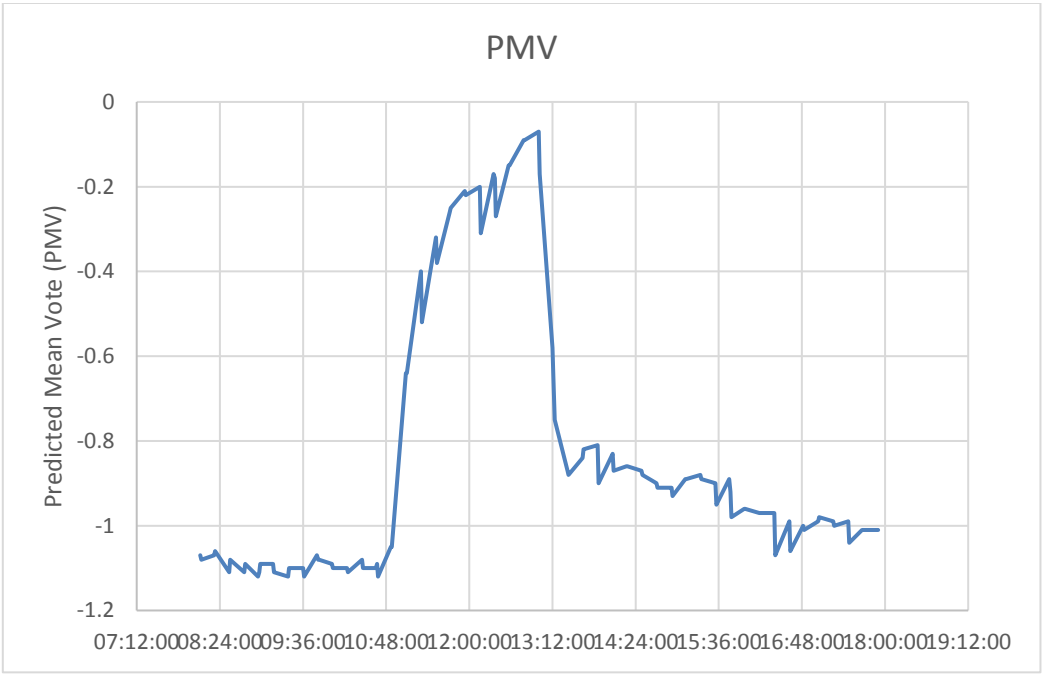

Figure 45 shows the PMV values from 8 am to 6pm.

The PMV is an indicator of what comfort conditions are. The limits of PMV should be between +0.5 and -0.5. The + sign is a warm sensation and the – sign is a cold sensation. Figure 6 shows negative values from 8 m through 6pm indicating space occupants experiencing a cold sensation.

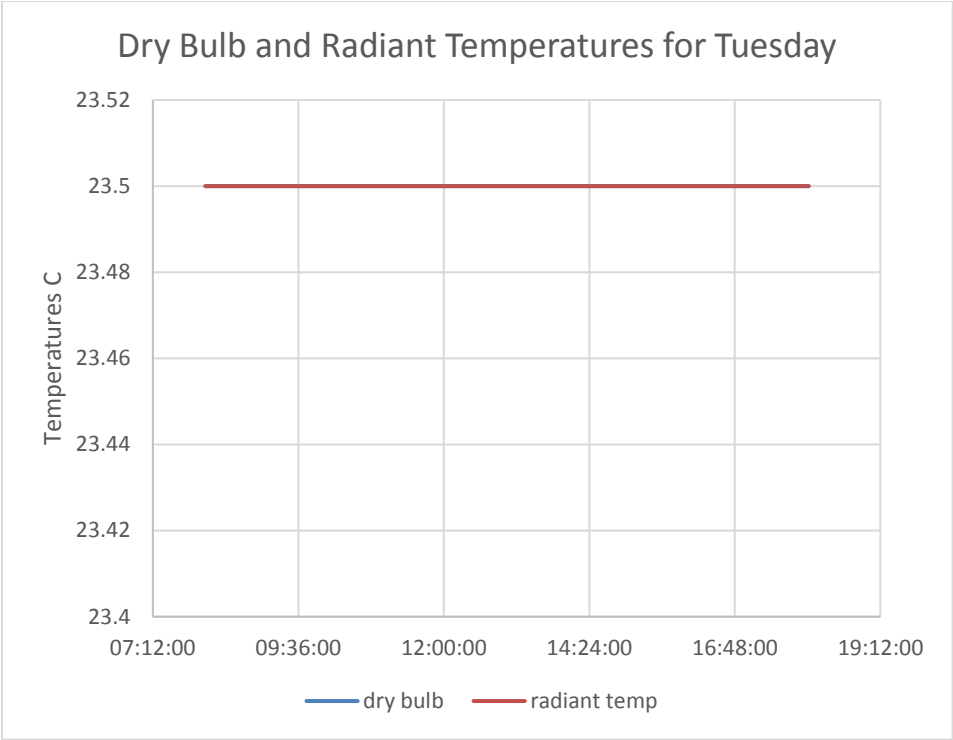

Figure 46 shows the dry bulb temperatures for Tuesday May 13th, 2014, for one of the 72 zones.

The recorded space conditions for this zone was 23.5 C for the whole of the day. As these results show the Dry Bulb temperature is equal to the Radiant temperature, the radiant temperature in this zone will have no negative impact on occupant comfort.

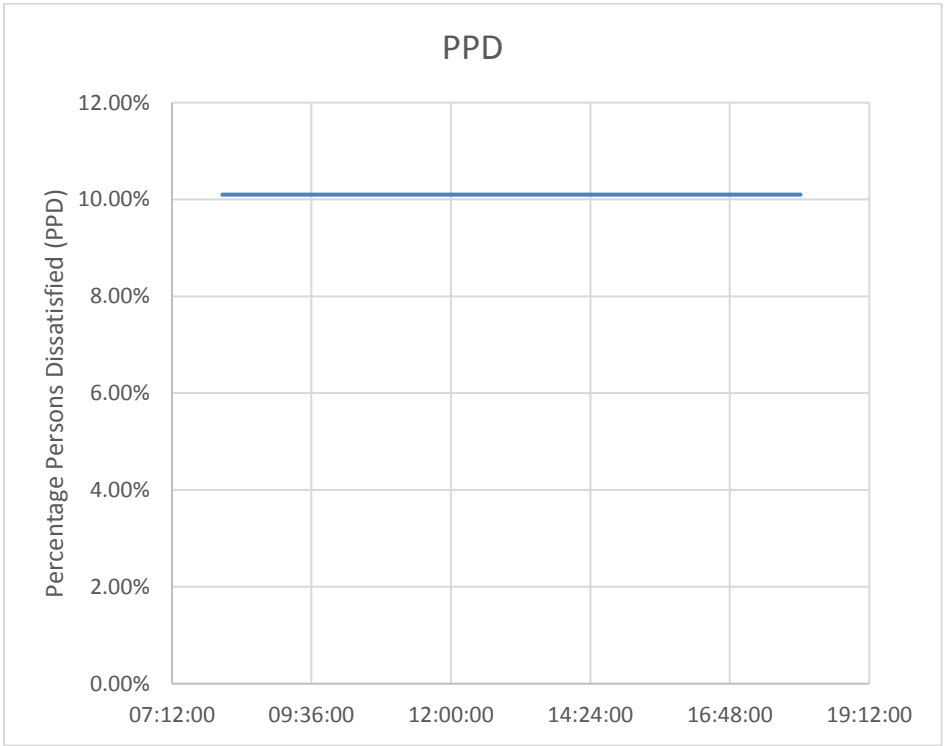

Figure 47 shows the PPD values recorded for the same zone as shown in figure 7.

The PPD values calculated for occupants having a Clo value of 0.85 are constant for the occupied period.

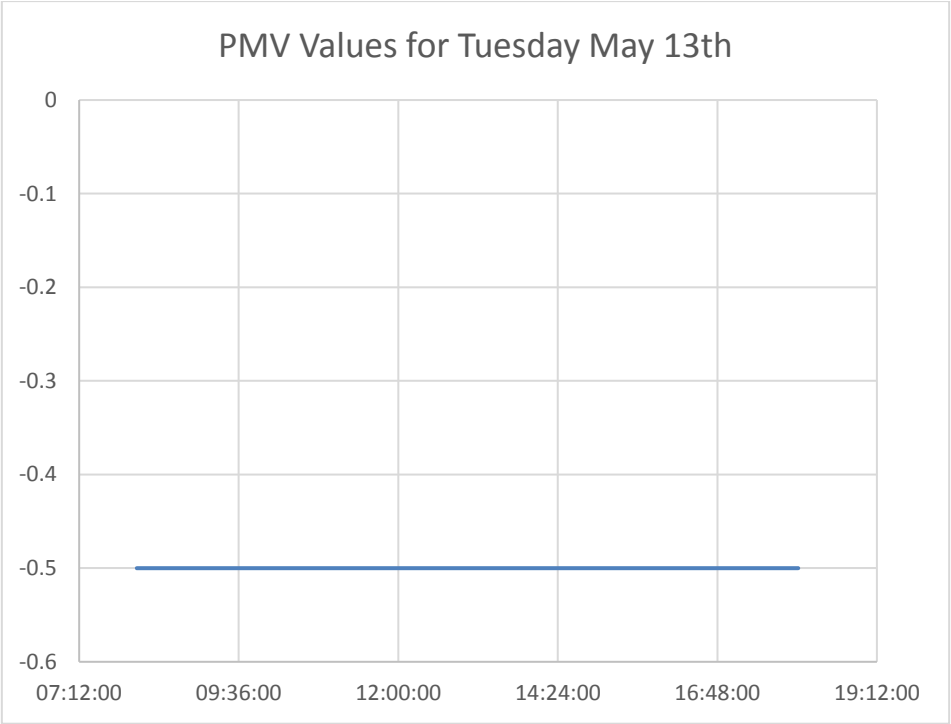

Figure 48 shows the PMV values recorded for the same zone as shown in figure 7.

The PMV values calculated for occupants having a Clo value of 0.85 are constant for the occupied period at about -0.5, this would mean the occupants are comfortable, but the sensation is approaching “cold”.

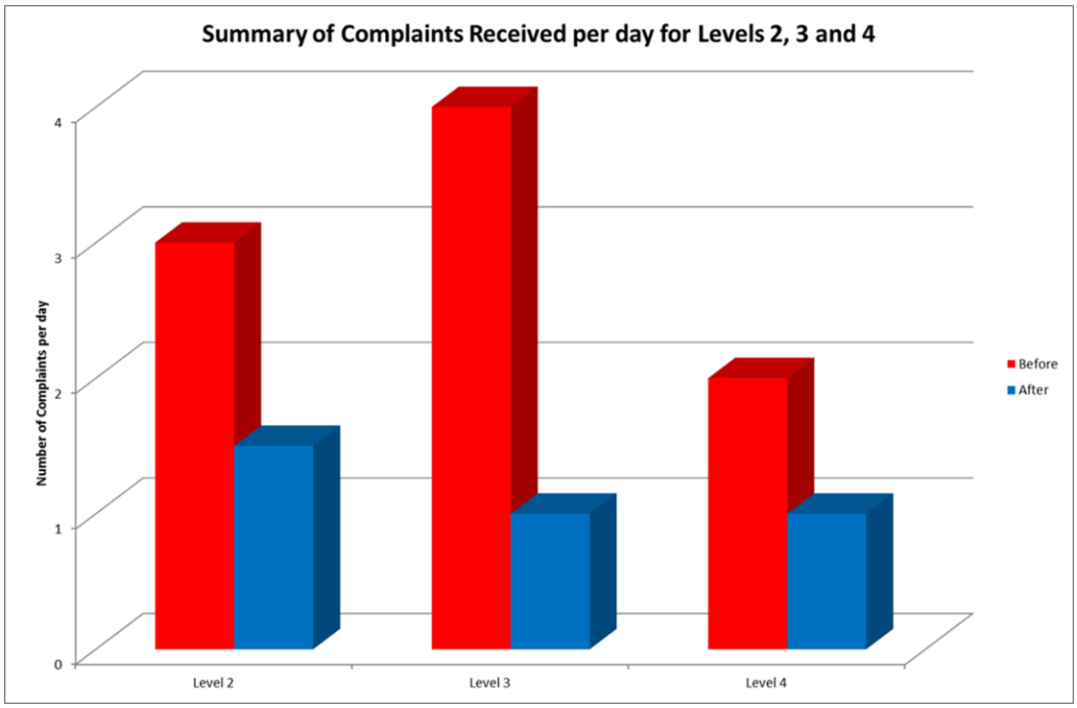

Figure 49 shows a summary of complaints for levels 2, 3 and 4

The number of complaints have dropped by more than 30%. Numerically even complaints of 3 or 4 per floor are far less than the 10% determined by Fanger.

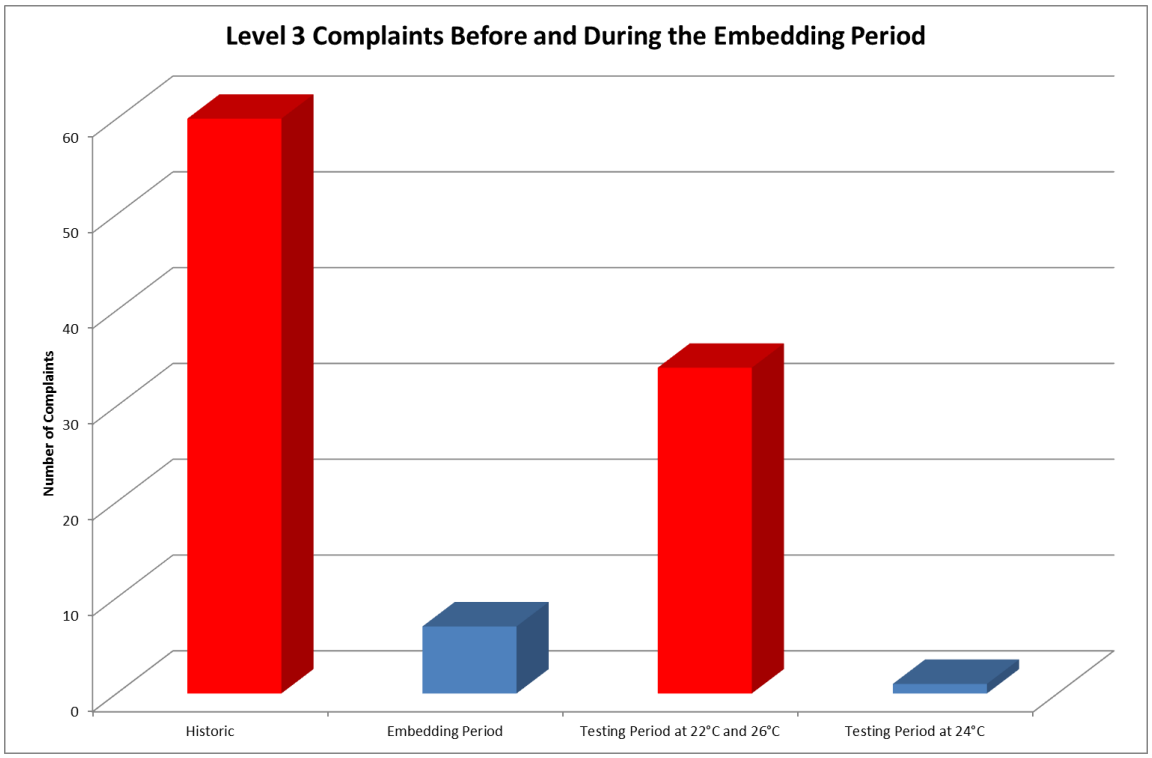

Figure 50 shows the number of complaints before and after the embedded period

On Monday May 12 there were 64 complaints, these were reduced to one on the second day when the zone temperature was re-set to 24C

7. STRATEGY FOR FM TEAM TO DEAL WITH THERMAL COMFORT DISSATISFACTION.

OBTAIN LOGGED COMPLAINTS VIA COMPLAINTS DESK

Identify issue, desk number, and name.

Provide thermal comfort questionnaire to assist FM team to deal with complaints.

IDENTIFY FAT ZONAL AREA CONCERNED

Identify the location of the zonal area on the floor plate and from what FAT unit it is served.

COLLATION OF DATA

Obtain screenshot of the FAT unit configuration and Thermal Comfort Index and take screenshots.

7.1 Equipment

Provide date and time on screenshots

Review screenshot for general issues with the performance of the equipment

(Alarms/ Faults/isolated etc.)

Identify if there are issues with the performance of the FAT units (primary /secondary air flows)

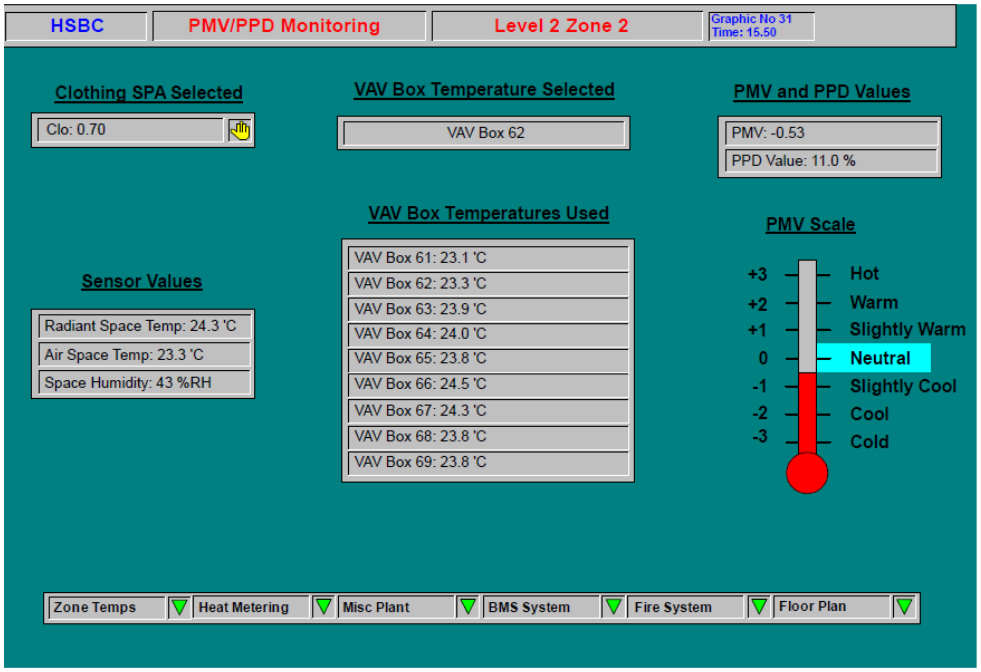

Figure 51 shows a screen shot from the BMS for a zone which shows the zone PPD and PMV conditions. The Clo value is 0.7 for these values.

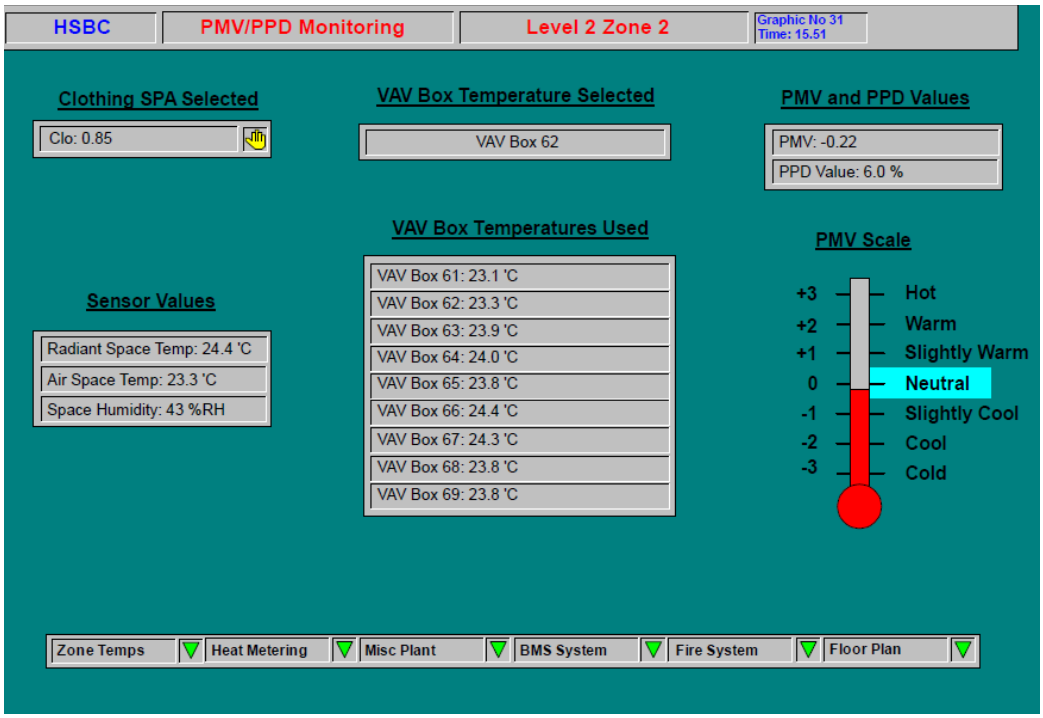

Figure 52 shows a screen shot from the BMS for a zone which shows the zone PPD and PMV conditions. The Clo value is 0.85 for these values.

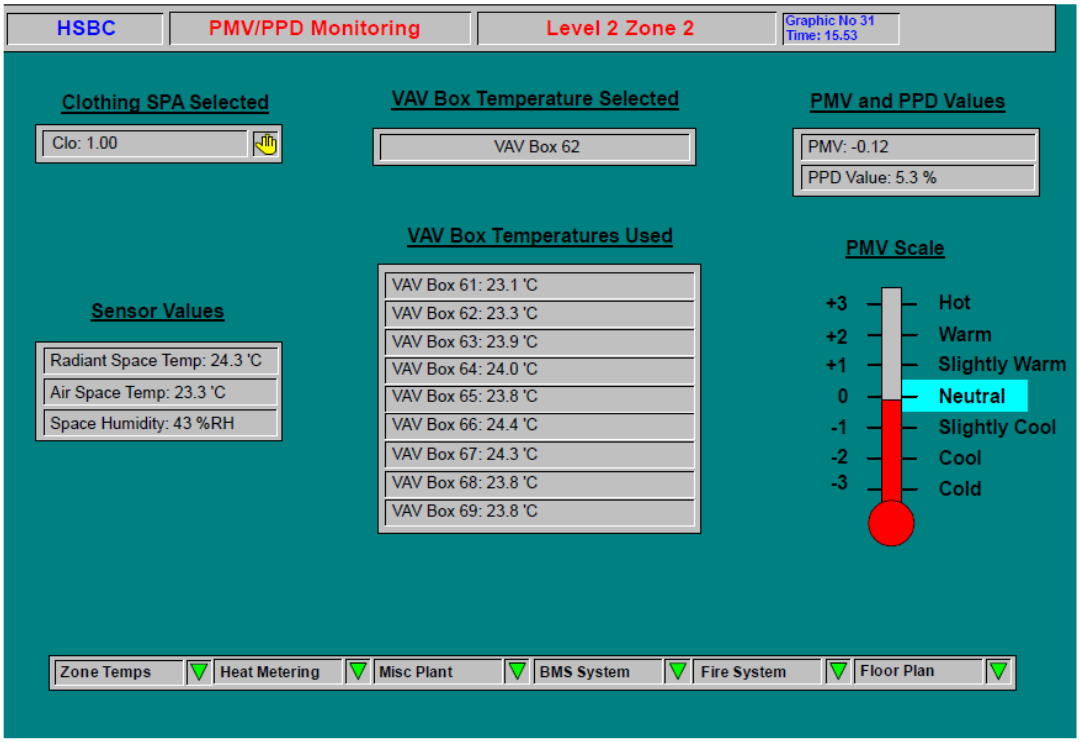

Figure 53 shows a screen shot from the BMS for a zone which shows the zone PPD and PMV conditions. The Clo value is 1 for these values.

7.2 Thermal Comfort (Parameters)

- Identify from data whether the temperature range is within design parameters
- (± 1.5 deg C from design set point)
- Review the PPD value recorded
- PPD range above 10% - Adjustment may be required to the zonal set points:
- (Meeting required between JLL/ HSBC representative and Design Engineer to agree approach to improve)
- PPD range between 7-10% - Acceptable comfort index range and may not require adjustment to systems.
- PPD range less than 7% - No Adjustment may be required to the zonal set points.

System is providing optimum thermal comfort in the zone.

PRELIMINARY ANALYSIS

Based on the above information review if there are inherent issues with the performance of the equipment /system and attend to issues if required via JLL BAU contract.

TRADER FEEDBACK

Based on the above information and analysis report back to the 'Traders'. This could be done in terms of one to one meeting set up by JLL discussing temperature ranges and comfort index.

If the system is working in accordance to the design and according to acceptable thermal comfort levels advise that the system is working in accordance with design parameters and thermal comfort indexes for the

Review if there are inherent issues with the performance of the equipment /system and attend to issues if required.

Identify if there are issues with the performance of the FAT unit (primary and secondary) air flows

Compare set design temperature and compared with space temperature (are these within 1.5°C of design)

Obtain Screenshot of PPD and PMV in the zone under consideration

Initially review screenshots that relate to FAT units concerned

8. CONCLUSION

Designing to comfort compliance (PPD <10% and PMV +/- 0.5) does provide further dimensions of HVAC and building designs which will enhance building performance and occupant comfort. Thermal Comfort parameters PPD and PMV, have been around since 1972, yet they have not been fully accepted or adhered to for many designs. Only in mostly completed buildings are complaints from HVAC systems analyzed for comfort compliance, but then it is mostly too late as the building has been constructed.

Comfort compliance can also be used in the design phase to assist in architectural designs and material selection, especially when large glazed areas are being considered. Comfort parameters can also identify the performance of radiant systems in HVAC design.

If comfort compliance is used during the design phase then the liability of the design team is also reduced.

9. REFERENCES

ASHRAE, Handbook-2013 Fundamentals. Atlanta: American Society of Heating, Refrigerating, and Air-Conditioning Engineers, Inc.

ASHRAE Standard 55--2013, “Thermal Environmental Conditions for Human Occupancy”. Atlanta: American Society of Heating, Refrigerating, and Air-Conditioning Engineers, Inc.

FANGER, P.O., 1972, "Thermal comfort analysis and applications in environmental engineering", McGraw-Hill, New York.

ISO 1984, "Moderate thermal environments - determination of the PMV and PPD indices and specification of the condition for thermal comfort." International Standard ISO 7730, International Organization for Standardization.

KREITH, Frank, 1969, “Principles of Heat Transfer”, 2d Ed.. International Textbook Company, Scranton Pennsylvania

Recknagel/Sprenger, 2000, “Taschenbuch fuer Heizung+Klima Technik, Oldenburg Verlag, Munich, Germany.

ROOM - A method to predict thermal comfort at any point in a space.Copyright OASYS Ltd., developed by ARUP Research and Development, London, England.

SIMMONDS, P, 2006, Using Standard 55 PMV scale: Radiant and Variables Control, ASHRAE annual meeting Quebec City, author

SIMMONDS, P, 2005, How to Design Building and HVAC Systems Based on Standard 55-2004, ASHRAE winter meeting, Orlando, author

SIMMONDS, P, 2003, Using the PMV to Control the Indoor Environment, ASHRAE/CIBSE conference, Edinburgh, author

SIMMONDS, P, 2003, Can the PPD/PMV Be Used to Control the Indoor Environment?, ASHRAE/CIBSE conference, Edinburgh, author

SIMMONDS, P, 1993, Dynamic Comfort Control, CIBSE National Conference, Manchester, England, author

SIMMONDS, P, 1993, Designing Comfortable Office Climates, ASHRAE Building Design Technology and Occupant Well-being in Temperate Climates, Brussels, Belgium, February 1993, author

SIMMONDS, P, 1993, Thermal Comfort and Optimal Energy Use, ASHRAE Transactions 1993 V99, Pt 1, author

SIMMONDS, P, 1992, The Design, Stimulation and Operation of a Comfortable Indoor Climate for a Standard Office, ASHRAE/DOE/BTEC conference, Clearwater Beach, FL, author

SIMMONDS, P, 1991, The Utilization and Optimization of A Buildings Thermal Inertia in Minimizing the Overall Energy Use, ASHRAE Transactions 1991 V97, Pt 2, author

SIMMONDS, P, 1991, A Building’s Thermal Inertia, CIBSE National Conference, Canterbury, England, author

WELTY, J.R., Wicks, C.E. and Wilson, R.E., 1969, "Fundamentals of Momentum, Heat and Mass Transfer". John Wiley and Sons, Inc., New York.

322: Solar thermal collector component for high-resolution stochastic bottom-up domestic energy demand models

PAUL HENSHALL, EOGHAN MCKENNA, MURRAY THOMSON, PHILIP EAMES

Centre for Renewable Energy Systems Technology (CREST), School of Electronic, Electrical and Systems Engineering, Loughborough University, LE11 3TU, UK. e.j.mckenna@lboro.ac.uk

High-resolution stochastic 'bottom-up' domestic energy demand models can be used to assess the impact of low-carbon technologies, and can underpin energy analyses of aggregations of dwellings. The domestic electricity demand model developed by Loughborough University has these features and accounts for lighting, appliance usage, and photovoltaic micro-generation. Work is underway at Loughborough to extend the existing model into an integrated thermal-electrical domestic demand model that can provide a suitable basis for modelling the impact of low-carbon heating technologies. This paper describes the development of one of the new components of the integrated model: a solar thermal collector model that provides domestic hot water to the dwelling. The paper describes the overall architecture of the solar thermal model and how it integrates with the broader thermal model, and includes a description of the control logic and thermal-electrical equivalent network used to model the solar collector heat output.

Keywords: Solar thermal collector, domestic, energy demand, dynamic

1. INTRODUCTION

Urban areas currently use over two-thirds of the world's energy and account for over 70% of global greenhouse gas emissions (International Energy Agency 2008). Furthermore, increasing urbanisation means that the proportion of the population living in urban areas is expected to rise from around 50% today to more than 60% in 2030, with urban energy use and emissions expected to rise as a consequence. With deep and binding carbon reduction targets in place in many nations (UK Government 2008, European Commission 2010), the urban environment has therefore become a critical area of focus for addressing the trilemma of secure, affordable and sustainable energy.

Accordingly, there is increasing research interest in urban energy and carbon modelling tools that quantify the economic and environmental impact of urban areas and low-carbon technological and behavioural interventions (Keirstead, Jennings et al. 2012). By helping to understand the energy-use of urban areas better, and providing an evidence-base for improving their performance, such models have the potential to detail the pathways to achieve significant carbon reductions.

The high-resolution 'bottom-up' domestic electricity demand model developed by Loughborough University accounts for electricity consumption and generation associated with domestic appliances, lighting and PV (Richardson, Thomson 2013) and can serve as a basis for urban energy modelling, particularly with a focus on quantifying the impacts of low-carbon technologies on low-voltage distribution networks (Richardson 2010). The model has been used widely within academia and industry (Navarro, Ochoa et al. 2013, EA Technology 2012, Collinson 2014), and work is underway at Loughborough to extend the existing model into an integrated thermal-electrical domestic demand model that can provide a suitable basis for modelling the impact of low-carbon heating technologies. This paper describes the development of one of the new components of the integrated model: a solar thermal collector model that provides domestic hot water to the dwelling. The integrated thermal-electrical demand model will be described elsewhere in forthcoming publications. The following sections describe the type of solar thermal system to be modelled, the thermal-electrical circuit analogy used to model the useful heat output of the system, how the solar thermal component integrates with the broader integrated domestic demand model, the model output calibration and validation, and finally a discussion of future work.

2. DOMESTIC SOLAR THERMAL COLLECTOR SYSTEMS

Domestic solar thermal systems are an example of low-carbon technology that will partially offset electricity and natural gas consumption for the hot water/heating requirements of a dwelling. There are a variety of solar thermal collectors available commercially for domestic purposes. Typically such collectors are either flat plate or evacuated tube varieties of solar thermal collector (Henshall, Moss et al. 2014). Advances in materials over the years has led to improvements in the collection efficiency and thermal insulation of these collectors thus making them more attractive for both the domestic and industrial process heat markets. This is especially the case for installation of such solar thermal collectors in locations of relatively variable climate, such as the UK. For example, recent research at Loughborough University is attempting to utilise a vacuum enclosure to thermally insulate a flat plate solar thermal collector. This would result in a flat plate collector that could reach higher temperatures at higher installed latitudes in comparison to conventional collectors.

The thermal energy generation from such systems is dependent on the variation of local external environmental factors, while thermal energy demand depends partly on the presence and activity of occupants. Generation of solar thermal energy will usually be greatest at solar noon while demand for hot water and heating is likely greatest in the morning and in the evening. This mismatch in generation and demand is buffered via the presence of local thermal energy storage systems, such as hot water cylinders. Accounting for these factors in the developed model is therefore important and will be accounted for as described in following sections.

One can expect the generation of solar thermal energy and the demand for hot water to be somewhat spikey in nature. Subsequently, it is useful to simulate the daily operation of such systems at high temporal resolution and with a common depiction of external irradiance and temperature with regard to generation and occupant activity. Loughborough's existing models produce simulation output at a resolution of 1-minute, and this will also be adopted for the solar thermal collector model described here.

Figure 54 shows the basic integration of a solar thermal collector with a dwellings hot water cylinder. A solar thermal collector is connected to a hot water cylinder via pipes which allow the circulation of a heat transfer fluid between the two components. The heat transfer fluid is typically water, mixed with an anti-freeze, and a pump enables the circulation of the fluid through the pipes. In the model, the pump controller monitors the temperature of the solar thermal collector and the hot water cylinder. If the temperature difference between the collector and the cylinder is greater than 2°C and the cylinder is above a maximum allowed temperature (70°C here) then the controller will turn the pump on and thermal energy will be added to the tank from the collector. If the temperature of the collector falls to within 2°C of the cylinder temperature or the maximum allowed cylinder temperature is exceeded, then the controller will turn the pump off. In the current model it is assumed that there is a perfect heat exchanger within the cylinder such that all the heat contained in the circulating fluid is transferred from the collector to the cylinder.

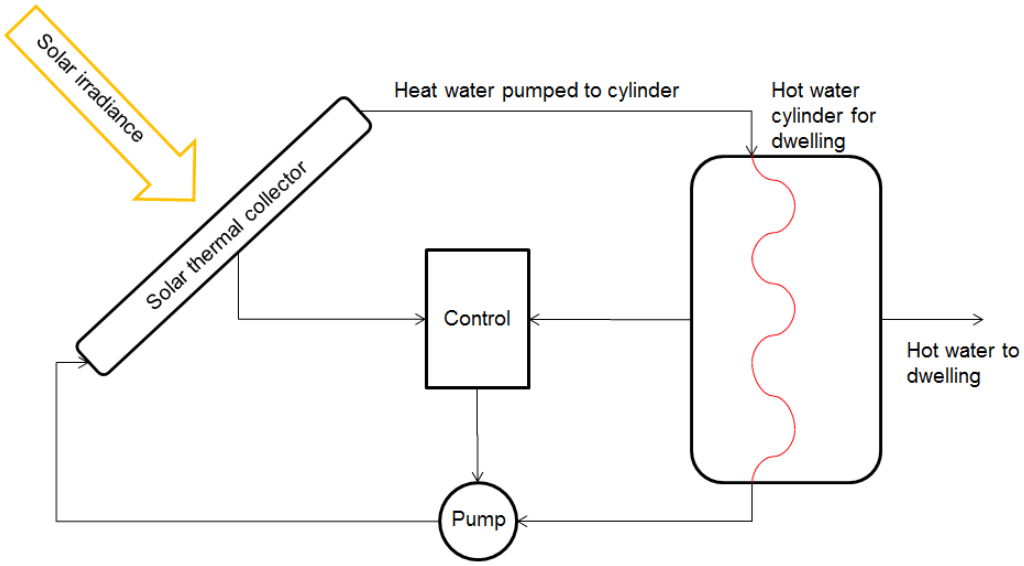

Figure 54: Block diagram of physical system for dwelling.

3. SOLAR THERMAL COLLECTOR COMPONENT MODEL

Stochastic high-resolution 'bottom-up' domestic integrated thermal-electricity demand models utilise a thermal-electric analogy networks for modelling the behaviours of the various systems (thermal emitters, hot water cylinder heater, etc…) of each dwelling (Good, Zhang et al. 2015, Cooper 2013). It is also common to use such an analogy when modelling the output of solar thermal collectors (Duffie, Beckman 1980, de Vries, Francken 1980, Sproul, Bilbao et al. 2012). The thermal-electric analogy network for the solar thermal collector system used in the model is presented in Figure 55.

In Figure 55, it can be seen that the model consists of a series of thermal-electric equivalent components such that:

- A node represents a part of the system represented in the model (units: K)
- A resistor represents a heat transfer coefficient between two nodes (units: W/K)
- A capacitor represents a thermal capacitance (units: J/K)
- A voltage source represents a source of constant temperature
- A current source represents a source of thermal power (W)

The thermal-electric equivalent network shown in Figure 55 is relatively simple in that it represents the temperature of components such as the collector and hot water cylinder via a single node with an attached capacitor. This level of simplicity is necessary such that the integrated "bottom up" model can use the solar thermal component to simulate a large number of dwellings quickly. However, despite the reduced order nature of the solar thermal collector model it will be shown to be a reasonable representation of actual solar thermal systems. More complex thermal-electrical network equivalents for modelling solar thermal collectors can be found in the following literature (de Vries, Francken 1980, Sproul, Bilbao et al. 2012).

In the thermal-electrical network depicted in Figure 55, there are two unknown temperatures to be solved for a given simulation time-step; these being the collector node and the cylinder node. Performing an energy balance at each of the nodes provides the equations to be solved during each time step:

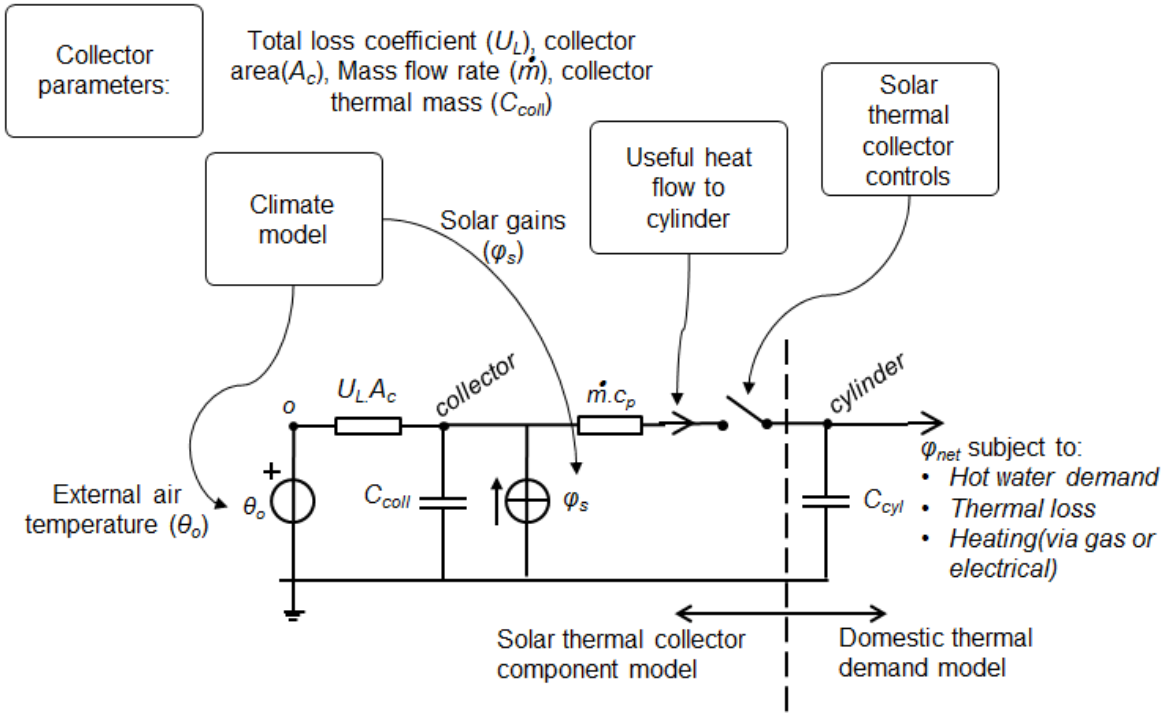

Figure 55: Thermal-electric equivalent network for an individual solar thermal collector and hot water cylinder.

Equation 5: Energy balance equation on collector node

$$\dot{\theta}_{coll} C_{coll} = \varphi_S A_c - U_L A_c \left(\theta_{coll} - \theta_0\right) - \dot{m} c_p \left(\theta_{coll} - \theta_{cyl}\right)$$

Where:

- A_c = collector area (m^2)
- C_{coll} = thermal mass of collector (JK^{-1})
- c_p = specific heat capacity of heat transfer fluid ($JK^{-1}kg^{-1}$)
- $\dot{m}$ = mass flow rate (kgs^{-1})
- U_L = total collector loss coefficient ($WK^{-1}m^{-2}$)
- θ_{coll} = collector temperature (K)
- θ_{cyl} = cylinder temperature (K)
- θ_0 = outside temperature(K)
- φ_s= solar gain (Wm^{-2}) = local solar irradiance (I) × collector transmission-absorption product ($\tau\alpha$)

Equation 6: Energy balance equation on cylinder node

$$\dot{\theta}_{cyl} C_{cyl} = \dot{m} c_p \left(\theta_{coll} - \theta_{cyl}\right) - \varphi_{net}$$

Where:

- C_{cyl} = thermal mass of cylinder (JK^{-1})
- φ_{net} = net heat flow from cylinder subject to demand, cylinder heat losses and gain from primary heating system

In the case of the cylinder, Equation 6 utilises a net heat flow (φ_{net}) to describe when it gains heat from an electrical (or gas) heater but also loses heat to the internal environment of the dwelling and when there is a demand for hot water. It should be noted that because the hot water cylinder temperature is represented as a single node, this model considers the hot water cylinder as fully mixed rather that stratified. In the model **Error! Not a valid bookmark self-reference.** and 2 are solved via Euler integration. With the inclusion of the thermal mass of the collector in **Error! Not a valid bookmark self-reference.** the model can provide an estimate of the dynamic behaviour of the solar thermal collector; this was deemed necessary to provide greater accuracy as the integrated model utilises high temporal resolution data.

As might be expected, as the thermal mass of a collector tends to zero, or the time step of the simulation tends to infinity, **Error! Not a valid bookmark self-reference.** will tend to a steady state equation (Equation 7) with a similar form to the well-known Hottel-Whillier-Bliss equation (Duffie, Beckman 1980), such that:

Equation 7: Steady state energy balance equation on collector node

$$\dot{m}c_p\left(\theta_{coll}-\theta_{cyl}\right)=A_c\left(\varphi_S-U_L\left(\theta_{coll}-\theta_0\right)\right)$$

Model architecture and component integration

A stochastic multi-dwelling domestic integrated thermal-electrical energy demand model is a collection of smaller components/models that work together to provide specific and aggregated energy demand data for a user specified number of dwellings. Based on historical climate data, occupancy/activity probability distributions and user specified control states the model generates multiple instances of dwellings for which presence and activity of occupants is stochastically calculated with each instance exposed to the same environmental conditions (Richardson, Thomson 2013, McKenna, Krawczynski et al. 2015). Based on the activity, calculations are performed to determine thermal and electrical energy required of each dwelling. This is then aggregated to provide electricity, gas and water demand for the group of dwellings.

A simple depiction of how the solar thermal component integrates with a thermal domestic energy demand model architecture is shown in Figure 56. A climate model provides solar irradiance and outside temperature data to the solar thermal model. In this paper the solar irradiance part of the climate model is the same model developed by Richardson and Thomson (Richardson, Thomson 2013) for the purpose of simulating electrical demand in dwellings with photovoltaic panels. The solar thermal collector model calculates useful heat gain based on the cylinder temperature of the dwelling. The temperature of the cylinder will be dependent on other components within the domestic demand model e.g. heat input from primary heating systems, losses to the indoor air, and domestic hot water draws. The useful heat gain from the solar thermal collector will partially offset energy demand associated with the dwelling's primary heating system e.g. gas demand, allowing the economic and environmental impact of the solar thermal collector to be evaluated.

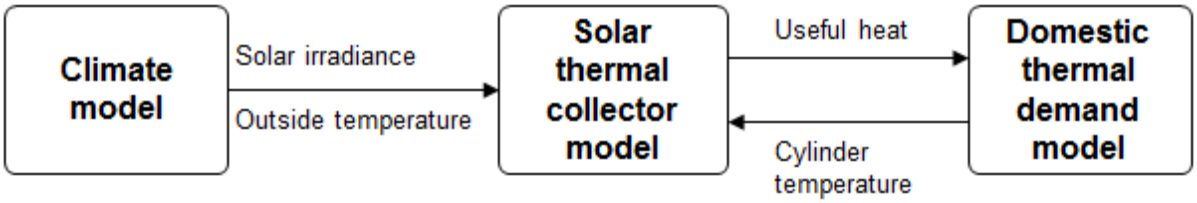

Figure 56: Simple domestic thermal energy demand model architecture.

4. CALIBRATION AND VALIDATION

To calibrate this model and ensure a representative output from the simulated collector, the physical characteristics of a commercial flat plate solar thermal collector were identified or otherwise estimated and are listed in Table 13. The collector area, pump mass flow rate, transmission-absorption product, and collector efficiency slope coefficient are based on a commercial flat plate solar thermal collector datasheet (Kingspan 2015). The heat removal factor is estimated based on a typical value from (Duffie, Beckman 1980). The total loss coefficient is then calculated as the collector efficiency slope coefficient divided by the heat removal factor. Finally, the effective thermal mass of the collector is estimated from (Hellstrom, Adsten et al. 2003).

Table 13: Characteristics of flat plate solar thermal collector for the solar thermal component model calibration

Characteristic	Value
Collector Area (A_c) (m^2)	2
Collector efficiency slope coefficient (k1) ($WK^{-1}m^{-2}$)	3.73
Pump mass flow rate ($\dot{m}$) (kgs^{-1})	0.03
Transmission-absorption product of collector ($\tau\alpha$)	0.87
Heat removal factor (F_R)	0.86
Total loss coefficient (U_L) ($WK^{-1}m^{-2}$)	4.34
Effective thermal mass of collector (C_{coll}) ($kJK^{-1}m^{-2}$)	7.5

From the characteristics listed in Table 13 a constant solar illumination test was run on a flat plate solar thermal collector circulating water to a 100 litre capacity hot water cylinder. The efficiency of the collector during the simulation was determined as the ratio of the useful heat flow to the cylinder to the product of the collector area (A_c) and the local solar irradiance (I). It should be noted the total loss coefficient (U_L) is considered constant for the solar thermal collector, which will result in a linear efficiency profile. The linear efficiency of the simulated collector was compared to the linear steady state efficiency reported for the commercial flat plate solar thermal collector (Figure 57). It will be the subject of future work to account for changes in U_L, this will be especially important for the consideration of high temperature solar thermal collector systems. The efficiency of the solar collector decreases as temperature of the cylinder increases as seen in Figure 57. The constant illumination simulation output of the flat plate solar thermal collector demonstrates a consistent behaviour to that of the commercial solar thermal collector. The constant illumination simulation demonstrates a relatively steady state response of the model, however, with dynamic illumination of the collector there will likely be a departure from this behaviour.

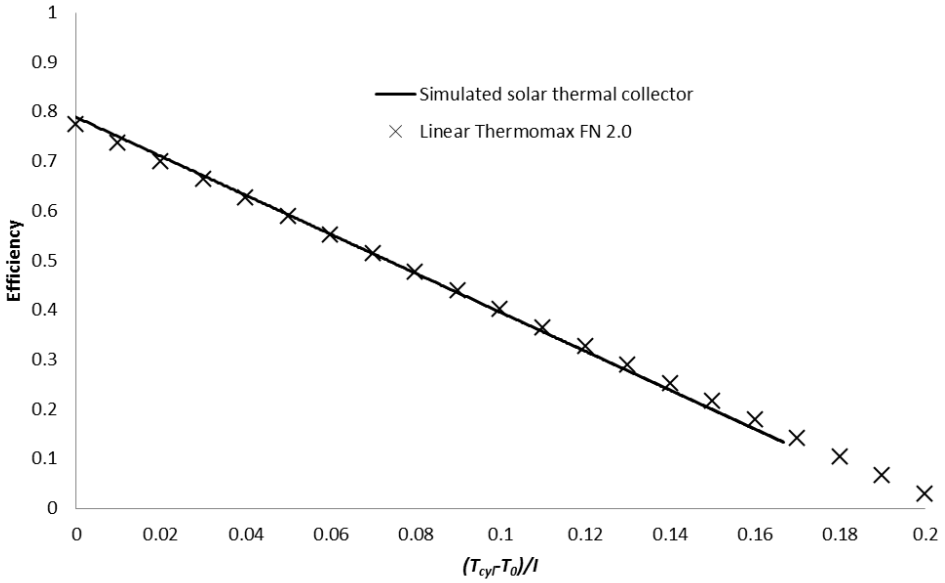

Figure 57: Linear efficiency of simulated and actual flat plate solar thermal collector

5. EXAMPLE OF DYNAMIC SIMULATION OUTPUT

The output from an example dynamic simulation of the solar thermal collector for an individual dwelling subjected to stochastically generated solar irradiance is seen in Figure 58 and 6. In this example the hot water cylinder is subject to a small but constant demand over the course of the day, equivalent to the UK household average of 122 litres / day. Figure 58 depicts the solar power incident on the dwellings solar thermal collector over the course of a day. The incident solar power is generated stochastically using the model developed by Richardson and Thomas (Richardson, Thomson 2013). Also shown in Figure 58 is the useful thermal energy flow from the collector to the hot water cylinder. Figure 59 depicts the temperature variation of the hot water cylinder, the solar thermal collector and the outside air temperature. The presence

of the horizontal line in Figure 59 indicates when the pump is on and heat transfer fluid is circulating between the solar thermal collector and the cylinder.

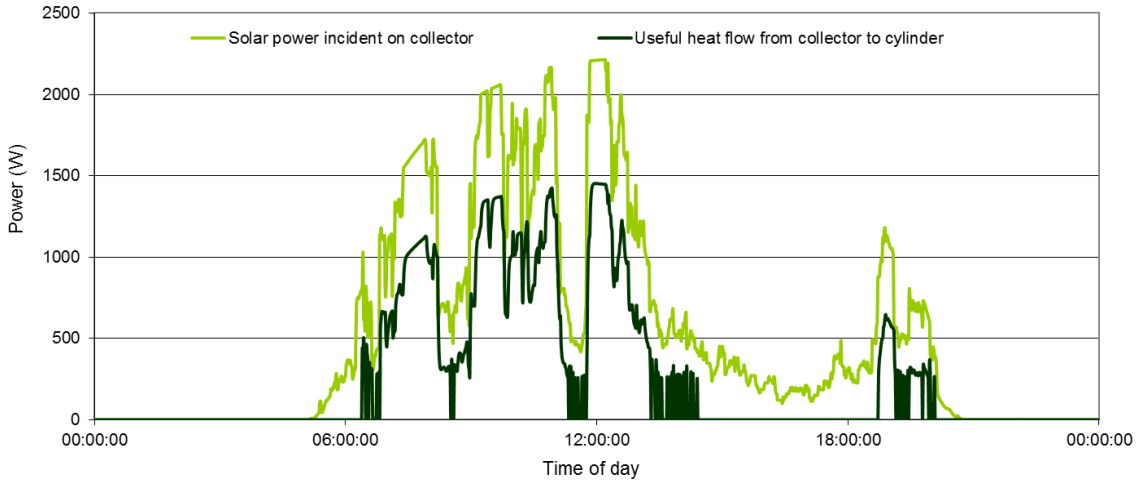

Figure 58: Solar irradiance on collector and useful heat flow from collector to cylinder

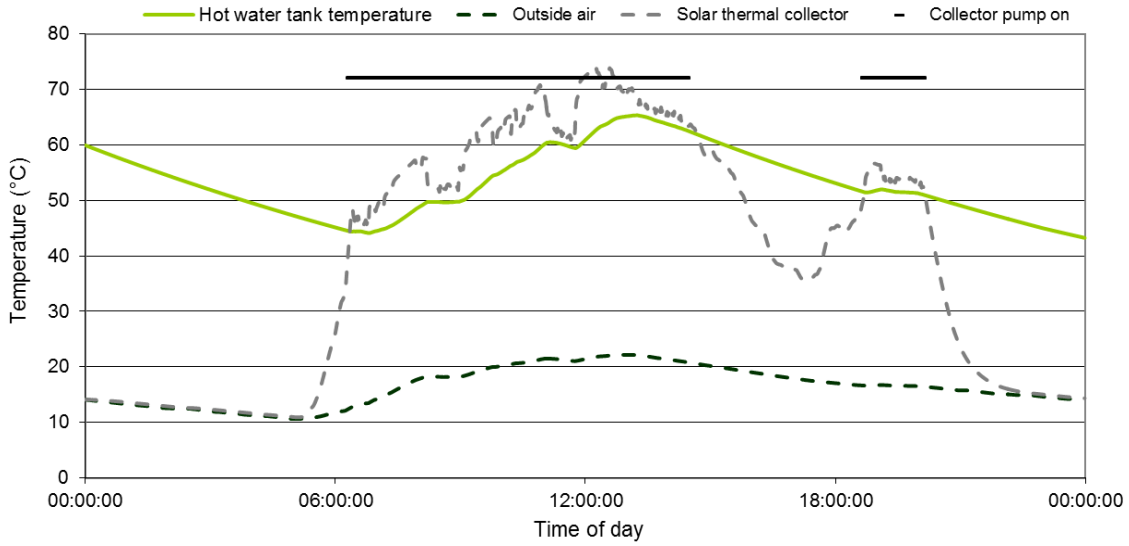

Figure 59: Variation of simulation node temperatures

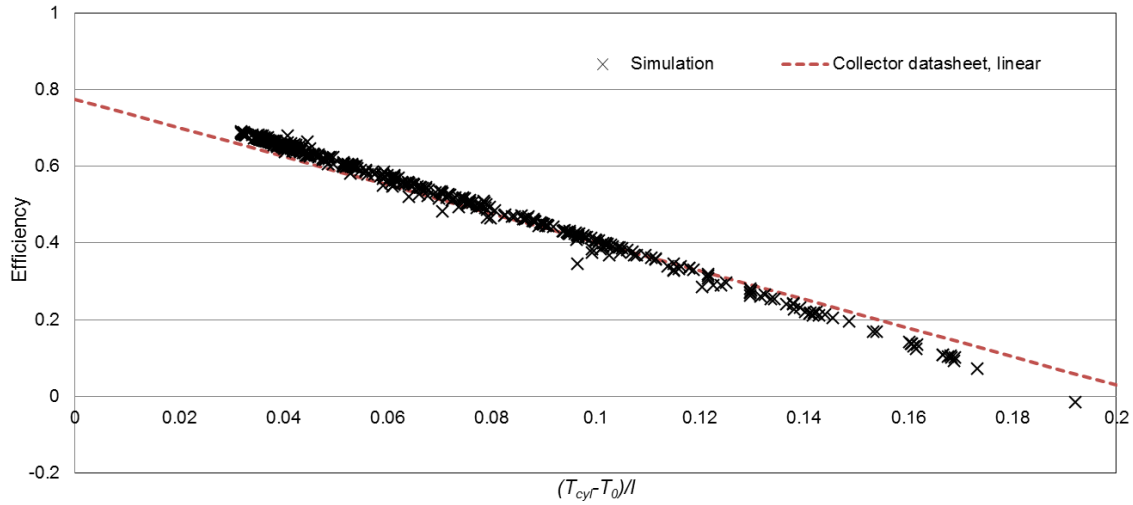

Figure 60: Instantaneous efficiency of simulated collector

In Figure 60 the instantaneous efficiency of the output of the solar thermal collector for the day shown above is plotted along with the steady state linear efficiency taken from the collectors data sheet (Kingspan 2015). It can be seen that for continuous operation the simulated collector behaves in a manner consistent with that of the steady state linear behaviour of the commercial collector. However, as to be expected there are instances when the instantaneous efficiency will depart from the linear trend, for example when the collector is heating up or cooling down.

6. FUTURE WORK

Future work will focus on publishing the open-source integrated thermal-electrical demand model with solar thermal component. This will allow the application of the model to evaluate the economic and environmental impact assessment of solar thermal systems and inform the extent to which they can contribute to a low-carbon urban environment. The solar thermal collector component will also be improved and extended to include more examples of solar thermal collector systems e.g. evacuated tube and evacuated flat plate, solar thermal for space heating, stratified hot water cylinders and systems with phase-change material storage buffers.

7. CONCLUSION

This paper described a simple linear solar thermal collector component model for use within stochastic multi-dwelling integrated thermal-electrical demand models to assess the large scale impact of domestic solar thermal systems. The model employs a linearized thermal-electric network analogy to calculate the instantaneous heat flow from the collector to a hot water cylinder simulated in an integrated thermal-electrical energy demand model. The simple nature of the model allows it to be utilised to quickly generate high temporal resolution data for a large number of dwellings, expediting the assessment of the impact of a variety of solar thermal collector technologies.

The integration of the solar thermal collector component into the larger model is described, detailing the inputs and outputs required. An example calibration and validation is performed based on the characteristics of an existing flat plate solar thermal collector. The solar thermal collector component model demonstrates behaviour consistent with the linear efficiency profile of the commercial solar thermal collector. Furthermore, the solar thermal collector component model is demonstrated responding to stochastically generated, high temporal resolution solar irradiance data. The solar thermal collector component again demonstrates a response consistent with the commercial collector. Subsequently, the solar thermal collector component model described is considered as a valid tool for use within stochastic multi-dwelling integrated thermal-electrical demand models. With further improvement to the component models accuracy and versatility it is expected to provide useful and representative data for domestic thermal energy demand simulations. Such simulations will help inform how current and future solar thermal technologies will impact domestic energy demand.

8. ACKNOWLEDGEMENTS

This project was supported by the Engineering and Physical Science Research Council within the High Performance Vacuum Flat Plate Solar Thermal Collector for Hot Water and Process Heat project (EP/K009230/1) and the Transformation of the Top and Tail of Energy Networks project (EP/I031707/1).

9. REFERENCES

COLLINSON, A., 2014. LV Network Management – A Challenge for Network Designers. SP Networks. Presentation given at LCNF Conference Brighton November 2013. Accessed 23 May 2014. .

COOPER, S., 2013. Thermodynamic Analysis of Air Source Heat Pumps and Micro Combined Heat and Power Units Participating in a Distributed Energy Future (Thesis). Accessed 6 May 2014.

DE VRIES, H.F.W. and Francken, J.C., 1980. Simulation of a solar energy system by means of an electrical resistance network. Solar Energy, **25**(3), pp. 279-281.

DUFFIE, J.A. and Beckman, W.A., 1980. Solar engineering of thermal processes. Wiley New York etc.

EA TECHNOLOGY, 2012. Assessing the Impact of Low Carbon Technologies on Great Britain's Power Distribution Networks. Accessed 23 May 2014. .

EUROPEAN COMMISSION, 28 Jan 2010, 2010-last update, Climate change: European Union notifies EU emission reduction targets following Copenhagen Accord. Accessed on 10th December 2012 [Homepage of Europa], [Online]. Available: http://europa.eu/rapid/pressReleasesAction.do?reference=IP/10/97&format=HTML&aged=0&language=EN&guiLanguage=en [27 Oct 2010, 2010].

GOOD, N., Zhang, L., Navarro-Espinosa, A. and Mancarella, P., 2015. High resolution modelling of multi-energy domestic demand profiles. Applied Energy, **137**(0), pp. 193-210.

HELLSTROM, B., Adsten, M., Nostell, P., Karlsson, B. and Wackelgard, E., 2003. The impact of optical and thermal properties on the performance of flat plate solar collectors. Renewable Energy, **28**(3), pp. 331-344.

HENSHALL, P., Moss, R., Arya, F., EAMES, P.C., Shire, S. and Hyde, T., 2014. An evacuated enclosure design for solar thermal energy applications, Grand Renewable Energy 2014 (GRE2014) International Conference and Exhibition, 27 July - 1 August 2014, © Grand Renewable Energy, pp. 4.

INTERNATIONAL ENERGY AGENCY, 2008. World Energy Outlook. Accessed on 10th December 2012. Paris, France: IEA.

KEIRSTEAD, J., Jennings, M. and Sivakumar, A., 2012. A review of urban energy system models: Approaches, challenges and opportunities. Renewable and Sustainable Energy Reviews, **16**(6), pp. 3847-3866.

KINGSPAN, 2015. Thermomax FN 2.0 Datasheet.

MCKENNA, E., Krawczynski, M. and Thomson, M., 2015. Four-state domestic building occupancy model for energy demand simulations. Energy and Buildings, **96**(0), pp. 30-39.

NAVARRO, A., Ochoa, L.F., Mancarella, P. and Randles, D., 2013. Impacts of photovoltaics on low voltage networks: A case study for the North West of England, Electricity Distribution (CIRED 2013), 22nd International Conference and Exhibition on 2013, pp. 1-4.

RICHARDSON, I., 2010. Integrated High-resolution Modelling of Domestic Electricity Demand and Low Voltage Electricity Distribution Networks (PhD Thesis), Loughborough University.

RICHARDSON, I. and Thomson, M., 2013. Integrated simulation of photovoltaic micro-generation and domestic electricity demand: a one-minute resolution open-source model. Proceedings of the Institution of Mechanical Engineers, Part A: Journal of Power and Energy, **227**(1), pp. 73-81.

SPROUL, A., Bilbao, J. and Bambrook, S., 2012. A novel thermal circuit analysis of solar thermal collectors, 50th Annual Conference of the Australian Solar Energy Society 2012.

UK GOVERNMENT, 2008. Climate Change Act 2008. London, UK:.

52: Numerical method to select chiller sequencing control concerning uncertainties

YUNDAN LIAO[1], GONGSHENG HUANG[2]

1 City University of Hong Kong, Tat Chee Avenue, Kowloon, Hong Kong. Email: ydliao2-c@my.cityu.edu.hk
2 City University of Hong Kong, Tat Chee Avenue, Kowloon, Hong Kong. Email: gongsheng.huang@cityu.edu.hk

Chiller sequencing control is used in multiple-chiller plants to switch on/off chillers according to building cooling load, aiming to achieve high energy-efficient while fulfilling the indoor thermal comfort demand. Various sequencing controls have been developed and implemented in practice, and typical ones include: total cooling load-based sequencing control, return water temperature-based sequencing control, direct power-based sequencing control, and bypass flow-based sequencing control. Each control uses a direct or an indirect indicator to represent building instantaneous cooling load and compares its indicator with pre-defined thresholds to determine sequencing action. Since different controls use different load indicators and thresholds, they suffer from different types of uncertainties and show different robustness to uncertainties.

To select the most suitable control for a given chiller plant, it is necessary to evaluate the performance of control alternatives and their robustness when subject to uncertainties. To this end, in-situ tests or detailed simulation should be carried out. However, in-situ tests may be time consuming and cost inefficient; while detailed simulation needs complex models of the chiller plant, which is knowledge/effort-intensive. To simplify the selection, a numerical method is proposed based on the fact that the sequencing is only determined by the load indicators and the switch-on/off thresholds and all the potential uncertainties can be shifted to the load indicators. Details of the numerical method will be given. Three performance indices, including chiller total switch number, under-cooling percentage and energy use, are used to quantify the performance and robustness of the typical controls. A multi-criterion decision making method is adopted to select the most suitable control. Case studies show that the proposed method can assess the performance of the candidate control strategies efficiently without any complex models of the chiller plant.

Keywords: chiller sequencing control, uncertainty shift, numerical method, decision making, robustness

1. INTRODUCTION

In a central air-conditioning system, a centralized chiller plant is commonly configured to provide cooling for indoor space so as to achieve indoor thermal comfort (ASHRAE, 2011: Page 42.3). The chiller plant usually represents the largest primary energy end-use in a central air-conditioning system and multiple chillers are always configured to improve operational feasibility and energy-efficiency under part load conditions (Chang et al. 2005). In this configuration, chiller sequencing control is used to switch on/off chillers according to building cooling load, aiming to achieve high energy-efficient while fulfilling the indoor thermal comfort demand (Huang et al., 2011).

Various chiller sequencing control strategies have been developed and implemented in practice. Typical control strategies include the chilled water return temperature-based (T-based) sequencing control, the bypass flow-based (F-based) sequencing control, the direct power-based (P-based) sequencing control, and the total cooling load-based (Q-based) sequencing control (Wang, 2010: Page 196). Each control strategy uses a direct or indirect indicator to represent the building instantaneous cooling load and compares its indicator with pre-defined thresholds to determine sequencing action. These control strategies are widely applied and their performance has significant impacts on control and energy performance of the chiller plant.

It is evident that the four typical control strategies are proved to be practicable for chiller sequencing control, but their performances are usually deteriorated by uncertainties (Huang et al., 2009). To guarantee a precise and reliable chiller sequencing control, uncertainty impacts cannot be neglected. Uncertainty refers to a state of having limited knowledge where it is impossible to exactly describe the existing state (Lindley, 2006). The existing of uncertainties in practice could easily result in unreliable control or energy waste. As presented in Huang et al. (2008), the measurement uncertainty in the total cooling load-based control resulted in more than 25% error in measured cooling load indicator, and chillers were controlled based on this inaccurate indicator either provided insufficient cooling or wasted energy. Furthermore, as discussed in Jiang et al. (2007), the lack consideration of uncertainties in operating conditions is an important reason why most multiple-chiller plants in commercial buildings were still sequenced by humans in a heuristic manner, despite of equipping with chiller sequencing controllers.

Since the typical chiller sequencing control strategies use different load indicator and thresholds for sequencing actions, they suffer from different types of uncertainties. In order to systematically analyse the impacts of associated uncertainties on the typical chiller sequencing control strategies, Liao et al. (2014) developed a method to shift various uncertainties to the load indicators of the corresponding sequencing control strategies. Using the developed method, case studies showed that the performances of control strategies were significantly deteriorated by uncertainties and the severity of uncertainty impacts on each control strategy were different.

Given the fact that uncertainties are widely existent in practice, to select the most suitable control for a given chiller plant, it is necessary to conduct robustness analysis for candidate control strategies to evaluate their performance and robustness when subject to uncertainties. To this end, in-situ tests or detailed simulation should be carried out. However, in-situ tests may be cost inefficient for the reason that to test all these typical strategies on the real plant under various working condition may take time and needs great efforts. While conducting robustness analysis on detailed simulation platform needs complex models of the chiller plant, in which all the components and subsystems of the multiple-chiller plant and the connections between them should be identified and properly configured. This method is knowledge/effort-intensive. Considering the fact that the configuration of multiple-chiller plant might vary from each application in details even they use the same system structure (e.g. decoupled multiple-chiller system), it is impractical to conduct robustness analysis based on detailed simulation platform for any given chiller plant.

Therefore, this paper proposes a simple numerical method for selecting proper chiller sequencing control by conducting the robustness analysis without using a detailed simulation platform. The method is developed based on the fact that the sequencing control is only determined by the load indicators and the switch-on and -off thresholds and all the potential uncertainties can be shifted to the load indicators. In this method, the multiple-chiller plant model is simplified with regression method, necessary information for robustness analysis are obtained from historical operation data and Monte Carlo method is adopted to simulate the stochastic characteristic of uncertainties. The performances of candidate control strategies are evaluated in terms of chiller total switch number, under-cooling percentage and energy use. Decisions for

selecting a proper control strategy is made with multi-criteria decision making techniques using a combined index.

The rest of the paper is organized as follows. Section 2 describes a multiple-chiller plant and the typical chiller sequencing control strategies. Meanwhile, the associated uncertainties are described, modelled and shifted. Section 3 introduces the methodology of the proposed numerical method. Section 4 presents case studies to verify the effectiveness of the developed numerical method. Finally, the conclusion remarks are given in Section 5.

2. CHILLER SEQUENCING CONTROL AND UNCERTAINTIES

2.1 Decoupled Multiple-Chiller Plant

A typical decoupled multiple-chiller plant is also named as constant primary/variable secondary pumping system. As illustrated in Figure 1, a bypass line (titled as decoupler) is installed between the header supply pipe and return pipe, dividing the system into two loops: the primary chilled-water production loop and the secondary chilled-water distribution loop. In the primary loop, chillers are arranged in parallel and each chiller is coupled with a constant-speed pump. The chilled supply water from each chiller (normally set at the same supply temperature) is mixed in the header supply pipe, flowing to the secondary loop or back to the chillers through the bypass line, depends on the load condition. In the secondary loop, the chilled water is distributed to air-handling units (AHUs) by multiple variable speed pumps. In AHUs, the chilled water exchanges heat with the supply air and the cooling down supply air is delivered to the space where cooling is needed. The flow rate of inlet (to AHUs) chilled water is controlled by control valve and the speed of the pumps are controlled by the differential pressure measured at the critical operating AHU.

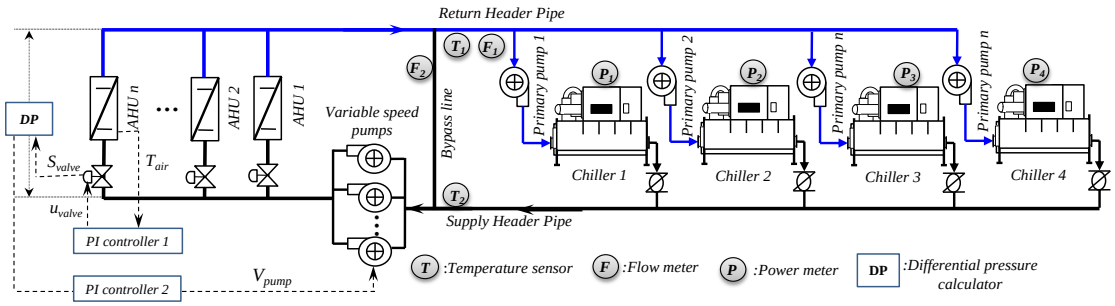

Figure 1: The structure of a typical decoupled multiple-chiller system

2.2 Chiller sequencing control

Figure 2 shows the principle of chiller sequencing control, where the x-axis is the building instantaneous cooling load, calculated by Equation 1.

Equation 1: Instantaneous cooling load of buildings

$$Q = c_w \dot{m}_p \left(T_{rtn} - T_{\sup}\right)$$

Where:

- c_w = chilled water specific heat capacity (kJ/kg·°C)
- $\dot{m}_p$ = chilled water mass flow rate in primary loop header pipe (kg/s)
- T_{rtn} = chilled water return (CHWR) temperature (°C)
- T_{sup} = chilled water supply (CHWS) temperature (°C)

Q_z^{th} and Q_{z+1}^{th}, which denote the ideal thresholds, are the intersection points of the total power curves of operating chillers. When the load is smaller than the threshold Q_z^{th}, the use of *z-1* chillers is better than *z* chillers in terms of energy efficiency.

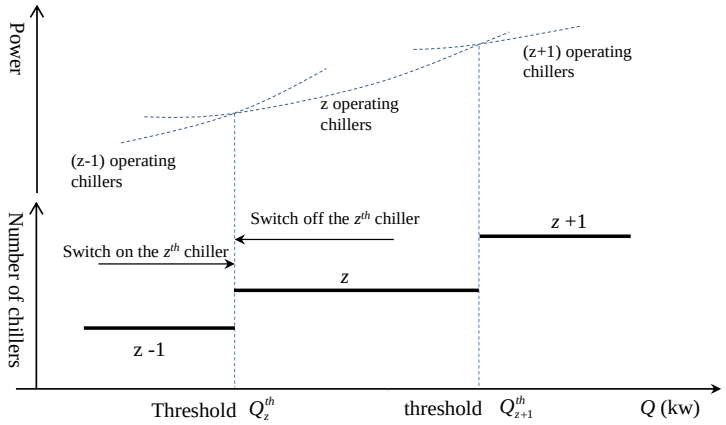

Figure 2: Basic principle of chiller sequencing control

In practice, multiple-chiller plants have various structure and configuration, and they may use different indicators to represent the building instantaneous cooling load. Therefore, different sequencing control has been developed, typically there are four strategies, including total cooling load-based (Q-based) sequencing control, return water temperature-based (T-based) sequencing control, direct power-based (P-based) sequencing control and bypass flow-based (F-based) sequencing control.

2.1. Uncertainties Associated with Chiller Sequencing Control

Shown by Liao et al. (2014), chiller sequencing control mainly suffers from measurement uncertainty, control uncertainty, operational uncertainty and threshold uncertainty, as shown in Table 1 below.

Table 1: Main uncertainties considered in the typical chiller sequencing controls

Control strategies	Measurement uncertainty	Control uncertainty	Operational uncertainty	Threshold uncertainty
Q-based control	√			
P-based control	√			√
T-based control	√	√	√	
F-based control	√	√	√	√

As the Q-based control follows the basic principle of chiller sequencing control and it needs to measure the building instantaneous load (by Equation 1), it therefore suffers from measurement uncertainty only.

In the T-based control, the CHWR temperature is used as the load indicator. It suffers from measurement uncertainty, control uncertainty and operational uncertainty. Because the T-based control needs to measure the CHWR temperature, measurement uncertainty exists. Control uncertainty exists because it assumes that the CHWS temperature is a constant, maintained at the setpoint level, which is actually controlled by a feedback controller and cannot track the setpoint perfectly. Given the assumption that the chilled water flow rate in the primary loop is constant, which actually oscillates due to the change of pump electrical conditions or/and the resistance variation inside the primary loop, operational uncertainty exists.

In the F-based control, the bypass flow rate in the decoupler is used to indicate the instantaneous cooling load, and it suffers from all four types of uncertainties. The need of measuring water flow rate results in measurement uncertainty. Due to the mass balance, the F-based control suffers from control uncertainty (caused by DP variations in secondary loop) and operation uncertainty (caused by flow rate variation in primary loop). Threshold uncertainty exists for the reason that, the switch-on/off thresholds of the F-based control are set according to the deficit flow and surplus flow in decoupler. Deficit flow only occurs when the cooling capacity of the online chillers cannot fulfil the demand which is larger than the standard switch-on threshold in Figure 2. The switch-off threshold needs the surplus flow in decoupler larger than 110%~120% of the rated flow of a chiller, which is smaller than the standard switch-off threshold in Figure 2.

In the P-based control strategy, a percentage of full load amperage (PFLA) is used as the load indicator, and it suffers from measurement uncertainty and threshold uncertainty. It needs to measure the electric current of the compressors so as the measurement uncertainty. Threshold uncertainty exists for the reason that we need to correlate the PFLA to the cooling load using COP curve of chillers in order to set up the

switch-on/off thresholds. Given the complex relationship between the electrical current and the associated cooling load, deriving an accurate correlation is not easy and may lead to uncertainty in the thresholds (WANG, 2010: Page 199).

2.3 Uncertainty Modelling

The measurement uncertainty in this study is assumed to be a normal distribution with zero bias as given by Equation 2, following the guideline of JCGM 100 (2008: Page15). The standard deviation σ is estimated from the operation data by statistic method.

Equation 2: Mathematical model of measurement uncertainties

$$\Delta \sim N(0,\sigma^2)$$

As shown in Liao et al. (2014), the control uncertainty and the operational uncertainty have the pattern of periodic variations. Fast Fourier transform on operation data shows that both the control uncertainty and operational uncertainty can be described by

Equation 3: Mathematical model of control and operational uncertainties

$$\Delta_{con,oper} = \sum_{i=1}^{n_c} c_i \sin(\omega_i t)$$

Where:

- n_c = number of components that should be taken into account
- ω_i , c_i = the frequency and amplitude of i^{th} component

Operation data analysis in Liao et al. (2014) indicates that the threshold uncertainty in the P-based control can be described using a Normal distribution with zero bias as shown in Equation 2. Differently, there is no need to model the threshold uncertainty of the F-based control since the threshold uncertainty in the F-based control is naturally integrated in the switch-on/off thresholds.

2.4 Uncertainty Shifting

Uncertainty shifting is to shift all potential uncertainties associated with a control strategy to the used load indicator. It is the key step for the realization of conducting robustness analysis with the developed numerical method. Details of the shifting process please refer to (Liao, 2014). Here only the final results representing the uncertainties after the shifting are shown as below.

In the Q-based control, the indicator is the measured cooling load Q_{meas}. After the shifting, the uncertainty associated with the indicator Δ_Q (the bias from its ideal indicator) is given by

Equation 4: Uncertainty associated with indicator used by the Q-based control

$$\Delta_Q = \Delta_{m,p,meas}\left(T_{rtn,meas} - T_{\sup,meas}\right) + \dot{m}_{p,meas}\left(\Delta_{T,rtn,meas} - \Delta_{T,\sup,meas}\right)$$

Where:

- $\dot{m}_{p,meas}$, $T_{rtn,meas}$, $T_{\sup,meas}$ = measurements of the chilled water mass flow rate, the CHWR temperature and the CHWS temperature, respectively
- $\Delta_{m,p,meas}$, $\Delta_{T,rtn,meas}$, $\Delta_{T,\sup,meas}$ = uncertainties in the measurements of the flow rate, the CHWR temperature and the CHWS temperature, respectively

In the T-based control, the load indicator is the measured CHWR temperature $T_{rtn,meas}$. After the shifting, the uncertainty associated with the indicator $\Delta_{T,rtn}$ is shown as

Equation 5: Uncertainty associated with the T-based control

$$\Delta_{T,rtn} = \frac{\Delta_{m,p,oper}}{\dot{m}_{p,r}}\left(T_{rtn,meas} - \Delta_{T,rtn,meas} - T_{\sup,st}\right) - \Delta_{T,\sup,cont}\left(1 + \frac{\Delta_{m,p,oper}}{\dot{m}_{p,r}}\right) - \Delta_{T,rtn,meas}$$

Where:

- $\Delta_{m,p,oper}$ = operational uncertainty from the constant pumps in the primary loop
- $\Delta_{T,\sup,cont}$ = control uncertainty in the CHWS temperature control
- $\Delta_{T,rtn,meas}$ = measurement uncertainty in CHWR temperature
- $\dot{m}_{p,r}$ = rated chilled water mass flow rate
- $T_{\sup,st}$ = set-point for the CHWS temperature

In the F-based control, the load indicator is the measured water flow rate in the decoupler $\dot{m}_{b,meas}$. After the shifting, the uncertainty associated with the indicator $\Delta_{m,b}$ (the bias from its ideal indicator) is described as

Equation 6: Uncertainty associated with the F-based control

$$\Delta_{m,b} = \Delta_{m,p,oper} - \Delta_{m,s,cont} + \Delta_{m,b,meas}$$

Where:

- $\Delta_{m,s,cont}$ = control uncertainty from DP control in the secondary loop
- $\Delta_{m,p,oper}$ = operational uncertainty from variation in primary loop
- $\Delta_{m,b,meas}$ = measurement uncertainty in bypass flow rate

In the P-based control, the load indicator is the electrical current of the compressor $\mathrm{I}_{\mathrm{meas}}$. After the shifting, the uncertainty associated with the indicator $\Delta_{I,z}$ is given by

Equation 7: Uncertainty associated with the P-based control

$$\Delta_{I,z} = \Delta_{I,meas} - \frac{\Delta_{COP}}{COP_r}\left(I_{z,meas}^{on} - \Delta_{I,meas}\right)$$

Where:

- $\Delta_{I,meas}$ = measurement uncertainty
- Δ_{COP} = threshold uncertainty
- COP_r = chiller rated COP value
- $I_{z,meas}^{on}$ = ideal switch on threshold represented by the electrical current

3. METHODOLOGY

The proposed numerical method is developed based on the fact that the sequencing control is only determined by the load indicators and the switch-on and -off thresholds and all the potential uncertainties can be shifted to the load indicators. As described in Section 2, all the load indicators used by the typical sequencing controls are based on the following variables: the power of operating chillers; the CHWS temperature, the CHWR temperature and the flow rate of the CHWS in the primary loop; the water flow rate in the decoupler. If these variables can be estimated without in-situ tests or a detailed simulation, but use historical operation data and the given load profile, the sequencing operation can be carried out without any in-situ test or detailed simulation. Considering that the uncertainties can be shifted to indicators (Section 2.5) and historical operation data is commonly available in energy management system (EMS) of the

buildings, a numerical method which makes use of the system operation data to estimate the robustness of control strategies is developed.

The structure of the proposed numerical method for robustness analysis is shown in Figure 3, which has three steps. Step 1 is to collect and analyse historical operation data to configure numerical simulation settings and extract uncertainty models. Step 2 is to perform the numerical simulation for each candidate control strategy under a typical load profile, where the Monte-Carlo method is adopted to capture the stochastic characteristic of uncertainties (Fishman, 1995). Step 3 is to compare the performance indices of each control alternative and make decisions with a multi-criteria decision making technique.

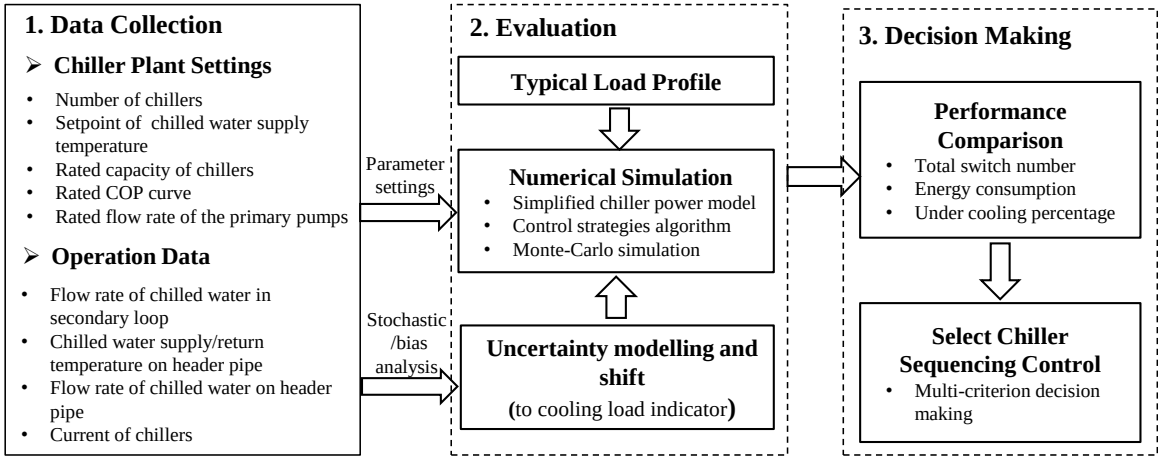

Figure 3: The algorithm of the numerical method

3.1 Data Collection

Data collection includes two aspects, first is to collect settings of the multiple-chiller plant to configure the chiller power model and control algorithms. Number and rated capacity of chillers are needed for determining the control rules in control algorithms; setpoint of SCHW temperature and rated flow rate of the primary pumps are needed for the calculation of cooling load (without uncertainty) and rated COP curve is needed to establish the simplified chiller power model so as to obtain the energy consumption of chiller plant. Second is to collect the historical operation data for uncertainty modelling and shifting. The uncertainties associated with the four control strategies mentioned in Section 2.3 should be abstracted and modelled. For example, the measurement uncertainties in SCHW/RCHW temperature and the primary flow rate should be modelled for the Q-based control strategy. The DP control oscillation should be extracted from the DP operation data, while the current of chillers should be used to identify the measurement uncertainty and threshold uncertainty for the P-based control. Details for uncertainty extraction and modelling please refer to (Liao, 2014).

3.2 Algorithm of Numerical Simulation

The algorithm of the developed numerical method for the typical multiple-chiller plant described in Section 2.1 is shown in Figure 4. Historical operation data is firstly regressed to identify the relationship between the part load ratio PLR and the *COP* (i.e. $COP = f_1(PLR)$) for the simplified energy model. Then regressed to identify the relationship between the chilled water flow rate in the secondary loop $\dot{m}_s$ and the cooling load *Q* (i.e. $\dot{m}_s = f_2(Q/Q_{\max}) \cdot \dot{m}_{\max}$), where, $\dot{m}_{\max}$ is the maximum flow rate in the secondary loop and $Q_{\max}$ is the maximum cooling capacity of the chiller plant, equals to the sum of the rated capacity of all the chillers. Given the cooling load at the *i*th time step $Q(i)$, user can calculate the actual load sent to the operating chillers $Q_{met}(i)$ by comparing $Q(i)$ with the capacity of online chillers $N(i) \cdot Q_c$. $Q_{met}(i)$ is then used to calculate the part load ratio $PLR(i)$, and the $COP(i)$ at time step *i*th. Similarly, the CHWR temperature $T_{rtn}(i)$, the CHWS temperature $T_{\sup}(i)$, the primary flow rate $\dot{m}_p$ as well as the total power of the operating chillers $P_{tot}(i)$ can be calculated using the equations given in Figure 4. With the calculated variables and the uncertainty modelled in pre-processor, the load indictors containing uncertainties are generated. By comparing the load indicator with the thresholds used in a control strategy, sequencing operation can be processed.

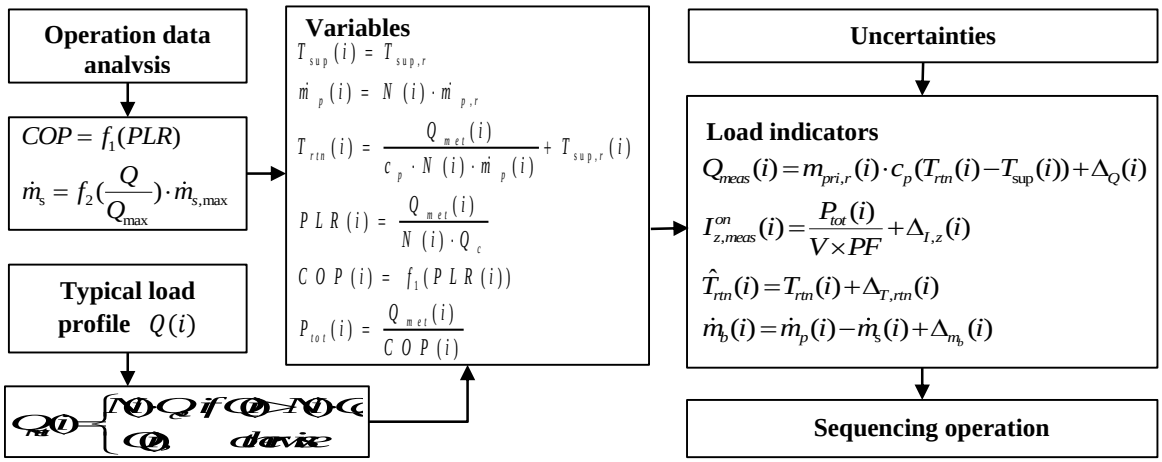

Figure 4: The algorithm of the numerical method

3.3 Performance indices and multi-criterion decision making

In order to quantitatively evaluate the control performance of the chiller sequencing control, three indices are defined, including the total chiller switch number (N_t), the energy use of the chiller plant (E_n), and the under-cooling percentage (P_{uc}). The total switch number, which quantifying the switch frequency, is increased by 1 whenever one chiller is switched on or off. The energy use, which indicating the energy performance of the plant under different control strategies during the test period, is the sum of energy consumption of all the chillers. Considering the main aim of chiller sequencing control is to provide indoor thermal comfort with energy efficiency, under-cooling percentage is employed to indicate insufficient cooling provided by the chiller plant (so as the indoor thermal comfort). If the chiller plant saves energy in the price of insufficient cooling, the energy saving is meaningless. This study assumes that the cooling supply is significantly insufficient when the CHWS temperature is higher than its setpoint by a certain value, say ε. Therefore, the under-cooling percentage is calculated by

Equation 8: Under-cooling percentage

$$P_{UC} = \frac{1}{\tau}\sum_k \zeta_k \Delta t \text{ with } \zeta_k = \begin{cases} 1, & if\ T_{\sup,act,k} > T_{\sup,r} + \varepsilon \\ 0, & otherwise \end{cases}$$

Where:

- τ = the total operation time period
- Δt = the time step
- ξ_k = a Boolean variable
- $T_{\sup,act,k}$ = the actual CHWS temperature
- ε = the user-defined parameter (was set to be 0.5°C in case studies)

Robustness is the ability of a system to resist change without adapting its initial stable configuration [17]. According to the definition, the robustness of the candidate control strategies should be evaluated by the performance variations comparing to the benchmark (theoretical cases without uncertainties). Therefore, the variations of performance indices, viz. the total switch number percentage variation ΔN_t, the increment of the under cooling percentage ΔP_{UC}, and the energy use percentage variation ΔE_n are defined as

Equation 9: Variations of performance indices

$$\Delta N_t = \frac{N_t - N_{t,0}}{N_{t,0}} \times 100\%,\ \Delta P_{UC} = P_{UC} - P_{UC,0},\ \Delta E_n = \frac{E_n - E_{n,0}}{E_{n,0}} \times 100\%$$

Where:

- $N_{t,0}, P_{UC,0}, E_{n,0}$ = the total switch number, the under-cooling percentage and the energy use when there is no any uncertainty, respectively

To select a suitable control strategy for a given chiller plant, decision maker needs to consider the three performance indices simultaneously and make trade-off between them. Given that decision maker may have different preferences for each performance index, a multi-criterion decision making method is adopted to calculate a combined index, which is defined as

Equation 10: Combined index for decision making

$$D = \sqrt{(w_1 \cdot \Delta N_t)^2 + (w_2 \cdot \Delta P_{UC})^2 + (w_3 \cdot \Delta E_n)^2} \text{ with } w_1 + w_2 + w_3 = 1$$

Where:

- D = the combined index; the smaller it is, the better robustness the corresponding control has
- w_1, w_2, w_3 = the weighting factors for each performance index given by the decision maker

4. CASE STUDIES

The effectiveness of the simple numerical method in selecting a most robust control strategy for a given chiller plant was evaluated by applying it to a random selected multiple-chiller plant (system structure is the same as shown in Figure 1) when subjected to various of uncertainties. The four typical control strategies were candidate controls. The control performances estimated from the numerical method were compared with results from detailed simulation conducted on commercial software TRNSYS 17. The detailed configurations of the detail simulation platform was shown in Liao et al. (2014). If the numerical method can provide similar results to the detailed simulation (using TRNSYS) but greatly simplify the selection procedure, the effectiveness of the developed numerical method can be verified.

4.1 Parameter Setup

In the studied multiple-chiller plant, four identical 600kW centrifugal chillers were connected in parallel in the primary loop. Four constant pumps with a rated flow rate 28.65L/s were interlocked with the four chillers. All the chillers shared the same CHWS temperature set-point, i.e. 7°C. The maximum chilled water flow rate in secondary loop was 114.6L/s. one-week of cooling load measured from a real building was adopted for simulation, the same as used in (Liao, 2014: page 194). Historical operation data was then applied to identify the functions f_1 and f_2 in algorithm of numerical method, shown as Equation 11 and Equation 12.

Equation 11: Actual COP of the selected chiller plant

$$COP = -6.3845 \cdot PLR^2 + 11.349 \cdot PLR - 0.0611$$

Equation 12: Relationship between chilled water flow rate in secondary loop and the cooling load

$$\dot{m}_s = [0.61 \cdot (\frac{Q}{Q_{\max}})^2 + 0.6955 \cdot (\frac{Q}{Q_{\max}}) - 0.02571] \cdot \dot{m}_{s,\max}$$

Table 2 lists the thresholds of the four control strategies, which were adopted by numerical method and detailed simulations. As discussed in Section 2, the Q-based control followed the principle of chiller sequencing control and was hypothesized as benchmark for threshold setup. The thresholds of the T-based control were directly derived from the thresholds of the Q-based control. The thresholds of the P-based control were set according to the rated COP curve and the thresholds of the Q-based control as well. For the F-based control, 120% of the rated flow rate of a chiller was selected to be the switch-off threshold. The uncertainties from which the selected chiller plant subjected is listed in Table 3. These values were used to generated uncertainty profiles for Monte Carlo simulations.

Table 2: Thresholds for chiller sequencing control strategies

Control strategy	Switch-on thresholds	Switch-off Thresholds

Q-based	From 1 to 2: Q > 592.8 kW From 2 to 3: Q > 1162.8 kW From 3 to 4: Q > 1732.8 kW	From 2 to 1: Q < 547.2 kW From 3 to 2: Q < 1117.2 kW From 4 to 3: Q < 1687.2 kW
T-based	From 1 to 2: T_{rtn} > 11.94 °C From 2 to 3: T_{rtn} > 11.85 °C From 3 to 4: T_{rtn} > 11.81 °C	From 2 to 1: T_{rtn} < 9.28 °C From 3 to 2: T_{rtn} < 10.10 °C From 4 to 3: T_{rtn} < 10.51 °C
P-based	From 1 to 2: *PFLA* > 98.13% From 2 to 3: *PFLA* > 95.34% From 3 to 4: *PFLA* > 94.45%	From 2 to 1: *PFLA* < 45.60% From 3 to 2: *PFLA* < 62.07% From 4 to 3: *PFLA* < 70.30%
F-based	The deficient flow > 0	The surplus flow > 120% of a chiller rated flow

Table 3: Uncertainties of a chiller system

Uncertainty type	Magnitude	Frequency (Hz)
Measurement uncertainty	Temperature: ±0.5°C /Flow rate: ±3% /Amperage: ±1%	--
Control uncertainty	T-based: ±0.25°C F-based: ±4%	T-based: 2.34×10^{-4} /1.8×10^{-4} F-based: 6.5×10^{-5} /2.6×10^{-4}
Operational uncertainty	±3%	2×10^{-4} /2.6×10^{-4}
Threshold uncertainty	±3%	--

4.2 Results and Analysis

The performance indices variations of the four alternatives were calculated by the proposed numerical method and compared with those calculated from the detailed simulation. As shown in Figure 5, the estimated results from the numerical method (the marks in red color) matched well with the results from detailed simulation (the marks in black color). The small difference was caused by the simplification of the chiller system model but do not change the relative performances of the four control strategies. The good match demonstrated that the proposed method can provide reliable robustness analysis for chiller sequencing controls without a complex detail simulation platform.

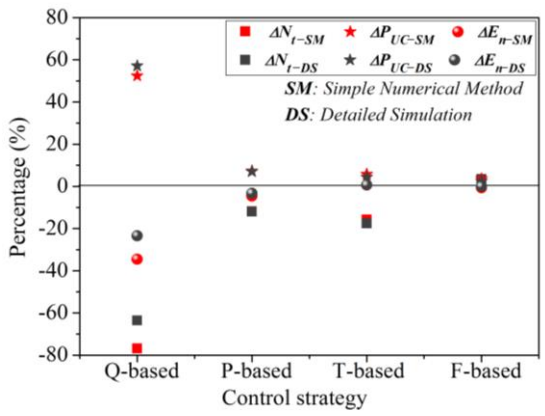

Figure 5: Performance indices from the simple numerical method and the detailed TRNSYS simulation

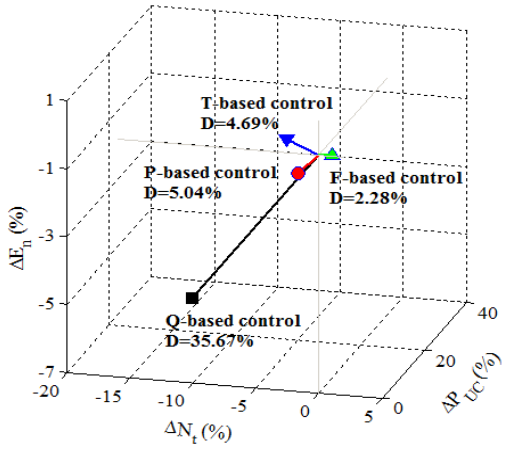

Figure 6: The combined index of the four candidate control strategies

Decision making was based on robustness of the control strategies and the preferences of decision maker. Assume the weighting factors for the performance indices were w_1=0.2,w_2=0.6,w_3=0.2, which meaning that the decision maker preferred to guarantee the indoor thermal comfort. Calculated with Equation 10, the combined index of each candidate control strategy was shown in Figure 6. It can be seen that the Q-based control had the largest combined index while the F-based control had the smallest combined index and correspondingly the best robustness to uncertainties. Therefore, the F-based control was suggested to be used under the uncertainty conditions listed in Table 10.

The convenience in selecting the most robust sequencing control for this random selected chiller plant which was subjected to various uncertainties has proved the effectiveness of the proposed numerical method. It is evident that for any given decoupled multi-chiller plant, the proposed simple numerical method

can provide similar results to the detailed simulations but greatly simplify the selection procedure, and thus it will be effective in practical applications.

5. CONCLUSION

In this paper, the authors have proposed a simple numerical method for selecting proper chiller sequencing control in preference of uncertainties by conducting the robustness analysis without using a detailed simulation platform. Instead of conducting complex simulation platform, this method makes use of historical operation data to identify the characteristic of the chiller plant and take account of potential uncertainties into the performance assessment of the candidate control strategies by shifting uncertainties to load indicators. The robustness of the alternatives is then evaluated by the variations of performance indices, viz. the total switch number percentage variation, the increment of the under cooling percentage and the energy use percentage variation. A multi-criterion decision making method is adopted to combine the robustness of the control strategies and the preferences of the decision maker. The developed numerical method was applied to a random selected multiple-chiller plant for chiller sequencing control selection in preference of various uncertainties. Case studies illustrated that this method provided similar performance assessment as the detailed simulation using TRNSYS simulation platform, and a most robust control strategy was selected easily with the combined index. Since a detailed simulation platform is avoided, the simple numerical method provides much convenience in selecting a proper chiller sequencing control according to the practical uncertainty conditions, and therefore it is feasible and effective to be implemented on practical applications.

6. REFERENCES

ASHRAE Handbook, 2011. ASHRAE Handbook-HVAC applications (SI), ASHRAE Inc., Atlanta, G.A. Chapter 42.

CHANG Y., Lin F., Lin C., 2005. Optimal chiller sequencing by branch and bound method for saving energy, Energy Conversion Management, 46, 2158-2172.

FISHMAN G.,1995. Monte Carlo: Concepts, Algorithms, and Applications, New York: Springer, USA.

HUANG G., Sun Y., Li P., 2011. Fusion of redundant measurements for enhancing the reliability of total cooling load based chiller sequencing control. Automation in Construction, 20, 789-798.

HUANG G., Wang S., Xiao F., Sun Y., 2009. A data fusion scheme for building automation systems of building central chilling plants, Automation in Construction,18, 302-309.

HUANG G., Wang S., Sun Y., 2008. Enhancing the reliability of chiller sequencing control using fused measurement of building cooling load. HVAC&R Research,14, 941-958.

LIAO Y., Huang G., Sun Y., Zhang L., 2014. Uncertainty analysis for chiller sequencing control. Energy and Buildings, 85,187-198.

LINDLEY D., 2006. Understanding uncertainty. Hoboken, NJ: Wiley-Interscience.

JCGM 100, 2008. Evaluation of measurement data - Guide to the expression of uncertainty in measurement.

JIANG W., Reddy T., Gurian P., 2007. General Methodology Combining Engineering Optimization of Primary HVAC&R Plants with Decision Analysis Methods--Part II: Uncertainty and Decision Analysis. HVAC&R Research, 13(1), 119-140.

WANG S., 2010. Intelligent buildings and building automation. London & New York: Spon Press.

SESSION 30: HEATING AND COOLING SYSTEM

53: A study on the effect of ground surface boundary conditions in modelling shallow ground heat exchangers

MARCO BORTOLONI[1], MICHELE BOTTARELLI[2], YUEHONG SU[3]

1 ENDIF-Engineering Department in Ferrara, via Saragat 1, 44122 Ferrara, Italy, marco.bortoloni@unife.it
2 Department of Architecture, via Quartieri 8, 44121 Ferrara, Italy, michele.bottarelli@unife.it
3 Department of Architecture and Built Environment, The University of Nottingham, University Park, Nottingham NG7 2RD, UK, yuehong.su@nottingham.ac.uk

The effect on numerical solution of different thermal boundary conditions at the ground surface was analysed in modelling HGHEs. Boundary conditions of the 1st, 2nd and 3rd kind have been alternately tested by means of a finite element numerical code, solving the unsteady-state heat transfer problem in a 2D domain.

An energy balance equation at the ground surface (3rd kind BC) has been developed and implemented in the numerical model. A preliminary simulation has been carried out in absence of the HGHE operating using real weather data. The solution has been validated with experimental data, and assumed as reference. The calibrated GSEB equation proved to properly predict the temperature in the soil.

The resulting heat flux and temperature at the top of the domain have been considered respectively as the 2nd and 1st kind of equivalent boundary conditions for two new models. Finally, all three models have been solved with the supposed HGHE operating, to analyse how the different BCs affected the numerical solution.

The results have been compared in terms of average temperature at the HGHE wall surface and in the ground. The use of a heat flux as BCs at the ground surface appeared as an extremely precautionary approach due to the resulting thermal drift in the soil. On the contrary, to assign an energy balance equation or a temperature as BCs on the ground surface seemed to have a limited effect in terms of temperature at the heat exchanger and in the soil.

Keywords: Ground surface energy balance, ground heat exchangers, numerical modelling, boundary conditions

1. INTRODUCTION

Reduce the building energy demand and greenhouse gases emissions are topics of great relevance in European policies of future planning. These policies sustain the spreading of renewable energy sources for space heating and cooling. Ground-coupled heat pumps (GCHPs) are regarded as a profitable and sustainable energy technology in this field, due to their high energy efficiency when the design is compliant with local environmental conditions (Chiasson 1999, Mustaf, 2008). In GCHPs the heat transfer is performed by means by means of ground heat exchangers, which can be installed vertically (VGHEs) or horizontally (HGHEs) as a loop placed in shallow diggings few meters deep in soil.

The performance of a GCHP system depends mainly on the thermo-kinetics coupling between the heat exchanger and soil. HGHEs use the ground as unsteady source/sink energy storage, related to the solar energy balance at ground surface. Although the close dependence on environmental conditions prevents thermal drifts after long-term operation (Gan, 2013: page 95), the seasonal temperature variation in shallow soil may lead to unfavourable working conditions for HGHEs, so the ground-coupling for a heat pump must be designed and sized accurately.

Several researches have been conducted to study the performance of HGHEs, following an analytical approach based on the line source theory and cylindrical heat transfer equations (Kavanaugh, 1997) or by means of numerical models. Anyway, attention should be paid to the correct assignment of the boundary condition at the ground surface, in order to treat realistically the effect of environmental conditions. The energy balance at the ground surface is usually reduced to a 1st kind boundary condition (BC). In (Lee, 2008) a sinusoidal temperature trend is assigned to the ground surface. A daily temperature time series is used as boundary condition in (Fujii, 2013), as calculated by means of a ground surface energy balance using real weather data. The similar 1st BC has been numerically converted to the 2nd equivalent kind BC by means of a heat flux in (Bottarelli, 2014), with the aim of considering the effect of the energy exploitation on the ground surface temperature. Despite the long computational time required, other numerical studies have been carried out including the mass transfer to take into account the effects of the soil moisture, as shown in (Piechowsky, 1999) or developing an energy balance equation at the ground surface, i.e. 3rd kind BC. In (Kupiec, 2015) only the convective heat flux between air and ground is considered. The external environmental conditions are included in the models by means of energy balance equation validated against experimental data, taking into account the effect of solar radiation, latent and sensible heat transfer (Demir, 2009). A ground surface heat balance is also used to study the performance of building foundation as heat exchanger in (Nam, 2014). The simultaneous heat and moisture heat transfer at the ground surface has been considered in modelling an earth-air tunnel in a ventilation system in (Gan, 2014).

This study aims to compare the effect on the solution of 1st, 2nd and 3rd kind BCs assigned at the ground surface in modelling HGHEs. A finite element numerical code has been applied solving the unsteady-state heat transfer problem in a 2D domain. An energy balance equation at the ground surface (3rd kind BC) has been developed, using real weather data and validated against experimental measurements. The resulting temperature and heat flux at the top of the domain have been considered respectively as the 1st and 2nd kind BCs for two other cases. Finally, an HGHE has been included in the simulations, applying alternately the different BCs.

2. NUMERICAL MODELLING

The commercial finite-element code COMSOL Multiphisycs V5.0 was used for the simulations, to solve the unsteady heat transfer problem in a 2D computational domain. A model of the energy balance at the ground surface has been developed, based on the ground surface properties (albedo and emissivity) and weather variables (solar radiation, air temperature, relative humidity, atmospheric pressure and wind speed). For a realistic simulation of the environmental conditions, weather data sets based on experimental data were used for simulations. A preliminary simulation was carried out to validate the proposed ground surface energy balance equation (GSEB) in absence of HGHEs, as described in the following. The simulated soil temperature has been compared with observed soil temperature at various depths, showing good agreement. Finally, simulations were carried out to test the energy performance of HGHE in heating and cooling, under the same environmental conditions. The GSEB equation, the resulting heat flux and temperature on ground surface have been used as boundary condition alternately, to analyse how the different BCs affected the numerical solution.

2.1 Model Domain

In this task, more attention was paid to the boundary conditions at the ground surface and to the modelling of the heat transfer induced by HGHEs in the soil. Hence, a 2D domain was modelled as a section of an HGHE and a large surrounding soil part (10 m wide and 10 m deep). A symmetric approach was applied to reduce the time required for calculations. The computational domain was taken to be sufficiently large to have a thermal undisturbed area by the HGHE operation. Here, the HGHE was assumed to be a flat-panel (FP), a novel type of ground exchanger invented at the University of Ferrara (Italy) that shows high energy performance, as reported in [Bottarelli, 2012]. In the model domain, the FP was simplified as a vertical line and introduced as boundary condition. The supposed FP is 1 m high and lay within shallow soil, between a depth of 1 and 2 m. A scheme of the model domain is shown in Fig.1 together with the full mesh.

The whole mesh is composed by up to 10000 triangular linear elements. To improve the solution, a higher concentration of elements is imposed near the FP and on the top edge of the domain, representing the ground surface. The mesh resolution was tested in order to produce reliable and mesh-independent results.

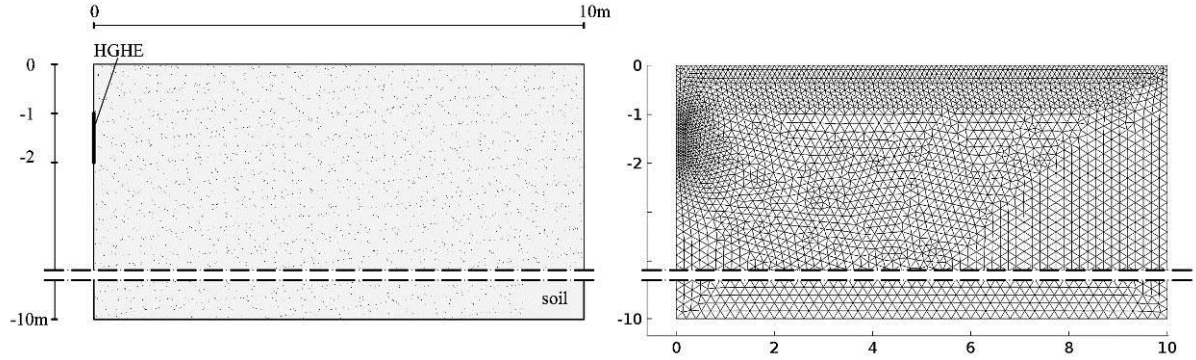

Figure 61: Sketch of the one-half symmetric model domain and mesh

The soil is supposed to be homogenous and isotropic over the entire domain. The thermo-physical properties of the soil were chosen according to UNI11466 (2012), the recent Italian standard regulation about ground source heat pump systems. The properties of the ground surface were taken from those reported in (Herb, 2008: page 331) for a bare soil. The thermo-physical properties of the soil and of the ground surface are reported in Tab.1.

Table 14: Physical properties of soil

Thermal conductivity	Density	Specific heat	Surface albedo (α)	Surface emissivity
(W/mK)	(Kg/m^3)	(J/kgK)	(-)	(-)
1.5	1800	1700	0.15	0.95

3. BOUNDARY CONDITIONS

Only the heat transfer problem has been solved in the model domain, so thermal boundary conditions were assigned to the outer domain boundaries. At the top, boundary conditions of 1st, 2nd and 3rd kind have been alternately imposed at the ground surface in modelling HGHEs. A GSEB equation was firstly used as the 3rd kind BC in a preliminary model to assess the equivalent heat flux (2nd kind BC) and the equivalent ground surface temperature (1st kind BC). A heat flux time series has been set to the HGHE, representing the heating and cooling demand. Finally, an adiabatic condition was assigned to the side and bottom boundaries of the domain. Full details of the BCs at the ground surface and of the energy demand at the HGHE are given below, in section 3.1 and 3.3 respectively.

To calculate the GSEB and to determine the HGHE heat flux at hourly scale, a complete set of 2014 weather data of Ferrara, a city in northern Italy, were used in simulations. Several weather variables (solar radiation, air temperature, relative humidity, atmospheric pressure and wind speed) have been collected on an hourly basis by means of a Davis Vantage Pro2 Plus weather station installed since 2012 at the Department of Architecture in Ferrara. Measurements of the downward longwave radiation have been kindly provided by ARPA-EM (the meteorological service of the Emilia Romagna region). Moreover, the weather station has been equipped with four temperature probes since 2013, to monitor in real time the soil temperature at

different depths (0.1, 0.8, 2.4, 4.2m). The sensors installed are thermistor with a resolution of ±0.5°C. The soil temperature time series for 2014 has been used to calibrate the parameters in the GSEB equation and to check the reliability of the model.

3.1. Energy Balance at the Ground Surface

The heat transfer between the ground surface and the underlying soil was supposed occurring only by conduction, in the model. The temperature in the soil is driven by the energy fluxes at the ground surface, so the heat flux deepening in soil is defined by the energy balance equation in his general and simplified form:

Equation 8: Energy balance at the ground surface.

$$G = R - H - LE$$

Where:

- G = soil heat flux (W/m^2)
- R = net radiative energy flux (W/m^2)
- H = sensible energy flux (W/m^2)
- LE = latent energy flux (W/m^2)

The effect of each component depends on the surface finishing. A grassy surface was taken as reference to have comparability with the available measurements of soil temperature at different depths. The introduction of a vegetated layer has a major effects on the surface heat transfer, and consequently on the surface temperature. A detailed modelling of the effect of the grass on GSEB would require an additional equation to solve energy balance of the vegetated layer, as reported in (Deardorff,1978, Best, 1998). To reduce the computational time, we opted for a simplification in modelling vegetation, neglecting a separate energy balance equation for vegetation and the underlying soil. The effect of the former one was introduced by means of appropriate coefficients of calibration for each energy flux.

The surface temperature is mainly driven by the radiative component, especially during the summer. The net radiative energy flux R (W/m^2) consider absorption and reflection of the incident shortwave radiation solar radiation into its components direct and diffused, and the longwave radiation received and emitted by the surface. The amount of shortwave and longwave solar radiation reaching the ground surface and the outgoing longwave radiation as well, are reduced by the shading due to the grassy layer, so a coefficient of shading (a_1) was introduced. The net radiative energy flux at the ground surface is given by:

Equation 2: Net radiative energy flux.

$$R = a_1\left[(1-\alpha)Rs + Rl_d - \varepsilon_s \sigma T_s^4\right]$$

Where:

- a_1 = calibration coefficient of shading
- α = surface albedo (W/m^2)
- Rs = shortwave solar radiation (W/m^2)
- Rl_d = downward longwave solar radiation (W/m^2)
- ε_s = surface emissivity
- σ = Stefan-Boltzmann constant (W/m^{2}K^4)
- T_s = surface temperature (K)

The convective energy flux between air and ground surface was calculated with Eq.3, where a coefficient of calibration (a_2) was introduced to take into account the sheltering effect of the vegetated layer as follows:

Equation 3: Convective energy flux.

$$H = a_2\left[h_{conv}(T_s - T_a)\right]$$

Where:

- a_2 = calibration coefficient of sheltering

- h_{conv} = convective heat transfer coefficient (W/m^{2}K)
- T_s = surface temperature (K)
- T_a = air temperature (K)

According to (Fujii 2012, Nam 2008), the convective heat transfer coefficient at ground surface was calculated by means of the following empirical Jürges equations:

Equation 4: Convective heat transfer coefficient.

$$\begin{cases} h_{conv} = 5.8 + 3.9v; (v < 5m/s) \\ h_{conv} = 7.1v^{0.78}; (v > 5m/s) \end{cases}$$

Where:

- v = wind speed (m/s).

The evapotranspiration from the vegetated surface has been calculated following the FAO Penman-Monteith model that proved to be reliable for different climates and time step (Allen, 1998). The equation allows the evapotranspiration calculation of a reference grass crop (ET_0), well irrigated and completely shading the ground, using standard weather data only. A calibration coefficient (a_3) was used to relate the calculated ET_0 to the latent energy flux at the ground surface, taking into account the condition of the vegetated layer taken as reference (not irrigated). Finally, the latent energy flux at the ground surface is given by:

Equation 5: Latent energy flux.

$$LE = a_3(lh \cdot ET_0)$$

where:

- a_3 = calibration coefficient
- lh = latent heat of evaporation (kJ/kg)
- ET_0 = reference evapotranspiration

3.2 Validation of the Model

The GSEB equation (Eq.1) was validated with the observed soil temperature data at different depths in 2014. The Eq.1 has been properly implemented in COMSOL to be tested as boundary condition at the ground surface, and a preliminary numerical simulation was carried out for a whole year in unsteady state. In this model, the heat flux representative of the HGHE was set to zero, so the variation in the soil thermal field was determined by the environmental conditions only. The weather conditions observed at the test field in 2014 were converted in hourly scale time series and used as input in Eq.2-5. The soil temperature was monitored with an hourly time step at different depths. The measured soil temperature data has been compared to the simulated temperature at the same depth to calibrate the parameters a_1, a_2 and a_3 in Eq.1 and thus to analyse the reliability of the model in predicting the soil temperature. Finally, a soil temperature profile for the 1st day of 2014 was obtained from the available soil temperature data and set as the initial condition for simulations.

The values of the three calibration parameters were set to reduce the difference between the simulated (s) and the measured (m) temperature in the soil. The calibration coefficient of shading (a_1) was set to 0.30. It represents the view factor between the ground surface and the sky/sun. It was assumed that the 70% of both incoming shortwave and longwave radiation were absorbed by the vegetated layer on the ground surface. The coefficient of sheltering (a_2) was set to 0.35. Finally, to account for the lack of a system of irrigation, the latent heat flux was reduced setting a_3 equal to 0.25.

The daily averaged values of soil temperature observed and simulated are reported in Fig. 2. Four temperature probes were considered (*T1*, *T2*, *T3* and *T4*) at four different depths (0.1, 0.8, 2.4, 4.2m respectively). Deviations are detectable mainly for shallow probes *T1* and *T2*, where fluctuations in temperature are greater. For shallow probes, the relationship between measured and simulated temperature is more stable in winter, when the radiative heat flux is low and the latent heat flux is nearly

zero. In this case the simulated temperatures are slightly higher than measured ones with a maximum error of 1.47°C. The model showed less accuracy in the estimating shallow soil temperature in summer, with a maximum error of 2°C. This could be a variation in the energy balance due to the natural growth cycle of the grass covering the ground surface, not accounted in the model, such as the rain. Finally, the temperatures are in good correspondence for both deep probes (T3 and T4) for the entire period of simulation.

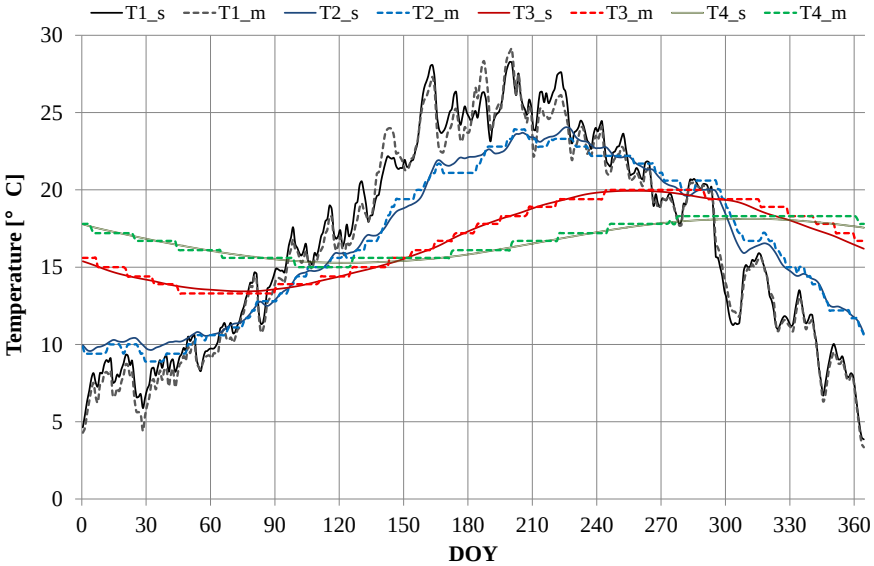

Figure 2: Daily averaged soil temperature at different depth (0.1, 0.8, 2.4, 4.2m): simulated (s) and measured (m).

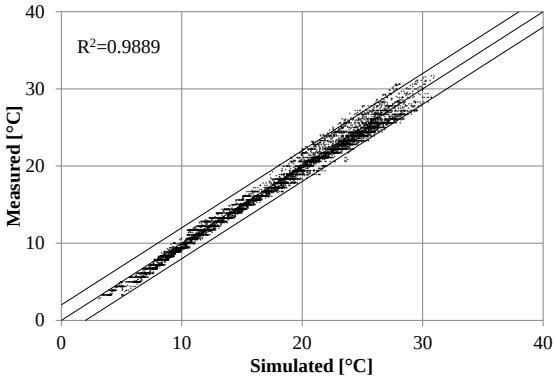

Figure 4: Scatter plot of the simulated and measured hourly temperature 0.1 m deep in soil

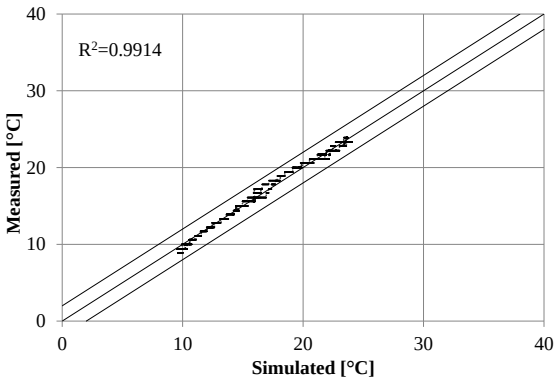

Figure 5: Scatter plot of the simulated and measured hourly temperature 0.8 m deep in soil

A scatter plot of the simulated soil temperatures versus the equivalent measured are shown in Fig. 4 for probe *T1* (depth 0.1m) and in Fig. 5 for probe *T2* (depth 0.8m), where the central line represents a perfect relationship between measured and simulated values, and the two others a span of 2°C. In both cases the slope of the relationship is close to 1:1, although slightly dispersion occurs for a temperature higher than 20°C. The overall mean root square error (RMSE) has been calculated for the entire simulation period, and reported in Tab. 2 for each temperature probes.

Table 2: Soil temperature simulation accuracy at different depths

Depth (m)	0.1	0.8	2.4	4.2
RMSE (°C)	0.79	0.46	0.29	0.25

The calibrated GSEB equation proved to properly predict the temperature in the soil. The discrepancies between the measured and simulated values were considered satisfactory. Furthermore, the error was reduced with increasing depth and then the thermo-physical properties of soil considered were plausible.

Fig. 6 shows the energy partition between each component of the GSEB, for 3 days in winter and summer. Both in winter and in summer, the conductive heat flux in soil (*G*) has a strong dependence on the net radiation (*R*) because the ground surface was supposed to be only partially shaded by the vegetation above. The convective heat flux (*H*) is low on average due to the sheltering effect by the vegetated layer. Moreover, the convective heat transfer coefficient is affected by the dependence on the low wind speed, here representative of an urban area. *H* is relatively stable and varies between +25 and -15W/m^2 depending on the temperature difference between air and surface. As expected, the heat loss from the surface due to the latent heat flux (*LE*) is nearly zero in winter. It is related to the air temperature and soil heat flux, thus an increase is observed in summer, with a daily oscillation between 25 and 5W/m^2 during daytime and nighttime.

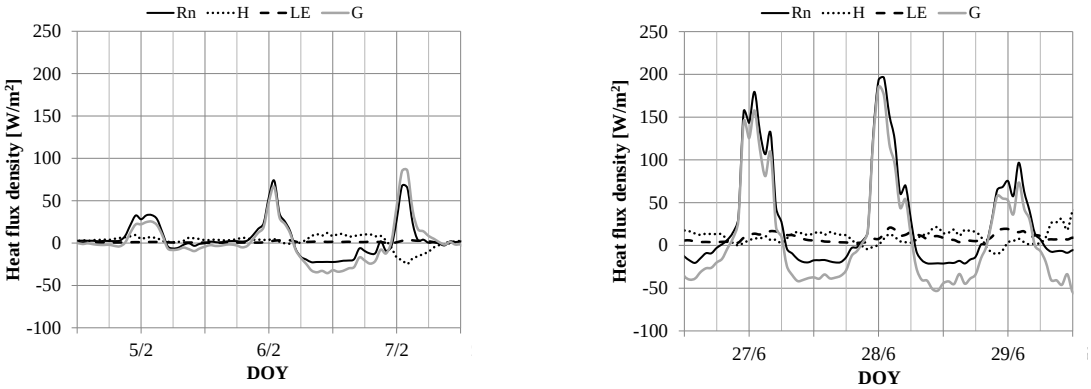

Figure 6: Energy partition of heat fluxes at ground surface during winter and summer.

A further case was simulated to analyse the relationship between the air temperature near the ground and the surface temperature. The hourly scale time series for the air temperature near ground in 2014 was used as 1st kind BC. The resulting daily averaged values of soil temperature are reported in Fig. 7, in comparison with the equivalent soil temperature data at different depths, observed in 2014. In this case, deviations are detectable in all probes and the estimated temperature at different depths is always lower than that the measured one. The air temperature is not directly applicable as BC, and a reliable correlation between the air and surface temperature could be a simple method to define a reliable BC at the ground surface in modelling HGHEs.

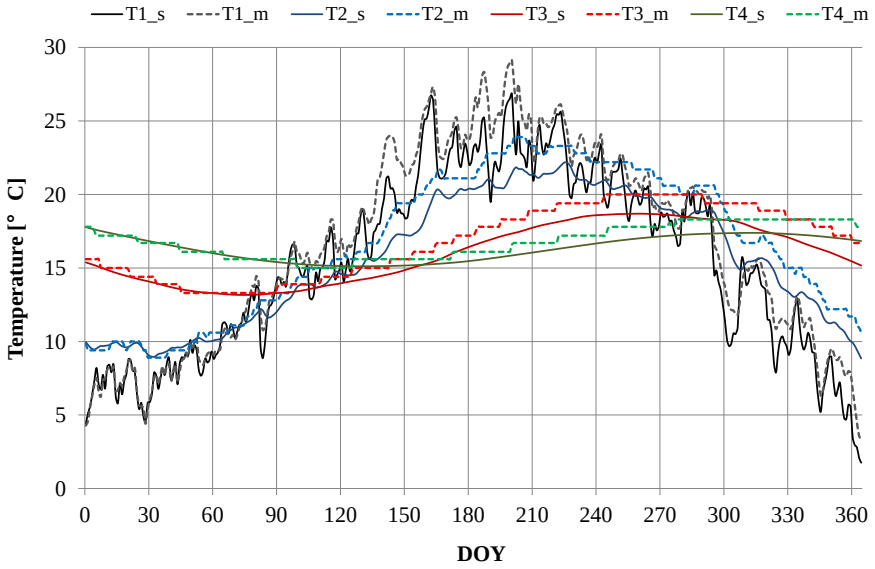

Figure 7: Daily averaged soil temperature at different depth: simulated (s) and measured (m).

3.3 Energy Requirements at the HGHE

The energy requirement for space heating and cooling is defined as the amount of energy needed to maintain a constant target value of the building indoor temperature. In GCHPs, the thermal energy is extracted/transferred from/to the ground by means of the ground heat exchanger.

To define an hourly energy requirement in heating and cooling mode we applied the methodology reported in (Bortoloni, 2015) where the energy requirement of a building was related to an outdoor air temperature time series. In this case, the real outdoor temperature of Ferrara in 2014 has been reduced to a sinusoidal and negative exponential variation of air temperature with Eq. 6:

Equation 6: Outdoor air temperature.

$$T_a(D) = T_M - A \cdot \cos\left[\frac{2\pi}{365}(D - D_0)\right]$$

where:

- T_a = daily average outdoor air temperature at Julian day D (C°)
- D_0 = Julian day with the lowest temperature
- T_M = annual average air temperature
- A = average annual amplitude of the air temperature

The parameters in Eq. 6 were chosen according to the available weather data. Then, the temperature time series on an hourly scale was obtained superimposing to the daily time series a sinusoidal oscillation ranging between the daily minimum and maximum/ air temperatures (night/ day) in winter and summer. The indoor, the outdoor temperature (calculated with Eq. 6) and the real outdoor temperature are shown in Fig.2 at a daily scale.

The building was simplified to a homogenous lumped and closed thermodynamic system whose internal energy variation only occurred owing to the heat transfer through its envelope only, as reported in (Bortoloni, 2015). The heating season is supposed from October 16th to April 30th, the cooling one from May 1st to October 15th. In the model, the heating/cooling system was set to operate for reaching and maintaining a defined target indoor temperature (20°C in winter and 24°C in summer). A time scheduling was supposed to represent typical working conditions for a residential building in a mild climate: 5-10 AM and 4-12 PM during working days, and 6 AM to 12 PM on the weekends.

Furthermore, it has been supposed that the heating and cooling power of the system could not exceed 40W for a cubic metre of building when it is turned on. For simplicity, the former energy demand has been considered as the full energy requirements for the closed loop. Finally, the resulting heat flux time series (W/m^2) has been directly applied as boundary condition at the FP in the numerical model. The daily energy demand at the FP is reported in Fig.8.

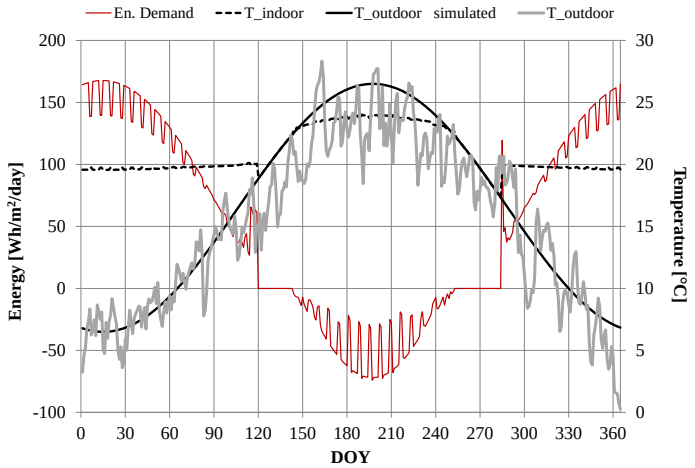

Figure 8: Outdoor air temperature, indoor temperature and energy requirements for space heating and cooling.

4. RESULTS

The effect of 1st, 2nd and 3rd kind BCs imposed at the ground surface in modeling HGHEs have been analysed. The proposed GSEB equation, the equivalent heat flux and temperature have been considered as BCs in three new simulations. As for preliminary analysis, a complete set of weather data of Ferrara for

2014 were considered. The soil temperature profile for the 1st day of 2014 was set as the initial condition. Simulations have been carried out with the supposed HGHE operating, for two consecutive years in each case, to check the thermal drift of the domain.

According to the simplifications and assumptions considered, the results were compared in terms of average temperature at the HGHE wall surface. This could be considered as the average temperature of the working fluid, and therefore it is representative of the HGHE performance with the different boundary conditions at the ground surface. Moreover, the temperatures in the surrounding soil were calculated by means of point probes at different depths to evaluate the evolution of the thermal field.

The resulting time series for each BCs of the daily average temperature at the HGHE wall are shown in Fig.9. For completeness, a weekly detail of the hourly HGHE operation, when the minimum temperature is reached in the heating period, has been included. In the diagram, an entire year is presented, starting in October, when heating season begins.

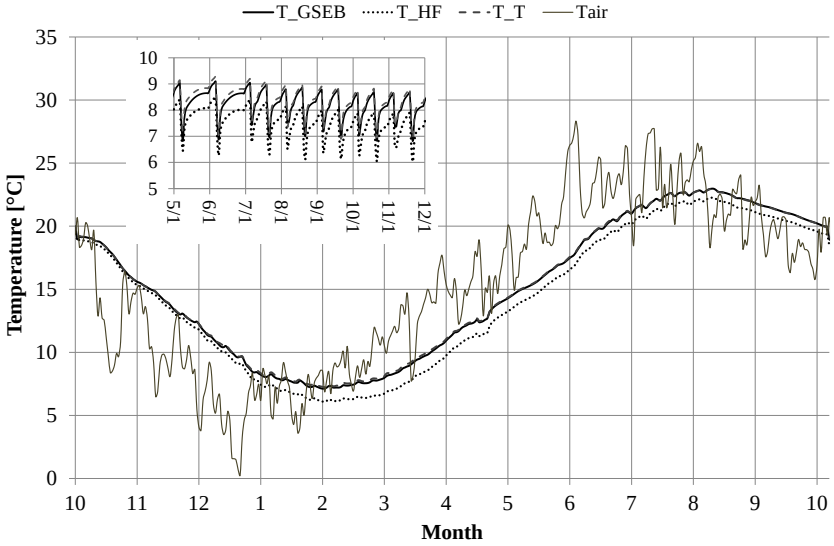

Figure 9: Daily average temperature on the HGHE surface for the three BCs and a week with hourly data.

The initial average temperature is around 20°C, and then it rapidly decreases. After two months of heat extraction, the temperature at the HGHE is 2.5°C lower than the equivalent undisturbed. The minimum temperature is reached in all three cases in the second half of February, with a lag of 45 days in comparison with the temperature at ground surface and that of air. The temperature drops more rapidly with the equivalent heat flux assigned to the surface (case *HF*) and shows a maximum difference of 1.3°C compared to the other two cases. Moreover, unlike the other cases (*GSEB* and *T*), a thermal drift of 0.6°C is detected after a year in HF, because the equivalent heat flux does not balance the heat demand of HGHE operating. On the contrary, a negligible discrepancy is observed between the case *GSEB* and *T*. Therefore the use of 1st kind boundary conditions could be considered an acceptable simplified boundary condition. Finally, it is noted that the daily average air temperature has more favourable values than soil temperature late in winter and in summer. As a consequence, it could be considered as an alternative energy source for the heat pump in space heating and cooling.

Fig.10 shows the hourly time series of soil temperature at two different points. The first temperature probe is above the HGHE, 0.8m deep in soil. The second probe is positioned at the average depth of the HGHE and 1m far from it. In the former one, the maximum difference between the case *HF* and the two other cases is 1.8°C. Moreover, a significant negative difference is maintained over the entire year. As for the temperature at the HGHE wall, the soil thermal field is comparable for *GSEB* and *T*.

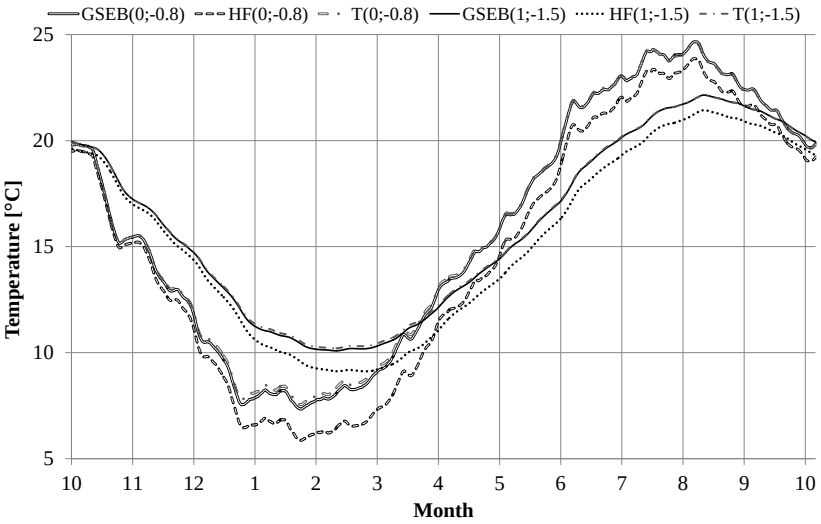

Figure 10: Average temperature in the soil for the three BCs.

5. REMARKS

The effect on numerical solution of different boundary conditions at the ground surface was analysed in modelling HGHEs. The commercial software COMSOL Multiphysics was used to solve the unsteady heat transfer problem in a 2D computational domain. A model of the energy balance at the ground surface (GSEB) based on the ground surface properties and weather variables was developed, and properly implemented in COMSOL to be tested as boundary condition at the ground surface. For a realistic simulation of the environmental conditions, weather data sets based on experimental data were used for simulations. It was validated with the observed soil temperature data at different depths in 2014, proving to properly predict the temperature in the soil.

Simulations were carried out to test the HGHE energy performance in heating and cooling, under the same environmental conditions. The GSEB equation, the resulting heat flux and temperature on ground surface were alternately used as boundary condition (BC) of the 1st, 2nd and 3rd kind in simulations. The solution of the equivalent heat flux at the ground surface diverged from the other two cases, and appeared as an extremely precautionary approach. On the other hand, to assign the temperature resulting from the energy balance on the ground surface has the significant limit to block the thermal effect of the heat exchanger on the surface. Consequently, to use a 3rd boundary condition in modelling HGHE is an acceptable approach to the problem, not affecting the calculation time. However, the correct estimation of surface temperature is of great importance also in this case, and a preliminary simulation with a GSEB could be required.

Finally, a simulation was conducted assigning the air temperature as 1st kind BCs at the ground surface. Although a tendency to underestimate the shallow soil temperature has been identified, a correlation between ground surface and air temperature could be developed in the future to determine more quickly a feasible boundary condition in modeling HGHEs.

6. REFERENCES

ALLEN, R.G., Pereira, L.S. Raes, D., Smith, M., 1998. Crop evapotranspiration. Guidelines for computing crop water requirements. FAO Irrigation and Drainage Paper, 56, Rome: FAO.

BEST, M.J., 1998. A model to predict surface temperatures. Boundary-Layer Meteorology. 88, 279-306.

BOTTARELLI, M., Bortoloni, M., Su, Y., Yousif, C., Aydin, A.A., Georgiev, A., 2014. Numerical analysis of a novel ground heat exchanger coupled with phase change materials. Applied Thermal Engineering, In press.

BOTTARELLI, M., Di Federico, V., 2012. Numerical comparison between two advanced HGHEs. Int. Journal of Low-Carbon Technologies. 7/2, 75-81.

BORTOLONI, M., Bottarelli, M., 2015. On the sizing of a Flat-Panel ground heat exchanger. International Journal of Energy and Environmental Engineering, 6, 55-63.

CHIASSON, A.D., 1999. Advances in modeling of ground-source heat pump systems. M.Sc. Thesis, Oklahoma: Oklahoma State University.

DEARDORFF, J.W., 1978. Efficient prediction of ground surface temperature and moisture with inclusion of a layer of vegetation. Journal of Geophysical Research, 83, 1889-1903.

DEMIR, H., Koyun, A. and Temir, G., 2009. Heat transfer of horizontal parallel pipe ground heat exchanger and experimental verification. Applied Thermal Engineering, 29, 224-233.

FUJII, H., Yamasaki, S., Maehara, T., Ishikami, T., Chou, N., 2013. Numerical simulation and sensitivity study of double-layer Slinky-coil horizontal ground heat exchangers. Geothermics, 47, 61-68.

GAN, G., 2013. Dynamic thermal modelling of horizontal ground-source heat pumps. International Journal of Low-Carbon Technologies, 8, 95-105.

GAN, G., 2014. Dynamic interactions between the ground heat exchanger and environments in earth-air tunnel ventilation of buildings. Energy and Building, 85, 12-22.

HERB, W.R., Janke, B., Mohseni, O., Stefan, H. G., 2008. Ground surface temperature simulation for different land covers. Journal of Hydrology, 356, 327-343.

KAVANAUGH S.P., Rafferty K., 1997. Ground source heat pumps-Design of geothermal systems for commercial and institutional buildings. ASHRAE Applications Handbook.

KUPIEC, K., Larwa, B., Gwadera, M., 2015. Heat transfer in horizontal ground heat exchangers. Applied Thermal Engineering, 75, 270-276.

LEE, K.H., Strand, R.K., 2008. The cooling and heating potential of an earth tube system in building. Energy and Buildings, 40, 486-494.

MUSTAF, O.A., 2008. Ground-source heat pumps systems and applications. Renewable and Sustainable Energy Reviews, 12/2, 344-371.

NAM, Y., Chae, H.,0 2014. Numerical simulation for the optimum design of ground source heat pump system using building foundation as horizontal heat exchanger. Energy, 1-10.

NAM, Y., OOka, R., Hwang, S., 2008. Development of a numerical model to predict heat exchange rates for a ground-source heat pump system. Energy and Buildings, 40, 2133-2140.

PIECHOWSKY M., 1999. Heat and mass transfer model of a ground heat exchanger: validation and sensitivity analysis. International Journal of Energy Research, 23, 571–588.

TODORVIC, M., Karic B., Pereira, L. S., 2013. Reference evapotranspiration estimate with limited weather data across a range of Mediterranean climates. Journal of Hydrology, 481, 166-176.

297: Soil temperature profile for some new cities in egypt: experimental results and mathematical model

AHMED A.SERAGELDIN[1], ALI K.ABDELRAHMAN[1],
AHMED HAMZA.H.ALI[2], MOHAMED R.O.ALI[3],SHINICHI OOKAWARA[4]

1 Egypt-Japan University of Science and Technology (E-JUST), Alexandria- Egypt, Ahmed.serageldin@ejust.edu.eg, ali.kamel@ejust.edu.eg
2 Assiut University , Assuit- Egypt, drahmedhamza@yahoo.com
3 Al-Minia University, Al-Minia-Egypt, mohamedroalin@mu.edu.eg
4Tokyo institute of Technology,Tokyo-Japan, Assuit- Egypt, sokawara@chemeng.titech.ac.jp

Egypt nowadays passes through an energy crisis in spite of the development of the building sector, represented by the plans of the Egyptian government to establish new cities over wide and different areas of the country, Earth-air heat exchanger (EAHE) systems are of the promising systems by which building electricity consumption can be reduced; through the reduction of energy needed for carrying air conditioning loads. Many parameters affecting the performance of such systems one of which is the soil temperature distribution profile. The aim of this research is to investigate experimentally the soil temperature variation with depth, in the avenue of the Egypt Japan university of Science and Technology (EJUST), New Borg Al-Arab city, Alexandria, Egypt during March 2015. In addition, an analytical model was developed to predict soil temperature distribution profile. The validation of the analytical model with the experimental results gave an error and correlation coefficient values of 5.59 % and 98 % respectively. The validated model was used with six different new cities in different areas in Egypt with four different ground surface cover conditions. The results of the model show that the type and nature of the surface cover affects directly the soil temperature profile especially when increasing the clay percentage.

Keywords: Earth Air Heat Exchanger, Soil Temperature, Analytical Model

1. BACKGROUND AND LITERATURE REVIEW

Soil thermal properties and soil temperature profile are of the most important parameters affecting the performance of geothermal (also known as ground source) engineering systems. One of the most promising applications with hot climate conditions is ground-coupled heat exchanger (GCHE) when used for buildings, (Abbas and Sanner 1999) demonstrated the feasibility of cold storage with borehole heat exchanger for the climatic environment of Cairo, Egypt. Two systems were evaluated a borehole thermal energy storage (BRES) in the limestone rocks of the cliff and an aquifer thermal energy storage (ATES) in the quaternary aquifer. ATES with limited number of wells was found more economically than BTES. (Adelrahim, Fahmy, and El-Fawal 2013) designed a geothermal hot water and space heating system to operate with three buildings; a school, a house, and an emergency hospital in a remote area on the Red Sea; approximately 20 km north Safaga city. In addition they illustrate design parameters and specification of case study of Umm Huweitat well. (El-din 1999) derived and developed a model for heat flux into ground based on energy balance Equation of the ground surface considering the periodic variation of solar radiation, atmospheric temperature and latent heat flux of evaporation. In addition, he calculated the corresponding ground temperature and damping depth. He concluded that ground temperature and the amplitude of the heat flux into the ground increase with increasing in the air relative humidity and the ground absorptivity. On the other hand, they decrease with increasing in the evaporation fraction and wind speed. Moreover, The values of the damping depth is almost the same while the corresponding ground temperature is influenced by the various parameters significantly. (Fargali, Fahmy, and Hassan 2010) used PV- Wind energy sources coupled with heating system in three different buildings in remote area in Egypt. In addition, they present complete mathematical modeling and MATLAB Simulink model for the system. (Gao et al. 2007) present approach to determine the soil thermal diffusivity and water heat flux density for four soil layer depths. They concluded that both of them change with increasing depth, which means that the soil thermal properties are heterogeneous in vertical column at this site.(Krarti 1995) present an analytical model to predict the temperature variation within a multilayered soil. The soil surface temperature was assumed to have a sinusoidal time variation for both daily and annual time scales. In addition, the soil thermal properties in each layer were assumed to be uniform. (Mihalakakou 2002) presents two methods, deterministic and neural network approaches. In order to model and estimate the daily and annually variation of soil surface temperature. Then, he tested and validated these two models with sets of measurements for bare and short grass covered soils in Athens and Dublin. He concluded that the models are adequate tools of estimating soil surface temperature variation. (Wang and Gao 2012) provide a general way to describe soil temperature under an infiltrating water source. They used Fourier series to describe soil surface temperature variations with time. one dimensional and unsteady conduction and convection heat transfer Equations with a multi-sinusoidal wave boundary condition were solved analytically using Fourier transformation and single sine wave model. Model's results were compared with field soil temperature at depths of 0.1 and 0.3 m (the results of comparison). It can be concluded that fourier series model estimates of field temperature that sin wave model.

In this research, a mathematical model for soil temperature profile was developed and validated experimentally. Three different soils samples were investigated (Loamy sand, sandy loam and clay) which are the soil types reported by Urban Communities Authority of the ministry of housing released for constructing 6 new cities in Egypt – **Error! Reference source not found.** – at 2013. The ground surface cover conditions was set to be bare and wet, bare and dry, cover and wet, and cover and dry which are the most possibilities of the ground surface conditions. Validation of this model was done through experiments conducted in the campus of Egypt-Japan University of Science and Technology (EJUST), New Borg Al-Arab, Alexandria, Egypt.

Figure 62: Egypt map shows the location of the cities considered in this research

2. EXPERIMENTAL SET-UP

To study soil temperature profile, experimental measurements were carried out at the garden of the Laboratories of Energy Resources Engineering Department located at the campus of the EJUST campus (Longitude/Latitude: E 29° 42' /N 30° 55'), where a 2x2x2 m^3 hole was dug. T type thermocouples were placed at depths (0m,0.5m,1m,1.5 and 2m) – shown by Figure 63 – to measure the soil temperature at these depths. The thermocouples were calibrated against a standard calibrated thermocouple type T (Beta calibrator TC-100 made in USA). The error was in the accepted range where the deviation between the thermocouples readings and that of the standard one was from +0.1 to +0.5 ˚C. A multi-point digital data logger (NEC DC 6100 remote scanning made in Japan) was used to store the temperatures and feed it to a Laptop to analysis it. The weather data parameters; wind speed and direction, outdoor air dry bulb temperature, relative humidity and rain fall were measured and recorded by Met one Portable Weather Station during period from 11to 13 of March 2015 every 1 hour – (Model Number 466A made in USA) which was placed in the same site of the soil temperature measurement unit.

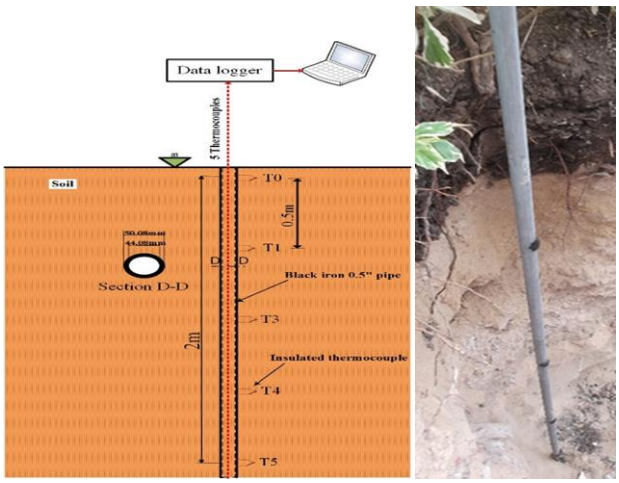

Figure 63 Schematic diagram and a picture of the temperature measurement unit

Figure 64 A Photograph of Portlog weather station

3. ANALYTICAL MODEL

Analytical model developed to predict soil temperature variation with depth. In addition soil temperature variation with time can be predicted.

3.1 Soil temperature profile

The following section presents analytical model (Wang and Gao 2012)for both soil surface and soil temperature profile as function of time and depth. From the energy balance of soil surface shown in Figure 65:

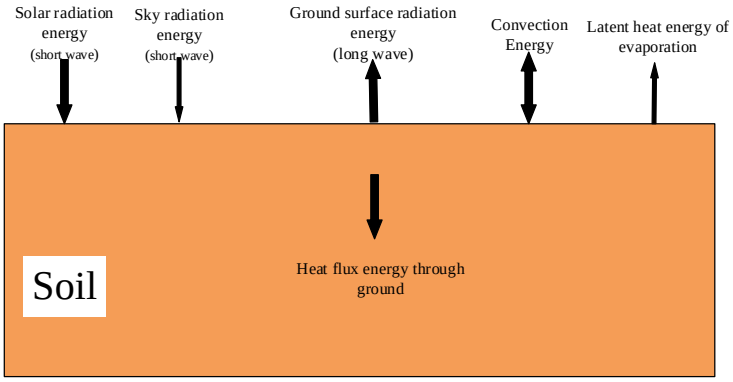

Figure 65 Energy balance of ground surface (Campbell and Norman 1998)

Equation 9: Energy balance of ground surface

$$-K(T)\left.\frac{\partial T_{sur}(t)}{\partial y}\right|_{y=0} = CE - LR + SR - LE$$

With the following assumptions:

- Steady state
- One dimension heat transfer by conduction
- Mass transfer neglected
- Soil properties independent of temperature

Where CE, LE, SR and LE indicate as follows:

*Equation 2: **CE** is convection energy*

$$CE = h_{sur}\left(T_a - T_{surf}\right)$$

Where:

- T_a is ambient temperature, (^{0}C)
- T_{surf} is ground surface temperature,(^{0}C)

Equation 3: h_{sur} is convection heat transfer at ground surface

$$h_{sur} = 2.8 + 3v$$

Where:

- v is wind speed at ground surface, (m/sec)

$$LR = \varepsilon \Delta R$$

*Equation 4: **LR** is ground surface long radiation energy*

Where:

- ε is long wave emissivity of the surface which varies from 0.93 to 0.96.(Campbell and Norman 1998)
- ΔR is radiation constant equal to 63 wm^{-2}.(Mihalakakou and Santamouris 1997)

$$SR = bS$$

*Equation 5: **SR** is short wave solar radiation*

Where:

- b is coefficient depends on surface absorptivity and illumination can be calculated as follows $b = 1 - A$
- A is albedo of the surface and it equals 0.1, 0.2, 0.3 for wet, moderate and dry soil respectively [10];
- S is global horizontal solar radiation, (w/m^2).

*Equation 6: **LE** is latent heat flux of evaporation at the ground surface*

$$LE = 0.0168 h_{sur} f\left[\left(aT_{sur} + b'\right) - r_a\left(aT_{a+b}\right)\right]$$

Where:

f *friction coefficient depends on ground cover and humidity level of the ground given by*

Equation 9: T_{se} *is solair-evaporation temperature coefficient*

$$T_{se} = \left[\left(1 + 0.0168\, far_a\right) h_{sur} T_{amb} + bS - \varepsilon\Delta R - 0.0168\, fb' h_{sur}\left(1 - r_a\right)\right] / h'$$

In order to calculate ground surface and soil temperature distribution profile solution of one dimensional, unsteady heat conduction equation must be obtained

- Table 15
- a=103Pa.k^{-1} and b=609 Pa at $263k \le T \le 303k$. (Mihalakakou and Santamouris 1997)
- r_a is relative humidity at ground surface.

So right hand side can be written as follows:

Equation 7:

$$-K(T)\left.\frac{\partial T_{sur}(t)}{\partial y}\right|_{y=0} = h'\left(T_{se} - T_{sur}\right)$$

Where:

- *Equation 8:* h' *is apparent convection heat transfer coefficient*

$$h' = (1 + 0.0168\, fa) h_{sur}$$

Equation 9: T_{se} *is solair-evaporation temperature coefficient*

$$T_{se} = \left[\left(1 + 0.0168\, far_a\right) h_{sur} T_{amb} + bS - \varepsilon\Delta R - 0.0168\, fb' h_{sur}\left(1 - r_a\right)\right] / h'$$

In order to calculate ground surface and soil temperature distribution profile solution of one dimensional, unsteady heat conduction equation must be obtained

Table 15 friction factor according to soil cover and moisture content, (Mihalakakou and Santamouris 1997)

Soil cover	f
Bar sat. soil	1
Bar moist soil	0.6-0.8
Bar dry soil	0.4-0.5
Grass cover sat. soil	0.7
Grass cover moist soil	0.42-0.56
Grass cover dry soil	0.28-0.35

Equation 10: heat conduction equation

$$\frac{\partial^2 T}{\partial z^2} = \frac{1}{D}\frac{\partial T}{\partial t}$$

By using sine wave approximation solution Equation 9 has a solution of the form of a sinusoidal wave.

Equation 11: a sinusoidal wave equation

$$T(z,t) = T_a + A_0 e^{-z/d} \sin\left[\frac{2\pi(t-t_0)}{365} - \frac{z}{d} - \frac{\pi}{2}\right]$$

Where:

- $T(z,t)$ *is the soil temperature at time t (day) and depth z (m),*
- T_a *is the average soil temperature, (°C)*
- *d is the damping depth (m) of annual fluctuation is given by* $d = \sqrt{\frac{2D_h}{\omega}}$
- D_h is Soil thermal diffusivity, (m^2/sec).
- $\omega = \frac{2\pi}{365}$ *in* d^{-1}

Substituting with z=0 in Equation 11 gives the ground surface temperature with time

Equation 12: ground surface temperature variation with time

$$T(z,t) = T_a + A_0 \sin\left[\frac{2\pi(t-t_0)}{365}\right]$$

Where:

- A_0 is the amplitude of the annual temperature function,
- t_0 it the time lag from an arbitrary starting date (selected as 1st of January in this case) to the occurrence of the minimum temperature in a year (El-din 1999).

A code was written and solved with MATLAB to solve this model; the next section presents the results of the model.

4. RESULTS AND DISCUSSION

4.1 Validation of the model results

Experiments conduct during the period from 11 to 13 of March 2015 and the results were recorded on hourly bases. Meteorological conditions were recorded simultaneously with experiments as shown in Figure 5. Where, the average values of relative humidity (r_a) and average horizontal solar radiation (THR) during the period of observations are 76 % and 450 W/m^2 respectively.

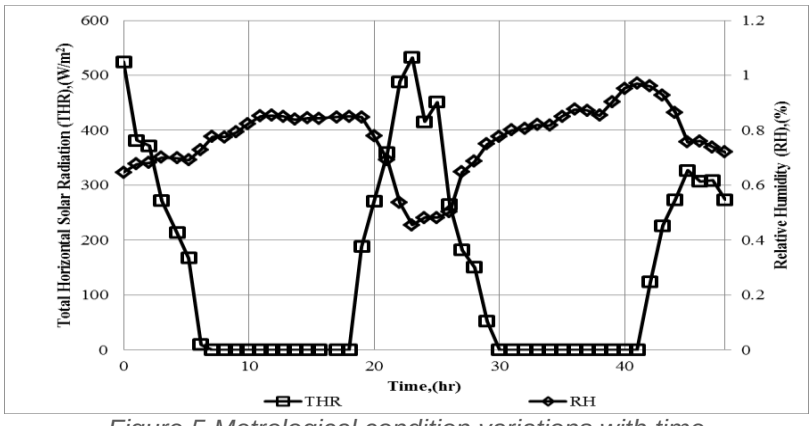

Figure 5 Metrological condition variations with time

Figure 6 presents comparison between experimental and modelling results for soil profile temperature of type loamy sand. The error and correlation coefficient are 5.59 % and 98% respectively calculated from equation 13, 14 respectively; (Morris 2001)

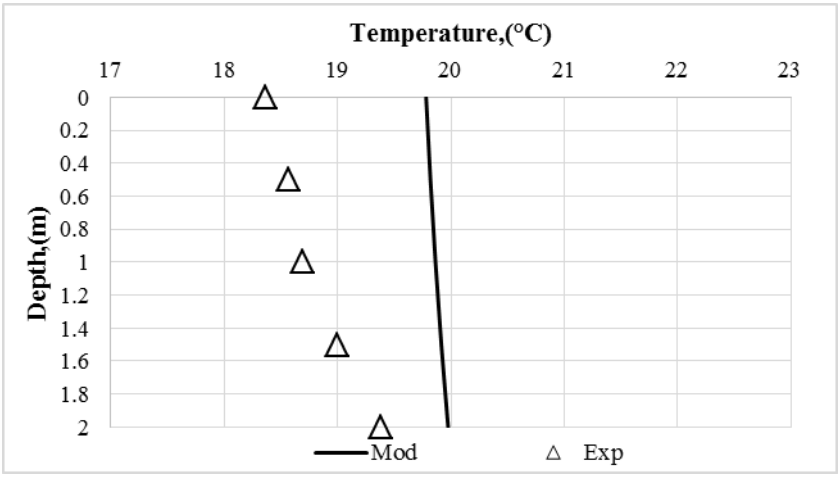

Figure 6 comparison between model results and experimental results for loamy sand sample picked from New Borg El-Arab City, Alexandria

Equation 13: absolute error e,

$$e=\sqrt{\frac{\sum\left[100\times\left(X_{sim,i}-X_{\exp,i}\right)/X_{sim,i}\right]^2}{N}}$$

Equation 14: correlation coefficient r,

$$r=\frac{N\left(\sum X_{\exp,i}\cdot X_{sim,i}\right)-\left(\sum X_{\exp,i}\right)\times\left(\sum X_{sim,i}\right)}{\sqrt{N\cdot\left(\sum X_{\exp,i}^2\right)-\left(\sum X_{\exp,i}\right)^2}\cdot\sqrt{N\cdot\left(\sum X_{sim,i}^2\right)-\left(\sum X_{sim,i}\right)^2}}$$

These values show that the developed model predicts accurately the temperature of the soil with variation of depth and weather conditions.

4.2 Soil temperature profile results

Validated model used to simulate the temperature profile of the six new cities shown in Figure 1 with three different soil composition; Loamy sand, Sandy clay and Clay. These soil types were reported by Urban Communities Authority of the Ministry of Housing. Thermo-physical properties (Density, heat capacity and thermal conductivity) of these soil samples are listed in Table 2.

Figure 66 shows average annually soil temperature profile output from modelling for six cities. It is observed that the temperature of the wet surface is lower than that of dry surface and this is a result of the effect of the heat of vaporization of wet soil surface and this agrees with the results found by G. Mihalakakou, Mihalakakou et al. and M. M. Salah.

It is also observed that the temperature of bare surface soil is lower than that of covered surface soil for all sites and this can be referred to the effect of evaporation too, because of the chance for evaporation with base coils is more than that with covered soils, where the fraction f for grass covered soils is 0.7 times that of the bare surface soils (Mihalakakou and Santamouris1997).

Table 2 Thermo-physical properties of different soil types, (Ali 2013)

Property	Loamy Sand	Sandy Clay	Clay
Density, Kg/m3	1680	1330	1230
Thermal conductivity, W/m.k	2.15	1.0796	0.8211
Specific Heat, J/kg.k	1187.8	1500.3	1622.3
Thermal diffusivity, 10-7 m2/s	10.774	5.41	4.115
City	Cairo, Luxor, El Minya, and Alexandria	Asyut	Sohag

As shown in Figure 66 the soil temperature profile of Cairo and Al-Minya are nearly the same with temperatures of 18.25, 18.5 and 20.2 ^{0}C respectively and this is due to the weather conditions and soil type of both sites are identical. For Alexandria soil condition of wet or dry does not affect the soil temperature

profile and this may be due to the effect of sir relative humidity of the sire because Alexandria is known by its high relative humidity of the atmosphere and the high wind speed where for the Alexandria site the wind speed has a yearly average of 6 m/sec. Sohag and Luxor have also nearly same profile with some little difference due to extreme ambient air temperature in Luxor which may be reaches to 45 °C in sometimes in the year.

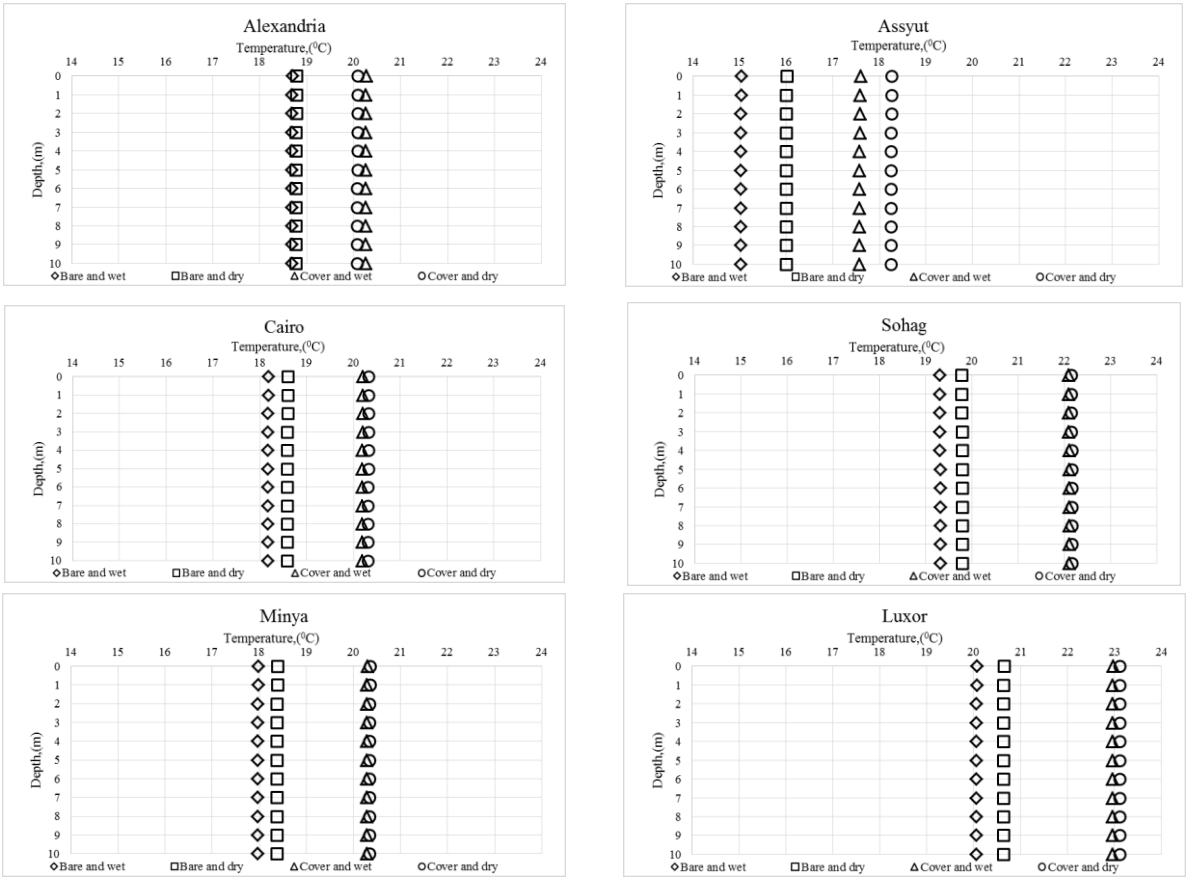

Figure 66 Soil temperature profiles of six cities at various ground cover conditions

Finally Asyut has different temperature profiles than other cities and this is due to the moderate condition with low humidity. Consequently, the amount of moisture content on the surface affects the average values of the temperature between bare and covered condition. Figure 67 indicates average monthly soil temperature distribution profile for Alexandria and Al-Minya. It can be found that on Sep, Oct, Nov, Dec, and Jan (winter season) the temperature profile begins with low temperature at the surface and increased with depth. This high temperature at depth can be utilized in heating purposes. On the other hand at Feb, Mar, Apr, May, June and July the reverse happened, which can be used in cooling purpose.

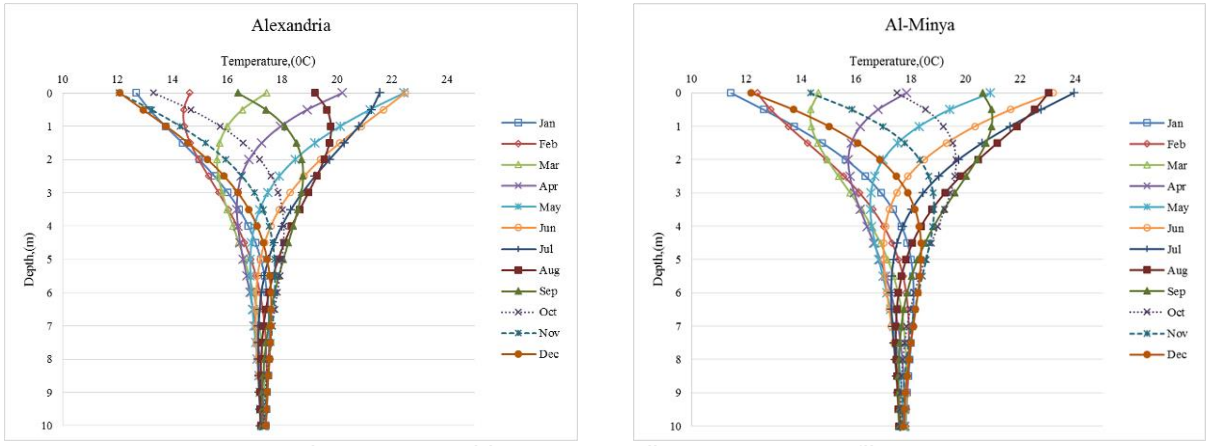

Figure 67 Monthly average soil temperature profiles

5. CONCLUSION

This paper presents experimental and analytical model of soil temperature distribution profile for new Borg Al-Arab city, Alexandria Egypt. Experimental work conducted during the period of 11 to 13 of March 2015. A good agreement achieved between modeling and experimental data with error values of 5.59 %. This model applied for 6 new cities. Thermal conductively of loamy sand, sandy clay and clay are 2.152, 1.6165 and 0.8211 W/m. k respectively. Average ground surface temperature over the period of experiments is 18.36 ^{0}C. Soil temperature increases with depth to reaches to 19.38 ^{0}C. So this paper can be taken as a reference in designing of EAHE applications in Egypt.

6. ACKNOWLEDGEMENT

The authors would like to acknowledge Ministry of Higher Education (MoHE) of Egypt for providing a scholarship to conduct this study as well as the Egypt Japan University of Science and Technology (E-JUST) for offering the facility, tools and equipment needed to conduct this research work.

7. REFERENCES

ABBAS, AM, and Burkhard Sanner. 1999. “Feasibility Investigations for Underground Cold Storage in Giza, Egypt.” *Bull. Hydrogeol* 17 (17). http://pangea.stanford.edu/ERE/pdf/IGAstandard/EGC/1999/Abbas.pdf.

ADELRAHIM, HM, FH Fahmy, and MAH El-Fawal. 2013. “Geothermal Hot Water and Space Heating System in Egypt.” In *2nd International Conference on Energy Systems and Technologies*. Cairo, Egypt. http://www.afaqscientific.com/icest2013/ICEST2013papertemplate.pdf.

ALI, Mohamed Reda Othman. 2013. “Modelling the Performance of Horizontal Heat Exchanger of Ground-Coupled Heat Pump Systems with Egyptian Conditions”. Ph.D thesis, School Of Mechanical, Aerospace, And Civil Engineering Manchester Univesity.

CAMPBELL, GS, and JM Norman. 1998. *An Introduction to Environmental Biophysics*. second edi. Springer. http://books.google.com/books?hl=en&lr=&id=v6UpE6lThCwC&oi=fnd&pg=PR5&dq=An+Introduction+to+Environmental+Biophysics&ots=JVd9WH9lwY&sig=kfWc1IpIelDUjJbB9TPrM9NJE3U.

EL-DIN, M M Salah. 1999. “On the Heat Flow into the Ground.” *Renewable Energy* 18: 473–490.

FARGALI, HM, FH Fahmy, and MA Hassan. 2010. “A Simulation Model for Predicting the Performance of PV/Wind–Powered Geothermal Space Heating System in Egypt.” *The Online Journal on Electronics and Electrical Engineering(OJEEE)* 2 (2): 321–330. http://www.infomesr.org/attachments/12-028.pdf.

GAO, Z., L. Bian, Y. Hu, L. Wang, and J. Fan. 2007. “Determination of Soil Temperature in an Arid Region.” *Journal of Arid Environments* 71 (2) (October): 157–168. doi:10.1016/j.jaridenv.2007.03.012. http://linkinghub.elsevier.com/retrieve/pii/S014019630700081X.

KRARTI, M. 1995. “Analytical Model to Predict Nonhomogeneous Soil Temperature Variation.” *Transaction of the ASME* 117 (May 1995). http://solarenergyengineering.asmedigitalcollection.asme.org/article.aspx?articleid=1455460.

MIHALAKAKOU, G. 2002. “On Estimating Soil Surface Temperature Profiles.” *Energy and Buildings* 34: 251–259. http://www.sciencedirect.com/science/article/pii/S0378778801000895.

MIHALAKAKOU, G, and M Santamouris. 1997. “On the Application of the Energy Balance Equation to Predict Ground Temperature Profiles.” *Solar Energy* 60 (97): 181–190. http://www.sciencedirect.com/science/article/pii/S0038092X97000121.

MORRIS, A.S. 2001 “Errors During the Measurement Process”, Measurements and Instrumentation Priciple, 3rd. Oxford, UK: BH, Chap. 3.

WANG, Linlin, and Z Gao. 2012. “An Analytical Solution to the One-Dimensional Heat Conduction–Convection Equation in Soil.” *Soil Science Society of America Journal*. doi:10.2136/sssaj2012.0023. https://dl.sciencesocieties.org/publications/sssaj/abstracts/76/6/1978.

383: Numerical investigation of heat transfer in the vertical tube of a supercritical water solar tower receiver

G. ZHANG, Y. LI, Y. J. DAI, R. Z. WANG

Institute of Refrigeration and Cryogenics, Shanghai Jiao Tong University, Shanghai 200240, China, liyo@sjtu.edu.cn

The higher incident radiation flux and the higher thermal to electric efficiency lead the solar tower power with supercritical water as heat transport fluid in central receiver to be one of the most promising solar thermal power. In this paper, heat transfer of supercritical water in a vertical tube of the solar tower receiver has been investigated using Computational Fluid Dynamics (CFD) method. A 3D simulation model is employed to really express distribution of heat flux in the circumferential direction of a circular tube heated by incident solar flux on one side. The RNG k-ε model with the standard wall function is employed to carry out numerical simulations and the results agree with experimental data well. The simulations reveal that the average heat transfer coefficient depends strongly upon the mass flux and incident solar flux. At sufficiently high mass fluxes, the average heat transfer coefficient reaches the peak value at a bulk temperature slightly less than the pseudo-critical temperature. At low mass flux relatively to the incident flux, heat transfer deterioration occurs in the pseudo-critical region. The buoyancy effect which is important factor causing heat transfer deterioration in supercritical water is obviously weakened in downward flow, even can be negligible. and h/h0 are modified to a limit of 10-6 for the onset of mixed convection and 0.45 for the onset of heat transfer deterioration when supercritical water in circular tube is heated by incident flux. And, the relations between the limit incident radiation flux above which the heat transfer deterioration occurs and mass flux for the supercritical water solar tower receiver is given as qin=0.453G

Keywords: supercritical water, incident solar flux, CFD, heat transfer

1. INTRODUCTION

Generally, the central receivers in solar tower power have higher solar-thermal conversion efficiency with higher acceptable incident radiation flux (Ho and Iverson, 2014). Indeed, the central receivers, which generally employ either molten nitrate salt or water/steam as the heat transfer fluid, have progressed in increasing the acceptable incident heat flux Since 1980s (Li et al., 2010). The receivers with water/steam in Solar One and CESA-1 promise an incident radiation flux of 300 kW/m^2, the molten salt solar receiver from Solar Two allows a peak flux of 800 kW/m^2. The increasing the allowable incident heat flux is not only helpful improving the solar-thermal conversion efficiency, but also reducing the Levelized Energy Cost (LEC) from concentrating solar power technologies.

Meanwhile, in order to reduce LEC, the research and development activities on higher efficiency power cycles (Ho and Iverson, 2014; Li et al., 2014) including air-Brayton, supercritical-CO_2, and ultra-supercritical steam cycles are being pursued. For the next generation of coal fired power plant, the live steam pressure and temperature for ultra-supercritical steam cycle are expected to reach 28~35 MPa and approximately 700 ^{o}C in the future. For nuclear power plant (Schulenberg et al., 2014), the Supercritical Water Reactor (SCWR) has been regarded as a leading candidate for electricity generation due to its advantages such as high efficiency (45%), elimination of steam generator and so on. However, the currently operating concentrating solar power plants mainly operate in subcritical Rankine power cycle with the gross thermal-to-electric efficiency between 30% and 40%. In view of the higher incident radiation flux and the higher efficiency power cycle, a supercritical water solar tower receiver is proposed to improve the solar thermal-to-electric conversion efficiency in this paper.

Due to the strong variation of thermal-physical properties of supercritical water in the pseudo-critical region, an unusually heat transfer behaviour (heat transfer enhancement or heat transfer deterioration) occurs in this region. Therefore, in terms of experiments and simulations, extensive research activities (Cheng et al., 2007; Kim et al., 2004; Yamagata et al., 1972) on heat transfer of supercritical water have been outgoing since the 1950s, mainly involving supercritical water as coolants in nuclear power plants. These investigations have revealed that the characteristics of heat transfer in supercritical water is strongly affected by heat flux, mass flux, flow direction and buoyancy. In simulations (Cheng et al., 2007; Kim et al., 2004; Yang et al., 2007), the reliability of the turbulence model is evaluated to exactly predict the characteristics of heat transfer in supercritical water, including Standard k-ε, RNG k-ε, Realizable k-ε, SST k-ω and so on. However, most studies focus on heat transfer in circular tube heated by uniform heat flux. Since the incident radiation flux is uniform and parallel arrangement, the distribution of heat flux around the heat exchanger tube of solar receiver is un-uniform. Unfortunately, there are limited data available for the supercritical water solar tower receiver proposed in this paper. Therefore, the study of heat transfer behaviour of supercritical water in circular tube heated by incident radiation flux is still required.

The objective of the present communication is to investigate the characteristics of heat transfer of supercritical water in circular tube heated by incident solar heat flux on one side using a commercial CFD program method. In order to really express the distribution of un-uniform heat flux in the circumferential direction of a circular tube, a 3D simulation is utilized. The RNG k-ε model with the standard wall function is employed to carry out numerical simulations and evaluated by comparing with experimental data. After the validation, the effect of incident flux and mass flux on heat transfer of supercritical water is analyzed. Furthermore, the buoyancy criterion and onset of heat transfer deterioration are also investigated in this paper.

2. MODELLING

2.1 Physical properties of supercritical water

Since the pressure drop inside the circular tube is relatively smaller than the inlet pressure 24.5 MPa which is the proposed operating pressure for supercritical water solar tower receiver in this paper, only the effect of temperature on supercritical water physical properties at 24.5 MPa is considered for simulation. NIST REFPROP software (National Institute of Standards Technology, 2007) is applied to calculate the water properties. Figure 1 gives the properties variations of water at 24.5 MPa based on NIST REFPROP. At 24.5 MPa, the pseudo-critical temperature is 383 ^{o}C. Near the pseudo-critical line, the special heat shows a sharp peak. The viscosity, the density and thermal conductivity decrease dramatically in this region. Beside the pseudo-critical region, the others are called as the liquid-like region and gas-like region.

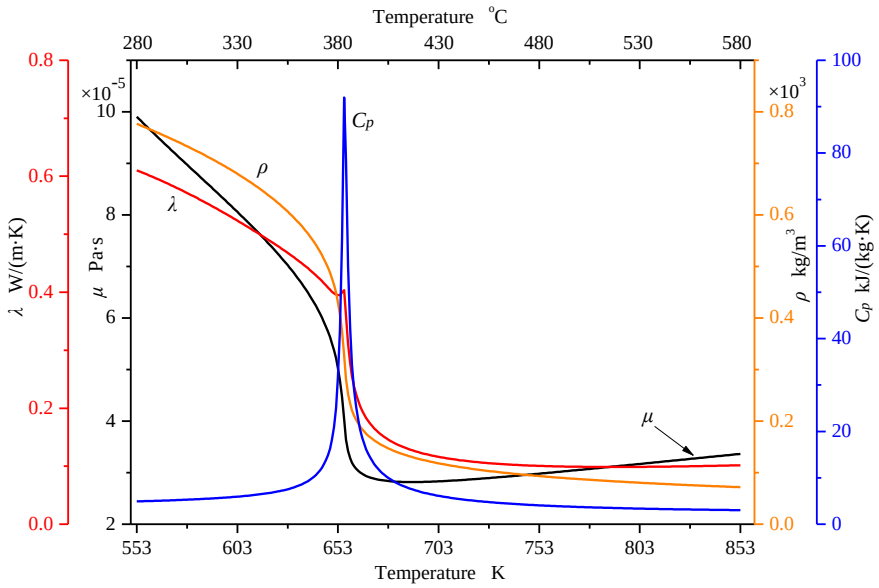

Figure 68: Water properties at 24.5 MPa

2.2 Geometry and distribution of heat flux

A cavity-type receiver with tubular panel is considered for the supercritical water solar tower receiver. The tubular panel receives the concentrated solar energy and converts it into available thermal energy in the supercritical water. In order to simplify the calculation model, an half circular tube is selected as the computational domain in this study. Figure 2 shows the cross section of the calculation model. The tube material was 316L stainless steel with conductivity equal to 24.5 W/(m•K). The inside and outside diameters of the tube are 7.5 mm and 11 mm respectively. the inside diameter of 7.5mm is almost always used in supercritical water cooled reactors (Schulenberg et al., 2014; Yamagata et al., 1972).To ensure calculation accuracy of model near pseudo-critical under low incident radiation flux, the tube length of 9 m is considered in this investigation.

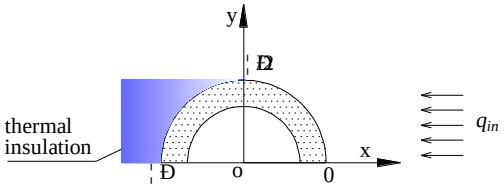

Figure 2: The cross section of the calculation model

For solar tower receiver, the available incident radiation converted into thermal-energy in heat transfer fluid can be represented as a percentage of the incident radiation on the receiver (Christian and Ho, 2012). Thus, in the present article, the available incident radiation is adopted and the thermal heat loss including conductive, convective, and radiative losses cannot be considered. Since the incident radiation flux is uniform and parallel arrangement and the left half of circular tube is thermally insulated, the heat flux distribution on the circumference of circular tube is non-uniform. This non-uniformity cannot be replaced by an equivalent heat flux in simulation due to the low conductivity of stainless steel. Therefore, the heat flux distribution on the circumference of circular tube must be really given, as following equation.

Equation 10: Distribution of heat flux

$$q_{(x,y,z)} = \begin{cases} q_{in} \sin\left(\frac{\pi}{2} \times \frac{x}{r_{out}}\right) & if \ x > 0 \\ 0 & if \ x \le 0 \end{cases}$$

Where:

$q_{(x,y,x)}$ = quantity of heat flux on (x, y, z) (kW/m^2)

q_{in}= incident heat flux (kW/m^2)

r_{out}= outside radius of tube (m)

x, y, z= directions

2.3 Turbulence Model

The turbulence model is the most significant factor which affects the accuracy of numerical simulation of heat transfer in supercritical water evidently. To evaluate the reliability of the turbulence model, various simulations are performed with turbulence models: Standard *k-ε*, RNG *k-ε*, SST *k-ω*, Realizable *k-ε* and so on. For the vertical flow of water in a circular tube, RNG *k-ε* with enhanced wall treatment is more accurate to predict heat transfer at supercritical pressure than other models. However, this turbulence model demands very small height of the first grid off the wall, which makes it not to be suitable for 3-D calculation with a complex or large geometry. On the other hand, the RNG *k-ε* with standard wall function is also found to have acceptable predicting capability. And, the grid requirement of the standard wall function is far loose than that of the enhanced wall treatment. Considering the accuracy of numerical simulation and computational cost and time, the RNG *k-ε* with standard wall function is employed in this paper.

In the wall function approach, the y^+ values are generally from about 5 to 100 in former studies (Yang et al., 2007). Accordingly in this study, this special mesh partition strategy is adopted. Meanwhile, to improve the precision of numerical simulation and accelerate the convergence of flow, the structured mesh is used.

2.4 Heat Transfer Coefficient

To evaluate the heat transfer of supercritical water in tube heated by incident radiation flux, the average heat transfer coefficient is employed in the current paper. However, the non-uniformity of heat flux distribution on the outside of circular tube makes the temperature distribution on the inside surface of circular tube to be non-uniform. In terms of solving the average heat transfer coefficient equation of supercritical water, it is important to evaluate the average temperature of tube inside surface. To express the average temperature of tube inside surface on the same cross section, the corresponding equation is given as following:

Equation 2: Average temperature of tube inside wall

$$T_{in,ave} = \frac{1}{n}\sum_{i=1}^{n} T_{in}\left(\frac{i\times\pi}{n}\right)$$

Where:

$T_{in,ave}$ = average temperature of tube inside wall on (°C)

$T_{in}(i\times\pi/n)$= temperature of the first grid off the inside wall of tube (°C)

n= number of the first grid off the inside wall of tube

3. Validation and mesh sensitive test

3.1 Validation

To verify the exactness of the turbulence model and simulation method, the comparison of the simulation data with the experimental data obtained by Yamagata et al. (Yamagata et al., 1972) has been carried out. The same working conditions are: the tube diameter 7.5 mm, the pressure 24.5 MPa, the inlet mass flux 1260 kg/m^{2}s, the uniform heat flux 233 kW/m^2. Figure 3 shows the comparison of the heat transfer coefficient between simulation and experiments. It is obviously that the simulated results agree with the experimental data well.

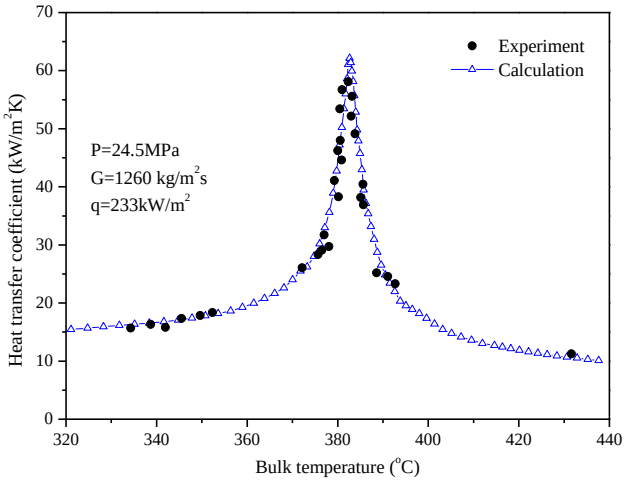

Figure 3: Comparison of the heat transfer coefficient between simulation and experiments

3.2 Mesh Sensitive Test

In order to ensure the CFD calculation accuracy and reduce the computational cost and time, the mesh sensitive test is performed. The tube length of 1.6 m is used in the mesh sensitivity. The incident radiation flux and the mass flux are 1000 kW/m^2 and 1500 kg/m^{2}s, respectively. Figure 4 gives the mesh sensitive test for the present study. It can be seen from this picture that the bulk temperatures at different position with different mesh numbers are coincident without evident differences. The maximum value of the absolute difference is less than 0.33 ^{o}C and the corresponding relative difference is no more than 0.1%. This illustrates the mesh partitions in Figure 4 are not sensitive for the circular tube calculations. Considering the computational time, for the current calculation model with the length of 9 m, the mesh number of 5130000 is fine enough. Therefore, the mesh number of 5130000 is adopted in this paper.

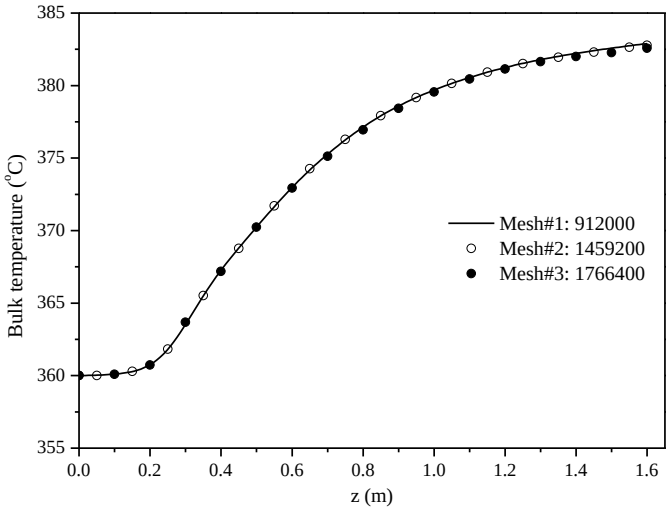

Figure 4: Mesh sensitive test

4. RESULTS AND DISCUSSION

Simulation involved in this study was performed at the pressure of 24.5MPa. The incident radiation flux ranges from 300 kW/m^2 to 800 kW/m^2, the mass flux is from 800 kg/(m^{2}s) to 1800 kg/(m^{2}s).

4.1 Effect of the Mass Flux

The effect of the mass flux on average heat transfer coefficient is given in Figure 5, for upward, at an incident flux of 600 kW/m^2. It is observed that the average heat transfer coefficient depends strongly upon the mass flux, and its value increases with increase of mass flux. Near the pseudo-critical region, the heat transfer enhancement occurs when the mass flux is equal or more than 1200 kg/(m^{2}s), while the heat

transfer deterioration takes place as the mass flux less than 1000 kg/(m^{2}s). So, for a certain incident radiation flux, an appropriate mass flux should be adopted in order to avoid the heat transfer deterioration.

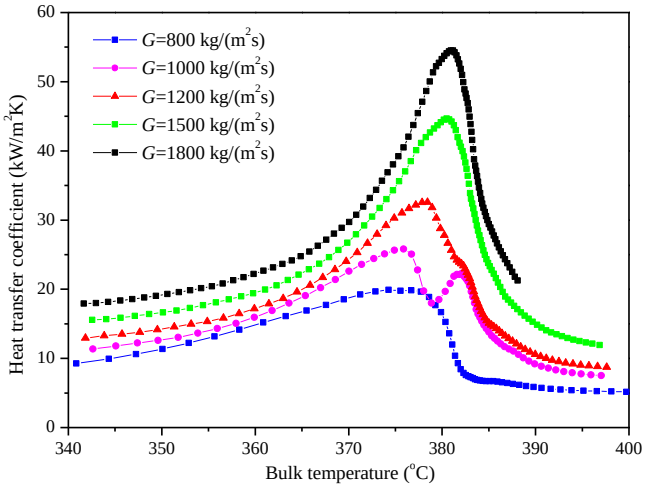

Figure 5: Comparison of heat transfer coefficient with various mass fluxes

4.2 Effect of the Incident Flux

Figure 6 shows the comparison of average heat transfer coefficient under various incident radiation fluxes. The flow direction of supercritical water is upward, the mass flux is 1000 kg/(m^{2}s). It can be seen from Figure 6 that the peak values of heat transfer coefficient decrease with the increase of incident radiation flux and the corresponding bulk temperature shift to low bulk temperature region, which is consistent with the heat transfer of supercritical water in tube in former work (Yamagata et al., 1972). Near the pseudo-critical region, the heat transfer deterioration occurs when the incident radiation flux are 600 kW/m^2 and 800 kW/m^2. The reason is that the increasing incident radiation flux results the increasing acceleration effect resulted by a sudden drop of density near the pseudo-critical line. Furthermore, the heat transfer coefficient is influenced.

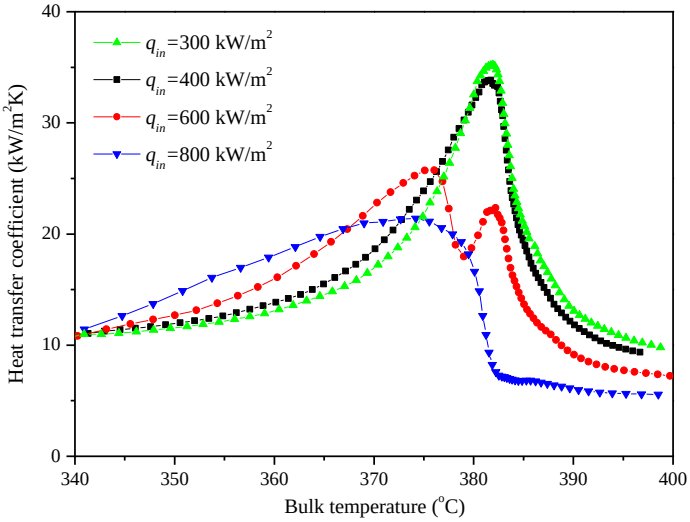

Figure 6: Comparison of heat transfer coefficient with various incident radiation fluxes

4.3 Effect of Flow Direction and Buoyancy Force

The variations of heat transfer coefficient with bulk temperature for different incident radiation fluxes is presented in Figure 7 for mass flux of 1000 kg/(m^{2}s). Upward and downward flows are considered and compared. For incident radiation flux of 400 kW/m^2, the values of heat transfer coefficient at different bulk temperature with upward flow and downward flow are coincident without evident differences. However, there is a noticeable distinction between the directions of upward and downward around the bulk temperature of 380 ^{o}C, for the incident radiation flux of 600 kW/m^2. The heat transfer deterioration occurred

in upward flow is not observed in downward flow. That is resulted from an enhancement of turbulent diffusion due to the different directions between the flow and buoyancy caused by the radial density gradient variations inside the flow field. In other words, the buoyancy effect which is important factor causing heat transfer deterioration in supercritical water is obviously weakened in downward flow, even negligible.

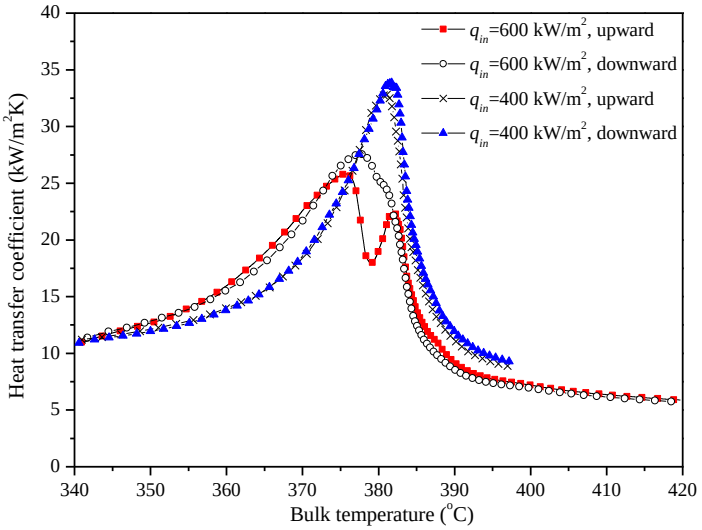

Figure 7: Comparison of heat transfer coefficient for upward and downward flow

However, for upward flow in circular tube, it is important to ascertain whether the effect of buoyancy is likely to be significant or not for given conditions. To evaluate the buoyancy effect on supercritical water in circular tube, a semi-empirical parameter defined by the comparison between the buoyancy forces and the inertial forces is proposed by Jackson and Hall (Jackson and Hall, 1979), and the criterion is given as following:

Equation 3: Criterion for onset of mixed convection

$$\frac{\overline{Gr}}{Re^{2.7}} < 1\times10^{-5}$$

Where:

$\overline{Gr}$ = average Grashof number

Re=Reynolds number

The limit value of 10^{-5} is applied for the onset of mixed convection. When the mixed convection takes place, the heat transfer coefficient is deteriorated in upward flow. But the criterion is developed on basis of uniform heat flux, which may be not suitable for the condition of incident radiation flux. A modified criterion is proposed to account for the buoyancy effect in this study. The evolution of the modified parameter $\overline{Gr}/Re^{2.7}$ with the dimensionless temperature T_b/T_{pc} is illustrated in Figure 8, for incident radiation flux of 400 kW/m^2 and 600 kW/m^2. The tendencies of the parameter $\overline{Gr}/Re^{2.7}$ are similar with the former works. The value of the ratio presents a peak value before the bulk temperature reaches the pseudo-critical temperature. Since the onset of mixed convection and the onset of heat transfer deterioration near pseudo-critical region are synchronized, the onset of heat transfer deterioration can be employed to determine the onset of mixed convection. Figure 9 shows the average inside wall temperature against bulk enthalpy at incident radiation flux of 400 kW/m^2 and 600 kW/m^2. The abrupt increases of the inside wall temperature resulted from heat transfer deterioration are observed for both of low mass fluxes. For the both high mass flux, the inside wall temperature rises gradually without abrupt increase. Combining Figure 8, the conclusion is confirmed: the modified criterion is the limit of 10^{-6} for the condition of incident radiation flux. The reason why the modified criterion is lower than the criterion proposed by Jackson and Hall is that the radial density gradient of fluid in circular tube is reduced due to the non-uniformity of temperature distribution on the circumference of circular tube caused by incident radiation flux.

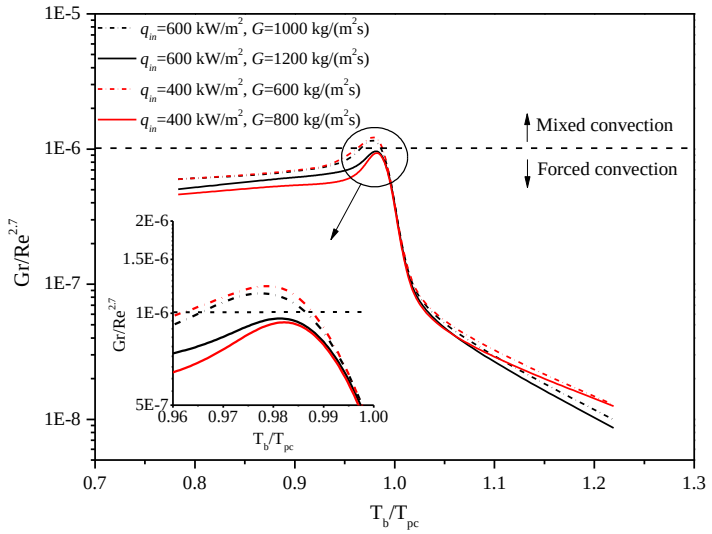

Figure 8: Evolution of the parameter $\overline{Gr}/Re^{2.7}$ with dimensionless temperature Tb/Tpc

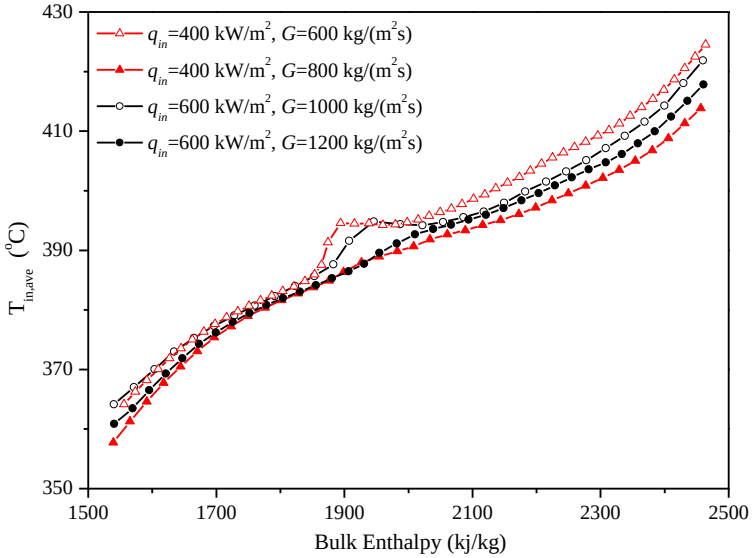

Figure 9: Variations of average inside wall temperature with bulk enthalpy

4.4 Onset of Heat Transfer Deterioration

The phenomenon of heat transfer deterioration in supercritical water is mainly caused by flow-acceleration as well as buoyancy effects resulted from a sudden drop of density near pseudo-critical region. It occurs for certain combinations of heat flux and mass flux, as shown in Figures 5 and 6. And, it is a slow and smooth behaviour. So, it is difficult to determine the onset point of heat transfer deterioration. In former works, different definitions were used, most of which are based on the ratio of the heat transfer coefficient (h) to a reference heat transfer coefficient (h_0) obtained from Dittus-Boelter equation. When the ratio h/h_0 equals 0.3, the onset of heat transfer deterioration is defined to occur. Based on experimental data in different diameters vertical tube, Styrikovich et al. (Styrikovich et al., 1967) and Yamagata et al. (Yamagata et al., 1972) proposed the following relationships between mass flux (G) and heat flux (q) for the onset of heat transfer deterioration:

Equation 4: Relation proposed by Styrikovich et al.

$$q_{Styrikovich} = 0.58G$$

Equation 5: Relation proposed by Yamagata et al.

$$q_{Yamagata} = 0.2G^{1.2}$$

Where:

q= heat flux (kW/m^2)

G=mass flux (kg/ m^2s)

However, the ratio of 0.3 may be not suitable for the heat transfer of supercritical water in tuber heated by incident radiation flux due to the non-uniformity of temperature distribution on the circumference of circular tube. Therefore, it is essential to reconfirm the criterion of the onset of heat transfer deterioration. Figure 10 shows the variations of the ratio h/h_0 with bulk temperature at the mass flux of 1000 kg/(m^2s). The value of the ratio h/h_0 reaches minimum at the pseudo-critical line for all incident radiation fluxes. In Figure 6, heat transfer deterioration occurs when the incident radiation flux is 600 kW/m^2. Considering Figures 6 and 10, the ratio h/h_0 of 0.45 should be adopted to be the criterion of the onset of heat transfer deterioration.

In terms of practical engineers, abrupt increase of the tube wall temperature resulted from heat transfer deterioration seriously affects the reliable and safe operation of facilities. Therefore, the relations between the limit incident radiation flux above which the heat transfer deterioration occurs and mass flux for the supercritical water solar tower receiver must be determined. Based on the ratio h/h_0 of 0.45, the relations between limit incident radiation flux and mass flux for deterioration in heat transfer is given in Figure 11. According the equations proposed by Styrikovich and Yamagata, the fitted curves are obtained using the least squares method. The adjusted R-square value of the relation 1 and relation 2 are 0.99 and 0.89, respectively. Therefore, the relation 1 is considered for the onset of heat transfer deterioration when supercritical water in circular tube is heated by incident radiation flux, as shown following:

Equation 6: Criterion for onset of heat transfer deterioration

$$q_{in} = 0.453G$$

Where:

q_{in}= incident heat flux (kW/m^2)

G=mass flux (kg/ m^2s)

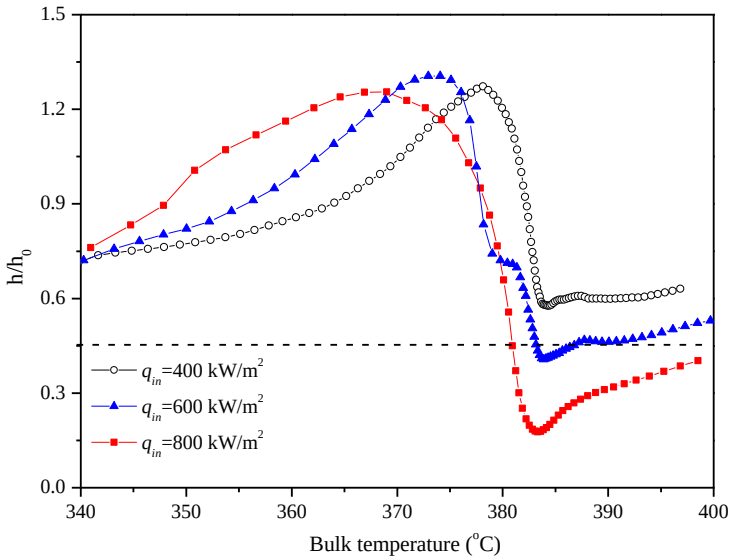

Figure 10: Variations of the ratio h/h0 with bulk temperature

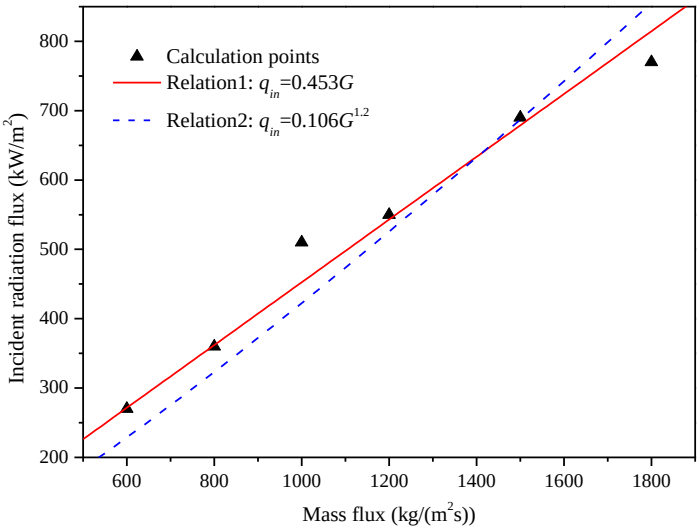

Figure 11: Relations between limit incident radiation flux and mass flux for deterioration in heat transfer

5. CONCLUSION

The characteristics of heat transfer of supercritical water in circular tube heated by incident radiation flux has been investigated using a commercial CFD program, FLUENT. The RNG *k-ε* model with the standard wall function is employed to carry out numerical simulations and evaluated by comparing with experimental data. After the validation, the effect of incident radiation flux and mass flux on heat transfer of supercritical water is analyzed. Then the criterions of onset of mixed convection and onset of heat transfer deterioration are reconfirmed. Some main conclusions can be drawn as following:

(1) The average heat transfer coefficient depends strongly upon the mass flux and incident radiation flux. At sufficiently high mass fluxes, the average heat transfer coefficient reaches the peak value at a bulk temperature slightly less than the pseudo-critical temperature. At low mass flux relatively to the incident radiation flux, heat transfer deterioration occurs in the pseudo-critical region.

(2) The buoyancy effect which is important factor causing heat transfer deterioration in supercritical water is obviously weakened in downward flow, even can be negligible.

(3) The non-uniformity of temperature distribution on the circumference of circular tube caused by incident radiation flux makes the radial density gradient of fluid in circular tube to be reduced. Furthermore, is modified to a limit of 10^{-6} for the onset of mixed convection.

(4) The ratio h/h_0 of 0.45 is adopted to be the criterion of the onset of deterioration in heat transfer instead of 0.3 when supercritical water in circular tube is heated by incident radiation flux. And, the relations between the limit incident radiation flux above which the heat transfer deterioration occurs and mass flux for the supercritical water solar tower receiver is given as q_{in}=0.453G.

6. ACKNOWLEDGMENTS

This work was supported by the national key technology R&D program under the contract No. 2012BAA05B06-6.

7. REFERENCES

CHENG, X., Kuang, B., Yang, Y.H., 2007. Numerical analysis of heat transfer in supercritical water cooled flow channels. Nucl. Eng. Des. 237, 240–252.

CHRISTIAN, J.M., Ho, C.K., 2012. CFD simulation and heat loss analysis of the solar two power tower receiver, in: ASME 2012 6th International Conference on Energy Sustainability Collocated with the ASME 2012 10th International Conference on Fuel Cell Science, Engineering and Technology. American Society of Mechanical Engineers, pp. 227–235.

HO, C.K., Iverson, B.D., 2014. Review of high-temperature central receiver designs for concentrating solar power. Renew. Sustain. Energy Rev. 29, 835–846.

JACKSON, J.D., Hall, W.B., 1979. Forced convection heat transfer to fluids at supercritical pressure. Turbul. Forced Convect. Channels Bundles 563–611.

KIM, S.H., Kim, Y.I., Bae, Y.Y., Cho, B.H., 2004. Numerical Simulation of the Vertical Upward Flow of Water in a Heated Tube at Supercritical Pressure, in: Proc. ICAPP.

LI, X., Kong, W., Wang, Z., Chang, C., Bai, F., 2010. Thermal model and thermodynamic performance of molten salt cavity receiver. Renew. Energy 35, 981–988.

LI, Y., Zhou, L., Xu, G., Fang, Y., Zhao, S., Yang, Y., 2014. Thermodynamic analysis and optimization of a double reheat system in an ultra-supercritical power plant. Energy 74, 202–214.

National Institute of Standards Technology, 2007. NIST Reference Fluid Thermodynamic and Transport Properties-REFPROP: NIST Standard Reference Database 23.

SCHULENBERG, T., Leung, L.K.H., Oka, Y., 2014. Review of R&D for supercritical water cooled reactors. Prog. Nucl. Energy 77, 282–299.

STYRIKOVICH, M.A., Margulova, T.K., Miropol'Skii, Z.L., 1967. Problems in the development of designs of supercritical boilers. Teploenergetika 14, 4–7.

YAMAGATA, K., Nishikawa, K., Hasegawa, S., Fujii, T., Yoshida, S., 1972. Forced convective heat transfer to supercritical water flowing in tubes. Int J Heat Mass Transf. 2575–2593.

YANG, J., Oka, Y., Ishiwatari, Y., Liu, J., Yoo, J., 2007. Numerical investigation of heat transfer in upward flows of supercritical water in circular tubes and tight fuel rod bundles. Nucl. Eng. Des. 237, 420–430.

SESSION 34: CARBON SEQUESTRATION

246: Carbon pump - a reinterpretation model for energy efficiency of CO2 capture

SHUAI DENG[1], RUIKAI ZHAO[1], YINAN LIU[1], HUASHAN BAO[2], ZHIWEI MA[2], LI ZHAO[1]

1 Key Laboratory of Efficient Utilization of Low and Medium Grade Energy (Tianjin University), MOE, Tianjin, China, SDeng@tju.edu.cn
2 Sir Joseph Swan Centre of Energy Research, Newcastle University, NE1 7RU, UK

The major barrier to a widespread adoption of CO2 capture is that imposed energy penalty commonly leads to at least 20% reduction in net output of retrofitted power plant. Such considerable energy requirement limits a scale-up development of near-term CO2 capture technologies. In contrary to the feasibility study on material and process in laboratory, the performance study on energy efficiency of various capture technologies should focus more on the scale of system by using specialized evaluation tools. However, the existing studies on such research field cannot present a satisfied performance "map" with a clear framework of energy efficiency for various CO2 capture technologies, so that three questions shown below cannot be directly answered:

1. What are the performance "windows" of energy efficiency for typical technologies in CCS industrial field? That is actually a "top ceiling" problem about the performance limitation of energy efficiency for various CCS technologies.

2. How to carry out a performance comparison of these typical technologies on a fair and clear platform of energy efficiency? The key to this problem is providing a standard methodology of performance evaluation which includes indicator, method and tool.

3. How to precisely indicate an effective pathway or possible directions for various CCS technologies to achieve energy-saving?

This paper presents a rethink on the methodology of energy-efficient analysis of CO2 capture using classical thermodynamic tools. A carbon pump model, which can be considered as an analogy from heat pump, was proposed with related principles, equation, and calculation method, based on the thermodynamic theory. Various aspects of possible applications of carbon pump model, especially on the performance evaluation, are discussed as well. In addition, several case studies on performance analysis are presented as a preliminary answer to above-mentioned three questions.

Keywords: carbon pump; carbon capture; thermodynamic cycle; energy efficiency; CCS

1. INTRODUCTION

Carbon capture and storage (CCS), which is widely accepted as a promising option to significantly reduce the greenhouse gas emission of human society, however, is an energy intensive process at the current stage. The large energy requirement, which leads to an efficiency decrease of 25% in the power plant when equipped with CCS (Kothandaraman, 2009, 1378), has already became a major barrier to a commercial application of near-term CCS technologies. A series of sustained global effort, which initiated with CCS development in the past several years to solve this problem, mainly focused on four aspects: advanced combustion technologies for low CO_2 emission (Wall, 2007, 45), innovation CCS technologies (Markewitz, et al., 2012, 7283), material in low energy requirement (Chaffee, et al., 2007, 14; Hedi, et al., 2013, 419; Sjostrom and Krutka, 2010, 1300), and renewable energy integration (Zhao, et al., 2015, 10).

However, existing studies on the topic of “energy efficiency of CCS technology” cannot present a satisfied performance "map" with a clear definition boundary of energy efficiency for various technical approaches available. For example, three questions on such a topic are shown below for discussion:

- What are the performance "windows" of energy efficiency for typical CO_2 capture technologies?

  That is actually a "top ceiling" problem about the performance limitation of energy efficiency for various CO_2 capture technologies. Some conclusions in published researches already shown that a blind pursuit of developing innovative solvents with a low heat of absorption and without enough theoretical considerations would lead to a misguided research direction on minimising the regeneration heat duty of post-combustion CO_2 capture (Oexmann and Kather, 2010, 36).

- How to carry out a performance comparison of typical CO_2 capture technologies on a fair and clear platform of energy efficiency?

  A performance comparison of various CO_2 capture technologies present not only a basic database for cost analysis and roadmap design, but also a deep understanding of technology development trend. The key to this problem is providing a standard methodology of performance evaluation which includes performance indicator, mathematical model, tool and method.

- How to precisely indicate a development pathway for specific CO_2 capture technology towards low energy consumption?

  For a specific CO_2 capture technology, an effective design of low-energy operation refers to several possible aspects. Taking the post-combustion capture by wet chemical absorption as an example, materials, mass transfer, separation process, system (Wilcox, 2012, 2) and renewable energy integration (Zhao, et al., 2015, 2) are main concerns. Thus, contributions of single factors and coupling effect of multi-factors to the energy efficiency of the entire system are needed to be clarified for a weight distribution of energy-saving potential on various sections of CCS technologies.

Thermodynamics is a branch of physics concerned with heat and work and their relations to energy efficiency of process, system and cycle. It has a complete theoretical framework for energy efficiency analysis of thermal system. Heat pump, which can use some certain amount of external power to accomplish a work of transferring energy from the heat source to the heat sink, is a classical concept in thermodynamic field. **Carbon pump** (CP), which can be considered as an analogy concept from heat pump, was proposed in this paper as a model for energy efficiency analysis of CO_2 capture process. The principles, equation, and calculation method related to carbon pump are presented as well. Various aspects of possible applications of carbon pump model, especially on the performance evaluation, are discussed. In addition, several case studies on performance analysis are presented as a preliminary answer to above-mentioned three questions.

2. LITERATURE RESEARCH

Carbon Pump (CP), which often appeared in combination terms of biological CP, microbial CP, ocean CP and marine CP, can be found via a historical literature research as an early appearance of term “ocean carbon pump”(Volk and Hoffert, 1984, 100). However, the main contribution to the development of ocean

CP mainly involves a global-scale research on CO_2 concentration gradient from ambient air to ocean surface, deep-water.

Another inspiration idea to carbon pump originates from the classical academic frame of separation process (SE). Most of textbooks about SE contain an independent chapter on energy efficiency of separation process based on a simplified version of separation model (King, 1980, 661; Seader, et al., 2011, 35). Based on the simplified separation model, the minimum separation work highly replies on two parameters: mole fraction of CO_2 in mixture before separation, and separation effect. This model has already been widely accepted in CCS research field to predict the energy consumption of ideal CO_2 capture process (Wilcox, 2012, 22; DOE/NETL, 2011, 19).

As shown in Fig.1, the idea of thermodynamic carbon pump originates from two sources: the concept adopts the term from researches on ocean carbon pump; the thermodynamic principles supporting the idea follow the thread of classical theory of separation process.

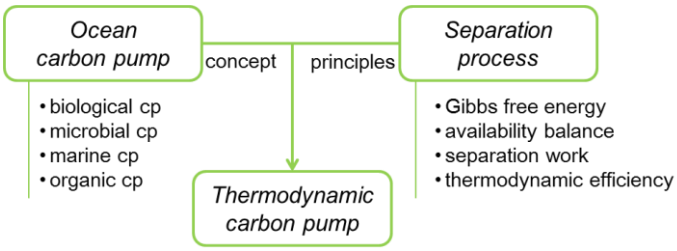

Figure 1: Flow diagram of literature research on CP

3. CONCEPT

Based on the existing knowledge pool of energy requirement in separation engineering, a reinterpretation model specifically for energy efficiency of CO_2 capture is discussed. Several important concepts in the model of carbon pump are presented in this section.

3.1 Analogy to heat pump

Driven by some amount of external work/thermal energy, a heat pump provides thermal energy from a source of heat to a destination called a "heat sink". Heat pumps are designed to move thermal energy opposite to the direction of spontaneous heat flow by absorbing heat from a cold space and releasing it to a warmer one. After a development lasting more than 100 years, the term "heat pump" currently refers to not only a heating device/facility, but also a thermodynamic cycle.

Using heat pump as a reference concept, carbon pump, which realize an enrichment of CO_2 from carbon source to carbon sink, was proposed. The feature comparison between heat pump and its analogy concept—carbon pump is shown in table 1.

Table 16: Comparison between heat pump and carbon pump

Features	Heat pump	Carbon pump
Source	thermal source: e.g., ambient air, river, etc.	CO_2 source: e.g., ambient air, flue gas, etc.
Sink	thermal sink: e.g., indoor air, etc.,	CO_2 sink, e.g., storage unit/ reservoir
Drive	Power/heat	Power/heat
Function	Heat transfer	CO_2 enrichment
Direction	Source → Sink	Source → Sink
Typical technology	Vapour-compression, absorption	Chemical absorption/adsorption

3.2 Carbon potential

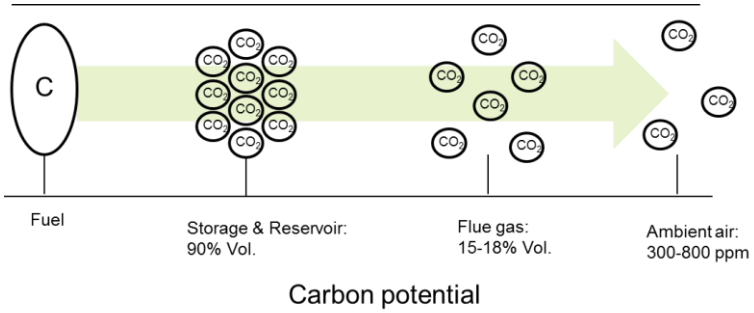

Figure 2: Carbon potential benchmarking for sink and source

An example of spontaneous process for CO_2 transfer is a concentration dilution process of CO_2 by N_2, as shown in fig.2. On the contrary, a reverse process from flue gas with a 15-18% CO_2 to the storage tank of captured CO_2 with 90% purity is a typical capture process without details between two status points. Thus, a parameter, which is termed carbon potential, is used as quantification benchmark along the transfer process of carbon. Depending on the evaluation aim on energy efficiency and specific application, the carbon potential can be expressed inside the classical thermodynamic framework by Gibbs free energy (Ruan, et al., 2014, 248) for pure material and mixtures, although it is a generalized concept of energy (Markewitz, et al., 2012, 7283). With the development of technology boundary, the definition and mathematical expression can be updated.

3.3 Carbon pump

The carbon pump model, as shown in Fig.3, is an updated one to the separation model of gas mixture. The CO_2 was "draw" by carbon pump, from a CO_2-inclusive carbon source. The carbon source, which can be a combustion exhaust, diluted bulk source or fuel, is generally at a low level of carbon potential. Through an energy input from source, the power or thermal energy was consumed to realize a continuous work of carbon pump. Compared to a spontaneous "dilution" process driven by the difference of carbon potential, CCS system is commonly meant to conduct a reverse process with an expense of energy.

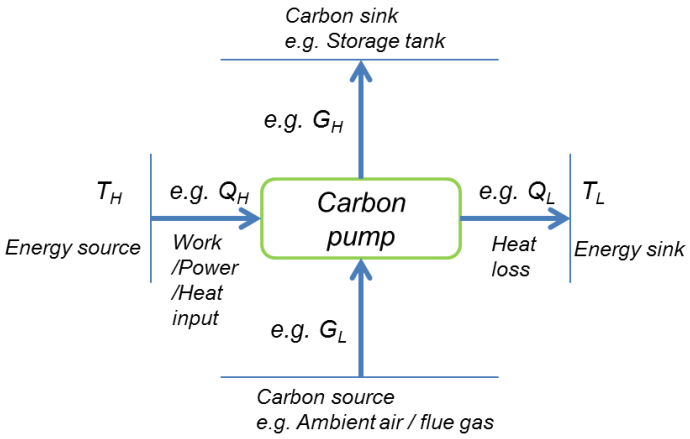

Figure 3: Carbon pump model

3.4 Carbon pump cycle

It is helpful that energy balance analysis would be carried out through the carbon pump model. However, carbon pump model was still a lumped model by which energy grade of input cannot be evaluated in a reasonable method. For example, various solvents in chemical absorption method for CO2 capture differ in regeneration temperatures of thermal source. Thus, energy grade of input energy is different. It is near impossible for a lumped model to do such a performance evaluation as inside details are neglected. In this case, a cycle model was proposed so that an energy relationship between CO_2 and its so-called carrier or

working media, can be further discussed at the various level of carbon potential inside the carbon pump model. Even optimized regeneration solution driven by solar energy in different concentration ratio can be discussed as a possible theoretical channel between energy supply and demand in different grades is presented via carbon pump cycle model.

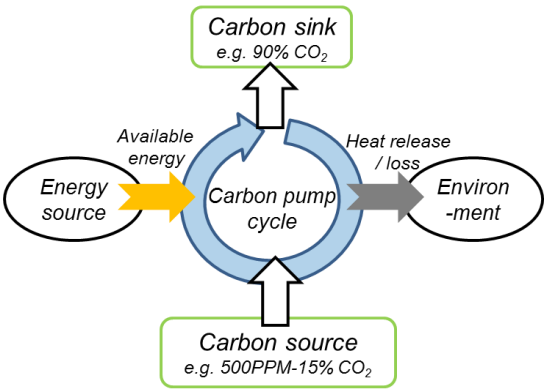

Figure 4: Carbon pump cycle

4. PRINCIPLES

Supported by mathematical tools, carbon pump cycle can also be expressed following the classical thermodynamic principles.

4.1 First law of thermodynamics in carbon pump cycle

The first law of thermodynamics is concerned with the conservation of energy inside the defined boundary of carbon pump cycle. Although energy and material flow across the boundaries, a steady-state energy balance form of first law can be established and is particularly useful for energy efficiency analysis as well as a mass balance.

$$M_{source} = M_{sink} + M_{loss} \quad (1)$$

$$W + Q = E_{sink} - E_{source} \quad (2)$$

In which M is mass flow of carbon pump cycle, W and Q are work/exergy/available energy and thermal energy flow cross the boundary of carbon pump. They are generally positive, as energy was necessary to a CO_2 migration process to compensate the gap of carbon potential (E) between sink and source. A typical evaluation parameters, which is used for the application of the first law of thermodynamic in CCS, is energy consumption per ton captured CO_2, For example, an experience data based on MEA method is that the heat duty is 3-4 GJ/ton CO_2.

4.2 Second law of thermodynamics in carbon pump cycle

The second law of thermodynamics, which focus on a performance distance between real cycle and ideal cycle, is concerned with entropy. In this case, a typical performance indictor, called 2nd-Law efficiency, is commonly used for thermodynamically perfectness evaluation and it is defined as:

$$\eta_{2nd} = W_{ideal} / W_{real} \quad (3)$$

in which W is actually work/exergy/available energy used for CO_2 capture. One case study using this indicator will be presented in the following section.

5. DISCUSSION

Three cases are presented in this section to show the development of energy analysis method of CCS technologies. The proposed method based on carbon pump model is applied in the third one.

Traditionally, the Second Law of Thermodynamics is an essential tool for process optimization through the application of exergy and exergy destruction (irreversibility) concepts. The exergy analysis method, which is proposed in the first case (Lara et al. 2011, 1046), is to provide a guide for identifying the irreversibility of power plant with CCS. Equation 4 shows the definition of exergetic efficiency mainly considered in calculations.

$$\eta_{ex} = \text{Products / Fuel} = (\text{product} + \text{waste\_energy} - (\text{heat} + \text{work})) / \text{fuel} \quad (4)$$

Fuel in Equation 4 is the main fuel used in the boiler and products are the produced steam, or hydrogen stream (in pre-combustion technologies) and waste energy coming from CO_2 capture system. Some examples of the application of the exergy analysis are presented for post-combustion, oxy-combustion and pre-combustion CO_2 capture technologies in Lara's work. The main target is to identify the equipment with larger irreversibilities and to propose items for future optimization.

Another case of exergy analysis is studied for an integrated gasification combined cycle power plant with CO_2 capture using hot potassium carbonate solvent (Li et al. 2014, 14814-14821). Exergy analysis is used to describe the destruction of the work availability that occurs, identify where the most inefficient parts of the process are, and also highlight the sub processes which require optimization in order to improve the whole plant efficiency. Equation 4 shows the exergy balance of a control volume at steady state conditions.

$$\int (1-T0/Tj)Q - W + \sum MinEin - \sum MoutEout - Xdes = 0 \quad (5)$$

The term $\int(1-T_0/Tj)Q$ and W refer to the heat exergy input or output and work input or output into a control volume ,respectively; M is the molar flow rate; E represents the specific exergy; X_{des} represents the amount of exergy destruction with the control volume due to irreversibilities.

The specific exergy includes both physical and chemical exergies, which is expressed in Equation 6.

$$E = E_{ph} + E_{ch} \quad (6)$$

On the basic of Equation 5 and 6, the exergy balance for each sub process of power plant with carbon capture can be obtained. Compared to the base power plant, the exergy destruction and emissions in the power plant with carbon capture can be calculated.

The above two cases focus more on the process optimization for the power plant with carbon capture. The applied exergy analysis method, although their detailed expression are different, are both used to optimize the energy consumption of a complex system including the original power plant and the new process. However, these thermodynamic evaluation indicators and relevant research method are both around a specific system.

The third case is studied to show the application feasibility of CP model in energy efficiency analysis of CO_2 capture. Its research aim and the related mathematical tool - 2nd law efficiency, as mentioned in section 2, are proposed to evaluate the development level of CCS technologies and the maturity distance to the ideal status of studies technologies.

This case is based on a simulation study on 800MW_e supercritical PC-fired power plant with CO_2 capture and compression. The setting parameters of reference plant are shown in tab 1 as well as simulated results. It can be found that the 2nd law efficiency of studied CCS technology – chemical absorption method via MEA is 14.93%. Based on the proposed CP model and existing researches, the performance map for various CCS technologies can be provided. A preliminary result is shown in fig. 5. Furthermore, the proposed CP cycle model, which has more details inside the CP model, can be applied in the discussion of efficient integration of solar energy into CCS.

Table 17: Parameters of case 1 (Sanpasertparnich et al., 2010, 502-504)

Parameters	Value
Setting parameter in reference:	
Mole fraction of CO_2 in flue gas (vol%)	14.98
Capture rate / efficiency (%)	90
Simulated result in reference:	
Reboiler heat duty (kJ/kg)	3973.13
Electricity consumption (kJ/kg)	52.85
Calculated result based on CP model :	
Ideal minimum work (kJ/kg)	154.67
Real consumed work (kJ/kg)	1035.73
Second law efficiency (%)	14.93

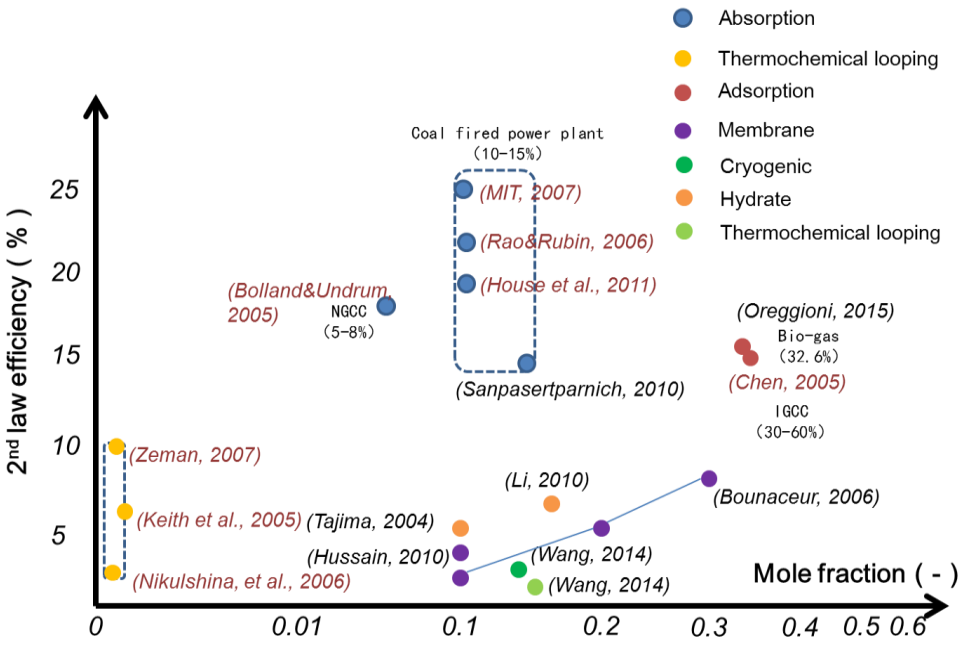

Figure 5: Performance windows for various CO_2 capture technologies

6. SUMMARY REMARKS

In summary, the application feasibility of proposed carbon pump model on the performance evaluation of CCS technology has been proved through a preliminary study. Three summary remarks are:

- Carbon pump model is proposed for the performance evaluation of various CCS technologies and it is an updated model of ideal separation process
- It is feasible for the CP model to evaluate the perfectness of various CCS technologies. The calculation, which is based on the existing results from publications and CP model, the 2nd law efficiency of chemical absorption method, is in the range of 15-25%, when the mole fraction of CO_2 in flue gas is 10-15%. The 2nd law efficiency of chemical adsorption method is about 10% based on results from two publication papers, however, the mole fraction of CO_2 before capture is from 30% to 35%, that is a typical range for bio-syngas or pre-combustion application.
- However, CP model is still a lumped model without inside details on carbon potential. Thus, it is near impossible to apply it to answer the question of “how to efficiently integrate the solar energy into CO_2 capture”. A CP cycle model is proposed so that possible integration solution of solar energy in different grades can be studied in the next step.

7. ACKNOWLEDGMENT

The authors thank for the financial support from 2015 research plan of application foundation and advanced technology of Tianjin city (Project: Guideline developing and optimization research on integrating solar energy utilization into CO2 capture system).

8. REFERENCES

CHAFFEE, A. L., et al., 2007. CO2 capture by adsorption: Materials and process development. International Journal of Greenhouse Gas Control. 1, 11-18.

DOE/NETL, 2011. Research and Development Goals for CO2 Capture Technology. http://www.netl.doe.gov/File%20Library/Research/Energy%20Analysis/Publications/DOE-NETL-2009-1366-R-DGoalsforCO2CaptureTech.pdf.

HEDIN, H., et al., 2013. Adsorbents for the post-combustion capture of CO2 using rapid temperature swing or vacuum swing adsorption, Applied Energy, 104, 418-433.

KING, C., 1980. Separation processes. 2nd. USA: McGraw-Hill. 1.

KOTHANDARAMAN, A., et al., 2009. Comparison of solvents for post-combustion capture of CO2 by chemical absorption. Energy procedia, 1, 1373-1380.

LARA, Yolanda, et al. 2011. Using the second law of thermodynamic to improve CO2 capture systems. Energy Procedia,4, 1043-1050.

LI, Sheng, et al. 2014. Energy and Exergy Analyses of an Integrated Gasification Combined Cycle Power Plant with CO2 Capture Using Hot Potassium Carbonate Solvent. Environmental science & technology, 48(24), 14814-14821.

MARKEWITZ, P., et al., 2012. Worldwide innovations in the development of carbon capture technologies and the utilization of CO2. Energy & Environmental Science, 5, 7281-7305.

OEXMANN, J., Kather, A., 2010. Minimising the regeneration heat duty of post-combustion CO2 capture by wet chemical absorption: the misguided focus on low heat of absorption solvents. International Journal of Greenhouse Gas Control, 4, 36-43.

RUAN, X. H., 2014. Chemical potential analysis for directing the optimal design of gas membrane separation frameworks. Chemical Engineering Science, 107, 245-255.

SANPASERTPARNICH, T., et al., 2010. Integration of post-combustion capture and storage into a pulverized coal-fired power plant. International Journal of Greenhouse Gas Control, 4(3), 499-510.

Seader, J. D., et al., 2011. Separation process principles: Chemical and Biochemical Operations. 3rd. USA: John Wiley & Sons. 1.

Sjostrom, S., Krutka, H., 2010, Evaluation of solid sorbents as a retrofit technology for CO2 capture, Fuel, 89, 1298-1306.

Wall, T. F., 2007. Combustion processes for carbon capture. 31st International Symposium on Combustion, 31: 31-47. 5-11, Aug, 2006. Heidelberg, Germany: Elsevier.

Wilcox, J. , et al., 2012. Carbon capture. 1st. USA: Springer. 1.

Zhao, R.K., et al., 2015. Energy-saving pathway exploration of CCS integrated with solar energy: literature research and comparative analysis. Energy conversion and management, DOI: 10.1016/j.enconman.2015.01.018.

312: Kinetics of direct CO_2 capture from ambient air Using K_2CO_3/Al_2O_3 composite sorbent

JANNA VESELOVSKAYA[1], VLADIMIR DEREVSCHIKOV[2], ALEKSEY OKUNEV[3]

1 Boreskov Institute of Catalysis, Pr. Ak. Lavrentieva, 5, Novosibirsk, 630090, Russia; Novosibirsk State University, Pirogova str., 2, Novosibirsk, 630090, Russia; Research and Educational Center for Energy Efficient Catalysis in Novosibirsk State University, Pirogova str., 2, Novosibirsk, 630090, Russia, jvv@catalysis.ru
2 Boreskov Institute of Catalysis, Pr. Ak. Lavrentieva, 5, Novosibirsk, 630090, Russia; Novosibirsk State University, Pirogova str., 2, Novosibirsk, 630090, Russia; Research and Educational Center for Energy Efficient Catalysis in Novosibirsk State University, Pirogova str., 2, Novosibirsk, 630090, Russia
3 Novosibirsk State University, Pirogova str., 2, Novosibirsk, 630090, Russia, Boreskov Institute of Catalysis, Pr. Ak. Lavrentieva, 5, Novosibirsk, 630090, Russia

The composite material K2CO3/Al2O3 is a promising solid absorbent for direct CO2 capture from ambient air. In the current work the kinetics of CO2 absorption by this composite material was studied in the perfectly mixed reactor. The dependence of CO2 absorption rate on temperature and characteristic grain size of the composite sorbent was investigated. It was revealed that the total CO2 uptake decreases in the temperature range from 50 to 80oC. Comparison of CO2 absorption kinetics of by fractions of the composite with characteristic grain sizes of 0.8-1.0 mm and 1.6-2.0 mm showed that the initial rate of CO2 absorption inversely depends on characteristic grain size of the composite material, which indicates that the absorption process is limited by mass transfer. The results obtained are of interest for the capture of air-borne CO2 with subsequent renewable methane production using H2 from alternative sources of energy.

Keywords: renewable energy storage, direct air capture, carbon dioxide, potassium carbonate, alumina

1. INTRODUCTION

The major challenge of our time is filling the gap between energy supply and demand with clean, reliable and inexpensive energy. Given depletion of fossil fuels, renewable energy technologies will need to play a bigger role in the future. However, there are still some unresolved problems that prevent these technologies from being economically viable on a large scale.

One of the main issues of power systems based on renewables, such as wind and solar energy, is volatility of the power supply. Hence, a storage technology is needed for electrical energy, produced by these fluctuating sources. The use of excess renewable electricity for production of synthetic fuels offers a realistic solution to this challenge, which enables an offsetting in the time gap between power production and its consumption.

The surplus electricity generated by renewables can be used for water electrolysis in order to produce hydrogen: $2H_2O \xrightarrow{electrolysis} 2H_2 + O_2$.

Hydrogen is considered to be a perspective fuel for low-carbon economy, but there are still unresolved safety problems regarding its transportation and storage. Therefore, it is reasonable to use the generated hydrogen for production of a conventional hydrocarbon fuel, e.g. methane, which can be obtained by Sabatier process: $CO_2 + 4H_2 \rightarrow CH_4 + 2H_2O$. The synthetic renewable methane, which corresponds to chemically normal natural gas, can be injected into the existing gas network or stored and utilized on demand.

It is very important for sustainable development that renewable methane can be produced using carbon dioxide captured from ambient air. It is well known that CO_2 is the major anthropogenic greenhouse gas which contributes to global climate change. Direct CO_2 capture from ambient air (a.k.a. “direct air capture”, DAC) offers more flexibility compared to conventional source point capture and can potentially be “carbon negative” if a renewable energy source is used to drive the process. Incorporation of the DAC unit with into the energy storage system offers an opportunity to use anthropogenic carbon dioxide as a valuable feedstock for the production of renewable methane which can be utilized in the heating market or as a fuel for transportation.

Carbon dioxide capture from ambient air is more challenging than conventional carbon capture from flue gases because of very low concentration of CO_2 in air (~ 400 ppm) and the necessity to operate in the presence of moisture excess at ambient temperature and pressure. The most developed DAC technologies are based on carbon dioxide absorption by aqueous alkali solutions. The major drawback of this approach is that the regeneration of these solutions is generally multi-stage and energy intensive.

Potassium carbonate is a well-known solid inorganic chemisorbent which reacts with atmospheric CO_2 in the presence of water vapour forming potassium bicarbonate: $K_2CO_3 + H_2O + CO_2 \rightarrow 2KHCO_3$.

The main problem with using bulk potassium carbonate for CO_2 absorption purposes is low carbonation rate (Okunev, 2000, p. 355). This problem can be solved by dispersing K_2CO_3 particles inside a porous support material. Composite materials “potassium carbonate inside a porous matrix” are known to be effective sorbents for capturing carbon dioxide from wet flue gases (Hayashi, 1998, p. 185; Lee, 2006, p. 385, Okunev, 2000, p. 355; Zhao, 2006, p. 4683).

Recently, it was also shown that K_2CO_3/γ-Al_2O_3 composite is a promising material for CO_2 capture directly from ambient air (Veselovskaya, 2013, p. 332). The composite was able to absorb CO_2 directly from ambient air without any pretreatment (such as drying) and showed great thermal stability in multiple temperature-swing absorption (TSA) cycles. However, a room for improvement of the composite materials CO_2 absorption properties still exists. The aim of this work was to study kinetics of CO_2 absorption form ambient air by K_2CO_3/γ-Al_2O_3 composite material in order to understand which factors define the rate of CO_2 capture.

2. MATERIAL AND METHODS

2.1 Composite Sorbent Preparation and Characterization

Composite sorbent K_2CO_3/γ-Al_2O_3 was prepared by dry impregnation method, described in detail in (Veselovskaya, 2013, p. 333). Granular γ-Al_2O_3 (A-64) produced by JSC «Angarsk Catalysts and Organic Synthesis Plant» was used as a host matrix. Cylindrical alumina granules with diameter of 3 mm and typical length of 4-6 mm were filled with 40 wt. % aqueous solution of potassium carbonate, dried at 100°C for 24 h and then calcinated at 300°C for 2 h. Potassium loading for the composite sorbent determined by means of atomic absorption spectroscopy is 12.5 wt. %, which is equivalent to 22.1 wt. % of K_2CO_3. The resulted product was crushed and sieved to obtain the desired particle size range fractions: 1.6-2.0 mm and 0.8-1.0 mm.

The phase composition for the samples of the composite sorbent was determined from powder X-ray diffraction (XRD) patterns which were obtained on a Brucker D8 Advance diffractometer using Cu K_α radiation. Diffraction intensities were measured with the LynxEye position sensitive detector (2.9° angular range). XRD patterns were collected in 2θ range 10-70°, with 0.02° step size and 2s collection time. Variation of the phase composition of the composite sorbent owing to heating and cooling of the composite sorbent in air were studied by XRD analysis *in situ* by Siemens D-500 X-ray diffractometer equipped with graphite monochromator on the diffracted beam using Cu K_α radiation. Diffraction patterns were detected in the 10°-50° (2θ) region by points with the 0.05° (2θ) step.

2.2 CO_2 absorption in the perfectly mixed reactor

CO_2 absorption kinetics by the composite material was studied using the perfectly mixed laboratory reactor), schematically shown in Figure 1. In a perfectly mixed reactor, concentrations and temperature are uniform and a high gas velocity around the particles of the sorbent allows avoiding interparticle transport limitations.

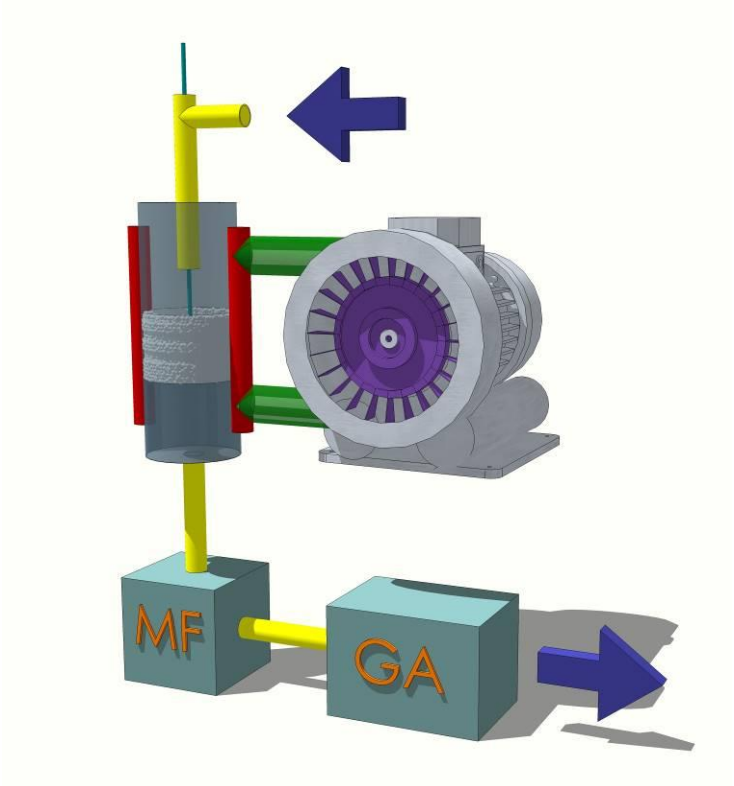

Figure 1. The perfectly mixed reactor for measuring CO_2 absorption from air (MF = mass flowmeter, GA = gas analyser).

The mixture of sorbent particles and quartz balls (D = 3 mm) was placed into a cylindrical steel tube reactor 18 mm ID located inside an electrical heater. Quartz balls were used for the improvement of heat and mass transfer in sorbent bed. The typical mass of the composite material loaded was 0.2 g.

Before the measurement of CO_2 absorption from air, a sample of the composite sorbent was regenerated at 300°C inside the reactor, as the air from compressed air line was purged directly through the reactor without any mixing. After that, the reactor was cooled down with no air purging. This temperature was maintained constant during the absorption experiments. Temperature monitoring during the whole experiment was carried out using a thermocouple, installed in the centre of the bed.

During the absorption experiment air from compressed air line was preliminarily humidified by passing it through a water evaporator, placed inside a thermostat at T=25°C. The outlet flow rate of air during the isothermal absorption experiment was controlled by the mass flowmeter SMC PFMV-5 and maintained 0.4 dm^3/min. Perfect mixing in the reactor was achieved by circulating air by means of the external pump. The rate of gas mixing in the reactor was 12 times more than outer flow rate. The initial CO_2 concentration in the air was 530-560 ppm. The outlet CO_2 concentration was measured by gas analyzer OPTOGAZ-500.4C.

3. RESULTS AND DISCUSSION

3.1 The effect of the characteristic grain size

CO_2 absorption kinetic curves for the samples with different characteristic grain size were measured in the perfectly mixed reactor at T=50°C (Figure 2). One can see that the minimal value of outlet CO_2 concentration differs significantly in these experiments, which indicates that the initial rate of CO_2 absorption depends on characteristic grain size of the sorbent.

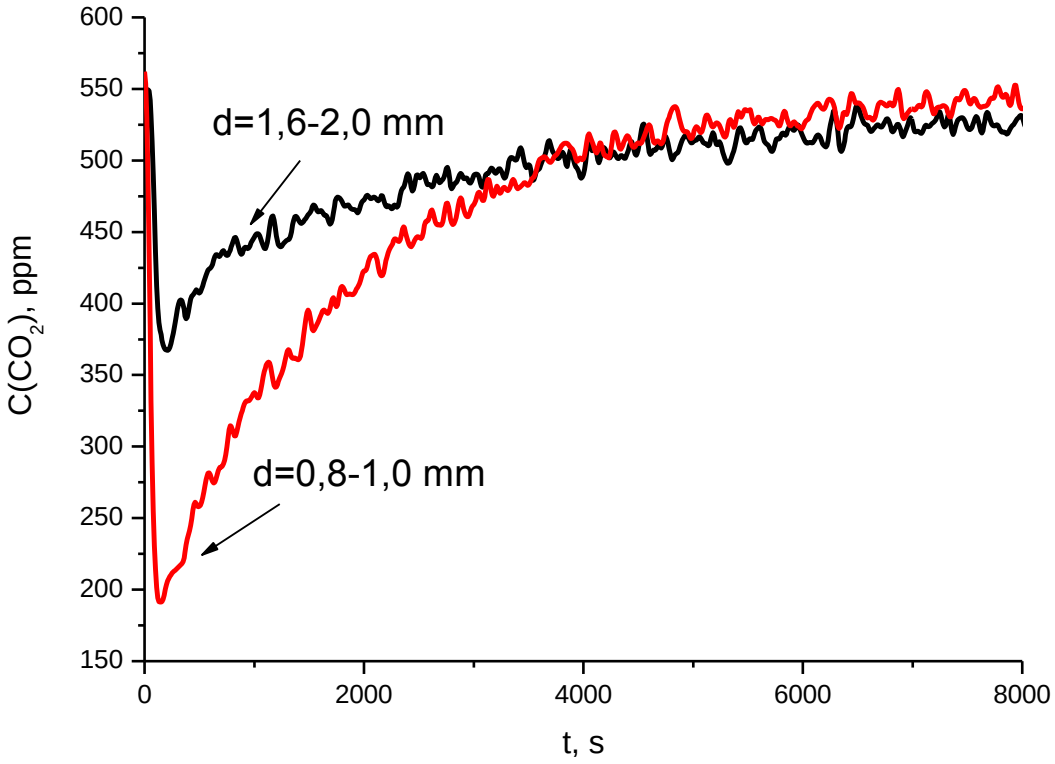

Figure 2. CO_2 absorption curves for the samples with different characteristic grain size (T=50°C, U=0.4 dm^3/min).

The maximal rate of CO_2 absorption was calculated as follows:

Equation 11: The maximal rate of CO_2 absorption

$$W_{max} = \frac{U \cdot (C_o - C_{min})}{m_s}$$

Where:

- W_{max} = the maximal rate of absorption for the sample (in $cm^3(CO_2)/min/g$)
- U = flow rate (in cm^3/min)
- C_0 = inlet CO_2 concentration (in vol.%/100%)
- C_{min} = minimal outlet CO_2 concentration (in vol.%/100%)
- m_s = mass of the sample (in g)

It was demonstrated that the maximal rate of absorption is inversely proportional to the characteristic grain size (Figure 3). The strong dependence of the rate of absorption on characteristic grain size indicates that the process of CO_2 absorption by the composite material is limited by mass transfer within the composite grain.

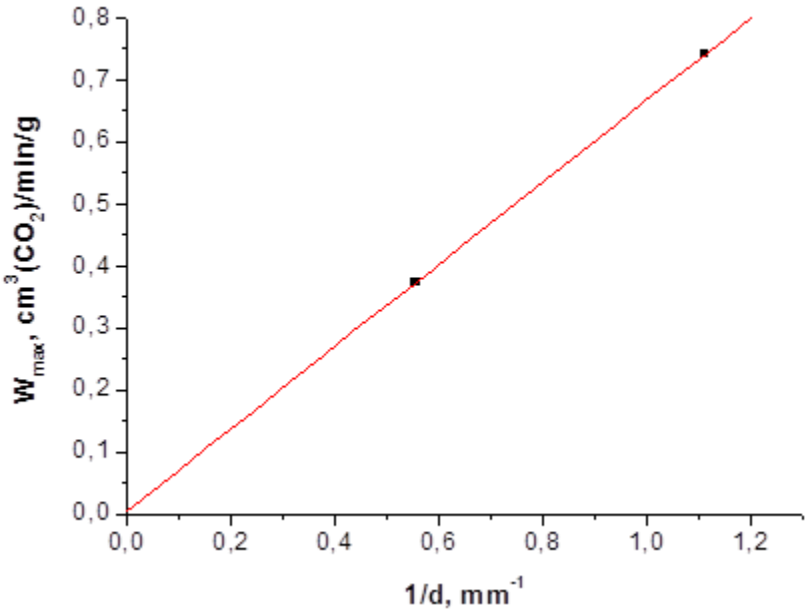

Figure 3. Maximal rate of CO_2 absorption versus reciprocal characteristic grain size of the composite particles (experimental conditions: T = 50°C, U = 400 cm^3/min, m_s = 0.2 g)

CO_2 uptake by the composite material was calculated as follows:

Equation 2: CO_2 uptake calculation

$$a(t) = \frac{U \cdot M_{CO_2}}{V_m \cdot m_s} \int_0^t (C_0 - C(t))dt$$

Where:

- $a(t)$ = *CO_2 uptake (in wt.%)*
- U = flow rate (in cm^3/min)
- C_0 = inlet CO_2 concentration (in vol.%)
- $C(t)$ = outlet CO_2 concentration (in vol.%)
- m_s = mass of the sample (in g)
- t = time (in s)
- V_m = the molar volume of the ideal gas at the standard conditions (24.4 dm^3/mol)
- M_{CO_2} is molar weight of CO_2 (44 g/mol)

The kinetic curves illustrating CO_2 uptake temporal evolution for the samples with different characteristic grain size are presented in Figure 4. One can see both samples reach the same level of total CO_2 uptake but the time of saturation is much shorter for the sample with characteristic grain size of 0.8-1.0 mm. Thus, reduction of the characteristic grain size allows shortening the duration of the absorption step in the TSA cycle, which is preferable for practical applications.

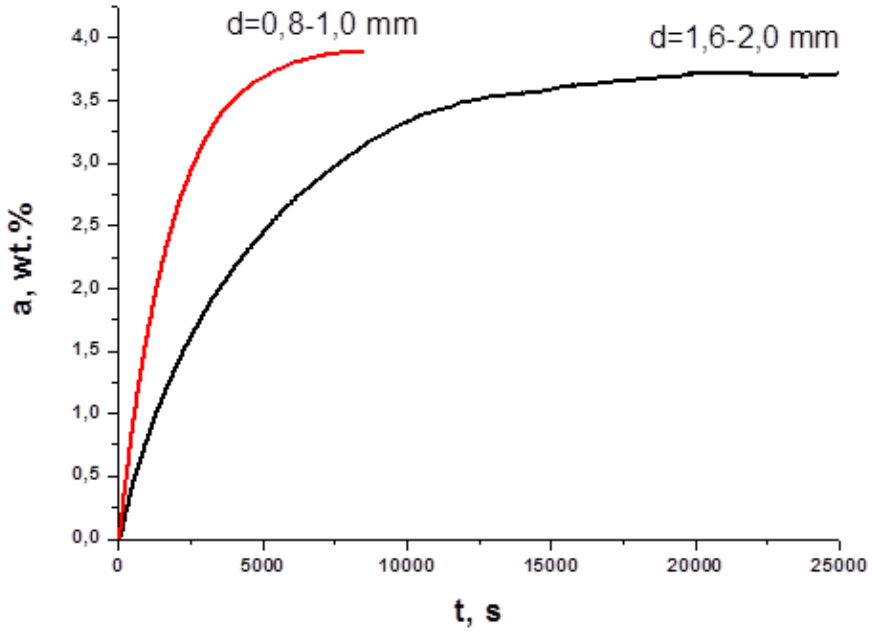

Figure 4. Kinetic CO_2 uptake curves for the samples with different characteristic grain size: d=0.8-1.0 mm and d=1.6-2.0 mm (T=50°C, U=0.4 dm³/min)

3.2 The effect of temperature

The effect of temperature on CO_2 absorption behaviour of the composite was studied for the sample with the characteristic grain size of 0.8-1.0 mm. CO_2 absorption curves were measured in the temperature range from 40 to 80°C. Integral kinetic CO_2 uptake curves calculated from experimental data are presented in Figure 5.

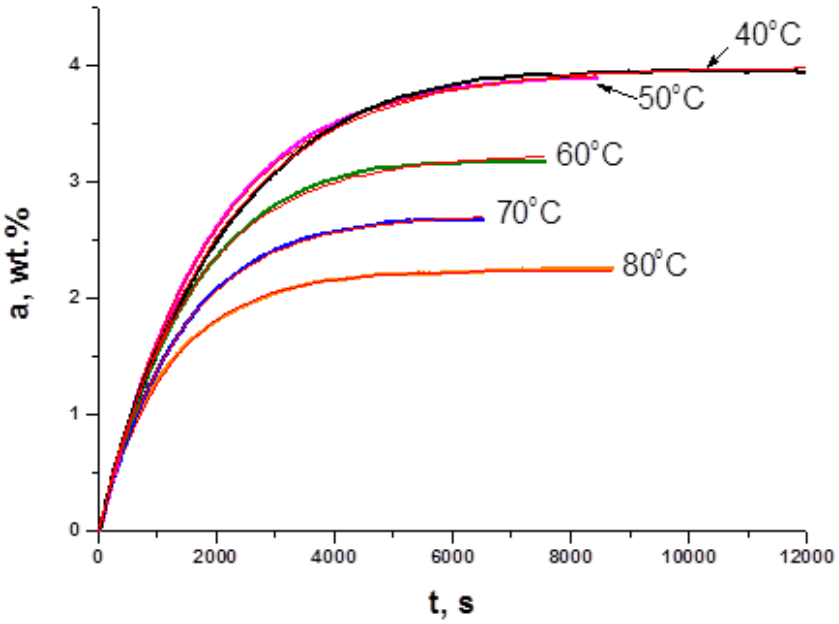

Figure 5. Kinetic CO_2 uptake curves for the samples with different characteristic grain size: d=0.8-1.0 mm and d=1.6-2.0 mm (T=50°C, U=0.4 dm³/min)

All the curves were approximated by exponential law:

Equation 3: CO_2 uptake approximation

$$a(t) = a_{tot} \cdot (1 - e^{-kt})$$

Where:

- $a(t)$ = CO_2 uptake (in wt.%)
- a_{tot} = *total CO_2 uptake* (in wt.%)
- k = rate constant (in s^{-1})
- t = time (in s)

The values of a_{tot} и k for all the experiments at different temperatures are presented in Table 1.

Table 18: The values of total CO_2 uptake and rate constant for different absorption temperatures

Temperature of absorption, °C	a_{tot}, wt.%	$k*10^4$, s^{-1}
40	4.0	5.0
50	4.0	5.3
60	3.2	6.4
70	2.7	7.1
80	2.2	8.3

It was demonstrated that total CO_2 uptake of the sample monotonously decreases in the temperature range from 50 to 80°C. On the other hand, the values of the total CO_2 uptake are the same for experiments conducted at T=40°C and T=50°C. Apparently, the total amount of CO_2 captured by the composite material is defined by absorption equilibrium in the system. In order to reach a maximal saturation of the material with CO_2 the absorption process should be conducted at temperature no higher than 50°C.

The crystalline products of CO_2 absorption at different temperatures have been characterized by means of XRD analysis (Table 2). It was demonstrated that phase composition is not the same for the samples saturated with CO_2 at 40 and 80°C. After CO_2 absorption at 40°C the crystalline phases of potassium bicarbonate $KHCO_3$ and potassium dawsonite $KAlCO_3(OH)_2$ are present in the sample, which is in line with our previous results (Veselovskaya, 2013, p. 335). On the other hand, XRD pattern for the sample after CO_2 absorption at 80°C does not show characteristic reflections for potassium bicarbonate or potassium dawsonite. The only crystalline phase detected for the latter sample is highly defected potassium carbonate K_2CO_3. Thus, the products of CO_2 absorption are X-ray amorphous if the absorption process takes place at 80°C. The observed difference in phase composition between these 2 samples confirms the hypothesis that absorption equilibrium in the system defines the value of CO_2 uptake at given temperature.

Table 2: Phase composition for samples of the composite (d=0.8-1.0 mm) after CO_2 absorption at different temperatures

Temperature of absorption, °C	Crystalline phases
40	$KHCO_3$, $KAlCO_3(OH)_2$
80	K_2CO_3 (defected)

4. CONCLUSIONS

Kinetics of CO_2 absorption by K_2CO_3/Al_2O_3 sorbent was studied in the perfectly mixed reactor. Two fractions of the sorbent (d=0.8-1.0 mm and d=1.6-2.0 mm) were investigated in order to study the grain size effect on kinetic performance of the material. It was shown that the maximal rate of CO2 absorption inversely depends on characteristic grain size of the composite material. Accordingly, the time of saturation with CO_2 (the end of absorption) is much shorter for smaller particles of the sorbent.

The effect of absorption temperature was studied for the sample with characteristic grain size of 0.8-1.0 mm. It was shown that total CO_2 uptake is stable in the temperature range 40-50°C and is decreasing in in

the temperature range 50-80°C. Apparently, the observed dependence of total CO_2 uptake on temperature is defined by absorption equilibrium of the material with CO_2.

By means of XRD analysis it was shown that temperature of CO_2 absorption also strongly affect phase composition of the composite material. Formation of the crystalline phases of potassium bicarbonate $KHCO_3$ and potassium dawsonite $KAlCO_3(OH)_2$ was observed as a result of CO_2 absorption at T=40°C. However, these crystalline phases were not formed after CO_2 absorption at T=80°C.

5. ACKNOWLEDGMENT

Authors thank Dr. Kardash T.Yu. for performing XRD analysis. The work was performed in the framework of the joint Research and Educational Center for Energy Efficient Catalysis (Novosibirsk State University, Boreskov Institute of Catalysis). The reported study was supported by RFBR, research project No. 14-03-31731 mol_a.

6. REFERENCES

HAYASHI, H., Taniuchi, J., Furuyashiki, N., Sugiyama, S., Hirano, S., Shigemoto, N., Nonaka, T., 1998. Efficient recovery of carbon dioxide from flue gases of coal-fired power plants by cyclic fixed-bed operations over K_2CO_3-on-carbon, *Ind. Eng. Chem. Res.* 37, p. 185-191.

LEE, S.C., Choi, B.Y., Lee, T.J., Ryu, C.K., Ahn, Y.S., Kim, J.C., 2006. CO_2 absorption and regeneration of alkali metal-based solid sorbents, *Catal. Today* 111, p. 385-390.

OKUNEV, A.G., Sharonov, V.E., Aristov, Yu.I., Parmon, V.N., 2000. Sorption of carbon dioxide from wet gases by K_2CO_3-in-porous matrix: influence of the matrix nature, *React. Kinet. Catal. Lett.* 71, p. 355-362.

VESELOVSKAYA, J.V., Derevschikov, V.S., Kardash, T.Yu., Stonkus, O.A., Trubitsina, T.A., Okunev, A.G., 2013. Direct CO_2 capture from ambient air using K_2CO_3/Al_2O_3 composite sorbent, *Int. J. Greenhouse Gas Control*, 17, p. 332-340.

ZHAO, C., Chen, X., Zhao, C., 2009. CO_2 absorption using dry potassium-based sorbents with different supports, *Energy Fuels*, 23, 4683-4687.

POSTER SESSION A

293: SOC management of BESS for frequency regulation with hysteresis loop control

JIN-SUN YANG[1], JIN-YOUNG CHOI[2], DONG-JUN WON[3],
IN-SUN CHOI[4], GEON-HO AHN[4], YEONG-JUN CHOI[4]

1 Dept. Electrical Engineering, INHA University, Inchoen, Republic of korea,sealvoeyjs@gmail.com
2 Dept. Electrical Engineering, INHA University, Inchoen, Republic of korea,djwon@inha.ac.kr
3 Dept. Electrical Engineering, INHA University, Inchoen, Republic of korea,jy128308@gmail.com
4 Dept. Power Grid Integration of R&D Center, Hyosung Corporation, Republic of Korea

For stably operation of BESS for frequency regulation, BESS needs a SOC management algorithm. This paper proposes that BESS changes a base point for the SOC management for stable operation to keep high performance score. To manage SOC of BESS providing frequency regulation, the base point is changed in accordance with a proposed hysteresis loop control when the SOC exceeds a limit, BESS provides the additional output as much as changed base point more than a regulation set point. Through this process, BESS recovers SOC and keeps stable operation range and high performance score. Three cases are observed: 1) without hysteresis loop control; 2) using hysteresis loop control; 3) using hysteresis loop control at high SOC. Cases simulated by using PSCAD/EMTDC. For the accuracy of simulation, this paper performs simulation based on real frequency regulation signal data of the PJM in USA. First case simulation shows that the SOC exceeds stable range and this situation finally causes shutdown the BESS because SOC reaches full. Second case simulation shows that SOC is managed in stable operating range. And final case shows that BESS is recovered from high SOC. This means BESS operators should set proper operation range and SOC limit for the SOC management. A simulation results show that if the proposed algorithm is applied to BESS for frequency regulation, the BESS is able to keep high performance score. Also proposed algorithm can be applied to BESS to perform other roles in power system.

Keywords: Battery energy storage system, state of charge management, regulation set point, base point, frequency regulation

1. INTRODUCTION

Today battery energy storage system (BESS) is widely used in power system by performing various purposes as peak shaving, integrated renewable sources, frequency regulation and etc. Recent related works have shown that the BESS can use various purposes. Reference [1] shows that proposed method can optimize size of the BESS and cost-benefit analysis when the BESS is applied voltage regulation and peak shaving in the high photovoltaic (PV) penetration. PV and wind farm usually installed BESS to solve their intermittent characteristics. In [2], study to reduce the fluctuation of the wind power and PV hybrid generation system (WPPVGS) using BESS is proposed. According to fluctuation, method in [2] effectively regulates power output of BESS and manages SOC. Reference [3] proposes a frequency regulation method with SOC feedback system using wind and BESS hybrid system. Power output is regulated according to frequency deviation and SOC feedback.

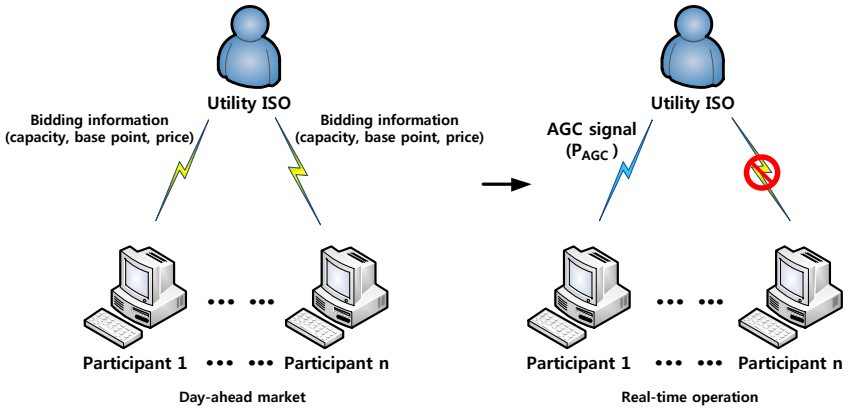

Figure 69: Frequency regulation market concept

In recent years, power system operators focus on participation in frequency regulation (or secondary reserve) of BESS because that quickly respond to signal due to fast ramping rate more than conventional resources. Recent studies include method and analysis of frequency regulation using BESS for microgrid and main grid [4-7]. For explanation, frequency regulation market concept described in Figure 1. In main grid scope, power system operators, such as independent system operators (ISOs) notify requirements in day-ahead market for frequency regulation. Each participant submits bid information (such as hourly bid capacity, hourly bid base point and price information) to succeed bidding in day-ahead market. In real-time operation, ISO sends automatic generation control (AGC) dispatch signal to the participants who bid successfully, participant provides power output to perform frequency regulation. Frequency regulation is the injection or withdrawal of active power by participants in response to an AGC signal to meet the needs of power system [8]. In case of BESS, performs charging or discharging in response to an AGC signal.

On October 20, 2011, federal energy regulatory commission (FERC) published Order No.755 [9] related to performance of resource providing the frequency regulation. If resource provides accurate output in response to AGC signal, resource receives high credits due to high performance score,

This paper proposes the SOC management algorithm of BESS providing frequency regulation to operate in stable range to keep high performance score. BESS for frequency regulation provides output according to a regulation set point and a base point. We proposes SOC management algorithm, which changes the base point through rebidding in frequency regulation market. Owing to the battery efficiency and power conversion system (PCS) efficiency, SOC slowly deviates from stable range whenever BESS preforms frequency regulation, and finally BESS will be shut down due to stable range deviation. Proposed algorithm performs additional charging or discharging by changing base point through rebidding to avoid shutdown of BESS and keeps high performance score. This paper provides a new contribution by managing the SOC through changing base point. In addition, to enhance justification of result, use real AGC signal data.

2. SOC MANAGEMENT ALGORITHM

BESS provides the frequency regulation through two signals. First signal is an automatic generation control (AGC) dispatching signal, which is so called “regulation set point”. This signal receives from the energy management system (EMS) of ISO. Second signal is a basic operation signal of the BESS, which is so called “base point” This signal is obtained from the economic dispatch of ISO or the request from operators.

The concept of output point, regulation set point and base point is depicted in Figure 2 (a). BESS basically provides output as much as base point. If base point is negative, basic output point of BESS is a discharging range. Whereas if base point is positive, basic output point of BESS is a charging range. Since the base point was set, BESS receives AGC signal and provides additional output as much as regulation set point. As a result, BESS provides output as base point plus regulation set point. Proposed algorithm changes base point through rebidding for SOC management. When the base point is changed, BESS provides output as a changed base point plus regulation set point. Due to changed base point, SOC recovers to stable range, and BESS will still performs frequency regulation according to AGC signal. This section explains output equation of BESS, SOC calculation equation, and SOC management algorithm through hysteresis loop control.

Output equation

Regulation set point and base point is per-unit (p.u) form. BESS provides the output as a regulation set point plus a base point [8].

Equation 12: Output of BESS for frequency regulation

$$OP_{.t} = SP_{.t} + BP_{.t}$$

Where

- $OP_{.t}$ = total output point of BESS for time t (p.u)
- $SP_{.t}$ = output point by the regulation set point for time t(p.u)
- $BP_{.t}$ = output point by the base point for time t (p.u)
- t = index of time (sec)

$BP_{.t}$ is changed every hour on the hour, $SP_{.t}$ is changed according to AGC signal cycle of ISO.

SOC calculation

SOC equation consist of charging equation and discharging equation. If $OP_{.t}$ is positive, BESS provides frequency regulation by charging. When receiving negative $OP_{.t}$, BESS performs discharging to provide frequency regulation. SOC is calculated as follow [10] :

Equation 13: SOC of BESS by $OP_{.t}$

$$SOC_{t+1} = SOC_t - \left(\frac{C_t \times (OP_{.t})}{C_{rate}} \times \Delta t \right) \times \eta \times 100\,[\%] \qquad (OP_{.t} > 0)$$

$$SOC_{t+1} = SOC_t - \left(\frac{C_t \times (OP_{.t})}{C_{rate}} \times \Delta t \right) \div \eta \times 100\,[\%] \qquad (OP_{.t} < 0)$$

- SOC_t = SOC of BESS for time t (%)
- C_t = bid capacity for time t (MW)
- C_{rate}= rated capacity of BESS (MWh)
- Δt = time difference (sec)
- η = BESS efficiency (%)

Hysteresis loop control

In this section, we explained hysteresis loop control. The $OP_{.t}$ is only $SP_{.t}$ when SOC in stable range through Equation 1 because $BP_{.t}$ is zero. Then SOC exceeds stable range, proposed algorithm changes $BP_{.t}$ for SOC management in stable range. Due to changed $BP_{.t}$, $OP_{.t}$ is set as $SP_{.t}$ plus BP_{ch} (or BP_{dis}) to perform additional output. But the bid capacity decreases according to changed base point as much as ratio of base point and maximum bid capacity.

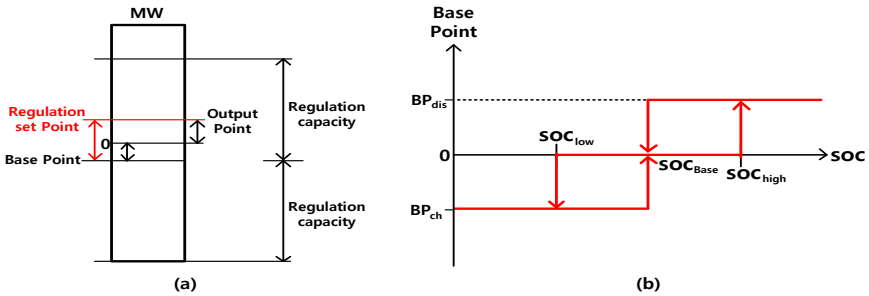

Figure 2: (a)concept of out point, regulation set point and base point (b)concept of hysteresis loop algorithm

As shown Figure 2 (b). When the SOC is between SOC_{low} and SOC_{high}, $BP_{.t}$ is set zero. Then the BESS operates only as much as $SP_{.t}$, that means BESS do not provide the additional output, thus this method is the best economical method because that can bid the maximum bid capacity. However it is difficult to manage SOC, due to the absence of control for SOC management. When the SOC is below SOC_{low}, $BP_{.t}$ is set BP_{ch}. Then the BESS operates as $SP_{.t}$ plus BP_{ch}, and provides as much as more BP_{ch} until the SOC crosses SOC_{base}. The algorithm manages the SOC by changing $BP_{.t}$. The BESS provides the output so as to recover the SOC in stable range. But the proposed algorithm reduces the bid capacity credit by the decrease of bid capacity. The same method is applied to the discharging case.

3. SIMULATION RESULTS

In this section, we observe simulation result to confirm the performance of proposed algorithm. Cases simulated by using PSCAD/EMTDC, and simulation time sets one day. Simulation used real frequency regulation signal data in 17 May, 2013 of the PJM in USA. The AGC signal cycle of PJM is 2 sec. Li-ion batteries are used as the BESS. The capacity of the Li-ion batteries is 4MW/2MWh, thus maximum bid capacity C_t is 4MW and C_{rate} is 2MWh. The charging/discharging efficiency η is 89%, stable operation range is between 40% and 80%. Other setting value is shown Table I. According to the PJM market rules, the base point can change every hour on the hour and then keeps 1hour.

Table 1: initial SOC and hysteresis loop control parameters

	initial SOC	SOC_{base}	SOC_{low}	SOC_{high}	BP_{ch}	BP_{dis}	algorithm
Case 1	65 %	60 %	40 %	80 %	-0.1	0.1	X
Case 2	65 %	60 %	40 %	80 %	-0.1	0.1	O
Case 3	85 %	60 %	40 %	80 %	-0.1	0.1	O

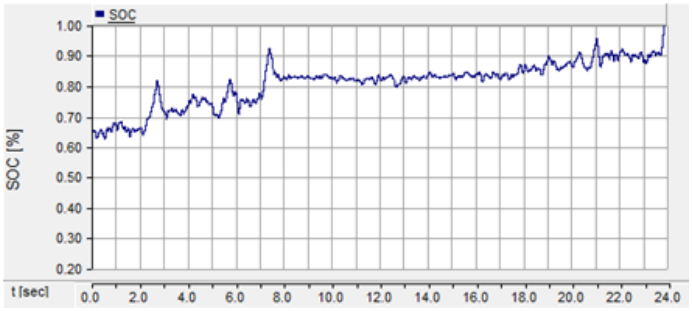

Figure 3: SOC without hysteresis loop control

Case 1 simulation result is shown in Figure 3, BESS performed frequency regulation in response to AGC signal without proposed algorithm. The SOC exceeded stable range at 2h and 5h. BESS operated at SOC above 80% since 7h, finally BESS were shut down because SOC reached 100% at 24h.

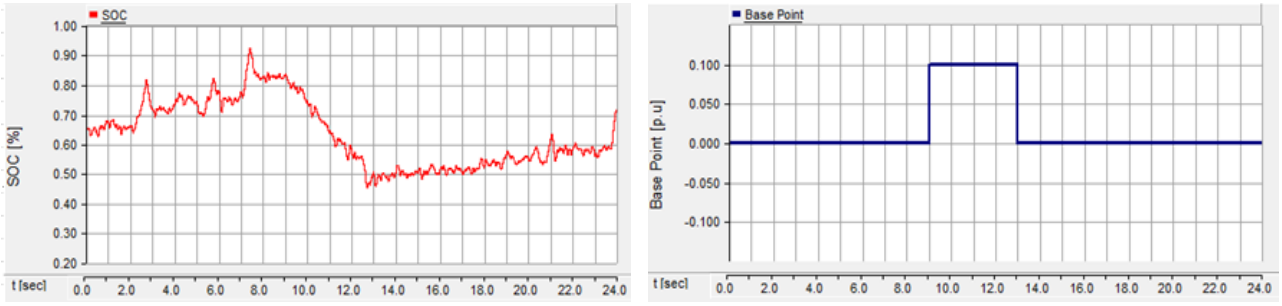

(a) (b)

Figure 4: (a) SOC with hysteresis loop control (b) base point with hysteresis loop control

As shown Figure 4, the same situation is observed in case 2 until 8h, proposed algorithm performed hysteresis loop control to decrease SOC by changing base point at 9h. Owing to changing base point by the BP_{dis}, BESS provided additional output for discharging. After 12h, SOC crossed $SOC_{base,}$ and then proposed algorithm is finished SOC management. According to the PJM market rules, proposed algorithm kept base point until 13h. Since then, BESS operated in stable range.

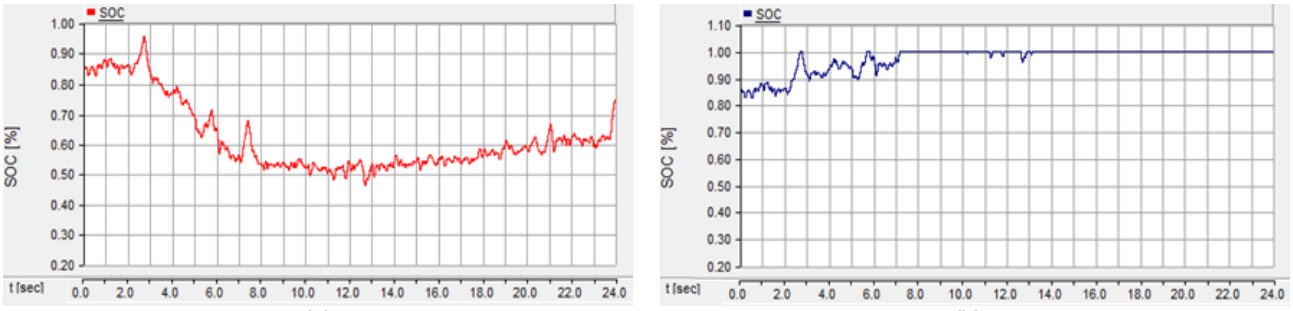

(a) (b)

Figure 5: (a) high SOC with hysteresis loop control (b) high SOC without hysteresis loop control

The SOC management result at high SOC with and without hysteresis loop control are compared in Figure 5. As shown Figure 5 (b). Owing to high initial SOC, since 7h BESS did not respond to AGC signal due to full charge. This situation causes loss, such as reduction in performance score, physical damage to BESS. In Figure 5 (a), SOC exceeded at 3h, but since 4h hysteresis loop control decreased SOC to manage the BESS and SOC stabilized after 7h.

4. CONCLUSION

In this paper, we proposed the SOC management algorithm of BESS by changing a base point. A Simulation results show that the proposed algorithm is successfully recovered the SOC. If the proposed algorithm is applied to BESS for frequency regulation, the BESS cannot only SOC management by itself without the generators but also BESS can receive high performance score because BESS can provide accurate output in response to AGC signal. Although the proposed algorithm reduces the capacity credit by the decrease of bid capacity, it will increase the total benefits through to keep high performance score.

This paper provides a new contribution by managing the SOC through changing base point. Also we used real AGC data to enhance justification of result. In frequency regulation market, BESS should have function to manage SOC because ISO don't manage SOC. Therefore proposed algorithm will be solution to solve this problem and promotes participation of BESS in frequency regulation. Also proposed algorithm can be applied to BESS to perform other roles in power system.

5. REFERENCES

[1] Ye YANG, Hui Li, Andreas Aichhorn, Jianping Zheng, Micheal Greenleaf, 2014.3. Sizing Strategy of Distributed Battery Storage System With High Penetration of Photovoltaic for Voltage Regulation and Peak Load Shaving, IEEE Transactions on smart grid, Vol. 5 No. 2, 982-991

[2] Xiangjun LI, Dong Hui, Xiaokang Lai, 2013.4. Battery Energy Storage Station (BESS)-Based Smoothing Control of Photovoltaic (PV) and Wind Power Generation Fluctuations, IEEE Transactions on sustainable energy, Vol 4. No 2, 464-473

[3] Jie DANG, John Seuss, Luv Suneja, Ronald G. Harley, 2014.3. SoC Feedback Control for Wind and ESS Hybrid Power System Frequency Regulation, IEEE Journal of emerging and selected topics in power electronics, Vol. 2 No. 1, 79-85

[4] Yi HAN, Peter Michael Young, Abhishek Jain, Daniel Zimmerle, 2015.3. Robust Control for Microgrid Frequency Deviation Reduction With Attached Storage System, IEEE Transactions on smart grid, Vol 6. No 2, 557-565

[5] Shichao LIU, Xiaoyu Wang, Peter Xiaoping Liu, 2015.4 Impact of Communication Delays on Secondary

Frequency Control in an Islanded Microgrid, IEEE Transactions on industrial electronics, VOL. 62, NO. 4, 2021-2031

[6] Ioan SERBAN, and Corneliu Marinescu, 2014.9. Control Strategy of Three-Phase Battery Energy Storage Systems for Frequency Support in Microgrids and with Uninterrupted Supply of Local Loads, IEEE Transactions on power electronics, Vol. 29 No. 9, 5010-5020

[7] Alexandre OUDALOV, Daniel Chartouni, and Christian Ohler, 2007.8. Optimizing a Battery Energy Storage System for Primary Frequency Control, IEEE Transactions on power systems, Vol. 22 No. 3, 1259-1266

[8] Alex D. PAPALEXOPOULOS, and Panagiotis E. Andrianesis, 2014.1. Performance-Based Pricing of Frequency Regulation in Electricity Markets, IEEE Transactions on power systems, Vol. 29 No. 1, 441-449

[9] Federal Energy Regulatory Commission. Order No. 755. Frequency Regulation Compensation in the organized Wholesale Power Markets, Oct. 2011. [Online], Available: http://www.ferc.gov/whats-new/comm-meet/2011/102011/E-28.pdf

[10] Massimo CERAOLO, 2000.11. New Dynamical Models of Lead-Acid Batteries, IEEE Transactions on power systems, Vol. 15 No. 4, 1184-1190

348: Assessing the benefits of installing energy storage in a household equipped with photovoltaic panels

CHRISTIAN KLUMPNER[1], ALAA EL BOUDALI[2]

1University of Nottingham, Faculty of Engineering, Department of Electrical and Electronic Engineering, University Park, Nottingham, NG7 2RD, UK, klumpner@ieee.org
2University of Nottingham, Faculty of Engineering, Department of Electrical and Electronic Engineering, University Park, Nottingham, NG7 2RD, UK, aelboudali@gmail.com

This paper evaluates the technical and financial impact of installing energy storage in a house equipped with Photovoltaic (PV) panels subject to the Feed-In Tariff (FIT). An additional benefit of installing energy storage is the possibility to purchase electricity off-peak (overnight) at a cheap rate and replace consumption during day/peak time and for this reason, the Economy7 tariff is considered.

The studies carried out are using real data of PV generation and household consumption continuously recorded over a week for each of the four seasons, from a UK installation. A functional model of the battery system is implemented that includes voltage dependency versus state of charge and maximum charging and discharging currents, that account for the limitations of the amount of charge - size dependant and current that can reflect the power capability of the battery to preserve high conversion efficiencies and lifetime.

As initial investigations point to a rather large battery system to maximize the synergy between PV and energy storage, the paper investigates how the performance indicators vary with the battery size. It is found that there may be a critical battery size up to which the peak rate consumption and the PV energy export decrease more rapidly. Above this critical point which in this study lies at around 25-30% of the battery size that would allow full local use of PV energy generated, the impact of increasing the battery size reduces, therefore the return of investment as a percentage decreases.

Keywords: battery sizing, energy storage, off peak tariff, photovoltaics

1. INTRODUCTION

Renewable energy is considered the main tool we have towards reducing greenhouse gas emissions that cause climate change. Wind power is typically exploited in large wind farms consisting of multi MW turbines whilst solar power can be converted directly into electricity via photovoltaic (PV) panels or into heat. Whilst a few large pilot solar power plants exist in the world, it is widely accepted that small scale (few kW) roof mounted installations deployed in tens of million houses have the capability to become a major contributor for reaching the 2020/2050 renewable energy production targets The reasons why the government supports this trend is that it can create a competitive market in the medium term, also producing the renewable energy closer to the point of consumption may in fact reduce losses of transporting and distributing electricity energy. Size of the installation remains low as there are limitations on the amount of power generated this way due to the fact that today's distribution systems are not designed to handle power travelling upstream.

Energy storage is seen as the critical technology to complement the unpredictability renewable energy. In the particular case of PV generation installed at the point of load, the use of energy storage may in fact prevent export of solar energy and therefore defer the upgrade of the distribution grids to allow bidirectional power flow. Regarding the energy storage technologies, electrochemical energy storage in the form of secondary (rechargeable) batteries is perhaps the most convenient way of storing PV energy. Various technologies exist and they have various applications and specific prices. The lead-acid batteries are still used in solar energy storage due to the low cost and also due to the predictable charging power which cannot exceed the PV panel power/current. They are however, quite heavy and bulky and for this reason, Lithium-Ion batteries, primarily used in transportation, are also been evaluated due to their small size and higher power/current capability but they are quite expensive which means these installations will be limited in terms of amount of energy that can be stored.

2. THEORETICAL POTENTIAL OF ENERGY STORAGE USED IN PV GENERATION

This study case is based on power data acquired from a UK household having installed PV generation (E.ON). The four weeks of input data that correspond for each of the seasons, of energy consumption and PV energy generation separately saved that are sampled every 5 minutes are shown in the left side of Figure 1. It is possible that by assuming an average daily export/import that can cancel the weekly deficit, to plot a weekly energy balance that can be used to estimate the theoretical size of the energy storage system that could prevent additional export of PV energy . The results are shown in the right side of Figure 1.

Table 1: Summary of the seasonal weekly consumption of a household with PV generation

	Energy Consumed	PV Energy generated	Excess(+)/Deficit(-)
Spring week	67.8kWh	52.2kWh	-15.6kWh
Summer week	62.3kWh	66.9kWh	+4.6kWh
Autumn week	77.9kWh	57.2kWh	-20.7kWh
Winter week	90.4kWh	28.4kWh	-62.0kWh
Annual (13x4week Sum)	3879.2kWh	2661.1kWh (68.6%)	

Table 2: Electrical energy price scheme consumed and generated considered in this study (spring 2014)

Single tariff	13.6p/kWh	
Econo7	Peak: 15.32p/kWh	Off peak: 6.92p/kWh
Feed in Tariff	14.9p/kWh	
Excess PV exported	4.64p/kWh	

By assuming the energy cost scheme highlighted in Table 2, it can be concluded that:

A. The cost of electricity for the household assuming that no PV is installed and that the electricity is charged at the single tariff, is £527.57. We may consider this case as our benchmark;
B. If the energy generated by the PV panels is considered, and it is assumed that the household is equipped with two meters, one counting the consumption on a single tariff as above and the second

to count the generation according to a FIT scheme including all PV as exported, the annual cost of energy becomes £527.57 - £519.98= £7.59 with the £519.98 benefit due to FIT counting as the yearly Return of Investment (ROI) for the PV equipment and installation;

C. It can be imagined that another situation is possible, where some of the PV energy generated during the day is used to cancel out instantaneous consumption and if a bidirectional single metering solution would be available, to detect each direction of power and assign to it the right tariff and therefore only count as export/import for the power excess (consumption – PV generation) as energy export, whilst still awarding the PV generation premium, a higher ROI would be possible. Whilst it may be possible to predict this with the current data available, it was considered irrelevant as this mechanism is expected to change the behaviour of the inhabitants with significant financial implications;
D. It is possible to estimate the potential to maximise the ROI by using energy storage to store the PV energy generation during day time and displace energy consumption during the evening and also be able to benefit from shifting loads to the off peak tariff. This means that if the energy storage is large enough to facilitate buying only the weekly deficit at cheap tariff, the amount of electricity that is acquired (all seasons except summer) becomes 1277.9kWh and its cost is £88.43, whilst during the three months of summer an energy excess of 59.8kWh is produced. If in this situation the premium for the PV energy generation but consumed locally is still awarded, the total energy cost becomes £88.43 – 2661.1kWh x 14.9p/kWh + 59.8kWh x 4.64p/kWh = -£310.85. This means a yearly ROI of £832.42 when compared to the noPV&no storage benchmark, that has to pay for both the installation of PV and the storage system, or when compared to the PV only case, a yearly ROI of £318.44 that could theoretically be available to pay back for the installation of the energy storage system;
E. If the FIT will not be paid for the PV energy that is generated but consumed locally, the ROI will dramatically change, as this accounted for -£399.28 whilst the real export accounted only for -£2.77 making therefore the situation significantly less economically viable that the PV only case.

The energy prices and the potential ROI quoted above are the maximum theoretical available that may in fact result for a very large energy storage system/battery that can deliver any power/current in order to cancel, when possible the export of PV energy, which may not be possible in practice or subject to significant costs. For this reason, it is recognised that it may be possible to find a higher ROI (in % of the investment) when exploring the trade-off between reduction/optimisation of the energy storage size/cost vs the decrease in the financial benefits due to battery limitations (state of charge, and current with impact also on lifetime).

It can be seen that a fairly large size for the energy storage is needed. Also whilst the hypothesis of importing/exporting the excess as a small constant continuous quantity may have an effect in smoothing the variation of the energy, it does not capitalises on the possibility to further buy cheap electricity overnight and displace additional consumption during day time typically charged at a higher rate when enrolled in an Economy 7 tariff. The second problem is that setting up a converter to handle in particular a low power level but of continuous nature, has a negative effect on the overall energy efficiency where shorter bursts of power set at the power level where the converter efficiency is the highest, leads to better overall energy efficiency. The last issue is that varying the size of energy storage may lead to poorer retention of the PV energy but it is expected that in relative figures (savings vs investment) smaller battery size may in fact offer a better Return of Investment (ROI) and the following investigation is designed to identify this optimum design point from the point of view of ROI.

3. METHODOLOGY

It is chosen to implement the battery assuming a simplified model of a 12.5V battery of variable capacity that assumes a voltage that is linearly dependent with the State of Charge (SOC) but neglecting internal resistance:

$$V_{batt}(SOC) = 10V + 5V*SOC(\%)/100\% \quad (1)$$

Following the update of the battery capacity and consequently of its SOC at the end of the previous sampling interval, the new battery voltage is determined using (1). This allows for the battery current to be calculated based on the power requirement for the energy storage. A limitation of the maximum charging and discharging battery current has also been implemented by assuming two situations: a cheap battery (lead acid) and a more expensive power battery (Li-ion). When the required battery current would exceed

the battery limit, the battery current will be clamped at the limit, the result being that the resulting power difference will be transferred to the grid power.

Table 3: Type of batteries used in this study

	Max charging current	Max discharge current
Cost-effective battery	0.2 C	0.5 C
Power dense battery	1.0 C	2.0 C

Also, in order to capitalise from the cheap rates of the Economy7 tariff, the energy storage system will perform battery charging overnight starting at midnight with the residual SOC at end of previous day and finalising at 5AM with a given target SOC for the battery, constant for the week. Two levels were tested: 35% SOC @5AM which works well for the seasons with energy excess or small deficits (spring, summer and autumn) and 70% SOC @5AM which seem to work better for seasons with larger deficits (winter).

Figure 2 shows the battery power versus the excess (consumption – PV) power when simulating the autumn week with a 12.5V/200Ah battery. In the left side the battery considered is a cost-effective type whilst in the right side, the battery has same capacity but is of a power dense type, both limits being stated in Table 3. Ideally, the power of the energy storage system should overlap the excess power at any time.

Figure 1: Left side: Power consumed (positive quantities) and PV power generated (negative quantities)

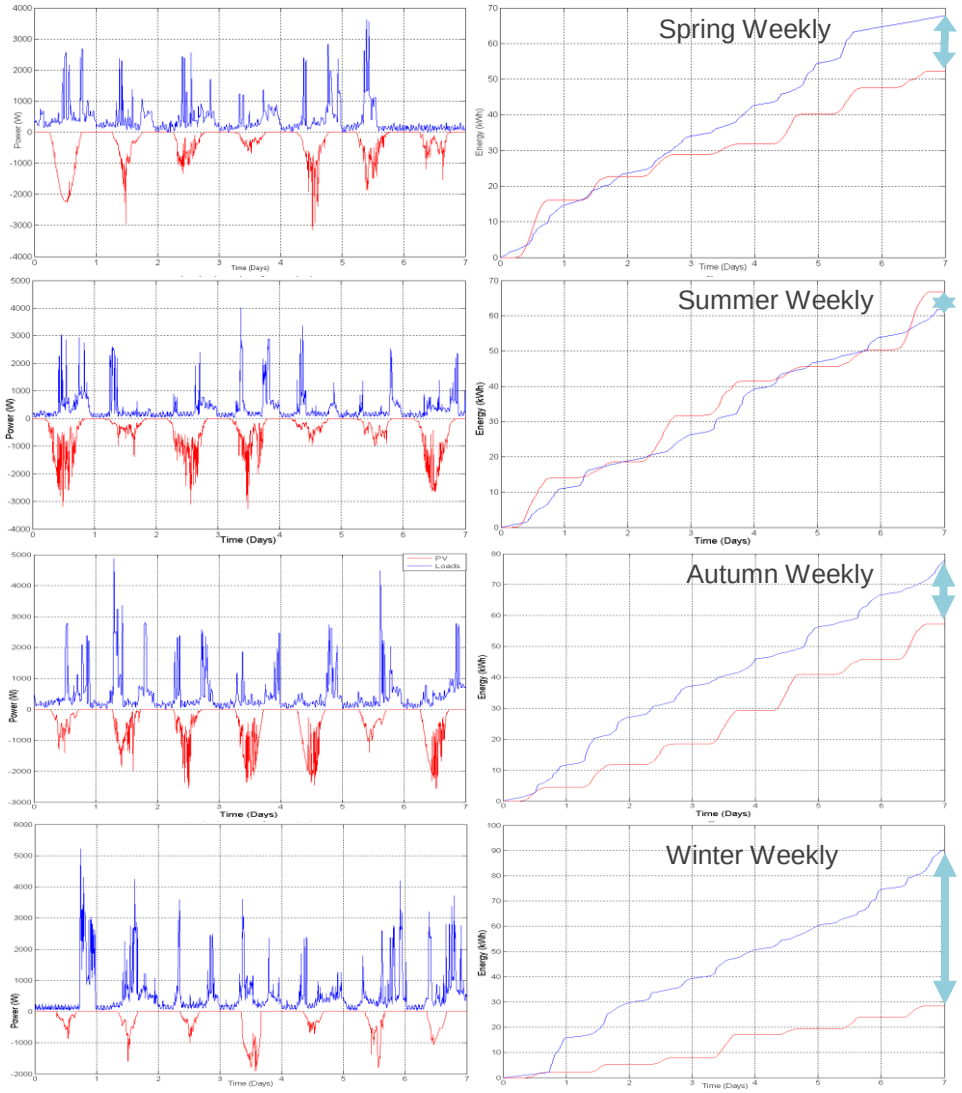

over a week for each season (spring =top; winter = bottom); Right side: the corresponding energy consumed and generated, highligting also the weekly energy excess or deficit.

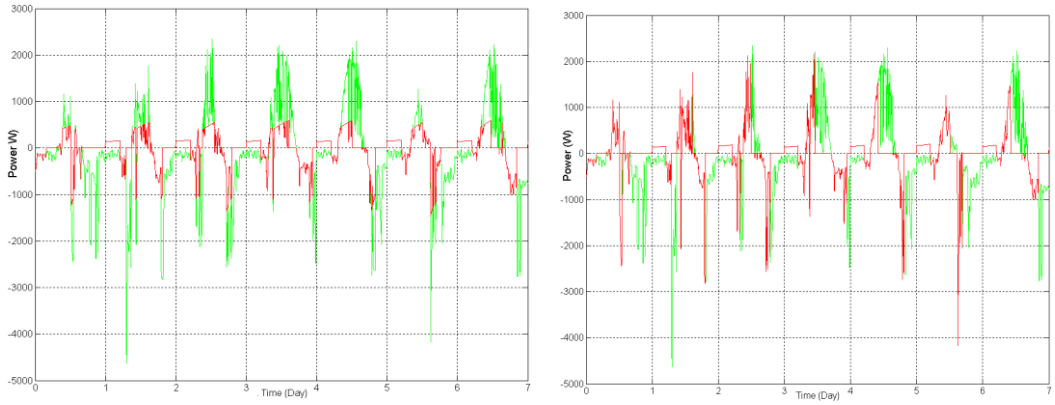

Figure 2: Power of the energy storage system (red) and the excess (consumed – PV) power (light green) showing the difference in ES behaviour when the battery has a weak (0.2C charging/0.5C discharging) current capability (left) vs power dense (1C charging/2C discharging). Battery parameters: 12.5V/200Ah; Season: autumn.

It is clear however that that is not always the case. First, thre are moments when the energy storage power drops to zero and the reason is that the battery becomes fully charged whilst the excess power points towards continuing the charging, or is fully discharged but the excess power points towards extracting power out of the battery. The second mismatch is in amplitude and may be due to the forced overnight charging (midnight-5AM) or is due to the battery current that would correspond to the excess power would exceed the current limits stated in Table 3. Typically, smaller battery sizes would be quite often subject to reaching the SOC limits due to lower energy storage capability, but they can also be affected by current limitation, as the current limits are also linked to capacity current.

Figure 3 shows the simulation of the household + PV + 12.5V/400Ah cost effective battery during a week of all four seasons. In the left side, the evolution of battery SOC is shown revealing that the overnight charging is equivalent to creating another charge/discharge partial cycle with impact in increasing profitability, but decreasing the lifetime. On the right side, the evolution of the energy bought at off—peak/cheap and peak rates are shown. The strategy of pre-charging the battery overnight at a predefined level compensates any use of grid power before the sunlight is powerful enough and results in minimisation of expensive energy purchases, obvious in the beginning and end of the spring and the middle and end of summer, and the reason is that weather changes significantly over 2-3 days in these two seasons. During autumn and winter, the weather seems more consistent and therefore imports of electricity are mainly due to the limited storage capability of the battery that cannot supply power for the whole evening. Further optimisation of the 5AM target SOC may be possible to further reduce peak energy consumption based eventually on weather forecast, but the aims of the study was first to determine the benefits of the system whilst using a very simple control that do not require often user interventions.

4. COMPARATIVE ANALYSIS

Figure 4 shows the percentage of PV energy exported out of the weekly PV energy generated. First, it suggests that without energy storage (extrapolate the curves for 0Ah battery, a large proportion (40+ to 60+ %) of the weekly energy generated by the PV is not met by instantaneous consumption by the household loads, having therefore to be exported. The curves show a steeper decaying slope until 250-300Ah battery capacity which means differential gains are higher at lower battery capacity. The PV energy export percentage can be reduced to under 30% when using a 325Ah battery or it can be reduced at 20% by using a 500Ah battery (note that in a summer week, there is an energy excess of 6.9% =4.6kWh/66.9kWh which has anyway to be exported which was omitted). During winter, the loads typically consume more power whilst the PVs are generating less energy and this is why the utilisation of PV energy looks so much better. There is a significant difference between the spring and the autumn curves even though the circumstances for the two seasons seem very similar (consumption and PV generation). However, the 20% difference in the PV energy utilisation which remains constant down to 50Ah battery capacity is perhaps due to a better synchronicity between PV energy availability and loads, which may be in fact the result of initial awareness and enthusiasm of the house inhabitants following PV installation and their desire to use locally as much of it as possible. It is widely accepted that this behaviour wears out with time.

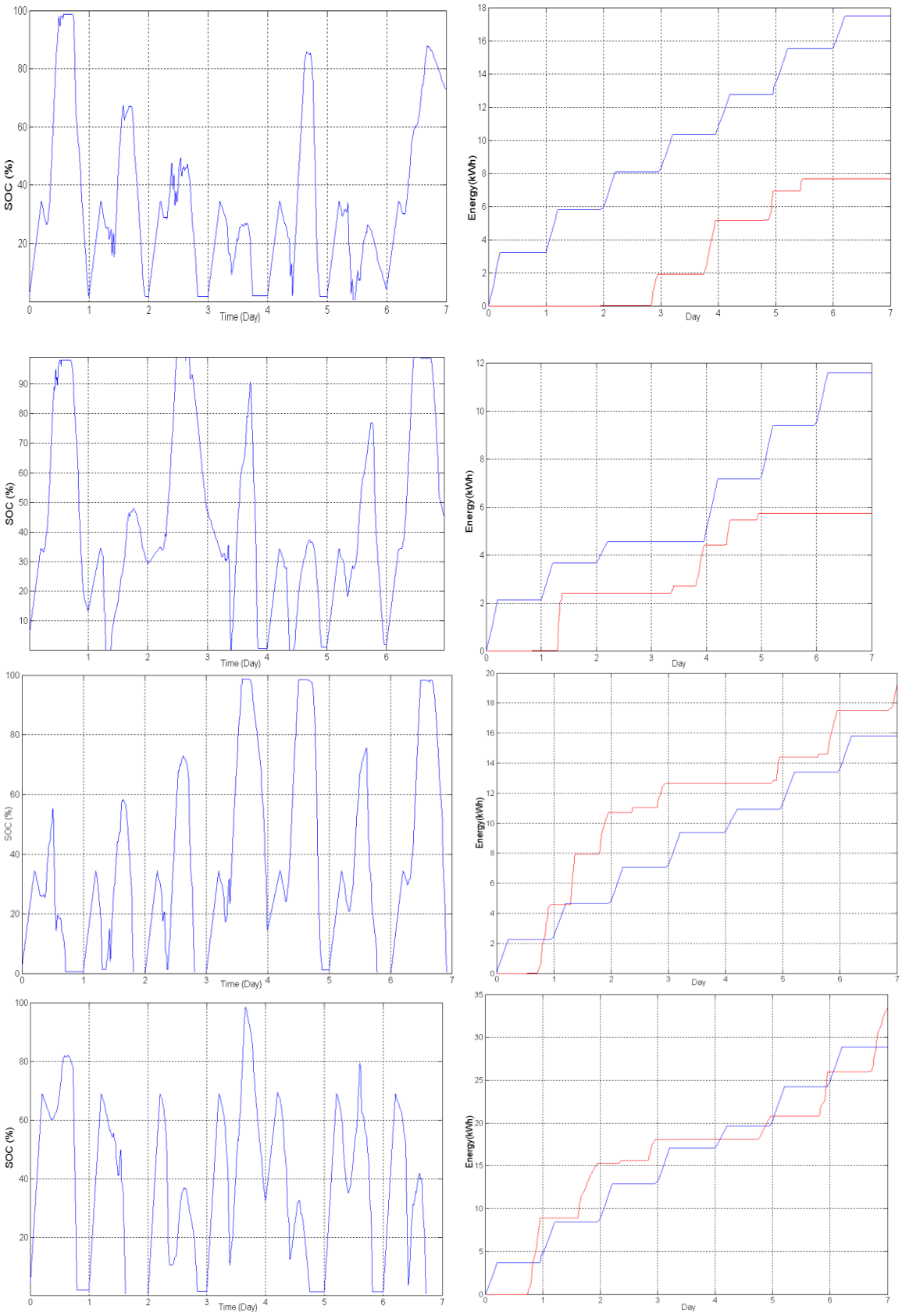

Figure 3: Weekly battery state of charge (left side) and peak (red) vs off-peak (blue) purchased energy (right side) for a 12.5V/400Ah battery system controlled to achieve 35% SOC at 5AM of each day of spring (top) – summer (2nd from top) – autumn (3rd from top) and 70% SOC at 5AM of each winter day.

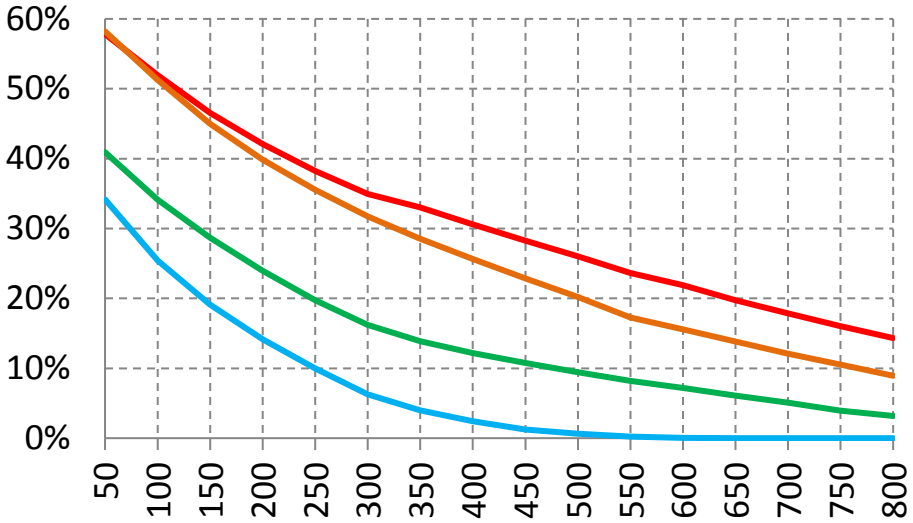

Figure 4:. Export of PV energy as percentage of overall weekly PV energy generation versus the 12.5V battery capacity. (green=spring; red= summer; amber=autumn; blue=winter).

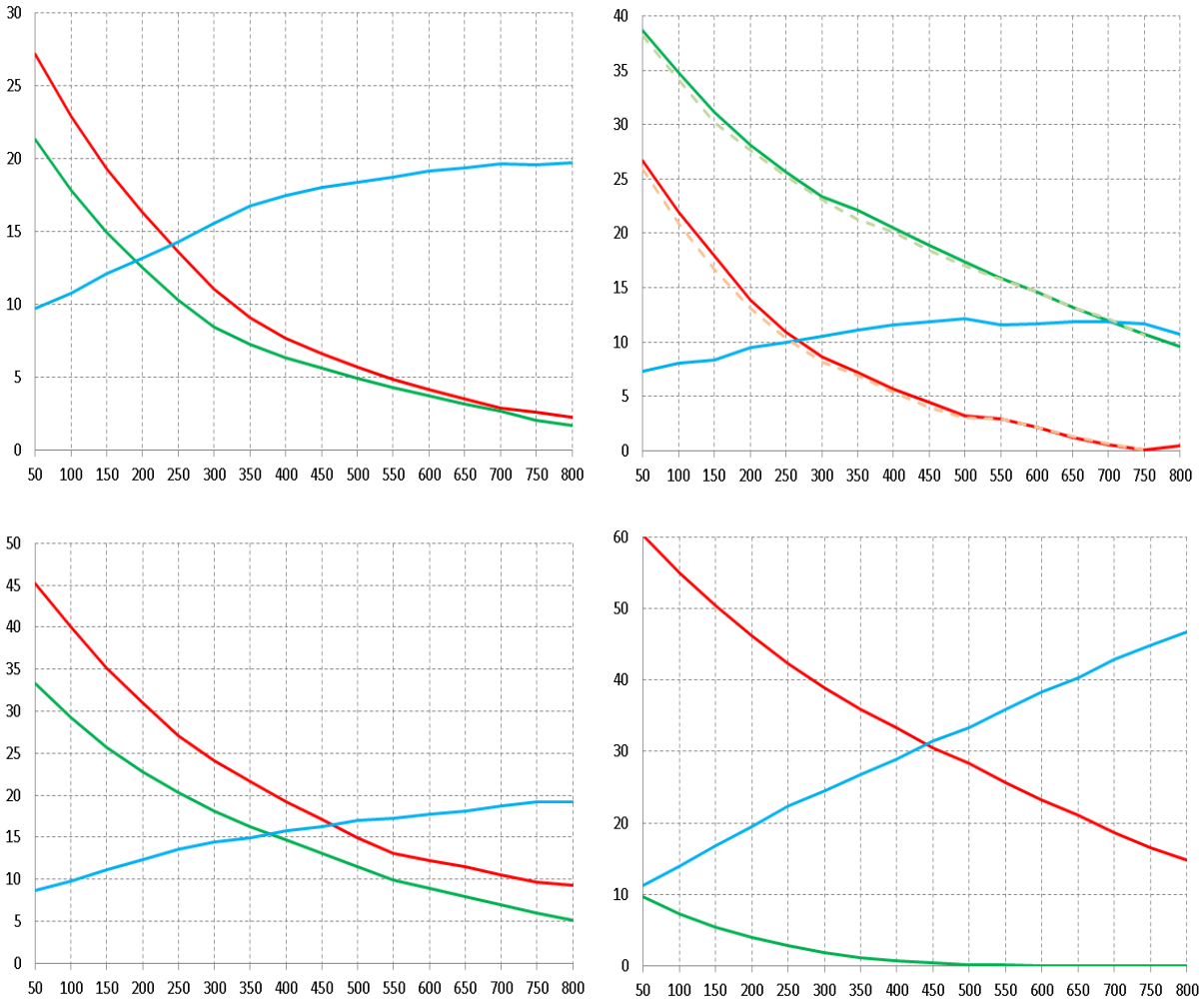

Figure 5: Weekly variation of the expensive purchased energy (red), PV exported energy (green) and cheap off-peak energy (blue) as a dependency on battery capacity for the the four considered seasons. Top -left: spring; -right: summer (dotted lines = curves corresponding to power dense battery); Bottom - left: autumn; -right: winter.

Looking at the curves in Figure 5 that shows expensive (red) and cheap (blue) energy purchased for each of the four season weeks, it can be noted that they exhibit one critical battery size beyond which the slopes change which means a given increase in battery capacity will result in smaller gains.

Increasing the battery size from 50Ah to 300Ah reduces to less than half the amount of expensive energy that has to be purchased at peak times in the spring. Above 300Ah battery size, the slope showing the amount of energy bought at peak time reduces which means lower gains are reached with same increase in battery size. The slope showing the PV energy sold due to limitations of the battery falls down quicker from 21kWh(40% of total PV energy captured) @50Ah to approx. 8kWh(18%)@300Ah. At higher battery capacity the slope (gains) reduces visibly. The Energy bought at cheap /off-peak rate raises fast from 10kWh @50Ah to 16.5kWh@350Ah above which the slope reduces. The battery size where the returns in percentage are higher seems to be in the range of 300-350Ah for the spring week data.

The results corresponding to the summer week data show two set of curves. In addition to the cost-effective battery (solid lines), the characteristics of a more powerful battery are shown. As expected at higher battery capacities, there is no difference between the two curves but at battery capacities below 200Ah, there are some slight gains in terms of being able to handle the desired power. However, due to size limitation, the capacity limits are triggered quicker and this explains the small differences. The critical battery size below which the slope of expensive/peak price range drops quicker is between 250-300Ah. The slope of the cheap energy curve raises slowest and above 450Ah, there is no visible gain. The autumn season shows a similar behaviour with the spring, with two critical points placed at 250Ah and 550Ah where the slope of the expensive/peak energy price reduces visibly twice. The other two curves show a fairly constant slope.

For the winter season, it can be noticed that increasing the battery size above 300Ah enables the full utilisation / disables the export of the PV energy generated by the household. In addition, by being able to charge overnight, it allows the reduction of electricity bought at peak time by a third (from 60kWh to just under 40kWh). The difference between the PV energy generated and the energy purchased at peak time represents an increase of energy bought at night which for battery sizes from 50-300Ah see a 2.5 times increase (from 10kWh to 25kWh). Further increase of the battery size is possible, but since there is no further improvement possible in utilisation of PV energy, the only mechanism for obtaining a ROI is to buy energy overnight cheap and displace expensive consumption during peak time. This is also reflected by the slightly slower decaying slope of the expensive energy curve. It can be noted that with a battery capacity of 1500Ah, it is possible to completely avoid purchasing expensive energy during the winter week under investigation.

Finally, it is possible to assign the price tag for each of the components in the energy bill. The cumulated variation of the financial benefits as a function of the battery size is shown in Figure 6. It is possible to compare this against the theoretical values calculated in §2B. The financial benefit from operating the PV + 50Ah battery is £570.83 which includes the FIT and the limited gains due to the buying cheap overnight electricity and replacing expensive electricity, thanks to the Econo7 dual tariff. Compared to the benefit of having only a PV system, which resulted in £519.98, this offers an additional of £50.85 to pay towards an energy storage system based on a 12.5V/50Ah battery. The financial benefit that correspond to a 1000Ah battery reaches £768.69 which is smaller than the theoretical gain of £832.42 as calculated in §2D which would represent the maximum available that could be achieved only with prior knowledge of the PV evolution and loads.

Looking at the financial benefit curve versus the size of the battery (Figure 6) it can be seen that the slope raises faster initially but the slope is continuously curved and is not possible to identify a clear critical point. However, it can be concluded that a battery capacity between 300-400Ah would offer the highest relative benefit (financial benefit related to cost/size of battery).

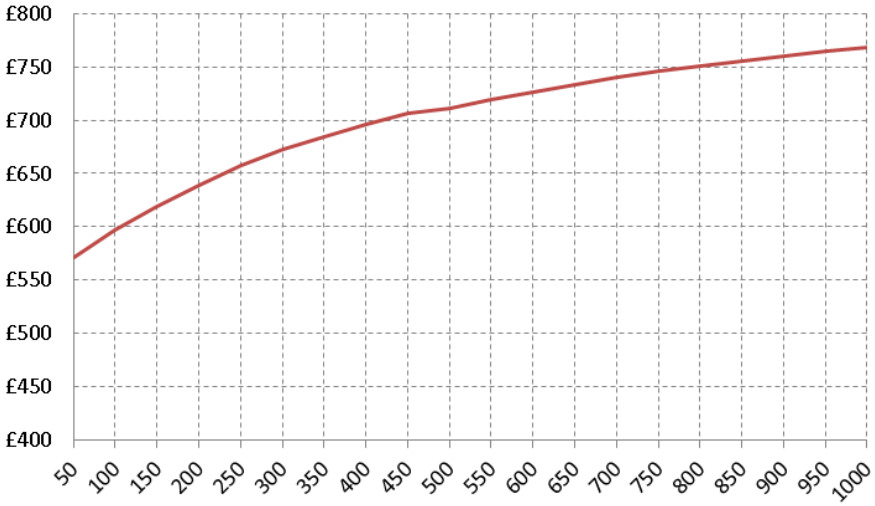

Figure 6: Financial benefit of PV+energy storage system versus battery capacity assuming a 12.5 V battery

5. CONCLUSION

This paper investigated the benefits that can be achieved by the addition of an energy storage system to a PV system installed in a UK household. Initially, the theoretical financial gains are derived based on idealistic assumptions. Then a realistic energy storage system based on a battery is modelled that can realistically model battery limitations in terms of size/capacity and current capability. A control algorithm based on a simple assumption of performing overnight charging to a predefined and constant state of charge level of 35% (spring-autumn) and 70% (winter) is implemented. The simulation model then quantifies separately the amount of PV energy that has to be exported due to limitations of the state of charge or current/power handling. The energy consumed during peak time and off-peak time are also separately quantified and represented as dependence of the battery capacity. Interesting trends emerge, that point to the possibility to achieve better financial benefits relative to the size of the battery (investment). This is finally confirmed by estimating the financial benefits versus battery capacity and comparing the ends of the range with the two theoretical values determined initially, showing reasonable consistency. Overall it could be concluded that the models may help determine a cost effective sizing of the energy storage system which may not fulfil the needs of storing all PV energy in all cases but may offer a faster return of the investment. Future work will include considering the losses in the battery and also the restriction in operation for the energy storage system emerging from the need to preserve high roundtrip efficiency.

6. ACKNOWLEDGEMENT

The project this report is based on was funded by E.ON as part of the E.ON International Research Initiative. Responsibility for the content of this publication lies with the author.

7. REFERENCES

Dickinson, M, Rabinowitz, R, Smith J, Ajiboye, P, 2012, Funding renewable energy projects: an introduction to the Feed-In Tariff and Renewable Heat Incentive schemes and associated funding options. BRE IP 12/18. Bracknell, IHS BRE Press 2012

E.ON, Representative household consumption and PV generation data, 2013, E.ON Thinking Energy programme.

Klumpner, C.; Asher, G.; Chen, G.Z., Selecting the power electronic interface for a supercapattery based energy storage system, 2009 IEEE Bucharest PowerTech, 1 - 7, DOI: 10.1109/PTC.2009.5281965

OFGEM, 2014, Feed-in-Tariff (FIT) Scheme, Ofgem, https://www.ofgem.gov.uk/environmental-programmes/feed-tariff-fit-scheme

Sharma, S.; Galipeau, D.W., Optimization of residential grid-tied PV systems without net-metering using load management, 2012, IEEE Third International Conference on Sustainable Energy Technologies (ICSET), 6 - 11, DOI: 10.1109/ICSET.2012.6357367.

Vazquez, S.; Lukic, S.M.; Galvan, E.; Franquelo, L.G.; Carrasco, J.M. Energy Storage Systems for Transport and Grid Applications, IEEE Trans on Industrial Electronics, Vol. 57, No. 12, 3881 - 3895, DOI: 10.1109/TIE.2010.2076414

POSTER SESSION B

105: Co-gasification of woody biomass and solid waste for clean energy production

PENGWEI DONG[1], THAWATCHAI MANEERUNG[1], ZHANYU YANG[1], YE SHEN[1,2], XIANG KAN[1,2], KOON GEE NEOH[2], CHI-HWA WANG[2], YEN WAH TONG[2], YANJUN DAI[3], CLIVE CHONG[4]

1 NUS Environmental Research Institute, National University of Singapore,1 Create Way, Create Tower #15-02, Singapore 138602
2 Department of Chemical and Biomolecular Engineering, National University of Singapore, 4 Engineering Drive 4, Singapore 117585
3 School of Mechanical Engineering, Shanghai Jiaotong University, #800 Dongchuan Road., Shanghai, China 200240
[4] BioPlas Energy Singapore PTE LTD, 1 Tuas Avenue 11, Singapore, 639067

Gasification is a promising alternative technology in solid waste management for megacities. It can reduce the volume of solid waste and recover heat and value-added products from this process. The feasibility test on co-gasification of different solid wastes with woody biomass has been conducted in this work using a 10 kW down-draft gasifier.

Food waste, horse manure, chicken manure and sewage sludge mixed with wood chips in different ratios were fed to the reactor continuously at the rate of 10 kg/h. The temperature in combustion and reduction zone was 900 oC and 850 oC respectively. In-situ analyses of the produced syngas were conducted using a gas analyser before the gases were burned in the chimney. The syngas composition varied with the type and ratio of solid waste due to difference in ash content, elemental composition and solid structure.

Keywords: co-gasification, downdraft gasifier, solid waste management, syngas.

1. INTRODUCTION

Solid waste management has been a great challenge for megacities around the world. The increasing demand for energy and the limited space for land fill have imposed restrictions on solid waste disposal and raised attention on environmental protection. About 7.5 million tonnes of solid waste were generated in Singapore in 2014 and only 60% of them were recycled according to the National Environmental Agency (2015). Some carbonaceous solid wastes such as horticultural waste, sludge, food and plastic etc. still have low recycling rate and require proper disposal in the future.

Some solid waste can be recycled by simple physical sorting while others need further disposal treatment. The most popular disposal method is through incineration which can reduce about 90% of solid volume. But it can only recover heat energy from combustion without considering the possible reuse of feedstock. Composting and digestion can produce fertilizer and bio-gas from solid waste. However, they are effective only for organic and bio-degradable waste and treatment process takes a long time. Gasification can convert carbonaceous solid waste into syngas (Cheng et al.) and other value-added products (Rong et al., 2015) besides recovering heat energy. The produced syngas can be burnt in a gas engine or be purified as feedstock for downstream processes. The solid residue such as bio-char or bottom ash can be modified as soil amendment in agricultural use or as catalyst in bio-fuel production (Maneerung et al., 2015). An integrated gasification combine cycle (IGCC) system can be considered as an alternative technology for waste disposal in megacities.

Down-draft gasifier has been widely used for biomass gasification and it can reduce tar production as compared with other types of gasifier so as to produce clean syngas for downstream utilization. But it has also some problems in dealing with different solid waste. In this work, the gasification of pure wood chips and co-gasification with other solid waste were conducted in a 10 kW down draft gasifier.

2. EXPERIMENTAL SECTION

2.1 Feedstock and apparatus

Four carbonaceous solid waste with low recycling rate in Singapore were chosen in this work. These were food waste from food court, sewage sludge collected from wastewater treatment plant, chicken manure from chicken farm and horse manure collected from Singapore Turf Club. All the solid wastes were dried in a dryer at 68 ^{o}C for 24 h before use. Proximate analyses were carried out on all samples using Shimadzu Thermal Gravimetric Analyzer in N_2 and Air. Ultimate analyses were conducted by Elementary Vario Micro Cube. Table 1 shows the properties of wood chips, chicken manure and horse manure. As shown in this table, the major components of each waste were similar but the content varied with waste types.

Solid waste was mixed with wood chips at different compositions. As for food waste, w/w (food/total feedstock) percentage was varied as 20, 30 and 40% in different runs. In contrast, w/w (sludge/total feedstock) percentage of sewage sludge was changed as 10, 20 and 30%, respectively. The horse manure and chicken manure were tested at the fixed composition of 30% w/w (horse/chicken manure/total feedstock). After mixing with wood chips, the mixture was added into the hopper. Feedstock was fed into the gasifier at 10 kg/h through a screw feeder. The temperature in the combustion zone and reduction zone were 900 ^{o}C and 850 ^{o}C, respectively. Syngas was conducted in-situ analyses using a gas analyser which could record the content of CO, H_2, CO_2, CH_4, C_nH_m, O_2 and the lower heating value of syngas. Bottom ash and bio-char were collected after each experiment.

Table 19: Proximate and ultimate analyses of solid waste

	Moisture (wt.%)	Volatile (wt.%)	Ash (wt.%)	F. C (wt.%)	HHV (MJ/kg)	C (wt.%)	H (wt.%)	N (wt.%)	S (wt.%)	O[8] (wt.%)
Wood Chips	8.5	69.2	6.3	16.2	18.2	44.2	6.1	0.9	0.5	42.5
Horse manure	75.7[a]	64.8	25.1	10.0	12.6	37.3	5.1	2.0	<0.5	55.6
Chicken manure	73.6[a]	61.4	28.1	10.5	18.8	28.2	3.5	8.1	1.1	59.1

*a: as received F. C: Fixed Carbon *: by difference*

3. RESULTS AND DISCUSSION

3.1 Feasibility test on co-gasification

The feasibility of co-gasification of wood chips and solid waste was evaluated from the operation state of the gasifier and the syngas composition. After one hour operation in steady state, the co-gasification of wood chips and sewage sludge was successfully conducted with 20% loading of sludge in the sludge wood chips mixture. When the composition of sludge was increased to 33%(w/w), the reactor was blocked due to agglomeration caused by the high iron content in ash. As for food waste, the co-gasification was conducted successfully with up to 30%(w/w) food waste of total waste. When this percentage was increased to 40%(w/w), the gasifier was blocked by the small char particle generated from small food waste particle. At the loading of 30%(w/w), horse manure and chicken manure were successfully co-gasified with wood chips.

3.2 Syngas composition

The syngas composition is a key indicator of gasification performance. In general, the content of CO_2 in syngas from co-gasification was lower than that from pure wood chips gasification while the CO and H_2 content increased in co-gasification. Figure 1 compares the syngas composition from three batches: gasification of pure wood chips, co-gasification with chicken manure and co-gasification with horse manure. As shown in this figure, the co-gasification of wood chips with manure increases the CO and H_2 content and reduces CO_2 content in syngas compared with pure wood chips. The ratio of H_2/CO changed with different feedstock, which indicated that the syngas composition could be tuned by changing the feedstock.

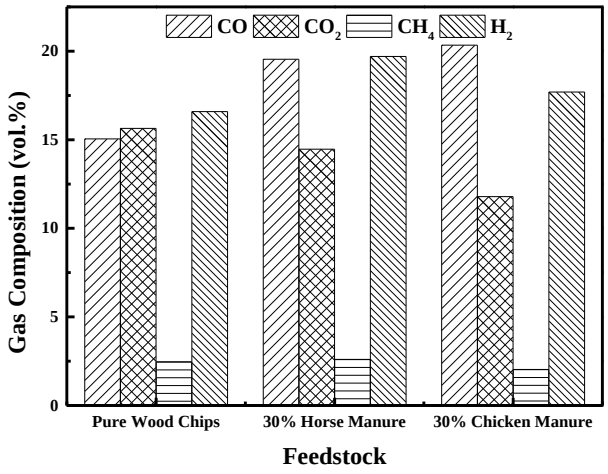

Figure 70: Syngas composition vs feedstock

4. CONCLUSIONS

The co-gasification of wood chips and different solid waste has been conducted successfully although a limiting factor is the solid loading ratio. The failure of co-gasification of sludge at 30% was due to the agglomeration from iron in the ash. The high fraction of small particles in food waste block can result in blockage of the gasifier after a long period of operation. The co-gasification with horse manure and chicken manure improve the syngas composition compared with pure wood chips. The syngas composition could be tuned by changing the feedstock. The effects of the variation of ash content, elemental composition and structure of solid wastes on the syngas quality were presented in this study.

5. ACKNOWLEDGEMENT

This research programme/project is funded by the National Research Foundation Singapore under its Campus for Research Excellence and Technology Enterprise (CREATE) programme.

6. REFERENCES

2015. Supplement Material [Online]. National Environmental Agency,Singapore. Available: http://www.nea.gov.sg/energy-waste/waste-management/waste-statistics-and-overall-recycling.

CHENG, Y., Thow, Z. & Wang, C.-H. Biomass gasification with CO2 in a fluidized bed. Powder Technology. In press

MANEERUNG, T., Kawi, S. & Wang, C.-H. 2015. Biomass gasification bottom ash as a source of CaO catalyst for biodiesel production via transesterification of palm oil. Energy Conversion and Management, 92, 234-243.

RONG, L., Maneerung, T., Ng, J. C., Neoh, K. G., Bay, B. H., Tong, Y. W., Dai, Y. & Wang, C.-H. 2015. Co-gasification of sewage sludge and woody biomass in a fixed-bed downdraft gasifier: Toxicity assessment of solid residues. Waste Management, 36, 241-255.

395: Fixed-bed staged gasification of biomass: rate-controlled equilibrium modelling

IGOR DONSKOY[1], ALEXANDRE KEIKO[2], ALEXANDER KOZLOV[3], VITALY SHAMANSKY[4], DENIS SVISHCHEV[5]

1 Melentiev Energy Systems Institute, Russian Academy of Sciences, Russia, 664033 Irkutsk, Lermontova st., 130, e-mail: donskoy.chem@mail.ru
2 Melentiev Energy Systems Institute, Russian Academy of Sciences, Russia, 664033 Irkutsk, Lermontova st., 130, e-mail: paragraph1@yandex.ru
3 Melentiev Energy Systems Institute, Russian Academy of Sciences, Russia, 664033 Irkutsk, Lermontova st., 130, e-mail: kozlov@isem.sei.irk.ru
4 Melentiev Energy Systems Institute, Russian Academy of Sciences, Russia, 664033 Irkutsk, Lermontova st., 130, e-mail: vita@isem.sei.irk.ru
5 Melentiev Energy Systems Institute, Russian Academy of Sciences, Russia, 664033 Irkutsk, Lermontova st., 130, e-mail: denis.svishchev@gmail.com

Biomass gasification is a technology suitable for small-scale power plants. This is a well-known and environmentally friendly way to convert biomass (such as forest and agricultural waste) into combustible fuel gas. However there are several disadvantages to overcome. Tarry gases call for a costly gas cleaning system, and the process is often unstable. These drawbacks are typical for widely used single-stage gasification processes.

Staged gasification as distinct from the single-stage one allows allothermal and autothermal conversion processes to be separated within the same plant. Separation of the devolatilization and char gasification stages makes tarry volatiles to burn and produce the gasification agent. Such process organization provides both low-tar gas production and better process heat utilization.

The plant being studied consists of two fixed-bed reactors and a gas combustion chamber. It has a number of feedbacks that cause a change in parameters of all reactors at a variation in any of them. A mathematical model is developed to predict staged process behaviour and to find stable operation modes. The model consists of blocks describing equilibrium gas combustion constrained by diffusion and kinetics. The results outline the control limits within which a stable and efficient gasification can be performed.

Keywords: gasification, biomass, staged process, mathematical modelling, equilibrium models, kinetic constraints.

1. INTRODUCTION

Biomass gasification has several obvious advantages. It can be implemented at small-capacity energy plants which are opportune to utilize sparsely distributed biomass fuels like forest and agricultural waste. Besides, it allows production of heat and power, pollution reduction, and mitigating climate change (Pereira, da Silva, de Oliveira et al., 2012).

Beside direct combustion there are many biomass-based energy technologies: fixed-bed (Erlich and Fransson, 2011), fluidized bed (Gomez-Barea and Leckner, 2010), and entrained-flow gasification (Hernandez J.J., Aranda G., Barba J. et al. 2012), pelletization (Stahl, Granstrom, Beghel et al., 2004) and briquetting followed by co-gasification with coals (Montiano, Fernandez, Diaz-Faes et al., 2015; Collot, Zhuo, Dugwell et al. 1999), catalytic conversion (Asadullah, Miyazawa, Ito et al., 2003), high-temperature processes (Ran and Li, 2012), etc. The main purpose of them is to convert biomass into a combustible gas to fuel boilers or engines.

A well-known drawback of biomass gasification is rather high content of tars in the producer gas that prevents its combustion in engines without a costly gas cleaning (Han and Kim, 2008; Asadullah, 2014). This motivates developing new methods of gasification process organization and control. The staged gasification is among such methods. At the staged gasification fuel pyrolysis and char gasification are separated. A general scheme of staged gasification process is shown in fig. 1. Such process organization has been studied e.g. at Technical University of Denmark (Henriksen, Ahrenfeldt, Jensen et al., 2006).

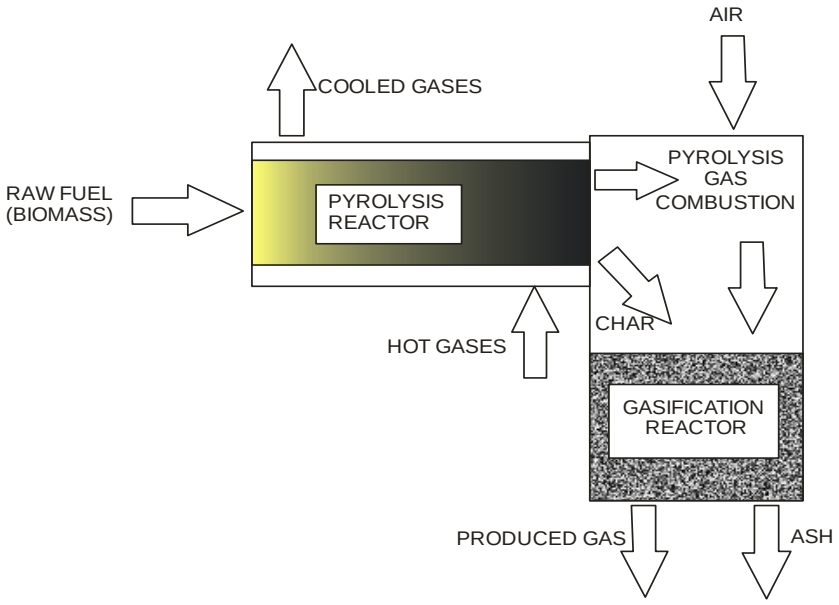

Fig. 1. Staged fixed-bed gasification: a general scheme

In the pyrolysis reactor (the first stage) raw biomass undergoes drying and devolatilization. The pyrolysis gas is combusted in the under-bed space of the gasification reactor (the second stage). The oxidation of pyrolysis products needs not to be complete because high temperatures provide elimination of tar due to secondary pyrolysis. Hot gases serve as a gasification agent at the second stage. The char gasification does not produce tars and fosters tar cracking. Thus, the produced gas is almost tar-free. Endothermic reactions of CO2 and H2O char gasification lessen thermodynamic heat loses.

To maintain a stable pyrolysis process, an additional heat is needed. At an autonomous plant this heat may be obtained by combustion of raw fuel, pyrolysis gas, char or syngas only. Herein we consider the case when the additional heat is supplied by syngas combustion products from the exhaust of a power unit.

Gasification plants based on the idea of staged process are investigated in several studies, e.g. (Henriksen, Ahrenfeldt, Jensen et al., 2006; Wang, He, Qin et al., 2015; van der Steene, Taguthou, Mermoud et al., 2010; Senachin et al., 2009), including both fixed-bed and fluidized-bed reactors (Gomez-Barea, Leckner, Perales et al., 2013). In all cases creation of sophisticated process schemes inevitably causes a complicated control to provide proper coordination of mass and heat flows.

Danish researchers developed mathematical models to provide theoretical base for staged gasification process operation and control. In the paper (Gobel, Henriksen, Jensen et al., 2007) they used one-dimensional diffusion-kinetic model to simulate dynamic behavior of a gasifier at fixed other parameters. They also used CFD-code to model underbed gas combustion and hydrodynamic flow modes in porous media (Gerun, Paraschiv, Vijeu et al., 2008).

In the paper (Keiko, Svishchev, Kozlov et al., 2012) a final-equilibrium thermodynamic model was used to determine the influence of a number of parameters on the thermodynamic limits of coal staged gasification. Among the independent parameters there were specific consumption of air and steam, conversion degree at pyrolysis, and others. In the work (Donskoy, 2013) a one-dimensional equilibrium model including diffusion-kinetics constraints was applied to obtain thermal stability boundaries for a coal staged gasification process. It was shown that the amount of heat recycled and air excess can be varied within certain ranges to maintain a stable process.

A rigorous and precise model of heterophase fuel conversion process still cannot be constructed due to lack of theoretical knowledge on the mechanisms of such reactions, leaving alone the high variability of natural fuels properties. That is why the explanatory potential of mathematical models in this area still dominates their predicting capabilities. This is a fortiori so for low-grade fuels which the biomass belongs to.

It is interesting to investigate staged biomass gasification process using a mathematical model able to predict such phenomena as process extinction (e.g. at insufficient heat recycling). It would help to determine the conditions at which staged gasification can be efficiently operated. Such model and some modelling results are discussed below.

2. MODEL ASSUMPTIONS AND STRUCTURE

The model structure is presented in fig. 2. The input parameters are: reactor sizes (diameters and lengths), raw fuel characteristics and its consumption, heat flow used for raw fuel pyrolysis, oxidizer excess ratio at gas combustion, and kinetic data on heterogeneous brutto-reactions of fuels. The latter can be obtained experimentally by the means of thermal analysis (Kozlov, Svishchev, Donskoy et al., 2012).

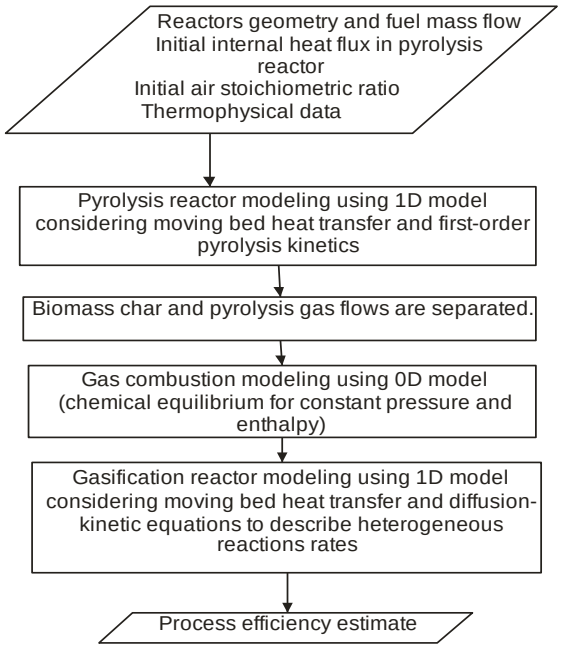

Fig. 2. Modeling algorithm structure.

The heat flux at the wall of pyrolyzer that is produced by exhaust gases could not be uniform, but we assume it to be so. A detailed study of heat flux distribution in pyrolyzer jacket is yet to be done. Fixed-bed reactors are represented as one-dimensional systems, lateral temperature gradients are neglected. Pyrolysis gas combustion is supposed to reach the complete chemical equilibrium under the conditions of

constant pressure and enthalpy. Thus, the key control parameters are the heat consumption in pyrolysis reactor and air stoichiometric ratio in the underbed combustion section.

The main features of a solid fuel conversion reactor model are discussed in (Donskoi, Keiko, Kozlov et al., 2013). It is one-dimensional model including two iteratively run submodels. One submodel describes heat transfer in a moving bed. The other one calculates final chemical equilibrium rate-controlled due to diffusion and reaction kinetics. The calculation starts from any reasonable closure of axial temperature profile, and the iterations stop when this profile's change becomes negligible, i.e. a steady state is achieved. The transitional states determined during iterations are not physical. The gas composition at each point along the reactor axis is equilibrium under the condition of incomplete fuel conversion derived from kinetic equations for drying, pyrolysis and gas-fuel heterogeneous reactions. Kinetic parameters for these reactions are obtained by thermal analysis and presented in the table 1.

Table 1. Kinetic parameters of heterogeneous reactions

Chemical reaction	Preexponential factor	Activation energy
Pyrolysis	$5.4\ 10^5\ s^{-1}$	96 kJ/mole
Char + CO_2	$7.0\ 10^{10}$ m/s	259 kJ/mole
Char + H_2O	$4.9\ 10^5$ m/s	175 kJ/mole

The tar produced in biomass pyrolysis is ascribed as a lumped substance with brutto-formula $CH_{0.6}O_{0.6}$. Since the combustion of pyrolysis products is implied to reach the final equilibrium the representation of tar is realistic enough.

3. MODELLING RESULTS

The reactor sizes chosen in this study are constant: diameter 0.5 m; height 1 m. Raw fuel consumption is taken 100 kg/hr. Fuel proximate analysis data are shown in table 2.

Table 2. Fuel characteristics

Property	Value
C(daf), %	49,5
H(daf), %	6,3
O(daf), %	44,2
V(daf), %	85
A(d), %	1
W(r), %	20

The above described model has been applied for a range of gasification regimes. Here we give one of them to provide our colleagues with the material for further discussion. The temperature, gas composition and fuel conversion degree axial profiles are presented at fig. 3. For this case heat flux in pyrolyzer comprises 24 kW; air ratio at pyrolysis gas combustion is 0.4. One can see that at the pyrolysis stage fuel moves in reactor and the most part of fuel does not react (fig. 3a,b). Only when the bed temperature rises up to 600 K an intensive pyrolysis starts. A lot of tar is produced during pyrolysis (fig. 3c). At the gasification stage hot gases react with char bed but output gas temperature is still very high (fig. 3f), so this heat may be utilized in pyrolysis reactor. Full regime map is presented at fig. 4.

It can be seen from fig. 4 that the more heat flux at pyrolysis stage the less oxidizer ratio is needed to achieve optimum cold gas efficiency. Pyrolysis starts when the heat flux makes up 5-7% of the fuel higher heating value. This is explained by the well-known kinetic feature – the exponential increase in reaction rate with a rise of temperature. At higher heat fluxes raw fuel is completely converted into char, tar and gas. Correspondingly, a larger share of fuel is converted in the pyrolyzer rather than in the gasifier. That is why at higher heat fluxes the gasification stage cannot provide enough combustibles to compensate their combustion in the underbed space. This, in turn, results in oxidation of the most part of biomass and lowers cold gas efficiency of the plant. The optimal values of air ratios range within 0.4-0.5. At lower air ratios the temperature of combustion products is insufficient to promote intensive gasification, and unreacted char leaves reactor with ash. Nevertheless, under very low air ratios unburnt pyrolysis gas has high heating value, so overall cold gas efficiency is near 70%.

There are still many questions to be answered. First of all, optimal distribution of heat flux at the pyrolysis stage is to be investigated. It is also important to improve the description of raw fuel pyrolysis kinetics, as the first-order Arrhenius kinetics is a rough approximation (Di Blasi, 2008). At last, it does make sense to

develop a model that would combine gasification system with the power unit. This would allow a comparison among different sources of additional heat for pyrolysis.

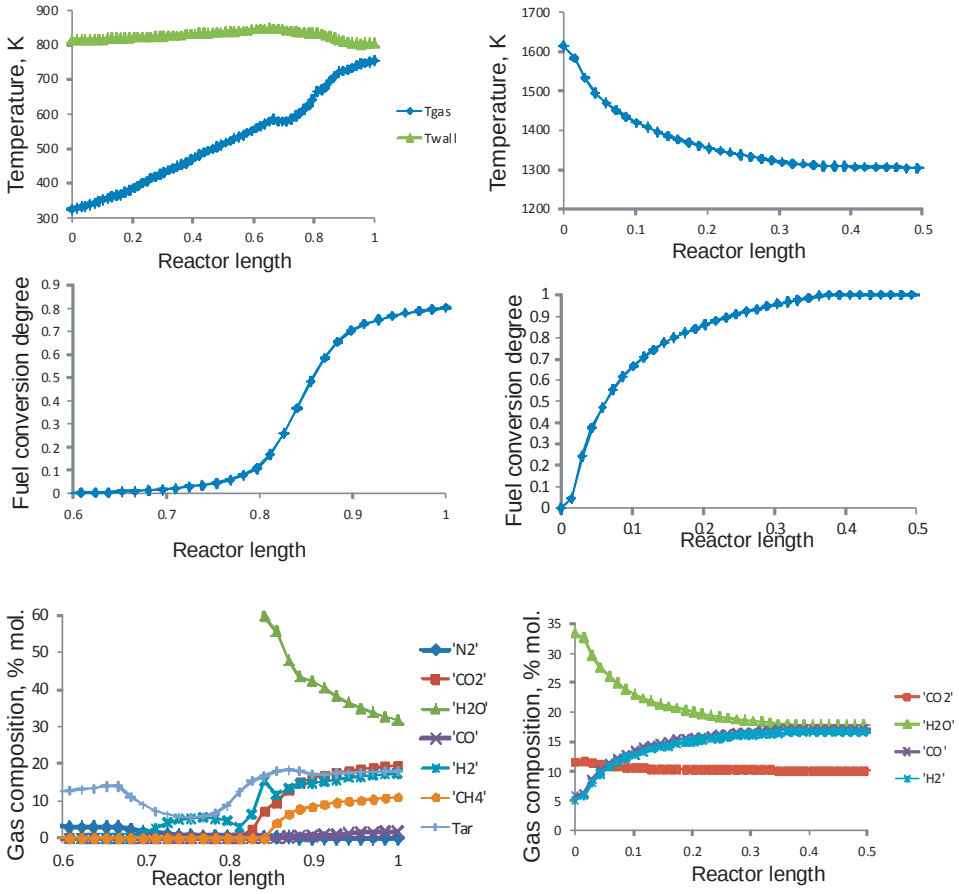

Fig. 3. Modeling results by stages: a, b, c – pyrolysis stage; d, e, f – gasification stage.

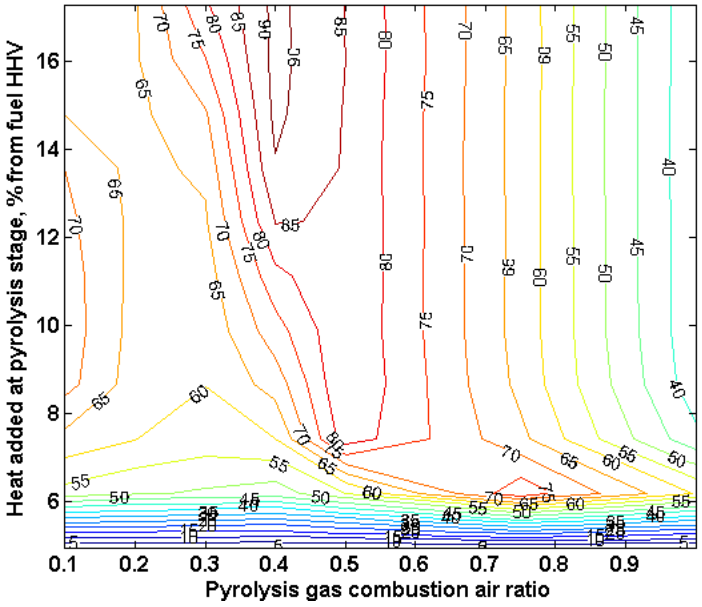

Fig. 4. Regime map for staged biomass gasification: cold gas efficiency vs. process parameters.

4. CONCLUSION

Processes of a staged fixed-bed gasification of biomass are studied using mathematical model. The whole process efficiency is shown to have two major control parameters: pyrolysing heat flux and air ratio at

pyrolysis gas combustion. There is a liminal value of the heat flux in pyrolysis reactor (5-7 % of the fuel higher heating value) that provides efficient fuel conversion. Air ratios have the range of optimal values within 0.4-0.5.

This study is supported by Russian Foundation of Basic Researches (grant No. 13-08-00281). Results of the study were obtained using the material and technical base of the Baikal Analytical Center for collective use of SB RAS.

5. REFERENCES

ASADULLAH, M., Miyazawa, T., Ito, S., Kunimori, K., Yamada, M. and Tomoshige, K. (2003) Catalyst development for the gasification of biomass in dual-bed gasifier. Applied Catalysis A: General 255; pp. 169-180.

ASADULLAH, M. (2014) Barriers of commercial power generation using biomass gasification gas: A review. Renewable and Sustainable Energy Reviews 29; pp. 201-215.

COLLOT, A.-G., Zhuo, Y., Dugwell, D.R. and Kandiyoti, R. (1999) Co-pyrolysis and co-gasification of coal and biomass in bench-scale fixed-bed and fluidised bed reactors. Fuel 78; pp. 667-679.

DI BLASI C. (2008) Modeling chemical and physical processes of wood and biomass pyrolysis. Progress in energy and combustion science 34; pp. 47-90.

DONSKOI, I.G., Keiko, A.V., Kozlov, A.N., Scishchev, D.A. and Shamanskii, V.A. (2013) Calculation of the fixed bed coal gasification regimes by the use of thermodynamic model with macrokinetic constraints. Thermal Engineering 60(12); pp. 904-909.

DONSKOY I.G. (2013) Mathematical modeling of the fixed bed staged coal gasification. Combustion and Plasmochemistry 12(4); pp. 376-382. [in Russian]

ERLICH, C. and Fransson, T.H. (2011) Downdraft gasification of pellets made from wood, palm-oil residues respective bagasse: Experimental study. Applied Energy 88; pp. 899-908.

GERUN, L., Paraschiv, M., Vijeu, R., Belletre, J., Tazerou, M., Gobel, B. and Henriksen, U. (2008) Numerical investigation of the partial oxidation in a two-stage downdraft gasifier. Fuel 87; pp. 1383-1393.

GOBEL, B., Henriksen, U., Jensen, T.K., Qvale, B. and Houbak, N. (2007) The development of a computer model for a fixed bed gasifier and its use for optimization and control. Bioresource Technology 98; pp. 2043-2052.

GOMEZ-BAREA, A. and Leckner, B. (2010) Modeling of biomass gasification in fluidized bed. Progress in Energy and Combustion Science 36; pp. 444-509.

GOMEZ-BAREA, A., Leckner, B., Perales, A.V., Nilsson, S. and Cano, D.F. (2013) Improving the performance of fluidized bed biomass/waste gasifiers for distributed electricity: A new three-staged gasification system. Applied Thermal Engineering 50; pp. 1453-1462.

KEIKO, A.V., Svishchev, D.A., Kozlov, A.N. and Ryzhkov, A.F. (2012) Modeling a solid-fuel staged gasification process. In: Proceedings of the 11th International Conference on Sustainable Energy Technologies (SET-2012). September 2-5, 2012. Vancouver, Canada.

KOZLOV, A.N., Svishchev, D.A., Donskoy, I.G. and Keiko, A.V. (2012) Thermal analysis in numerical thermodynamic modeling of solid fuel conversion. Journal of Thermal Analysis and Calorimetry 109(3); pp. 1311-1317.

HAN, J. and Kim, H. (2008) The reduction and control technology of tar during biomass gasification/pyrolysis: An overview. Renewable and Sustainable Energy Reviews 12; pp. 397-416.

HENRIKSEN, U., Ahrenfeldt, J., Jensen, T.K., Gobel, B., Bentzen, J.D., Hindsgaul, C. and Sorensen, L.H. (2006) The design, construction and operation of a 75 kW two-staged gasifier. Energy 31; pp. 1542-1553.

HERNANDEZ, J.J., Aranda, G., Barba, J. and Mendoza, J.M. (2012) Effect of steam content in the air-steam flow on biomass entrained flow gasification. Fuel Processing Technology 99; pp. 43-55.

MONTIANO, M.G., Fernandez, A.M., Diaz-Faes, E. and Barriocanal, C. (2015) Tar from biomass/coal-containing briquettes. Evaluation of PAHs. Fuel 154; pp. 261-267.

PEREIRA, E.G., da Silva, J.N., de Oliveira, J.L. and Machado, C.S. (2012) Sustainable energy: a review of gasification technologies. Renewable and Sustainable Energy Reviews 16; pp. 4753-4762.

RAN, J. and Li, C. (2012) High temperature gasification of woody biomass using regenerative gasifier. Fuel Processing Technology 99; pp. 90-96.

SENACHIN, P.K. (Ed.) (2009) Fixed bed gasification technologies, Barnaul: "Altay publishing house". [in Russian]

STAHL, M., Granstrom, K., Berghel, J. and Renstrom, R. (2004) Industrial processes for biomass drying and their effects on the quality properties of wood pellets. Biomass and Bioenergy 27; pp. 621-628.

VAN DER STEENE, L., Taguthou, J.P., Mermoud, F., Martin, E. and Salvador, S. (2010) A new experimental Continuous Fixed Bed Reactor to characterise wood char gasification. Fuel 89; pp. 3320-3329.

WANG, Z., He, T., Qin, J., Wu, J., Li, J., Liu, G., Wu, J. and Su, L. (2015) Gasification of biomass with oxygen-enriched air in a pilot scale two-stage gasifier. Fuel 150; pp. 386-393.

POSTER SESSION C

75: Experimental research on cooling effect of battery pack with liquid flow heat exchange structure

TIANSHI ZHANG [1,2], QING GAO [1,2*], YANLONG GU [1,2],
GUOHUA WANG [1,2] , KAIPENG ZHANG [1,2] CONG XIAO [3] , Y.Y. YAN [4]

1State Key Laboratory of Automotive Simulation and Control, Jilin University, 130025, Changchun, China
**Corresponding Email: gaoqing@jlu.edu.cn*
2 College of Automotive Engineering, Jilin University, 130025, Changchun, China, zhangtianshi@jlu.edu.cn
3 R&D Centre, China First Automobile Works Group Corp, 130011, Changchun, China, xiaocong@rdc.faw.com.cn
4Faculty of Engineering, University of Nottingham, Nottingham, NG72RD, UK, Yuying.Yan@nottingham.ac.uk

Abstract: In order to realize high efficiency and lightweight of battery thermal management (BTM), we designed a new liquid flow heat exchange structure which used flat tube bundle and graphite layer with high thermal conductivity. In different battery pack cooling processes, series of experiment were conducted to investigate basic heat transfer characteristics include temperature variation, temperature uniformity, thermal response and temperature fluctuation. The experimental results showed that the designed structure not only ensured cooling effect and temperature uniformity of battery pack, but also reduced volume and weight of liquid flow. At the same time, through adopting variable temperature cascade cooling method, cold shock were alleviative and temperature uniformity was promotion during battery pack cooling process. In addition, battery cooling effect was not sensitive to variation of liquid flow within experimental conditions, and this characteristic will facilitated to achieve low flow resistance and low pump power consumption.

Keywords: BTM; liquid flow heat exchange; flat tube bundle; graphite layer; cooling effect

1. INTRODUCTION

With the development of electric vehicle, high-capacity battery pack received more and more attention. Battery will generate large heat during charging or discharging process and the electrochemical reaction is extremely sensitive to temperature environment. In fact, it will produce strong heat accumulation, heat transfer difference, temperature nonuniformity inside the battery pack because of the compact structure and positional difference of each cell. At the same time, electrochemical reaction uniformity and internal resistance uniformity of each cell will be deteriorated seriously, and affect the cycle life of battery pack, even generate internal friction and thermal runaway[1-4]. So power battery pack not only need good cooling, also require strict temperature uniformity regulation.

Generally, battery thermal management (BTM) method is divided into air cooling method and liquid cooling method. Air cooling system has simple structure and lower cost compared with liquid cooling system, but the heat transfer coefficient is very small between the air and battery pack and the cooling speed is slower. Thus, air cooling method is usually adopted for low capacity battery pack. Now, Liquid medium has rapid thermal response and higher heat transfer capability, these characteristics will meet the needs of summer cooling and winter preheating at the same time, and facilitate to realize double thermal management for battery pack. Therefore, liquid flow heat transfer system has gaining increasing attentions for high-capacity battery pack [5-7].

There have been some primary researches and applications of the battery thermal management system (BTMS) by liquid flow heat transfer in the worldwide. In 2011, Pendergast et al. used the 18650 batteries and housed them inside a triangular aluminum module, then put them under water. Their experiment can be also seen as a early simple liquid BTM solution [8]. Anthony designed a thin metal battery cooling plate for BTM, which include serpentine-channels. Heat is conducted from the batteries into the cooling plate, and transported away by the coolant. The computational fluid dynamics (CFD) optimization results indicated that the design can satisfy both pressure and average temperature objectives, but at the expense of temperature uniformity [9]. In 2012, Yuan designed a liquid cooling plate for BTM aim to keep the battery average temperature and temperature difference in the optimum range. Results showed that system's overall flow was balanced and battery operating temperature and temperature uniformity were well in the steady state [10].

In addition, the international vehicle manufacturers are developing new BTMS and integrated vehicle thermal management system (VTMS) by liquid flow heat transfer. In 2010, TESLA electric cars adopted liquid circulation BTMS for the large number of 18650 column type battery combination [11]. In 2011, GM designed T type battery pack which combine liquid circulation heat exchange structure with laminated sheet battery, and adopted it to the extended range EV "Chevrolet Volt"[12-13]. In addition, BMW Active E, i3 and Ford Focus EV have attempted to use the liquid circulation thermal management system [14].

However, the above battery pack adopted full contact cooling plate as heat exchanger, and this kind of structure is large and not conducive to lightweight. Also, to explore more simple, compact and efficient liquid heat exchange structure has become key technology that need to be breakthrough for liquid flow BTMS. Therefore, we designed a new liquid flow heat transfer structure that simplified cooling plate into flat tube bundle for BTM, aim to achieve good heat transfer capability, reduce the liquid flow volume, and realize lightweight.

Furthermore, the previous researches of BTM only analyzed and evaluated in battery temperature steady state. In fact, applications in temperature unsteady state are objective existence and practical need for BTMS. At present, some we attempt to use vehicle-mounted refrigeration system to rapidly cool battery pack in high temperature and heavy load. But the battery electrochemistry reaction is extremely sensitive to temperature, and the large temperature difference heat transfer conditions will lead to battery temperature uniformity rapidly deteriorate, affect cycle life and even may cause thermal runaway[15-16].

Therefore, it is necessary to investigate basic heat transfer characteristics of BTM in large temperature difference heat exchange conditions, and explore cooling methods to suppress the battery temperature uniformity rapidly deteriorate during the cooling progress.

2. EXPERIMENTAL SYSTEM AND METHODS

In order to make battery thermal management become more efficient and lightweight, we fabricated a flat tube bundle liquid flow heat exchange structure and built experiment system. Meanwhile, different cooling methods and experimental condition parameters were set up.

2.1System Loop and Facilities

The battery thermal management experimental system consisted of simulated battery pack, environment chamber, low temperature refrigerating system, water tank, heater, temperature control unit, expansion tank, battery cooling radiator, refrigerating system radiator, agitator, circulating pump, flow distributor, temperature control unit, regulating valve, circulating pump, filter and so on. The experimental system loop and bench were presented in Fig.1 (a) and Fig.1 (b) respectively.

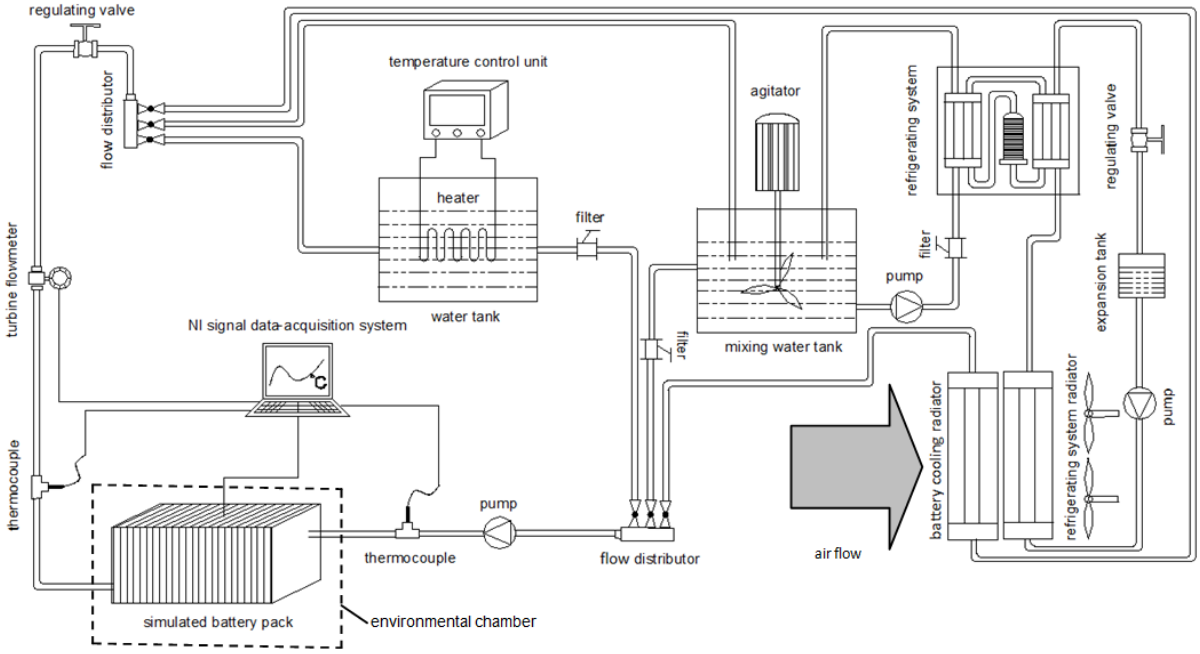

(a): System loop

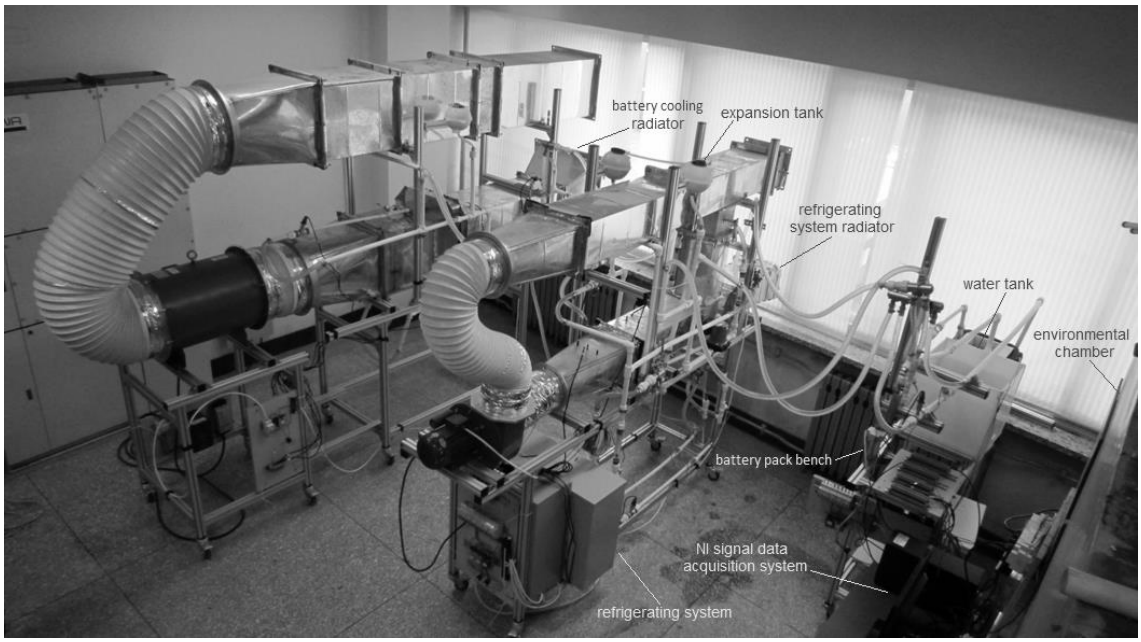

(b): Experimental bench

Figure 1: Battery thermal management experimental system composition

Experimental battery pack consisted of 20 pieces of simulation battery and flat tube bundle heat exchange structure. Flat tube bundle heat exchange structure was mainly composed of end plate, aluminum flat tube bundle, high thermal conductivity material layer, entrance and exit of water pipes, as shown in Fig. 2 (a).Two columns of flat tube bundle were staggered arrangement on both sides of battery surface, and each column consisted of three flat tubes that was taken as heat exchange channel between liquid flow and battery pack. This structure could further reduce liquid volume and flow path compare with full contact cooling plate, and adopt graphite layer with high thermal conductivity as the liner to ensure battery surface temperature uniformity and heat transfer effect. Simulated batteries used carbon fiber heaters to simulate heat generation from real batteries operating. Liquid flow temperature was regulated by water tank, low temperature refrigerating system and radiator. Expansion tank was used to maintain the system pressure and added liquid. The liquid flow was ethylene glycol aqueous solution of 50% volume concentration. Battery pack was in a environment chamber during the experiment process, and system pipes were adopted insulation measures to reduce the environment impact.

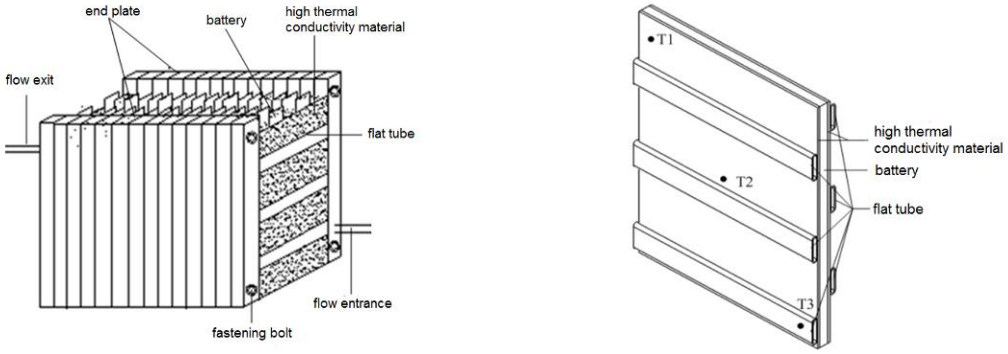

(a*): battery pack* *(b): temperature measured points*

Figure 2: Battery pack structure and temperature measured points' layout

In addition, test system mainly includes NI(National Instrument) signal data acquisition system, the turbine flowmeter, thermocouple, etc. Measurement parameters included temperature of measured points in battery pack, liquid flow temperature of battery pack entrance and exit, liquid flow rate of battery pack entrance and water tank temperature, etc. The 6^{th} and 14^{th} cells were chosen as the measured batteries, and three temperature measured points called T1, T2, T3 were set up on the positive side of each battery respectively. At the same time, symmetric position of T1 was located in the bottom of flat tube on the negative side of battery. T2 and its symmetric position were located out of flat tube in the two sides, and they were also the centre of battery. T3 was located in the bottom of flat tube. Three points' locations were shown in Fig. 2 (b).

2.2 Methods and Parameters

Experiments of BTM were conducted to investigate and analysis characteristics of temperature distribution inside the battery pack under different heat flow conditions. The main cooling methods included synchronized cooling and temperature difference threshold cooling and cascade cooling. by regulating liquid flow rate and liquid flow temperature, to adapt heat load from battery pack in different charging and discharging process, and to seek the most effective cooling methods to achieve good temperature uniformity.

Table 1: Temperature difference threshold cooling methods and parameters

Cooling Methods	Synchronized	Low Temperature Difference	Medium Temperature Difference	High Temperature Difference
Thresholds	0	10℃	20℃	30℃

In order to simulate battery thermal management process, we defined several basic cooling methods that include synchronized cooling, low temperature difference threshold cooling, medium temperature difference threshold cooling and high temperature difference threshold cooling by setting the temperature difference threshold. Synchronized cooling means that circulation pump was started while the battery operating simultaneously. Temperature difference threshold cooling means that circulation pump was started while there is a temperature difference value between battery pack and liquid flow, and threshold values were shown in Table 1. Cascade cooling means that battery pack was cooled by progressive variable

temperature liquid flow which according to the order of 40℃, 30℃ and 20℃ gradually decreased in a 90 s time interval when the batteries in high temperature, and keep liquid flow inlet temperature 20℃ until it reach steady state.

Table 2: Experimental condition parameters

Liquid flow rate/L•min^{-1}	Cell heat load/W	Flow inlet temp/℃	Batteries initial temp/℃
3		40	
4.5	20	30	20
6		20	

Furthermore, selecting battery pack initial temperature 20℃, liquid flow inlet temperature 20℃, liquid flow rate 4.5 L/min, cell heat load 20W as the basic experimental condition, and parameter values of each condition were shown in Table 2. While temperature of battery pack was less than or equal to 1℃ in 5 minutes, it can be seen reach steady state, and balance response time length was from the cooling beginning to the steady state.

3. RESULTS AND ANALYSIS

We mainly explored basic heat transfer characteristics of flat tube bundle liquid flow structure, such as temperature variation, temperature uniformity, thermal response and temperature fluctuation, etc. In order to further promote the temperature uniformity in battery pack cooling process, also proposed the variable temperature cascade cooling method and conducted experimental researches.

3.1 Basic Cooling Effect

Synchronized cooling was adopted for battery pack under basic condition, and the cooling process was compared with no cooling. Meanwhile, by detecting the chosen cells and their measured points' temperature in the battery pack, we investigated the 6th and 14th cells temperature variation characteristics.

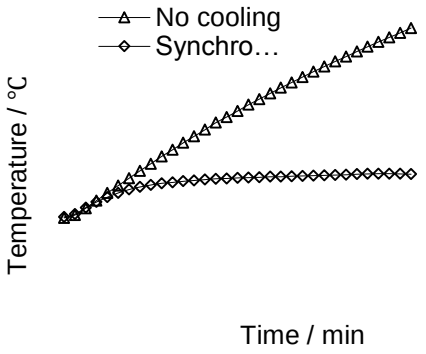

Figure 3: Temperature of the 14th cell's centre

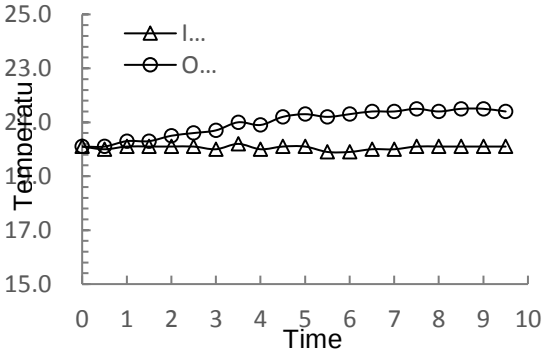

Figure 4: Temperature of liquid flow inlet and outlet

The experimental results were shown in Fig. 3. In the no cooling process, the centre of 14th cell temperature started rising at 4.3℃/min heating rate, then reached about 85℃ from the initial temperature of 20℃ in 15 minutes. In the process of synchronized cooling, the centre of cell heating rate was bigger due to the small temperature difference between battery and liquid flow at initial stage. The battery temperature was gradually risen, and temperature rise rate was decreased until reach steady state after 6minutes. The battery balanced temperature was 33.6℃ ultimately.

At the same time, the temperature of liquid flow inlet and outlet during synchronized cooling process was shown in Fig. 4. Liquid flow inlet temperature was kept 20℃ approximately. The outlet temperature was risen gradually in the experimental process, and it was balanced after 6 minutes. The temperature difference between inlet and outlet was about 1.4℃ at steady state. Thus, the thermal exchange power between the structure and battery pack could be calculated by Equation 1. The total thermal exchange power was 410.9 W and each cell thermal exchange power was 20.5 W. It was consistent with the simulated battery thermal load.

Equation 1: Thermal exchange power between the heat exchange structure and battery pack

$$Q_P = \rho Q_V C_P \Delta T$$

Where:

- Q_P=total thermal exchange power(410.9W)
- Q_V=volume flow rate(5L/min)
- C_P=specific heat capacity of liquid flow(3.281kJ/kg•K)
- ΔT=temperature difference between inlet and outlet(1.4℃)
- ρ=liquid flow density(1073.35kg/m^3)

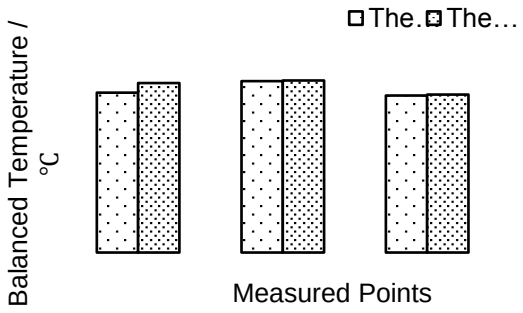

Figure 5: Temperature contrast of measured points at balance time

The measured points' temperatures were compared at steady state as shown in Fig. 5. When the battery temperature reached balance, the measured points' temperature were presented variation caused by different positions. T2's temperature was the highest, and T3's temperature was lowest. The maximum temperature difference was 2.8℃ among three measured points of the 6th cell, and the 14th cell's maximum temperature difference was 2.7℃. The maximum temperature difference between two cells (6th and 14th) was 2.9℃. Therefore, we found that the designed liquid flow heat exchange structure could realize good cooling effect for battery at steady state.

3.2 Comparing Four Cooling Methods

Due to the battery electrochemistry reaction was very sensitive to temperature, so the selection of cooling moment was also very important in battery operating process. Then we analyzed temperature variation rate of four kinds of cooling methods which contained synchronized cooling, low, medium and high temperature difference threshold cooling. The 14th cell of battery pack was chosen as measured batteries to carry out the investigation and analysis.

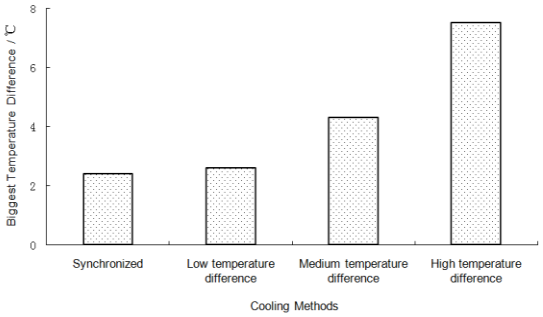

Figure 6: Largest temperature difference of centre measured point

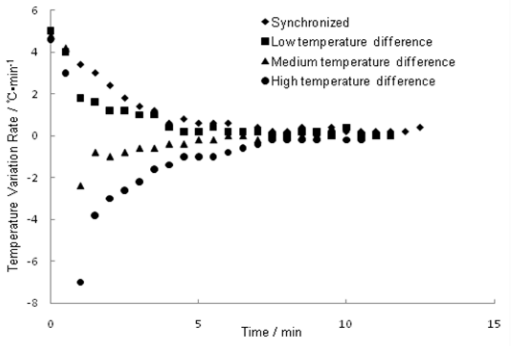

Figure 7: Temperature fluctuation characteristics of centre-measured point

Through comparing the maximum temperature difference of battery's centre under four kinds of cooling methods, we found that the maximum temperature difference was lowest in synchronized cooling process, and this method could ensure good temperature uniformity of battery. The maximum temperature difference rose rapidly with the increase of temperature difference threshold, and it increased to 7.5℃ in high temperature difference threshold cooling method, as shown in Fig. 6.

In addition, in order to further explore temperature fluctuations characteristics inside battery pack, we compared temperature variation rate of the centre points in four kinds of cooling methods, and found that temperature fluctuations were more remarkable than the latter within the first 5 minutes in four kinds of cooling process, as shown in Fig. 7. The centre temperature fluctuation characteristic curve's slope was minimum in synchronized cooling process, and low temperature difference threshold cooling's was bigger. High temperature difference threshold's was significantly greater than other cooling methods, and it presented cold shock to battery pack, which seriously deteriorated temperature uniformity, even may cause thermal runaway.

3.3 Impact Factors Analysis

Obviously, with temperature difference increasing between battery pack and liquid flow, the cooling speed was rising, but temperature uniformity became worsen. Therefore, liquid flow temperature was an important impact factor in battery pack cooling process. Furthermore, the experiment adopted 3 kinds of liquid flow included 3L/min, 4.5L/min and 6L/min, and investigated flow rate change characteristics in medium temperature difference threshold cooling method. At the same time, battery pack initial temperature was 20 ℃, liquid flow inlet temperature was 20℃, and cell heat load was 20W. We found that the temperature variations of centre measured point were basically identical while changing the liquid flow rate, and it had little impact on balanced temperature and response time, as shown in Fig. 8.

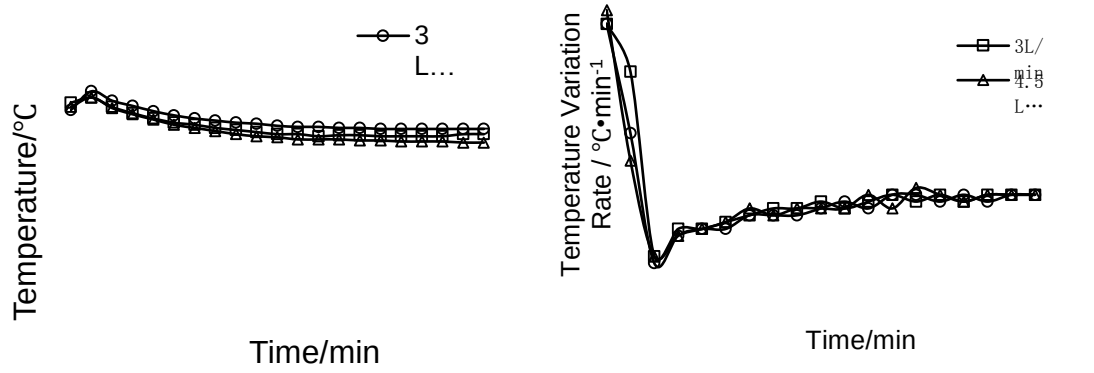

(a) Temperature variation of centre measured point *（b）Temperature variation rate of centre measured point*

Figure 8: Impact of fluid flow rate in the battery cooling process

Through above investigation, we could conclude that the battery cooling effect was not sensitive to variation of liquid flow rate within experimental condition parameters. This characteristic will facilitated to realize low flow resistance and low pump power consumption. At the same time, by comparing with the two impact factors (temperature& flow rate), battery cooling effect was dominated by liquid flow temperature, so making good balance between cooling speed and cooling effect of battery pack had become a key problem need to be solved.

3.4 Effect of cascade cooling method

Although synchronized cooling method presented very good cooling effect and cooling synchronicity in the cooling process of battery pack, it usually need to be open while battery starts working and will cause more power consumption. In fact, it is unnecessary to start synchronized cooling method in early working stage until temperature difference between battery and liquid flow reach set value. Through above analysis we known that low temperature difference threshold cooling method could not achieve rapid cooling response, and high temperature difference threshold cooling method caused temperature uniformity deterioration and cold shock for battery pack.

Therefore, we proposed a cascade cooling method which was a progressive cooling method aim to keep balance between cooling speed and cooling effect, and reduce the negative impact of the high temperature difference threshold cooling.

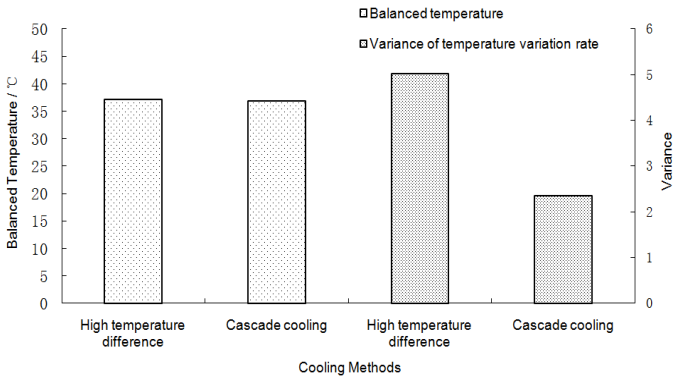

Figure 9: Comparison of cascade cooling and cooling high temperature difference threshold

The experiment was conducted in basic experimental condition, and took 14th cell as the measured batteries. When battery pack temperature rose from 20℃ to 50℃, cascade cooling was started. The liquid flow temperature of battery pack inlet according to the order of 40℃, 30℃ and 20℃gradually decreased with a 90 s time interval, and keep liquid flow inlet temperature 20℃ until it reach steady state. In order to analyze the differences between cascade cooling and high temperature difference threshold cooling, we compared balanced temperature and temperature variation rate by variance statistical method.

The experimental result showed that the final balanced temperatures of battery were equal for two cooling methods, as shown in Fig. 9, but the variance of temperature variation rate in cascade cooling was far less than the temperature difference threshold cooling. It could be seen during large temperature difference rapid cooling process, to adopt the variable temperature cascade cooling method could reduce the negative impact and promote temperature uniformity of battery pack

4 CONCLUSION

(1)Flat tube bundle liquid flow heat exchange structure not only ensured cooling effect of battery pack, but also reduced volume and weight of liquid flow. The balanced temperature of battery pack were kept within 35℃, the cell maximum surface temperature difference was about 2.8℃ and the maximum temperature difference among all cells was about 2.9℃.Meanwhile, synchronized cooling method presented very good cooling effect and cooling synchronicity, but it will consumed more power consumption.

(2)By comparing the effect of high temperature difference threshold cooling method and cascade cooling method, the final balanced temperature of battery pack were equal, but cascade cooling method reduced the impact of cold shock rapidly and promoted temperature uniformity.

(3) In experiment conditions, the impact of liquid flow temperature was remarkable， and the battery cooling effect was not sensitive to variation of liquid flow rate, it will facilitated to realize low flow resistance and low pump power consumption.

5 ACKNOWLEDGEMENTS

The authors gratefully acknowledge the financial support from the NSFC (National Natural Science Foundation of China) under the grant No.51376079 and the Department of Science and Technology of Jilin Province development plan item (No.20130204018GX).

6 REFERENCES

[1] KENNEDY B, Patterson D, Camilleri S, 2000. Use of lithium-ion batteries in electric vehicles[J]. Journal of Power Sources, 90(2):156-162.

[2] VETTER J, Novak P,Wagner M R, et al, 2005. Ageing mechanisms in lithium-ion batteries [J]. Journal of Power Sources, 147(1/2):269-281.

[3] ANMAD A, Pesaran, 2001. Battery Thermal Management in EVs and HEVs: Issues and Solutions[C].Advanced Automotive Battery Conference, Las Vegas, Nevada.

[4]Q. WANG a, B. Jiang a, Q.F. Xue b, H.L. Sun b, B. Li a, H.M. Zou a, Y.Y. Yan, 2014. Applied Thermal Engineering[J], 7,1-7

[5] A.A. PESARAN, S. Burch, and M. Keyser, May 24.27, 1999. An Approach for Designing Thermal Management Systems for Electric and Hybrid Vehicle Battery Packs. In: Fourth Vehicle Thermal Management Systems Conference and Exhibition , London, UK.

[6] HALLAJ S Al, Selman S R, 2002. Thermal modeling of secondary lithium batteries for electric vehicle/hybrid electric vehicle application [J] . Journal of Power Sources, 110: 341-348.

[7] TIANSHI Zhang, Chun Gao, Qing Gao(*), Guohua Wang, MingHui Liu, Yuanke Guo, Cong Xiao, Y.Y. Yan, 2011. Status and development of electric vehicle integrated thermal management from BTM to HVAC, Applied Thermal Engineering,76（2）:76-100.

[8] PENDERGAST DR, De Mauro EP, Fletcher M, Stimson E, Mollendorf JC, 2011. A rechargeable lithium-ion battery module for underwater use. Journal of Power Sources;196(2):793-800.

[9]Anthony JARRETT, Il Yong Kim, 2011. Design optimization of electric vehicle battery cooling plates for thermal performance. Journal of Power Sources 196, 10359 – 10368.

[10]Yuan HAO, Wang Lifang, Wang Liye, 2012. Battery Thermal Management System with Liquid Cooling and Heating in Electric Vehicles. Automotive Safety and Energy, Vo1. 3 No.4.

[11] Peter Dore RAWLINSON, Nicholas Hayden Herron, Bruce Phillip Edwards, Gregory Michael Goetchius, 2013. Vehicle battery pack thermal barrier, us Patent 20130153317A1.

[12] Derek R. WEBER, Roger Michael. Brisbane, 2001. Cooling plate for lithium-ion battery pack, US Patent 2011/0162820A1

[13] Leonid C. LEV, Nikolay Kondratyev, 2013. Cooling system for automotive battery, US Patent 2013/0209856A1.

[14] Admin, 2010. Ford Focus pure electric version of the lithium-ion battery pack will use liquid cooling management program. New energy vehicles Focus.

[15]TETSUYA Kawamura, ARISHISA Kimura, et al, 2002. Thermal stability of alkyl carbonate mixed-solvent electrolytes for lithium ion cells [J]. J Power Sources, 104(2): 260-264.

[16] ROTH E P, Doughty D H, Pile D L, 2007. Effects of separator breakdown on abuse response of 18650 Li-ion cells[J]. J Power Sources, 174(2): 579-583.

81: Numerical investigation of the thermal performance of water based closed loop oscillating heat pipe (CLOHP)

SIEGFRIED YEBOAH[1], JO DARKWA[2]

1 The University of Nottingham Ningbo China, 199Taikang East Road, Ningbo China, Siegfried.yeboah@nottinghamedu.cn
2 The University of Nottingham, University Park, Nottingham, NG7 2RD, UK, J.Darkwa@nottingham.ac.uk

The enhanced capabilities of Oscillating/Pulsating Heat Pipes (OHPs/PHPs) are often curtailed by a gamut of factors that affects their optimum thermal performance. These factors ranging from their design parameters to operating conditions may not make it feasible to develop experimental prototypes through trial and error as optimum thermal performance cannot be ascertained a priori.

In this study, an Eulerian Volume of Fluid (VOF) model coupled with a Level Set Method has been used to numerically investigate the thermal performance of a five-turn water based CLOHP with volume fractions 0.3, 0.5 and 0.7 in vertical and horizontal modes. The capabilities of this computational fluid dynamics (CFD) approach to help predict the optimum thermal performance of OHP/PHPs is well established in literature.

A summary of the results from this investigations show that more convective heat transfer rate occurs from the liquid phase than from the vapour phase. Also orientation was found to significantly influence pressure distribution within the CLOHPs. Finally it was observed that thermal resistance was significantly influenced by volume fraction/fill ratio rather than by orientation of the device.

Keywords: Closed Loop Oscillating Heat Pipe, Volume of Fluid (VOF), Computational Fluid Dynamics (CFD), Thermal Performance

1. INTRODUCTION

Oscillating/Pulsating heat pipes (PHP/OHP) developed by Akachi in the early 1990s are two-phase heat transfer devices that rely on the oscillatory flow of liquid slug and vapour plug. Capable of transporting heat without any additional power input, they offer enhanced heat transfer through passive, two-phase heat transfer mechanism with no wick structure [(Zhang and Faghri, 2008) (Lin et al, 2011) (Bhuwakietkumjohn and Rittidech, 2010)]. Their overall resistance is typically greater than that of traditional heat pipes and can operate at higher heat fluxes (Bejan and Kraus, 2003). A typical system consists of an evaporating section, an adiabatic section, and a condensing section with heat transferred from the evaporating section to the condensing section through forced convection and phase-change (Ma et al, 2008).

Their extensive application range is widely reported in literature [Meena et al (2007) and Meena and Rittidech (2008),]. However their performance is also well documented to be dependent on a host of parameters and properties including the working fluid type, fill ratio, channel geometry, number of serpentine-arranged turns, operating orientation and heating/cooling areas (Thompson et al, 2011). For instance, start-up behaviour is known to be dependent on the working fluid type (Qu et al, 2012). Senjaya and Inoue found that fill ratio also has significant impact on their thermal performance. A critical diameter is required for their design due to the dominance of surface tension (Qu, and Wang, 2013). Other than that the working fluid settles by gravity and no longer pulsates (Khandekar et al, 2003). For the same heat load, a shorter evaporator length translates to higher heat flux and higher evaporator temperature (Qu, and Wang, 2013). Their adiabatic length has considerable effect on thermal performance (Dilawar and Pattamatta (2013) however their number of turns needs to satisfy a critical value for them to operate in the horizontal orientation and vice versa (Khandekar et al, 2003). Katpradit et al (2005) found that a high number of turns may lead to dry-out phenomenon in the evaporator section. The effect of inclination angle essentially reflects the influence of gravity on OHPs/PHPs (Qu et al, 2012). Smoot et al (2011) tested OHPs vertically with the evaporator at the bottom and found that the heat transfer performance was much better than that tested horizontally. Jahani et al (2013) showed that the thermal resistance increases in the horizontal heating mode in comparison to the vertical heating mode.

The varied considerations needed to be made in the design of an effective CLOHP that can achieve optimum thermal performance makes it crucial for theoretical studies to be carried out. This is perceived to invariably limit the trial and error development of experimental prototypes which may have its own associated material cost especially as optimum thermal performance cannot be ascertained a priori. To this end, an Eulerian Volume of Fluid Model coupled with the Level-Set Method a computational fluid dynamics approach is used for the numerical investigation of the thermal performance of water based CLOHP. To avoid significant influence of inclination on a CLOHP with lower number of turn and a possible dry-out in the evaporator section of a higher one, a five-turn system is designed and used for this investigation.

2. PHYSICAL AND NUMERICAL MODELS

2.1 Physical Model Description

Figure 1a and 1b shows a simple annotated 2D geometry and 3D model in the z-x plane of a five-turn Closed Loop Oscillating Heat Pipe (CLOHP) system designed using Rhinoceros 5 and imported into ANSYS Fluent R15.0 respectively. The CLOHP is made of copper tube with internal diameter 2mm. The actual diameter value determined from equation (1) was around 1.5mm but for simplicity in modelling a round off value of 2mm is used in the investigations. Heat input at the evaporator section is rejected at the condenser section. Table 1 provides the typical dimensions of the model.

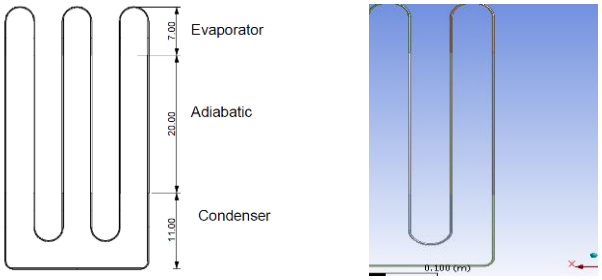

Figure 71: (a) Annotated 2D Geometry of CLOHP in Rhinoceros 5 (b) A 3D Model in ANSYS R15.0 in z-x Plane

Table 20: CLOHP Specification

Parameter	Value	Units
Internal Diameter	2	mm
Pipe Thickness	1	mm
Condenser Length	11	cm
Evaporator Length	7	cm
Adiabatic Length	20	cm
Number of Turns	5	-

The mesh is an automatic mesh generated with 28158 elements and 33660 nodes.

Mathematical Models

Surface tension predominate the two-phase flow in a CLOHP hence the critical diameter should be satisfied (Qu, and Wang, 2013) equation (1)

$$.D_{crit} = 2L = 2\sqrt{\frac{\sigma}{g(\rho_l - \rho_v)}} \quad (1)$$

The VOF Model tracks the interface between phases via a continuity equation for the volume fraction given by (ANSYS, 2012);

$$\frac{1}{\rho_q}\left[\frac{\partial}{\partial t}(\alpha_q\rho_q) + \nabla.(\alpha_q\rho_q\vec{v}_q) = S_{\alpha q} + \sum_{p=1}^{n}(\dot{m}_{pq} - \dot{m}_{qp})\right] \quad (2)$$

The density in each cell is given by;

$$\rho = \alpha_2\rho_2 + (1-\alpha_2)\rho_1 \quad (3)$$

In the general form, the volume fraction averaged density is:

$$\rho = \sum \alpha_q\rho_q \quad (4)$$

ANSYS Fluent solves the Momentum equation by:

$$\frac{\partial}{\partial t}(\rho\vec{v}) + \nabla.(\rho\vec{v}\vec{v}) = -\nabla p + \nabla.[\mu(\nabla\vec{v} + \nabla\vec{v}^T)] + \rho\vec{g} + \vec{F} \quad (5)$$

The energy equation for the phases is given by:

$$\frac{\partial}{\partial t}(\rho E) + \nabla.\left(\vec{v}(\rho E + p)\right) = \nabla.\left(k_{eff}\nabla T\right) + S_h \quad (6)$$

For the VOF model, energy E and temperature T are mass averaged variables determined as follows:

$$E = \frac{\sum_{q=1}^{n}\alpha_q\rho_q E_q}{\sum_{q=1}^{n}\alpha_q\rho_q} \quad (7)$$

For the Continuum Surface Force (CSF) Model in ANSYS Fluent, the pressure drop across the surface depends on the surface tension coefficient and the surface curvature measured by two radii in orthogonal directions:

$$p_2 - p_1 = \sigma\left(\frac{1}{R_1} + \frac{1}{R_2}\right) \quad (8)$$

The CSF is computed from local gradients in the surface normal $n = \nabla\alpha_q$

The curvature, $\kappa = \nabla.\hat{n}$ where $\hat{n} = \frac{n}{|n|}$

The level-set function, the signed distance to the interface is given by

$$\varphi(x,t) = \begin{cases} +|d| \; if \; x \in the \; primary \; phase \\ 0 \; if \; x \in \Gamma \\ -|d| if \; x \in the \; secondary \; phase \end{cases} \quad (9)$$

Where

- $\Gamma = \{x|\varphi(x,t) = 0\}$ in a two phase system
- d - the distance from the interface

For the surface tension force, the normal and curvature of the interface are needed

$$; \vec{n} = \frac{\nabla\varphi}{|\nabla\varphi|}\Big|_{\varphi} = 0 \quad (10)$$

$$\kappa = \nabla.\frac{\nabla\varphi}{|\nabla\varphi|}\Big|_{\varphi} = 0 \quad (11)$$

The evolution of the level set is given by equation $\frac{\partial\varphi}{\partial t} + \nabla.(\vec{u}\varphi) = 0$

The momentum equation is therefore written as

$$\frac{\partial}{\partial t}(\rho\vec{u}) + \nabla.(\rho\vec{u}\vec{u}) = -\nabla p + \nabla.\mu[\nabla\vec{u} + (\nabla\vec{u})^T] - \sigma\kappa\delta(\varphi) + \rho\vec{g} \quad (12)$$

$$\delta(\varphi) = \frac{1+cos\left(\pi\varphi/a\right)}{2a} \text{ if } |\varphi| < a, \quad \text{otherwise } \delta(\varphi) = 0.\sigma$$

Where, a=1.5h, h is the grid spacing and $\vec{u}$ is the underlying velocity field

Thermal Resistance (R) according to Hao et al (2014) is determined by

$$R = \frac{\bar{T}_e - \bar{T}_c}{Q_e} \quad (13)$$

3. MODELLING AND SIMULATION METHODOLOGY

The CLOHP model was designed in Rhinoceros 5 and imported into ANSYS Design Modeler where new parts consisting of the condenser, adiabatic and evaporator sections formed. The geometry was then automatically meshed and loaded into Fluent for simulation. The VOF model was chosen because it has

the capability to model two or more immiscible fluids by solving a single set of momentum equations whilst tracking the volume fraction of each of the fluids throughout the domain (ANSYS, 2012). Nagwase and Pachghare (2013) and Liu and Chen (2014) also successfully used this model in investigating the performance of Closed Loop Pulsating Heat Pipes.

For this present study, a pressure based transient model with consideration for acceleration due gravity was used. For the flow, laminar viscous model was selected and viscous heating activated. The chosen working fluid was water hence the two phases in this model are water liquid and water vapour. Since the physical model is a closed loop and oscillation of fluid within the loop was expected, translational periodic boundary conditions were created for the evaporator and condenser sections using sliding meshes. Phase interaction was enabled for surface tension coefficient a text command used to activate the relevant equations during the simulation. At the walls, contact angle of 67.42° for water in a capillary tube obtained from literature (Kumar et al, 2014) was used.

The level set (LS) method was coupled with the VOF model due to the VOF method's weakness in the calculation of its spatial derivatives (ANSYS, 2012). According to Sun and Tao (2010) by using the level set function, inaccuracy of curvature and bad smoothness of discontinuous physical quantities near interfaces, can be overcome. Authors such as Lv et al (2010), Ningegowda and Premachandran (2014) and Wang et al (2013) have also used VOF coupled with LS in their investigations.

The evaporator temperature was 393K whilst the condenser and adiabatic sections were maintained at the default temperature of 300K. Translational periodic condition at a velocity of 1m/s was set in the z and y orientations. The Pressure-Implicit with Splitting of Operators (PISO) algorithm coupled with pressure-velocity scheme and a geometric reconstruction scheme was then used to solve the related transport equations. The volume fraction/fill ratio of the liquid phase was patched to all cell zones for the two orientations. The solver was then initialized at the respective volume fractions. Convergence was set to absolute criteria where residuals were expected to go below 0.001 for all transport equation and 1e-06 for energy. 120 time steps of size 0.0002791947 empirically determined was used for a maximum iteration of 40 per time step. The case and data files from the simulation which had results of the geometry and simulation were loaded in ANSYS CFD Post for quantitative analysis. Here expressions and locations were created for the numerical processing of results and the qualitative display of variables for analysis. Transient data was generated via CFD Post for analysis.

4. RESULTS AND DISCUSSIONS

The results provide a perspective of the transient performances of the CLOHPs under the chosen fill ratios and orientations. On the x-axis of the graphs, ctstep created through expressions in ANSYS CFD Post represents the current time step whilst the variables of interest are represented on the y-axis. Three graphs headed with their respective volume fractions (VF) are plotted per figure for relevant thermal properties.

4.1 Evaporator Temperature

Figure 2a and 2b shows a relatively constant input temperature at the evaporator sections of the CLOHPs under the two orientations considered. Here the typical trend shows a sharp rise in temperature from about 320K to a steady temperature of 393K throughout the simulation. For both orientations and all volume fractions, the figures show that the steady 393K input temperature was reached after 5 time steps.

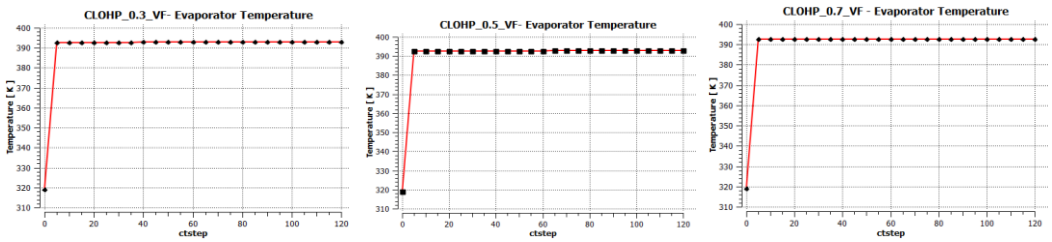

Figure 2a: Evaporator Temperature for CLOHPs – Vertical Orientation

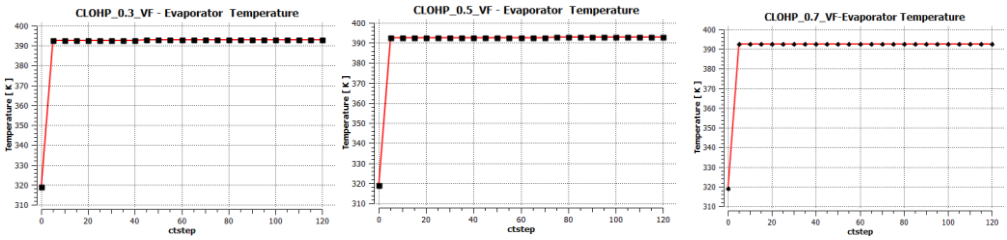

Figure 2b: Evaporator Temperature for CLOHPs – Horizontal Orientation

4.2 Condenser Temperature

The condenser section on the other hand provides an entirely different perspective of the working condition of the CLOHPs. From Figures 3a and 3b, it can be seen that the condenser temperature varied significantly for each CLOHP under the two orientations. For Figure 3a, the profiles clearly shows different activities at different fill ratios for the condensers. What is common to the CLOHPs in Figure 3a is that before the 30th time step they were relatively at the same temperature and at the end of the simulation they all settled at the same temperature. Other than that their transient histories shows different fill ratios peaked at different temperatures. It is important to note that these temperature variations, although appear wide, are variations within a small temperature range. The profiles in Figure 3a also show that the lower fill ratio CLOHP condenser had a wider variation of temperature and momentary peak condenser temperature.

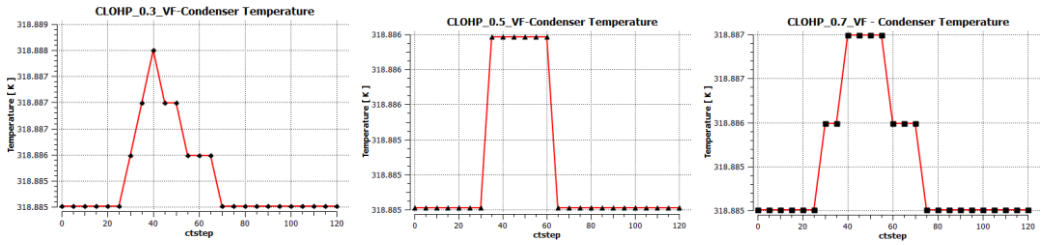

Figure 3a: Condenser Temperature for CLOHPs – Vertical Orientation

The profiles shown in Figure 3b are generally different for corresponding fill ratios in Figure 3a. However, an oddity in condenser performance is observed for fill ratio 0.7 in Figure 3b and fill ratio 0.5 in Figure 3a. A closer look shows that these two CLOHPs share a similar condenser performance profiles. The profiles for the other two in Figure 3b are also similar although their values vary slightly. They both seem to show a sharp decline in temperature after the 60th time step.

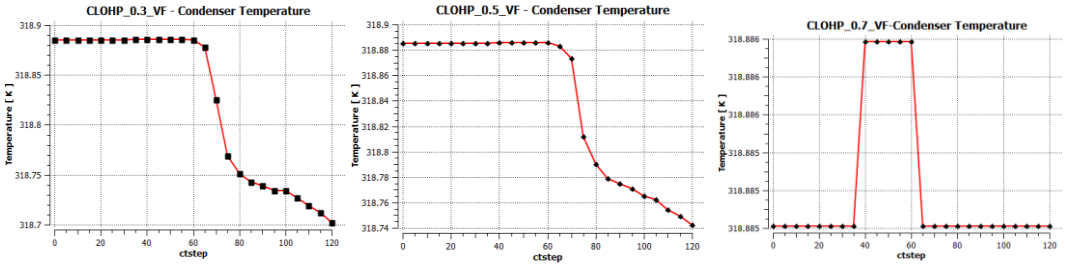

Figure 3b: Condenser Temperature for CLOHPs – Horizontal Orientation

4.3 Evaporator Wall Heat Flux

The trends for the wall heat flux shown in Figure 4a and 4b were similar in profile for all the CLOHPs and same for specific fill ratios. From the beginning of the simulation till time step 5, the input flux profile sharply increased to a peak value for all fill ratios and orientations capturing a similar trend as their temperature profiles. For the same evaporator temperature for all fill ratios, the wall flux plots in Figure 4a and 4b shows varying input flux for each fill ratio. It is evident from the plots that the input flux increased with fill ratio for the same input temperature requirement.

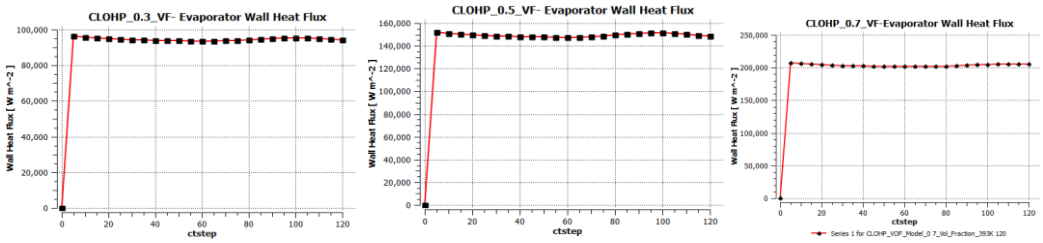

Figure 4a: Evaporator Wall Heat Flux for CLOHPs in Vertical Orientation

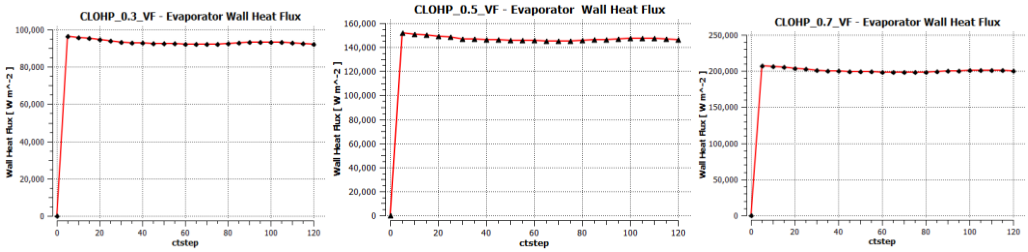

Figure 4b: Evaporator Wall Heat Flux for CLOHPs in Horizontal Orientation

4.4 Condenser Wall Heat Flux

The negative heat fluxes shown for the condenser section for the CLOHPs in Figure 5a and 5b signifies the heat rejection by the CLOHP. This typically reflects the cooling capacity of the CLOHPs studied. The plots indicated an initial sharp decline of the wall heat flux to a lower value until a gradual rise from the 5th time step. From the plots it is evident that the condenser wall heat flux decreases with increasing fill ratio for both orientations.

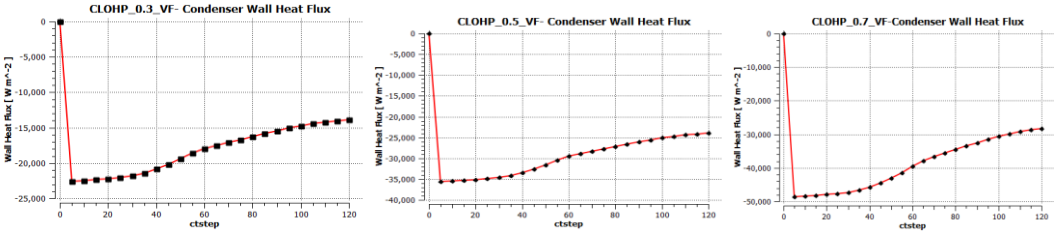

Figure 5a: Condenser Wall Heat Flux for CLOHPs– Vertical Orientation

However on further iterations, it can be seen from both figures that the condenser wall heat flux remains at a lower value when horizontally inclined than when vertically inclined. In fact the difference after 40 time steps is very significant between the two orientations.

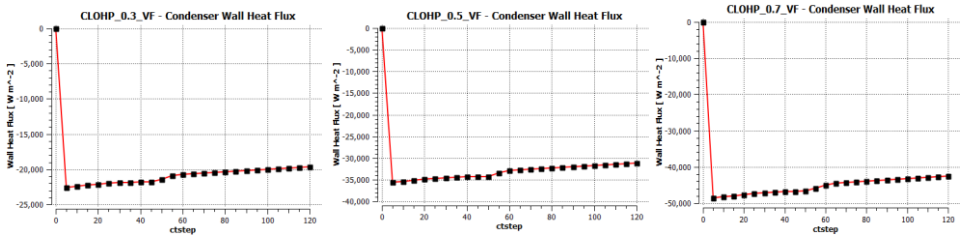

Figure 5b: Condenser Wall Heat Flux for CLOHPs – Horizontal Orientation

4.5 Evaporator Surface Heat Transfer Coefficient

The evaporator surface heat transfer coefficient increased with increasing fill ratio. This is evident from Figures 6a and 6b, as the values are typically higher for CLOHPs with greater proportion of liquid volume fraction demonstrating that more convective heat transfer rate is expected from the liquid phase than from the vapour phase. For both orientations, surface heat transfer coefficient for the evaporator section increased with increasing fill ratios.

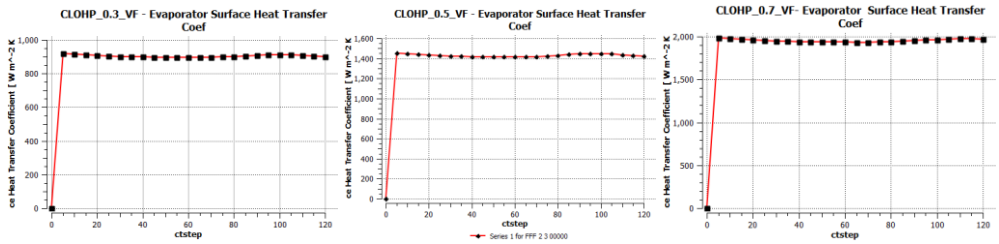

Figure 6a: Evaporator Surface Heat Transfer Coefficient for CLOHPs– Vertical Orientation

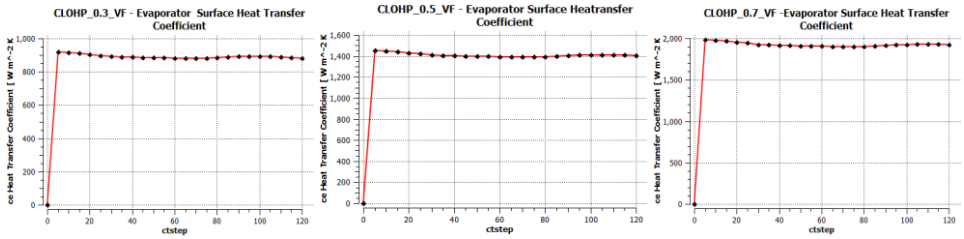

Figure 6b: Evaporator Surface Heat Transfer Coefficient for CLOHPs– Horizontal Orientation

4.6 Condenser Surface Heat Transfer Coefficient

The condenser surface heat transfer coefficient as related to the wall heat flux also reflected the heat rejection (See Figures 7a and 7b). The trends once again were similar showing an initial sharp decline to a lower value before a steady rise for all fill ratios and orientations.

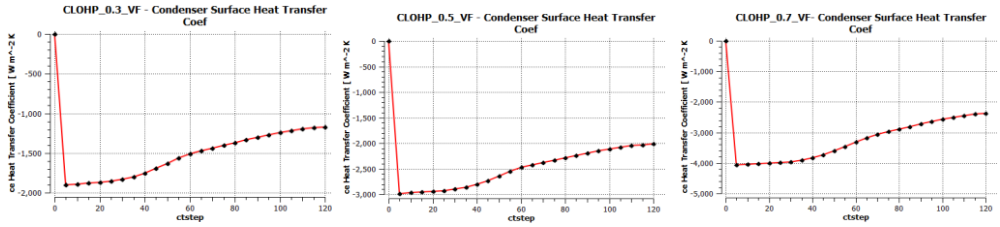

Figure 7a: Condenser Surface Heat Transfer Coefficient – Vertical Orientation

Similar to the wall heat flux, this parameter for both orientations decreased with fill ratio. The significant differences can be seen for respective volume fractions between the vertically inclined and horizontally inclined CLOHPs.

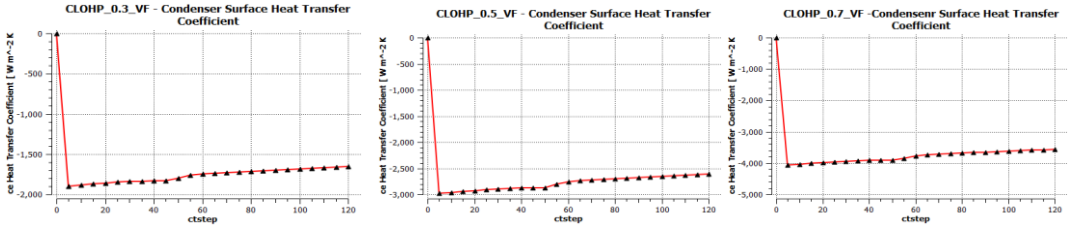

Figure 7b: Condenser Surface Heat Transfer Coefficient for CLOHPs– Horizontal Orientation

4.7 Evaporator Pressure

For the vertical orientation, the pressure within the evaporator section increased with decreasing fill ratio as can be seen in Figure 8a. At the beginning of the simulation, the pressure increases sharply to a high value on input of energy into the evaporator. From Figure 8a it is evident that the pressure in the evaporator is largely due to the vapour phase as the pressure in the CLOHP with fill ratio of 0.7 is about half the pressure in the CLOHP with fill ratio of 0.3.

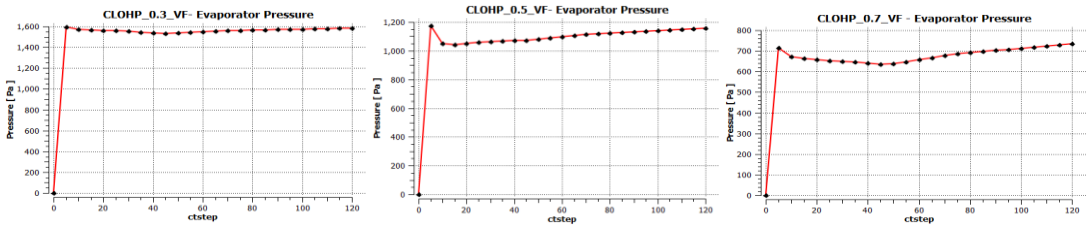

Figure 8a: Evaporator Pressure for CLOHPs in Vertical Orientation

For the horizontally oriented CLOHPs (Figure 8b), the trend is somewhat opposite that of the vertically oriented. Here the pressure declines sharply on commencement of the simulation. It is however evident from both Figures 8a and 8b that the sharp increase or decrease in pressure gradually enters a steady regime from the 5th time step possibly demonstrating the time at which oscillations begun in the CLOHPs.

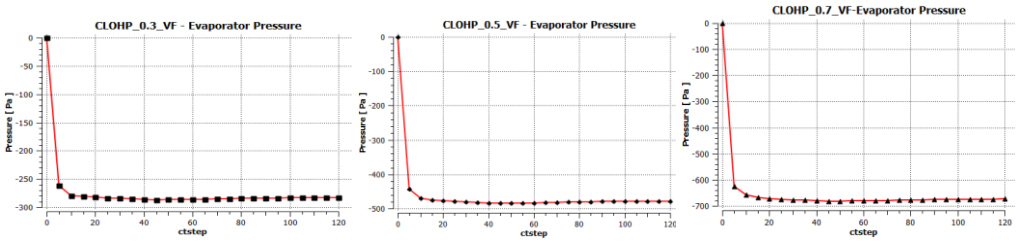

Figure 8b: Evaporator Pressure for CLOHPs in Horizontal Orientation

4.8 Condenser Pressure

The condenser pressure for the vertically oriented CLOHPs follows a similar trend as their evaporator (see Figure 9a). However for the CLOHPs with fill ratios 0.5 and 0.7, it is evident from the plots that on further iterations the pressure in the condenser increases slight above their respective evaporator pressures.

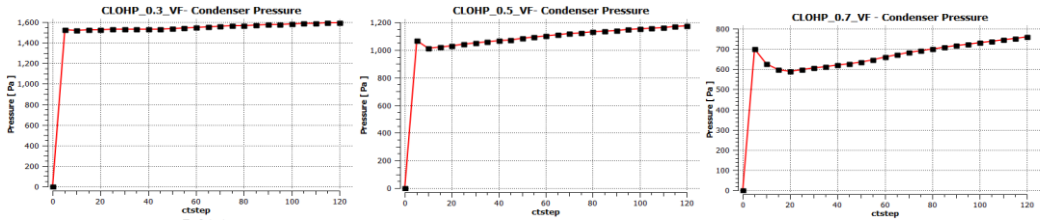

Figure 9a: Condenser Pressure for CLOHPs in Vertical Orientation

For the horizontally inclined CLOHPs, the pressures in the condensers are opposite that of their evaporator pressures. In Figure 9b it can be seen that the condenser pressure increases with increasing volume fraction/fill ratio. This is also the opposite to that of the condenser pressure in the vertically inclined CLOHP where the pressure decreases with fill ratio (see Figure 9a).

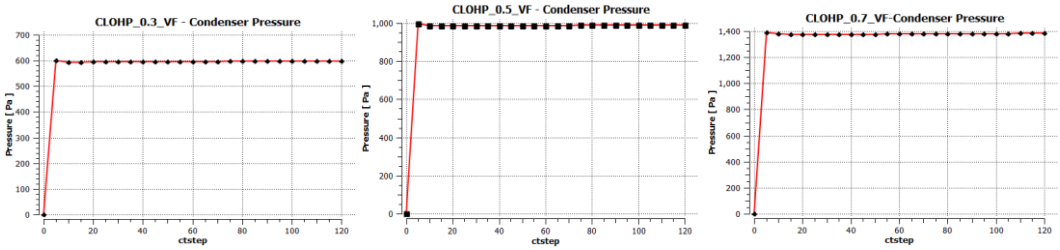

Figure 9b: Condenser Pressure for CLOHPs in Horizontal Orientation

4.9 Influence of Orientation on Pressure Distribution

Contours shown in Figures 10a and 10b clearly shows the influence of gravity on pressure distribution for the two orientations. In Figure 10a, it can be seen that the influence of gravity does not allow the even

distribution of pressure across the various sections namely the evaporator, condenser and adiabatic sections.

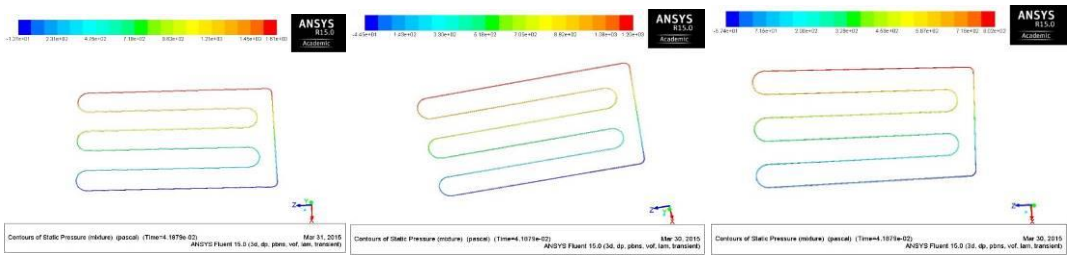

Figure 720a: Contours of Static Pressure in Vertical Orientation. From Left to Right, CLOHPs with Volume Fractions 0.3, 0.5 and 0.7 Respectively

Contrary to the trend demonstrated for the vertically inclined CLOHP, for the horizontally inclined, the pressure distribution is even across the CLOHP sections. In Figure 10b, it can be seen that the maximum pressure is at the condenser section whilst the least pressure is shown at the evaporator section. It is also evident from the two orientations that volume fraction only has influence on the pressure values but not the distribution.

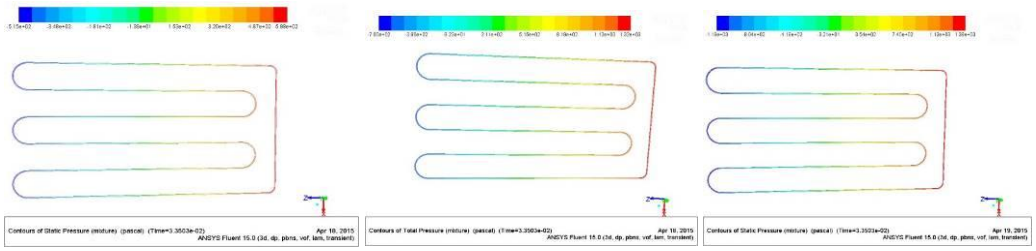

Figure 730b: Contours of Static Pressure in Horizontal Orientation. From Left to Right, CLOHPs with Volume Fractions 0.3, 0.5 and 0.7 Respectively

4.10 Thermal Performance

The thermal Performance of the vertically and horizontally oriented CLOHPs was determined using equations (13) and plotted on Figure 11. It is evident from the plot that thermal resistance decreases with increasing volume fraction/fill ratio.

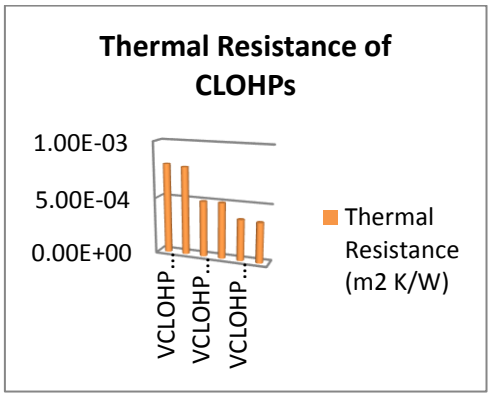

Figure 11: Thermal Resistance Plots of CLOHPs. VCLOHP Represents CLOHP in Vertical Orientation and HCLOHP Represents CLOHP in Horizontal Orientation

Between CLOHPs of same volume fraction but different orientations, the results show that the vertically inclined CLOHPs had a higher thermal resistance than their horizontal counterpart consistent with the findings from (Smoot et al, 2011).

5. CONCLUSION

An Eulerian Volume of Fluid (VOF) model coupled with a Level Set Method has been used to numerically investigate the performance of a five-turn water based CLOHP. Volume fractions 0.3, 0.5 and 0.7 were studied in vertical and horizontal modes. From the results; the following major observations were made:

- At a constant evaporator temperature of 393K, the condenser temperature varied significantly for each CLOHP under the two orientations although their temperature ranges were largely common per orientation. The CLOHP with volume fraction of 0.5 in vertical orientation and the one with volume fraction of 0.7 in horizontal orientation shared similar temperature profile.
- For both orientations the evaporator wall heat flux increased with fill ratio for the same input temperature requirement. For the condenser, the wall heat flux decreased with increasing fill ratio for both orientations although values were reasonably lower in the respective horizontally inclined CLOHPs.
- The surface heat transfer coefficient for the evaporator also increased with increasing fill ratios for both orientations. The trends were similar for the condenser section as their respective wall heat fluxes.
- For the vertically orientated CLOHPs, the pressure within the evaporator section increased with decreasing fill ratio whereas in horizontal orientation the opposite was true.
- The pressure profile was similar for the condenser section and its corresponding evaporator section in vertically oriented mode whilst the opposite occurred in the horizontal mode.
- The pressure distribution within the CLOHPs appeared not be influenced by their fill ratios. However, orientation was found to have profound influence. In horizontal mode, the condenser was found to have the maximum pressure whereas in vertical mode the pressure distribution was uneven for each section.
- For the thermal performance, the simulations show that thermal resistance decreases with increasing volume fraction. In terms of orientation, the study shows that the differences are slight but the thermal resistance was higher in vertically oriented mode than in the horizontally oriented mode for the same fill ratio.

Overall, it was observed that, more convective heat transfer rate occurs from the liquid phase than from the vapour phase. Also orientation significantly influences pressure distribution within the CLOHPs with thermal performance significantly influenced by volume fraction/fill ratio rather than by orientation.

6. NOMENCLATURE

- D_{crit} - Critical diameter (m)
- $\vec{F}$ is a body force
- g – Acceleration due to gravity (m/s^2)
- L - Laplace constant which represents the bubble diameter at departure for pool nucleate boiling
- n - the number of phases
- p_1 and p_2 are the pressures in the two fluids on either side of the interface
- Q_e - input power.
- R-Thermal Resistance
- $S_{\alpha q}$ - the mass source
- $\bar{T}_e$ - the average surface temperature of the evaporation section,
- $\bar{T}_c$ - the average surface temperature of condensation section,
- $\bar{T}_v$ - the vapour temperature, which can be replaced by the average adiabatic section temperature $\bar{T}_a$
- $\vec{V}_v$ is the vapour phase velocity
- $\vec{v}_m$ is the mass averaged velocity
- $\vec{v}_{dr,k}$ is the drift velocity for the secondary phase k; $\vec{v}_{dr,k} = \vec{v}_k - \vec{v}_m$

- *v* - the vapour phase
- α_k -the volume fraction of phase k
- α - the vapour volume fraction
- ρ_L – Density of saturated liquid (kg/m^3)
- ρ_m - the mixture density; $\rho_m = \sum_{k=1}^{n} \alpha_k \rho_k$
- ρ_v - the vapour density (kg/m^3)
- σ – Surface tension (N/m)
- μ_m the viscosity of the mixture; $\mu_m = \sum_{k=1}^{n} \alpha_k \mu_k$
- coeff - coefficient that needs to be fine-tuned and can be interpreted as a relaxation time.

7. REFERENCES

AKACHI, H. (1990) “Structure of a heat pipe”, U.S. Pat., 4921041.

ANSYS, Inc. (2012) ANSYS Fluent Theory Guide. February 2012. Release 14.5 - © SAS IP, Inc.

BEJAN, Adrian. and Kraus, Allan D. (2003). Heat Transfer Handbook. John Wiley & Sons

BHUWAKIETKUMJOHN, N. and Rittidech, S. (2010) Internal flow patterns on heat transfer characteristics of a closed-loop oscillating heat-pipe with check valves using ethanol and a silver nano-ethanol mixture. Experimental Thermal and Fluid Science, Volume 34, Issue 8, Pages 1000-1007

DILAWAR, Mahendra and Pattamatta, Arvind (2013) A parametric study of oscillatory two-phase flows in a single turn Pulsating Heat Pipe using a non-isothermal vapor model. Applied Thermal Engineering, Volume 51, Issues 1–2, Pages 1328-1338

HAO, Tingting. Ma, Xuehu. Lan, Zhong. Li, Nan. Zhao,Yuzhe and Ma, Hongbin. (2014) Effects of hydrophilic surface on heat transfer performance and oscillating motion for an oscillating heat pipe. International Journal of Heat and Mass Transfer, Volume 72, Pages 50-65

JAHANI, Kambiz. Mohammadi, Maziar. Shafii, Mohammad Behshad. and Shiee, Zahra. (2013) Promising Technology for Electronic Cooling: Nanofluidic Micro Pulsating Heat Pipes. Journal of Electronic Packaging ASME, Vol. 135 / 021005-1

KATPRADIT, T. Wongratanaphisan, T. Terdtoon, P. Kamonpet, P. Polchai,A. and Akbarzadeh, A. (2005) Correlation to predict heat transfer characteristics of a closed end oscillating heat pipe at critical state. Applied Thermal Engineering, Volume 25, Issues 14–15, Pages 2138-2151

KHANDEKAR, Sameer. Charoensawan, Piyanun. Groll, Manfred., and Terdtoon. Pradit (2003) Closed loop pulsating heat pipes Part B: visualization and semi-empirical modeling. Applied Thermal Engineering, Volume 23, Issue 16, Pages 2021-2033

KUMAR, Sushant. Mehta, Balkrishna. Bajpai, Ashish. and Khandekar, Sameer (2014) LOCAL THERMO-HYDRODYNAMICS OF A LIQUID PLUG PULSATING INSIDE A DRY CAPILLARY TUBE. Proceedings of the 4th European Conference on Microfluidics - Microfluidics 2014 - Limerick,

LIN, Zirong. Wang, Shuangfeng. Huo, Jiepeng. Hu, Yanxin. Chen, Jinjian. Zhang, Winston and Lee, Eton (2011) Heat transfer characteristics and LED heat sink application of aluminum plate oscillating heat pipes. Applied Thermal Engineering, Volume 31, Issues 14–15, Pages 2221-2229

LIU, Xiangdong and Chen, Yongping (2014) Fluid flow and heat transfer in flat-plate oscillating heat pipe. Energy and Buildings, Volume 75, Pages 29-42

LV, Xin. Zou, Qingping. Zhao,Yong and Reeve, Dominic (2010)A novel coupled level set and volume of fluid method for sharp interface capturing on 3D tetrahedral grids. Journal of Computational Physics, Volume 229, Issue 7, Pages 2573-2604

MA, H. B. Borgmeyer, B. Cheng, P. and Zhang, Y. (2008) Heat Transport Capability in an Oscillating Heat Pipe. J. Heat Transfer 130(8), 081501

MEENA, P., Rittidech, S. and Poomsa-ad, N. (2007) Application of closed-loop oscillating heat-pipe with check valves (CLOHP/CV) air-preheater for reducing relative humidity in drying systems, Applied Energy 84, pp. 553–564.

MEENA, P. and Rittidech, S. (2008) Waste Heat Recovery by Closed-Loop Oscillating Heat Pipe with Check Valve from Pottery Kilns for Energy Thrift. American J. of Engineering and Applied Sciences 1 (2): 126-130,

NAGWASE, Subhash Y. and Pachghare, Pramod R. (2013) Experimental and CFD Analysis of Closed Loop Pulsating Heat Pipe with DI-Water. Energy Efficient Technologies for Sustainability (ICEETS), 2013 International Conference, Page(s):185 - 190.

NINGEGOWDA, B.M. and Premachandran, B. (2014) A Coupled Level Set and Volume of Fluid method with multi-directional advection algorithms for two-phase flows with and without phase change. International Journal of Heat and Mass Transfer, Volume 79, Pages 532-550\

QU, Jian and Wang, Qian (2013) Experimental study on the thermal performance of vertical closed-loop oscillating heat pipes and correlation modeling Original Research Article. Applied Energy, Volume 112, Pages 1154-1160

QU, Jian. Wu, Huiying, and Cheng, Ping. (2012) Start-up, heat transfer and flow characteristics of silicon-based micro pulsating heat pipes. International Journal of Heat and Mass Transfer, Volume 55, Issues 21–22, Pages 6109-6120

SENJAYA, Raffles and Inoue, Takayoshi (2013) Oscillating heat pipe simulation considering bubble generation Part I: Presentation of the model and effects of a bubble generation. International Journal of Heat and Mass Transfer, Volume 60, Pages 816-824

SENJAYA, Raffles and Inoue, Takayoshi (2014) Effects of non-condensable gas on the performance of oscillating heat pipe, part I: Theoretical study. Applied Thermal Engineering, Volume 73, Issue 1, Pages 1387-1392

SMOOT, C. D. Ma, H. B. Wilson, C. A. and Greenberg, L. (2011) Heat Conduction Effect on Oscillating Heat Pipe Operation. Journal of Thermal Science and Engineering Applications, Vol. 3 / 024501-5

SUN, D.L .and Tao, W.Q.(2010) A coupled volume-of-fluid and level set (VOSET) method for computing incompressible two-phase flows. International Journal of Heat and Mass Transfer, Volume 53, Issue 4, Pages 645-655

THOMPSON, S.M. Cheng, P. and Ma, H.B. (2011) An experimental investigation of a three-dimensional flat-plate oscillating heat pipe with staggered microchannels. International Journal of Heat and Mass Transfer, Volume 54, Issues 17–18, , Pages 3951-3959

WANG, Tai. Li, Huixiong. Feng, Yongchang. and Shi, Dongxiao. (2013) A coupled volume-of-fluid and level set (VOSET) method on dynamically adaptive quadtree grids. International Journal of Heat and Mass Transfer, Volume 67, Pages 70-73

ZHANG, Yuwen and Faghri, Amir (2008) 'Advances and Unsolved Issues in Pulsating Heat Pipes', Heat Transfer Engineering, 29:1, 20 – 44

88: The environmental impact of thermal discharge of warm water from a heat pump in commercial building to a canal

PORNPUT JARUMONGKONSAK[1], SHENYI WU[2], YUYING YAN[3]

1 HVACR & Heat Transfer Research Group, University of Nottingham, UK NG7 2RD, ezxpj@nottingham.ac.uk
2 HVACR & Heat Transfer Research Group, University of Nottingham, UK NG7 2RD, lazsw@nottingham.ac.uk
3 HVACR & Heat Transfer Research Group, University of Nottingham, UK NG7 2RD, lazyy@nottingham.ac.uk

Using natural water sources like rivers, lakes, canals etc. to remove heat from heat pump or air-conditioner systems is a good practice in terms of improving the system efficiency and running costs. However, the rise of water temperature due to the discharge of heat could potentially impact on the near-by environment and animals. In order to minimise the impact, measures have to be taken to make sure the discharge complying with the regulations. Currently, this is done case by case, which is accurate but time consuming. A general and reliable model of thermal discharge is a useful tool for this purpose; however, this has not yet been sufficiently developed. This study is a step towards this direction and develops an exact solution through applying the advection-diffusion equation for temperature with the known boundary conditions. By assuming that the thermal diffusion in the canal is similar to plume diffusion in the river, the general equations of both vertical and transverse turbulent diffusivities were found from the combination of Manning's equation and Fischer's common formula. A Matlab model based on this has been developed and the solution from this model was verified by the referred experiment data with 3-5% difference. The results from the exact solution show that the major influence factors to the thermal diffusion in the canal are the ground friction, the hydraulic radius and the depth of the canal. They influence the turbulent vortices and eddy in vertical and transverse directions through shear forces. Meanwhile, the variation of velocity of discharged warm water in the turbulent range is unaffected to the temperature decay when is higher enough to reach the maximum limit of turbulent diffusion on its specific canal condition.

Keywords: Heat pump, Thermal discharge, Environmental impact

1. INTRODUCTION

Heat pumps or air-conditioner systems are essential part of current commercial buildings Taking water from natural or artificial canals to cool the systems and then discharging it back is one of the system improvements (Figure 1). The system benefits from both lower operating cost and higher efficiency. The reduction in total system's energy consumption also means a reduction to CO_2 emission. However, this approach could have a local environment impact which cannot be ignored. The regulations require that temperature and other properties of the public water resources have to be controlled within the allowance and routinely recorded if they are used as heat sink. These criteria are varied from countries to other countries. In the UK, 28°C is the maximum ambient canal water temperature (Ali, 2011) to prevent the de-oxygenation, which is a risk for local aquatic life. The mathematic model to predict the temperature rise is useful for this application at the design stage. Therefore, this research has an aim to develop a more general but still reliable model of the thermal discharge to a canal.

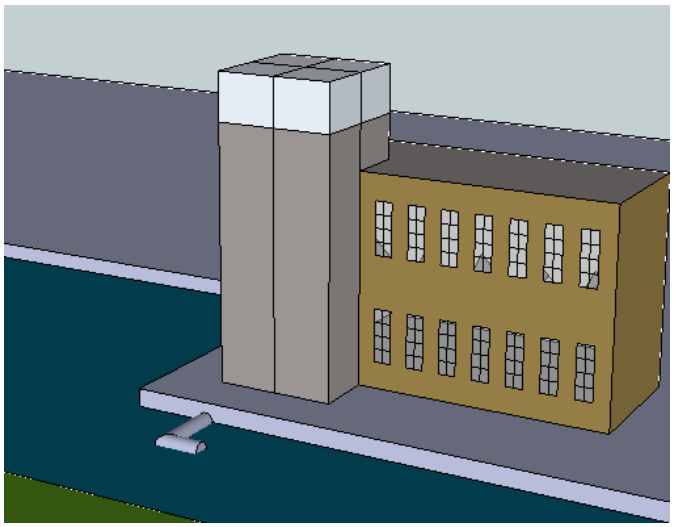

Figure 74: Thermal discharge to a canal from a commercial building

2. MATHEMATICAL MODEL

The turbulent advection-diffusion equation for temperature (Equation 1) consists of advection terms, which are occurred from water flow, on the left side of the equation and two different kinds of diffusion term on the right side. The first diffusion is molecular diffusion from thermal conductive ability, while the second, known as rapid mixing, is thermal turbulent diffusion. Since the turbulent diffusivity is much greater than the molecular diffusivity, all three directional the molecular diffusions are neglected. Besides, from typical discharging characteristic of warm water into a shallow canal in Figure 2, the traverse and vertical velocities are very small and can be neglected. The influence of the buoyant force can be neglected due to small temperature difference in the water. Since the heat transport due to the longitudinal velocity is much larger than that due to turbulent diffusion in the same direction when discharging with high velocity (Roberts and Webster, 2002), the longitudinal turbulent diffusion can be neglected. Then, the remaining terms in steady state condition are shown in Equation 2.

Equation 14:

$$\frac{\partial T}{\partial t}+\left(U\frac{\partial T}{\partial X}+V\frac{\partial T}{\partial Y}+W\frac{\partial T}{\partial Z}\right) = \left(\frac{k_X}{\rho Cp}\frac{\partial^2 T}{\partial X^2}+\frac{k_Y}{\rho Cp}\frac{\partial^2 T}{\partial Y^2}+\frac{k_Z}{\rho Cp}\frac{\partial^2 T}{\partial Z^2}\right)+\left(D_X\frac{\partial^2 T}{\partial X^2}+D_Y\frac{\partial^2 T}{\partial Y^2}+D_Z\frac{\partial^2 T}{\partial Z^2}\right)$$

Where:

- T = temperature (K)

- U= longitudinal velocity in X direction (m/s)
- V= traverse velocity in Y direction (m/s)
- W= vertical velocity in Z direction (m/s)
- k_X= thermal conductivity in X direction (W/mK)
- k_Y= thermal conductivity in Y direction (W/mK)
- k_Z= thermal conductivity in Z direction (W/mK)
- ρ = density (kg/m^3)
- Cp= specific heat (J/kgK)
- D_X= longitudinal turbulent diffusivity in X direction (m^2/s)
- D_Y= traverse turbulent diffusivity in Y direction (m^2/s)
- D_Z= vertical turbulent diffusivity in Z direction (m^2/s)

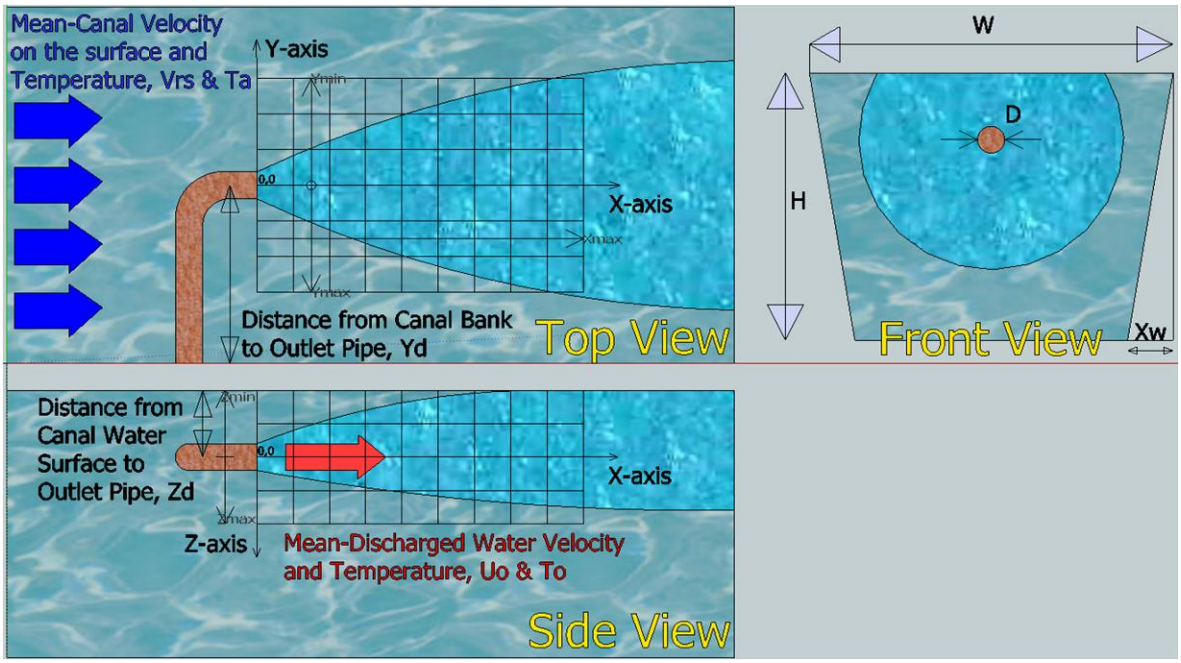

Figure 2: Flow configuration

Equation 2:

$$U\frac{\partial T}{\partial X} = D_Y\frac{\partial^2 T}{\partial Y^2} + D_Z\frac{\partial^2 T}{\partial Z^2}$$

3. TURBULENT DIFFUSIVITY

In order to solve Equation 2, the turbulent diffusions must be determined first. They can be found from taking data on-site or theoretical calculation according to theory of fluid mechanics (Ali, 2011). The result showed that the on-site empirical data provide more accurate than the theoretical data. However, the case-by-case solution is not suitable to use for other canal conditions. This study used an alternative method to determine the turbulent diffusion. Figure 3 presents the conceptual eddy motions that generate the turbulent diffusions. By assuming most of the vortices and eddies are caused by traverse and vertical shear velocities from the boundary frictions in the shallow canal condition, this thermal dispersion now behaves as a plume diffusion in the river. Then, the equations known as Fischer's common formula for river flow (Fischer, 1979) can be applied to find both turbulent diffusivities (Equation 3 and 4).

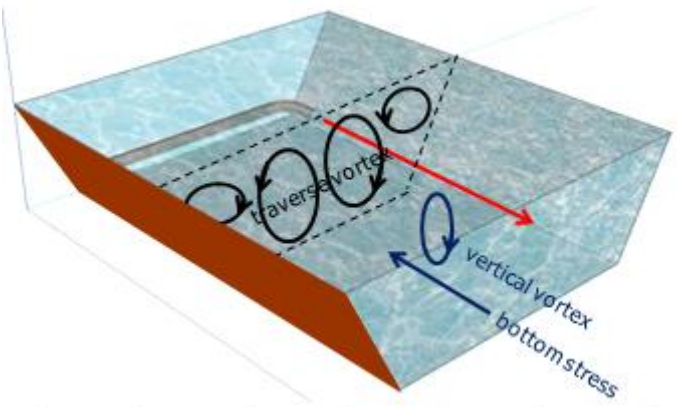

Figure 3: Vortices as the cause of turbulent diffusivities

$$D_Y = 0.15HU^*$$

Equation 3:

Equation 4:

$$D_Z = 0.067HU^*$$

Where:

- H= height (depth) of river channel (m)
- U*= shear velocity (m/s)

Fischer is not only one provided turbulent diffusivities in empirical term of shear velocity and river depth, but Bansal (1971), Yotsukura and Sayre (1976), Deng et al (2001) and Albers and Steffler (2007) were all proposed the same equation with just different constant coefficient number. However, Gujer (2008) and Fernando (2013) suggested that Fischer's equation is commonly accepted for the uniform straight channel, while others are for bend channel with strong secondary flow or natural large stream with non-uniform depth. So, the Fischer's equation is more satisfactory to the thermal discharge into a canal. Then, Manning (1891) proposed that shear velocity is related to average velocity by assuming that the river flow is only driven by gravity force (Equation 5). The shear velocity is also influenced by river channel dimension and friction. The Manning's equation can be used in various different channels due to there are many empirical Manning coefficients that suits to each different friction characteristics, as shown in Table 1. Afterwards, this equation was developed to be one of the well known equations in the field of civil engineering, Manning equation.

Equation 5:

$$U^* = \left(\frac{n\sqrt{g}}{R_h^{1/6}}\right)\overline{U}$$

Where:

- n = Manning coefficient ($s/m^{1/3}$)
- g = gravitational acceleration (m/s^2)
- R_h = hydraulic radius or cross-sectional area per wetted perimeter (m)
- $\overline{U}$ = average velocity (m/s)

Table 21: Manning coefficient

Channel condition		n
Lined channel with	Concrete surface	0.0145
	Brick/masonry surface	0.0200
Unlined channel with	Earth surface	0.0215
	Rock (gravel) surface	0.0250
	Weed surface	0.0300
Natural river	-	0.0350
Laboratory model channel	Perspex surface	0.0090

Finally, the traverse and vertical turbulent diffusivities can be determined and the exact solutions in both X-Y and X-Z planes (Equation 6 and 7) can be solved from Equation 2 when applying sufficient boundary conditions.

Equation 6:

$$T(X,Y)=\left(\frac{T_O-T_a}{2}\right)\left(erf\left(\frac{b-Y}{2\sqrt{\left(D_Y/U\right)X}}\right)+erf\left(\frac{b+Y}{2\sqrt{\left(D_Y/U\right)X}}\right)\right)+T_a$$

Equation 7:

$$T(X,Z)=\left(\frac{T_O-T_a}{2}\right)\left(erf\left(\frac{b-Z}{2\sqrt{\left(D_Z/U\right)X}}\right)+erf\left(\frac{b+Z}{2\sqrt{\left(D_Z/U\right)X}}\right)\right)+T_a$$

Where:

- T_O = water discharging temperature (K)
- T_a = canal water temperature (K)
- b = discharging pipe radius (m)

4. RESULT AND DISCUSSION

In this section, the general exact solution was verified and compared with the actual measured data on the on-site thermal discharge through Matlab software before was used for parametric study.

4.1 Accuracy of the current model

To examine the accuracy of the current solution, the published on-site measured data by Ali (2010), for discharging warm water into a canal that performed as the model developing condition, was chosen as the reference case. Ali (2010) presented the data of temperature decay at the centreline in X-Y plane when discharging warm water through 0.15m pipe diameter on the canal surface with 1.23m/s constant longitudinal velocity into the typical concrete lined British Waterways canal with 1.5m depth and having common average 10m width and near-stagnant velocity (assumed to be 0.001m/s). All temperature date were recorded and measured by calibrated K type thermocouples. The data of on-site experiment was recorded for discharging water temperature at 297K and the canal temperature at the 290K. The current model was used the same to find the exact solution. Figure 4 shows both the on-site measured and calculated data plots of temperature decay. It can be found that the model prediction is good and accurate. The difference between them is within 5% along the X direction.

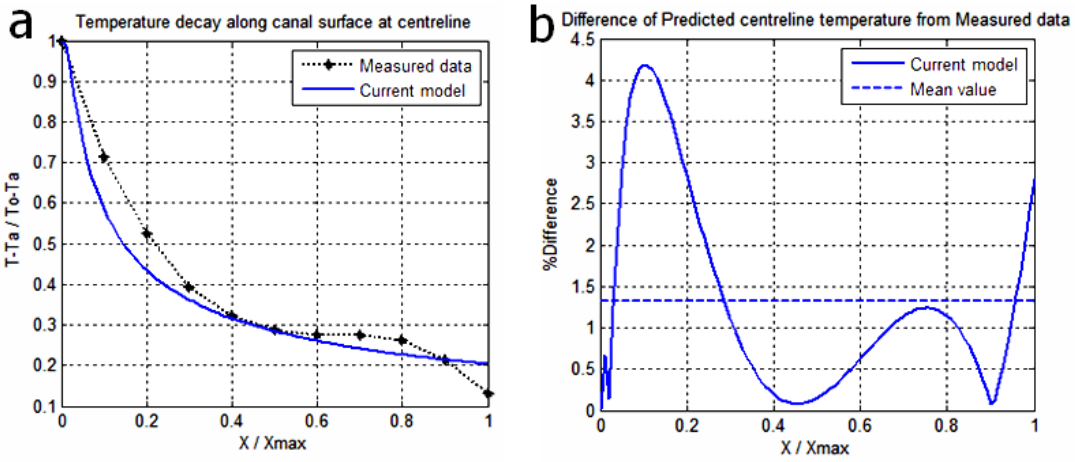

Figure 4: (a) Temperature decay along the centreline of canal by current model and on-site measured data (Ali, 2010) (b)%Difference of centreline temperature between by current model and on-site measured data (Ali,2010)

4.2 Parametric Analysis

According to results from the mathematic model, the canal's ground friction, the canal's depth and the hydraulic radius are the factors that influence the thermal distribution of the discharge, while the velocity is not. Figure 5 confirms that the bottom surface friction is a strong factor to the thermal distribution of the discharge. In other words, when the roughness (equivalent to Manning coefficient, n) is increasing from case a, b to c, while other factors are constant, the thermal mixing areas are expanding in both X-Y and X-Z planes and average temperatures in both planes are dropping. The Figure 6 shows the thermal distribution area changes with the canal depth, H. They were obtained under a constant hydraulic radius, i.e., the canal depth, H and the canal width, W changed accordingly to maintain the hydraulic radius unchanged. It can be found that the increase of depth has the same result influence to the thermal distribution area as the canal friction. Therefore, the thermal discharge into the deeper section of canal with higher roughness bottom surface will provide the better thermal mixing and reduce the impact to environment of canal.

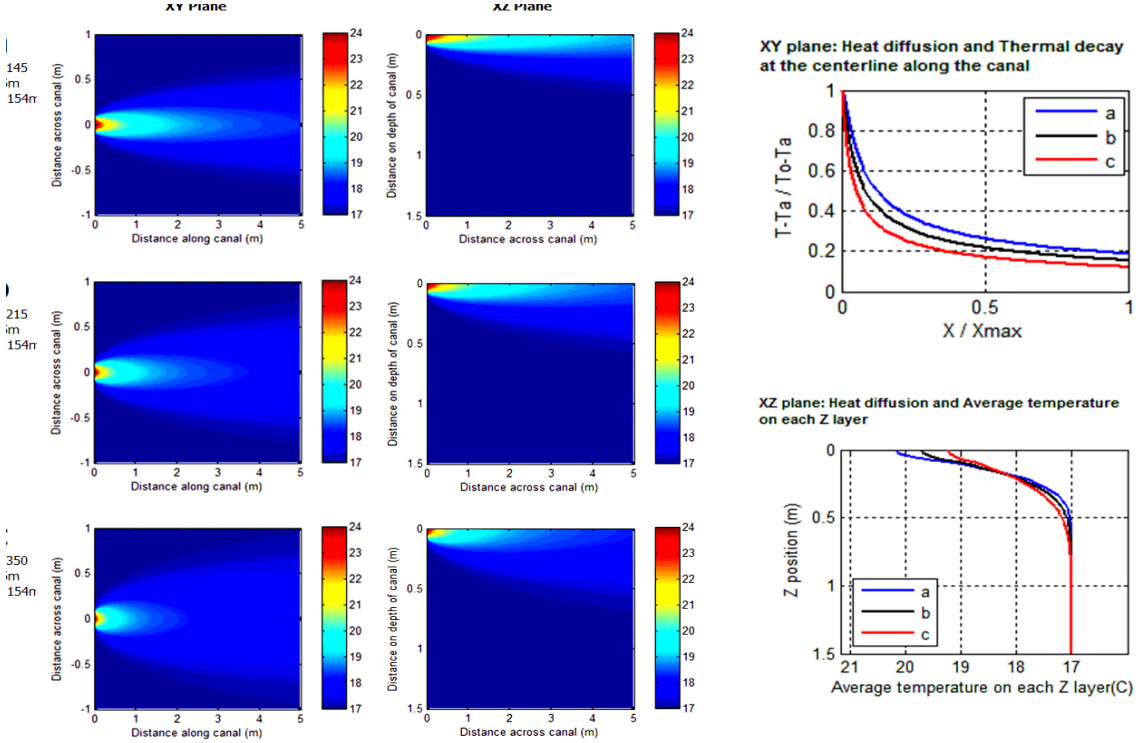

Figure 5: Temperature decay at the centreline in X-Y and central X-Z planes with (a) n 0.0145 (b) n 0.0215 (c) n 0.0350

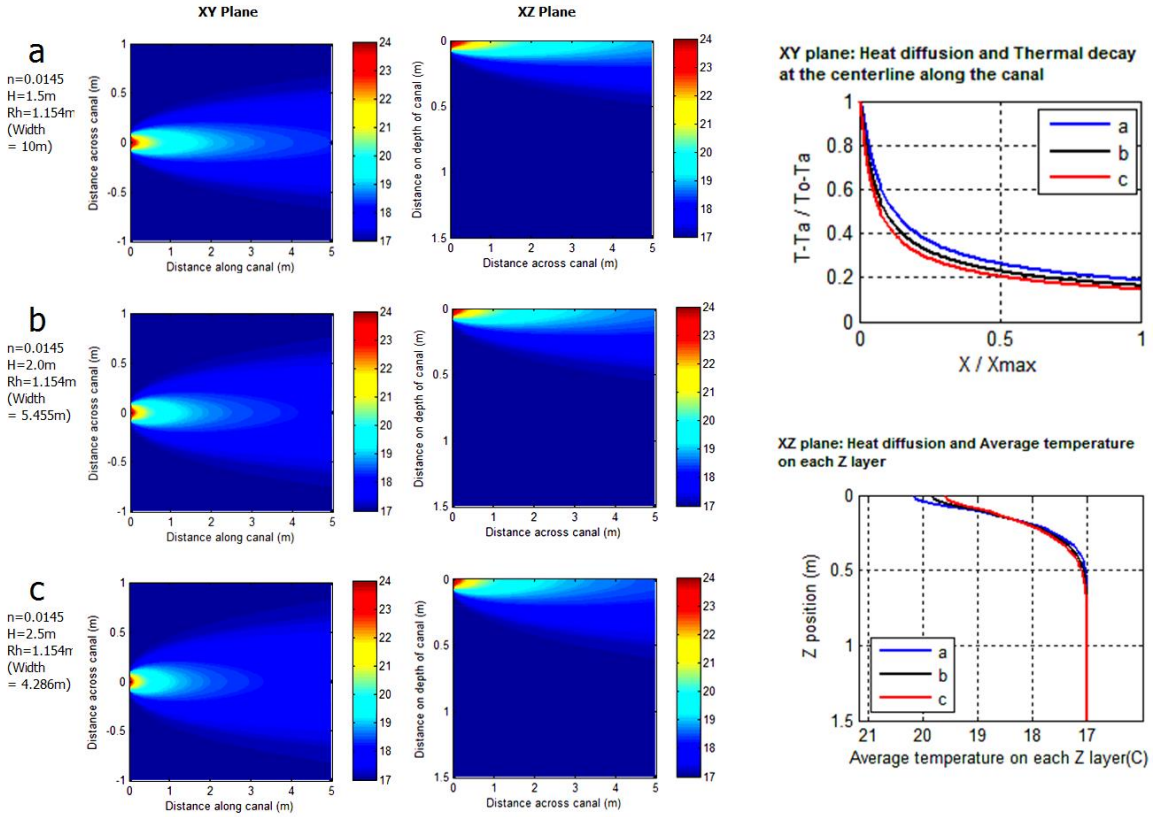

Figure 6: Temperature decay at the centreline in X-Y and central X-Z planes with (a) H1.5m (b) H2.0m (c) H2.5m

Figure 7 shows the influence of the hydraulic radius. The variation of the canal hydraulic radius was via through changing the width of canal. It can be found that the impact from this factor is inversely. This means the thermal distribution area in both planes are smaller and the average temperatures are higher when increasing the canal hydraulic radius from case a to case b. The reason might be the proportion of water mass to friction force is lower when expanding the width of the canal. This leads to generate weaker shear velocity, which is the source of diffusivity. Nevertheless, the impact from this factor is much lower than others due to the changing of temperature decay is very small, as shown in Figure 7.

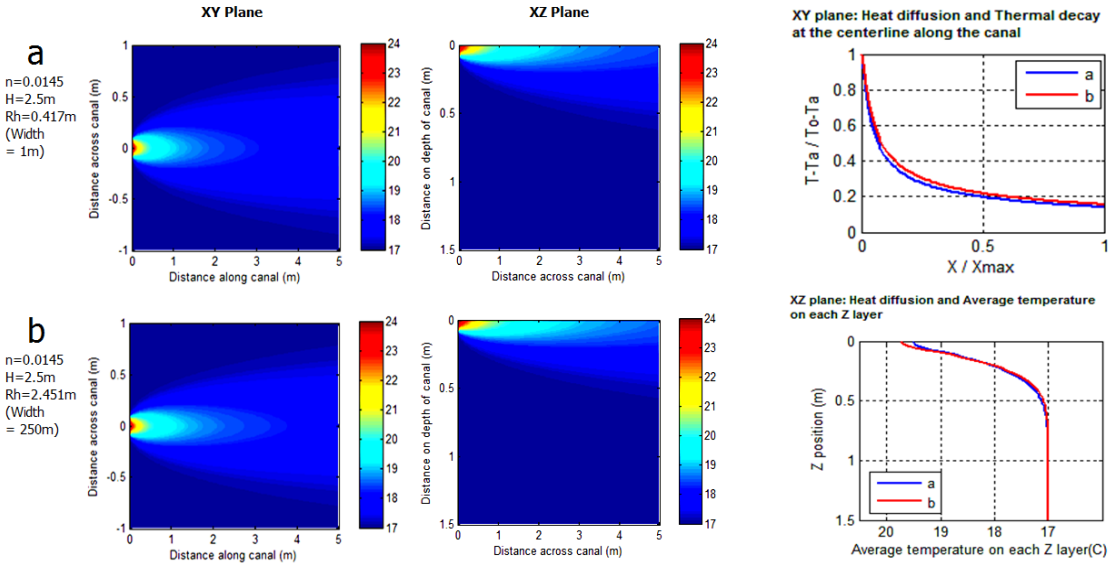

Figure 7: Temperature decay at the centreline in X-Y and central X-Z planes with (a) R_h 0.417m (b) R_h 2.451m

Next, The discharging velocity was varied but maintained above 0.01m/s (10 times higher than canal velocity) in order to neglect the influence of turbulent diffusivity at the same direction. Figure 8 shows that the thermal mixing area and average temperature are almost indifferent even though the velocity is very dissimilar. The cause of this result can be that the temperatures in Equation 6 and 7 now depend on the division of diffusivity and longitudinal discharging velocity. However, the diffusivity is also the product of plume velocity (summation of canal and discharging velocities). As the result, due to the discharging velocity is always very higher than canal velocity by the assumption, the division of velocities is into value of 1 even highly changing quantity of the discharging velocity.

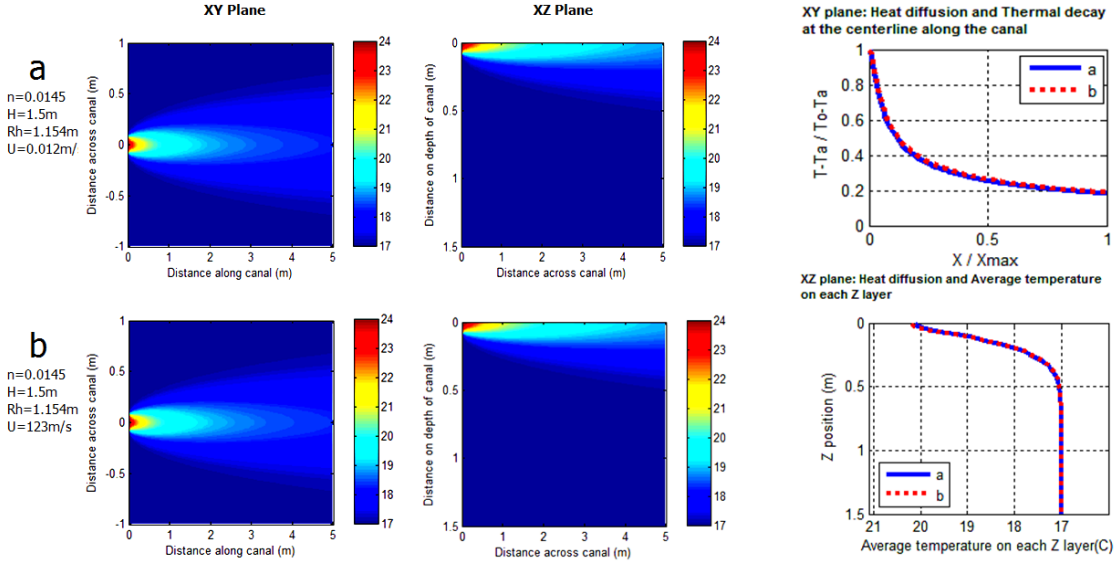

Figure 8: Temperature decay at the centreline in X-Y and central X-Z planes with (a) U 0.0123m/s (b) U 123m/s

5. CONCLUSION

By assuming the turbulent diffusivities are majorly caused by canal boundary friction, the general model of thermal discharge could be developed from the theory and experiment study of plume diffusion in river flow. The exact solution from the model provided good reliable result with only less than 5% difference from the actual result on the reference case. The model showed that the major influence factors to the thermal mixing are all canal's characteristics, namely the bottom surface friction, depth of the canal and hydraulic radius. The higher quantity of the first two factors provides the stronger vortices and eddies, and it leads to larger area heat spreads and better mixing. For the hydraulic radius, the impact is in reverse way and is lower than previous two factors. Moreover, it seems to be that the thermal mixing is independent from water discharge characteristics. When the water discharge is still in high velocity state (for a reason to keep neglecting longitudinal turbulent diffusivity), the increasing more or decreasing less of that velocity is unaffected to thermal mixing. Then, the environmental impact for using commercial water cooling type heat pump can be minimized and under the regulation by reasonably discharging warmer water into the high effective region of the near-by canal.

6. REFERENCES

ALBER, C.,P., Steffler, 2007. Estimating traverse mixing in open channels due to secondary current-induced shear dispersion. Hydraulic Engineering, ASCE, 133, 186-196.

ALI, Jafar, Fieldhouse, John, TALBOT, Chris, 2010. Numerical Modelling of three-dimensional thermal surface discharges. Engineer Applications of Computational Fluid Mechanics, 5(2), 201-209.

ALI, Jafar, Fieldhouse, John, TALBOT, Chris, 2011. Turbulent cooling water discharge into still body of water. Nuclear Engineering and Design, 241, 2006-2012.

BANSAL, M.K., 1971. Dispersion in natural steams. Hydraulic Engineering, ASCE, 97(11), 1867-1886.

DENG, Z-Q, V.P.,Singh, L., Bengtsson 2001. Logitudinal dispersion coefficient in straight rivers. Hydraulic Engineering, ASCE, 130, 919-927.

FERNANDO, H.J.S., 2013. Handbook of Environmental Fluid Dynamics-systems, pollution, modeling, and measurements volume two. USA: CRC press.

FISCHER, Hugo B., 1979. Mixing in Inland and Coastal Waters. United Kingdom: Academic press inc. (London) ltd.

GUJER, Willi, 2008. Systems Analysis for Water Technology. USA:Springer.

MANNING, Robert, 1891. On the flow of water in open channels and pipes. Transactions of the Institute of Civil Engineers of Ireland, 20, 161-207.

ROBERT PJW., Wedster, DR., 2002. Environmental Fluid Mechanics. Chapmen & Hall.

YOTSUKURA, N., W., Sayre, 1976. Traverse mixing in natural channels. Water Resource Research, 12, 695-704.

171: Experimental study of an adsorption heat storage systems for building applications

NORHAYATI MAT WAJID[1], BLAISE MEMPOUO[2], AUWAL DODO[3],SIDDIG OMER[4], SAFFA RIFFAT[5]

1Mrs, Department of Architecture and Built Environment, Faculty of Engineering, University Park, University of Nottingham, NG7 2RD United Kingdom, ezxnm@nottingham.ac.uk
2Dr, Department of Architecture and Built Environment, Faculty of Engineering, University Park, University of Nottingham, NG7 2RD United Kingdom, ezzbm@exmail.nottingham.ac.uk
3Dr, Department of Architecture and Built Environment, Faculty of Engineering, University Park, University of Nottingham, NG7 2RD United Kingdom, ezzam2@exmail.nottingham.ac.uk
4Associate Professor, Department of Architecture and Built Environment, Faculty of Engineering, University Park, University of Nottingham, NG7 2RD United Kingdom, Lazsao@exmail.nottingham.ac.uk
5 Professor, Department of Architecture and Built Environment, Faculty of Engineering, University Park, University of Nottingham, NG7 2RD United Kingdom, Lazsbr@exmail.nottingham.ac.uk

In this paper an Adsorption Heat Storage System (AdHS-HFC134a)/heating system utilising Vermiculite and Calcium Chloride composite adsorbent material was experimentally investigated. The main aim of the experimental investigations is to carry out preliminary tests on a small scale Adsorption Heat Storage Systems (AdHS-HFC134a) using a heat pump circuit as the regeneration heat source. The test rig was constructed using Vertical Glass Pipes with a heat pump circuit using a miniature compressor for transporting the refrigeration gas as a heat source for desorption cycle. The system also incorporates condenser coils, evaporator coils, and an expansion valve. The integration with a heat pump circuit is to analyse the performance of an AdHS-HFC134a using off peak power in desorption/charging cycle and utilising renewable energy sources to minimise energy demands from fossil fuels. The refrigerant gas used for the regeneration cycle is HFC R134a due to its low global warming potential (GWP), and no Ozone Depletion Potential (ODP), adopted for the proposed systems. Firstly, the regeneration phase occurs during night hours, when cheap off peak electricity is available under the 'Economy 7' tariff that is more suitable for households with night storage heaters or if we use lots of electricity at night. Secondly, in the heat pumping phase/adsorption loop which will occur during the day. The useful heat of adsorption in the adsorbent pipe could be used for underfloor heating (35°C-40°C), or for domestic hot water production (55°C-°60°c) during the day. The maximum temperature lift observed from the adsorption process is 68.62°C (adsorption pipe) with corresponding COP of 0.55 to 1.39.

Keywords: Thermochemical, Adsorption, Desorption, heat storage, HFC134a

1. INTRODUCTION

In Europe, the building sector constitutes to about one third of the total energy consumption of the union (International Energy Agengy 2014; Eurostat 2010), and heat production for housing (heating and domestic hot water (DHW)) represents from 19% (International Energy Agengy 2014) to 24% (Eurostat 2010) of the overall energy consumption of the UE-27. Approximately 20% is produced from renewable energy sources like wood, wastes or hydropower. Therefore, this means that approximately 80% of the heat generated in residential buildings comes from fossils resources. As cooling and heating demand for climate control rises in the future, it wills frontrunner to increasing energy consumption. This instinctively leads to a faster depletion of known fossil fuel reserves, more carbon dioxide emissions and a higher peak electricity demand. Such environmental issues have intensified research efforts on the development of environmentally benign refrigerants and energy saving cooling and heating technologies, and renewed interest in heating applications. Consequently, adsorption heat storage systems, considered more environmentally friendly with the ability of using water as the refrigerant for the heating and cooling. Some advantages have been recognised by adopting adsorption heating/cooling systems, as given by Hamdan et al. 2013);

- These systems can be driven by waste heat.
- The energy density is much higher compared to existing liquid absorption heat pumps because of the much higher reaction heat.
- The primary process has no moving parts which offer advantages with respect to maintenance.
- These systems have an inherent heat storage capability.
- Heat or cold can be stored for longer time periods.

Furthermore, adsorption heat storage/Thermochemical heat storage is a promising technology to solve the mismatch between seasonal heat supply and demand as a typical problem for temperate climate zones. Such systems are able to make use of solar irradiation during the summer time to cover for the heat demand during the winter time. Adsorption heating/cooling were extensively investigated to compete with the conventional vapour compression systems. The key of possessing high energy density and high sorption capacity is crucial to improved coefficient of performance (COP) of the adsorption systems against its counterparts. One way to solve these problems is by using composite materials in the adsorbent bed. The composite material also known as “composite salt inside matrix” have recently been recognized as the promising materials for adsorption systems due to their enhanced sorption capacity to common working fluids such as water, methanol and ammonia (Gordeeva & Aristov 2012). Extensive work on material syntheses of these composite materials have been conducted by (Casey et al. 2014).The high energy density with low regeneration temperature of composite adsorbents makes adsorption systems ideal alternative to conventional heating and cooling systems. Thus, this paper aims to investigate the performance of an Adsorption Heat Storage System (ADHS) incorporated composite adsorbent material ($CaCl_2$/vermiculite), and water as the working media. The regeneration for desorption process is achieved by utilising a heat – pump circuit. The regeneration refrigerant gas used in these experiments is 1, 1, 1, 2-tetrafluoroethane (HFC R134a). The integration with a heat pump circuit is to analyse the performance of an AdHS-HFC134a using an off peak power in desorption/charging cycle and utilising renewable energy sources to minimise energy demands from fossil fuels.

2. PRINCIPLE OF ADSORPTION HEAT STORAGE SYSTEMS (ADHS)

AdHS/Thermochemical energy storage (TES) is based on performing reversible chemical reaction (Shkatulov et al. 2012). The principle of sorption in Thermochemical ES is based on performing a reversible chemical reaction (desorption) which allows adsorption of heat in the course of decomposition (desorption) process that is endothermic (Hauer 2007; Ding & Riffat 2012). The reversible physic-chemical reaction, C is the thermochemical material (TCM). With the heat supply C, can be dissociated into components A and B, which can be any phase and stored separately. Both A and B are reactants as working pairs or sorption couple, and C will be formed with a heat release when put A and B together. A reverse synthesis reaction is exothermic that results in giving a stored heat back (Shkatulov et al. 2012).

C + Heat <=> A+ B

Basically, thermochemical ES processes (Figure 1) divided in three phases which consists of; i) Charging, which normally known as endothermic reaction. Heat source is required for the dissociation process of C, ii) Storing, this stage occurrs after the charging process and A and B will be formed and stored, iii)

discharging, where A and B associated in an exothermic reaction and material C is regenerated and the recovered energy released.

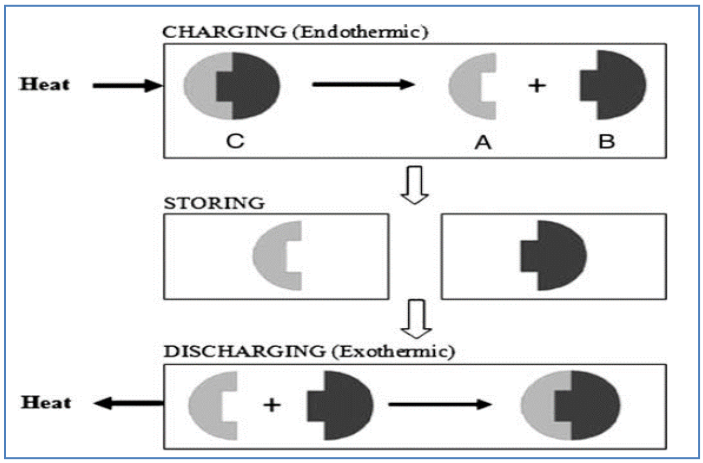

Figure 75: Processes involved in a thermochemical energy storage cycle. Adapted from (Abedin & Rosen 2012)

3. SYSTEM DESIGN AND EXPERIMENTAL RIG SET-UP

The experimental investigation was carried out using a small-scale laboratory model located at the Sustainable Research Building Laboratory of the Department of Architecture and Built Environment, University of Nottingham, UK. The prototype system is illustrated in

Figure 76. The AdHS-HFC134a system consists of two main separate component systems, namely the heat storage system, and the regeneration system. The heat storage systems consists of the adsorption pipe, evaporator pipe and the vacuum pump. The regeneration system employs a common heat pump circuit which consist of a mini-compressor, an expansion valve, a receiver, and coil pipe circulating the adsorption pipe and evaporator pipe. The adsorption/evaporator pipes are two separate vertical glass vessel QVF DN50 pipes, connected by a valve, and equipped with thermocouples probes and pressure transmitter for the measurement of temperature and pressure, respectively.

3.1 Experimental procedure and instrumentation

The detail descriptions of main system components have been given in Table 22. For this particular rig the K-type thermocouples were chosen with the temperature range of (-50°C -2000°C) and the accuracy of +/- 1° C. This thermocouple are highly accurate on the temperature range of -10°C to 70°C and in this experiments, they provide the best fits in glass vessel on reducing the possibility of air leakage. The pressure and temperature measurement points are illustrated in

Figure 76. Additionally, measurement of temperature in the refrigerant circuits was done using a compression fitting type for more accurate data measurements. Pressure were measured with UNIK 5000 GE pressure transmitter, which is a multipurpose, high performance stainless steel 7-28V output transducer transmitting at 4-20mA output range. The pressure range is -1 to 1.6 bar. It is a temperature compensated strain gauge technology with a +/- 0.04% accuracy full scale. The test rig was also equipped with data logging equipment DT500 for the recording of experimental data on a computer. The leakage tests were conducted before the experiments begun using a vacuum pump. The adsorption pipe and evaporator pipe were fully insulated to minimise heat loss during the experiments (see Figure 77).

Firstly, the experiment started with the adsorption process by un-evacuated the Swagelok ball valve that separating the adsorption and evaporation pipes. During the adsorption process, the water vapour from the evaporator pipe below will flows to the condenser pipe due to pressure different in the systems. The adsorption process will be monitored until there is no temperature different in the adsorption pipe. Secondly, desorption process will be conducted. During desorption process, the adsorption pipe receives heat from the coil pipe fill with refrigerant gas from the compressor, and then transfer heat to the adsorbent material. During this process, the condensate water returns back to the evaporator by opening the Swagelok ball valve. The temperature and pressure were measured every one second interval. The adsorption process

was monitored for 3 hours and desorption process was monitored for 4 hours period. The compressor power was also measured every 30 minutes of desorption process to validate the manufacturer data against theoretical analysis. Finally, the mass of adsorbent material and water were weight before and after adsorption and desorption processes. Two (2) experiments were conducted with different mass of adsorbent material and water in order to analyse the effect of mass of working pair to the temperature variation for the adsorption and desorption processes. The first test of using a relatively an equal ratio (1:1) of mass of adsorbent material and mass of water (Vermiculite+$CaCl_2$:63g, water: 61g). Then the second test is by using 1:2 ratio which is (vermiculite+$CaCl_2$: 44g, water: 80g). This experiment focused on the temperature lift in the condenser pipe and temperature drop in the evaporator pipe and sorption capacity (kg of dry adsorbent: kg of water) during the adsorption desorption process.

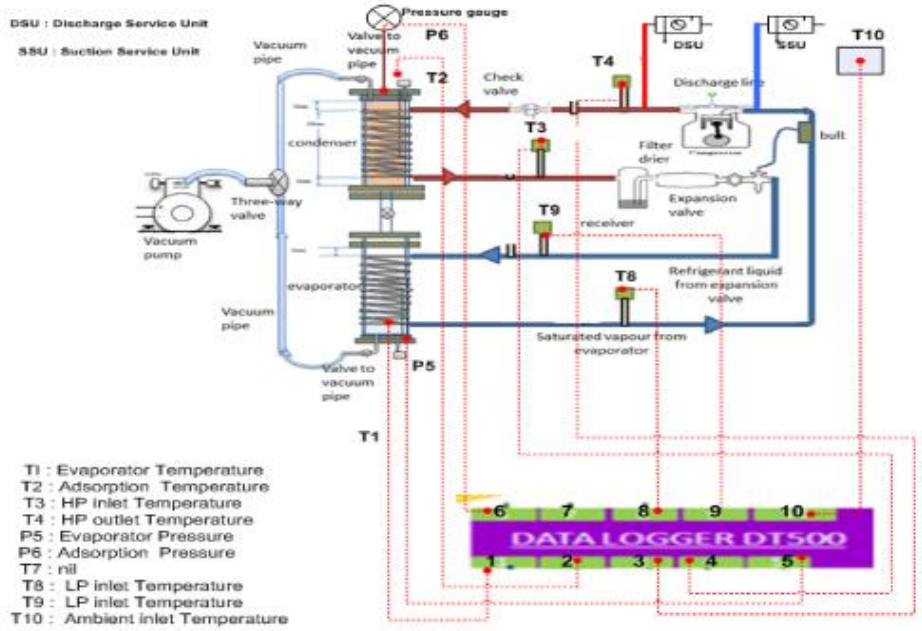

Figure 76: Schematic Of AdHS-HFC134a system

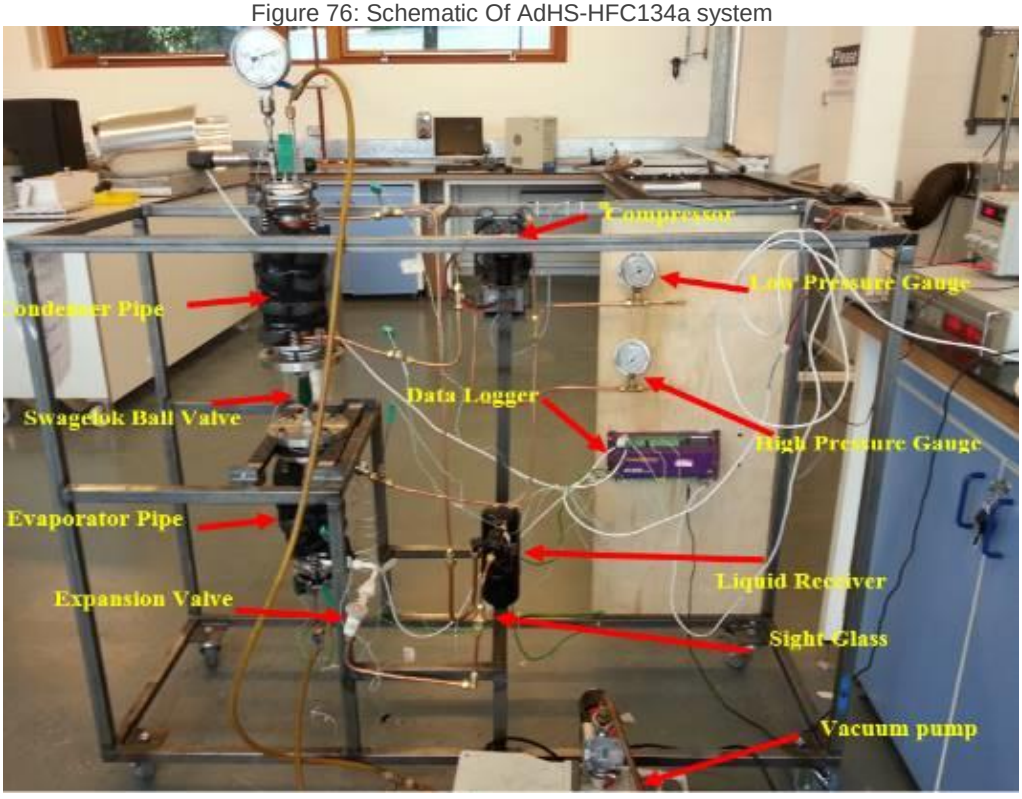

Figure 77: The AdHS-HFC134a systems and components

Table 22: Details description of main components

No	Name	Type	Description
1	Compressor	Closed rotary hermetic	miniature DC inverter compressor (ZH2024, Greatcool) displacement of 1.9cm^3/rev, input power of 220W
2	Condenser pipe	Cylindrical borosilicate Glass	QVF glass , ID 50mm, L: 250mm, maximum pressure 4 bar$_g$, maximum temperature :200°C , heat transfer area: 448 cm^2, thermal conductivity (λ: 1.2 W/m.K), Density: 2.23 kg/dm^3, specific heat : 0.8 KJ/kg.K
3	Evaporator pipe	Cylindrical borosilicate Glass	QVF glass , ID 50mm, maximum pressure 4 barg, maximum temperature :200° C , heat transfer area: 448 cm^2, thermal conductivity (λ: 1.2 W/m.K), Density (ρ): 2.23 kg/dm^3, specific heat (cp): 0.8 KJ/kg.K
4	Expansion Valve	Thermostatic Expansion Valve (TXV)	Universal, TN2 Danfoss , Control device, it has a sensing bulb attached to the outlet of the evaporator

3.2 Experimental design

The amount of energy released (Vaporised) from the evaporator at any temperature is:

Equation 15: Energy release to evaporator $Evap = Mv\ x\ Qst\ x\ \Delta w$

Where;

- Mv = the amount of water vaporized (kg)
- Qst = the isosteric heat of adsorption (3490 kJ/kg)(Aristov et al. 2000)
- Δw = sorption capacity (kg/kg)

This amount of released energy is the same that water will lose leading to a drop in its temperature, this energy drop (Qcooling) may be expressed by:

Equation 16: Energy drop in evaporator $Qcool = Mw\ x\ Cpw\ x\ \Delta T$

Where;

- M_w = the mass of liquid water (kg)
- C_{pw} = specific heat of water (4.18 kJ/kgK)
- ΔT = Temperature drop (°C)

As water vapour is absorbed by the composite material, the composite material will experience a temperature rise. Thus, this will give the amount of heating by;

Equation 17: Energy release from Vermiculite+CaCl₂ $Qheat = Ms\ x\ Cps\ x\ \Delta T_{Vermiculite_{CaCl_2}}$

Where;

- Ms = Mass of Vermiculite+$CaCl_2$
- Cps = Specific heat of vermiculite+$CaCl_2$ (0.91 kJ/kgK)(Aydin et al. 2015)
- ΔT = Temperature rise (°C)

During the regeneration/charging process, the heat from the condenser coils will be transfer to the wall of adsorbent pipe. By using the P-H diagram (Pressure - Enthalpy diagram) the heat in the condenser coils can be determine as;

Equation 18: Heat source from heat pump $\boldsymbol{Q_{heatpump} = \dot{m}(h_{2\_} h_3)}$

Where,

- $\dot{m}$= the volumetric flowrate of the refrigerant (m^3/s),
- h_2 = the enthalpy heat refrigerant from the discharge pipe of the compressor (kJ/kg)
- h_3 = the enthalpy of refrigerant from the outlet of the condenser coils of the system (kJ/kg). The enthalpy heat determined via thermo-physical properties libraries available in the EES software.

The COP of AdHS circuit at any time (t) instant was calculated as;

Equation 19: COPadhs

$$COP_{adhs} = \frac{Q_{heat}(t)}{Q134A(t)}$$

Where;

- *Qh = The heat gain through the adsorption process (KJ)*
- *$Q134A$ = The heat gain from the regeneration source (KJ)*

4. RESULT AND DISCUSSION

The experimental data for adsorption and desorption/regeneration tests using Vermiculite - $CaCl_2$ adsorbent, conducted using the glass pipes rig assembly was analysed and the results are discussed below.

4.1 Adsorption test

Adsorption test was initially carried out using the Vermiculite - $CaCl_2$ adsorbent (mass ratio of 1:1) and the results of temperature variations at the adsorption and evaporation vessels of the rig have been shown in Figure *78.* The temperature in the adsorption pipe increase gradually from initial temperature of 24.6°C to the highest temperature of 54.56°C. The temperature was notice to be drop sharply from 54.56°C to 45°C in 8 minutes and gradually drop to its initial temperature (22.08°C) in 75th minute of the whole adsorption process. The temperature gain gives the maximum heating of 1727J/s and maximum cooling of 2012 J/s. The initial mass of adsorbent material of 63g increased to 67g which give the sorption capacity of 0.06 kg dry adsorbent/kg water. The sorption capacity was considered very low and some further improvement should be entailed in order to achieve this. Apart from low sorption capacity, this test evidences that the composite adsorbent material could increase the temperature through adsorption process to a useful temperature appropriate for heating applications. Contrariwise, sharp rise in the adsorption pipe of 68.08°C from its initial temperature of 24.92°C for Test 2 during the adsorption process (see Figure 79). It is an evidence that the mass ratio of 1:2 could achieved the adsorption process relatively 20 minutes quicker than the mass ratio of 1:1. Therefore, this could be a future reference to optimize the quantities between adsorbent material and water for a larger scale design. Apart from that, the initial mass of the adsorbent material of 44g increase to 54g after the adsorption process. This gives a sorption capacity of 0.18 and relatively 0.66% higher than Test1. Furthermore the heat release and energy drop is higher than in test 1, which is 1750J and 2280J respectively. Thus, the developed prototype is practicable and can discharge large amount of heat (68°C) for hot water or heating demand and high sorption capacity with an appropriate ratio of adsorbent material and water mass.

4.2 Desorption Test

It is necessary for the adsorbent material of choice for use in the AdHS prototype system to be regenerate at a relatively low desorption temperature, in order for low heat energy sources to be used during the charging of adsorbent. As per discussed in section 3.2, the regeneration was carried out using a heat pump circuit utilising HFC134a as the refrigerant gas. The volumetric flowrate of refrigerant gas were constant at 1.9 cm^3/rev through the 4 hours of regeneration. Figure 80 illustrates the temperature variation from desorption process for Test 1. It can be seen that the HP (high pressure) inlet temperature increased gradually from an initial temperature of 24°C to 62.13°C in 100 minutes. Then the (HPinlet temp) remain constantly about 63°C through 4 hours of regeneration. The temperature in the adsorption pipe (AdsTemp) increased from 25°C to 49°C in the first 66 minutes. Then, the (Adstemp) remain constant at 54°C in 4 hours of regeneration process. This result showed that there was approximately 9°C temperature difference from the coils pipe to the (Adstemp). Therefore, these experiments suggest that that there are some heat losses

from the copper pipe transferring the heat through the glass vessel which is technically low thermal conductivity of 1.2 W/m^{2}K. Thus, some further improvement need to be entailed on using a high thermal conductivity for the adsorbent reactor such as stainless steel pipe or copper pipe to improve the heat transfer in the systems. Then, the liquid refrigerant were being transfer through copper coils from the adsorbent pipe to the evaporator pipe. The temperature variant to the evaporator pipe is indicate as (evaptemp) and the refrigerant gas flows through copper coils is indicate as LPinlet/outlet temp. It can be seen that in the (LPinlet) and (evapTemp) has temperature different about 7°C which indicates that temperature loss also occurs in the evaporation sections. Thus, similar improvement need to be entailed in the piping construction as has been suggested in the adsorption section. However, lower temperature of average of 1.5°C is sufficient enough condensate the water vapour from the desorption process. In a real scale of AdHs systems, the ground heat source shall be utilize as a heat source for the heat pump and improve the performance of the whole systems. Similarly, in Figure 81, temperature variant in the adsorption section and evaporator section experiencing a temperature loss of approximately about 10 °C. However the temperature in the evaporator pipe is higher that Test 1. This may be due to the fact that the amount of water used is more than in Test1 where longer time was needed to condense the water vapour. Additionally, the mass of adsorbent and water were re-weight after desorption process and the same amount of water being desorb after this process. Therefore, these experiments suggest that the regeneration temperature for Vermiculite+$CaCl_2$ is in the range of 55 °C to 65 °C. Thus, a low grade regeneration system such as flat plate collector or ground source heat pump could be utilized in order to reduce demand of using a conventional energy source from a fossil fuel.

4.3 Overall system performance

Table 23, showing the overall performance of the AdHS-HFC134a of different mass ratio which is 1:1 and 1:2 respectively. The heat storage were analyse base on the average density of vermiculite and calcium chloride which is 175 kg/m^3 as according to (Aydin et al. 2015). The heat store ($Q_{heating}$ store) of Test 2 is higher than TEST 1 by approximately 30% more. It can be seen that the heat storage is strongly influenced by the increase of mass of adsorbent material. Furthermore, the time (s) for temperature lift to maximum values (ΔTmax) for Test 2 was approximately 70% quicker than that of Test 1. This would affect adversely to the COP of the systems which is the maximum COP for Test 2 is 1.98 compared to 1.16 for Test 1 respectively. Therefore, overall performance of the system is highly dependent on the mass of the working pair and the temperature lift during the adsorption process. Thus, these experiments suggests that an actual scale systems should use a most appropriate mass for working pair in order to enhance the heat store and COP the whole systems. In addition, the heat source should be constructed inside the reaction vessel (adsorption vessel) in order to enhance the heat transfer and improve the dissociation of water vapour during the desorption process.

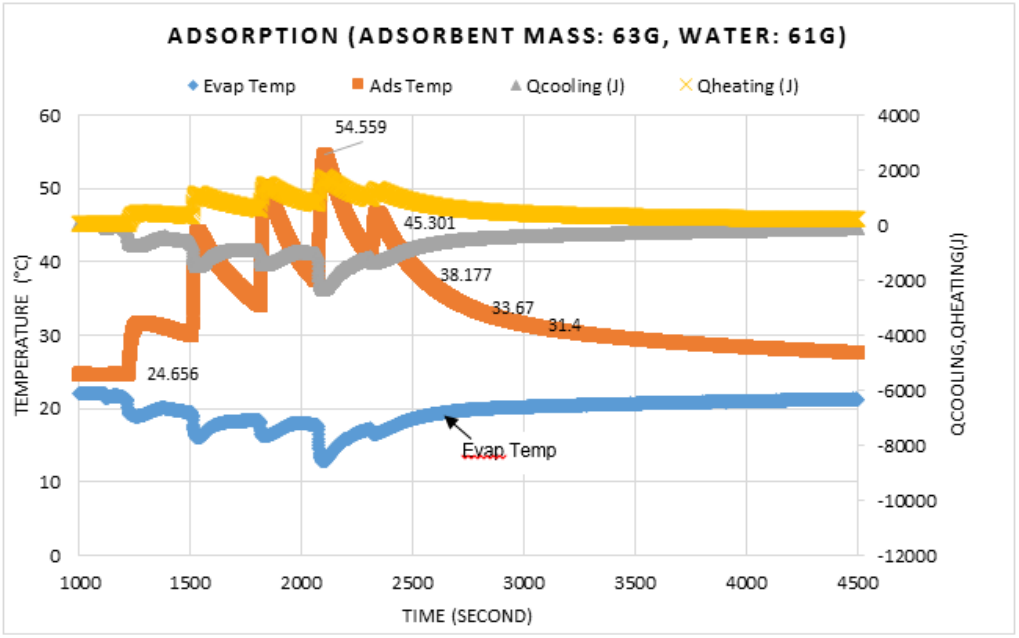

Figure 78: Test 1, Temperature variation and Heat release from adsorbent material ($Q_{heating}$) and Energy drop ($Q_{cooling}$) from the water vapor.

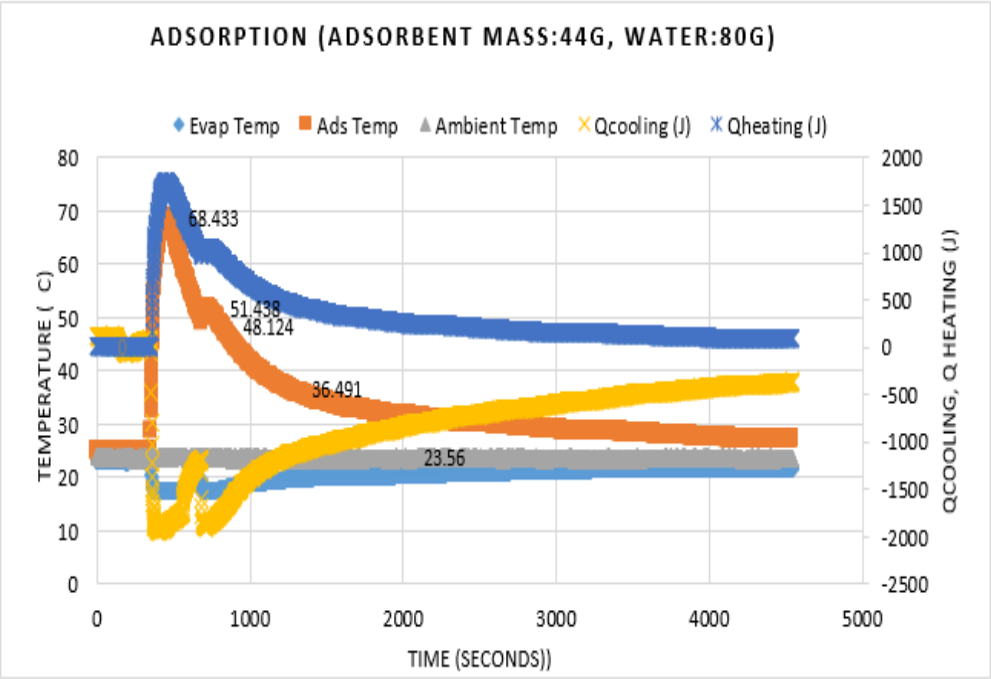

Figure 79: Test 2, Temperature variation and Heat release from adsorbent material (Qheating) and Energy drop (Qcooling) from the water vapor.

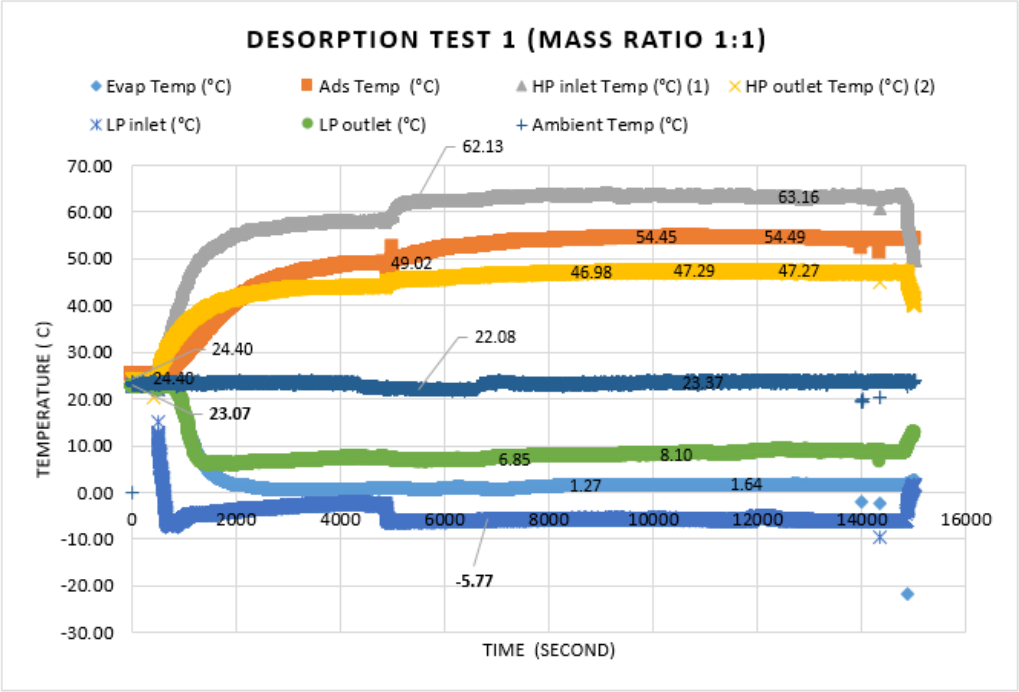

Figure 80: Desorption test for test 1(mass ratio: 1:1), HPinlet/outlet (gas HFC134a from compressor and to the expansion valve), LPinlet/outlet (liquid from HFC134a from expansion valve to compressor)

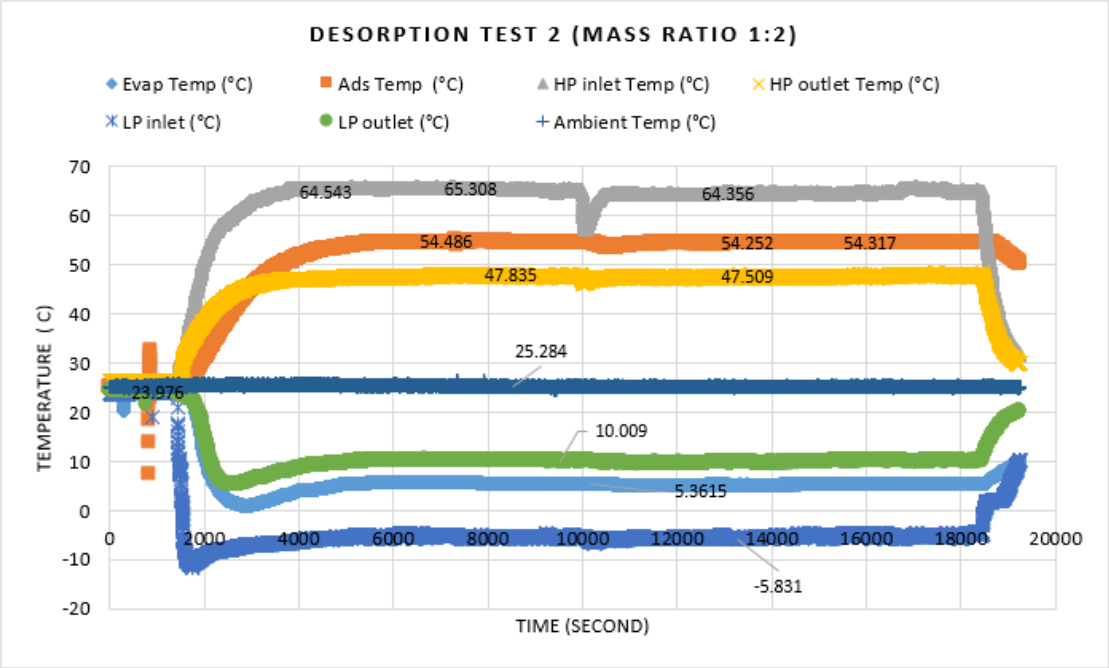

Figure 81: Desorption test for test 2 (mass ratio: 1:2)

Table 23: Performance comparison between Test 1 and Test 2

	TEST 1	TEST 2
Mass ratio (mass of dry adsorbent: mass of water)	1:1	1:2
$Q_{heating}$ store (kWh/m^3)	1.34	1.97
Adsorption cycle (min)	35 - 75	7 – 60
COP	0.55 – 1.16	0.98 to 1.39
Maximum Adsorption Temperature (°C)	54.55	68.08
Δ w (kg/kg)	0.06	0.18

5. CONCLUSION AND RECOMMENDATIONS

This paper represent the experimental investigation of a prototype scale of an Adsorption heat storage system using heat – pump circuit (HFC134a) as a heat source for regeneration. The following remarks can be drawn from the present study:

- The temperature rise during adsorption process was strongly influenced by the amount of water used in the evaporator. Thus, the amount of water required in the evaporator need to be optimized in order to achieve better vapour transport and temperature drop in the evaporator.
- To maintain a constant adsorption temperature, proper insulation is crucially during the adsorption process.
- For real scale AdHS systems, the adsorbent pipe and the evaporator pipe should be constructed with a high thermal conductivity material to enhance heat transfer performance in the system.
- The heat transfer coils need to be constructed inside of the condenser and evaporator pipes to prevent heat loss in the systems.
- The number of coil turns should be optimized to ensure that the heat from high pressure inlet can be transfer to the whole adsorption pipe.
- Maximum COP using 1:1 mass ratio is 1.16, while 1.97 for mass ratio of 1:2 respectively.

6. REFERENCES

ABEDIN, A.H. & Rosen, M., 2012. Closed and open thermochemical energy storage: Energy- and exergy-based comparisons. *Energy*, 41(1), pp.83–92.

ARISTOV, Y.I. et al., 2000. Selective Water Sorbent for Multiple Applications.11 CaCl2 Confined to Expanded Vermiculite. *React.Kinet.Catal.Lett.*, 71(2), pp.377–384.

AYDIN, D., Casey, S.P. & Riffat, S., 2015. Numerical analysis of solar-assisted seasonal “open” thermochemical heat storage. *International Journal of Low-Carbon Technologies*, pp.1–8.

CASEY, S.P. et al., 2014. Salt impregnated desiccant matrices for “open” thermochemical energy storage—Selection, synthesis and characterisation of candidate materials. *Energy and Buildings*, 84, pp.412–425.

DING, Y. & Riffat, S.B., 2012. Thermochemical energy storage technologies for building applications: a state-of-the-art review. *International Journal of Low-Carbon Technologies*, 8(2), pp.106–116.

Eurostat, 2010. *Energy - early statistics 2008*, Luxembourg: Publication Office of the European Union. Available at: http://epp.eurostat.ec.europa.eu/portal/page/portal/product_details/publication?p_product_code=KS-PC-10-001.

GORDEEVA, L.G. & Aristov, Y.I., 2012. Composites “salt inside porous matrix” for adsorption heat transformation: a current state-of-the-art and new trends. *International Journal of Low-Carbon Technologies*, (June), pp.288–302.

HAMDAN, M.., Rossides, S.D. & Haj Khalil, R., 2013. Thermal energy storage using thermo-chemical heat pump. *Energy Conversion and Management*, 65, pp.721–724.

HAUER, A., 2007. A Sorption storage for solar thermal energy—possibilities and limits. In *Thermal Energy Storage for Sustainable Energy Consumption*.

International Energy Agengy, 2014. 2014 Key World Energy Statistic. *IEA Energy Statistic*. Available at: http://www.iea.org/publications/freepublications/publication/KeyWorld2014.pdf.

SHKATULOV, A. et al., 2012. Composite material “Mg(OH)2/vermiculite”: A promising new candidate for storage of middle temperature heat. *Energy*, 44(1), pp.1028–1034.

235: Preliminary performance investigation of a novel direct contact evaporative cooling system

PINAR MERT CUCE[1*], KEMAL GANI BAYRAKTAR[2], SAFFA RIFFAT[1], SIDDIG OMER[1]

1 Department of Architecture and Built Environment, Faculty of Engineering, University of Nottingham, University Park, NG7 2RD Nottingham, UK
2 Izocam Tic. ve San. A.S., Altaycesme Mah., Oz Sokak, No:19, Kat:3-5-6, P.K. 34843, Maltepe, Istanbul, Turkey
**Corresponding email: ezxapm@nottingham.ac.uk, Tel: +44(0)747 327 8285*

Buildings are responsible for about 47% of total energy consumption in the world. The energy consumed is mainly for cooling, heating and ventilation. It is noted that energy requirement for cooling reached 14.6% per annum between 1990 and 2000. Energy demand of buildings will continue to rise in near future owing to long-term use of buildings, increasing comfort demand of occupants and growth in population. In this regard, the aim of evaporative cooling systems is to mitigate the energy consumption and cost of operating a building by transferring heat between two fluids. An evaporative cooling system simply works as increasing the moisture contents of the air with use of water. When hot and dry air welcomes water, the water starts to evaporate with help of energy taken from the air. Thus the air becomes cooler whereas its relative humidity ratio goes up. The evaporative cooling system can be categorised as direct contact or indirect contact with respect to interaction between the streams. In this paper, domestic application of a novel direct contact evaporative cooling system is experimentally investigated. Within the concept of this research, performance evaluation of the system is introduced. For different temperatures of inlet fresh air, outlet temperatures are measured time-dependently and the level of cooling achieved is determined. Proper temperature and relative humidity measurements are performed for a reliable performance assessment. The results indicate that the efficiency of evaporative cooling is very promising. Even if extreme weather conditions are considered for air at the inlet, more than 20 oC temperature difference can be obtained with a remarkably high range of COP. In this respect, it can be easily concluded that the system provides very promising results for hot and arid climates.

Keywords: Evaporative cooling, HVAC, building applications

1. INTRODUCTION

HVAC is an indispensable part of a building and causes a significant amount of energy loss. Therefore it is considered as a key solution for remarkable energy savings in buildings. Cooling constitutes an important part of heat loss due to HVAC. There are many types of cooling systems that provide cool fresh air for domestic or commercial use. The choice of any system directly affects the energy consumption along with the carbon dioxide emissions from system. Evaporative cooling is a novel technology that supplies cool air to the occupants as well as providing a promising way to reduce carbon emissions and energy consumption. Evaporative cooling is a concept that is defined as making air cool via increasing its water vapour content. In other words, air becomes cooler while its humidity level increases.

An evaporative cooling system simply works as increasing the moisture contents of the air with use of water. When hot and dry air welcomes water, the water starts to evaporate with help of energy taken from the air. Thus the air becomes cooler whereas its relative humidity ratio goes up. The evaporative cooling system can be categorised as direct contact or indirect contact with respect to interaction between the streams as illustrated in **Figure 1**. The direct contact evaporative cooling systems are utilised to cool the intake air in hot and dry climatic conditions. It is possible to get adequate cooling by use of this system, but the increasing level of the air humidity might make the occupants uncomfortable. On contrary to direct contact system, an indirect contact evaporative cooling system can deal with undesired living conditions for the occupants owing to its characteristic configuration.

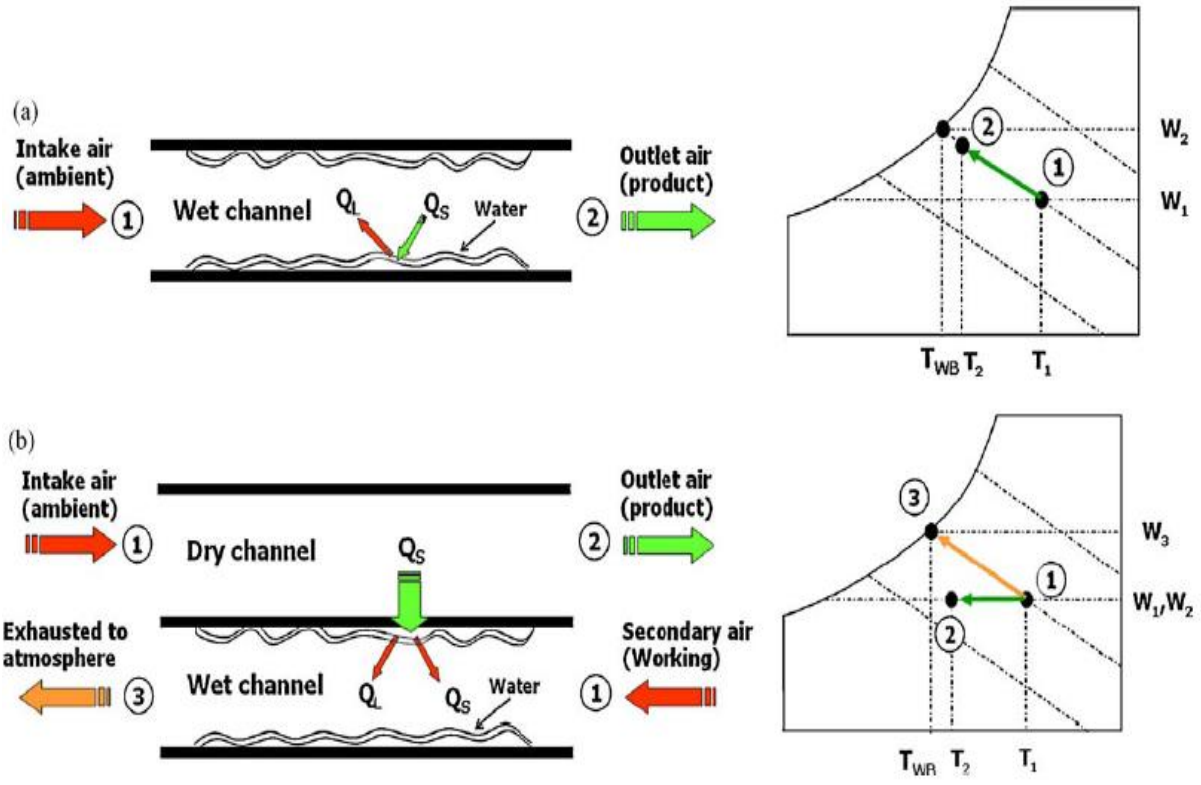

***Figure 1**. Direct evaporative cooling (a) and indirect evaporative cooling (b).*

As reported by Hasan [**1**] in a recent work, the demand for cooling increases day by day as a consequence of the growing demand for better thermal comfort conditions in buildings. Cooling can be performed in several ways, and one of those is evaporative cooling. Evaporative cooling has a high potential to meet cooling demands at low energy costs. Riangvilaikul and Kumar [**2**] note that the evaporative cooling is a good alternative to mechanical vapour compression for air conditioning applications since it requires about four times less electric power than vapour-compression refrigeration [**3**]. Current available evaporative cooling systems can be classified as direct-contact and indirect-contact evaporative coolers. In a direct evaporative cooling system, working air to be cooled is in a direct contact with a liquid water film. Cooling is accomplished by the adiabatic heat exchange between the working air and the liquid water film [**4**].

Direct-contact evaporative cooling systems are appropriate for use only in dry, hot environmental conditions, or in rooms needing both cooling and humidification [5]. On the other hand, in an indirect-contact evaporative cooler, the inlet air is cooled by so-called working (secondary) air which is cooled through evaporation [6]. Thermodynamically, the wet passage absorbs heat from the dry passage by evaporating water, and thus cools the dry passage, while the latent heat of vaporizing water is dissipated into the working air. Within the scope of this research, only the evaporative cooling test and its results are introduced.

Evaporative cooling systems are widely used in building sector nowadays as an alternative to conventional air conditioners. Energy consumed in HVAC systems accounts for about 20% of the total world energy consumption [**7**], and hence novel solution to mitigate this figure is of vital importance due to growing significance of environmental issues [**8**]. Evaporative cooling technology offers a wide range of opportunities for buildings to fulfil this purpose owing to low retrofit costs, high efficiency ranges, insignificant maintenance and attractive payback periods [**9**].

2. DESCRIPTION OF A NOVEL ECS (EVAPORATIVE COOLING SYSTEM)

Cooling energy has an important part in buildings' energy consumption levels. As reported by Hasan [**1**] in a recent work, the demand for cooling increases day by day as a consequence of the growing demand for better thermal comfort conditions in buildings. Evaporative cooling has a high potential to meet cooling demands at low energy costs [**10**]. Riangvilaikul and Kumar [**2**] note that the evaporative cooling is a good alternative to mechanical vapour compression for air conditioning applications since it requires about four times less electric power than vapour-compression refrigeration [**3**].

ECS, which has been recently developed, is a novel system that can be used for both ventilation and air conditioning purposes. A comprehensive description of the system is illustrated in **Figure 2**. The system is capable of meeting cooling demand at hot and arid climatic conditions. The working principle is definitely the same with a standard humidifier. First, outside air at any temperature is welcomed at the humidifying channel via a low power circulating fan. Humidification is achieved via adiabatically saturated wicks which are specially designed and filled with water. In the system proposed here, fresh air is exposed to humidification and its temperature reduces to the thermal comfort level. Drained water is collected at the bottom of the humidification channel and pumped to the water tank, which is fixed at the top of ECS.

ECS is devised to be used as a roof application. In this respect, its design is compatible with the roof pitch of existing UK building stock. External dimensions of the wooden structure of ECS are 1 m wide, 1.5 m length and 1.5 m height. Dimension optimization of ECS is expected to yield a slimmer and lighter construction. At this stage, the focal point is to investigate the thermal performance efficiency of ECS for different climatic conditions.

3. EXPERIMENTAL SETUP AND ANALYSIS OF ECS

The test rig of a novel evaporative cooling system is built in the Department of Architecture and Built Environment at the University of Nottingham. Real indoor and outdoor thermal conditions are assumed during the experiments. A multi-functional digital environmental chamber is used to adjust the temperature and the humidity ratio of incoming fresh air. Two water tanks, a pump and a blower fan are utilised to run the system properly. The system is simulated and designed as to be a roof application of a real house. For a real house case of the proposed system, rain water will be collected to a tank and will be delivered to the system to use it for cooling purposes instead of tap water. Thus, it is achieved to save large amount of tap water. As it is underlined here, the aforementioned system helps to save both energy and water, and contributes to reduce greenhouse gas emissions.

In this part of the research, evaporative cooling performance of a novel ECS is investigated. In this respect, for different conditions of fresh air from environmental chamber, time-dependent outlet temperature and outlet relative humidity of air are measured. Following the relevant measurements, coefficient of performance of the aforesaid cooling system is determined for each case. The results are comprehensively analysed for a reliable evaluation and easier understanding.

***Figure 2**. Detailed view of ECS.*

4. RESULTS AND DISCUSSION

In this section, experimental results of the system are introduced. **Figure 3** shows the temperature measurement results of the system. As a natural consequence of evaporative cooling process, air temperature remarkably decreases at the outlet. Steady-state measurements reveal that the average temperature of fresh air at the inlet is 36.9 ^{o}C, whereas it is 22.9 ^{o}C at the outlet. The temperature difference of 14 ^{o}C achieved by ECS is very promising.

Figure 4 illustrates the relative humidity change during the measurement. The outlet relative humidity of fresh air almost reaches the adiabatic saturation condition as clearly shown. The average humidity values at the inlet and outlet are measured to be 37.2 and 97.7%, respectively.

Following the relevant measurements of temperature and relative humidity at the inlet and outlet, the coefficient of performance (COP) of ECS is calculated as shown in **Figure 5**. The average COP of the test is found to be 5.0.

This research basically aims at demonstrating the feasibility of this novel system to reduce the cooling demand of buildings in hot and arid environmental conditions. The preliminary test results for the evaporative cooling system clearly reveal that the system developed is very promising for hot and arid climatic conditions. In the next stage, the system will be powered with desiccant filled wicks, and the experiments will be repeated for humid conditions of incoming air.

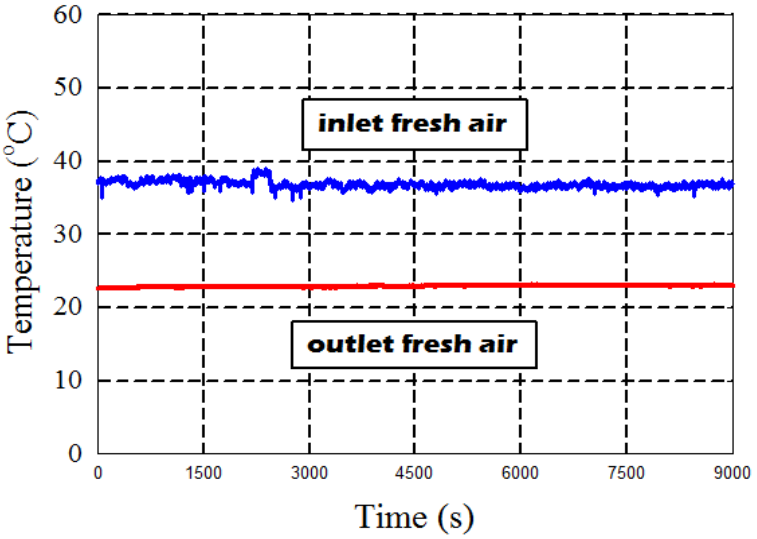

***Figure 3**. Temperature measurement of a novel evaporative cooling system (ECS).*

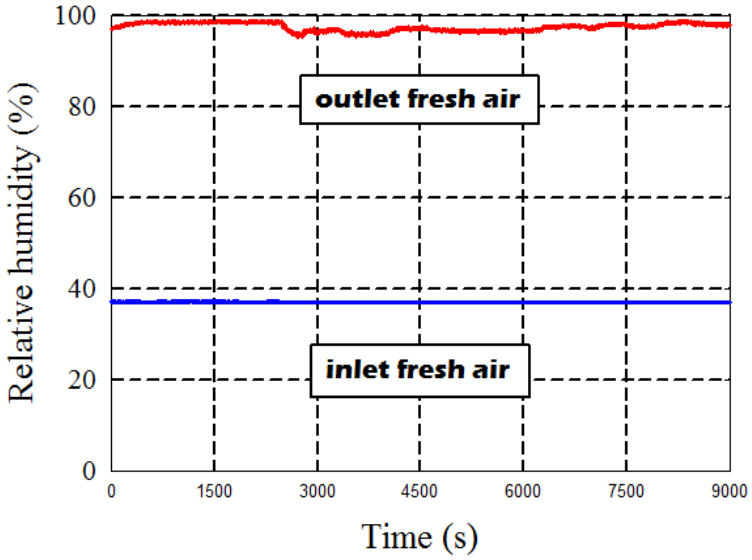

***Figure 4**. Relative humidity measurement of a novel evaporative cooling system (ECS).*

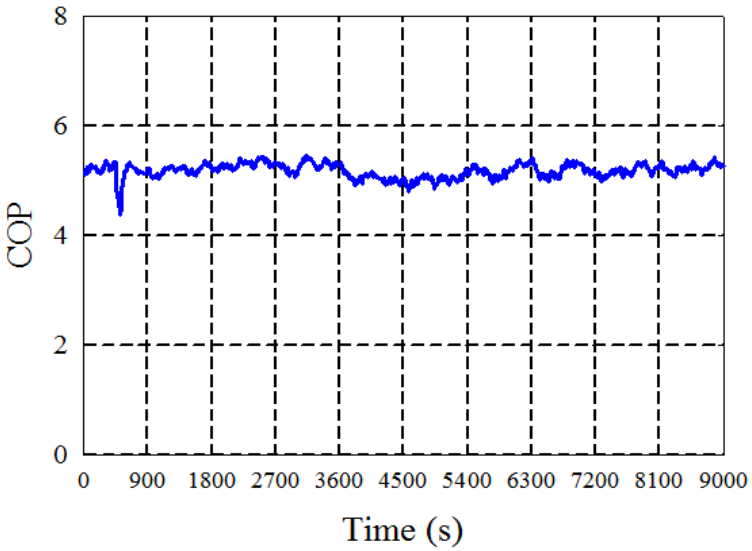

***Figure 5**. Coefficient of performance (COP) value of the proposed system.*

5. CONCLUSIONS

An intelligent building is defined as maximising the efficiency of the service with a minimum cost [**11**]. Energy consumption of the building sector increases say by day due to good thermal comfort demand of the occupants. That's why, use of energy-efficient technologies in buildings is of prime concern for anyone wishing to save both energy and money [**12**].

In this work, a novel evaporative cooling system (ECS) is introduced to mitigate energy consumption in buildings arising from cooling and air conditioning. The results show that the evaporative cooling systems have a great potential to save energy in hot and arid climatic zones. It also seems that this novel solution is a very cost effective way compared to the alternative air-conditioning applications. This technology has a good efficiency/effectiveness value as well as a good COP range. The next step will be based on integrating desiccant filled wicks into the system and repeating the tests as characterising the humid climates.

6. ACKNOWLEDGEMENTS

The authors gratefully acknowledge the financial support of EU through the research project 'HERB'.

7. REFERENCES

1. HASAN A. Indirect evaporative cooling of air to a sub-wet bulb temperature. Applied Thermal Engineering 2010; 30: 2460–2468.

2. RIANGVILAIKUL B, Kumar S. An experimental study of a novel dew point evaporative cooling system. Energy and Buildings 2010; 42: 637–644.

3. CERCI Y. A new ideal evaporative freezing cycle. International Journal of Heat and Mass Transfer 2003; 46: 2967–2974.

4. GUO XC, Zhao TS. A parametric study of an indirect evaporative air cooler. International Communications in Heat and Mass Transfer 1998; 25(2): 217–226.

5. ZHAO X, Li JM, Riffat SB. Numerical study of a novel counter-flow heat and mass exchanger for dew point evaporative cooling. Applied Thermal Engineering 2008; 28: 1942–1951.

6. JIANG Y, Xie X. Theoretical and testing performance of an innovative indirect evaporative chiller. Solar Energy 2010; 84: 2041–2055.

7. CHENGQIN R, Nianping L, Guangfa T. Principles of exergy analysis in HVAC and evaluation of evaporative cooling schemes. Building and Environment 2002; 37: 1045–1055.

8. CUCE E, Cuce PM. A comprehensive review on solar cookers. Applied Energy 2013; 102: 1399–1421.

9. DELFANI S, Esmaeelian J, Pasdarshahri H, Karami M. Energy saving potential of an indirect evaporative cooler as a pre-cooling unit for mechanical cooling systems in Iran. Energy and Buildings 2010; 42: 2169–2176.

10. SAN JOSE ALONSO JF, Rey Martinez FJ, Velasco Gomez E, Alvarez-Guerra Plasencia MA. Simulation model of an indirect evaporative cooler. Energy and Buildings 1998; 29: 23–27.

11. GONZALEZ PA, Zamarreno JM. Prediction of hourly energy consumption in buildings based on a feedback artificial neural network. Energy and Buildings 2005; 37: 595–601.

12. LI X, Bowers CP, Schnier T. Classification of energy consumption in buildings with outlier detection. IEEE Transactions on Industrial Electronics 2010; 57(11): 3639–3644.

260: A Review on desiccant cooling system

KHALID ALSALEH , SAFFA RIFFAT

Institute of Sustainable Energy Technology, Faculty of Engineering, University of Nottingham, Nottingham ng7 2rd, UK, ezxka1@nottingham.ac.uk

World are planning for signification deployments of Renewable and Nuclear energy to produce energy from clean and sustainable source. Renewable energy will save hydrocarbons and oil that are currently used to generate energy which will reflect in the environmental pollution.

The roadmap for Solar PV will envision up to 16% of global electricity. According to IEA, "6 300 TWh generated in 2050, up from the 4 500 TWh foreseen in the 2010 roadmap. Total global capacity overtook 150 gigawatts (GW) in early 2014".(IEA, 2014)

About half the large PV deployment would take place on buildings or nearby such as over parking. The prospects for self-consumption are higher in hot countries, where air-cooling loads partly drive consumption, and for buildings other than residential.(IEA, 2014)

According to the U.S. Energy Information Administration (EIA), heating and cooling accounted for 72% of the energy used in household in the United States. Air conditioning is claimed to account for over 65% of the energy consumption in Gulf Cooperation Council (GCC) country.(SEEC, 2013)

Desiccant cooling system has been growing rapidly since 2004 from 60 systems to more than 1000 system installed in less than ten years. However, compared to the potential of using solar energy to generate cooling, deployment levels are very low. In the Sunbelt region, where cooling demands are quickly rising, there are still only a few demonstration plants and studies available. (IRENA, 2015)

The demand for cooling in hot and humid regions is more than heating which showed excellent opportunity to develop renewable cooling system in that region.(IEA, 2007) The need of a solar assisted desiccant system is more important today especially in regions of high humidity.(Elsarrag, 2008)

This paper aims to presents a review of the available cooling technologies; followed by a pros and cons analysis of the different solar cooling processes as well a market study will be carried.

Keywords: desiccant, cooling, solar, market, policy

1. INTRODUCTION

Worldwide the energy consumption for cooling the buildings is increasing dramatically.(Heimo Staller, 2011)

Hot and humid regions such as in the desert area, Caribbean and Mediterranean regions are suffering from high temperature which effect in the demand on the cooling system. In the past several years the EU severing from high temperature that caused by climate change.

In addition to climate change effect there more than one reason need to be considered for cooling development such as:

- Inefficient design for building (commercial, hospital, etc…)
- Increase of internal loads such asIT-equipment, lighting.
- Misconduct of the occupants.
- Climate change aspects.
- Inefficiency of conventional cooling systems.
- Cooling demand and peak of solar gains are at the same time (mainly in the summer period)

Nowadays, the interest of cooling technologies become more widely in the EU as they introduce several project such as “Removing market barriers to the uptake of efficient heating and cooling solutions” and **“**Technology for district heating and cooling” with total budget exceed € 66M.(European Commission, 2013)

This paper will introduce brief of solar cooling technologies, policy for solar cooling technologies and marketing issue.

2. SOLAR COOLING TECHNOLOGIES

The present technologies for cooling systems driven by solar heat can classified into two type: closed systems and open systems.((IEE), 2008) In general two concepts are possible to classified solar cooling:

2.1 Cooling with PV collectors

“A conventional vapour compression machine is operated by electricity provided by PV collectors. As the only difference to conventional cooling systems is solar produced electricity, as systems with thermal collectors are emerging and as systems with thermal collectors offer, promising approaches (both from energy efficiency and financial aspects”.(Martin Treberspurg, 2011, Marc Delorme, 2002)

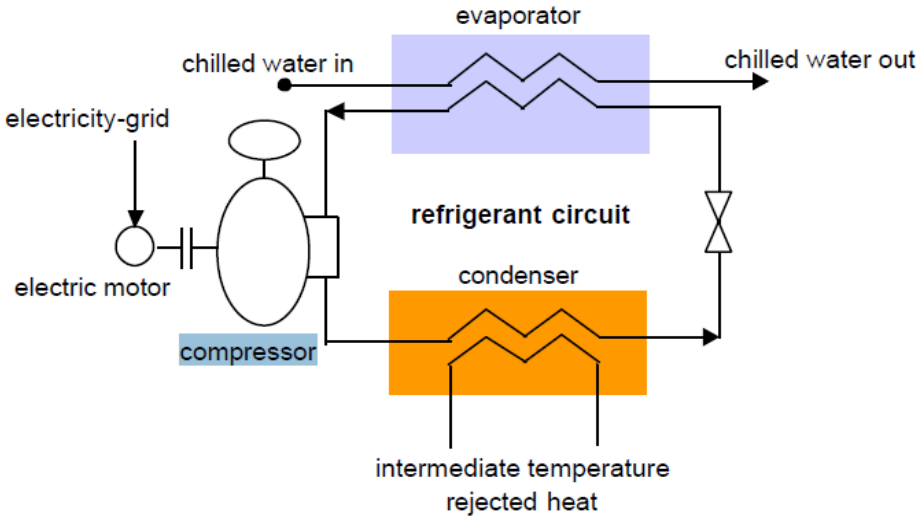

Fig. 1 Vapour Compression Chiller.

2.2 Cooling with thermal collectors

There are three thermal driven systems:

- Absorption cooling with chilled water
- Adsorption cooling with chilled water
- Desiccant cooling for air based cooling systems

Absorption chillers

“Solar powered absorption chillers use hot water from solar collectors to absorb already pressurized refrigerant from an absorbent/refrigerant mixture. Condensation and evaporation of the refrigerant vapour provide the same cooling effect as that provided by mechanical cooling systems. Although absorption chillers require some electricity for pumping the mixture, the amount is small compared to that consumed by a compressor in a conventional electric air conditioner. Absorption chillers are the most widely used chillers throughout the world although most of the installations are located in countries with mild climate such as southern Europe, China and the Mediterranean”. (Marc Delorme, 2002, Martin Treberspurg, 2011, Allouhi et al., 2015)

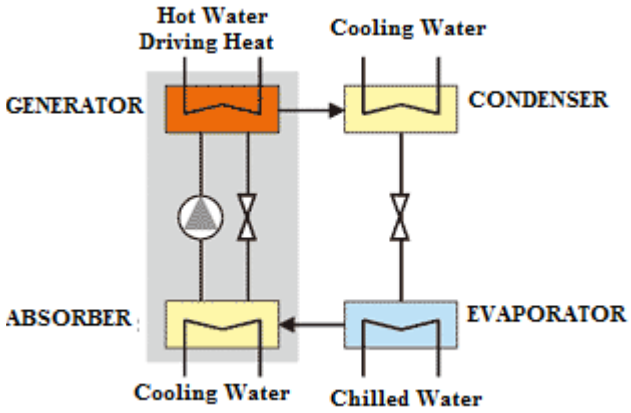

Figure. 2 Diagram of absorption chiller for Air Conditioning

Adsorption chillers

“Market available systems use water as a refrigerant and silica gel as a sorbent. The machines consist of two sorbent compartments, one evaporator and one condenser. Under typical operation conditions, with a driving heat temperature of about 80°C, the systems achieve a thermal COP of about 0.6, but the operation is possible even at heat source temperature of approx. 60°C. The capacity of the chillers range from 50 to 500 kW chilling power. The simple mechanical construction of adsorption chillers and their expected robustness is an advantage. There is no danger of crystallization and thus no limitations in the heat rejection temperatures. An internal solution pump does not exist and hence only a minimum of electricity is consumed. A disadvantage is that they are much heavier”. A significant potential for improvements of the heat exchangers in the adsorption compartments is expected.(Marc Delorme, 2002, Martin Treberspurg, 2011, Allouhi et al., 2015)

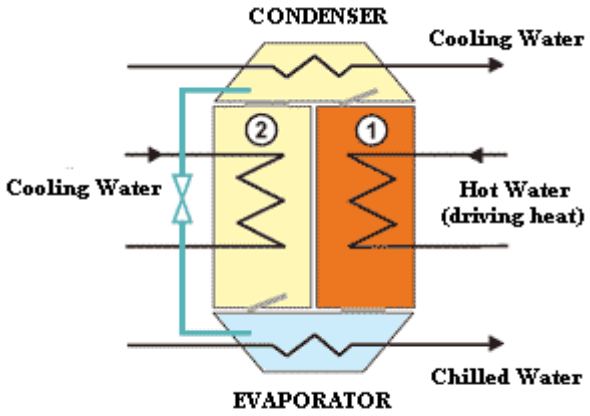

Figure. 3 Diagram of adsorption chiller for Air Conditioning.

Desiccant cooling system

"Desiccant cooling systems are open cycle systems, using water as a refrigerant in direct contact with air. The thermally driven cooling cycle is a combination of evaporative cooling with air dehumidification by a desiccant, e.g a hygroscopic material. For this purpose, liquid or solid materials can be employed. Only water is possible as a refrigerant since a direct contact to the atmosphere exists. The common technology applied today uses rotating desiccant wheels, equipped with silica gel or lithium chloride as sorption material. Solar assisted desiccant cooling used solar thermal energy to dry out or regenerate the desiccant".(Allouhi et al., 2015, Martin Treberspurg, 2011, Marc Delorme, 2002)

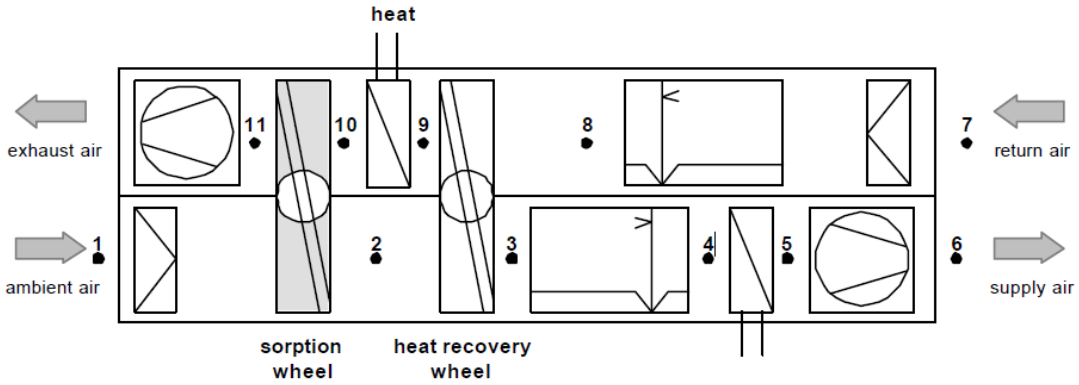

Figure. 4 Schematic drawing of a desiccant cooling unit

2.3 Solar Cooling Disadvantages & Advantages

There several advantages for implement solar cooling technologies and some disadvantage that affected of growth for these technologies. (Ayadi, 2011, Abdel-Salam et al., 2014, Baniyounes et al., 2014)

Advantages

- There is an increased consciousness of the environmental problems which created by the use of non-sustainable energy.
- The use of standard working fluids (refrigerants), with their ozone-depleting, has become a serious environmental problem.
- The impact of air-conditioning in increasing the peak power demand and contributing to shortages in the electricity supply have caused serious problems in several countries. A growing number of

countries experience a switch of peak power from winter to summer; this underlines the need to implement advanced, new concepts in building air-conditioning.
- Solar energy is available almost at the same time when cooling required.
- Comparatively little noise and vibration-free operation of thermally driven chillers.

Disadvantages

There are some barriers confronting the solar air conditioning industry in adapting to the market. (Ayadi, 2011, Abdel-Salam et al., 2014, Baniyounes et al., 2014)

- High costs are the main barrier to the market deployment.
- Technical barriers, Hardware and Software (e.g. planning guidelines, training)
- Lack of awareness of solar cooling will become a key barrier to growth shortly potential users such as hospitals, museums, libraries

3. SOLAR COOLING POLICY, REGULATOR & STANDARD

In Europe, there are just two ways in which solar thermal heating and cooling is supported, and that is through encouragements or tax reductions, which is used in different counters such as France and Germany; or having laws and responsibilities to use solar thermal in new houses or renovations, as in Spain and some prt in Germany. (Larsen, 16 July 2010)

Solar heating and cooling has been in the agenda of the International Energy Agency (IEA) since 1977 (IEA, 2012, IEA, 2014, Naukkarinen, 2007).

The governmental of United Kingdom introduce the Enhanced Capital Allowance (ECA) Scheme to improve energy efficiency and energy consumption in the country. Which support companies to be qualify for tax relief in renewable energy, heating and cooling.(Services, 2014)

European and National standards refer mainly on general issues of air conditioning systems and equipment and indoors comfort conditions. EN 14511 “Air conditioners, liquid chilling and heat pumps with electrically driven compressors for space heating and cooling” is the most representative standard among an extensive set of technical documents.

ISO 7730:2005 ”Ergonomics of the thermal environment -Analytical determination and interpretation of thermal comfort” is the most recognized standard in this area.(ISO, 2009) International Electrotechnical Commission (IEC) take consider the need of implement heating and cooling standard in solar technologies.

Till now the standard on solar air conditioning systems is not programmed. A pre-standard activity is ongoing in the framework of International Energy Agency Task 38 “Solar Air Conditioning and Refrigeration” activities”.(EU, 2007, IEA, 2012)

4. SOLAR COOLING MARKET

Throughout the 4th international conference solar air-conditioning in Cyprus, October 2011, (Henning) estimated the number of installed solar cooling system in the world to be about 1000 systems.Nevertheless, in 2015 the world will add 57GW solar PV with 30% growth compare with 2014, 17GW in China only.

Solar heat for cooling could reach a contribution of 1.5 EJ per year from an installed capacity of more than 1000 GWth for cooling, accounting for nearly 17% of energy use for cooling in 2050.(IEA, 2014) The number of installations shows that the solar cooling market is still a weak market, which is under development and not economical yet.(Kühn, 2013)

A desiccant technology is novel and disruptive, so bringing it into the entrenched conventional air conditioner market will create some market risk. The desiccant air-condition will increase site water use by approximately 60 gal/day for a typical home which equal to three-ton air conditioner. Some counteries face localized water supply issues, however, desiccant A/C in these locations may not be acceptable.(Eric Kozubal, 2011)

Table 1: Solar Cooling Market Summary.(Johnston, 2006)

Market	Prognosis	Best Opportunities
Industrial	Application suited to dry air requirements and harnessing of waste heat	Agriculture, pharmaceuticals, sweets
Commercial Buildings	Most favourable target for initial installations	Hotels, modest government offices (owner occupied or long term lease)
Residential Buildings	Large market but hurdles relating to maintenance and defining system standard	Combi-systems (space and domestic water heating), Desiccant systems (in tropical hot humid climate)

The running cost of the system mostly depends on the desiccant regeneration hence it is difficult to adopt desiccant A/C where thermal energy sources are limited.(Sultan et al., 2015)

Essentially, in Europe today for administrative buildings, the ROI (Return on Investment) of about 10-15 years, in some cases with high electricity costs or long operating times even under 10 years is possible. For solar cooling kits for residential buildings or small offices, the ROI is depending on the boundary conditions between 12 and 18 years.(Kühn, 2013)

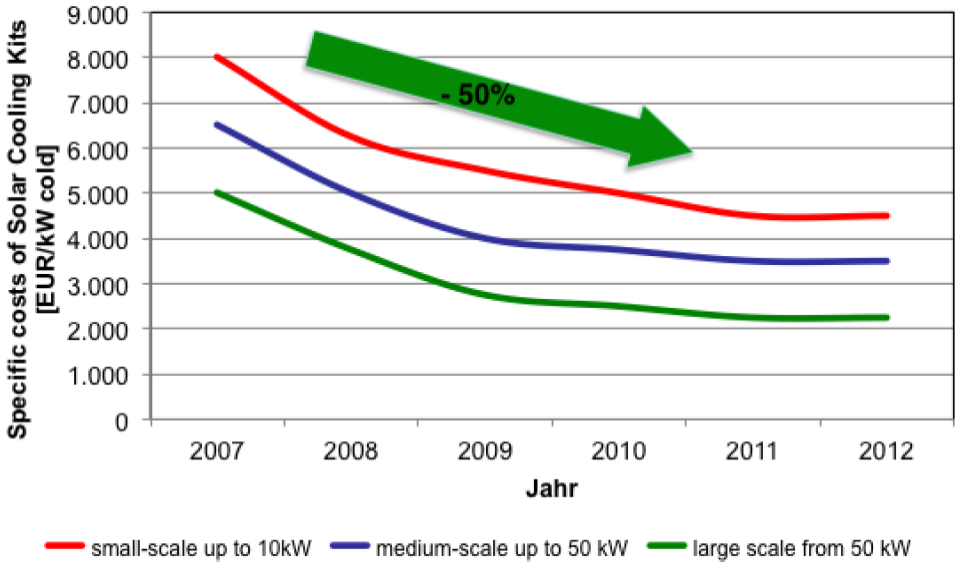

Figure. 5 Specific total costs of solar cooling kits(Kühn, 2013)

4.1 Market Barriers

(Allouhi, 2015) defined the market barriers into three groups: economic, technological and others(Allouhi et al., 2015).

The main market barriers for solar cooling have been identified as(P. Kohlenbach, 2010):

- Low electricity prices
- Low-cost conventional air conditioning
- Cross-subsidy of conventional cooling system by all electricity customers who have to pay for network and generation infrastructure
- Most components manufactured overseas and imported
- Low number of installed systems
- System complexity
- Lack to professionals training.
- A standardized solar cooling system for large counter to be implemented.

4.2 Market Opportunities

In this century, the position and needs for solar cooling have been increased. On 18 July 2013, the London School of Hygiene and Tropical Medicine reported that the first nine days of the heat wave had caused up to an additional 760 deaths in the UK.(Wikipedia, 2013)

Government measures towards intelligent use of energy, building upgrades, and peak reduction have been implemented, as well as various funding programs for sustainable energies. These include(P. Kohlenbach, 2010):

- Implementation of time of use metering for end users
- Building owners' recognition for energy efficient.
- Renewable Energy Credits for solar systems.
- implementation of tradable certificates for energy saving activities.

Increased ventilation rates, need for indoor air quality and effective humidity control, phase out of CFCs, national standards requiring higher efficiency for cooling systems, desire for lowered peak electric demands and utilization of clean renewable energy sources, and the ability for desiccant systems to solve specific problems, are the factors driving desiccant technologies to the mainstream of the A/C market.(Buker and Riffat, 2015)

5. REFERENCES

(IEE), I. E. E. 2008. Promotion of Solar Assisted Heating and Cooling in the agrofood sector.

ABDEL-SALAM, A. H., Ge, G. & Simonson, C. J. 2014. Thermo-economic performance of a solar membrane liquid desiccant air conditioning system. Solar Energy, 102, 56-73.

ALLOUHI, A., Kousksou, T., Jamil, A., Bruel, P., Mourad, Y. & Zeraouli, Y. 2015. Solar driven cooling systems: An updated review. Renewable and Sustainable Energy Reviews, 44, 159-181.

AYADI, O. 2011. <Solar Cooling Systems Utilizing Concentrating Solar Collectors.pdf>.

BANIYOUNES, A. M., Ghadi, Y. Y., Rasul, M. G., Alomari, M. H. & Manasreh, A. 2014. An Overview of Solar Cooling Technologies Markets Development and its Managerial Aspects. Energy Procedia, 61, 1864-1869.

BUKER, M. S. & Riffat, S. B. 2015. Recent developments in solar assisted liquid desiccant evaporative cooling technology—A review. Energy and Buildings, 96, 95-108.

ELSARRAG, E. 2008. Evaporation rate of a novel tilted solar liquid desiccant regeneration system. Solar Energy, 82, 663-668.

ERIC KOZUBAL, J. W., Burch, J., Boranian, A., AND Merrigan T., 2011. Desiccant Enhanced Evaporative Air-Conditioning (DEVap) Evaluation of a New Concept in Ultra Efficient Air Conditioning. US: NREL.

EU 2007. <Solar Heating and Cooling of Buildings.pdf>.

EUROPEAN COMMISSION, R. I. 2013. Removing market barriers to the uptake of efficient heating and cooling solutions [Online]. Available: https://ec.europa.eu/research/participants/portal/desktop/en/opportunities/h2020/topics/2375-ee-14-2015.html#tab2 28 May 2015].

HEIMO STALLER, A. T. 2011. State of the Art Report - Innovative cooling concepts for office buildings.

IEA 2007. Renewable Heating Cooling.

IEA 2012. 2012 Solar Heating Cooling Roadmap.

IEA 2014. Technology Road map Solar Photovoltaic Energy _2014edition.

IRENA 2015. Solar Heating and Cooling for Residential Applications.

ISO. 2009. ISO 7730:2005 [Online]. Available: http://www.iso.org/iso/catalogue_detail.htm?csnumber=39155 27 May 2015].

JOHNSTON, W. 2006. SOLAR AIR CONDITIONING OPPORTUNITIES AND OBSTACLES IN AUSTRALIA.

KÜHN, A. 2013. Thermally driven heat pumps for heating and cooling, Berlin, iversitätsverlag der TU Berlin.

LARSEN, K. 16 July 2010. Heating and cooling Europe with solar [Online]. Available: http://www.renewableenergyfocus.com/view/10931/heating-and-cooling-europe-with-solar/ 27 May 2015].

DELORME, R. S., Sabrine Berthaud, Daniel Mugnier,Jean-Yves Quinette, Nadja Richler, Frank Heunemann, Edo Wiemken,Hans-Martin Henning,Theocharis Tsoutsos,Effie Korma, Giuliano Dall 'O,Paola Fragnito,Luca Piterà, Pedro Oliveira,Joao Barroso, José Ramón López, ,SANTIAGO TORRE ENCISO 2002. Promoting Solar Air Conditioning.

TREBERSPURG, M. D., Heimo Staller 2011. Solar heating & cooling.

NAUKKARINEN, P. 2007. <Solar air conditioning and its role in alleviating the energy crisis of the Mediterranean hotels.

P. KOHLENBACH, M. A., M. Dennis, M.Airah, 2010. Solar Cooling in Australia The future of AC.

SEEC 2013. cooling consumption in GCC.

SERVICES, B.-D. A. C. 2014. Is Air Conditioning Bad for the Environment? [Online]. Glasgow: B-DACS Air Conditioning Services Available: http://www.bdacs.com/is-air-conditioning-bad-for-the-environment/ [Accessed 19 May 2015.

SULTAN, M., El-Sharkawy, I. I., Miyazaki, T., Saha, B. B. & Koyama, S. 2015. An overview of solid desiccant dehumidification and air conditioning systems. Renewable and Sustainable Energy Reviews, 46, 16-29.

WIKIPEDIA. 2013. 2013 heatwave in Ireland and the United Kingdom [Online]. Available: http://en.wikipedia.org/wiki/2013_heatwave_in_Ireland_and_the_United_Kingdom 28 May 2015].

274: The review of solid and liquid desiccant cooling technologies in sustainable energy development

MOHD ANAS MOHD SABRI[1], SIDDIG OMER[2], SAFFA RIFFAT[3]

1Mohd Anas Mohd Sabri, Institute of Sustainable Energy Technology, University of Nottingham, United Kingdom, ezxmam@nottingham.ac.uk
Department of Mechanical & Manufacturing Engineering, Faculty of Engineering & Built Environment, Universiti Kebangsaan Malaysia, Malaysia
anas@eng.ukm.my
2Siddig Omer, Institute of Sustainable Energy Technology, University of Nottingham, United Kingdom, Lazsao@exmail.nottingham.ac.uk
3Saffa Riffat, Institute of Sustainable Energy Technology, University of Nottingham, United Kingdom, Lazsbr@exmail.nottingham.ac.uk

In a fast moving and very competitive world, high energy requirement could be very demanding for engineers and researcher. Nevertheless, it sometimes misled to unwanted pollution and destruction to the environment. Energy cooling in buildings in a hot and humid country is one of the biggest contributors to this problem. Main reason is because of vapour compression cycle system requires high energy to dehumidify the air. This conventional air-conditioning system can be replaced by using desiccant cooling technologies. The objective of this paper is to review the development and application of solid and liquid desiccant cooling technologies. We will be looking on the basics and further enhancement of both solid and liquid desiccant technologies. For solid desiccant, we studied the classic desiccant-based rotor wheel and also other type of dehumidifier such as fixed bed solid desiccant. For liquid desiccant, we studied the single stage and multiple stage liquid dehumidification system and hybrid liquid desiccant cooling system. We also focus on the dehumidification mechanism for heat and mass transfer and also liquid desiccant solution. From the review, we can use as guidelines to develop a new desiccant cooling technology.

Keywords: solar energy, solid desiccant, liquid desiccant, vapour compression cycle, dehumidification

1. INTRODUCTION

Cooling is important for space conditioning of most buildings in warm climates and humid country. Removal of moisture from the air represents a considerable portion of the air conditioning load. Conventionally, air conditioning systems have to lower the air temperature below its dew point to accomplish dehumidification. This act will resulting wet cooling coil surface that led to the growth of mould and bacteria which could lead to unwanted health issue and bad indoor air quality in conditioned space (Ge et al., 2011, page 1499). After that, the air has to be reheated in order to reach the desired comfort level. Following this traditional process consumes extra energy and increases peak electricity demands. All these disadvantages of conventional air conditioning can be resolved by desiccant cooling system (Alizadeh, 2008:page 564). Solar air conditioning is regarded as one of the highest technical level whose advantages lie in its great match with the season. The greater solar radiation, the larger refrigeration output the solar radiation can produce. Desiccant cooling systems has a solution to meet the humidity and temperature requirements of buildings via decoupling latent and sensible loads. Desiccant cooling system also considered as suitable option where humidity control is the main concern in buildings such as supermarket, green house and clean room. This humidity control can be done by using desiccants to humidify the air. Desiccant materials have strong attraction towards present of water vapour in air. The driving force for this absorption of water vapour is due to the vapour pressure difference between the air and desiccant material (JAIN & Bansaal 2006: page 862). There are three types of thermally activated desiccant cooling technologies which are solid desiccant, liquid desiccant and hybrid desiccant system (Enteria et al, 2011: page 2119).

The main components of a desiccant cooling system are the dehumidifier and the regenerator. The desiccant material that has been brought into contact with the air absorbs the moisture from the air and gets diluted in the dehumidification process. After that, the desiccants must be regenerated to a useful level of concentration so that it can absorb moisture again in dehumidification. The minimum temperature required for regeneration depends on the capability of desiccant material. It varies from 50 ^{o}C for lithium chloride to 60 ^{o}C for silica gel (Bourdoukan et al., 2008: page 1210). Desiccant can be regenerated by low grade heat with low temperatures, such as solar energy and industrial exhaust gas. For the economical aspect point of view, solar energy such as solar thermal was selected because it is one of the most abundant energy sources and without any environmental pollution. One way to collect solar thermal energy is by using solar thermal collector. This is a device which absorbs the incoming solar radiation, converts it into heat energy, and transfers it through a fluid (usually air, water, or oil) for useful applications and for this case, regenerating desiccant material.

The solid desiccant cooling system is the most commonly used in application of desiccant cooling system. This is due to the simplicity of handling of desiccant materials. The desiccant material is typically implemented a honeycomb designed wheels or of the cross-flow heat exchangers. Although, it has some drawback compare to liquid desiccant, solid desiccant is easy to maintained and less complex for handling. Usually solid desiccant was used in form of desiccant wheel, fix bed and combination or modified type.

Liquid desiccant air dehumidification had gained much progress recently due to the clear qualities of this technology. It was highly efficient and it had no liquid water condensations. Packed beds, in which the liquid desiccant and the airstream exchanged heat and moisture indirect contact, were the traditional equipment to realize air dehumidification. Selected permeable membranes had been combined to the liquid desiccant air dehumidification to form a new kind of liquid desiccant air dehumidification system which is called membrane-based liquid desiccant air dehumidification system. This was been done to eliminate the cross-over problem that always happen in packed beds. The liquid desiccant system has the following advantages compared to the solid desiccant system: (1) It is easier to remove the latent heat due to the fluidness of the liquid desiccants compare to solid desiccant.(2) It has more potential of storing chemical energy (3) It can improve the air quality by absorbing the dust, bacteria, and so on.

A comprehensive literature review has been carried out and a patent search was conducted for desiccant cooling systems design, structure and operation. This review is to investigate the current development in solid and liquid desiccant cooling, as well as exploring a new innovation that can be implementing in to this technology.

2. SOLID DESICCANT COOLING

The solid-based system uses solid desiccant materials that can hold off water vapour. There are several kinds of solid desiccant materials which is silica gel, titanium silicates, calcium chloride, activated aluminas,

zeolite, molecular sieve, lithium chloride, organic-based desiccants, polymers, compound and composite desiccants. (Abdulrahman et al., 2013a: page 2)

2.1 Basic Principle

This type of desiccant cooling system used solid-based desiccant materials in controlling air moisture content. Air moisture control mechanism can come through by an absorption or adsorption. It is a solid, inorganic, crystalline desiccant which are impregnated in inert materials and used in a unit with a honeycomb type heat-wheel. They are widely used for commercial HVAC applications. Solid desiccant systems are available in single-wheel and dual-wheel packaged units. The single wheel units only include a desiccant wheel, cooling coil and reheat coil. Fresh air from outside is dehumidified by the desiccant wheel. Then, a cooling coil reduces the air temperature to the desired dew point, and the reheat coil raises the air to the desired dry bulb temperature. The dual-wheel units use a two desiccant-based wheel and a sensible-only heat wheel along with the conventional chilled water or direct expansion coil. During the cooling mode the sensible-only wheel is used as a post-cooler or to reheat the over-cooled dehumidified air. Heat is required to regenerate or reactivate the desiccant material by drive off the absorbed water vapour and discharge it outdoors using an air stream. Natural gas and solar energy is usually used to provide the heat for regeneration in single wheel units. Sometimes a combination of exhaust air and gas heat may be used on dual-wheel systems.

2.2 Development in Solid Desiccant Cooling

Figure 1 shows air handling unit system which is composed of two wheel type and sometimes called the Munter Cycle (Halliday et al., 2000: page 2). It's an open heat driven cycle which comprise a desiccant wheel parallel with a thermal wheel, with a supplementary cooling coil on supply air and evaporative cooler in the return air stream before the thermal wheel. A regeneration coil located in the return air stream and subsequently drives whole cycle. The regeneration coil is usually use a low or medium temperature hot water coil. The author creates the model utilises meteorological data to compare the actual performance of the case study. It was found that during summertime air temperature from the system can reached 23 ^{o}C, with 70% gas energy saving was achieved annually. The application of the desiccant wheel as the air dehumidifier has several elements to be considered.

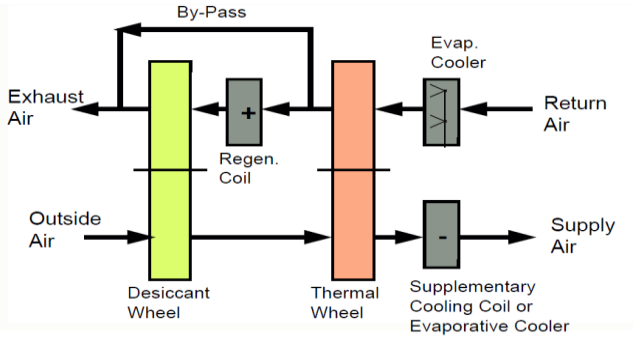

Figure 1: Air Handling Unit (AHU) configuration (Halliday et al., 2000: page 2)

The performance of the desiccant-based cooling i.e. dehumidification system relies much on the desiccant material in moisture sorption capacity. Kodama et al. 2001: page 1673 shows that there is an optimal speed rotating desiccant wheel can lead to high sorption rate. The optimal speed increases with increasing regeneration air flow rate, decreasing desiccant wheel depth, and decreasing bulk density of rotor. The optimal wheel speed decreases with higher humidity and lower regeneration temperature. It shows also that the sorption rate is relative to the air relative humidity. Zhang and Niu 2002: page 1359 show that the sorption performance of the desiccant wheel depends on the wheel rotational speed and the number of the transfer units. Thus, it was suggested that desiccant wheel should have number of transfer units of 2.5.

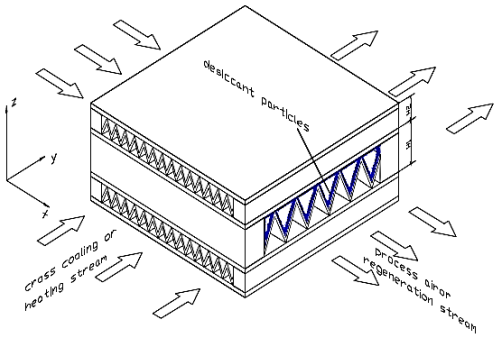

Figure 2: Desiccant coated cross-cooled compact dehumidifier (Yuan et al. 2008: page 2258)

Apart from desiccant wheel type, the fixed bed solid desiccant cooling system is another type of the system. The advantage of the bed system is the sorption process which can be done through isothermal means. It means that the air after passing the desiccant material, its temperature is not increased. Hence, the sorption process is increased due to the removal of heat of sorption. Yuan et al., 2008: page 2258 proposed a cross-cooled compact solid desiccant dehumidifier. The objective of the design is to make the dehumidification process cooler due to the heat exchange between the dehumidified air and the secondary air. It was shown in the author's result that the performance of the design is better than without secondary cooling. Figure 2 shows the cross-flow fixed bed type air-dehumidifier with cooler. Zhang et al., 2014: page 431 studied the dehumidification performances with ten kinds of solid desiccants, as the wall materials for honeycomb-type adsorbent beds, are compared. He found that the COPs of various solid desiccants tend to remain unchanged with a higher regeneration temperature under humid operating conditions, but they decrease with regeneration temperature increasing under dry operating conditions. He also concluded that among various desiccants, the silica gels type B, 3A and RD always perform better than other candidates for air dehumidification under most operating conditions, when low grade waste heat is used as the driving energy

In most design, the operation of solid desiccant cooling system is through dehumidification-humidification process. With such process, air dehumidification is done at very low humidity content for the application of evaporative cooling. With such process, the required regeneration temperature is increased. Thereof, constant dehumidification process is another option to avoid the deep dehumidification which will be applicable to hot and humid climate. Enteria et al., 2010: page 281 presented the constant humidity air cooling cycle of the desiccant as presented in Figure 3. Ando et al. 2005: page 632 shows the double stage dehumidification process. In the double stage dehumidification process, two desiccant wheels are employed as shown in Figure 4. The main purpose of the double stage dehumidification is to reduce the air moisture content in the case of humid air with lower regeneration temperature requirements.

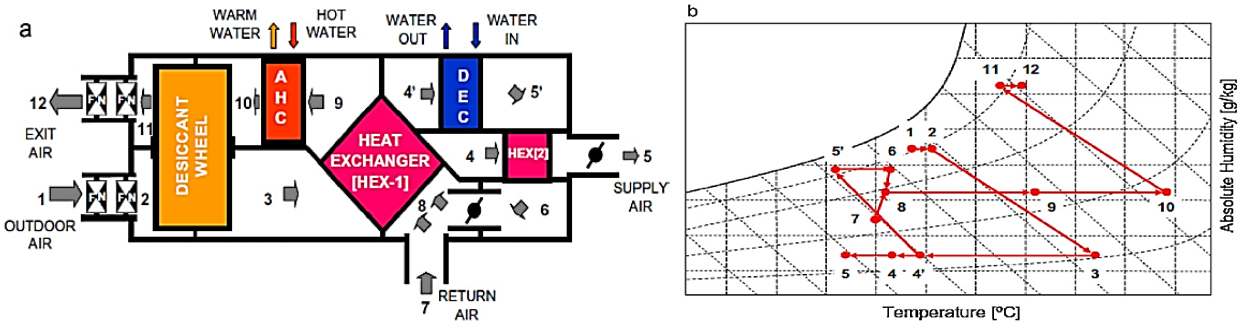

Figure 3: Constant humidity supply air desiccant cooling system . (Enteria et al. 2010: page 281)

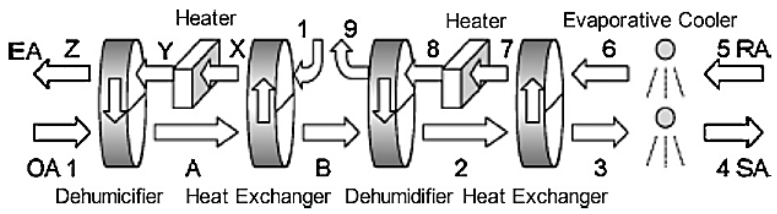

Figure 4: Double stage dehumidification desiccant cooling system (Ando et al. 2005: page 632)

3. LIQUID DESICCANT COOLING

The liquid desiccant cooling system uses the liquid desiccant in controlling air moisture content. The process of air moisture reduction is through absorption process. For reduction of the air moisture content, the air is passed in the same way as in the air cooling done in the solid desiccant cooling system. There are several types of liquid desiccants which are calcium chloride, lithium chloride, lithium bromide, tri-ethylene glycol, and a mixture of 50% calcium chloride and 50% lithium chloride and so on (Abdulrahman et al., 2013b: page 23). These liquid desiccants have general properties, but their requirements are not fully answered by any single desiccant. These requirements include low vapour pressure, low crystallization point, high density, low viscosity, low regeneration temperature, and low cost

3.1 Basic Principle

Air is dehumidified when in contact with strong liquid desiccants and subsequently, it will provide sensible cooling to the dehumidified air before air is sent to the conditioned space. When the solution is weakened by absorption of moisture, it is sent directly to the regeneration process to release the moisture using external heat resources. This process is called regenerating the desiccant. The simplest liquid-desiccant system configuration, shown in Figure 5, consists of a conditioner, regenerator, a heat exchanger to heat the solution, and another heat exchanger to cool the solution (Rutherford, 2000: page 11) The solution attracts moisture from the air in the conditioner or dehumidifier, which weakens the solution. The weak solution is sent through the heat exchanger for heating and then sprayed into the regenerator. In the regenerator, the air carries away the water vapour from the solution. After this process, the solution is sent to the conditioner across the heat exchanger for cooling. Liquid desiccant dehumidification often requires two desiccant air-contact devices which is absorbers and regenerators. A liquid desiccant absorber/regenerator system has three configurations which is packed tower, spry chamber, and spry coil arrangement.

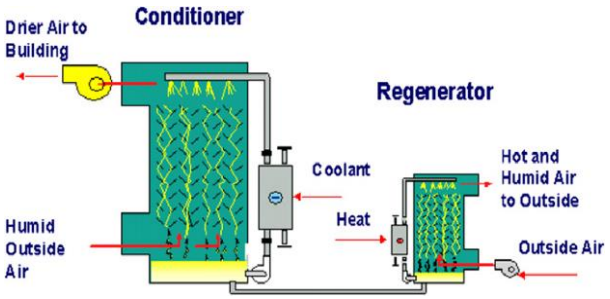

Figure 5: Liquid desiccant system (Rutherford, 2000: page 11)

3.2 Development in Liquid Desiccant Cooling

The development of the liquid desiccant cooling has taken the lime light in by several authors and engineers in recent years compared to solid desiccant cooling. This is because it can offer great advantages such as lower regeneration temperature and capability for easier storing. The following is the recent development that has been done in liquid desiccant cooling

Typical single stage liquid dehumidification system

The single stage liquid desiccant can be heated by electric heater which is used to simulate the solar collector. The layout of the experimental setup is given in Figure 6. JAIN et al., 2011: page 2464 used paper as indirect contact air-desiccant that allows moisture transfer, triggered by a difference in partial water vapour pressure between desiccant and the air. He studied a wide range of desiccant flow rates, concentration, temperatures and ambient condition. Nevertheless his studies were limited by moisture transfer characteristics of the surface in the contactor.

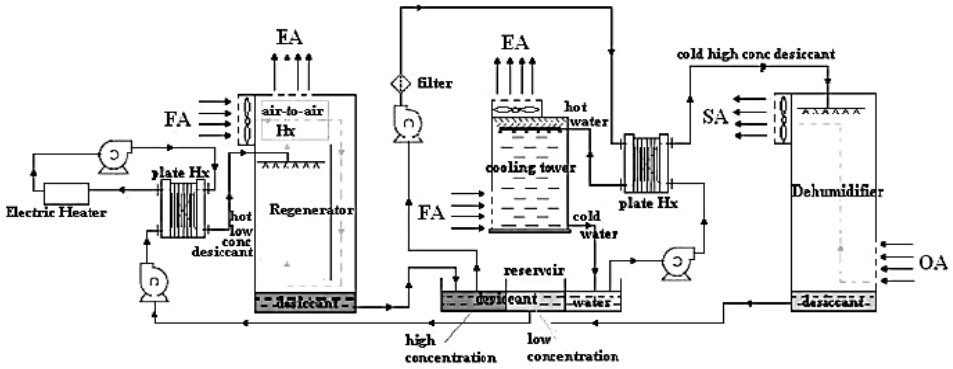

Figure 6: Liquid desiccant cooling by JAIN et al, 2011: page 2464

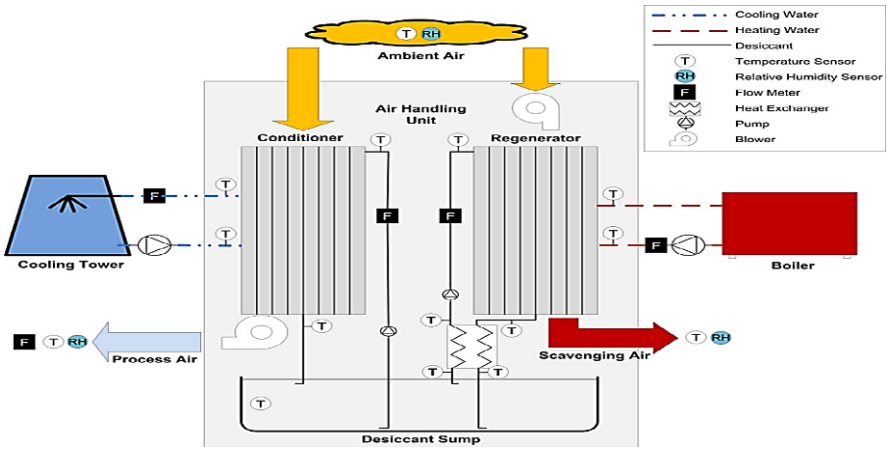

Figure 7: Schematic of liquid desiccant air conditioning equipment and instrumentation used (Croffoot & Harrison, 2012: page 545)

Croffoot & Harrison, 2012: page 545 installed a liquid desiccant air conditioning that uses low-flow parallel plate heat and mass exchanger as both the conditioner and regenerator in Canada (Figure 7). Desiccant flows in a thin wick down the outside of the plates, while cooling/heating water is circulated through the plates internally. The low-flow design eliminates carryover of desiccant into the air stream and improves the storage capacity due to the higher air to desiccant mass flow ratio. The system was tested for the duration of the summer in Ontorio, Canada. The average latent cooling power was 13.2 and average total cooling power was 12.3kW. Over the days of operation a thermal COP of 0.47 was observed. Solar collector efficiency was 56% and solar energy was able to provide 63% of the heat to drive the liquid desiccant air conditioning. Performance is expected to improve as weather gets hotter and more humid. Over the winter between October until March 2012, the solar array was operated with a dry cooler. 18,800kWh were collected with an average efficiency of 61%.

There was also a study by Audhah et al., 2011: page 3728 in utilising single stage liquid desiccant cooling system powered by the solar energy to meet fresh water and cooling needs at minimum cost (Figure 8). Parabolic solar concentrators will be the heat source for regenerating the liquid desiccant. The water condensate will be captured from the air leaving the regenerator. The regenerator exit humidified air is directed to a cooling coil submerged in cold sea water where condensation happens and distilled water is collected. They find out that heat sink temperature is a critical optimization parameter and dictates the appropriate regeneration temperature within the constraints of operation of the system to deliver its outputs of fresh water and dry cool air stream.

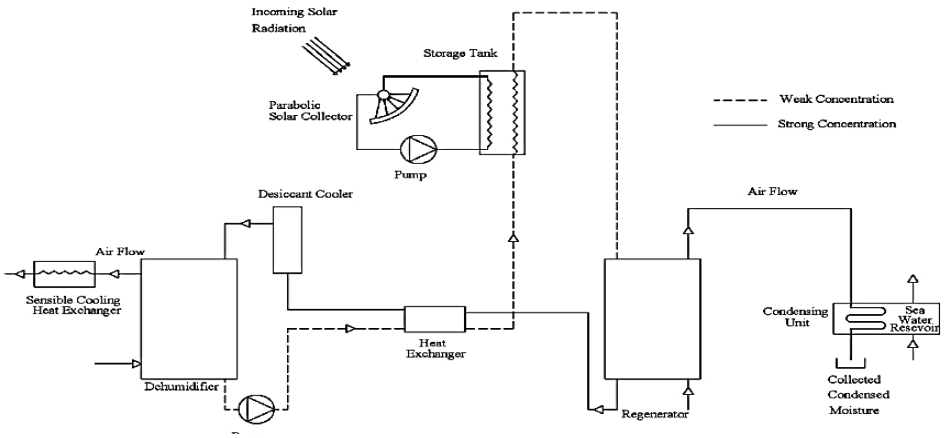

Figure 8: Schematic diagram of the liquid desiccant system (Audhah et al., 2011: page 3728).

Multi-stage liquid dehumidification system

Xiong et al., 2009: page 1210 investigated the two stage hybrid desiccant cooling system using the lithium bromide as the primary dehumidifier assisted by the calcium chloride powered by solar energy as shown in Figure 9. The results show the improvement of the energy storage capacity compared to the ordinary liquid desiccant system, also, better dehumidification performance due to the effect of pre-dehumidification. The performance of the system is higher than the ordinary liquid desiccant by 15.8% in TCOP and 32% in COP. The cost of the liquid desiccant sections decreased by 5% as long as there is abundant solar energy source. Meanwhile Li et al., 2005, page 588 introduced the design of the liquid desiccant total heat exchanger shown in Figure 10. The simulated energy efficiency ratio, EER for the air processor is 6.3 to 7.3 in summer condition.

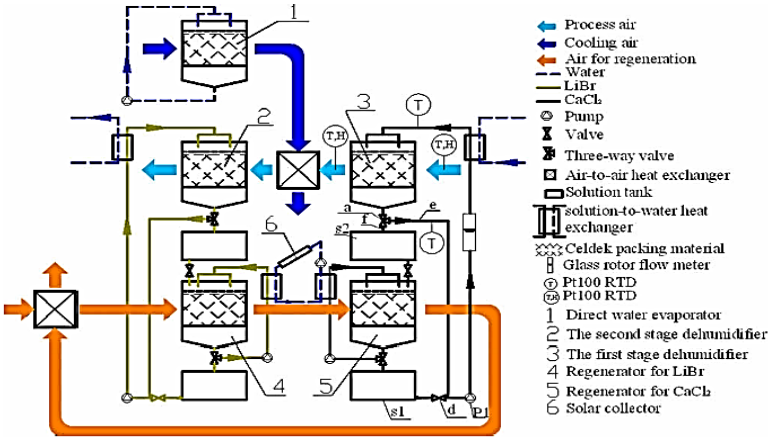

Figure 9: Solar two-stage liquid desiccant based hybrid system (Xiong et al., 2009:page 1210)

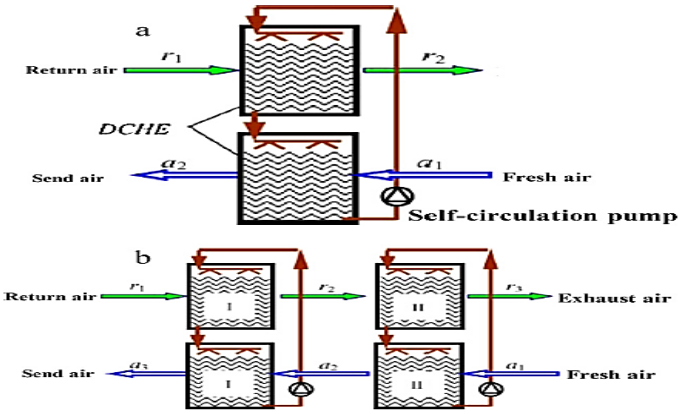

Figure 10: Liquid desiccant total heat exchanger: (a) single stage and (b) double stage (Li et al., 2005, page 588)

Hybrid liquid desiccant cooling system

Hybrid liquid-desiccant air-conditioning system is a combination of the capability of the liquid desiccant dehumidification process in removing latent load and the ability of the cooling unit to meet sensible cooling load. The main classification of the hybrid liquid desiccant cooling system is based on the cooling units used in the reduction of the dehumidified air temperature. Using hybrid system, the dehumidifier can absorb enough moisture with the smaller size of the dehumidifier and lowering the required regeneration temperature needed by the desiccant cooling system from (70– 80) ^{o}C to (50–60) ^{o}C. Al-Farayedhi et al., 2002: page 508 combined a 5-ton-capacity vapour compression unit with a packed dehumidifier and regenerator as shown in Figure 11. A gauze-type structure was used as packing towers with the following dimensions: height=2.6 m; diameter=50 cm; and thickness=0.5 cm. Calcium chloride was used as liquid desiccant to dehumidify the air inside the dehumidifier. The results showed that the hybrid cooling system provided higher COP than the conventional system. The COPs of the hybrid desiccant system for different modes of regeneration process were as follows: desiccant heating=1.164; air heating=1.616, and desiccant and air heating=1.4221; the COP of the vapour compression unit was 0.989.

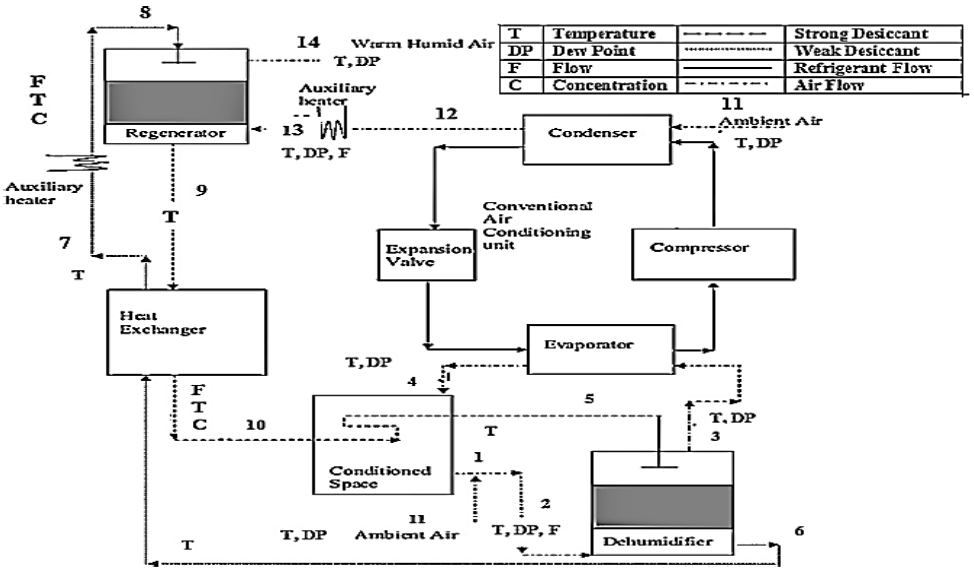

Figure 11: Experimental set-ups for hybrid cooling system. (Al-Farayedhi et al., 2002: page 508)

Dai et al., 2001: page 1188 established a hybrid air-conditioning system consisting of a vapour-compression unit, desiccant dehumidification, and evaporative cooling, as shown in Figure 12. The desiccant dehumidification unit consisted of packing honeycomb paper. The COP of the system increased by approximately 23.1% compared with the COP of the conventional vapour system when the dehumidification section was considered. It increased by 15.3% when the dehumidification and evaporative sections were taken into account.

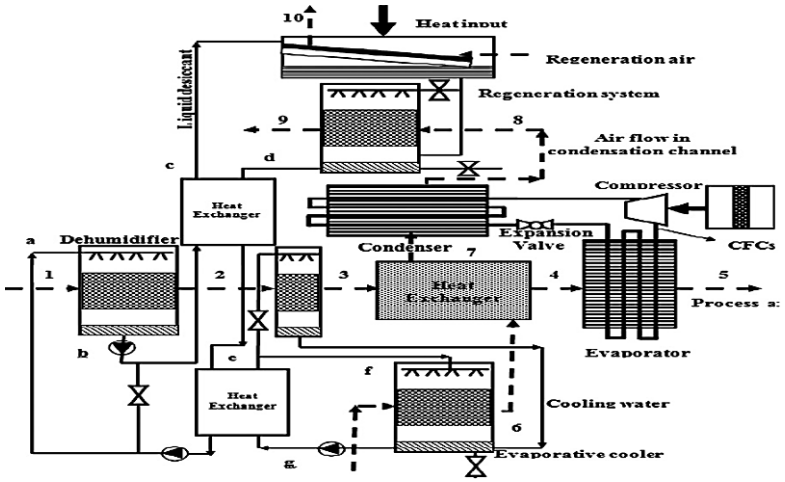

Figure 12 Schematic of the hybrid cooling system (Dai et al., 2001: page 1188)

3.3 Liquid desiccant solution

The selection of desiccant will have a significant effect on the design of the liquid desiccant cooling system. Glycols and solutions of halide salts are regularly used in industrial equipment and both have an important advantages and disadvantages. Halide salts such as lithium bromide and lithium chloride are very strong desiccants. A saturated solution of lithium bromide can dry air to 6% relative humidity and lithium chloride to 11%. (Lowenstein, 2008:page 824). However, halide salts are corrosive to most metals. Glycols such as propylene glycol and triethylene have low toxicity, and their compatibility with most metals has made the suitable to use in liquid desiccant cooling system. However, the volatile effect that glycol has make it less practical in liquid desiccant cooling application. A mixture of 96% triethylene glycol and 4% water will dry air to the same dew point as a 42% lithium chloride solution. Nevertheless, at equilibrium, the molar concentration of the glycol in the air will be on the order of 1% that of the water vapour. In an HVAC application where a 10,200 m^3/h liquid desiccant cooling system operates for 2000 hours per year, the annual loss of triethylene glycol in the conditioner would be more than 4500 kg. This fact alone has shown significant approve that glycols can bring bad an environmental effect if it used in HVAC system. According to Mei ad Dai, 2006 page 666, Lithium-based solution is the most stable desiccant with advantageously low vapour pressure, but its cost is slightly higher compared with others. A large amounts of anhydrous salt for lithium bromide and chloride cost USD6.60 and USD 9.68 per kilogram, respectively. Although the tank for desiccant storage such an uninsulated plastic tank is relatively inexpensive, the cost of the lithium chloride and lithium bromide alone would discourage desiccant storage of more than a fraction of an hour. For calcium chloride, it was found that it is the cheapest and readily available desiccant, but its vapour pressure at a given temperature is relatively high. Its application is limited due to unstable conditions depending on inlet air conditions and desiccant concentration in solution.

Salts of weak organic acids has been identified as less corrosive and non-volatile compare to halide salts. Examples of the salts is potassium formate, sodium formate and acetate. Formate salts such as potassium formate have the advantage of being significantly less viscous than acetate salts at concentrations with equivalent equilibrium relative humidities. Several companies market potassium formate as a low-viscosity heat transfer fluid and biodegradable de-icing solution (Dynalene, 2001: page 1). Although potassium formate it is a significantly weaker desiccant than lithium bromide or lithium chloride, the ability to dry air below 30% relative humidity could make it as good alternative desiccant solution in liquid desiccant cooling application. Several authors has successfully used potassium formate in the design of liquid desiccant cooling system. Jardi and Riffat 2014: page 88 has used potassium formate (HCOOK) as liquid desiccant in biomass-fuelled micro-scale tri-generation system. With flow rate of 3.5 l/s and air intake of 0.12kg/s, and capable to reduce the relative humidity from dehumidifier inlet to outlet from 87% to 57.1%. Mehta and Rane, 2013: page 690 has used the solution for liquid desiccant based solar air conditioning with evacuated tube collector. The volume flow rate is up to 300 l/h and an accuracy of 0.5% of measured value. The concentration change from 18.5% to exit concentration of 70.4% mixture of potassium formate and water.

4. CONCLUSION

The review shows that desiccant cooling system is a complicated technology but yet simple enough to improve the performance of the system. Some ways to improve the COPs of the system is to designed an efficient dehumidifier, multi-stage dehumidifier/ regeneration, double output (water condensation), and combining with conventional vapour compression unit. Due to discussed advantages desiccant cooling, it is clearly to say that liquid desiccant will be continued to be future research instead of solid desiccant. Nevertheless, we could not simply the other advantages from desiccant wheel as it to use, simple and compact. It is also noted that the use of salts of weak organic such as potassium formate would be a viable choice for liquid desiccant cooling system because it is less corrosive and non-volatile This review can be perfect guideline on how to fabricate a new type of desiccant cooling system which that can integrate the best features of both technologies.

5. REFERENCES

ABDULRAHMAN, T.M., Mat, S., Sulaiman, M.Y., Sopian, K., Al-Abidi, 2013a, A. A., Survey of liquid desiccant dehumidification system based on integrated vapor compression technology for building applications, Energy and Buildings, Vol 62, page 1–14

ABDULRAHMAN, T.M., Mat, S., Sulaiman, M.Y., Sopian, K., Al-AbidI, A. A., 2013b, Historical review of liquid desiccant evaporation cooling technology, Energy and Buildings, Vol 67, page 22–33

AL-FARAYEDHI, A, Gandhidasan, P, Antar, M.A, Abdul Gaffar, M.S., 2002, Experimental study of hybrid liquid desiccant based vapor compression system. In: Proceedings of the 6th Saudi engineering conference 5, Saudi;

ALIZADEH, Shahab, 2008, Performance of a solar liquid desiccant air conditioner – An experimental and theoretical approach, Solar Energy, Vol 82, page 563–572

ANDO, K, Kodama, A, Hirose, T, Goto, M, Okano, H., 2005, Experimental study on a process design for adsorption desiccant cooling driven with a low-temperature heat. Adsorption, Vol 11, page 631–636.

AUDAH, N., Ghaddar, N., Ghali, K. 2011, Optimized solar-powered liquid desiccant system to supply building fresh water and cooling needs. Applied Energy, Vol 88, page 3726–3736

BOURDOUKAN, P, Wurtz, E, Joubert, P, Sperandio, M., 2008, Potential of solar heat pipe vacuum collectors in the desiccant cooling process: modeling and experimental results. Solar Energy, Vol 82, page 1209–1219.

CROFOOT, Lisa & Harrison, Stephen, 2012, Performance evaluation of a liquid desiccant solar air conditioning system, Energy Procedia, Vol 30, page 542 – 550

DAI, R.Z.W.Y.J., ZHANG, H.F., YU, J.D., 2001, Use of liquid cooling to improve the performance of vapor compression air conditioning, Applied Thermal Engineering, Vol 21, page 1185–1202.

DYNALENE. 2001. Dynalene Heat Transfer Fluid HC—Engineering Guide, Dynalene Inc.

ENTERIA, N, Yoshino, H, Satake, A, Mochida, A, Takaki, R, Yoshie, R, 2010, Development and construction of the novel solar thermal desiccant cooling system incorporating hot water production. Applied Energy, Vol 87, page 478–486.

ENTERIA, Napoleon & Mizutani, Kunio, 2011, The role of the thermally activated desiccant cooling technologies in the issue of energy and environment, Renewable and Sustainable Energy Reviews, Vol 15, page 2095–2122

GE, G.M, Xiao, F., Niu, X.F., 2011, Control Strategies for Liquid Desiccant air Conditioning system, Energy and Buildings, Vol 43, page 1499-1507

HALLIDAY, S.P., Beggs, C.B. & Sleigh, P.A., 2000, The Potential for Solar Desiccant Cooling in the UK. Dublin Paper

JAIN, Sanjeev & Bansal, P.K, 2006, Performance analysis of liquid desiccant dehumidification systems, International Journal of Refrigeration, Vol 30, page 861-872

JAIN, Sanjeev, Tripathi, Sagun, Das, Rajat Subhra., 2011, Experimental performance of a liquid desiccant dehumidification system under tropical climates, Energy Conversion and Management, Vol 52, page 2461–2466

JRADI, M & Riffat, S. 2014, Experimental investigation of a biomass-fuelled micro-scale tri-generation system with an organic Rankine cycle and liquid desiccant cooling unit, Energy, Vol 71 page 80-93

KODAMA, A, Hirayama, T, Goto, M, Hirose, T, Critoph, R., 2001, The use of psychrometric charts for the optimization of a thermal swing desiccant wheel. Applied Thermal Engineering, Vol 21, page 1657–1674.

LI, Z, Liu, X, Jiang, Y, Chen X., 2005, New type of fresh air processor with liquid desiccant total heat recovery. Energy and Buildings, Vol 37, page 587–593.

LOWENSTEIN, Andrew, 2008, Review of Liquid Desiccant Technology for HVAC Applications, HVAC&R Research, Vol 14 page 819-838

MEHTA, J.R & Rane M.V, 2013, Liquid desiccant based solar air conditioning system with novel evacuated tube collector as regenerator, Procedia Engineering, Vol 51, page 688-693

MEI, L & Dai, Y.J, 2008, A technical review on use of liquid-desiccant dehumidification for air-conditioning application, Renewable and Sustainable Energy Reviews, Volume 12 page 662–689

RUTHERFORD, Thomas R., 2000, Desiccant Cooling Technology: Resource Guide, Science Applications International Corporation,

XIONG, Z.Q, Dai, Y.J, Wang, R.Z., 2009, Investigation on a two-stage solar liquid-desiccant (LiBr) dehumidification system assisted by $CaCl_2$ solution. Applied Thermal Engineering. Vol 29, page1209–1215.

YUAN, W, Zheng, Y, Liu, X, Yuan, X. 2008, Study of a new modified cross cooled compact solid desiccant dehumidifier. Applied Thermal Engineering 28; 2257–2266.

ZHANG, L, Niu, J., 2002, Performance comparisons of desiccant wheels for air dehumidification and enthalpy recovery. Applied Thermal Engineering, page 1347–1367.

ZHANG, Li-Zhi, Fu, Huang-Xi, Yang, Qi-Rong, XU, Jian-Chang, 2014, Performance comparisons of honeycomb-type adsorbent beds (wheels) for air dehumidification with various desiccant wall materials, Energy, Vol 65, 430-440

329: Computational Investigation of Unsteady Conjugated Heat Transfer in Microchannel Active Magnetic Regenerator

MUHAMMAD SAJID KAMRAN[1,2], JIE SUN[1,3], HASSAN ALI[2],
HU ZHANG[4], YI LONG[4], HUA SHENG WANG[1*]

1School of Engineering and Materials Science, Queen Mary University of London, Mile End Road, London E1 4NS, UK
2Department of Mechanical Engineering, University of Engineering and Technology, Lahore, Pakistan
3 Institue of Engineering Thermophysics, Chinese Academy of Sciences, Beijing 100190, China
4School of Materials Science and Engineering, University of Science and Technology Beijing, Beijing 100083, China
**Corresponding author: h.s.wang@qmul.ac.uk*

Materials such as Gd and LaFeCoSi alloy show significant entropy or temperature change during magnetisation and demagnetisation in a varying magnetic field. This is referred to as the magnetocaloric effect (MCE) on which room temperature magnetic refrigeration operation is based. An active magnetic regenerator (AMR), made of magnetocaloric material (MCM), is one of the key components of a room temperature magnetic refrigerator/heat pump. The working fluid, normally water, oscillates in the AMR and therefore the heat transfer in the AMR is essentially transient. The AMR in the present work is a microchannel heat exchanger made of Gd MCM. The paper describes a computational model of the transient conjugated conductive heat transfer in MCM microchannel wall and convective heat transfer in fluid flow in channels. The model is solved using Ansys Fluent. The temperature span, transient variation of Nu and effect of the ratio of channel spacing to diameter (porosity) are examined. Heat transfer enhancement and AMR dimension optimisation are presented.

Keywords: Magnetic refrigeration, Active magnetic regenerator, Transient conjugate heat transfer, Heat transfer enhancement, Numerical simulation

1. INTRODUCTION

Magnetocaloric effect (MCE) is a fundamental property of ferromagnetic materials (e.g. Gd, Mn, La, Tb and their alloys) and is observed as entropy or temperature change of the materials under varying magnetic field intensity. Materials exhibiting MCE are known as magnetocaloric materials (MCM). The MCE is the result of interaction between internal energy and magnetic energy of the material (Morrish (1965)), Tishin and Spichkin (2003)). Upon exposure/removal of MCM to a varying magnetic field, magnetic domains of the MCM become aligned (misaligned) and consequently the magnetic entropy of the MCM decreases (increases), respectively. If the variation in magnetic field intensity occurs under adiabatic (constant entropy) condition, the change in magnetic entropy must be balanced by an equal increment (decrement) in internal energy which can be observed as rise (drop) in temperature of the MCM. Neglecting the effect of magnetic hysteresis, MCE is a reversible property of MCMs (Tishin and Spichkin (2003)).

For cooling/heating purpose, an established temperature span along the regenerator length (made of MCM e.g. Gd, see

Figure 83) is necessary. This can be progressively achieved by a cyclic regenerative process, known as active magnetic regenerative (AMR) cycle. The cycle consists of four stages; namely (a) adiabatic magnetization: magnetic field intensity is increased resulting in temperature rise of the MCM; (b) cold blow: fluid flows in one direction (from cold to hot side); (c) adiabatic demagnetization: magnetic field intensity is decreased resulting in temperature drop of the MCM; (d) hot flow: fluid flows in opposite direction (from hot to cold side). The continuous repetition of the cycle leads the temperature at one end of the MCM regenerator to rise and that at the other end to drop. The temperature variation of the MCM with time during the four stages of the cycle is schematically shown in *Figure 82*(a). *Figure 82*(b) schematically shows the periodically steady temperature gradient established within the MCM regenerator.

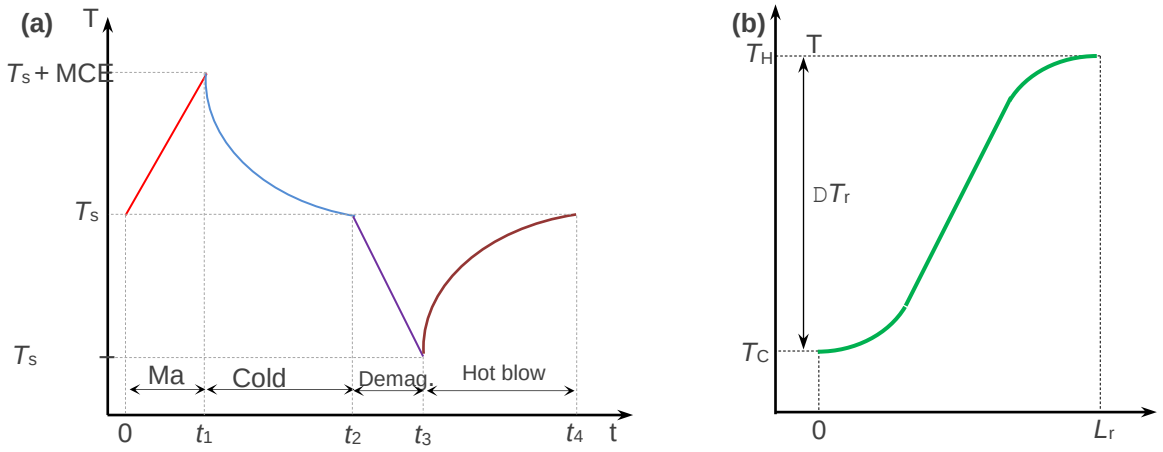

Figure 82: (a) Temperature variation in regenerator during four-stage AMR cycle; (b) Temperature gradient inside the MCM regenerator.

Compared with heat transfer in condenser and evaporator in the conventional vapour-compression refrigeration systems, heat transfer in regenerators has the following features: (1) water or water-based fluids are used as the working fluid and heat transfer is single-phase; (2) fluid periodically flows through the regenerator and heat transfer is transient; (3) convective heat transfer of the fluid and conductive heat transfer in MCM solid are coupled; (4) MCE occurs periodically as an energy source (heating and cooling) within the MCM solid. It is apparent that heat transfer in the regenerators plays an important role in developing applicable magnetic refrigeration systems. So far, parallel-plate and spherical particle bed MCM regenerators have been employed in the magnetic refrigerator prototypes (Pecharsky and Gschneidner (2006), Nielsen (2010), Yu et al. (2010), Go´mez et al. (2013)) and little investigation has been conducted for microchannel regenerators. Microchannel heat exchangers have proved to be both compact and effective as a condenser (Wang and Rose (2005), Wang and Rose (2011)). In the present work, heat transfer through a microchannel in a magnetocaloric solid is numerically simulated. The temperature span, transient variation of *Nu* and effect of channel spacing to diameter ratio (porosity) are investigated.

2. PHYSICAL MODEL AND GOVERNING EQUATIONS

As shown in

Figure 83(a), a microchannel active magnetic regenerator, consisting of many channels with an optimum inter-channel spacing (Wang and Rose (2011), is considered in the present work. The circular channels are drilled in MCM (Gd) solid. Water is used as the working fluid. Assuming symmetry and uniform flow rate distribution among channels, only one channel (see

Figure 83(b)) is chosen for the computational simulation in order to reduce the computer time. The diameter of the circular channel is *d* and the MCM solid has a width δ_x, height δ_y and length *L*. The MCM undergoes magnetisation (demagnetisation) process, resulting in temperature rise (drop), respectively, due to MCE. Heat is transferred from MCM (water) to water (MCM) periodically in cold (hot) blow following a sequence shown in *Figure 82*(a).

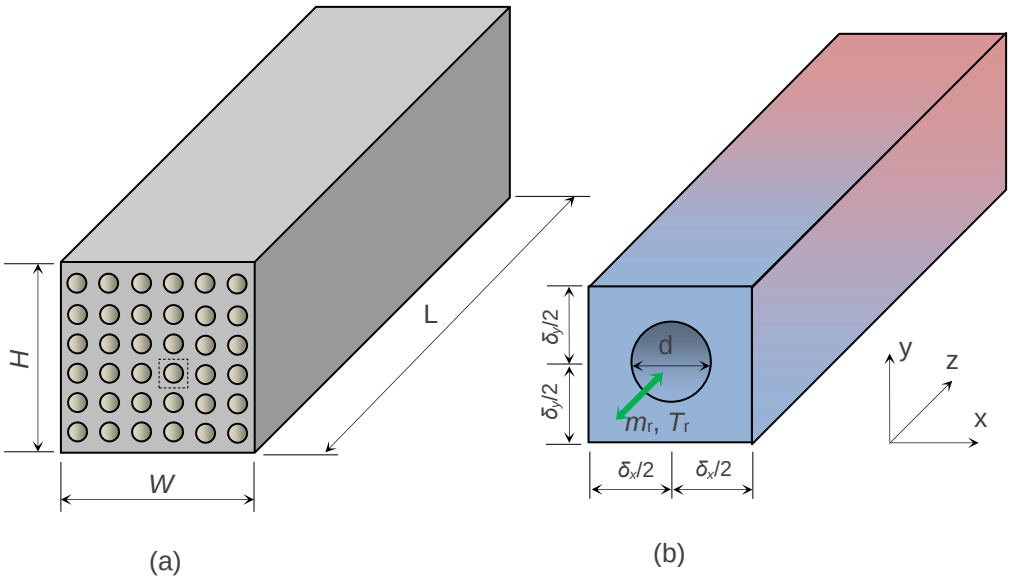

Figure 83: Physical model of conjugated heat transfer in microchannel regenerators

To model the conjugated convective and conductive heat transfer, the following assumptions are made: 1) Magnetic field intensity is uniform in the regenerator and the internal demagnetizing field is neglected; 2) Thermal and magnetic hysteresis in the MCM are negligible; 3) Properties of the MCM are independent of temperature and magnetic field intensity; 4) Flow is incompressible; 5) Thermophysical properties of water are taken to be constant; 6) Viscous dissipation is neglected.

The conservation of mass, momentum and energy are:

Equation (1)
$$\nabla \cdot \boldsymbol{u} = 0$$

Equation(2)
$$\rho_{\mathrm{f}}\left(\frac{\partial \boldsymbol{u}}{\partial t} + \boldsymbol{u}\cdot\nabla\boldsymbol{u}\right) = -\nabla P + \mu_{\mathrm{f}}\left(\nabla^2\boldsymbol{u}\right)$$

Equation (3)
$$\frac{\partial T_{\mathrm{f}}}{\partial t} + \boldsymbol{u}\cdot\nabla T_{\mathrm{f}} = \alpha_{\mathrm{f}}\left(\nabla^2 T_{\mathrm{f}}\right)$$

Equation (4)
$$\rho_{\mathrm{s}} c_{\mathrm{P,s}}\frac{\partial T_{\mathrm{s}}}{\partial t} = \lambda_{\mathrm{s}}\left(\nabla^2 T_{\mathrm{s}}\right) + \dot{q}_{\mathrm{MCE}}$$

where $\boldsymbol{u}$ is the velocity of water, *t* is time, T_{f} and T_{s} are temperatures of water and MCM solid, respectively, ρ_{f}, $c_{\mathrm{P,f}}$, λ_{f} and μ_{f} are the density, specific heat capacity, thermal conductivity and dynamic viscosity of water, respectively. ρ_s, c_s and λ_s are the density, specific heat capacity and thermal conductivity of Gd,

respectively, α_f is the diffusivity of water and α_s is the diffusivity of Gd, $\dot{q}_{MCE}$ is the MCE source term given by Eq. (5) (Nielsen (2010)).

Equation (5)

$$\dot{q}_{MCE} = -\rho_s T_s \frac{\partial m}{\partial T}\frac{dB}{dt}$$

where m is the magnetization determined by the mean field model given by Eqs. (6)-(8) (Morrish (1965)), dB/dt is the rate of change in magnetic field intensity.

Equation (6)

$$m(B,T_s) = Ng\mu_B J B_J(X)$$

Equation (7)

$$B_J(X) = \frac{2J+1}{2J}\coth\left(\frac{2J+1}{2J}X\right) - \frac{1}{2J}\coth\left(\frac{1}{2J}X\right)$$

Equation (8)

$$X(B_J, B, T_s) = \frac{Jg\mu_B}{K_B T_s}B + \frac{3JT_{Cu}}{J+1}\frac{B_J(X)}{T_s}$$

where K_B = 1.381×10^{-23} J/K is the Boltzmann Constant, μ_B = 9.274×10^{-24} J/T is the Bohr magneton, N_A = 6.022×10^{23} mol^{-1} is the Avogadro's number, G = 2 is the Lande factor, J = 3.5 h is the angular momentum, N_s = 3.83×10^{28} kg^{-1} is the number of magnetic spins, T_{Cu} = 294.0 K is the Curie temperature of Gd, T_{De} = 173 K is the Debye temperature.

Figure 84(a) shows the variation of temperature rise of the MCM, when exposed to the variations in magnetic field intensity ΔB for 0.8, 1.0, 1.2, 1.4 and 1.6 T, with MCM temperature as predicted by the mean field model. As is seen from *Figure 84*(a), the temperature rise gradually increases with increasing temeprature, takes the maximum value at the Curie temperature T_{Cu} of the MCM and gradually decreases with further increasing temperature. *Figure 84*(b) plots the temperature dependent heat source incorporated in Eq. (4) to approximately treat the actual $\dot{q}_{MCE}$ as given by Eq. (5). The simplified source term (see *Figure 84*(b)) given by Eqs. (9) and (10) is employed in the present simulation to avoid the iterative process involved in the solution of Eqs. (5) – (8).

Equation (9)

$$\dot{q}_{MCE}(T_s, \Delta B = 1.0\text{T}) = a_4 T_s^4 + a_3 T_s^3 + a_2 T_s^2 + a_1 T_s + a_0 \quad \text{for } T_s \le T_{Cu}$$

Equation (10)

$$\dot{q}_{MCE}(T_s, \Delta B = 1.0\text{T}) = b_4 T_s^4 + b_3 T_s^3 + b_2 T_s^2 + b_1 T_s + b_0 \quad \text{for } T_s > T_{Cu}$$

where a_4 = -72.996834, a_3 = 8.210825×10^4, a_2 = -3.461445×10^7, a_1 = 6.4822174×10^9, a_0 = -4.549999×10^{11}, b_4 = -89.634816, b_3 = 1.104078×10^5, b_2 = -5.096618×10^7, b_1 = 1.044936×10^{10} and b_0 = -8.028107×10^{11}. Equations (9) and (10) are obtained for ΔT_{ad} at ΔB = 1.0 T, the Curie temperature of Gd 294.0 K, in time period of 1 s with Δt = 0.1 s.

The present work is conducted for the periods of the magnetisation, demagnetisation, cold blow and hot blow to be 1 s, respectively, leading to the period of four-stage AMR cycle to be 4 s (see *Figure 82*(a)).

The source term is taken to be positive during magnetisation, negative during demagnetisation and zero during the cold and hot blows. This simplified method considerably reduces the computational time for the solution of a 3D problem.

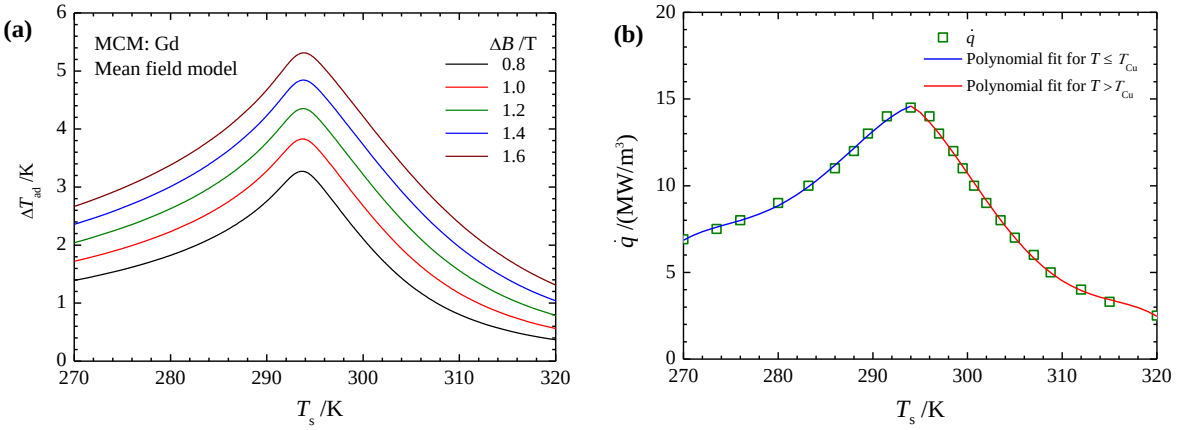

Figure 84: (a) Variation of ΔT_{ad} with MCM temperature for ΔB values of 0.8, 1.0, 1.2, 1.4 and 1.6 T, predicted by the mean field model for Gd; (b) Source term used in Eq. (4) for ΔB = 1.0 T.

2.1 Boundary Conditions

The boundary conditions are described below considering the case where $\delta_x = \delta_y = \delta$;

$q = 0, u = v = w = 0$ at $0 < (x^2 + y^2 - d^2/4) < \delta/2$, $z = 0$, $z = L$

$\lambda_f \left(\frac{\partial T_f}{d\mathbf{n}} \right) = \lambda_s \left(\frac{\partial T_s}{d\mathbf{n}} \right)$ at $x^2 + y^2 - d^2/4 = 0$, $0 \le z \le L$

$\frac{\partial T_s}{d\mathbf{n}} = 0$ at $\delta/2 < x < \delta/2$, $y = \delta/2$, $0 \le z \le L$

$\frac{\partial T_s}{d\mathbf{n}} = 0$ at $x = \delta/2$, $\delta/2 < y < \delta/2$, $0 \le z \le L$

During magnetisation

$u_{r,c} = 0$ at $x^2 + y^2 - d^2/4 < 0$, $z = 0$

During cold blow

$u_{r,c} = \frac{m_r}{\rho_f A_{ch} n_{ch}}, T_{r,c} = T_{r,c,in}$ at $x^2 + y^2 - d^2/4 < 0$, $z = 0$

$\frac{\partial \boldsymbol{u}}{\partial \mathbf{n}} = 0, \frac{\partial T_f}{\partial \mathbf{n}} = 0$ at $x^2 + y^2 - d^2/4 < 0$, $z = L$

$q_{MCE} = 0$

During demagnetisation

$u_{r,h} = 0$ at $x^2 + y^2 - d^2/4 < 0$, $z = L$

During hot blow

$$u_{\mathrm{r,\,h}} = \frac{m_{\mathrm{r}}}{\rho_{\mathrm{f}} A_{\mathrm{ch}} n_{\mathrm{ch}}}, T_{\mathrm{r,\,h}} = T_{\mathrm{r,\,h,\,in}} \quad \text{at} \quad x^2 + y^2 - d^2/4 < 0,\ z = L$$

$$\frac{\partial \mathbf{u}}{\partial \mathbf{n}} = 0, \frac{\partial T_{\mathrm{f}}}{\partial \mathbf{n}} = 0 \quad \text{at} \quad x^2 + y^2 - d^2/4 < 0,\ z = 0$$

$$q_{\mathrm{MCE}} = 0$$

The time averaged Nusselt number is calculated by

Equation (11)

$$\overline{Nu_{\mathrm{av}}} = \frac{1}{\tau_{\mathrm{flow}}} \int_0^{\tau_{\mathrm{flow}}} Nu_{\mathrm{av}} \mathrm{d}t$$

where

- $Nu_{\mathrm{av}} = \frac{1}{L} \int_0^L Nu_z \mathrm{d}z$ and $Nu_z = \frac{\alpha_z d_{\mathrm{h}}}{\lambda_{\mathrm{f}}}$

The utilization is defined as the ratio of thermal mass of the fluid to thermal mass of the solid given by Eq. (12)

Equation (12)

$$\varphi = \frac{m_{\mathrm{r}} c_{\mathrm{P,\,f}} \tau_{\mathrm{f}}}{m_{\mathrm{s}} c_{\mathrm{s}}}$$

where m_r is the mass flow rate, τ_f is the flow time and m_s is the mass of the MCM.

3. SOLUTION PROCEDURE

Equations (1) - (4) together with the corresponding boundary conditions were solved using Fluent. The SIMPLE algorithm was chosen to couple the pressure and velocity and the QUICK scheme was used to discretise the convective terms in the momentum and energy equations. The first order implicit scheme was used to discretise the transient terms. The properties of water were taken at a reference temperature of 20 ^{o}C. The density, specific heat capacity, thermal conductivity and dynamic viscosity of water are taken to be ρ_{f} = 1000 kg/m^3, $c_{\mathrm{P,f}}$ = 4180 J/kg K, λ_{f} = 0.58 W/m K and μ_{f} =1.003 Pa.s, respectively. The *Pr* number of water is taken to be constant of 7 and the *Re* number varies from 1 to 400. The density, specific heat capacity and thermal conductivity of Gd are ρ_s = 7900 kg/m^3, c_s = 290 J/kg K and λ_s = 10.6 W/m K, respectively.

The four stages of the cycle are simulated in the following way:

(1) *Magnetization*: The regenerator moves into the magnet field and the intensity of the magnet field increases from B_{min} to B_{max}. The MCE is implemented as positive source term and temperature of the MCM solid increases. The control volumes with $T_s \leq T_{\mathrm{Cu}}$ are updated using Eq. (9) while for control volumes with $T_s > T_{\mathrm{Cu}}$ Eq. (10) is used.

(2) *Cold blow*: During cold blow, the regenerator retains in the magnet field (B_{max}), the working fluid flows forwards (cold blow) through the microchannels and the MCM solid is cooled down.

(3) *Demagnetization*: The regenerator moves away from the magnetic field and the magnetic field intensity decreases from B_{max} to $B_{\mathrm{min.}}$ The MCE is implemented as negative source term and consequently the local temperatures of the MCM solid decreases.

(4) *Hot blow*: The regenerator retains outside the magnet field (B_{min}), the working fluid flows backwards (in the reverse direction of cold blow) through the microchannels and the MCM solid is heated up.

More details of the method are given in Kamran et al. (2012).

3.1 Grid independence

The computational domain for the conjugated heat transfer is shown in *Figure 85*. The fluid (channel for water flow) and solid (MCM) zones are shown by green and black colours, respectively. The domain was discretised into hexagonal cells. To study grid indepence, steady-state flow and heat transfer of water as specified in *Table 1* was computed (single blow, flow from one direction only) using various grid spacings $n_{\Delta x}$, $n_{\Delta y}$ and $n_{\Delta z}$ along *x*, *y* and *z* directions, respectively. As can be seen from table 1, the average Nu converges as the number of the mesh increases. A grid size of 10×10×90 was therefore selected.

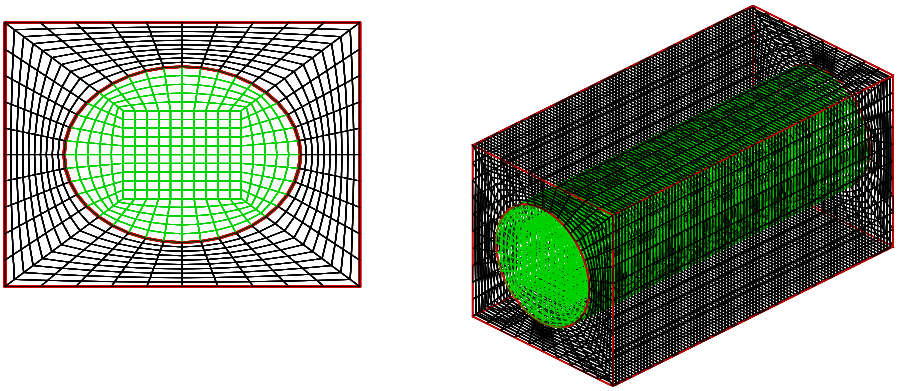

Figure 85: Grid for a single microchannel

Table 1 Mesh depenance study at $\delta_x/d = \delta_y/d = 1.5$, $L/d = 90$, $Re = 500$, $Pr = 7.0$

$n_{\Delta x}$	$n_{\Delta y}$	$n_{\Delta z}$	n_{CV}	Nu_{av}
8	8	60	24480	5.71
8	8	90	36720	5.70
8	8	120	46080	5.58
8	8	150	57600	5.59
10	10	60	37200	5.59
10	10	90	55800	5.57
10	10	120	74400	5.55
10	10	150	93000	5.64
15	15	60	48960	5.59
15	15	90	73440	5.57
15	15	120	97920	5.55
15	15	150	122400	5.54

3.2 Validataion

To validate the present model and numerical schemes used, steady-state conjugated heat transfer for simultaneously (thermally and hydrodynamically) developing laminar flows was performed and compared with the results of Shah and London (1978) for constant surface temeprature and constant heat flux conditions and Kroeker et al. (2004) for conjugated condition, as shown in *Figure 86*. Kroeker et al. (2004) presented their results, the variation of *Nu* with the dimensionless longitudinal dimension Z^+ defined as

Equation (13)

$$Z^+ = \frac{z}{d_{ch} Re\, Pr}$$

where *z* is the axial distance in the flow direction, *d* is the channel diameter, $Re = \rho_f u d / u_f$ is the Reynolds number and $Pr = \mu_f c_{P,f} / \lambda_f$ is the Prandtl number. As is seen from *Figure 86*, the present results are in good agreement with those of Shah and London (1978) and Kroeker et al. (2004).

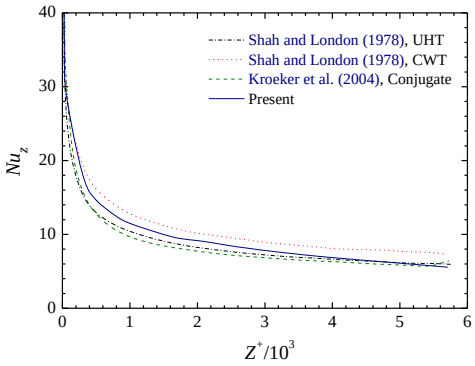

Figure 86: Comparison of longitudinal variation of local Nusselt number of present numerical simulation with those of Shah and London (1978) and Kroeker et al. (2004); for δ_x/d = 4, δ_y/d = 2, L/d = 20, Re = 500, Pr = 7.0, λ_s/λ_f = 668.3 (copper-water).

4 RESULTS AND DISCUSSION

Various calculations have been performed. The results are discussed for the temperature profile, temperature span, mass flow rate, Nusselt number and porosity.

4.1 Temperature profile

Figure 87(a) and (b) show periodical temperature profiles at the cold and hot ends for δ/d = 1.2 and δ/d = 1.5, respectively, when a steady-state temperature span is established. The temperatures at the cold end T_c and the hot end T_h are measured by integrating circumferential temperature in the *xy*-planes at the locations of z/L = 0.01 and z/L = 0.99, respectively. The average temperatures at two ends behaviour differently during cold and hot blows. During cold blow, the average temperature at the hot end decreases linearly while that at the cold end decreases non-linearly. Vice versa is the case during the hot blow. However, average temperature profiles during magnetisation and demagnetisation follow similar linear trends at both of the cold and hot ends.

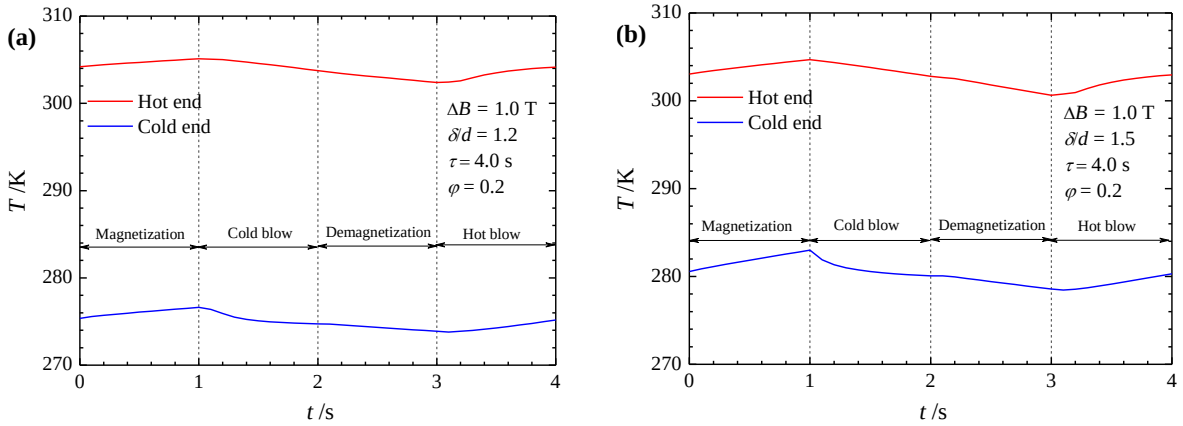

Figure 87: Periodic steady-state temperature profiles at cold and hot ends; (a) δ/d = 1.2, ΔB = 1.0 T, φ = 0.2, τ = 4.0 s and (b) δ/d = 1.5, ΔB = 1.0 T, φ = 0.2, τ = 4.0 s.

4.2 Temperature span

Figure 88 shows the variation of the cross-sectional averaged temperature in MCM solid along z-direction with time. The initial temperature along z-direction is 293.0 K. As the microchannel regenerator is subjected to the four-stage AMR cycle, the temperature at one end drops and the temperature at the other end rises.

The rate of change in temperature gradually decreases with time till it finally becomes zero. The temperature profile stabilises and a steady-state temperature gradient is reached at t ~ 800 s.

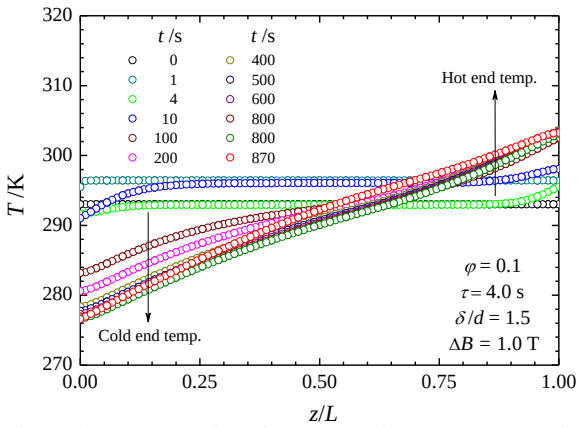

Figure 88: Variation of cross-sectional averaged temperature along the channel.

Figure 89 shows the contours of transient development of temperature gradient. Figure 89(a) shows slices along x direction while Figure 89(b) shows slices along z direction. The temperature contours are shown for different stages of AMR cycle. At t = 600 s the temperature contours for the cold blow are shown while at t = 800 s the temperature contours for the hot blow are shown.

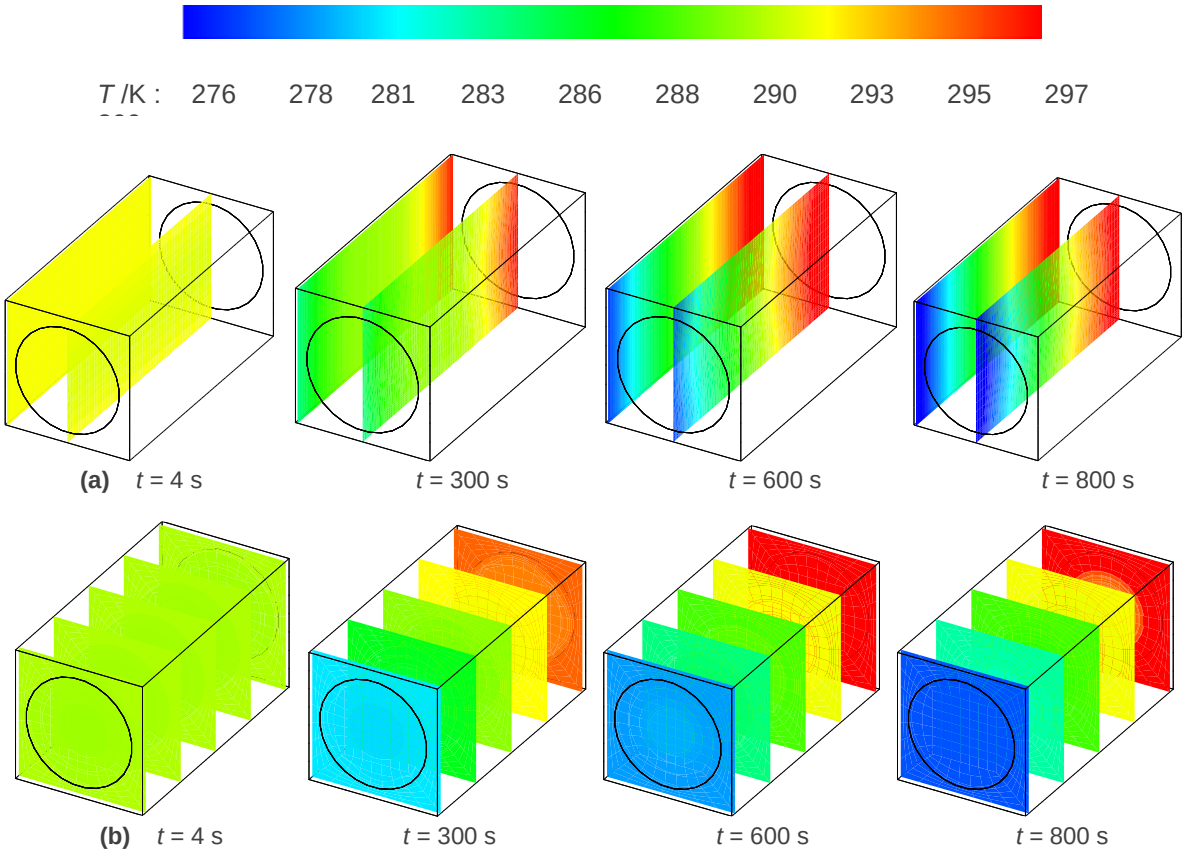

Figure 89: Contours of transient response of microchannel regenerator δ/d = 1.5, Re = 20, φ = 0.2, τ = 4.0 s; (a) contour slices along x-direction and (b) contour slices along z-direction.

4.3 Mass flow rate

The temperature span ΔT_r of the regenerator was calculated for different *Re* and different values of *δ/d*. *Re* is varied by changing the mass flow rate of water resulting in variation in utilization *φ*. The transient

variations in temperatures at the hot end and colds of the regenerator are shown in *Figure 90*(a) – (d). The temperatures profiles at two ends commence to depart from each other from the first cycle and the deviation grows to a periodically steady state temperature gradient in the MCM. The temperature span is the difference between the average temperatures at the hot and cold ends. The variation in temperature span with utilization takes the maximum value at φ = 0.1. A sufficiently higher temperature span is required in magnetic refrigeration in order to make the system workable in practice. The time required to reach a steady-state temperature span decreases as the mass flow rate increases.

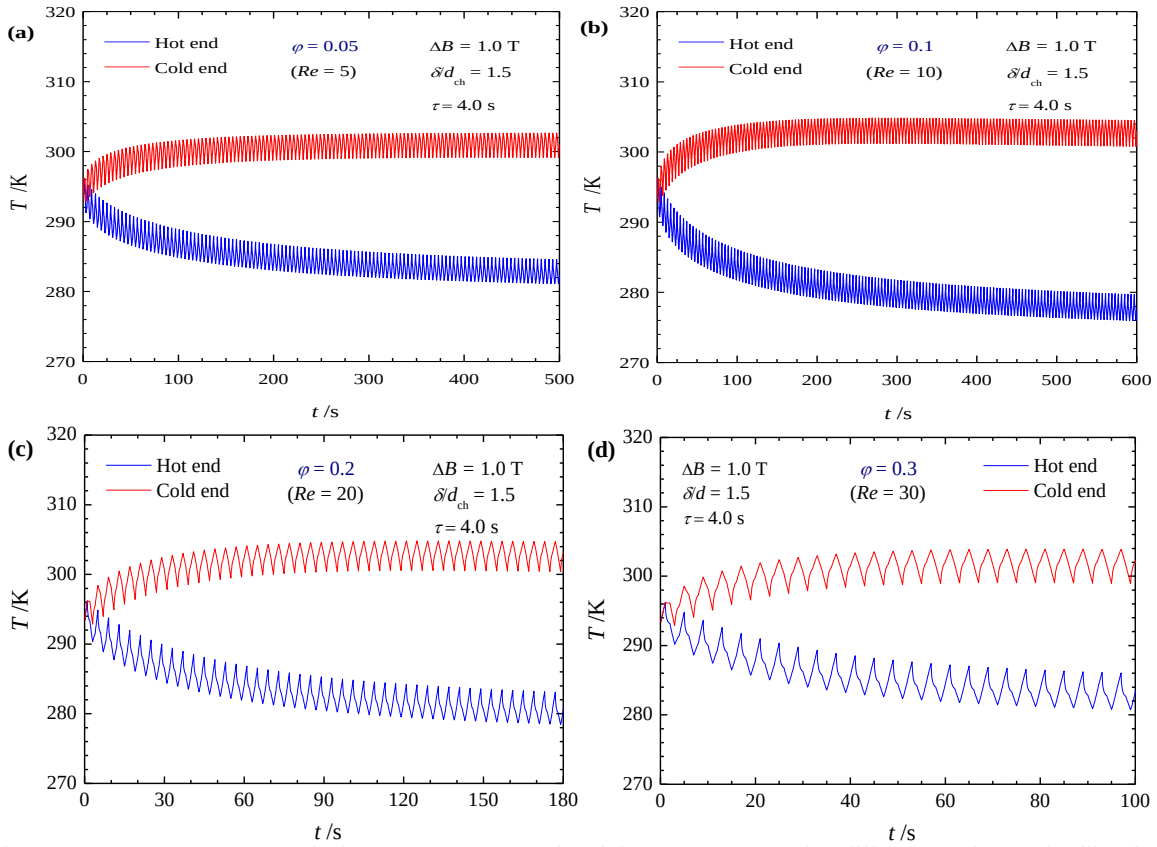

Figure 90: Temperature variation across two ends of the regenerator for different values of utilization.

4.4 Nusselt number

The circumferentially averaged Nusselt number along z-direction is shown in

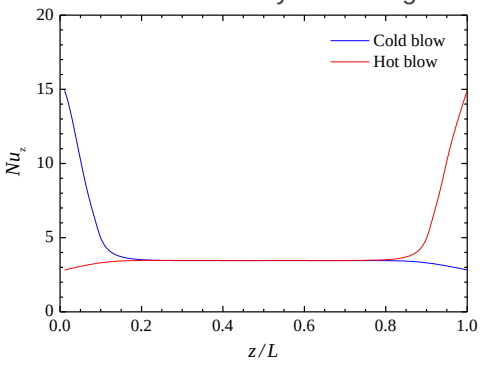

Figure 91. During the cold blow the Nu at z = 0 is the highest and the value gradually drops to the average value while during the hot blow the Nu at z = L. is the highest and the values gradually drops to the average value.

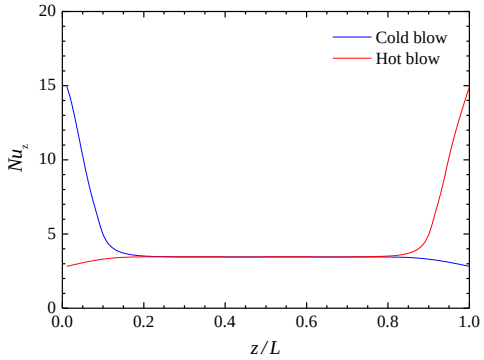

Figure 91: Variation of cross-sectional circumferentially averaged Nu along the channel.

4.5 Porosity

The effects of the utilization and porosity on the temperature span were examined by computing the cases given in *table 2*. The results are shown in *Figure 92*. For a give+n value of ε, as the utilization φ is increased the temperature span quickly increases, takes a maximum value and decreases gradually. For φ = 0.2, the temperature span increases with increasing ε, reaches its maximum value for ε = 0.55 and then decreases with further increase in porosity. For smaller porosity (larger volume of MCM), more heat is dispersed (conducted) within the MCM as compared to the heat transported by fluid resulting in lower cooling capacity and opposite is the case for larger porosity (smaller volume of MCM) where more convection heat transfer rate is higher than heat conduction rate within the MCM insufficient to develop a temperature gradient.

Table 2 Dimensions used to study the effects of utilization and porosity

Case	*L/d*	δ_x/d	δ_y/d	ε
I	90	1.1	1.1	0.65
II		1.2	1.2	0.55
III		1.5	1.5	0.35
IV		2.0	2.0	0.2
V		2.5	2.5	0.13
VI		3.0	3.0	0.09

Figure 92: Variation of temperature span with utilization for different ε values.

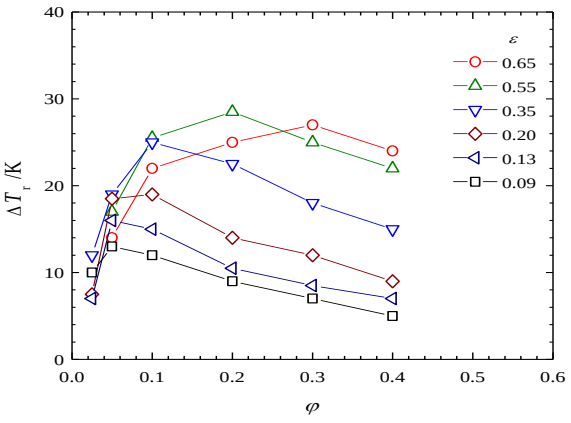

The solid line is a guide for the eye.

5 CONCLUSIONS

Three-dimensional numerical simulations have been performed using Fluent to investigate flow and heat transfer through a circular microchannel made of magnetocaloric materials (Gd). The volumetric energy source due to the magnetocaloric effect is determined by the local temperature. The mass flow rate of the fluid is found to have limited operating range to yield the optimal performance. The ratio δ/d or porosity greatly influences the achievable regenerator temperature span and the largest temperature span is obtained when the value of δ/d being 1.2. The best performance is achieved when Biot number is less than 0.1. A prototype magnetic refrigerator employing Gd microchannel regenerator is under construction and the numerical results will be compared with experimental data when they become available.

6 ACKNOWLEDGMENT

A PhD studentship by University of Engineering and Technology Lahore, Pakistan and EU research grant FP7-2010-IRSES-269205 are gratefully acknowledged.

7 REFERENCES

GOMEZ, J. R., Gracia, R. F., Carril, J. C. and Gomez, M. R., 2013, A review of room temperature linear reciprocating magnetic refrigerators, Renewable and Sustainable Energy Reviews 21, 1–12.

KAMRAN, M. S., Sun, J., Wu, J. H., Chen, Y. G. and Wang, H. S., Numerical simulation of room temperature microchannel regenerator magnetic refrigerator; In proc. Fifth IIF-IIR INTERNATIONAL CONFERENCE ON MAGNETIC REFRIGERATION AT ROOM TEMPERATURE, THERMAG V, Grenoble, France, 17-20 September 2012.

KROEKER, C. J., Soliman, H. M. and Ormiston, S.J., 2004, Three-dimensional thermal analysis of heat sinks with circular cooling micro-channels, International Journal of Heat and Mass Transfer 47, 4733–4744.

MORRISH, A.H., 1965, The Physical Principles of Magnetism, John Wiley & Sons, Inc.

NIELSEN, K. K., 2010, Numerical modelling and analysis of the active magnetic regenerator, PhD Thesis, TDU, Denmark.

PECHARSKY, V. K. and Gschneidner, K., 2006, Advanced magnetocaloric materials: what does the future hold?, International Journal of Refrigeration 29, 1239 – 1249.

SHAH, R. K. and London, A. L., 1987, Laminar Flow Forced Convection in Ducts, Academic Press, New York.

TISHIN, A. M. and Spichkin, Y. I., 2003, The Magnetocaloric Effect and its Applications. Institute of Physics Publishing.

WANG, H. S. and Rose, J. W., 2005, A theory of film condensation in horizontal non-circular section microchannels, ASME Journal of Heat Transfer, 127(10), 1096-1105

WANG, H. S. and Rose, J.W., 2011, Theory of heat transfer during condensation in microchannels, International Journal of Heat and Mass Transfer, 54, 2525-2534

YU, B. F., Liu, M., Egolf, W., and Kitanovski, A., 2010, A review of magnetic refrigerator and heat pump prototypes built before the year 2010, International Journal of Refrigeration, 33(6), 1029-1060.

363: Building applications of heat recovery systems: a review

PINAR MERT CUCE[1*], KEMAL GANI BAYRAKTAR[2], SAFFA RIFFAT[1], SIDDIG OMER[1]

1 Department of Architecture and Built Environment, Faculty of Engineering, University of Nottingham, University Park, NG7 2RD Nottingham, UK
2 Izocam Tic. ve San. A.S., Altaycesme Mah., Oz Sokak, No:19, Kat:3-5-6, P.K. 34843, Maltepe, Istanbul, Turkey
**Corresponding email: ezxapm@nottingham.ac.uk, Tel: +44(0)747 327 8285*

In the early 21st century, energy consumption levels were specified by sector and the results interestingly indicated that buildings play an important role on global energy consumption. Buildings have a long life span lasting for 50 years or more and thus, minimization of energy consumption levels of buildings has a notable potential to contribute in mitigating greenhouse gas concentrations for longer periods. Most of the energy losses in buildings occur in heating, ventilation and air conditioning systems. Therefore, recovering the waste heat from HVAC systems may considerably contribute to efficient energy utilization and hence, in degrading gas emissions. In this paper, a comprehensive review on building applications of heat recovery systems is presented. The review is given as a clear and understandable summary of the previous works. The review covers detailed description of heat recovery systems with working principle and system components, current typical heat recovery technologies including the building applications. Moreover, environmental impacts of heat recovery systems are evaluated. Future scenarios for heat recovery technologies including some recommendations are also considered in the study. It is concluded from the results that the heat recovery systems are very promising to mitigate the fuel consumption amounts of buildings. Heat recovery system (HRS) provides cost-effective and environmentally friendly energy. Thus, they can remarkably contribute in reducing greenhouse gas emissions in the atmosphere.

Keywords: HVAC, heat recovery, building applications

1. INTRODUCTION

There is a growing concern about energy use and its impacts on the environment. The latest reports of the Intergovernmental Panel on Climate Change (IPCC) have enhanced the public awareness of energy use and its environmental impacts [**1-3**]. Furthermore, intensive efforts have been made in recent years to expand the proportion of alternative energy resources in global energy production. However, fossil fuel based energy consumption still predominate with a lion's share and hence, renewable energy sources are not able to supply the global energy demand. From this point of view, minimization of energy consumption levels in all sectors has become significant in the last decades. In the early 21st century, energy consumption levels were specified by sector and the results interestingly indicated that buildings play an important role on global energy consumption. Moreover, buildings are responsible for a 20–40% of the total annual energy consumption of the world [**4,5**]. It was also reported that buildings account for more than 30% greenhouse gas emissions in most of the developed countries. On the other hand, energy consumption levels of buildings increase as a consequence of economic development, growing of building sectors and rising heating, ventilation and air conditioning (HVAC) demand. Buildings have a long life span lasting for 50 years or more and thus, minimization of energy consumption levels of buildings has a notable potential to contribute in mitigating greenhouse gas concentrations for longer periods. Most of the energy losses in buildings occur in heating, ventilation and air conditioning systems. Therefore, recovering the waste heat from HVAC systems may considerably contribute to efficient energy utilization and hence, in degrading gas emissions.

2. HEAT RECOVERY SYSTEM

Ventilation air is the major source of moisture load in air conditioning. For instance, ventilation air constitutes approximately 68% of the total moisture load in most commercial buildings as seen in Figure 1. For this reason, HVAC system is required to remove the moisture from the life space. It is a fact that in most of the countries, the energy consumption by HVAC sectors account for one third of the total energy consumption of the whole society [6]. Therefore heating, cooling and ventilation of buildings using heat recovery have become more significant in recent years since it contributes in decreasing energy demand for HVAC.

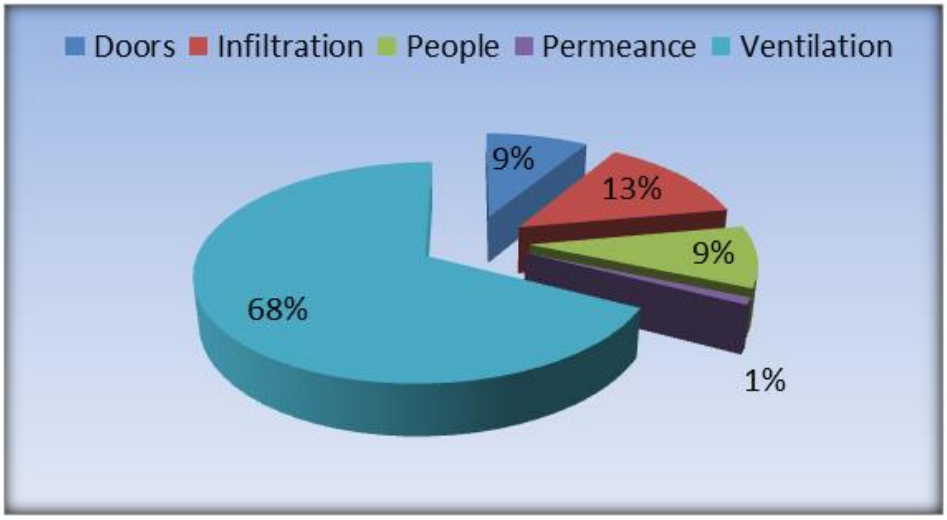

Figure 1. Sources of moisture loads in a medium size retail store [6].

Heat recovery term is commonly known as an air-to-air heat or energy recovery system which works between two sources at different temperatures. In other words, it is based on heating the incoming air via the recovered waste heat and hence, decreasing the heating loads. Heat recovery systems have many types to transfer waste heat (energy) from the stale air to the incoming air. However, all those heat recovery systems generally fall into two main categories namely sensible heat recovery systems and enthalpy heat recovery systems. A typical heat recovery system in buildings comprises of a core unit, channels for fresh air and exhaust air, and blower fans. Roof space is generally considered for the mounting of heat recovery systems. Current heat recovery systems are able to recycle about 60 to 95% of the waste energy which is

very promising. HRSs have a significant potential to reduce the heating demand of buildings in a cost-effective way. The need of effective ventilation for the places without window like bathrooms and toilets can also be maintained by heat recovery technologies [7].

3. APPLICATIONS OF HEAT RECOVERY SYSTEM IN BUILDINGS

Heating, ventilation and air conditioning (HVAC) systems are an indispensable necessity for comfortable and healthy indoor environment for residents of a building. However, energy saving in buildings becomes more significant due to the high energy demand of buildings for HVAC systems. Recent efforts have been made by researchers to reduce energy consumption used by HRSs and to improve the thermal efficiency of HRSs. Recently, Mardiana-Idayu and Riffat [8] develop an enthalpy recovery system and the performance of the system is analysed. The sensible energy efficiency is found to be roughly 66% whereas it is 59% for latent energy. Abd El-Baky and Mohamed [9] design a horizontal staggered heat pipe as seen in Figure 2. They use heat pipe heat exchanger to cool fresh air in air conditioning application. The aim of the study is to examine the effectiveness and thermal performance of HRS by connecting the stale air and fresh air with heat pipe heat exchanger. The results indicate that the temperature changes of fresh and exhaust air increase with increasing fresh air temperature. The heat recovery also reaches about 85% with increasing fresh air temperature. In addition to those results, the thermal effectiveness rises with increasing fresh air temperature.

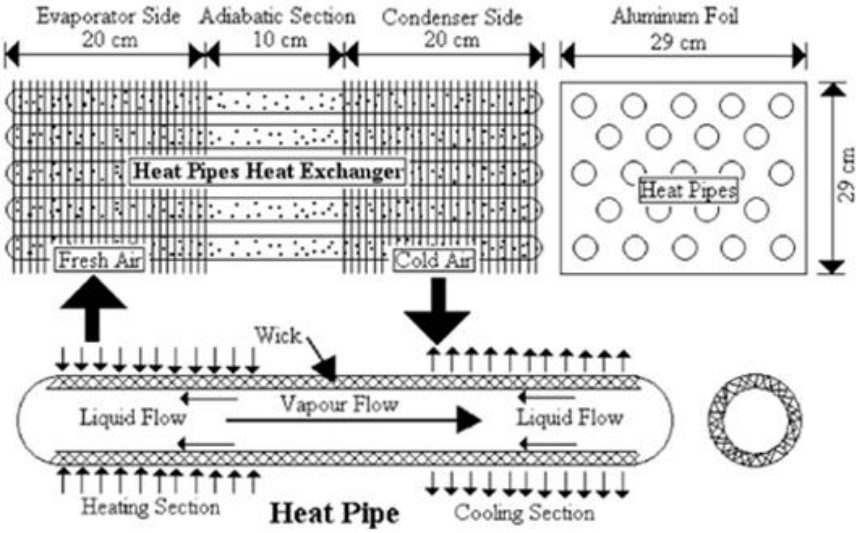

Figure 2. A schematic of a horizontal heat pipe heat exchanger [1159].

Energy consumption of buildings increases with a rapid rising in urbanisation. Therefore, it is a necessity to save this energy. It is possible to save considerable amounts of HVAC energy using heat recovery system. Ke and Yanming [**10**] carry out a study in order to estimate the applicability of energy recovery ventilators by selecting eight cities in four different climates in China. It is stressed in the study that the single heat exchanger cannot meet the energy demand in the aforementioned climate zones. Therefore, the double heat exchanger should be used in ventilation systems to adapt the requirement of energy recovering in ventilation systems. An air source heat pump system with none, single and double heat recovery capabilities is built and tested by Nguyen et al. [**11**]. The analyses show that a heat pump system with double heat recovery mechanism is found to be the most efficient in terms of energy saving performance compared to the other variations.

In recent years, the air source air-conditioner/heat pump (AC/HP) system is one of the most common used heating and cooling equipment in buildings in China. The outdoor air is used as a heating or cooling thermal source by aforementioned system. A new heat recovery technique for the AC/HP system is urged by Gong et al. [**12**]. The technique uses a compound air cooling and water cooling condensing module to replace the sole air-cooling system in the conventional AC/HP system. The results of the experiments lasting four seasons represent that the new heat pump system works steadily and efficiently. Gu et al. [**13**] described a heat recovery system using phase change materials (PCMs) to store the sensible and latent heat. It is observed from the analysis that the integrative energy efficiency ratio (IEER) of the system has an effective

improvement when all exhaust heat is recovered. Besides contributing the carbon dioxide emission reduction, PV systems are very promising in the upcoming future due to limited energy reserves and rapidly growing importance of environmental issues [**14-23**]. Sukamongkol et al. [**24**] carry out an experimental tests conducting condenser heat recovery integrated with a PV/T air heating collector. The results show that saving energy of 18% is possible using aforementioned system.

Liu [**25**] develops a novel heat recovery/desiccant cooling system as illustrated in **Figure 3** utilizing plate type air-to-air heat exchanger. Several parameters sre analysed in terms of their impacts on heat recovery efficiency. The results indicate that the heat recovery efficiency exponentially increases with heat exchanger length and the ratio of exchanger width to length. On the other hand, it remarkably decreases with the mass flow rate of fresh air.

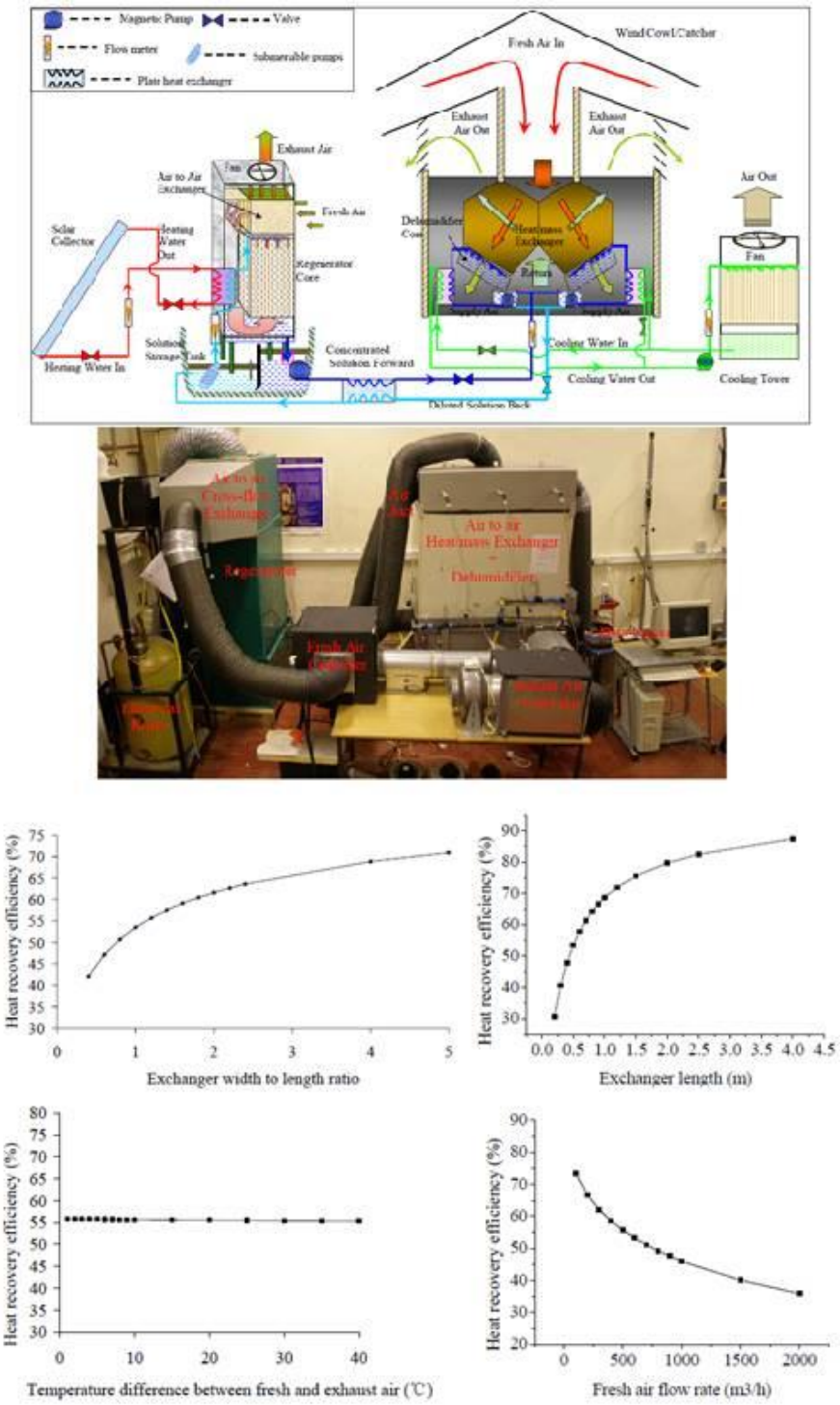

Figure 3. Schematic, test rig and results from a novel heat recovery system [25].

4. ENVIRONMENTAL IMPACTS OF HEAT RECOVERY SYSTEMS

Energy saving is one of the key issues for both fossil fuel consumption and protection of global environment [**26**]. The rising cost of energy and the global warming underline that development of the improved energy systems is necessary to increase the energy efficiency while reducing greenhouse gas emissions. The most effective way to reduce energy demand is to use energy more efficiently [**27**]. Therefore, waste heat recovery is becoming popular in recent years since it improves energy efficiency. About 26% of industrial energy is still wasted as hot gas or fluid in many countries [**28**]. However, during last two decades there has been remarkable attention to recover waste heat from various industries and to optimise the units which are used to absorb heat from waste gases [**29,30**]. Thus, these attempts enhance reducing of global warming as well as of energy demand.

5. CONCLUSIONS

Heat recovery systems are very promising technologies since they provide considerable energy savings in various sectors especially in domestic and industrial buildings. As clean energy generation becomes important day by day, efficient utilization of the energy appears much more significant due to the rising cost of energy production. Therefore, heat recovery systems draw attention throughout the world for their potential of saving energy and mitigating greenhouse gas concentrations in the atmosphere. The current cost of the heat recovery systems completely depends on the technology that they have. The payback period of them varies from a couple of years to 15 years with respect to the heat recovery technology [**7**] and their lifetime is mostly greater than 30 years. As reported by Crawford et al. [**31**] for a building integrated photovoltaic system with heat recovery unit, heat recovery systems have a dominant impact on reducing the payback period of the energy supplying system. Future predictions indicate that the heat recovery systems will play an important role in the energy sector as a consequence of the developments in material sciences and growing significance of environmental issues [**32-35**].

In this study, a detailed review on building applications of heat recovery technologies is presented. It is noted from the results that there are many different type of HRSs in the market today. However, as previously reported by Mardiana and Riffat [**7**], heat pipe, fixed plate, run-around and rotary wheel heat exchangers are the most common types, and rotary wheel heat recovery systems still have the highest efficiency levels as shown in Table 1. The results from the literature analysis indicate that heat recovery systems have a remarkable potential to mitigate the energy demand of buildings, and thus the greenhouse gas emissions in the atmosphere.

Table 1. A comparison of heat recovery types by their efficiency ranges and potential advantages [97]

System type	System efficiency	Advantages
Fixed-plate	50-80%	Compact, highly efficient due to high heat transfer coefficient, no cross contamination, can be coupled with counter-current flow which enabling to produce close end-temperature differences.
Heat pipe	45-55%	No moving parts, no external power requirements, high reliability, no cross contamination, compact, suitable for naturally ventilated building, fully reversible, easy cleaning.
Rotary-wheel	above 80%	High efficiency, capability of recovering sensible and latent heat.
Run-around	45-65%	Does not require the supply and exhaust air ducts to be located side by side, supply and exhaust duct can be physically separated, no cross contamination.

6. REFERENCES

WAN KKW, Li DHW, Liu D, Lam JC. Future trends of building heating and cooling loads and energy consumption in different climates. Building and Environment 2011; 46: 223–234.

IPCC, Climate Change 2007: The physical science basis. Solomon S, Qin D, Manning M, Marquis M, Averyt K, Tignor MMB, Miller HL, Chen Z. Contribution of the working group I to the fourth assessment report of the Intergovernmental Panel on Climate Change. Cambridge University Press 2007, Cambridge.

IPCC, Climate Change 2007: Mitigation of climate change. Metz B, Davidson OR, Bosch PR, Dave R, Meyer LA. The Physical Science Basis. Contribution of the working group III to the fourth assessment report of the Intergovernmental Panel on Climate Change. Cambridge University Press 2007, Cambridge.

PEREZ-LOMBARD L, Ortiz J, Pout C. A review on buildings energy consumption information. Energy and Buildings 2008; 40: 394–398.

LIU D, Zhao FY, Tang GF. Active low-grade energy recovery potential for building energy conservation. Renewable and Sustainable Energy Reviews 2010; 14: 2736–2747.

ZHANG LZ. Total heat recovery: Heat and moisture recovery from ventilation air. Nova Science Publishers, Inc. 2008, New York.

MARDIANA-IDAYU A, Riffat SB. Review on heat recovery technologies for building applications. Renewable and Sustainable Energy Reviews 2012; 16: 1241–1255.

MARDIANA-IDAYU A, Riffat SB. An experimental study on the performance of enthalpy recovery system for building applications. Energy and Buildings 2011; 43: 2533–2538.

ABD EL-BAKY MA, Mohamed MM. Heat pipe heat exchanger for heat recovery in air conditioning. Applied Thermal Engineering 2007; 27: 795–801.

KE Z, Yanming K. Applicability of air-to-air heat recovery ventilators in China. Applied Thermal Engineering 2009; 29: 830–840.

NGUYEN A, Kim Y, Shin Y. Experimental study of sensible heat recovery of heat pump during heating and ventilation. International Journal of Refrigeration 2005; 28: 242–252.

GONG G, Zeng W, Wang L, Wu C. A new heat recovery technique for air-conditioning/heat pump system. Applied Thermal Engineering 2008; 28: 2360–2370.

GU Z, Liu H, Li Y. Thermal energy recovery of air conditioning system–heat recovery system calculation and phase change materials development. Applied Thermal Engineering 2004; 24: 2511–2526.

RIFFAT SB, Cuce E. A review on hybrid photovoltaic/thermal collectors and systems. International Journal of Low-Carbon Technologies 2011; 6(3): 212–241.

CUCE PM, Cuce E. A novel model of photovoltaic modules for parameter estimation and thermodynamic assessment. International Journal of Low-Carbon Technologies 2012; 7(2): 159–165.

CUCE E, Cuce PM. A comprehensive review on solar cookers. Applied Energy 2012; 102: 1399–1421.

CUCE PM, Cuce E. Homotopy perturbation method for temperature distribution, fin efficiency and fin effectiveness of convective straight fins. International Journal of Low-Carbon Technologies 2014; 9(1): 80–84.

CUCE E, Cuce PM. Homotopy perturbation method for temperature distribution, fin efficiency and fin effectiveness of convective straight fins with temperature-dependent thermal conductivity. Proceedings of the Institution of Mechanical Engineers, Part C, Journal of Mechanical Engineering Science 2013; 227(8): 1754–1760.

CUCE PM, Cuce E. Optimization of configurations to enhance heat transfer from a longitudinal fin exposed to natural convection and radiation. International Journal of Low-Carbon Technologies 2013; doi:10.1093/ijlct/ctt005.

CUCE E, Cuce PM. Energetic and exergetic performance assessment of solar cookers with different geometrical designs. International Journal of Ambient Energy 2013; doi: 10.1080/01430750.2013.823111.

CUCE E, Cuce PM, Wood CJ, Riffat SB. Toward aerogel based thermal superinsulation in buildings: A comprehensive review. Renewable and Sustainable Energy Reviews 2014; 34: 273–299.

CUCE E, Cuce PM, Wood CJ, Riffat SB. Optimizing insulation thickness and analysing environmental impacts of aerogel-based thermal superinsulation in buildings. Energy and Buildings 2014; 77: 28–39.

CUCE PM, Cuce E. Effects of concavity level on heat loss, effectiveness and efficiency of a longitudinal fin exposed to natural convection and radiation. 10th International Conference on Sustainable Energy Technologies, Istanbul, September 4-7, 2011.

SUKAMONGKOL Y, Chungpaibulpatana S, Limmeechokchai B, Sripadungtham P. Condenser heat recovery with a PV/T air heating collector to regenerate desiccant for reducing energy use of air conditioning room. Energy and Buildings 2010; 42: 315–325.

LIU S. A novel heat recovery/desiccant cooling system. Ph.D. Thesis, University of Nottingham, 2008.

GHODSIPOUR N, Sadrameli M. Experimental and sensitivity analysis of a rotary air preheater for the flue gas heat recovery. Applied Thermal Engineering 2003; 23: 571–580.

YILMAZ M, Sara ON, Karsli S. Performance evaluation criteria for heat exchangers based on second law analysis. Exergy International Journal 2001; 1(4): 278–294.

TEKE I, Agra O, Atayilmaz SO, Demir H. Determining the best type of heat exchangers for heat recovery. Applied Thermal Engineering 2010; 30: 577–583.

BUTCHER CJ, Reddy BV. Second law analysis of a waste heat recovery based power generation system. International Journal of Heat and Mass Transfer 2007; 50: 2355–2363.

REDDY BV, Ramkiran G, Kumar KA, Nag PK. Second law analysis of a waste heat recovery steam generator. International Journal of Heat and Mass Transfer 2002; 45: 1807–1814.

CRAWFORD RH, Treloar GJ, Fuller RJ, Bazilian M. Life-cycle energy analysis of building integrated photovoltaic systems (BiPVs) with heat recovery unit. Renewable and Sustainable Energy Reviews 2006; 10: 559–575.

CUCE E, Cuce PM, Bali T. An experimental analysis of illumination intensity and temperature dependency of photovoltaic cell parameters. Applied Energy 2013; 111: 374–382.

CUCE E, Cuce PM. Improving thermodynamic performance parameters of silicon photovoltaic cells via air cooling. International Journal of Ambient Energy 2013; doi: 10.1080/01430750.2013.793481.

CUCE E, Cuce PM. Theoretical investigation of hot box solar cookers having conventional and finned absorber plates. International Journal of Low-Carbon Technologies 2013; doi:10.1093/ijlct/ctt052.

PACCA S, Horvath A. Greenhouse gas emissions from building and operating electric power plants in the Upper Colorado River Basin. Environmental Science and Technology 2002; 36(14): 3194–3200.

460: Assessment methods for selecting organic absorbents of HFC refrigerant in absorption system

WENJIE GUAN[1], ZHANGZHANG YANG[2], HANRU YU[3],
XIAOGANG QIAO[4], XIAOHONG HAN[5], GUANGMING GHEN[6]

1 Key Laboratory of Refrigeration and Cryogenic Technology of Zhejiang Province, Institute of Refrigeration and Cryogenics, Zhejiang University, Hangzhou, China, 21327109@zju.edu.cn
2 Key Laboratory of Refrigeration and Cryogenic Technology of Zhejiang Province, Institute of Refrigeration and Cryogenics, Zhejiang University, Hangzhou, China, yzhangzhang@126.com
3 Key Laboratory of Refrigeration and Cryogenic Technology of Zhejiang Province, Institute of Refrigeration and Cryogenics, Zhejiang University, Hangzhou, China, 237781472@qq.com
4 Zhejiang College of Construction, Hangzhou, China, 370936192@qq.com
Key Laboratory of Refrigeration and Cryogenic Technology of Zhejiang Province, Institute of Refrigeration and Cryogenics, Zhejiang University, Hangzhou, China, hanxh66@zju.edu.cn
5 Key Laboratory of Refrigeration and Cryogenic Technology of Zhejiang Province, Institute of Refrigeration and Cryogenics, Zhejiang University, Hangzhou, China, hanxh66@zju.edu.cn
5 Key Laboratory of Refrigeration and Cryogenic Technology of Zhejiang Province, Institute of Refrigeration and Cryogenics, Zhejiang University, Hangzhou, China, gmchen@zju.edu.cn

Absorption refrigeration is one of the refrigeration methods which can make use of low quality heat sources. Some HFC refrigerants have been put forward in the absorption refrigeration systems for their good properties. R161 and R134a are both potential refrigerants. However, which absorbent is more suitable for them in the common absorbents, and how to evaluate the HFC working fluid pairs have not been clearly presented. On the basis of these, we need to obtain an assessment method for selecting organic absorbents of HFC refrigerant. In this work, R161 and R134a were selected as the refrigerants. DMEDEG/DMAC/NMP/DMF were selected as the absorbents of R161, and DMEDEG/MEGDME/DMETrEG/DMF were selected as the absorbents of R134a. Firstly, a single-grade absorption refrigeration cycle simulation was adopted, and the coefficient of performance (COP), the circulation ratio (f) and the power consumption of solution pump (Wp) of the systems with the investigated working pairs were evaluated. Secondly, three assessment criteria including bubble point pressure (p), excess Gibbs free energy (GE) and deflation ratio (dR) were estimated with NRTL model. By comparing the relationships between the criteria and system performance, it could be found that: 1) Bubble point pressure (p) influenced the pressure differential in system but had little relationship with system performance; 2) The GE influenced the system performance remarkably, and the working pair whose extreme value of excess Gibbs free energy (GEmax) within an appropriate range had the best thermal performance, and for R161 and R134a working pairs the range was -400 J/mol ~ -300 J/mol; 3) The bigger dR meant the better cycle performance, and when dR > 6%, the preferable performance could be achieved. Overall, the combined assessment method can preliminarily evaluate the performance of the organic absorbents of HFC refrigerant and help us to select suitable absorbent for the specified refrigerant in absorption system.

Keywords: absorption refrigeration system; working pair; HFC; assessment method.

1. INTRODUCTION

Under the back ground of energy shortage and environment pollution, traditional energies need to be replaced by clean renewable energies. The absorption refrigeration is a refrigeration method that could make use of low quality heat sources such as waste heat and solar energy. In the past several decades, researchers have developed a series of studies about absorption refrigeration driven by heat (IBARRA-BAHENA, 2014: page 751). The properties of working pairs have significant influence on the performance of absorption system. As HFC refrigerants can be used in a wide temperature range with good environmental acceptability, some HFC refrigerants have been put forward in the absorption refrigeration system (SUN, 2012: page 1899-1904). To make the HFC refrigerants better applied in the absorption refrigeration system, selecting suitable absorbent for the specified refrigerant is one of the key tasks. While, it is impossible to study all kinds of working pair in absorption system by experimental method. Thus, using theoretical assessment methods to evaluate and select a better absorbent for the specific refrigerant is very important.

Thermodynamic properties are important factors which affect the application of working pairs in absorption cycle. Many researchers have studied the influence of working pairs' thermodynamic properties and put forward some assessment methods. The investigation on the optimum interaction between the working fluid and absorbent in absorption heat pump was conducted by EISA et al. They found that there existed an optimum negative deviation from Raoult's law, which depended on operating conditions (EISA, 1987: page 107). NARODOSLAWSKY et al. pointed out that the latent heat of vaporization and the size and location of G^E (excess Gibbs free energy) of working pair greatly affected system performance. The working pairs with higher latent heat of vaporization and lower extreme value of G^E could show better performance (NARODOSLAWSKY, 1988: page 221). MATTHYS et al. considered that the working pair having highly non-ideal solubility behaviour would show better intersolubility in absorber (MATTHYS, 1989: page 327). KERNEN et al. suggested that the sharply increase of G^E function of temperature could cause good separation effect (KERNEN, 1995: page 42). ZHENG et al. suggested that G^E_{max} can be used to evaluate working pairs. The research result indicated that the smaller G^E_{max} led to smaller circulation ratio, and there existed an optimum G^E_{max} where absorption system can achieve the best performance (ZHENG, 2001: page 834).

The assessment methods introduced above can evaluate some thermodynamic properties of working pairs of absorption system in certain scope. However, whether they are able to estimate HFC working pairs remain some uncertainties. In addition, the G^E was studied extensively and deeply, while the other assessment criteria have not been discussed in detail. G^E is correlated with the intersolubility of binary solution, and high-solubility means hard to separate, which leads to large f (circulation ratio) and W_p (power consumption of solution pump). Moreover, G^E failed to describe Δp (pressure differential) in absorption system, which influences equipment reliability remarkably. There remain some unavoidable limitations when only G^E is considered. Therefore, we combine the assessment criteria including p (bubble point pressure), G^E and d_R (deflation ratio), and to tentatively evaluate the organic absorbents of HFC refrigerant more fully. In this work, R161 was selected as the working fluid for its good environmental acceptability and thermodynamic properties. R134a was also selected as the working fluid for it's a transitional refrigerant widely used. For HFC refrigerants well dissolved in organic absorbents, DMEDEG/DMAC/NMP/DMF were selected as the absorbents of R161, and DMEDEG/MEGDME/DMETrEG/DMF were selected as the absorbents of R134a. On the basis of comparing the advantages and disadvantages of the three assessment criteria—p, G^E and d_R, we attempt to obtain an assessment method for selecting organic absorbents of HFC refrigerant in absorption system.

2. THE MODEL OF ASSESSMENT CRITERIA

Bubble point pressure p

Experimental data were correlated by the Non-Random Two-Liquid (NRTL) equation (RENON, 1968: page 137). NRTL activity coefficient model can describe the phase equilibrium of binary solution well.

Equation 20: NRTL model for calculating binary solution.

$$\ln\gamma_1 = x_2^2\left[\tau_{21}\left(\frac{G_{21}}{x_1 + x_2 G_{21}}\right)^2 + \frac{\tau_{12}G_{12}}{\left(x_2 + x_1 G_{12}\right)^2}\right]$$

$$\ln\gamma_2 = x_1^2\left[\tau_{12}\left(\frac{G_{12}}{x_2 + x_1 G_{12}}\right)^2 + \frac{\tau_{21}G_{21}}{\left(x_1 + x_2 G_{21}\right)^2}\right]$$

$$G_{12} = \exp(-\alpha\tau_{12}), \quad G_{21} = \exp(-\alpha\tau_{21})$$

Where:

- γ_1 and γ_2 are the activity coefficient of refrigerant and absorbent.
- x_1, x_2 are the mole fraction of refrigerant and absorbent in liquid phase.
- G_{12}, G_{21}, τ_{12}, τ_{12}, α, are model parameters.

In this paper, better correlation results could be obtained when τ_{12} and τ_{21} took the following form.

Equation 21: Model parameters of NRTL model

$$\tau_{12} = A_0 + A_1 \ln T$$

$$\tau_{21} = B_0 + B_1 \ln T$$

Where:

- A_0, A_1, B_0, B_1 are model parameters regressed from NRTL model.
- T= temperature of the system (K).

Excess Gibbs free energy

According to the research of TUFANO et al. (TUFANO, 1998: page 171), absorption system would get better performance when working pairs expressed negative deviation from Raoult's law. However, it doesn't mean that the bigger negative deviation, the better system performance can be obtained. G^E was proposed to evaluate the performance of working pairs by NARODOSLAWSKY et al. (NARODOSLAWSKY, 1988: page 221) and ZHENG et al. (ZHENG, 2013: page 9480), respectively. G^E is a function of temperature, mole fraction.

Equation 22: Excess Gibbs free energy calculated by NRTL model (J/mol).

$$\frac{G^E}{RT} = x_1 x_2\left[\frac{\tau_{21}G_{21}}{x_1 + x_2 G_{21}} + \frac{\tau_{12}G_{12}}{x_2 + x_1 G_{12}}\right]$$

Deflation ratio

G^E represents the solubility property of working pairs to some extent. Nevertheless, just good intersolubility between refrigerant and absorbent is not enough, good separability is also required in generator (ZHENG, 2013: page 9480) . This means that the solubility should have obvious difference between absorber and generator, and deflation ratio represents this difference of mass fraction of refrigerant.

Equation 23: Deflation ratio.

$$d_R = w_a - w_g$$

Where:

- w_a and w_g are the mass fraction of refrigerant in absorber and generator.
-

3. THERMAL PERFORMANCE CHARACTERISTICS OF ABSORPTION REFRIGERATION SYSTEM

We chose COP, f and W_p to represent the thermal performance of absorption refrigeration cycle. Energy consumed by the solution pump is high-grade which should not be neglected. Thus, W_p was also selected as the thermal performance characteristic in this work. In order to compare the relationships among the

assessment criteria and the thermal performance characteristics, a single-grade absorption refrigeration cycle simulation was adopted. The schematic diagram of the single-grade absorption refrigeration cycle is shown in Figure 93, and Figure 94 shows the thermodynamic cycle of the system on *p-T* coordinates.

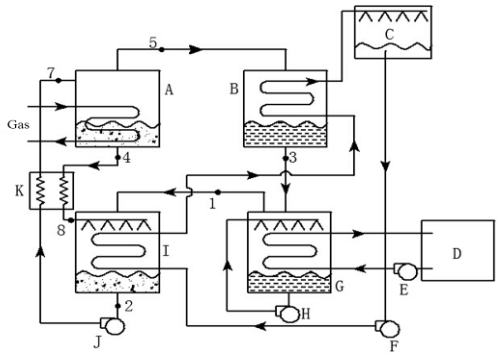

Figure 93. The schematic diagram of the single-grade absorption refrigeration cycle

A-generator B-condenser C-cooling tower D-air condition E/F-water pump G-evaporator H-refrigerant pump I-absorber

J-solution pump K- solution heat exchanger

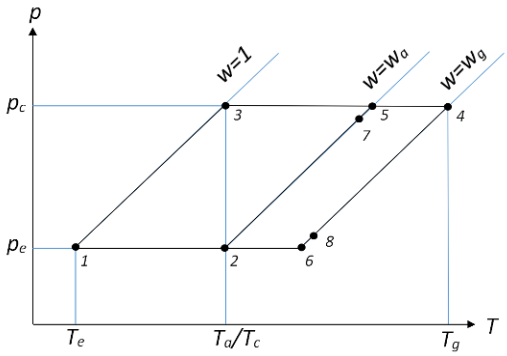

Figure 94. The thermodynamic cycle of the system

The temperatures of generator, absorber, evaporator and condenser were set to 80-100℃, 30℃, 0℃ and 30℃, respectively. The total refrigeration capacity is 10kW. The following assumptions are made for the thermodynamic analysis:

- The absorption refrigeration system operates at steady state.
- All the heat exchangers are ideal and have 100% efficiency.
- The heat loss and the pressure drop in the system can be neglected.
- The solution streams at the exit of generator and absorber are at the equilibrium state.
- The exit gas stream of generator is pure refrigerant.

The operating pressures of the absorption refrigeration system are determined by the saturation pressures of condenser temperature and evaporator temperature. The temperatures at various state points are shown clearly in Figure 94. As the exit solution streams of generator and absorber are at the equilibrium condition, the mass fraction of refrigerant in the exit streams of absorber and generator, w_a and w_g, could be calculated by phase equilibrium data (DENG, 2014 page:180-181) (JING, 2013 page: 3292-3293) (ZEHIOUA, 2010 page: 2772) (CHAUDHARI, 2008 page: 30-31) (HAN, 2011 page: 1824). Thus, the mass fractions at various state points can also be obtained. The circulation ratio is determined by Equation 24,

Equation 24: Circulation ratio.

$$f = \frac{1 - w_g}{w_a - w_g}$$

The power consumption of solution pump is defined by Equation 25,

Equation 25: Power consumption of solution pump (W).

$$W_p = \frac{f \cdot \Delta p \cdot \Phi_0}{\rho \cdot \eta \cdot \Delta h}$$

Where:

- ρ = density of solution (kg/m^3).
- η = efficiency of solution pump which was set to 0.5.
- Δp = differential pressure between the inlet and outlet of the solution pump (Pa).
- Φ_0 = total cooling capacity (W).
- Δh = latent heat vaporization of the refrigerant at 0℃(J/kg).

The COP of absorption refrigeration system is defined as,

Equation 26: COP of absorption refrigeration system.

$$COP = \frac{\Phi_0}{\Phi_g + W_p}$$

Where: Φ_g is the total thermal load of generator (W).

4. RESULTS AND DISCUSSION

The effects of temperature of generator (T_g) on the thermal performance characteristics of absorption refrigeration system are shown in Figures 3-5. Figure 95 reveals that, for the systems with R161 as the refrigerant, the R161-NMP has the highest COP followed by R161-DMAC, R161-DMF, R161-DMEDEG; for the systems with R134a as the refrigerant, R134a-DMEDEG has the highest COP followed by R134a-MEGDME, R134a-DMETrEG, R134a-DMF. Though the circulation ratios of R161 working pairs are larger than those of R134a working pairs (Figure 96), the COPs of R161 working pairs are still higher compared to R134a working pairs. That is because the latent heat of vaporization of R161 (378.815 kJ/kg) is much larger than R134a (198.596 kJ/kg) at 0℃.

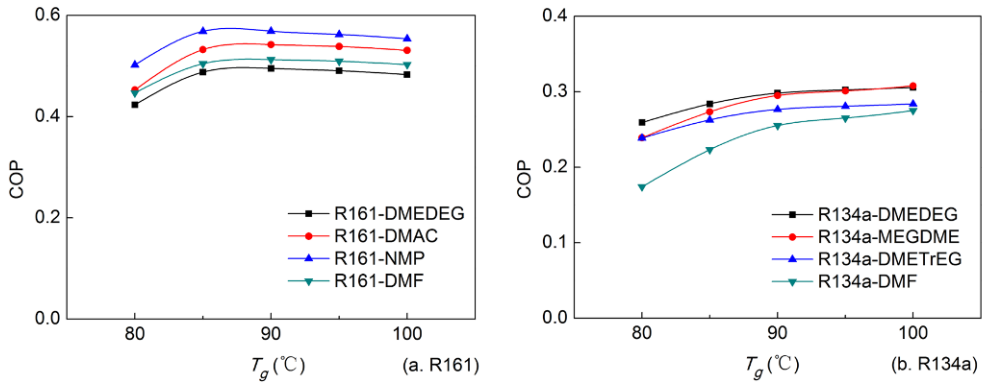

Figure 95. Variation of COP with T_g

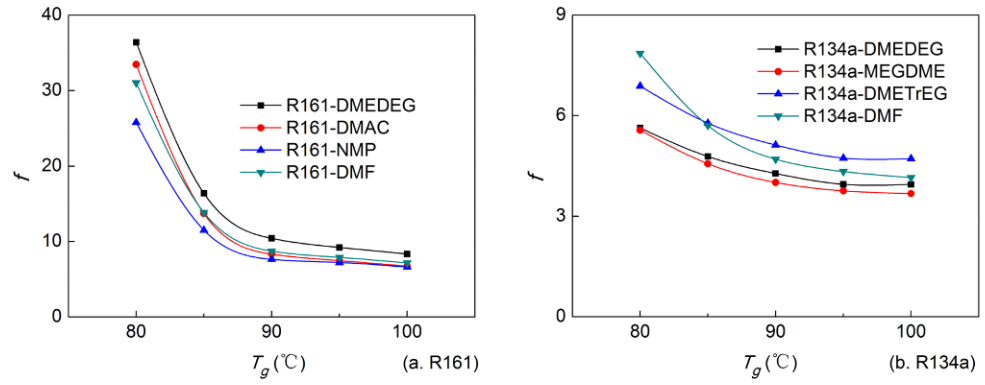

Figure 96. Variation of f with T_g

Figure 97 shows the W_p of the systems and W_p decreases with the increase of generator temperature T_g. On the whole, the absorption working pair with larger COP has smaller W_p at the same time, and obtain better thermal performance.

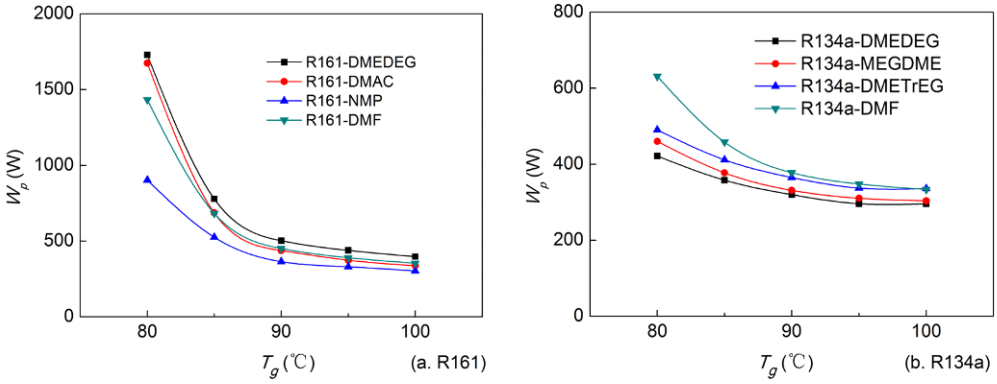

Figure 97. Variation of W_p with T_g

4.1 Bubble Point Pressure

Figure 98 gives the *p-T* cycle diagram of R161-DMEDEG and R134a-DMEDEG when T_g is 80℃. As Figure 98 illustrates, in the same condition, the condenser pressure and evaporator pressure of R161-DMEDEG are higher than those of R134a-DMEDEG. And R161-DMEDEG has large pressure differential between condenser and evaporator, that may results in the increase of W_p. According to Clausius–Clapeyron equation, the working pair with flat pressure curve has smaller latent heat of vaporization (GENG, 1983: page 32). Therefore, R134a has smaller pressure differential in advantage but low COP in disadvantage.

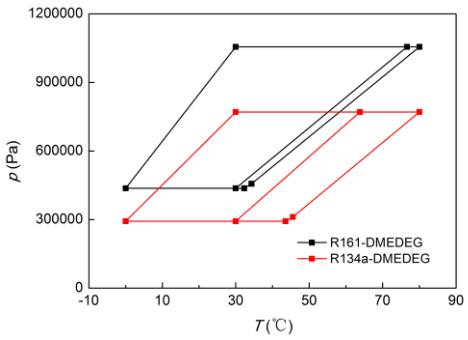

Figure 98. The p-T cycle diagram of R161-DMEDEG and R134a-DMEDEG when T_g is 80 ℃

Figure 99 provides the curves of bubble point pressure of R161 working pairs and R134a working pairs at 30℃. The working pairs with the same refrigerant and different absorbents have little difference in bubble point pressure. This suggests that *p* has little relation with system performance, and we can't compare the thermodynamic properties of different working pairs through bubble point pressure only.

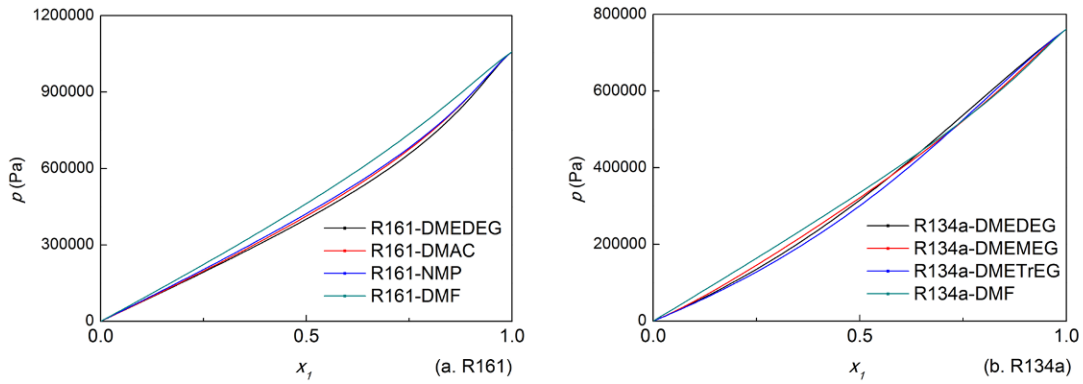

Figure 99. Variation of p with x_1 at 30 ℃

4.2 Excess Gibbs Free Energy

The G^E of working pairs at 30℃ (absorber temperature) is shown in Figure 100. It can be found that G^E keeps negative with the mole fraction of refrigerant changing, and a minimum value exists at a certain value of the fraction.

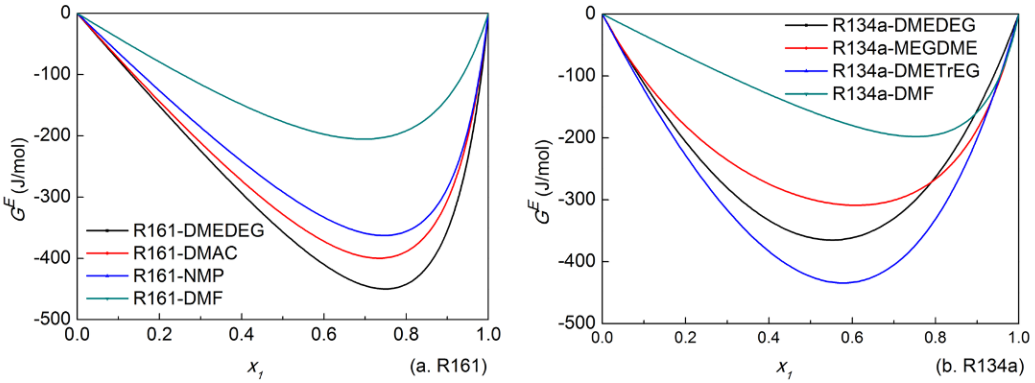

Figure 100. Variation of G^E with x_1 of working pairs at 30 ℃

ZHENG et al. considered that this minimum value, G^E_{max} represented the ability of absorbent to absorb refrigerant. The smaller G^E_{max} meant stronger absorptive capacity (ZHENG, 2013: page 9487). Table 24 lists our calculation result of the G^E_{max} of working pairs.

Table 24. The extreme value of excess Gibbs free energy G^E_{max} (30 ℃)

Working pair	R161-DMEDEG	R161-DMAC	R161-NMP	R161-DMF
G^E_{max} (J/mol)	-450.1	-399.8	-362.7	-205.2
Working pair	R134a -DMEDEG	R134a –MEGDME	R134a -DMETrEG	R134a -DMF
G^E_{max} (J/mol)	-364.9	-308.8	-434.3	-197.9

By analyzing the relationship of G^E_{max} and system performance, it can be seen that G^E_{max} can evaluate the HFC working pairs. Figure 101 and Figure 102 show variation of COP with G^E_{max} and variation of f with G^E_{max} when T_g is 90℃, respectively. An optimum value of G^E_{max} is within the range of -400 J/mol ~ -300 J/mol, and that's where f is minimum and COP is maximum. The similar character can also be found when T_g is within the scope of 80-100℃. However, when T_g is below 90℃, the f of R161 working pairs are always high, which will lead to the increase of W_p.

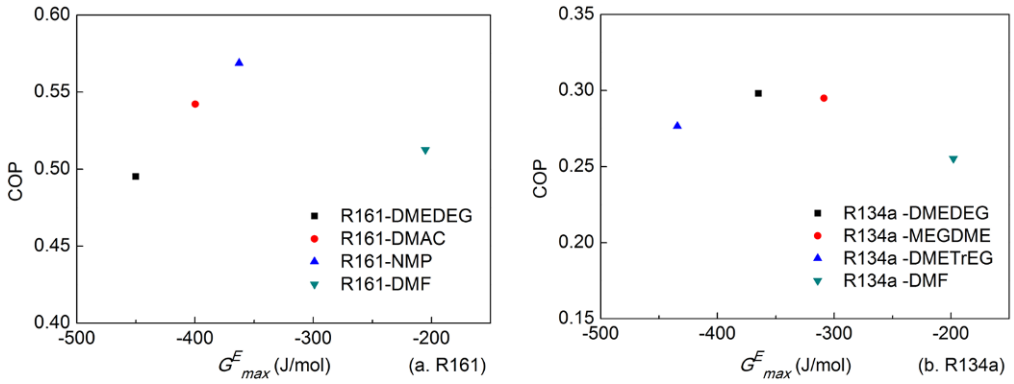

Figure 101. Variation of COP with G^E_{max} when T_g is 90 ℃

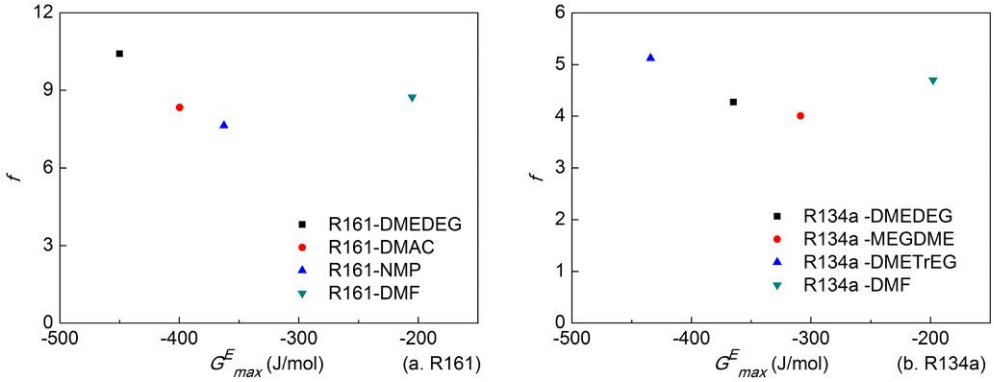

Figure 102. Variation of f with G^E_{max} when T_g is 90 ℃

The relationship between G^E_{max} and W_p when T_g is 90℃ is shown in Figure 103. It can be seen that the working pair with G^E_{max} of -400 J/mol ~ -300 J/mol has lowest W_p for both R161 and R134a working pairs. However, according to the calculation, when T_g is below 90℃, the W_p of the system with R161 working pairs is really high. For example, the W_p of the system with R161-DMEDEG occupies 7.3% of the whole system consumption when T_g is 80℃. In addition, the solution pump consumes the electric energy, which belongs to high-grade energy. Hence, it is necessary to introduce a new assessment criterion to evaluate HFC working pairs.

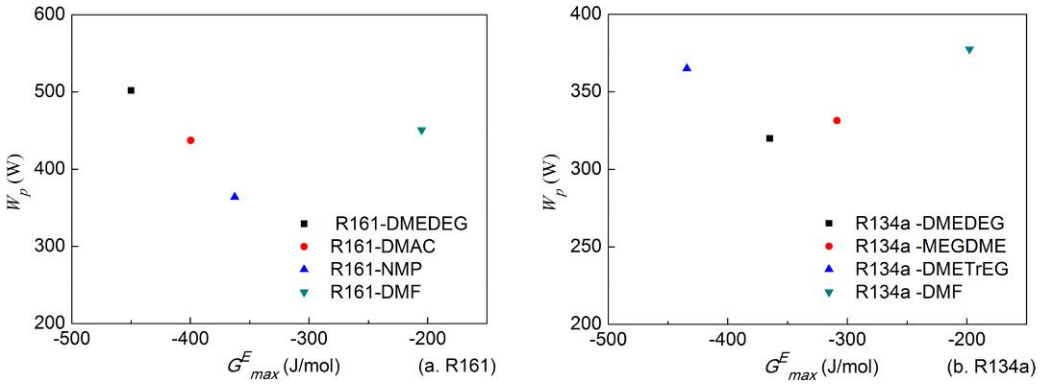

Figure 103. Variation of W_p with G^E_{max} when T_g is 90 ℃

4.3 Deflation Ratio

Deflation ratio is related to temperature and pressure of operating condition, according to the calculation results, d_R increases with the increase of T_g. The relationship between d_R and COP when T_g is 90℃ is presented in Figure 104. When T_g is 90℃, the COP increases with the increase of d_R for both R161 and R134a working pairs. It can be found in Figure 105 that, for R161 working pairs, f decreases with the increase of d_R. For R134a working pairs, there exists an optimum value of d_R, and the R134a-DMETrEG has the lowest f. Overall, when d_R is larger than 6%, f is always lower than 10.

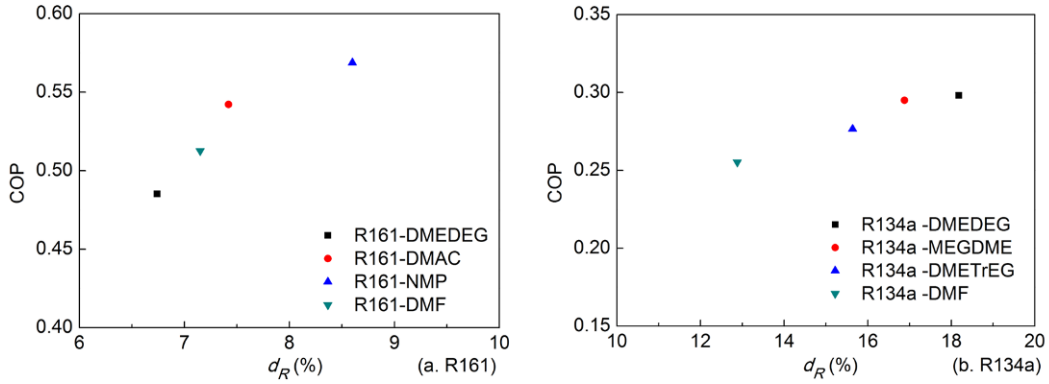

Figure 104. Variation of COP with d_R when T_g is 90 ℃

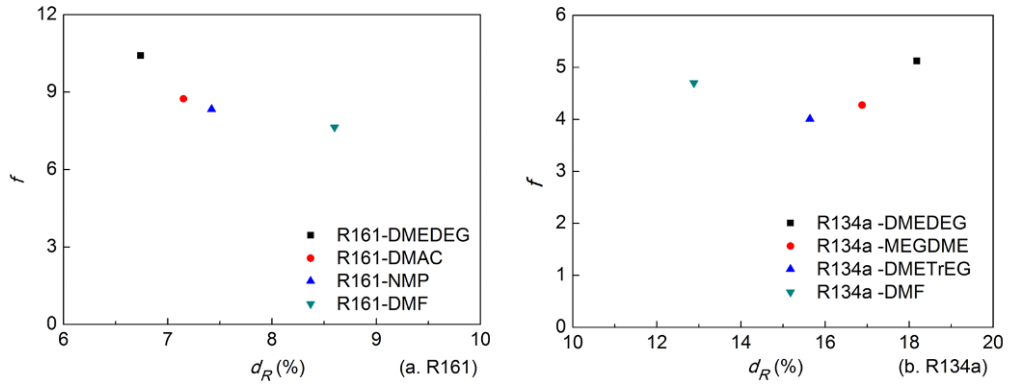

Figure 105. Variation of f with d_R when T_g is 90 ℃

Figure 106 presents the variation of W_p with d_R when T_g is 90℃. There is a negative correlation between d_R and W_p. Overall, when d_R is larger than 6%, W_p is always lower than 600W. And all the relationships between d_R and COP, f, W_p when T_g is 90℃ can also be found when T_g is within the scope of 80-100℃.

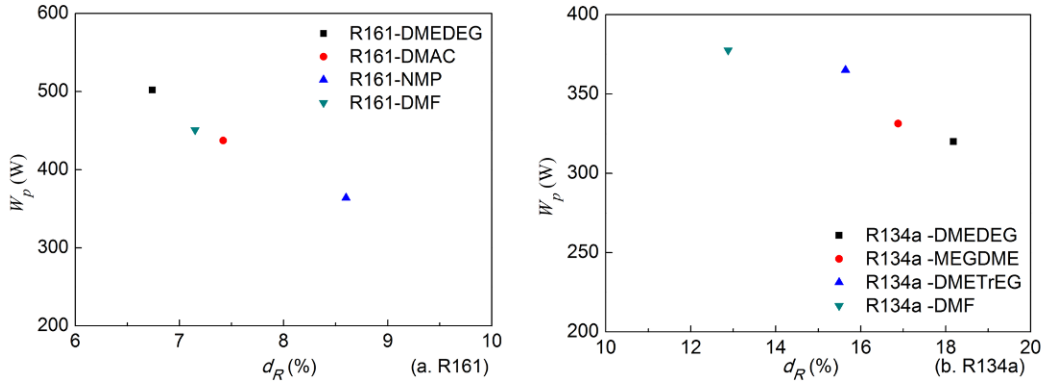

Figure 106. Variation of W_p with d_R when T_g is 90 ℃

With the analysis and comparison of these assessment criteria, some relationships can be found and used in evaluating and selecting working pairs. Table 25 summarizes the relationships between assessment criteria and thermal performance of absorption refrigeration system. All the assessment criteria have their advantages and disadvantages.

Table 25. Relationships among assessment criteria and thermal performance of system

	Δp	COP	f	W_p
p	Qualitatively estimate	No relationship	No relationship	Qualitatively estimate
G^E_{max}	No relationship	Exist optimum value	Exist optimum value	Exist optimum value
d_R	No relationship	Positive correlation	Negative correlation	Negative correlation

By using the three criteria in combination, the thermal performance of HFC working pairs can be evaluated. Firstly, we have to judge if the pressure difference is within acceptable range according to bubble point pressure. Secondly, we need to calculate G^E_{max} in order to determine which absorbent fits the selected refrigerant best. Thirdly, calculate the d_R of this working pair under specified operating condition to estimate the suitability of its application in absorption refrigeration system. Then the potential working pair can be selected.

4.4 Application of assessment criteria

R236fa-DMAC and R236fa-DMEDEG (ZHANG, 2014: page 3916-3917) were taken for example to test the assessment criteria described above. Experimental data were correlated with NRTL model, and p, G^E_{max}, d_R were calculated. These assessment criteria were compared to the simulation results of absorption refrigeration system which had been described in the third section. The results are provided in Table 26.

Table 26. Calculation results of R236fa-DMAC and R236fa-DMEDEG

	R236fa-DMAC					R236fa-DMEDEG				
T_g (℃)	COP	f	W_p (W)	d_R (%)	G^E_{max}(30℃) (J/mol)	COP	f	W_p (W)	d_R (%)	G^E_{max}(30℃) (J/mol)
80	0.4632	4.861	151	7.23		0.4729	3.937	124	13.01	
85	0.4584	3.708	115	10.32		0.4601	3.201	101	17.39	
90	0.4499	3.121	97.4	13.20	-1156	0.4459	2.778	87.7	21.55	-1095
95	0.4400	2.767	86.4	15.85		0.4315	2.505	79	25.47	
100	0.4297	2.533	79.1	18.28		0.4174	2.315	73	29.16	

The results show that the system with R236fa-DMEDEG has higher COP, lower f and lower W_p compared to R236fa-DMAC. The G^E_{max} of R236fa working pairs is much smaller than those of R161 and R134a working pairs. The optimum value of G^E_{max} could not be determined with only two working pairs, but it could be seen that too small G^E_{max} may be unfavorable, because R236fa-DMAC has smaller G^E_{max} but smaller COP. And the results also present the large d_R for R236fa-DMAC and even larger d_R for R236fa-DMEDEG. Therefore, the assessment criteria that the working pairs with larger d_R can have better performance can also be applied here. The d_R of R236fa-DMAC and R236fa-DMEDEG is both much larger than 6%, so their f and W_p are much lower than 10 and 600W, respectively, which is similar to the law found above. Hence, R236fa-DMAC and R236fa-DMEDEG are potential working pairs. Assessment criteria summarized above could evaluate the performance of R236fa working pairs well.

5. CONCLUSIONS

In this work, R161 was used as refrigerant in combination with one of the absorbents of DMEDEG/DMAC/NMP/DMF, and R134a was used as refrigerant in combination with one of the absorbents of DMEDEG/MEGDME/DMETrEG/DMF. A single-grade absorption refrigeration cycle simulation was adopted, and COP, f and W_p were obtained as performance parameters. The assessment criteria including p, G^E and d_R were estimated by NRTL activity coefficient models. Through the contrastive analysis of assessment criteria and system performance, the following conclusions could be drawn: 1) Bubble point pressure (p) influenced the pressure differential in system, which is related to system reliability. But the working pairs with the same refrigerant and different absorbents had similar bubble point pressure, so we couldn't assess the working pairs through p only; 2) G^E was closely related to the system performance, and the working pair with G^E_{max} within an appropriate range had the optimum thermal performance. For R161 and R134a working pairs, this range of G^E_{max} was -400 J/mol ~ -300 J/mol; 3) The bigger d_R meant the better cycle performance, especially for COP and W_p, and when d_R > 6%, nice system performance could be achieved. The assessment criteria also could be well applied to evaluate the thermal performance of R236fa working pairs. Overall, the combined assessment criteria can preliminarily evaluate the properties of the organic absorbents of HFC refrigerant, and help us to select potential working pairs for absorption refrigeration system.

6. ACKNOWLEDGEMENT

This work has been supported by the Nation Natural Science Foundation of China (Grant No. 51176166) and the Key Laboratory of Low-grade Energy Utilization Technologies and Systems (Chongqing University), Ministry of Education of China, Chongqing University, Chongqing 400044, China (No. LLEUTS- 201510).

7. REFERENCES

CHAUDHARI, S.K., Salavera, D., Esteve, X., Coronas, A., 2008. Vapour–liquid equilibria of the system 1,1,1,2-tetrafluoroethane+monoethylene-glycol dimethylether from 283.15 to 353.15K: New modified UNIFAC parameters. Fluid Phase Equilibria, 271(1-2), 28-33.

DENG, Rulei, Jing, Xuye, Zheng, Danxing, LI, Xiaoxiao, 2014. Vapor–liquid equilibrium measurements and assessments of fluoroethane + N,N-dimethylformamide and fluoroethane + dimethylether diethylene glycol systems for the hybrid refrigeration cycle. International Journal of Refrigeration, 43, 176-186.

EISA, M.A.R., Holland, F.A., 1987. A study of the optimum interaction between the working fluid and the absorbent in absorption heat pump systems. Heat Recovery Systems and CHP, 7 (2), 107-117.

GENG, Huibin, 1983. Working pairs of absorption heat pump. Refrigeration technology, (04), 30-42.

HAN, Xiaohong, Gao, Zanjun, Xu, Yingjie, Qiu, Yu, Min, Xuwei, Cui, Xiaolong, Chen, Guangming, 2011. Solubility of refrigerant 1,1,1,2-Tetrafluoroethane in the N,N-Dimethyl Formamide in the temperature range from (263.15 K to 363.15)K. Journal of Chemical & Engineering Data, 56(5), 1821-1826.

IBARRA-BAHENA, Jonathan, Romero, Rosenberg J., 2014. Performance of Different Experimental Absorber Designs in Absorption Heat Pump Cycle Technologies: A Review. Energies, 7(2), 751-766.

JING, Xuye, Deng, Rulei, Zheng, Danxing, 2013. Measurement and Correlation of Isothermal Vapor–Liquid Equilibrium of Fluoroethane + N,N-Dimethylacetamide, Fluoroethane + N-Methyl-2-pyrrolidone, and 1,1,1,2-Tetrafluoroethane + N,N-Dimethylacetamide Systems. Journal of Chemical & Engineering Data, 58(11), 3289-3296.

KERNEN, M., Lee, L.L., Perez-Blanco, H., 1995. A study of solution properties to optimize absorption cycle COP. International Journal of Refrigeration, 18(1), 42-50.

MATTHYS, H., Trepp, Ch., 1989. Working fluids for high temperature sorption cycles. International Journal of Refrigeration, 12(6), 327-331.

NARODOSLAWSKY, M., Otter, G., Moser, F., 1988. Thermodynamic criteria for optimal absorption heat pump media. Heat Recovery Systems and CHP, 8(3), 221-233.

RENON, Henri, Prausnitz, J.M., 1968. Local Compositions in Thermodynamic Excess Functions for Liquid Mixtures. AIChE journal, 14(1), 135-144.

SUN, Jian, Fu, Lin, Zhang, Shigang, 2012. A review of working fluids of absorption cycles. Renewable and Sustainable Energy Reviews, 16 (4), 1899-1906.

TUFANO, Vincenzo, 1998. Simplified criteria for the development of new absorption working pairs. Applied Thermal Engineering, 18(3), 171-177.

ZEHIOUA, Raouf, Coquelet, Christophe, Meniai, Abdeslam-Hassen, Richon, Dominique, 2010. p−T−x Measurements for Some Working Fluids for an Absorption Heat Transformer: 1,1,1,2-Tetrafluoroethane (R134a) + Dimethylether Diethylene Glycol (DMEDEG) and Dimethylether Triethylene Glycol (DMETrEG). Journal of Chemical & Engineering Data, 55(8), 2769-2775.

ZHANG, Min, Zheng, Danxing, Yang, Wenzhi, Li, Xiaoxiao, 2014. Measurement and Correlation of Isothermal Vapor-Liquid Equilibrium of 1,1,1,3,3-Pentafluoropropane + N,N-Dimethylacetamide and 1,1,1,3,3,3-Hexafluoropropane + N,N-Dimethylacetamide /Diethylene Glycol Dimethyl Ether Systems. Journal of Chemical & Engineering Data, 59(11), 3912-3919.

ZHENG, Danxing, Ji, Peijun, Qi, Janping, 2001. Maximum excess Gibbs function of working pairs and absorption cycle performance. International Journal of Refrigeration, 24(8), 834-840.

ZHENG, Danxing, Dong, Li, Wu, Xianghong, 2013. New Approach for Absorbent Species Selection with Excess Gibbs Function. Industrial & Engineering Chemistry Research, 52(27), 9480-9489.

POSTER SESSION D

56: Method theory research on determining the phase-change temperature arrange of pcm integrated into building envelopes theory analysis on the determination method

XI MENG[1], WEI ZHANG[2], CAIXIA WANG[3], YANRU LI[4], ENSHEN LONG[5]

1 Sichuan University, No. 24, First loop south first section, Chengdu, China, mengxihvac@163.com
2 Sichuan University, No. 24, First loop south first section, Chengdu, China, xskin821@163.com
3 Sichuan University, No. 24, First loop south first section, Chengdu, China, caixiawang11@163.com
4 Sichuan University, No. 24, First loop south first section, Chengdu, China, 429506492@qq.com
5 Sichuan University, No. 24, First loop south first section, Chengdu, China, longes2@163.com

PCM (Phase change material) can be integrated into building envelopes to decrease the building energy consumption, refine the indoor thermal comfort, shift and reduce the peak electricity load due to its relatively large latent heat. However, only when the phase change of PCM occurs can the phase-change heat storage property be played. Therefore, the reasonable selection on the PCM phase-change temperature arrangements directly affect the PCM effect. At present, there always a lack of a relative method to determine the PCM phase-change temperature arrange due to its complexity and too many factors.

In this study, the determination method on the PCM phase-change temperature arrange is theoretically researched and proposed on the basis of the traditional wall heat transfer theories. This method couples all affecting factors including wall structure, material properties, outdoor climate conditions, indoor thermal environment and so on.

This method can provide some meaningful guides for the selection for the PCM phase-change temperature arrange in the engineering practices.

Keywords: PCM, Phase-transition temperature, Building envelopes

1. INTRODUCTION

With the continuous improvement of living standard and indoor comfort, the building energy consumption is growing very quickly and the building energy efficiency has been very urgent (Long (2005) and Meng et al (2015)). Energy storage can reduce the time or rate mismatch between energy supply and demand, thereby playing a vital role in energy conservation (Jin (2014)). Compared with the sensible heat storage system, the phase change material (PCM) becomes popular due to its higher energy storage density and the smaller masses and volumes of material. So PCM has been widely used in many engineering, such as heating and cooling (Zhang(2007), solar energy storage (Esen (2000)), food preservation (Gin (2010)), cooling of electronic components (Weng,2011)) and so on.

In recent years, the PCM building envelopes have been researched by many researchers (Memon(2014) and Waqas (2013)). Compared with the traditional building envelopes, the thermal mass of the PCM envelopes integrated with the PCM layer was increased greatly, which would reduce the building energy consumption, improve the indoor thermal comfort, and shift the peak electricity load (Jin (2014)).

Yan et al.(2012) experimentally researched the thermal properties of the PCM wall formed by three different methods. Their results shown the addition of PCM in traditional walls can decrease building consumption and reduce the indoor air temperature fluctuation. And the energy-saving effect of the phase change walls prepared by lamination interpolation method is better than walls prepared by the direct mixing method.

Mandilaras et al. (2013) built a two-story typical family house outfitted with PCM walls. The results showed that the wall thermal mass was enhanced during late spring, early summer and autumn. The decrement factor was reduced by 30-40% and the time lag was increased by approximately 100 min. Evers et al. (2010) presented thermal performance of frame walls enhanced with paraffin and hydrated salt PCM and found that the average peak heat flux and the total daily heat flow were reduced by up to 9.2% and 1.2%, respectively.

Zhang et al. (2011) analyzed indoor wall surface temperature response of brick wall filled with PCM under outdoor fluctuating air temperature. The results indicated that PCM applied in the brick walls was beneficial for thermal insulation, temperature hysteresis and thermal comfort. Meanwhile, increasing the filled amount of PCM could make the indoor wall surface temperature fluctuation be significantly smoothed. Ding and Ye [(2011) compared the effects of PCM on energy saving of buildings located in five typical cities of China and found that the inner wall integrating with PCM could make indoor environment comfortable and reduce energy consumption of air conditioning system in summer.

In addition, Jin et al. (2014) experimentally studied the placement of a PCM thermal shield within the cavity of buildings walls. Their results show, compared to a wall without a PCM layer, the peak heat flows were reduced by as much as 11% when the thermal shield was placed in the inward-most location next to the internal surface of the gypsum wallboard within the wall cavity. The PCM thermal shield produced only small effects on the peak heat flows when it was placed half way between the enclosing surfaces of the internal cavity of the wall and there is almost no effect when it was placed next to the internal surface of the outermost layer.

Wang et al. (2013) studied the ultrathin envelope thermal performance improvement of the prefab house by integrating with PCM numerically under the Chengdu climates. Results show that the small PCM heat conductivity coefficient, the large phase change latent heat of PCM, the low phase transition temperature range and the PCM layer locating at inner side can obtain the excellent thermal performance of ultrathin envelope integrated with PCM.

The above research shows that the PCM layer has a obvious effect on decreasing the building energy consumption, refining the indoor thermal comfort, shifting and reducing the peak electricity load in particular. However, the above research focuses on the improvement effect of PCM on buildings and there lacks of the coupling studies of PCM thermal physical properties with envelope structures, indoor and outdoor thermal environment. In particular, the phase-change temperature arrangement of PCM is the most important factor owing to the fact that the phase-change temperature arrange influences the phase change degree.

If the phase-change temperature arrange is far away from the temperature change of the PCM layer in building envelopes, PCM would always be solid or liquid without any phase change. Meanwhile, if the phase

change temperature arrange is much bigger than the temperature change of the PCM layer, the part of PCM would have no phase change and the best effect of phase change would not be obtained. In addition, if the phase-change temperature arrange is much smaller than the temperature change of the PCM layer, PCM will lose the phase change effect owing to the full phase change during the partial period with high or low temperature, when there is often the peak time of electricity consumption for air conditioning or heating. Therefore, it is of great importance to determine the phase-change temperature arrange for PCM properly according to envelop structures, indoor and outdoor environment.

The research of Wang et al. (2013) shows the phase change temperature range of 12-22°C is a better choice for the prefab house with one polystyrene foam board of 40 mm in the Chengdu city, China. Meng et al. (2015) numerically researches the influence of the PCM thermal physical properties on the temperature and the heat flow of inner surface in the Chengdu climates. Their research shows the best phase change temperature range is 14-26°C for he sintered brick wall of 240mm integrating with the PCM layer of 20mm.

Although some optimized phase change temperature ranges are proposed for the certain the wall under the given climate condition in some published papers, the optimization method is always lacked on phase change temperature range with the consideration of wall structures, indoor and outdoor thermal environment, the PCM thermal physical properties and so on. Only when this main problem is solved could PCM be widely used in building envelops with the high efficiency. In our study, the determination method is researched about the PCM phase-change temperature arrange, based on the theory analysis of heat transfer laws, and the optimization equations are proposed on the optimum phase-change temperature arrange. Meanwhile, the influence of all factors, such as wall structures, thermal environment and PCM thermal physical properties, is analyzed on PCM phase-change temperature arrange qualitatively and the numerical simulation is also used to research the accuracy of the mathematic correlation on PCM phase-change temperature arrange quantitatively by suing the validated heat transfer model of walls integrating with PCM.

2. DETERMINATION PRINCIPLE OF THE PCM PHASE-CHANGE TEMPERATURE ARRANGEMENT

When PCM is integrated into building envelopes, the phase-change heat storage will be expected in a certain period, which maybe summer, transition season or the whole year. However, no matter under any period, there are high and low temperatures for outdoor thermal environment and the relatively constant temperature for indoor thermal environment owing to air-conditioning and heating. In our study, it is considered that PCM has the efficient phase change heat storage property in the whole year with indoor air temperature of 20°C in winter and 25°C in summer.

Figure 1 shows the schematic diagram on wall temperature distribution under the heating in winter and the air-conditioning in summer. And the basic principle is shown on the full phase change of PCM in the Figure 1. As shown in the Figure, wall temperature always increases from outside to inside during the winter, while wall temperature always decreases from outside to inside during summer. Therefore, if the full phase change of PCM can occur, the PCM phase-change temperature arrange must be satisfied as follows:

Equation 1: the restricted relationship of the full phase change of PCM in winter

$$T_S < T_{\text{P-out,win}} < T_{\text{P-in,win}} < T_L$$

Equation 2: the restricted relationship of the full phase change of PCM in summer

$$T_S < T_{\text{P-in,sum}} < T_{\text{P-out,sum}} < T_L$$

Where:

- T_S = solidus temperature (K)
- T_L = liquidus temperature (K)
- $T_{P\text{-}out,win}$ = the outer surface temperature of the PCM layer in winter (K)
- $T_{P\text{-}in,win}$ = the inner surface temperature of the PCM layer in winter (K)
- $T_{P\text{-}out,sum}$ = the outer surface temperature of the PCM layer in summer (K)
- $T_{P\text{-}in,sum}$ = the inner surface temperature of the PCM layer in summer (K)

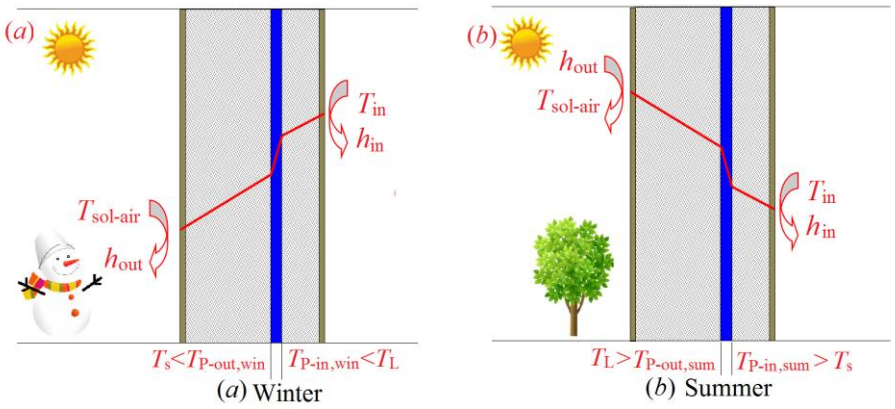

Figure 1: The temperature distribution of wall under (a) the winte, and (b) the summer

In addition, PCM has also the phase change effect, for the transition seasons when the PCM phase-change temperature arrange can meet the demand the full phase change in the summer and the winter.

Moreover, there are two relative constraint conditions.

(I) The PCM phase-change temperature arrange should be as small as possible under the conditions of the PCM full phase change;
(II) Wall temperature in winter is much less than that in summer and there is the littlest temperature difference in inner surface under the conditions of winter heating and summer air-conditioning.

In generally, indoor design air temperatures are 20°C in winter and 25°C in summer for the residential and public buildings respectively, so the corresponding relations of wall inner surface temperatures between winter and summer is following:

Equation 3: the corresponding relations of wall inner surface temperatures

$$T_{\text{P-in,sum}} - T_{\text{P-in,win}} \geq T_{\text{W-in,sum}} - T_{\text{W-in,win}} > T_{\text{in,sum}} - T_{\text{out,win}} = 25°\text{C} - 20°\text{C} = 5°\text{C}$$

Where:

- $T_{in,win}$ = indoor air temperature in winter (K)
- $T_{out,sum}$ =outdoor air temperature in summer (K)
- $T_{W\text{-}in,win}$ = the outer surface temperature of wall in winter (K)
- $T_{W\text{-}in,sum}$ = the inner surface temperature of t wall in summer (K)

Combination with Equations 1-3, Equation 4 on the determination principle of the PCM phase-change temperature arrange can be obtained as follows:

Equation 4: the determination principle of the PCM phase-change temperature arrange

$$T_S < T_{\text{P-out,win}} < T_{\text{P-in,win}} < T_{\text{W-in,sum}} < T_{\text{W-out,sum}} < T_L$$

According to Equation 4, outside surface temperature of the PCM layer is the basic solidus temperature in winter, while outside surface temperature of the PCM layer is the basic liquidus temperature in summer. Therefore, how to determine the outside surface temperature of the PCM layer is a key problem on the optimization of the PCM phase change temperature arrange

3. DETERMINATION METHOD ON OUTSIDE SURFACE TEMPERATURE OF THE PCM LAYER

In general, outdoor thermal environment changes alternately all the year round, but outdoor thermal environment is more similar in a shorter period such as a week, a mouth and even a season. Therefore, under the certain period, the average temperature of any layer in a day can be approximately considered to be constant. Meanwhile, at the period of 24h, the transient temperature has a certain fluctuation due to

the alternation of day and night. Therefore, the temperature fluctuation arrange of any wall layer can be defined as follows:

Equation 5: the temperature fluctuation arrange of any wall layer

$$T_{\text{L-base}} - A \le T \le T_{\text{L-base}} + A$$

Where:

- $T_{L\text{-}base}$ = the average value of any layer temperature in a day (K)
- A = the temperature fluctuation of any layer temperature in a day (K)

According to Equation 5, it can be found that any layer temperature can include the base temperature and the fluctuation temperature. For the base temperature, the stable algorithm is adopted. According to the thermoelectricity analogy method (Paschkis and. Baker (1942) and Lombard and Mathews (1999)), Figure 2 shows the thermoelectricity analogy circuit diagram of the multilayer wall integrating with the PCM layer. According to the thermoelectricity analogy circuit diagram, outer surface temperature of the PCM layer can be obtained as following:

Equation 6: the computer method on the outer surface temperature of the PCM layer

$$T_{\text{base}} = \frac{T_{\text{sol-air,avg}} - T_{\text{in}}}{\frac{1}{h_{\text{out}}} + \sum_{i=1}^{n} \frac{\delta_i}{\lambda_i} + \frac{1}{h_{\text{in}}}} \cdot \left(\sum_{i=k}^{n} \frac{\delta_i}{\lambda_i} + \frac{1}{h_{\text{in}}}\right) + T_{\text{in}}$$

Where:

- δ_i = the thickness of of the ith layer (m)
- λ_i = the thermal conductivity of the ith layer (W/(m·K))
- h_{in} = inside convective heat transfer coefficient (W/(m·K))
- h_{out} = outside convective heat transfer coefficient (W/(m·K))
- $T_{sol\text{-}air,avg}$ = the average value of outdoor comprehensive temperature (K)

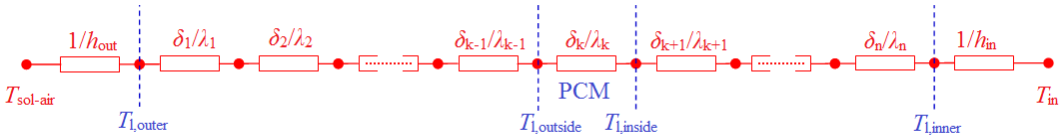

Figure 2: Thermoelectricity analogy circuit diagram of multilayer wall

The thermal fluctuation of outer environment is the power source of wall temperature fluctuation. Outer comprehensive temperature wave, which transfer from outer surface to inner surface, must be damped due to the thermal inertia of the wall layer. The damping decrement of outdoor temperature wave is mainly affected by wall thermal inertia, wall surface thermal storage coefficient in the interface between two different materials and so on. Due to the fact that the full phase change of PCM is necessary, so the damping decrement of outdoor comprehensive temperature wave can be calculated under the consideration of the full phase change of PCM as following:

Equation 7: the damping decrement of outdoor comprehensive temperature wave

$$\frac{A_{sol-air}}{A_{W-in}} = e^{\frac{\sum D}{\sqrt{2}}} \cdot \frac{S_n + h_{\text{in}}}{S_n + Y_n} \cdots \frac{S_k + Y_{k+1}}{S_k + Y_k} \cdots \frac{S_1 + Y_2}{S_1 + Y_1} \cdot \frac{h_{out} + Y_1}{h_{out}}$$

Where:

- D = wall thermal inertia
- $A_{w\text{-}in}$ = the temperature amplitude of inner surface (K)
- Y_i = the surface heat storage coefficient of the ith layer (W/(m²·K))
- S_i = the wall material heat storage coefficient of the ith layer (W/(m²·K))

- $A_{sol\text{-}air}$ = the temperature amplitude of outdoor comprehensive temperature (K)

Y_i is defined as following:

Equation 8: the computer method on surface heat storage coefficient

$$Y_n = \begin{cases} \left(\frac{\delta_n}{\lambda_n} S_n^2 + h_{in}\right) \Big/ \left(1 + \frac{\delta_n}{\lambda_n} h_{in}\right) & i = n \\ S_i & D \geq 1 \text{ and } i < n \\ \left(\frac{\delta_i}{\lambda_i} S_i^2 + Y_{i+1}\right) \Big/ \left(1 + \frac{\delta_i}{\lambda_i} Y_{i+1}\right) & D < 1 \text{ and } i < n \end{cases}$$

D is wall comprehensive inertia and can be calculated as following:

Equation 9: the computer method on wall thermal inertia

$$D = \sum_{i=1}^{k} \frac{\delta_i}{\lambda_i} \cdot \sqrt{\frac{2\pi\lambda_i C_{Pi} \rho_i}{z}}$$

Where:

- z = outdoor comprehensive temperature fluctuation period, 86400s
- ρ_i = the material density of the ith layer, (kg/m^3)
- C_{pi} = the heat capacity of the ith layer (J/(kg·K))

The phase-change latent heat of PCM can be equivalent to heat capacity by the following method:

Equation 10: the equivalent method on the phase-change latent heat of PCM

$$C'_{PCM} = C_{PCM} + \frac{L_{PCM}}{T_{\text{P-out,sum}} - T_{\text{P-out,win}}}$$

Where:

- L_{PCM} = the PCM latent heat (J/kg)
- C_{PCM} = the oringinal heat capacity of PCM, (kg/m^3)

When outdoor air comprehensive temperature wave arrives at the outer surface of the PCM layer, which is assumed as the kth layer, the damping decrement can be calculated owing to the outside wall of the PCM layer as following:

Equation 11: the equivalent method on the damping decrement owing to the outside wall of the PCM layer

$$\frac{A_{sol-air}}{A_{P-out}} = \frac{S_{k-1} + Y_k}{S_{k-1} + Y_{k-1}} \cdots \frac{S_1 + Y_2}{S_1 + Y_1} \cdot \frac{h_{out} + Y_1}{h_{out}} e^{\frac{\sum D_{P-out}}{\sqrt{2}}}$$

Where:

- $D_{P\text{-}out}$ = outside wall thermal inertia of the PCM layer
- Y_i = the surface heat storage coefficient of the ith layer (W/(m^2·K))
- $A_{\text{P-out}}$ = the outer surface temperature amplitude of the PCM layer (K)

And the outer surface temperature amplitude of the PCM layer can be obtained by Equation 11 as following:

Equation 12: the equivalent method on outer surface temperature amplitude of the PCM layer

$$A_{P-out}=\frac{A_{sol-air}}{\frac{S_{k-1}+Y_k}{S_{k-1}+Y_{k-1}}\cdots\frac{S_1+Y_2}{S_1+Y_1}\cdot\frac{h_{out}+Y_1}{h_{out}}e^{\frac{\sum D_{P-out}}{\sqrt{2}}}}$$

From the above, the outer surface temperature change arrange of the PCM layer can be obtained as following:

Equation 13: the equivalent method on the outer surface temperature change arrange of the PCM layer

$$\frac{T_{\text{sol-air,avg}}-T_{\text{in}}}{\frac{1}{h_{\text{out}}}+\sum_{i=1}^{n}\frac{\delta_i}{\lambda_i}+\frac{1}{h_{\text{in}}}}\cdot\left(\sum_{i=k}^{n}\frac{\delta_i}{\lambda_i}+\frac{1}{h_{\text{in}}}\right)+T_{\text{in}}-\frac{A_{sol-air}}{\frac{S_{k-1}+Y_k}{S_{k-1}+Y_{k-1}}\cdots\frac{S_1+Y_2}{S_1+Y_1}\cdot\frac{h_{out}+Y_1}{h_{out}}e^{\frac{\sum D_{P-out}}{\sqrt{2}}}}$$

$$<\ T_{P-out}\ <$$

$$\frac{T_{\text{sol-air,avg}}-T_{\text{in}}}{\frac{1}{h_{\text{out}}}+\sum_{i=1}^{n}\frac{\delta_i}{\lambda_i}+\frac{1}{h_{\text{in}}}}\cdot\left(\sum_{i=k}^{n}\frac{\delta_i}{\lambda_i}+\frac{1}{h_{\text{in}}}\right)+T_{\text{in}}+\frac{A_{sol-air}}{\frac{S_{k-1}+Y_k}{S_{k-1}+Y_{k-1}}\cdots\frac{S_1+Y_2}{S_1+Y_1}\cdot\frac{h_{out}+Y_1}{h_{out}}e^{\frac{\sum D_{P-out}}{\sqrt{2}}}}$$

4. DETERMINATION METHOD ON THE PHASE-CHANGE TEMPERATURE ARRANGE OF PCM

According to Equation 4, outer surface temperature of the PCM layer in winter is the PCM solidus temperature, while outer surface temperature of the PCM layer in summer is the PCM liquidus temperature. However, the outer surface of the PCM layer fluctuates with outdoor air temperature naturally. Therefore, solidus and liquidus temperatures should be considered the downward fluctuation in winter and the upward fluctuation in summer, respectively. Combining with the above analysis, solidus and liquidus temperatures can be obtained as following, respectively:

Equation 14: the equivalent method on solidus temperature

$$T_{\text{S}}=(T_{\text{in}})_{\text{win}}+\frac{(T_{\text{sol-air,avg}}-T_{\text{in}})_{\text{win}}\cdot\left(\sum_{i=k}^{n}\frac{\delta_i}{\lambda_i}+\frac{1}{h_{\text{in}}}\right)}{\frac{1}{h_{\text{out}}}+\sum_{i=1}^{n}\frac{\delta_i}{\lambda_i}+\frac{1}{h_{\text{in}}}}-\frac{A_{sol-air,\text{win}}}{\frac{S_{k-1}+Y_k}{S_{k-1}+Y_{k-1}}\cdots\frac{S_1+Y_2}{S_1+Y_1}\cdot\frac{h_{out}+Y_1}{h_{out}}e^{\frac{\sum D_{P-out}}{\sqrt{2}}}}$$

Equation 15: the equivalent method on liquidus temperature

$$T_{L}=(T_{\text{in}})_{\text{sum}}+\frac{(T_{\text{sol-air,avg}}-T_{\text{in}})_{\text{sum}}\cdot\left(\sum_{i=k}^{n}\frac{\delta_i}{\lambda_i}+\frac{1}{h_{\text{in}}}\right)}{\frac{1}{h_{\text{out}}}+\sum_{i=1}^{n}\frac{\delta_i}{\lambda_i}+\frac{1}{h_{\text{in}}}}+\frac{A_{\text{sol-air,summer}}}{\frac{S_{k-1}+Y_k}{S_{k-1}+Y_{k-1}}\cdots\frac{S_1+Y_2}{S_1+Y_1}\cdot\frac{h_{out}+Y_1}{h_{out}}e^{\frac{\sum D_{P-out}}{\sqrt{2}}}}$$

5. CONCLUSIONS

Owing to the fact that the PCM phase-change temperature arrange is a important factor affecting the phase-change degree of PCM integrated into building envelops and that there is no any method to determine the PCM phase-change temperature arrange according to climate conditions, wall structures and so on, our study proposes the determination methods on the PCM phase-change temperature arrange based on the traditional wall heat transfer theories. In addition, the accuracy of this determination methods has been verified by experiment and numerical simulation, which not be shown in this paper due to the page limitation. Therefore, this determination methods, which considers indoor and outdoor thermal environment, wall structures and wall material properties, provides some meaningful guides for the selection for the PCM phase-change temperature arrange in the engineering practices.

6. REFERENCES

ESEN M., 2000. Thermal performance of a solar-aided latent heat store used for space heating by heat pump, Solar Energy, 69, 15-25

GIN B.J., Farid M.M., 2010. The use of PCM panels to improve storage condition of frozen food. Journal of Food Engineering, 100, 372-376

JIN X., Zhang S.L., Xu X.D., Zhang X.S., 2014. Effects of PCM state on its phase change performance and the thermal performance of building walls, Building and Environment, 81, 334-339

JIN X., Medina M.A., Zhang X.S., 2014. On the placement of a phase change material thermal shield within the cavity of buildings walls for heat transfer rate reduction. Energy, 73, 780-786

LOMBARD C., Mathews E.H., 1999. A two- port envelope model for building heat transfer. Building and Environment, 34,19 -30.

LONG E.S., Zang Z.X., Ma X.F., 2005. Are the energy conservation rates (RVRs) approximate in different cities for the same building with the same outer-wall thermal insulation measures?, Building and Environment, 40(4), 537-544.

MANDIARAS I. Stamadiadou M., Katsourinis D., Zannis G., Founti M., 2013. Experimental thermal characterization of a mediterranean residential building with PCM gypsum board walls. Building and Environment, 61, 93-103

WANG J., Long E.S., Qin W., Xu L., 2013. Ultrathin envelope thermal performance improvement of prefab house by integrating with phase change material. Energy and Buildings, 67, 210-216

MEMON S.A., 2010. Phase change materials integrated in building walls: A state of the art review. Renewable and Sustainable Energy Reviews, 31, 870-906.

MENG X., Gao Y.N., Long E.S., 2015. Optimization research on the multilayer wall integrated with a PCM layer, Journal of Asian Institute of Low Carbon Design. 1, 49-54.

MENG X., Gao Y.N., Wang Y., Yan B., Zhang W., Long E.S., 2015. Feasibility experiment on the simple hot box-heat flow meter method and the optimization based on simulation reproduction. Applied Thermal Engineering, 83, 48-56.

PASCHKIS V., Baker H.D., 1942. A method for determining unsteady- state heat transfer by means of an electrical analogy. Transact ions of the American Society of Mechanical Engineers. 64, 105-112.

WAQAS A., Din Z.U., 2013. Phase change material (PCM) storage for free cooling of buildings - a review, Renewable and Sustainable Energy Reviews, 18, 607-625.

WENG Y.C., Cho H.P., Chang C.C., Chen S.L., 2011. Heat pipe with PCM for electronic cooling. Applied Energy, 88, 1825-1833.

YAN Q.Y., Huo R., Li L.S., 2012. Experimental study on the thermal properties of the phase change material wall formed by different methods. Solar Energy, 86, 3099-3102.

ZHANG C.B., Chen Y.P., Wu L.Y., Shi M.H., 2011. Thermal response of brick wall filled with phase change materials (PCM) under fluctuating outdoor temperature, Energy and Buildings 43, 3514-3520.

ZHANG Y.P., Zhou G.B, Lin K.P., Zhang Q.L., Di H.F., 2007. Application of latent heat thermal energy storage in buildings: state-of-the-art and outlook. Building and Environment, 42, 197-209.

73: Numerical study of laminar heat transfer and pressure drop of phase change material emulsion (PCME) in coiled tubes

JINGJING SHAO[1], JO DARKWA[2], GEORGIOS KOKOGIANNAKIS[3]

1 Faculty of Engineering, University of Nottingham, University Park, NG7 2RD Nottingham, UK, epxjs5@nottingham.ac.uk
2 Faculty of Engineering, University of Nottingham, University Park, NG7 2RD Nottingham, UK, J.Darkwa@nottingham.ac.uk
3 Sustainable Buildings Research Centre, University of Wollongong, Wollongon NSW2522

Phase Change Emulsion (PCME) is a multifunctional fluid consisting of a Phase Change Material (PCM) and a carrier fluid. PCMEs have the potential of reducing energy consumption in air conditioning systems due to their higher latent heat capacities than water, which enable the same amount of cooling energy to be achieved at reduced flow rates. However optimum design of an integrated system requires a good understanding of flow behaviour and heat transfer characteristics of PCME in heat exchangers which cannot currently be readily deduced from manufacturer's data or published data. In this paper, the flow behaviour and heat transfer characteristics of a phase change emulsion (PCME) in coiled tubes have been investigated to establish its true potential as a heat transfer fluid in air conditioning systems. The result showed higher Nusselt number and heat transfer coefficient as well as reduction in flow rate by 20-40%. However, the pressure drop was found to be much higher than water due to its relatively higher viscosity which could affect the overall energy reduction capability of the PCME. Further enhancements are therefore recommended.

Keywords: CFD simulation, Phase change emulsion, heat exchanger, heat transfer, pressure drop

1. INTRODUCTION

Phase change material emulsions (PCMEs), consist of Phase Change Materials (PCMs) and a carrier fluid, have the potential of reducing energy consumption in air conditioning systems due to their higher latent heat capacities than water, which enable the same amount of cooling energy to be achieved at reduced flow rates. PCMEs can also simultaneously act as cold energy storage for shifting peak-load to off-peak time and thereby improving coefficient of performance of cooling systems (Zhang and Ma, 2012).

However optimum design of an integrated system requires a good understanding of flow behaviour and heat transfer characteristics of PCME in heat exchangers which cannot currently be readily deduced from manufacturer's data or published data. This is due to the fact that most of the published data cover straight pipes and not coiled pipes. Even though some technical data on various types of heat exchangers (e.g. air-emulsion direct-contact heat exchanger (Inaba and Morita, 1996), double-coiled heat exchanger (Zhao et al., 2002, Inaba and Morita, 1995)) are available, there is limited information regarding fin-and-tube heat exchangers which are the types commonly used in air conditioning systems.

To this end computational fluid dynamics (CFD) investigation was carried out to analyse the flow behaviour and heat transfer characteristics of a commercially available PCME in a fin-and-tube heat exchanger.

2. CFD MODELLING

2.1 Physical Model

Figure 107 shows the views of the fin-and-tube heat exchanger which was considered for the modelling exercise. It consists of horizontal tubes with coiled ends and thin vertical fins meant to increase the heat transfer area. The physical parameters are given in Table 27.

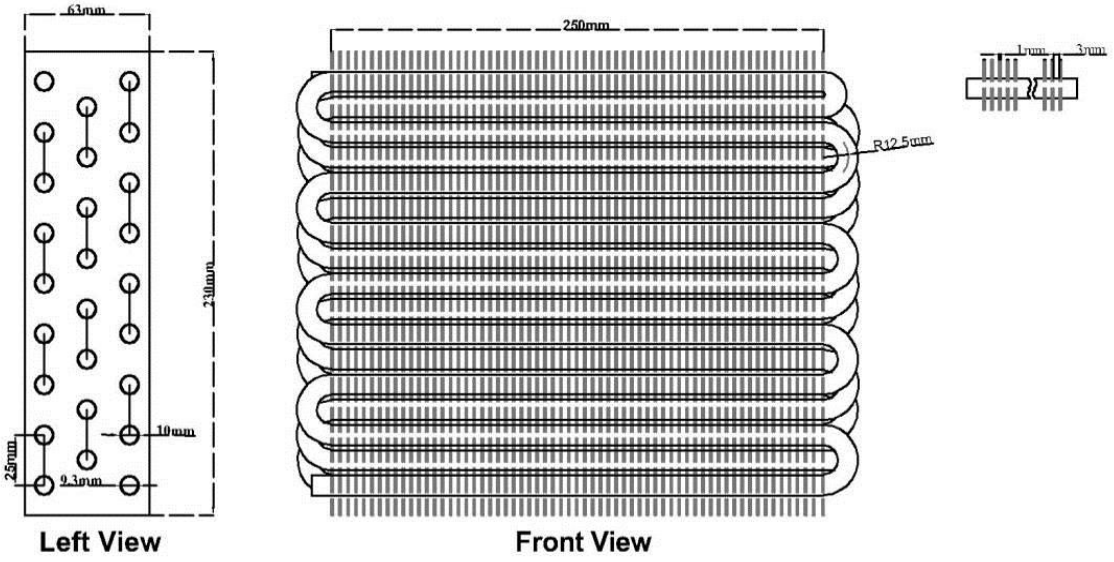

Figure 107: Views of the fin-and –tube heat exchanger

Table 27: Fin-and-tube coil data

Coil Dimensions	
Finned-tube length	250mm
Number of circuits	3
Distance between rows	22mm
Number of tubes per circuit	9
Distance between columns	25mm
Tube material	Copper
Tube inner diameter D	9.3mm
Tube wall thickness	0.35mm
Fin material	Aluminium
Fin thickness	1mm
Face area	250*236

2.2 Mathematical Modelling

The following assumptions were considered:

- The PCME was treated as an incompressible, steady state, homogeneous single-phase fluid with negligible effect of viscous heating.
- Fluid properties were assumed to be constant with respect to temperature, except heat capacity of material.
- Phase change process was assumed to take place within a specific temperature range but volume change was neglected.
- Buoyancy effects were neglected as density was assumed to be constant.
- Inter-particle interaction and particle-wall interactions were neglected.

The governing equations can be written as follows (ANSYS, 2013):

Equation 27: Conservation of mass

$$\frac{\partial \rho}{\partial t} + \nabla \cdot (\rho \vec{v}) = 0$$

Equation 28: Conservation of momentum

$$\frac{\partial}{\partial t}(\rho \vec{v}) + \nabla \cdot (\rho \vec{v}\vec{v}) = -\nabla P + \nabla \cdot \left[\mu \nabla \vec{v} - \frac{2}{3} \mu \nabla \cdot \vec{v} \right] + \rho \vec{g} + \vec{F}$$

Equation 29: Conservation of energy

$$\frac{\partial}{\partial t}(\rho E) + \nabla \cdot (\vec{v}(\rho E + P)) = \nabla \cdot (k_{eff} \nabla T) + S_E$$

Where:

- v = the velocity of fluid
- ρ = the density of fluid
- P = static pressure
- μ=molecular viscosity
- k_{eff} = effective conductivity of fluid
- E=sensible enthalpy of fluid

The SST K-ω turbulence model was used to simulate turbulent flow. SST k-ω model was developed by Menter (Menter and Y., 2010) to effectively blend the robust and accurate formulation of the k-ω model in the near-wall region with the free-stream independence of the k-ω model in the far field. Transport equations for SST K-omega model are expressed as:

Equation 30: Transportation equation-k

$$\frac{\partial}{\partial t}(\rho k) + \nabla \cdot (\rho k \vec{v}) = \nabla \cdot [(\mu + \frac{\mu_t}{\sigma_k}) \nabla k] + G_k - Y_k + S_k$$

Equation 31: Transportation equation-ω

$$\frac{\partial}{\partial t}(\rho \omega) + \nabla \cdot (\rho \omega \vec{v}) = \nabla [(\mu + \frac{\mu_t}{\sigma_\omega}) \nabla \omega] + G_\omega - Y_\omega + D_\omega + S_\omega$$

Where,

- σ_k = constant turbulent Prandtl numbers for k
- σ_ω = constant turbulent Prandtl numbers for ω
- Y_k = the dissipation of k due to turbulence
- Y_w = the dissipation of ω due to turbulence.
- D_w = the cross-diffusion term

2.3 Thermo-physical Properties of PCME

In the present work, the phase change material emulsion CryoSol^{PLUS} 10 from Fraunhofer UMSICHT was used. The emulsion contains 1.5wt% surfactant, 2.5wt% nucleating agent and 30wt% of RT10.

The heat transfer of the PCME was modelled using effective heat capacity model (Alisetti, 1998). In this model, the heat storage capacity of PCME at different temperature range was directly incorporated into the energy equation by assuming specific heat capacity of the phase change emulsion to be a function of temperature.

The heat capacity was therefore calculated by using Equation 32 and the thermo-physical properties of the emulsion listed in Table 28.

Equation 32: Specific heat capacity at different range

$$C_{\mathrm{p,m},eff}(T) = \begin{cases} X_{\mathrm{W}} C_{\mathrm{p},w} \Delta T + X_{\mathrm{PCM}} C_{\mathrm{p},PCM} \Delta T & T < T_1 \\ X_{\mathrm{W}} C_{\mathrm{p},w} \Delta T + X_{\mathrm{PCM}} C_{\mathrm{p},PCM} \Delta T + X_{\mathrm{PCM}} \Delta h / \Delta T & T_1 < T < T_2 \\ X_{\mathrm{W}} C_{\mathrm{p},w} \Delta T + X_{\mathrm{PCM}} C_{\mathrm{p},PCM} \Delta T & T_2 < T \end{cases}$$

Where:

- X_{PCM} = mass fraction of PCM
- $C_{p,PCM}$ = specific heat capacity of PCM in solid phase
- h = the latent heat of PCM
- T_1 and T_2 are onset and end phase change temperatures of PCM

Table 28: Specification for CryoSol^{PLUS} 10 (Huang et al., 2010)

	T<3 7°C	3.7°C<T<11.4°C	T>11.4°C
Density ρ (kg/m3)	940	940	940
Droplet size distribution (μm)	1-10	1-10	1-10
Specific heat capacity $C_{p,p}$ (KJ/kg K)	3.6	8.9	3.6

CryoSol^{PLUS} 10 is a non-Newtonian fluid and shows a shear-thinning behaviour. The viscosity η of non-Newtonian fluid can be described as a function of rate shear γ using Equation 33:

Equation 33: Ostwald Equation

$$\eta = K \times \gamma^{n-1}$$

Where, K and n are coefficients and given in Table 29.

Table 29: Coefficients K and n of CryoSol^{PLUS} 10 at 10°C and 20°C (Huang and Petermann, 2015)

T (°C)	k	n
10	0.1510	0.5429
20	0.1197	0.5442

2.4 Boundary Conditions

The simulation was subjected to the following boundary conditions. Velocity inlet boundary condition was applied at the inlet. The inlet fluid temperature was fixed at 7°C with velocity ranging from 0-1.5m/s. The turbulence intensity was fixed at 5% with a hydraulic diameter pipe of 9.3mm. The pressure at outlet was assumed to be 0. Heat transfer coefficient of 35W/m^{2}K was applied at the external wall surface of the pipe with free-stream air temperature of 300K. A no-slip and no-penetrating boundary conditions were also imposed on the wall surface of the pipe.

2.5 Solution Control

For the purpose of comparison, water was also modelled as a cooling. The pressure-velocity coupling was done using coupled scheme and the pressure discretization was achieved by the PRESTO procedure. Second order upwind scheme was employed to discretize the convection terms, diffusion terms and other quantities resulting from the governing equations.

3. RESULT AND DISCUSSION

3.1 Flow Behaviour

Figure 108 shows the pressure drop per unit length for pure water and PCME versus the flow velocity at different temperatures. It can be seen that at the same velocity, the emulsions produced much bigger pressure drops due to high viscosities. Moreover, the pressure loss of the emulsion without phase change (liquid condition of PCM) is lower than that with phase change at low temperature.

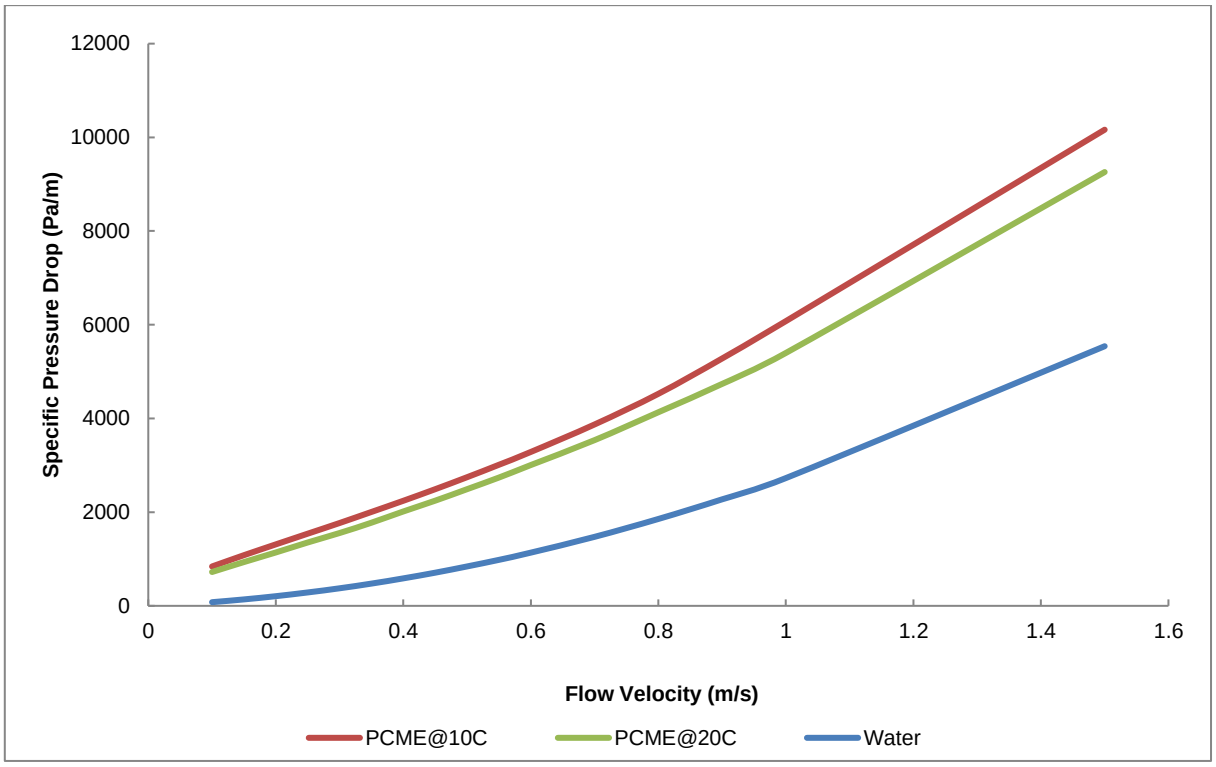

Figure 108: Pressure drop and pump power v/s flow velocity plot.

3.2Heat Transfer Characteristics

The temperature profiles at the exit of the heat exchanger for PCME and water are given in Figure 109. The average outlet temperature of PCME was lower than water due to the differences in their heat capacities. The heat capacity of PCME is twice as much as that of water hence the smaller temperature variation at the outlet.

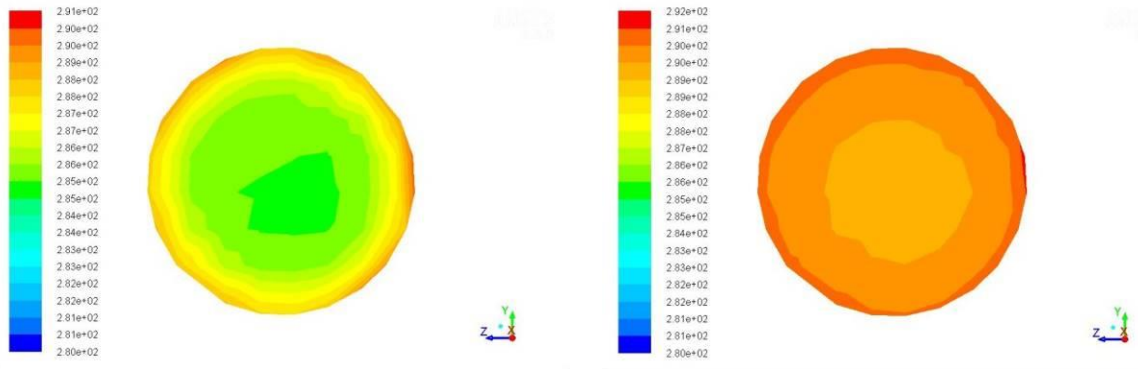

(a) PCME *(b) Water*

Figure 109: Temperature contour plot for outlet at inlet velocity 0.3m/s

Figure 110 compares the heat transfer performance of PCME and water. It can be seen that the PCME transferred about 10% more heat within the velocity range of 0.1m/s to 0.4m/s before gradually dropping to the water level. In chilled water air conditioning system, water enters the cooling coils at 0.2-0.5m/s (Lu, 2007). Therefore in that velocity range, 20-40% less PCME is required to deliver same amount of heat.

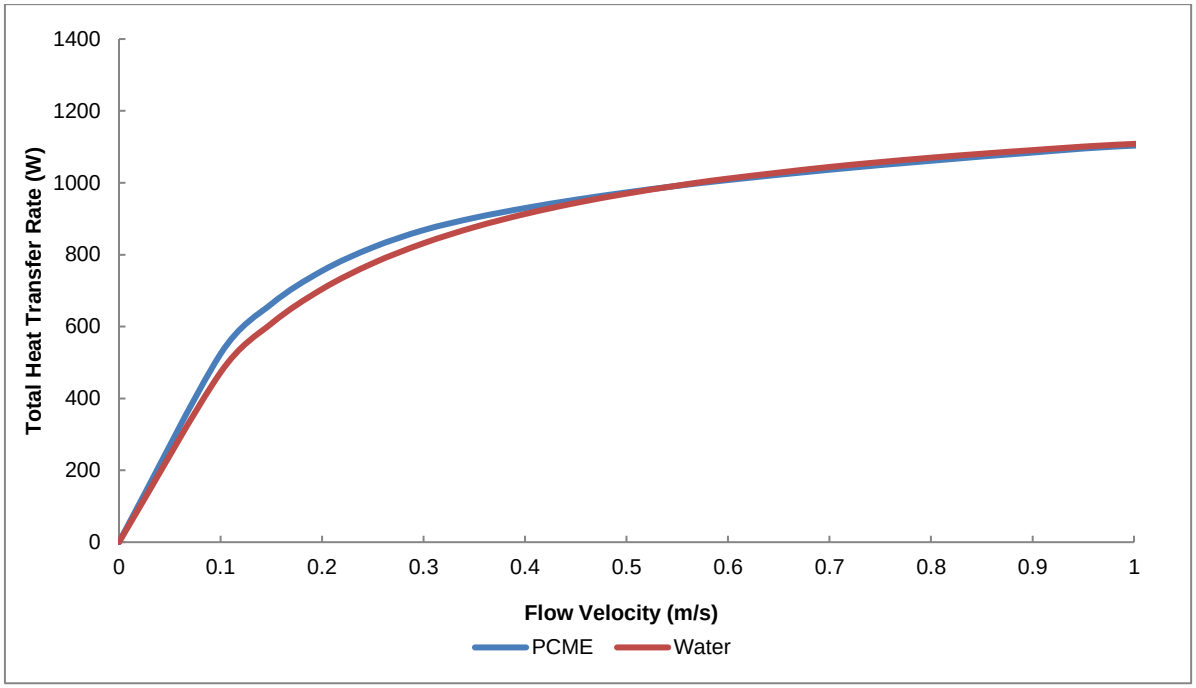

Figure 110: Temperature contour plot for outlet at inlet velocity 0.3m/s

The convective heat transfer coefficient and Nusselt number for PCME were calculated from the following equations:

Equation 34: Heat transfer coefficient

$$h = \frac{Q}{T_{wall} - T_f}$$

Equation 35: Nusselt Number

$$Nu = \frac{hD}{k}$$

Equation 36: Reynolds Number

$$\mathrm{Re} = 8^{1-n}\left(\frac{3n+1}{4n}\right)^{-n}\frac{\rho u^{2-n} D^n}{\eta}$$

Where, Q, T_{wall} and T_f are surface flux (W/m^2), average temperature (°C) of tube wall and fluid, respectively. For water, which is a Newtonian fluid, n=1.

Figure 111 represents the average Nusselt number versus Reynolds number for water and CryoSol^{PLUS} 10 in laminar flow region. It is shows that by increasing the Reynolds number the Nusselt number also increases.

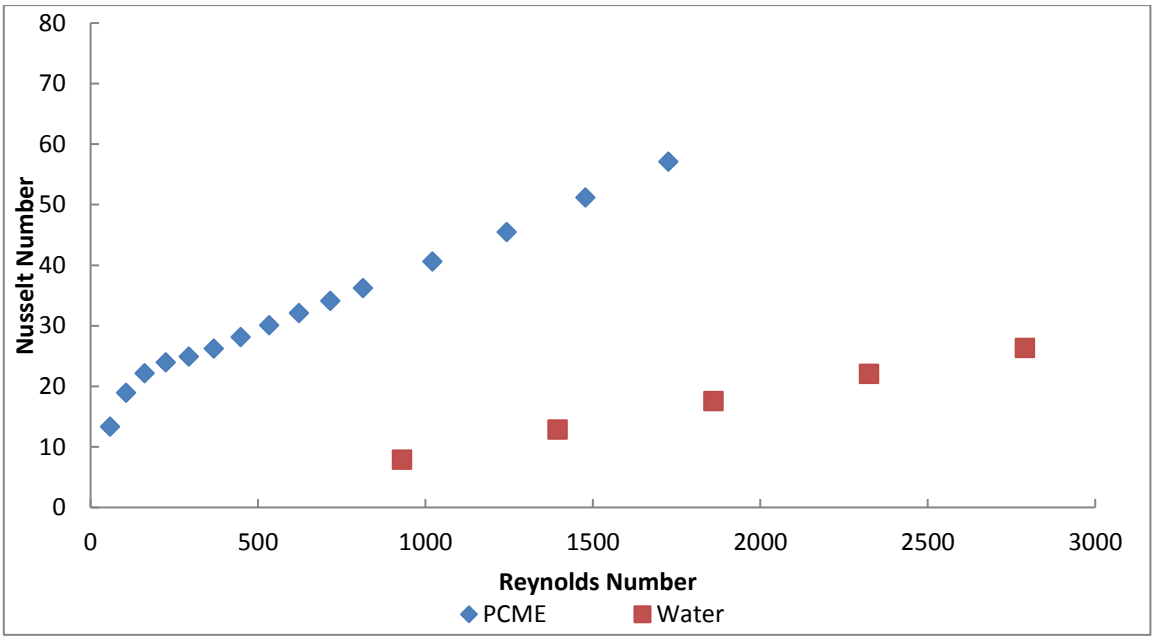

Figure 111: Nusselt number v/s Reynolds number plot.

4. CONCLUSION

In this paper, a computational fluid dynamics (CFD) study has been carried out to assess the heat transfer and pressure drop characteristics of a commercially available PCME (CryoSol^{PLUS} 10) in fin-and-tube heat exchangers and the results of heat transfer parameters have been compared with water under the same geometrical and operating conditions. The result showed higher Nusselt number levels and heat transfer coefficient for the PCME with a reduction in flow rate by 20-40%. However, the pressure drop was found to be much higher than that of water due to its relatively higher viscosity. This means that its application in coiled tubes could affect the overall energy reducing capability as a heat transfer fluid in air conditioning systems. Further investigation towards reducing the viscosity effect is therefore encouraged.

5. REFERENCES

ALISETTI, E. 1998. Forced convection heat transfer to phase change material slurries in circular ducts. PhD, University of Miami.

ANSYS 2013. ANSYS Fluent Theory Guide Version 15.0, Canonsburg, PA.

HUANG, L., Doetsch, C. & Pollerberg, C. 2010. Low temperature paraffin phase change emulsions. International Journal of Refrigeration, 33**,** 1583-1589.

HUANG, L. & Petermann, M. 2015. An experimental study on rheological behaviors of paraffin/water phase change emulsion. International Journal of Heat and Mass Transfer, 83**,** 479-486.

INABA, H. & Morita, S. 1995. Flow and cold heat-storage characteristics of phase change emulsion in a coiled double tube heat exchanger.

INABA, H. & Morita, S. 1996. Cold heat-release characteristics of phase-change emulsion by air-emulsion direct-contact heat exchange method. International Journal of Heat and Mass Transfer, 39**,** 1797-1803.

LU, Y. 2007. Design manual for domestic heating cooling and air conditioning, Beijing China, China Building Industry Press.

MENTER, F. & Y., E. 2010. The scaled-adaptive simulation method for unsteady turbulent flow prediction Part 1: Theory and Model description. Journal Flow Turbulence and Combustion, 85**,** 113-138.

ZHANG, P. & Ma, Z. W. 2012. An overview of fundamental studies and applications of phase change material slurries to secondary loop refrigeration and air conditioning systems. Renewable and Sustainable Energy Reviews, 16**,** 5021-5058.

ZHAO, Z., Shi, Y., Zhang, Y. & Gai, P. 2002. Flow and heat transfer characteristics of phase -change emulsion in a coiled double-tube heat exchanger. Journal of Engineering Thermophysics, 23**,** 730-732.

83: Thermal simulation of a laminated microencapsulated multiphase change material drywall

WEIGUANG SU[1], JO DARKWA[2], GEORGIOS KOKOGIANNAKIS[3]

1 University of Nottingham Ningbo China, Centre for Sustainable Energy Technologies (CSET), 199 Taikang East Road, Ningbo, 315100, China, Weiguang.Su@nottingham.edu.cn
2 University of Nottingham, Faculty of Engineering, University Park, Nottingham, NG7 2RD, UK, J.Darkwa@nottingham.ac.uk
3 University of Wollongong, School of Mechanical, Materials and Mechatronic Engineering, Sustainable Buildings Research Centre, 1 Pitt Street, Loftus, New South Wales 2232, Australia, gkg@uow.edu.au

Phase change materials (PCMs) possess the potential of reducing energy consumption in buildings because of their relatively large energy storage capability at constant temperatures. However, currently available PCMs have single phase change temperatures and therefore unable to be tuned to multiphase change temperature applications. In this regard the thermal performance of a proposed laminated microencapsulated multiphase change material (MEMPCM) drywall has been theoretically evaluated. The simulation results showed that the MEMPCM was able to reduce the maximum peak room temperatures by 2.86℃ to 6.67℃ from May to October while the overall thermal comfort period was enhanced by 25.4% in a selected location. Future experimental evaluation is however recommended to establish its practical potential.

Keywords: Simulation, ESP-r, Fluent, microencapsulated multiphase change material

1. INTRODUCTION

Microencapsulated phase change materials (MEPCMs) have been recognized as potential energy saving materials because they can be used to reduce the mismatch between heating and cooling demands in buildings (Fokaides et al., 2015, Waqas et al., 2015). For example, an experimental study carried out on a novel translucent full scale passive solar MEPCM wall by Berthou et al. (Berthou et al., 2015) revealed that it could be used to provide significant improvement of indoor temperatures in both cold and sunny climates. Silva et al. (Silva et al., 2015) evaluated the thermal performance of a novel PCM window shutter in a room and obtained a reduction in the maximum and minimum peak temperatures by 6% and 11% respectively. Darkwa et al. (Darkwa et al., 2012) developed a non-deform MEPCM (Darkwa et al., 2012) for thermal energy storage application and further evaluated its thermal performance (Zhou et al., 2015) in a model room to achieve a maximum temperature reduction of 5 °C. Another experimental investigation (Kuznik and Virgone, 2009) also achieved air temperature reduction of 4.2 °C with a composite copolymer composite microencapsulated phase change material (MEPCM) wallboard. Investigation by Schossig et al. (Schossig et al., 2005) revealed that an integrated MEPCM gypsum board could reduce the cooling demand in lightweight buildings.

However, all these studies were carried out with commercially available MEPCMs which are only able to operate at specific phase change melting temperatures and therefore unable to satisfy all year seasonal thermal energy storage application within wide range ambient conditions. To this end a novel MEMPCM was recently developed and tested in our research laboratory at the University of Nottingham. This was based on combining two manufactured MEPCMs (n-eicosane and n-octadecane as the core materials) to form a composite MEMPCM which is capable of storing and releasing energy at two different predetermine phase change melting temperatures. This study was therefore focused on simulating the performance of a proposed composite laminated microencapsulated multiphase change material (MEMPCM) drywall in an indoor environment.

2. SIMULATION WITH ANSYS FLUENT

Whole building simulation software ESP-r was used for the evaluation due to its capability in importing historical weather data as boundary conditions. However ESP-r is able to define only one MEPCM in a particular zone at a time and not able to handle multiple materials with different melting points. For this reason Ansys Fluent software was initially employed to establish suitable directional arrangement for the MEPCM elements to represent MEMPCM layer before the simulation exercise took place. As a test case, Hangzhou city in China was selected as suitable and corresponding indoor location for the samples (Yi, 2005).

2.1. Physical model

For the benefit of comparison and for achieving the best performance for the MEMPCM, the MEPCM cells were arranged in horizontal and vertical directions as shown in Fig.1. In Fig (1a), the MEPCM cells are arranged in a non-uniform manner and segmented into two units of cells. It was therefore necessary to examine different unit cell sizes (such as 2x2mm, 10x10mm and 50x50 mm) in order to promote uniform heat transfer distribution in the proposed drywall. As shown in Fig.1b, the vertical type is arranged in two separate but uniformly distributed MEPCM unit cells in the direction of heat transfer direction. Therefore it does not require examination of different unit cell sizes.

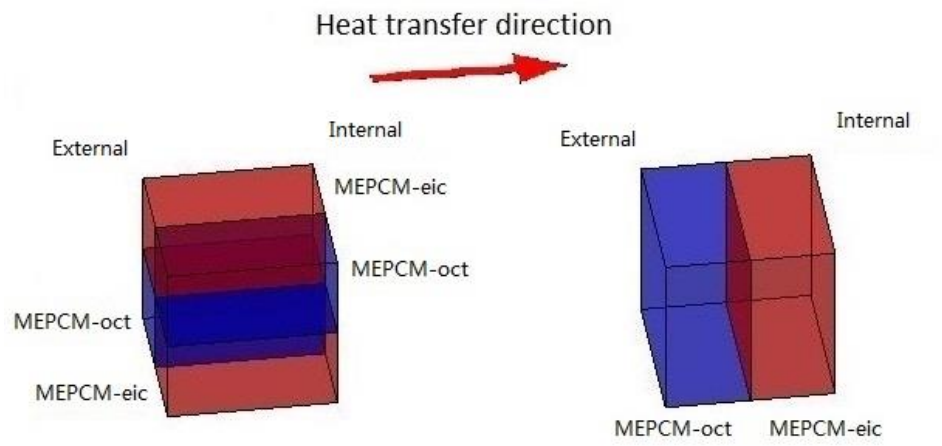

(a) Horizontal arrangement *(b) Vertical arrangement*

Figure 1: Composite MEPCMs layers

2.2. Heat transfer model

Since there is no internal heat generation and mass transfer, the governing equation during solidification/melting process for the latent energy storage layer can be expressed as (Inc., 2007a):

$$\frac{\partial}{\partial t}\left(\rho_e H_P\right) = \nabla \cdot (k_e \nabla T) \quad (1)$$

The total enthalpy of the MEMPCM (H_P) is computed as the sum of the differential specific heat enthalpy (H_e) and the latent heat enthalpy (ΔH):

$$H_P = H_e + \Delta H \quad (2)$$

Where

$$:H_e = \int_{T_0}^{T} C_{p,eff} dT \quad (3)$$

$$c_{p,eff} = \begin{cases} C_{p,s} & T < T_{s1} \\ C_{p,s} + \frac{\Delta h}{T_l - T_s} & T_{s1} < T < T_{l1} \\ C_{p,l} & T > T_{l1} \end{cases} \quad (4)$$

$$\Delta \boldsymbol{H} = \boldsymbol{\beta L} \quad (5)$$

The liquid fraction can also be calculated with the equation below (Inc., 2007b) as:

$$\beta = \begin{cases} 0 & \text{if} \quad T < T_s \\ \frac{T - T_s}{T_l - T_s} & \text{if} \quad T_s < T < T_l \\ 1 & \text{if} \quad T > T_l \end{cases} \quad (6)$$

For the MEPCM layer the specific heat (Cp) is a constant value, so that the total enthalpy (H_P) is computed as the sum of the sensible heat enthalpy (h) and the latent heat enthalpy (ΔH).

Therefore Eq. 2 becomes:

$$H_P = h + \Delta H \quad (7)$$

Where:

$$h = \int_{T_0}^{T} C_p dT \quad (8)$$

2.3. Boundary conditions and materials properties

The external boundary conditions were defined as natural convection for the exposed surface and adiabatic for the insulated surface. The variations in the external ambient temperatures were described as sinusoidal and defined by Eq.9 and Eq.10 with user-defined-functions (UDF) in Fluent as:

For high temperature cycle (303.15-313.15K) situation,

$$T = 5\sin\left(2 * \frac{\pi}{84600} * t - \frac{\pi}{2}\right) + 308.15 \quad (9)$$

For low temperature cycle (293.15-303.15K) condition the temperature is expressed as;

$$T = 5\sin\left(2 * \frac{\pi}{84600} * t - \frac{\pi}{2}\right) + 298.15 \quad (10)$$

Based on previous work the thermophysical properties of the MEPCMs samples were summarized in Tab.1. The properties for the MEMPCM (MEPCM-oct/MEPCM-eic at 50/50wt%) were however obtained with the uniform mixing theory (Darkwa and Su, 2012) and Eq.4 and Eq.5.

Table 1: Physical properties of MEPCM layers

Name	ρ(kg/m3)	Cp (J/kg)	k (W/m•K)	Mt(℃)	Ml(℃)	H(J/kg)
MEPCM-oct	658	2202	0.154	23.55	25.55	179000
MEPCM-eic	684	2115	0.166	34.99	36.99	194000

Table 2: Physical properties of MEMPCM in Fluent

Name	ρ(kg/m3)	$Cp_{s,l}$ (J/kg)	Cp_{eff} (J/kg,296.7-298.7K)	Mt_2 (℃)	H (J/kg)	k (W/m•K)
MEMPCM	671	2158.5	44750	34.99	97000	0.160

2.4. Heat transfer analysis

The heat transfer process for different arrangement of MEMPCM layers can be quantified by considering the mean absolute deviation (MD) (Wikipedia, 2015) of temperature (MD_T) and heat flux (MD_{HF}) in the unit cells with Eq. 11 and Eq. 12 as shown below:

$$MD_T = \frac{1}{n}\sum|T_{MEPCM} - T_{MEMPCM}| \quad (11)$$

$$MD_{HF} = \frac{1}{n}\sum|HF_{MEPCM} - HF_{MEMPCM}| \quad (12)$$

Fig. 2 shows the inside temperature and the external surface heat flux profiles for the low and high temperature cycles. It can be observed that the temperature and heat flux profiles followed the same corresponding trends for the various arrangements. For instance, during the phase change periods (296.70-298.70K and 308.14-310.14K) in the low and high temperature cycles, the differential temperatures dropped while the heat flux values increased rapidly. That was because the latent heat component was much higher than the sensible heat. As demonstrated in Fig.2 (b) and (d) the energy storage periods started from 0-12 hours and later discharged from 12-24 hours thus showing a balance in the thermal cycling process.

However, analysis of the MD_T and MD_{HF} values in Tab. 3 is shows a significant difference between the horizontal and the vertical arrangements. Although the MD_T and MD_{HF} values for the 'horizontal 2mm' cell unit were relatively small for both low and high temperature cycles, the values did increase when the size was changed to 50 mm. That means the similarity between horizontal arrangements and MEMCPM was strongly affected by the cell sizes. Hence to achieve good similarity millions of tiny horizontal MEPCMs cells would be needed to substitute the MEMPCM drywall in the ESP-r simulation programme which would be impracticable. In comparison with the horizontal arrangement the vertical arrangement showed a significant advantage. For instance the MD_T and MD_{HF} values for the two thermal cycles were found to be lower than most of the values under the horizontal arrangement. It was therefore decided to adopt the vertical arrangement for the simulation of the laminated MEMPCM drywall system.

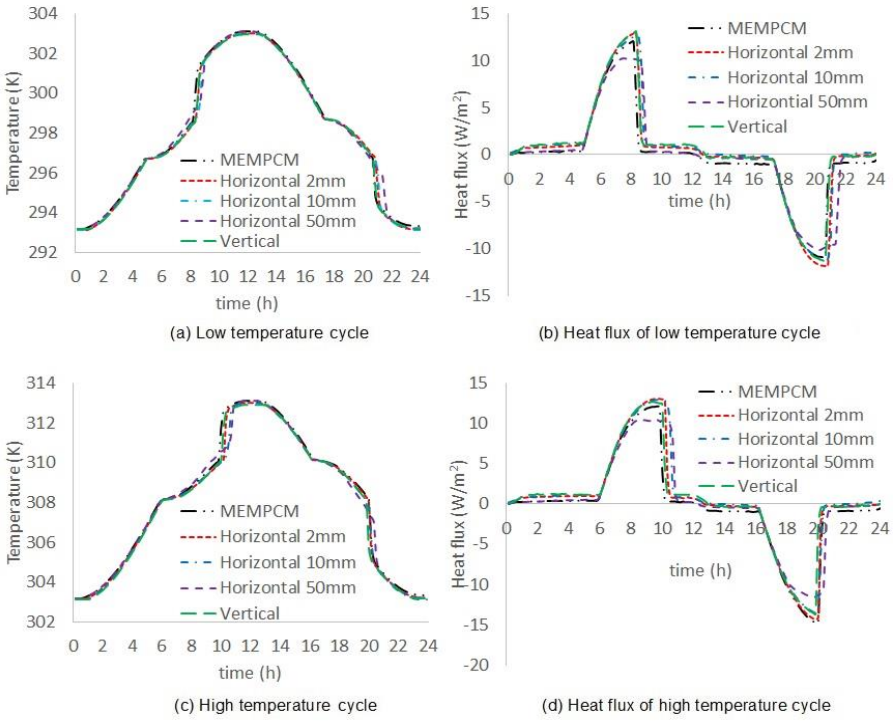

Figure 2: Temperature and heat flux profiles of MEMPCM and various arrangements of MEPCMs layers

Table 3: Comparison of various MEMPCM arrangements

Thermal cycles	Arrangements	MD_T (℃)	MD_{HF} (W/m²)
Low temperature cycle	Vertical	0.13	0.07
	Horizontal 2mm	0.14	0.07
	Horizontal 10mm	0.22	0.29
	Horizontal 50mm	0.24	0.40
High temperature cycle	Vertical	0.13	0.08
	Horizontal 2mm	0.14	0.07
	Horizontal 10mm	0.27	0.33
	Horizontal 50mm	0.31	0.48

3. SIMULATION WITH ESP-R

3.1 Model building description

Fig. 3 shows a pictorial view of a model building measuring 5m x 4m on ground and 2.7m high with a south facing door (1.2X2.1m) and a north located window (2X1m). It is a lightweight building construction based on data from 'BESTBEST '(Judkoff and Neymark, 1995) but the inside walls and roof are laminated with 5mm MEMPCM drywall layer. For the purpose of analysis of thermal performance, other cases covering

standard walls/roof without PCM and walls/roof with laminated MEPCM-oct and MEPCM-eic layers were simulated and compared with that of the MEMPCM model.

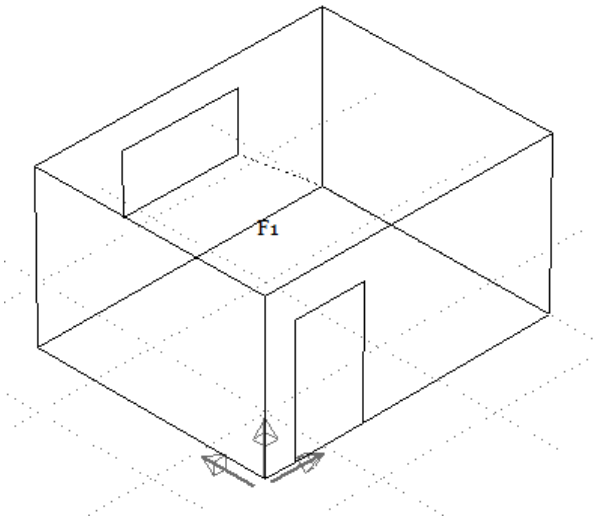

Figure 3: Physical model

3.2 Governing equations

According to ESP-r code the differential equation of transient heat conduction with variable thermo-physical properties is given by Eq.13 (Heim and Clarke, 2004):

$$\frac{\partial}{\partial t}(\rho(T)h(T)) = \nabla \cdot [k(T)\nabla T(\vec{r},t)] + g(\vec{r},t) \tag{13}$$

Where T is temperature, ρ is density, h is enthalpy, k is thermal conductivity and g is the heat generate rate.

In order to simplify the mathematical model, the following assumptions were made:

- The MEMPCM layer was represented by two uniform layers of MEPCM-oct and MEPCM-eic. (Physical and thermal properties are shown in Tab.1).
- There was no heat source in the building.

Hence $\frac{\partial \rho}{\partial t} \approx 0$, $g(\vec{r},t) = 0$ and $\frac{\partial h}{\partial t} = \frac{\partial h}{\partial T}\frac{\partial T}{\partial t} = C_{\mathrm{p,eff}}(T)\frac{\partial T}{\partial t}$, where $\mathrm{C_{p,eff}(T)}$ is the effective specific heat capacity as given in Eq.4,:

Therefore Eq. (13) becomes:

$$\rho(\mathrm{T})\mathrm{C_{p,eff}}(\mathrm{T})\frac{\partial \mathrm{T}}{\partial \mathrm{t}} = \nabla \cdot [\mathrm{k(T)}\nabla \mathrm{T}(\vec{\mathrm{r}},\mathrm{t})] \tag{14}$$

3.3 Analysis of building thermal performance case study

Based on weather history profile for Hangzhou a six-month period (May to October) building thermal performance was simulated with the ESP-r software. According to the simulation results in Fig.4 (a), the monthly indoor average temperatures for various wall conditions were even higher than the environmental temperature due to the effects of solar radiations (Vautherot et al., 2015). Although there were not many differences between the average indoor air temperatures and different wall conditions, the building containing laminated MEMPCM walls demonstrated relatively low average temperatures. As shown in Fig.4 (b), the MEMPCM drywall was also able to reduce the peak indoor temperature far more than the other materials by about 2.86-6.67℃. This means that the building with MEMPCM would consume less energy to achieve an acceptable thermal comfort level.

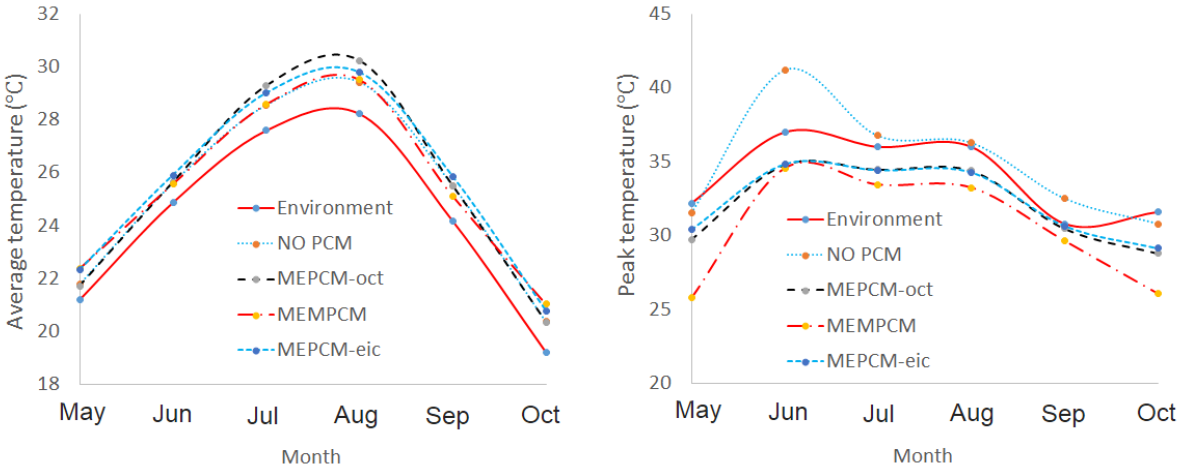

(a) Average temperature *(b) Peak temperature*

Figure 4: Monthly temperature profiles

The six-month simulation period of 4416 hours (184 days) were separated into three zones based on ASHRAE Standards 55-2013 (ASHRAE, 2013) and the indoor temperatures, i.e. cold (temperature less than 21℃), comfort (21-28℃) and hot (temperature over 28℃). As summarized in Tab.4, the thermal comfort time zone was significantly increased with the laminated MEMPCM drywalls as compared with others, and increased the thermal comfort time zone by about 25.4% in the Hangzhou area.

Table 4: Total times for various MEMPCMs

Zone	NO PCM (h)	MEPCM-oct (h)	MEMPCM50 (h)	MEPCM-eic (h)
Cold	916	864	589	720
Comfort	**2155**	**2174**	**2703**	**2258**
Hot	1345	1378	1124	1439

4. CONCLUSION

This study was focused on evaluating the thermal performance of a proposed composite laminated MEMPCM drywall in an indoor environment. Due to the complex nature of the heat transfer process Ansys Fluent software was initially used to establish the most suitable directional arrangement for the MEPCM cells before a whole building simulation process with ESP-r software was carried out. The results based on a selected location for a six-month period showed that the laminated MEMPCM wall performed thermally better than the other types of walls considered in the simulation. The specific findings may therefore be summarised as follows:

- The Fluent simulation results showed that vertical arrangement of MEPCM cells was more suitable than the horizontal arrangement for simulating the performance of the MEMPCM drywall layer in ESP-r.
- The ESP-r simulation showed that the MEMPCM drywall was able to reduce the peak indoor temperature far more than the other materials by 2.86-6.67℃. It was also able to increase the thermal comfort time zone by about 25.4% in the selected location.

5. REFERENCES

ASHRAE 2013. Standard 55-2013 : Thermal Environmental Conditions for Human Occupancy.

BERTHOU, Y., Biwole, P. H., Achard, P., Sall E, H., Tantot-Neirac, M. & Jay, F. 2015. Full scale experimentation on a new translucent passive solar wall combining silica aerogels and phase change materials. Solar Energy, 115, 733-742.

DARKWA, J. & Su, O. 2012. Thermal simulation of composite high conductivity laminated microencapsulated phase change material (MEPCM) board. Applied Energy, 95, 246-252.

DARKWA, J., Su, O. & Zhou, T. 2012. Development of non-deform micro-encapsulated phase change energy storage tablets. Applied Energy, 98, 441-447.

FOKAIDES, P., Kylili, A. & Kalogirou, S. 2015. Phase change materials (PCMs) integrated into transparent building elements: a review. Materials for Renewable and Sustainable Energy, 4, 1-13.

HEIM, D. & Clarke, J. A. 2004. Numerical modelling and thermal simulation of PCM–gypsum composites with ESP-r. Energy and Buildings, 36, 795-805.

INC., A. (ed.) 2007a. Fluent 6.3 User Guide.

INC., A. (ed.) 2007b. Fluent 6.3 User Guide.

JUDKOFF, R. & Neymark, J. 1995. International Energy Agency Building Energy Simulation Test (BESTEST) and Diagnostic Method. National Renewable Energy Laboratory.

KUZNIK, F. & Virgone, J. 2009. Experimental assessment of a phase change material for wall building use. Applied Energy, 86, 2038-2046.

SCHOSSIG, P., Henning, H. M., Gschwander, S. & Haussmann, T. 2005. Micro-encapsulated phase-change materials integrated into construction materials. Solar Energy Materials and Solar Cells, 89, 297-306.

SILVA, T., Vicente, R., Rodrigues, F., Samagaio, A. & Cardoso, C. 2015. Performance of a window shutter with phase change material under summer Mediterranean climate conditions. Applied Thermal Engineering.

VAUTHEROT, M., Mar Chal, F. & Farid, M. M. 2015. Analysis of energy requirements versus comfort levels for the integration of phase change materials in buildings. Journal of Building Engineering.

WAQAS, A., Ali, M. & Ud Din, Z. 2015. Performance analysis of phase-change material storage unit for both heating and cooling of buildings. International Journal of Sustainable Energy, 1-19.

WIKIPEDIA. 2015. Average absolute deviation [Online]. Available: http://en.wikipedia.org/wiki/Average_absolute_deviation.

YI, J. 2005. China Standard Weather Data for Analyzing Building Thermal Conditions, Beijing, China Building Industry Publishing House.

ZHOU, T., Darkwa, J. & Kokogiannakis, G. 2015. Thermal evaluation of laminated composite phase change material gypsum board under dynamic conditions. Renewable Energy, 78, 448-456.

84: Research on PCM thermal storage structure of the size and mixing melting points sphere packing

GUOHUA WANG[1,2], QING GAO[1,2], CHUN GAO[1,2] ,
WENLONG XU[3], TIANSHI ZHANG[1,2] , Y.Y. YAN [4]

1 State Key Laboratory of Automotive Simulation and Control, Jilin University, Changchun, China, gqing@jlu.edu.cn
2 State Key Laboratory of Automotive Simulation and Control, Jilin University, Changchun, China, wanggh@jlu.edu.cn
3 China FAW Group Corporation R&D Center, Changchun, China
4Faculty of Engineering, University of Nottingham, Nottingham, NG72RD, UK, Yuying.Yan@nottingham.ac.uk

Electric vehicles as a main development direction of future car development, the technology of parking heat storage and heat recovery storage is very important to solve the winter heating and battery cold start. Through using the phase change thermal storage at sphere packing structure, the temperature equalizing and controlling stability of battery power system can be ensured. The research works focus on heat flux characteristics of phase change thermal storage at sphere packing structure, by combining the model of numerical simulation analysis and experimental verification. And, the further analysis focuses on the sphere diameter, multi melting points mixture by uniformity and layered structure. The research shows that the good temperature adaptability and heat flux characteristics in this thermal storage device, by using the way of small diameter and mixing melting points.

Keywords: Thermal Storage; PCM; Sphere Packing; Sphere diameter; Mixing Melting Points

1. INTRODUCTION

Electric vehicles (EV) as a main development direction of future car development, the technology of parking heat storage and heat recovery storage is very important to solving the heating and battery cold start in winter. So the heat storage technology by using phase change materials (PCM) has been given attention [1-3]. By the selection of transition temperature can determine the dominant operating temperature, and achieve energy cascade storage using the combination of mixing melting points. Because of the transition temperature, PCM is good at heat transfer. And different transition temperatures can be using as the working temperatures. It can make for heat storage in different temperatures.

In the different application fields at home and abroad, a lot researches have been made on the heat storage device by using PCM. Faghri et al. have used the internally finned tube to analyse the heat transfer enhancement in latent heat thermal energy storage system [4]. Ismail et al. have done a research through experiment and numerical calculation with the straight rib in the columnar phase change thermal storage unit [5]. Khodadadi et al. have used the PCM sphere to analyse the thermal storage characteristic in natural convection state [6]. Inaba et al. have used the simulation method to analyse the thermal storage characteristic for fin effect [7]. Stritih et al. have done an experimental study enhanced heat transfer in rectangular PCM thermal storage [8]. Agyenim et al. have used the annular rib and longitudinal rib plate to do a comparison of heat transfer enhancement [9]. Chen et al. have used experiment and numerical calculation to analyse the thermal storage characteristic of form-stable PCM [10]. Wang Zengyi et al. have used experimental to study on heat transfer characteristics of a heat pipe heat exchanger [11]. Zhou Sujuan al. has used dynamic simulation on heat storing process of bushing heat storage vessel with PCM [12]. Liao Haijiao al. have used numerical simulation to analyse the thermal storage characteristic of fin-plate thermal storage [13]. Lv minghui al. have used Material naphthalene as PCM to analyse the thermal storage characteristic of fin-plate thermal storage [14].The aim of these studies is enhancing heat transfer, and strengthening the thermal response capability of phase change heat storage equipment. So it can adapt to different applications.

In recent years, PCM energy storage in the energy field has been continuously research and application, and new phase change materials and structure continue to appear. The small scale accumulation of particles is one of them. With the gaps state of the accumulation, the good heat transfer and flow characteristics can also be achieved. But there are less researches of PCM thermal storage Structure using sphere packing. Especially, researches are less about the different melting point combinations and scale characteristics. The aim of this paper was to obtain the thermal storage characteristic of PCM thermal storage Structure using sphere packing. The method of combining numerical simulation and experimental verification is used. Study on the thermal properties of different small scale accumulation void space and different melting point mixture in PCM thermal storage.

2. MODEL AND CALCULATION METHOD

The experiment method and numerical calculation method are used in this research. The numerical calculation is tested by experiment, and further analysis is made to conduct by numerical calculation method.

2.1 Geometric Model

The disorder accumulation of spheres is used in the device. The method of the Particle Flow Code (PFC) and Monte Carlo random is adopted to realize the disorder accumulation of spheres. The geometrical structure is shown in Figure 1. To simplify the analysis, the hypothesis is as follows: (1) Isotropic and uniform of phase change materials; (2) The physical parameters of phase change materials do not change with temperature.

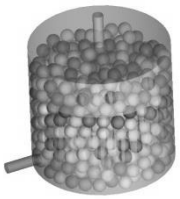

Fig.1 Geometric model

2.2 Calculation Method

The calculation method is based on finite volume method. Non-coupled implicit model, unsteady model, standard turbulence model and solidification / thawing model are selected. The direction of gravity acceleration is defined as –z. Material physical parameters of PCM and Spherical shell PE are shown in Table 1 and in Table 2. The circulating fluid uses ethylene glycol aqueous solution, and the volume fraction is 50%.

Table1. Physical parameters of PCM

Parameters	Units	25#PCM	36#PCM	48#PCM
Density	kg/m^3	1600	1500	1460
Specific Heat	kJ/(kg·K)	2.1	2.0	3.0
Thermal Conductivity	W/(m·K)	1.1 (Solid) 0.6 (Liquid)	0.6(Solid) 0.5 (Liquid)	1.0(Solid) 0.6 (Liquid)
Viscosity	kg/(m·s)	0.034	0.034	0.034
Latent Heat	kJ/kg	200	232	226
Transformation temperature	℃	25	36	48

Table2. Physical parameters of PE

Material	Specific Heat kJ/(kg·K)	Conductivity, W/(m·K)	Density, kg/m³
PE	2.3	0.42	921

3. EXPERIMENT VERIFICATION

According to the calculation results of the model, the experimental verification and analysis are carried out.

3.1 Experimental System

The experimental system includes PCM device, test device, water tank for heating and mixing. The function of water tank for heating and mixing is providing the stable heat source. Test device is composed of temperature sensors, flow sensors and data acquisition systems. The experimental system is shown in Figure 2.

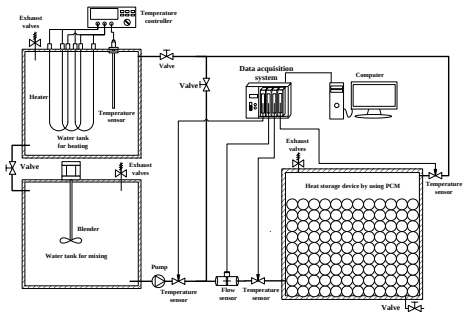

Fig.2 Experimental system for phase change energy storage

3.2 Verification of Experimental Results

36#PCM is used as the PCM in the experimental and computational analysis. The diameter of sphere is 20mm. Fluid inlet velocity condition is 5L/min, initial temperature of storage heat is -5℃, initial temperature of release heat is 60℃, and ambient temperature is -10℃.

By comparison, the difference between the experimental and the calculation is not significant in the process of heat storage and heat release. Most of the regions are in good temperature agreement, and the average value of deviation is kept within 1℃. It shows that the mathematical model and the method of calculation have good reliability. However, the differences are mainly in the phase change heat transfer stage. The

main reason is that the simulation of the phase change process can not accurately reproduce the heat transfer caused by the small flow of liquid in the solid gap.

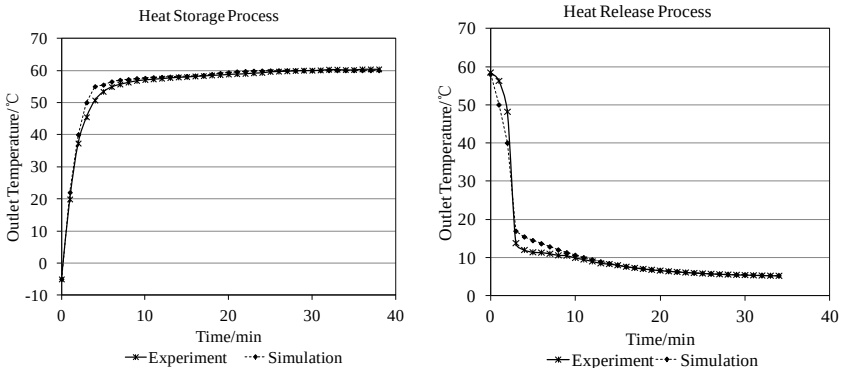

Fig.3. Experiment and calculate data of outlet temperature

4. BASIC CHARACTERISTIC ANALYSIS

For the analysis, the sampling points were set up in the simulation model. A sphere at the centre is selected, and 4 points along the centreline is selected. From the inside to the outside number are P1, P2, P3 and P4.

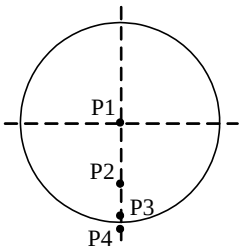

Fig.4. Location of sampling points

The thermal storage process mainly experiences three stages. It is the initial stage, the main storage stage and the stable stage.

In the initial stage, the outlet temperature is rising rapidly, and above 40℃ in a short time. But the average liquid fraction is always below 0.2. The reason is that the high temperature water gets into device and exchange heat with cold water quickly. This leads to water temperature rising rapidly. And the mean temperature difference is increased between water and sphere surface. So the PCM near the sphere surface begin to melt and the average liquid fraction is increased. However, because of the response time of transition and the structure of sphere, most of PCM has not begun to melt and still in the sensible heat transfer.

In the main stage, the average liquid fraction begins to increase greatly. But the outlet temperature is not high, close to about 10℃. The heat is absorbed by PCM, which makes the outlet temperature increase slowly. But, there is slight difference in the moment of initial phase change. P4 also maintains for a long time of phase change temperature. The reason is that the heat absorbed by PCM is in balance with the heat released by high temperature water. The result is that the surface temperature of the sphere is little change. With the end of latent heat change, the temperature of P4 is beginning to increase with the small heat absorption. The heat storage process steps to the stable stage of the heat storage, and the rise of the outlet temperature is slightly higher.

In the stable stage, the outlet temperature is increased gradually to the inlet temperature. The reason is that PCM has mostly melted. So sensible heat transfer is main heat transfer mode in this stage, and the average liquid fraction is difficult to rise.

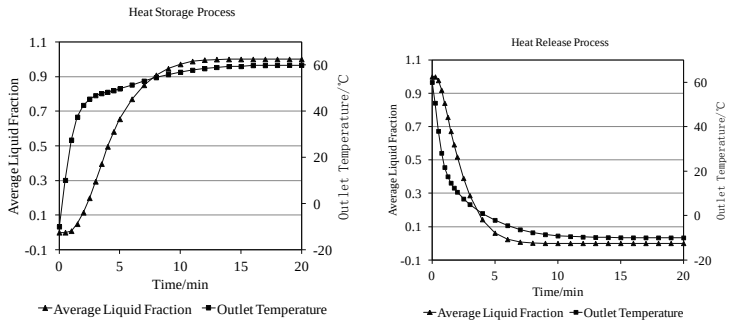

Fig.5. Average liquid fraction and outlet temperature curve

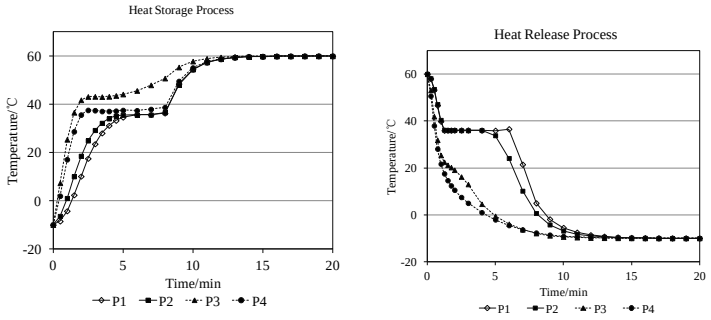

Fig.6. PCM sphere temperature curve

In the initial release stage, the average liquid fraction and the outlet temperature are dropping quickly. The outlet temperature and the sphere temperature are also dropping quickly. From the curve we can see that the phase transition is happened lightly. The reason is that temperature of the inlet region dropped quickly.

In the start of the main release stage, the dropping rate of outlet temperature is smaller, but the dropping rate of the average liquid fraction is still dropping quickly. At the end of the stage the dropping rate of the average liquid fraction is slower; the dropping rate of outlet temperature is bigger. The reason is that the temperature dropping quickly make the temperature of surface sphere drop to the phase-transition temperature. This leads to phase transitions of PCM occurring. And because the PCM solid thermal resistance is less than the liquid, when the liquid of surface sphere is solidified, the heat transfer rapidly to the outside sphere, which makes the internal phase change almost simultaneously. At this time the large amount of latent heat released into the fluid, the decrease of the outlet temperature is slowed. So the temperature maintains a higher temperature grade in a longer time. As shown in Figure 5, the outlet temperature is maintained at above 20℃ within 5 minutes. And this is good to the power system of the electric power system such as the power battery. In the stable stage of the heat release, the outlet temperature gradually approaches the inlet temperature. The average liquid fraction tends to 1, the heat release is end.

5. NUMERICAL ANALYSIS OF SCALE AND MULTI MELTING POINT MIXTURE

Because of the sphere structure, the rate of thermal storage is restricted. The PCM sphere with different diameters is calculated and analyzed. In addition, considering the influence factors of energy utilization of the thermal storage device, the multi melting point mixture model is used for calculation and analysis.

5.1 Analysis of Scale Factor

36#PCM is also as the phase change material in the computational analysis. And diameters of sphere are 10mm, 20mm and 40mm. The phase change material in the different diameters is same, and the calculation condition is consistent with the basic working.

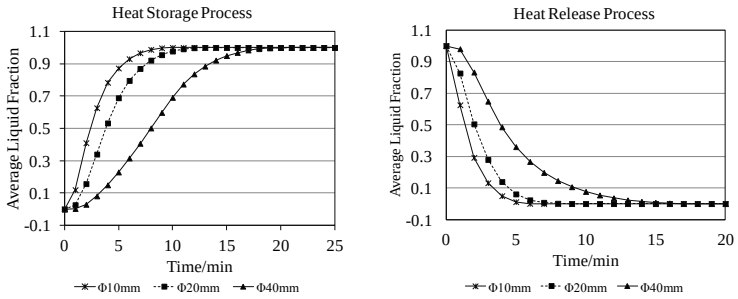

Fig.7. Average liquid fraction curves

As shown in figure 7, it has a greater impact on increase or decrease of PCM sphere diameters. At 5 minutes of heat storage, the average liquid fraction valve is 0.87, 0.69 and 0.23. At 5 minutes of heat release, the average liquid fraction valve is 0.01 , 0.06 and 0.36.The reason is the larger diameter increases the internal heat transfer resistance of the sphere in the heat storage stage, And this leads to the temperature change rate of sphere central region is slower than smaller diameter. Thus the overall increasing rate of average liquid fraction is reduced. So the rate of heat storage and heat release is largely influenced by the size of sphere.

As shown in figure 8, the outlet temperature of larger sphere is easier to reach the stable temperature of thermal stage. The reason is that the larger sphere has larger heat transfer resistant, and the heat inside the sphere is hard to transfer. So the heat storage and release of stable stage is longer. In release stage, the heat is not good to use because of the low temperature.

Above all, the diameter of sphere has great influence on the thermal storage. And using the thermal storage technology to preheat the electric power system and the power battery pack, the influence of diameter should be taken into account.

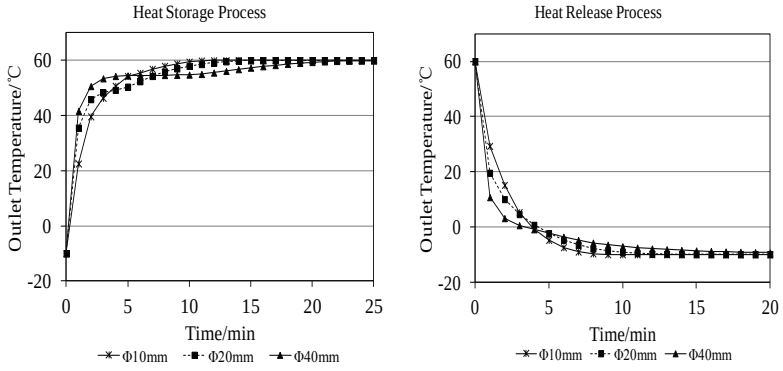

Fig.8. Outlet temperature curve

5.2 Analysis of multi melting point mixture

There are four modes in the analysis, 36#PCM, Mixed # PCM, 25-36-48#PCM and 48-36-25#PCM. The diameter of them is 20mm, and the numbers of sphere is same. The mode of Mixed # PCM means making the three different PCM spheres evenly mix together. The mode of 25-36-48#PCM and 48-36-25#PCM is using the hierarchical mode. It means making the spheres arrange from the inlet region to the outlet region by layering.

As shown in figure 10, it has a little impact on increase or decrease of PCM thermal storage. The influence of the heat storage process is mainly within the range of 5~15min. The average liquid fraction is 0.97798, 0.91367, 0.8808 and 0.93138 at 10 minutes. The influence of the heat release process is mainly within the range of 3~10min. The average liquid fraction of the four modes is 0.06118, 0.07431, 0.05003 and 0.09946 at 5 minutes. It shows that the PCM spheres of different types are mixed in different ways, which have some effect on the main storage stage and the main heat release stage.

So the mixed mode has the same thermal storage characteristic as the mode using 36#PCM. But the mixed mode has the characteristics of heat storage and heat release in different temperatures at the same time. So it has better adaptability than single melting point when it is needed for wide range of heat storage and heat release temperature. And by adjusting the order of the melting point of the mixed mode, the performance of the heat storage or the heat release can be improved to some extent.

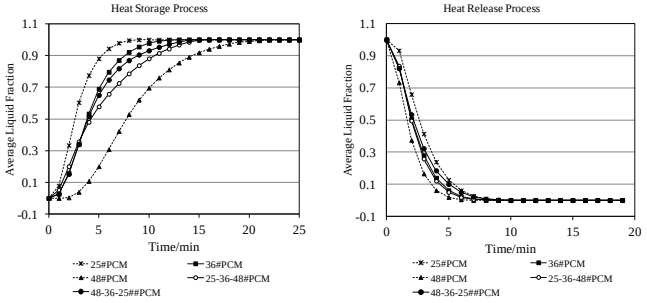

Fig.9. Average liquid fraction curve

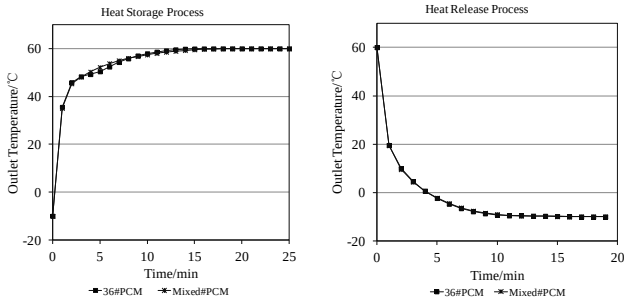

Fig.10. Outlet temperature curve

6. CONCLUSION

(1) The basic PCM thermal storage structure of sphere packing is using the material of 36#PCM. And the experimental verification is made, which shows that the numerical simulation can instead the experiment.

(2) The thermal storage process mainly experiences three stages. It is the initial stage, the main storage stage and the stable stage. The outlet temperature is maintained highly at a certain time at the heat release stage which is good to the power system of the electric power system such as the power battery.

(3) The diameter of sphere has great influence on the thermal storage. And using the thermal storage technology to preheat the electric power system and the power battery pack, the influence of diameter should be taken into account.

(4) The mixed mode has the same thermal storage characteristics with single melting point mode. But the mixed mode has the characteristics of heat storage and heat release in different temperatures at the same time. So it has better adaptability than single melting point when it is needed for wide range of heat storage and heat release temperature.

7. REFERENCES

[1] N. JAVANI, I. Dincer, G.F. Naterer, B.S. Yilbas. Heat transfer and thermal management with PCMs in a Li-ion battery cell for electric vehicles. Int J of Heat and Mass Transfer, 72（5）, 2014：690-703

[2] Ziye LING, Zhengguo Zhang, etc. Review on thermal management systems using phase change materials for electronic components, Li-ion batteries and photovoltaic modules. Renewable and Sustainable Energy Reviews, 31(3), 2014: 427-438

[3] Guoquan SHI, Xiaoming Fang, etc. Heat transfer in phase change materials for thermal management of electric vehicle battery modules. Int J Heat Mass Transfer, 53(12), 2010:5176-5182

[4] Y. W, ZHANG, A. Faghri. Heat transfer enhancement in latent heat thermal energy storage system by using the internally finned tube.[J]. Heat Mass Transfer, 1996,39(15):3165-3173.

[5] K. A. R. ISMAIL, C. L. F. Alves, M. S..Modesto. Numerical and experimental study on the solidification of PCM around a vertical axially finned isothermal cylinder[J]. Applied Thermal Eng,2001, 21: 53-77.

[6] J. M. KHODADADI, Y. Zhang. Effects of buoyancy-driven convection on melting within spherical containers[J]. Heat Mass Transfer,2001, 44 :1605-1618.

[7] H. INABA, K. Matsuo, A. Horibe. Numerical simulation for fin effect of a rectangular latent heat storage vessel packed with molten salt under heat release process [J]. Heat Mass Transfer,2003,39:231–237.

[8] U. STRITIH. An experimental study of enhanced heat transfer in rectangular PCM thermal storage.[J]. Heat Mass Transfer,2004, 47: 2841-2847.

[9] Francis AGYENIM, Philip Eames, Mervyn Smyth. A comparison of heat transfer enhancement in a medium temperature thermal energy storage heat exchanger using fins[J]. Solar Energy, 2009,83:1509-1520.

[10]Chen CHAO, Jian Ruihuan, Jiao Zhuangying, Xia Zhiguo, Li Xiangling, Numerical and experimental analysison heat-storage and discharge characteristics with form-stable PCM[J]. Acta Energiae Solaris Sinia, 2005,26(6): 857-862.

[11]Wang ZENGYI, Liu Zhongliang, Ma Chong-Fang, Experimental study on heat transfer characteristics of the process of charging/discharging of a heat pipe heat exchanger with latent heat storage[J], Journal of Engineering Thermophysics, 2005, 26(6): 899-991.

[12] Zhou SUJUAN, Zhang Xiaosong, Yin Yonggao, Dynamic simulation of heat storing process of bushing heat storage vessel with phase change material[J], Fluid Machinery, 2008(1):58-61.

[13]Liao HAIJIAO, Ling Xiang, Numerical simulation of phase change heat transfer in high temperature fin-plate thermal storage[J], Acta Energiae Solaris Sinia, 2010.31(3):345-350.

[14]Lv MINGHUI, Ling Xiang, Experimental study on thermal storage performance of fin-plate heat thermal storage[J], Fluid Machinery, 2009,27(2):65-68.

[15] EPPINGER.T, Seidler.K, Kraume.M. DEM-CFD simulations of fixed bed reactors with small tube to particle diameter ratios[J]. Chemical Engineering Journal,2011,166(1):324-331.

[16]Han ZHANZHONG, Lan Xiaoping. FLUENT- fluid process simulation calculation example and application[M]. Beijing: Beijing Institute of Technology press, 2010:18-19.

[17]Zhu HONGJUN, Lin Yuanhua, Xie Longhan. The hydrodynamic analysis and Simulation of practical course[M]. Beijing: People's Posts and Telecommunications Press, 2010.

POLICIES & MANAGEMENT

Keynote Speaker Chris Twinn: "The goalposts are changing– are we ready for the new direction?"

Chris Twinn is the CEO of Twinn Sustainability Innovation.

Chris specialises in the design and delivery of projects where sustainability - with its environmental impact, social and financial aspects - is a key issue. His background is multi-disciplinary building design, from architectural engineering, through M&E systems, to building physics & sustainability. He has also built up extensive experience of using planning policy, business strategies and regulatory frameworks to deliver sustainability win-win benefits.

He has more than 35 years of experience in the design and construction of the built environment. His continuing in-depth involvement in the design of fabric and systems for environmentally sensitive buildings, together with their 'Total Design' approach for integrating planning and policy, architecture engineering, and economics, has resulted in recognition as a world leader in this field. Chris has a unique combination of experience in policy formulation, planning, design and delivery of projects seeking to achieve advanced sustainability.

After 28 years at Arup, latterly as a director and Arup Fellow, he decided to set up his own specialist practice to focus on where sustainability is heading next. Based in China and Australasia for much 2010 to 2013, he has worked on numerous eco-cities, zero carbon and similar projects.

He has demonstrated the ability to recognise the most appropriate design, policy and business solutions by drawing on his extensive experience of applying locally suitable solutions in many different markets around the world.

SESSION 4: ENVIRONMENTAL ISSUES AND THE PUBLIC

304: Income growth and sustainable behaviour motivation in developing countries

Understanding the relationship according to the environmental kuznets curve (ekc): the case of Cairo, Egypt

AMIRA ELBORTOKALY[1], NIHAL ABDELGAWWAD[2], AHMED SHALABY[3]

1 Teaching Assistant, Architecture Department – Faculty of Engineering – Cairo University, Giza, amera_elbortokaly@yahoo.com
2 Lecturer Assistant, Architecture Department – Faculty of Engineering – Cairo University, Giza, nihal.abdelgawwad@hotmail.com
3 Professor of Architecture and Urban Development, Architecture Department – Faculty of Engineering – Cairo University, Giza, amshalaby@gmail.com

Enhancement of the urban environment quality has been the point of interest of numerous researches that studied and analysed the factors affecting sustainable practices and behaviours. The most prominent of which is the environmental Kuznets curve (EKC), that hypothesizes that environmental quality and sustainability are enhanced as income grows. However, the EKC seems to miss variables that may affect the environmental quality as public awareness and support for environmental protection. Additionally, it does not represent the majority of slower growing economies where consumerism is at its highest as in the case of developing countries. The paper focuses on Greater Cairo Region (GCR), Egypt as an example, where citizens live a consumer's lifestyle since the 1980s Sadat's liberalizing policies. The issue – among other triggering reasons as the over population of the CBD – that caused the swoop of suburbanization, represented in upscale gated communities providing only 10% of the housing stock scattered in the desert's outskirts, claiming to offer a more sustainable lifestyle for the high-income and luxury segments that present 8% of the country's population and receive almost 65% of the GDP. The research, accordingly, aims at examining the applicability of the EKC in a developing country's city and questions: do urban communities of high level income groups necessarily represent a more sustainable behaviour and environment than communities of lower level income groups?. To achieve the said aim, the paper compares the sustainability indices of two urban areas of high and low- income groups in GCR, through a multi-criterion framework (environmental, social, economic and institutional) for assessing these areas' sustainability. The framework includes quantitative indicators that can be measured simultaneously for the two chosen areas as the noise levels, quantity of solid waste generated, residential density, mean travel time and distance to work, etc. The paper concludes that income level clearly influences the sustainability of urban areas, however, in cities of developing countries, sustainability may be proven to be higher in urban areas with a lower income level where hidden potentials and motivation for sustainable behaviour can be found.

Keywords: Sustainability Index, Income Growth, Environmental Kuznets Curve (EKC), Developing Countries, Sustainable Behaviour, Consumption and Production Patterns

1. INTRODUCTION

Sustainability has become one of the most widespread slogans on the world's policy agenda. Almost all governments have included sustainability in their developments, by integrating economic welfare, environmental quality, social coherence and institutional effectiveness. Accordingly, a strong need for a comprehensive assessment of developments and dimensions that affect sustainability arouse. This assessment is of extreme importance to the extent that if cannot be clearly understood and addressed, will be problematic and will leave consequences hard to upgrade (Böhringer and Jochem, 2007: page 1). Despite that several bodies and organizations worldwide call for embracing more sustainable strategies, relatively little has been done on the practical level so far, attributing this to the fact that sustainability is a complex issue comprising several dimensions that cannot by fully understood and practically measured and evaluated (Azapagic and Perdan, 2000: page 243).

Several studies have been carried out to examine the effect of different developments on the sustainability of localities. Among the first relationships to take extensive and intellectual attention is the one between economic development and growth, environmental quality, and the achievement of a sustainable future (Howarth, 2012: page 32). In this course, the traditional economic theory posits that there exists a controversial relationship based on a trade-off between economic growth and environmental quality. However, rapidly expanding empirical and theoretical literature since the early 1990s suggests that this relationship could be positive (Lee et al., 2005: page 2). Since economic visionors first postulated a theoretical relationship between income changes and environmental quality, its representation in what is known as the Environmental Kuznets Curve (EKC) became the benchmark in almost all conversations and studies related to sustainability and environmental quality (Yandle et al., 2012: page 1). The primordial form of the EKC was first introduced by Simon Kuznets in 1954 while discussing "Economic Growth and Income Inequality." He suggested that as per capita income increases, income inequality and difference in income levels also increases, however, after reaching a certain turning point, income inequality starts to decline. Kuznets believed that the distribution of income becomes more unequal at early stages of income growth but that the distribution eventually moves back toward greater equality as economic growth continues (Kuznets, 1955: page 25). Accordingly, this changing relationship between per capita income and income inequality can be represented by a bell-shaped curve – now known as the Kuznets Curve – as in Figure 112.

In 1991, the Kuznets Curve occupied a new presence. Studies that examined the relationship between measured levels of environmental quality through certain indicators as the concentration of sulphur dioxide emissions, and per capita income proved that this relationship follows a distinctive pattern. The pattern implies that the environmental quality initially declines as poorer cities develop, but as the economic growth continues, a turning point in environmental decline is revealed, and thereafter, environmental quality improves as income increases. This relationship was figured out as economists were able to collect data on the environmental indicators for larger models of countries and income levels. Accordingly, another curve was plotted between the level of environmental degradation and measured per capita income. This new curve is proved to follow the same inverted U-shaped relationship as does income inequality and per capita income in the original Kuznets curve as in Figure 113 (Kahn, 2006: page 30). When first revealed, EKCs achieved an amazing effect and popularity. Prior to the advent of the EKCs, visionors believed that richer economies damaged and even destroyed their natural resources at a faster rate than poorer ones. They thought that higher environmental quality could only be achieved by giving up industrialization, as well as the desire for higher incomes. These contradictions between what was previously thought before the EKC and what the EKC tried to prove inspired further research. Knowledge about the ties between economic growth and environment are now far more than before 1991 (Yandle et al., 2012: page 3).

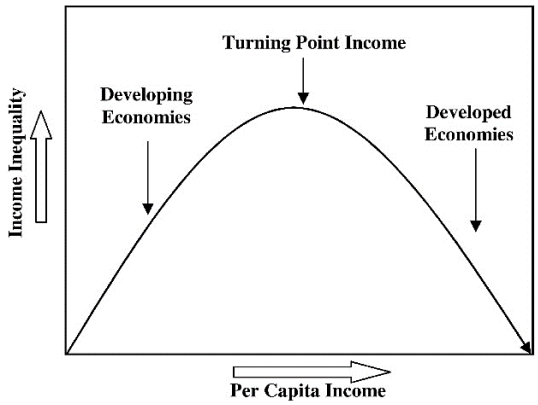

Figure 112: The general form of the original Kuznets curve (Yandle et al., 2012: page 2)

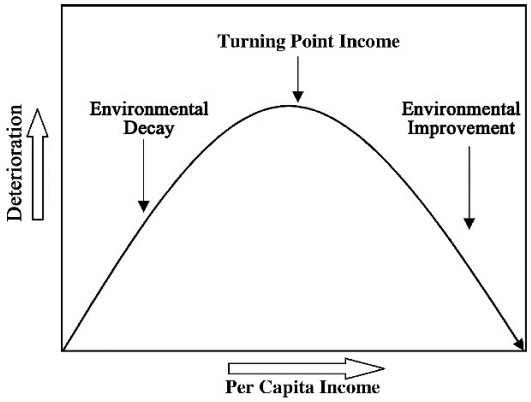

Figure 113: The environmental Kuznets curve (Yandle et al., 2012: page 3)

However, the EKC seems to neglect variables that may seriously affect the environmental quality, as public awareness and support for environmental protection. Moreover, it does not represent or signify the majority of slower growing economies where consumerism is at its highest form, as in the case of developing countries. Another point that should be taken into consideration is that EKC only deal with indicators of environmental quality, leaving behind other social and economic dimensions and indicators that can affect the environment. These facts can lead to a change in the main concept on which the EKC is based, which argues that with income growth environmental quality is enhanced. Accordingly, the purpose of this paper is dedicated mainly to empirically examine the relationship between income growth and various measures of the environmental quality in slower growing economies, i.e. developing countries, focusing on the case of Cairo, Egypt. However, prior to proceeding in the empirical study, it is worth clarifying and reviewing the meaning of sustainability and its fundamental measures.

Basically, the world's standard definition of environmental sustainability is sustainable development, which in turn is identified as the development which achieves both quality of life and lasting satisfaction of human needs under the condition that ecosystems are not threatened (Devuyst, 2000: page 96). Many cities around the world have fostered sustainable development plans for guiding their urbanization processes towards an enhanced future status of urban sustainability. Several sustainability indicators have been selected by various studies as key elements for measuring the performance of the practice. These indictors assist in defining how successful the strategies and policies imposed are, and whether they help in the achievement of sustainability objectives or not, as diverse practices use different indicators consistent with their particular needs and objectives (Shen et al., 2011: page 17). The concept of sustainability assessment is an ongoing continuous process that needs institutional arrangements (George and Kirkpatrick, 2007: page 25). This process is closely related to the context in which the development takes place and is developed through practical applications in order to merge into a framework of overall systems (Gibson et al., 2005: page 142). Several approaches of sustainability assessment have been proposed and derived in attempts to aid and evaluate the shift towards sustainability. Among these approaches – which are mostly oriented towards environmental assessment – are the environmental impact assessments (EIA), the strategic environmental assessment (SEA), the objectives-led SEA, the EIA-based integrated assessment, the objectives-led integrated assessment. However, lately, assessments based on integrated approaches are being used in addressing sustainability issues, these approaches include the social, economic and institutional dimensions, as the triple bottom line approach which covers environmental, economic and social dimensions (Pope et al., 2004: page 595). Different indicators have been compiled by Shen et al. (2011) to form a comprehensive list for assessment. The International Urban Sustainability Indicators List (IUSIL). The IUSIL includes a wide variety of indicators covering the four sustainable development dimensions; the environmental, economic, social and institutional. The list includes the quality of air, noise pollution, waste and water recycling as environmental indicators, consumption and production patterns, services and taxes prices as economic indicators, travel time, mode and distance, sense of safety, and social harmony as social indicators (Shen et al., 2011: pages 26-29).

Upon displaying the importance of an integrated approach for assessing the sustainability of developments, and reviewing the advent and development of the Environmental Kuznets Curve and the relationships it argues their existence, a number of questions are raised. The present research's objective is to answer these questions which are as follows:

- Does studying/analysing the relationship between income growth, income levels, and sustainability depend only on addressing the environmental quality as what Environmental Kuznets Curve implies?
- Does income growth or increase in the income level enhance the sustainable behaviour, which in turn affect sustainability as a whole?
- Are EKC's concepts applicable in the case of slow growing economies in the developing countries like Egypt?

2. METHODS AND DATA

To answer the questions previously set and to examine the applicability of the EKC in a developing country, the researchers limit the scope of the study to residential areas, as these area are where the sustainable behaviour can be monitored. Accordingly, the research progresses through four main consecutive stages. The first is the variables identification stage, it involves the selection of a group of relatively independent variables relevant to the sustainability of residential areas. The second stage is a multi-step statistical analysis to extract two sustainability assessment criteria (factors), one from the medium level income residents' point of view and the other from the high income level residents' point of view. The third stage involves the collection of data concerning the two extracted factors from the two study areas – the high and medium level income residential areas. Lastly, two pairs of sustainability indices are calculated for the two residential areas in order to analyse the sustainable behaviour of residents in relation to their income levels.

2.1 Identification of Variables

Based on the literature reviewed in the previous section, sustainability related issues – whether development, rating, or behaviour – must be studied and analysed as multi-dimensional involving environmental, economic, social, and institutional aspects. Accordingly, this stage of the study aims at reaching a suite of sustainability variables or indicators that are small in number, and as independent on each other as possible to obtain a reliable and comprehensive measurement of sustainability of a residential area. The study reviews a great body of literature that deals with sustainability indicators, it then complies those that are related to small scale urban areas. 28 independent sustainability variables or indicators are concluded, and categorized under the four main dimensions; environmental, economic, social, and institutional as in (Figure 114).

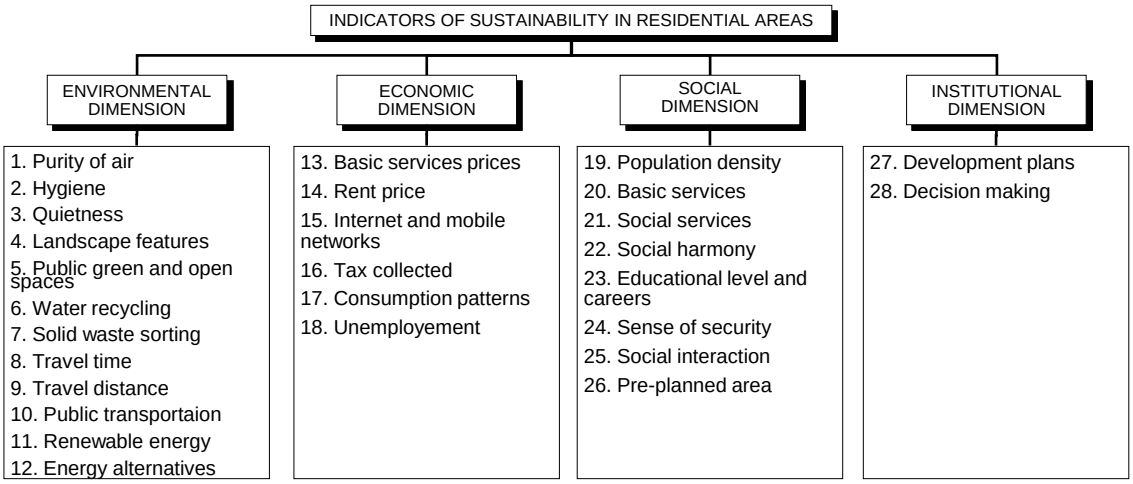

Figure 114: Indicators of sustainability in residential areas (The Authors)

2.2 Extraction of Sustainability Assessment Criteria (Factors)

In order to assess the sustainability of residential areas of two different income levels, two assessment criteria (factors) have to be used. This methodology is two-fold, it is adapted for two reasons: first, to examine whether residents of different income levels assess sustainability the same way or not, and second, it seems unfair to compare the sustainability of different areas in features and characteristics based on a fixed criterion for both areas, as what affects sustainability according to residents of medium level income is not necessarily relevant to residents of high level income.

The assessment criteria (factors) are extracted through a multi-step statistical analysis of the results of a questionnaire. Two identical questionnaires are distributed evenly among two samples of participants; one sample consists of 37 members who reside in medium level income neighbourhoods and areas in Cairo and Giza as Cairo Downtown area, el-Mohandesein, el-Manial, and el-Dokki, the other sample consists of 37 members who reside in high level income gated communities in 6th of October City, el-Sheikh Zayed City, and New Cairo City. The questionnaire is an indirect structured one that involves 28 Likert scale questions. Each question represents a variable and is translated in the questionnaire as a factor that affects the sustainability of the residential area. Each respondent is then asked to mark in the Likert scale whether this factor has no, a little, or a large impact on his/her area's sustainability from his/her point of view. To perform statistical analysis, the results of the questionnaires are transformed into numerical values in which no, little, and large impacts are given the values 0, 1, and 2 respectively.

Using SPSS (Statistical Package for the Social Science) program, the extraction of sustainability assessment factors is preceded by a KMO and Bartlett's Test to examine the sampling adequacy that turned above 0.5 for both samples which is considered the bare minimum. The statistical analysis of each questionnaire's results is then proceeded by the application of a three-round factor analysis to the values assigned by the participants to the 28 variables previously mentioned. Each round of the factor analysis helps in reducing the number of insignificant variables affecting the assessment of sustainability (from each income level group's point of view) by suppressing variables that score coefficients below 0.4 in each round. The third round of factor analysis for each sample results in a minimum number of variables that prove to be affecting the sustainability of residential areas. For each variable of the final round, the statistical analysis calculates a coefficient by which this variable contributes in the sustainability index. The sustainability index in turn represents a value calculated for each area and constitutes its ranking among other areas compared with the same variables and same coefficients.

Table and Table 31 show the factors extracted for the medium and high level income sustainability respectively. For the medium level income factor, variables that scored the highest coefficients (above 0.5) are the variables related to the use of clean energy sources and recycling, followed by variables that assure the existence in a healthy social context that offers social services, social interaction, moderate consumption level, adequate public transport systems, short travel time, and public green and open areas outside the area that residents can easily access. For the high level income factor, variables that scored the highest coefficients (above 0.5) are the variables related to the design of the residential area as the population density, quietness and the existence of the residential unit in a pre-planned area own by a reliable and a reputable body, and the richness of the landscape of the area. Social harmony and the high educational level and reputable professions of neighbours, and the sense of security also scored high among the variables selected by the members of the high level income group.

Table 30: Medium level income sustainability component matrix[a]

Variable Code	Variable Name	Variable Coefficient
V01	Purity of Air	---
V02	Hygiene	---
V03	Quietness	---
V04	Landscape Features	---
V05	Access to Public Spaces Outside Area	0.552
V06	Water Recycling	0.591
V07	Solid Waste Sorting	---
V08	Short Travel Time	0.506
V09	Short Travel Distance	0.439
V10	Public Transportation	0.557
V11	Renewable Energy	0.625
V12	Energy Alternatives	0.651
V13	Basic Services Low Prices	---
V14	Low Rent Prices	---
V15	Access to Internet & Telephone Networks	0.470

Table 31: High level income sustainability component matrix[a]

Variable Code	Variable Name	Variable Coefficient
V01	Purity of Air	---
V02	Hygiene	---
V03	Quietness	0.774
V04	Landscape Features	0.571
V05	Access to Public Spaces Outside Area	---
V06	Water Recycling	---
V07	Solid Waste Sorting	---
V08	Short Travel Time	---
V09	Short Travel Distance	---
V10	Public Transportation	---
V11	Renewable Energy	---
V12	Energy Alternatives	---
V13	Basic Services Low Prices	0.710
V14	Low Rent Prices	0.409
V15	Access to Internet & Telephone Networks	0.49

V16	Low Taxes	0.416
V17	Moderate Consumption Patterns	0.544
V18	Low Unemployment Level	0.425
V19	Low Population Density	0.407
V20	Access to Basic Services	---
V21	Access to Social Services	0.576
V22	Social Harmony	0.533
V23	High Educational Level & Reputable Careers	---
V24	High Security Level	0.470
V25	Social Interaction	0.596
V26	Pre-planned Area	---
V27	Development Plans	---
V28	Decision Making	---

Extraction Method: Principal Component Analysis.
a. 1 components extracted.

V16	Low Taxes	---
V17	Moderate Consumption Patterns	---
V18	Low Unemployment Level	---
V19	Low Population Density	0.885
V20	Access to Basic Services	---
V21	Access to Social Services	---
V22	Social Harmony	0.595
V23	High Educational Level & Reputable Careers	0.669
V24	High Security Level	0.58
V25	Social Interaction	---
V26	Pre-planned Area	0.750
V27	Development Plans	---
V28	Decision Making	---

Extraction Method: Principal Component Analysis.
a. 1 components extracted.

2.3 Study Areas and Collection of Data

Two residential areas, a high level income area and a medium level income one are chosen to apply the two extracted factors and to calculate the sustainability indices to examine the relationship between income growth and sustainable behaviour. Hay el-Ashgar (an Arabic translation for the Trees District) gated compound in 6th of October City and a sector of Cairo downtown area are chosen to be studied as the high and medium level income study areas respectively (Figure 115). The medium level income group represents citizens who earn an average monthly income of around 2000 EGP equivalent to 2600 $ (USD) and 170 £ (GBP), while high level income group represents those whose average monthly income is around 5000 EGP equivalent to 650 $ (USD) and 420 £ (GBP) (ElHusseiny, 2004: page 160). The study excluded the other two income level groups; the low and elite ones as they represent two extremes which would lead to unreliable readings and analysis.

Hay el-Ashgar is a gated compound of an area of 200 feddans (84 hectares), 90% of the area dedicated to residence is constituted of apartment blocks of areas 120 to 215 m^2, another 7% is constituted of townhouses, the remaining 4% is constituted of detached villas (Sims, 2005: page 30). The compound is very well-known as it represents the first compound planned and built in the 1990s in the range of gated communities dedicated to high level income residents in the desert's outskirts of Cairo. On the other hand, the sector chosen in Cairo downtown is of an area of 211 feddans (88.7 hectares). The area is formerly known as the major business and commercial district in the city of Cairo as it includes a diversity of land use. Mixed use constitutes the majority of downtown's land use as 48% of the buildings are registered as commercial/residential ones, located along the major axes and squares. The second and third highest percentages of buildings are occupied by office and exclusively residential use, representing 15.8 and 14% respectively of the total number of buildings in the area (Institut de Recherche pour le Développement, 2002: page 4/9). Due to the mixed use nature of the downtown area, and its containment of proximity to a large number of public and governmental buildings, and the decrease in the rents after 1952 revolution, the area became one of the most crowded spots of the city, the fact that expelled the elite out and replaced them with medium level groups (El Kadi, 2012: page 86)

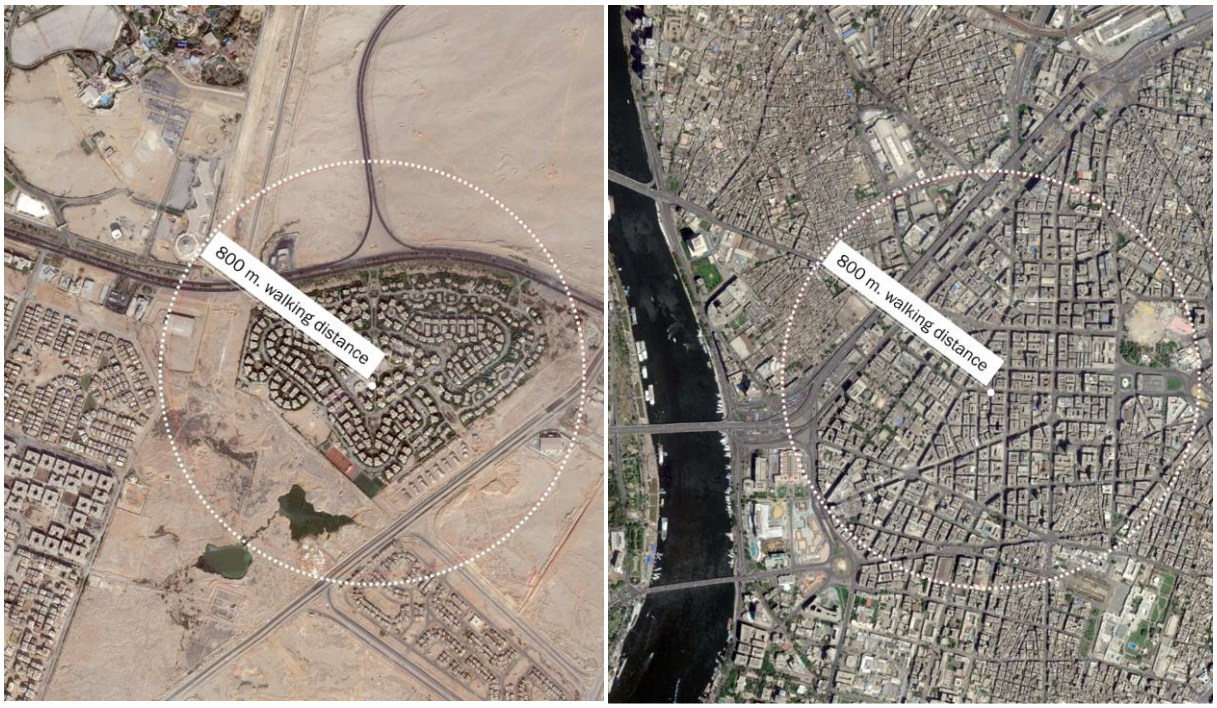

Figure 115: The two selected study areas, Hay el-Ashgar (L) and Downtown Cairo (R) (Google Earth, 2015)

In order to assess the sustainability indices of both selected areas, two factors or assessment criteria are extracted as previously elaborated. However, it is impossible to compare the two sustainability indices that are calculated, as each index is derived from a factor different than the other. Accordingly, to be able to compare the sustainability indices calculated for the two chosen areas through two different factors, two pairs of sustainability indices are computed for the two areas using the two extracted factors. These two pairs of indices include two sustainability indices for Hay el-Ashgar computed one time using the factor extracted for the high level income group point of view, and the other time using the other factor extracted for the medium level income group point of views. The same procedure is then applied to the Downtown Cairo area to obtain the other pair of indices. This methodology helps in performing a multi-level comparison between the indices (Figure 116). One level of comparison is between the two sustainability indices of the same residential area to examine the differences in the sustainability assessment according to the different income groups. The other level of comparison is between the sustainability indices of the two chosen areas when computed using the same factor to examine which will score higher according to the factor used in calculations.

The calculation of the sustainability index for each of the two chosen areas is carried out by the authors, in which each variable in the two extracted factors is measured and given a value according to the methods shown below (

Table 32: Study variables and data

). By using the coefficients obtained for each variable in the two extracted factors in the previous steps of analysis, the reading of each variable is multiplied by its coefficient. Finally, the actual values of variables of each factor (coefficient multiplied by reading) are all added together to give the sustainability index for each of the two chosen areas.

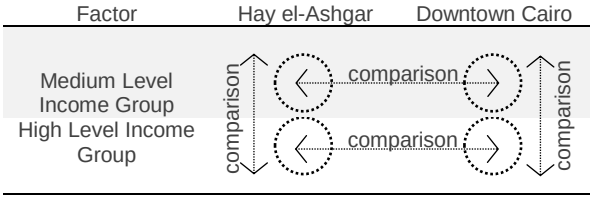

Figure 116: Methodology of sustainability indices comparison (The Authors)

Table 32: Study variables and data

Variable Code	Variable Name	Description	Method of Measurement
V03	Quietness	Noise level in a main street at 14:00 hrs. compared to allowed levels[1]	Researchers by measuring noise level in dB using noise level measuring apparatus divided by 60 dB in downtown and 50 dB in gated compounds[1]
V04	Landscape Features	Landscape features (tress, grass, fountains, …) areas	Researchers by measuring % of landscape features areas (trees, grass, fountains, …) to total area (variable is given 1 if 30%, 2 if >30%, -1 if <30%)
V05	Public Spaces Outside Area	Access to public green and open spaces within 800 m./a 15 minute-walk[2]	Researchers by measuring % of public green and open spaces areas to the 800 m. radius circle's area (variable is given 1 if 15%, 2 if >15%, -1 if <15%, 0 if none)
V06	Water Recycling	Omitted variable due to shortage of information and lack of implementation systems in Egypt	
V08	Travel Time	Average time consumed to reach work or frequent services from residence	Researchers through a questionnaire asking about the average travel time of 10 residents (variable is given 1 if moderate, 2 if short, -1 if long)
V09	Travel Distance	Average distance to work or frequent services from residence	Researchers through a questionnaire asking about the average travel distance of 10 residents (variable is given 1 if moderate, 2 if short, -1 if long)
V10	Public Transport-ation	Access to public transport stations within 800 m./a 15 minute-walk	Researchers by counting the number of public transport stations
V11	Renewable Energy	Omitted variable due to shortage of information and lack of implementation systems in Egypt	
V12	Energy Alternatives	Omitted variable due to shortage of information and lack of implementation systems in Egypt	
V13	Basic Services Prices	Average electricity bill compared to monthly income	Researchers through a questionnaire asking about the average % of electricity bill of average monthly income (variable is given 1 if moderate, 2 if low, -1 if high)
V14	Rent Prices	Average rent price of apartment/villa/townhouse	Researchers through a questionnaire asking about the average current rent amount inside area (variable is given 1 if moderate, 2 if low, -1 if high)
V15	Internet & Telephone Networks	Access to internet and mobile connections	Researchers through a questionnaire asking about the availability of internet and mobile connections (variable is given 1 if available, 0 if not available)
V16	Taxes	Average tax collected per month in return of supplementary services	Researchers through a questionnaire asking about the average % of tax collected of 10 residents per month of average monthly income (variable is given 1 if moderate, 2 if low, -1 if high)
V17	Consumption Pattern	Domestic merchandise consumption	Researchers through a questionnaire asking about the average % of domestic merchandise consumption of average monthly income (variable is given 1 if moderate, 2 if low, -1 if high)
V18	Unemploy-ment Level	Omitted variable due to shortage of reliable statistical information and difficulty of measurement	
V19	Population Density		Number of residents per unit area (feddan) (variable is given 1 if 100, 2 if <100, -1 if >200)
V21	Social Services	Access to social services (library, social club,….) within 800 m./a 15 minute-walk	Researchers through measuring % of social services area within 800 m. of standard required area
V22	Social Harmony	Existence of homogeneous social classes	Researchers through a questionnaire asking about the evaluation of extent of social harmony (variable is given 1 if Yes, 0 if No)
V23	Educational Level & Careers	High level of education and reputable careers	Researchers through a questionnaire asking about the evaluation of level of education and careers reputation (variable is given 1 if Yes, 0 if No)

V24	Security Level	Sense of security and safety	Evaluation of level of security (variable is given 1 if Yes, 0 if No)
V25	Social Interaction	Rate of existence of social interaction venues	Researchers through measuring the gross area of cafés /population (variable is given 1 if 0.05, 2 if >0.05, -1 if <0.05)[3]
V26	Pre-planned Area	Existence of residential unit in a pre-planned area	Researchers through investigating the existence of pre-planning party (variable is given 1 if Yes, 0 if No)

Any questionnaire involves 10 residents in each study area
[1] Allowed noise levels according to the Egyptian law no. 4 for the year 1994 on the protection of the environment
[2] 800 m. corresponding to a 15 minute-walk is measured from the centre of the area according to New Jersey Department of Transportation (1994)
[3] 0.05 m^2 is the minimum rate of social services per person

2.4 Calculations of Sustainability Indices

In this stage, site visits were performed by the authors where readings for the previously discussed variables were recorded according to methods and descriptions mentioned before. Table 33 and Table 34 represent the steps by which the sustainability index of each of the two area is calculated. In each table the first column indicates the variables, the second and third columns represent the coefficients extracted for the selected variables by each income level group in the second stage. The fourth column is the core of this stage, its represents the readings of each variable. The fifth and last columns indicate the sustainability index for each residential area, calculated by multiplying each variable coefficient and its reading then adding all values to obtain one index.

Analysing the readings of the variables can give insights to the physical and social features of the two areas. Downtown Cairo scored higher in the noise level (V03) than Hay el-Ashgar, due to the fact that its streets are occupied by a large number of private cars and public transport vehicles. In the same course, the Downtown area's density (V19) came out greater than 100 persons/feddan and thus was given the value -1, compared to the very low population density of Hay el-Ashgar (whose occupancy is approximately 30%) which was given the value 2. Concerning travel time and distances, the majority of respondents in downtown work in areas near the CBD and consume moderate travel time (around 30 minutes) in reaching their daily trips to work, thus these variables (V08 and V09) were given the value 1. On the contrary, the majority of respondents in Hay el-Ashgar assured that they work in areas far away from the compound (12 to 30 km) (7 to 19 miles), mostly in the CBD, consuming an average of 90 minutes per day to reach their work, thus the variables were given the value -1. Addressing the landscape aspect, Downtown Cairo's high population density gives limited chances for landscaped spaces inside the area, on the contrary, a considerably large area in hay el-Ashgar is dedicated to landscape, thus this variable (V04) is given the values -1 and 2 for the downtown area and Hay el-Ashgar respectively. Concerning the economic level, most respondents in the downtown area confirmed that they pay a low electricity bill, while in Hay el-Ashgar, the majority of respondents agreed that the electricity bills are average, thus this variable (V13) is given the values 2 and 1 for the downtown area and Hay el-Ashgar respectively. The same procedure is applied for all the variables to obtain the readings in the two following tables.

Table 33: Data and Sustainability Indices (SI) of Downtown Cairo

Variable Code	High Level Income Coeff.	Medium Level Income Coeff.	Readings	High Level Income SI	Medium Level Income SI
V03	0.774	0	1.33	1.032	0
V04	0.571	0	-1	-0.571	0
V05	0	0.552	2	0	1.104
V06	0	0.591	0	0	0
V08	0	0.506	1	0	0.506
V09	0	0.439	1	0	0.439
V10	0	0.557	6	0	3.342
V11	0	0.625	0	0	0
V12	0	0.651	0	0	0
V13	0.71	0	2	1.42	0
V14	0.409	0	1	0.409	0
V15	0.49	0.47	1	0.49	0.47
V16	0	0.416	-1	0	-0.416
V17	0	0.544	2	0	1.088

Table 34: Data and Sustainability Indices (SI) of Hay el-Ashgar

Variable Code	High Level Income Coeff.	Medium Level Income Coeff.	Readings	High Level Income SI	Medium Level Income SI
V03	0.774	0	1.1	0.851	0
V04	0.571	0	2	1.142	0
V05	0	0.552	0	0	0
V06	0	0.591	0	0	0
V08	0	0.506	-1	0	-0.506
V09	0	0.439	-1	0	-0.439
V10	0	0.557	0	0	0
V11	0	0.625	0	0	0
V12	0	0.651	0	0	0
V13	0.71	0	1	0.71	0
V14	0.409	0	-1	-0.409	0
V15	0.49	0.47	1	0.49	0.47
V16	0	0.416	1	0	0.416
V17	0	0.544	1	0	0.544

V18	0	0.425	0	0	0
V19	0.885	0.407	-1	-0.885	-0.407
V21	0	0.576	0	0	0
V22	0.595	0.533	0	0	0
V23	0.669	0	0	0	0
V24	0.58	0.47	0	0	0
V25	0	0.596	2	0	1.192
V26	0.75	0	1	0.75	0
				2.645	**7.318**

V18	0	0.425	0	0	0
V19	0.885	0.407	2	1.77	0.814
V21	0	0.576	0	0	0
V22	0.595	0.533	1	0.595	0.533
V23	0.669	0	1	0.669	0
V24	0.58	0.47	1	0.58	0.47
V25	0	0.596	1	0	0.596
V26	0.75	0	1	0.75	0
				7.148	**2.898**

3. RESULTS

Different income level groups assess sustainability from different point of views and this is obvious from the results of the questionnaires distributed among high and medium level income groups. Figure 117 elaborates this through comparing the scores (coefficients) of variables in the two extracted factors. As for the factor extracted from the medium level income group questionnaire results, variables that scored the highest coefficients (above 0.5) are the variables related to the use of clean energy sources and recycling, followed by variables that assure the existence in a healthy social context that offers social services, social interaction, moderate consumption level, adequate public transport systems, short travel time, and public green and open spaces outside the area such that residents can easily access them. On the other hand, in the factor extracted from the high level income group questionnaire, variables that scored the highest coefficients (above 0.5) are the variables related to the design of the residential area as the population density, quietness and the existence of the residential unit in a pre-planned area owned by a reliable and a reputable body, and the richness of the landscape of the area. Social harmony and the high educational level and reputable professions of neighbours, and the sense of security also scored high among the variables selected by the members of the high income level group.

Results that also echo the previous one are the values of sustainability indices (SI) calculated in the previous stage of the study. Comparing the four calculated sustainability indices, it is noted that the high level income group area (Hay el-Ashgar) scored higher in SI (7.148) than the medium level income group area (Downtown Cairo) (2.898) when the SI is calculated using the high level income factor. This indicates that members of the high level income group considers Hay al-Ashgar a more sustainable area than Downtown Cairo, and that Hay el-Ashgar residents' behaviours are more sustainable than those of Downtown Cairo. The same is noticed for the medium level income group area, which scored almost the same value of SI (7.318) when calculated using the medium level income factor, while the high level income group area scored lower (2.645) using the same factor in the SI calculation. This indicates that members of the medium level income group considers Downtown Cairo a more sustainable area than Hay el-Ashgar, and that its residents' behaviours are more sustainable than those of Hay el-Ashgar.

Difference in the comprehension and appreciation of sustainability according to the income level is also revealed from the number of variables chosen in the questionnaires. The high level income respondents chose variables that are much less in number than those chosen by the medium level income respondents. This indicates the appreciation of the medium level income groups to every variable affecting sustainability and their feeling of sustainable behaviour importance.

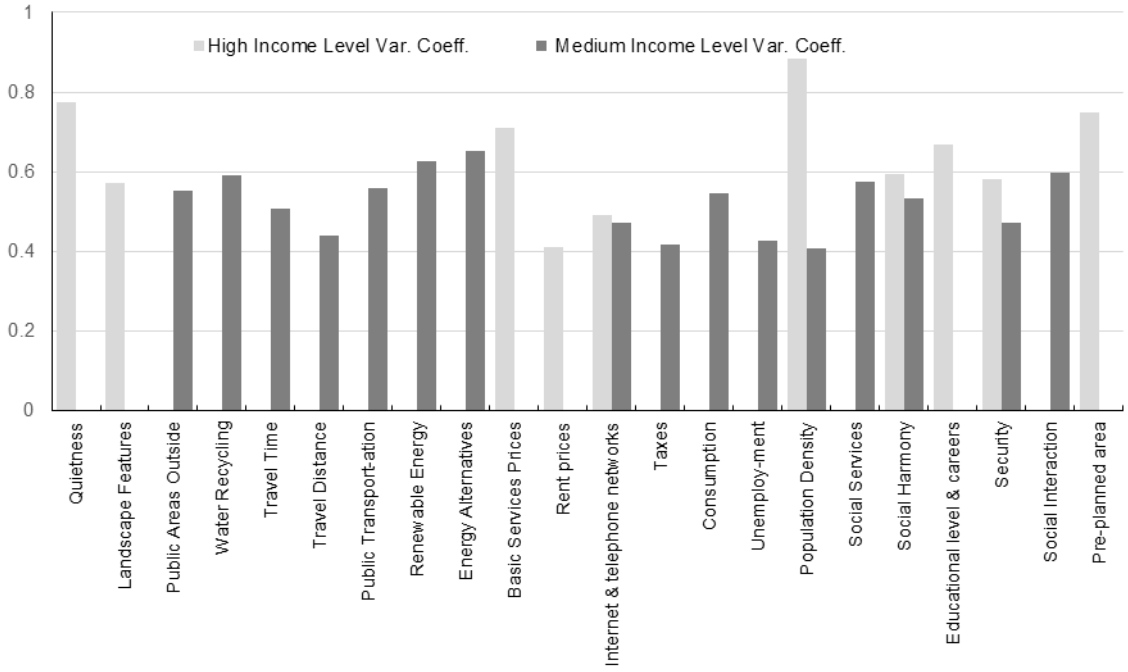

Figure 117: Variables scores in the two extracted factors of the different income groups

4. DISCUSSION

The methodology, statistical analysis, and quantitative approach of the research succeeded in enabling the researchers to judge – to a great extent – the relationship between income growth and the sustainable behaviour of residents. The same methodology and steps can be used to calculate and compare SI for different areas f approximately the same areas. Through the calculated values of SI, the study was able to conclude that high income level groups assess sustainability based on a consuming individual preference, as they chose the design of the residential area, population density, richness of the area's landscape, social harmony, high educational level and reputable professions of neighbours as the variables that most affect sustainability. On the other hand, they marginalized relatively important variables that can noticeably affect sustainability. This fact obviously appeared in their ignoring for most of the important variables in the environmental dimension such as the purity of air, and water and wastes recycling. However, medium income groups seemed to assess sustainability based on moderation. Their choices of variables are oriented towards applying – even without acknowledging – the principals of the New Urbanism and compacted cities, as living in a dense area and a healthy social context with adequate transit systems and moderate consumption.

Much of the consumption patterns exercised by the Egyptian consumers and discussed above are governmentally based. In Egypt, as a developing country, and since Sadat's liberalizing policies, market forces orient people towards scaling up their consumption instead of purchasing high quality items in less quantities. This sounds unlike what EKC assumed, that with income growth, more sustainable choices are taken represented in high quality consumption patterns a s a result of higher educational levels and awareness of consumers.

5. CONCLUSION

This research represents a response to the call for sustainability assessments that consider social, economic and institutional dimensions of the context. Through a quantitative analysis and calculations, the study integrated all of the four dimensions and extracted one SI that can be related to the income level and growth. Accordingly, the research proved that sustainability assessment and indices do not merely represent values and numbers extracted from analysis. They rather represent indicators that should be compared with each other, and that governments and decision makers should notice and give concern in order to enhance their environments' quality for better future. However, the study does not represent a comprehensive methodology for quantitatively measuring the SI of large areas and scales as cities. Accordingly, the research suggests

building upon the methodology used herein to reach a methodological quantitative approach for comparing sustainable behaviour in large scale localities.

6. REFERENCES

AZAPAGIC, A. & Perdan, S., 2000. Indicators of Sustainable Development for Industry: A General Framework. *Process Safety and Environmental Protection,* 78**,** 243–261.

BÖHRINGER, C. & Jochem, P., 2007. Measuring the Immeasurable: A Survey of Sustainability Indices. *Ecological Economics,* 63**,** 1-8.

DEVUYST, D., 2000. Linking Impact Assessment and Sustainable Development at the Local Level: The Introduction of Sustainability Assessment Systems. *Sustainable Development,* 8**,** 67-78.

EL KADI, G., 2012. *Le Caire, Centre en Mouvement,* Marseille, IRD Éditions: Institut de Recherche pour le Développement.

ELHUSSEINY, N. 2004. *Evaluation Criteria for the Marketing Trends of Real Estate Investment Projects - A Marketing Feasibility Study to Achieve a Balance of Supply and Demand in New Urban Communities - Case Studies: 6th of October and Sheikh Zayed Cities.* Masters of Science, Cairo University.

GEORGE, C. & Kirkpatrick, C. H. (eds.) 2007. *Impact Assessment and Sustainable Development: European Practice and Experience,* Cheltenham: Edward Elgar Publishing.

GIBSON, R. B., Holtz, S., Tansey, J., Whitelaw, G. & Hassan, S., 2005. *Sustainability Assessment: Criteria, Processes and Applications,* London, Earthscan.

HOWARTH, R. B., 2012. Sustainability, Well-Being, and Economic Growth. *Minding Nature - Center for Humans and Nature,* 5**,** 32-39.

INSTITUT DE RECHERCHE POUR LE DÉVELOPPEMENT, 2002. *Heritage Conservation and Management in Egypt and Syria (HERCOMANES),* Cairo, Center for Architectural and Engineering Design Support - Faculty of Engineering - Cairo University.

KAHN, M., 2006. *Green Cities: Urban Growth and the Environment,* Washington, D.C., Brookings Institution Press.

KUZNETS, S., 1955. Economic Growth and Income Inequality. *The American Economic Review,* 45**,** 1-28.

LEE, H.-H., Chung, R. K. & Koo, C. M. On the Relationship between Economic Growth and Environmental Sustainability. The 5th Ministerial Conference on Environment and Development in Asia and the Pacific, 2005 Seoul, Korea.

NEW JERSEY DEPARTMENT OF TRANSPORTATION, 1994. *Planning for Transit-Friendly Land Use: A Handbook for New Jersey Communities,* New Jersey, New Jersey Department of Transportation.

POPE, J., ANNANDALE, D. & MORRISON-SAUNDERSB, A., 2004. Conceptualising Sustainability Assessment. *Environmental Impact Assessment Review,* 24**,** 595–616.

SHEN, L., OCHOA, J. J., SHAH, M. N. & ZHANG, X., 2011. The Application of Urban Sustainability Indicators - A Comparison between Various Practices. *Habitat International,* 35**,** 17-29.

SIMS, D., 2005. Guide to Field Work for First Registration in Nasr City, Sixth of October, and El Maadi - Egypt Financial Services Project. United States Agency for International Development (USAID).

YANDLE, B., VIJAYARAGHAVAN, M. & BHATTARAI, M., 2012. The Environmental Kuznets Curve: A Primer. *PERC Articles (Property and Environment Research Center)*.

202: Empirical study of the energy saving potentials in Shanghai residential buildings through human behaviour change

XINGXING ZHANG[1], JINGCHUN SHEN[1], JINLU SI[1], TONG YANG[1], WU DENG[1], LLEWELLYN TANG[1], YUPENG WU[2]

[1] *Department of Architecture and Built Environment, University of Nottingham, China, 199 Taikang East Road, Ningbo, 315100, China. Xingxing.zhang@nottingham.edu.cn; Jingchun.Shen@nottingham.edu.cn; zy09747@nottingham.edu.cn; Tong.Yang@nottingham.edu.cn; Wu.Deng@nottingham.edu.cn; Llewellyn.Tang@nottingham.edu.cn*

[2] *Department of Architecture and Built Environment, University of Nottingham, UK, NG7 2RD Yupeng.Wu@nottingham.ac.uk*

Smart meters and in-home displays (IHD) have been recently adopted to help give residential consumers more control over energy consumption, and to help meet environmental and security of supply objectives. The paper aims to identify the effectiveness of smart meters and real-time IHDs in reducing Shanghai household energy consumption. A first pilot in Shanghai city with an effective sample of 131 respondents was arranged to two groups as IHD households and non-IHD households. A statistical analysis model was developed to investigate the characteristics and the regulations of electricity consumption in these two groups, such as check frequency, electricity consumption reduction and shifting, energy bill saving, and standby power. The research results demonstrate IHD could lead to around 9.1% (11.0%) in reduction of monthly electricity consumption (bill). A general comparison of the electricity consumption reduction between this research and the average UK case was further made. The overall research is expected to contribute some empirical evidence on how IHD feedback could influence household electricity consumption in the Chinese context. It will further provide a social-technical basis for the electricity-economic leverage of government and the bidding competitiveness of power-related industries.

Keywords: In-home display; Residential building; Behaviour change; Electricity consumption.

Nomenclature

ave	average	***Greek***	
C	current, A	*σ*	standard deviation
d	daily		
h	hourly	***Subscripts***	
k	day number	*B*	electricity bill
m	monthly	*cf*	check frequency
max	maximum value	*E*	electricity energy
min	minimum value	*i*	recording number
n	number of household with IHD	*j*	hour number
N	number of household without IHD	*on-peak*	on-peak period
p	power, W	*off-peak*	off-peak period
R	ratio	*sb*	standby
V	voltage, V		

1. INTRODUCTION

Climate change and energy security have defined the landscape of energy policy in the 21st century. With its potential for reducing carbon emissions and strengthening energy security, energy demand reduction is essential to the low-carbon energy transition. Moreover, by avoiding the need for additional energy infrastructure, lower energy demand can enhance the economic efficiency of energy system. On the international level, while there is extensive experience of employing policies (e.g. energy performance standards, labelling and various subsidies) to increase the market penetration of efficient products, there is an emerging policy interest in influencing how energy is used at the consumer end. One strategy is to provide consumers with feedback on their energy use, with the aim of increasing the visibility of energy consumption and mediating energy-conservation actions. The energy feedback can be given in many ways: in-home displays (IHDs), mobile phone applications, websites, enhanced or informative bills, ambient displays and so forth. They may differ in many important aspects such as the content (e.g. current/historical consumption levels, costs), format (e.g. in numbers or graphs) and frequency (e.g. real-time) of feedback.

There is abundant evidence in the existing literature on the potential of energy feedback in promoting energy demand reductions. Darby found the ranges for energy savings to be 5-15% and 0-10% for direct and indirect feedback programmes respectively (Darby, 2006). In the review of 91 international feedback-only programmes, VaasaETT found those involving IHDs, websites and informative billing/leaflets had achieved the average energy use reduction of 8.54%, 5.35% and 4.72% (Lewis et al., 2014). An earlier study of VaasaETT also analysed how energy feedback could influence the impacts of time-of-use (TOU) tariffs (Dromacque, 2012). Based the review of over 200 TOU trials, it found that total energy consumption for TOU projects with some kind of energy feedback was lower by 4% whereas those without energy feedback saw 1% increase in total energy use, and that reduction in peak electricity use in TOU projects with energy feedback is on average 40% higher than those without any form of feedback. Similarly Faruqui et al., discovered in their review of international IHD programmes that the average rate of energy saving in these programmes is around 7% if prepayment is not involved, and that IHDs have the potential of enhancing 'the impact of time-of-use rates' (Faruqui et al., 2010: p.1598-1608). Besides such quantitative assessments of the impacts of energy feedback on energy use, other scholars employ more qualitative approach to understanding of the process whereby energy feedback promotes demand reduction, thus underlining the socio-technical underpinnings of energy feedback (Hargreaves et al., 2010: p.6111-6119).

Energy feedback sits at the heart of the policy of many countries to promote energy demand reduction. For instance, in the European Union, the Energy Efficiency Directive coming into effect in 2012 requires metering systems to provide information of energy consumption on 'actual time of use' and historical consumption data (European Parliament & EU Council, 2012). In UK, IHDs will be provided as part of the smart metering rollout to domestic consumers, thus enabling them to manage and eventually reduce their

electricity and gas consumption (DECC Energy Trends, 2011). Many IHD programmes, with or without pricing products, have also been set up in North America and Asia (Hargreaves et al., 2010: p.6111-6119). While considerable progress has been made in China in terms of rolling out smart or advanced metering infrastructure, the focus seems to be on the technical or engineering aspects of development. In fact there seems to be a lack of evidence or study on whether and how energy feedback, especially that enabled by smart metering technologies like IHDs, could influence the residential energy use in China.

The electricity use in the residential sector takes up only a small share in the total final electricity use in China. Based on the electricity consumption data published by the National Energy Administration, households consumed 679.3 TWh in 2013, constituting only about 12% of the total electricity use nationwide (China Energy Monthly Report, 2014). While the share of residential electricity use is relatively small, there is still great value in exploring the potential of reducing household electricity consumption, through energy feedback and/or others. Firstly, the absolute value of residential electricity use is significant, which is more than twice the total final electricity consumption of the UK in 2013 (DECC Energy Investment Report, 2014). Secondly, the annual growth rate of residential electricity use reached 9.2%, outpacing the rate of increase of 7.5% averaged across all sectors in China. With the trend of urbanization going on, there is prospect for the residential sector taking up higher shares in the total electricity use.

This paper reports on the results of a first IHD pilot in Shanghai, which is intended to contribute empirical evidence on how energy feedback could influence household electricity consumption in the Chinese context. It implemented the smart meter and IHDs based on the information and communication technologies (ICTs) in order to identify the residential behaviour change behind electricity consumption. The research result is expected to lead residents to become more aware of their energy consumption, change their corresponding behaviours, and provide social-technical basis for future economic leverage of government and the bidding competitiveness of power-related industries. Figure 1 shows the main significance of this research.

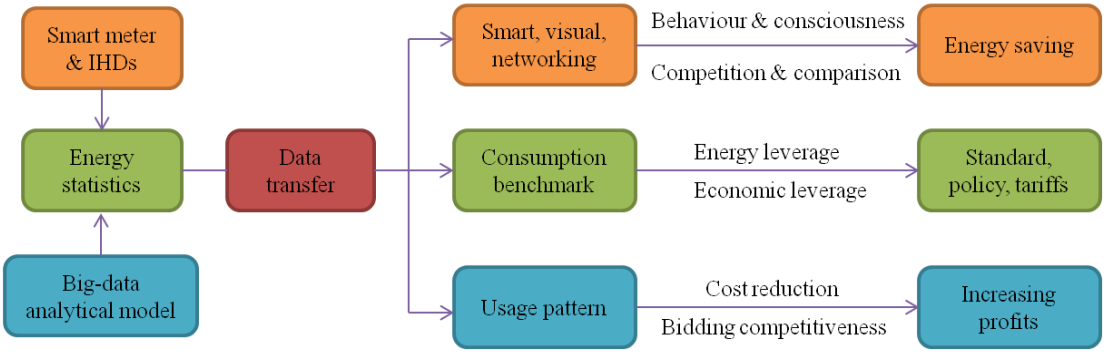

Figure 1: Primary research significance of the smart meter and IHD

2. TECHNOLOGY BEHIND THE PILOT

It is clear about the importance of immediate feedback in making energy information more visible and more amenable to understanding and control. Philip Lewis indicated that consumption reduction is highest for real time feedback while other feedback channels such as web pages and informative bills are a valuable addition to IHDs. Savings from web pages are around half that of IHDs. The ICT based smart meter and IHD framework is therefore proposed as an efficient way of contributing to above objectives. Figure 2 presents the real images of key devices that were utilized in the pilot project, such as IHD, smart meter and their onsite installation. Schematic of the smart meter and the IHD framework is illustrated in Figure 3. The whole system includes the smart meter unit, IHDs, data transfer network, three databases, statistical analytical unit, web server and customers' personal computers. The electricity data is automatically collected by the smart meter from the individual electricity box in each household and further transmitted to the IHDs and the GPRS terminals through the ZigBee network. Thanks to the GPRS terminals, a remote and secure transmission of the electricity data to the databases can be achieved. There are three databases established in this system: (1) the first database is to store the raw electricity data from the GPRS terminals; (2) the second database is designed for storage of the statistical data; and (3) the third database has the function to store the background information of the pilot, such as customer account, household information, home appliances, building location, collecting point IP address. A website based interface

(http://www.ihomee.com.cn/) is also developed for customers to check energy bills online, compare local energy utilization, save history electricity data, and seek potential energy-saving suggestions. The pilot has been conducted on first generation display products consisting of functions like weather conditions, room air temperature, numeric displays and CO_2 savings on the environment. Best practice concerning IHDs and the frameworks are continuing to improve. Savings from IHDs are therefore expected to improve further in the future develops.

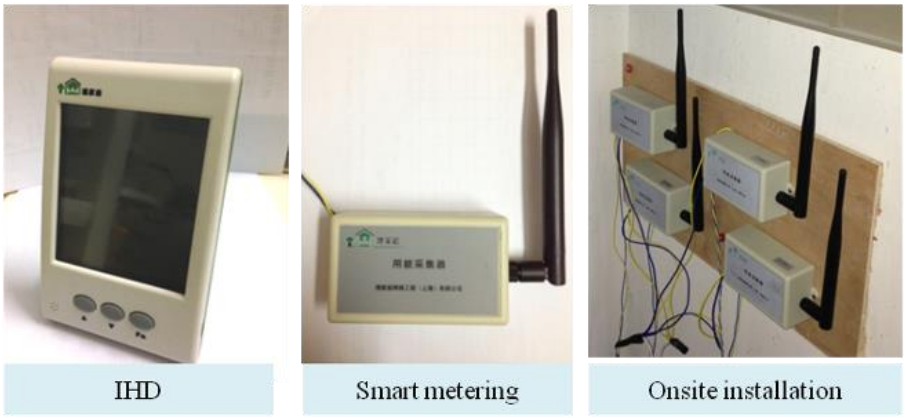

Figure 2: Real images of IHD, smart meter and onsite installation

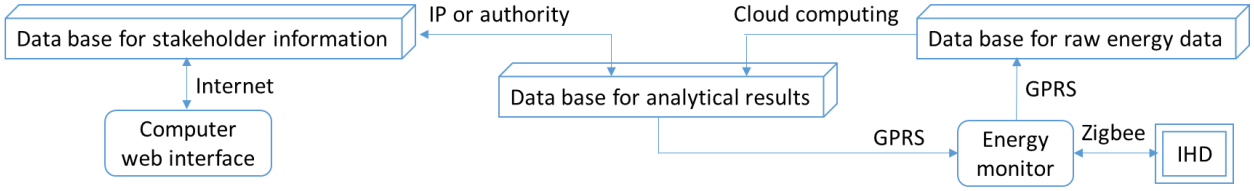

Figure 3: Framework of the smart metering and IHD networks

3. DESCRIPTION OF THE PILOT

The purpose of the pilot is to seek the potential effectiveness of smart meter and IHDs to the energy saving in China context. The pilot project was carried out at two economic apartments with the average household areas of 60.24 and 50.25 m^2 respectively in Shanghai, China.The effective research sample comprised 131 respondents at the standard apartments, which was arranged as 2 groups for discussions as shown in Figure 4: 55 with IHD (sample A) and 76 without IHD (sample B). These samples were designed to embrace a spread of family number, age, income, gender, and district. A check responder was specially designed inside the IHDs which would automatically record the customers' check frequency (the multiple IHD checks in 5 minutes regarded as 1 check action). There were 4 smart metering device installed on each floor while only 1 GPRS terminal installed in each building. The data collecting frequency is set at 15 minutes. Although the whole system starts to work from August 2013, some missing data still occurs during practical operation. As a result, we selected a group of relatively complete electricity data in whole November 2013 for detailed analysis in this paper. The multi-step domestic electricity charging conditions in Shanghai are listed in Table 1. The on-peak and off-peak periods for electricity usage in Shanghai are respectively from 06:00 to 22:00 and 22:00 to 06:00 (+1). Their corresponding electricity tariffs vary from 0.307 to 0.977 CNY/kWh depending on different electricity consumption volumes.

Table 1: Multi-step electricity tariffs in Shanghai, China (Xinhuanet energy, 2014)

Mode	Electricity (kWh/household/month)	Time	electricity tariffs (CNY/kWh)
1	0-260	On peak	0.617
		Off peak	0.307
2	260-400	On peak	0.677
		Off peak	0.337
3	Above 400	On peak	0.977
		Off peak	0.487

4. STATISTICAL ANALYSIS MODEL

4.1 Single Household's Level

Equation 1: The electric power of a single household at i recording number in j hour.

$$P(i, j) = C(i, j) \times V(i, j)$$

Where:

- *j* = the hour number varying from 1 to 24
- *C* = the current values (A)
- *V* = the voltage values (V)

Equation 2: The hourly average electric power of a single household in j hour.

$$Pave(j) = \frac{1}{4}\sum_{i=1}^{4} P(i, j)$$

It's needed to address that owing to the frequency of data collection at 15 minutes, the total hourly recording number should be equal to 4.

Equation 3: The hourly electric energy consumption of a single household

$$h_E(j) = Pave(j) \times 1hour/1000$$

.

Equation 4: The daily electricity energy consumption of a single household

$$d_E = \sum_{j=1}^{24} h_E(j)$$

Equation 5: The overall electricity energy consumption of a single household with IHD.

$$m_E = \sum_{k=1}^{30} d_E(k)$$

Where:

- k = the day number in one month varying from 1 to 30.

Equation 6: Calculation of relative electricity bills considering the electricity consumption at different time and different usage level

$$\begin{cases} 0 \le m_E \le 260, \begin{cases} 06-22 : m_B = m_E \times 0.617 \\ 22-06 : m_B = m_E \times 0.307 \end{cases} \\ 260 < m_E \le 400, \begin{cases} 06-22 : m_B = m_E \times 0.677 \\ 22-06 : m_B = m_E \times 0.337 \end{cases} \\ 400 < m_E, \begin{cases} 06-22 : m_B = m_E \times 0.977 \\ 22-06 : m_B = m_E \times 0.487 \end{cases} \end{cases}$$

4.2 Multiple Households' Level

Equation 7: The monthly maximum ($mmax_{cf}$), minimum ($mmin_{cf}$), average ($mave_{cf}$) and standard deviation (σ_{cf}) values of their check frequency for the households with IHD.

$$\begin{cases} mmax_{cf} = \max\left[m_{cf}(n) \right] \\ mmin_{cf} = \min\left[m_{cf}(n) \right] \\ mave_{cf} = \dfrac{1}{55} \sum_{n=1}^{55} m_{cf}(n) \\ \sigma_{cf} = \sqrt{\dfrac{1}{55} \sum_{n=1}^{55} \left[m_{cf}(n) - mave_{cf} \right]^2} \end{cases}$$

Equation 8 &9: The monthly maximum ($mmax_E$), minimum ($mmin_E$), average ($mave_E$), on/off-peak ($mave_{E,on/-off-peak}$), on/off-peak ratio ($R_{E,on/-off-peak}$) and standard deviation (σ_E) values of the electricity consumption among all the households in both sample A and B are respectively.

$$\begin{cases} mmax_E = \max\left[m_E(n) \right] \\ mmin_E = \min\left[m_E(n) \right] \\ mave_E = \dfrac{1}{55} \sum_{n=1}^{55} m_E(n) \begin{cases} 06-22 : mave_{E,on-peak} \\ 22-06 : mave_{E,off-peak} \end{cases} \\ R_{E,on-peak} = mave_{E,on-peak} / mave_E \\ R_{E,off-peak} = mave_{E,off-peak} / mave_E \\ \sigma_E = \sqrt{\dfrac{1}{55} \sum_{n=1}^{55} \left[m_E(n) - mave_E \right]^2} \end{cases} \qquad \begin{cases} mmax_E = \max\left[m_E(N) \right] \\ mmin_E = \min\left[m_E(N) \right] \\ mave_E = \dfrac{1}{76} \sum_{n=1}^{76} m_E(N) \begin{cases} 06-22 : mave_{E,on-peak} \\ 22-06 : mave_{E,off-peak} \end{cases} \\ R_{E,on-peak} = mave_{E,on-peak} / mave_E \\ R_{E,off-peak} = mave_{E,off-peak} / mave_E \\ \sigma_E = \sqrt{\dfrac{1}{76} \sum_{N=1}^{76} \left[m_E(N) - mave_E \right]^2} \end{cases}$$

Where,

- n = the household number with IHD: n=1,2…,55;
- N = the household number without IHD: N=1,2,…76.

Equation 10 &11: The monthly maximum ($mmax_B$), minimum ($mmin_B$), average ($mave_B$), on/off-peak ($mave_{B,on/-off-peak}$), on/off-peak ratio ($R_{B,on/-off-peak}$) and standard deviation (σ_B) values of the electricity bills among all the households in sample A and B are respectively.

$$\begin{cases} mmax_B = \max\left[m_B(n)\right] \\ mmin_B = \min\left[m_B(n)\right] \\ mave_B = \frac{1}{55}\sum_{n=1}^{55} m_B(n) \begin{cases} 06-22 : mave_{B,on-peak} \\ 22-06 : mave_{B,off-peak} \end{cases} \\ R_{B,on-peak} = mave_{B,on-peak} \big/ mave_B \\ R_{B,off-peak} = mave_{B,off-peak} \big/ mave_B \\ \sigma_B = \sqrt{\frac{1}{55}\sum_{n=1}^{55}\left[m_B(n) - mave_B\right]^2} \end{cases} \qquad \begin{cases} mmax_B = \max\left[m_B(N)\right] \\ mmin_B = \min\left[m_B(N)\right] \\ mave_B = \frac{1}{76}\sum_{n=1}^{76} m_B(N) \begin{cases} 06-22 : mave_{B,on-peak} \\ 22-06 : mave_{B,off-peak} \end{cases} \\ R_{B,on-peak} = mave_{B,on-peak} \big/ mave_B \\ R_{B,off-peak} = mave_{B,off-peak} \big/ mave_B \\ \sigma_B = \sqrt{\frac{1}{76}\sum_{N=1}^{76}\left[m_B(N) - mave_B\right]^2} \end{cases}$$

Equation 12: The monthly average electric power at multiple household's level at i recording number in j hour.

$$mPave(i, j) = \frac{1}{55}\sum_{n=1}^{55} P(i_n, j_n)$$

5. RESULTS AND DISCUSSIONS

The quantitative and qualitative research analysed for this pilot provides an insight into the impact of IHDs on the residential electricity consumption. The characteristics behind the impact in this section include electricity consumption reduction/shifting and energy bill saving. A general comparison was finally made between the analysed results in Shanghai, China and that in the UK.

5.1 Electricity Consumption Reduction and Shifting

The direct comparison results in electricity energy saving between the two samples with or without IHD are presented in Figure 4. The standard deviations of monthly electricity consumption were 36.7 and 53.8 respectively in sample A and B. Such high standard deviations indicate that the data points were spread out over a large range of values, possibly owing to some uncertainties like different appliances, home-stay period and some other unpredictable factors in the households. The monthly average electricity consumption by the households with IHD was about 91.0 kWh while it increased to nearly 100.1 kWh in the households without IHD, leading to around 9.1% in reduction of electricity consumption. The maximum electricity consumption in the households without IHD reached nearly 287.5 kWh while only there was 180.6 kWh consumed in the households with IHD. This results in the maximum reduction of electricity energy consumption by nearly 37.2%. However, the minimum electricity consumption in the households with IHD was almost 35.0 kWh, which is unexpectedly higher than that in households without IHD (6.5 kWh). This

might because the households with IHD stayed longer at home - it is mainly concluded from the processes of IHD dispatch and installation of smart meter. As a result, if the factor of home-stay period is also considered in the future implementation, the energy-saving potential of IHD should be even higher. But in general, the positive impact of the IHD on electricity consumption could be easily observed from the average and maximum values.

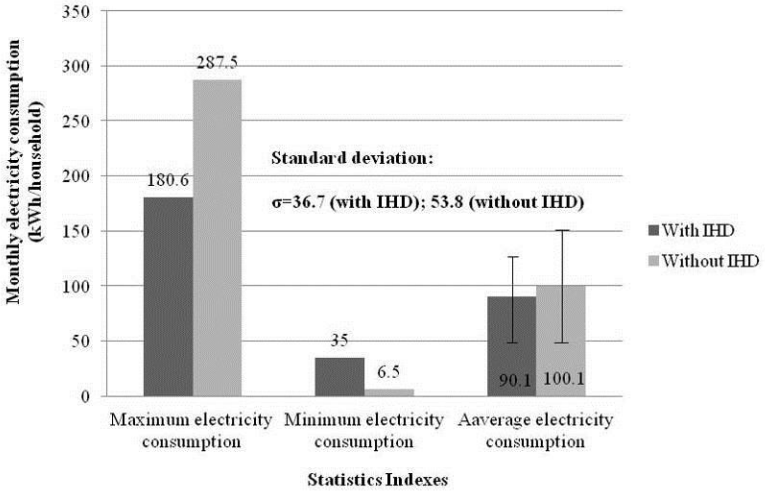

Figure 4: Monthly electricity consumption of the households with or without IHD

The monthly average on/off-peak electricity consumption of the households with or without IHD and their corresponding ratios to the monthly average electricity consumptions are given in Figure 5 and Figure 6. During the on-peak (off-peak) period, the households with IHD and without IHD respectively consumed about 45.5 (44.6) kWh and 52.3 (47.8) kWh electricity on average. By comparing the two samples, the relative electricity consumptions savings in households with IHD have been found with 13% for on-peak time, and 6.7% for off-peak period. A major reduction of the electricity consumption was achieved in the on-peak time. In addition, the ratio of off-peak electricity consumption in the households with IHD has risen up to 49.5% when only 47.7% was found in the households without IHD. It means there was a trend in shifting the electricity consumption from the on-peak time to the off-peak time through the effects of IHD's TOU functions to people's behaviour change.

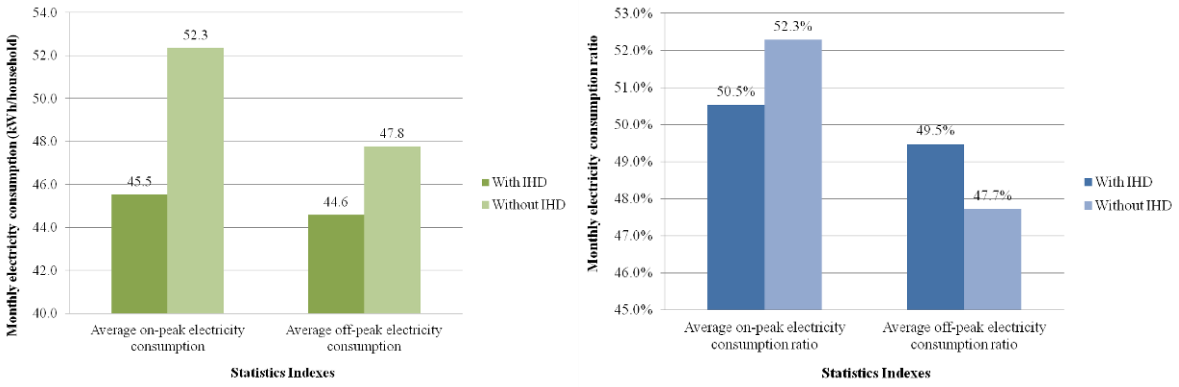

Figure 5 & 6: Average on/off peak electricity consumption & average on/off peak electricity consumption ratio of the households with or without IHD

5.2 Monthly Electricity Bill Saving

Figure 7 displays the comparison results in electricity bills saving between the two samples with or without IHD. The standard deviations of monthly electricity bills were 28.4 and 36.5 respectively in sample A and B. Such high standard deviations indicate that the data points were spread out over a large range of values, mainly due to some uncertainties like different electricity tariffs and on/off-peak electricity consumption. The monthly average electricity bill of the households with IHD was about 41.8 CNY while it climbed up to nearly 46.9 CNY in the households without IHD, leading to around 11.0% in reduction of electricity bill. The maximum electricity bill in the household without IHD achieved nearly 148.0 CNY while only there was 83.9

CNY spent in the household with IHD, leading to the maximum reduction in electricity bill at almost 43.3%. Similar as the electricity consumption, the minimum electricity bill in the households with IHD was about 16.2 CNY, higher than that in households without IHD. This might because the households with IHD stayed longer time at home and consumed much more electricity. In future pilot implementation, the energy bill saving potential of IHD could be even higher if the factor of home-stay period is also considered in two samples. But general speaking, the positive impact of the IHD on the energy bill could be obviously observed from the average and maximum values.

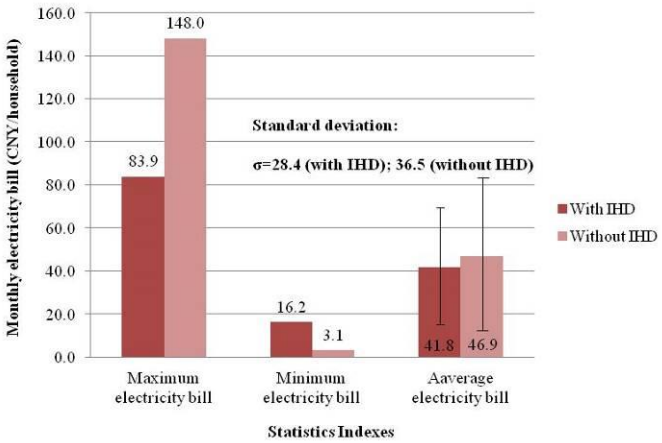

Figure 7: Monthly electricity bill of the households with or without IHD

The monthly average on/off-peak electricity bill of the households with or without IHD and their corresponding ratios to the monthly average electricity bill are shown in Figure 8 and Figure 9. The households with IHD and without IHD respectively spent about 28.1 (13.7) CNY and 32.3 (14.7) CNY in electricity on average during the on-peak (off-peak) period. When comparing the bills of two samples against the time, the relative savings in households with IHD were nearly the same as the electricity consumptions with 13% for on-peak time, and 6.7% for off-peak period. It is obvious that the much more savings in bill was gained at the on-peak time. Besides, the ratios of on-peak (off-peak) electricity bill in the households with IHD and without IHD were nearly 67.2% (32.8%) and 68.7% (31.3%) respectively. There was absolute 1.5% of the electricity bill shifting from the on-peak time to the off-peak time depending on the impacts of the IHD to people's behaviour change.

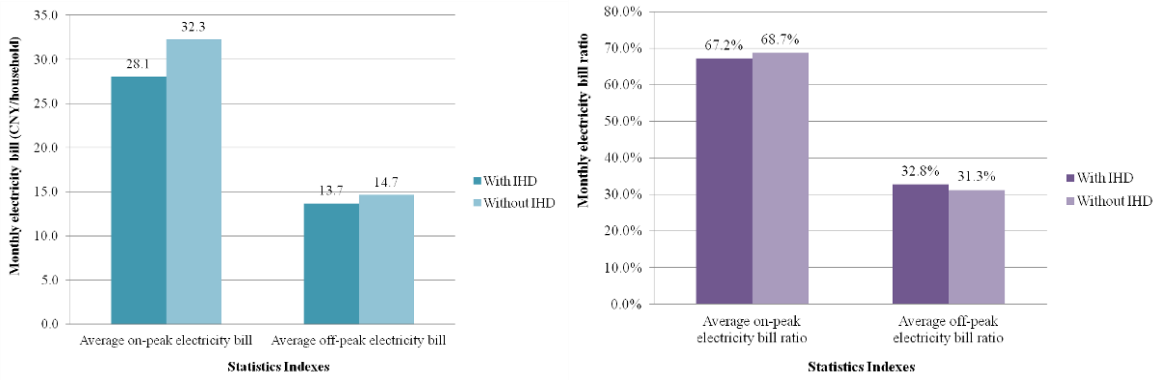

Figure 8&9: Average on/off peak electricity bill & average on/off peak electricity bill ratio of the households with or without IHD

5.3 Comparison with the UK Case

A general comparison between the result from this research and the average UK case is made in Figure 10. Electricity consumption reductions by other channels are also presented to see the potential of IHD depending on the UK case. According to the average results of trials in the UK, electricity savings from only IHD are over 11.3% in the households (Lewis et al., 2014). Although there was only 9.1% in reduction of electricity consumption achieved in this pilot investigation, it is still expected to increase significantly in the future if the related educational and disseminations activities are implemented in Shanghai. As indicating in Figure 16, the IHD has already been proven as the most effective method among the different channels

for consumption feedback, enabling almost double reduction in electricity consumption. However in fact, it will be a better option if IHD works with other channels, i.e., webpage or informative bill, to form up multiple feedback networks since they could complement each other.

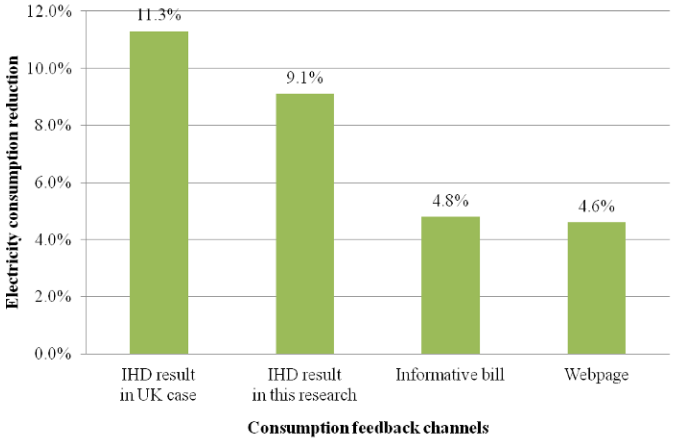

Figure 10: Electricity consumption reduction by channel

6. CONCLUSION

This paper reports on the results of a first IHD pilot in Shanghai, which is intended to contribute empirical evidence on how energy feedback could influence household electricity consumption in the Chinese context. The monthly average electricity consumption and bill reductions achieved by the households with IHD were about 9.1% and 11.0% respectively. A major reduction in either the electricity consumption or electricity bill was found in the on-peak time. There was a trend in shifting the electricity consumption or the electricity bill from the on-peak time to the off-peak time through the effects of IHD's TOU functions to people's behaviour change. Macroscopically speaking, such shifting would further influence the electricity tariffs, the related governmental policy and the operation of power infrastructures. The general comparison between the result from this research and the average UK case indicated that although there was smaller electricity consumption achieved in this pilot investigation, it is still expected to increase significantly in the future if the related educational and disseminations activities are implemented in Shanghai. In addition, it will be a better option if IHD works with other channels to form up multiple feedback networks since they could complement each other. The overall investigation is expected to open up the IHD research in China context, which will lead residents to become more aware of their energy consumption, change their corresponding behaviours, and provide social-technical basis for future economic leverage of government and the bidding competitiveness of power-related industries.

7. ACKNOWLEDGEMENT

The authors would acknowledge our sincere appreciation to the financial supports from Energy Foundation: China sustainable energy program (G-1210-17040) and the Ningbo Natural Science Foundation (2015A610039).

8. REFERENCES

DARBY, S. (2006). The effectiveness of feedback on energy consumption: a review for defra of the literature on metering, billing and direct displays, University of Oxford.

LEWIS, P., Bogacka, A., Grigoriou, R.,and Xu,S. (2014). Assessing the Use and Value of Energy Monitors in Great Britain, vaasaETT.

DROMACQUE, C.(2012). European Residential Energy Price Report, vaasaETT.

FARUQUI, A., Sergici,S., Sharif, A.(2010). The impact of informational feedback on energy consumption - A survey of the experimental evidence, Energy 35, pp.1598–1608.

HARGREAVES, T., Nye, M. And Burgess, J.(2010). Making energy visible: A qualitative field study of how householders interact with feedback from smart energy monitors, Energy Policy 38, pp.6111-6119.

Article 9 and 10 of Directive 2012/27/EU of the European Parliament and of the Council of the European Union.

DECC Energy Trends (2011). Measured using Renewable Energy Directive methodology.

BUCHANAN,K., Russo,R., and Anderson,B. (2014). Feeding back about eco-feedback: How do consumers use and respond to energy monitors?, Energy Policy 73, pp.138–146.

ANDA, M. and Temmen, J. (2014). Smart metering for residential energy efficiency: The use of community based social marketing for behavioural change and smart grid introduction, Renewable Energy 67, pp. 119-127.

CARROLL, J., Lyons, S., and Denny, E. (2014). Reducing household electricity demand through smart metering: The role of improved information about energy saving, Energy Economics 45, pp. 234–243.

CHIANG, T., et al. (2014). Inducing [sub]conscious energy behaviour through visually displayed energy information: A case study in university accommodation, Energy and Buildings 70, pp. 507–515.

BONINO, D., Corno, F., and Russis, L.D. (2012). Home energy consumption feedback: A user survey, Energy and Buildings 47, pp. 383–393.

China Energy Monthly Report (2014). [viewed 2 December 2014]. Avaliable from: https://www.gov.uk

DECC Energy Investment Report (2014).

Xinhuanet, energy (2014). Multi-step electricity tariffs in Shanghai, China. [viewd 3 December 2014]. Avaliable from:

<http://www.xinhuanet.com/energy/jiage/jg3.htm.>

HAZEWINKEL ,M.(2001). "Quadratic deviation"- Encyclopedia of Mathematics, Springer, ISBN 978-1-55608-010-4.

Standard deviation, assessed on 09/12/2014, http://en.wikipedia.org/wiki/Standard_deviation

495: The role of community-based energy management schemes in supporting resilience

TRAVIS O'DOHERTY [1], LUCELIA RODRIGUES [1*], MARK GILLOTT [1]

[1] Department of Architecture and Built Environment, Faculty of Engineering, University of Nottingham, United Kingdom, University Park, NG7 2RD
* Lucelia.Rodrigues@nottingham.ac.uk

The world's first energy suppliers were all community-based schemes, in its simplest form a group of people managing a water wheel on a nearby river. The community produced, managed and used its own energy. Eventually, energy production was privatised and today in the UK there are only six large energy suppliers controlling 95% of the market. Energy production and management have become centralised and consumers have become disengaged with the process. This has not only several infrastructure implications but also impacts greatly on people's behaviour and, consequently, energy use.

Localised or distributed energy ownership, common in many European countries but rare in the UK mostly due to existing policy framework, could be of great advantage for society. From a grid perspective, it could lead to a reduction of voltage fluctuations, increased power and improved stability. From a customer perspective, it could help improve energy security, increase power quality, reduce costs and fuel poverty. In addition, from a community perspective, it could give consumer behaviour a role in driving system efficiency and help develop social networks.

The definition of community resilience involves change and adaptation in response to key interventions and the management of local capacities. Some of these interventions are easily quantifiable, such as changes to infrastructure, whereas others, like social change, can only be recognised over time. In this work, the authors explored how the resilience of communities (infrastructure and social) can be affected by distributed energy ownership, greater use of renewable energy, better energy efficiency and improved community resilience. The conclusions are focused on suggestions for the development of a case study in a deprived residential neighbourhood in Nottingham. This neighbourhood is currently the focus of a regeneration scheme, which seeks to reduce the environmental impact of the area and redevelop its reputation.

Keywords: Social Resilience, Community Resilience, Energy Management, Behavioural Change

1. INTRODUCTION

The growing list of environmental problems such as climate change, dependence on fossil fuels, urban sprawl and habitat destruction indicate how current patterns of resource and land use are unsustainable. There is a realisation that time is running out for finding ways to counteract major environmental problems, especially climate change, necessitating rapid shifts in socio-technological systems (Brown and Vergragt, 2008, p109). At present much of the world's energy is produced and consumed in ways which could not be sustained if technology were to remain constant or if energy use were to increase substantially (Baris and Kucukali, 2012, p377). Greater greenhouse gas (GHG) emissions reductions will be required in order for the EU to meet its 2050 target of an emissions reduction of 80-95% (EEA, 2015, p12). Approximately two-thirds of anthropogenic GHG emissions come from the energy sector, therefore action in the energy sector is essential to tackling climate change (IEA, 2015, p20). Key measures required to achieve these GHG emissions reductions include reducing the carbon intensity of electricity production, increasing energy efficiency and behavioural changes (IPCC, 2014, p28). The prospect of global climate stability will depend largely on whether in the near future a transition to more sustainable patterns of energy consumption can occur.

Renewable technologies such as solar, wind, wave, hydro, biomass, biofuels and geothermal energy can increase security of supply by reducing demand for fossil fuels, contribute to diversification of the fuel mix and may assist in decoupling economic growth from environmental degradation. Despite the drop in oil and gas prices in 2014, investment in renewables did not relent, with an estimated increase of 128GW globally in 2014, of which 37% was wind power, approximately one third solar power and one quarter from hydropower (IEA, 2015, p21). However, renewable energies are at a disadvantage as they are competing in a market dominated by fossil fuels which are competing without external costs being fully taken into account, and renewable energy technologies often incur large initial capital costs (Roulleau and Lloyd, 2008, p1843). The age of cheap oil is over, as the future availability of oil decreases there will be a greater need for energy use become less intensive. Here the authors examine the benefits and challenges associated with the implementation of localised or distributed energy ownership in a community in Nottingham.

2. AN OVERVIEW OF THE ELECTRICITY MARKET IN THE UK

In 1881 the world's first electricity supply company was set up in the UK, electricity was generated using a water wheel and used to power street lighting and lights in local businesses, in 1882 the Electric Lighting Act allowed individuals, local authorities and companies to set up their own electricity supply systems (OVO Energy, 2014, p6). In 1948 the UK energy supply industry was nationalised, privatisation of the energy industry then began starting with the privatisation of the British Gas Corporation in 1886. Between 1995-2002 consolidation of the market took place and the 'Big Six' vertically integrated energy companies emerged in the U.K (OVO Energy, 2014, p6). As energy production and management has become centralised consumers have become almost completely disengaged with the process. Distributed energy storage or community energy storage offers a means of reengaging communities in energy matters, and allows the community to take ownership in their energy futures. Energy Service Companies (ESCOs) are companies created to produce and manage the local delivery of energy. Often ESCOs can support the regeneration of a community, and they can play an important part role in facilitating community scale reductions in GHG emissions. In 2014 the UK Department of Energy and Climate Change published the first Community Energy Strategy for the UK (Department of Energy and Climate Change, 2014). This is significant as the UK government now recognises the role community energy schemes will have in meeting the UK's future energy targets.

The main challenges facing the energy industry in the UK are affordability, security of supply and the need to reduce GHG emissions (OVO Energy, 2014, p8). Security of energy supply and climate change are increasingly important drivers of energy policy and there are potential synergies between these two issues (Bazilian et al., 2011, p3750). While renewables are an essential part of the UK's commitments to reducing carbon emissions and increasing security of supply there are challenges associated with the intermittency of renewables, in particular wind and solar (Hoff and Perez, 2012, p2177).

As the share of wind and solar photovoltaics (PV) increases, there will be a need to manage peak loads efficiently alongside changes in consumer behaviour (OVO Energy, 2014, p12). One of the main drivers of new investment in the UK energy system is the need to cope with periods of peak demand, which determines the need for additional transmission and distribution lines and associated infrastructure (OVO

Energy, 2014, p12). Battery energy storage can help customers manage peak loads more efficiently, enabling more households to produce their own energy, reducing the amount of electricity bought from utilities. Furthermore, the combination of PV and battery storage allows households to move from being net consumers to becoming net producers of electricity (Joshi et al., 2009, p1114).

3. POLICY IMPLICATIONS FOR COMMUNITY ENERGY STORAGE

As fossil fuel prices increase and technology improves, renewables are becoming increasingly competitive. In Germany, community-owned energy schemes make up over 40% of the country's renewable energy generation capacity. By contrast, in the UK community-owned energy schemes constitute approximately 1% of UK's renewable energy generation (OVO Energy, 2014, p18). There is clearly potential for growth of community energy schemes in the UK. Distributed energy storage schemes provide a mechanism to address the issues of affordability, energy security and the need to reduce GHG emissions, however community leadership is an important factor (OVO Energy, 2014, p15). Estimates by the Department of Energy and Climate Change indicate that there is potential for local energy community schemes to supply enough electricity for 1 million homes by 2020 (Department of Energy and Climate Change, 2014, p15). Installed solar PV capacity in the UK of up to 10 GW can be accommodated on the electricity transmission system without major difficulties in the operation of the transmission system (National Grid, 2012, p3). As shown in Figure 1 there has been a rapid expansion globally of installed PV capacity in recent years, strong PV technology price decreases and increases in the cost of electricity have increased the competitiveness of PV (European Photovoltaic Industry Association, 2014, p10).

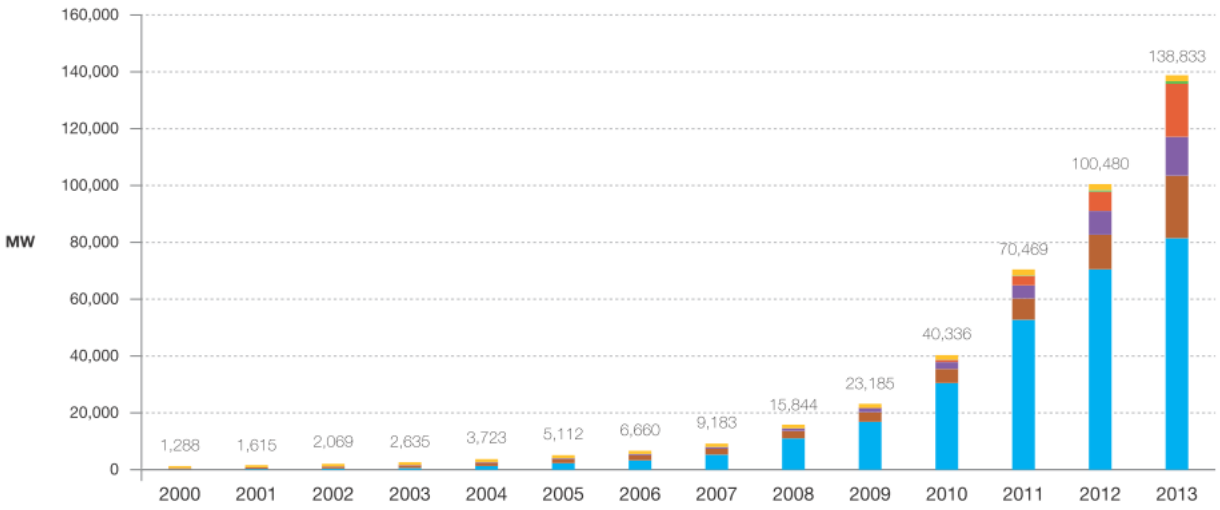

	2000	2001	2002	2003	2004	2005	2006	2007	2008	2009	2010	2011	2012	2013
RoW	751	807	887	964	993	1,003	1,108	1,150	1,226	1,306	1,590	2,098	2,098	2,098
MEA	n/a	n/a	n/a	n/a	1	1	1	2	3	25	80	205	570	953
China	19	24	42	52	62	70	80	100	140	300	800	3,300	6,800	18,600
Americas	21	24	54	102	163	246	355	522	828	1,328	2,410	4,590	8,365	13,727
APAC	368	496	686	916	1,198	1,502	1,827	2,098	2,628	3,373	4,951	7,513	12,159	21,992
Europe	129	265	399	601	1,306	2,291	3,289	5,312	11,020	16,854	30,505	52,764	70,489	81,464
Total	**1,288**	**1,615**	**2,069**	**2,635**	**3,723**	**5,112**	**6,660**	**9,183**	**15,844**	**23,185**	**40,336**	**70,469**	**100,480**	**138,833**

RoW: Rest of the World. MEA: Middle East and Africa. APAC: Asia Pacific.
Methodology used for RoW data collection has changed in 2012.

Figure 118: Global cumulative installed PV capacity 2000-2013 (European Photovoltaic Industry Association, 2014, p17)

The intermittency of solar radiation is one of the limiting factors in the application of solar PV, however integrating solar PV with battery energy storage can help resolve this issue, another benefit of solar PV is that it does not emit GHGs during its operation (Joshi et al., 2009, p1887). The addition of energy storage does raise the investment cost, but an economic analysis by Joshi et al. (2009, p1113) found that battery energy storage in Germany is currently profitable for small scale residential purposes under eight scenarios for investment costs and electricity prices without policy supports over the period from 2013 to 2022. Over

this time period the optimal PV system and storage size increases such that by 2015-2021 households become net exporters of electricity (Joshi et al., 2009, 1115). However, it was noted that barriers still remain to the implementation of solar PV as financial returns from investment in solar PV are uncertain due to market price fluctuations (Joshi et al., 2009, p1113). Policy makers may take decisions in future to change the profitability of energy storage, for example reduction in the UK Feed-in-Tariffs (FITs) in 2012 has reduced uptake rates for solar PV. Optimising the size of the PV system and the energy storage system is necessary to maximise the efficiency of the system, however, this is a difficult to predict as load patterns change over time (Joshi et al., 2009, p113).

4. THE ROLE OF BEHAVIOURS IN ENERGY MANAGEMENT

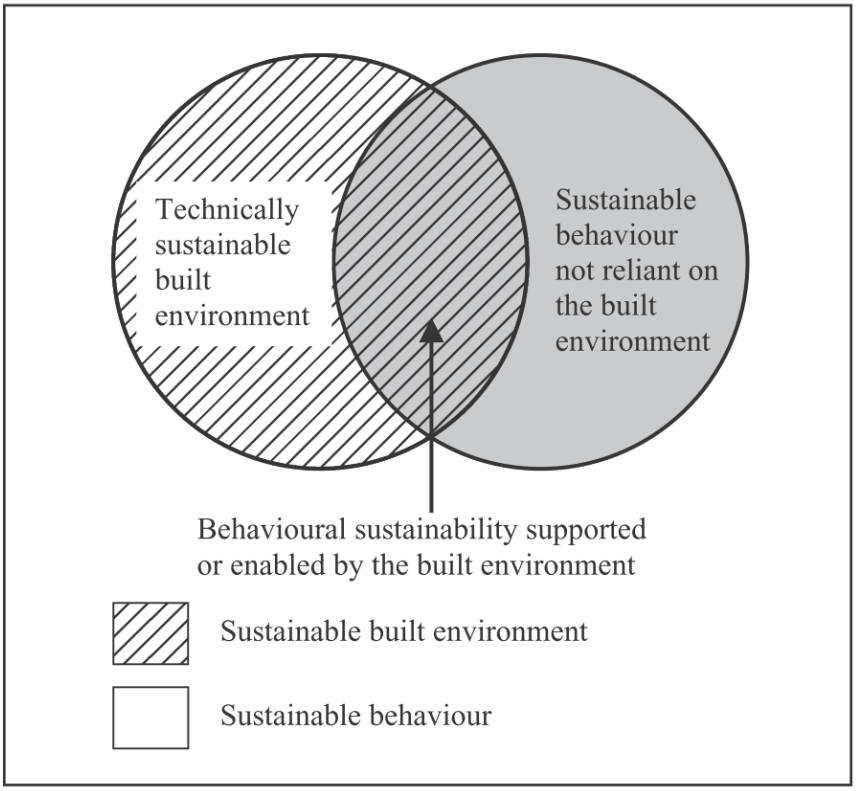

Figure 2: Technical and behavioural sustainability (Katie and Carol, 2007, p161)

The sustainability of the built environment depends on two aspects, namely technical and behavioural sustainability (Figure 2). Technical sustainability refers to the ability of technologies to perform effectively and contribute to sustainability. Behavioural sustainability refers to the actions of inhabitants of urban areas. It is argued that certain elements of the built environment can encourage behaviour change: however, unless used properly these features will not contribute to sustainability (Katie and Carol 2007, pp161-162). Social acceptance is a key factor in the adoption of policies aimed at creating more sustainable consumption patterns (van den Bergh et al., 2007, p249). Energy use and associated GHG emissions are heavily influenced by lifestyle, behaviour and culture. Emissions can be substantially lowered through implementation of technological and structural changes alongside behavioural and lifestyle changes (IPCC, 2014, p101).

Consumers make choices about the products and services they use and their lifestyles determine their consumption patterns (Caeiro et al., 2012, p73, Halme et al., 2004, p126). Baiocchi et al. (2010, p67) found that in the UK 75% of GHG emissions were associated with lifestyle choices, and the household and transport sectors accounted for the largest shares. Consumption habits and lifestyles can be difficult to change, and need to be understood in order to promote new sustainable modes of consumption. Triandis (1979) developed an integrated model of personal behaviour which recognised the key role which emotions and social norms have in informing intentions and behaviours (see Figure 3).

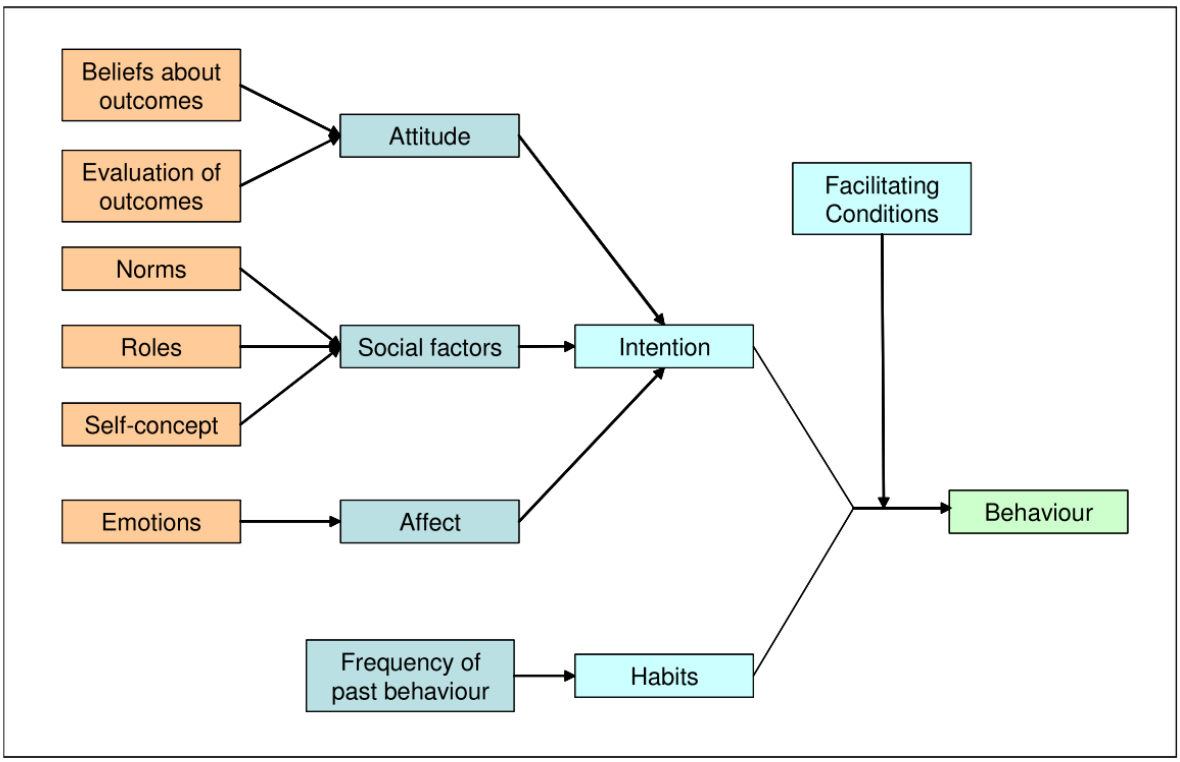

Figure 3: Triandis' theory of interpersonal relationships (Triandis 1979 cited in Jackson 2005)

Attitudes and behaviours have a role to play in determining whether renewable technologies are adopted, knowledge about investment opportunities and overcoming behavioural barriers are important considerations (Joshi et al., 2009). A significant barrier to greater renewable energy uptake levels is the high initial capital cost (Balcombe et al., 2014, p404). In a survey of 132 non-adopters of microgeneration technology in the UK conducted by Caird and Roy (2010), the main barriers to uptake of were the purchase price (86% of the respondents), uncertainty regarding the payback period (68% of respondents) and size of available grants (60% of respondents). Uptake rates would be expected to increase if incentives were introduced to assist with the high initial capital costs. Governments have an important role to play in terms of incentivising renewable technology, for example, in Germany, in 2013 the government introduced an incentive scheme supporting the purchase of solar energy storage, covering up to 30% of the installation costs (Mayer, 2013).

Energy demand side management (DSM) programmes aim to modify consumer behaviours through for example, reducing peak demand, total demand and demand fluctuations. DSM programmes aimed at domestic electricity users can take the form of information campaigns, incentives and changes to the structure of electricity tariffs (Dulleck and Kaufmann, 2004, p1025). Managing electricity demand during periods of high and low load demand can significantly reduce GHG emissions. In an analysis by Papagiannis of the economic and environmental impacts of demand side management systems in the EU, results indicate that reductions in CO_2 emissions by weight of 1.5-5% can be achieved (Papagiannis et al., 2008, p176). Customer information campaigns, which aim to decrease energy demand through the provision of information on efficient energy use techniques, form an important part of DSM programmes.

In determining uptake of microgeneration technologies, environmental concerns appear to be a major factor (Balcombe et al., 2013, p659). Caird and Roy (2010), surveyed 832 considerers and adopters of renewable technologies in the UK on their motivations for considering or adopting microgeneration technologies and found that reducing carbon emissions was the most important motive, followed by financial savings. There is clearly interest in reducing their GHG emissions among UK energy consumers. One fifth of respondents stated that they were either working in a field related to renewable energy or had an interest in the subject, hinting at the importance of renewable energy pioneers in urban communities.

5. IMPLICATIONS FOR THE MEADOWS COMMUNITY IN NOTTINGHAM, UK

The Meadows is a community centrally located on the south side of Nottingham city centre, in close proximity to both the railway station and to the River Trent. It was originally a large area of wetland that was drained and gradually developed for a variety of uses, incorporating terraced housing, public houses, factories, warehouses and public buildings such as libraries and swimming baths. The Meadows is a mostly residential community, which is centrally located for access to the city centre, rail station, nearby green spaces and the river. There is a tight community structure in the Meadows and a high level of community cohesion. In recent years the majority of new developments in Nottingham have occurred in the suburbs outside of the city boundaries, this has had the effect of hollowing out in the city centre and polarization of the population. The Meadows is one of the poorer areas of Nottingham city and the fuel poverty rates are relatively high.

The Meadows Ozone Energy Services (MOZES) is an Energy Service Companies formed in October 2009, with the assistance of the Meadows Partnership Trust and Nottingham Energy Partnership. MOZES aims to tackle issues relating to fuel poverty and greenhouse gas emissions in the community, it is a grassroots organisation formed by members of the local community. MOZES in collaboration with the University of Nottingham was recently awarded an EU-funded grant for the installation or energy storage in the Meadows. Led by Siemens in Germany, the project titled Storage Enabled Sustainable Energy for Buildings and Communities (SENSIBLE) aims to address the issues surrounding energy storage, both thermal and electrical, in homes and communities. The addition of energy storage to the Meadows will assist the community in managing peak loads more efficiently, reducing the amount of electricity bought from utilities. In addition MOZES collaborates on another European Project called TURAS, which examines how urban communities become more resilient and more sustainable.

It can be argued that provision of local services, amenities, and businesses helps support sustainable community development by supporting local supply chains, increasing social interaction and retaining money within the local economy (Katie and Carol, 2007pp170-171). There has been awareness that many environmental problems have a local origin and global environmental issues often manifest at a local level (Finco and Nijkamp, 2001, p290). Communities should aim to make it easy for residents to adopt sustainable lifestyles and reduce their environmental footprint, whilst providing a high quality of life in an attractive environment (Sevier, 2008, p37). There is a need for more aspirational housing in Nottingham in order to attract high quality talent to the city, enhance retention rates of universities and create intercity competition for talent. There have been a number of regeneration projects in the Meadows. Green Street is a regeneration project completed by Blueprint, phase 1 was completed in 2012 and consists of 38 energy efficient three and four bedroomed homes, a further 21 homes were constructed in phase 2 in 2015. Homes make use of natural light and have high levels of insulation and air tightness. Due to its green credentials the development aims to attract urban pioneers who will embrace and champion the principles of sustainability in the community.

MOZES has strong links with Nottingham City Council and the University of Nottingham. Since its inception MOZES has offered a number of programmes to address energy related issues in the community, engaging with the local community at a grassroots level to address both technical and behavioural aspects of sustainability. MOZES offers advice on energy efficiency and debt issues to the local community, providing knowledge to help overcome barriers and inform attitudes towards renewable energy. Community information sessions and energy workshops are organised adding to the social cohesion of the community. In addition there are volunteer and employment opportunities in MOZES and primary school education campaigns are undertaken to engage children in energy efficiency matters. The University of Nottingham sits on the board of MOZES and collaborates with MOZES on several academic research projects. Building trust and rapport with the local community takes considerable time and effort, the work since 2009 has built a platform on which future energy projects can build.

MOZES has the ability to draw down funding from large organisations or state agencies. Supported by Scottish Energy, MOZES offered interest free loans for energy retrofit measures for some of the most vulnerable households in the community. In addition MOZES was awarded a grant to install wall insulation or energy efficient boilers. In partnership with British Gas, MOZES was awarded £500,000 funding in 2009 from the Department of Energy and Climate Change (DECC) to install solar PV in 65 homes, 3 schools and 2 community buildings in the Meadows, excess electricity is fed into the national grid. However, there have been difficulties, for example in accessing FITs due to Government State Aid Regulations. MOZES have highlighted this issue with government.

A cohesive community benefits both individuals and organisations and empowers citizens to become involved in shaping their community. The benefits of 'bottom-up' community engagement are widely publicised. In close consultation with the local community a range of programmes were devised allowing local residents to take ownership in their energy futures. MOZES board members and local community give their time on a voluntary basis for the advancement of the community as a whole. A key factor in the development of MOZES is the presence of a local community champion who has been instrumental in guiding the development of the community.

6. CONCLUSIONS

Local, regional and national differences between areas mean that it is not possible to analyse urban sustainable development on the basis of universal principles alone. Although the experiences in the Meadows are relevant to other communities, there is a need to consider the implications of time and space when transferring project actions. The Meadows community in Nottingham is an example of a cohesive community. The presence of an active community group (MOZES) and a local champion who has an intimate knowledge and trust within the community have been instrumental to the success of MOZES. The community in the Meadows have been engaged through a wide variety of dissemination activities.

The addition of battery energy storage to the Meadows is an exciting prospect for the development of the community, which will likely to change the future of energy use and distribution in the community. The award of EU funding for the installation of battery energy storage overcomes the initial capital costs of installation, which is one of the main barriers to uptake of the technology. Over the course of the SENSIBLE project further monitoring of the technical and social aspects of the project will be conducted, yielding further insights into sustainable community development.

The authors have examined some of the barriers to increased uptake of PV energy storage systems, and how a community in Nottingham has tackled many of these barriers. The increasing profitability of PV energy storage is a positive step, however major challenges remain in terms of investment in technical infrastructure in order to support community energy projects. Monitoring of the development of battery storage in the Meadows will have benefit to other communities considering similar measures.

7. ACKNOWLEDGEMENTS

The authors would like to thank the EU for funding this research via the TURAS project (Grant No 282834).

8. REFERENCES

BAIOCCHI, G., Minx, J. & Hubacek, K. 2010. The impact of social factors and consumer behavior on carbon dioxide emissions in the United Kingdom. *Journal of Industrial Ecology,* 14**,** 50-72.

BALCOMBE, P., Rigby, D. & Azapagic, A. 2013. Motivations and barriers associated with adopting microgeneration energy technologies in the UK. *Renewable and Sustainable Energy Reviews,* 22**,** 655-666.

BALCOMBE, P., Rigby, D. & Azapagic, A. 2014. Investigating the importance of motivations and barriers related to microgeneration uptake in the UK. *Applied Energy,* 130**,** 403-418.

BALCOMBE, P., Rigby, D. & Azapagic, A. 2015. Energy self-sufficiency, grid demand variability and consumer costs: Integrating solar PV, Stirling engine CHP and battery storage. *Applied Energy,* 155**,** 393-408.

BARIS, K. & Kucukali, S. 2012. Availability of renewable energy sources in Turkey: current situation, potential, government policies and the EU perspective. *Energy Policy,* 42**,** 377-391.

BAZILIAN, M., Hobbs, B. F., Blyth, W., Macgill, I. & Howells, M. 2011. Interactions between energy security and climate change: A focus on developing countries. *Energy Policy,* 39**,** 3750-3756.

BRAND, C. & Boardman, B. 2008. Taming of the few - the unequal distribution of greenhouse gas emissions from personal travel in the UK. *Energy Policy,* 36**,** 224-238.

BROWN, H. S. & Vergragt, P. J. 2008. Bounded socio-technical experiments as agents of systemic change: The case of a zero-energy residential building. *Technological Forecasting and Social Change,* 75**,** 107-130.

CAEIRO, S., Ramos, T. B. & Huisingh, D. 2012. Procedures and criteria to develop and evaluate household sustainable consumption indicators. *Journal of Cleaner Production,* 27**,** 72-91.

CAIRD, S. & Roy, R. 2010. Adoption and Use of Household Microgeneration Heat Technologies. *Low Carbon Economy,* 1**,** 61-70.

DEPARTMENT OF ENERGY AND CLIMATE CHANGE 2014. Community Energy Strategy: Full Report. London, UK: Department of Energy and Climate Change.

DULLECK, U. & Kaufmann, S. 2004. Do customer information programs reduce household electricity demand? - the Irish program. *Energy Policy,* 32**,** 1025-1032.

EEA 2005. Household consumption and the environment. Copenhagen, Denmark: European Environment Agency.

EEA 2009. Annual European Community greenhouse gas inventory 1990–2007 and inventory report 2009. Submission to the UNFCCC Secretariat. Brussels: European Environment Agency, .

EEA 2010. The European environment state and outlook 2010 synthesis. Copenhagen: European Environment Agency.

EEA 2015. The European environment state and outlook 2015 synthesis report. Luxembourg: European Environment Agency.

EUROPEAN PHOTOVOLTAIC INDUSTRY ASSOCIATION 2014. Global Market Outlook for Photovoltaics 2014-2018. Brussels, Belgium: European Photovoltaic Industry Association.

FINCO, A. & Nijkamp, P. 2001. Pathways to urban sustainability. *Journal of Environmental Policy and Planning,* 3**,** 289-302.

HALME, M., Jasch, C. & Scharp, M. 2004. Sustainable home services? toward household services that enhance ecological, social and economic sustainability. *Ecological Economics,* 51**,** 125-138.

HAMIN, E. M. & Gurran, N. 2009. Urban form and climate change: balancing adaptation and mitigation in the U.S. and Australia. *Habitat International,* 33**,** 238-245.

HOFF, T. E. & Perez, R. 2012. Modelling PV fleet output variability. *Solar Energy,* 86**,** 2177-2189.

IEA 2015. Energy and Climate Change - World Outlook Special Report. Paris, France: International Energy Agency.

IPCC 2014. *Climate Change 2014: Synthesis Report. Contribution of Working Groups I, II and III to the Fifth Assessment Report of the Intergovernmental Panel on Climate Change* Geneva, Switzerland, IPPC.

JACKSON, T. 2005. Motivating sustainable consumption. A review of evidence on consumer behaviour and behavioural change. Guildford, Surrey: Sustainable Development Research Network.

JOSHI, A. S., Dincer, I. & Reddy, B. V. 2009. Performance analysis of photovoltaic systems: A review. *Renewable and Sustainable Energy Reviews,* 13**,** 1884-1897.

KATIE, W. & Carol, D. 2007. A framework of sustainable behaviours that can be enabled through the design of neighbourhood-scale developments. Sustainable Development, 15, 160-173.

MAYER, J. 2013. STATE INCENTIVE PROGRAM IS LAUNCHED FOR SOLAR STORAGE SYSTEMS [Online]. Available: http://www.solarenergystorage.org/en/staatliche-forderung-von-solarstromspeichern-gestartet/.

NATIONAL GRID 2012. Solar PV Briefing Note. London: DECC.

OVO ENERGY 2014. Community Energy White Paper April 2014.

PAPAGIANNIS, G., Dagoumas, A., Lettas, N. & Dokopoulos, P. 2008. Economic and environmental impacts from the implementation of an intelligent demand side management system at the European level. *Energy Policy,* 36**,** 163-180.

ROBERTS, P. 2009. Sustainable Communities Policy, Practice and professional development: A model for Europe. *In:* Cooper, I. & Symes, M. (eds.) *Sustainable Urban Development Volume 4: Changing Professional Practice.* Abingdon: Routledge.

ROULLEAU, T. & Lloyd, C. R. 2008. International policy issues regarding solar water heating, with a focus on New Zealand. *Energy Policy,* 36**,** 1843-1857.

SAHELY, H. R., Kennedy, C. A. & Adams, B. J. 2005. Developing sustainability criteria for urban infrastructure systems. *Canadian Journal of Civil Engineering,* 32**,** 72-85.

SEVIER, L., Henderson, M. & Naidu 2008. Ecovillages: a model life? . *Ecologis,* 38**,** 36-41.

TRIANDIS, H. C. 1979. Values, attitudes, and interpersonal behavior. *Nebraska Symposium on Motivation,* 27**,** 195-259.

UNEP 2011. Paving the way for sustainable consumption and production. The Marrakech process progress report. Towards a 10 year framework of programmes on sustainable consumption and production. Paris, France: United Nations Environment Programme.

VAN DEN BERGH, J. C. J. M., van Leeuwen, E. S., Oosterhuis, F. H., Rietveld, P. & Verhoef, E. T. 2007. Social learning by doing in sustainable transport innovations: ex-post analysis of common factors behind successes and failures. *Research Policy,* 36**,** 247-259.

SESSION 8: ENERGY AND ENVIRONMENT SECURITY

456: The need for UN climate change policy reformation

SHARAF ELDIN I. BANNAGA

Director, Physical Environmental centre of Khartoum, 471, Mamoun Behary St. (63rd street) Alamarat, PO Box 2256 Khartoum, Khartoum, SUDAN
Tel: +249 155145853, +249 155 662773
shbannaga@yahoo.com

This paper discusses the global warming, its causes and consequences. The paper assesses the impact of the polices adopted by the UN organizations including the Intergovernmental Panel on Climate Change (IPCC) to mitigate global warming, and the consequences following failure of the Kyoto Protocol to mitigate global warming. The key issues discussed here include the ineffectiveness of the UN climate change policies and the role of urbanization in greenhouse gases emissions mitigation. It is evident that the UN efforts to combat climate change through mitigation of global warming are ineffective due to many issues. These are summarised in the increasing causes of urbanization and development of "megacities" around the world, and particularly in the less developed nations due to the current global polices and the economic model which favour urbanization.

Keywords: Climate change, UN policies reform, Carbon dioxide, IPCC

1. INTRODUCTION

1.1 Global Warming and Consequences

Scientists have spent decades searching the causes of global warming, and now it is widely believed that, the main cause of the current global warming trend is the human expansion of the "*greenhouse effect". Global* warming occurs when Green House Gases (GHGs) including carbon dioxide, methane, water vapor, nitrous oxides, chlorofluorocarbon and Halocarbons collect and trap heat and light from the sun in the earth's atmosphere. A stronger greenhouse effect will warm the oceans and partially melt glaciers and other ice causing sea level to rise. Ocean water also will expand if it warms, contributing further to sea level rise. Warmer conditions will probably lead to more evaporation and precipitation overall, but this may vary at individual regions, some becoming wetter while others become dryer

Currently, extreme weather events in different parts of the globe such as extreme precipitation rate, severe draughts, floods, hurricanes, typhoons and cyclones are frequent and increasing in ferocity and frequency. Satellite images and research have revealed that the ice caps are melting faster and our sea levels are rising higher (COPs, 2012). Cities and towns are heavily vulnerable to climate change. Hundreds of millions of people in urban areas across the world will be affected by rising sea levels, increased precipitation, inland floods, more frequent and stronger cyclones and storms.

1.2 Roles of the Intergovernmental Panel on Climate Change (IPCC)

The Intergovernmental Panel on Climate Change (IPCC) was established in 1988 by the United Nations Environment Programme (UNEP) and the World Meteorological Organization (WMO) in order to provide scientific view from the information, findings and data available on climate change and its impact on the environment and socio- economic values worldwide (IPCC website, 2015). In addition to the IPCC, the gateway to the UN systems and links to the UN Partners on Climate Change, including UNEP, WMO, UNFCCC and UNDP are all working on projects to mitigate the effect of Climate Change.

The findings of IPCC on the climate change were accepted in its second assessment in 1995. Since then it has been undeniable that the Earth's climate is warming, which is evident from models and observations at global and continental levels, produced by IPCC (IPCC website, 2015). These findings clearly show that there was an increase of 0.74°C between 1906 and 2005.

Table 1, shows the annual trend of Carbon Dioxide (CO_2) concentrations as measured by the Earth System Research Laboratory (ESRL, of the National Oceanic and Atmospheric Administration (NOAA), US Department of Commerce. This laboratory has grown to become the premier long-term atmospheric monitoring facility and it is a credible laboratory where the concentrations of global atmospheric carbon dioxide are measured.

Table 1. Annual trend of Carbon Dioxide (CO2) concentrations as measured by the Earth System Research Laboratory. Source of Annual CO2 Data: NOAA-ESRL Data File Created January 6, 2015.

Year	CO_2 (ppm)	Notes
2014	398.55	
2013	396.48	
2012	393.82	
2011	391.63	
2010	389.85	
2009	387.37	Copenhagen Accord
2008	385.59	
2007	383.76	
2006	381.90	
1997	363.71	Kyoto Protocol
1992	356.38	Earth Summit in Rio de Janeiro
1987	349.16	The year when the annual CO_2 level was less than 350 ppm
1959	315.97	The first year with a full year of instrument data

It can be observed that the annual increase in CO2 concentration in the period 1959 to 2006 was at 1.4 ppm, while this value has increased to 2.1 ppm in the period from 2006 to 2014. This clearly indicates that the rate of CO2 concentration is increasing, regardless of all the efforts made to mitigate this. This is also mirrored in the 5th report of IPCC which was produced in October 2013 (IPCC website, 2015). The main findings of the report are:

- The continuous emissions of greenhouse gases will cause further warming and changes in all components of the climate system.
- In order to reduce the impact of the climate change a substantial and sustained reductions of greenhouse gas emissions is required.
- The understanding of the effects of all the gases together requires scientists to consider all greenhouse gases in terms of the equivalent amount of CO2.
- Since 1990, yearly emissions have gone up by about 6 billion metric tons of "carbon dioxide equivalent" worldwide, more than a 20% increase.

In 2011 and according to IPCC report (IPCC website, 2015), the concentration of CO_2 was 391 ppm, rising from 280 ppm in 1750. The average annual concentration of CO_2 in the atmosphere at present (2014) is 398.55 parts per million (ppm), 0.522% up from2013 figures.

2. ROLE OF URBANIZATION IN GREENHOUSE GASES (GHGS)

It is well recognized that the major source of GHGs is burning of fossil fuel and similar non-renewable energy products. These are used in transportation, electricity generation, and many activities including activities at homes, workplaces and factories. Another malpractice is loss of forests and vegetation cover to development since trees and other plants collect CO_2 from the atmosphere. Therefore, it is obvious that cities are the prime driver of global warming since they are directly contributing to GHG emissions as a result of a range of activities that are undertaken by the urban residents. Associated with increased rates of energy consumption, cities' energy consumption is several times greater than rural areas. Energy consumption of Khartoum for example amounts to 70-75% of total national energy consumption, with only 16% of Sudan population.

Encroach on land that may previously have been covered with vegetation – thereby reducing its potential to absorb CO2, cities are continuing to sprawl because they are inhabited by higher concentrations of people with fast population growth. Anna Tibaijuka (Anna Tibaijuka, 2006), who addressed the High Level Plenary in Bali, stated that three-quarters of global energy consumption occur in cities, and an equally significant proportion of GHGs emissions are produced by other urban areas. Thus climate change is a creation of cities. Besides population, cities concentrate disproportional parts of the economy, resource consumption and the decision making power in most countries. According to the Institute of the Advanced Study of Sustainability, UNU 75% of the global economic production takes place in urban areas. Cities are responsible for 67% of the total global energy consumption and more than 70% of greenhouse gas emissions and these trends significantly intensify the severity of some of the two great challenges of our time; climate change and energy security.

With the process of urbanization, the building sector fundamentally impacted by people's daily life is one of the main contributors to carbon emissions. Buildings consume about 40% of our energy for heating, cooling and lightening. One of the key goals of urban sustainable development is to promote energy and resource efficiency in the building sector and to provide good, healthy and affordable buildings for people in cities.

On the other hand, the issue of emissions from transportation in cities is particularly important in countries where motor vehicle ownership is expanding rapidly. The increased dependence on private motorized vehicles is a major source of urban GHG emissions

Fuelwood is another source of GHG, as many families consume charcoal and fuel wood in households while all residents rely on inward flows of food and consumer goods that may result in GHG emissions from areas outside the city. For example in Sudan, forests contribute to between 70% – 80% of the total energy consumption, as it is the easiest way of producing energy for cooking. This results in deforestation, which is the permanent removal of trees from forests without planting new trees and the consequential increase in levels of carbon dioxide in the atmosphere because trees are not there to absorb CO2 for photosynthesis. As a result, the carbon cycle is affected, and according to National Geographic, agriculture is the primary

cause of deforestation. Farmers remove trees on a large-scale basis to increase acreage for crops and livestock.

Engineering networks is another serious source of GHG, represented in energy used for power generation together with other municipal services. Activities including production and distribution of fresh water, collection and treatment of wastewater, and the reclaimed water recycling and discharge, collection of solid waste etc constitute a large percentage of GHGs emissions.

Industrial activities in urban areas over the past century have significantly increased the amount of carbon in the atmosphere, mainly in the form of carbon dioxide primarily by burning fossil fuels for different manufacturing activities. It has to be noted that many polluting and carbon intensive manufacturing processes are no longer located in developed countries, but have been sited elsewhere in developing cities to take advantage of lower labour costs and less rigorous environmental enforcement.

Another contributor to GHG effect is the "Dust Dome", a local mega city phenomenon called “Urban Microclimate”, which usually evolves as a result of the city intensive industrialization, its location characteristics and the population habits. The dust clouds and smoke that hang over the city in the biosphere and accumulate in the air or sink don’t disappear except at great altitudes thus, forming a foggy blanket or SMOG on cities’ skies. The suspended particulates and the smoke together with water vapour, create a ‘DUST DOME’ or what is known as 'Heat Island Effect'/’Greenhouse Effect’. Table 2 shows the share of Cities in global energy consumption and related CO_2 generation.

Table 2. Share of cities on global energy consumption and related CO_2.

Cities share in	**2006**	**2030 (%)**
Global energy consumption	67 **(%)**	73 **(%)**
Global energy- related CO_2	71 **(%)**	76 **(%)**
Global anthropogenic GHG emissions	40 - 70 **(%)**	43 - 70 **(%)**

Despite these activities and the consequential risks, many cities have not yet addressed climate change and particularly developing cities. The reasons include lack of capacity and resources in developing cities together with lack of public awareness on climate variability. This is why the majority of developing cities lacks implementation of relevant city policies and action plans; existence of regulations on urban planning and environment which have not been adjusted to manage climate change.

3. UN EFFORTS TO COMBAT CLIMATE CHANGE

The United Nations Framework Convention on Climate Change (UNFCCC), is an international environmental treaty, and its objective is to "stabilize greenhouse gas concentrations in the atmosphere at a level that would prevent dangerous anthropogenic interference with the climate system". The treaty provides a framework for negotiating specific international treaties called "protocols" that may set binding limits on greenhouse gases. The parties to the convention have met annually from 1995 in Conferences of the Parties (COP) to assess progress in dealing with climate change. In 1997, the Kyoto Protocol was concluded and established legally binding obligations for developed countries to reduce their greenhouse gas emissions. The Kyoto Protocol has had two commitment periods, the first was in the period 2005-2012, and the second is in the period 2012-2020. By the time the first commitment period expired on the 31st December 2012, the Protocol had 83 signatories worldwide, unfortunately, only 55 of the original signatories ratified the agreement. The United State one of the largest polluters is among those who did not ratify the Kyoto Protocol.

One of the first tasks set by the UNFCCC was for signatory nations to establish national greenhouse gas inventories of greenhouse gas (GHG) emissions and removals, which were used to create the 1990 benchmark levels for accession of Annex I countries to the Kyoto Protocol and for the commitment of those countries to GHG reductions. Updated inventories must be regularly submitted by Annex I countries. The last meeting or the 20th COP took place in Peru in December 2014 where a new 2015 agreement on climate change, expected to be signed in Paris, will harness action by all nations. This agreement took a further important step forward in Lima following two weeks of negotiations by over 190 countries.

The Climate Change meeting held in Doha, Qatar (COP18/CMP8), in November/ December 2012 was considered fruitful since it has opened up a new gateway driving governments to take the essential steps in the global response to climate change. Countries in Doha endorsed the completion of new institutions and agreed ways and means to deliver scaled-up climate finance and technology to developing countries and are committed to implement (COP18/CMP8) as follow:

- ✓ Continue the Kyoto Protocol's Market Mechanisms – the Clean Development Mechanism (CDM), Joint Implementation (JI) and International Emissions Trading (IET) as of 2013.
- ✓ Continue operating JI with the agreed technical rules allowing the issuance of credits, once a host country's emissions target has been formally established.
- ✓ Speedily work toward a universal climate change agreement covering all countries from 2020, to be adopted by 2015, to curb emissions so that the world can stay below the agreed maximum 2 degrees Celsius temperature rise.
- ✓ Establish a pathway to provide the most vulnerable populations with better protection against loss and damage caused by slow onset events such as rising sea levels.
- ✓ Implement National Adaptation Plans for least developed countries including linking funding and other support
- ✓ Further clarify ways to measure deforestation, and to ensure that efforts to fight deforestation are supported.

It should be noted that the overall processes of the UNFCCC and the adopted Kyoto Protocol have been criticized by not having achieved its stated goals of reducing the emission of carbon dioxide as discussed above. The failure to achieve meaningful progress and reach effective CO_2 reducing-policy treaties among the parties over the past eighteen years have driven some countries like the United States to never ratify the UNFCCC's because according to US the treaty didn't cover developing countries which some of them are now considered the largest CO_2 emitters. Other air polluting countries may follow US as reported in COP documents but for different reasons. In 2010 in Cancun, Japan stated that it will not sign up a second Kyoto term, because it would impose restrictions on it not faced by its main economic competitors, China, India and Indonesia. A similar indication was given by the Prime Minister of New Zealand in November 2012 in Doha. At the 2012 conference in Doha, last minute objections at the conference by Russia, Ukraine, Belarus and Kazakhstan were ignored by the governing officials, and they have indicated that they will likely withdraw or not ratify the treaty. These defections place additional pressures on the UNFCCC process.

4. INEFFECTIVENESS OF THE UN CURRENT POLICIES

The nations met in Lima concluded by elaborating the elements of the new agreement, scheduled to be agreed in Paris in late 2015, while also agreeing the ground rules on how all countries can submit contributions to the new agreement. The expected agreement may restore a faith in UN process if implemented but does not reduce temperatures as needed in the near future. This is in addition to the defections expected from some influential countries that declared not to fulfill their obligations. UN Program appears to be concentrating on combating the effects of climate change rather than targeting the main grassroots causes of climate variations. The main cause of climate change is that we are making more cities than villages. UN effort is primarily exerted at present in assisting communities to cope with adverse effects of climate change rather than working for diluting the concentration of urban centers to appropriately distribute the urban population. UN policy is to mitigate the impacts of climate change and thus engage countries to climate change adaptation and through facilitation of actions – like implementing energy efficiency standards for buildings or adding bus rapid transit lanes – aim to reduce greenhouse gas emissions and improve urban resilience to climate change.

Of course, any deal that ignores developing countries as noted by the US is meaningless. An accelerating rate of energy consumption is the situation that will prevail in the near future in developing countries if preventive measures are not imposed to control CO2 emissions by developing countries. This is primarily caused by fast urbanization and for this reason UN climate change efforts will be aborted and its programme to counteract climate change will not succeed when considering the following:

4.1 Developing Cities are Growing Extremely Fast and so Will Consume More Energy.

In 1970, 37% of the world population was in urban areas, while 63% was in rural areas. In 2000 this percentages have changed to 47% urban and 53 rural, and in 2030, the urban population is expected to grow to reach 60% of the total population, while the rural population will drop to 40% only. The growth is expected to be very high in the less developed countries, while it is nearly nil in the more developed countries, as shown by Figure 1.

Worldwide, there are more than 20 cities with population exceeding 10 million, and the pattern is on increase in particular with less developed countries, as shown in Figure 2. It is noted that most of the mega-cities and large urban centers are growing in the South and that large cities such as Bangalore, Mexico City or Cairo are found morphing into new spatial configurations in which they amalgamate other cities and towns of various sizes within their economic orbit. In other cases, two or more large cities, such as Mumbai and Delhi in India, Sao Paulo- Rio de Janeiro in Brazil, or Ibadan-Lagos-Accra in Africa form transport corridors for the purposes of industrial development, business services or trade.

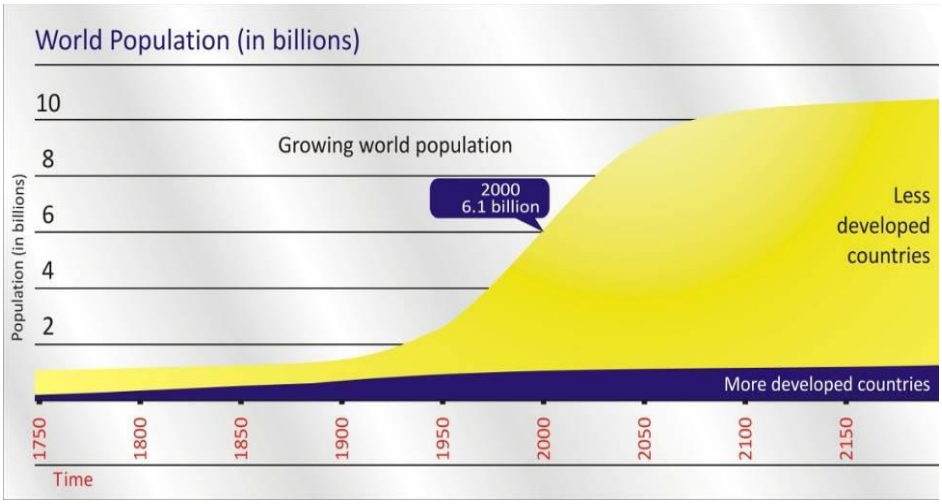

Figure 1: Rate of population growth in developed countries compared to less developed countries.

Rapid urban growth habitually could end up with serious social and environmental challenges, such as urban poverty and various forms of pollution. In order to keep up with rapid urban expansion and urban population growth, more resources as well as more consumption and production are required. The ever-increasing production and consumption in cities result in serious environmental problems in terms of the pollution of air, water and land as well as the degradation of ecosystems.

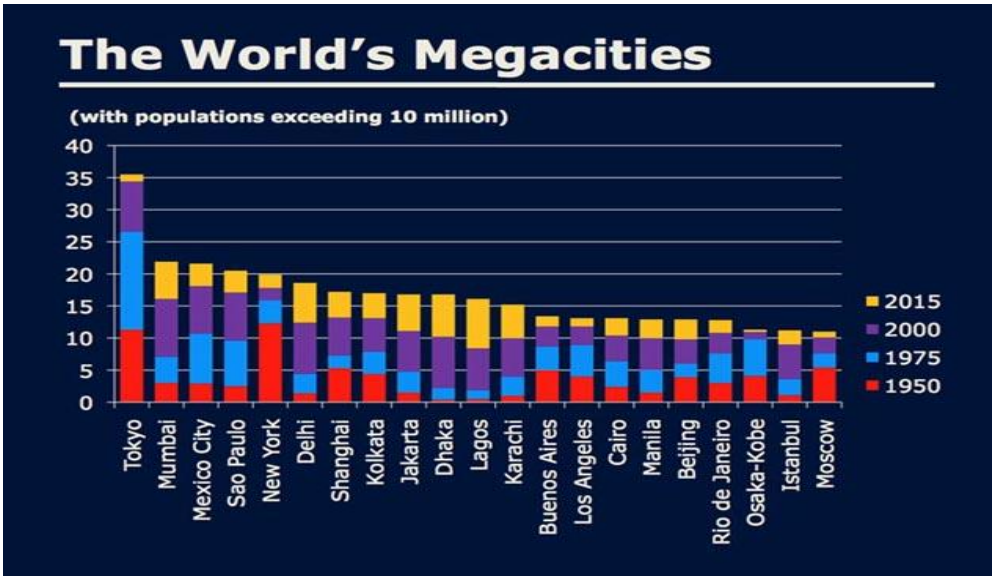

Figure 2: Population of the world Megacities

4.2 Pattern of Urban Development versus Compact City Model

It is known that a negative correlation exists between population density and atmospheric GHG emissions; spatially compact and mixed-use urban developments have generally significant benefits in terms of GHG emissions reduction. The development pattern adopted by the majority of developing cities is urban sprawl which is contrary to 'Compact City' model resulting in reduction of energy and services cost. The incessant displacement of rural people, the continuous exodus towards cities; and the excessive expansion of makeshift settlements and uncontrolled development produce huge subdivisions of sprawled physical development overwhelmed by poor dwellers living in shanty settlements. The substantial horizontal expansion of Greater Khartoum in Sudan is a typical example and has been encouraged by abundance of land serviced with water, construction of cheap building forms and lack of development control.

4.3 Climate Change Effects are Driving Rural Population to Leave their Land

Recurrent and prolong periods of droughts in some developing countries are now lowering the yield of crops, decreasing animals' grazing areas and causing poverty, death of livestock as well as triggering social, economic and political tensions and repetitive armed conflicts. This results in further migration towards cities. It is known that the poor will always be a threat to the environment through their malpractices. Some go searching for firewood as it is the easiest way of producing energy for cooking besides cutting the scattered trees for building their shacks, using the available few grass for roofing and forage for their animals. Desertification has affected the physical, social and economic life of most African communities. It accounts for loss of soil fertility, vegetation cover and reduction of rainfed agriculture.

4.4 Change of the Economy from Rural to Urban

Developing cities have become places for production and economic growth. The World Bank (World Bank Report, 2000) estimated that 65% - 80% of the gross domestic products GDP of countries are produced in cities according to the bank report for the year 2000. The cities are now known as engines of economic growth where their contribution in the gross domestic product in the developing countries is substantial.

4.5 Relationship Between Global Economic Development Model and Urbanisation

The negative and unsustainable outcomes of current urban economies, which are based on high production and consumption of industrial goods, have become more visible. Developing cities are following the steps of the industrial cities and most developing cites prefer industrial development as a means for economical growth. Developing countries have rushed for implementing industrial programmes despite the fact that they are well equipped for expansion in agricultural activities rather than for industrial development. This is because industrial products are more valuable and profitable than agricultural commodities.

While manufacturing has declined in importance in developed countries, it has expanded rapidly in some developing countries. Countries such as Brazil, China, India and South Africa – encouraged by economic and geopolitical changes – are now centres for global manufacturing. Their industries have been intensified, expanded and their production is increased to meet the needs of the global market. Even the peripheral areas in some cities in the developing world receive global funding, in terms of the high tech industries and other industrial service, which are concentrated and developed without feasibility studies or prior planning, as is currently happening in some cities of East Asia.

In the near future, developing cities will become centres of great consumption and wealth and are likely to have higher per capita GHG emissions than previous eras. Developing cities are therefore expected soon to emit very large volumes of GHGs more than what developed cities are generating noting that China has already surpassed USA in GHG emission. Brazil, China, India, Indonesia and South Africa – although not part of the legally binding framework to reduce emissions but their substantial emissions compel them to take a more progressive role in international climate negotiations. Countries status with regard to CO2 emission has already changed and new countries like India and Brazil are now on the run. According to data from Statista, the largest five producers of CO2 emissions worldwide in 2014, based on their share of global CO2 emissions were China 23.4%, US 16.69%, India 5.7%. Russia 4.87% and Brazil 4.17%

The evidences from the IEA Annual Reports (2014) and Statista Website (2015) show that the CO2 emissions of OECD countries has dropped from 66.1% in 1983 to 41% in 2010 and to 38% in 2012. The

CO2 emission of Non-OECD Europe and Eurasia has dropped from 16.2% in 19873 to reach 8.6% in 2012 while the CO2 emissions of China increased from 5.9% in 1973 to 24.1% in 2010 and 26% in 2012. The CO2 emissions of Africa have almost doubled from 1973 at 1.8% to 3.3% in 2012, while that of Asia has more than tripled, increasing from 3% to 11.6% in 2012. The CO2 emissions of Middle East have jumped from 0.8% in 1973 to 5.2% in 2012.

4.6 Inability to Adopt Green Technology by Most Developing Countries

Poor countries are unable to implement policies that provide safe energy supply because of the prohibitive cost envisaged for the reduction of GHGs which requires use of alternate or renewable energy. They will not consider using alternative energy unless it becomes affordable to their nations noting that they are in need for the use of whatever type of energy and to whatever extent to run their factories and provide mobility to their urban dwellers considering that their electricity supply is short even for the use of very essential functions. Table 3 below reflects the huge deficit in energy consumption in most developing countries when compared to that of the developed ones. United States or Canada presently consumes more than 20 times that of an IGAD country and contribute more than 20 times to CO2 emission.

Table 3: Energy use (kg of oil equivalent per capita) in Selected Countries

Country name	2008	2009	2010
Australia	5,779	5,739	5,593
Canada	7,946	7,434	7,380
Finland	6,639	6,227	6,787
Iceland	16,868	16,905	16,882
Luxembourg	8,610	7,939	8,343
Norway	6,250	5,831	6,637
United States	7,488	7,057	7,164
Benin	392	400	413
Congo, Dem. Rep.	356	357	360
Eritrea	137	142	142
Ethiopia	396	398	400
Kenya	461	476	483
Mozambique	421	428	436
Nepal	332	338	341
Senegal	261	270	272
Sudan	364	374	371
Tanzania	449	446	448

Source: IAE Statistics and World Bank Data

4.7 Inability to Establish Large Capacity Public Transport Systems

Nothing can be done by most developing countries to solve the transportation problem. Insufficient public transport capacities and the low traffic speed in addition to limited network of paved roads while growth rates of private vehicle ownership in the developing world continue to soar despite the fact that the rates of private cars ownership in the developed countries is exceptionally high and it surpasses tens of times of the number in the developing countries. According to World Bank data (2003), for example the number of motor vehicles in some European countries e.g.; Finland and the Unites State varies between 612 and 797 vehicles per 1000 people respectively, while this number is in the range 3 - 27 in Ethiopia and Sudan respectively. Large capacity systems such as trains, metros, transit rails, large capacity buses, etc, are not expected to operate in the near future instead, private vehicles utilization rates will increase because cities will not inhibit their use due to absence of alternatives.

5. UN POLICY REFORMATION

A major shift in climate change combat approach by the UN, state governments and the international community is urgently required. Financial support alone is meaningless without global and national policy reformation. Urgent actions are required, at first, to correct the distortions from CC impacts and pre-empt the total environmental disaster. A new strategy supported by sound policies should be put in place to

restore rural life, promote reforestation and enhance eco-agriculture for making the countryside a more appealing place to live in and work. This strategy should be engraved in the minds of those who draft UN Climate Change Programme. Accordingly the following policies need to be replaced by new policies that serve the designated strategy:

5.1 Policies Encouraging Rapid Urbanisation

Bias policies that encourage fast urban growth must be revised and replaced by policies that reverse the population movement towards cities or at least normalizes the process of urban growth. Currently global policies influencing the urbanization processes include:

* The structural adjustments packages imposed by international financial institutions on the developing countries to integrate into the international economy: these have opened the door for the capitalist economic model and promoted knowledge-based economic activities thus, paving the way for industrialization while retarding traditional economies and agriculture. This is a global order drive in which the rich countries seek to shape the world according to their interests, influence and ideological presuppositions. Also the multinational giant companies increased their role and strengthened their power in the global economy.

* The World Trade Organization and the current system of trade, monetary flow, production and consumption, allow few of the rich people to increase their wealth at the expense of others. “Science and Technology” is almost in the hands of the giant companies and lack of control by the community is encouraging these companies to over-exploit resources for profit.

* Reduction of the opportunities of exports from developing countries to the international markets because cost of agricultural production has increased. This is primarily due to the increased cost of the agriculture inputs exported from industrial countries. In addition, agricultural products produced by farmers in industrial countries are subsidized and this lowers the prices of agricultural commodities in the international markets.

5.2 Irrational National Policies

Good governance has not been enforced worldwide to bring governments closer to people and to reform global institutions to bring justice to all Earth inhabitants. UN has to push hard for implementation of good governance in developing countries so as to abandon policies that:

- ✓ Result in uprooting of huge influxes of IDPS and migrants who flood developing cities. Most developing countries are not distributing fairly physical development which is an important means for settling regional disparities and directing population movements.
- ✓ Trigger wars - fighting has been going on in a number of developing countries primarily related to human rights violations, lack of security, marauding and social disturbance, and religious intolerance, racial, ethnic and cultural prejudices, etc. Some of these wars are still raging because external forces stock them with arms and ammunition.
- ✓ Aggravate desertification and poverty - poverty is in most cases attributed to the impacts of climate change such as desertification, soil fertility decline, deforestation, depletion of resources and the loss of biodiversity. These are all having devastating consequences for the livelihoods of the world’s poor. Thus, the poor nations of developing countries will continue to strive for a better way of living because of the threats of poverty, and this would have impact on the environment.
- ✓ Spread poverty due to the unevenness of distribution of economic wealth and other opportunities. This generates group tensions and conflicts and consequential migration of rural people, resulting in megacities resulting in further GHG emissions.

5.3 Local and Global Injustices

It is clear that the world order as a whole needs to undergo a structural transformation in order to bring justice to all Earth inhabitants. This is not so at present since:

Over using the environmental resources through excessiveness of the rich is not checked. The basic environmental problem thus, facing humanity is the continual extravagant usage and depletion of natural resources by developed countries. Many of the developed countries exceeded their Kyoto baseline emissions (e.g. Canada by 54%).

The dominance of the rich over the poor, giving assistance to the poor is seen as charity, not a right or social justice? Since 1986, international organizations and the UN agencies have talked about poverty reduction but in fact the global poverty has increased and the rich countries have become richer. For example in Porto Novo, Benin the percentage of poor families has increased from22% in 1993 to 49% in 2003. Likewise the poverty figures have increased in Sana'a, Yemen from 14% in 1993 to 63% in 2003. Even in countries with high GDP such as Nigeria, the percentage of poor population in Lagos has increased from 53% in 1993 to 62.5% in 20103. In Rio de Janeiro in Brazil, the poor families' percentage increased from 17.5% in 1993 to 30% in 2003.

6. CONCLUSIONS

The global warming, its causes and consequences have been discussed in this paper. The investigation included the ineffectiveness of the polices adopted by the UN organizations to mitigate global warming. A number of ineffectiveness causes are identified while those which led to the failure of the Kyoto protocol to mitigate global warming are highlighted. These included the current developed economic model which was found in this study to favour urbanization mode of life, and has severely impacted the UN policies for greenhouse gases emissions mitigation. There are many drivers of rapid urbanization including development of "megacities" around the world, particularly in the less developed nations need to be addressed if any future polices has to succeed in mitigating the issue of the man made global warming phenomenon.

7. NOMENCLATURE:

IPCC = Intergovernmental Panel on Climate Change

UNEP = United Nations Environment Programme

WMO = World Meteorological Organization

UNFCCC = United Nations Framework Convention on Climate Change

UNDP = United Nations Development Program

8. REFERENCES

TIBAIJUKA, Anna (2006). "UN-HABITAT address at the High Level Plenary", COP13, Bali, Indonesia.

COPs: The 18th, 19th and 20th Sessions of the Conference of the Parties to the UNFCCC and in particular the 18th session of the Conference of the Parties 26 November to 8 December 2012. The Qatar National Convention Centre. Doha, Qatar.

IEA Annual Reports, 2012-2014. "Key World Energy Statistics, 2012-2013 and 2014"

IPCC website (2015). IPCC website www.ipcc.ch and the IPCC WGI AR5 website www.climatechange2013.org

KUMAR and Barrett (2008). State of World Cities, 2012- 2013 (p.24) ; figures for Lusaka were obtained for the local study prepared for this Report

Statista Website (2015): Available online at www.Statista.com,

UN-HABITAT (2001). "World Population Growth 1950 – 2020" World Urbanization Prospects

UN-HABITAT (2007). Global Urban Observatory.

World Bank Report (2015) available online at http://www.worldbank.org

360: Renewable energy options and the nigerian built environment

FERDINAND F O DAMINABO[1]; SAMUEL C DIKE[2]

1 Department of Architecture, Rivers State University of Science and Technology, Port Harcourt, Rivers State, Nigeria. Email: ferdydaminabo@yahoo.com
2 Faculty of Law, Rivers State University of Science and Technology, Port Harcourt, Nigeria. Email: chisadike@yahoo.com

The year 2014, saw the Nigerian economy rebased as the largest in the African continent ahead of South Africa but a critical assessment however exposes huge holes in its energy independence and security with gross underperformance in power security. To adequately unbundle the nation's economic and industrial potentials as well as significant inflow of foreign investments which includes energy, the question of energy poverty needs be addressed. More than 60% of Nigerians' population is not connected to the National grid and power is epileptic which has compelled the Nigerian government to set out plan to launch a National policy on Renewable Energy and Energy efficiency to boost power supply in the country. A 7% renewable energy use by 2025 is the government's assumed target taking advantage of new scientific breakthroughs in energy efficiency and delivery of renewable energy technologies and to attain 30,000MW of renewable electricity within a decade. This paper therefore seeks to examine the necessary renewable energy options with attendant advantages to the environment and use of green energy in off-grid locations across the country for up to 60% of a population of 170 million people which is a huge market for Renewables. The existing templates of renewable energy platforms including foreign participation as well as the market in Nigeria will be in sharp focus. A progress report submitted by the presidential task force committee on power reforms in Nigeria in a 2011 assessment showed the largest gap between demand and supply of electricity in the world and this reinforces the need for this research to harness and provide focal point for both national and international efforts on alternative energy options away from fossils and with futuristic perspectives and use within the Built Environment.

KEYWORDS: Renewable Energy, Power Security, Built Environment

1. INTRODUCTION

Africa's most populous nation, Nigeria is on a knife edge as regards energy poverty sustained by decades of ineffective infrastructural as well as institutional framework and lack of appropriate energy policies that has rendered 60% of its teaming 170 million population without any form of power.

The existing beleaguered generation, distribution and supply networks leave much to be desired in the face of massive supply disruptions. However, with demand growing at the rate of 8.2% annually the need to consider other routes to power generation cannot be overemphasized especially in the area of alternative power generation with renewable options in sharp focus.

The Kyoto protocol and the apparent threat from climate change has made the need for green and sustainable environment a global phenomenon as governments and stakeholders of industries and the scientific community call for a rethink on fossil energy as main energy base and to refocus on cleaner and environmentally friendly energy sources across the globe to mitigate climate change impacts due to global warming.

However, the response is slow even with the greatest emitters like the US and china and it is wisdom to refocus on this challenge across board knowing that our continued existence on this planet depends on the actions we take to mitigate and slow down the process of systematic self-annihilation because of economic advantage and gluttony and ignoring the ethos of the protocol.

2. EXISTING RENEWABLE PLATFORMS AND PILOT PROGRAMS

Nigeria with over five decades of independence is still experiencing vast energy crises in all sectors of its national life and in the renewable sector just a few platforms are in existence or at the preliminary stages of execution. The existing platforms and pilot programs [1] are mostly those instituted by the Nigerian government through the Federal Ministry of Environment and sometimes collaborating with private bodies from international destinations like India and with some state governments in Nigeria.

Some of these are; Global Biofuels Ltd now developing a biofuel production Complex at ilemeso in the northern part of Ekiti state of Nigeria under the platform of Renewable Energy Programme of the Ministry of Environment. Similar plants are slated for Ondo, Kwara, Osun, Oyo, Kogi, Kaduna, Kano, Zamfara, Benue, Plateau, Nasarawa and such other states in Nigeria that lie between latitudes 7o and 14° North of the Equator[1]. Renewable Energy Program office, Adamawa State Government and Green Carbon Afrique is developing sugarcane based biofuel plants in Girei and Demsa Local Government Areas of Adamawa State covering 2,000 hectares plantation.

This initiative is to produce sugar for local use and export, ethanol and ultimately electricity. This integrated project is being replicated in ten states of the country. However, working in conjunction with Carbon Quest and Adamawa State, the Renewable Energy Program office is establishing an integrated Rice Processing and Power Generating Facilitator the economic benefit of the investing State, by bringing home the advantages of large scale Rice production, self-generated Power from rice-husk as well with 85%, availability of power to the urban and rural communities.

3. RENEWABLE ENERGY AND THE BUILT ENVIRONMENT

The Abuja Green City is an initiative of the Renewable Energy Programme of the Federal Ministry of Environment together with Green carbon Afrique Creation Environmental Services and Integra integrated' Renewable Energy services[1]. The Project has the full commitment of the Federal government, the Federal Capital Territory and the Federal Ministry of Environment.

This will increase Abuja city green credentials with low carbon emission and when completed will be the first in Africa and second in the world after Masdar city in United Arab Emirates. The low-carbon development is using a combination of local electricity generation, improved insulation, and energy efficient devices for the apartments. However, to deepen and engrave Renewable energy use in the psyche of the nation, energy efficiency in buildings and a cocktail of renewable energy options must be incorporated into the energy mix to achieve a maximum, durable and sustainable result in the medium and long term basis in Nigeria and most developing countries, Figure 1.

This is based on the unanimous submissions from all sources as well as climate change experts and the scientific community that global warming is occurring on larger scale than initial predictions, thus all mitigation channels must be exploited to slow down the process including Eco design solutions Figure 2, as buildings, their construction and operations constitutes the greatest source of greenhouse gas.

A/. Wind Energy *B/. Solar*

Figure 1

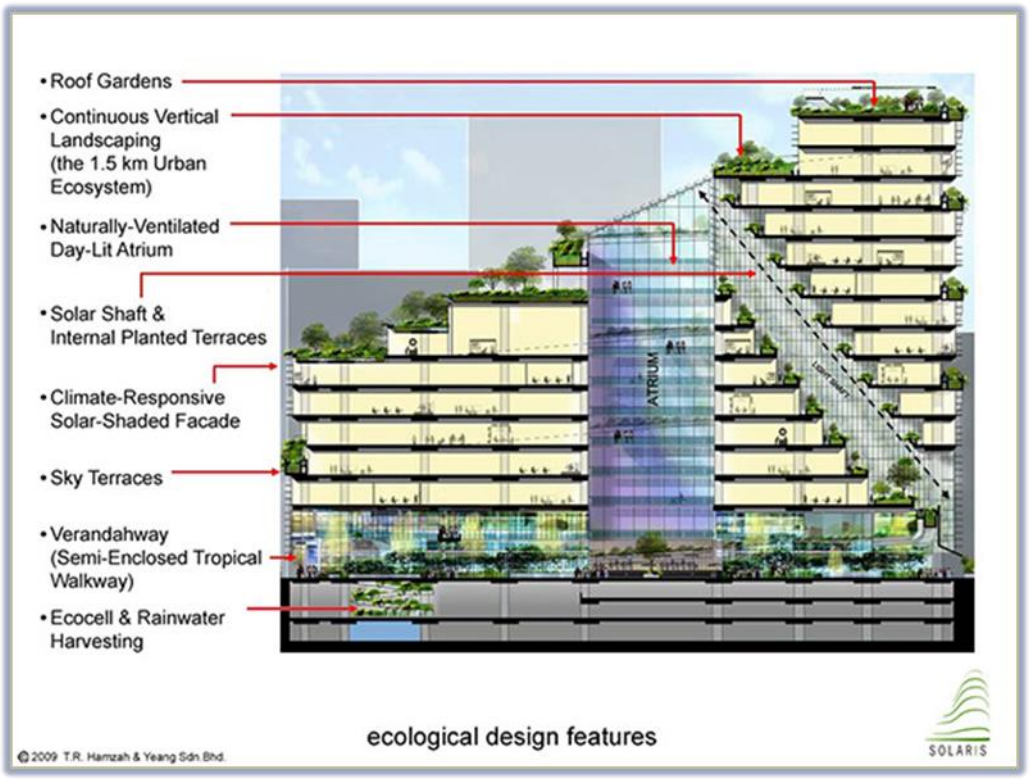

Figure 2. Solaris Singapore, an example of a green building

all mitigation channels must be exploited to slow down the process including Eco design solutions Figure 2, as buildings, their construction and operations constitutes the greatest source of greenhouse gas emissions causing global warming. It is by virtue of its size, one of the largest users of energy, material resources, and water, and also a formidable polluter of the environment [2, 3].

The Report Emissions for Greenhouse Gases in the United States [4], estimates that around half of all non-renewable resources mankind consumes are used in housing construction, making it one of the least sustainable industries in the world. A quick evaluation of the role of buildings in the global warming matrix is the aggregation of their embodied energy, transport energy and operational energy constituting a greater percentage of GHG emissions from all sources.

Despite the Kyoto protocol, many industrial nations including the US ignore the clarion call to do something about our warming planet for some unspecified reasons mostly economical but time is ticking as we all are at the verge of a major global catastrophe now or in the future and third world countries are at risk as their minimal resources can hardly protect them from the consequences of climate change when compared to the developed world who have benefitted from the production of GHG and by implication have more resources to protect themselves from the consequences of climate change. On the other hand, third world countries with their expanding population emit less GHG, and have less benefit from the production of GHG but will bear the consequences of emissions far from their shores.

As an expression of the principles of sustainability, [5] it is highly desirable that buildings have substantial capacity to self-regulate use of energy, temperature and water use as it responds to daily and seasonal temperature and precipitation cycles and more so reducing emission level of greenhouse gases, of which the built environment and construction activities contribute the highest proportion of atmospheric and environmental pollutants thus exacerbating the precarious disposition of the global climate. The current level or stock of greenhouse gases in the atmosphere is equivalent to around 430 parts per million (ppm) CO2 [6], compared with only 280ppm before the Industrial Revolution. These concentrations have already caused the world to warm by more than half a degree Celsius and will lead to at least a further half degree warming over the next few decades, because of the inertia in the climate system. [7]

4. RENEWABLE POWER PROJECTION

The International Energy Agency (IEA) has projected that renewable power generation in Nigeria Table 1, and others would increase by 60 per cent by 2017[8], given the increasing relevance of the new technology in the global power mix despite the economic uncertainties and insecurity of most developing countries. Current indicators are reassuring as government at various levels strive to maintain a grip on the result of the rebasing of the Nigerian economy of which the impact has not been felt by a sizeable section of the population but nevertheless a positive green shoot.

Federal Ministry of Environment (Renewable Energy Program), Federal Ministry of Women Affairs and International Centre for Energy Environment and Development (ICEED) through the Alliance for Clean Stoves initiated a sensitization campaign to effectively change the mind-set of the average Nigerian about firewood and introduce them to the healthier and cheaper option of clean cook stoves.

The main thrust of the alliance is to distribute 30 million clean and energy efficient cook stoves in the next 5 years. Considering the prospect of solar energy in a developing economy like Nigeria, the Synergent Powershare Group of Company is investing in a 50 MW solar farm in Kaduna which was officially launched by the Honorable Minister of Environment and Kaduna State Governor in September 2011, a major contribution to the energy matrix in the country with Table 2 indicating sectorial energy consumption in Nigeria,

Table 1: Renewable Energy Potentials [8]

Resource	Capacity	Remark
Large Hydropower	11,500 MW	Only 1972 MW exploited
Small Hydropower	3,500 MW	Only about 64.2 MW exploited
Solar	3.5 kW/m/day – 7.0 kW/m/day	Refer to solar radiation map
Sunshine Hrs	(4-7.5)hrs/day	
Wind	2-4 m/s @ 10m height mainland	Electronic Wind Information disk (WIS) available
Biomass	Fuelwood	11 million hectares of forest and woodland
	Animal Waste	245 million assorted in 2001
	Energy Crops and Agric Residue	72 million hectares of Agric. Land

Sources: (i) Nigerian National Petroleum Corporation (NNPC) 2007)

(ii)Renewable Energy Masterplan (REMP) 2005

(iii)Ministry of Mines and Steel Development (2008)

Table 2: Percentage Electricity Consumption by Sector [8]

S/N	Sector	1988	1989	1990	1995	1999	2002
1.	Industrial (%)	30.2	30.2	25.7	21.9	21.7	24.1
2.	Commercial & Street Lighting (%)	12.8	12.8	23.8	25.6	26.8	25.9
3.	Residential (%)	57.0	57.0	50.5	52.5	51.5	50.0
	Total (billion kWh)	7.865	8.854	7.944	9.435	8.576	12.118

Source: Central Bank of Nigeria (CBN) (1990), Federal Office of Statistics (FOS) (2002)

5. RENEWABLE ENERGY POLICY, REGULATION AND LEGISLATION

The 2003, National Energy Policy of the Federal Government was approved to encourage the optimal utilization of the country's energy resources and renewables was top on the list of the energy options for a sustainable national development with the active private sector participation. The following policies are articulated for solar energy, biomass and wind [8]:

Solar Energy:

- The nation shall aggressively pursue the integration of solar energy into the nation's energy mix

- The nation shall keep abreast with worldwide developments in solar energy technology.

Biomass:

- The nation shall effectively harness non-fuelwood biomass energy resources and integrate them with other energy resources

- The nation shall promote the use of efficient biomass conversion technologies.

Wind:

- The nation shall commercially develop its wind energy resource and integrate this with other energy resource.

- The nation shall take necessary measures to ensure that this form of energy is harnessed at sustainable costs to both suppliers and consumers in the rural areas.

Regulation and Legislation

In 2005, the Energy Commission of Nigeria in collaboration with the United Nations Development Program (UNDP) drafted a Renewable Energy Masterplan [8] from the National Energy Policy strategies. The masterplan provides a roadmap or activities that will enable the implementation of the policies on renewable energy, with targets/milestones and timelines in the short, medium and long terms.

In 2007, a biofuel policy initiated by the country's National Petroleum Corporation (NNPC), was approved by the Federal Government. The policy articulates amongst other things, a seeding, program within which up to 10% mixture of ethanol in premium motor spirit (E10) and 20% of biodiesel in petro-diesel (B20) by volume are to be imported and used as automotive fuels in the country.

6. MAJOR RENEWABLE ENERGY APPLICATIONS IN NIGERIA

The renewable energy matrix in Nigeria Figure3 and 4 are in the area of;

- Electricity generation

- Biofuel

- Other thermal energy mix (cooking, drying, heating, etc.)

The coordination of the national policies on energy in all its ramification rests on the Energy Commission of Nigeria, established by law in1979.Generally, the Nigerian electricity sector was liberalized by the Electric Power Sector Reform Act of 2005, and a strong regulatory institution, the Nigerian Electricity Regulatory Commission (NERC) was thereafter established.

NERC has the general mandate to regulate the entire electricity sector in the country with regards to tariff setting and regulation, supervision of market rules, performance monitoring, and overseeing the orderly transformation of the power sector to a more competitive environment. Licenses are required for generation of 1MW aggregate and above at a site; and distribution of power of capacity greater than 100kW in aggregate at a site. Generally, automotive fuels in Nigeria are regulated by the Department of Petroleum Resources (DPR). Automotive fuels include both mineral fuels and biofuels.

Other relevant regulatory institution to renewable energy is the Standard Organization of Nigeria (SON), charged with responsibility of setting and enforcing standards of goods and services in Nigeria.

Therefore, the quality standards of solar PV modules, inverters, batteries, solar cookers, improved woodstoves, biogas digesters etc. should be enforced by SON; after the standards have been set in conjunction with relevant bodies like the Energy Commission of Nigeria, Manufacturers Association of Nigeria, Nigeria Society of Engineers, NERC and others.

The National energy Masterplan, which includes renewable energy, as well as the masterplan are yet to be passed into law through an Act of National Assembly.

The National Assembly is, however, being sensitized to facilitate the consideration of an energy bill that would enable the enactment of the National Energy Policy and Masterplan into law.

Figure 3: Solar Street Lighting in Uyo, Cross River State

Figure 4: Solar PV at Ilaje, Ondo State of Nigeria

7. FOREIGN PARTICIPATION AND INVESTMENT

Nigeria now boast as the largest economy in Africa despite the fall in oil prices by a half. With over 60% of Africa's' most populous nation of over 170 million, the market cannot be better for investing in both energy production and distribution and more so in the renewable energy sector. The International Energy Agency (IEA) has projected that renewable power generation in Nigeria and others would increase by 60 per cent by 2017[8]. Again the National Energy Policy of the Federal Government was approved in 2003[10] to encourage the optimal utilization of the country's energy resources and renewables was top on the list of the energy options for a sustainable national development with active private sector participation.

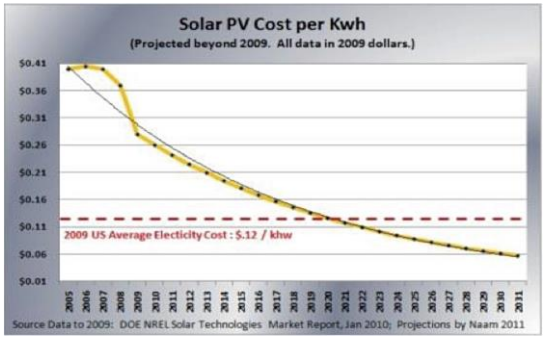

Figure 5: Solar PV cost per Kwh. Source: Nigeria Low Carbon Plan: Power Sector – Interim Presentation, October 2011.

The Abuja Green City, an initiative of the Renewable Energy Program of the Federal Ministry of Environment together with Green carbon Afrique, Creation Environmental Services and Integra integrated' Renewable Energy service are strong pointers that business will be good with impetus from the federal government of Nigeria through its ministries and various agencies. Another governmental contribution is to insist on advancing the renewable option based on its long term benefits.

For instance, If a typical household has a choice of a solar lantern with no ongoing energy costs priced at N3,000 ($19) and a kerosene lantern with constant fuel needs costing N300, the likely result, where money supply is not flexible, is to choose the lantern that is cheaper in the short term.

Translated to a larger scale, an investment of N40, 000 for a generator with weekly fuel costs of N3, 000 will win over a small solar/inverter combination costing N250, 000, Figure 5. Cheap startup capital or loans, together with education to improve awareness of the long-term benefits and increasing reliability of solar-powered products, could go a long way to making the alternative renewable choices a possibility. [10] But would be foreign investors are skeptical about investing in renewables or any other business because of security challenges.

Currently, the new administration of President Buhari has promised to deal decisively with security matters and create a secure platform for business to thrive thus allaying the fears of foreign investors and the international community. However, it is worthy to note that despite the security challenges in Nigeria, it is not just as bad as it is in Baghdad, Afghanistan or Syria and so business can be good in Nigeria as only small section of the Northeast and Southern Nigeria is experiencing minor disruptions.

8. DISCUSSIONS

The renewable energy sector in Nigeria is still in its infancy and the government and its various agencies are now turning to alternative sources of energy to make up for its shortfall in energy supply. Current levels are ridiculously low with massive disruptions that have impacted negatively on the economy. Power supply from the grid is epileptic, coupled with infrastructural decay and vandalization of existing facilities. Sustained decades of energy poverty due to ineffective infrastructural as well as institutional framework and lack of appropriate energy policies has rendered 60% of Nigeria's teaming 170 million population without any form of power.

The existing beleaguered generation, distribution and supply networks leave much to be desired in the face of massive supply disruptions and gas shortages. This makes it a viable investment heaven as current operators of the renewable sector are small scale with limited impact on the Nigerian renewable market. Government must commit to renewable energy by creating and supporting systematic policymaking, research and finance for the development of the sector [10].

Other measures by governments to promote the renewable energy market include educational campaigns aimed at policy makers, businesses and the populace to understand the immense benefits of renewable energy as a potent alternative to fossil based energy. State governments should consider reducing business costs for renewable energy companies in order to lower barriers to product expansion [10]. Renewable energy developers and financiers need to work together to make the case for renewable energy in both homes and businesses with a clear path to affordable options for customers with very different needs.

There are few companies, and organization that are dealing with the renewable energy technology in Nigeria which are the Luminous Inverter, Solar mate engineering limited, Chevron, Avatar Energy, new Era Energy, CREN, ICEED etc. Chevron is one of the companies that handle renewable energy sector in the country. They are the world leader in delivering and developing energy from oil and gas which is still the world the most important source of energy for years to come. [11]

The Nigerian Green Energy Company (Avatar Energy) is one of the renewable energy companies in the country that is inspired by the need for a continuous positive impact, diversity, growth and development, in the renewable energy and agricultural sector. [12] The new Era Energy is a specialized company that was created and based in Nigeria to source; maintain and supply renewable energy solution for the Council for Renewable Energy Nigeria (CREN), a non-profit (NGO) multi-stakeholder organization or association which promotes the utility of renewable energy technologies in Nigeria. [13]

9. CONCLUSION

The implications of promoting renewable energy sector is not just something exclusive to Nigeria but a global pursuit that must be encouraged and sustained to save our planet. The Nigerian scenario is that of not plugging all the holes that will ensure energy security and bring over 60% of her population out of energy poverty.

This massive shortfall however creates a huge energy market in Nigeria that should invigorate foreign investors in this sector with Nigeria benefiting from a slush of investment funds and infrastructure thus breathing new life into the economy that despite the rebasing of the economy as the largest in Africa has suffered setbacks from the fall in oil prices.

However, with concerted effort on the part of government and the private sector in creating an enabling environment, renewable energy businesses in Nigeria will thrive and leaving a green energy footprint beneficial to all as the world must come together to confront greenhouse gas emissions and the resultant changes in weather patterns due to global warming.

10. REFERENCES

[1] http://www.ngrguardiannews.com; (Accessed; May, 2015).

[2] DING, Lei, Roberto G. Quercia, Wei Li, and Janneke Ratcliffe. 2010, May 17. “Risky Borrowers or Risky Mortgages: Dis- aggregating Effects Using Propensity Score Models.” Working Paper. Durham, NC: Department of Urban Studies and Planning and the UNC Center for Community Capital.

[3]. DING, G.K.C. (2008) Sustainable construction – The role of environmental assessment tools, Journal of Environmental Management, Vol. 86 No.3, pp.451-64.

[4]. United States Department of Energy (USDOE). (2010). Energy Efficiency and Renewable Energy. Federal Energy Management Program. 1-34.

[5] KOSTER, Egbert. (1998) Natuur onder architectuur: Architecture for nature Schuyt & Co.: Haarlem, P 7.

[6] EPA (forthcoming) ‘Global Anthropogenic non-CO2 greenhouse gas emissions: 1990-2020’, USEnvironmental Protection Agency, Washington DC. Emissions data obtained from correspondence with EPA team. Environmental Change Institute (2004), ‘Methane UK’, Environmental Change Institute: Oxford, United

[7] IPCC (2001) .pp 4-5

[8] SAMBO, A.S., (2010). A Paper Presented at the World Future Council\strategy Workshop on Renewable Energy, Accra, and Ghana.pp19-24.

[9] NAN – http://www.nannewsngr.com; (Accessed; May, 2015).

[10] NEWSON, Chris, (2014). Renewable energy potential in Nigeria: Low carbon approaches to energy delivery through renewables. Pp 1-2.

[11] Chevron Webpage 2012; General&utm_medium=cpc&utm_source=Google&utm_term=renewable_energy

[12] Avatar Energy (2011).http://www.avatarenergyltd.com/

[13] Council for Renewable Energy in Nigeria 2011 (Accessed May, 2015) http://renewablenigeria.org/

240: Risk assessment in a central receiver system

SAMANIEGO DANYELA.[1], FERREIRA ALMERINDO D[2], GAMEIRO DA SILVA MANUEL[3]

1 Department of Mechanical Engineering, University of Coimbra, Portugal, danyela.samaniego@gmail.com.
2 ADAI-LAETA, Department of Mechanical Engineering, University of Coimbra, Portugal, almerindo.ferreira@dem.uc.pt
3 Department of Mechanical Engineering, University of Coimbra, Portugal, manuel.gameiro@dem.uc.pt

Sun is used as a renewable source for electricity production by the concentrated power systems (CPS). Among the CPS technologies available, the central receiver system (CRS) is becoming more popular within the options in the promising future of solar thermal industry. Basically the CRS technology consists in the concentration of sunrays on the receiver by reflecting them in heliostats' surfaces (mirrors). The reflections can be differently classified based on the concept of human-interacting situations, e.g. the reflection aimed the sky, reflections from one single heliostat, the reflected irradiance from the receiver or concentrated solar radiation from the field of heliostats. Since solar radiation has the potential to interact positively and/or negatively with biological human systems, and adding that CPS facilities are usually located in sunny environments, those situations might exhibit scenarios of potential risks for human health. The workers sometimes developed their duties under lower protection. Those stages could happen, for instance, to people located up in the central tower, workers who stand in front of a heliostat surface, and also people in the near surroundings. Based on simulations of the irradiance flux in a CRS, through the usage of software SolTRACE®, this paper aims to provide information about the assessment of eye exposures.

Keywords: Solar energy, environmental conditions, risk assessment, concentrated power systems, central receiver systems

1. INTRODUCTION

Natural light is present in solar thermal power plants in a daily basis. Due to the countries´ motivation of using renewable energy sources for electricity production instead of fossil fuels, the thermal solar power plants are increasing its capacity of power generation and quantity over the world. One of the several types of solar thermal technology is based on the concept of the concentration of sunrays, also known as the concentrated solar power (CSP) systems, using the solar radiation as a renewable source for electricity production through a thermodynamic cycle (Hamilton, 2011; IRENA, 2013).

Behar, et al., (2013) recognized that among all the CSP technologies available in the late years, the one that uses central receiver system (CRS) is the type of technology moving to the forefront. Basically these systems concentrate the sunrays on the receiver by reflecting the sun light through heliostats' surfaces (mirrors). The receiver absorbs the concentrated solar energy and transfers it to a circulating fluid (Kalogirou, 2009). The heated fluid is pumped into storage tanks and passed across a heat-exchanger, where steam is produced. This steam drives a generator in order to produce electricity (Hamilton, 2011; IRENA, 2013; Romero, et al., 2002). The heliostat' surface is designed to focus the beams on the receiver where the reflected light will be scattered on a degree that increases proportionally to the distance between the heliostat and the focal point.

According to Franck, et al., (2010) those reflections can be classified in different human-interacting situations. The reflection aimed at the sky (potential risk for airplane pilots), non- concentrated reflection from one single heliostat (potential risk for a person standing in front of the mirror), concentrated solar radiation from the heliostats field (potential risk for workers located in the solar tower) and solar field and beyond (potential risks for people located outside the heliostats field although near, e.g. roads). Otherwise other scenarios are also added according with Ho, et al., (2011) e.g., the diffuse radiation from the receiver, the reflection from the mirrors when they are moving from the standby mode or stowed position and when they are not orientated toward the receiver.

Also the CRS has to be submitted to a regular heliostats cleaning and maintenance operations because those activities will allow maximum reflectivity from the heliostats surface to achieve the desired productivity levels. The cleaning activities can be rather accomplished by a cleaning system based on wet brushing (robot) (SENER, 2012) or/and by manual activities (Kattke, and Vant-Hull, 2012), in cases with the presence of some environmental agents, such as: material that could become chemically attached to the heliostat surface, i.e. blow down from cooling tower, and smog or air contaminants. In other hand, no specific information was found about heliostats reparation or installing replacements (SENER, 2012; Kattke, and Vant-Hull, 2012)

James Hamilton in 2011, classified some of the duties, among solar thermal facilities, as repetitive, physically demanding and sometimes developed under inclement weather conditions, especially those workers in charge of the control and operation of pump manifold systems and the ones in charge of the installation, maintenance and reparation of the pipe systems.

The CPS facilities are usually located in sunny environments with a high solar ultraviolet index. The solar radiation has the potential to impact in biological systems. Those impacts are direct or indirectly alterations (effects) which produce a physiological, biochemical or behavioural changes; resulting from that process several types of damage to the eyes (Kwan- Hoong, 2013; Franck, et al., 2010; Brauer, 2006; Carrasco, 2003; Stanojevic, et al., 2004). Within some relevant literature, such as standards, a classification of health pacts to the eye is provided in the *Table. 1.*

In 2014, Ho, C. K., et al., developed a study which was requested by the personnel of the solar power plant Ivanpah located in United States. Such request was based on the reports submitted by pilots and air traffic controllers about the glare coming from that facility. The fact drove to the evaluation of glare in order to understand the causes and health impacts. Once quantified the irradiance in the facility and identified the potential ocular impacts of the glare, mitigation measures were taken. The results showed that the intense glare was caused by heliostats surfaces when in standby mode, i.e. when deviated to the side of the receiver, had the potential to cause an after-image effect (temporary blind spot on a sight) up to a distance of 10 km.

Environments with these characteristics might represent an indirect drawback because working places under that kind of environmental conditions seems to allow possible scenarios of potential risks for human

health where it might be necessary to analyse the environmental conditions in order to ensure the occupational health and safety in future facilities. With the help of the software SolTRACE®, this paper aims to evaluate the eye exposures based on simulations of the irradiance flux in a CRS.

Table. 1. Solar radiation irreversible and reversible ocular effects in health. Literature adaptation.2

Reversible physiological effects					
wavelength (nm)	**Affected area**	**Primary effect**	**Description**	**Secondary effects**	**Side effects**
400 – 780 nm VL	ocular	**Afterimage**	Blind spot in the visual field which persists from seconds to a few minutes after the light in no longer in the visual perimeter.		Accidents, falls, injuries
400 – 780 nm VL	ocular	**Glare (dazzle)**	Refers to temporary inability to see details in the area of the visual field around a bright light.		Accidents, falls, injuries
400 – 780 nm VL	ocular	**Glare disability**	Veiling luminance (the scattered light that overlays the retinal image) in the human eye reduces the contrast in the scene.		Accidents, falls, injuries
400 – 780 nm VL	ocular	**Flash blindness**	An immediate and temporary loss of vision produced when the retinal light – sensitive pigments are bleached by light more intense than that to which the retina is physiologically adapted at the moment.	Dazzle, temporary scotoma or afterimage,	Accidents, falls, injuries
400 – 780 nm VL	ocular	**Luminance flicker**	Temporal intensity modulations of bright lights	Vertigo, disorientation, mild headaches, muscle spasm to convulsions and epileptic seizures (the effect of increase with the intensity of the source and also depends of the photosensitivity of the person).	Accidents, falls, injuries

Irreversible physiological effects					
wavelength (nm)	**Affected area**	**Primary effect**	**Description**	**Secondary effects**	**Side effects**
380-1400 nm UVA – VL – IR	ocular	**Thermal eye lesions**	Most of the useful vision is lost	Burns in the retinal tissue	
1400 – 3000 nm-10 μm IR-B, IR-C	ocular		Protein coagulation of the front and middle layers, ulcers.	Burns in the cornea	
315- 400 nm UVA; 780 – 3000 nm IR	ocular		Opacities in the lens	Cataracts	
180 - 400 nm UV	ocular		Inflammation on the cornea (the effect of feeling sand in the eye)	keratitis	
400 - 700 nm VL; 780 – 3000 nm IR	ocular		vision loss in a portion of the visual field	scotoma	
300 – 700 nm UV-VL	ocular		Inflammation of the retina of the eye	Retinitis	

2. METHODOLOGY

The eye is significantly sensitive to solar radiation. Even though, it is protected against the bright light by natural responses that commonly are the action of blink or deviating the looking to other sides instead the bright source, ending this process in a momentary exposure. Even if the workers are exposed to lower momentary intensities, the cumulative exposures might cause an acute damage (Franck, et al., 2010; Sliney, 1994; Sliney, et al., 2005).

Ho, et al., (2009) and Brumleve (1984) proposed a short-term exposure parameters in order to assess the bright light sources in CPS installations. In those studies two variables were defined as a necessary for the evaluation of the impact of solar radiation in the eyes: retinal irradiance (E_r), which is the power of the solar radiation that strikes a surface, and the subtended angle (Equation 1) of the glare source (ω).

Equation 37: Subtended angle of a glare source

$$\omega = d_s / r$$

Where:

- d_s = source size
- r = distance between the eye and the source

Since the radiation in the frontal plane of the cornea E_c (W/m^2) has to be known, the estimation of it can be measured with a radiometer or rather simulated by using a software, i.e. SolTRACE* (http://www.nrel.gov/csp/soltrace/download.html) . Then the E_r (retinal irradiance) can be calculated by the total power that enters in the pupil and the area of the retinal image (Equation 2):

Equation 2: Retinal irradiance

$$E_r = E_c\left(\frac{dp^2}{dr^2}\right)\tau$$

Where:

- d_p = daylight adjusted pupil diameter (~2mm) (Brumleve, 1984)
- $d_r = f\omega$; The product of focal length of the eye (0.017) and the subtended angle (Sliney and Freasier, 1973).
- τ = transmission coefficient (~0.5) (Brumleve, 1984).

The relation of the subtended angle and the retinal irradiance with the potential risk to the eye resides in the moment that ω increases and the safe threshold for E_r decreases proportionally. In other words the delivery of power into the retina occurs in larger amount and then permanent eye damage might occur. It can be represented by Er,burn (burn in the retina in W/cm2). According to Brumleve (1984) the threshold should be delimited by the equation 3:

Equation 3: Burn in the retina threshold

$$E_{r,burn} = \frac{0.118}{\omega} \; for \; \omega < 0.118 rad$$

$$E_{r,burn} = 1 \; for \; \omega \geq 0.118 rad$$

As the burns in the retina, the temporary blindness caused by a flash (after-image effect) also depends on the size of the subtended angle of the source but differs on the severity of impact. The authors (Ho, et al., 2009; Brumleve, 1984) affirm that the size of the after-Image and the impact would be lower with small angles. The potential threshold of after- image ($E_{r,flash}$) (W/cm^2) can be calculated through equation 4:

Equation 4: Potential threshold of after- image

$$E_{r,\,flash} = \frac{3.59x10^{-5}}{\omega^{1.77}}$$

Once the values of E_r are calculated, they can be compared with security metrics provided by Ho, et al. in 2011. The figure 1 resume the potential impacts in the eye in a short-term exposure, where three potential risks of impact regions are defined: the risk of permanent damage to the eyes or retinal burn in 0.15 seconds (typical average time of blink response), potential for a temporary after-Image effect (flash blindness), and low potential to produce after-Image effect.

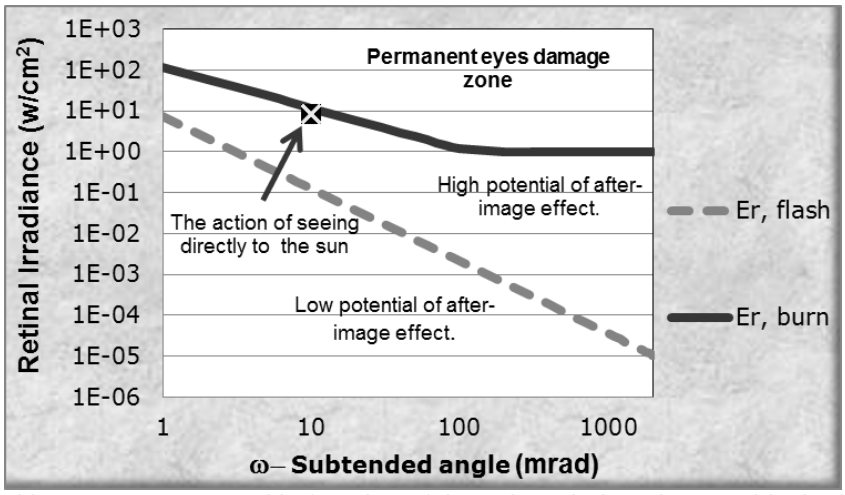

Figure 1: Potential impacts represented in function of the subtended angle. Graphical adaptation of Ho K. C., et al. (2011).

It is important to notice the fact that the quantified metrics and retinal irradiance estimations do not considered all the factors and situations, e.g., the atmospheric attenuation, when a person is wearing sun glasses, human factors and behaviours, and also multiple beams from adjacent receiver (Brumleve, 1984).

The action of seeing the reflection from the receiver can be simulated as a diffuse source because it is designed to absorb the concentrated solar radiation coming from the heliostats field (Brumleve, 1984). In 2012, (Samaniego, et al., 2012), proposed a way to evaluate the reflected irradiance coming from diffuse sources. The angular size of the source is determined by the effective area reflected on the receiver' surface which is seen by the observer (Figure 2). The effective area seen by the observer (A_{obs}) it can be calculated by equation 5 and it depends on the total illuminated area on the receiver' surface and the angle of the observer respect to the receiver. At the same time it depends on the tower height and the distance.

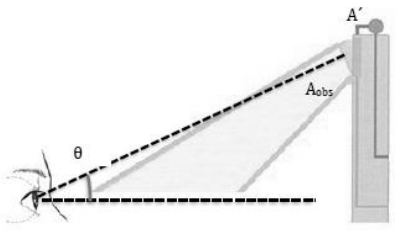

Figure 2: Observer respect to the receiver.

Equation 5: Effective area seen by the observer

$$A_{obs} = A^{'} \cos\theta$$

Where:

- $A^{'}$ = Area of the reflecting surface

Once the total illuminated area is known, the reflected irradiance (E_{ref}) can be calculated (equation 6) by multiplying it by the reflection coefficient (ρ), which varies from 0.8 to 0.2.

Equation 6: Reflected irradiance

$$E_{ref} = \rho E^{'}$$

Where:

- ρ = Reflection coefficient
- $E^{'}$ = Irradiance of the reflecting surface

However, there is a difference between the total reflected radiation that is seen by the observer and the total amount of radiation just outside of the eye cornea. The main reason is the distance and the angle in which the observer is located respect to the receiver. The irradiance outside of the cornea (E_c in W/cm^2) is defined by equation 7:

Equation 7: Irradiance outside of the cornea

$$E_c = E_{ref} A^{'} \frac{X_{obs}}{\left(z_{obs}{}^2 + X_{obs}{}^2\right)^{\frac{3}{2}}}$$

On the other hand, the energy (per cm^2) that enters through the pupil (E_r) is equal to the average of the energy that is outside of the cornea; the area of the pupil for a determined distance (location of the observer) over the area seen by the observer. With a transmission coefficient of τ=0.5 and a focal length of the eye of f=0.017m, the E_r is calculated by equation 8:

Equation 8: Energy per cm^2 that enters through the pupil

$$E_r = \frac{E_c A_p \pi r_{obs}{}^2}{A_{obs} f^2}$$

Where:

- A_p = Projected area
- A_{obs} = Observed area
- r_{obs} = observer distance

The E_r calculation refers to the amount of radiation on the retina produced by a single heliostat. Therefore, the amount of radiation that reaches the retina in **n** heliostats is determined by an equivalent area (equation 9) for an equivalent irradiance (equation 10).

Equation 9: Equivalent area

$$A_{equiv} = \sum_{i=1}^{n} \frac{A'_n E'_n}{E'_n}$$

Equation 10: Equivalent irradiance

$$E_{equiv} = \sum_{i=1}^{n} E'_n$$

Where:

- A_n and E_n are the area and irradiance, respectively of each of the ***n*** heliostats.

3. DESIGN OF THE ASSESSMENT

In Ivanpah (Ho, et al., 2014), over 170,000 heliostats with 2.6 million square meters of mirrors reflect and concentrate sun irradiance. It counts with three receivers of the 140 m (459 ft) of height that produce steam for the power cycle. In order to assess the case of glare coming from the receiver' surface and a heliostat in its focal point, sibling to the activity of cleaning the heliostat' surface, a design of evaluation is proposed.

The method seeks to evaluate the situation of seeing the diffuse radiation from the receiver when the heliostats are reflecting the sun beams on it. The analysis is accomplished in order to find an analytical solution to evaluate the radiation from sources (heliostats and receiver of the tower). The software "SolTrace", tool developed at the National Renewable Energy Laboratory (NREL, 2014), allows the simulation of the irradiance flow according to the distance.

There are two scenarios of evaluation. In the first situation a heliostat is simulated at different distances, passing through its focal point, i.e. the point with the highest concentration of aces. The data with more relevance, is the irradiance peak flow, since what is being sought is to detect the worst possible situations. The second situation summarizes the irradiance and ocular impact of the glare of the receiver in the top of the tower. The equivalent irradiance (E_{equiv}) refers to the sum of the irradiance of ***n*** heliostats' images overlapping in the receiver' surface. Taking into account the characteristics of the facility Ivanpah, the heliostats within 3 km are candidates to simulations (figure 3).

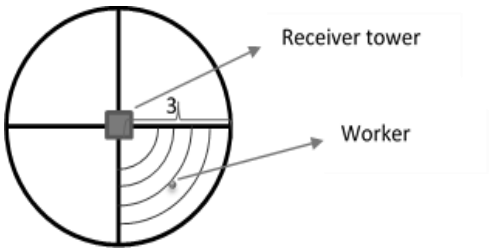

Figure 3: Observer respect to the glare of the receiver.

Heliostats groups are defined and the average of each of the group's irradiance is taken.

H4, a 50 m, represents 20 heliostats (grup 1)

H15, a 100 m, represents 40 heliostats (grup 2)

H45, a 500 m, represents 201 heliostats (grup 3)

H60, a 1000 m, represents 403 heliostats (grup 4)

H80, a 200 m, represents 80 heliostats (grup 5)

Subsequently a comparison with the security metrics established by the authors (figure 1) and after that the areas of risk depending on the distance can be define.

4. RESULTS

The application of the method and the equations developed in the part of methodology (section 2), were applied in the following characteristics: E_c coming from simulations, d_p= 0.002m, f =0.017m, β= 0.0115 y τ = 0.5, y E_{DNI} de 1000 W/cm^2.

In figure 4, the irradiance reaching the retina as a result of the refection of the heliostat' surface in its focal point is compared with $E_{r,\,flash}$ and $E_{r,\,burn}$ settled by the authors of the literature reviewed (fig. 1). As a result the power of the irradiance coming from the heliostat surface is sufficiently high to cause a permanent damage in the eye.

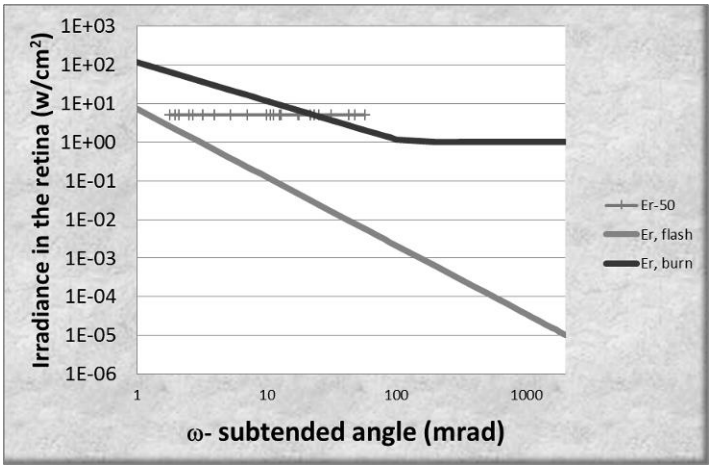

Figure 4: The action of viewing directly the heliostat' surface.

The figure 5 represents the establishment of the distances at which the irradiance received in the retina of the eye is powerful enough to cross the limit of permanent damage, delimited by the $E_{r,burn}$.

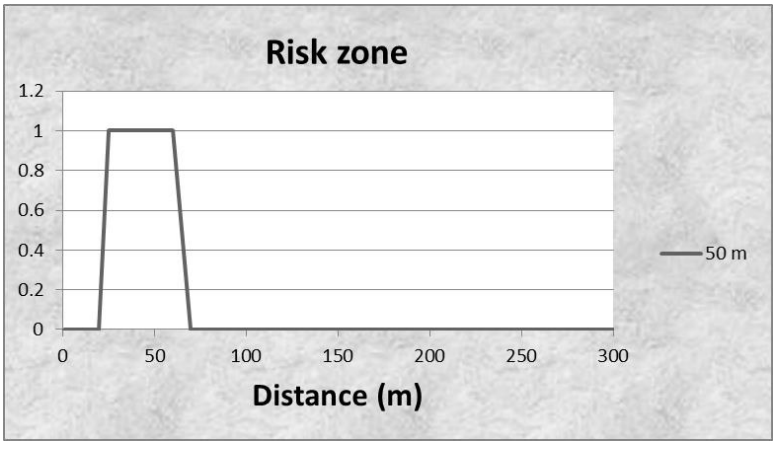

Figure 5: Risk zone of the action of viewing directly the heliostat' surface

The second situation consists in the evaluation of the reflection of the sunlight on the surface of the receiver, subject area that is seen by the observer and its particular angle, as well as the distance (1 to 3km). Supposedly 744 heliostats' images overlapping on the receiver were evaluated. After that, a comparison with limits of E_r, burn and E_r flash provided by other authors was made. The results show that the irradiance

has sufficient power to create a post-Image effect (Figure 6). On the other hand the area of risk within 150 m where there is a post image effect might occur are shown in Figure 7.

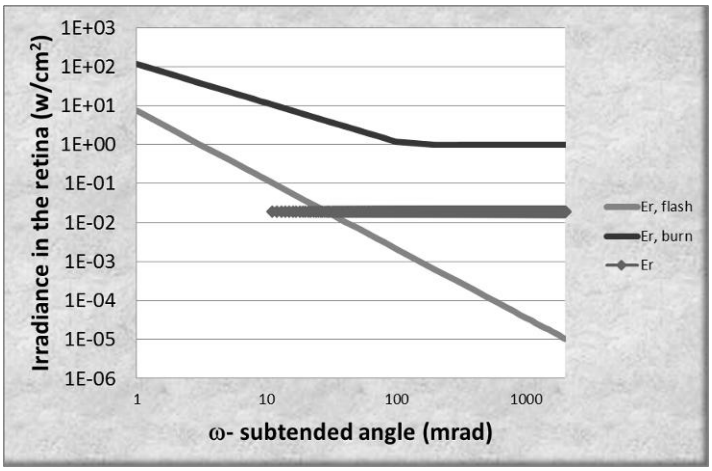

Figure 6: The diffuse radiation from the receiver.

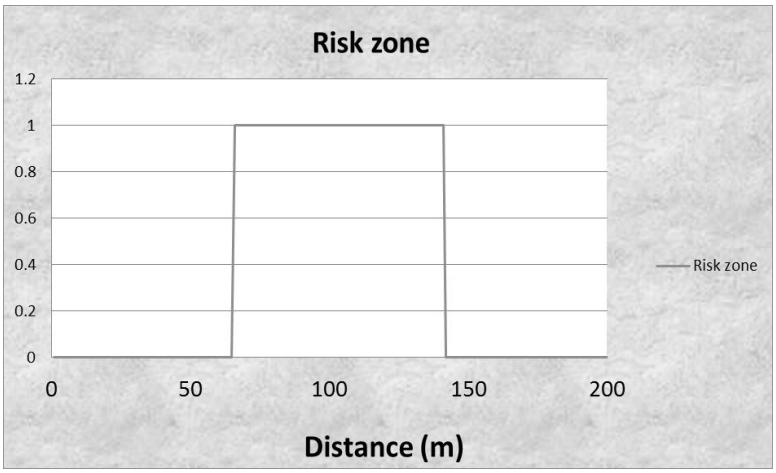

Figure 7. The diffuse radiation from the receiver risk zone.

5. CONCLUSIONS

There exists an increase in publishing studies on health effects as a result of exposure to the sun by working in outdoors. In order to ensure occupational health and safety based on the concept of prevention, the assessment of potential risks due to exposure become necessary in solar industry.

Such analyses help to detect situations where the maximum permissible limits of exposure are exceeded and ends in a potential damage or post-Image effect. The risky areas are based on the distance in which the individual sees directly the surface of heliostats as well the glare of the receiver. Otherwise a real data assessment, which might be compared with the information presented in this paper, is recommended.

Present work aims to contribute with the development of standard procedures to ensure the safety work of the workforce in the future solar industry.

6. REFERENCES

BEHAR, O., Khellaf, A., & Mohammedi, K. (2013). A review of studies on central receiver solar thermal power plants. Renewable and Sustainable Energy Reviews, 23, 12-39.

BRAUER I. R., 2006. “Safety and health for engineers”, 2nd ed., Nonionizing radiation, A JOHN WILEY & SONS, INC., ch.21, pp.382-460.

BRUMLEVE, T.D., 1984. 10 MWe Solar Thermal Central Receiver Pilot Plant: Beam Safety Tests and Analyses, SAND83-8035, Sandia National Laboratories, United States of America.

CARRASCO J.L., 2003. Radiaciones ionizantes y no-ionizantes, aplicaciones y riesgos. Hospital U, Málaga, [online] Available at: http://www.marcoshurvitz.com.ar/Archivos/Docen/ISFT%20190/Radiaciones%20y%20patologia.pdf, [Accessed 11 of November 2014].

FRANCK D., Walzer S. and Chernin O., 2010. Assessment and resolution of potential optical safety hazards from a power tower: SolarPACES, Perpignan, Francia, septiembre 2010.

HAMILTON J., 2011. Careers in solar power. Green jobs: solar power. [online] The Bureau of Labor Statistics. Available at: http://www.bls.gov/green/solar_power/solar_power.pdf, [Accessed 13 of November 2014].

HO, C. K., Sims, C. A., & Christian, J. M., 2014. Evaluation of Glare at the Ivanpah Solar Electric Generating System. Ivanpah Solar Electric Generating System California Energy Commission (07-AFC-5C) Bureau of Land Management (CACA-48668, 49502, 49503, and 49504) Condition of Certification TRANS-3.

HO, C.K., Ghanbari, C.M., & Diver, R.B., 2009. Hazard analyses of glint and glare from concentrating solar power plants: SolarPACES, September 2009, pp.15-18

HO, C.K., Ghanbari, C.M., & Diver, R.B., 2011. Methodology to Assess Potential Glint and Glare Hazards from Concentrating Solar Power Plants: Analytical Models and Experimental Validation, SAND2010-2581C, in proceedings of the 4th International Conference on Energy Sustainability, ES2010-90053, Phoenix, AZ, May 17-22, 2010.

International Commission on Non-Ionizing Radiation Protection (ICRNIRP), 2004. BfS- R, Guidelines on limits of exposure to ultraviolet radiation of wavelengths between 180 nm and 400 nm (incoherent optical radiation), Matthes, Ingolstaedter Landstr. 1, 85764 Oberschleissheim, Germany.

International Commission on Non-Ionizing Radiation Protection (ICNIRP 14), 2007. Protecting workers from ultraviolet radiation. Germany: International Commission on Non-Ionizing Radiation Protection; ISBN 978-3-934994-07-2

International Commission on Non-Ionizing Radiation Protection (ICNIRP), 2010. Statement—protection of workers against ultraviolet radiation. Germany; Health Physics, vol. 99, no. 1, pp. 66-87. DOI: 10.1097/HP.0b013e3181d85908.

IRENA (International Renewable International Agency), 2014. Renewable energy and jobs, Pp.7. [online] Available at: http://www.irena.org/publications/rejobs-annual-review-2014.pdf, [Accessed 13 of November 2014].

IRENA (International Renewable International Agency). 2013. Concentrating Solar Power, Technology Brief. Pp.12. [online] Available at: http://www.irena.org/DocumentDownloads/Publications/IRENA-ETSAP%20Tech%20Brief%20E10%20Concentrating%20Solar%20Power.pdf

KALOGIROU S., 2009. Solar energy: Introduction, 1era ed, Ch 1, pp. 23- 26, Elsevier, San Diego: USA.

KATTKE, K., & Vant-Hull, L., 2012. Optimum target reflectivity for heliostat washing: SolarPACES, Marrakesh, Morocco. September 2012.

KWAN-HOONG, Ng., 2003, Non-Ionizing Radiations – Sources, Biological Effects, Emissions and Exposures: proceedings of the international conference on Non- Ionizing Radiation, UNITEN, ICNIR2003. Available at: http://www.who.int/peh-emf/meetings/archive/en/keynote3ng.pdf.

NERL (National Renewable Laboratory), 2014. SolTrace. [online] Available at: http://www.nrel.gov/csp/soltrace/download.html, [Accessed 30 of Arpil 2015].

ROMERO, M., et al., 2002. An update on solar central receiver systems projects and technologies. J. Energy Engine. Vol. 124, no. 2, pp. 98-108.

SAMANIEGO, D., Arancibia, C., & León, J., 2012. Estimación de riesgos oculares por reflexión de radiación solar concentrada en una instalación de torre central, in proceedings of the 10th International Conference on OPR, Occupational Risk Prevention, Bilbao, España, 2012.

SENER, 2012. HECTOR, cleaning robot systems for heliostats. [online] Available at: http://www.sener-aerospace.com/AEROESPACIAL/pdf_preview.php?id=cw4efc4f1de8b47, [Accessed 26 of November 2014].

SLINEY, D. H., 1994. Ocular hazards of light, International Lighting in Controlled Environments Workshop, p. 183-189. In: T.W.Tibbitts (ed.). NASA-CP-95-3309.

SLINEY, D. H., 2000. Ocular radiation hazards. Handbook of Optics, vol 3.

SLINEY, D. H., et al, 2005. Adjustment of guidelines for exposure of the eye to optical radiation from ocular instruments: statement from a task group of the International Commission on Non-Ionizing Radiation Protection (ICNIRP). Applied optics, vol. 44, no. 11, pp. 2162-2176.

STANOJEVIĆ, M. R., et al, 2004. Ultraviolet radiation and melanogenesis. Archive of Oncology, vol. 12, no. 4, pp. 203-205.

39: Techno-economic assessment of an integrated solar combined cycle power plant in semi-arid region in Algeria

BOUALEM ZEROUAL[1], ABDELHAFIDH MOUMMI[2], AREZKI SMAÏLI[3]

1 Laboratoire de Génie Civil, Hydraulique, Développement durable et Environnement, LAR-GHYDE, Université Mohamed Khider de Biskra, BP 145, RP, 7000,Biskra,Algeria, boualem.zeroual@gmail.com
2 Laboratoire de Génie Civil, Hydraulique, Développement durable et Environnement, LAR-GHYDE, Université Mohamed Khider de Biskra, BP 145, RP, 07000, Biskra, Alegria, abdelhafidh.moummi@gmail.com
3 Ecole Nationale Polytechnique, Laboratoire de Génie Mécanique et Développement, B.P. 182 El-Harrach, 16200, Algiers, Alegria, arezki.smaili@enp.edu.dz

A number of solar thermal power plants have been planned by the Algerian state for the horizon of 2030, for the purpose to achieve the self-sufficiency from solar electricity and its exportation. The main objective of the present paper is annual performance and economic assessment of an Integrated Solar Combined Cycle System (ISCCS-18) of 68.2 MWe with 18 MWe solar field, using parabolic trough collectors. This power plant has been designed and simulated through the software IPSEpro for Naâma site in Algeria. For this purpose five power plants cases have been investigated in terms of performance and economics analysis, namely, (i) Gas turbine, (ii) conventional combined cycle, (iii) ISCCS without fossil-fuel back-up system, (iv) ISCCS with fossil-fuel back-up system, and (v) Solar Electric Generating System (SEGS). The parameters of the annual performance analysis include annual energy production, net annual efficiency and capacity factor. The economic analysis includes environmental, investment, fuel and Operation and Maintenance (O&M) costs, and the Levelized Electricity Cost (LEC) calculation. The obtained results have shown that the LEC of the ISCCS-18 is 4.22 ¢/kWh; about 43% higher than the combined cycle with consideration of environmental cost, and saves around 21 million US$ in fuel consumption and reduces about 0.45 million tons in CO2 emissions in 30 years operating period in comparison with conventional combined cycle. Also, the results have shown that about 4 % improvement in the net annual efficiency of the ISCCS-18, as well as the annual solar share is 8.0 %. According to this solar share and to the Algerian regulations, the project owner will receive premium of 100 % of the LEC of the total produced electricity by the ISCCS-18.

Keywords: Solar thermal power plants; parabolic trough collector; combined cycle; economical assessment; performance analysis

1. INTRODUCTION

Integration of solar energy to fossil fuel -natural gas- and increasing the solar contribution gradually, with the technological improvement and development of the Concentrating Solar Power (CSP), will be promising solution to reduction of the CO_2 emissions and to the increasing demand of electricity. In 2014 the world CO_2 emission reached 40 billion ton, the big share of these emissions is from the power generation using fossil energy. Basically there are four CSP technologies: parabolic trough, solar tower, Linear Fresnel, and solar dish technology. Among these CSP technologies, parabolic trough power plants have the biggest share, that is in operation, under construction, and planned all over the world, estimated by 56.4 %, in September 2010 (Günter, Jeanne and Csambor, 2012, p.8), due to their simplest design and integration with conventional combined cycles.

For successful solar thermal power plant several related aspects and topics must be considered, which are given as follows: (i) the choice of the suitable site to build the power plant, (ii) the thermo-economic design optimization, (iii) annual performance assessment, (iv) the Levelized electricity cost calculation, and (v) environmental analysis. Several works on CSP plants and their related topics have been already tackled and are available in literatures. Here, we focus on the published works concerning North Africa region. The prospective and potential role of concentrated solar power in Africa and Europe for horizon 2050 have been discussed and analyzed previously (Viebahn, Lechon and Trieb, 2011, p.4420), it has been shown that significant long-term reductions in LEC, to figures within 4-6 ¢/kWh in 2050, and important greenhouse gas emission reductions up to 18 g CO_2-equivalents/kWh_e.. The potential and projects development of the parabolic trough power plants in Algeria have been reported in recent work (Boukelia and Mecibah, 2013, p. 288). Mainly, the following three points have been addressed: (i) the Algerian government program for the period 2011-2030, to promote renewable energy; (ii) an overview on the first ISCCS of Hassi R'mal, started in operation in May, 2011, and (iii) the three other hybrid power plants that will be completed by 2018.

An interesting comparison of dry cooling and wet cooling of steam for CSP power plants (Liqreina and Qoaider, 2014, p.417) for the arid-regions of the Middle East and North Africa (MENA), has shown that dry cooling is the most suitable option for arid-regions with high solar radiation in terms of performance and economics. The instantaneous performance analysis of the Algeria's first integrated solar combined cycle system of Hassi R'mal, has been carried out (Behar, Kellaf, Mohamedi et al., 2011, p.185). Comparison of parabolic trough power plant under Mediterranean and arid climate conditions in Algeria has been conducted (Abbas, Belgroun, Aburidah et al. 2013, p.93), using the NREL's SAM software (System Advisor Model); the comparison is based on the annual energy output, capacity factor, annual water usage, and LEC. Nowadays, Algeria gives a great importance to renewable energy in its sustainable development and energy politics. A program consists of installing up to 22 000 MW of power generating capacity in which 40 % from renewable resources has been planned for the horizon of 2030 (Ministry of Energy and Mines, 2011). The program includes a number of solar thermal power plants, such as ISCCS systems. Among the factors that encourage the CSP power plants implementation in the southern regions of Algeria are; high yearly direct normal irradiation, the land availability with flat topography, and fuel for hybrid power plants operation.

In this paper, an integrated solar combined cycle power plant, that utilizes line-focus parabolic trough collectors has been designed and simulated under climatic conditions of Naâma site in Algeria. Naâma is semi-arid region located in the west region of Algeria, (33.26 °N, 0.31 °W). The annual Direct Normal Irradiation (DNI) is above 2300 kWh/m^2 (SoDa, 2013). The measured annual mean sunshine duration is 9.26 h/day. The cycle heat balance calculation and the simulation are performed using the software IPSEpro, (IPSEpro, 2012). The main annual performance parameters, namely, net annual efficiency, annual energy production, and capacity factor are presented and discussed. The economic analysis including environmental, investment, fuel and O&M costs, and the LEC calculation are presented and compared for the following five power plant cases:

1- Gas Turbine power plant (GT): 32.2 MW gas turbine;
2- Combined Cycle power plant (CC): 32.2 MW gas turbine + 18 MW steam turbine;
3- Integrated Solar Combined Cycle power plant with 18 MWe solar field (ISCCS-18): 32.2 MW gas turbine +18 MW steam turbine +18 MWe solar field;
4- Integrated Solar Combined Cycle power plant with 18 MWe solar field and fossil-fuel back-up system as Auxiliary Firing (ISCCS18-AF): 32.2 MW gas turbine + 18 MW steam turbine +18 MW solar field +18 MW fossil-fuel back-up system; and
5- Solar Electric Generating System (SEGS): 18 MW solar field + 18 MW fossil-fuel back-up system.

2. PRESENTATION OF THE SOFTWARE IPSEpro

The software package IPSEpro is from SimTech Simulation Technology in Austria (IPSEpro, 2012). It is a highly flexible and comprehensive environment for modeling, simulation, analysis and design of components and processes for energy and chemical engineering. Besides, IPSEpro has been designed to solve problems that you can represent by a network of discrete components. These components are interconnected with streamlines to build up the process scheme. Currently, SimTech offering five models libraries: Advanced Power Plants, Gas Turbine, CSP, Low Temperature, and Desalination library. All these libraries contain the needed physical properties. The user can also add new physical properties. IPSEpro is provided with a Model Development Kit (MDK) for building new specified user components or modifying existing components. The MDK permits also to use two or more libraries together for a system design and analysis. There are also other tools or extension modules available for IPSEpro which are: (i) PSOptimize which allows to the user to specify and run formal optimization calculations in order to find the process parameters that optimize the criterion that can be freely define. (ii) PSValidate gives the possibility to enter measured values directly into the process flow sheet and specify the accuracy of the measurements of real power plant. And (iii) PSExcel allows the user to connect and exchange the calculations data between IPSEpro project and MS-Excel. Other software tool which is PSEconomy for analyzing and optimization the economics of process is available. The Part-load calculations are also available.

For the design and simulation of the present hybrid power plant, the MDK has been used to build a new model library that contains the all needed components of the system. The obtained library is a mixture of components of Advanced Power Plant library (for combined cycle) and components from Concentrating Solar Power library (for the solar field). The equations model of parabolic trough collector field, type LS-3 used in our power plant, is created and introduced to the new obtained model library using the MDK. The model developed can be simulated for different geographical areas changing the geographical coordinates and the input of meteorological data, and for different sizes of solar field. The solar collector model can be integrated with power cycle model to simulate the whole system.

3. INTEGRATED SOLAR COMBINED CYCLE POWER PLANT

The configuration of the integrated solar combined cycle power plant under study shown in Figure 1 The design point is at 830 W/m^2 of Direct Normal Irradiation (DNI) and 21.0°C of ambient temperature. The power plant consists of gas turbine in Brayton cycle, a conventional combined cycle in Rankine cycle, with Heat Recovery Steam Generator (HRSG) to collect the heat from the exhaust hot flue gases of the gas turbine.

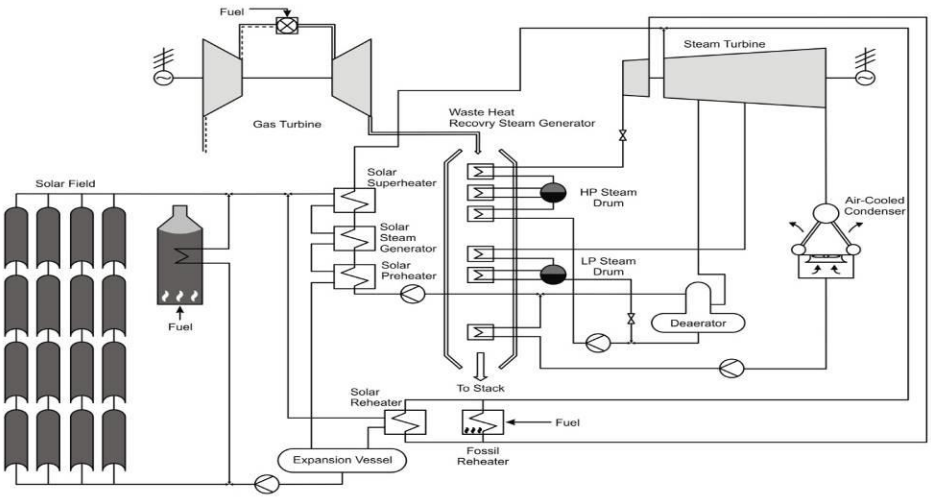

Figure 1: Schematic diagram of the integrated solar combined cycle power plant

The HRSG has two pressure levels; high pressure of 129.7 bar with 512°C and low pressure level of 3.28 bar with 236°C. The steam turbine has fossil/solar reheater to improve steam properties at the inlet of the second stage of the steam turbine at 380°C. The combined cycle is integrated with solar filed of parabolic trough collectors type LS-3 (LUZ solar collector). The solar field consists of 114,954 m^2 of total aperture area, and it consists of 210 Solar Collector Assemblies (SCAs) or 35 loops; each loop has 6 solar collector

assemblies connected in series of 3284.4 m^2 aperture area. The spacing between two rows is taken 17 m, with no-storage; therefore the solar multiple is 1. The collectors are fitted with a vacuum receiver tube of Schott's 2008 PTR70 type presented in (Burkholder and Kutscher, 2009). The collectors are aligned in the north-south direction and they track the sun from east to west. The synthetic oil (Therminol VP-1) is used as heat transfer fluid to collect thermal energy from the collectors to the Rankine cycle (power block), via heat exchangers train; pre-heater, steam generator and super-heater. The steam generated from the solar field feeds the second section of the steam turbine at pressure of 13.2 bar with 385°C, to increase its production capacity. Hence some components of the power block, such as steam turbine, deaerator, and the condenser of ISCCS must be larger than the corresponding components of a conventional combined cycle, due to the increased steam mass flow rate generated by the solar field. The solar field is also coupled in parallel with fossil- fuel back-up system to work at peak electricity demand at later evening. The exhaust steam from the last steam turbine section goes into air cooled condenser (ACC) of 0.22 bar and 62 °C to be condensate and starts the cycle again. Because using the cooling tower needs water make-up to compensate the evaporation rate, which is between 1 and 1.5% (El-Wakil, 1984) of the total circulating water flow rate. The use of air cooled condenser for solar thermal power plant is still the best solution in hot arid-regions with high solar radiation in terms of performance and cost (Liqreina and Qoaider, 2014, p.417).

4. PERFORMANCE ANALYSIS CRITERIA

In order to evaluate the performance of the proposed power plant, the following parameters and criteria have been used. The first of which is the capacity factor, given by the relationship:

Equation 1: Capacity factor

$$CF = E_{el\_an} / P_N.8760$$

Where:

- E_{el_an} = annual electrical energy production (kWh)
- P_N = power plant nominal power (kW)

For the purpose of thermal performance comparison, the fuel based annual net efficiency, is calculated as the net annual energy production of the plant divided by the total annual thermal energy provided from the fuel which is given by the relationship:

Equation 2: Plant annual net efficiency

$$\eta_{net} = E_{net\_an} / m_f.LHV$$

Where:

- E_{net_an} = net annual energy production (kWh)
- m_f = total annual mass of fuel (kg)
- LHV = Lower Heating Value of natural gas (46 595.3 kJ/kg)

For combined cycle and ISCCS, E_{net_an} is the sum of annual net output energy of the gas turbine and the output energy of steam turbine. For the SEGS, the annual net efficiency is calculated assuming that the SEGS works in fossil back-up system, so m_f is the total annual mass of fuel consumed by the fossil-fuel back-up system in (kg). The third criterion or figure of merit used in this paper to evaluate such power plant is called the annual solar to electric efficiency, this is used as a measure of the product of the efficiencies of the solar field, the power block, and the steam turbine generator; which can be calculated as:

Equation 3: Annual solar to electric efficiency

$$\eta_{solar\_to\_electric\_an} = E_{el\_solar\_an} / A_c.DNI_{incident\_an}$$

Where:

- $E_{el\_solar\_an}$ = annual electricity produced from solar energy (kWh)
- A_c = total aperture area of solar field (m^2)
- $DNI_{incident\_an}$ = annual incident direct normal irradiation (kWh/m^2)

The last parameter is the annual solar share (Dersch, Geyer, Herrmann et al. 2004, p. 952) for the ISCCS-18, which is used as a measure of the solar contribution in the annual energy produced by an ISCCS system, which can be calculated with the following equation:

Equation 4: Annual solar share

Ss=1-(annual fuel consumption per kWh) of ISCCS/ (annual fuel consumption per kWh) of CC ref. plant

5. .ECONOMIC ASSESSMENT

The objective of the economic analysis is to help assess economic profitability to compare different cases. The best method which may be used is the Levelized Electricity Cost (LEC) method, which is defined as the annual expenditure of plant divided by the annual produced energy. The lowest LEC determines the best choice. Therefore, the investor has to calculate the LEC of power plant before starting the investment. The LEC is given in the units of currency per kilowatt-hour (e.g., ¢/kWh), and it can be calculated as:

Equation 5: Levelized Electricity Cost

$$LEC = (CRF.C + O\&M + PVF)/E_{el\_an}$$

Where:

- CRF = Cost Recovery Factor
- C = total investment cost (US$)
- O&M = operation and maintenance cost (US$)
- PVF = annual fuel cost (US$)
- $E_{el\text{-}an}$ = annual electrical energy produced (kWh)

Equation 6: Cost Recovery Factor

$$CRF=R/ (1-(1+R)^{-N})$$

Where:

- R = discount rate
- N = expected lifetime of power plant (Year)

The expected lifetime is estimated as 20 years for gas turbine, and 30 years for steam unit and ISCCS plant. The total investment cost for ISCCS is the sum of gas turbine cost, steam unite cost, and solar unite cost. The Operation & Maintenance costs (O&M) include labor, spare parts, consumables and normal maintenance equipment requirements; which can be estimated as follows**:**

Equation 7: Operation and maintenance cost

$$O\&M = k_gC_g+k_sC_s+k_{sol}C_{sol}$$

Where:

- k_g = 5, k_s = 2, and k_{sol} = 1.5, operation and maintenance cost factors of gas unit, steam unit and solar unit respectively (Hosseini, Soltani and Valizadeh, 2005, p.1549)
- C_g = specific cost of gas unit is 314 US$/kW, - C_s = specific cost of steam unit is 1052 US$/kW,

(Bakos and Parsa, 2013, p.601), and - C_{sol} = specific cost of solar unit is 295 US$/kW, (Turchi, Mehos, Ho et al. 2010, p.4).

Economical assumptions and key data for calculating the LEC in different cases are shown in (table 2). The cost of the fossil-fuel back-up system is taken approximately 9% of the total investment cost of the SEGS system. Substituting these values and the annual fuel price into (equation 5) will give us the LEC. For this objective a computer program was developed. (Equation 5) calculates the LEC without considering the environmental effects, but when considering the environmental effects, it should add, the annual CO_2 emission cost to the numerator.

6. RESULTS AND DISCUSSIONS

Simulations over a one-year period for the location of Naâma have been carried out, to evaluate the annual performance of the subjected power plant, 1 h step was chosen in the annual simulation. Table 1 shows the produced energy of the cases mentioned above, capacity factors and annual work hours for (full load) operation. Energy production of the power plant is considerably influenced by ambient conditions of the location of the power plant: ambient temperature and relative humidity for gas turbine and CC power plant, and by ambient temperature, direct normal irradiation (DNI) and wind speed for the solar power plants. The annual energy produced is known by considering 45 days for power plant overhauls. As shown in (Table 1), the capacity factor of the SEGS system is 36.4 % in which 20.0 % from solar energy, which depends on the design and the incident DNI of the site, and 16.4 % for fossil energy. This latter value can be increased by increasing of fossil-fuel back-up mode working hours.

Figure 2 shows the energy production obtained in different seasons for ISCCS-18. As it can be seen that the energy production for conventional power plant is minimum in summer day, but for solar power plant, it is compensated by the solar energy, which is maximum in summer. The ISCCS-18 plant works in the solar dispatching mode, i.e. without given specific load profile, the gas turbine functioning at full load for 24 h. The output of the gas turbine and steam turbine then depend only on the ambient temperature. If incident solar radiation is sufficient to produce work on steam turbine, the steam turbine is boosted and the total plant output increases. No fossil-fuel back-up system is used in this mode. Figure 3 shows a comparison of the net electricity generation between combined cycle and ISCCS-18, in summer day. It can be noted that when electricity generation in conventional combined cycle decreases, the power generated by ISCCS is maximal. The operation of the ISCCS18-AF follows somewhat the scheduled load curve during the later evening.

Table 1- Annual gross energy production in different cases

Power plant	Annual energy production (MWh)	Capacity factor (%)	Annual work hours (Full load)
GT	255,445	90.5	7927
CC	402,582	91.5	8015
ISCCS-18	434,230	72.7	6368
ISCCS18-AF	459,984	77.0	6745
SEGS:	57,402	36.4	3188
From solar energy	31,648	20.0	1752
From fossil fuel	25,754	16.4	1436

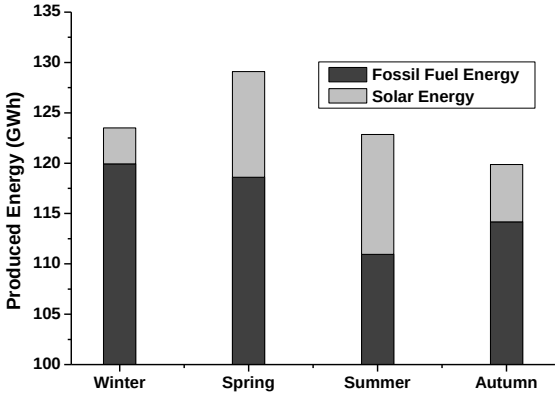

Figure 2: Energy production variation of ISCCS-18 for different seasons

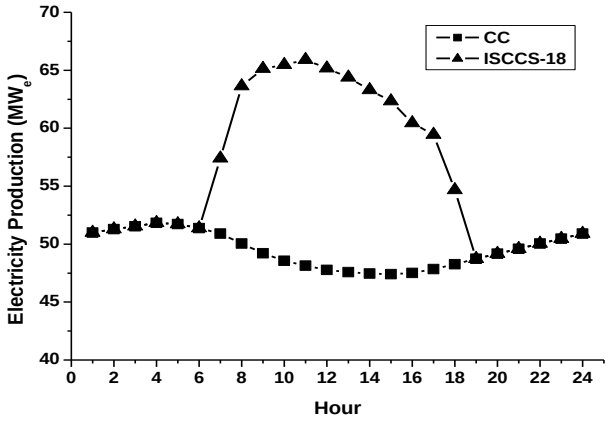

.

Figure 3: Net electric power variation of ISCCS-18 and combined cycle in a summer day

If the ISCCS18-AF fossil-fuel back-up system works continuously at non-solar hours, this produces more fuel consumption (natural gas), and the motor of the compressor of the back-up system consumes more electric power. It is more than 60 % of the produced energy by the back-up system, somewhat like the compressor of the gas turbine; hence the fossil-fuel back-up system should not work more than 4 or 5 h per day.

One of the main parameters in annual performance evaluation of power plants is the fuel based annual net efficiency which is shown in Figure 4, for five cases. It can be seen that during the days with high solar radiation, the generated steam mass flow rate increases, therefore the efficiencies of SCCS-18 and ISCCS18-AF power plants are higher than the conventional combined cycle and gas turbine.

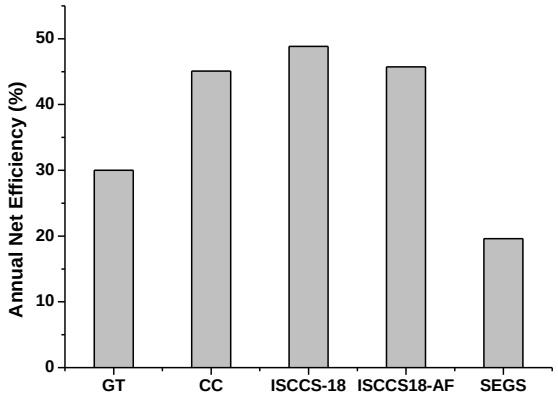

Figure 4: Annual net efficiency of different cases

The efficiency of the SEGS power plant is calculated assuming that the SEGS system works only 5 h for winter and 4 h per day for other seasons with fossil-fuel back-up mode, which is lowest because of the high power consumption of the compressor of the fossil fuel back-up system, but the value of global efficiency of the SEGS system is 33.3 %. The solar to electric efficiency of the ISCCS is calculated using (Equation 3), this yields;
12.0 %. The solar share or the annual solar contribution in ISCCS power production is calculated using (Equation 4) and is found to be 8.0%. Figure 5 shows the specific fuel consumption for the five cases given in (kg/MWh); it is clear from this figure that the fuel consumption in gas turbine is more than the other power plants, followed by combined cycle.

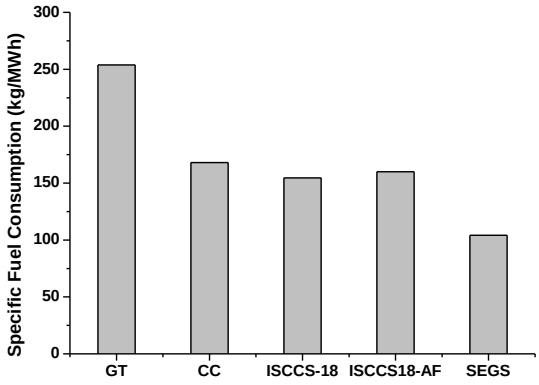

Figure 5: Natural gas specific consumption for different cases

In this analysis the conventional combined cycle is taken as reference power plant. The ISCCS-18 and the ISCCS18-AF are 8% and 4.75% lower than the CC power plant in fuel consumption respectively. It can be said that if the fossil fuel back-up system works more, the fuel consumption is increased and can exceed the consumption of the CC power plant, hence this working mode is not economical viable. The SEGS is the lowest owing to the solar contribution and the limit hours of using the fossil back-up system. The increase of solar field area produces the lower fuel consumption but the capital cost is also increased considerably because of the high specific cost of solar parts.

Figure 5 and Figure 6 permit to conclude that the CO_2 emissions is proportional to the fuel consumption by power plant, these two parameters depend on the air excess used in gas turbine, fossil-fuel back-up system, and the in the reheater. CO_2 production in the gas turbine is maximal and decreases in conventional combined cycle, ISCCS18-AF, ISCCS-18, and SEGS power plant respectively; ISCCS-18 and ISCCS18-AF produce 7.55% and 4.3 % lower than conventional combined cycle.

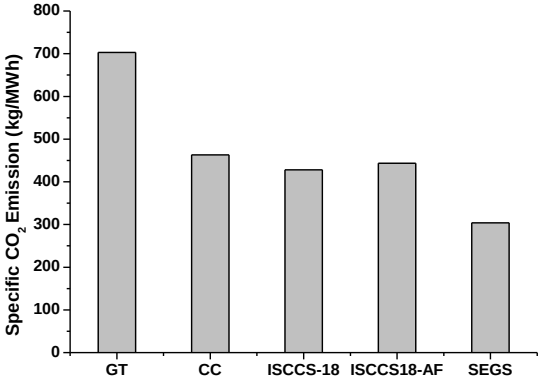

Figure 6: Specific CO_2 emission for different cases

Figure 7 and Figure 8 show the calculated LEC for different cases. In Figure 7, the LEC is divided into three fragments, as investment cost, O&M cost, and fuel cost.

Table 2- Key data and economic assumptions for calculating the LEC in different cases

Parameter	Symbol	Unit	Value
Natural gas price	C_f	¢/m^3	7.2
Annual fuel price escalation rate	C_{fes}	%	2.0
Cost of CO_2 emission	C_{co2}	US$/ton	9.9
Internal consumption of GT	A_{GT}	%	1.5
Internal consumption of CC	A_{CC}	%	1.9
Internal consumption of ISCCS-18	$A_{ISCCS-18}$	%	2.35
Internal consumption of ISCCS18-AF	$A_{ISCCS18-AF}$	%	5.27

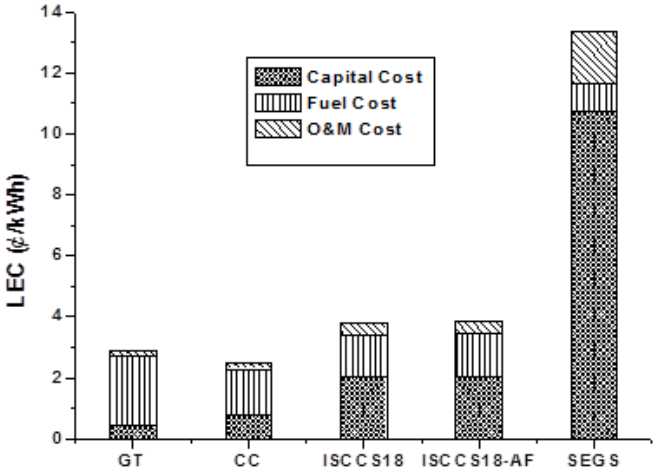

Figure 7: LEC of different cases without considering CO_2 emission cost

In Figure 8, the LEC is the same as in Figure 7 but it takes into account the CO_2 emission cost, because the pollutant emission increases the LEC. The LEC is greatly affected by the specific cost of power plant, especially for solar power plant, because the cost of the solar parts is very high compared to the fossil parts. In Figure 7, when the CO_2 emission cost is not taken into consideration, the combined cycle has the lowest LEC followed by the gas turbine power plant. In this case, the LEC of ISCCS-18 is 52 % and ISCCS18-AF is 54 % higher than the CC. The LEC of the SEGS is approximately 5.32 times more than conventional combined cycle. In Figure 8, when the CO_2 emission cost is considered, assuming that the CO_2 emission cost of 9.9 US$/ton, the LEC of the CC is the lowest, In this case, the LEC of ISCCS-18 is around 43 %, ISCCS18-AF is 44.6 %, and the ESGS is 4.6 times higher than combined cycle. ISCCS-18 produces 0.45 million ton of CO_2 and 0.27 million ton for the ISCCS18-AF and SEGS lower than combined cycle over 30 years operating period. If we assume that the fuel price (natural gas) 7.2 US¢/m^3, the ISCCS-18 saves about 21.11 million $ through 30 years of operating period and 13.16 million $ for ISCCS18-AF and SEGS, these results and the calculated LEC of the different cases are summarized in Table 3.

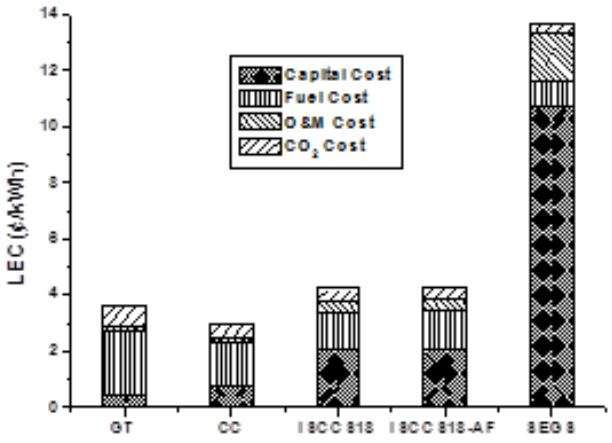

Figure 8: LEC of different cases with considering CO2 emission cost

Table 3: General technical and economical specifications of different cases for the ISCCS

Parameter	Unit	GT	CC	ISCCS-18	ISCCS18-AF	SEGS
Nominal power	MW_e	32.2	50.2	68.2	*68.2*	18
Investment cost	Million US$	10.11	29.06	81.91	86.98	57.92
Specific cost	US$/kW	314	578.9	1201	1275.4	3217.8
Fuel saving in 30 years	Million US$	-	-	21.11	13.16	13.16
Avoided CO_2 mission in 30 years	Million ton	-	-	0.45	0.27	0.27
LEC[a]	¢/kWh	2.91	2.50	3.8	*3.85*	13.30
LEC[b]	¢/kWh	3.60	2.96	4.22	*4.28*	13.60

[a] *Without considering environmental cost.*

7. CONCLUSIONS

The annual performance and economical assessment of different cases of the integrated solar combined cycle power plant (ISCCS-18) has been simulated under the climatic conditions of Naâma site in Algeria, using the software IPSEpro. The obtained results show that the LEC of the combined cycle is the lowest, with and without considering the environmental effects. The LEC of the ISCCS-18 is of 3.80 ¢/kWh, about 52 % higher than conventional combined cycle without considering the CO_2 emission cost, and 4.22 ¢/kWh, when the environmental effects is considered, is around 43 % higher than the combined cycle. The present study shows also that the ISCCS-18 saves about 21.11 million US$ in fuel consumption and reduces about 0.45 million ton in CO_2 emission in 30 years of power plant operation period. Also, the results have shown that about 4 % improvement in the net annual efficiency of the ISCCS-18, as well as the annual solar share is 8.0 %. According to this solar share and to the Algerian regulations, the project owner will receive premium of 100 % of the LEC of the total produced electricity by the ISCCS-18. Finally, the integration of fossil fuel - Natural gas – with solar energy will be a very attractive option for electricity generation in Algeria.

8. ACKNOWLEDGEMENTS

The authors wish to thank Mr. Erhard W. Perz and Mr. Stefan Bergmann of the SimTech Simulation Technology, for their explanations and valuable information about their software IPSEpro. Our thanks are extended to Pr. Sophia Haussener of the Laboratory of Renewable Energy Sciences and Engineering (LRESE), de l'Ecole Polytechnique Fédérale de Lausanne (EPFL), Switzerland, due to her help and encouragement during realization of the present study.

9. REFERENCES

ABBAS, M., Belgroun, Z., Aburidah, H., Kasbadji Merzouk, N., (2013). Assessment of a solar parabolic trough power plant for electricity generation under Mediterranean and arid climate conditions in Algeria. Energy Procedia, 42, pp. 93-102.

BAKOS, G.C., Parsa, D., (2013). Technoeconomic assessment of an integrated solar combined cycle power plant in Greece using line-focus parabolic trough collectors. Renewable Energy, 60, pp. 598-603.

BEHAR, O., Kellaf, A., Mohamedi, K., Belhamel, M., (2011). Instantaneous performance of the first Integrated Solar Combined Cycle System in Algeria. Energy Procedia, 6, pp. 185-193.

BOUKELIA, T. E., Mecibah, M. S., (2013). Parabolic trough thermal power plant: Potential, and projects development in Algeria. Renewable and Sustainable Energy Reviews, 21, pp .288-297.

BURKHOLDER, F., Kutscher, C., (2009). Heat loss testing of Schott's 2008 PTR70 parabolic trough receiver, National Renewable Energy Laboratory, NREL/TP-550-45633, May 2009.

DERSCH, J. , Geyer, M., Herrmann, U., Jones, S. A., Kelly, B., Kistner, R., Ortmanns, W., Pitz-Paal, R., Price, H., (2004). Trough integration into power plants-a study on the performance and economy of integrated solar combined cycle systems. Energy, 29, pp. 947-959.

EL-WAKIl, M. M., (1984). Power plant technology. New York, McGraw-Hill.

GÜNTER, M., Jeanne, M., Csambor, S., (2012). EnerMENA, Advanced CSP teaching materials: Parabolic Trough Technology. The German Aerospace Center (DLR), Germany.

HOSSEINI, R., Soltani, M., Valizadeh, G., (2005).Technical and economic assessment of the integrated solar combined cycle power plants in Iran. Renewable Energy, 30, pp.1541-1555

IPSEpro-Heat balance and process simulation package, (2012). SimTech GmbH, Graz, Austria. Available from: http://www.SimTechnology.com/

LIQREINA, A., Qoaider, L., (2014). Dry cooling of concentrating solar power (CSP) plants, an economic competitive option for the desert regions of the MENA region. Solar Energy, 103, pp. 417-424.

Ministry of Energy and Mines, (2011). Programme des énergies renouvelables et de l'efficacité énergétique, Algeria, Algiers. Available from: http://www.mem-algeria.org. [Accessed in 2011].

SoDa-Solar radiation Data, Solar Energy Services for Professionals, (2013) Available from: http://www.soda-is.com/eng/services/services_radiation_free_eng.php. [Accessed in 2013].

TURCHI, C., Mehos, M., Ho, C. k., and Kolb, G. J., (2010). Current and future costs for parabolic trough and power tower systems in the US market, SolarPACES, Perpignan, France.

VIEBAHN, P., Lechon, Y., Trieb, F., (2011). The potential role of concentrated solar (CSP) in Africa and Europe - A dynamic assessment of technology development, cost development and life cycle inventories until 2050.Energy Policy. 39, pp. 4420-4430.

SESSION 12: ENERGY AND ENVIRONMENT POLICIES

26: JIC Green Initiative Project (GIP) toward environment friendly college

MOHAMMED I. Y. ALEID[1], SHAREEF SHEKSHAKI[2], MOHAMMED ABDUL BASEER[3], FOUAD ZAYADIN[4], MOHSEN AL-SHAKHOURI[5], VADREVU KAMARAJU[6], MOHAMMAD HANIFA[7], MOHAMMAD ABU AJRA[8]

1 Mechanical Engineering Department, Jubail Industrial College (JIC), Jubail Industrial City –Saudi Arabia
2 Electrical Engineering Departments, Jubail Industrial College (JIC), Jubail Industrial City –Saudi Arabia
3 Mechanical Engineering Department, Jubail Industrial College (JIC), Jubail Industrial City –Saudi Arabia
4 Mechanical Engineering Department, Jubail Industrial College (JIC), Jubail Industrial City –Saudi Arabia
5 Mechanical Engineering Department, Jubail Industrial College (JIC), Jubail Industrial City –Saudi Arabia
6 Electrical Engineering Departments, Jubail Industrial College (JIC), Jubail Industrial City –Saudi Arabia
7 Chemical Engineering Departments, Jubail Industrial College (JIC), Jubail Industrial City –Saudi Arabia
8 Electrical Engineering Departments, Jubail Industrial College (JIC), Jubail Industrial City –Saudi Arabia

In Jubail Industrial College (JIC) a team of engineers and researchers started to lay out what is known as Green Initiative Project (GIP). The main objective of this project is to implement renewable energy technology in our routine life. The project intends to touch many different aspects of life in the coastal Industrial City of Jubail. JIC is an educational organization located in a very vital region in the Middle East and near giant Petrochemical Industries in what is known as Jubail Industrial City.

Our location in Kingdom of Saudi Arabia made us to lay the foundation and initiate a special project. The project of its kind is unique, which chiefly focuses on environment protection utilizing renewable energy technology. It enables us to become a role model to all the educational Institutions and Industries around the globe.

A greener and pollution free atmosphere combined with hands on practical experience would lead us to utilize the power from the natural resources like wind and solar energy. This would strengthen the perception of future

An electronic survey was conducted on GIP involving one hundred and forty (140) faculty and staff members. The feedback of nearly 90 % of the members is quite encouraging and supportive, later the project has become the pool of innovative ideas and project team were inquired about its details interestingly.

Our team of members proposed to utilize solar energy which is very promising; we tried to gear three essential needs together, the need for parking lot, the need of shadow and the need of solar energy. We analysed the wind speed at different locations of coastal city Jubail and we found that renewable energy from wind is feasible in Jubail Industrial City in general.

Bio-gas energy is to be produced from food and vegetable waste collected in JIC restaurants, canteens and dormitories as well as green grass clippings to generate a green fuel that is most friendly to our environment.

Keywords: Renewable Energy, Solar Energy, Bio-Gas, Renewable Energy Centre, Wind Energy, Zero-car emission

1. INTRODUCTION

As shown in the Figure 1 the total cost of nine months power consumption in JIC is about 2 million US dollar that is 28,817.200 Mega Watt hour as shown in Figure 2.

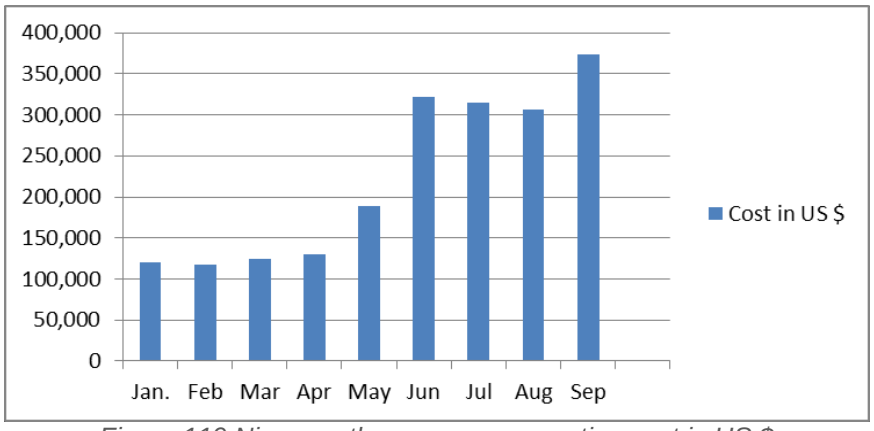

Figure 119 Nine months power consumption cost in US $

The projected annual consumption of power in JIC is about 2.5 million US dollar, which is about 38,817.600 MWh, that is a lot of power and money.

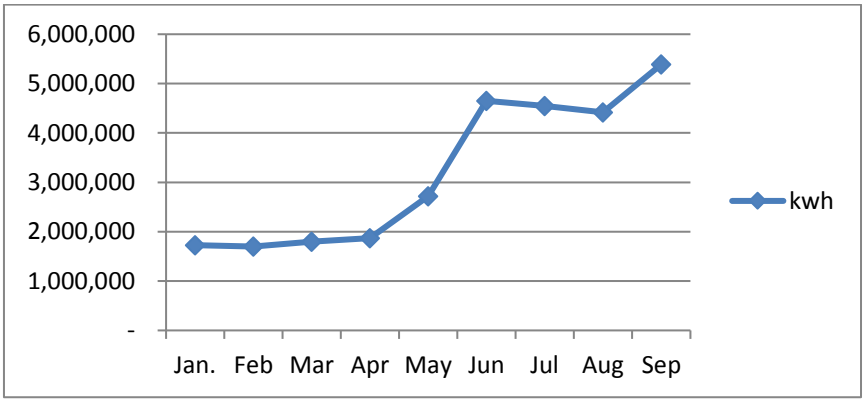

Figure 120 Nine months power consumption in kWh

Maximum power consumption was in September as the weather is extremely hot and HVAC systems will consume more power in the summer see Table 1

Month	kwh	Cost in SR	Cost in US $
Jan.	1726500	448920	119712
Feb	1699200	441822	117819
Mar	1800300	468108	124829
Apr	1870900	486464	129724
May	2720200	707282	188609
Jun	4651000	1209290	322477
Jul	4544300	1181548	315079
Aug	4416500	1148320	306219
Sep	5388300	1400988	373597

Table 35 Power consumption in JIC (January 2012 to September 2012)

In this project our target is reducing the emissions and minimizing the dependence on the fossil fuel to power the facility inside Jubail Industrial College (JIC). To start with, our aim to reduce the power cost at JIC by 25% i.e. the annual power cost would be the present 9 month cost (see table 2 below)

Total KWH	28,817,200
Total SAR	7,492,742
Total US $	1,998,065

Table 36 total cost and kWh consumption

Financially speaking our project target is to save 2.5 million dollars annually.

2. JIC GREEN INITIATIVE PROJECT (GIP)

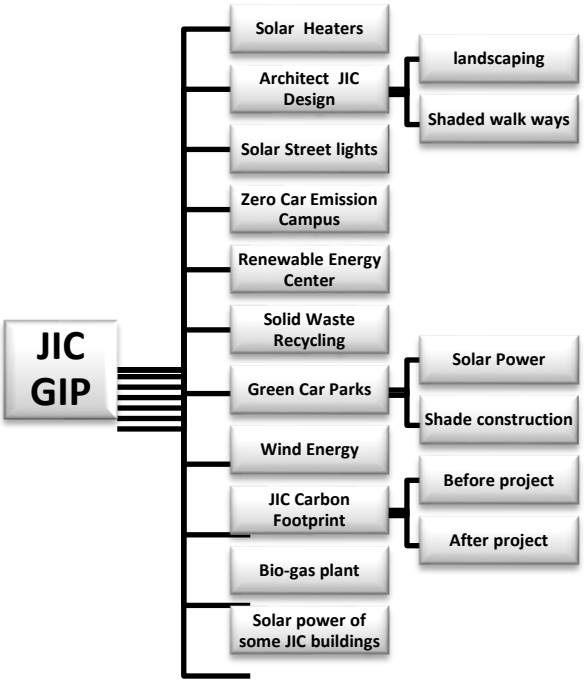

Figure 121 JIC Green Initiative Project skeletons

As in Figure 3 above the JIC GIP project is divided into eleven segments:

1- Solar heaters
2- Architect design
3- Solar street light
4- Zero car emission campus
5- Renewable energy center
6- Solid waste recycling
7- Green car parks
8- Wind energy
9- Carbon foot print calculation
10- Biogas plant
11- Solar power of some buildings

3. SURVEY ABOUT JIC GIP

We started the project by executing a survey of 154 participants that included staff members as well as students, among the participants 84% were staff members and 24% were students see Figure 4.

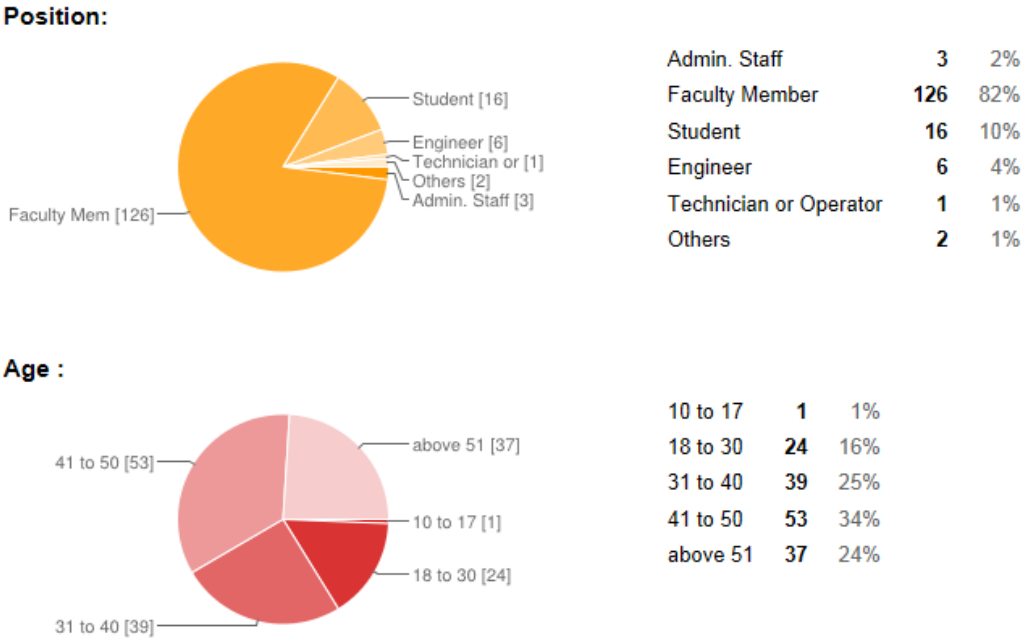

Figure 122 Survey participation

The questionnaire was electronic questionnaire and Google Drive was used to execute the questionnaire [16]. The target of the survey is to investigate community awareness of pollution problem in Jubail Industrial City in general and in Jubail Industrial College (JIC) in specific, then to measure to what extend Jubail Industrial College students and staff are interested to contribute in solve the problem if they think that there is a problem.

The first question was “Is there a pollution problem in Jubail Industrial City?” see Figure 4, 92% of participants think that there is a pollution problem in Jubail Industrial City see Figure 5. 84 % of people would like to participate in solving the pollution problem see Figure 6.

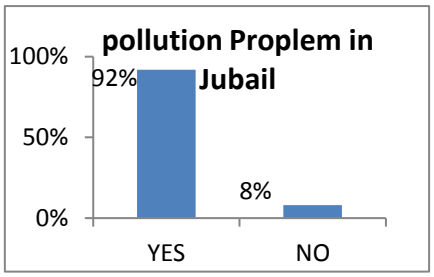

Figure 124 Pollution pro Industrial C

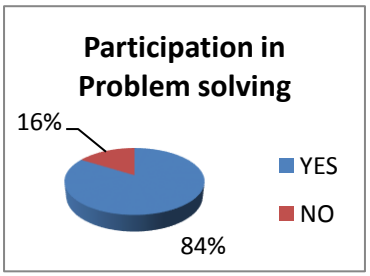

Figure 123 Participation in solving the problem

96% of survey participants know that vehicles are responsible for increasing the carbon footprint in our environment by releasing harmful gases into the air see Figure 7.More than 93% of staff and students know that vehicles are responsible for sound pollution see Figure 8.

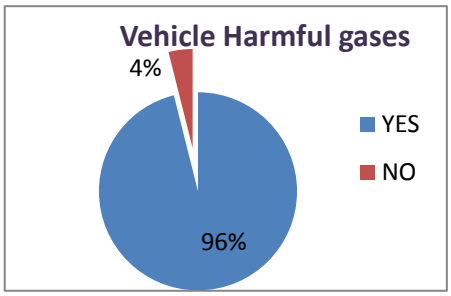

Figure 125 96% of people are aware of vehicle pollution

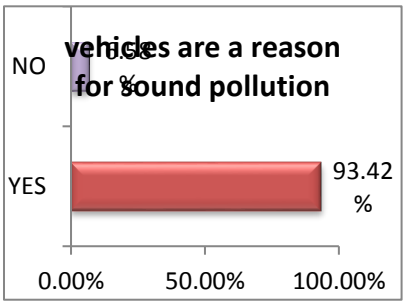

/ehicles are responsible for sound pollution

In JIC 86% of staff and students recommend riding bicycle instead of driving cars for students inside JIC campus see Figure 9.

Nearly 70 % recommend riding bicycle instead of driving cars for staff inside JIC campus see Figure 10.

30 % of staff would disagree riding the bicycle that is because of the Saudi Arabia tradition and the custom address “Thoub” see Figure 11 and maybe some staff already used to using the car inside the campus very close to their teaching location.

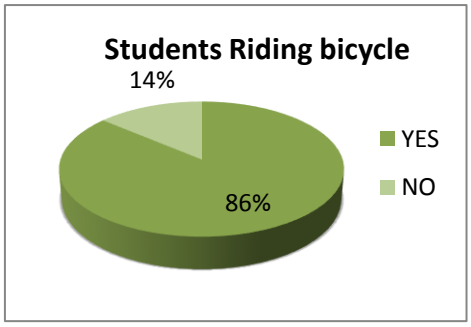

Figure 128 Riding bicycle instead of driving cars for students

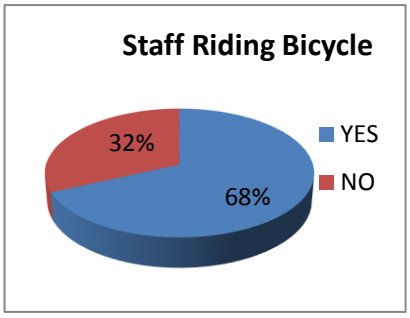

'7 Riding bicycle instead of riving cars for staff

Figure 129 Riding bicycle with "Thoub" address for Saudi Staff [1]

As we asked the following question “Do you think that banning gasoline/ diesel powered cars from the JIC campus can improve air quality and reduce pollution?” 74% think that banning fossil fuel cars will improve air quality see Figure 12.

71% of car users in general inside JIC campus agreed to Park their gasoline/diesel powered cars outside the JIC (Just across the road) campus see Figure 13.

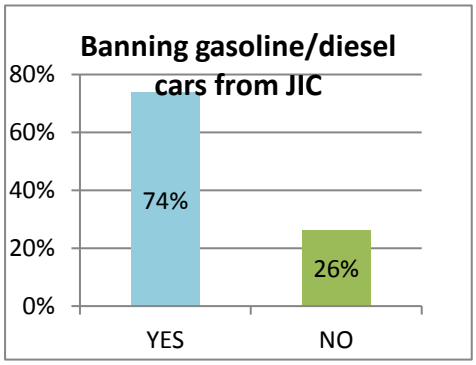

Figure 130 Campus has 74% supports banning gasoline/diesel cars in JIC

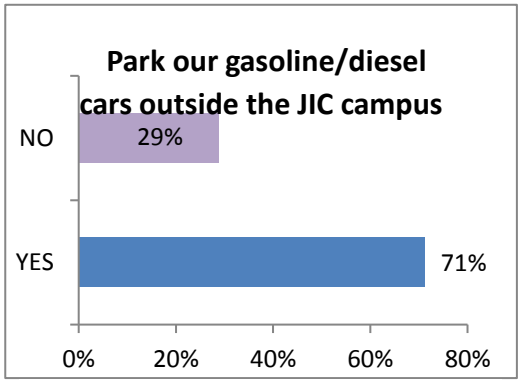

Figure 131 Parking fossil fuel cars outside JIC campus

Staff and students still agree to the last question even if it will take them an extra ten minutes to reach their destination inside JIC after parking outside the campus (transportation inside JIC will be by bicycle or electric bus/shuttle bus) see Figure 14.

85% of the survey output thinks it is a good idea to recycle solid waste inside JIC campus see Figure 15.

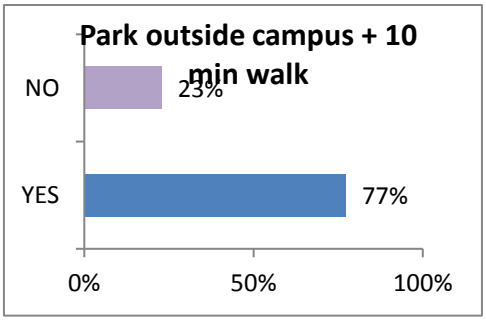

Figure 133 80% response to walking after parking the car

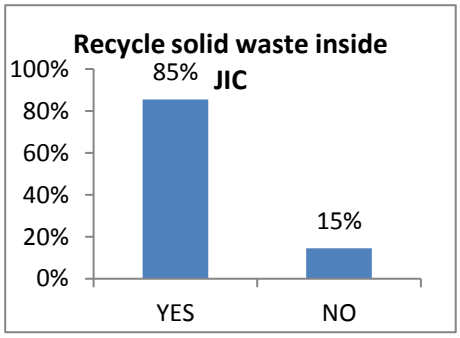

Figure 132 Strong response to solid waste recycling inside JIC

9% of college people thinks it is a good idea to convert all street lights inside JIC to solar energy powered lights instead of the current electric powered ones see Figure 16

85% of JIC staff and student would accept having wind turbines inside JIC see Figure 17.

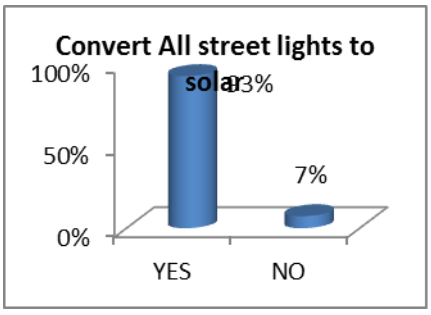

Figure 134 Response to solar street lights conversion

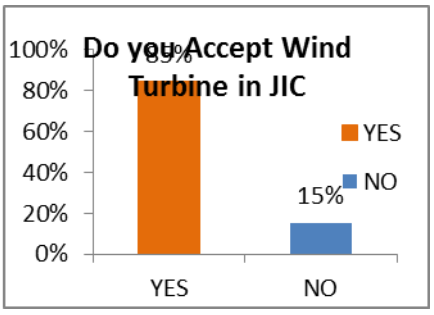

Figure 135 Wind turbine installation support

95% of survey contributors says it a good idea to establish a Renewable Energy Center to educate the community and students about renewable energy see Figure 18.

Survey participants when they were asked if they support converting some buildings inside JIC into solar powered buildings, 97% said yes see Figure 19.

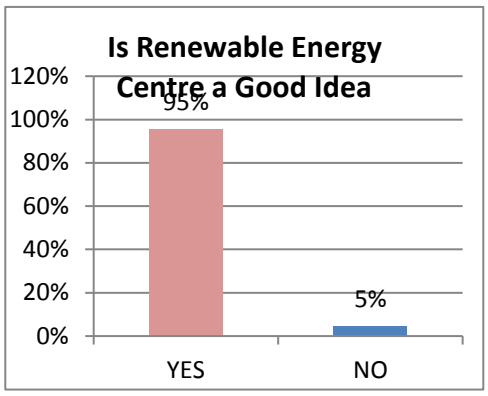

Figure 137 Renewable Energy Centre support

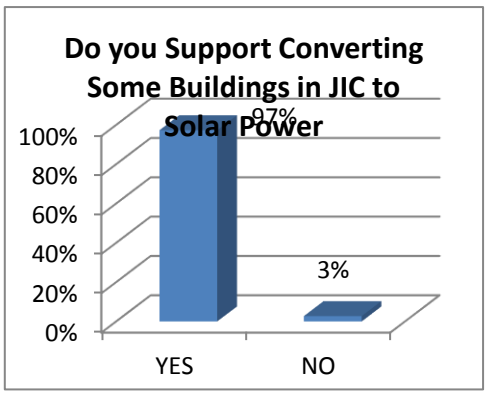

Figure 136 Converting some JIC buildings to solar power

Generally we can conclude that all different aspects of the green project were supported by faculty and students.

4. SOLAR STREET LIGHTS

Figure 138 Solar Street light by Sun co.

Very essential part of our main project is to replace the traditional method of the street lighting using the grid power by the solar power see figure 20.

It is too obvious that after about 15 years, the world's electricity production will be mainly relied on solar energy. Solar energy is a non-polluted energy source, abundant and of course not costly. Maintenance is almost free and hazards are none, see Figure 20.

Batteries (which are a secured supply - DC) store the solar power from the solar plates and deliver it to the lights. If AC loads need to be supplied, DC can be converted into AC. Smart -self / 24 a day controller is used to control the lighting according to the sky brightness. The normal lamps will be replaced by LED lamps.

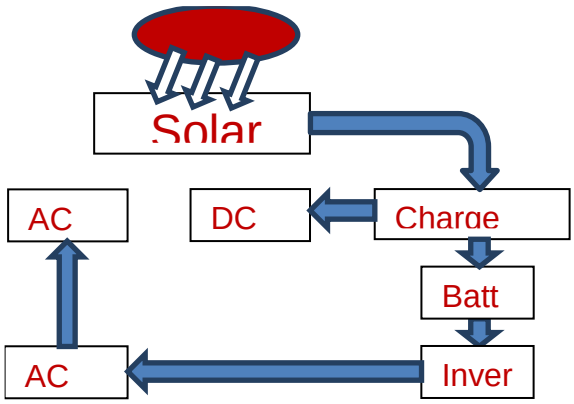

Figure 139 Solar energy system

Figure 21 shows how the sun light is absorbed by the solar cells then transferred to the DC and / or AC loads.

By surveying our JIC lights, the following different types have been monitored:

Street Lights, Global Lights, Pathway Lights, Bollard Lights, Parking Shed Lights. JIC Main entrance gate is seen in Figure 22.

Figure 140 JIC Main entrance gate [2]

The attached table 3 shows the wattages, the quantities and the costs according to the different types of lights.

The following Figures and results must be highly considered:

The total price of lights is **259,776 US$** which means about **1M SAR**
The total Power is **88.404 kW**.
The annual total Energy is **258,846.91** kW**h**
The total annual Billing is **67,300.197 SAR** ~ **18,000 $ US**

It is clear that the payback period will be 14 years and 5 months.

S. No.	Type of Lights	Wattage	Quantity	Total Wattage (W)	Price/ Unit (USD)	Total Price (USD)	Remarks
1	Street Lights	(1*400W)	125	50000	1019	127375	
2	Global Lights	(4*100W)	4	1600	1019	4076	
3	Global Lights	(4*15W)	50	3000	175	8750	
4	Global Lights	(1*15W)	111	1665	85	9435	
5	Bathway Lights	(1*80W)	52	4160	230	11960	
6	Bathway Lights	(1*125W)	111	13875	350	38850	
7	Bollard Lights	(1*26W)	24	624	85	2040	
8	Parking Shed Lights	(1*40W)	337	13480	170	57290	
	Total	-	-	88.404 (Kw)	-	259,776	~ 1 M SAR

Table 3 statistics of all types of lights in JIC campus

5. SOLAR POWER CHEMICAL DEPARTMENT BUILDING

5.1 Introduction

This paper proposes a Photovoltaic system model to supply electricity to the Chemical Department Building, (seen in Figure 23) occupying 4160 square meter area in Jubail Industrial College, as a part of its upcoming Green initiative project. The aim of this project is to implement renewable energy technology there by reducing its dependency for power on the Electricity Distributing Company. This paper chiefly discusses about proper selection of the PV panel system with solar charge controllers combined with battery bank for energy storage, inverter module for energy conversion and further utilization. The maximum demand at all the time needed by the building is 2000 kW. The proposed PV model is designed in such a way to cater the needs of energy in the building completely. The proposed PV system would supply the maximum demand. If the demand for electricity exceeds the maximum demand then the electricity Distribution Company would supply the additional demand [1]. There would be a change over switch to connect the power supply to the electricity distribution company if this situation demands. The battery bank would be used to store the surplus amount of energy if the load is less than the maximum demand.

Figure 23 Chemical Department Building

5.2 Proposed PV system model:

Figure 24 below shows the proposed PV system model consisting of the group of Solar panels fixed on 45 degrees angle in the north south direction. The output of the solar panels is connected to the control unit. The control unit monitors the solar panels and the battery bank connected. In the event of the complete charge of the battery bank, the solar panels are disconnected from the battery bank by the control unit. In the event of the excessive load the loads are connected to the electricity distribution company to meet the additional maximum demand.

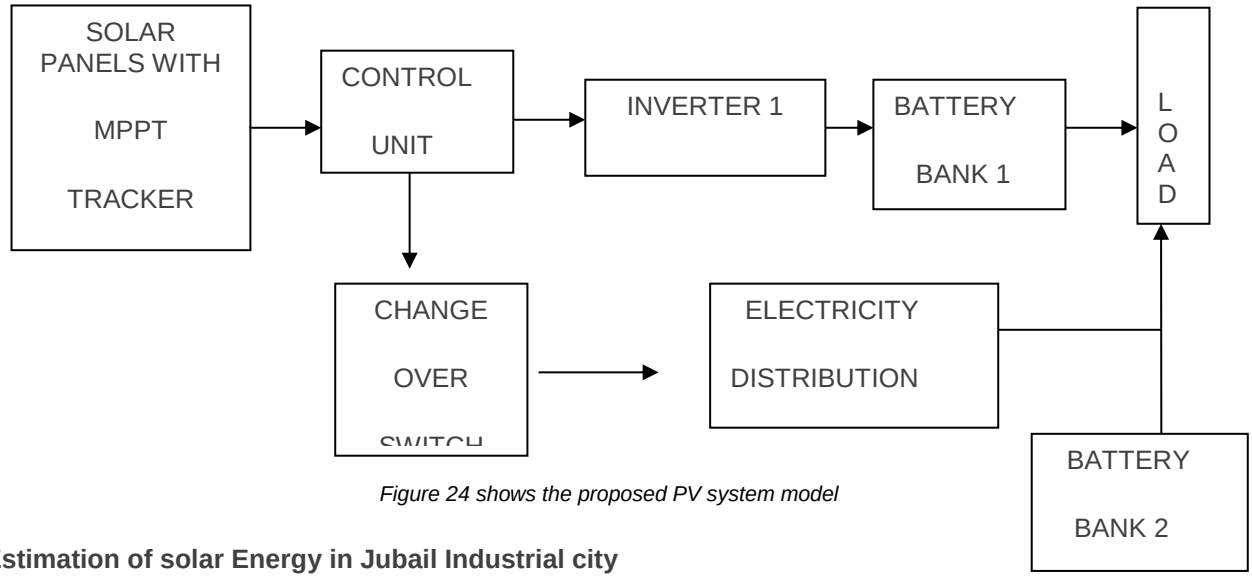

Figure 24 shows the proposed PV system model

Estimation of solar Energy in Jubail Industrial city

The global formula used for estimation of the electricity generated in output of a photovoltaic system [4] is

E = A×r×H×PR…… Where

E =Energy in kilo watt hours (kWh)

A = Area of the solar panel in (m^2)….. (a)

r= solar panel yield in percentage…… (b)

H =annual average solar radiation on tilted panel (shadings not include)…..(c)

PR = performance ratio is the coefficient for losses (range between 0.5 and 0.9, default value =0.75)…..(d)

r is the yield of the solar panel given by the ratio.

The Electrical power of one solar panel can be estimated by using above formula as follows.

Area of solar panel is 1.6 m^2…. (a)

The solar panel yield for 250w peak power with area of 1.6 m^2 is 0.25/1.6 =15.6 %.....(b)

Month	Day	Total Daily Radiation (H), W/m^2
Jan	17	4235.0
Feb	16	4028.7
March	16	5121.9
April	15	6996.7
May	15	6307.8
June	11	6312.9
July	17	6644.1
Aug	16	6960.7
Sep	15	5990.1
Oct	15	4991.3
Nov	14	4208.1
Dec	10	2963.1

Table 4 statistics of Total Daily Radiation in Jubail Industrial City

Table 4 demonstrates statistics of Total Daily Radiation in Jubail Industrial City.

For the purpose of analysis the Global Solar Radiation (GSR) for location via Jubail Industrial city is 6996 w/m^2 from [5].

H = 6356 W/m^2 annual solar radiation for Jubail Industrial city ……. (c)

PR = 0.75 …… (d)

Substituting a,b,c,d, in equation (1) we get

E =A×r ×H × PR

= 1.6 ×15.6 ×6996 ×0.75

=130965W or 131 kwh/year

The annual power produced by one photovoltaic solar panel can be estimated according to [6],taking into consideration that one watt of peak power produces an annual energy of about 2 kWh [7].

The solar energy generated by one silicon crystalline panel as per the formula, can be estimated to have a peak power of 119 kwh. So a single photovoltaic panel produces about 240 kwh / year. The surface of the panel is 1.6 m^2.

Maximum Demand Assessment:

The maximum demand assessment for the Chemical Department Building having a maximum demand of 2000 KW has been assessed based on the procedure adapted in [2] as follows.

The maximum demand required = 2000 kW

No of hours the entire loads are in operation = 2000 kW * 15 = 30,000 kWh

(Morning 6 am to Night 9 am); 15 hours in total.

6. SOLAR POWERED GREEN CAR PARK

JIC ambitious plan for creating a zero emission environment inside the campus has led to the idea of establishing a Green Car Park near JIC campus and next to the Royal Commission Building.

6.1 Current status:

Currently the college is hosting 4000 students in addition to educational and supporting staff; daily car movement within JIC campus is creating the following effect:

1- Car emissions are present inside the campus
2- Slow car movement increases emissions per distance.
3- Internal transportation is car-dependent; which results in further amount of emissions
4- Cars are subject to increased temperature during parking time, which requires more fuel consumption for cooling
5- Moving vehicles present a safety issue for students and facilities
6- Parking areas within JIC are consuming areas that can better be used for student and staff wellbeing

Furthermore, JIC is expanding in plans to accommodate 14000 students with an increased number of staff within five years; the same problems will dramatically increase leading to a deficiency in the current structure

6.2 Ambition

Our ambition is to create a zero emission campus, an environment that promotes healthy activities in addition to education; where the student will learn and practice healthy behavior that will positively reflect on the society and the working environment.

6.3 Methodology

A Green Car Park (see Figure 26)will assure the following:

1- the park will allow for quick entering and parking to reduce engine running time
2- the park will be well ventilated to allow release of engine emissions
3- car shading will be provided by PV cells
4- the Park will have sufficient natural illumination at day time
5- night time illumination will be provided by electricity from PV cells in the morning
6- electricity saving system will be applied
7- electrical energy produced that exceeds the need of the park will be directed to other buildings
8- the park will provide a charging station for electrical vehicles powered by PV cells
9- rain water harvest system will be applied, collected water either will be sent to the grid or used internally

10- exits of the park will allow for easy departure to reduce engine running time

6.4 Case Study

The eastern area (see figure 25) has an insolation (incoming solar energy) of 1700 kWh/m^2 as displayed by the solar map below. Available photo voltage cells have an average productivity of 15%.

Actual calculation of electrical power generated is calculated on annual basis since the daily weather will affect productivity

To calculate annual productivity [8]:

Annual productivity = insolation x efficiency x area

Annual productivity for our Green Car Park is 1700 kWh/m^2 x 0.15 x 30,000 m^2

Equals 7650000 kWh that is: 7.65 GWh

With expected losses of 15% due to current conversion and unexpected weather conditions the resulting total will be 6.5GWh

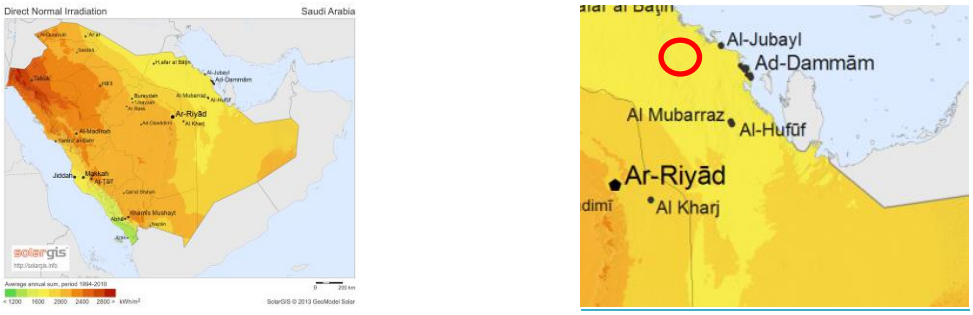

Figure 25 Saudi Arabia Eastern area has an insolation (incoming solar energy) of 1700KWh/m^2

While a more efficient PV cell can be used, the cost will increase; although this point is discussable knowing that other factor affecting insolation such as humidity and dust are present. Figure 25 shows the situation of Jubail city in Saudi Arabia, Eastern region which has an insolation (incoming solar energy) of 1700KWh/m^2

6.5 Environmental Impact

Measured and calculated depending on oil consumption to produce electricity, the following types and amounts of gases are produced [9]: see table 5

Gas	*Emission (kg/MWh)*	*Actual emissions to be prevented (ton)*
carbon dioxide	758.4	5,801,760
sulfur dioxide	5.4	41,310
nitrogen oxides	1.8	13,770

Table 5 Actual emissions to be prevented

In addition to reducing emissions from vehicles will reduce 27 kg/h [10] of emissions for each car, assuming a car travelling inside JIC is comparable to car in idle state. Compared to JIC electrical consumption, the previous amount to be produced will cover the needs of JIC and the extra can be utilized to power additional buildings or facilities; see Figure 26

Figure 26 proposed actual Car Park to be converted into Green Car Park

7. WIND SPEED AND POWER CHARACTERISTICS AT JUBAIL INDUSTRIAL CITY

7.1 Introduction

To assess the feasibility of wind power generation at Jubail industrial college (JIC), five years weather data was collected from nine weather stations (see Figure 27). Weather station 1, 2 and 8 were found to be closer the JIC. Site 1 was closest to JIC and weather data at this site is collected at three different heights, 10 m, 50 m and 90 m.

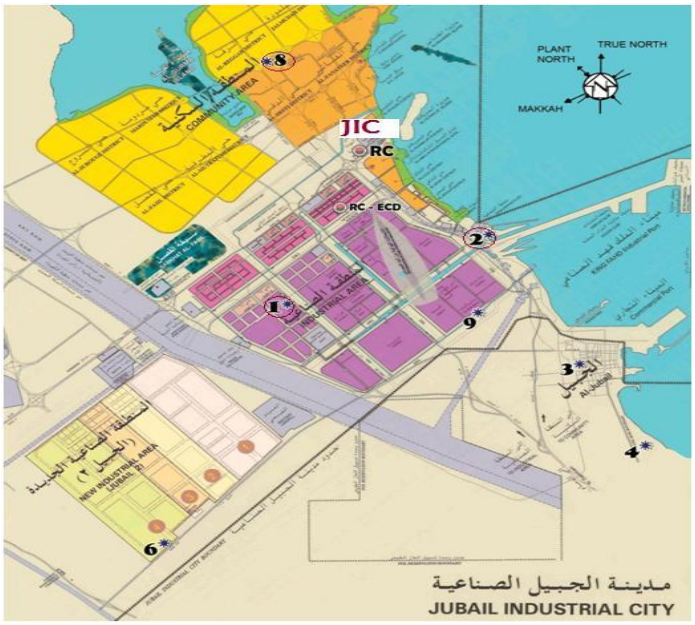

Figure 27: Nine weather stations [12]

7.2 Results and Analysis:

The yearly average wind speed at 10 m, 50 m and 90 m hub height were found to be 3.3 m/s, 4.8 m/s and 5.3 m/s respectively. The seasonal variation of wind speed at these different heights is given in Figure 11. It was observed the wind speed was highest in the month of February and lowest in the month of October.

The seasonal variation of average wind power density is given in Figure 28.

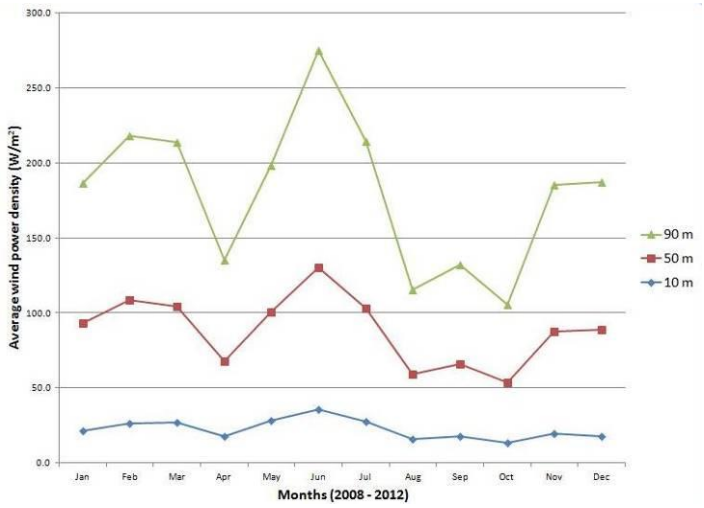

Figure 28: Seasonal variation of wind power density at different hub heights

A typical medium capacity vertical wind turbine of 3 kW rated power was selected for the feasibility analysis, since the Weibull distribution of the wind speed at 50 m hub height shows 90% availability see Figure 29 of more than cut-in wind speed which is 1.5 m/s. (See the power curve, Figure 30)

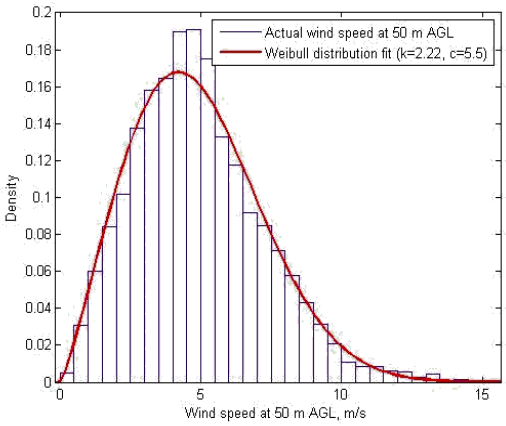

Figure 29: Weibull distribution of wind speed at 50 m hub height.

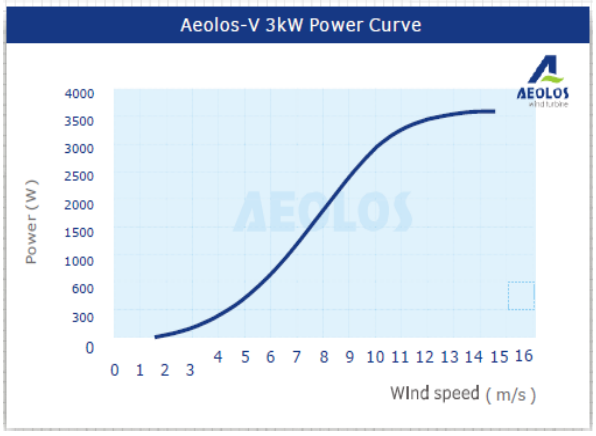

Figure 30: Power curve for a typical 3 kw rated power vertical wind turbine.[12] speed at 50 m hub height.

8. RENEWABLE ENERGY CENTER

To establish a renewable energy centre at Jubail Industrial College

8.1 Introduction

Saudi Arabia is largely dependent on exporting oil as well in Saudi up to now depends on fossil fuels to produce the electric power. The business of the sustainable and renewable energy technology is growing business but still it is slower in Saudi Arabia than the others therefore education of replacement of fossil fuels by various sources of renewable energy is needed especially because the renewable energy technologies are becoming internationally recognized as a dynamic input towards a sustainable energy future. By shifting some of the fossil fuel plant to renewable energy Saudi Arabia will export more oil and sell it with the international price and more saving for the environment by reducing the pollutions that produced by fossil fuel plants.

8.2 Mission Statement

Our mission is to provide training courses in renewable energy technology an to apply the use of renewable resources and practices as educational opportunities to the community as well the school's students and colleges with long and short training programs in renewable energy.

8.3 Vision Statement

To discover the use of alternative energy in helping our excellent local resources for the purpose of implementing and supporting successful country development.

Establishing renewable energy centre at Jubail Industrial College as cornerstones of a renewable energy school and research centre in future will help to provide the community as well as the industry with a proper location with proper and full facility to study the latest technology and the applications in the field of renewable energy. The renewable energy centre will provide elective courses for the colleges and university for Royal commission for Jubail and Yanbu as well as to provide special programs for schools boys/girls

8.4 The renewable energy centre will be fully equipped to serve the educational program as well the researchers:

The renewable energy centre and the program will consist of such as:

- Solar energy technology
- Wind energy technology
- Geothermal energy technology
- Residential energy management
- The centre will be powered by solar and wind energy
- Solar vehicle as well as hybrid vehicle as training aid
- Solar energy stations to be used as research and training aid
- Wind turbine stations to be used as research and training aid
- Solar pumps, solar compressors, solar air-conditions and lighting to be used as examples of some application of using solar energy.
- Geothermal training system
- Combined renewable energy stations to be used as research and training aid.

8.5 Who will benefit from the renewable energy centre?

The renewable energy centre will serve different institutions at different level; as well will serve the schools from primary up to secondary level.

The renewable energy centre as well will serve more than 20 petrochemical factories by providing a well-equipped renewable centre for their engineers to do their research.

The renewable energy centre will provide long training programs as will a short program for the community to encourage the community to use the renewable energy in their homes.

8.6 The size and location of the renewable energy centre

The centre will be established inside Jubail Industrial College which is in the middle between the community's houses and the industrial factories therefore the location will be suitable for both and easy to reach for outside visitors.

The size of the renewable energy centre will be around 3000 square meter and it will consist of renewable energy workshop, lab for research, class room, and lecture hall with a capacity of 100 seats, offices, and stores.

8.7 List of equipment's needed for renewable energy to be used by researchers

1) Programmable gas analysers for thermal conductivity analysis
2) Renewable Energy Training System Teaching Aids
3) Solar raining kit, for demonstration and training
4) Renewable Energy Education Set
5) Hydrogen car, fuel cell
6) Electric vehicle, charged by solar
7) Wind turbine
8) Solar water pump
9) Solar air compressor
10) Split unit air condition
11) Water heater
12) Electronic multi meters
13) Workshop tool box
14) Class room chairs
15) Data Projector
16) White Boards
17) Office table and chairs
18) Electronic board
19) Store shelves
20) Power full computers with laser printers
21) Meeting table and chairs
22) Workshop benches

8.8 Similar project in the world

Figure 31 Ecotech Institute's campus received the Leadership in Energy and Environmental Design (LEED)

Ecotech institute as seen in Figure 31, college of renewable energy and management in in Aurora, Colorado focuses on generating graduates to work in the field of rapidly grown sustainable and renewable energy technology. It offers associate's degrees in solar energy technology, wind energy technology and some other majors. In 2011, their building was legally certified from the US Green Building Council. The building has a very good environment which helps students build expertise they need for their clean energy carriers. However, it includes twelve roof top solar panels and eight wind turbines generating more than 65000 kilo watt per hour each year. The institute owns elite faculty members. When a student is inside, he will not be sitting in a classroom for all the day, and that because of the availability of well-equipped labs with the latest technologies. Wind energy students benefit from various wind turbine trainers and that is just an example. [13]

9. BIOGAS PROJECT IN JIC

1. Biogas is produced from anaerobic decay (decay that occurs without oxygen)

Anaerobic Digestion (AD) is a process whereby organic waste is broken down in a controlled, oxygen free environment by bacteria naturally occurring in the waste material. Methane rich biogas is produced thus facilitating renewable energy generation. As a result, materials that are currently going to landfill can be utilized; natural methane emissions are reduced and conventional generation with its associated carbon emissions is displaced. The residual nutrient rich liquor and digestive is suitable for use as fertilizer on the farmland surrounding such a plant, reducing the need for artificial fertilizer. [2] See Figure 32

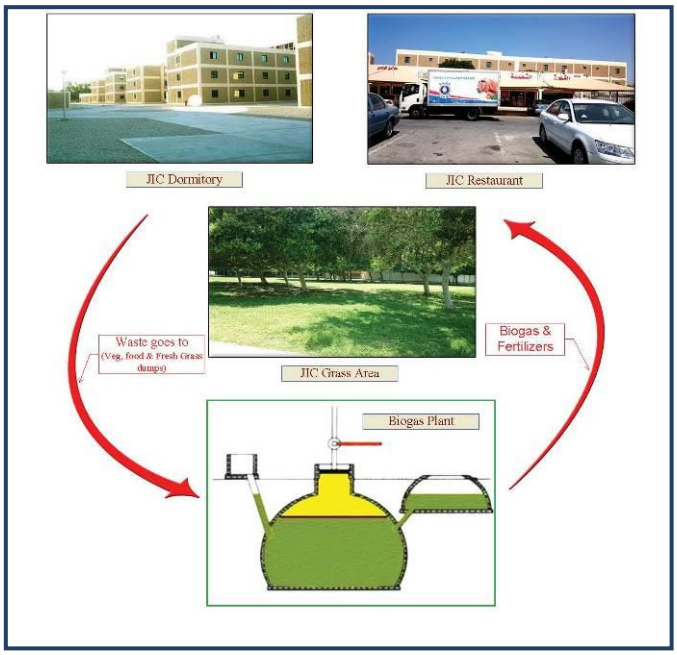

Figure 32 Proposed Biogas cycle in JIC

2. During biogas process anaerobic digestion will take place which will convert the organic matter to more soluble and biologically available forms, providing a more predictable bio fertilizer. These fertilizers are rich in nutrients which benefit to the plants. Other nutrient recovery technologies may be employed to reduce the nutrient content of the digested wastewater. Biogas is produced based on to satisfy the conversion system load that can serve the need. Storage systems will be designed to smooth out variations in gas production rate, gas quality and gas consumption rete. The storage component will operate at a constant pressure. Biogas can be used readily in all applications designed for natural gas such as direct combustion including absorption heating and cooling, cooking, space and water heating, drying, and gas turbines can be used in for vehicle use in the form of compressed gas. [14]

3. General Components of Biogas:

   • ± 60% CH_4 (methane)

   • ± 38% CO_2 (carbon dioxide)

   • ± 2% N_2, O_2, H_2, & H_2S

4. Amount of biogas depends on the waste itself and design of the digester. *Some digesters can yield 20 liters of biogas per kilogram of waste up to 800 liters per kilogram. Factors: waste quality, digester design, temperature, system operation, presence of oxygen. [15]*

   Average fuel value of methane = 1000 BTU/ft^3

Average fuel value of propane = 2500 BTU/ft^3

1 BTU/ft3 = 37.2589 KJ/m^3

Approximate cost to have a BIOGAS plant (see figure 33) in JIC premises which can fulfil the requirement of JIC is 100,000.00 SAR that is approximately 27000 US$. See the proposed location for Bio-Gas Plant in Figure 33

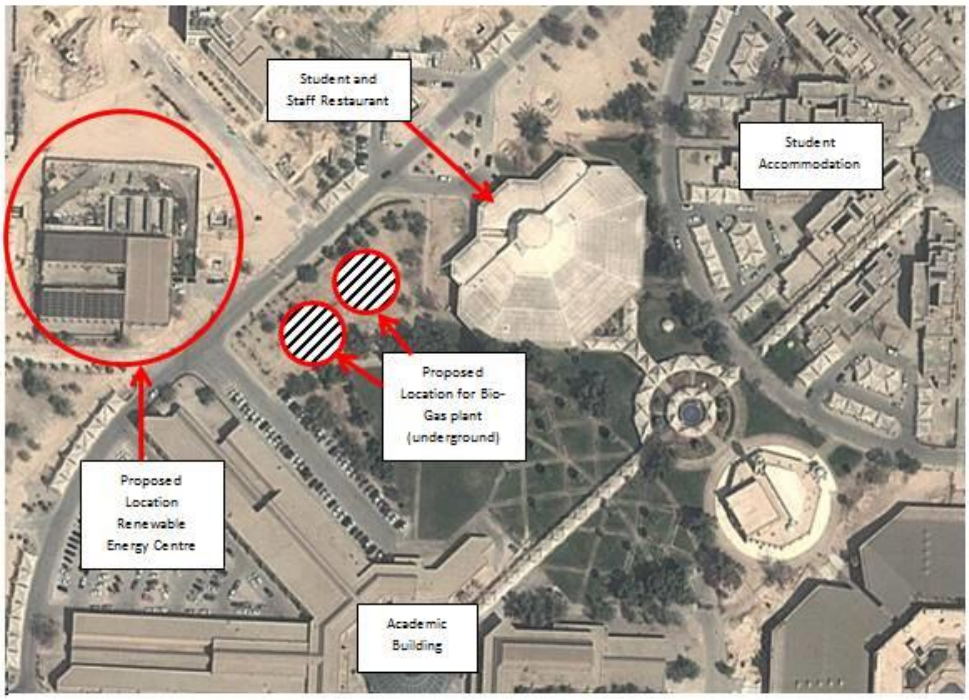

Figure 33 Proposed location for Bio-Gas Plant

10. ZERO CAR EMISSION CAMPUS

As shown in Figure 34 JIC campus will be proposed as a Zero Car Emission Campus that is fossel fuel, the proposer parking will be just across the border and it will be linked to the campus by bridge or tunnel see Figure 35. Elecctric Vehicle and bicycles are proposed to substitute fossel fuel cars with total cost of 449,000 US $ see Table 6

Figure 34 JIC Campus

Figure 35 Proposed Zero Car Emission Campus

Sr.	quantity	describtion	Cost (SAR)
1	4 pcs.	Nissan leaf car	432,000
2	8 Pcs.	Golf cars	150,000
3	10 pcs.	E.V. Chargers for green park	37,775
4	12 pcs.	External parkings E.V. chargers	98,775
5	10 pcs.	Shuttle bus – 14 passenger For students	421,875
6	5 pcs.	Shuttle bus – 14 passenger For staff	210,937
7	1	Car port with EV chargers (10 cars capacity)	247,500
8	2	EV mainenance truck	84,750
9	50	Men bicycle for students	37,500
Total		US $ 449,000	1,683,338

Table 6 Total cost of zero emission campus in SAR

11. CONCLUSIONS

The project could be established with a resonable cost and the pay pack is expected to be within a resonable time, the huge amout of heat in Saudi Arabia because of weather could be converted into solar energy that could reduse the pollution in an industrial city like Jubail Industrial City.

12. ACKNOWLEDGMENT

Thanks to Mr. Haris Jayah JIC Mechanical Department Chairman for his follow up and great support to this research, adding to this the JIC contractor NASMA CO. for their cooperation and help, Nabaa Construction Contractor and responsible engineer Mr. Khan for support in the new chemical building, also Mr Khalid AlHakami from JIC maintenance, also many thanks to service department in Royal Commission represented by Mr Yasser Arafat, we are also very grateful to both Electrical Department and Chemical Engineering Department in JIC for their support to finish this research and finally special thanks to Mr. William Carl Peterson who proof checked the questionaire and all JIC staff and students who articipated in the questionaire.

13. REFERENCES

[1] http://thedailyq.org/2013/09/25/why-bicycles-will-never-work-in-education-city/, accessed 6/12/2014.

[2] https://ssl.panoramio.com/user/1226242, accessed 6/12/2014.

[3] www.ecotechinstitute.com, accessed 6/12/2014.

[4]. K EUN H.Lee and P.K.Sen "Conceptual Design and Cost Estimate for A Stand Alone Residential Phovoltaic System"pp 1-5.

[5].http:// photovoltaic-software.com /PV-solar –energy-calculation.php

[6].Adel M.AL-NASSER "Performance and Economics of a solar thermal power generation plant in Jubail,Saudi Arabia: Parabolic Trough Collector" pp 754.

[7].REHMAN,S and Halawani, T.O, "Global Solar Radiation over Saudi Arabia Emperical model development"Applied Energy pp 3.

[8] Solargis: http://solargis.info/doc/88

[9] EPA (2012). Inventory of U.S. Greenhouse Gas Emissions and Sinks: 1990-2010. Chapter 3 (Energy), Tables 3-12, 3-13, and 3-14. U.S. Environmental Protection Agency, Washington, DC. U.S. EPA #430-R-12-001 (PDF)(481 pp, 16.6MB, About PDF)

[10] Wikipidia http://en.wikipedia.org/wiki/Motor_vehicle_emissions. 6/12/2014.

[11] Royal commession for Jubail, environment department, http://www.rcjy.gov.sa/en-US/Pages/default.aspx 6/12/2014.

[12] http://www.windturbinestar.com/vertikale-windkraftanlagen-preise.html 6/12/2014.

[13] http://www.ecotechinstitute.com/ 6/12/2014.

[14] https://biogas.ifas.ufl.edu/biogasdefs.asp

[15] www.anaerobic-digestion.com/index.php

[16] https://docs.google.com/forms/d/1ZFO8KC5qxB9OB0dg4z-JQFHNBgEX8LE0SlDT3m8gUqI/viewform accessed 6/12/2014

445: Energy uses and climate change mitigation: assessing the roles of robust energy efficiency practices

SAMUEL C DIKE[1], FERDINAND DAMINABO[2]

1. Energy Law Consultant and Lecturer in Faculty of Law, Rivers State University of Science and Technology, Port Harcourt, Nigeria. Email eme.olive@yahoo.co.uk
2. Department of Architecture, Rivers State University of Science and Technology, Port Harcourt Nigeria Corresponding email: ferdydaminabo@yahoo.com

Energy uses, security of supply of energy and tackling climate change risks, have been regarded as the most important issues that occupied the 21st century. This is due to the difficulties of ensuring adequate supply of commercial energy to more than 1billion population of the world that are energy poor and the challenges posed by climate change risks. Consequently, policy makers and researchers have proffered different solutions for addressing these existential issues of our time. Some of the remedies proffered are the benefits of diversifying energy supplies away from the conventional energy forms to renewable energy sources and the employment of energy efficiency practices. From the perspective of a cost effective approach or a tested legal framework, and due to the slow pace of penetration of renewable energy sources to the world's global energy mix, it has been posited that adopting a robust energy efficiency practice in our homes, industries and institutions, would be the magic wand needed to reduce or stabilise the Greenhouse Gas effect which are responsible for the disturbing growth of climate change risks. The objective of this paper therefore is to examine the benefits of energy efficiency practices in promoting climate change mitigation.

Keywords: energy uses, security of supply, climate change, renewable energy sources and energy efficiency practices

1. INTRODUCTION

The objective of this paper is to consider the benefits of adopting robust energy efficiency practices in our homes, industries, business, residential houses, building, transportation and other sundry sectors in a way that will reduce carbon emissions while promoting sustainable development .Energy is the golden thread that connects economic growth, increase social equity, and create an environment that allows the world to thrive. (UN 2012). Energy is very vital to the development of every nation and the attainment of Millennium Development Goals.(MAUGHNAUTEN, 2011:32). However, making energy available faces three" trilemmas": delivering security of supply, ensuring sustainability of energy systems and providing access to affordable energy to all (MAUGHNATEN 2011).

Energy is seen as an input into the production of desired energy services and is also employed in various ways namely: in electricity for generation, cooling and heating of buildings, lightings and fuels for transportation. All these needs for useful energy are called energy services.(JASSEN, 2011: 241). Energy services are economic goods produced by the deployment of useful energy while useful energy is obtained directly from ambient energy flows, from solar or any other energy carrier including electricity (JASSEN, 2011: 241).

The disruption of the flow of useful energy and the inability to meet substantially any or all human and industrial requirements for energy services leads to energy insecurity. Energy security has been defined by many authors (SOVACOOL, 2011:3), but (BOHI and TOMAN, 1996: 2) stated that energy insecurity stems from the loss of welfare that may occur as a result of a change in price or availability of energy. However, for Elkind, energy security is the availability, affordability, reliability, accessibility and sustainable energy supplies and services (ELKIND, 2010:121) .For energy to meet all energy service requirements; it must be readily available and affordable to the consumer. Furthermore, the access to cheap energy must not be costly or unreliable or intermittent in supply. Above all, energy sources and service must be sustainable that is, must be delivered in an environmentally friendly manner. (ASCLE R.S INDIRIYANTO, 2011:96).

Energy insecurity has become prevalent because energy demand outstrips its supply hence some countries, especially countries of the sub-Saharan Africa and those of Asia population, are deprived of this essential commodity (/OECD/IEA 2010 a). According to the International Energy Agency, more than 1.4 billion people globally lack access to electricity, 85% of them in rural areas, and the number of people relying on traditional biomass for cooking was estimated to be around 2.7 billion (OECD/IEA, 2010c).(MOOWAN. et al, 2011). In 2015, almost 1.2 billion more people who need access to electricity and 1.9 billion more people that require access to modern fuels can still not meet these energy services, thus heightening their poverty levels. It is now an acknowledged fact that making energy available, reliable and sustainable and economical affordable is a difficult task unless drastic actions are taking towards improving energy efficiency practices and renewable technologies.(OECD/ IEA 2014) (UNSE4 ALL 2014).

The failure to deliver energy sustainably contributes to the disturbing growth of green house gas and the ensuring climate variability (IPCC 2007a) The term" climate change" means any change in climate over time, whether due to natural variability or as a result of human activity (IPCC 2007a).These changes lead to various risks to flora, fauna and ecosystem. Climate change risk is now very unequivocal. According to the IPCC's special report on climate change and renewable,, "Climate change exposes people, societies and ecosystems to risk. Risk is the potential for consequences when something of value is at stake and the outcome is uncertain, and recognizing the diversity of values (MOOWAN et al, 2011).

The past and current Inter governmental Panel Report on Climate change(IPCC) reports showed that the unabated rise in green house gases in the atmosphere leading to climate change risks, contribute to energy crisis globally (MOOMAW. et al, 2011), (IPCC 2007a) and (IPCC 2014). This is due to the casual link between anthropogenic actions, energy uses and increase in green house gas emission. Some of the conventional energy sources namely: crude oil, natural gas, coal are major carriers of green house gasses such as carbon dioxide, methane and nitrous oxide.(IPCC 2014). Oil is the most traded commodity globally, with higher green house gas GHG potential. It is also the primary source of fuel for transportation and oil will continue to contribute over 80% of the global energy mix for some decades to come (EL BADIRE, 2011:14) (Dike 2014:142).

Natural gas is fast gaining global attention and is cleaner than oil and more environmentally sustainable. Coal which was the "king" of fossil fuels, is gradually regaining its popularity due to the huge price of oil and billion of investments required to bring cheap oil and gas to the market place. (OECD/ IEA, 2014 c). All

fossil fuels are finite and are precursors to climate change and other environmental risks.(IPCC 2014) Furthermore, the combustion of fossil fuels accounted for 56.6% of all anthropogenic GHG emissions (CO2eq) in 2004 .To maintain both sustainable economy that is capable of providing essential goods and services in both developed and developing countries, energy must be delivered sustainably and efficiently.(WORLD ENERGY ASSESSMENT 2000) AND (DEIETE et al, 2009 :18452).

According to Taverne, some climate change-related fossil fuel policies that also promote sustainable development are: First curbing the consumption of fossil fuels through fiscal measures such as carbon tax and abolishing fuel road transport subsidies (Tavern 2013). It also includes ambitious energy efficiency measures both at the supply-side and demand- side. Second, is the setting up a Cap and Trade framework scheme such as the European Union Emission Trading Scheme ETS. Third, is the expansion of the production of non-fossil fuel electricity through nuclear power station, hydro and other renewable electricity or Coal seems fitted with carbon capture. Fourth, is the introduction of alternative transport system such as electricity cars, hydrogen and bio-fuels powered cars. Fifth is fuel switching whereby coal could be replaced by natural gas or biomass and, finally, by replacing fossil fuels' use in building by electricity. Another ambitious strategy is to put a price on GHG emissions (OECD/IEA 2011).

In addition, such pricing must promote research and development (R&D) in the area of energy-saving and climate-friendly technologies. In this paper, however, a broad mix of policy instruments will have to be analysed, which, at the same time, must be cost effective because the problem is not about climate reduction alone but also promoting energy security. This is where energy efficiency is considered ahead of other strategies. Energy efficiency has been defined as a decline in energy intensity of total primary energy which is due to the application of efficiency methods and process in energy uptake (NATHALIE ET al, 2011). Energy efficiency means producing one unit of GDP with less energy input .It means conserving and storing energy. In this paper, energy efficiency is defined as the energy services provided per unit of energy input. For example, the energy efficiency of an air conditioner is the amount of heat removed from air per kilowatt-hour (kWh) of electricity input. At the individual product level, energy efficiency can be thought of as one of a bundle of product characteristics, alongside product cost and other attributes (NEWELL et al. 1999:75). It is both behavioural as well as an activity chains.

Apart from deploying energy efficiency practices, nuclear energy has been identified to mitigate climate change hence a source of sustainable energy. Nuclear power is the largest source of low-carbon electricity in OECD countries with an 18% overall share of electricity production in 2013. Globally, it is the second-largest source, with an 11% share (OECD/IEA 2015 N) .The continuing deployment of nuclear energy in most western nations and OECD countries, faces both social acceptance challenge, Health and safety challenges and political constraint due to occasional catastrophes (SOVACOOL,2008),(WEA 2000).For instance, the Furkinshima Daiichi incident contributes to the negative acceptance of nuclear as part of the continuing global energy mix (OECD/IEA 2015N)

Renewable energy which is energy produced from renewable sources in a sustainable manner include bio-energy, geothermal energy, hydropower, ocean (including wave and ocean energy); solar energy and wind energy (IRENA 2009) and (BOYLE, 2004). Renewable technologies seem to be the magic wand to both supply security and sustainability, but regrettably, it is yet to gain wide acceptance due to high upfront capital cost and social problems, (BOYLE 2014). Renewable sources contribute about 19% of the global energy mix. However, there are economic, social and political challenges facing the penetration of renewable energy sources into the global energy mix. These challenges are also encountered in both advanced and developing countries and hinder their wide deployment.

It is to address these challenges that the United Nations developed the centre for sustainable energy for all in 2011(UN SE4all 2011). The UN considered the various options and strategies for making energy available to the unreached population and in a manner that will reduce carbon emission, while stimulating economic growth. This would be achieved through renewable energy and the deployment of efficient energy sources and services. Energy efficiency EE practices have been found to address both demand -side and supply- side impacts of energy supply. Therefore, it is necessary to evaluate the cost-effectiveness of energy efficiency which is essential in identifying how much of a country's potential for energy efficiency resources will be captured.

Some of these measures have economic, social and political implications, which affect either their wide spread application or their acceptance. In the united states of America, for instance, studies carried out showed that energy efficiency resources may be able to meet 50 % or more of the expected load growth

by 2025 (NATIONAL ACTION PLAN FOR ENERGY EFFICIENCY 2008).for this reason, it has become necessary to define what cost effectiveness means and by defining c**ost-**effectiveness, would help **EF** measures to compete with the broad- range of the case of renewable energy and climate change mitigation**.**

This paper will critically examine the energy efficiency gains in various sectors and make recommendation on how to develop a cost effective, pragmatic, legal, regulatory and administrative framework that would promote energy efficiency practices ahead of renewable energy technologies. The paper is divided into the followings: Part one is the introduction. Part two will adumbrate on various legal and regulatory measures for promoting energy uses, highlighting the case for renewable energy sources and their advantages to the mitigation of climate change. Part three will dwell mainly on energy efficiency practices, methodologies and its gains while part 4 will conclude and make recommendations.

2. THE CASE OF RENEWABLE ENERGY AND CLIMATE CHANGE MITIGATION

This section examines the contributions of renewable technologies to the global energy mix and in mitigation of climate change risks. The renewable energy (RE) technology is one of the options canvassed for the reduction of the disturbing growth of green house gas emission globally (INTERNATIONAL RENEWABLE ENERGY AGENCY IRENA 2009). In 2012, renewable energy contributed an estimated 19% of global final energy consumption. Of this total share, modern renewable accounted for approximately 10%, with the remainder 9% coming from traditional biomass. Heat energy from modern renewable sources accounted for an estimated 4.2% of total final energy use; hydropower made up about 3.8%, and an estimated 2% was provided by power from wind, solar, geothermal, and biomass, as well as by bio fuels. (REN 21, 2014)

For IRENA, RE contributes to environmental preservation, through limiting pressure on natural resources and reducing deforestation, desertification and biodiversity loss to climate protection, economic growth and social cohesion, including poverty alleviation and sustainable development, access to security of energy supply to regional and inter generational responsibility (IRENA, 2009) Whereas, the authors do not deny the robust role of RE technologies in achieving the above -stated objectives, we are concerned that the organised cost of many RE technologies is currently higher than existing energy prices, though in various settings, RE is already economically competitive.

Therefore ,whether renewable or energy efficiency practices is being canvassed, an evaluation of any portfolio of mitigation options would require an examination of their respective mitigation potentials in addition to their associated risks, costs and their contribution to sustainable development. Consequently, some researchers have shown that the increasing demand for energy services is expected to drive RE growth. Therefore, the remit of the present paper is to examine how far RE could go in mitigating climate change risk while promoting security of supply, considering the numerous challenges that it faces.

A close examination of hydro power (HP), the most common renewable shows that HP produced 3,288 TWh equivalent to 16.3% of global electricity production in 2008 and contributed but has its the limitation. The global technical exploitable HP is more than 16400TWh per year(OECD/ IEA 2008 H) .According to IEA, climate change may affect water resources and cause changes in the availability of HP energy sources. The HP potential would remain unaffected at the global scale. HP, which provides the single largest share of renewable electricity worldwide, is being used increasingly to balance systems with high shares of variable renewable sometimes, with the aid of pumped storage (REN 21 2014). The generation cost of HP plant is about USD 50 to 100 MWH and a typical plant could last between 50 to 100 years, thus cancelling out the cost. However, HP is affected both by social acceptance problems and negative environmental impacts, namely-the likely emission of carbon and methane in fresh reservoirs. This indicates that notwithstanding the security of supply potential, HP contributes to greenhouse gas emissions**.**

Solar energy (SE) is energy from the sun and one of the largest energy sources of RE. It can be available as solar thermal for electricity generation and sola photovoltaic's usually mounted on roof tops. (BOYLE, 2009:92). The cost of PV includes capital cost and running cost. The initial cost is usually high while the running cost is low. The environmental effect of PV is minimal due to the use of silicon and cadmium as chemicals. Therefore, the use of solar for electricity generation would help in mitigating climate change but the cost of photovoltaic system has been found higher than the conventional electricity .(QUASCHNING, V. 2005).

Bio energy (BE) is another source of renewable energy mainly from biomass wood or bio fuels, and the main source of fuels in some African countries. This energy source is also derived from waste or agricultural plants. The paradox about bio- energy is that it may not be possible to fuel all vehicles on the planet with bio- fuels at their current low engine efficiencies, but if vehicles' fuel efficiency were greater, a larger fraction of vehicles could run on bio fuels thus reducing the demand on conventional oil and gas thereby saving the climate. Biomass energy depends importantly on plants and agricultural crops hence affect food security. It is for this reason, that the continuing contribution of Biomass to climate change mitigation and security of supply is contested (GROUTIOUS et al, 2011). The combustion of biomass generates carbon dioxide but these Co_2 is offset by growing plants. However, Biomass contributes to indoor air pollution, respiratory problems and emission of carbon due to inefficient combustion. Methane is also produced during the anaerobic digestion of biomass (BOYLE, G 2009).

Wind energy is a form of renewable energy from the natural wind. The atmospheric pressure is enhanced by the use of wind turbine to generate electricity. However, most wind turbines contribute to noise pollution and create visual negative impacts. They are likely to affect migratory birds and offshore wind farms affect fish and other marine lives which support human and natural systems (BOYLE, 2011:276). There is also a negative public attitude to wind farms as people in the UK are generally opposed to wind farms hence the acronym NOT in MY Back Yard (NYMBY) (BOYLE, G 2008; 274). Deploying wind energy requires detailed planning and approval in some countries and this may offset the gain in the industry due to years of bottlenecks and delayed approvals. This has negative impacts on the wide deployment of wind energy. Also, offshore wind farm is gaining prominence in some developed countries, such as Germany, Denmark and the UK both in investment and heat generation.(REN21 2014) However, the penetration is low in developing countries due to lack of capital and innovative technology. For example, throughout 2013, wind power met 33.2% of electricity demand in Denmark and 20.9% in Spain but in Italy, solar PV met 7.8% of total annual electricity demand. This is in addition to the apparent intermittency of wind which means that it cannot be guaranteed all year round. Therefore, wind energy may not be the magic wand needed to drive the reduction in climate change.

The Intergovernmental Panel on Climate Change (IPCC 2011) has observed a huge challenge of maintaining system reliability due to their cost. However, a suite of complementary RE technologies is one solution to reducing the risks and costs of RE integration (IPCC 2011).IPCC further stated that the costs associated with RE integration, whether for electricity, heating, cooling, gaseous or liquid fuels, are contextual, site-specific and generally difficult to determine. They may include additional costs for network infrastructure investment, system operation and losses, and other adjustments to the existing energy supply systems as needed. The available literature on integration costs is sparse and estimates are often lacking or vary widely. This is not so for energy efficiency devises.(IPCC 2011).Similarly, Climate change might have adverse impacts on renewable technologies while it is not so in the case of energy efficiency devises .(IPCC 2011 d) The authors thus argue for a wide- spread adoption of energy efficiency in our homes, industries and in Buildings.

3. ENERGY EFFICIENCY PRACTICES AND CLIMATE CHANGE MITIGATION

This section considers the advantages of deploying energy efficiency practices and their cost effectiveness. As already noted, energy efficiency is the ratio of useful energy or other useful physical outputs obtained from a system, conversion process, transmission or storage activity to its energy input (measured as kWh/kWh, tonnes/kWh or any other physical measure of useful output like tonne-km transported, etc (NATHALIE and PETER, 2011; 222) . We argue that EF should be preferred ahead of R E.

Energy efficiency can be understood as the reciprocal of energy intensity; hence the fraction of solar, wind or fossil fuel energy that can be converted to electricity is the conversion efficiency. Alternatively, energy efficiency output is measured in terms of populations (i.e., per capita) or monetary units such as the gross domestic product (GDP) or total value of shipments or similar terms. In most countries, energy intensity is the ratio of total domestic primary (or final) energy use to GDP. Energy intensity can be decomposed as a sum of intensities of particular activities weighted by the activities' shares of GDP (NATHALIE, 2011:218).

The benefits of energy efficiency practices is that energy consumption per unit of output from efficient process and technologies is one third to less than-half that of typically available equipment. The advantage of EF includes its contribution to hold consumption of energy services constant. This makes EF different in character from many other product attributes for which there may not be a well-defined notion of what constitutes optimal or "rational" behaviour on the part of the individual (GILLINGHAM, Kenneth et al, 2009.)

.How is energy efficiency optimised.? We also consider EF as being optimised by the way energy is supplied, consumed and conserved; by avoiding loss of energy at end-use and promoting energy savings.

The changes that bring about energy efficiency are noticeable in the way buildings are constructed and habited; and the way energy is employed in cooling and heating of our buildings; and in power for electricity generation; the way transport fuels are used and the way manufactures and business employ energy. The intensity of energy depends on the aggregate effect of total primary energy consumed per unit of GDP. If it is less, then there is a higher efficiency but if it is low, then the energy source is unsustainable. (NATHALIE and TAYLOR, 2011: 236). This leads us to consider the case for the adoption of energy efficient technologies.

3.1 Methodologies for the Deployment of Energy Efficiency Practices and Why Energy Efficiency should be preferred.

Energy efficiency can be applied first, by supply side-efficiency of energy conversion, transmission and distribution, including combined heat and power as well as improved demand-side efficiency in, buildings, industrial and agricultural processes, transportation, heating, cooling, lighting (IPCC, 2014). Second, a shift from high GHG energy carriers such as coal and oil to lower GHG energy carriers such as natural gas, nuclear fuels and RE sources.

Third, by the utilization of carbon capture and storage (CCS) to prevent post-combustion or industrial process of CO_2 from entering the atmosphere after the combustion of biomass sources of energy (see also IPCC, 2007). Fourth, an attitudinal changes for a better managed energy use or the use of fewer carbon and energy-intensive goods and services (see also DIETZ et al., 2009). This behavioural pattern cost little but may require a retrofit of equipments from energy intensive burners, for instance, to an efficient burner, in the case of gas or coal combustion or distillation.

In the United States of America, evaluating the cost-effectiveness of energy efficiency is essential to identifying how much of the country's potential for energy efficiency resources will be captured. It has been shown that energy efficiency resources may be able to meet 50 percent or more of the expected load growth by 2025 (National Action Plan for Energy Efficiency, 2008). Defining cost-effectiveness helps energy EF compete with the broad range of other resource options in order for EF to get the attention and funding necessary to succeed. (NATIONAL ACTION PLAN, 2008) . .Accordingly, the National Action Plan, outlined measures for integrating into the energy regulatory frameworks, cost effective frame work, to be complied by stake holders. These measures are contained in the Ten Implementation Goals of the National Action Plan for Energy Efficiency Vision for 2025 and they include the following goals:

1. a framework for change and this involves the establishing of a cost-effective energy efficiency as a high-priority,
2. developing processes to align utility and other program administrators' incentives such that efficiency and supply resources are on a level playing field,
3. the establishment of cost-effectiveness tests,
4. the establishment of evaluation, measurement, and verification mechanisms,
5. the establishment of effective energy efficiency delivery mechanisms,
6. the development of the State policies to ensure robust energy efficiency practices,
7. the aligning of customer pricing and incentives to encourage investment in energy efficiency,
8. establishing state of the art billing systems,
9. the Implementation of the State of the Art efficiency Information sharing and delivery system
10. Implementing advanced Technologies..

The main objective of these goals is to assist utility regulators and others in meeting the 10 implementation goals of the National Action Plan for Energy Efficiency's Vision to achieve all cost-effective energy efficiency by 2025. Thus, looking at the cost-effectiveness tests together helps decision makers to determine whether some measures are too costly; whether some incentives are too costly or low and what adjustments need to be made to improve distribution of costs and benefits among stakeholders. Using the US Southern California Edison (SCE) Residential Energy Efficiency Incentive Program, which provides customers incentives for efficient lighting and appliances (not including HVAC), It was found that the reduced energy consumption achieved as a result of the program resulted in $188 million avoided cost savings to the utility; $278 million in bill savings to the customers (and reduced revenue to SCE). 1; reduced nitrogen oxides

(NOx), PM10, and carbon dioxide (CO2) emission. This is a welcome development for other states in the US to adopt and for other countries to adopt in the wide- spread application of EE Program.

At an aggregate macro level, energy intensity stated in terms of energy per unit of GDP or in energy per capita is often used for a sector such as transportation, industry or buildings, or to refer to an entire economy. The transport sector has recorded some improvement given the utilization of engineering improvements in traditional internal combustion engines to reduce fuel consumption rather than enhancing acceleration and performance (AHMAN and NILSSON, 2008). Also, there are many gains from the substantial CO_2 emission reductions achieved through the hybrid electric systems, low battery electric systems and fuel cells

Other gains achieved by applying energy efficiently include an improved supply- side efficiency of energy conversion, transmission and distribution through a combined heat and power and an improve demand-side efficiency in the respective sectors and applications(e.g. buildings industrial and agricultural processes, transportation, heating, cooling, lighting) . Further, the benefits include the fact that properly sized variable-speed electric motors, improved efficiency compressors for refrigerators, air conditioners and heat pumps can lower primary energy use in many applications (SIMS et al., 2007).

Similarly, efficient houses and small commercial buildings which are air tight, well insulated from their design, may require only about one-tenth the energy of more conventional dwellings (PASSIVHAUS, 2010).) Similarly, EF design of high-rise buildings in tropical countries and other areas, could reduce emissions from cooling at a substantial cost savings ((AMBROS, 2009). Much gain had also been realised from the electricity sector by the deployment of efficient appliances for lighting such as the compact fluorescent or light-emitting diode lamps, which uses less electricity to produce a lumen of light than does a traditional incandescent lamp (NATHALIE AND PETER, 2011). With respect to the transport sector in the OECD countries, for instance, passengers light duty vehicles account for over half of transport demand for oil and light duty vehicle, are the largest consumers of energy accounting for over 87 % of passengers transport energy consumption. Therefore, reducing the fuel intensity of cars in these OECD countries, has meant the reductions in the dependence on oil and a mitigation of climate change.(NATHLIE and PETER, 2011). Similarly, among OECD countries, the overall energy intensities in relation to their GDP is estimated at 65% of the total decline in energy per GDP and this signalled the promotion of energy efficiency and sectorial energy uses ((NATHALIE AND PETER, 2011)

With respect to the industrial sector, it has been noted that industry contributes 37 % of global green house gas and industrial GHG emission is estimated at 12 $GTco_2$. (WORREL, et al 2009). Energy intensity of most industries is 50% of the base line. There are enough potential for green house gas mitigation through energy efficiency practices and energy audit in these industries. Energy uses is the largest source of GHG in industries and this has been estimated at 83% . Petroleum industry has had a long standing efficiency program for refineries and chemical plants with which they often integrated. These efforts had yielded significant results. For instance, Exxon Mobil and other companies had reported much gain from energy efficiency measures between 1974- 1999. Similarly, 65% of electricity consumed by industries is used by motor driving system. Therefore improving the winding system of these motors would help to reduce carbon emissions of GHG.

Also, mitigation potential through cogeneration – which produces both heat and cool through efficiency method contribute to added efficiency in the electricity sector (WORREL, et al, 2009) .Thus a cost effective energy savings of 5%--40% are found in process integration analyses in almost all industries. (SORREL et aL, 2009). In order to access the cost effectiveness of these measures, the researcher or industry should determine the quantity of avoided carbon dioxide (CO_2) emissions from the efficiency program. Once the amount of CO_2 reductions, has been determined, the economic value of the voided Co_2 can be calculated and added to the net benefits of the energy efficiency measures used to achieve the reductions. Currently, some jurisdictions use an explicit monetary CO_2 value in cost-benefit calculations and some do not. (NATIONAL ACTION PLAN, 2009) (NEWELL et al., 1999).It has also been found that the responsiveness of energy-efficient product innovation to energy prices increased substantially after product labelling was required.

Measure of energy efficiency includes energy savings from reduced energy intensity by changing the activities that demand energy inputs. A good example is seen by turning off lights when not needed, by walking instead of transportation, changing the controls for heating or air conditioning to avoid excessive heating or cooling or eliminating a particular appliance and doing such a task in a less energy intensive

manner. (DIETZ et al., 2009). It could be unarguable that these have recorded positive gains in reducing energy intensity, lowering carbon emission and promoting security of supply with minimal cost that cannot be achieved by the employment of renewable energy. Consequently, wide -spread energy efficiency practices can be said to be a head of renewable energy technologies with respect to the lowering of carbon emissions, and promoting security of supply of energy.

Energy efficiency is also a form of savings in that energy savings can be gained by organisation through, institutional and structural changes and by a changed behaviour. This can also be achieved by voluntary agreements between the government and industries and business to lower energy use or dedicated special management regulations that direct staff to lower energy uptake in their offices or establishment with or without rewards. It could be argued that reducing energy needed at the energy services delivery stage is an important means of reducing the primary energy required for all energy supply fuels and technologies. More so, energy savings at the end-use stage may utilize one form of renewable technology or the other for a specific energy service. (TWIDELL and WEIR, 2005).

This leads us to uncover the interdependence between energy efficiency and Renewable Portfolio standard compliance (RPS). RPS goals are an emerging issue in energy efficiency. This is so because unlike supply-side investments, energy efficiency, through load shedding, can reduce the amount of renewable energy that must be procured pursuant to RPS targets. This reduces RPS compliance cost, which is a benefit that should be considered in energy efficiency cost-effectiveness ahead of an outright deployment of various suites of renewable with higher cost margin. There are challenges to the deployment of energy efficient measures. One of the challenges is that energy savings, resulting from efficiency measures are not always fully realized in practice due to rebound effect in which some fraction of the measure is offset. This is because the lower the total cost of energy required to perform a specific energy service, may lead to utilization of more energy services. Rebound effect is also in the nature of carbon leakage if a wide spread energy efficiency method is adopted by particular jurisdiction. Carbon leakage is a situation where the increase in CO_2 emissions outside of the countries taking domestic mitigation action divided by the reduction in the emissions of these countries.. (NATHALIE and TAYLOR, 2011:222). There are two scenarios to the impact of a rebound effect.

First is that a successful energy efficiency measure may lead to lowering energy costs for the entity subject to the measure because it uses less energy. Another impact is that the full energy saving may not occur because a more efficient vehicle reduces the cost of operation per kilometre, so the user may drive more kilometres. Or a better-insulated home may not achieve the full saving because it is now possible to achieve greater comfort by using less energy intensive appliance. Thus, mitigation policies are not applied uniformly across different sectors and jurisdictions, then it is possible for carbon-emitting activities that are controlled in one place to move to another sector or country where such activities are not restricted (KALLBEKKEN, 2007: 198) (OECD/ IEA, 2008a). Recent research suggests, however, that estimates of carbon leakage are too high. However, rebound effect has been addressed by saturation effects leading to a chance of between 10 and 30% for home heating and vehicle use in OECD countries, and the negative impact is very small for more efficient appliances and water heating (SORRELL et al., 2009:4).

In the light of the above potential and actual benefits of deploying EF practices, it can safely be concluded that that the decline in the overall energy intensities of various energy end- use led to energy savings and this decline was due to attitudinal changes than investment in energy savings devices. However, we further argue that energy efficiency measures will continue to lower energy prices and hence, lead to economic development. This is because, an efficiency measure that is successful in lowering economy -wide energy demand, lowers the price of energy as well. This means that there is a huge gain by applying energy efficiency behaviours and adequate investment in promoting energy access and in addressing climate change mitigation. The cost of energy efficient infrastructures places it ahead of the adoption of renewable energy technologies. This is because, energy efficiency at the end-use stage facilitates the use of renewable and the lowest cost option is to reduce end-use energy demand through efficiency measures, which include both new technologies and more efficient practices (AMBROSE, 2009:240). A good example is the deployment of efficient appliances for lighting, as well as heating and cooling in the building sector (IPCC 2007).

Consequently, five key cost-effectiveness tests for energy efficiency program evaluation have been developed. These are the participant cost test (PCT), the utility/program administrator cost test (PACT), the ratepayer impact measure test (RIM), the total resource cost test (TRC), and the societal cost test (SCT) National Action Plan EE 2006) .The most common primary measurement of energy efficiency cost-effectiveness is the TRC, followed closely by the SCT. A positive TRC result indicates that the program will

produce a net reduction in energy costs in the utility service territory over the lifetime of the program. The distributional tests (PCT, PACT, and RIM) are then used to indicate how different stakeholders are affected. Historically, reliance on the RIM test has limited energy efficiency investment, as it is the most restrictive of the five cost-effectiveness tests.

Finally the benefits of deploying energy efficient measures include enhanced energy security, reduced investment in energy infrastructure, lower fossil fuels dependency, increased competitiveness and improved consumer welfare. There is also improvement in environmental benefits efficiency such as mitigation of green house gas and indoor air pollution. Similarly, energy efficiency measures have been known to have yielded additional satisfaction which cannot easily be quantified through additional benefits (and costs) beyond energy savings. This is in the area of improved comfort, productivity, health, convenience and aesthetics. Some jurisdictions choose to include costs in some of the cost-effectiveness tests, often focusing on specific issues, emphasized in state policy (MOOWAN, et al 2011) . It is also possible to measure energy efficiency through the established indicators provided by policy makers and this measures the pattern of end- use energy, providing where greater efficiency lies. By combining data on fuel efficiency with information about car uses and ownership, it was possible to ascertain the energy efficiency of cars and transportation sector in some OECD countries (NATHALIE and TAYLOR, 2011:232). This means that a robust energy efficiency measure has greater potential in lowering energy uptake in industries, electricity, households and building, while reducing green house gas emission

4. CONCLUSIONS

The authors have been able to examine the relationship between energy uses, energy efficiency and climate change mitigation, stating the advantages of employing wide -spread energy efficiency technologies ahead of renewable energy sources .In this paper, the authors argued that reducing energy needed at the energy services delivery stage is an important means of reducing the primary energy required for all energy supply fuels and technologies hence the importance of energy efficiency. Assessing the relative strength and weakness of deploying energy efficient measure and renewable energy technologies in climate change mitigation is a difficult one due to inadequate data from many countries. Except in OECD countries and USA, where the data on energy consumption and supply of different mix are available, there are inadequate information to guide a researcher to validate this claim in some developing countries due to the continuing dependence of their sizable population on the traditional biomass to meet their energy uptake

However, It is necessary to examine the total cost of end-use efficiency measures plus RE technology, and then determine whether there is rebound effect for a specific case. Rebound effect have been offset in the case of energy efficiency application and it is more cost effective than the application of inchoate renewable technologies which are bedevilled with social acceptance challenge, upfront capital cost, and the lack of political will in some countries. Although, renewable, technologies have been chosen as one way of reducing GHG effect but, has been found not the magic wand needed for the delivery of a zero growth in climate change risk. In this paper, the authors argued for the wide -spread adoption of energy efficiency technologies ahead of renewable by integrating energy efficiency practices into policy and legal frameworks of all countries and to promote voluntary energy efficiency behaviours with a reward This would be a win- win sum for both access to energy services and the mitigation of climate change.

5. REFERENCES

AMBROSE, M. 2009. Energy-efficient Planning and Design. In: Technology, Design, and Process Innovation in the Built Environment. P. Newton, K.D. Hampson, andR. Drogemuller (eds.), Taylor and Francis, New York, pp. 238-249.

AHMED M and Nilsson L J, 2008. Path Dependency and the Future of advanced Vehicles and Biofuels. Utilities Policy, 16(2), pp. 80-89.

ASCLEPIAS, R S Indriyanto, DWI ARI Fauzi and ALFA Firdaus 2011. The Sustainable Development Dimension of Energy Security in Benjamin Sovacool (ed) The Routledge Hand book of Energy Security Routledge, New York , PP 96-97.

BOHI, D.R., Toman, M.A 1996. The Economics of Energy Security, Kluwer AcademicPublishers, Boston/Dordrecht/London 2

Bohi, DR and Toman, M‘1993. Energy Security: Externalities and Policies ‘Energy Policy 1093.

BOYLE, Godfrey. 2008 Renewable Energy: Power For Sustainable Future. Oxford University Press, 275-276,

DIETZ T, Gardner, G. Gilligan, T, Stern, P. C, Vandenburgh, M.P 2009. Household Actions can Provide a Behavioural way to Rapidly Reduce US carbon Emissions. Proceedings of the National Academy of Sciences, 106(44), pp.18452-18456

DIKE, S C, 2014 Appraising the Legal Relationship between Operator, Non Operator and Operating Committee in a Joint Venture—the UK Example International Energy Agency Law Review p 142

DIETZ, T, York, R, Rosa, E 2009. Environmentally Efficient Well-Being: Rethinking Sustainability as the Relationship between Human Well-being and Environmental 16 (1) Society of For Human Ecology.

ELBADRI, A S 2011`Energy Security: the Supply side of the Equation` in: World Energy Council , World Energy insights World energy Council 14-15

ELKIND, Jonathan 2010 .Energy Security: A Call for a Broader Agenda in: Energy Security, Economic, Politics, Strategies and Implications, Elkind J and Pascal C, Brookline Institutes USA Pp 121-124

FIGURES, C 2008. Bridging the Gaps What would Constitute Success at Durban? in: World Energy insights World Energy Council 1

GROOTHUIS, P.A., Groothuis J D , Whitehead J C 2008. Green vs. green: Measuring the compensation required to site electrical generation windmills in a viewshed. Energy Policy, 36(4), pp. 1545-1550

GALLUFT, Anne Konn and ESHITA Gupta 2011. Energy Security and Climate Change: A Tenuous link In: Introduction; Defining, Measuring and Exploring Energy Security in the Routledge hand book of Energy Security Benjamin Sovacool, (ed) Routledge. New York pp 43-56

JAAP C Jansen and Adrian J Van der Welle (2011)The Energy Services Dimension of Energy Security in :The Routledge Hand Book on Energy security .Benjamin Sovacool, Routledge, New York 239-241

IPCC 2007a. Climate Change 2007: Synthesis Report. Contribution of WorkingGroups I, II and III to the Fourth Assessment Report of the Intergovernmental

Panel on Climate Change. Core Writing Team, R.K. Pachauri, and A. Reisinger (eds.), Cambridge University Press, 104 pp

IPCC 2007d. Climate Change 2007: Mitigation of Climate Change. Contribution of Working Group III to the Fourth Assessment Report of the Intergovernmental

Panel on Climate Change. B. Metz, O.R. Davidson, P.R. Bosch, R. Dave, and L.A. Meyer (eds.), Cambridge University Press, 851 pp.

IPCC 2014, Climate Change, Synthesis Report Summary For Policy Makers AR5 SYR Final SPM.

KATRINA PIELLI U.S. Environmental Protection Agency Office of Air and Radiation Climate Protection Partnerships Division <http://www.epa.gov/cleanenergy/documents/suca/cost-effectiveness.pdf> accessed 26/may 2015

GILLINGHAM ,K Richard G. Palmer, N K 2009. Energy Efficiency Economics and Policy National Bureau of Economic Research Working Paper 15031 http://www.n ber.org/papers/w15031 accessed May 2015

MAC NAUGHTON, J 2011. Delivering Sustainability through Effective Policy` in :World Energy Council: World Energy insights World Energy Council 32

MOOMAW, W., Yamba, F, Kamimoto M,. Maurice,, N, Urama L J K,. Weir T, 2011: Introduction. In IPCC Special Report on Renewable Energy Sources and Climate Change Mitigation [O. Edenhofer, R. Pichs-Madruga, Y. Sokona, K. Seyboth, P. Matschoss, S. Kadner, T. Zwickel, P. Eickemeier, G. Hansen, S. Schlömer, C.von Stechow (eds)], Cambridge University Press, Cambridge, United Kingdom and New York, NY,.

NATIONAL ACTION PLAN FOR ENERGY EFFICIENCY 2008. Understanding Cost-Effectiveness of Energy Efficiency Programs: Best Practices, Technical Methods, and Emerging Issues for Policy-Makers. Energy and Environmental Economics, Inc. and Regulatory Assistance Project. www.epa.gov/eeactionplan accessed May 2015

NEWELL R, Jaffe, Stavins, A R. 1999. The induced innovation hypothesis and energy-saving technological change. Q. J. Econ. 114:941–75

OECD/IEA 2008 Climate Change Mitigation: What Do We Do OECD Paris

OECD/ IEA 2010a. World Energy Outlook 2010. Energy Poverty: How to make modern

energy access universal., International Energy Agency, Paris, France.

OECD/IEA 2014 C Coal < ://www.iea.org/topics/coal/> accessed May 2014. Coal to reach 9 billion tonnes per year in 2019

WORLD ENERGY ASSESSMENT, 2000 Energy and the Challenge of Sustainability UNDP. UNESC

OECD/IEA (2015N). What is Nuclear. http://www.iea.org/aboutus/faqs/nuclear/ accessed May 2015

REN21 RENEWABLE ENERGY POLICY NETWORK FOR THE 21St CENTURY, RENEWABLE ENERGY: GLOBALSTATUS REPORT 2014 <mpactshttp://www.ren21.net/portals/0/documents/resources/gsr/2014/gsr2014_full%20report_low%20res.pdf> accessed May 2015

United Nations 2012, Decades of Sustainable Energy for all 2014-2024,> http://www.se4all.org/decade/>General Assembly Resolution 65/151 designated 2012 the “International Year of Sustainable Energy for All” accessed May 2015

RYAN L Campbel, N (2012) Spreading the Net:the Multiple Benefits of Energy efficiency in Improvements in energy efficiency Can Deliver a Range of Benefits to the Economy and Society OECD /IEA. Paris.

SIMS, R.E.H., Rogers H H and Gregory, K 2003a: Carbon Emission and Mitigation cost comparisons between fossil fuel, nuclear and renewable energy resources for electricity generation. Energy Policy, 31, pp. 1315-1326.

NATHALIE, T ,Peter, Taylor G 2011.The Energy efficiency Dimension of Energy Security in : The Routledge Hand Book of Energy Security B Sovacool (ed) Routledge , New York, 222-223.

SOVACOOL, Benjamin 2008. Valuing the Emissions From nuclear Power: a critical survey. Energy Policy, 26, pp. 2940-2953

SORRELL, S., J. Dimitropoulos J and Sommerville M 2009. Empirical estimates ofthe Direct rebound Effect: a Review. Energy Policy, 37, pp. 1356-1371

SOVACOOL ,Benjamin 2011. The Routledge Hand book of Energy Security Routledge New York pp3-6,

The Statute of the International Renewable Energy Agency on the 26 January 2009 IRENA/FC/dcc.1

QUASCHNING, V 2005. Understanding Renewable System Earth scan, pp.238

PASSIVHAUS 2010. What is a Passive House? Passivhaus Institute, Darmstadt, Germany. Available at: www.passiv.de/07_eng/index_e.html .

REN21 2010. Renewable 2010: Global Status Report. Renewable Energy Policy

Network for the 21st Century Secretariat, Paris, France, 80 pp

TWIDELL, J., and Weir, A D (2005). Renewable Energy Resources. 2nd Ed. Taylor & Francis, London, UK and New York, NY, USA

KALLBEKKEN, S. 2007 Why the CDM will reduce carbon leakage. Climate Policy, 7, pp. 197-211.

TAVERN, B. 2013. Petroleum Industry and Governments: A Study of the Involvement of Industry and Governments in Exploring for and Producing Petroleum (3rd ed.) Wolter Kluwer Netherland. 94-96

United Nations, 2010. Secretary-General Advisory Group on Energy and Climate New York <http://www.un.org/wcm/webdav/site/climatechange/shared/Documents/AGECC%20summary%20 report %5B1%5D.pdf> accessed 29 July 2014

342: Sustainable educational buildings: A proposal for changes to investment evaluation policies in Chile through the incorporation of thermal comfort and air quality criteria

JAIME SOTO-MUÑOZ[1], MAUREEN TREBILCOCK[2], ALEXIS PÉREZ-FARGALLO[3]

1 Universidad del Bío-Bío, Departamento de Ciencias de la Construcción, Collao 1202, Concepción, Chile, jsotom@ubiobio.cl
2 Universidad del Bío-Bío, Departamento de Teoría y Diseño de la Arquitectura, Collao 1202, Concepción, Chile, mtrebilc@ubiobio.cl
3 Universidad de Sevilla, Departamento de Construcciones Arquitectónicas II, Avda. Reina Mercedes, 4 A, 41012-Sevilla. España, alexisfargallo@us.es

The constructive configuration of an educational institution influences its indoor comfort variables; while at the same time comfort variables have an effect on the metabolism and stress of students and teachers. In turn, each architectural project depends on the factors that define its design. When the investment is assessed, costs are determined to compare alternative architectural strategies for the project. However, public policies in most countries in Latin America do not consider factors related to thermal comfort or air quality in their educational indicators since it has not been possible to gauge the effect of physical variables on school outcomes in the Southern Cone. This study addresses the current constructive reality of public schools located in different geographic areas of Chile. Data was obtained on temperature, humidity, CO2 concentration and other indicators of environmental conditions using sensors installed in 4th-grade classrooms in summer and winter. Fieldwork demonstrated that the quality of the indoor environment in schools is deficient and therefore it is necessary to establish strategies for economic evaluation when heating and cooling systems are not present. Taking into consideration this information, Chilean state policies and methods of investment evaluation were reviewed. Mandatory criteria were determined and a proposal for public policy improvements was developed that integrates indicators and monitoring of student productivity and energy efficiency variables based on the data collected. This has the potential to encourage energy savings and increase understanding of the value of an optimal indoor environment that includes thermal comfort and air quality as factors conducive to better learning. If these comfort parameters are adequate, they will positively influence the development of education in regards to student productivity and learning.

Keywords: educational buildings, sustainability, energy and environmental policies, educational indicators, indoor environmental comfort.

1. INTRODUCTION

Sustainability has been considered as a way forward since the United Nations Conference on Environment and Development held in Rio de Janeiro in 1992. As a result, the energy performance of buildings has become especially relevant in the international arena in order to reduce consumption and CO_2 emissions. Accordingly, sustainable schools take into consideration the integration of social, economic and environmental concepts; under this logic, educational buildings use resources during construction and operation in more efficient and less polluting manners than buildings that meet minimum construction requirements. They also use more natural light, and have better air quality and generally superior indoor comfort conditions; thus, these buildings contribute to better learning and student health, thereby improving the productivity of classroom activities (Wargocki & Wyon, 2013). However, in most Latin American countries, policies on the social evaluation of public investment projects for new building or renovation have not changed to include the value of sustainable construction. These social evaluation policies give evidence of different criteria using methodological manuals with specific procedures. According to Candia, Perrotti and Aldunate (2015), in 2010, the Network of National Public Investment Systems (SNIP Network) was created to improve the management of public investment in 15 countries and has subsequently made contributions to different national systems. In Chile, the social evaluation of projects is understood as the act of determining whether to execute a project from the perspective of society as a whole, considering the positive and negative effects the project has on other economic agents. Although the procedures for the evaluation of investment in building projects do not take into consideration sustainability issues, in recent decades there has been a public effort incorporate the value of energy efficiency and indoor environmental quality into the design, construction and life cycle of buildings. In this sense, the weaknesses in the evaluation of investment in design strategies and their incorporation into building designs require changes in the way benefits are valued by the population. For example, in the case of educational buildings, students and teachers require the inclusion of thermal comfort and air quality in classroom design and construction. Thermal comfort is defined as satisfaction with the thermal environment and is a subjective decision (ASHRAE, 2010). In this regard, in Chile, Supreme Decree 548 is the main document governing educational infrastructure; it establishes the different areas within an educational establishment and gives requirements for both the design and construction of these buildings. This decree establishes the minimum standards of comfort for educational institutions, but makes no mention of how these requirements should be tested or verified. In particular, CO_2 concentration levels in classrooms are not established, only the requirement of 3 m^3 of air per person, which is only partially complied with in the country. In 2012, terms of reference were developed by the Chilean Energy Efficiency Agency that modify the criteria to an airflow greater than 5 l/s/pp or 0.6 l/s/m^2. References such as the British Building Bulletin 101: Ventilation of School Buildings (BB 101) and the American ASHRAE standard 62.1-2013, Ventilation for Acceptable Indoor Air Quality are used, but informally. Previously, international studies have detected amounts of up to 5,000 ppm in classrooms, in comparison with the average outdoor CO_2 level worldwide of just 360 ppm (Mumovi, 2009). CO_2 concentrations above 1,000 ppm can produce negative effects on humans such as decreased attention span and reaction times (Bako-Biro, 2012).

However, temperature is the most influential variable in the sensation of comfort in an enclosed area according to studies by Lee (2012). Men and women are affected in distinct manners and cold and hot ambient temperatures produce different effects. Heat decreases overall performance in activities and produces the physiological response of perspiration, while cold causes a reduction in motor skills and in the speed of task completion. To calculate temperature, there are two complementary approaches: adaptive thermal limits and the Fanger method (de Dear & Brager, 2002). Thermal comfort has gained a position in the country as a result of the emergence of environmental conditioning techniques. In the case of educational buildings, said techniques translate into more comfortable classrooms. However, models are not used to evaluate the performance of thermal comfort or air quality in schools. From Yaglou (1923) through Fanger (1970), these physical variables have come to be recognized in buildings, and only now in the present are there methods for evaluating the variables that influence man-environment thermal exchanges. This assessment makes it possible to identify wellbeing and measure the costs/benefits of an investment project in educational building. Nevertheless, in Chile, the Ministry of Social Development's Division of Social Evaluation (MIDESO), when using the National Investment System (SNI) in order to make a decision on investment or the technical-economic convenience of executing a project, does not establish sustainability criteria in its public profitability procedures, such as saving energy by including energy efficiency in passive strategies in the envelope or having better air quality inside classrooms.

Internationally, advanced tools exist and are used to quantify the impact of the incorporation of energy efficiency in buildings. Almost without exception, these use two methodologies currently recognized to be universal, as a base to define their objectives, criteria, standards, databases, and assessment procedures,

among others. The first is referred to as Life Cycle Assessment (LCA), which mainly focuses on the study of environmental impact throughout the life of a product, from the cradle to the grave; the second, called Life Cycle Cost (LCC), is used more in the assessment of the total cost of an asset over time, including its acquisition, operation, maintenance and deconstruction costs. Their use is supported by scientific backing and standards from recognized international bodies such as the International Organization for Standardization (ISO) and the American Society for Testing and Materials (ASTM).

Countries are organized and their policies made based on observations of reality, and the observable evolution of quality of life and sustainability indicators. The existence of psychological, cultural and social factors in Latin American schools suggests that concepts of well-being in the classroom and not just corporate-economic principles should be taken into consideration. This is directly related to the obligations assumed by Latin American states in the Declaration of the Rights of the Child (1959) and updated in the 2002 special session of the United Nations "A World Fit for Children". In this regard, the social vulnerability factor in Chilean schools is taken into consideration with the School Vulnerability Index (IVE) indicator. This is part of the National System for the Equitable Allocation of Scholarships from the National Student Aid and Scholarship Board (JUNAEB), which was created in the 1960s to support educational efforts in the country. The IVE does not explain vulnerability, but rather each year generates information for educational support programs. For example, these include access to free meals in the most vulnerable schools throughout the academic year, which is a factor directly associated with the ability to use memory, and therefore collaborative learning. Then, the IVE can be used as a benchmark for the development of environmental and social policies regarding design criteria and the incorporation of architectural strategies in public education buildings, while studies have found that most classrooms do not meet the minimum standards of comfort (AChEE, 2012). The effect of air quality in classrooms and thermal comfort in the most vulnerable schools is the opportunity to take into account the difficult reality faced by students and therefore their teachers, when trying to learn content, procedures and attitudes for their future development.

2. OBJECTIVES

Chile has a total of 12,116 educational establishments that are divided into: 5,820 public institutions; 5,536 government-subsidized establishments; 681 private institutions; and 70 establishments managed by business associations or private corporations, with public financing (Espinoza, 2012). The aim of this study is to analyse the importance of the effect of indoor climate conditions in Chilean public schools when faced with other determinants such as student social level. This involves analysing the relationship that may exist between academic performance, social factors and the comfort of learning spaces, in order to determine the factors that have a greater impact on the productivity of students.

It aims to establish a logical foundation for the development of government policies related to the evaluation of public investments for the consideration of sustainable strategies that favour the improvement of learning in the classroom.

3. METHODOLOGY

Research primarily involved obtaining information in order to carry out an objective analysis of the aspects that most greatly influence the academic performance of students. To this end, 15 public schools in Chile were selected based on: geographical location according to the climatic zoning in Chilean Standard NCh1079; urban location; and an enrolment of more than 30 students per classroom. The selected schools were in the cities of Iquique in northern Chile, Puerto Montt in the south, and the Metropolitan Region of Santiago in the centre of the country. Also, these three urban centres are located in different climatic zones, 1NL, 3NVT and 4CL, and a high percentage of the country's population resides within the analysed zones.

A second factor taken into account in sample selection was the previously mentioned School Vulnerability Index (IVE). A high vulnerability value index implies a low socio-economic level and vice versa. The IVEs of the sample range from 37.6% to 93.10%, thus including all socio-economic levels in order to analyse the relationship with academic performance as a starting point in public schools (see Table 1).

Table 1: Classroom data used in the study

School	Municipality	Climatic zone	IVE	Attendance	SIMCE	Pass rate
IQ1	Iquique	1NL	71.30%	78.23%	222	80.49%
IQ2	Iquique	1NL	79.10%	86.52%	224	86.52%
IQ3	Iquique	1NL	80.60%	80.92%	237	84.00%
PM1	Puerto Montt	4CL	67.40%	91.75%	235	97.78%
PM2	Puerto Montt	4CL	71.80%	84.07%	243	93.75%
PM3	Puerto Montt	4CL	92.40%	84.62%	232	88.89%
PM4	Puerto Montt	4CL	93.10%	86.70%	249	86.44%
SC1	La Florida	3NVT	62.13%	84.40%	253	96.06%
SC2	La Granja	3NVT	75.83%	80.91%	232	84.08%
SC3	La Granja	3NVT	83.31%	81.20%	231	80.70%
SC4	Ñuñoa	3NVT	37.6%	87.22%	313	93.68%
SC5	Providencia	3NVT	41.56%	82.59%	264	91.01%
SC6	Providencia	3NVT	43.3%	87.25%	268	95.50%
SC7	Quinta Normal	3NVT	80.0%	84.33%	276	91.49%
SC8	Renca	3NVT	68.81%	90.51%	233	91.30%

Table 2: Data on thermal comfort and indoor air quality in classrooms

	Winter				Summer			
School	T °C	PPM CO_2	PMV	PPD	T °C	PPM CO_2	PMV	PPD
IQ1	21.19	1,461.57	-0.014	31.01%	24.38	892.48	0.42	37.42%
IQ2	17.37	657.94	-0.42	22.01%	22.19	920.68	0.55	34.50%
IQ3	19.11	1,384.11	0.25	43.57%	21.89	1,404.56	0.46	41.71%
SC1	17.99	2,023.91	0.14	27.29%	20.46	1,402.07	0.48	24.51%
SC2	17.92	1,592.73	0.22	27.76%	19.43	1,311.41	0.05	22.03%
SC3	14.42	1,834.74	-0.23	42.74%	18.85	1,311.66	0.25	22.17%
SC4	15.33	1,519.28	-0.062	25.59%	18.39	1,184.51	0.10	28.89%
SC5	12.53	1,539.29	-0.27	42.76%	25.34	652.20	1.15	60.42%
SC6	12.23	1,363.87	0.03	19.81%	24.34	693.11	0.57	38.43%
SC7	11.77	1,343.95	-0.31	29.29%	26.04	560.26	0.72	53.21%
SC8	13.95	1,874.14	-0.27	28%	25.047	524.59	0.128	31.2%
PM1	12.98	1,027.91	-0.022	19.57%	24.48	590.73	0.71	42.67%
PM2	13.65	1,326.47	-0.2	22%	26.03	648.75	0.34	27.23%
PM3	13.58	1,766.44	-0.02	43%	24.69	879.49	0.63	40.26%
PM4	11.23	1,858.20	-0.56	21.53%	22.83	1,191.56	0.15	21.43%

Fieldwork was conducted to characterize the buildings using monitoring equipment installed for 4-day periods. Measurements of air temperature, radiant temperature, relative humidity, wind speed and CO_2 concentrations in PPM were taken in winter and summer (see Table 2). Data collection made it possible to characterize each educational building and show its unique features, such as: envelope composition and equipment, and resources, among others.

Likewise, through daily perception surveys for students and teachers, information to estimate thermal comfort was collected using the Fanger method. Data was obtained on activities done before the survey, thereby providing information about metabolic rate. Both students and teachers were asked about the type of clothing they were wearing when responding to the survey. The above-mentioned information was used to obtain CLO and MET data. In turn, these data were used to obtain the PMV and PPD indices (see Table 2).

Finally, data on academic performance, student pass rate, performance on the System for the Measurement Educational Quality (SIMCE) test, and attendance were collected (see Table 1).

4. DATA ANALYSIS

4.1 Relationship between attendance, IVE and performance

Nationally, recent studies indicate that school dropout rates in primary education are negligible; in the study sample, dropout rates range from 1.11% to 11.40%. However, Espinoza (2012) indicates that for the 1992-2002 period the dropout rate is directly related to socio-economic level and ranges from 1.5% to 6.5%, the latter corresponding to the poorest fifth of Chilean society. Therefore, at first glance it could be said that this percentage is not randomly distributed, but rather it is the poorest groups that suffer to a greater extent due to this problem (Espíndola and Leon, 2002).

From an educational and policymaking standpoint, it seems appropriate to indicate that there should be a direct relationship between poverty, vulnerability, exclusion, school dropout, school attendance and academic performance. In the sample under study in this research, it was found that there was no direct relationship between the dropout rate and the vulnerability index of students; instead, there was a correlation between the percentage of attendance and dropout, with lower student dropout rates in educational establishments with higher attendance. Also, it could be expected that attendance rate and vulnerability index are linked. As can be seen in Figure 1, it is not possible to corroborate this claim, as no such trend exists in the data.

On the other hand, it can be said that in the classrooms analysed there is no evidence that dropout and school performance are directly related to the socio-economic status of the students. However, there is a relationship between the passing rate, the dropout percentage and attendance, with better results in both areas in those schools where attendance is higher (see Figures 1 and 2).

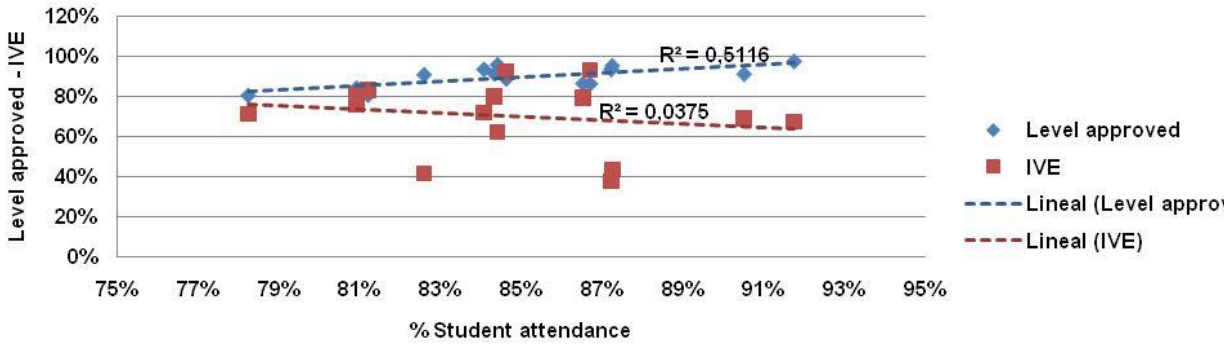

Figure 141: Relation between IVE, attendance and pass rate

Most studies on academic performance formulate hypotheses about socio-economic levels and pedagogical practices and mainly indicate that students at risk of social exclusion need special programs to increase academic performance. This suggests that low performance and grade repetition are related to living in poverty or social exclusion, thus indicating a higher chance of school failure (Román, 2003).

The SIMCE is the National Education Quality Measurement System that consists of a set of standardized tests to measure the level achieved in different content areas and is administered in grades four, eight and ten. Upon observing Figure 2, in which student SIMCE results in the classrooms studied are related with attendance, it can be seen that there is a general trend in which attendance relates to test value; as described previously, attendance is not linked to socio-economic level. Therefore, it can be affirmed that academic results are not directly related either.

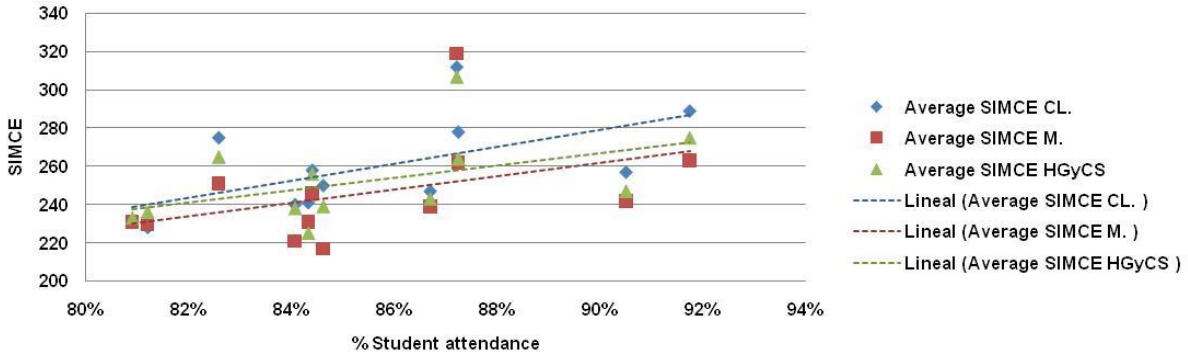

Figure 2: Relationship between attendance and SIMCE results

4.2 Relationship between attendance and comfort

The concept of thermal comfort has emerged fairly recently in the discussion on the design of public schools in Chile. It is understood to be the subjective manifestation of conformity or satisfaction with the existing thermal environment (Passive design manual, 2012), depending on the perception of four physical variables (air temperature, radiant wall temperature, relative humidity, air velocity) and two personal variables (clothing insulation (CLO) and metabolic rate) (Fanger, 1970; ASHRAE 55-2013; ISO 7730: 2005).

The assessment of thermal comfort was born out of the new climate control techniques; the heating the cooling of an enclosed area is intended to make people feel comfortable and for this reason methods were developed to measure user satisfaction. Currently, there are two theories to define thermal comfort; both have their limits and potentials. On the one hand, there is the theory of heat balance and on the other, adaptive theory. Adaptive theory is applicable to field work. As such, it was used in this research. Proposed by Povl Ole Fanger in 1973, this theory involves calculating two indices called the Predicted Mean Vote (PMV) and the Predicted Percentage of Dissatisfied individuals (PPD) based on the evaluation of one's dress, metabolic rate, air temperature, mean radiant temperature, air speed and relative humidity. Nevertheless, it cannot be ignored that the thermal comfort criterion is in turn linked to culture and weather conditions, lifestyle and even socio-economic level. From the previous, the theory of adaptive thermal comfort was born. Its mission is to analyse the real acceptability of thermal environments according to their context, in this case the nation's schools; the performance of the building during the school year; and student expectations. Adaptive theory argues that people create their own thermal preferences based on their interaction with the environment, and modify their behaviour or gradually adapt themselves (Brager & de Dear, 1998). Three categories of adaptation can be created: adjustment of behaviour, physiological (occurs in extreme situations and therefore not in buildings) and psychological (altered perception).

For an initial analysis of comfort, the PPD was associated with the PMV and with the percentage of class attendance. As can be seen in Figures 3 and 4, a relationship was not observed between student attendance and classroom comfort conditions due to the great dispersion of data in both summer and winter. Due to the above, the decision was made to perform an analysis to relate average classroom temperatures with student attendance.

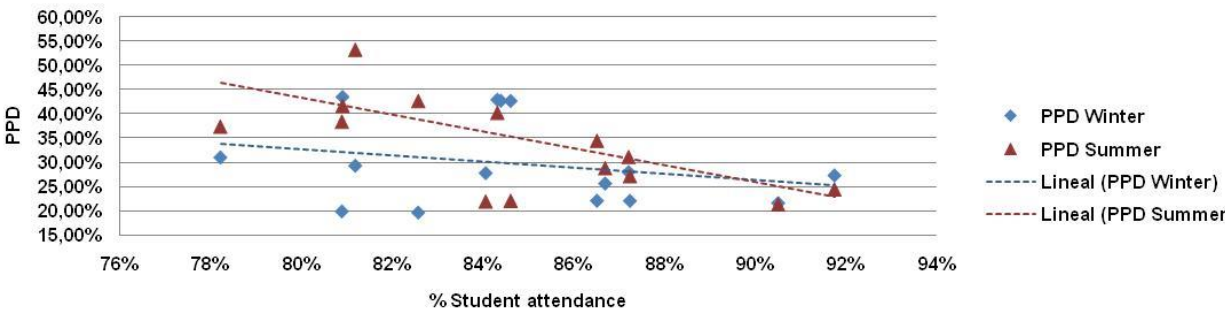

Figure 3: Relationship between attendance and PPD.

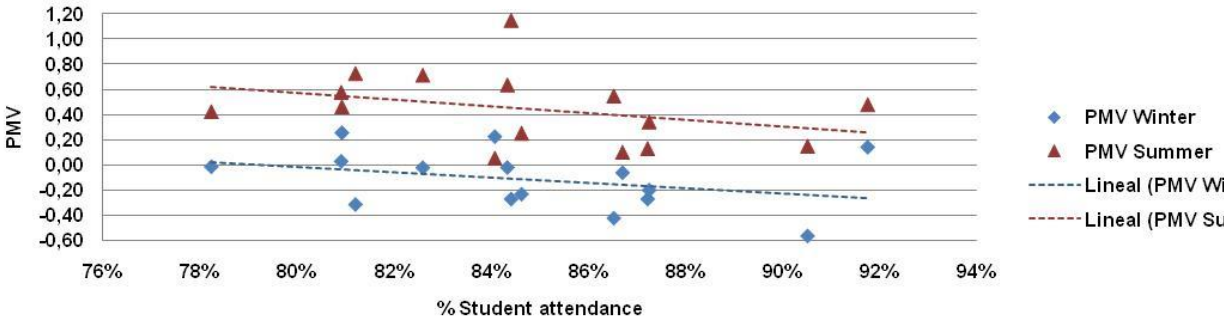

Figure 4: Relationship between attendance and PMV.

It has been demonstrated that there are limitations to the evaluation methods used to calculate thermal comfort. Some authors have obtained errors of close to 15% regarding the estimation of individual metabolic rate, which translates into a variation of approximately 0.3 in PMV (Havenith et al. 2002).

Of the values used for obtaining the PMV, that which shows greater relevance is metabolic rate since it determines the level of an individual's clothing insulation (Gauthier & Shipworth, 2012). These values are tabulated by ISO standard 8996:2004, based on adults averaging 30 years of age, weighing 60 to 70 kg and having body surface area of 1.6 to 1.8 m². As the present study is on primary school children, whose age is between 9 and 11 years, and whose weight and body surface values do not correspond to those tabulated to obtain metabolic levels, it is quite possible that there is an approximation error in the values obtained for the evaluation of thermal comfort. For this reason, it is possible that the PMV and PPD values from young individuals are not sufficiently accurate for analysis. More exact values of metabolic rate would have to be obtained to minimize error.

Schofield (1985) designed a series of equations to calculate the basal metabolic rate (BMR) of individuals based on data from a representative sample.

Equation 38: BMR calculation for boys between 3 and 10 years old.

$$BRM = 0{,}095w + 2{,}11$$

Equation 2: BMR calculation for boys between 10 and 18 years old.

$$BRM = 0{,}074w + 2{,}754$$

Equation 3: BMR calculation for girls between 3 and 10 years old.

$$BRM = 0{,}085w + 2{,}033$$

Equation 4: BMR calculation for girls between 10 and 18 years old.

$$BRM = 0{,}056w + 2{,}898$$

Where:

- w = weight of the individual (kg)

It was observed that even with Schofield's suggested corrections to the BMR calculation, there is no relationship between attendance and thermal comfort as seen in Figures 3 and 4; therefore, it was decided to directly carry out an analysis of student attendance and average classroom temperature.

In Figure 6, student attendance and average classroom temperature are correlated. Here, it can be observed that the dispersion of data is large and thus it is not possible to say that there is a link between classroom temperature conditions and attendance. However, if the values obtained from the schools located in the colder climates (Santiago, Puerto Montt) are analysed (see Figure 6), it can be seen that there is a tendency of greater attendance the higher the classroom temperature in winter. It should be mentioned that the temperatures in Iquique in winter correspond to summer weather in the other two populations, as this city has a warmer climate. Therefore, it was important to take this information into consideration in the study.

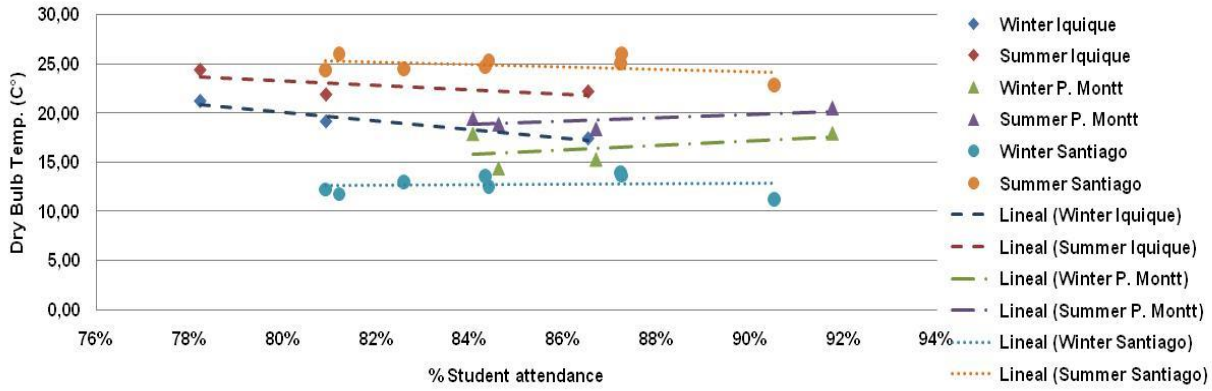

Figure 5: Relationship between attendance and classroom dry bulb temperature in winter by location

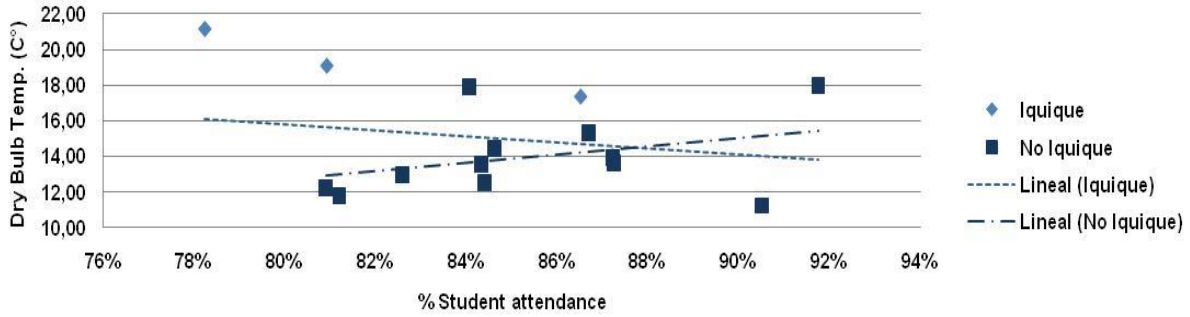

Figure 6: Relationship between attendance and classroom dry bulb temperature in winter

Regarding summer temperatures (see Figure 8), it was noted that even with some dispersion among the values, the lower the classroom temperature, the greater the student attendance; although, winter temperatures (see Figure 7) are the most grouped values. The relationship between temperature and winter attendance is related to the rise in temperatures from internal gains due to higher classroom occupancy; an increase in indoor temperature results from greater attendance, which translates into greater thermal comfort. This phenomenon is more difficult to observe in the summer temperatures since the opening of windows makes the relationship between temperature and attendance not so linear. This is largely due to the fact that its value will depend on the amount of ventilation surface area and whether there is cross ventilation. For this reason, the values are more dispersed. However, it is still possible to observe that at a lower classroom temperature there is a relatively higher percentage of attendance.

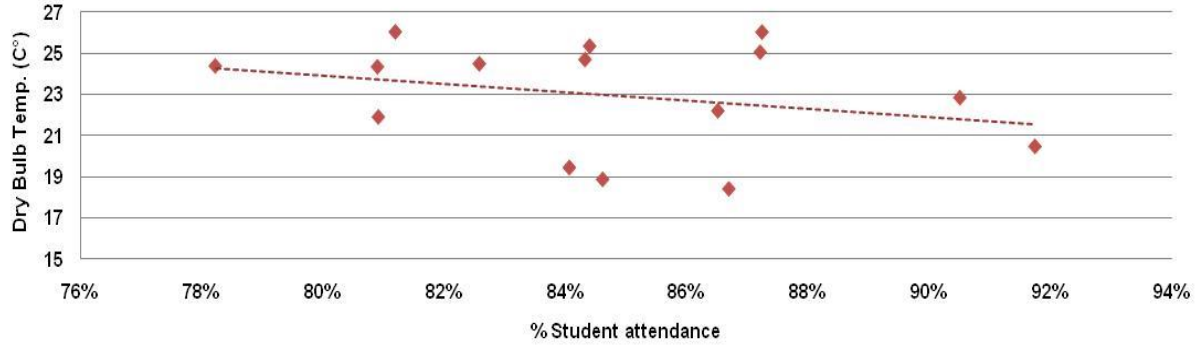

Figure 7: Relationship between attendance and classroom temperature in summer

Therefore, it became clear that the PMV and PPD values of the children were unrelated to attendance and as such are not valid indicators for analysis; whereas, average classroom temperatures apparently do correlate with attendance.

4.3 Relationship between attendance and air quality

Air quality is measured by the level of pollutants in a space that positively influence or negatively affect or even cause health problems for occupants (Passive Design Manual, 2012).

The assessment of air quality in classrooms was directly linked to the concentration of parts per million of CO_2 measured during classroom occupancy hours. Through the process of respiration, living beings convert oxygen into carbon dioxide. Nevertheless, there are also other environmental pollutants such as formaldehyde, organic vapours, dust or fibres. These are due to multiple factors, amongst which construction materials stand out and were not measured in the present research.

Various studies indicate that CO_2 concentrations in occupied spaces with little or no ventilation can reach more than 5,000 ppm, which is well above the permissible range for humans (1,000-1,500 ppm) (Bakó-Biro, 2012). High concentrations of carbon dioxide can significantly lower reaction speed and reasoning ability, thereby decreasing the academic performance of students under this circumstance by approximately 30% (Wargocky, 2013). It was observed that the phenomenon of high CO_2 concentration in classrooms is perceived by students as a consequence of raising the room temperature, although some teachers did perceive the situation and eventually took action to ventilate by briefly opening windows.

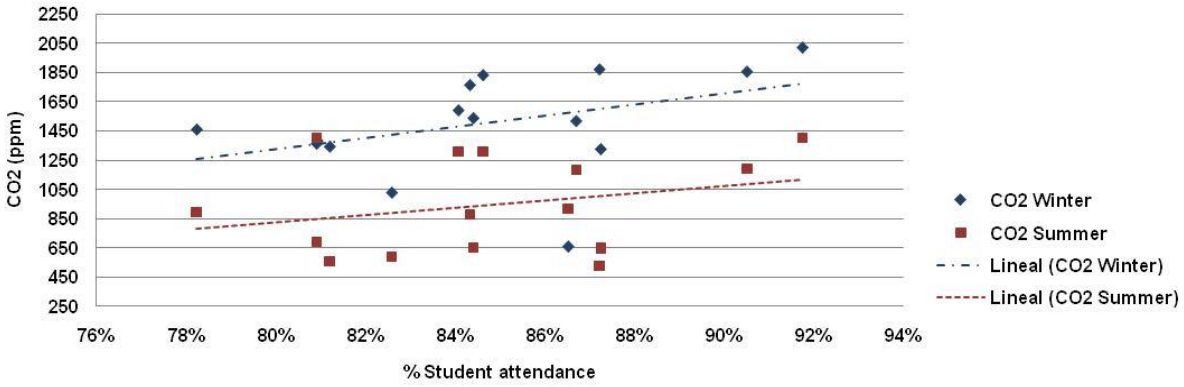

Figure 8: Relationship between attendance and CO_2 concentration (ppm).

With respect to CO_2 concentrations (see Figure 8), it was observed that even with some dispersion in the values, in winter the higher the attendance, the greater the concentration of carbon dioxide in classrooms. The relationship between CO_2 concentration and attendance in winter is related to greater room occupancy; hence, the increase in carbon dioxide emissions results in poorer air quality. In summer, this phenomenon is more difficult to observe because the opening of windows causes the relationship between carbon dioxide concentration and attendance to be not so linear. This value largely depends on the amount of surface area for ventilation and if there is any cross ventilation. Consequently, the values are more dispersed.

4.4 Public investments in state-managed schools

Accordingly, how should the factors discussed be considered in decision making for public investments? First, by defining social assessment strategies, such as for example the achievement of national learning and curriculum aims linked to the concept of educational space in the classroom. In this analysis, it was observed that there are differences between an area referred to as a "classroom" and an educational space. As reflected in the data collected, it is possible to distinguish that there exist classrooms that are actually enclosed spaces that do not take into consideration visual, auditory or other perceptive factors that favour a suitable environment for mental concentration. Ideally, the environmental factors of educational spaces decrease student stress and promote health by minimizing disturbances, such as for example, lower incidence of respiratory diseases with proper management of fresh air and temperature conditions that promote immunity to sickness.

With that said, it is logical to develop an academic productivity indicator based on elements such as the relationship between the degree of inclusion of sustainable strategies in the building, physical-environmental variables, student health and academic performance. This indicator must be able to measure physiological and behavioural changes in students resulting from an inadequate environment. Thus, when

making an initial investment or investing in renovations, the incorporation of passive strategies that favour an educational space will be valued (see Figure 9).

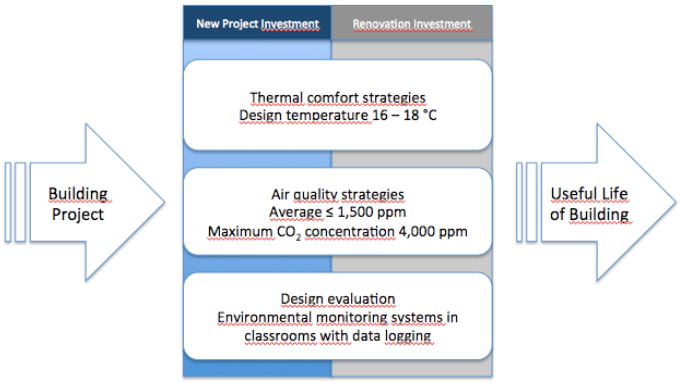

Figure 9: New considerations for policies on the evaluation of public investment in educational buildings

The proposal involves the modification of the Ministry of Social Development's project evaluation procedures and policies, by making information available that enables formulators and analysts of initiatives for investment in public buildings to consider costs and benefits in their design or analysis. This relates to the implementation of measures to promote a better quality of student learning in the classroom, including greater opportunities for development throughout their primary and secondary education.

5. CONCLUSIONS

In the search for a logical foundation for new government policies on investments in educational building in Chile that includes sustainable strategies for transforming a classroom into a better educational space, the previously described methodology was employed. From this research, evidence emerged demonstrating that in Chilean public schools thermal comfort and air quality conditions are not satisfactory for the welfare and academic performance of students.

Regarding the difficulties in obtaining valid data, primarily related to the PMV and PPD values, the young individuals are apparently inconsistent in their analysis of environmental conditions in the classroom thereby causing difficulties in applying the Fanger method. Also, unlike other authors mentioned in the study, no direct relationship was found between the dropout rate and the vulnerability index IVE, exclusion or the poverty rate; but rather, was more related to the percentage of attendance. Therefore, there is no evidence that dropout rates and school performance are directly related to the socio-economic status of students in the classrooms analysed; likewise, the connection between the pass rate and attendance also emerged from this research. This made it possible to determine that the percentage of attendance was the factor most closely related to thermal comfort and air quality conditions.

Concerning the analysis of PPD and PMV, it was found that even after making the corrections recommended by Schofield for the calculation of BMR, there was no relationship between the factors analysed; hence, it was decided to carry out a direct analysis between student attendance and average classroom temperature. It should be noted that adequate procedures still do not exist for assessing the thermal comfort values established by Fanger with children.

In the analysis of attendance and average classroom temperature, it was observed that the dispersion of data was very wide due to the inclusion of a region (Iquique) where the winter weather corresponded to the summer weather in the other populations (Santiago, Puerto Montt). However, from the data obtained from schools located in the colder climates it was found that there is indeed a trend of increasing classroom temperature in winter, the higher the attendance; this circumstance may be due to greater internal gains, but implies more comfort and even lower risk of sicknesses related to low temperatures. With regard to summer temperatures, it was observed that there was still some dispersion of the values, which is explained by the natural ventilation in classrooms. Nevertheless, it was possible to relate lower classroom temperature with higher student attendance. Accordingly, it can be concluded that it is necessary to obtain indoor

classroom temperatures in both winter and summer that promote lower student absenteeism and thus increase productivity in educational institutions.

The comfort conditions described above strongly affect indoor air quality because as it has been demonstrated, a higher level of attendance implies a greater concentration of carbon dioxide in classroom air; in winter a large number of classrooms exceed concentrations of 1,500 ppm when attendance surpasses 84%. Consequently, it follows that increasing the standard classroom temperature will increase occupancy and therefore mechanisms should be installed to help achieve indoor air quality for optimum student performance.

It can be concluded that classroom temperature should be between 18 and 21 degrees Celsius to increase attendance rates and consequently lower the dropout rate and increase student performance. In this way, a drop-out rate close to 1% and a pass rate of close to 98% could be achieved. It can also be stated that students from more vulnerable socio-economic groups acquire a better attitude toward classroom temperatures, in this way increasing their comfort range compared to students from less vulnerable socio-economic groups.

The absence of systematic evidence involving data on physical-environmental variables in classrooms makes it impossible analyse the problem of lack of comfort and poor air quality. Considering the absence of systems to monitor environmental conditions in classrooms and recognizing the variability of these factors according to the different climates in Chile, it is necessary to include temperature, humidity and CO_2 concentration sensors in the design of educational buildings.

Finally, a method of evaluation of public investment exists in the country. However, it does not take into consideration the learning opportunities generated for students by including strategies that produce educational spaces in Chilean schools. Therefore, there is an opportunity to develop policies in this respect and foster the development of a standard for better education in the future.

6. ACKNOWLEDGMENTS

The authors belong to the Sustainable Architecture and Construction Research Group (GACS) at the University of the Bío-Bío and would like to acknowledge that this paper is part of the FONDECYT research project 1130596 “Methodology for the dynamic analysis of thermal comfort during the design process of school buildings” funded by the Chilean National Commission for Research in Science and Technology.

7. REFERENCES

ASHRAE, 2013. Standard 55-2013 -- Thermal Environmental Conditions for Human Occupancy

ASHRAE, 2013. Standard 62.1-2013 - Ventilation for Acceptable Indoor Air Quality

BAKÓ-BIRÓ, Zs., Clements-Croome, D.J., Kochhar, N., Awbi, H.B., & Williams, M.J., 2012. Ventilation rates in schools and pupils’ performance, Building and Environment, 48, p. 215-223.

BRAGER, Gail, & De Dear, Richard, 1998. Thermal adaptation in the built environment: a literature review. Energy and buildings, 27(1), p.83–96

CANDIA, Jorge, Perrotti, Daniel E., Aldunate, E., 2015. Evaluación social de proyectos Un resumen de las principales metodologías oficiales utilizadas en América Latina y el Caribe. 1ed. Santiago de Chile: Cepal. 1

CITEC UBB, & Decon UC, 2012. Manual de Diseño Pasivo y Eficiencia Energética en Edificios Públicos, p. 112. Santiago de Chile

DE DEAR, R, & Brager, G. 2002. Thermal comfort in naturally ventilated buildings: revisions to ASHRAE Standard 55, Energy and Buildings. Volume 34, Issue 6, July 2002, p. 549–561

EDUCATION FUNDING AGENCY, 2014. Building Bulletin 101: ventilation for school buildings

ESPINOZA, O., Castillo, D., González, L.E. & Loyola, J., 2012. Factores familiares asociados a la deserción escolar en Chile: un estudio de caso. Revista de Ciencias Sociales.

ESPÍNDOLA, E. y León, A. (2002). La deserción escolar en América Latina: Un tema prioritario para la agenda regional. Revista Iberoamericana de Educación, 30, 39-62.

FANGER, P.O., 1970. Thermal comfort: analysis and applications in environments engineering, Danish Technical Press Copenhagen

INSTITUTO NAICONAL DE LA NORMALIZACIÓN, 2008. Nch 1079/Of 2008: Arquitectura y construcción - Zonificación climático habitacional para Chile y recomendaciones para el diseño arquitectónico

ISO, 2006. Standard 7730:2006- Ergonomía del ambiente térmico: Determinación analítica e interpretación del bienestar térmico mediante el cálculo de los índices PMV y PPD y los criterios de bienestar térmico local

MUMOVI, D. & Santamouris, M. eds, 2009. A Handbook of Sustainable Building Design and Engineering

ROMÁN, M. 2003. Resultados IV Encuesta Actores Sistema Educacional Chileno. Santiago de Chile: CIDE

WARGOCKI, P., & Wyon, D.P., 2013. Providing better thermal and air quality conditions in school classrooms would be cost-effective. Building and Environment, 59(0), 581–589

427: Supply side initiatives for overcoming electricity crisis in Pakistan

M. ASLAM UQAILI, NAYYAR HUSSAIN, ABDULLAH MENGAL, KHANJI HARIJAN

Mehran University of Engineering and Technology, Jamshoro; Sindh-Pakistan

Pakistan is a developing country having a population of approximately 199 million and coping severe electricity crisis for nearly a decade. The electricity shortage during year 2014 remained in excess of 6000 that was estimated to be between 1,000 and 2,000 MW in 2007. This situation has not only adversely affected its common population i.e. domestic consumers facing 12 hours electricity outages but also various industries which have been either shut down or have slowed down the production. These crises over the time have worsened instead of improving supply and distribution of electricity. As such, now it is need of the hour to undertake output based projects which should deliver as soon as possible. Alternatively these crises may worsen in coming years with increase in demand. Dealing with this challenge the present government announced the new power policy in 2013. The goal of this power policy is to develop electricity generation capacity that can meet nation's energy demand appropriately. To achieve this goal on long term basis government has undertaken various power generation projects throughout the country with focus on low-cost indigenous resources. This paper provides a review and analysis of the power policies of Pakistan and various power projects currently undertaken or to be undertaken as per governments' plans to overcome the electricity crisis.

Keywords: *Electricity Crisis, Power Policy, Power Project*

1. INTRODUCTION

Energy is key to growth for any country thus nations which has managed their energy resources appropriately has attained development across various sectors of the economy. Electricity as a form of energy is now nearly termed as a commodity which is essential for the masses. Pakistan is blessed with various indigenous primary energy resources, however, inappropriate planning, policy guideline and even implementation of these have plunged country as energy deficient. As a result, today demand and supply gap of electricity stands between 5-7GW (Abdullah Mengal, 2014)

Energy Planning attained much importance after the Oil embargo of 1970's. The focus of energy planning then mainly looked efficient supplies only. However, later various other parameters have been added to the planning paradigm most important of these are least cost and environment friendliness. This planning paradigm is now replaced with more focussed and accepted approach i.e. addressing sustainability and targeting the sustainable development.

The various mathematical and statistical model were initially developed to ensure supply of energy, however, with advancement in technology and more due to modern computers available since 1980's various computer based models has had been developed which duly consider sustainability concerns and address the sustainable development.

Pakistan had somehow focused on energy and power sector much belatedly and country which secured independence in 1947 had announced its first ever formal energy policy in 1994 (PPIB, 2015). There have been even concerns from various quarters on this policy which have been addressed later in subsequent policies. This paper provides a review and analysis of the power policies of Pakistan and various power projects currently undertaken or to be undertaken as per governments' plans to overcome the electricity crisis.

2. PAKISTAN'S POWER SECTOR

Like other developing countries Pakistan's power sector mainly owned by government and comprises of vertically integrated utilities i.e. generation companies (WAPDA and GENCOS) , transmission company (NTDC) and distribution companies (DISCOS) except in the City of Karachi where privatized K-Electric is entrusted to manage generation, transmission and distribution. Pakistan has abundant primary energy resources; however, issues relating harnessing these resources have halted the desired growth.

Pakistan depends greatly on two fossil fuels for meeting its commercial energy demand i.e. oil and gas. As such, electricity in Pakistan is mostly generated from the fossil fuels like imported oil, indigenous natural gas and minimum amount from local coal. Massive potential of hydro, other renewable and coal is available in the country but these have not been significantly exploited. The total installed capacity which was 19420 MW in 2008 increased only (14.86%) to 22812 MW in 2013 as shown in Figure 1. The major increase (85%) was in thermal capacity with soaring tariff of IPPs (Kessides, 2013; NEPRA, 2013; Yearbook, 2011)

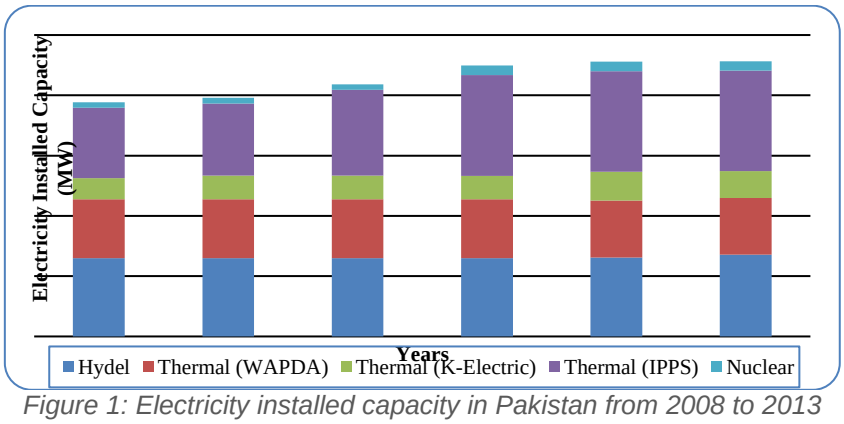

Figure 1: Electricity installed capacity in Pakistan from 2008 to 2013

Consequently, the gap between supply and demand has widened continuously as Figure 2. The economic development of county is, as such, adversely affected by this widened gap between the supply and demand of electricity.

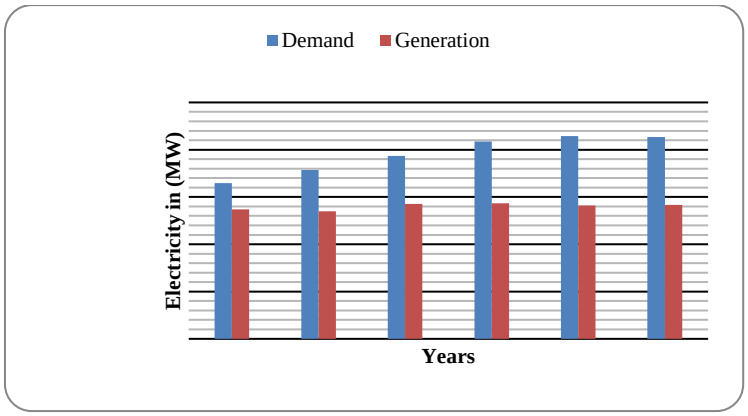

Figure 2: Electricity demand and generation in Pakistan

Further, the country's generation of electricity is dominated by thermal power plants which are about 36% running on expensive imported oil. This has also contributed the present power crisis since dwindling economy of the country cannot provide adequate fuel to these power plants (NEPRA, 2013; Yearbook, 2012).

During the financial year 2012-13 the total electricity generation in the country remained 96,122 GWh of which the thermal electricity generation (oil, gas & coal) was 61,711GWh (64.2%), hydel power plants produced 29,857 GWh (31%) and nuclear power plants contributed 4,553 GWh (5%) as shown in Figure 6 (Yearbook, 2012).

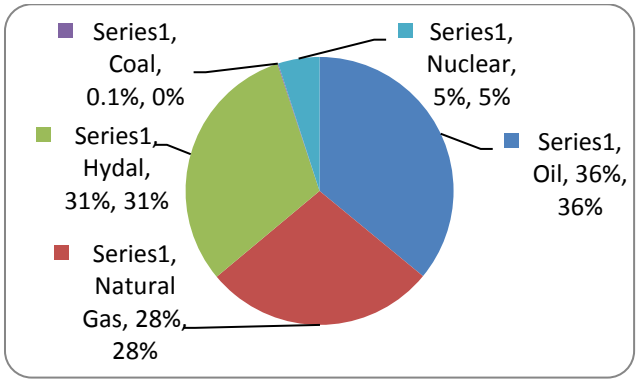

Figure 3: Share of electricity generation from different

However, one of very important concern is that total electricity generation is about 50% of the actual installed capacity owing to inappropriate fuel mix, low maintenance of power plants leading to overall lower output efficiency (Yearbook, 2012).

If current trend to generate electricity from imported fossil fuels continue then it would be a regular burden on Pakistan's financial resources which may also result in constant raise in the prices of energy resulting country's exports becoming less competitive, the prices of goods and consumables for utilisation in local industry would become higher too. Consequently some of industries could be forced to shut down and causing an overall economic stress may go on a wide scale. As such, it has become very essential now that consistent energy policies may be introduced as well as implemented which should result in meeting the electricity demand and address efficiency and affordability altogether.

3. ENERGY AND POWER POLICIES OF PAKISTAN

Since the surfacing of energy crisis more than a decade ago all governments of the country has had been putting serious efforts towards rational policy formulation. Most of energy/power policies of country mainly focus readily available primary energy sources or on least cost solutions to overcome the crisis and generally private sector has been attracted for investments. Ministry of Water and Power of Pakistan with support from Energy Wing of Planning Commission are mainly responsible for policy formulation. Various studies are usually undertaken before policy formulation and Council for Common Interests (CCI) headed

by Prime Minister generally approves these polices for implementation. However, so far none of the various energy/power polices has delivered to the expectation owing to various reasons of which implementation remains at the top of the list. Following are the various energy/power polices so far announced by the Government of Pakistan with key features of the each policy briefly highlighted.

- **1994 : First Formal Energy Policy** (PPIB, 2015)
  - The first ever energy conservation program initiated
  - Electricity generation of 13000 MW aimed through IPPS.
  - Guaranteed payment of fixed "capacity price" to IPPs regardless of generation of electricity.
  - Immunity from various taxes and surcharges such as : income tax, customs duties and sales tax, for importing equipment by IPPs'
  - Bulk tariff of US cents 6.5/kwh for WAPDA to purchase electricity from IPPS
  - Fuel supply and power purchase agreements introduced.
  - Foreign exchange risk insurance
  - Simplified one window procedures for IPPs

- **1995: Hydropower Power Policy** (PPIB, 2015)
  - Encourage proposals for power generation based on indigenous hydel resources.
  - All the fiscal incentives of 1994 policy extended to this policy
  - A bulk tariff of US cents 6.1/kwh to be charged to WAPDA
  - The ownership of the hydro power project will be transferred to GOP after 25 year, free of cost.
  - Protection against specific force majeure risk is provided
  - Protection against changes in certain taxes and duties also provided
  - Guaranteed foreign exchange conversion facility.

- **1998: Policy for New Private Independent Power Project** (PPIB, 2015)
  - Amended/Revised 1994 Policy with more rationalization.
  - Tariffs based on open bids, denominated in Rupees.
  - Bidders to quote in two parts: (1) Energy Purchase Price and (2) Capacity Purchase Price
  - Provided protection against specific force majeure risk.
  - Provided protection against changes in certain taxes and duties.
  - IPPS allowed to raise finance in local and foreign currency
  - Guaranteed foreign exchange conversion facility.

- **2002: Policy for Power Generation** (PPIB, 2015)
  - This Policy promoted private, public-private and public sector projects.
  - Two distinct options for investors introduced. One is the Unsolicited Proposal option and the other is Bidding Process.
  - The participating bidder were proposed to be selected on the basis of minimum levied tariff through competitive bidding for the solicited proposal or based on negotiation for raw sites.
  - Competitive tariffs comprised an Energy Purchase Price (EPP) and a Capacity Purchase Price (CPP) with sufficient provision for escalation
  - Fuel supply and power purchase agreements ensured.
  - Encouraged local industry to form joint ventures to develop power projects to attain a capacity of 20000 MW by 2015

- In **2005**, under Pakistan's Vision for 2030 the Energy Security Action Plan (2005-2030) was announced to to ensure secure energy supplies. The key features of this plan pertaining energy are as under: (GOP, PC, 2007)
  - It emphasized increasing electricity generation capacity, from 19,540 MW of electricity to 162,590 MW by the year 2030.
  - Energy mix comprising nuclear, hydro and other renewable energy resources was proposed to generate 143,050 MW as additional capacity under a phased program.

- **2006 : Policy for Development of Renewable Energy for Power Generation** (PPIB, 2015)
  - Encouraged Small Hydro, Wind, and Solar and Bio Fuel Technologies.
  - Exemptions from custom duties/sale tax were allowed for machinery for the projects utilizing renewable energy resources.
  - Exemption from income tax.

- Equity and dividends partition freely allowed.
- IPPS allowed raising local and foreign finance.
- Zakat exemption was allowed for non-muslins and non residents from company dividends.

- **2010-2012 : National Energy Policy** (PPIB, 2015)
  - Following a three-day national energy conference in Islamabad during the month of April 2010, then Prime Minister announced on 22 April 2010 “energy policy”.
  - This Policy focused Energy Conservation, Short Term and Long Term Plan for generation of Electricity which included RPPs and Rehabilitation of existing public sector power plants and investment by IPPS to cater energy needs of the country.

- **2013- Present: National Power Policy** (PPIB, 2015)

  The Newly Elected Government following May 11, 2013 Elections announced ambitious National Power Policy with varied Goals to achieve, such as:
  - Develop electricity generation capacity to meet country’s energy needs sustainably.
  - Energy conservation culture promoted
  - Emphasized affordable electricity generation from indigenous primary energy resources. .
  - Upfront tariff and competitive bidding to lower the cost of the electricity.
  - Reduction of subsidies
  - Switching to cheaper fuels
  - Minimize pilferage and adulteration in fuel supply as well as loss/theft of electricity

It may be noted that focus of each of these energy policies varies (e.g., 1994 Energy policy focuses on “attracting IPPs”, 1995 Energy Policy targets hydel power, 1998 Energy policy introduced competitive open bidding process, 2006 RE policy provides incentives for renewable generation, and 2013 National Power Policy initiates shifts to cheaper fuels (i.e., indigenous coal and hydro projects), the common thrust is to attract IPPs investments in the electricity sector of Pakistan.

All these policies were developed with serious efforts behind them; however, in all cases absence of thorough implementation mechanism and causes of failure of any policy had hardly been addressed. It is, therefore, very important that current energy policy should be implemented with great spirit taking into consideration the past experiences, focusing the depletion of indigenous fossil fuel resources, addressing the environmental concerns and affordability appropriately.

4. OVERCOMING POWER CRISIS IN PAKISTAN

Government of Pakistan is determined to overcome the existing power crisis through development of various power projects based on coal, hydel and renewable sources into energy mix of the country. As result of these efforts, it is expected that about 16 to 20 GW of power generation capacity will be added to national grid during next four to five years which will reduce the load shading duration (Yousuf et al., 2014)The brief these future power projects undertaken or to be undertaken in light of current national power policy are discussed as under:

4.1 Hydel Power

The hydroelectric power has a huge potential in the country which can produce low cost electricity. Government have provided medium and long-term plans of hydropower capacity expansion under the current power policy. Six projects totalling 384 MW are expected to be completed during year 2015 as power policy 2013. The Gulpur and Patrind hydal projects of smaller capacities are anticipated to be completed by the end of year 2017 which will add 247 MW to the grid. Further, around 969 MWs are expected from Neelum-Jhelum project by November 2016. A number of hydel projects are anticipated to come on line in 2017 including the fourth and fifth Tarbela expansions which have potential of generating electricity to the tune of 1910 MW. The detail engineering design for projects at Patan 2,800 MW, Dasu of 2,160 MW, and Thakot 2,800 MW (Table 1) has been undertaken or expected to be undertaken under current power policy. Some other long-term projects are as Bunji 7,100 MW, Kohala 1,100 MW and Diamer-Bahasha 4,500 MW. Completion of these projects may secure country from energy crises (WAPDA, 2011, 2013; Yousuf et al., 2014). Brief detail of these projects is listed in Table 1 below.

Table 37: Proposed hydro power plant

Name of Power Plant	Capacity (MW)	Executing Agency	Expected Date of completion
Hydro NeelumJehlum	969	WAPDA	2016
Tarbela 4th ,5th extension	1910	WAPDA	2017
Patrind Hydro power	147	IPP	2017
Akhori dam project	600	WAPDA	2018
Sehra Hydropower Project	130	IPP	2019
Dasu Hydropower Project	4320	WAPDA	2019
DiamerBasha Dam	4500	WAPDA	2020
SukiKinari Hydropower	870	IPP	2020
KarotHydropowerProject	720	IPP	2020
Bunji hydropower	7100	WAPDA	2022
Azad Pattan Hydropower	640	IPP	2022
Lower Palas Hydropower	665	IPP	2022
Lower Spat GahHydropower	496	1PP	2022
Kohala Hydropower Project	1100	IPP	2023
Mahl Hydropower Project	590	IPP	2023
Thakot hydropower	2800	WAPDA	2024
Patan hydropower	2800	WAPDA	2025
Munda dam project	740	WAPDA	-
Mohmand dam hydropower	800	WAPDA	-
Shyok dam project	690	WAPDA	-
Chakoti-Hattan Hydro Project	500	IPP	-

4.2 Coal Power

Pakistan is blessed with 6th largest reserves of the coal in the world. These deposits are found in all four provinces of the country; as well as in Azad Jammu and Kashmir. The total reserve is estimated to 186,000 million tons (Mt) out of which major reserves 185,000 million tons (Mt) are in the province of Sindh. Realizing the benefit of coal based power generation the government has decided to install coal power plants at different locations of the country through public and private investment basis. Initially 10 power unit on coal each of 660 MW, with a total of 6600 MW will be established at Gaddani Energy Park in the Balochistan province. Further, in future coal power plants are proposed to be installed in various districts of the Punjab on local/indigenous coal. Sindh Engro Coal Mining Company (SECMC) in joint venture with Sindh Government and Engro power Company is also developing a coalmine block in Thar. SECMC is expected to complete construction of a 660 MW power plant in the first phase by 2017 while in the second phase another 660 MW power plant would be commissioned by 2019. In Block III of Thar coalmines, 5000 MW power plant is expected to be installed by various companies whereas 7,500 MW power plants by Sino Sindh Resources (Pvt) Limited (SSRL) China will be established in Block I of coalmines at different Phases. Three power plants each of 1320 MW are proposed to be in installed at Jamshoro, Lakhra and port Qasim by PEPCO and K-Electric (Coutinho et al., 2014; TCEB; Yousuf et al., 2014). Table 2 summarises Coal based power plant under current power plans of government.

Table 2: Proposed coal power plants

Name of Power Plant	Capacity (MW)	Executing Agency	Expected Date of Completion
Imported Coal			
Coal power plants at Punjab	2x660	PEPCO	2018
Coal power plants at Punjab	5280	IPP	Different Phases
Coal power plants at Jamshoro	2x660	PEPCO	2018
Coal power plants at Gaddani	2x660	PEPCO	2018
Coal power plants at Gaddani	8x660	IPP	Different Phases
Coal power at Port Qasim	2x660	IPP	3-4 Years
Conversion of Jamshoro Power Plant from Oil to Coal	850	PEPCO	Different Phases
Conversion of MuzafarGarh Power Plant from Oil to Coal	1350	PEPCO	Different Phases
Conversion of Guddu Power Plant from Oil to Coal	640	PEPCO	Different Phases
Conversion of K-Electric Power Plant from Oil to Coal	1260	K-Electric	2018
Conversion of HUBCO Power Plant from Oil to Coal	1292	IPP	Different Phases
Local coal			
Sino Sindh Resources (Pvt.) Limited (SSRL)(China	7500	IPP	Different Phases
Thar Power Company Ltd. (THARCO) SECMC	5000	IPP	Different Phases

Oracle Coalfields UK	1400	IPP	Different Phases
GENCOS	1320	PEPCO	3-5 Years
Sindh/ETON Japan Power	3960	IPP	Different Phases

4.3 Nuclear power

Pakistan Atomic Energy Commission (PAEC) is responsible for planning, construction and operation of nuclear power plants in the country. PAEC is presently operating three nuclear power plants i.e. Karachi Nuclear Power Plant (KANUPP), Chashama Nuclear Power Plant Unit-1 (C-1) and Unit-2 (C-2). The construction of two more plants at Chasma, C-3 and C-4 of 340 MW each are in progress and are expected to be commissioned by the end of 2016. The ground breaking ceremony of two Karachi Coastal Nuclear Power Plants (K-2) and (K-3) of 1,100 MW each was held in November, 2013 and they are expected to be completed in 2020. About 2200 MW nuclear power project is proposed at costal belt of Baluchistan near Hub as well (PAEC). Summary of Nuclear power plants under current power policy is given in Table 3.

Table 3: Proposed Nuclear power plants

Name of Power Plant	Capacity (MW)	Executing Agency	Expected Date of Completion
Chashma Nuclear Power Plant Units-3 (C-3) and Unit-4 (C-4)	680	PAEC	2016 – 2017
Karachi Nuclear Power Plants (K-2) and (K-3)	2200	PAEC	2020
Chashma Nuclear Power Plant Unit-5	1000	PAEC	Proposed
Coastal Nuclear Power Hub Balochistan	2200	PAEC	Proposed

4.4 Renewable Power

Pakistan has immense potential of renewable energy (RE) resources and if explored effectively they can play a significant role in the contributing towards energy security and energy independence. In 2003 Alternative Energy Development Board (AEDB) was established to work as a central agency for development, promotion and facilitation of renewable energy technologies and by making appropriate policies and plans. The Government of Pakistan has given a task to AEDB to ensure 15% of total power from renewable energy up to 2030 (AEDB, 2014; Javaid et al., 2011; News). Solar, wind and biomass are the main RE resources in the country and each this potential is discussed as under:

Solar Energy

Pakistan can take the advantage of solar energy technologies appropriately being in the sunny region. The mean global radiation is recorded as 200-250 watt per m2 per day. This potential is feasible for both PV and solar thermal applications. Realizing this potential Government has taken steps to harness power from solar. A 1000 MW of solar PV plant has been undertaken at “Quaid-e-Azam Solar power Park” in district Bahawalpur Punjab province on 9th May, 2014. Another 500 MW solar based power plant is also on the cards to be set up by Canadian Company at “Quaid-e-Azam Solar power Park” which will be completed in two years [20].

Wind power

Costal belt of Pakistan is blessed with a God gifted wind corridor that is 60 km wide (Gharo-Keti Bander) and 180 Km long (up to Hyderabad). In addition to that there are other wind sites available in coastal area of Balochistan and some Northern areas. The wind potential of Pakistan estimated by National Renewable Energy Laboratory USA in collaboration with USAID is 346 GW but in spite of this potential wind power is not utilized in Pakistan. Only two power plants “Fuji Fertilizer Energy Company limited (FFCEL)” and Zurlu Wind Energy” with cumulative /installed capacity of 106 MW are connected to National grid. Other wind power plants i.e. 50 MW Foundation Wind energy I, 50 MW Foundation Wind energy II, 50 MW Sapphire Power, 50 MW Metro and 50 MW China Three Gorges are at final stages. In addition to these Letter of Intents have also been issued for450 MW of wind energy projects. An additional 2,276 MW of wind power projects are currently in the feasibility process. (Bhutto et al., 2013; WAPDA, 2013) The brief of renewable energy project already undertaken or to be undertaken as per governments plans are given in Table 4.

Table 4: Proposed Renewable (other than hydro) power plants

Name of power plant	Capacity (MW)	Executing Agency	Expected Date of completion
Solar PV power park Punjab	1000	AEDB	Different Phases
Canadian solar Company	500	AEDB	2016
Zurlu Wind Energy Sindh	56	AEDB	2014
Fuji Fertilizer Energy Sindh	50	AEDB	2014
Capacity of wind power Commissioned	2726	AEDB	2016
Bagasse based power plant	83	AEDB	-

Biomass power

Pakistan is basically an agricultural country, its livestock and agricultural sector produces massive amount of biomass resources in the form of crops residues, animal wastes such bagasse, dung, rice husk etc. Pakistan is world's fifth largest producer of sugarcane with an average production of about 50 million tons of sugarcane annually. This of amount sugarcane crushing in 80 sugar mills of country which produce 10 million tons of bagasse can be an immense source of energy. Pakistan has potential to produce 3,000 MW electricity from bagasse and 5,000 MW from livestock. The national power policy 2013 stipulated to produce 83 MW of electricity from bagasse. Letter of Intents (LOIs) have been issued to different bagasse based power plants by Alternative Energy Development Board (AEDB) such Biomass to energy power plant at Jhang, Faisalabad Punjab, at Mirpurkhas, Sindh and at Mardan Khyber Phakhtunkhua (Farooqui, 2014; Perwez and Sohail, 2014; Zuberi et al., 2013).

5. CONCLUSION

It is evident from above analysis and discussion that although Pakistan is currently facing energy crisis but has enormous potential of indigenous energy resources to overcome these crisis with consistent policies and implementation announced polices more importantly. Current governments ambitious National Power Policy of 2013 is being currently well pushed and implementation same resulting in completion of the various power projects discussed in this paper are expected to bring relief for nation no later than in 3-5 years. Reduction in line losses both at transmission and distribution level should also be on government's priority. Further, it would be worthwhile that government together with these supply side initiatives may also appropriately focus on demand side management with specific focus on energy conservation to archive the desired balance between supply and demand of energy.

6. ACKNOWLEDGEMENTS

The Authors would like to acknowledge the Mehran University of Engineering and Technology, Jamshoro, Pakistan, Higher Education Commission (HEC), Government of Pakistan and PSSP-USAID for supporting this study.

7. REFERENCES

Abdullah MENGAL, K. H., Mohammad A. Uqaili, and Nayyar Hussain, 2014, Electricity Demand and Emissions under Different Policy Scenarios for Pakistan. International Conference on Energy, Environment and Sustainable Development, Mehran University of Engineering and Technology, Jamshoro, Pakistan

AEDB, 2014. Alternative Energy Development Board, Pakistan.

BHUTTO, A.W., Bazmi, A.A., Zahedi, G., 2013. Greener energy: Issues and challenges for Pakistan—wind power prospective. Renewable and Sustainable Energy Reviews 20, 519-538.

COUTINHO, M., Butt, H.K., Rauf, S., 2014. Environmental Impact Assessment Guidance for Coal Fired Power Plants in Pakistan. by: IUCN Pakistan (National Impact Assessment Programme).

FAROOQUI, S.Z., 2014. Prospects of renewables penetration in the energy mix of Pakistan. Renewable and Sustainable Energy Reviews 29, 693-700.

GoP, PC (2007): Pakistan in the 21st Century, Vision 2030, Planning Commission, Government of Pakistan. Islamabad

JAVAID, M.A., Hussain, S., Maqsood, A., Arshad, Z., Arshad, A., Idrees, M., 2011. Electrical energy crisis in Pakistan and their possible solutions. International Journal of Basic & Applied Sciences 11, 38-52.

KESSIDES, I.N., 2013. Chaos in power: Pakistan's electricity crisis. Energy policy 55, 271-285.

NEPRA, 2013. National Electric Power Regulatory Authority. National Electric Power Regulatory Authority

News, D., PM launches solar power plant in Bahawalpur, Dawn.

PPIB. 2015. Power Policies of Pakistan [Online]. Private Power Infrastructure Board (PPIB). Available: http://www.ppib.gov.pk/N_cpp.htm [Accessed June 05 2015].

PAEC, Pakistan Atomic Energy Commission Government of Pakistan.

TCEB, Thar Coal Energy Board. Government of Sindh Pakistan.

WAPDA, 2011. Hydro Potential Pakistan. Water and Power Development Authority.

WAPDA, 2013. National Power Policy 2013. Ministry of Water and Power, Government of Pakistan.

Yearbook, P.E., 2012. Hydrocarbon Development Institute of Pakistan. Ministry of Petroleum and Natural Resources, Government of Pakistan,

YOUSUF, I., Ghumman, A., Hashmi, H., Kamal, M., 2014. Carbon emissions from power sector in Pakistan and opportunities to mitigate those. Renewable and Sustainable Energy Reviews 34, 71-77.

ZUBERI, M.J.S., Hasany, S.Z., Tariq, M.A., Fahrioglu, M., 2013. Assessment of biomass energy resources potential in Pakistan for power generation, Power Engineering, Energy and Electrical Drives (POWERENG), 2013 Fourth International Conference on. IEEE, pp. 1301-1306.

POSTER SESSION A

144: CFD simulation of wind environment around a high-rise building at pedestrian level in Hong Kong

DEQI WANG[1*], LIN LU[1], PING CUI[2,3], YU JIANG[1]

1 Renewable Energy Research Group, The Hong Kong Polytechnic University, Hong Kong, China
2 Shandong Key Laboratory of Building Energy-saving Technique, Jinan, China
3 Key Laboratory of Renewable Energy Utilization Technologies in Buildings, Ministry of Education, Shandong Jianzhu University, Jinan, China

Recently, increasing number of high-rise buildings are built in Hong Kong, especially in the urban area. Wind environment of existing buildings is affected significantly by the high-rise buildings. Flow distribution of high-rise buildings closely interacts with existing building, which may influence pollutant distributions at the height of activity of human being. In this paper, the finite volume method was used to investigate the effect of a new high rise building on wind environment of existing buildings, and the pulsating flow was simulated by RNG k-ε model. A suitable computational grid was generated by special methods. A comparison experiment was conducted between the isolated buildings with high-rise building and without high-rise building. A ventilation threat area has been found with its wind speed reaching above 12m/s and an updraft area has also been detected in the case of high-rise building, which may lead to a contamination threat to the downstream buildings.

Keywords: CFD, Wind environment, Urban area, High-rise building

1. INTRODUCTION

A great progress of computer and computational fluid dynamics (CFD) software has been achieved in the recent years, which enables the wind environment can be modelled and predicted in the design stage. Compared with traditional wind tunnel studies, CFD is a more cost-saving and multifunctional technology in modeling the wind environment around buildings. As a reliable simulation model can provide detailed information in whole flow field, CFD is applied to study different wind environment problems, such as air pollution (Moonen, Dorer et al., 2011), natural ventilation (Wakes, Maegli et al., 2010), wind-driven heat transfer (Karava, Jubayer et al., 2011), wind erosion and wind comfort (Blocken, Janssen et al., 2012).

The issue concerning wind comfort and safety is considered as an essential requirement for urban areas, in particular for the level of pedestrian (Stathopoulos, 2006, Metje, Sterling et al., 2008). According to the report (Lawson and Penwarden, 1975), when individuals exposure to high wind conditions, a dangerous situation, even life-threatening, may occur. To study the local wind comfort and safety, meteorological data with aerodynamic information and wind safety criteria should be an important and necessary part. The aerodynamic information can transform the statistical meteorological data from weather conditions to the building site, and then, it can be used to estimate the local wind environment with a comfort/safety standard. In this study, the simulation models are judged by a classical standard for wind comfort (NEN 8100) and a practice guideline (NPR 6097) which declared that the user could choose wind tunnel modelling or CFD to determine the design-related contribution.

In this paper, 3D steady simulation models, which contain 1) a high-density community with a high-rise building and 2) a high-density community with no high-rise building, have been established to study the influence of the high-rise building on the wind environment in Hong Kong. Special attention has been paid around the high-rise building with a high mesh resolution. Different wind conditions have been taken into consideration based on the meteorological data from the Hong Kong Observatory. A detailed comparison and discussion of these simulation models will be presented at the last section of this paper.

2. GENERAL ASPECTS OF THE HIGH-DENSITY COMMUNITY

Hong Kong is one of the high-density city all over the world. Seven and a half million inhabitants live in a limited area of 1000 km^2. In this study, the Whampoa Garden, shown in **Error! Reference source not found.** is selected as the research object. It is the largest private housing estate located in Kowloon (Hong Kong). It was built on the site of the former Whampoa Dockyards by Hutchison Whampoa Property and completed in 1991. As shown in **Error! Reference source not found.**, there are 30 buildings and two main roads (marked with yellow line) in this high-density area, including 24 residential buildings, 4 primary schools (marked with blue point in Figure 1), 3 commercial buildings 1 supermarket and 1 high-rise hotel building. The design of the residential buildings is quite same, and the total height of each building is 47.35 m. The narrowest building space between the residential buildings is 3 meters.

Figure 142 Aero view of Whampoa Garden in Kowloon

This community is in the west of the high-rise building. Two primary schools are located in the central of our research area, the Alliance primary school and the Whampoa Garden primary school. The new high-rise building is located near the sea site with a total height of 233 meters (763 foot) and mainly use for the residential purpose.

2.1 Statistical meteorological data

Whether data is collected from a nearby meteorological station, Star Ferry of the Hong Kong Observatory, which is reasonable to represent the wind direction and wind velocity of the building site. It provides hourly mean wind speed and wind direction at 10m of the Star Ferry station. The wind rose covering a period from 1981 to 2010 (**Error! Reference source not found.**) shows that it the wind direction fluctuate around 90 degree, but the east wind is prevailing wind direction and the wind velocity are commonly from 3.3 m/s to 8.2m/s.

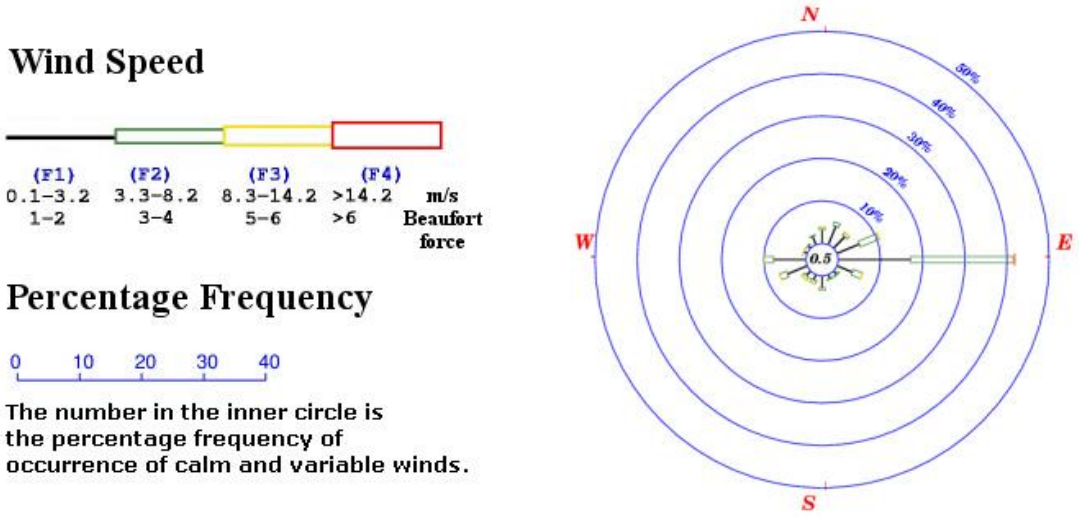

Figure 143 Wind rose from the meteorological station

2.2 Comfort criterion

The wind can influence the individual activities in different ways, such as cooling the body, flipping the cloth, flying the dust. Pedestrians will feel discomfort when the wind speed become strong, and then individuals will begin to annoy and try to avoid the wind. Different wind comfort criterions have been reported and used in the past decades. However, the majority of these criterions are based on the threshold wind speed and the probability of it (Durgin, 1992, Williams, Soligo et al., 1992). An overview of published discomfort thresholds has been given in Table , created by Bottema (2000). Different threshold criterions can be used to different locations or different human activities.

Table 38: Overview of published discomfort thresholds (Bottema, 2000)

Threshold	Used/applicable for	Threshold	Used/applicable for
$U + \sigma_u > 6$ m/s	Applied to all human activities	$U + 3(\sigma_u^2 + \sigma_v^2)^{0.5} > 6$ m/s	For activities very sensitive to wind
U(Beaufort) > 6B=7.6 m/s	Walking fast	$U + 3(\sigma_u^2 + \sigma_v^2)^{0.5} > 9$ m/s	For most activities to be unaffected
U(Beaufort) > 5B=5.6 m/s	Strolling, skating	U_3 (daily max.) > 10 m/s	Applied to all human activities
U(Beaufort) > 4B=3.9 m/s	Standing/sitting; short	U_3 (daily max.) > 15 m/s	Applied to all human activities
U(Beaufort) > 3B=2.4 m/s	Standing/sitting; long	$u(t) > 4.2$ m/s	Sitting
U(Beaufort) > 6B=7.6 m/s	Roads, car parks	$u(t) > 6.1$ m/s	Standing
U(Beaufort) > 5B=5.6 m/s	Walking	$u(t) > 8.3$ m/s	Walking
U(Beaufort) > 4B=3.9 m/s	Standing, entrances	$U + 4\sigma_u > 5$ m/s	Preliminary, all activities
U(Beaufort) > 3B=2.4 m/s	Covered areas	$U > 5$ m/s	Remedial action of shop owners
$U > 5$ m/s	Applied to all human activities		

3. NUMERICAL APPLICATION

3.1 Geometry and grid modelling

Two geometry model were established in this study. One is the high-density community without high-rise building, the original model (OM). Another one contains the high-rise building, called the tall building model (TM). The narrowest openings space is 1.5 m, so accurately geometrical models are required in this study. To reduce the effect of the boundaries, a large enough space has been created around each building community. The OM without the high-rise building has a dimension of $L \times W \times H = 1500 \times 700 \times 300\ m^3$. The length of this area is 3.5 times of the key observation area, and the width is two times of the key observation area. The highest building in this model is 82 m. The total height of the calculation area is 300m. Due to complex construction, several structure simplifications are adopted in the modelling process for saving the computer resource and improving computation efficiency. Based on the OM, the new high-rise building is established and become the TM. The length and width of this calculation are same as the original model with a dimension of 1500m (L) and 600m (W), respectively. Because the highest building is 233m in the TM, the total height of the calculation domain is set as 500m.

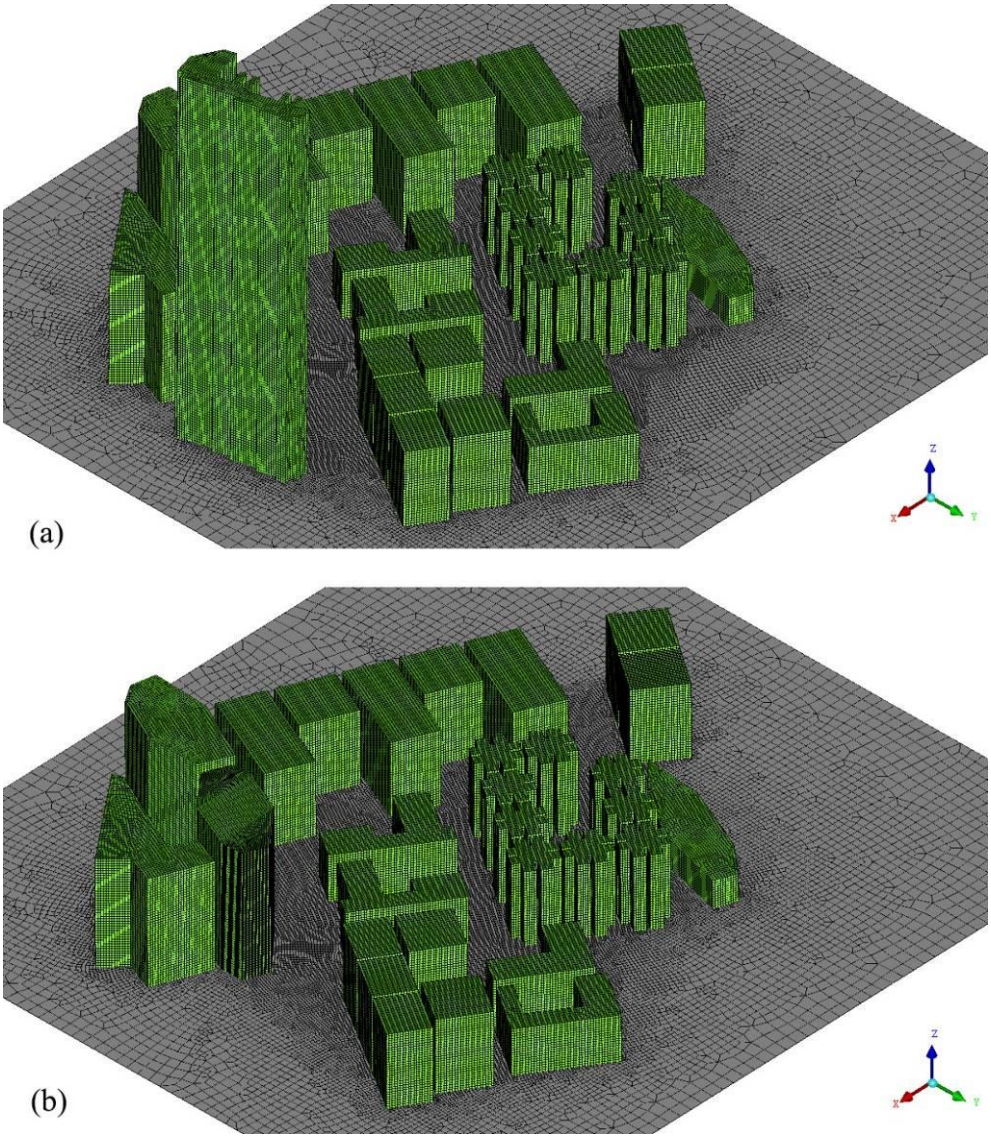

Figure 144 Corresponding high-resolution computational grid, (a) original model and (b) tall building model

Due to the complex geometry of the high-rise building and a large difference between the smallest dimension (1.5m) and the largest dimension (1500m) of the modeling domain, a good quality mesh strategy is required in each model. Generally, for buildings model meshing, there are two opposite sides that should be balanced. For one thing, to simulate the air flow more accurately and to get more details about the street

flow status, the grid size should be as small as possible. For another, to consider the efficiency and speed of the simulation and the requirement to the computer hardware, larger grid size is needed. So, to balance these two things, a suitable grid size or grid number should be considered to make the grid both robust and accurate. Special mesh technique, presented by van Hooff and Blocken (2010), has been applied to develop a high-quality mesh, which contain only hexahedral or prismatic cell and do not have the tetrahedral one. By using this technique, a high resolution can be easily obtained with the second-order discretization schemes. Images of the mesh of two models are shown in **Error! Reference source not found.**. It can be seen clearly that the building surface has a more dense mesh with the maximum setting of 0.5m. There are 6,334,195 elements in the OM and 9,584,055 elements in the TM. The meshing process is accomplished in ANSYS ICEM v14.0.

3.2 Governing equations

In this study, the airflow bowling around the buildings is governed by Eulerian conservation equations and the Renormalization Group (RNG) *k-ε* turbulence model is used to simulating its turbulence behaviour. For an incompressible turbulent flow, the continuity and Reynolds mean momentum equations are as follows:

Equation 39: $$\frac{\partial \overline{u_i}}{\partial x_i} = 0$$

Equation 2: $$\frac{\partial \overline{u_i}}{\partial t} + \overline{u_j}\frac{\partial \overline{u_i}}{\partial x_j} = -\frac{1}{\rho}\frac{\partial \overline{p}}{\partial x_i} + \frac{1}{\rho}\frac{\partial}{\partial x_j}\left(\mu\frac{\partial \overline{u_i}}{\partial x_j} - \rho\overline{u_i' u_j'}\right)$$

Where:

- $\mu_t = \rho C_\mu k^2/\varepsilon$ = the eddy viscosity
- $k = \overline{u_i' u_j'}/2$ = the turbulent kinetic energy
- ε = the turbulent dissipation rate
- $\overline{s_{ij}}$ = the mean tensor of the strain rate

Using the RNG $k-\varepsilon$ turbulence model to close the equation 1 and 2. The equations of turbulent kinetic energy *k* and turbulent dissipation rate ε are:

Equation 3: $$\frac{\partial k}{\partial t} + \overline{u_k}\frac{\partial k}{\partial x_k} = \frac{\partial}{\partial x_k}\left(\frac{\alpha_k \mu_t}{\rho}\frac{\partial k}{\partial x_k}\right) + 2\frac{\mu_t}{\rho}\overline{s_{ij} s_{ij}} - \varepsilon$$

Equation 4: $$\frac{\partial \varepsilon}{\partial t} + \overline{u_k}\frac{\partial \varepsilon}{\partial x_k} = \frac{\partial}{\partial x_k}\left(\frac{\alpha_\varepsilon \mu_t}{\rho}\frac{\partial \varepsilon}{\partial x_k}\right) + C_{1\varepsilon}\frac{\varepsilon}{k}\left(2\frac{\mu_t}{\rho}\overline{s_{ij} s_{ij}}\right) - C_{2\varepsilon}\frac{\varepsilon^2}{k} - R_\varepsilon$$

Where $C_{1\varepsilon}$=1.42, $C_{2\varepsilon}$=1.68, C_μ=0.085, $\alpha_k = \alpha_\varepsilon \approx 1.393$.

3.3 Boundary conditions

A finite volume method is applied in the solver of ANSYS CFX. An atmospheric boundary layer inflow was given at the inlet of the calculation domain, which include the mean wind profile and turbulence dissipation rate. The inlet velocity profile is set to be a uniform distribution of 3.0/3.5/4.0/4.5m/s at the turbulence intensity of 5% and length scale of 0.1m. The inlet velocity magnitude is the average wind speed at 10m above ground level the latest 22-year wind data gotten from the Hong Kong Observatory. At the outlet and the lateral sides, an opening boundary condition are used. At the top side, free boundary conditions are applied. Ground and building surfaces are viewed as wall in the simulation. Standard wall function is applied to deal with the near-wall treatment. The air properties is set by default in the CFX, i.e. density is 1.225 *kg/m* and viscosity is 1.7894×10 *kg /ms* at normal air pressure.

4. RESULTS AND DISCUSSION

The wind velocity distribution at 2m high is significant because it indicates the available ventilation of pedestrians among the assessed areas. When the inlet mean velocity is 4.5m/s, the cut planes of velocity vectors at Y=2m for case OM and case TM are shown in (a) and (b), respectively.

It can be seen clearly that the high-rise building has a significant strengthening effect to the wind in the main roads, especially to the area around the high-rise building. Compared with the safety standard in Table , for the case of OM, the wind distribution was uniform among the residential buildings and only a high wind speed area occurs at the cross section of two main roads. But for the case of TM, a dangerous wind area can be found on the sides of the high-rise building. As shown in (b), the wind speed at the south of the high-rise building reach above 12.0m/s, which may not only lead to a discomfort feeling for the pedestrians, but also a health threatening for the old people. For safety concerning, some wind-weaken strategy should be applied to slow down the wind speed to a reasonable level, such as wind-resistant plants. By comparing the wind profile between (a) and (b), the air ventilation of the residential buildings in the south is weakened by the high-rise building and a ventilation stagnation area can be found at the south-east.

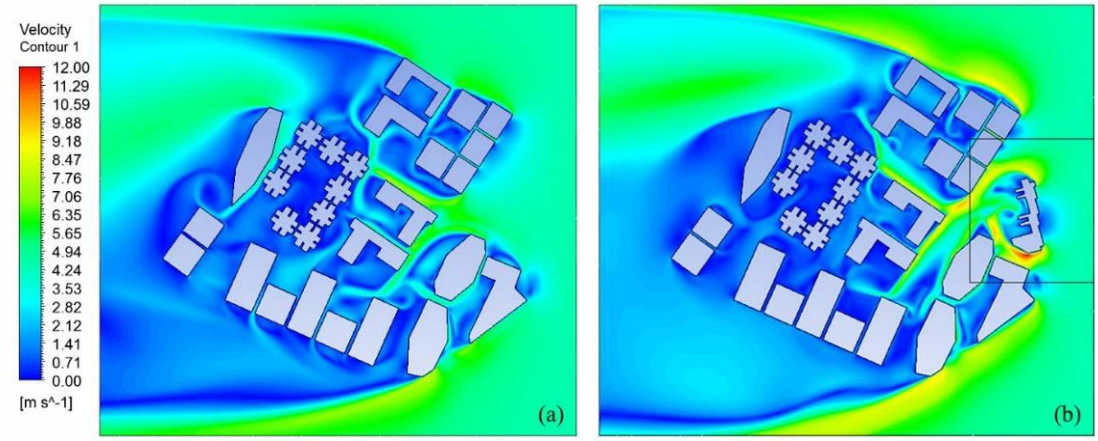

Figure 145 Wind distribution at the pedestrian level of (a) OM and (b) TM with inlet mean velocity of 4.5m/s

To more clearly understand the effect of the high-rise building on the air ventilation of the community. The cut planes crossing the high-rise building is shown in **Error! Reference source not found.**. The highest buildings form a wall and the velocity in the leeward area is obviously lower than that in the windward area. For the case of TM, it can be noticed that the wind blows from the edge, flows inward at the back of the high-rise building and collide with each other forming an updraft. The updraft can easily carry the pollutants into the air ventilation and has damage to the downstream buildings. This updraft cannot be observed in the case of OM, which means more attention should be paid on the pollution control for the case of TM. In this study, it seems that the four primary schools will suffer directly for the air pollution, if there is no specific pollution control.

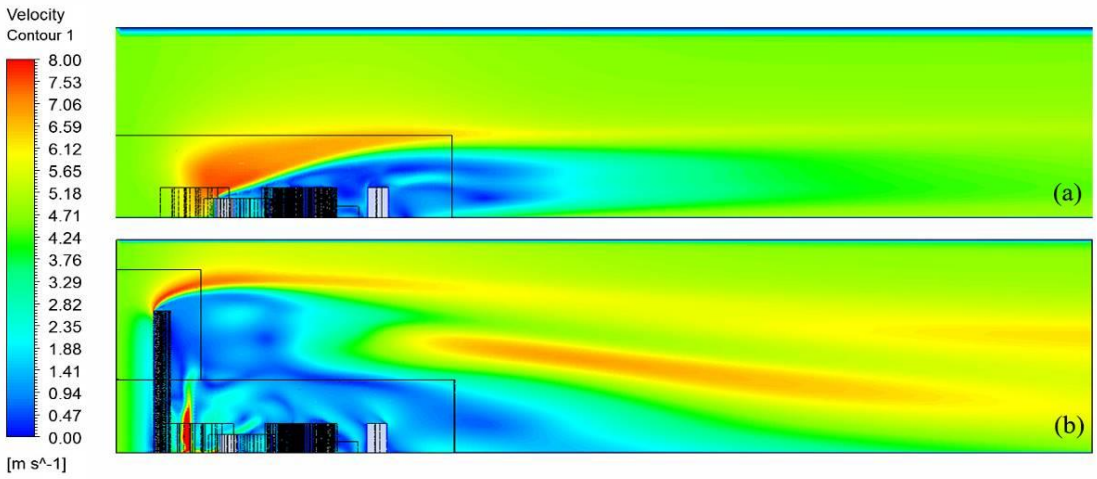

Figure 146 Wind distribution crossing the high-rise building of OM (a) and TM (b)

5. CONCLUSION

Estimation of the steady-state velocity field in the high-density community for the effect of high-rise building using the code ANSYS CFX and a subsequent comparison with available numerical results was carried out. The Renormalization Group (RNG k--ε) equations together with the finite volume approach was used to simulate the air ventilation in this study. Some conclusions can be drawn by analysing the results:

a) The higher buildings in front of short buildings weakened the ventilation in the streets.

b) In the case of high-rise building, a high danger area with the wind speed reaching above 12.0m/s occurs at the cross section of two main roads, which could be a threat to the pedestrian

c) An updraft area has been found in the case of high-rise building, which may lead to a contamination threat to the downstream buildings.

6. ACKNOWLEDGEMENTS

The numerical simulations reported in this paper were supported by the Hong Kong Polytechnic University, a grant from CII-HK Limited, Hong Kong, China (5-ZJF2).

7. REFERENCES

BLOCKEN, B., Janssen, W. and van Hooff, T., 2012. CFD simulation for pedestrian wind comfort and wind safety in urban areas: General decision framework and case study for the Eindhoven University campus. Environmental Modelling & Software, 30: 15-34.

BOTTEMA, M., 2000. A method for optimisation of wind discomfort criteria. Building and Environment, 35 (1): 1-18.

DURGIN, F.H., 1992. Pedestrian level wind studies at the Wright Brothers facility. Journal of Wind Engineering and Industrial Aerodynamics, 44 (1): 2253-2264.

KARAVA, P., Jubayer, C.M. and Savory, E., 2011. Numerical modelling of forced convective heat transfer from the inclined windward roof of an isolated low-rise building with application to photovoltaic/thermal systems. Applied Thermal Engineering, 31 (11): 1950-1963.

LAWSON, T. and Penwarden, A., 1975. The effects of wind on people in the vicinity of buildings. Proceedings 4th International Conference on Wind Effects on Buildings and Structures, Cambridge University Press, Heathrow.

METJE, N., Sterling, M. and Baker, C., 2008. Pedestrian comfort using clothing values and body temperatures. Journal of Wind Engineering and Industrial Aerodynamics, 96 (4): 412-435.

MOONEN, P., Dorer, V. and Carmeliet, J., 2011. Evaluation of the ventilation potential of courtyards and urban street canyons using RANS and LES. Journal of Wind Engineering and Industrial Aerodynamics, 99 (4): 414-423.

STATHOPOULOS, T., 2006. Pedestrian level winds and outdoor human comfort. Journal of wind engineering and industrial aerodynamics, 94 (11): 769-780.

VAN HOOFf, T. and Blocken, B., 2010. Coupled urban wind flow and indoor natural ventilation modelling on a high-resolution grid: a case study for the Amsterdam ArenA stadium. Environmental Modelling & Software, 25 (1): 51-65.

WAKES, S.J., Maegli, T., Dickinson, K.J. and Hilton, M.J., 2010. Numerical modelling of wind flow over a complex topography. Environmental Modelling & Software, 25 (2): 237-247.

WILLIAMS, C.J., Soligo, M.J. and Côté, J., 1992. A discussion of the components for a comprehensive pedestrian level comfort criterion. Journal of Wind Engineering and Industrial Aerodynamics, 44 (1): 2389-2390.

422: Pakistan's energy system: integrated energy modeling and formulation of national energy policies

NAYYAR HUSSAIN[1], M. ASLAM UQAILI[1], KHANJI HARIJAN[1], GORDHAN VALASAI[2]

1Mehran University of Engineering and Technology, Jamshoro; Sindh, Pakistan
2Quaid e Awam University of Engineering, Science and Technology, Nawabshah, Pakistan

Pakistan is facing multiple challenges for harnessing the various indigenous energy resources and devise the energy policy for meeting the ever increasing demand of energy by various sectors of the economy. The country which is believed to have substantial indigenous primary energy resources i.e. Fossil fuels and renewables is facing energy supply gap of over 5,000 megawatts, ending up frequent outages and load shedding. Energy planning in Pakistan was given little consideration before 1980's mainly owing to limited industrial growth and small urban population. However, in the following years there has had been substantial urbanization and industrial growth in the country emphasized to devise the rational energy polices. From 1994 to 2013 various energy polices have been formulated and implemented. The focus of formulation of these policies have varied from policy to policy with major polices devised without undertaking integrated energy modelling exercise, although there has been some efforts at government level as well as by the academicians. Popular energy modelling tools such as MARKAL/TIMES; LEAP, ENPEP and MESSAGE have been developed and successfully used by nations to devise the energy policies. This paper provides brief on Pakistan's Energy System, review of energy modelling tools and their possible application in Pakistan for the formulation of energy policies.

Keywords: Energy Modelling, Energy Planning, Energy Policies

1. INTRODUCTION

Energy is essential for development of an economy and closely associated sustainable development –a significant subject discussed and debated now at various levels.. Energy planning attained much of the formal attention followed by the oil crisis of 1970s. The planning approaches then only emphasized on identifying the efficient supply options. This followed development of much recognized planning approaches wherein it is a process to explore the minimum cost solution that meets the present and future power and energy demands. Other criteria, such as environmental concerns and the reliability of supply, are given monetary values, and included on the cost criteria, thus considered only as constraints(Hussain et al., 2013). Much of these energy planning approaches are now being well worked away using various computer based energy modelling tools. MARKet Allocation (MARKAL), ENergy and Power Evaluation Program (ENPEP), and Long Range Energy Alternatives Planning System (LEAP) are well recognized energy modelling tools used for energy planning at various levels. These models help to organize large amount of data, reflect complete system in understandable form and provide a consistent framework for testing hypothesis. These energy tools are extremely useful for various energy planning applications which are diverse in terms of the regions they analyse, the technologies they consider, and objective they fulfil (Heaps, 2002, Connolly et al., 2010).

Energy planning using energy modelling tools are contributing significantly in devising the energy policies for various nations and used around the world for this very purpose. The next sections of this paper provides brief on Pakistan's Energy system, review of energy modelling tools and their application in Pakistan for the formulation of energy policies.

2. PAKISTAN'S ENERGY SYSTEM

Energy has played a vital role in Pakistan's advancement and growth. Energy is also an essential ingredient of socio-economic development and economic growth. Without sufficient energy into usable forms and at affordable prices, there is a little prospect of development or improving the economy of a country and the living conditions of the people. Pakistan has abundant primary energy resources, however, with growth in population during past two decades, there has had been planning and implementation issues for disposal and utilization these valuable energy resources. As a result of this about half and one-fourth of the Pakistan's population has no access to electricity and natural gas respectively, and per capita consumption of energy is one of the lowest in the world. About 65% of the country's population live in rural areas and most of them have no access to commercial energy and use biomass and kerosene for cooking, heating and lighting (Harijan, 2008).

At present, the people are facing severe load shedding/blackout problems due to a shortage of 5-7 GW power supply. The natural gas demand grows beyond the transmission/supply capacity and the large users mainly industries, power plants, cement industries and transport sector (CNG stations) are curtailed especially during winter to ensure supplies to domestic, commercial and small industries or fertilizer. The energy crisis in the country has forced thousands of industries to shut down operations, affecting industrial production and the livelihoods of thousands of families. It has been a major drag on the economy and a serious impediment to growth with an estimated cost of 10% of the GDP over the past 5 years. Pakistan's energy crisis, if not tackled at both operating and strategic levels in the immediate future, might become a national security threat (Uqaili et al., 2007, Sahir, 2007).

Pakistan relies mainly on oil and gas for meeting its energy demand. The national energy system of Pakistan for various energy sources for the year 2012-13 is shown in Figure 1, whereas primary energy supplies, consumption, energy mixes for power generation for the year 2012-13 and electricity supply and demand curve are shown in Figure 1.

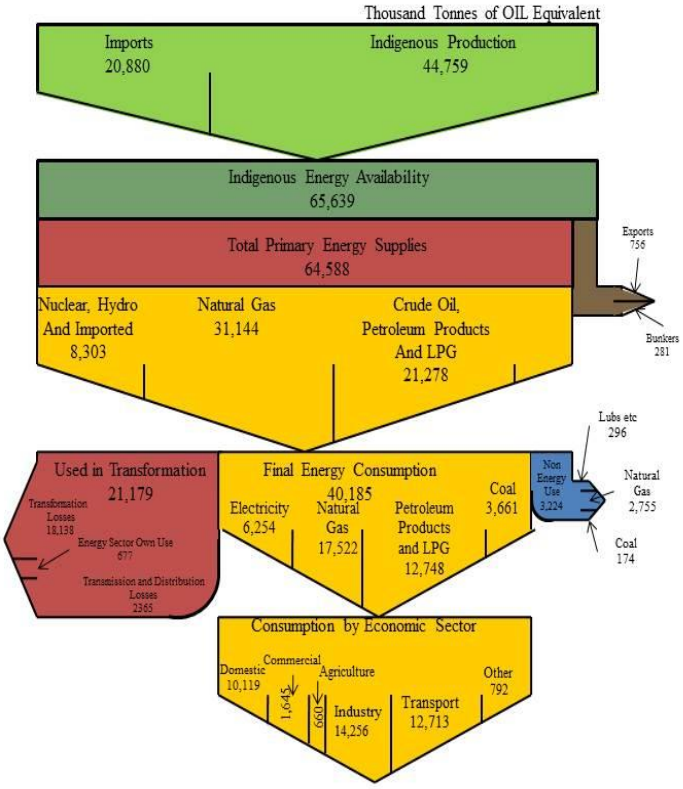

Figure1: Energy flow 2012-2013 in National Energy System of Pakistan(HDIP, 2012)

It is evident from the above data that the shares of different sources in primary commercial energy consumption (64.6 MTOE) in 2012-13 were: gas – 48.2%; oil – 32.5%; hydro and nuclear electricity – 12.8%; and Coal– 6.0%. The major consumers of primary commercial energy in Pakistan are power, transport, industrial and domestic sectors. The power generation sector utilizes about 35.2% of oil, 29.0% of gas and only 0.01% of coal in the country. Fossil fuels, hydropower and nuclear energy have 64.5%, 30% and 5.8% shares respectively in the total electricity generation. The transport sector accounts for about 31.4%, the industrial sector utilizes about 37.6%, domestic sector 23.4% of total primary energy supplies. The commercial, agriculture and others consume 4.0%, 1.8% and 1.9% of the total energy as given in Figure 2 (b).

The indigenous resources of oil and gas are limited and the country is heavily dependent on the import of oil. With the present rate of production, the indigenous recoverable reserves of oil and gas will get exhausted after 13 and 16 years respectively. Though there is huge coal potential (185 billion tonnes) in the country, but has not been explored and utilized to its full potential due to poor quality, financial constraints, location disadvantage, and lack of experience in modern clean coal utilization technologies. The country is meeting about 85% of oil demand from imports by spending around US$ 14.5 billion per annum. The oil import bill is a serious strain on the country's economy and has been deteriorating the balance of payment situation. The production and combustion of fossil fuels also degrade the environment (Harijan, 2008).

With the economic development and with efforts to provide enhanced access to commercial energy, the energy demand in the country is expected to grow rapidly. It has been projected that the primary commercial energy demand would increase at 4.3, 7.3 and 10.4% per annum average growth rates and would reach at 150, 320 and 670 MTOE by the year 2030 under LEG (low economic growth), BAU (business as usual), and HEG (high economic growth) scenarios respectively. The government of Pakistan has planned to bridge the energy demand-supply gap (about 57% in 2030) by importing energy. The development of options for importing gas has been constrained by the sensitive regional security environment, special technical issues, and complexities associated with commercial and operating arrangements typical of large projects requiring inter-country agreements(Uqaili et al., 2007).

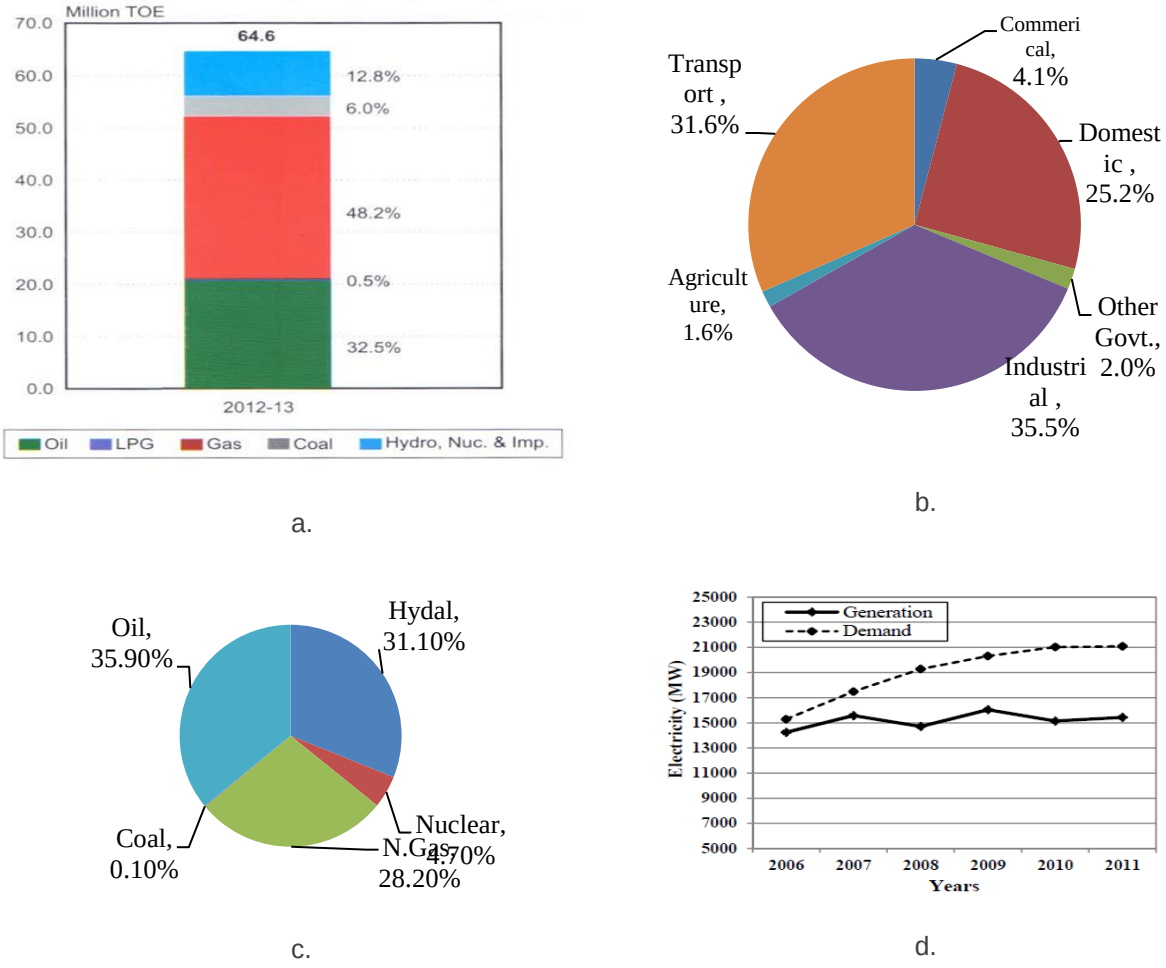

Figure 2: a. Primary Energy Supplies by Source, b. Energy Consumption by Sector, c. Electricity Generation by Source, d. Electricity Supply and Demand Gap (HDIP, 2012)

It is evident from above illustration and discussion that Pakistan needs to push for maximum diffusion of renewables in the energy mix instead of imported fossil fuels (oil and coal mainly) which not only impact the foreign exchange reserves of the country but also result in the increased upfront tariff of various forms of energy. This situation may also cause increase in the prices of local goods being used in the industry and resultant affect shall be that either these industries may face forced shutdown or may not achieve the production targets. Implementation of best practices of energy conservation is another avenue which Pakistan need to explore to minimise the energy supply and demand gap.

3. ENERGY MODELLING TOOLS

Energy planning practice may be traced back with the early industrialization of economy, however, the scope and level of planning remained quite limited. Later on, when Governments started devising economic policies, energy was considered as one of the tradable commodities and its supply and demand was documented. National level energy policies were evolved during and after Second World War period (Sahir, 2007). However, some formal planning approaches have evolved only after the oil crises of 1970. Several researchers and policy makers are engaged to find most feasible solution for the long term sustainable energy planning options at their level of concern. Technological developments paralleled with exponential growth in population, energy consumption, multiple objectives, and various constraints have made energy planning a complex process. However, modern computers for their ability to handle numerous data and complexities very efficiently by the end of last century became a vital assistant for energy planning problem.

Energy security, environmental concerns, social acceptability, economic feasibility, risk and uncertainties are key challenges being dealt with in long term sustainable energy planning problem. In order to address all these and other specific issues several computer based energy modelling tools being developed at various levels and are in use for analysis of the long term strategic energy planning. A comprehensive review of the methodological advances in energy modelling between 1970 and 1990 has been presented by Griffen(Griffin, 1993). The energy models essentially help to integrate the supply and demand side database to the socio-economic and techno-economic constraints for a consistent application of the analytical techniques and generate direct and indirect solutions for policy planning(Sahir, 2007). Jebaraj (Jebaraj and Iniyan, 2006) has carried out another review on energy planning using various models at different levels of energy system. Whereas, Giatrakos(Giatrakos et al., 2009) have briefly reviewed the three important methodologies used by energy planning models as of Optimisation, Simulation and Accounting Frameworks.:

D. Connolly (Connolly et al., 2010) has also completed a detailed review of various energy modelling tools used for energy planning.

Energy planning involves consideration of a complex array of issues in national as well as global perspective. Energy models are found to be often useful when analysing such complex system with a large amount of data (Worrell et al., 2003). The advent of powerful personal computers, greatly facilitated the in development of various energy modelling tools. Energy Models currently available are based on different fundamental approaches and concepts, and employ a range of mathematical algorithms. For nearly four decades, substantial work on improvement of such models has been carried out and these models are now widely used across the globe by various nations. Therefore, in practice it is not feasible to develop own models for energy planning exercise by energy planner or researchers instead more effective is to use existing models with appropriate selection that could cater the planning requirements(Dementjeva and Siirde, 2009). Amongst various computer tools being used for energy modelling MARKAL, LEAP and ENPEP are the classic system tools with long lasting success, growing user base, continuous training of researchers, institution and governments (Blarke, 2005). Each of these tools is briefly discussed here.

MARKAL is energy/economics tool developed in a collaborative effort under the auspices of the International Energy Agency's "Energy Technology System Analysis Program", which started in 1978. MARKAL have been used by various studies and at the moment it is used in 70 countries by 250 institutes(Connolly et al., 2010). MARKAL uses principles of market-economics and optimization so that it becomes the model that identifies which technologies should be preferred (Blarke, 2005). The total costs (MARKAL plus user-interface plus GAMS and solvers) range from about 3,300 USD for academic users up to 15,000 USD for unaffiliated commercial users.

ENPEP-Balance uses a combination of techno-economic bottom-up analysis and optimization to compare the demand for energy with available resources and technologies. It was developed by Argonne National Laboratory in the USA in 1999 and it is used in over 50 countries(Connolly et al., 2010, Blarke, 2005).

LEAP was developed in 1980 in the USA and currently maintained by the Stockholm Environment Institute. It is an integrated modelling tool (based on accounting framework) that is usually used to analyse the national energy system by tracking energy consumption, production and resource extractions in all sectors of economy. LEAP is freely available to qualified users in developing countries. Currently LEAP has over 5000 users in 169 countries (Heaps, 2008).

These and various other energy planning tools used towards building national energy models have been greatly useful by providing analytical support for the generation and evaluation of alternative energy scenarios to be considered as policy options.

4. APPLICATION OF ENERGY MODELLING IN PAKISTAN FOR ENERGY POLICY FORMULATION

Energy models are widely used around the world for devising energy policies. The modeling results do not provide itself the policies instead guide decision makers to devise the appropriate path in formulation of these polices. Various computer modeling tools, as discussed in section 3 of this paper, are very popular and actively used by governments, academician and other institute to support policy making. The application of these models in not only restricted for the national level instead they are also used to analyze energy systems at regional and local level. More over these models, at the same time, may be used for the integrated energy planning or sector specific analysis.

Application of energy modeling tools both at government and academic level for analyzing energy system and further utilizing model results for policy formulation in Pakistan are minimum compared to other developing countries. As such, these modeling exercises undertaken both at government and academic level are reviewed in this section.

National Level Government Efforts

There has had been no formal integrated energy modeling exercise found in literature before mid 1980s. Instead, most of the time organization level energy and power forecasts based on past trend were used to plan for the future. However, two national level efforts by government that also came as grant or Technical Assistance (TA) from two international institutions, i.e. United States Agency for International Development (USAID) and Asian Development Bank (ADB) are found in literature. Both of these integrated energy modeling efforts are reviewed briefly as under:

RESPAK Model

In Mid 1980's Energy Wing of Planning Commission was supported by USAID in the development of RESPAK model which was an optimization planning framework model (IRG). The model predicted total energy requirements based on sectoral economic growth, but incorporates adjustment factors for technological change, increased energy efficiency and swap between fuel types. This forecast was prepared for the years 1988 to 2013 (SHYDO, 2006). However, model fell into disuse due to much needed retention of expertise as well as lack of team and capacity building of other staff for using this model. Further, in early 1990s owing to privatization of the power sector, least cost economic modeling was considered no longer necessary(IRG). The RESPAK model, as such, was mainly used for couple of years for the power forecasting and during this period, government of Pakistan not announced any policy. In fact first formal energy policy was announced by Pakistan was in 1994 wherein no reference to RESPAK model is made.

Pakistan Integrated Energy Model (Pak-IEM)

In October, 2007 ADB approved a Technical Assistance (TA) grant named as TA 498-PAK: Integrated Energy Model (PAK-IEM). Following TA signing in November 2007 the project consultants lead by International Resource Group (IRG) were mobilized during the month of June 2008 (Kawawaki, 2009). The purpose of this effort by ADB was to develop an integrated energy model of Pakistan by bringing various key energy sector players in country closer to develop the capacity so that energy policies are devised rationally.

PAK-IEM was first of its sort integrated energy planning effort in Pakistan, as such; various ministries, organization and academia interacted with the development of institutional structure of the model. Energy Wing, Planning Commission had main lead and coordinating role in the model development.

Pak-IEM had utilized the TIMES model which is the successor to the MARKAL modeling framework and has been conceived, developed and continuously supported by International Energy Agency (IEA) under Energy Technology System Analysis Program (ETSAP). The model employs the VErsatile Data Analyst (VEDA) and model management system to organize and handle the input and data process. The development of the model input data is organized into a set of Excel workbooks that are managed by VEDA-FE (Front End) to form the complete model for calibration(Loulou et al., 2007). In Pak-IEM the model had been calibrated for the year 2006-2007 and development of reference scenario out to 2030, and beyond(IRG). Various alternate scenarios had been developed to introduce a different energy mix as future options. The structure of Pak-IEM Model is shown in Figure 3.

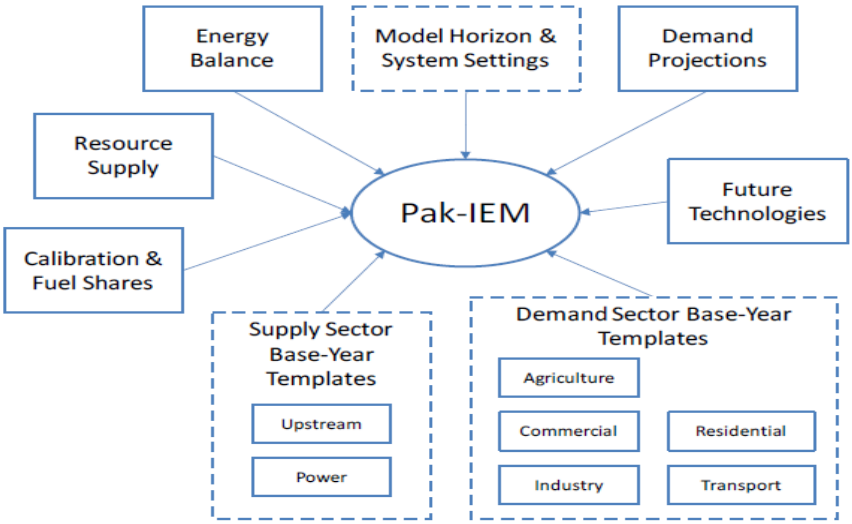

Figure 3: The structure of Pak-IEM Model

The Pak-IEM model provide analysis of the options Pakistan's energy system to advance over the next 20 years to achieve the growth projections based on 5.6% average GDP up to 2030. These analysis suggested that in order sustain economic growth Pak-IEM Called for(IRG) a four-fold increase in electricity generation from – 94,000 GWh to 410,000 GWh is essential thus require addition of 82,000 MW of new electricity generation capacity as well as three-fold increase in consumption of high value petroleum products from 6.2 MTOE to 18 MTOE

These analyses further suggested that without quick government action, averting the looming Energy Security crisis by 2030 may become difficult because as per existing practices and policies, proven conventional natural gas reserves will be depleted causing an increase in the energy imports from 27% to 45% of the total supply. This situation may go worse if proposed energy projects are delayed.

Pak-IEM Model suggested significant annual savings by introducing Smart Policies (best practices) since eliminating the load shedding shall avoid Rs. 524 billion in economic losses. Reducing electricity transmission and distribution losses by 7% saves Rs. 7.3 billion (gross). Improving end-use energy efficiency saves Rs. 41 billion (net) and successful exploration to deliver 20% more gas saves an additional Rs. 37 billion (gross).

Briefly, these policies are expected to reduce dependency on imported energy sources by 20 MTOE by year 2030. Further focus on non-hydro renewable can ensure security by reducing imports by 38% in 2030.

The actual TA completion date which was 31 March 2009 had been twice extended and this study was completed on 31 Dec. 2011. Three volumes of model report were produced as under:

- Volume-I: Model Design Report
- Volume-II: Policy Analysis Report
- Volume-III: User Guide

Although this study is rated successful by ADB, however, since publication of these reports and closure of project there is little known as what further updates has had been to made model and that has any recommendations of "this study are taken as input for subsequent energy polices. The energy policy document of 2013 titled "National Power Policy 2013" announced by Ministry of Water and Power even makes no reference to this study.

Academia level Efforts

There is substantial work done by the researchers on Pakistan's energy system, however, this review only takes on account the work whereby energy modeling has been undertaken for national level energy planning. Some of these efforts are given in Table 1 with brief review at the end.

Table 1: National level energy modeling efforts in Pakistan

S. No.	Research Title	Authors	Year	Model Used
1.	Energy System Modeling and Analysis of Long Term Sustainable Energy Alternatives for Pakistan	Mukhtar Hussain Sahir (Sahir, 2007)	2007	Linear Regression
2.	Modeling & Analysis of the Potential Demand for Renewable Resources of Energy in Pakistan.	Khanji Harijan (Harijan, 2008)	2008	Linear Regression
3.	Modelling Diversified Electricity Generation Scenarios for Pakistan	Mariam Gul, Waqar A. Qureshi (Gul and Qureshi, 2012)	2012	LEAP
4.	Energy, environmental and economic effects of Renewable Portfolio Standards in a Developing Country	Muhammad Khalid Farooq, S.Kumar, Ram M.Shrestha (Farooq et al., 2013)	2013	MARKAL
5.	Electricity Demand and Emissions under Different Policy Scenarios for Pakistan	Abdullah Mengal, Khanji Harijan, Mohammad A. Uqaili, and Nayyar Hussain Mirjat (Abdullah Mengal, 2014)	2014	LEAP
6.	Modeling and Forecasting of Energy Scenario in Pakistan with Application of Decentralized Energy Planning	Maira Shakeel Sye, Dr. Ijaz Ahmad Chaudhry, Muhammad Farooq, Adnan Qamar (SYED et al., 2014)	2014	LEAP

These studies are found to be useful and were undertaken as a result of research work by various academician/researchers. The first two studies are PhD thesis wherein conventional Linear Regression models were adopted for Integrated Energy Planning and Analysis of Renewable Energy Potential respectively. Both of these are comprehensive and national level studies. The studies at S.No. 03, 05 and 06 have been undertaken using LEAP Energy Modeling tool wherein only electricity supply side has been considered with different fuel mix as scenarios. The study at S.No. 5 also consider the environmental emissions as a result of different energy mix options considered. The paper at S.No. 04 has analyzed the potential of renewable energy for power generation and its environmental and economic implications in Pakistan, using MARKAL framework.

These and further similar research efforts, however, are rarely considered in energy policy formulation at national level despite the substantial contribution by these researchers.

5. ENERGY POLICIES OF PAKISTAN

The energy policies in Pakistan are prepared and implemented mainly by Ministry of Water and Power with support and coordination of Energy Wing of Planning Commission. Pakistan's Energy sector organisations have sort of complex structure and comprises of several entities each with their different but related functions and area of jurisdiction, as shown in Table 2..

Table 2: The Key Energy Sector Players in Pakistan

Function/Sector	Organization/Institute
Coordination on Policy Formulation, legislation and regulation	Energy Planning Commission
Policy formulization and Implementation	Ministry of Water & Power
Regulation	National Electric Power Regulatory Authority (NEPRA) Oil and Gas Regulatory Authority (OGRA) Private Power and Infrastructure Board (PPIB)
Oil & Gas (Production and Distribution)	Oil and Gas Development Company Limited (OGDCL), Pakistan Petroleum Limited (PPL),Pakistan State Oil (PSO) Private multinationals
Electricity (Production, transmission and Distribution)	Water and Power Development Authority(WAPDA) Pakistan Electric Power Company (PEPCO) Generation Companies(GENCOS) National Transmission and Distribution Company (NTDC) Distribution Companies (DISCOS)
Research & Development	National Energy Conservation Centre (ENERCON) Various Academic Institutes Alternative Energy Development Board (AEDB) Pakistan Council for Renewable Energy Technologies (PCRET)

Since 1994 Government has formally focused on the Energy Policy formulation, however, most of polices announced so far focus on either readily available primary energy sources or least cost solutions. Ministry of Water and Power is generally responsible for development these policies supported by the Energy Wing of the Planning Commission. Various studies and integrated energy modeling exercise has been undertaking couple of time for the rational policy formulation. However, the outcome of these efforts yielded very low owing to implementation issues thus Pakistan has not witnessed any substantial economic activity,

growth or development across various sectors as per set targets. Listing with brief focus (PPIB, 2015) of the various energy/power polices so far announced by the Government of Pakistan is given in Table 3.

Table 3: Various energy/power policies by the Government of Pakistan

Year	Policy	Focus
1994	Energy Policy (First Formal Policy)	Introduced Independent Power Producers (IPPS) and emphasized energy conservation.
1995	Hydropower Power Policy	1994 Power Policy extended for Hydropower Generation.
1998	Revised Policy for New Private Independent Power Projects	Amended/Revised 1994 Policy with more rationalization i.e. introducing completion/bidding.
2002	Power Generation Policy	This policy encourages investment from private, public-private and public sector organizations
2005	Energy Security Action Plan (2005-2030)	The objectives of Pakistan's Vision 2030 for reliable and quality energy supplies addressed in this policy,
2006	Development of Renewable Energy for Power Generation	Focused on development of Small Hydro, Wind, and Solar and Bio Fuel Technologies.
2010-2012	National Energy Policy	This Policy focused Energy Conservation, Short Term and Long Term Plan for generation of Electricity which included RPPs and Rehabilitation of existing public sector power plants and investment by IPPS to cater energy needs of the country.
2013	National Power Policy	Focuses on development of electricity generation and energy conservation projects to overcome energy crisis.

It may be noted that focus of each of these energy policies varies (e.g., energy policy 1994 focuses on "attracting IPPs", Energy Policy 1995 targets hydel power, Energy policy 1998 introduced competitive open bidding process, RE policy 2006 provides incentives for renewable generation, and National Power Policy 2013 initiates shift to cheaper fuels (i.e., indigenous coal and hydro projects), the common thrust is to attract IPPs investments in the electricity sector of Pakistan.

All these policies were developed with serious efforts behind them; however, integrated energy modelling efforts undertaken by either planning commission or academia were generally not referred in these policy document. It is, therefore, need of the hour that Pakistan now should focus rational approaches for energy planning and policy formulation taking into account the uncertainties of global energy market, social and environmental aspects to attain energy security and sustainable development.

6. CONCLUSION

Based on the review of Pakistan's current energy status, the modeling efforts undertaken and national energy policies devised so far it is concluded that:

- The institutional capacity building is need of the hour to have coordination between various ministries, organizations and academia to work jointly for common goal i.e. the rational energy policy for the nation for averting the energy crisis of today and the future.
- Multiple integrated energy modeling efforts may be encouraged with reliable and adequate date for common period instead of analyzing the national energy system on a single model and relying on same.
- The integrated energy modeling efforts must be considered by decision and policy makers as key input for the future policies as of practiced around the world
- Continued update of integrated energy models should be ensured to analyze the national energy system to various changes.

7. ACKNOWLEDGMENT

The authors acknowledge highly thanks PSSP-USAID and Mehran University of Engineering & Technology, Jamshoro for their financial and technical support for completing this research work.

8. REFERENCES

ABDULLAH MENGAL, K. H., Mohammad A. Uqaili, AND Nayyar Hussain Mirjat Electricity Demand and Emissions under Different Policy Scenarios for Pakistan. International Conference on Energy, Environment and Sustainable Development, 2014 Mehran University of Engineering and Technology, Jamshoro, Pakistan.

BLARKE, M. B. 2005. Integrated Resource Planning: General Methodology and Assumptions, A report prepared under the Malaysian-Danish Environmental Cooperation Programme. *Renewable Energy and Energy Efficiency Component Economic Planning Unit, Malaysia*.

CONNOLLY, D., Lund, H., Mathiesen, B. V. & Leahy, M. 2010. A review of computer tools for analysing the integration of renewable energy into Various energy systems. *Applied Energy,* 87**,** 1059-1082.

DEMENTJEVA, N. & Siirde, A. 2009. *Energy Planning Models Analysis and Their Adaptability for Estonian Energy Sector*, TUT Press.

FAROOQ, M. K., Kumar, S. & Shrestha, R. M. 2013. Energy, environmental and economic effects of Renewable Portfolio Standards (RPS) in a Developing Country. *Energy Policy,* 62**,** 989-1001.

GIATRAKOS, G. P., Tsoutsos, T. D. & Zografakis, N. 2009. Sustainable power planning for the island of Crete. *Energy policy,* 37**,** 1222-1238.

GRIFFIN, J. M. 1993. Methodological advances in energy modelling: 1970-1990. *The Energy Journal***,** 111-124.

GUL, M. & Qureshi, W. A. Modeling diversified electricity generation scenarios for Pakistan. Power and Energy Society General Meeting, 2012 IEEE, 2012. IEEE, 1-7.

HARIJAN, K. 2008. *Modelling and analysis of the potential demand for renewable sources of energy in Pakistan.* PhD Thesis, Mehran University of Engineering and Technology, Jamshoro, Pakistan.

HDIP 2012. Hydrocarbon Development Institute of Pakistan. *Ministry of Petroleum and Natural Resources, Government of Pakistan***,** 39.

HEAPS, C. 2002. Integrated energy-environment modelling and LEAP, SEI Boston and Tellus Institute, Boston.

HEAPS, C. 2008. An introduction to LEAP. *Stockholm Environment Institute*.

HUSSAIN, N., Nallagownden, P. & Ibrahim, T. 2013. Long Term Sustainable Energy Planning for Malaysia: A Modelling and Decision Aid Framework. *Journal of Energy and Environment,* 3.

IRG 2009. Pakistan Integrated Energy Model (Pak-IEM). Asian Development Bank and Ministry of Planning and Development, Government of Pakistan.

JEBARAJ, S. & Iniyan, S. 2006. A review of energy models. *Renewable and Sustainable Energy Reviews,* 10**,** 281-311.

KAWAWAKI, F. C. 2009. TECHNICAL ASSISTANCE COMPLETION REPORT - TA 4982-PAK: Integrated Energy Model CWEN.

LOULOU, R., Goldstein, G. & Noble, K. 2007. Documentation for the MARKAL family of models. 2004. *IEA Energy Technology Systems Analysis Programme*.

PPIB. 2015. *Power Policies of Pakistan* [Online]. Private Power Infrastructure Board (PPIB). Available: http://www.ppib.gov.pk/N_cpp.htm [Accessed June 05 2015].

SAHIR, M. H. 2007. *Energy System Modeling and Analysis of Long Term Sustainable Energy Alternatives for Pakistan.*

SHYDO 2006. Machai Hydropower Feasibility Study. *Renewable Energy Development Project.* Sarhad Hydel Development Organization

SYED, M. S., Chaudhry, I. A., Farooq, M. & Qamar, A. 2014. Modeling and Forecasting of Energy Scenario in Pakistan with Application of Decentralized Energy Planning. *JOURNAL OF FACULTY OF ENGINEERING & TECHNOLOGY,* 21**,** 23-36.

UQAILI, M. A., Harijan, K. & Memon, M. (2007) Prospects of renewable energy for meeting growing electricity demand in Pakistan. Renewable Energy for Sustainable Development in the Asia Pacific Region,. AIP Publishing, 53-61.

WORRELL, E., Ramesohl, S. & Boyd, G. 2003. Towards increased policy relevance in energy modeling. *Lawrence Berkeley National Laboratory*.

155: Existing metrics, codes and technologies for HVAC design of energy-efficient data centre: a literature review

ZISHANG ZHU[1], YAN LU[2], XUDONG ZHAO[1*] , YANYI SUN[3]

1 School of Engineering, University of Hull, UK, HU6 7RX
2 China Academy of Building Research Southwest Institute, China
3 Department of Architecture and Building Environment, University of Nottingham, UK

The data centre energy demand increased rapidly because the explosion of IT industry, and the annual increasing rate will keep as high as 20% in the predictable future. Until 2013, there are over 1000 large colocation data centres from 24 countries in EU and 562 from China, taken 1.3% and 1.2% energy from the whole social energy consumption respectively. However, in a typical EU data centre, 40% energy is used for HAVC and 10% is relevant to the building itself, both of which have a huge energy saving potential by applying advanced HAVC technologies and proper building design strategies.

This paper reviewed the codes and standards for energy-efficient data centre, as well as relevant techniques in term of data centre HVAC system design. The most widely used data centre energy efficacy metrics and benchmarks are studies, the requirements of codes from main countries are compared and analysed, such as Chinese "DB31/651-2012: The norm of Data centre Unit Energy Effectiveness" and "The EU Code of Conduct on Data Centres". Meanwhile, a number of data centre adoptable energy saving system (mainly represent by cooling system) are investigated.

By investigation and comparison of metrics, code and techniques mainly including cooling and energy recovery, the energy efficiency requirements emphasis and the features of available energy saving techniques for data centre are summarised in this paper. Although the code requirement is higher and higher, and the technologies are keep improving, obvious shortcomings still exist in sustainability and economic aspects which are discussed in the end of this review.

Keywords: Energy efficiency; Data centre; Building service, HVAC, codes, metrics, techniques;

1. INTRODUCTION AND CURRENT SITUATION

Ever since the third industrial revolution, the rise of information technology (IT) has brought great reform to human life. Data centers (DCs), which include all the buildings, facilities, and rooms that contain data servers, telecommunication equipment, cooling equipment and power equipment [1], are developing quickly as an important part of IT industry [2,3]. Currently, there are around 1000 main colocation data centers with more than 200 racks in Europe, similar number can be found for United States, meanwhile, for China the number is around 150 with rapid increasing rate. Without consideration of the scale, there are 3.5 M data centres in the world, most of them have no more than 5 racks in 100m^2, half of which located in Europe and US. The worldwide distribution for main data centres and distribution in Europe countries can be seen in Fig. 1 and Fig. 2 [4] below.

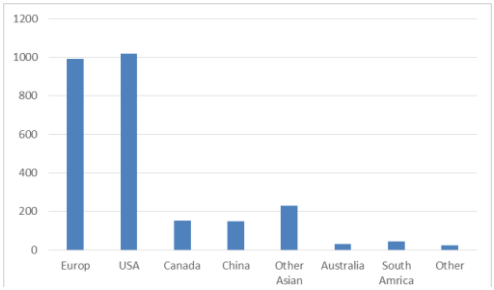

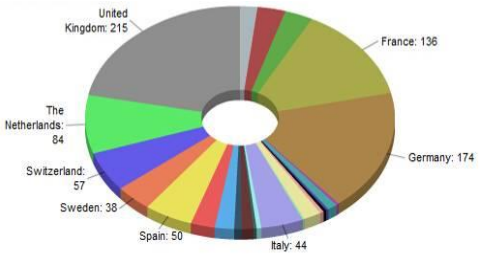

Fig.1 The worldwide distribution for main data centres Fig.2 Europe Main Data Center distribution Statistics

The global electricity usage by data centers doubled from 2000 to 2005, even though in 2008 when the economic slowdown due to financial crisis, this number still increased 56% from 2005 to 2010 [5]. In 2010, electricity used by data centers took about 1.3% of world whole electricity consumption. European data centre consumed 56 TWh electric in 2007 and will increase to 104 TWh per year by 2020 as predicted, which are equivalent to over 13MW and 24MW of power plant capacity respectively [6]. In China, an analysis conducted in 2010 showed that the energy consumption of the data centers accounted for 1% of total electricity consumption [7]. Meanwhile, in the foreseeable future, the predictions for annual increases in data center power demand are as high as15–20% [8].

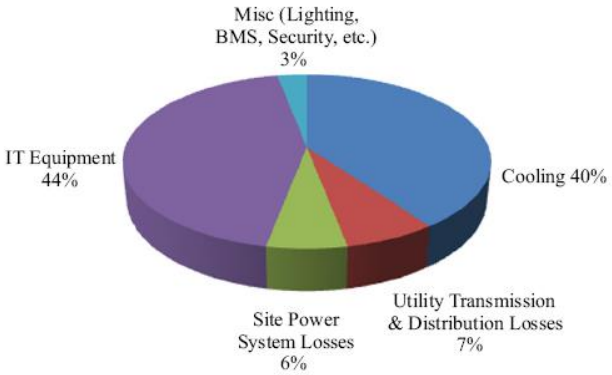

Fig. 3 Example of data center energy split [8]

Apart from the electricity used by IT equipment, other energy consumption from building service system, such as cooling and lighting, which is not computing power relevant, take more than 50% of total energy usage in most data centres. Cooling equipment is one of the main energy consumer in data centers because heat dissipation has become a major determinant factor of availability and reliability. Traditional cooling system of data centers is computer room air conditioner (CRAC) based on mechanical vapour compression refrigeration. Its energy consumption takes up even around 30–50% of the total energy demand [9–11]. An example of data center energy split is shown in Fig. 3 [9] below. To overcome the high demand from none computing power relevant system, while computer and IT engineers are focusing on developing more efficient hardware and software, building service system researchers have made effect on high efficacy cooling, lighting, energy recovery and power supply system. A number of techniques

including raised floor air supply, cold/hot aisle, spot cooling units, free cooling, renewable energy and waste heat reuse etc. are recently developed for improving the energy efficiency of data center. Relevant design codes, such as European Code of Conduct for Data Centers, were developed by government or association to promote the build and upgrade of high energy efficiency data center and setting energy consumption limitation. More benchmark tools are adopted in this field recently to help with the implementation of design codes.

This review will describe the existing main DC energy efficiency metrics, benchmarks, codes and DC building service system as well as their recent improvements. Their principle, application, advantage and disadvantage are listed and compared in a critical way.

2. THE DEVELOPMENT OF DC ENERGY EFFICIENCY METRICS, BENCHMARKS AND CODES

2.1 Energy efficiency metrics for DCs

For the purpose of DCs energy measurement and monitoring, dedicated energy performance metrics are developed recently. The most two widely adopted metrics are Power usage effectiveness (PUE) and its reciprocal, Data center infrastructure efficiency (DCiE), both developed in 2007 by The Green Grid [12]. PUE is the ratio of total amount of energy used by a computer data center facility to the energy delivered to computing equipment. It measures the energy efficiency of computer data center, specifically how much energy is used by the IT equipment against building service system [13]. The mathematic equation and scope definition of PUE can be seen as equation 1 and Fig 4. The PUE range start from 1.0 to infinity. Theoretically, PUE achieving 1.0 indicate 100% efficiency that all energy is used by IT equipment only. Currently, there are no comprehensive study which show the recent distribution of the PUE for datacenters among countries, but, Lawrence Berkley National Labs [14] investigate 22 data centres and found their PUE range from 1.3 to 3.0. It is obviously that average PUE keep improving year by year, and great PUE difference exist between recent and old DCs. In 2006, some researches figure that a PUE of 3.0 or greater widely exist especially in earlier cases, however, they can be improved to 2.0 with proper design and reasonable investment [15]; at the same year, Belady [16] stated that a PUE value of 1.6 is also achievable for new cases with dedicated design and equipment. However, in 2013 the average PUE is between 1.8 and 1.89 by surveys carried out by Uptime Institute. Great energy efficiency improvement can be found through the reduction of PUE, although the study of accurate or statistical relationship of PUE against building service selection and investment is still missing currently.

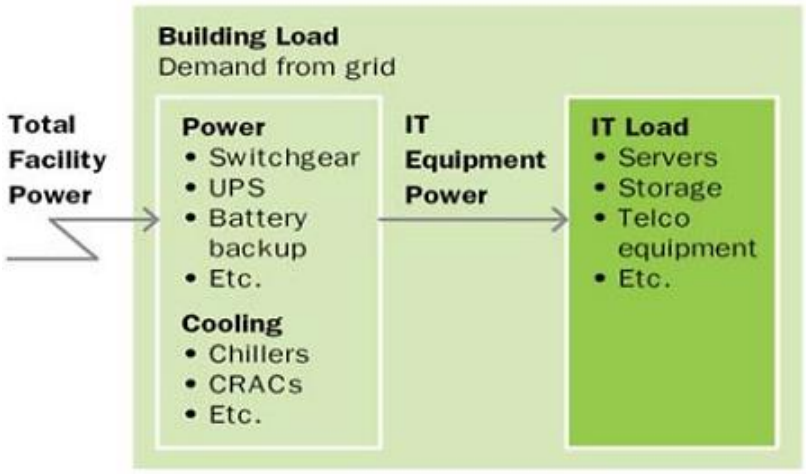

Fig. 4: The PUE scope definition

Equation 1:
$$\mathrm{PUE} = \frac{\text{Total Facility Energy}}{\text{IT Equipment Energy}}$$

2.2 Existing problems and improvement in current metrics

Although PUE (and DCiE) is widely used as a common metric for energy efficiency of DCs, its issues and shortcomings are figured quite a lot as well.

- The definition for scope of energy use is not clear

The problem that most likely accord in practice is that the scope of total facility energy is not specifically defined. Some PUE reporting does not involve the energy using by “unnecessary” devices [17], such as lighting, elevator, and security system, which are not directly affect the computing performance. A case study carried out in 2009 [18] shows that the proportions energy used by IT servers, HVAC system, power network and conditioning facilities and lighting are 56%, 30%, 13%, and 1% respectively. In this case, take lighting into account or assume that it is total switched off during operation will resulting in different PUE of 1.79 or 1.77. Thus, tactfully ignore some part of building service system that not necessary for server operation but essential for whole DCs will obviously resulting in an improved PUE value.

Besides, the definition of power input is not clearly defined also, as well as the calculation when adding on-site energy generation into account. A typical 10% to 20% difference will be made by whether involving energy input before the transformer or after.

- The great mismatch form design PUE and real PUE
  The real PUE in operation stage is always different than estimated value in design stage, the most important reason for this, apart from undetailed consideration, is the inaccurate design data taken from design codes [19]. To make sure that the DCs can operate in worst design conditions and meet all building and IT codes, as well as maximize the redundancy of cooling and power supply, designer trend to use the max value in suggestion range of design code and choose higher capacity for building service system. As a consequence, the infrastructures servicing the IT devices including HVAC and power transformer always operate in under-loaded condition, which lead inefficiency operation and higher PUE than design value.

- Reflect opposite information in some cases
  The reason to introduce the metric PUE into IT industry is to reflect the CDs energy efficiency in an intuition way. But in some DC renovation cases, power consumption form IT devices was reduced while keeping the same computing ability by upgraded CPUs to updated products, however, the successful renovation may lead the PUE became worse. The reason for this unusual phenomenon is that the energy consumption for building service system and power supply devices (numerator in PUE calculation) are not able to be reduced as much as the proportion reduced of IT devices (denominator in PUE calculation) [20]. Thus, highly decrease of computing device energy need may cause worse PUE, although the whole DC is more energy efficiency after renovation.

To overcome the existing problems and shortcomings in DC energy efficiency metrics, the improved metrics has been proposed by IT industry and associations. The “Partial PUE” (pPUE) metrics have been developed by Green Grid in 2011 to help improving the accuracy of PUE and address the scope definition problem. The pPUE describe DC`s power efficiency by account energy consumption within a specific boundary instead of the whole DC building. The boundary are normally defined for a zone or floor (e.g., the server floor zone) that contains the data centre function [21]. The pPUEs for each data centre zones present the power efficiency of data center function within a multipurpose building. Thus, energy consumption form other non-DC-related zones, such as staff living, meeting, and storage space, will not interfere the power efficiency metric. Unfortunately, although pPUE may work for rooms in a multipurpose building, the sum of the pPUE for each zone may not represent the overall PUE of the facility [22]. Besides, member of the Green Grid are also developing metrics that can reflect the power efficiency of specific systems in DC, such as cooling load factor (CLF) and power load factor (PLF) [23] which present the proportion of cooling system load and power supply system against IT load separately. These metrics exclusive for dedicated systems are able to contribute the comparison and benchmarking of building service design in DC.

2.3 Benchmarks and codes for DCs` energy efficiency

To minimize DCs energy demand and provide guidance for engineering design, a number of compulsory and voluntary building code and rating system are adopted in data centre building. The building code allocate the maximum power allowance of specific infrastructure or device such as HVAC, lighting and power supply system. The most world wildly used building energy codes, such as The International Energy Conservation Code (IECC) developed by DOE [24] and the American Society of Heating, Refrigerating, and Air-Conditioning Engineers (ASHRAE) Standard [25], set the limitation for specific building system based on building/space type or function. For instance, according to ASHRAE the maximum power for space lighting in normal office building is 9.15W/m^2, thus, the lighting annual energy consumption can be calculated by apply proper lighting schedule. Although they have become to the baseline for many national building energy code applied in different countries, only a few clauses in these codes are suitable for data

centre, as they are mainly designed for the building to house people not servers. Some energy codes specifically designed for data centre are developed in recent years, represent by U.S. Code 17112 - Energy efficiency for data center buildings (compulsory) [26], EU Code of Conduct on Data Centres Energy Efficiency (voluntary) [27] and its associated annual best practice guidelines [28] and Chinese code of The norm of Data centre Unit Energy Usage Effectiveness (compulsory) [29]. Both energy consumption limitation for detailed DC infrastructure and current/future PUE limitation for whole DC building are involved in these code, as well as scores for energy saving strategies in DC energy rating system. The specific features of world mainly energy code related to DCs can be seen in table1 below.

Table 39: The features of world mainly energy code related to DC

Codes/guides name	*Range*	*Specialized for DC*	*Aspects applied to DC building*
Telecommunications Infrastructure Telecommunications Infrastructure Standard for Data Centers Standard for Data Centers ANSI/TIA-942	World wide	Y	Specific infrastructure requirement
ENERGY STAR Data Center Rating	World wide	Y	Whole DC energy rating
U.S. Code 17112 - Energy efficiency for data center buildings	USA	Y	Requirements by law
EU Code of Conduct on Data Centres Energy Efficiency	EU	Y	Specific technologies and energy performance suggestion
Technology specification and evaluation methods for occupancy of resources, energy efficiency and emission of IDC	China	Y	Specific infrastructure requirement, whole DC energy rating
CEEDA	UK	Y	Specific infrastructure rating, whole DC energy rating
Green Data Centre - Energy and Environmental Management, SS 564:2010	Singapore	Y	Specific infrastructure requirement, whole DC energy rating
Best Practices Guide for Energy-Efficient Data Center Design	USA	Y	Practices guide and energy performance suggestion
Best Practices: The EU Code of Conduct on Data Centres	EU	Y	Practices guide and energy performance suggestion
The International Energy Conservation Code	World wide	N	Cooling, Ventilation, Lighting
American Society of Heating, Refrigerating, and Air-Conditioning Engineers Standard	World wide	N	Cooling, Ventilation, Lighting
LEED, BREEAM, CASBE, DGNB, Chinese Evaluation standard for green building, .etc.	National	N	Sustainability rating for landing, water, energy, resources using

3. THE AVAILABLE ENERGY EFFICIENCY TECHNICAL MEASURES

3.1 Air-cooled system, air flow management and free cooling

Air cooling system are used in most of existing DCs and certain part of new DCs. In air cooled DC, the server racks are placed into hot and cold aisles. The front side of racks with air inlet stand face to each other in cold aisles, meanwhile, the back side of racks with air outlet line the hot aisles. The chilled air provided from air vents in floor or ceiling of cold aisles, go through the server racks and reach the hot racks where it has been become warm air and then return to cooling units [30]. Current research shows that the supplied and exhausted air typically at 25^{o}C and 40 ^{o}C, with temperature difference of 15 ^{o}C in an efficient air cooling system [31]. Air flow rate (AFR) can be vary depend on server racks power density and rack arrangement. According to Schmidt etal.[32], a typical 0.5MW dater centre with 50 server racks can be operate at AFR of 1500CFM per rack, the temperature difference between cold and hot aisles is 10.5 ^{o}C. A high efficiency air-cooled system [33] involving variable speed fans servicing for 28 high power density racks were studied, the maximum AFR is 2400CFM, and maximum temperature difference is 40 ^{o}C when the cold aisles at 15 ^{o}C, the cooling energy demand is 10%-15% lower than air –cooling system with fixed speed fan. A chiller or cooling tower is normally used to remove the heat returned from hot aisles to external environment. Temperature of water in chiller can be vary by system design, but researches [34] point out the typical supply and return water temperature range of 10 ^{o}C -13 ^{o}C and 15.5 ^{o}C -18.4 ^{o}C separately. Based on the statistic research of air-cooled cases, typical parameters of air-cooled system in DC was summarised by researchers [35, that paper] in table 2 below.

Table 2: The typical parameters of air-cooled system in DC

Parameter	*Value range*
Cold aisle supply temperature	10 °C -32 °C
Hot aisle return temperature	50 °C -60 °C
Temperature rise between server	10 °C -20 °C
Air flow rate per rack	200CFM-2500CFM
Chiller supply water	7 °C -10 °C
Chiller return water	35 °C

The proper air flow management in air-cooled DCs can significantly improve the cooling efficiency. The core strategy of air flow management is to minimize bypass air, which returns to the cooling units without performing cooling and the resultant recirculation and mixing of cool and hot air increasing equipment intake temperatures. A number of parameters will affect the air flow efficiency, such as width of hot and cold aisles, room height, distance between server rack`s top and ceiling [35]. The airflow recirculation, created by the turbulent mixing of hot and cold airs over the racks, was identified as the major cooling problem in air flow management designs. To overcome the effect of hot air recirculation, cooling unit air supply temperatures are frequently reduced or air flow volumes increased, which has an energy penalty. Addressing these issues will deliver more uniform equipment inlet temperatures and allow set points to be increased (with the associated energy savings) without the risk of equipment overheating. Thus, the space shape and racks arrangement need to be carefully designed, normally by the help of CFD simulation in recent successful cases.

Free cooling designs use cool ambient conditions, water and/or air, to meet part or all of the facilities cooling requirements hence compressor work for cooling is reduced or removed, which can result in significant energy reduction. As the updated generation of microprocessors have ability to work at as high as 100 °C [36], although most electronics thermal management researches consider 85 °C [37] as a safety set point and some DCs set the maximum temperature at 60 °C [38] to ensure other components` (memory and HDD) reliability for long-term operation, it is still far more higher that external air temperature in most regions, this lead the natural air cooling become a viable option. Using mechanical cooling only when the outside air temperatures become too high to cool datacentres is an effective strategy to make datacentres green. A typical free air cooling system involves air filters, dehumidification device air channel and fans, to catch particles, ensure the correct humidity levels and optimum air flow rate. DCs with free cooling design are investigated that about 25% and 35% of cooling energy need can be reduced compare to traditional case.

3.2 Water–cooled system and two-phase cooled system

Water-cooled system and two-phase cooled system normally exist in recent or new DCs, the reason is that newer DCs always housing high performance computing units with extremely high power and heat density, which cause lead to inefficiency by apply an air-cooled system alone. The single or two-phase cooled system with liquid coolant were developed to provide high cooling ability and energy efficiency by sending the coolant to heat source surface directly and enhancing the thermal conductivity between heat source and coolant. In a water-cooled system, the copper tube with cold plates are designed as close as possible to heat source components, such as microprocessor and memory, or joint together with component surface [39, 3]. The thermal conductivity (the ability of removal heat from component) can easily reach 200W/cm^2, which is 5 times higher than air-cooled system [39, 3]. Better conductivity and heat capacity lead to lower temperature rise across the system, typical temperature difference will be 10 °C between a server rack with a water flow rate of 0.7L/min, which means the input water can be as high as 75 °C to keep the heat source component below 85 °C [39]. The high temperature of return water provide high quality waste heat and high energy recovery efficiency, that means the need for chillers can be eliminated by recovered heat, thus reduce the energy consumption. According to a recent case [40], a DC equipped with water-cooled system to cooling the processor and memory, using circulated air to cooling the other components. The internal water loop brings to external coolant loop by heat exchanger, and eventually transfer to external air by a dry-cooler. Due to the major heat is removed by water, the size of air tunnels and fans can be can be significantly reduced. In that case, the proportion of cooling energy need to total energy need reduce from standard of 45% to 3.5% [41]. Besides, through control the temperature at a 60 °C -85 °C, the application of water-cooled system in server or rack level are able to increasing the processor`s performance by 33% [42]. Based on the statistic research of air-cooled cases, typical parameters of water-cooled system in DC was summarised by researchers [35] in table 3 below.

Table 3: The typical parameters of water-cooled system in DC

Parameter	*Value range*
Water supply to server	20 °C -60 °C(std), 70 °C -75 °C (max)
Water temp. rise over server	2 °C -5 °C
Water flow rate per rack	50-10 GPM
Temp. difference between water and heat source surface	5 °C -18 °C
Heat exchanger flow rate	5-10 GPM
Heat exchanger supply temp.	3 °C -5 °C above ambient

For the DCs with extremely high heat density, especially over 1Kw/cm^2, the two-phase cooled system is considered instead of water-cooled system. The application of two-phase cooled system can be found from the surface heat flow between 0.7 Kw/cm^2 to 27Kw/cm^2 [35] due to its high heat transfer efficiency from internal evaporation and huge effective heat exchange area given by micro-channel heat pipe. Compare to water-cooled system, benefited from high efficiency of heat absorption by coolant evaporation, the mass flow rate, facility size and pumping power demand for a typical two-phase cooling system is separately 4 times, 2 times and 10 times less than the water-cooled system for same server [43]. According to simulation [44], the microprocessor temperature can be 13 °C lower by using two-phase cooling than water-cooling with same pump power. Another advantage is that the temperature rise over microprocessors is far lower than water-cooled system, a case show that there is only 0.2 °C rise when coolant goes over a typical microprocessor, while the rise will be 2 °C by applying water-cooled system. Thus, the outlet temperature can reach as high as 80°C which is easy to drive the compressor and benefit for waste heat recovery. Based on the statistic research of air-cooled cases, typical parameters of two-phase cooled system in DC was summarised by researchers [35, that paper] in table 4 below.

Table 4: The typical parameters of two-phase cooled system in DC

Parameter	*Value range*
Coolant supply to evaporator	60 °C(std), 70 °C -75 °C (max)
Coolant exit from evaporator	62 °C (std), 75 °C -80 °C (max)
Condenser cooling fluid inlet	30 °C
Condenser cooling fluid outlet	45 °C -90 °C

3.3 DC waste heat recovery

To recovery and reuse the removed heat form servers, some techniques are developed and applied to DCs. To meet the characteristics of waste heat from DC, the techniques must able to operate for mid-low temperature and high volume waster heat. The market available heat recovery and reuse techniques for DCs are list and discussed as follow.

- Building heating or hot water production
  The most common recovery method for low temperature heat is in domestic heating or hot water system. The waste heat can be used for space heating for DC itself firstly, and then provide the remaining heat to other building users. The range are vary, depending on the size of DC and other building`s heating demand. A calculation [45] shows that by converting the recovered heat to the normal energy price, an annual $280-$325 will be payback per server by providing heating and hot water to an apartment or primary school. When the temperature of waste heat is slightly higher, such as recycled from water-cooling system, district heating can be considered. The heat can be transport in form of stream through stream tubes and delivered to a wide range.

- Power plant co-location
  The power plant co-location strategy can be considered if high temperature waste heat can be recovered. Two –phase cooling system with outlet temperature above 65 °C -70 °C are able to satisfy the system requirement [46]. The recovered heat will be used in the pre-treatment (pre-heat) process of input water of power plant`s boiler which will operate in Rankine cycle to generate power. The pre-heated water will reduce the energy need from boiler, therefore, contribute the overall fossil fuels consumption. A simulation shows that the wasted heat form a super DC housing 100,000 servers will improving 2.2% boiler efficiency of a 175MW power plant by reheat its input water, which will lead to a $46M total saving including the saving from coal consumption and carbon emission tax [47].

- Absorption cooling

  The absorption cooling system are used to replace the traditional vapor compression refrigeration system in some new DCs to provide constant cooling output. The main benefit for this replacement is that the absorption refrigeration system can be directly driven by DC waste heat. A typical DC absorption cooling system is studied previously [48], a 10 ton single effect lithium bromide-water absorption cooling unit was driven by the server waste heat of studied DC with two-phase cooling system, cooling requirement can be fully satisfied and the excess waste heat will be stored in a water-based heat storage. When 50.2 Kw waste heat can be provided at 88 ^{o}C, 35.2Kw cooling can be produced by the absorption cooling unit, which means a 0.7 COP. The available temperature range of waste heat for absorption cooling system is 70 ^{o}C - 90 ^{o}C that can be provided by most DCs equipped with water-cooled or two-phase cooled system.

- Electricity generation

  The DC waste heat are used to generate power by mechanical or electronic systems. Organic rankine cycle power generation unit is a simply mechanical system that works similar as steam rankine cycle by using lower boiling point organic fluids. It`s low boiling point brings the adoptability of DC waste heat. A typical rankine cycle power generation unit are able to operate with waste heat at temperature 65 ^{o}C or higher, the overall efficiency of power generation are vary form 5%-20% depend on the temperature of waste heat and working fluid [49]. Due to the limitation of boiling point, rankine cycle unit can only reuse the waste heat form water or two-phase cooling system, waste heat from air-cooled system are not able to be reused without additional heat source.

  The thermoelectric technology is adopted in DCs` waste heat reuse, which are able to convert heat to electricity directly. The thermoelectric modules are designed based on Seebek effect [50], by apply temperature to two different materials with different conduction energy band levels respectively, certain voltage are able to be generated. The hot side of a typical thermoelectric module reaches 10 ^{o}C -175 ^{o}C by using DC waste heat while up to 70 ^{o}C temperature difference are managed. Although the size of thermoelectric module are small and compact, only 2%-5% efficiency can be reached, and the cost of thermoelectric module is high as well, these disadvantage severely limit its application.

  Apart from heat-electricity converting methods, other energy can be recovery from DC as well, using techniques such as piezoelectric generation. The piezoelectric generation unit always installed in the air outlet of DC air-cooled system, converting the mechanical energy, such as vibration and gas expansion near air supply, into small amount of electricity. Although the overall efficacy is very low less than 1%), this electricity can be used to drive LED lights, fans or indicators that hard to wiring from main power supply, thus benefit for energy saving and weak-current wiring simplification.

4. CONCLUSION

This paper comprehensively reviewed the DC energy efficiency metric, code and techniques. In recent years, the common PUE reduced from 3.0 to 1.6, target of of lower PUE is established in many counties for new build DC as well. Great improvement of DC building service system energy efficiency has been achieved, operation temperature can be keep at 60 ^{o}C -80 ^{o}C by air-cooled, water-cooled or two-phase cooled system, meanwhile as high as 70% of waste heat are able to be recovered in different ways. Although codes limitation become higher and such improvement of the DC efficiency has been made, the research of energy efficiency of DC`s building service system are still not as practical as other building types, such as residential of commercial building. Two shortcoming still exist in DC`s building service system researches, which are discussed below.

- The current using metrics and codes have no interactive relationship with sustainability. Although the current or improved metrics, such as PUE, DCiE and pPUE, are able to reflect the overhead energy consumption by DC building service systems, but there is no relationship established with sustainability. All these metric are based on the calculation of electricity instead of energy, thus, the energy grade are not be involved in consideration. A DC with cooling system using high-grade energy (e.g. electricity) while proved low-grade energy (e.g. low temperature water) to nearby resident by heat recovery will certified same PUE with the one using same amount of low-grade energy for cooling while provide high-grade energy by heat recovery, the last one is more energy efficient and practical in real world, which cannot be reflect by PUE their PUE value.

The factor of external climate effect is not involved in current metric as well. A DC located in Shanghai (average temperature in summer is 27.8 °C) with PUE 2.0 is not efficient than anther DC in Stockholm (average temperature in summer is 15°C) with PUE of 1.4 in term of definition of current metrics. But if the consideration of climate difference is involved, the first DC might be more sustainable and more energy saving design is adopted in it to achieve that PUE in such a hot climate condition.

Current DC efficiency code are based on the calculation of metrics, thus, although the requirements from codes are higher and higher, sustainability factor are still not been defined in a proper way.

- Lack of comprehensive economic study of DC energy efficiency techniques. The cost of DC`s building service system are vary, depending on its energy efficiency techniques, moreover, similar techniques will give different cost and efficiency when applied to devised servers. For instance, same type of water based cooling system will require different investment and maintenance cost while apply it to servers with different heat density. Although cost researches can be found in the area of high efficiency DC cooling, ventilation or lighting device, but most of them are alone without combined consideration of weather condition, payback and possible changing with server upgrading. Therefore, more comprehensive study is required, involving the high energy efficacy technique's` initial investment, extension ability and cost with server upgrading, operation and maintenance cost, payback and their interaction. Besides, the economic feature of different system type need to be compared and a practical economic methodology of DC building service system choosing and sizing should be established in near future.

5. REFERENCES

[1] European Commission. Code of conduction data centres energy efficiency-version 2.0. Ispra,Italy ;November 20, 2009.

[2] CHO, J., Kim, B.S., Evaluation of air management system's thermal performance for superior cooling efficiency in high density data centers. Energy Build 2011;43:2145–55.

[3] SHEHABI, A., Masanet, E., Price, H., Horvath, A., Nazar off WW. Data center design and location: consequences for electricity use and green house-gas emissions. Build Environ2011;46:990–8.

[4] http://www.datacentermap.com/western-europe/, [accessed on 12/12/2014]

[5] Analytics Press. Growth in data center electricity use 2005 to 2010, Available at http://www.analyticspress.com/datacenters.html⟩ [August1,2011].

[6] EUROPEAN COMMISSION Institute for Energy, Code of Conduct on Data Centres Energy Efficiency 1.0, 30 October 2008.

[7] GU, L. J., Zhou, F. Q., and Meng, H., Research on Data Center Energy Consumption and Energy Efficiency Level, Energy of China, vol. 32, no. 11, pp. 42–45, 2010.

[8] BRUNSCHWILER, T., Smith B, Ruetsche E, Michel B. Toward zero-emission data centers through direct reuse of thermal energy. IBM J Res Dev 2009;53(3):1–13 (11).

[9] EBRAHIMI K, Jones GF, Fleischer A S. A review of data center cooling technology, operating conditions and the corresponding ow-grade waste heat recovery opportunities. Renew Sustain Energy Rev 2014; 31:622–38.

[10] JOHNSON, P., Marker, T., Data center energy efficiency product profile. Pitt &Sherry, Report to Equipment Energy Efficiency Committee (E3) of the Australian Government Department of the Environment, Water, Heritage and the Arts(DEWHA);2009.

[11] MEIJER G. I. Cooling energy-hungry data centers. Science 2010; 328:318–9.

[12] The Green Guide, "Green Grid Metrics: Describing Data Center Power Efficiency", 2007

[13] The Green Grid, " The Green Grid Data Center Power Efficiency Metrics: PUE and DCiE", 2008

[14] GREENBERG, S., E. Mills, B. Tschudi, P. Rumsey, and B. Myatt. (2006). "Best Practices for Data Centers: Results from Benchmarking 22 Data Centers."

[15] PATTERSON, M.K., Pratt, A., Kumar, P., "From UPS to Silicon, an End-to-End Evaluation of Data Center Efficiency", Feb 2006

[16] BELADY, C., "How to Minimize Data Center Utility Bills," September, 2006

[17] RASMUSSEN, N. (2005). Electrical efficiency modeling for data centers. Schneider Electric, Data Center Science Center, London, UK

[18] PELLEY, S., Meisner, D., Wenisch, T.F., & VanGilder, J.W. (2009). Understanding and abstracting total data center power. In Proceedings of the Workshop on Energy-Efficient Design, Austin, TX.

[19] RASMUSSEN, N. (2005). Guidelines for specification of data center power density. Schneider Electric, Data Center Science Center, London, UK

[20] LONGBOTTOM, C. (2012). Data centre cases where PUE or power usage effectiveness doesn't work. Retrieved on 1st Jun 2015 from: http://www.computerweekly.com/tip/Data-centre-cases-where-PUE-or-power-usage-effectiveness-doesnt-work.

[21] AZEVEDO, D., Blackburn, M., Cooley, J., & Patterson, M. (2011). Data center efficiency-PUE, Partial PUE, ERE, DCcE. The Green Grid, Beaverton, OR

[23] YUVENTI, J. & Mehdizadeh, R., (2013) A Critical Analysis of Power Usage Effectiveness and Its Use as Data Center Energy Sustainability Metrics, CIFE Working Paper at WP131, February 2013, STANFORD UNIVERSITY

[23] BELADY, C., (2008) GREEN GRID DATA CENTER POWER EFFICIENCY METRICS: PUE AND DCIE, Microsoft Cooperation.

[24] US Department of Energy, 2015 International Energy Conservation Code, (2015), the world code council,

[25] ASHRAE, The ASHRAE Advanced Energy Design Guides(2014)

[26] U.S. codes, 42 U.S.C. 17112 - ENERGY EFFICIENCY FOR DATA CENTER BUILDINGS, United States Code, 2006 Edition, Supplement 4, Title 42 - THE PUBLIC HEALTH AND WELFARE

[27] Code of Conduct on Data Centres Energy Efficiency (2010), EC, Institute for Energy, Renewable Energies Unit

[28] 2014 Best Practices, The EU Code of Conduct on Data Centres, EC, Institute for Energy, Renewable Energies Unit

[29] Code of The norm of Data centre Unit Energy Usage Effectiveness, China Ministry of Industry and Information Technology

[30] PATEL, C.D. A vision of energy aware computing from chips to data centers. In: Proceedings of ISMME . Japan; Dec 1– 3, 2003.

[31] BASH, C.E, Patel C.D., Sharma RK. Efficient thermal management of data centers– immediate and long-term research needs. HVAC&R Res 20 03;9(2):137– 52.

[32] SCHMIDT, R.R, Cruz E.E., Iyengar M.K., Challenges of data center thermal management. IBM J Res Dev 20 05;49(4/5):709– 23.

[33] RAMBO, J, Joshi Y. Modeling of data center airflow and heat transfer: state of the art and future trends. Distrib Parallel Database 2007;21:193–225 .

[34] Maximizing cooling efficiency in a currently maintainable and fault tolerant data center. San Jose (CA, USA): Silicon Valley Leadership Group; 2009.

[35] RAMBO, J., Joshi Y., Modeling of data center airflow and heat transfer: state of the art and future trends. Distrib Parallel Database 20 07;21:193–225 .

[36] SCHMIDT, R.R., Notohardjono BD. High-end server low-temperature cooling. IBM J Res Dev 20 02;46(6):739 – 51.

[37] PATEL, C.D., A vision of energy aware computing from chips to data centers. In: Proceedings of ISMME 20 03. Tsuchiura, Japan; Dec 1– 3, 2003

[38] 600 GByte,3.5″ ,15,000rpm disk drive specification – 6Gb SAS-2 interface. Sun Microsystems, Inc.

[39] BRUNSCHWILER, T., Smith B , Ruetsch E., Michel B., Toward zero-emission data centers through direct reuse of thermal energy. IBM J Re s Dev 20 09;53(3):1 –13 (11).

[40] IYENGAR, M., David, M., Parida, P., Kamath, V., Kochuparambil, B., Graybill, D., Serverliquid cooling with chiller-less data center design to enable energy savings.In: Proceedings of the 28th IEEE SEMI-THERM symposium. San Jose (CA, USA);18–22 March ,

[41] DAVID M.P., Iyengar, M., Parida, P., Simons, R., Schultz, M., Schmidt, R., et al. Experimental characterization of an energy effi cient chiller-less data center test facility with warm water cooled servers. In: Proceedings of the 28th IEEE SEMI-THERM symposium. San Jose (CA , USA); March 18 – 22, 2012. p. 232– 7.

[42] ELLSWORTH, M.J., Iyengar, M. K., Energy efficiency analyses and comparison of air and water cooled high-performance servers. In: Proceedings of IPACK

[43] HANNEM, an n R , Marsala, J., Pitasi, M., Pumped liquid multiphase cooling . In: Proceedings of IMECE00 4 .Anheim (CA , USA); November 13 –19,2004.p.469 –73

[44] THOME, J.R., Bruch, A., Refrigerated cooling of microprocessors with micro-evaporation heat sink s: new developments and energy prospects for green data centers. IOR Proceedings, vol. 105; 20 08/9.

[46] LIU, J., Goraczko, M., James, S., Belady, C., Lu, J., Whitehouse, K.. The data furnace: heating up with cloud computing. In: Proceedings of 3rd USENIX work shop on hot topics in cloud computing. Portland (OR, USA); June 14 – 15, 2 0 11.

[47] Waste heat recovery: technology and opportunities in US industry. US Department of Energy; 2008.

MARCINICHEN, J.B., Olivier, J.A., Thome, J.R., On-chip two-phase cooling of data- centers: cooling systems and energy recovery evaluation. ApplThermEng 2012;41:36– 51.

[48] HAYWOOD, A., Sherbeck, J., Phelan, P., Varsamopoulos, G., Gupta, S.K.S., A sustain-able data center with heat-activated cooling. In: Proceedings of ITHERM 2010, 12th intersociety conference. Las Vegas (NV, USA); June 2– 5, 2010.

[49] VÉLEZ, F., Segovia, J.J., Martín, M.C., Antolín, G., Chejne, F., Quijano, A., A technical, economical and market review of organic Rankine cycles for the conversion of low-grade heat for power generation. Renew Sustain Energy Rev 2012;16 (6):4175 – 89.

[50] MARTÍN-GONZÁLEZ, M., Caballero-Calero, O., Díaz-Chao, P., Nano engineering thermoelectrics for 21st century: energy harvesting and other trends in the field. Renew Sustain Energy Rev 2013;24:288– 305

206: Transportation energy consumption and emissions - a view from City of Indonesia

IWAN SUKARNO[1], HIROSHI MATSUMOTO[2]

1Architecture and Civil Engineering, Toyohashi University of Technology, Japan, iwan_sukarno81@yahoo.com
2 Architecture and Civil Engineering, Toyohashi University of Technology, Japan, matsu@tut.ace.jp

The transportation sector in a city is one of the fundamental aspects of social – economic system which includes moving people and trade in an increasingly globalized world, as well as for improving standards of living. No doubt that transportation sector cannot be separated from the fuel consumption. Every country applied different policies and scenarios to introduce alternative fuel and technology to reduce the road transportation that is dependent on fossil fuel and the environmental impacts. However, in the last decade, global energy consumption in the transport sector was increased continuously. In the city context, transportation sector should be put on the long term urban planning toward sustainable development.

The purpose of this study is to investigate the energy consumption and road emissions of the transportation sector to predict the future energy consumption and emissions interactions. A system dynamics model for transportation sector was developed in this study to model the transportation energy consumption and road emission trends. The basic data on energy consumption, transportation data and emissions factor were used as the basic input parameters. Results show that total fuel consumption and GHG emission in Padang road transport is predicted 65 times in 2050 compared to 2013 levels. Increase of private vehicles plays a very essential role in road emissions reduction activities of Padang. The modelling results also show that reducing of private vehicles and integrated public transportation has reduced the fuel consumption and GHG emission to about 34% in 2050. All these results will provide essential information and can be used for policy maker to meet challenges of decision making to support the urban development process.

Keywords: Transportation, Energy Consumption, Road Emission, System Dynamic

1. INTRODUCTION

In the last decades, the energy consumption and emission become a serious concern for researchers and policy maker and strategic options have to be taken to face this situation. Data under the International Energy Outlook 2011 shows that world energy consumption of fossil fuels increase from 354 quadrillion Btu in 1990 to 770 quadrillion Btu in 2035 (EIA, 2011). Increase in energy consumption is especially in Non-OECD countries such as Malaysia, Singapore, Brunei, and 40 other countries, including Indonesia. In the last three years, transportation sector experienced the largest annual growth rate reached 6.45% per year compared to the other sector (IEO, 2013).

From the total energy consumption, 30% of that was consumed in the transportation sector. Almost all energy used in the transportation sector (97% of total transportation sector) using oil fuel (ESDM, 2012). In the transportation sector, road transports contribute more than 90% of total oil consumption, and is the main responsibility of an increase concentration of Greenhouse gases (GHG). The road transportation unit includes light-duty vehicles, such as automobiles, sport utility vehicles, minivans, small trucks, and motorbikes, as well as heavy-duty vehicles such as large trucks used for moving freight and buses for passenger travel (EIA, 2011). Greenhouse gas emissions from transportation sources include carbon dioxide (CO2), methane (CH4), nitrous oxide (N2O), carbon monoxide (CO), hydrocarbon (HC) and particulate matter (PM) (Azhaginiyal, 2014). In 2010, Indonesia`s road transport produce 91% of total GHG (Figure 1).

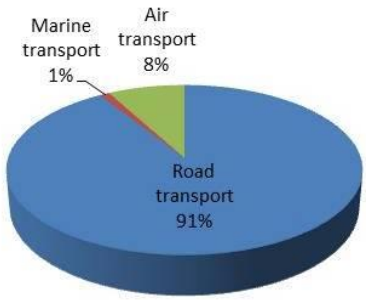

Figure 1: Share of GHG emissions by Transportation mode (ESDM, 2012)

Moreover, as mentioned above, the transportation sector is set to grow over 6% per annum on the back of Indonesia economic rising and it will lead increasing of GHG emission from road transportation. According to the Transport department`s official report, the total of vehicles continuously increased almost 90 million in 2012 (Figure 2). Motorcycles population zoomed to 77 million in 2012 from 13 million in 2000 while the number of passenger car jumped to 10 million in 2012 from 3 million in 2000.

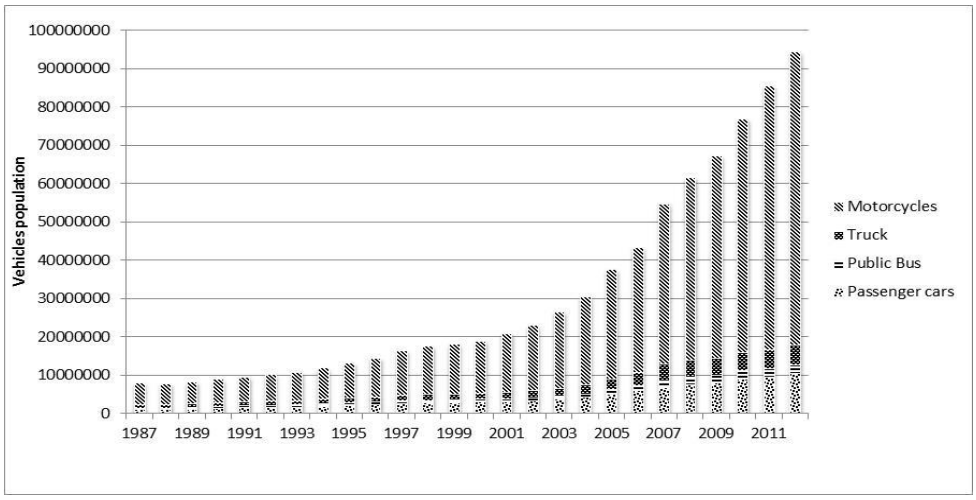

Figure 2: Vehicle population in Indonesia

Globally, the growth of the transportation sector, mainly driven by road transportation will dependently on the availability of oil. In fact that from total energy consumption, 58% still comes from fossil source and it is

quite alarming that fossil-based energy reserve in Indonesia was estimated only for 18-30 years (ESDM, 2012). As a result, the transportation sector is one of the main keys to decrease the GHG emissions driven by oil consumption. Hence, collective effort and constructive policy are needed to face these challenges.

Based on that condition, the aim of these studies is:

a. To understand the current condition of Transportation demand and supply.
b. To acquire data on energy consumption and emissions in road transportation.
c. To estimate and analyse the future trend of energy and emissions through a dynamic model of the transportation sector
d. To investigate the potential improvement to achieve the sustainability of energy and transportation.

2. METHODOLOGY AND DATA

A transportation model has been developed to estimate energy consumption and emission in a city of Indonesia. Energy consumption and road transport emission between 2013 and 2050 have been estimated using this model. Data related to transport vehicles, energy usage in the basic year has been collected and simulated to find the future energy demand. The level of road emissions from the present year and future has also been identified. Three scenarios have been designed to represent the present and the future plan of the development strategies for Indonesia`s road transport sector in term of energy and road emissions. A comparison of the results has been carried out to determine the advantages of the policy measures to be adopted.

2.1. Overview of the study area

Padang is the largest city on the western coast of Sumatera island, and the capital city of West Sumatera province, Indonesia. Covers an area of about 694.96 km^2 and has a population of about 876,678 (Padang yearbook, 2013). Padang consists of 11 districts, Bungus, East Padang, Koto Tangah, Kuranji, Lubuk Begalung, Lubuk Kilangan, Nanggalo, North Padang, Pauh, South Padang, and West Padang (Table 1 and Figure 3).

Table 1. Details of the case study city

Aspects	Information
Land area	694.96(km^2)
Number of sub districts	11
Population (2013)	876,678 (Person)
Population density	1218.4(Person/km^2)
GDP (2013)	12,792.18 million Rupiah
GDP per capita (2013)	32.50 billion Rupiah

Sources :Padang Yearbook, 2013

Figure 3: Case Study (Padang, Indonesia)

Similar of another city in developing countries, Padang is facing rapid transformation, with a growing population, business, and also increasing of transportation vehicles. Padang is the largest city among the other big cities such as Jakarta, Medan, Makassar and Surabaya (Table 2).

Table 2: City sizes

Cities	Size area (km²)	Population (2013)
Jakarta	649.81	9,603,417
Padang	694.96	876,678
Medan	265.10	2,602,612
Makassar	199.26	1,612,413
Surabaya	374.80	2,719,859

After the earthquake in 2009, the local government attention to continue recovery in all sectors of social-economic system, accelerated development of housing, health and educational facilities, public infrastructure and improvement of urban transportation systems. To support the recovery and development process, this city should have a comprehensive study of urban energy consumption. This study can be integrated with the long-term urban planning toward sustainable development.

Related to the transportation sector, according to the Indonesian transportation department, the ratio of private vehicles to public vehicles is 98% : 2%. During the period 2000-2013, the growth of private vehicles reaches to 12% per year while public transport only 2% per year and continues decreased. Motorcycles showed the fastest growth with ownership per 1000 population is 250 respectively. These increases in vehicle population and fuel consumption have resulted in an increase of GHG emissions that become serious concerns of government. According to Environment Impact Control (BAPEDALDA) reported that 70% of air pollution was caused by motor vehicles, 20% by industrial activities, and the other from garbage and cigarettes.

2.2. Causal map

In order to understand the relationships among the various variables in the transportation sector and road emissions, a causal lops has been developed (Figure 4).

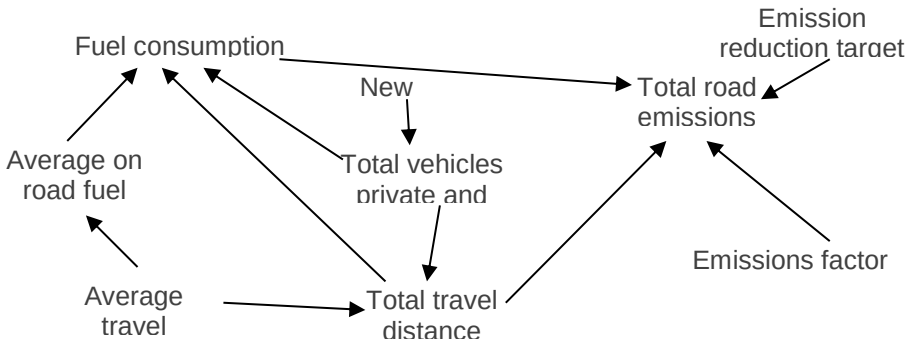

Figure 4: Causal loop of transportation sector

The main driver of fuel consumption is represented by the total kilometres of travel distances and vehicle population. The strong link between road emissions and fuel consumptions provide an important description on the growth of the transportation demand.

In this study, a system dynamic modelling was developed for estimating and prediction of transportation and emissions trends in Padang. In light of these study goals, the model was designed as two models, i.e., transportation model and emission model.

2.3. Transportation Sector

As described above, Padang as the capital city as well as areas with high population density compared to other regions. One of the effects which is quite alarming today is the issue of transportation. The high numbers of vehicles on the road are not comparable to the growth of road infrastructure. Congestion, fuel consumption increased, and air pollution becomes a critical issue to immediately look for the solution. The Number of private vehicles and public vehicles was estimated from the historical data of Padang City from 1994 to 2013. Travel distance by public transportation was estimated by multiplying the average distance by the average trip per day. Fuel consumption of vehicles was estimated from the standard fuel consumption of different type vehicles. Table 3 shows an assumption that is used in the calculation of energy consumption.

Table 3: Average Fuel Consumption

Type of vehicle	Average Travel Distance (km/day)	Fuel Consumption (km/l)	Fuel Consumption (l/vehicles/year)
Car	18	12	548
Motorcycle	18	43.85	150
Microbus (petrol)	100	12	3,042
Buses (diesel)	126	10	4,599
Taxi	24	12	730

2.4. Emissions Sector

With respect to the emissions sector, the data related GHG emissions and the other urban pollutants from fuel combustion were calculated based on fuel consumption and kilometre travel distance by different transport modes. Emission factors for tracing GHG gas emission from various types of vehicles was estimated from the EURO emissions standard as shown in Table 4.

Table 4: Emission Factors (g/km)

Pollutant/ vehicle	Car	Motorcycle	Auto Rickshaw	Microbus	Bus	Taxi
CO2	223.6	26.6	26.6[a]	515.2	515.2	208.3
CO	2.2[a]	2.2[a]	5.5[a]	4[a]	3.6	0.9
NOx	0.2	0.19	0.3[a]	12	12	0.5
CH4	0.17	0.18	0.18	0.09	0.09	0.01
SO2	0.053	0.013	0.029	1.42	1.42	10.3
PM	0.03	0.05	0.2	0.56	0.56	0.07
HC	0.25	1.42	1[a]	0.87	0.87	0.13

Source: Ramachandra and Shetmala, 2009

[a] Ministry of environment regulation, No.04/2009

3. MODEL DEVELOPMENT

The system dynamic model for Padang transportation and emissions has been developed based on a causal loop diagram (Figure 5). The models were divided into three parts which consist of private transport, public transport and vehicle emissions. The various parameters considered in this model are growth rate (GR), fuel consumption (FC), average distance (AD), fuel per kilometre (Fkl), total vehicles by different transport modes, split mode between private and public transport, total travel distance (TTD), and various emission factors.

Transportation and emissions models provide an overview of the development of the vehicle population and GHG emissions. The transportation sector taken into account was commonly private passenger car (4-7 seats), motorcycles, and public transportation (city bus, microbus, taxi). The vehicle growth was assumed from the past trend using government official report by the Padang statistical agency. In addition, the vehicle population was verified using the real data of Padang vehicles population from 2001 to 2013 by Padang Statistical Yearbook 2014.

In this transportation and GHG emissions model, it was assumed that the future energy consumption and GHG pollution trend would mainly be affected by vehicles growth, emissions standard, and split mode between private and public uses as shown in Table 5. Three test scenarios were carried out on this model to investigate and predict the future transportation trends and GHG emissions by fuel exhausting. Scenario 1 is called a reference scenario whereby it was assumed that the simulation runs based on the existing trend of growth rate of vehicles and transportation splits mode. Scenarios 2 and 3, it was assumed that starting year 2020 it has major change in several conditions. Prior to 2020, the trends would be same as scenario 1, and based on the implementation of Transport Master Plan of Padang 2030 some of major improvement on the public transportation system would be taking place on/after 2020. Detailed overview of the test scenarios and the stock - flow diagram of transportation and emission mode is given in Table 5 and Figure 5.

Table 5: Detail of simulation scenarios

Variables	Scenario 1	Scenario 2	Scenario 3
	Normal Growth (reference scenario)	*Partial effort*	*Integrated transportation*
Private vehicles growth	continues increase: 12% p.a	continues increase: 12% p.a	starting 2020, level gradually decreases to 8%
Public Transport growth	gradually decreases to1% p.a (bus type) and gradually increase to 2% p.a (microbus type)	From 2020 level gradually increase to 1% (Bus rapid transit)	From 2020 level gradually increase to 3% p.a (integrated transportation (Bus rapid transit, rail transport)
Emissions standard	Euro II	Euro III	Euro III
split mode between private and public transportation	53:47 (based on 2010 condition)	starting 2020 level of public transportation gradual increase to 50%	from 2020, level gradual increase to 70%

1. The above assumptions of future trends are adapted from Transport Master Plan of Padang 2030, and the authors` own rationales.
2. Emission standard is adopted from Ministry of Environment Regulation.

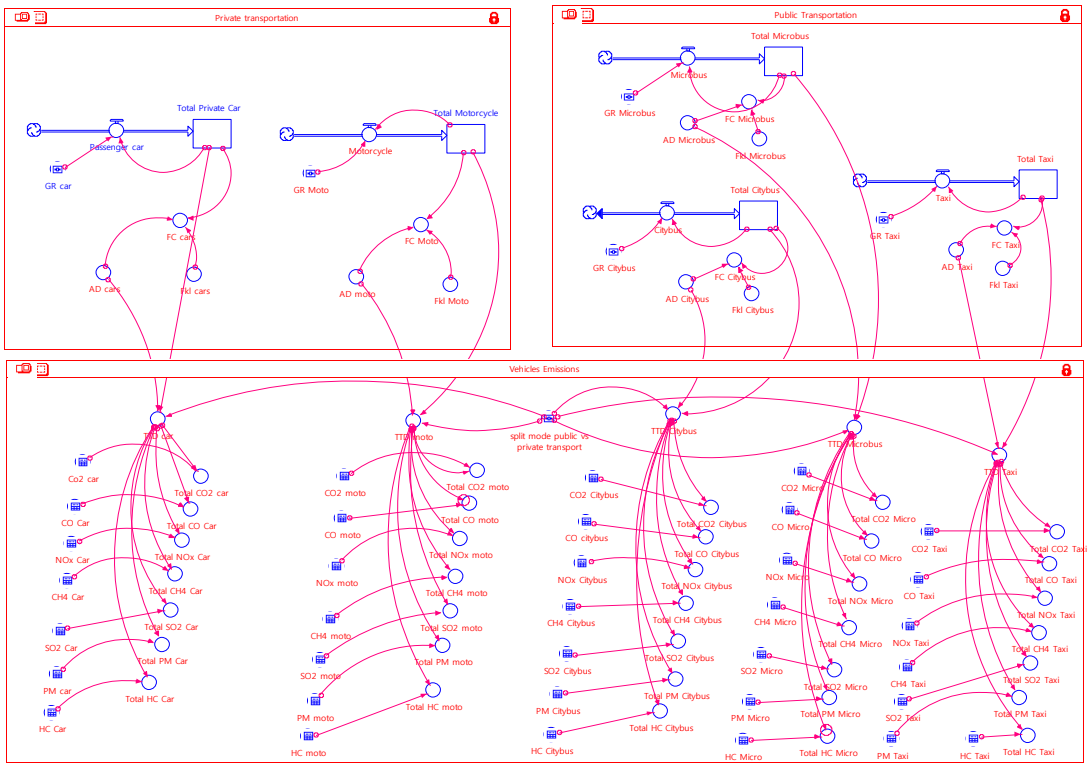

Figure 5: The stock - flow diagram of transportation and emissions model

4. RESULT AND DISCUSSION

4.1 Reference Scenario

In the reference scenario, the existing growth rate trend of various type vehicles still continues till the year 2050 without any major interruption from the present policy. A part of public transportation, the growth rate of city bus gradually decreases 1% per year, while microbus continuously increase 2 % per year. Decrease of city bus was caused by decreasing passenger using city bus and move to other vehicles such as motorcycle or microbus. This phenomenon can be seen from General Plan for Road Transport Network (RUJTJ) Padang City Year 2004-2013 report (Figure 6).

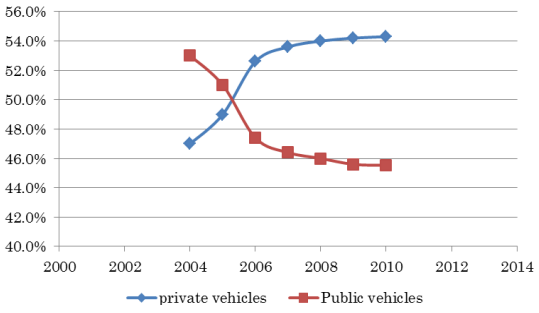

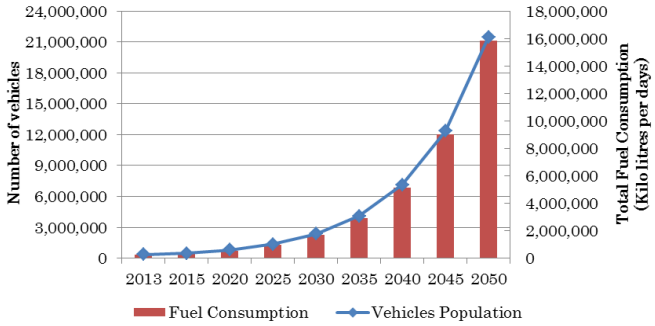

Figure 6: Trend of transportation modes *Figure 7: Scenario 1- vehicles population and Fuel Consumption*

Based on the existing growth rate and with the split mode between private vehicles and public vehicles have been taken as 53:47, the number of vehicles, fuel consumed by each transport mode and the corresponding emissions level have been simulated as shown in Figure 7. Due to the exponential growth of vehicles population and fuel consumption, road emissions in 2050 is more than 65 times of 2013 level (Table 6)

Table 6: Scenario 1- Total GHG emissions from road transport (Kg/km)

Vehicles type	2013							2050						
	CO_2	CH_4	CO	HC	Nox	PM	SO_2	CO_2	CH_4	CO	HC	Nox	PM	SO_2
City bus	4,424	0.8	30.9	7.5	103	4.8	12.2	3,050	0.5	21.3	5.2	71	3.3	8.4
Microbus	50,850	8.9	395	85.9	1,184	55.3	140.2	105,803	18.5	821	178.7	2,464	115.0	291.6
Taxi	1,115	0.8	11.0	1.2	1.0	0.1	0.3	1,611	1.2	15.9	1.8	1.4	0.2	0.4
Car	170,652	130	1,679	191	153	22.9	40.4	4,138,954	3,147	40,723	4,628	3,702	555.3	981.1
Motorcycle	74,860	507	6,191	5,403	535	141	37	4,958,141	33,551	410,072	357,881	35,415	9,320	2,423

4.2 Overall Simulation

Figures 8 and 9 illustrate the vehicle population of private and public vehicles.

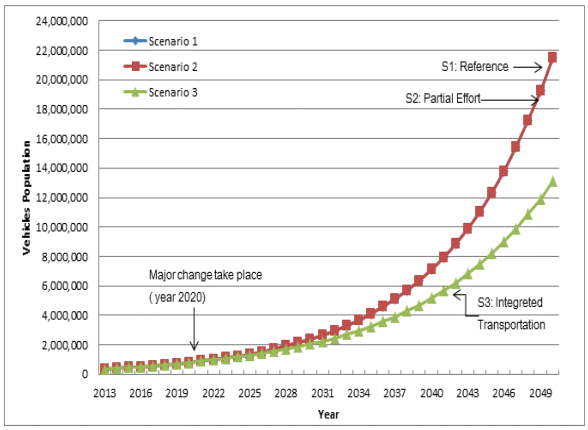

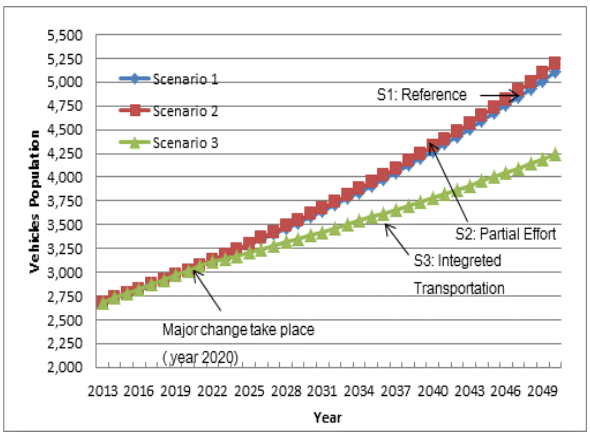

Figure 8: Private vehicle population *Figure 9: Public vehicle population*

As explained before, the major changes in the scenarios 2 and 3 were made in year 2020. Hence, overall results are same till 2020 as shown in the figure above. Due to the various change starting from year 2020 such as vehicle growth rate, implemented of rail transport and split mode transportation, several results of scenarios were seen after year 2020. Under the reference scenario (S1), both of vehicles population (private and public) experience a steady increase until year 2050. A part of private vehicles, the number of motorcycles is more than 66 times of 2013 level while passenger car only 24 times of 2013 level. With partial effort by implementing the bus rapid transit (BRT) the number of private vehicles stills same with the reference scenario. Slight increase of the public transportation showed in this scenario due to the increase of the city bus. According to the master plan of Padang transportation 2010-2030, implementation of BRT is one of the alternative solutions to decrease the private transportation usage. In the scenario 3 with integrated transportation between BRT, and rail transport, generally the total of public transportation is decreased due to the decrease of microbus (7 passengers). With integrated of mass transportation such as BRT and train, lead to the reduction of microbus and private vehicles. Under scenario 3 micro bus can be pressed 30% of current condition of 2050.

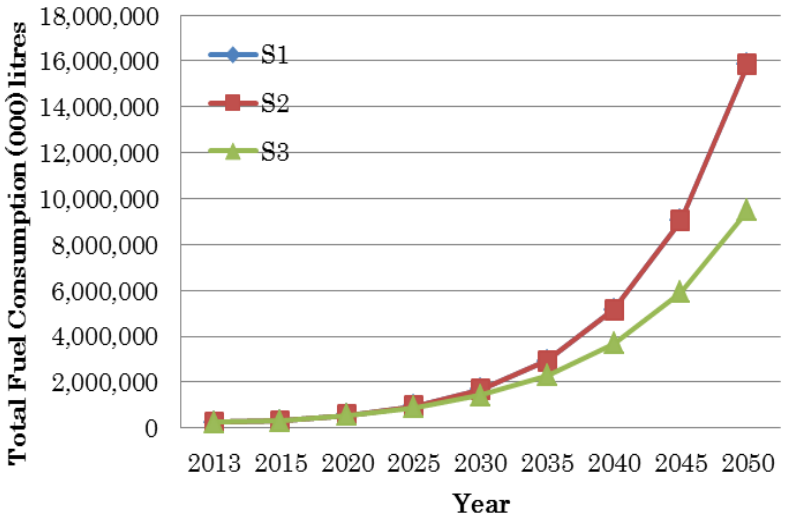

Figure 10: Public vehicles population

In terms of fuel consumption, the simulation result can be shown in Figure 10. In Scenarios 1 and 2 the total fuel consumption almost has same pattern due to a partial effort on the scenarios. Even though in Scenario 2 the population city bus was made in 2020 growth up to 1% per year, however the microbus also getting decrease in the same level. The Better result is shown in Scenario 3. The total fuel consumption in 2050 is successfully suppressed 36 times of 2013 level in consequence of integrated public transportation.

With an integration of public transportation in 2020, the concomitant decrease in road emissions level of GHG emissions from vehicles can be observed in Table 7. Emission level of vehicles under scenario 3 has reduced to about 34% and 17% in consideration with Scenario 1 and 2 respectively. The important point of these results is the motorcycle emissions. From these results, it can be concluded that the reduction of private vehicles and integrated public transportation are very significant in decreasing GHG emission from road transport. Presently, about 70% of GHG pollutant from road transport was caused by motorcycle.

Table 7: GHG Emissions of Scenario 3- year 2050 (Kg/day)

Vehicles type	CO_2	CH_4	CO	HC	Nox	PM	SO_2
City bus	6,140	1.1	43	10	143	7	17
Microbus	50,750	9	394	86	1,182	55	140
Taxi	1,028	0.8	10	1.1	0.9	0.1	0.2
Car	4,223,145	3,211	37,774	4,722	3,777	567	1,001
Motorcycle	3,883,347	26,278	291,981	43,797	21,899	7,300	1,898

Thus from the overall results it has been found that achieving a split mode 70:30 between private and public transportation of giving good results in connection with fuel consumption and GHG emissions. But in fact, that to achieve this scenario at the same time is also not an easy way. Hence, these elements should be

prioritized in the futuristic urban energy study and integrated with the long-term urban planning toward sustainable development.

5. LIMITATION OF THE MODEL

The main purpose of this model is to capture the overview of the energy consumption and emissions trend from road transportation rather than detailed modeling of each sector, therefore various simplifications had been made in this model.

1. The fuel consumption and GHG pollutant only calculated by common road transportation as mentioned in these models.
2. In this model, it was assumed that future energy consumption and GHG emissions trends from road transport mainly be affected by five general road vehicles as used in this model. In fact, there are several other vehicle types that exclude from this model due to the lack of the official data, such as medium truck, three wheeled motorcycle and private bus.

Even though there are limitations in the model, the current results are believed to be sufficient to reveal the transportation energy consumption and GHG emissions. However , the present model will be improved in the further study.

6. CONCLUSIONS

In order to project the transportation and GHG emission from the road sector in Padang over 2013 to 2050, an integrated dynamic model was developed under three different scenarios. Although it was a basic model with various limitations as mentioned above, it provides to capture the energy consumption and GHG emissions trends. The results show that Padang in the small scope is to be confronted with a heavy burden of fuel consumption and GHG emissions, which will need serious concern for decreasing energy consumption and GHG emissions in the future. Particularly, with the existing vehicles growth trends, the total energy consumption and GHG emissions only from road transportation is predicted to be 65 times higher than that of 2013. From the above test scenarios, the main driving forces of the road fuel consumption and emissions is from private vehicle which are passenger car and motorcycle. Hence, these results should be prioritized in the future context to reduce private vehicle usage and move to public transportation. Despite it is difficult to force society in the case of private vehicle ownership. Nevertheless, integrated public transportation is one of the key points to press the fuel consumption and GHG emissions from road transport.

7. REFERENCES

Ministry of Mineral Resources. Assessment of Greenhouse Emissions: Transport Sector. 2012 (in Indonesia version)

AZHAGINIYAL. A., Umadevi.G. System dynamics simulation Modeling of Transport, Energy and Emissions Interaction. Civil Engineering and Architecture 2 (4):149-165, 2014.

EIA, Energy International Outlook 2011. Energy Information Administration, U.S. Energy Information Administration

IEO, Indonesia Energy Outlook 2013. Agency for the Assessment and Application of Technology,

Ministry of Transportation Republic Indonesia, 2013.

Ministry of Mineral Resources. Indonesia. http://www.esdm.go.id.

http://www.bps.go.id/linkTabelStatis/view/id/1413. Accessed on May 2015

BAPEDALDA. http://www.padang.go.id. Accessed on February 2015

Ministry of environment Regulation, No.04/2009 concerning threshold limit of vehicles exhaust emissions

RAMACHANDRA, T.V., Shwetmala, (2009). Emission from India`s transport sector: Statewise synthesis. Government of India Report. New Delhi. February 2010.

Padang Statistical Yearbook, 2013

POSTER SESSION D

173: Potential integration of sustainable technology in office building in Ghana: exploratory study

EUNICE ADJEI[1], SIDDIG OMER[2], YUPENG WU[3]

1 University of Nottingham, NG7 2RD, Nottingham, UK. Email: laxeaa@nottingham.ac.uk
2 University of Nottingham, NG7 2RD, Nottingham, UK. Email: Siddig.Omer@nottingham.ac.uk
University of Nottingham, NG7 2RD, Nottingham, UK. Email: Yupeng.Wu@nottingham.ac.uk

Building sector energy consumption has overtaken all other sectors energy use, hence this contributing significantly to the global greenhouse emission levels. It is well known that building performance is influenced by several factors, including architectural design, occupant's behaviour, building service equipment, regulations, technologies applied among others. Integration of sustainable technologies in buildings for solving the above problem remains one of the essential areas in global research, but remains at very slow rate.

This paper seeks to explore typical sustainable technologies with potential integration into office buildings in Ghana for enhanced buildings performance. The research is accomplished through administration of online survey questionnaire using Bristol Online Survey Tool and snowball sampling technique among building professionals in Ghana. The research has concluded three major findings and these are thought to have played a role in the current building energy consumption rate in Ghana. Firstly, only 14% of building professionals in Ghana access building performance of design stage and post occupancy stage. Secondly, most building professionals have little knowledge on performance of typical office building in Ghana. Thirdly, the research did not trace any significant sustainable technology that has been integrated into office building envelope in Ghana which could have affected the building performance positively.

In conclusion, sustainable technologies integrated into office buildings in Ghana is insignificant irrespective of the existing valuable research carried out in other parts of the world. This is due to the prescriptive nature of the building regulations of Ghana; hence it is recommended that the building regulation should be modified into performance based to facilitate the enhancement of performance.

Keywords: Sustainable technology, building regulation, building professionals, building performance, air sealing.

1. INTRODUCTION

There is a growing concern about rise in energy consumption in buildings above other end-use sectors like industrial, transportation, and the other sectors in the world (Lombard et al, 2008; Iwaro and Mwasha ,2010; Sadineni et al, 2011 and Devabhaktuni et al, 2013). It has been estimated that buildings (both commercial and residential) accounts for up to about 40% of world energy end-use; it is responsible for about 24% of world's CO_2 emissions and overall rise in fuel prices leading to high increase in energy prices, (IEA, 2008a and World Energy Council, 2013). The energy consumption is mainly due to the country's economic growth, population, demographic and service equipment demand, (IEA, 2008a; Kwok and Rajkovich, 2010 and Fumo et al, 2010). Though, the energy consumption of a country is mainly due to the above indicators, the research focuses on the factors which influence service equipment demand.

The energy performance of buildings, their needs and consumption, have long been an issue in the debate of construction and real estate sectors Fabbri et al, 2012. Energy saving and environmental sustainability will be the next challenge in architecture, especially as far as technologies and energy plant system solutions are concerned Fabbri et al. (2012) . In tropical climate, demand for indoor environmental comfort in modern building designs has led to reliance on mechanical cooling for larger part of the year. Usually vapour compression air-conditioning systems are used for both ventilation and the dehumidification of the air resulting to high electricity consumption. It has been concluded that air-conditioning is the dominant building service equipment in tropical climate consuming up to about 50% of the total electricity end-use ,(Korolija et al, 2011; Hughes et al, 2011; Chua et al,2013 and Vakiloroaya et. al, 2014).

From reviewed scientific and technical journals as well as published documentations on Ghana, the following issues were identified: 1.Inadequate documentation on electricity end-use in office buildings. 2. Building regulation of Ghana is prescriptive with no technical guidelines. 3. Insignificant building professionals carry out building performance assessment from early design stage to post occupancy. 4. Energy certificate is not a requirement for issuance of building permit. 5. Rise of percentage increase in electricity consumption in commercial and institutional building sector above residential sector, Ghana electricity outlook 2012. The issues identified above are in consistent with an earlier research carried out by Koranteng and Mahdaviv, 2011 and Amos-Abanyie, 2009. It is established, that building performance is affected by the following factors: architectural factors, building service equipment, technology, regulations, climate and occupants. In view of the identified above issues, the typical actual office building performance of Ghana is unknown. Some of the key issues identified above, falls under the factors which affect the building performance. Hence it is undoubted that, the increase in electricity consumption in commercial and institutional building above residential sector has contributed significantly by some of the key issues indicated above. Consequently, improving energy efficiency in buildings is today a prime objective for global energy policy makers, Chua et al, 2013.

In view of the increasing electricity consumption arising from air conditioning systems in buildings; several integrated building approaches have been used to enhance performance. Among them are: technologies, codes/regulations, control strategies, envelope design, building fabric, among others, (Yu et al, 2011; Zhao and Magoulès, 2012; Chua et al, 2013; Devabhaktuni et al, 2013; Haq et al, 2014; Lamnatou et al,2015; Buker and Riffat 2015 and Cuce and Riffat 2015) .

Though, all the above approaches for minimizing electricity consumption have proven to be effective; the research is focusing on the use of technology. According to Oxford dictionary, technology is the application of scientific knowledge for practical purposes. There are several technologies integrated into building for comfortable indoor environment and efficient energy at cost-effective way. It is well known that technologies integrated in buildings which have direct impact on building performance can be classified into two; passive and active.

Active technologies include: active solar thermal technology, smart grids, photovoltaics , building control, building demand, occupancy control, lighting control, desiccant air-conditioning, heat recovery, thermo-active, heat exchanger, among others, (Lamnatou et al 2015, Goyal et al 2015 and Buker and Riffat 2015).

Passive technology include: Insulation, Air tightness, Natural light, Solar gain, Natural Ventilation, building fabric technologies (Phase change materials, Nanomaterial technology etc.), shading, thermal mass, renewable energy technologies(solar power, wind power and fuel cell) among others, (Zhivov et al., 2012, International Energy Agency 2013 and Haung et al 2014,). According to International Energy Agency 2013, hot climate developing economy typically concentrate on building envelope technology for optimized

natural/mechanical ventilation; reflective roofs and wall coatings; low SHGC windows; interior and exterior shading. Studies by some researchers have concluded that integration of technology enhances energy saving in buildings, (Mardiana-Idayu and Riffat 2012; Devabhaktuni et al. 2013 and Buker and Riffat 2015). The rationale for selecting air sealing technology as an energy saving technologies is that air sealing technology alone can reduce electricity for cooling/heating by 20% to 30%, International Energy Agency 2013 and Zhivov et al., 2012. From International Energy Agency 2013, most advanced building programmes in the world focus on very low leakage rates, although specified requirements still vary considerably from 0.2ACH for typical very tight new building with ventilation to 20ACH old leaky houses.

1.1 Research Aim and Objectives

To provide statistically detailed robust data acquired from building professionals in Ghana to enhance the knowledge of researchers on the appropriate cost effective potential sustainable technology for improved electricity consumption in commercial building sector. The specific objectives in achieving the aim have been outlined; among them are: 1. critically review the trend of electricity utilization in commercial building sector and its impact on total increasing electricity consumption concern. This would be achieved through technical and scientific journals review. 2. To investigate the current sustainable technology integrated into commercial building sector by building professionals in Ghana. This would be accomplished through online survey questionnaire using Bristol Online survey tool. 3. To critically review Ghana building regulation regarding building performance to ascertain the technical measure outlined in mitigating the rising electricity consumption in commercial building sector.

2. METHODOLOGY

Critical review of scientific and technical journals were carried out to ascertain technologies and trend of electricity utilization in commercial building sector and its impact on increasing electricity consumption in Ghana. The reviews of journals were followed by designing of the questionnaire and acquisition of ethical certificate for data collection through the questionnaire administration. The questionnaires were mixed open and close format, designed with knowledge of standard building performance questionnaire and literature. The questionnaires were designed for building material manufacturers, building service engineers, architects and government agencies (Ministry of Water and Housing, Ghana Standards Boards and Building Permit Authorities).

2.1 Samples of the Questionnaires

1. If not adequate, to what extent do you agree with the necessity to modify (change to improve quality) the building regulation of Ghana which was enacted in 1996?

- Strongly agree
- Agree
- Turn to agree
- Neither agree nor disagree
- Turn to disagree
- Disagree
- Strongly disagree

2. From your design considerations, what are the typical factors do you consider in sizing air-conditions for office building? (Select all that apply)

- Building envelope materials
- Occupants metabolic activities
- External weather conditions
- ASHRAE standards for indoor environment comfort specification
- CIBSE Guides for indoor environment comfort specification
- Affordability
- Aesthetics
- Building efficiency
- Function of the office space
- Ghana Building regulation
- Other (please specify):

3**.** Do you perform Whole Building Simulation to assess the building performance before handling the building design over to clients?

- Yes
- No
- Other (please specify):

4. What type of window pane/glass do you used mostly in your office building designs? (Select all that apply)

- Single glazing
- Double glazing
- Solar gain reflector
- Low emission
- Triple glazing
- Louvres
- kappa DG internal blind
- SG cool-lite

5. What is the trend of office building designs since the first electricity crisis in Ghana?

- Complicated building design with about 70% glass
- Simple building design with about 30% glass
- There is no change
- Sustainable building design with bioclimatic and passive technology incorporated
- Other (please specify):

6. If a client intends to retrofit an office building to improve building performance, what best advice would you offer? (Select all that apply)

- Insulate the whole building
- Seal all leakages to minimize infiltration
- Efficient building service equipment
- Use bright coloured indoor shading device
- Use daylighting and minimize artificial lighting
- Use thermostatic air condition system
- Use desiccant cooling system
- All of the above
- Other (please specify):

Multistage sampling technique was used for the data acquisition across the building professionals in Ghana. The steps involved include: identifying the cluster of the institutions and buildings; Sample size of participants in each institutions; Generating the username and passwords for the four separate questionnaire link. The four questionnaires links were Architecture; Building Service Engineers; Building Material Manufacturing; Government Agencies (Ministry of Water and Housing, Ghana Standards Boards and Building Permit Authorities). Hence, the multistage sampling technique were categorised into two major stages.

Stage 1: Identifying the cluster of the institutions and building service companies. The clusters of institutions were selected using the knowledge from the critical literature review and snowball sampling technique. Rationale for the selected approach for data sampling technique was as a result of the disperse nature of all the building service engineers companies and institutions to get a representative data for generalisation for the whole Ghana. The anticipated influencing factors on the identification of the cluster selection were: 1. Aside the Architecture, and Government agencies who have registered Institutions; the remaining clusters are disperse all over Ghana. 2. Significant number of institutions in Ghana have its Headquarters in Accra, hence any data acquired in Accra (study area) would be a representative functions of what is happening in the rest of Ghana.

Stage 2: Sample size of participants in each cluster of institutions and building service companies. The administrators of registered institutions stated above; known large scale companies of Building Service Engineers. In order to increase the sample size among building professionals, an initial email was sent to administrators of all building professional institutions and some registered building service companies inquiring their willingness to participate in the study. Out of about 150 emails sent; 55% of the institutions and registered building service companies expressed their willingness to participate in the survey

Among the constraints identified are: 1. Security reasons for participants, no details (name or email address) of an individual in the institution and building service company can be given to me. 2. Username and passwords should be submitted to the administrators for distribution to participants using stratified random sampling i.e. based on the participant speciality or section relating to the study. 3. Limitation of numbers of username and password logins to be sent.

Limitations of the study: 1. Due to the online administration of the questionnaires, the response rate are average. 2. Due to the disperse nature of Building Service Engineers and Building Materials Manufacturing industries, small scale manufacturers were not included in the survey. 3. Average Sample size.

The data was administered and acquired through the launching of questionnaire link from Bristol Survey Tool to participants via emails. Bristol Online Surveys (BOS) is an easy-to-use service that allows you to develop, deploy and analyse surveys via the Web. No complicated set-up or technical knowledge is required and the service is offered free to University of Nottingham postgraduate research students and staff through the Graduate School.

3. CRITICAL REVIEW ON GHANA ELECTRICITY C+ONSUMPTION

From Ghana Electricity outlook 2013, a similar trend of electricity consumption in residential and commercial buildings are observed However, percentage mean growth of electricity consumption in commercial buildings exceeds residential buildings and Industry by 2.8% and 5.1% respectively from 2000 to 2012 . Compared electricity sector end-use of Ghana from both International Energy Agency 2011 and Electricity Company of Ghana 2013, shows a consistent data from 2000 to 2011. However, Electricity Company of Ghana data indicated is not detailed compared to International Energy Agency hence International Energy Agency data source was used for further discussion in this research. The International Energy Agency 2011 data source outlined the total energy generated, domestic supply, electricity losses, final electricity consumption, residential building, commercial and public service building, industry, transport, fishing, other non-specified, and Agricultural and forestry. However, there is insignificant data on transport, fishing, other non-specified, and Agricultural and forestry hence not discussed.

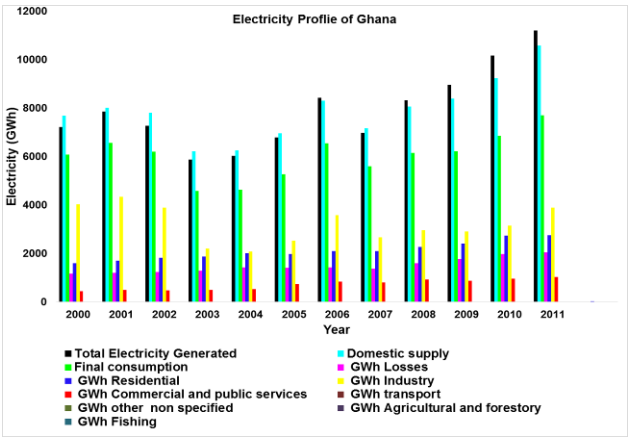

Figure 1: Electricity Profile of Ghana

Source: International Energy Agency, 2011

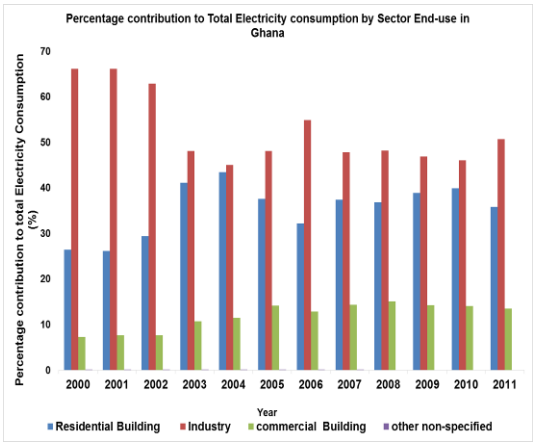

Figure 2: Electricity consumption of Sector end-use

Source: International Energy Agency, 2011

In general, from figure 1, it can be concluded that within 2000 to 2011, the final electricity generated and total electricity consumed have been very dynamic. The total electricity end-use sector by residential and

commercial buildings have increased by 41.7% and 57.2% respectively. However there has been a decline of 3.3% of electricity consumption in the industrial sector within the said period. It is worth mentioning that the total electricity losses have steadily increased by 42.8% within 2000 to 2011; however electricity losses are beyond the scope of this research. From Figure 1, there was electricity deficit in 2000 to 2005 and 2007 that is, the total domestic electricity supply exceeded the total electricity generation hence an import of electricity from neighbouring countries. Within this period, there was corresponding increase of electricity consumption in residential from 1610GWh to 2095GWh and commercial building sectors from 445GWh to 802GWh with corresponding decrease in electricity consumption in the industrial sector from 4027GWh to 2677GWh. The electricity deficit in 2000 to 2005 and 2007 resulted to load allotment ('Dumsor, Dumsor') among all sectors which adversely impacted on the economic development of the country. From Figure1, in 2006 and 2008 to 2011 total electricity generation exceeded the total domestic electricity supply hence electricity was exported to neighbouring countries. Within this period, there was corresponding increase of electricity consumption in residential from 2105GWh to 2761 GWh , commercial building sectors from 842GWh to 1040GWh and industrial sector from 3593 GWh to 3900GWh.

From figure 2, in 2000 and 2001, the percentage share contribution of sector end-use to the total electricity consumption in Ghana remained constant for all sectors with the Industrial sector being the highest above other sector. However, the percentage share of building (residential and commercial) sector to total electricity consumption increased from 2002 to 2005 with decreased Industrial sector. Although there was a reverse trend in 2006, however from 2007 to 2010 there was rise and fall pattern observed in all the sectors. In 2011, there was a significant growth in the industrial sector with a decline in the building (residential and commercial) sector. This notwithstanding, there is an increasing percentage share of the building (residential and commercial) sector to industrial sector in Ghana. In conclusion, inferring from figure 2, the percentage share of building (residential and commercial) sector to total electricity consumption increases with decreasing percentage share in industrial sector. Hence the economic development of Ghana is strongly dependent on increasing percentage share of total electricity consumption by the industrial sector and commercial and public building service sector; this observed trend is in consistent with World Bank Africa Energy Group 2013 report.

4. ANALYSIS AND DISCUSSION

The survey questionnaires were sorted and categorized along the following clusters for analysis: 1. Building regulation appraisal. 2. Sustainable technology used in building materials manufacturing 3. Sustainable technology used in building design and specification and 4. Sustainable technology used in building service selecting and sizing.

4.1 Building Regulation Appraisal

The building regulation appraisal carried on building professionals in Ghana have been summarized from figure 3 to 8. The appraisal was based on 10 factors; however those of relevance to this study include codes/regulations used in Ghana for performance assessment, sizing and selecting equipment; cost effectiveness in implementing the Ghana building regulation; empirical basis of the regulation; need for modification of the regulation to assist in minimizing electricity consumption; government effectiveness in implementing the modification as well as the existing regulation and common non-compliances encountered during issuance of building permit.

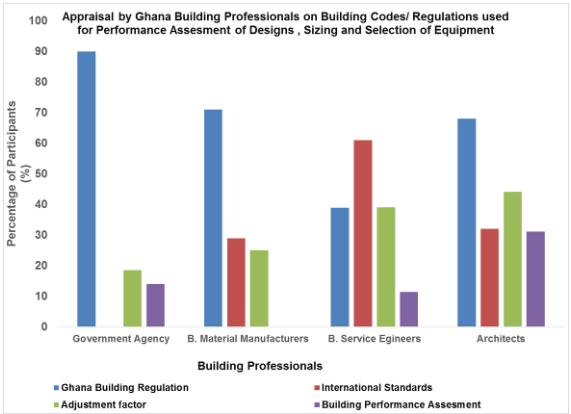

Figure 3: Typical Codes/regulations Use

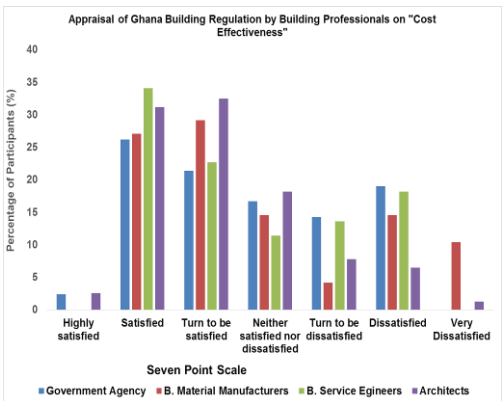

Figure 4: Cost Effectiveness

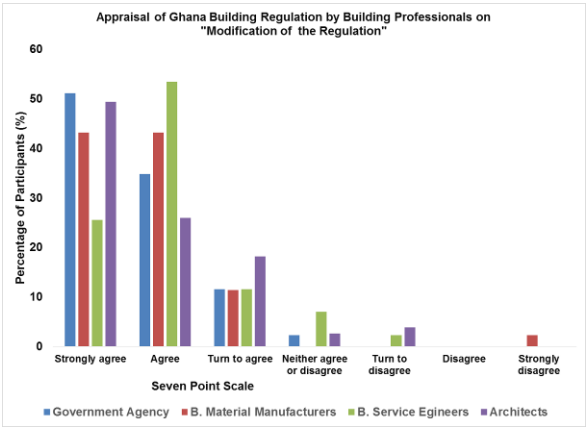

Figure 5: Recommendation for Modification

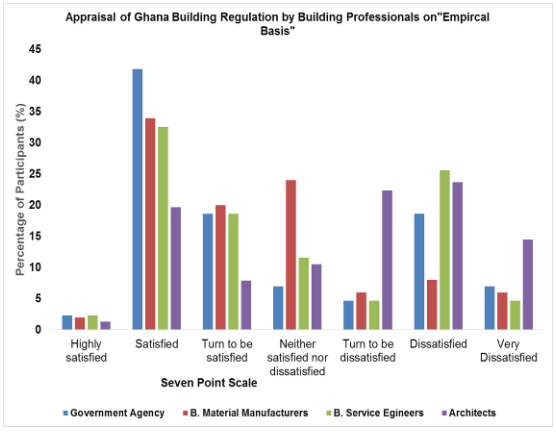

Figure 6: Empirical Basis

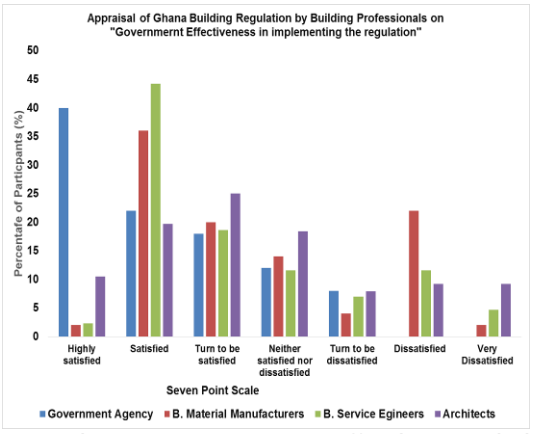

Figure 7: Government Effectiveness in implementation

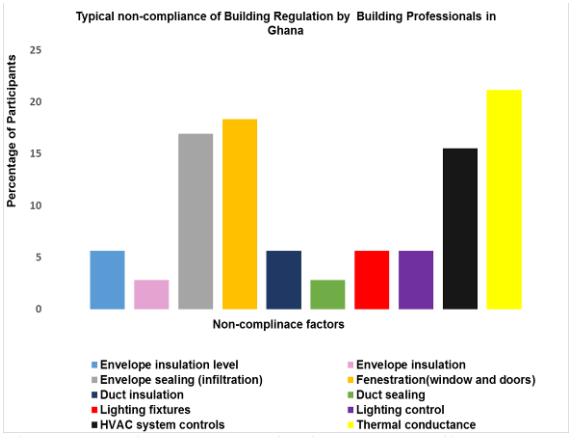

Figure 8: Typical non-compliance

From figure 3 to 8; the appraisal is analysed along strength, weakness, opportunities and threats, which is known as SWOT analysis. Strength of the building regulation as assessed by all building professionals can be seen in figure 3, 4 and 6. From figure 3, significant participants above 60% of building professionals use Ghana building regulation except building service engineers who dominantly use International codes/regulations. Finally, from figure 3, insignificantly average of 14% of all building professionals undertakes building performance assessment except building material manufacturers with insignificant percentage of participants. From figure 4, on the seven point scale used, the responses were significantly dispersed along all seven point scales. In detail, an average of 30% of all building professional participants was satisfied with the cost effectiveness in implementing the building regulation. With only 2.4% and 2.6% of government agency (Ministry of Water and Housing, Ghana Standards Boards and Building Permit Authorities) and architects respectively were highly satisfied. Conversely, 10.4% and 1.3% of building service engineers and architects respectively were highly dissatisfied. From figure 6, the responses were also significantly dispersed along all the seven point scales. In detail, an average of 2% of building professionals are highly satisfied with empirical basis of Ghana building regulation; with an average of 8% of all building professionals highly dissatisfied. However, a dominant number of average participants of 32.05 of building professionals were satisfied. On weakness, based on the fairly dispersed nature of all the above factors along the seven point scale; there is no significant weakness identified within the appraisal of the building regulation. On opportunities; figure 5 and 7 shows that the building regulation needs modification and the government is effective in implementing the building regulation as well as any recommended modification by building professionals. On threats, figure 8 shows typical non-compliance of the building regulations during the issuance of building permit. The significant percentage of typical non-compliance by all building professional from figure 8 are: 22%; 19%; 17% and 16% for thermal conductance of materials (concrete blocks, roofing materials); fenestration (window and doors); Envelope sealing (infiltration) and HVAC system controls respectively. In conclusion, based on these typical non-compliance issues above which have significant impact on building performance and subsequently energy usage; there is an opportunity for potential sustainable technology to be integrated in buildings in Ghana.

4.2 Sustainable technology used in Building Materials Manufacturing

From the respondents, 79% indicated that, they have not used any other binding materials such as fly ash, blast furnace slag and silica fumes as a replacement of ordinary Portland cement or as an admixture. Although, the use of local building materials policy (mud bricks; bamboo; straw and clay block) which are environmentally sustainable materials; have been enacted into law in 2010 in Ghana, however the local building materials listed above are not the dominant materials manufactured except bamboo. The principal reasons these local environmentally sustainable materials are not produced in commercial quantities for office building in Ghana are: 24%; 22%; 19% and 14% are poor mechanical properties; technology for refining and enhancing properties; equipment and durability respectively. Typical building material manufacturers materials manufactured and practices are summarized in figure 9 and 10.

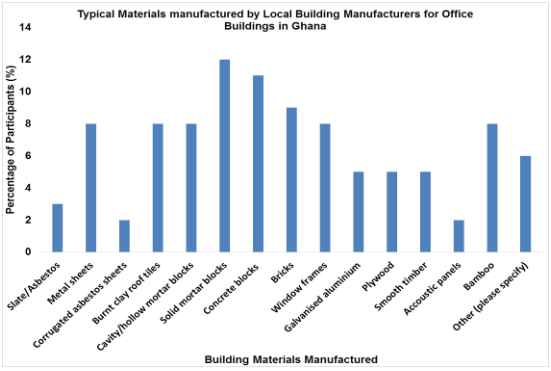

Figure 9: Typical manufactured materials

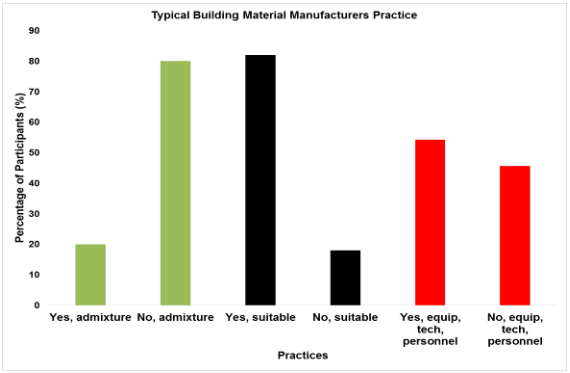

Figure10: Typical building manufacturer's practices

Figure 9 shows typical materials manufactured by local Building Manufacturers for office buildings in Ghana. The typical responses of participants for building materials manufactured as shown in figure 9 are as follows: metal roofing sheets, burnt clay roofing tiles, cavity/hollow mortar blocks, window frames, bamboo were all 8% each; the most significant materials were 12%, 11% and 9% respectively for solid mortars, concrete blocks and bricks respectively.

From figure 10, 80% of the participants do not add any admixture to the materials produced in figure 9. The challenging issue is that, from figure 10, 82% of the participants indicated that the materials produced in figure 9, are suitable for Ghana climate.

From figure 10, there was a slight percentage difference of 8.6% among participants who indicated that they have technology, equipment and personnel to manufacture these sustainable environmental materials.

4.3 Sustainable technology used in building design and specification

From the survey questionnaire, 52.6% architect respondents admitted that there is difference in parameters when designing natural cooling and air-conditioned office building envelope design whiles 41% responded that there is no difference. From architects, the trend of office building designs since the first electricity crisis in Ghana have been 57.1% and 24% representing complicated building design with up to about 70% glass and no change respectively; with only 10% indicating the integration of sustainable building design with bioclimatic and passive technology in their designs. Substantial percentage of 63% participants indicated that fully passive multi-story office building cannot be designed and constructed at efficient cost, low energy utilization and comfortable indoor environment under Ghana climate. Conversely, architect participants indicated that, typical factors which influence their design and specification of new multi-story office buildings are: 12% each for (Minimizing negative environmental impacts eg. Pollution, cost, Sustainable construction materials among others) and 11% each for (Thermal performance (R-value, heat capacity etc); Durability and Clients specifications). Significant architects indicated that in future if the building performance assessment of an existing typical multi-story office building is not acceptable; they would most likely recommend the following: 24%; 17% and 16% been change building design of wall, roof and window pane; Use efficient building service equipment and Improve building sealing to minimize

infiltration respectively. The summary architect participants for different questions on typical passive technologies used in designing and specifying building envelope elements as shown in figure 11.

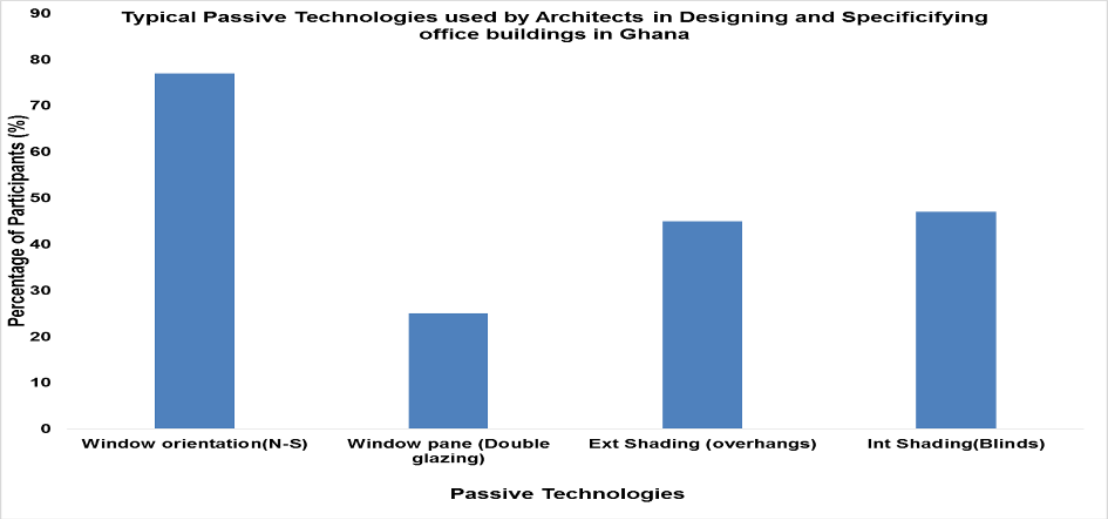

Figure 11: Typical Passive Technologies

From figure 11, it can be deduce that the typical passive technology used in building design and specification is window orientation 77% followed by, 47% for the use of blinds for internal shading; 45% for use of overhangs for external shading and finally, 25% for double glazing window pane. Although significant passive technologies are integrated into building design and specification; they are based on the affirmation of typical technologies described by International Energy Agency 2013 in above.

4.4 Sustainable technology used in building service equipment selection and sizing.

Significant Building Service Engineers participants of 59%, indicated that office buildings in Ghana does not require Energy certificate for operation. Interesting, 96% of the participants agree that the government should introduce energy certificate and target CO2 emission rate (TER) for office building operation in Ghana to help solve energy crisis and environmental emissions arising from building service equipment. Substantial participants of 78% indicated that mechanical cooling type is used in Ghana office buildings; with 34%; 30% and 29% been the typical mechanical cooling type of central; split and window air-conditioning systems. Unfortunately, 87% of participants indicated that, typically they do not use building simulation software in sizing the air-condition equipment. Typical factors consider by participants in selecting building service equipment for office buildings in Ghana are 24% each for efficiency and long life span; and 17% for the office space usage. Participants indicated that cooling load in Ghana office buildings are dominantly contributed by 30%; 25% and 22% equipment; solar gain and dehumidifying load respectively. Interestingly, significant percentage of participants 66%; indicated that building fabric used currently in Ghana's climate is suitable.

The summary of all technologies typically recommended to clients by building service engineers are summarized in figure 12.

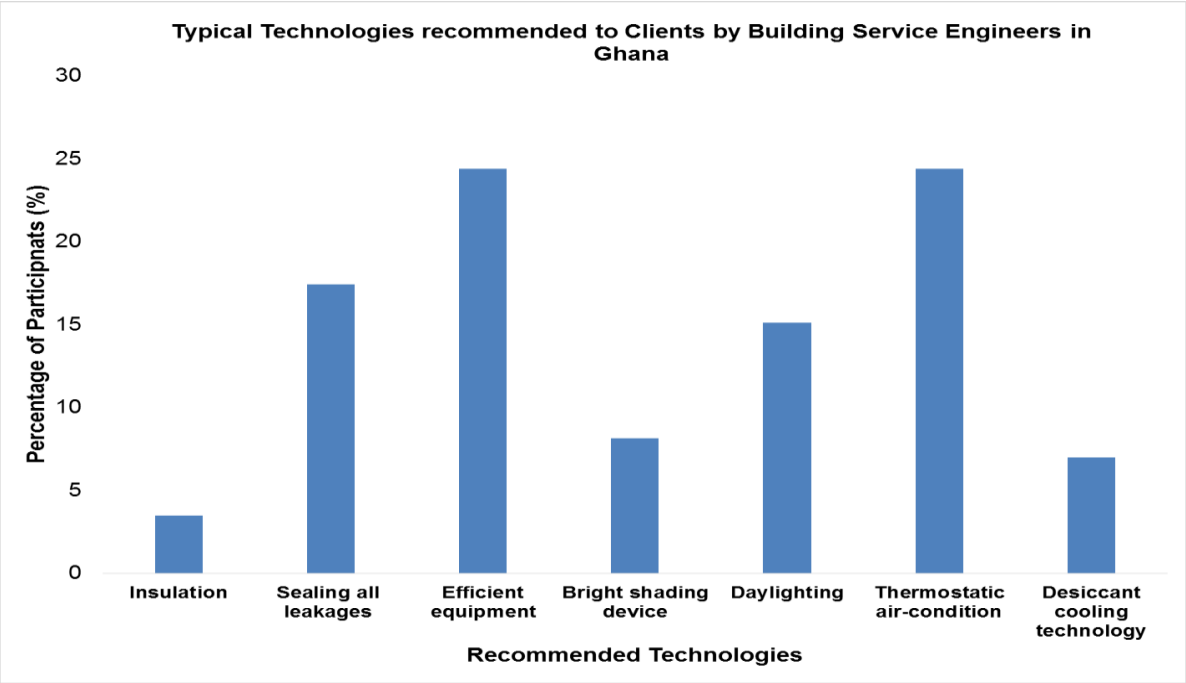

Figure 12: Typical Technologies used by Building Service Engineers for office building retrofit

From figure 12, Participant's indicated that, if client intends to retrofit an office building to improve building performance they recommend the following: 24.4% each for use of efficient building service equipment and thermostatic air-condition system; 17.4% for sealing all leakages to minimize infiltration; 15.1% for the use of daylighting and 8.1% for use of bright coloured indoor shading device. Conversely, only 7% and 3.4% recommended for use desiccant cooling system and insulate the whole building respectively.

4 CONCLUSION AND RECOMMENDATION

The following conclusions have been outlined from this research: 1. insignificant percentage of all building professionals do undertake building performance assessment. 2. Insignificant percentage of sustainable technologies are presently integrated into building design, specification and selection. 3. The overall appraisal of Ghana building regulation by building professionals shows satisfactory assessment; however there was a strong recommendation for modification. 4. Improving building sealing to minimize infiltration was considered as a future recommendation by architects and building service engineers for enhancing building performance. 5. Finally, all building professionals agreed that the building fabric used for office building is suitable for Ghana's climate.

In recommendation, the building regulation of Ghana should be modified into performance based regulation. This would encourage building professionals in undertaking performance assessment of design, selection and sizing equipment; integrate sustainable building technology and minimize high electricity consumption caused by high cooling load arising in commercial and institutional buildings.

5 REFERENCES

AMOS-ABANYIE, S., Akuffo, F.O. and Quagrain, V., 2009. Unveiling Energy Saving Techniques for Cooling in Residential Buildings in Ghana.‖ International Journal of Ventilation, Vol. 8, Issue 1, Coventry, UK, pg. 23-35.

Ben Richard HUGHES, Hassam Nasarullah Chaudhry, and Saud Abdul Ghani, 2011. A review of sustainable cooling technologies in buildings. Renewable and Sustainable Energy Reviews 15 (2011) 3112– 3120

Christian KORANTENG and Ardeshir Mahdavi, 2011. An investigation into the thermal performance of office buildings in Ghana. Energy and Buildings 43 (2011) 555–563

Hai-xiang ZHAO and Frédéric Magoulès, 2012. A review on the prediction of building energy consumption. Renewable and Sustainable Energy Reviews 16 (2012) 3586– 3592

IEA, 2008a: Energy Technology Perspectives, 2008: Scenarios & Strategies to 2050: in Support of the G8 Plan of Action. International Energy Agency (IEA) of the Organisation for Economic Cooperation and Development (OECD), Paris, France.

Joseph IWARO and Abraham Mwash, 2010 .A review of building energy regulation and policy for energy conservation in developing countries. Energy Policy 38 (2010) 7744–7755

Kwok AG, Rajkovich NB, 2010. Addressing climate change in comfort standards. Building and Environment 2010; 45(1):18-22.

Kristian FABBRI, Marco Zuppiroli, and Keoma Ambrogio,2012. Heritage buildings and energy performance: Mapping with GIS tools. Energy and Buildings 48 (2012) 137–145

KOROLIJA I, Marjanovic-Halburd L, Zhang Y, Hanby VI, 2011. Influence of building parameters and HVAC systems coupling on building energy performance. Energy Build 2011; 43:1247–53

K.J. CHUA, S.K. Chou, W.M. Yang and J. Yan, 2013. Achieving better energy-efficient air conditioning – A review of technologies and strategies. Applied Energy 104 (2013) 87–104

Mahmut Sami BUKER and Saffa B. Riffat, 2015. Recent developments in solar assisted liquid desiccant evaporativecooling technology—A review. Energy and Buildings 96 (2015) 95–108

Nelson, Fumo; Pedro, Mago and Rogelio, Luck, 2010. Methodology to estimate building energy consumption using EnergyPlus Bench Models. Energy and Buildings 42(2010)2331-2337.

Pérez-Lombard L, ORTIZ J, Pout C, 2008. A review on buildings energy consumption information. Energy and Buildings 2008; 40(3):394e8.

Suresh B. SADINENI, Srikanth Madala, and Robert F. Boehm, 2011. Passive building energy savings: A review of building envelope components. Renewable and Sustainable Energy Reviews 15 (2011) 3617–3631

Siddharth GOYAL, Prabir Barooah and Timothy Middelkoop, 2015. Experimental study of occupancy-based control of HVAC zones. Applied Energy 140 (2015) 75–84.

Vijay DEVABHAKTUNI, MansoorAlam, Soma Shekara Sreenadh Reddy Depuru, Robert C. Green II, DouglasNims, and CraigNear, 2013. Solar energy: Trends and enabling technologies. Renewable and Sustainable Energy Reviews 19 (2013) 555–564

Vahid VAKILOROAYA, Bijan Samali ,Ahmad Fakhar and Kambiz Pishghadam, 2014. A review of different strategies for HVAC energy saving. Energy Conversion and Management 77 (2014) 738–754

Zhun YU, Benjamin C.M. Fung, Fariborz Haghighat, Hiroshi Yoshino, Edward Morofsky, 2011, A systematic procedure to study the influence of occupant behaviour on building energy consumption. Energy and Buildings 43 (2011) 1409–1417

ZHIVOV, A., D. Herron, J.L. Durston and M. Heron, 2012. Achieving good air tightness in new and retrofitted US Army buildings, presented at TightVent Europe Workshop, Brussels, 28-29 March.

184: The studies of nanotechnology applications on the development of energy and technology teaching material

CHIENKUO KU[1], CHIALING WEI[2]

1 University of Taipei, No.1, Ai Kuo West Road, Chung Zheng District, Taipei,2007ckku@gmail.com
2 University of Taipei, No.1, Ai Kuo West Road, Chung Zheng District, Taipei, chialing@mail.mhups.tp.edu.tw

Energy storage devices have the characteristics of high activity, large surface area, ultrafine crystal grain characteristic and particular electro-optic properties, and hence energy storage devices are actively developed worldwide, attempting to provide high capacity of energy storage system which is better than the current capacity of batteries. Taiwan has developed high capacity power storage elements and electro-optic batteries, aiming at enhancing the usage efficiency and reducing the waste consumption. Besides, the nanotechnology in power saving has designed new form of solar panels, which are able to absorb sunlight more efficiently. At present, schools in Taiwan have not provided any courses related to nanotechnology. In order to promote energy and nanotechnology education, related supplementary teaching material is developed. This research aims at using ADDIE teaching mode to develop the nanotechnology applied on energy teaching material. To analyse learners and teaching requests and opinions, students and teacher are interviewed. Then the integration and analysis of related literature, K-12 curriculum, and learners' characteristics are completed, in order to design the teaching material structure. Stories as teaching material are outlined based on the structure. Education, nanotechnology and energy experts are invited to review the accuracy and appropriateness of the content. The teaching material is designed for three-hour classes, and the participants are grade-six 25 students. This teaching material is presented as stories and hands-on experiments. The teaching time is arranged after school, and the length is 90 minute. It will take two classes to complete the teaching. The review and improvement of the teaching material are made through qualitative interview. The teaching material is shared through the website.

Keywords: nanotechnology , energy, K-12 curriculum , Elementary Schools , picture Books

1. INTRODUCTION

Taiwan energy resource is limited, and the power generation is mainly depending on fire plants (Legislation Yuan, 2009). At the same time, Taiwan is located in Tropic of Cancer, with sufficient sunlight. To solve the problems of relying on imported fossil fuel, we should focus on enhancing power generating, developing high efficient battery and solar power generation. At the moment, energy in Taiwan relied mainly on fire plants, which will cause high carbon emission.

In the future, the raising of the temperature and extreme climate change is inevitable. In Taiwan many companies have developed high capacity power storage elements and electro-optic batteries, aiming at enhancing the usage efficiency and reducing the waste consumption. Besides, the nanotechnology in power saving has designed new form of solar panels, which are able to absorb sunlight more efficiently. At present, schools in Taiwan have not provided any courses related to nanotechnology. At the moment, elementary schools and high schools have the structure of curriculum and text books regulated by the government, and teachers have the schedule for the teaching, therefore the nanotechnology and energy issue is seldom mentioned. If elementary teachers are provided with the nanotechnology and energy supplementary teaching material, reducing the time for designing, teachers will be motivated to teach more about the related topic, and the students will get to know more about the present and future issue of nanotechnology and energy. A number of researchers thinks that the stage of elementary school is the effective and appropriate time to promote energy education.(Jin-Zhong, Zhou, 2003, You Guang-Zhao 2004, Lin Yun Hong, 2006.) However, government's promotion of energy education should face up the accurate and attitude of teacher's energy knowledge, they will then integrate the correct energy knowledge into proper teaching and related activities. What kind of teaching material should we provide to help teachers in nanotechnology and energy teaching? Comic booksor picture books can enlighten children's cognition, attitude and personality (Ming Yi, Lin, 2000). The best Comic books are experiences with the written text (Kiefer, 2010). And Comic books are the good teaching material for forming the concept.

Moreover, Taiwan students should stress on science reading. If the teaching material can combine with reading classes, then science learning can extend to language classes. According to the Culture Councils of Legislative Yuan, comic books or picture books are the children book which uses pictures to tell stories. Comic books or picture books are the story book which combines story and picture, besides conveying messages, it will strengthen the content (Yang Ya-Shu, 2010). Using teaching material with illustrations, after practicing for a few times, children can reach the goal of learning (Xu Su-Xia, 2002). The words used in the comic books or picture books are fewer, and more illustrations are used to express the knowledge (Lewis, 2001). Even though comic books or picture books are simple, but the meaning expressed through illustration is deep (Splocha, 2007), and the illustrations provided by the comic books or picture books will reduce the gap between reading and writing. Lin Mei-Zhi (2009) thinks that ecological picture books teaching can improve students' emotion, motor skill, and social responsibility. And Sheng Jia-Yan (2009) after the teaching of picture books, the experiment group and control group have significant difference. Xie Yi-Ting (2008) points out that the picture books on science, including nanotechnology and energy ,are rare for k-12 students in Taiwan. This kind of theme and publishers are yet to be developed. However, Taiwan needs to develop nano-energy related comic books or picture books to reflect environmental problems. The purpose of this research is as following: Understanding the teachers' and students' opinions of the layout and content of picture books, Developing the nanotechnology and energy related picture books as a supplementary teaching material.

2. METHOD

This research used the teaching mode of ADDIE, which is divided into analysis, design, develop, implementation and evaluation.

2.1 Analysis

Investigate teachers' opinions on nanotechnology and energy teaching and understand teacher's individual background, in order to understand the current nanotechnology and energy teaching status and also the needs for teaching materials. A total of seven experts who comprises of two energy education experts, one nanotechnology experts, four elementary nature subject teachers who have the nanotechnology and energy teaching experience. Through the analysis of text books, we get to know students' concept of energy and nanotechnology, and also through interviews of three six-grade students, students' opinions of comic

books or picture books as supplementary, influences of fossil fuel power generation and environmental impact, and also the energy solution by using nanotechnology are analyzed.

2.2 Design and Development

The design stage is created based on the analysis result of the teaching materials structure. The planning of the content:

(1) **Energy:** The natural resources in Taiwan are limited, and the energy power is imported. More than 60% of power comes from fossil fuel. Taiwan needs to save energy, reduce carbon emission and develop renewable energy.
(2) **Energy technology**: Taiwan has developed high capacity power storage elements and electro-optic batteries, aiming at enhancing the usage efficiency and reducing the waste consumption.
(3) **Nanotechnology**: in power saving has designed new form of solar panels, which are able to absorb.

The development stage is created based on the related information to draw the illustration in the design stage. And turn the content of the book into teaching material, and after the suggestions of experts, we have finalized the picture books. In order to design the teaching material structure, stories as teaching material are outlined based on the structure. Education, nanotechnology and energy experts are invited to review the accuracy and appropriateness of the content.

2.3 Implementation

The students should undergo teaching according to the design of teaching material, comic books book, they should watch the teaching demonstration, comparing to self-teaching idea, or they can have students to prepare for the related information and pre-studying the learning material, and the learning effect will be better. The teaching material is designed for three-hour classes, and the participants are grade-six 25 students. This teaching material is presented as stories and hands-on experiments. The teaching time is arranged after school, and the length is 90 minute. It will take two classes to complete the teaching.

2.4 Evaluation

After the script of the books, teaching material, is finished, the concept of students on nanotechnology and energy issues is applied before and after the teaching. The review and improvement of the teaching material are made through qualitative interview.

2.5 Tools

The research tools are self edited by the researcher, which include: the interview of teachers' and students' opinion, the pre and post tests of nanotechnology and energy teaching.

(1) The interview of teachers' and students' opinions of the supplementary teaching material of nanotechnology and energy

Interview teacher in terms of teaching demand, aims at understanding teachers' demand on the supplementary teaching material of nanotechnology and energy issues. During the interview, with the permission of the interviewees, the interview is recorded and transferred into word files. And students are interviewed, also, in order to develop teaching material and teacher's manual.

(2) The learning achievement of teaching material

The books used in the research is developed by the researcher and illustrated by an artist. In order to reach the purpose of learning, after the teaching activities, teacher will test the students' learning achievement for ten minutes, to revise the book, so that the picture books will be finalized.

(3) Data processing

This research used SPSS for Windows to carry out statistic analysis: the overall information was gained from descriptive statistic analysis.

3. RESULTS AND DISCUSSION.

3.1 Understanding teachers' and students' opinions of the supplementary teaching material of nanotechnology and energy

According to interview, teachers' related sources obtained from television and websites. Relatively, information obtained from seminars is fewer. Teachers' view on nanotechnology and energy related teaching material and pedagogical demand. The comic books or picture books are far more interesting than text books, and will arouse students' interest. Teachers point out that teaching material should emphasize on energy technology research in Taiwan, and examples of the research done by Taiwan scholars. Comic books or picture books are the best supplementary tools. Students' understanding on the burning of fossil fuel will emit greenhouse gas, besides petroleum, they have limited knowledge on coal and natural gas. They have limited knowledge on solar power, hydropower and wind power. Students aware that global warming will cause the melting of ice in south and north pole, leading to sea level rising, ecological disappearing. Through the content of picture books, students will get to know these disasters, and face the future environmental challenge.

On the part of students, they generally think that the application of nanotechnology, the nanotechnology research done by Taiwan scholars, and how nanotechnology can solve energy problems are not mentioned in the classes. They also suggest that when introducing nanotechnology and energy concept, hands-on experiments should be implemented.

3.2 Developing the nanotechnology and energy related comic books as a supplementary teaching material

We developed nanotechnology and energy supplementary text books using comic books, which divided into three parts:

1.Clean energy: We introduce different kinds of solar panels, including single crystalline, polycrystalline silicon, thin film, and also biofuel.

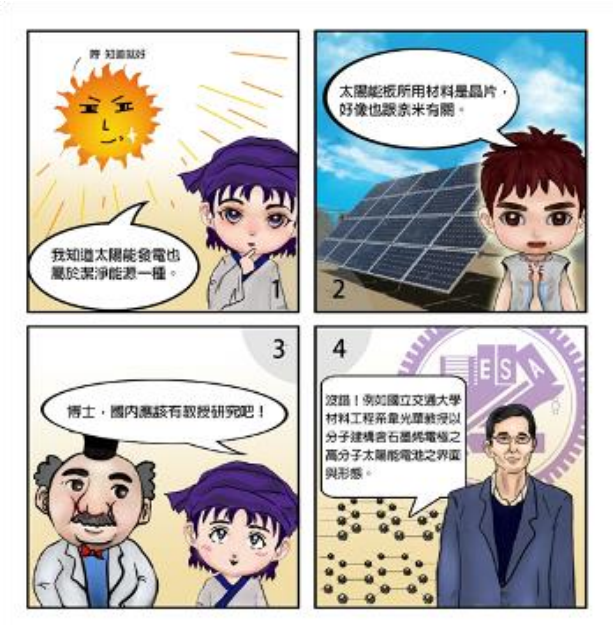

Figure 1: Introducing solar panels and researchers

Figure 2: alcohol biofuel

2. Storage battery: We introduce lithium battery types and principals, and also researchers in Taiwan.

Figure 3: Introducingbatteries and researchers.

3. Illumination and electronics appliance: We introduce commonly seen lightings, efficient lightings, and also energy saving advantages.

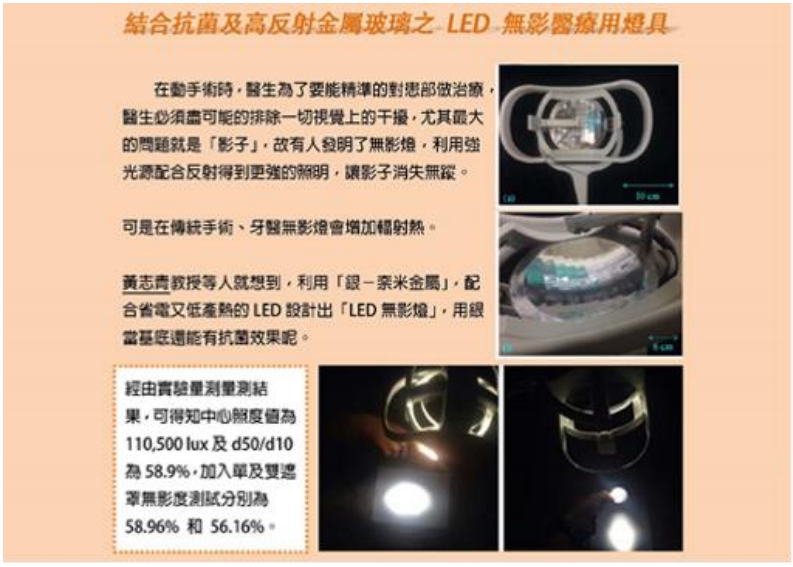

Figure 4: Efficient lightings.

3.3 The concept of students on nanotechnology and energy issues is applied before and after the teaching

Two experts and two elementary school teachers reviewed the comic books, and undergo three-hour teaching (picture 5). Students are interested in the comic books, and felt that they are interesting, practical and learning response was good. Besides, students also went through interaction games to evaluate students' understanding on the contents(picture 6).


Figure 5: Discussion.


Figure 6: Students'responses were active


Figure 7: online interaction games.

To understand students's learning, before and after teaching, evaluation of nanotechnology and energy concept would be carried out. The study shows that before classes, students are correct about what is nanotechnology or nanotechnology labels, but for the application or the relation between nanotechnology and energy, the accuracy was only 40~50%. After classes, the accuracuy reached 60%-90%, showing comic books books teaching helped improve the learning of nanotechnology and energy field, see table 1.

Table 1 The comparison of before and after nanotechnology comic books teaching.

Questions	Concept testings%	
	Pre	Post
1. What is nanotechnology?	48.3	100.0
2. Which of the following is not nano structure or phenomena existed in the nature?	31.0	44.8
3. What is nanotechnology?	96.6	96.6
4. When using wood to be fossil fuel, what is the special fact about the black outer surface of the pot	13.8	75.9
5. Which is the nanotechnology label?	93.1	100.0
6. Which is the energy application of nanotechnogy?	48.3	69.0
7. What is the characteristics of nano CD rom?	48.3	58.6
8. What is the main function of the nano windshield coating?	48.3	75.9
9. What is reason for adding nanoparticles into beverage?	24.1	62.1
12. What is the reason for nanofabrics?	93.1	79.3
13. Which battery belongs to nanotechnology?	69.0	75.9
15. Which tools use solar panels to generate power?	82.8	89.7
16. Can nanotechnology improve the exhaust gas emitted by cars?	55.2	72.4
19. Which tools are not using heat to transfer into electricity?	24.1	41.4

4. CONCLUSION

1. Teachers' demand for comic books or picture books are very high, as nanotechnology and energy issues are seldom appear in elementary schools. Teachers mainly integrate the theme into subjects of social, language and nature, which can be a reference for future lesson planning. Students like joyful and warm stories with vivid and rich colours. Every student is able to say something about solar energy, and highly concern about the effect of global warming after reading comic books.
2. We develop comic books, based on teachers' demand on nanotechnology and energy supplementary teaching material, and surveys on senior elementary school students' books.
3. Comic books teaching significantly improves students' learning on nanotechnology and energy. Comic books teaching helps building up students' consciousness toward nanotechnology and energy issue. After the statistic analysis of comic books teaching, the learning would be easier if it is taught through comic books.. Students highly affirm comic books integration into teaching.

5. ACKNOWLEDGEMENT

The financial support from the National Science Council (MOST 103－2120－S－845－001) of Taiwan is gratefully acknowledged.

6. REFERENCES

ARIZPE, E. & Styles, 2003, Children Reading Pictures; interpreting visual texts, Routledge Falmer, Londen.

CAI, D.-X. , 2007, Love San-Chong: Old Photos tell Story. San-Chong City Office, P.173.

KIEFER, Barbara Z.,2010, Charlotte Huck's Children's Literature. New York, McGraw-Hill.

LEWIS, D., 2001, Reading Contemporary Picture Books, Routledge Falmer, London.

LIN, W.-J., 2009, The Analysis of the climate change concept in Elementary and High School text books , 2009 Environmental Education Conference B-116.

SHEN, J-Y., 2009, The Study of teaching effectiveness in Developing ADDIE mode in wind power animation and picture books supplementary teaching material for senior elementary students, Taipei Municipal University of Education, Taipei.

STRASSER, J. & Seplocha, H., 2007, Using picture books to support young children's literacy, *Childhood Education*, 83, 219-224.

XU, S.-X., 2002, The Guidance to Taiwan Children Picture Books. National Taiwan Arts Education Center, P14-15.

ZHOU, J.-Z, 2009, The Study of Taipei Elementary School Teachers' Attitude toward Energy, Taipei Municipal University of Education.

Grade 1-9 Curriculum Guideline, 2010, Key Issue Environmental Education. Browsing date: 2010/5/18. http://teach.eje.edu.tw/9CC/discuss/discuss3.php

Picture Book Arts Museum, Culture Council, Executive Yuan , 1999, Knowing Picture Book, Browsing date: 2009/12/15. http://children.cca.gov.tw/children/gallery/know.php

Water Resource Agency, Ministry of Economic Affairs. Tamshui River, Browsing date: 2010/5/20. http://www.wra10.gov.tw/service0111.asp

Taiwan Environmental Information Society , 2010, Boundless Earth Day in Tuvalu(1) Paint My Home, Browsing date: 2010/5/20. http://www.wretch.cc/blog/totaltotal/21219828

Facing Global Warming, Taiwan's Response (2008). Global Climate and Greenhouse Gases, Browsing date: 2010/5/20. : http://www.tri.org.tw/unfccc/

@SET_Conference

www.facebook.com/SustainableEnergyTechnologies

www.set2015.org